

## **Probing and perturbing the oligomerization of membrane protein utilizing nanoparticle plasmon coupling and Deep learning**

**Dr. Abu S. M. Mohsin, Associate Professor**  
**BracU,EEE, 66 Mohakhali,Dhaka-1212,Bangladesh**

**Challenges:** Membrane proteins are the first line of communication between the extracellular environment and the cell interior. This communication in cellular systems is largely under the control of complex spatial and temporal networks of macromolecular interactions called signaling pathways [1]. Traditional biochemical tools such as yeast-two-hybrid [2], co-immunoprecipitation [3] together with gene [4] and protein arrays [5] provides critical information on the constituents of interaction networks. Recently it has been known that the activation of epidermal growth factor receptor (EGFR) occurs via dimerization [6,7,8] or higher order oligomerization however the precise geometry, stoichiometry, and relevance to signaling pathways is not known at this time [9].

More recently several state-of-the-art fluorescence based non-destructive, non-invasive super resolution imaging techniques has been used in lateral micrometer and sub-wavelength range to track and analyse the biological molecules, interaction and oligomerization. However, due to the photo blinking and photo bleaching property of fluorophore and destructive nature of imaging these techniques cannot be utilized in live-cell imaging or to examine dynamic information about the uptake or aggregation. In order to investigate the oligomerization of membrane protein and subsequent activation pathway we proposed to use plasmonic nanoparticle and deep learning-based image segmentation technique in human cervical carcinoma (HeLa) cells. Plasmonic nanoparticle will be used as multifunctional probes and nano-spacers in a model cell system to investigate the organization of membrane proteins and to determine how receptor spatial arrangement influences cell behavior. The findings of this study will be helpful in spatial structuring, receptor organization and cellular function and drug delivery. Most importantly, the novelty of our work lies in the presentation of a pioneering technique that allows in-vitro cellular studies of membrane protein interaction in a non-destructive setting under the diffraction limit.

**Proposed Project:** The aim of the project is to determine the role of spatial organization on the function of membrane proteins. The objective of the project is as follows: **(a)** Investigate the light matter interaction of nanoparticle & structure using analytical models (Mathematica/Matlab) & numerical methods (Lumerical-FDTD). **(b)** Probe the spatial organization of membrane proteins (EGFR). **(c)** Control the spatial organization of membrane proteins. **(d)** Determine how receptor spatial arrangement influences cell behaviour.

**Expected Outcome: Expected outcome from aim 1:** Investigate the light matter interaction of single particle and cluster on the 10-100 nm scale. We will provide evidence how the shape, size and geometry of the particle influence the plasmonic property. **Likely Impact from aim 1:** The results will be useful for understanding the fundamental properties of plasmonic nanoparticles and structures and employ them in several applications. This will help to investigate monomer-dimer transitions at the molecular scale. We expect to have one peer reviewed paper from these findings.

**Expected outcome from aim 2:** We will probe the spatial organization of membrane proteins (EGFR) using nanoparticle as a probe or nanospacer. We will demonstrate perturbation of spatial organization through the creation of clusters of different size, spatial extent and geometry. **Likely impact from aims 2:** The impact from this study will be high because it will address the issues of creating clusters with defined size and geometry directly. We expect to have one peer reviewed paper from these findings.

**Expected outcome from aim 3:** We will determine how cellular function is linked to spatial organization of membrane proteins. **Likely impact from aims 3:** The concept of spatial organization appears to be important for polyvalent ligand-receptor interactions where ligand-mediated receptor cross-linking brings components into molecular contact. However being able to ascertain the role of different sizes and geometries has been challenging because of the numerous species on the cell surface. Our novel approach will provide the link between spatial structuring, receptor organization and cellular function. We expect to have one peer reviewed paper from these findings.

The proposed project will help to address SDG 3-Good Health and Wellbeing, SDG4 Quality education and SDG 9 Industry, Innovation, and Infrastructure and help to create skilled workforce for Industry 4.0.

# Probing and perturbing the oligomerization of membrane protein with plasmonic nanoparticles and deep learning

## I. INTRODUCTION

Membrane proteins are the first line of communication between the extracellular environment and the cell interior. This communication in cellular systems is largely under the control of complex spatial and temporal networks of macromolecular interactions called signaling pathways [1]. Traditional biochemical tools such as yeast-two-hybrid [2], co-immunoprecipitation [3] together with gene [4] and protein arrays [5] provides critical information on the constituents of interaction networks. Recently it has been known that the activation of epidermal growth factor receptor (EGFR) occurs via dimerization [6,7,8] or higher order oligomerization however the precise geometry, stoichiometry, and relevance to signaling pathways is not known at this time [9].

More recently several state-of-the-art fluorescence based non-destructive, non-invasive super resolution imaging techniques has been used in lateral micrometer and sub-wavelength range to track and analyse the biological molecules, interaction and oligomerization state without the use of any contrasting agent. However, due to the photo blinking and photo bleaching property of fluorophore and destructive nature of imaging these techniques cannot be utilized in live-cell imaging or to examine dynamic information about the uptake or aggregation. In order to investigate the oligomerization of membrane protein and subsequent activation pathway we proposed to use plasmonic nanoparticle and deep learning-based image segmentation technique in human cervical carcinoma (HeLa) cells. Plasmonic nanoparticle will be used as multifunctional probes and nano-spacers in a model cell system to investigate the organization of membrane proteins and how receptor spatial arrangement influences cell behavior. The findings of this study will be helpful in spatial structuring, receptor organization and cellular function and drug delivery. Most importantly, the novelty of our work lies in the presentation of a pioneering technique that allows in-vitro cellular studies of membrane protein interaction in a non-destructive setting under the diffraction limit.

## II. LITERATURE REVIEW

The optical properties of plasmonic nanoparticles have fascinated many scientists since ancient times [1-5]. The topic has generated renewed interest among researchers, beginning with the developments of classical electromagnetic theory. Gustav Mie [6] deduced Maxwell's equation to explain the strong absorption of the gold nanosphere (AuNS) while illuminated under plane waves, offering a rigorous scientific foundation for understanding these phenomena. More recently, plasmonic nanoparticle has created a considerable amount of interest in the scientific community due to excellent optical properties, especially for nanoparticle plasmon coupling. [7-15] To understand this phenomenon, sufficient knowledge of the electromagnetic properties of interacting metallic nanoparticles at close proximity is required. This property has been introduced in several applications such as solar cells [16-20], data storage [5, 21, 22], biological imaging, [23-27] bio labeling and sensing, [28, 29] diagnostics, [26, 30-32] photo thermal cancer therapy, [33, 34] drug and gene delivery, [28, 35-37] and probing membrane proteins. [38, 39] Recently, the prospect of these plasmonic particles as therapeutic cancer agents and probing membrane protein has grown enormously, which necessitates the particles to be internalized or uptaken by cells. [40-47] Consequently, the study of AuNP uptake of cells has been a major research focus in which the effect of size, [41] shape, [41] surface coatings [42] and concentration have been intensively studied. Previously several research have been conducted on micrometer scale on ensembles however there have been very few research conducted on single particle at nanometer scale. The main objective of this study is to conduct a systematic study to investigate the oligomerization of membrane protein utilizing plasmon coupling and deep learning-based image segmentation technique.

Unlike Forster resonance energy transfer (FRET), there has very few studies conducted to investigate the higher-order spatial organization or oligomerization on the length scale of protein diameters (1 – 10 nm). Therefore, in search of higher-level ordering of receptor clusters, we require a technique that can probe the size regime in 10 – 100 nm. To address such issue, we propose to use plasmonic nanoparticle aided deep learning analysis on nanoparticle (NP)-antibody-EGFR complexes.



# Probing and perturbing the oligomerization of membrane protein with plasmonic nanoparticles and deep learning

Recently Artificial Intelligence (AI) and deep learning methods plays a crucial role in understanding, diagnosing, and treating diseases and analyzing cell images. For microscopic image segmentation, Generative Adversarial Networks (GANs) [48] and other image segmentation technique such as UNet, SegFast etc. has been applied to image segmentation, disease detection, cell or nuclei detection, counting numbers of cells, and cell structure analysis for cancer detection [49]. The primary challenge with this domain is the lack of a bulk amount of data for challenging diseases and variety in the quality of images due to the different types of imaging devices involved.

## III. AIM & OBJECTIVES

**AIM:** To determine the role of spatial organization on the function of EGFR membrane proteins.

**OBJECTIVES:** The objectives are as follows:

- a) Investigate the light matter interaction (of nanoparticle and structure) using analytical models (Mathematica/Matlab) and numerical methods (Lumerical-FDTD).
- b) Probe the spatial organization of membrane proteins (EGFR)
- c) Control the spatial organization of membrane proteins
- d) Determine how receptor spatial arrangement influences cell behaviour.

## IV. EXPECTED OUTCOMES OF THE RESEARCH

**Expected outcome from aim 1:** Investigate the light matter interaction of single particle and cluster on the 10-100 nm scale. We will provide evidence how the shape, size and geometry of the particle influence the plasmonic property. **Likely Impact from aim 1:** The results will be useful for understanding the fundamental properties of plasmonic nanoparticles and structures and employ them in several applications. This will help to investigate monomer-dimer transitions at the molecular scale. We expect to have one peer reviewed paper from these findings.

**Expected outcome from aim 2:** We will probe the spatial organization of membrane proteins (EGFR) using nanoparticle as a probe or nanospacer. We will demonstrate perturbation of spatial organization through the creation of clusters of different size, spatial extent, and geometry. **Likely impact from aims 2:** The impact from this study will be high because it will address the issues of creating clusters with defined size and geometry directly. We expect to have one peer reviewed paper from these findings.

**Expected outcome from aim 3:** We will determine how cellular function is linked to spatial organization of membrane proteins. **Likely impact from aims 3:** The concept of spatial organization appears to be important for polyvalent ligand-receptor interactions where ligand-mediated receptor cross-linking brings components into molecular contact. However, being able to ascertain the role of different sizes and geometries has been challenging because of the numerous species on the cell surface. Our novel approach will provide the link between spatial structuring, receptor organization and cellular function. We expect to have one peer reviewed paper from these findings.

## V. RESEARCH DESIGN

**Conceptual framework:** To utilize gold/silver plasmonic nanoparticle (such as NRs) as both multifunctional probes and nano-spacers of membrane protein (EGFR) organization and combine them with cell biology to determine consequences for cellular function.

**Design:** The experimental design consists of gold/silver nanorods as probes, nano-spacers and a model cell system for investigating receptor function.

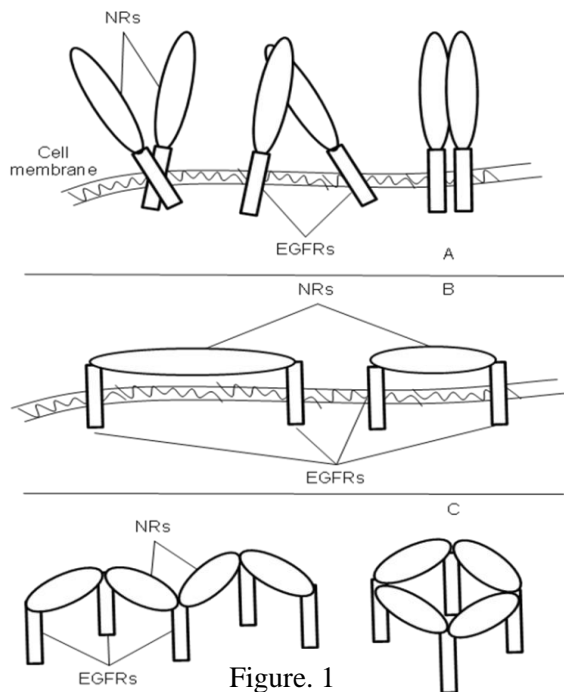
**Nanorods as probes:** We will create gold/silver plasmonic NRs of varying lengths (tunable between 10 nm -100 nm, width can be fixed at anywhere 10 - 20 nm). The synthesized NRs will then be conjugated to antibodies specific to the EGFR (clone 29.1.1 Sigma) using available protocol [13] and the resulting conjugates will be added to the surface of intact normal cells expressing the EGFRs. To measure the size (number of receptors) and average distance between receptors (10-100 nm scale) on the surface of intact cells we will deploy plasmon resonance coupling. The separation distance and conformational information will be determined from the shift of the Plasmon resonance from dark field scattering spectroscopy [30], while the intensity of scattered light will provide information on the number of receptors per cluster

# Probing and perturbing the oligomerization of membrane protein with plasmonic nanoparticles and deep learning

Numerical simulation (finite difference time-domain methods, Lumerical) or analytical Mie-Gans theory [31] on light wave interaction with coupled NRs will be used to calculate SPR shifts with respect to coupling geometries of NRs and subsequent scattering results. Experimental results will then be compared to theoretical simulations to discover conformational geometries of EGFRs. These experiments will be performed on resting (unactivated) cells and cells activated with ligand for the EGFR.

**Nanorods as nano-spacers:** We will then use NRs of specific lengths as steric spacers of receptor-receptor association. We will prepare antibody-nanorod conjugates at low antibody-to-nanorod ratio and add them to cells expressing EGFR with a fluorescent protein tag on the c-terminus as a fluorescence probe of the receptor. We will create NRs of the form antibody-nanorod-antibody to bivalently cross-link receptors at defined spacing. This will enable the effect of space on receptor organization and function. To create higher-level ordering, we will use the antibody-nanorod-antibody system described above and use secondary antibodies against the primary antibodies. By varying the secondary antibody to antibody-nanorod-antibody concentration ratio, and the nanorod length, clusters with different spatial extents and valency will be able to be produced.

Simplistic possible geometric configurations of such higher orderings for 4-5 EGFR receptor monomers or clusters are shown in Figure 1B and Figure 1C. Obviously many different variations in number and configuration are expected.



**Figure 1.** Schematic depiction of membrane protein (EGFR) organization with plasmonic NRs attached as probe or nano-spacers **A.** Receptor pair attached with NRs, and their possible coupling configuration in oligomerization. The signatory SPR shifts induced from these configurations will be detected to unveil their conformational geometries. **B.** NRs used as variable length nano-spacers (10-100nm) between receptor pair or cluster pair. **C.** Possible higher-level ordering involving 4-5 EGFR monomer/dimer/tetramers with NRs as preset nano-spacers

**Model cell system:** We will use a model cell system, Hela cell or BaF/3 cells, which enable the function and biophysics of the EGFR to be studied without the complications of other cell types. This cell line is devoid of other EGFR family members or secreted ligands which would otherwise confound experiments of this type. The EGFR can be expressed in these cells as physiological levels and biophysical and cell biological assays are well-established for this cell system.

## VI. RESEARCH SCHEDULE AND DELIVERABLES

**Specific aim 1: Investigate the light matter interaction (of nanoparticle and structure) using analytical models (Mathematica/Matlab) and numerical methods (Lumerical-FDTD).**

**Year 1, 1<sup>st</sup> half:** We will investigate the light matter interaction of Ag, Au, Al, Ge, Si, Ga using available analytical models (such as Mie and Mie Gans theory) and Numerical Simulations (Lumerical-FDTD). We will determine the effect of size, shape, and geometry of plasmonic nanoparticles and structures and determine the optical and electrical property. This will have a huge impact because, specially providing a guideline to synthesize or fabricate customized nanoparticles or structure. Hence the fabricated structure/device will be helpful in the development of biosensor, plasmonic solar cells, plasmonic nanoantenna, plasmonic circuitry, and other biological applications. We expect to have one peer reviewed paper from this section.

## Probing and perturbing the oligomerization of membrane protein with plasmonic nanoparticles and deep learning

### **Specific aim 2: Probe the spatial organization of membrane proteins (EGFR)**

**Year 1, 2<sup>nd</sup> half:** We will firstly create model clusters of nanoparticles for probing oligomerization. We will vary the concentration of antibodies relative to nanoparticle (nanorod/bipyramid) concentration to control the valency per nanoparticle (nanorod/by pyramid) and inject the secondary antibodies for cross-linking and clustering nanoparticle in solution. We will use confocal/dark field micro-spectroscopy (spectrum and polarization selective light scattering) to probe the spatial organization of Nanoparticle-antibody complexes. Electron microscopy will be employed to get a clear geometry of clustering and correlated optical images will be analysed. Dark field imaging will be performed using Nikon trinocular upright LED microscope ready to operate at Brac University, EEE Nanobiophotonics lab along with chemical synthesis and bio lab. Consumables such as Nanoparticle precursors, antibodies, EGF ligands and fluorophores will be required.

### **Specific aim 3: Control the spatial organization of membrane proteins**

**Year 2, 1<sup>st</sup> half:** We will perform numerical simulation of various geometry of predetermined nanoparticle cluster by commercial Lumerical (finite difference time domain simulation –FDTD software). For the experimental purpose we will prepare nanoparticle-antibody complex in a model cell system (HeLa/BaF/3 cells), for linking with EGFRs. Nanoparticle containing only one antibody will be used to probe cell surface organization of EGFR. We will also investigate spatial organization which means-identify number of receptors per cluster and the average distance between clusters. We will use three types of nano-spacers to perturb the spatial organization of nanoparticle-antibody complex on model cell system. The first type of experiment will be nanoparticle-antibody complex, second experiment antibody-nanoparticle antibody and the third experiment polyvalent complex. The 2<sup>nd</sup> and 3<sup>rd</sup> will be useful to determine average distance and identify number of receptors per cluster. The number of receptors per cluster will be determined from the scattering strength of plasmon resonance. Also the average distance between receptor will be determined from the shift of plasmon resonance as previously identified from numerical simulations. The generative adversarial network (CGAN) or other Deep learning algorithm (SegFast) will be used for probing the spatial organization. For that purpose, we will build our image library capturing dark field images of nanoparticle-antibody complex, later level the image, test and train the image for further analysis. Consumables such as tissue culture reagents and microscope substrates, immersion oil, coverslip glass and lamp will be required

### **Specific aim 4: Determine how receptor spatial arrangement influences cell behaviour.**

**Year 2, 2<sup>nd</sup> half:** We will probe and control the spatial organization of the EGFR monomers and clusters in higher-level oligomerization. The dark field images of nanoparticle-antibody complex will be analysed utilizing plasmon coupling concept. Later the findings will be verified using deep learning algorithm to identify best complex which have effect on spatial organization. Standard cell biological assay will be used to determine the impact on receptor organization, cellular proliferation, and survival

**Execution Plan:** Dr. Abu S. M. Mohsin (PI), BracU, BD will lead the project and responsible for nanoparticle cell interaction section, (Aim 1-3), Professor Dr. Mohsin Kazi (CO-PI), King Saud University will be responsible for bio-conjugation and cell signaling (Aim 3-4).

#### Time schedule

Aim	Task	GANTT CHART (months)											
		2	4	6	8	10	12	14	16	18	20	22	24
Goal 1	Finding Gap in Literature												
Goal 2	Analytical + Numerical												
Goal 3	Synthesis/Fabrication												
Goal 4	Experiment (Dark field)												
Goal 5	Data processing using Deep learning												
Goal 6	Results & Publication												

## VII. IMPACT & RELEVANCE TO THE INSTITUTE AND COUNTRY

# Probing and perturbing the oligomerization of membrane protein with plasmonic nanoparticles and deep learning

**How the research is significant and how the research addresses an important problem:** Membrane proteins are significant because (1) They make up 30% of proteins encoded in the human genome, (2) They perform critical functions in normal physiology, (3) They are targets for the majority of drugs in the pharmaceutical industry. EGFR is an archetypical type 1 membrane receptor protein that controls cellular processes such as proliferation, migration and survival. However, the way in which a single receptor can mediate a variety of cell pathways is poorly understood. This research will examine an aspect of membrane-protein structure of EGFR in which the higher-level cluster-cluster oligomerization and 2D spatial organization on a cell surface alters cellular functioning. This is significant because up to relatively recently this aspect of membrane protein structure has been largely explored using methods that destructively extract proteins from the cell surface or imaging methods that don't have the resolution to deal with interactions in the 10-100nm scale [28].

**How the outcomes will advance the knowledge base of the discipline with novel and innovative aims and concepts:** The outcomes will advance the knowledge base of the discipline by providing the following novel information; (1) New understanding on the association of an important membrane receptor (EGFR) on the 10-100 nm scale. Up to now, only information on the 1-10 nm or beyond 250 nm scale has been obtainable on living cells. This goal is achievable using our expertise in the exploitation of the novel optical properties of anisotropic plasmonic nanoparticles such as NRs. (2) New understanding on the role of spatial organization with respect to size and geometry of receptor clusters on cellular behavior. This goal is achieved using our expertise in plasmonic NRs, multidimensional microscopy and EGFR biophysics.

**Environmental, social or economic benefits:** Bangladesh is a developing country and through this innovative project Bangladeshi researcher is going to endorse their footprint in the scientific innovation of biological science, structural biology and immunology. There is a need, however, to develop new basic technologies, grounded in fundamental physics and biology that can probe the internal structure and dynamics of living cells. This application spans several priority areas and makes use of frontier technologies (bio) photonics and deep learning to understand a fundamental yet complex problem. The project relates directly to the research priority area Frontier Technologies for Building and Transforming Bangladeshi Industries since its outcomes will spawn development of new biophotonic-based/deep learning-based assays which have potential use in the biotechnology or pharmaceutical industry. The project will provide multidisciplinary training across cell biology, pharmacist, biophysics, biochemistry, nanotechnology and deep learning for developing researchers such as postgraduate research students. Furthermore, the project is consistent with a growing need to draw together different disciplines for the study of complex systems/problems. The proposed project will help to address SDG 3-Good Health and Wellbeing, SDG4-Quality education and SDG 9 -Industry, Innovation, and Infrastructure. Most importantly, this project will help to create an educated skilled workforce who will be able to face the challenges put forward by the industry 4.0 revolution.

## VIII. CONCLUSION

To conclude, this proposal spans several priority areas and makes use of frontier technologies (bio photonics) to understand a fundamental yet complex problem to develop new basic technologies, grounded in fundamental physics, biology and chemistry which have potential use in the biotechnology and pharmaceuticals industry. Furthermore, the project is consistent with a growing need to draw together different disciplines for the study of complex systems/problems.

## REFERENCES

- [1] A. S. M. Mohsin and M. B. Salim, "Probing the Plasmon Coupling, Quantum Yield, and Effects of Tip Geometry of Gold Nanoparticle Using Analytical Models and FDTD Simulation," *IEEE Photonics Journal*, vol. 10, no. 3, pp. 1-10, 2018, doi: 10.1109/JPHOT.2018.2825435.
- [2] W. Rechberger, A. Hohenau, A. Leitner, J. R. Krenn, B. Lamprecht, and F. R. Aussenegg, "Optical properties of two interacting gold nanoparticles," *Optics communications*, vol. 220, no. 2003, pp. 137-141, 2003.

# Probing and perturbing the oligomerization of membrane protein with plasmonic nanoparticles and deep learning

- [3] C. Sonnichsen, M. L. ReinhardBjorn, and A. P. Jan Alivisatos, "A molecular ruler based on plasmon coupling of single gold and silver nanoparticles," *Nat Biotechl.*, vol. 23, no. 6, pp. 741-745, 2005.
- [4] B. M. Reinhard, M. Siu, I. H. Agarwa, A. P. Alivisatos, and J. Liphardt, "Calibration of Dynamic Molecular Rulers Based on Plasmon Coupling between Gold Nanoparticles," *Nano Letters*, vol. 5, no. 11, pp. 2246-2252, 2005.
- [5] Z. Peter, W. M. C. James, and G. Min, "Five dimensional optical recording mediated by surface plasmons in gold nanorods," *Nature*, vol. 459, pp. 410-413, 2005.
- [6] G. Mie, "Beitrage zur Optik truber Medien, speziell kolloidaler Metallosungen," *Annalen der Physik*, vol. 330, no. 3, pp. 377-445, 1908, doi: 10.1002/andp.19083300302.
- [7] J. Aaron, T. Kor, N. Harrison, and K. Sokolov, "Dynamic Imaging of Molecular Assemblies in Live Cells Based on Nanoparticle Plasmon Resonance Coupling," *Nano letters*, vol. 9, no. 10, pp. 3612-3618, 2009.
- [8] T. A B, K. J, and C. J W M, "Detuned surface plasmon resonance scattering of gold nanorods for continuous wave multilayered optical recording and readout," *Optics Express*, vol. 20, no. 5, pp. 5069-5081, 2012.
- [9] M. J. Crow, K. Seekell, J. H. Ostrander, and A. Wax, "Monitoring of Receptor Dimerization Using Plasmonic Coupling of Gold Nanoparticles," *ACS Nano*, vol. 5, no. 11, pp. 8532-8540, 2011, doi: 10.1021/nn201451c.
- [10] A. M. Funston, C. Novo, T. J. Davis, and P. Mulvaney, "Plasmon Coupling of Gold Nanorods at Short Distances and in Different Geometries," *Nano Letters*, vol. 9, no. 4, pp. 1651-1658, 2009, doi: 10.1021/nl900034v.
- [11] M. N. C. Hu and A. Funston, "Dark-field microscopy studies of single metal nanoparticles: understanding the factors that influence the linewidth of the localized surface plasmon resonance.,", *Journal of materials chemistry*, vol. 18, no. 17, pp. 1949-1960, 2008.
- [12] U. V. Kreibig, "Optical Sizing of Immunolabel Clusters through Multispectral Plasmon Coupling Microscopy," *Optical Properties of Metal Clusters: Springer-Verlag: Berlin*, 1995.
- [13] P. K. Jain, W. Huang, and M. A. El Sayed, "On the Universal Scaling Behavior of the Distance Decay of Plasmon Coupling in Metal Nanoparticle Pairs A Plasmon Ruler Equation," *Nano Letters*, vol. 7, no. 7, pp. 2080-2088, 2007.
- [14] P. Nordlander, Coubre, E. Prodan, K. Li, and M. I. Stockman, "Plasmon Hybridization in Nanoparticle Dimers," *Nanoletters*, vol. 4, no. 5, pp.899-903, 2004.
- [15] H. Wang, G. Rong, B. Yan, L. Yang, and B. r. M. Reinhard, "Optical sizing of immunolabel clusters through multispectral plasmon coupling microscopy," *Nano letters*, vol. 11, no. 2, pp. 498-504, 2011.
- [16] X. Chen *et al.*, "Broadband Enhancement in Thin-Film Amorphous Silicon Solar Cells Enabled by Nucleated Silver Nanoparticles," *Nano Letters*, vol. 12, no. 5, pp. 2187-2192, 2012/05/09 2012, doi: 10.1021/nl203463z.
- [17] V. E. Ferry, L. A. Sweatlock, D. Pacifici, and H. A. Atwater, "Plasmonic Nanostructure Design for Efficient Light Coupling into Solar Cells," *Nano Letters*, vol. 8, no. 12, pp. 4391-4397, 2008/12/10 2008, doi: 10.1021/nl8022548.
- [18] P. Yu, Y. Yao, J. Wu, X. Niu, A. L. Rogach, and Z. Wang, "Effects of Plasmonic Metal Core -Dielectric Shell Nanoparticles on the Broadband Light Absorption Enhancement in Thin Film Solar Cells," (in eng), *Sci Rep.* vol. 7, no. 1, pp. 7696-7696, 2017, doi: 10.1038/s41598-017-08077-9.
- [19] K. R. Catchpole and A. Polman, "Plasmonic solar cells," *Opt. Express*, vol. 16, no. 26, pp. 21793-21800, 2008/12/22 2008, doi: 10.1364/OE.16.021793.
- [20] H. A. Atwater and A. Polman, "Plasmonics for improved photovoltaic devices," *Nature Materials*, vol. 9, no. 3, pp. 205-213, 2010/03/01 2010, doi: 10.1038/nmat2629.
- [21] A. B. Taylor, P. Michaux, A. S. M. Mohsin, and J. W. M. Chon, "Electron-beam lithography of plasmonic nanorod arrays for multilayered optical storage," *Opt. Express*, vol. 22, no. 11, pp. 13234-13243, 2014/06/02 2014, doi: 10.1364/OE.22.013234.
- [22] V. B. Kumar, A. K. Sahu, A. S. M. Mohsin, X. Li, and A. Gedanken, "Refractive-Index Tuning of Highly Fluorescent Carbon Dots," *ACS Applied Materials & Interfaces*, vol. 9, no. 34, pp. 28930-28938, 2017, doi: 10.1021/acsami.7b08985.
- [23] P. Zijlstra, J. W. Chon, and M. Gu, "Five-dimensional optical recording mediated by surface plasmons in gold nanorods," *Nature*, vol. 459, no. 7245, pp. 410-413, 2009.
- [24] K. Sokolov *et al.*, "Real-time vital optical imaging of precancer using anti-epidermal growth factor receptor antibodies conjugated to gold nanoparticles," *Cancer research*, vol. 63, no. 9, pp. 1999-2004, 2003.
- [25] J. Aaron, K. Travis, N. Harrison, and K. Sokolov, "Dynamic imaging of molecular assemblies in live cells based on nanoparticle plasmon resonance coupling," *Nano letters*, vol. 9, no. 10, pp. 3612-3618, 2009.
- [26] I. H. El-Sayed, X. Huang, and M. A. El-Sayed, "Surface plasmon resonance scattering and absorption of anti-EGFR antibody conjugated gold nanoparticles in cancer diagnostics: applications in oral cancer," *Nano letters*, vol. 5, no. 5, pp. 829-834, 2005.
- [27] R. Mercatelli *et al.*, "Quantitative measurement of scattering and extinction spectra of nanoparticles by darkfield microscopy," *Applied Physics Letters*, vol. 99, no. 13, p. 131113, 2011.
- [28] C. J. Murphy *et al.*, "Chemical sensing and imaging with metallic nanorods," *Chemical Communications*, no. 5, pp. 544-557, 2008.
- [29] J. M. Pingarrón, P. Yáñez-Sedeño, and A. González-Cortés, "Gold nanoparticle-based electrochemical biosensors," *Electrochimica Acta*, vol. 53, no. 19, pp. 5848-5866, 2008/08/01/ 2008, doi: <https://doi.org/10.1016/j.electacta.2008.03.005>.
- [30] X. Huang, I. H. El-Sayed, W. Qian, and M. A. El-Sayed, "Cancer Cells Assemble and Align Gold Nanorods Conjugated to Antibodies to Produce Highly Enhanced, Sharp, and Polarized Surface Raman Spectra: A Potential Cancer Diagnostic Marker," *Nano Letters*, vol. 7, no. 6, pp. 1591-1597, 2007/06/01 2007, doi: 10.1021/nl070472c.
- [31] X. Huang, P. K. Jain, I. H. El-Sayed, and M. A. El-Sayed, "Gold nanoparticles: interesting optical properties and recent applications in cancer diagnostics and therapy," *Nanomedicine*, vol. 2, no. 5, pp. 681-693, 2007/10/01 2007, doi: 10.2217/17435889.2.5.681.
- [32] P. Weerathunge, R. Ramanathan, R. Shukla, T. K. Sharma, and V. Bansal, "Aptamer-Controlled Reversible Inhibition of Gold Nanozyme Activity for Pesticide Sensing," *Analytical Chemistry*, vol. 86, no. 24, pp. 11937-11941, 2014/12/16 2014, doi: 10.1021/ac5028726.
- [33] X. Huang, I. H. El-Sayed, W. Qian, and M. A. El-Sayed, "Cancer cell imaging and photothermal therapy in the near-infrared region by using gold nanorods," *Journal of the American Chemical Society*, vol. 128, no. 6, pp. 2115-2120, 2006.
- [34] A. Wijaya, S. B. Schaffer, I. G. Pallares, and K. Hamad-Schifferli, "Selective release of multiple DNA oligonucleotides from gold nanorods," *Acs Nano*, vol. 3, no. 1, pp. 80-86, 2008.
- [35] C.-C. Chen *et al.*, "DNA-gold nanorod conjugates for remote control of localized gene expression by near infrared irradiation," *Journal of the American Chemical Society*, vol. 128, no. 11, pp. 3709-3715, 2006.

## Probing and perturbing the oligomerization of membrane protein with plasmonic nanoparticles and deep learning

- [36] N. L. Rosi, D. A. Giljohann, C. S. Thaxton, A. K. R. Lytton-Jean, M. S. Han, and C. A. Mirkin, "Oligonucleotide-Modified Gold Nanoparticles for Intracellular Gene Regulation," *Science*, 10.1126/science.1125559 vol. 312, no. 5776, p. 1027, 2006. [Online]. Available: <http://science.sciencemag.org/content/312/5776/1027.abstract>.
- [37] A. K. Salem, P. C. Searson, and K. W. Leong, "Multifunctional nanorods for gene delivery," *Nature Materials*, vol. 2, p. 668, 09/14/online 2003, doi: 10.1038/nmat974.
- [38] A. H. Clayton *et al.*, "Ligand-induced dimer-tetramer transition during the activation of the cell surface epidermal growth factor receptor-A multidimensional microscopy analysis," *Journal of Biological Chemistry*, vol. 280, no. 34, pp. 30392-30399, 2005.
- [39] C. Sönnichsen, B. M. Reinhard, J. Liphardt, and A. P. Alivisatos, "A molecular ruler based on plasmon coupling of single gold and silver nanoparticles," *Nature biotechnology*, vol. 23, no. 6, pp. 741-745, 2005.
- [40] A. M. Alkilany, P. K. Nagaria, C. R. Hexel, T. J. Shaw, C. J. Murphy, and M. D. Wyatt, "Cellular uptake and cytotoxicity of gold nanorods: molecular origin of cytotoxicity and surface effects," *Small*, vol. 5, no. 6, pp. 701-708, 2009.
- [41] B. D. Chithrani, A. A. Ghazani, and W. C. Chan, "Determining the size and shape dependence of gold nanoparticle uptake into mammalian cells," *Nano letters*, vol. 6, no. 4, pp. 662-668, 2006.
- [42] C. Grabinski *et al.*, "Effect of Gold Nanorod Surface Chemistry on Cellular Response," *ACS Nano*, vol. 5, no. 4, pp. 2870-2879, 2011, doi: 10.1021/nn103476x.
- [43] A. Albanese and W. C. W. Chan, "Effect of Gold Nanoparticle Aggregation on Cell Uptake and Toxicity," *ACS Nano*, vol. 5, no. 7, pp. 5478-5489, 2011, doi: 10.1021/nn2007496.
- [44] T. S. Hauck, A. A. Ghazani, and W. C. Chan, "Assessing the effect of surface chemistry on gold nanorod uptake, toxicity, and gene expression in mammalian cells," *Small*, vol. 4, no. 1, pp. 153-159, 2008.
- [45] C. J. Murphy *et al.*, "Gold Nanoparticles in Biology: Beyond Toxicity to Cellular Imaging," *Accounts of Chemical Research*, vol. 41, no. 12, pp. 1721-1730, 2008, doi: 10.1021/ar800035u.
- [46] R. Levy, U. Shaheen, Y. Cesbron, and V. See, "Gold nanoparticles delivery in mammalian live cells: a critical review," *Nano reviews*, vol. 1, 2010.
- [47] P. P. Joshi, S. J. Yoon, W. G. Hardin, S. Emelianov, and K. V. Sokolov, "Conjugation of antibodies to gold nanorods through Fc portion: synthesis and molecular specific imaging," *Bioconjugate chemistry*, vol. 24, no. 6, pp. 878-888, 05/14 2013, doi: 10.1021/bc3004815.
- [48] Ding, C., Xia, Y., and Li, Y., Supervised segmentation of vasculature in retinal images using neural networks. In: Orange technologies (ICOT), 2014 IEEE International Conference on, IEEE, pp. 49-52, 2014
- [49] Humayun Irshad, Antoine Veillard, Ludovic Roux, and Daniel Racoceanu. 2014. Methods for nuclei detection, segmentation, and classification in digital histopathology: A review—Current status and future potential. *IEEE Reviews in Biomedical Engineering* 7 (2014), 97–114.

## **Efficient Models for Photonic Functional Devices for Future Optical Communication**

### **Category: Information Summary**

The continuous growth of the telecommunication market has led to a huge demand of high-density low-power high-speed nanoscale systems. Recently, the excessive demand on mobile and communications networks during the COVID-19 pandemic adds pressure to the network, which affects service quality and levels. This rising demand can create a ripple effect as companies across various sectors are in the ongoing shift to remote work and implement remote-work plans. Therefore, we should put a lot of research efforts to investigate the future of ICT amid the challenges.

The global photonics market is estimated to rise from USD 802.5 billion in 2021 to USD 1267.3 billion by 2028 according to Fortune Business Insights™. According to its latest research report titled “Photonics Market, 2021-2028”, the optical communication technologies are listed top of “Key Market Trends”. Because photonics, as a new technology, can help address some of the challenges facing ICT. For instance, plasmonics, as a promising branch of photonics, is playing a vital role in the realization of many devices and systems beyond the diffraction limit penetrating a wide range of applications from telecoms, integrated optics, sensing, and others. However, understanding the physical effects behind plasmonic devices is still a challenge and needs much more considerable effort to deeply understand light-matter interaction enabling plasmonic effect. On the other hand, silicon photonics shows promise to realize a wide range of photonic devices for future ICT applications. However, modeling such high-index-contrast nature between silicon and surrounding materials is still a challenge facing numerical techniques to be able to capture the correct rapid variation of the field at the interfaces.

In this regard, this proposal will focus on developing new powerful computational modeling tool for fundamental physical understanding and correctly analyzing photonic devices with high-index-contrast like in plasmonics or even silicon photonics. This proposal aims at:

- Demonstrating a study for the physical explanation of the challenges facing existing modeling techniques of such high-index-contrast structures.
- Recommending the best techniques for each photonic device and based on its physical nature in both classical and quantum regimes.
- Developing more accurate and efficient numerical modeling techniques based on semi-vectorial/ full-vectorial modal analysis and bidirectional beam propagation method for 3D photonic devices.

This proposal can lead to the following outcomes:

- New efficient computational tool capable of accurately characterizing and design both 2D and 3D photonic devices such as couplers mandatory for future ICT.
- 1-2 publications in high impact factor open access OPTICA journals (targeting Opt. Express).
- Participating in one international conference.

This proposal will give me a good opportunity to extend some of existing open research possibilities related to my PhD, and future work may include other extensions to solve the following problems:

- Coupling my quantum solver with Poisson solver to be able to apply external bias ( $V=x$ ) to characterize more features of modern quantum devices.
- Making use of the parallel implementation of my algorithm to speed up the analysis.



# Efficient Models for Photonic Functional Devices for Future Optical Communication

## Category: Information

### Literature Review

Since plasmonic effects allowed devices in the nanoscale regime, the fields have become more localized. Also, other high-index contrast structures show rapid changes in the fields like in silicon photonics. Thus, solving such high field values requires huge computational resources. In addition, the finite elements method (FEM) and the finite difference method (FDM) are mesh-based methods. Therefore, they require a special treatment to handle infinite or semi-infinite computational domains. A domain truncation, using PMLs, or variants of transparent boundary conditions, is one common approach. However, FEM based on “Master” and “Slave” nodes require a considerable amount of logic for coupling the related degrees of freedom and do not easily lend itself to developing programs as extensions to existing general-purpose finite-element packages. Moreover, FEM based on “edge elements” of leaving the normal component of the expanded function free to jump across common faces of adjacent elements was shown to be a possible source of spurious surface charges on those faces and led to nonsymmetric systems of linear, algebraic equations and may lead to singularity. In addition, these edge elements-based technique is computationally more expensive in terms of both storage requirements and efficiency of iterative solvers. Otherwise, superposition of an auxiliary continuous function on linear nodal elements resulting in lower accuracy. All these results suggest the need for a new type of vectorial expansion function that combines the regularity properties of the nodal elements with the capability of modeling the behavior of the field strength across interfaces. Fortunately, Generalized Cartesian Finite Elements Method (GCFEM) [1] presented a new family of vectorial expansion functions that can accurately and consistently model the behavior of the electric and the magnetic field strengths both at interfaces between media with different constitutive parameters and inside interface-free subdomains, but it has never been used for photonic devices before. In this regard, we would like to develop, for the first time to the best of our knowledge, a new Generalized Cartesian Finite Elements Method for photonic devices.

On the other hand, semi-analytical techniques that use global basis functions, which are defined over the whole domain, are successful alternatives. These methods are known as spectral methods, and conformal maps can be incorporated into the basis functions to allow their definition on semi-infinite or infinite domains such as Laguerre or Hermite basis functions. These methods have a very high convergent rate  $O(e^{-kN})$ , where the constant  $k$  is real and positive. Equipped with domain decomposition, the so-called pseudo-spectral methods have been utilized for the modal analysis of plasmonic and dielectric waveguides. Appropriate conformal maps are used to redefine the basis functions over finite or semi-infinite subdomains, eliminating the need for PMLs. Moreover, the pseudo-spectral methods have the ability to properly apply the physical boundary conditions at the interfaces of the discontinuity between metal and dielectric materials. Although pseudo-spectral methods have been successfully adopted for the accurate and fast modal analysis of photonic devices, they have never been used for the propagation analysis of photonic devices [2,3].

Beam propagation methods (BPMs) are well known for their simplicity and speed and are frequently used in the analysis of photonic devices based on dielectric materials. Bidirectional beam propagation methods (BiBPMs) are upgraded versions of BPMs without neglecting reflections from each discontinuity interface in the propagation direction. Therefore, BiBPMs can be considered as very efficient techniques to account for multiple longitudinal discontinuities structures. One of the advantages of BPMs, in general, is their compatibility with any discretization technique/modal solvers. The main step of BiBPMs, which controls the accuracy and the stability





	<b>Applying quantitative measures:</b> <ul style="list-style-type: none"> <li>Validation using Lumerical &amp; FEM, COMSOL software</li> </ul>																																						
3	Developing new 2D full-vectorial modal analysis. <b>Applying quantitative measures:</b> <ul style="list-style-type: none"> <li>Validation using Lumerical &amp; FEM, COMSOL software</li> </ul>																																						
4	Developing 3D propagation modeling technique based on the Blocked Schur algorithm and the developed 2D modal analysis <b>Applying quantitative measures:</b> <ul style="list-style-type: none"> <li>Validation using FDTD, Lumerical software</li> </ul>																																						
	Reporting results in publications and conference.																																						

**Outcome(s)**

- New efficient computational tool capable of accurately characterizing and design both 2D and 3D photonic devices such as couplers mandatory for future ICT.
- 1-2 publications in high impact factor open access OPTICA journals (targeting Opt. Express).
- Participating in one international conference.

**Impact**

Energy consumed by communication systems and networks has been continuously increasing over the past decade. The world is becoming more and more dependent upon information communication technology (ICT) with the number of internet users increasing and demand

growing for online services, especially after the COVID-19 pandemic, which in turn requires faster networking, increased data processing, and data storage capabilities. The collective knowledge accumulated by mankind since the beginning of history to 2000 ad is estimated to be around five exabytes ( $5 \times 10^9$  gigabytes), according to a report published by the Microphotonics Center at the Massachusetts Institute of Technology in the USA. According to Google, an additional latency of 0.5 s when loading a search result page causes a 20% decrease in search traffic. Similarly, Amazon reported that each additional 100 ms of page loading time decreased sales by 1%. In 2011, the total energy required to power the Internet, including data centers, network nodes, and user terminals, amounts to about 3% of the world's energy generation capacity – this is more than is used for global air traffic! With Internet traffic growing at nearly 50% each year, the energy used as a result of Internet traffic is expected to comprise 10% of the world's total energy usage in 2018 [5].

That is why we need new generations of optical telecommunication devices, systems, and network which provide more efficient services, cover the traffic growth and reduce energy consumption in the next years. Therefore, the proposed project will aim at researching efficient models for photonic functional devices. For instance, plasmonics offers strong light localization into subwavelength dimensions beyond the diffraction limit. Therefore, photonics has a significant impact on realizing nanoscale photonic devices for future ICT, our focus in this project. The computational modeling of high-index contrast structures like in plasmonics and silicon photonics provides a fundamental understanding of the relying physics. However, computational modeling of these devices is still a challenge as some of the existing modeling techniques fail to capture the correct physical behavior of plasmonic devices. The high index contrast nature produces a huge spectrum of surface, radiated, evanescent, and even nonphysical waves. Therefore, it is quite important to have new technology for future ICT and to look closer at the accurate design of photonic devices which we introduce in this project.

## References

- [1] Lager, Ioan Ernest, and Gerrit Mur. "Generalized Cartesian finite elements." *IEEE transactions on magnetics* 34, no. 4 (1998): 2220-2227.
- [2] A. Abdrabou, A. Heikal, and S. S. A. Obayya, "Efficient rational Chebyshev pseudo-spectral method with domain decomposition for optical waveguides modal analysis," *Opt. Express* 24, 10495–10511 (2016).
- [3] **Said, Afaf**, Atia, K.S.R., Obayya, S.S.A., "On modeling of plasmonic devices: Overview", *Journal of the Optical Society of America B: Optical Physics*, 2020, 37(11), pp. A163–A174 (**Invited review article**)
- [4] **Afaf. M. Said**, A. Heikal, N. F. Areed, and S. S. A. Obayya, "Why do field-based methods fail to model plasmonics?" *IEEE Photon. J.* 8, 4802613 (2016).
- [5] M. Asghari, and A. V. Krishnamoorthy, "Silicon photonics: Energy-efficient communication," *Nature Photonics* 5, 268-270 2011.

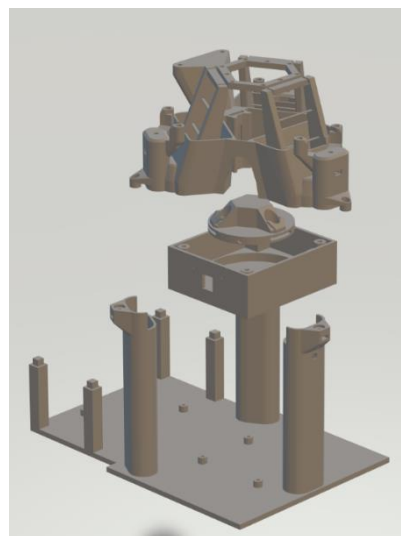
# Global Modular Microscopy (G-ModMicro)

## Executive Summary

Global Modular Microscopy (G-ModMicro) is an ambitious project that will leverage optical technologies, additive manufacturing and low-cost innovations for making diagnostics affordable, tackling the key problem of disparate healthcare capabilities globally. A step-change in research and diagnostics will be a direct result of the current proposal to make advanced microscopy hardware accessible at a fraction of the cost of proprietary systems. G-ModMicro was designed to bridge the gap between microscopy technology access and diagnostic needs, with a focus on developing countries. The proposal is shaped through conversations and existing collaborations with pathologists in Visakhapatnam (India), microscopy needs for malaria diagnostics in Malawi and Tanzania (Africa), as use cases, and researchers in the UK.

The proposal outlines the novel development of hardware for three techniques – confocal microscopy, structured illumination microscopy (SIM) and stimulated emission depletion (STED) – as a step towards solving an ever-present imbalance of hardware access due to high costs. Simultaneously, the project will build strategic partnerships to deploy currently available and subsequent novel hardware in pathology labs in India and Africa with a focus on cancer and malaria diagnostics, respectively. Building on the OpenFlexure project<sup>1</sup>, this proposal will innovatively design imaging hardware using additive manufacturing, novel light sources and in-house electronics to build all-inclusive and openly accessible microscopy systems.

G-ModMicro suite brings together a complete range of 3D-printed microscopy hardware and a bill of materials that enables users to build and apply multiple microscopy techniques to research and diagnostics. The suite of tools has thus far adopted the OpenFlexure project as a template for (1) bright field microscopy, applied to machine learning-based classification, (2) epifluorescence microscopy with bespoke components (Figure 1) for zebrafish imaging<sup>2</sup> and (3) polarised light microscopy for imaging malarial parasites in tissue samples from Malawi, in collaboration with parasitologists at the University of Glasgow. This research has received prior support from the University of Glasgow Knowledge Exchange Fund, Engineering and Physical Sciences Research Council (EPSRC) Impact Acceleration Accounts (IAA), SPIE, IEEE Photonics Society and the Institute of Physics. Subsequent support through this Award will see both additional research and development, and deployment in the UK, India and Africa (the latter is in progress with the University of Glasgow Research and Innovation team).



*Figure 1 – G-ModMicro's epifluorescence microscope costs £150 per unit, fully equipped with an objective, filters and light sources.*

G-ModMicro will provide the global community, irrespective of the economic standing, access to dependable hardware. This will directly enhance the capabilities of research institutions, and improve capabilities and reduce diagnostic waiting times in healthcare.

---

<sup>1</sup> <https://openflexure.org/>

<sup>2</sup> Our system costs £150 vs. standard systems that can cost between £2,000 to £40,000

## Global Modular Microscopy (G-ModMicro)

Microscopy has long been a domain restricted to either those who use basic bright-field techniques or well-funded research groups, institutions and medical facilities with large budgets for advanced techniques. However, the ability to achieve high resolution for diagnostics, material sciences, and medical applications is an aspiration that is shared globally. Many microscopy techniques remain out of reach in developing countries primarily due to their costs. While some of the costs are unavoidable, the supporting hardware can be innovated using additive manufacturing. The imbalance of access is the status quo this proposal will challenge and has the potential for a step-change in the field of microscopy. There is a need for cost-effective solutions now more than ever, with COVID-19 illustrating the necessity for open access to diagnostic technologies globally [1]–[7].

### Problem Statement and Objective

The problem statement this proposal address is the overall imbalance of access to advanced microscopy techniques due to expensive hardware costs. This ranges from access to multiple brightfield microscopes to enhance the capability of diagnostic laboratories to superresolution imaging in institutions for healthcare-related research. The objective of this proposal is two-fold:

- To develop novel hardware from a common starting point, with bespoke components, for realising advanced microscopy techniques (Figure 1), with alternative light sources, optical components and in-house electronics. The OpenFlexure project is used as a template and components are designed for sustainable reuse and realise multiple techniques minimally yet effectively. The hardware will be designed for:
  - o Confocal microscopy
  - o Structured illumination microscopy (SIM)
  - o Stimulated emission depletion (STED) microscopy
- Deploy existing microscope hardware (Figure 1) through strategic partnerships with the support of this Award, the University of Glasgow Research and Innovation teams and collaborations in Visakhapatnam (India), Malawi and Tanzania (Africa). All entities (Research and Innovation (University of Glasgow), research- and country-specific collaborations) for ensuring the success of this step are in place.

### Proposal

Microscope hardware is expensive and beyond the reach of small research labs and/or developing countries. Being dominantly commercial, they are heavily dependent on maintenance support from the manufacturer. Through previous work and the proposed project, the application of 3D printing technologies will be extended to low-cost designs for effective modular imaging. The suite of tools will eventually contain the majority of the optical microscopy techniques available through combinations of novel designed parts to allow for interoperability, quick repair and rapid usage.

This proposal will tackle preparing three arrangements for microscopy – Confocal, SIM and STED (Figure 1), along with the principles of these well-known techniques as shown in Figure 2. Confocal imaging will facilitate 3D imaging through biological samples, SIM is capable of using structured light to achieve enhanced resolutions in low light conditions, and STED microscopy can beat the diffraction limit and image beyond, achieving superresolution. These advancements build on completed illustrations of brightfield, epifluorescence and polarised light microscopes currently being used for hemozoin imaging for malaria diagnostics. This hardware is aligned with ongoing research at the University of Glasgow into sub-diffraction

imaging [8], [9], bridging optical techniques and microscopy. This facilitates multiple avenues of application of the research proposed for this Award.

The proposal, within the scope of the Optica Award, includes research and development of novel hardware for the mentioned microscopy techniques. A modular philosophy will be explored, with parts used in different configurations for efficient and sustainable designs. Further, simultaneously, existing collaborations and partnerships will be put in place to deploy the microscope hardware that is currently ready. For the latter, discussions with the University of Glasgow's teams are ongoing, with eventual governmental partnerships in the future. These will happen with pathologists in India and Africa, utilising existing collaborations.



Figure 1 – Optical microscopy currently covers multiple techniques, each with specialised hardware. Of these techniques, our research has achieved three techniques (light microscopy applied in Archibald et al. [10], an epifluorescence system, and a polarised light microscope capable of imaging hemozoin crystals related to malarial parasite research) illustrated in green. This proposal will develop bespoke hardware for techniques shown in orange, with future plans to tackle those shown in black. The intended outcome is to develop novel hardware designs at a greatly reduced cost of specialised systems from tens and hundreds of thousands to less than £1000 per arrangement.

Confocal microscopes consist of moving stages, detectors and common optical components. Using a general design for reference, the epifluorescence microscope will be redesigned to accommodate all the parts. The system will be tested in comparison with standard laboratory confocal microscopes available in the School of Physics and Astronomy. SIM and STED microscopy are more complex systems. For SIM, a grating or a scanning mirror is needed to structure the light before it is incident on the sample. This structured light interacts with the



sample and results in an improved point spread function that can achieve higher resolution. For STED, the three-dimensional point spread function is achieved when combinations of depletion and excitation lasers are used in combination with dichroic mirrors and filters. All the optical components needed for realising the three microscope designs are available within the Optics group, with consumables purchased from this proposal completing the necessary kit. The design of all three microscopes will undergo intense design considerations while building from a common baseline to enhance the modular nature of the hardware. All three systems will be tested with biological samples with Dr Amanda Wright at the University of Nottingham.

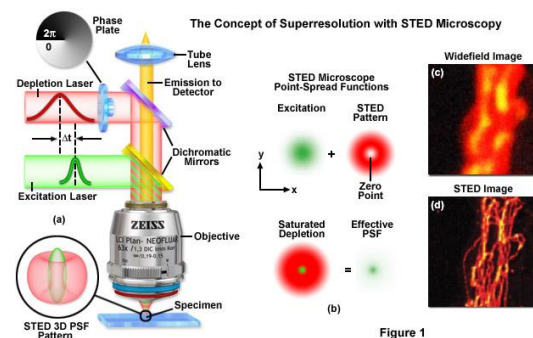
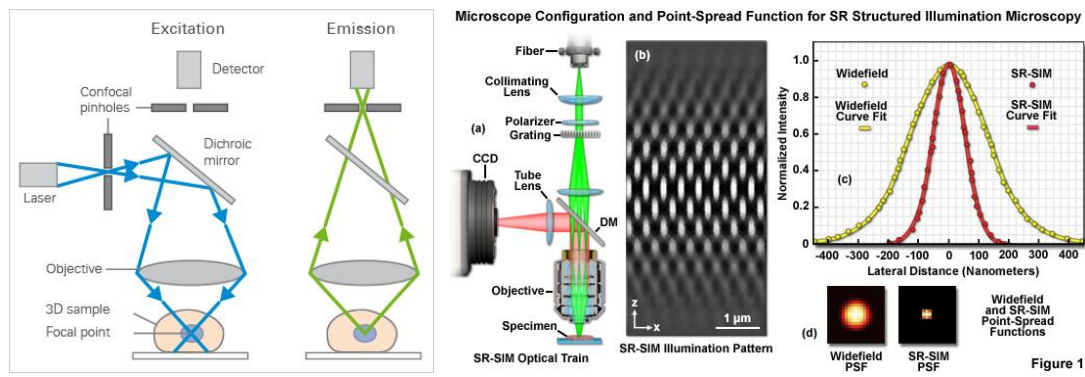


Figure 2 – All three microscope techniques (confocal, SIM and STED) are illustrated here. These techniques, commercially available and widely used, require a bespoke design using 3D printing to achieve modular and global utility. The modular nature will allow a common baseline upon which each system can be developed. This allows interoperability, reduction of necessary parts and a plug-and-play modality previously unavailable in advanced microscopy.

The project builds on skills, researcher expertise and experience [10], [11] and past research projects. The brightfield microscope from the OpenFlexure project was adopted for machine learning research. Subsequently, an epifluorescence microscope was developed through a 2021 EPSRC Impact Acceleration Account project, titled [ModMicro](#). The device was rapidly prototyped in just 2 months and is now in Dr Jonathan Taylor's (UofG) lab to image zebrafish, with output due to be published. The polarised light microscope is acquiring hemozoin distribution images in malarial parasite slides, in collaboration with Dr Matt Gibbins and Prof Matthias Marti (UofG).

## Outcomes

The immediate outcomes of this project will be three novel and cost-effective solutions to advanced microscopy techniques. These are achieved at a fraction of the cost (by a factor of 50 or more), making the systems useful around the world independent of budgetary challenges. While certain optical components will remain necessary, the overall build and assembly of

systems are where this technology will have a significant impact. The value of research-grade techniques being available in any socioeconomic setting cannot be understated. Secondly, a strategic partnership to deploy the microscopes in India and Africa will be in place, to send the microscopes, adequately packaged, to these sites through agreements.

## Impact

This proposal will revolutionise the ability of small laboratories and clinical institutions around the world to access and benefit from high-resolution, advanced microscopy. Immediate impact is made possible through collaborations in India and Africa. The need for imaging tools is clear and present, mainly due to the high cost of proprietary systems in developing countries. This results in a lack of access and/or long delays for the analysis of samples. The solution proposed here will also reduce the lack of access to high-resolution imaging and allow rapid diagnostics. While commercial systems cannot be replaced, reduced dependence on access can reduce the overall time needed for diagnosing key medical conditions.

In the long-term, the possibilities of the approach in this proposal are endless, with a global community needing more effective, precise yet cost-effective solutions. While commercial equipment is available, integrating low-cost microscopes in different research fields from bi-imaging to quantum science is promising.

## References

- [1] P. P. Vallejo Ramirez *et al.*, “OptiJ: Open-source optical projection tomography of large organ samples,” *Scientific Reports* 2019 9:1, vol. 9, no. 1, pp. 1–9, Oct. 2019, doi: 10.1038/s41598-019-52065-0.
- [2] J. P. Sharkey, D. C. W. Foo, A. Kabla, J. J. Baumberg, and R. W. Bowman, “A one-piece 3D printed flexure translation stage for open-source microscopy,” *Review of Scientific Instruments*, vol. 87, no. 2, pp. 025104 1–7, 2016, doi: 10.1063/1.4941068.
- [3] “The OpenFlexure project.” <https://openflexure.org/> (accessed Aug. 31, 2021).
- [4] J. P. Sharkey, D. C. W. Foo, A. Kabla, J. J. Baumberg, and R. W. Bowman, “A one-piece 3D printed flexure translation stage for open-source microscopy,” *Review of Scientific Instruments*, vol. 87, no. 2, pp. 025104 (1–7), Feb. 2016, doi: 10.1063/1.4941068.
- [5] J. T. Collins *et al.*, “Robotic microscopy for everyone: The OpenFlexure Microscope,” *Biomed Opt Express*, vol. 11, no. 5, pp. 2447–2460, 2019, doi: 10.1101/861856.
- [6] J. Stirling and R. Bowman, “The COVID-19 Pandemic Highlights the Need for Open Design Not Just Open Hardware,” *Design Journal*, vol. 24, no. 2, pp. 299–314, 2021, doi: 10.1080/14606925.2020.1859168.
- [7] J. Stirling *et al.*, “The OpenFlexure Project. The technical challenges of co-Developing a microscope in the UK and Tanzania,” 2020. doi: 10.1109/GHTC46280.2020.9342860.
- [8] A. Kallepalli, D. Stellinga, M.-J. Sun, R. Bowman, and E. Rotunno, “Ghost imaging with electron microscopy inspired, non-orthogonal phase masks,” *ArXiv*, Dec. 2021, doi: 10.21203/RS.3.RS-1111193/V1.
- [9] A. Kallepalli *et al.*, “Computational ghost imaging for transmission electron microscopy,” *ArXiv*, Apr. 2022, doi: 10.48550/arxiv.2204.09997.
- [10] R. Archibald, G. M. Gibson, S. T. Westlake, and A. Kallepalli, “Open-source microscopic solution for classification of biological samples,” in *Proceedings of SPIE 11879, Frontiers of Biophotonics and Imaging*, Oct. 2021. doi: 10.1117/12.2599435.
- [11] R. Archibald, S. Westlake, G. Gibson, and A. Kallepalli, “OPEN-BIOset: A dataset of microscope images collected using the OpenFlexure Delta Stage Microscope.” University of Glasgow, Glasgow, UK, 2021. doi: 10.5525/gla.researchdata.1149.



## **Executive summaries**

Name of Challenge Project: “**Design and Development of Cost and Energy Efficient TWDM Optical Wireless Link for High Speed Reliable Communication**”.

### **Category: Information**

**Problem Statement/Objective:** To Design and Develop Flexible TWDM Optical Wireless Link for Reliable, Cost Effective and Energy Efficient Connectivity. The designed link is expected to enhance the reliability of the high speed wireless link with low cost and power requirements.

The major objectives of the proposal are: -

- To simulate and analyze the performance of 20 Gbps and beyond optical wireless link at different geographical locations.
- Evaluation of the bit error performance (BER) of the designed link for real time variable network conditions and various parameters.
- Designing and development of 20 Gbps and beyond test bench link for physical network connectivity.
- FPGA implementation for real time effective resource allocation and link switching.
- Reliability, cost and power effective analysis of developed TWDM optical wireless link bench.

### **Outcome(s) and deliverables**

- Designed and developed 20 Gbps link is expected to provide the high speed, energy and cost efficient reliable broadband wireless connectivity.
- The implementation of FPGA in the designed link is expected to utilize the available central office resources effectively and can allocate the bandwidth dynamically as per real time requirements and network conditions.
- The complete project report with the technical details
- Research papers having potential to get published in the Optica journals and conferences.

### **Impact**

- The proposed and designed link can provide the reliable wireless broadband connectivity to the rural areas and can overcome the technological gap between the rural and urban communities and therefore can reduce the population density fluctuations.
- Dissemination of the major findings of the project with the industry, academia and research personals through symposia and spread the knowledge to the scientific community.
- The delivered major findings and technical aspects will help the telecom operators to provide the reliable, energy efficient and cost effective connectivity to the rural areas and can boost the rural development.

Name of Challenge Project: “**Design and Development of Cost and Energy Efficient TWDM Optical Wireless Link for High Speed Reliable Communication**”.

**Dr. AMIT KUMAR GARG**, Assistant Professor,

Indian Institute of Information Technology Kota, [amitgarg.ece@iiitkota.ac.in](mailto:amitgarg.ece@iiitkota.ac.in), 7568707248

## **Literature Review**

For getting a better quality of life, more employment opportunities, and accessibility of smart services; the urbanization across the globe is increasing very fast and people are migrating towards the cities. As per the forecast of the United Nations in context of India, approximately 814 million Indians will live in cities by 2050 [1]. This will create a huge population density fluctuations and increasing density gaps between cities and villages. Highly dense cities may face several challenges in the coming future including lack of sufficient resources such as livable land, availability of usable water, food grains, breathable air, hospitals, roads, etc. Therefore, to keep the population balance between the cities and villages, the migration of people from rural areas to cities must be stopped by providing them with the smart services and growing opportunities in line with the cities.

The smart villages are expected to stop the migration of people from rural areas to urban areas by bridging the technological gap and providing various essential smart services. The lack of- skill development, quality education, better healthcare, and employment opportunities, etc are a few of the major concerns of existing rural areas that force its dwellers to migrate towards the more technologically advanced urban areas. The migration of people from rural and remote areas statically overburdening the cities and becoming the major barrier for the realization of the concept of smart cities. i.e. the planning and development of smart villages is equally important as the smart cities and must be done parallelly [2].

With the exponential growth of internet applications/users/devices, there is a much need for planning and development of smart, reliable, and efficient ICT infrastructure in rural as well as urban areas. i.e. already deployed ICT infrastructure needs to be upgraded and in its absence, new ICT infrastructure needs to be deployed. Most of the urban areas are being connected and serviced by private vendors but due to the lack of return on investment opportunities, the majority of rural areas are still untouched.

To provide high-speed internet services to the end-users, many technologies are emerging day by day. 5G technology is just at its beginning and within a couple of years, 6G services are also expected.

Fiber-optic communication played an important role in transmitting high-speed data up to a few 100GHz in the core as well as access networks. In the present scenario, the optical networks are in a much-advanced stage that provides highly reliable and efficient internet services with very little energy consumption and operational cost [3]. However, the internet services provided by the fiber optic networks are point to point or point to multipoint serving only at predefined fixed locations. In smart communities, due to the use of various IoT-enabled devices, there is much demand for movable broadband connectivity. Also in some geographically or legally restricted areas, the installation of fiber is still a challenge and that needs to be planned and developed by

means of some other technology including the free-space optics(FSO) and satellite communication [3], [4].

Almost two decades ago (1999), Singapore initiated the development of the intelligent island to encourage the use of various ICT services in urban energy consumption, traffic jamming, and pollution management. In 2007, France began the development of smart Paris and its flexible Public Bicycle Sharing (PBS) system is one of the key successful projects, which reduces major carbon footprints, traffic consumption intelligently. In 2010, Portugal's Cisco driven IT valley initiative developed the network of smart devices to cope up with the increased waste management and related energy consumption issues. At the beginning of the last decade, during 2013-2015, urbanization gained speed and many countries including India came in the front. In 2013, the Government of India, initiated the BharatNet project (Earlier National Optical Fiber Network, NOFN) to provide broadband connectivity to the 2.5 Lakh gram panchayats (GPs) covering approximately ~ 6.4 Lakh Indian Villages. The broadband connectivity in rural areas is expected to provide smart services and promote the reverse migration from the cities to the villages to breathe fresh air, eat organic food and live in a pleasant environment [5], [6].

The UK, Korean, US government launched various citizen-centered, IT-driven, and intelligent projects to tackle various issues with the efficient use of technology [7]. In 2015, India initiated the development of 100 smart cities in the next few years. At present, many countries are managing various issues such as intelligent public transportation and traffic management, smart solar plants, smart grids, smart agriculture, smart healthcare, smart sewage, smart disaster management, smart and accurate weather predictions, smart governance, smart education etc [8].

Daniel Minoli et al (DVI Communications, Inc. New York, NY, USA) presented various real-time aspects of integration of 5G networks for different IoT applications in smart cities which opened the various research aspects for the developing communities [9]. Suzana Miladić-Tešić et al (University of East Sarajevo, Bosnia and Herzegovina) studied various optical technologies that are also very essential for the realization of smart cities. Energy-efficient and high data rate transmission for fifth-generation networks could be possible with the use of optical fiber at the back end, and mobile wireless access network at the front end [10]. Véronique Georlette et al (University of Mons, Mons, Belgium) studied various existing data transfer technology and observed the optical wireless technology as one of the best technology that doesn't require licensing as the paid and limited spectrum RF technology [11]. For various innovative and useful indoor and outdoor applications, light fidelity (Li-Fi), FSO transmission and Visible light communication (VLC) [11] are also being used in smart communities for medium to high data rate transmission for low to medium distances. VLC based optical camera communication (OCC) technology was also investigated for 5G networks that can serve various IoT services including E-health, smart industry, smart grids, vehicle to everything networks etc. [12].

### **Problem Statement/Objective**

To Design and Develop Flexible TWDM Optical Wireless Link for Reliable, Cost Effective and Energy Efficient Connectivity. The designed link is expected to enhance the reliability of the high speed wireless link with low cost and power requirements.

The major objectives of the proposal are:-.

- 1) To simulate and analyze the performance of 20 Gbps and beyond optical wireless link at different geographical locations.
- 2) Evaluation of the bit error performance (BER) of the designed link for real time variable network conditions and various parameters.
- 3) Designing and development of 20 Gbps and beyond test bench link for physical network connectivity.
- 4) FPGA implementation for real time effective resource allocation and link switching.
- 5) Reliability, cost and power effective analysis of developed TWDM optical wireless link bench.

### **Outline of tasks/Work Plan**

- 1) Initially, 20 Gbps TWDM link covering different modulation schemes such as OOK, BPSK & DPSK will be simulated with the help of Optisystem Simulation Tool.
- 2) The impact of various system parameters (such as transmission reach, data rate, transmission environment, available power budget etc) will be observed for effective BER performance.
- 3) Development of TWDM Optical Wireless test bench for high speed and reliable network connectivity. The implementation of time division multiplexing will provide the effective resource sharing and also reduce the power and cost requirement. The wavelength division multiplexing will provide the dedicated wavelengths to the users for secured, high speed and reliable connectivity.
- 4) Implementation of FPGA in the designed link for dynamic wavelength and bandwidth allocation, real time link switching for cost, energy and bandwidth efficient services for various real time network scenarios. Depending on the requirement, the FPGA will switch the multiplexing technique from TDM to WDM and vice versa.
- 5) Preparation of the project report on the major findings, progress and submission of the results to the Optica journals and conferences. Organization of the symposiums to disseminate the major findings with the industry, academia professionals. Submission of the final report to the Optica Foundation.

### **Year-wise work plan:**

#### **Year1:**

- A. Purchasing of the various required and approved components/ simulation tools. A full-time junior research fellow (JRF) will be employed who will assist the prize winner in carrying out the research activities related to the project.
- B. Concrete literature surveys associated with the project, technological advancement related to the different modulation techniques, coding techniques, forward error correction codes will be carried out. The training of the hired JRF will also be done.
- C. Simulation analysis of reliable, cost & energy efficient TWDM optical wireless link will be done. With the help of the Vivado/ MATLAB tool, the designed link will be realized for TDM or WDM depending on the requirement.

- D. Preparation of project annual report and research paper. Major findings will be submitted to the Optica journals and conferences.
- E. Organization of the symposia to disseminate the major findings with the industry, academia professionals.

**Year2:**

- F. Designing TWDM optical wireless test bench for high data rate 20Gbps and beyond.
- G. Implementation of FPGA based efficient resource allocation system for effective OPEX, energy and bandwidth services. FPGA will enable the multiplexing technology switching by connecting the power combiner or arrayed waveguide grating in the network.
- H. Comparative analysis of simulation results with the designed test bench for different network conditions.
- I. Preparation of project annual report and research paper.
- J. Submission of the major findings to the Optica journals. Submission of major findings to the Optica journals and conferences.
- K. Organization of the symposia to disseminate the major findings with the industry, academia professionals.
- L. Submission of the final report to the Optica Foundation.

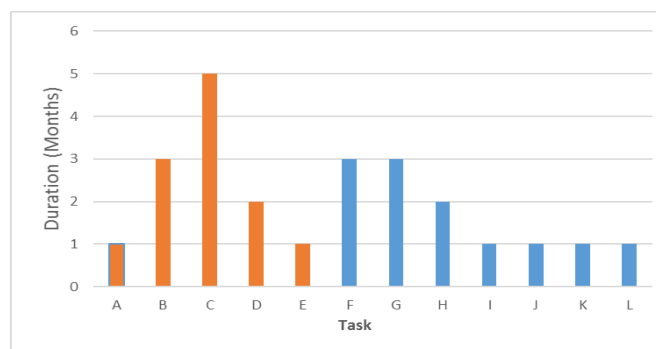


Figure: Activity and duration chart

**Outcome(s) and deliverables**

- Designed and developed 20 Gbps link is expected to provide the high speed, energy and cost efficient reliable broadband wireless connectivity.
- The implementation of FPGA in the designed link is expected to utilize the available central office resources effectively and can allocate the bandwidth dynamically as per real time requirements and network conditions.
- The complete project report with the technical details
- Research papers having potential to get published in the Optica journals and conferences.

**Impact**

- The proposed and designed link can provide the reliable wireless broadband connectivity to the rural areas and can overcome the technological gap between the

rural and urban communities and therefore can reduce the population density fluctuations.

- Dissemination of the major findings of the project with the industry, academia and research personals through symposia and spread the knowledge to the scientific community.
- The delivered major findings and technical aspects will help the telecom operators to provide the reliable, energy efficient and cost effective connectivity to the rural areas and can boost the rural development.

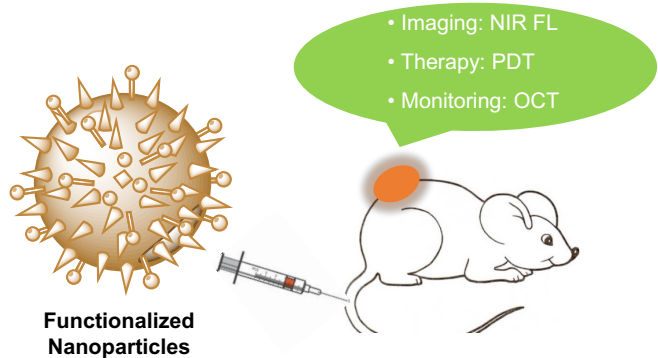
## **Bibliography**

1. <https://www.un.org/development/desa/en/news/population/2018-revision-of-world-urbanization-prospects.html>.
2. S. P. Mohanty, U. Choppali and E. Kougianos, "Everything you wanted to know about smart cities: The Internet of things is the backbone," in IEEE Consumer Electronics Magazine, vol. 5, no. 3, pp. 60-70, July 2016. doi: 10.1109/MCE.2016.2556879.
3. Stotaw Talbachew Hayle, Yibeltal Chanie Manie, Guan-Ming Shao, Po-Han Chiu, Tsung-Yuan Yeh, Song-Lin You, Peng-Chun Peng, Integration of fiber and FSO network with fault-protection for optical access network, Optics Communications, Volume 484, 2021, 126676, ISSN 0030- 4018, <https://doi.org/10.1016/j.optcom.2020.126676>.
4. C.H. Yeh, J.R. Chen, W.Y. You, C.W. Chow, Hybrid WDM FSO fiber access network with Rayleigh backscattering noise mitigation, IEEE Access 8 (2020) 96449–96454.
5. <http://usof.gov.in/usof-cms/NOFN.jsp>
6. <http://www.bbnl.nic.in/index1.aspx?lsid=249&lev=2&lid=21&langid=1>
7. 5G Smart Cities Whitepaper, Compiled by Deloitte jointly with China Unicom, June 2020. <https://www2.deloitte.com/content/dam/Deloitte/cn/Documents/technology-media/telecommunications/deloitte-cn-tmt-empowering-smart-cities-with-5g-white-paper-en-200702.pdf>
8. An ICT approach to rural metamorphosis: A white paper – PwC, 2017, <https://www.pwc.in/assets/pdfs/publications/2017/an-ict-approach-to-rural-metamorphosis-a-white-paper.pdf>.
9. D. Minoli, B. Occhiogrosso, "Practical Aspects for the Integration of 5G Networks and IoT Applications in Smart Cities Environments", Wireless Communications and Mobile Computing, vol. 2019, Article ID 5710834, 30 pages, 2019. <https://doi.org/10.1155/2019/5710834>.
10. S. D. M.-Tešić, G. Z. Marković, and N. P. Nonković, "Optical Technologies in Support of the Smart City Concept" January 2020 Tehnika 75(2):209-215. File No.: SRG/2021/000806/ES | Page 14 of 24
11. V. Georlette, V. Moeyaert, S. Bette and N. Point, "Visible Light Communication Challenges in the Frame of Smart Cities," 2020 22nd International Conference on Transparent Optical Networks (ICTON), Bari, Italy, 2020, pp. 1-4, doi: 10.1109/ICTON51198.2020.9203463.
12. Chowdhury, M.Z.; Shahjalal, M.; Hasan, M.K.; Jang, Y.M. The Role of Optical Wireless Communication Technologies in 5G/6G and IoT Solutions: Prospects, Directions, and Challenges. Appl. Sci. 2019, 9, 4367. <https://doi.org/10.3390/app9204367>.

## Executive Summary of Research Proposal

### FUNCTIONALIZED NANOPARTICLES FOR CANCER DIAGNOSIS, THERAPY, AND MONITORING USING OPTIC TECHNOLOGIES

We propose an all-in-one approach to cancer research using optical technologies in this proposal. New organic-based nanoparticles will be developed as biomarkers for NIR fluorescent imaging. Photodynamic therapy will be used as a treatment option. Finally, optical coherence tomography (OCT) will be used to track the progress of the therapy.



Premature clearance by the reticuloendothelial system (RES) and

insufficient penetration into the tumor frequently impede the effective delivery of actively targeted nano constructs to deep tumor sites. A recent pre-targeting strategy based on the administration of a polyethylene-glycol (PEG)-coated nano-carrier to the tumor-bearing subject has been designed to overcome these shortcomings. This PEG-coated nanocarrier has the ability to (i) evade RES capture and clearance, (ii) increase nano-drug accumulation in tumors via the enhanced-permeability-retention-effect (EPR), and (iii) enhance the performance of photosensitizers via drug-loaded-PEG-nano-carrier.

We hypothesize that the PEG-coated nanocarrier will enhance the photophysical properties including photo-stability, biocompatibility, singlet oxygen quantum yield, and fluorescent quantum yield of our synthesized photosensitizer. In addition, the nano complex is expected to evade RES and immunosurveillance and the near-tumor-vasculature and is capable of penetrating deep into the tumor, which can be seen by fluorescent imaging. After that, the light will be given to activate the photosensitizer of the complex to generate singlet oxygen that harms cancer cells. Moreover, the progress of tumor ablation will be non-invasively monitored via OCT.

The OCT setup will be a custom-built frequency domain OCT (FD-OCT). The high-speed spectrometer will be built to detect two bands of the spectral interference signal, namely at approximately 850 nm light wavelength for high-resolution imaging of superficial skin and 3D cell culture and at approximately 1300 nm light wavelength for deep imaging at low resolution beneath the skin surface. OCT system will enable non-invasive real-time 3D imaging of 3D culture cells and/or artificial skin to track the development of skin cancers as well as to track the progress of PDT treatment.

The goal of this work is to create a research network between Thai researchers and researchers from other countries such as the United States, Malaysia, and China. In terms of wellness and healthcare, this project will have a significant impact on society. The outputs and outcomes will include the graduation of at least two students, the production of two well-trained post-docs, at least three international publications, and the filing of one patent application. Furthermore, a strong bond will be formed among the researchers. Finally, and most importantly, the international network will foster the development of deep technology and platform knowledge.



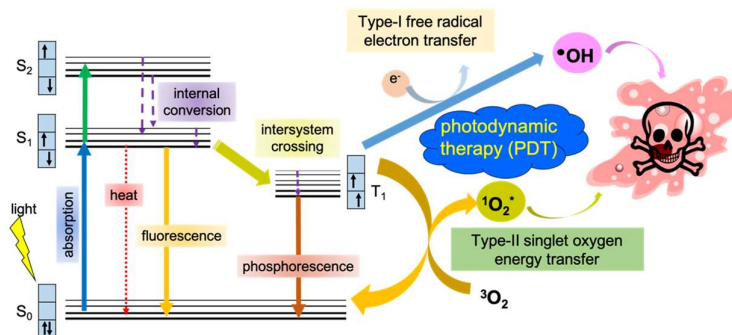
## FUNCTIONALIZED NANOPARTICLES FOR CANCER DIAGNOSIS, THERAPY, AND MONITORING USING OPTIC TECHNOLOGIES

Currently, many researchers have explored a better method to reduce the rate of cancer. In clinical, radiation therapy, surgery and chemotherapy are the mainstream procedures for cancer treatment. However, there are some serious side effects of those treatments including; (i) surrounding tissues damage in radiation therapy, (ii) wound complication and poor healing from surgery, and (iii) unexpected results occurring from chemotherapy, for example, individual response to the chemo drug and more side effect such as nausea, vomiting or immune depression.<sup>1-2</sup> Thus, finding an alternative/better way to cure cancer is urgent. Recently, nanotechnology plays important role in cancer research. The development of nanosystems to deliver imaging and/or therapeutic agents more efficiently is extensively explored.

In this proposal, we offer nanosystems that utilize a noninvasive treatment which is photodynamic therapy (PDT), approved to be used in the clinic, for cancer therapy. To improve cancer treatment, molecular imaging has become a tool for standard care of cancer. This technique allows scientists and physicians to see what is happening in the body at a cellular level by offering unique information to assist in the detection, diagnosis, evaluation, treatment, and management of cancer.<sup>3</sup> In addition to nanoparticles, we will develop a combined OCT and NIR fluorescence imaging system to visualize our prepared nanoparticles in an animal model. This system enables simultaneous imaging of tissue morphology and molecular information combined field of view of 3D OCT imaging and fluorescence imaging with about 30x30 mm scanning field of view. In the future, this system could be used in the small animal facility and clinical imaging. Moreover, with larger-scale studies, we can obtain the sensitivity and specificity for OCT/FL in the detection of cancer cells. This imaging technique could potentially enhance the clinician's capability in early diagnosis. At the end of the program, we expect to see Thai people aware of the importance of early diagnosis. We will introduce the country to the noninvasive light cancer treatments that might be included in the healthcare plan or a treatment option for patients who resistance to existing treatment procedures.

Light penetrates through tissues as a function of wavelength, the shorter wavelength lights absorb surface of the tissues. The longer wavelength lights travel depth tissue and are used for *in vivo* imaging and pre-treatment by PDT. Major components of human tissue are hemoglobin and water; hemoglobin strongly absorbs light at wavelengths lower than 650 nm and water absorbs light at wavelengths higher than 900 nm. The optical window optimum wavelength is between 650-900 nm for *in vivo* imaging.<sup>4</sup>

The therapeutic properties of light have been known for thousands of years, but it was only in the last century that PDT has been developed.<sup>5-6</sup> PDT is known as a treatment that uses a drug called a photosensitizer (PS) or photosensitizing agent, and a particular type of light. When PSs are exposed to a specific wavelength of the light source, they produce a form of oxygen that kills nearby cells (Figure 1).



**Figure 1.** Schematic represents type I and type II reactions of photodynamic therapy (PDT).



Indocyanine green (ICG), also referred to as Cardio Green, is a FDA approved dye for medical applications in the early 1950's.<sup>7</sup> ICG has also been explored as a potential PS but an extremely low singlet oxygen quantum yield ( $\Phi = 0.077$ ) has limited its practical utility. Singlet oxygen generation in PDT involves energy transfer from the sensitizers excited triplet state to the ground state of molecular oxygen. Excited triplet states are formed from excited singlet states via a process known as intersystem crossing (ISC). As fluorescence occurs as a result of radiative deactivation from a fluorophore's excited singlet state, the fluorescence and singlet oxygen quantum yields are invariably linked, with good fluorophores typically being poor sensitizers and vice versa.

Iodinated cyanine dye (I<sub>2</sub>-IR783) was recently developed<sup>8</sup> with high photostability, and strong fluorescence which made them more suitable than conventional cyanine dyes as fluorescence probes. Addition of heavy atoms to the structural skeleton of conjugated aromatics is known to increase the ISC process and improve singlet oxygen generation. Naturally, this usually comes at a price of reduced fluorescence emission. The effect of these structural modifications was proved to be a good imaging agent as well as a PDT material. Furthermore, the NIR activated PDT efficacy of I<sub>2</sub>-IR783 was also investigated in a mouse model.<sup>8</sup>

However, cyanine derivatives including I<sub>2</sub>-IR783 are not photo stable, making them difficult to use in preclinical study.<sup>9</sup> To circumvent this limitation, many researchers encapsulated the PS in a polymer to create nanoparticles (NPs), which have been shown to improve blood circulation and thus tumor accumulation.<sup>10-15</sup> Encapsulating PSs within functional amphiphilic polymers such as polyethylene glycol (PEG) resulted in the development of polymeric-based cyanine dyes NPs for cancer theranostic applications.<sup>9, 16-17</sup> To target tumors, hydrophilic nanomedicines use an enhanced permeability and retention (EPR) effect.<sup>18</sup> By allowing particles preferential access to tumors due to their size and persistence in circulation, EPR provides a strong justification for the development of nano-sized drug carriers. In comparison to normal tissues and organs, most solid tumors have a higher vascular density (hyper vasculature), *i.e.* angiogenesis, which is one of the most important properties of tumors to maintain their rapid growth.<sup>19-20</sup> Blood vessel breaches allow nanoparticles to infiltrate tumor tissue due to the rapid formation of new blood vessels.<sup>21</sup>

Currently, biomedical imaging is an indispensable tool in clinical diagnosis and evaluation, allowing non-invasive, highly sensitive, and specific observation of pathological and physiological changes related to human diseases,<sup>22</sup> and the detection of changes in tumor tissue before spreading remains a major goal in cancer clinical trials.<sup>23</sup> Optical Coherence Tomography (OCT) is an emerging medical imaging technology that enables micron-scale, cross-sectional imaging of microstructure in biological tissue in real-time.<sup>24-31</sup> OCT is a truly noninvasive, high resolution imaging modality that provides histological cross-sectional tomographic images and allows highly sensitive imaging of microvascular structures. One advantage of using OCT is that no exogenous contrast agents or cell engineering are required for stable labeling with fluorescent or bioluminescent tags. Acquisition speed is faster when compared to many other preclinical imaging modalities (such as MRI or PET). Furthermore, OCT can be successfully combined with other modalities (such as fluorescence confocal) for data validation and co-registration. In conjunction with fluorescence imaging, which provides molecular information by measuring the fluorescence intensity of fluorescent bio-markers that target specific molecules, clinicians can obtain more information for disease diagnosis. Moreover, OCT systems are attractive for imaging tumor response to PDT for several reasons. First, OCT systems typically utilize wavelengths of light ranging from 850 to 1350 nm, where absorption due to hemoglobin in blood is low and beyond the absorption of most PSs with insufficient energy for photodynamic action. Second, OCT systems use relatively low irradiances in the range of hundreds of microwatts. These characteristics of OCT make it a safe imaging technique compatible with PDT for visualizing tumor volume and microvascular networks before and after PDT without activating or photobleaching the PS. Third, real-time, high speed OCT systems enable online monitoring of tumor structural changes during PDT, making it a viable candidate for clinical translation as is already becoming the case in cardiovascular applications.<sup>32-35</sup>

## Objectives

The long-term goal of our program is to develop a theranostic platform relied on the inherent properties of nanomaterials which can be truly beneficial to our proposed nanotheranostic. Other objectives include:

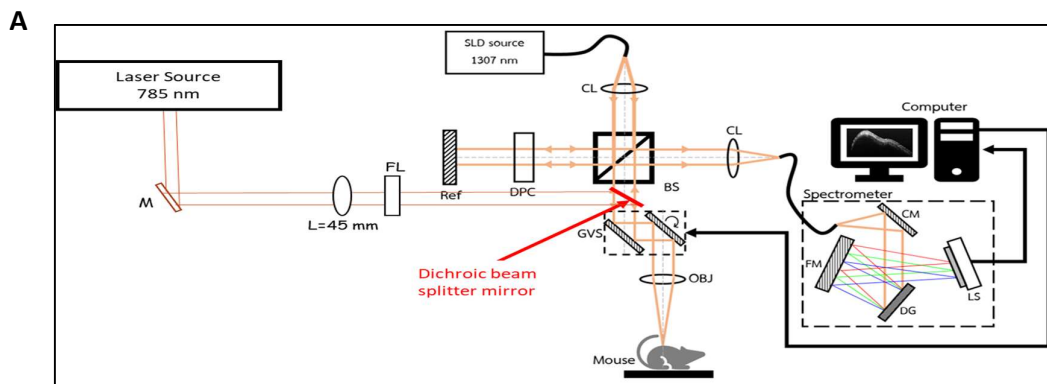
- 1) To develop the prototypes and up-scale production of nanomaterials. We endeavor to pay attention to *in vivo* tests. These tests are vital to achieve a high degree of efficacy of the prototypes.
- 2) To build up an optical imaging systems. *In vitro* studies of proposed nanotheranostic will be tested to lay the groundwork for the *in vivo* tests. Reproducibility is a key requirement of our research. The imaging facility will be setup as a research facility.

## Methodology

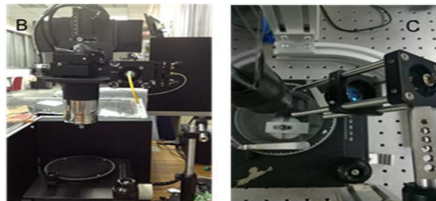
### 1<sup>st</sup> year plan:

1. Nanoparticles synthesis and characterizations.
2. *In vitro* tests.
3. Optical imaging system setup.

Along with the preparation of NPs, an optical imaging system will also be set up. We proposed a combined OCT and NIR fluorescence imaging system. This system enables simultaneous imaging of tissue morphology and molecular information combined field of view of 3D OCT imaging and fluorescence imaging with about 30x30 mm scanning field of view.



CL = Collimating lens; BS = Beam splitter; DPC = Dispersion compensator; GVS = Galvanometer scan mirror; OBJ = Objective lens; CM = Collimating mirror; FM = Focusing Mirror; LS = Line scan sensor

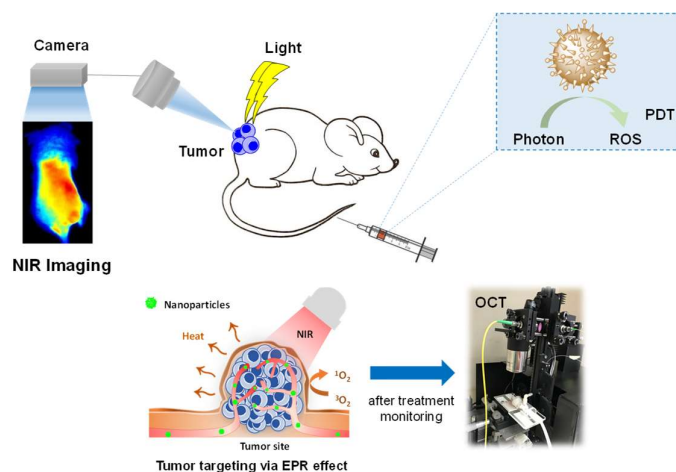


**Figure 2.** (A) Schematics of the combined OCT/NIR Fluorescence imaging system. (B) Photograph of OCT used a SLD at 1307 nm and (C) Full-Field Fluorescence Imaging

### 2<sup>nd</sup> year plans:

1. Develop tumor models for *in vivo* OCT and NIR imaging to monitor the optimal time for light irradiation in PDT.
2. Protocol validation.

*All experiments with animal model, we will use our home-made imaging system in comparison with a commercial imaging system.*



**Figure 3.** Schematic represents protocols in *in vivo* studies.

### Schedule for the entire project and expected output

year	activity	output	
		products	processes
1	1. Nanoparticles syntheses and characterizations. 2. Development of a home-made optical imaging system (OCT&FL)	a good nano systems to be used in vivo test 1 machine	a method to prepare NPs 1 prototype
2	Animal model and in vivo experiments using our homemade imaging system in comparison with a commercial imaging system.	2 publications 2 master students 2 post-docs training	1 patent application

### Impact

Cancer is inevitably problems worldwide. Our proposed program could create a remarkable network among young researchers in Thailand. This domestic connection could provide a crucial impact as a result of a wide range background from the team members, which is a prerequisite for a multidisciplinary research. Likewise, we also aim to build up new researchers in the field of nanomaterial-based biomedicine through our students and postdoc researchers. Ultimately, the novel prototype will be a high value equipment with a lower cost of production.

### References

1. Goldsmith, H. S., Clinical advances in the treatment of cancer. *Am J Surg* **1969**, *118* (3), 368-76.
2. Petrelli, N. J.; Winer, E. P.; Brahmer, J.; Dubey, S.; Smith, S.; Thomas, C.; Vahdat, L. T.; Obel, J.; Vogelzang, N.; Markman, M.; Sweetenham, J. W.; Pfister, D.; Kris, M. G.; Schuchter, L. M.; Sawaya, R.; Raghavan, D.; Ganz, P. A.; Kramer, B., Clinical Cancer Advances 2009: major research advances in cancer treatment, prevention, and screening--a report from the American Society of Clinical Oncology. *J Clin Oncol* **2009**, *27* (35), 6052-69.
3. Weissleder, R., Molecular Imaging in Cancer. *Science* **2006**, *312* (5777), 1168-1171.
4. Weissleder, R., A clearer vision for in vivo imaging. *Nature Biotechnology* **2001**, *19* (4), 316-317.
5. Dolmans, D. E.; Fukumura, D.; Jain, R. K., Photodynamic therapy for cancer. *Nat Rev Cancer* **2003**, *3* (5), 380-7.
6. Dougherty, T. J.; Gomer, C. J.; Henderson, B. W.; Jori, G.; Kessel, D.; Korbely, M.; Moan, J.; Peng, Q., Photodynamic therapy. *J Natl Cancer Inst* **1998**, *90* (12), 889-905.
7. Alander, J. T.; Kaartinen, I.; Laakso, A.; Patila, T.; Spillmann, T.; Tuchin, V. V.; Venermo, M.; Valisuo, P., A review of indocyanine green fluorescent imaging in surgery. *Int J Biomed Imaging* **2012**, *2012*, 940585.
8. Atchison, J.; Kamila, S.; Nesbitt, H.; Logan, K. A.; Nicholas, D. M.; Fowley, C.; Davis, J.; Callan, B.; McHale, A. P.; Callan, J. F., Iodinated cyanine dyes: a new class of sensitizers for use in NIR activated photodynamic therapy (PDT). *Chemical Communications* **2017**, *53* (12), 2009-2012.

9. Zhang, L.; Jia, H.; Liu, X.; Zou, Y.; Sun, J.; Liu, M.; Jia, S.; Liu, N.; Li, Y.; Wang, Q., Heptamethine Cyanine-Based Application for Cancer Theranostics. *Front Pharmacol* **2021**, *12*, 764654.
10. Liu, Y.; Shen, G.; Zhao, L.; Zou, Q.; Jiao, T.; Yan, X., Robust Photothermal Nanodrugs Based on Covalent Assembly of Nonpigmented Biomolecules for Antitumor Therapy. *ACS Appl Mater Interfaces* **2019**, *11* (45), 41898-41905.
11. Xing, R.; Zou, Q.; Yuan, C.; Zhao, L.; Chang, R.; Yan, X., Self-Assembling Endogenous Biliverdin as a Versatile Near-Infrared Photothermal Nanoagent for Cancer Theranostics. *Adv Mater* **2019**, *31* (16), e1900822.
12. Li, S.; Zou, Q.; Li, Y.; Yuan, C.; Xing, R.; Yan, X., Smart Peptide-Based Supramolecular Photodynamic Metallo-Nanodrugs Designed by Multicomponent Coordination Self-Assembly. *J Am Chem Soc* **2018**, *140* (34), 10794-10802.
13. Zou, Q.; Abbas, M.; Zhao, L.; Li, S.; Shen, G.; Yan, X., Biological Photothermal Nanodots Based on Self-Assembly of Peptide-Porphyrin Conjugates for Antitumor Therapy. *J Am Chem Soc* **2017**, *139* (5), 1921-1927.
14. Kamaly, N.; Yameen, B.; Wu, J.; Farokhzad, O. C., Degradable Controlled-Release Polymers and Polymeric Nanoparticles: Mechanisms of Controlling Drug Release. *Chem Rev* **2016**, *116* (4), 2602-63.
15. Liang, C.; Xu, L.; Song, G.; Liu, Z., Emerging nanomedicine approaches fighting tumor metastasis: animal models, metastasis-targeted drug delivery, phototherapy, and immunotherapy. *Chem Soc Rev* **2016**, *45* (22), 6250-6269.
16. Dereje, D. M.; Pontremoli, C.; Moran Plata, M. J.; Visentin, S.; Barbero, N., Polymethine dyes for PDT: recent advances and perspectives to drive future applications. *Photochemical & Photobiological Sciences* **2022**, *21* (3), 397-419.
17. St. Lorenz, A.; Buabeng, E. R.; Taratula, O.; Taratula, O.; Henary, M., Near-Infrared Heptamethine Cyanine Dyes for Nanoparticle-Based Photoacoustic Imaging and Photothermal Therapy. *Journal of Medicinal Chemistry* **2021**, *64* (12), 8798-8805.
18. Kang, H.; Rho, S.; Stiles, W. R.; Hu, S.; Baek, Y.; Hwang, D. W.; Kashiwagi, S.; Kim, M. S.; Choi, H. S., Size-Dependent EPR Effect of Polymeric Nanoparticles on Tumor Targeting. *Adv Healthc Mater* **2020**, *9* (1), e1901223.
19. Maeda, H.; Fang, J.; Inutsuka, T.; Kitamoto, Y., Vascular permeability enhancement in solid tumor: various factors, mechanisms involved and its implications. *International Immunopharmacology* **2003**, *3* (3), 319-328.
20. Iyer, A. K.; Khaled, G.; Fang, J.; Maeda, H., Exploiting the enhanced permeability and retention effect for tumor targeting. *Drug Discov Today* **2006**, *11* (17-18), 812-8.
21. Maeda, H.; Bharate, G. Y.; Daruwalla, J., Polymeric drugs for efficient tumor-targeted drug delivery based on EPR-effect. *Eur J Pharm Biopharm* **2009**, *71* (3), 409-19.
22. Weissleder, R.; Nahrendorf, M., Advancing biomedical imaging. *Proceedings of the National Academy of Sciences of the United States of America* **2015**, *112* (47), 14424-14428.
23. Hussain, T.; Nguyen, Q. T., Molecular imaging for cancer diagnosis and surgery. *Advanced Drug Delivery Reviews* **2014**, *66*, 90-100.
24. Huang, D.; Swanson, E. A.; Lin, C. P.; Schuman, J. S.; Stinson, W. G.; Chang, W.; Hee, M. R.; Flotte, T.; Gregory, K.; Puliafito, C. A.; et al., Optical coherence tomography. *Science* **1991**, *254* (5035), 1178-81.
25. Koustenis, A., Jr.; Harris, A.; Gross, J.; Januleviciene, I.; Shah, A.; Siesky, B., Optical coherence tomography angiography: an overview of the technology and an assessment of applications for clinical research. *Br J Ophthalmol* **2017**, *101* (1), 16-20.
26. Marschall, S.; Sander, B.; Mogensen, M.; Jorgensen, T. M.; Andersen, P. E., Optical coherence tomography-current technology and applications in clinical and biomedical research. *Anal Bioanal Chem* **2011**, *400* (9), 2699-720.
27. Fujimoto, J. G., Optical coherence tomography for ultrahigh resolution in vivo imaging. *Nat Biotechnol* **2003**, *21* (11), 1361-7.
28. Nam, A. S.; Vakoc, B.; Blauvelt, D.; Chico-Calero, I., Optical Coherence Tomography in Cancer Imaging. In *Optical Coherence Tomography: Technology and Applications*, Drexler, W.; Fujimoto, J. G., Eds. Springer International Publishing: Cham, 2015; pp 1399-1412.
29. Vakoc, B. J.; Lanning, R. M.; Tyrrell, J. A.; Padera, T. P.; Bartlett, L. A.; Stylianopoulos, T.; Munn, L. L.; Tearney, G. J.; Fukumura, D.; Jain, R. K.; Bouma, B. E., Three-dimensional microscopy of the tumor microenvironment in vivo using optical frequency domain imaging. *Nat Med* **2009**, *15* (10), 1219-23.
30. Wang, J.; Xu, Y.; Boppart, S. A., Review of optical coherence tomography in oncology. *J Biomed Opt* **2017**, *22* (12), 1-23.
31. Vakoc, B. J.; Fukumura, D.; Jain, R. K.; Bouma, B. E., Cancer imaging by optical coherence tomography: preclinical progress and clinical potential. *Nature Reviews Cancer* **2012**, *12*, 363.
32. Jung, Y.; Klein, O. J.; Wang, H.; Evans, C. L., Longitudinal, label-free, quantitative tracking of cell death and viability in a 3D tumor model with OCT. *Sci Rep* **2016**, *6*, 27017.
33. Jung, Y.; Nichols, A. J.; Klein, O. J.; Roussakis, E.; Evans, C. L., Label-Free, Longitudinal Visualization of PDT Response In Vitro with Optical Coherence Tomography. *Isr J Chem* **2012**, *52* (8-9), 728-744.
34. Makita, S.; Yasuno, Y., In vivo photothermal optical coherence tomography for non-invasive imaging of endogenous absorption agents. *Biomed Opt Express* **2015**, *6* (5), 1707-25.
35. Yang, T. D.; Park, K.; Kim, H. J.; Im, N. R.; Kim, B.; Kim, T.; Seo, S.; Lee, J. S.; Kim, B. M.; Choi, Y.; Baek, S. K., In vivo photothermal treatment with real-time monitoring by optical fiber-needle array. *Biomed Opt Express* **2017**, *8* (7), 3482-3492.

**Name of the Project:** Piloting an affordable and real-time Water Assessment System (WAS) for detection of fecal coliforms in drinking water

**Category :** Environment

**The Problem:**

- 40% of water consumed globally is not tested,
- an estimated 2 billion people globally use drinking water contaminated with feces,
- >829,000 people (with >297,000 children) die each year from diseases transmitted via fecal-oral route because of fecal contamination of water,
- traditional approaches to testing water for fecal contamination require infrastructure (>30k\$), testing-time (>18 h), training (~2Y post high-school) and/or expensive consumables (~5\$/test), so are not conducive for implementation in the developing countries where such tests are mostly needed.

**Our solution:** A reagentless system, based on our unique flat Fresnel lens working in the deep-UV, to detect fecal contamination in water based on native fluorescence of tryptophan-based proteins synthesized by the fecal coliforms

**Capabilities:**

- Real-time (<1 min), low-cost (<\$300 for a basic system), portable (< 1000 cm<sup>3</sup> ; < 1 kg) and user-friendly (basic traffic-light indicators according to WHO risk categories)
- 96% sensitivity to detect fecal contamination
- Detection of other contaminants in drinking water

**Applications to real-world issues:** early-warning detection of fecal contamination in resource-limited settings

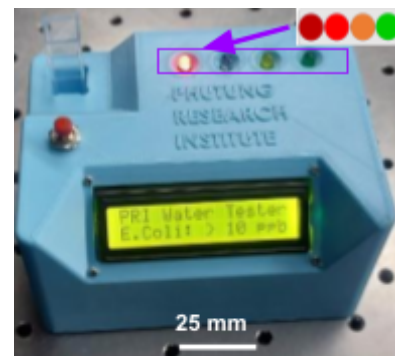
**Outcomes of the proposed project:** By the end of the project, we will have piloted 20 beta models (Technological Readiness Level-8) WAS devices with >6 community-managed water user groups, >6 households, >2 municipalities in Nepal, and > 6 food and water-related industries in Nepal. While doing so, we will have:

1. obtained >18 early adopters paying a discounted price, and obtained a rating of >7/10 from the users based on their overall experience with our device,
2. adapted our system designs according to the corresponding user's key requirements,
3. improved the method of manufacturing the optical system on our premises in Nepal using a low-cost polymer process, with a performance comparable (within 10%) to those made using methods requiring high-end lithography,
4. improved methods to manufacture electronics and assemble the whole system to yield 99% consistency in performance across all devices,
5. secured ~\$200,000 of seed funding for a new company to scale up and expand the sales in the countries around the globe (focused on developing countries).

**Long-term Impact**

- Reduction of water-borne diseases, especially in developing countries, improving lives and livelihood of billions of people around the globe,
- Direct economic impact on the country of Nepal, and to its scientific, R&D and innovation ecosystem.
- Acting as a role model by giving confidence to other researchers and entrepreneurs.

**Collaborators/Advisors:** Prof. Thomas Kraus (Nanophotonics), Prof. Marcel van der Horst (Electronics design), Mr. Arjan Rensema (New Business Development), Prof. Prof. Annelies Bobelyn (Product Design).



**Fig. 1:** A prototype WAS model with simple traffic light indicators and a LCD display to indicate level of fecal contamination.

## Literature Review

**The Problem.** Waterborne diseases such as diarrhea, typhoid etc, which are transmitted by the fecal-oral route, remain one of the major causes of death of children and vulnerable populations in developing countries. The WHO reports [1] that at least 2 billion people globally use a drinking water source contaminated with feces, and >829,000 people (with >297,000 children) die each year from diarrhea. The problem will only exacerbate due to extreme weather conditions and climate change [2-3]. In Nepal alone, studies have estimated that waterborne diseases cause as much as 263,836 years of life losses and 10,500 deaths due to diarrheal diseases [4]. The problem is particularly acute in low-income, less-educated families, and vulnerable groups, such as pregnant and nursing women. The economic impact due to treatment costs and morbidity of the breadwinners are approximately twice their average daily wage [5].

Therefore, detection of fecal contamination of drinking and environmental water is of paramount importance. WHO recommends the enumeration of fecal indicator organisms (FIO) such as thermotolerant coliforms (TTCs), including *Escherichia coli*, to quantify the level of fecal contamination in water samples [6]. Microbiological methodologies, such as membrane filtration and plate counting of cultured FIOs have been in use for tens of decades for quantifying or detecting the presence of TTCs. Colorimetric (eg. H<sub>2</sub>S test ) or fluorometric (eg. Colilert test) methods have also been developed in recent decades to indirectly quantify the cultured bacteria by utilizing their biochemistry. However, these methods are not reliable (H<sub>2</sub>S), they take > 18 h of culturing the sample in optimal laboratory conditions (Colilert), and/or require extensive sets of reagents, laboratory infrastructure and skilled personnel. These methods are therefore unsuitable for most developing countries and are used little in practice in low-resource settings. The 2022 progress report [7] of the United Nations Sustainable Development Goal 6 on Water and Sanitation, reveals that the quality of water consumed by at least 3 billion people is unknown due to lack of accessible monitoring tools. **Hence, real-time, in-situ, portable and low-cost methods and tools to monitor drinking and environmental water are badly needed.** Demonstrating this need, UNICEF has provided [8] Target Product Profile of rapid, portable and low-cost tests for quantifying the level of fecal contamination in drinking water and classifying the samples according to the WHO risk categories.

Several studies [9-12] have demonstrated a strong correlation between the intensity of Tryptophan-like Fluorescence (TLF, Excitation/Emission = 280 nm / 350 nm) from environmental water samples and the number of colony forming units (CFU) of TTCs present in the sample. TLF is emitted by indole-containing organic compounds which have similar fluorescence properties as the L-Tryptophan (Trp) amino acid. These compounds are produced and metabolized in relatively large quantities by active microorganisms, such as TTCs [10]. Based on experiments using water samples collected from five countries, Sorensen et al suggested that a TLF threshold of 1.3 ppb (equivalent to standard tryptophan solution) can predict the presence of TTCs  $\geq 10$  CFU/100 ml in real-time. Unfortunately, Sorensen et al. used high-cost (US\$8-20k) fluorimeters designed for specialists that are out of reach for users in developing countries. Clearly, low cost fluorimeters with 1 ppb sensitivity are needed.

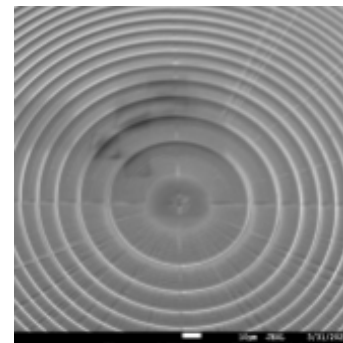


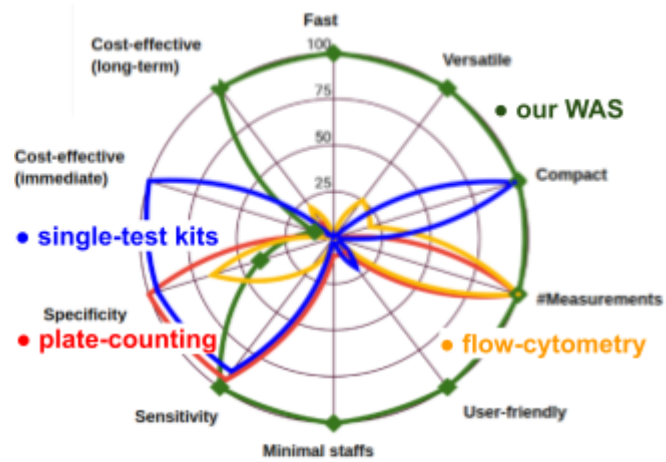
Fig. 2: Flat fresnel lenses operating in the UV implemented in our fluorimeters (from [13]).

**Our solution.** We recently reported [13] a fluorometer that can be built from very low cost (<\$150) components but with detection limits comparable to commercial fluorimeters. A key aspect of our fluorometer is the optical system - instead of using conventional bulk lenses, which are costly and complex to align, we use flat Fresnel lenses operating in the deep UV



(Fig. 2) that can be etched directly into a glass substrate or transfer-printed using UV-grade polymers such as Polydimethylsiloxane (PDMS). We have been able to demonstrate a very high signal collection efficiency with these flat lenses. In addition, we have developed a bespoke electronic transimpedance amplifier that allows us to use simple silicon pin diodes compared to the bulky and expensive photomultiplier tubes used in traditional systems. Altogether, when accounting for all the operational, materials and manufacturing costs, our business model predicts that fluorometers can be made and sold for less than \$300 while still generating a small profit.

To verify the performance of the instrument, we collected 157 samples of drinking and environmental water in the Kathmandu Valley, Nepal, and were able to demonstrate (manuscript in preparation) a sensitivity ( $\frac{\# \text{True positives}}{\# \text{Total positives}}$ ) of 96% to detect TTCs with plate counting as the reference. The corresponding receiver operating characteristic (ROC) of our system has an area of 0.82 squared units, which is considered to be a very good prediction test. Therefore, being low-cost, portable, reagentless, and operating in real-time, our system has significant potential as a water quality surveillance tool for resource limited settings. When comparing its performance indicators to established methods (Fig 3 top), our WAS system excels in most indicators, except in terms of specificity, where plate counting is the accepted gold standard; in terms of immediate cost-effectiveness, single-test kits such as  $\text{H}_2\text{S}$  are cheaper but also have much lower performance and are costly in the long-term.



**Fig. 3: (Top)** Performance comparison against competing technologies for various indicators. The comparison is relative to the best performing one - which is assigned a value of 100. **(Bottom)**. A picture from the end-user-feedback workshop we organized recently to understand user requirements.

### Problem Statement/Objective

To date, we have built 4 working prototypes of the design shown in fig. 1 that are aimed at minimally trained users in Nepalese communities. Our youtube video illustrates the operation: [https://youtu.be/borlcJgN\\_Ro](https://youtu.be/borlcJgN_Ro). We also organized an end-user engagement workshop (Fig 3 Bottom), and set up four demonstration booths in public exhibitions in Nepal. As a result, we have obtained oral and written feedback from 300 potential users. All of these users were enthusiastic about the system and stated that they want to see the system in the market as soon as possible. When our device is ready for implementation in the field, the Ministry of Science and Technology and the Nepal Bureau of Standards & Metrology have promised their support in facilitating accreditation and integration of the instrument into the national standard system. Additionally, Tarakeshwor municipality has committed \$10,000 support to develop 10 units for their distribution system. However, different potential customers requested different product profiles depending on their use, as

described in Table I. Therefore our main objectives will be focused on finding product-market-fit, eg. by addressing the customer needs and adapting our system for enhanced access and utility.

Customer Profile			Customer Requirements	
No	User	Use	Features	Price
1	Community-managed Water User groups (non-technical), General	Community level tests, Household tests	Dip-in system, portable, simple procedure, non-technical readout in native language	<\$200
2	Community-managed Water User groups (semi-technical), Municipalities, surveillance	Surveillance of distribution system	In-line continuous monitoring, remote alarm, minimal maintenance	<\$1000
3	Hotels, restaurants, dairy, food, drinks and water packaging industries	Detection of contamination or inefficiency in process pipelines	Continuous monitoring, remote alarm, spectral analysis	<\$5,000
4	Municipalities, health	Water-communicable diseases	Specificity for Water-communicable diseases	<\$20,000
5	Wild-life conservation	Environmental	Specificity for human-wildlife transmissible diseases	<\$10,000
6	Research	Environmental	Specificity, Fe <sup>+</sup> , Mn, NH <sub>4</sub> etc	<\$20,000

**Table 1. Customer profile of the different end-user groups**

### Objectives

- Adapt designs to develop pilot models according to user requirements** for enhancing product-market fit and long-term impact. As addressing the requirements of all the customer profiles is not possible within the time-frame of this project, we will focus on obtaining and addressing the needs of >6 early adopters from each Customer profiles No. 1, 2 and 3 (see Table 1), prepared to pay a discounted price of \$150, \$750, and \$3,750 respectively. Through at least two design-and-pilot cycles, we aim for a rating of >7 (out of 10), when rated by our >300 potential customers for ease of use, user experience and accuracy, and >50% of them willing to purchase our device.
- Develop low-cost transfer-printing methods to locally manufacture lenses.** In our current prototypes, we use flat-Fresnel lenses etched directly on quartz substrate with in-kind technical support from the group of Prof. Thomas Krauss at the University of York, UK. The manufacture involves a dry etching process, which requires cleanroom and dry-etching infrastructure and consumables. To be able to produce the lenses in Nepal in large volume without investing in such infrastructure, we are currently developing methods to transfer the lens structure into a thin layer of UV-grade PDMS polymer. Currently, the yield of the transfer printing is low because the PDMS bonds the mold and the substrate together resulting in damage of the transferred structure during the removal process. With Prof. With Krauss' in-kind support, we will identify suitable materials that will act as anti-adhesive layers and develop a mechanical system that can apply a well-distributed and optimum pressure to remove the substrate without damaging the transferred structures. We aim for >90% yield within 10% of performance compared to lithographically made lenses.
- Develop a consistent production process** for the volume manufacturing of the transimpedance amplifier in Nepal with in-kind support from Amsterdam University of

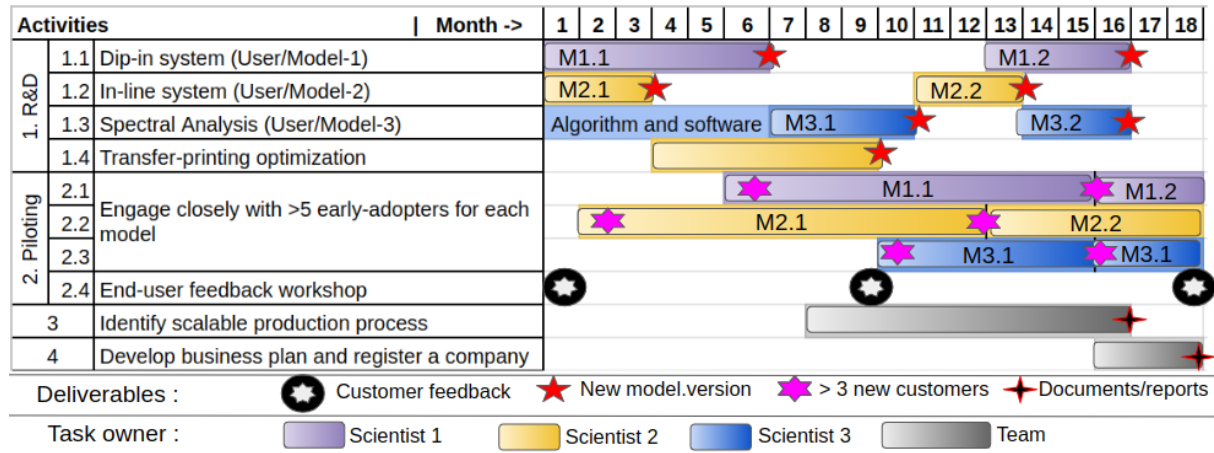


Applied Sciences and Technical University of Eindhoven, with whom we are already engaged. Our goal is to achieve 99% consistency of the performance across 6 units of each of the three models we will focus on.

4. **Develop a scaling plan** for manufacturing and distribution in Nepal and for expansion beyond Nepal into other developing countries (with in-kind support from Global School for Entrepreneurship, Amsterdam, with whom we are already engaged with the same goal). By the end of this project we aim to register a new company and obtain >\$200,000 seed funding from local investors and impact funders to scale up.

### Outline of tasks/Work Plan

An outline of the activities and work-plan is provided in Fig. 2.



**Fig. 4: Outline of the key deliverables with project activities**

We will employ three scientists (3x 0.66FTE =2 FTE) to perform the tasks related to R&D and piloting. In addition to receiving direct feedback from our early adopters, we will conduct three comprehensive end-user feedback workshops with > 100 additional potential customers in each workshop (>300 users in total) to understand their needs and adapt our models and develop business plans accordingly.

To do these tasks, we will **collaborate** and seek advice from Prof. Thomas Krauss, University of York (Fresnel lenses), Prof. Marcel van der Horst, Amsterdam University of Applied Sciences (Electronics design), Prof. Annelies Bobelyn, Technical University of Eindhoven (Product design) and Mr. Arjan Rensema, Global School for Entrepreneurship, Amsterdam (New Business Development).

### Outcome(s)

Key deliverables of our project activities are indicated in Fig 4, which includes: (1) > 6 early adopters from each customer profile willing to pay a discounted price of \$150, \$750, and \$3,750 respectively, (2) >18 and 2 versions of beta models designed and developed to meet customer requirements, (3) a transfer-printing technology to manufacture flat lenses in Nepal using UV-grade PDMS polymer with >90% yield within 10% of performance compared to lithographically made lenses, (4) detailed customer feedback, both oral and written from 3 end-user feedback workshops with which we will reach-out to >300 potential end-users, (5) manufacturing process standards and documents to obtain 99% consistency, (6) a registered company to scale-up production and marketing, (7) >\$ 200,000 investment for scaling.

### Impact

The proposed activities are the first steps towards bringing our TRL-7/8 technology to 40% of the world population, who have been consuming untested water. By providing a tool to

strengthen water surveillance in the developing countries, in remote locations of developed countries, and in locations impacted by the natural disasters, we expect that our system will mitigate threats from fecal contamination of drinking and environmental water to the lives and livelihood of billions of lives around the globe in the long-run. Assuming that we directly or indirectly reach only 5% of the key stakeholders due to our system, of which 50% take necessary preventive steps (eg. decontamination, policy planning, regulation, chlorination, identification and isolation of the sources of contamination), facilitated by people whom we closely engage with, our innovation has the potential to proportionally reduce mortality, morbidity, treatment costs due to waterborne diseases in the neediest population around the globe by 2.5% (=50%\*5%).

Additionally, as the project is led by Nepali team and the production is planned in Nepal, one of the least developed countries in the world, there will be direct and invaluable economic impact to Nepal, and to its scientific, R&D and innovation ecosystem. The technological achievements and corresponding knowledge generated from our R&D activities will also have a long-term academic and societal impact. Last but not the least, we hope that our activities and outcomes will provide a role model for innovation and applications of optics by giving confidence to other researchers and entrepreneurs operating in the developing countries to address their local problems by using photonics.

#### References:

1. WHO fact sheet: <https://www.who.int/news-room/fact-sheets/detail/drinking-water>
2. WHO Nepal policy: <https://www.who.int/globalchange/resources/wash-toolkit/review-of-policy-documents-on-climate-change-wash-and-pulic-health-in-nepal.pdf>
3. UNICEF WASH climate: <https://www.unicef.org/wash/climate>
4. Nepal Burden of Disease country report, Nepal Health Research Council: [http://nhrc.gov.np/wp-content/uploads/2019/04/NBoD-2017\\_NHRC-MoHP.pdf](http://nhrc.gov.np/wp-content/uploads/2019/04/NBoD-2017_NHRC-MoHP.pdf)
5. Malik, Afifa, et al. "Water-borne diseases, cost of illness and willingness to pay for diseases interventions in rural communities of developing countries." *Iranian journal of public health* 41.6 (2012): 39-49.
6. Guidelines for Drinking-water Quality, 4th Edition Incorporating the First Addendum, WHO (2017)
7. Report of the Secretary-General, Progress towards the Sustainable Development Goals- E/2022, United Nations. [https://sustainabledevelopment.un.org/content/documents/29858SG\\_SDG\\_Progress\\_Report\\_2022.pdf](https://sustainabledevelopment.un.org/content/documents/29858SG_SDG_Progress_Report_2022.pdf)
8. UNICEF, 2017. Target Product Profile: Rapid *E. Coli* detection. Version 2.0.
9. Goffin, Angélique, et al. "Temperature, turbidity, and the inner filter effect correction methodology for analyzing fluorescent dissolved organic matter in urban sewage." *Environmental Science and Pollution Research* 27.28 (2020): 35712-35723.
10. Cumberland, Susan, et al. "Fluorescence spectroscopy as a tool for determining microbial quality in potable water applications." *Environmental technology* 33.6 (2012): 687-693.
11. Sorensen, James PR, et al. "Real-time detection of faecally contaminated drinking water with tryptophan-like fluorescence: defining threshold values." *Science of the Total Environment* 622 (2018): 1250-1257.
12. Bridgeman, John, Magdalena Bieroza, and Andy Baker. "The application of fluorescence spectroscopy to organic matter characterisation in drinking water treatment." *Reviews in Environmental Science and Bio/Technology* 10.3 (2011): 277-290.
13. Bohora, Sanket et al. "A Low-cost Fresnel Lens Fluorometer to Detect Fecal Contamination in Drinking Water in Realtime" CLEO 2022 (AM5M.8)

Executive summary for proposal to the 20th anniversary challenge in the field of environment:

## **Tunable dual-comb spectrometer for real-time high sensitivity multi-species environmental sensing**

One of the major challenges today is the emission of greenhouse gases and air pollutants by industry, intensive agriculture and traffic in urban environments leading to global warming and health issues with enormous costs for society. In order to be able to take appropriate measures, a suitable data basis must be created. Since the currently known trace gases are harmful even at very low concentrations in the parts-per-billion range, highly sensitive measurement methods are required. With modern instruments, such measurements are relatively easy to perform as point measurements. But precise multispecies large-area measurements are still not very widespread. However, such measurements are of particular importance in order to study the exact relationships between emissions and their environmental effects and to identify main sources.

The problem can be addressed with open-path dual-comb spectroscopy measurements. These high-precision time-resolved multi-species measurements have been successfully demonstrated for the detection of methane leaks, agricultural monitoring and urban pollution monitoring.

So far, however, such measurements have been extremely costly and mostly limited to proof of principle experiments, since the underlying optical system, consisting of two stabilized optical frequency combs, is complex and expensive. Furthermore, the measurements have so far suffered from limited sensitivity. This is due to the fact that attempts were made to measure a broad optical spectrum simultaneously in order to achieve a good species selectivity. Also, these first measurements were predominantly performed in the near-IR at 1.6  $\mu\text{m}$  where the trace gases show only relatively weak absorption features. This in turn has forced long integration times on the minute to hour scale and integration distances on the km scale.

Here, we propose a setup superior to these systems, which has a simpler architecture and at the same time offers higher performance. The performance gain can be achieved by sequential narrowband measurements in the mid-IR optical spectrum (2  $\mu\text{m}$  to 5  $\mu\text{m}$ ), the molecular fingerprint region of trace gases, at identical total integration times. We access this regime by a combination of a low-noise single-cavity dual-comb solid-state pump laser operated at 1  $\mu\text{m}$  in combination with a wavelength tunable single-cavity dual-comb optical parametric oscillator (OPO) for highly efficient frequency conversion into the mid-IR. At the core of this system is our special recipe for the realization of low noise, solid-state single-cavity dual-comb lasers. We spatially multiplex the optical cavity by the insertion of a biprism that allows for the coexistence of two slightly detuned but mutually coherent frequency combs in the same cavity. Further we transfer the same concept to the OPO cavity to obtain a synchronously pumped single-cavity dual-comb OPO. This allows us to realize a wavelength tunable system with optical frequency combs in the mid-IR pumped by a simple to realize dual-comb laser at 1  $\mu\text{m}$  with excellent noise performance in free-running operation. The low intensity noise and timing noise of the laser is crucial for dual-comb measurements for two reasons: Measurements are typically shot-noise limited and high sensitivity will be obtained through a coherent averaging approach.

In the framework of this project, we will design and assemble a mechanically optimized and portable prototype system of the proposed tunable dual-comb spectrometer, validate it under laboratory conditions and apply it for open-path environmental sensing.

# Tunable dual-comb spectrometer for real-time high sensitivity multi-species environmental sensing

## Problem statement/Objective

Air quality control in urban environment and mitigation of emission of greenhouse gases is one of the major challenges of the 21<sup>st</sup> century. In addition to the suffering for the individual, both generate substantial costs for society. Treatments of diseases caused by poor air quality alone generated worldwide annual costs of 8.1 trillion USD in 2019 [1] and the increased occurrence of natural catastrophes enhanced by global warming is estimated to cost up to 23 trillion USD by 2050 [2]. Efficient measures and scientific guidance of political decisions require a good understanding of these man-made environmental impacts and their interrelationship. For this purpose, a reliable and accurate data situation is important. In recent years, there have been significant efforts to provide such data and thus identify important emission products and their sources. The most important greenhouse gases known today include carbon dioxide (CO<sub>2</sub>), methane (CH<sub>4</sub>), ammonia (NH<sub>3</sub>) and nitrous oxide (N<sub>2</sub>O). Air pollutants of direct health concern include carbon monoxide (CO), nitric oxide (NO), nitrogen dioxide (NO<sub>2</sub>), ozone (O<sub>3</sub>) and sulfur dioxide (SO<sub>2</sub>) [3]. A large proportion of these gases is emitted by the combustion of fossil fuels at high temperatures or by modern intensive agriculture. There is also high interest in detection of volatile organic compounds, aerosols, and other trace gases in the context of human health. The combined occurrence of certain species allows to draw conclusions about the exact source of the pollution and whether they are man-made.

There has been a major effort in science and industry to develop systems that simultaneously provide high sensitivity, high dynamic range, wide species selectivity, fast measurement update rates, and insensitivity to other environmental fluctuations. Further, for environmental monitoring a large area coverage is required. In this sense open-path multi-species line-integrated measurements of up to several km range can be beneficial compared to point measurements provided by most sensor systems on the market today.

Here, we propose a new approach for such open-path measurements based on a free-running tunable dual-comb spectrometer with increased sensitivity and at the same time reduced system complexity compared to existing demonstrations with broadband coherent sources.

## Literature review

Commercial point measurement systems can currently reach ppb (parts per billion) to even ppt (parts per trillion) sensitivity in second integration time [4]. In contrast to classical high precision spectroscopy methods like gas chromatography, mass spectrometry and chemiluminescence – all suffering from complicated sample preparation and slow measurement update rates – these highest performance measurements are enabled by absorption spectroscopy. Typically, a continuous wave (CW) laser is swept over an absorption feature and the signal is detected via lock-in detection. Further enhancement of the signal is achieved in optical multi-pass cell arrangements, where the effective interaction length between the light and the target gas is increased to the 100-m scale.

Of particular interest for the detection of trace gases is the mid-IR wavelength range (2  $\mu\text{m}$  to 5  $\mu\text{m}$  and its extension to  $>10 \mu\text{m}$ ), also called molecular fingerprint region. Here, many of the above listed molecules exhibit strong absorption features based on their (ro-) vibrational transitions as can be seen

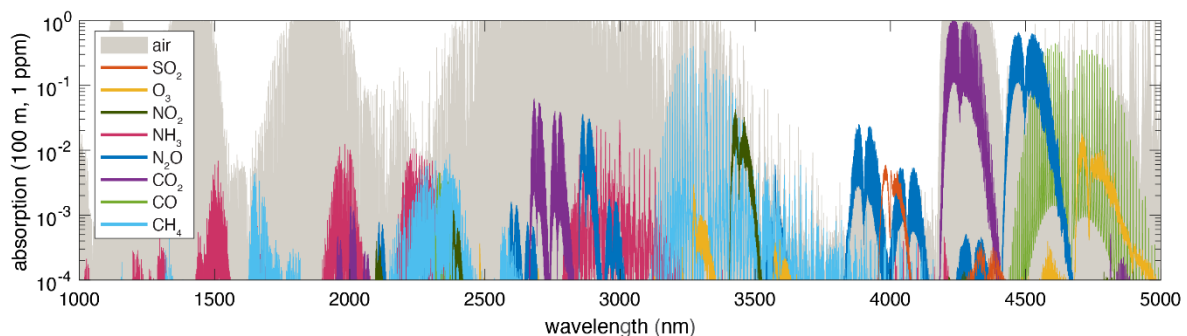


Figure 1: HITRAN calculated absorption features of a selection of prominent greenhouse gases and air pollutants at a concentration of 1 ppm and integration path of 100 m as a function of wavelength. Note that the background from air is calculated for standard conditions and mostly governed by water and CO<sub>2</sub> absorption.

in Figure 1. Because of the lack of high brightness light sources, this wavelength regime has been traditionally accessed with Fourier transform spectrometers (FTIR). While FTIRs with black-body sources offer excellent spectral coverage, they are limited in resolution, sensitivity and speed and have moving parts. Recently, quantum-cascade lasers (QCLs) have matured enough to enable spectroscopy systems in the mid-IR spectral range, allowing for sub-ppb detection efficiencies within an integration time of around 1 second. Unfortunately, individual QCL emitters offer only very limited wavelength tunability and thus have to be tailored to a specific trace gas component. This drives the cost of such systems and makes them restrictive in case new gases with other absorption features are to be investigated. Furthermore, QCLs have difficulties to access the interesting frequency band from 2  $\mu\text{m}$  to 4.5  $\mu\text{m}$ .

A very promising method that has emerged in the past years is dual-comb spectroscopy (DCS) [5]. A pair of slightly detuned optical frequency combs, e.g. generated by two mode-locked femtosecond lasers with repetition rates of  $f_{rep}$  and  $f_{rep} + \Delta f_{rep}$ , creates a beating between the pairs of optical comb-lines and transfers the spectroscopic information from the optical frequency domain to the RF domain in the frequency range  $[0, f_{rep}/2]$ . The update rate of the spectroscopy measurement is given by  $1/\Delta f_{rep}$ . To increase the sensitivity, coherent averaging of multiple periods is necessary. Therefore, the coherence time of the dual-comb system needs to be sufficiently high. Until now, this has been achieved by full stabilization of both of the combs, but this implies a high complexity and cost.

The optical comb line spacing, given by  $f_{rep}$ , should be chosen according to the width of the absorption features to be measured in order to optimize the sensitivity. For example, for gas phase studies under standard pressure and temperature conditions (1 atm, 25°C), the individual absorption features are several GHz wide due to collisional and Doppler broadening. Therefore, higher repetition rates of around a gigahertz are favorable since they offer sufficient spectral resolution, high update rates (below 1 millisecond), and high power per comb line. However, traditional systems based on fiber lasers are limited to the few-100-MHz range. In recent work, researchers switched to solid-state lasers to enable high repetition rates [6], although still with complex fully stabilized combs.

With the advances in dual-comb technology, it has been possible in the past years to demonstrate that dual-comb laser sources can be successfully used for trace gas sensing both in the laboratory and in field experiments. The latter have so far been demonstrated in the near-IR region around 1.6  $\mu\text{m}$  via supercontinuum generation [7–11], and covering the 4.5  $\mu\text{m}$  to 5.0  $\mu\text{m}$  range in the mid-IR via optical rectification [12]. Field experiments include methane leak detection [10], monitoring beef cattle feedlots [11], greenhouse gas emission from road traffic [9] and urban air pollution [8,12] where the latest experiments have reached (sub-)ppb level sensitivity for the trace-gases on 100-m to 1-km scale open paths. Common to these experiments was the requirement for a rather long integration time of minutes to hours to reach the desired sensitivity since measurements were performed with ultra-broadband spectral coverage and low  $\Delta f_{rep}$ . We believe that a system combining the spectral coverage of comb-based sources with the sensitivity of QCLs could represent an important step in advanced environmental and industrial monitoring applications.

### Outline of tasks/Work plan

Here, we propose a specific scheme for practical dual-comb generation in the near- and mid-IR range up to 5  $\mu\text{m}$  that will allow for high sensitivity while addressing the limitations discussed above. Based on [13], splitting the full spectral measurement in DCS into  $N$  separate spectrally narrowband measurements reduces the averaging time required by  $\sqrt{N}$ . This scaling law favors a tunable mid-infrared gigahertz source with sufficiently low noise to perform coherent averaging even in free-running operation. Development of a portable prototype source and proof-of-principle open-path measurements with it are the main goals of the proposal. While this approach has several potential advantages compared to existing ultra-broadband dual-comb sources, it has received less attention due to several technological challenges. Our system concept to overcome these challenges is illustrated in figure 2. It is comprised of a dual-comb modelocked laser pumping a single dual-comb OPO cavity.

We will realize this concept through our new dual-comb spatial multiplexing technique for generating both combs in a single cavity arrangement. In our first demonstration with this technique, we developed a dual-comb modelocked solid-state laser source at 80 MHz repetition rate [14]. In two recent efforts, we scaled the laser repetition rate to 1 GHz [15,16], and used a 250-MHz laser to drive a

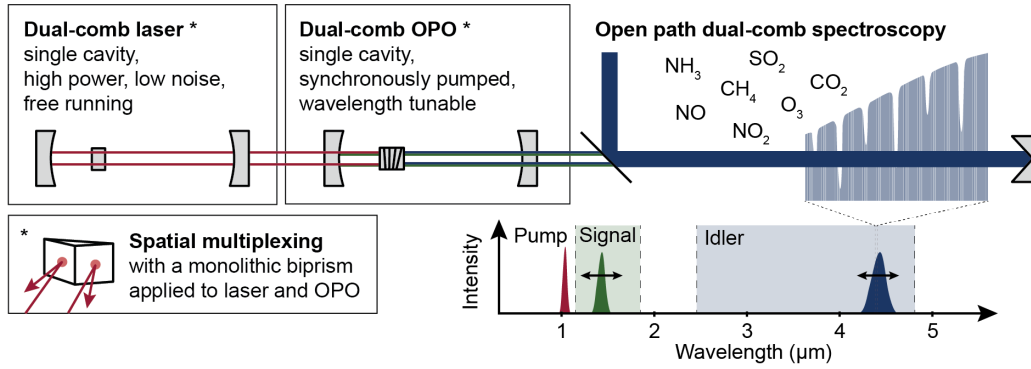


Figure 2: Schematic representation of the proposed tunable dual-comb spectrometer in the mid-IR wavelength regime for open path environmental monitoring applications.

single-cavity synchronously pumped optical parametric oscillator (OPO) for efficient wavelength conversion [17]. OPOs represent an ideal approach for wavelength conversion since they preserve the spectral brightness, timing jitter, and relative intensity noise (RIN) characteristics of our ultralow noise dual-comb pump lasers. By choosing a single-cavity architecture for both the laser and OPO subsystems, we greatly reduce system complexity while drastically reducing noise. Here we propose to combine these developments into a portable prototype system and perform a first proof of principle demonstration of open-path dual-comb spectroscopy with free-running single-cavity dual-combs. The estimated timeline and parallel processing of the work packages is summarised in figure 3. The first four work packages will leverage on existing technology and knowledge in the research group and therefore can be implemented highly efficiently. The last work package will involve collaboration with experts in the spectroscopy community.

month 1-3	month 4-6	month 7-9	month 10-12
Workpackage 1 prototype design			
	Workpackage 2 prototype assembly		
	Workpackage 3 dual-comb data processing electronics		
		Workpackage 4 prototype validation under lab conditions	
			Workpackage 5 open path experiments

Figure 3: Work package overview with estimated duration for execution.

#### Work package 1: Mechanically-optimized laser and OPO design

In the first step we design a mechanically isolated and optimized single-cavity dual-comb pump laser and a single-cavity dual-comb OPO. The mechanical prototype design will provide robustness against environmental changes and suppression of acoustic noise sources, which is crucial for low noise operation and mutual coherence of the two combs system. Such coherence is required for computational tracking of the radio frequency comb lines, which in turn enables coherent averaging of the dual-comb interferogram data that contains the spectroscopic information. Slow feedback loops will be included to prevent drifts of the repetition rate difference and maintain OPO synchronicity over long timescales.

The laser and OPO will be implemented for 1 GHz repetition rate. This allows for significant optical power per comb line (which is needed for high-sensitivity detection), and for fast sampling rates of more than 10 kHz (which mitigates the influence of disturbances due to air turbulence in the open path experiments). The instantaneous optical bandwidth and the repetition rate difference will be chosen in a compromise for parallel coverage of trace-gas absorption features for good species selectivity, the sensitivity of the system and speed of sampling. For a system operating up to an idler wavelength of 5  $\mu\text{m}$  periodically poled lithium niobate (PPLN) is an ideal choice for the nonlinear crystal in the OPO and supports continuous wavelength tuning. This will enable sufficient spectral coverage needed to detect the targeted gas species. Future work could extend the approach to longer wavelengths using OP:GaP nonlinear crystals or a longer wavelength pump laser at 2  $\mu\text{m}$ .

#### Work package 2: Mechanically-optimized laser and OPO implementation and validation

The custom mechanical parts for the laser and OPO prototype system will be fabricated inhouse by the mechanical workshop of ETH. This ensures a quick turnaround and mitigates risks in case small modifications are required. We have extensive experience with such prototype design from the successful implementation of a 80 MHz single-cavity dual-comb pump laser and OPO [14]. The

available diagnostic devices in our research group allow for a thorough characterization and – if required – optimization of the prototype system with a special focus on the noise performance. This will be beneficial for the use of the tunable, yet free-running dual-comb spectrometer to the environmental sensing applications. The completed work package will provide a portable rugged dual-comb OPO system with computer-controlled tuning of the OPO output wavelengths.

*Work package 3: Processing electronics and routines for dual-comb data*

Operating a dual-comb system in free-running mode requires active tracking of the optical comb-line positions for coherent averaging. We have recently shown that this is possible in a computationally efficient way by tracking the carrier envelope phase of the individual interferograms. This continuous tracking is achieved with our single-cavity dual-comb platform due to the ultra-low timing noise performance [16]. The underlying algorithm will be transferred to a real-time data processing unit that allows for extended coherent integration of the dual-comb signal. This will allow for real-time phase correction and adaptive sampling of the interferograms, the prerequisite for coherent averaging and memory efficient storage of the acquired dual-comb time domain spectroscopy data.

We plan to send out simultaneously the three colors of pump, signal and idler along the same open path and detect them spectrally filtered on individual photodiodes and digitalizing channels. Active use of the available additional optical power in the near-IR has the following advantages: Due to minimal spectral overlap of the pump comb with atmospheric absorption feature, it can serve as a reference for the phase correction of the dual-comb data. The additional signal comb can serve as a parallel reference measurement for inline calibration of e.g. the strength of water absorption that might be superimposed with the signal in the mid-IR wavelength regime. A quantitative analysis of the trace gas concentrations along the integrated path will be performed with a numerical fitting routine against the individual species absorption data precalculated from the line-by-line data from spectroscopic databases.

*Work package 4: Sensitivity validation and open path experiments*

The sensitivity of the dual-comb system can be best tested under laboratory conditions in a multi-pass cell filled with reference gas compositions, mimicking the open-path experiments. These controlled conditions will further allow to validate the optimal dual-comb signal detection, especially the suitability of high bandwidth HgCdTe detectors covering the mid-IR wavelength range. A backup plan for too strong detector limitations is nonlinear up-conversion of the returned mid-IR combs to the near-IR spectral range where high performance photodiodes are widely available.

*Work package 5: Environmental sensing experiments and interpretation of data*

The portable dual-comb spectrometer will be used in an open-path experiment with multi-100-m integration length. This part of the proposal we plan to execute in collaboration with an institute specialized in environmental monitoring – we are already in contact with the Swiss institute EMPA – to identify an interesting environmental monitoring target (urban, industrial, or undeveloped area).

The beam preparation and steering are of special importance here. Diffraction of the beam requires 10-cm-scale beams at the emitter side for up to km length propagation, which will be optimally achieved with a fiber coupled front end and off-axis parabolic mirror telescopes. The light will be directed back to the emitter side with a retro-reflector for insensitivity to beam pointing fluctuations. We plan to combine the two optical frequency combs prior to the open path propagation. Although this means that the spectral phase of the absorption lines is not available, it reduces the sensitivity to wavefront aberrations that arise from air turbulences.

To make best use of the tunability and increased sensitivity of the source compared to directly broadband dual-comb source we will identify the optimal spectral bands for each trace gas in terms of selectivity against the background (dominated by water absorption) and restrict the measurement to those frequency sub-bands. Our collaborators will help to best interpret the recorded data, extract correlations between the monitored compounds, and help with dissemination of the results to the environmental monitoring community.

**Outcome(s)**

The successful project will deliver a portable prototype system of a tunable mid-IR spectrometer based on our unique concept for single-cavity dual-comb OPOs synchronously pumped by a free-running single-cavity low-noise solid-state dual-comb laser oscillator. By combining limited instantaneous optical spectral coverage with a broadband tunability of the source throughout the molecular fingerprint



region in the mid-IR, this system will enable the next step in sensitivity on the sub-ppb range in open-path sensing applications of dual-comb spectrometers. The performance of the fully prototyped system shall be directly demonstrated in the second part of the proposed project by open-path environmental sensing. The findings of these experiments will be reported at international scientific conferences, open-access journals, and other publicly accessible sources such as our group website.

## Impact

The proposed tunable dual-comb spectrometer has the potential for a new cost-effective high-performance system that shall be specifically suited for large area environmental monitoring tasks. The dual-comb measurement is an inherently calibration free measurement that can benefit from the increased sensitivity and lower update rate compared to reported results in literature so far. On the long run such systems can improve the high-quality data situation for environmental monitoring, allowing for the development of advanced models and efficient measures for improved air quality and reduction of greenhouse gas emission.

The proposed system will not be restricted to environmental monitoring task but also open up dual-comb spectroscopy for a wider range of applications including exhaust monitoring under difficult conditions with high temporal variability, industrial process control and medical diagnostic via breath analysis for early detection of diseases. In industrial applications, the source can especially show its strength against narrowband QCL and ICL sources when a wide tunability is needed to switch regularly between different species to be monitored.

By mastering the optical design of such single-cavity dual-comb OPO systems, the proposed free-running system can be implemented with very low complexity, low cost and high performance. These features could allow for a wider adaptation of dual-comb spectroscopy by overcoming the high complexity and cost of current commercially available systems.

## References

1. World Bank, *The Global Health Cost of PM<sub>2.5</sub> Air Pollution: A Case for Action Beyond 2021* (World Bank, 2022).
2. J. Guo, D. Kubli, and P. Saner, "The economics of climate change: no action not an option," *Swiss Re Inst. Switz.* (2021).
3. D. Weidmann, "4 - Atmospheric trace gas measurements using laser heterodyne spectroscopy," in *Advances in Spectroscopic Monitoring of the Atmosphere*, W. Chen, D. S. Venables, and M. W. Sigrist, eds. (Elsevier, 2021), pp. 159–223.
4. M. Shahmohammadi, F. Kapsalidis, M. J. Süess, E. Gini, M. Beck, M. Hundt, B. Tuzson, L. Emmenegger, and J. Faist, "Multi-wavelength distributed feedback quantum cascade lasers for broadband trace gas spectroscopy," *Semicond. Sci. Technol.* **34**, 083001 (2019).
5. I. Coddington, N. Newbury, and W. Swann, "Dual-comb spectroscopy," *Optica* **3**, 414–426 (2016).
6. N. Hoghooghi, S. Xing, P. Chang, D. Lesko, A. Lind, G. Rieker, and S. Diddams, "Broadband 1-GHz mid-infrared frequency comb," *Light Sci. Appl.* **11**, 264 (2022).
7. E. M. Waxman, K. C. Cossel, G.-W. Truong, F. R. Giorgetta, W. C. Swann, S. Coburn, R. J. Wright, G. B. Rieker, I. Coddington, and N. R. Newbury, "Intercomparison of open-path trace gas measurements with two dual-frequency-comb spectrometers," *Atmospheric Meas. Tech.* **10**, 3295–3311 (2017).
8. G. B. Rieker, F. R. Giorgetta, W. C. Swann, J. Kofler, A. M. Zolot, L. C. Sinclair, E. Baumann, C. Cromer, G. Petron, C. Sweeney, P. P. Tans, I. Coddington, and N. R. Newbury, "Frequency-comb-based remote sensing of greenhouse gases over kilometer air paths," *Optica* **1**, 290–298 (2014).
9. E. M. Waxman, K. C. Cossel, F. Giorgetta, G.-W. Truong, W. C. Swann, I. Coddington, and N. R. Newbury, "Estimating vehicle carbon dioxide emissions from Boulder, Colorado, using horizontal path-integrated column measurements," *Atmospheric Chem. Phys.* **19**, 4177–4192 (2019).
10. S. Coburn, C. B. Alden, R. Wright, K. Cossel, E. Baumann, G.-W. Truong, F. Giorgetta, C. Sweeney, N. R. Newbury, K. Prasad, I. Coddington, and G. B. Rieker, "Regional trace-gas source attribution using a field-deployed dual frequency comb spectrometer," *Optica* **5**, 320–327 (2018).
11. D. I. Herman, C. Weerasekara, L. C. Hutcherson, F. R. Giorgetta, K. C. Cossel, E. M. Waxman, G. M. Colacion, N. R. Newbury, S. M. Welch, B. D. DePaola, I. Coddington, E. A. Santos, and B. R. Washburn, "Precise multispecies agricultural gas flux determined using broadband open-path dual-comb spectroscopy," *Sci. Adv.* **7**, eabe9765 (2021).
12. F. R. Giorgetta, J. Peischl, D. I. Herman, G. Ycas, I. Coddington, N. R. Newbury, and K. C. Cossel, "Open-Path Dual-Comb Spectroscopy for Multispecies Trace Gas Detection in the 4.5–5  $\mu\text{m}$  Spectral Region," *Laser Photonics Rev.* **15**, 2000583 (2021).
13. N. R. Newbury, I. Coddington, and W. Swann, "Sensitivity of coherent dual-comb spectroscopy," *Opt. Express* **18**, 7929 (2010).
14. J. Pupeikis, B. Willenberg, S. L. Camenzind, A. Benayad, P. Camy, C. R. Phillips, and U. Keller, "Spatially multiplexed single-cavity dual-comb laser," *Optica* **9**, 713–716 (2022).
15. B. Willenberg, J. Pupeikis, C. R. Phillips, and U. Keller, "SESAM-mode-locked gigahertz solid-state dual-comb oscillator with flexible repetition rate difference," in *Solid State Lasers XXXI: Technology and Devices* (SPIE, 2022), Vol. PC11980, p. PC1198008.
16. C. R. Phillips, J. Pupeikis, B. Willenberg, A. Nussbaum-Lapping, S. L. Camenzind, F. Callegari, A. Benayad, P. Camy, and U. Keller, "Dual-comb modelocked laser oscillators with high power and low noise," in *Europhoton 2022* (2022).
17. C. P. Bauer, J. Pupeikis, B. Willenberg, Z. A. Bejm, N. Pezzoli, C. R. Phillips, and U. Keller, "Spatially-multiplexed tunable dual-comb optical parametric oscillator at 250 MHz," in *Europhoton 2022* (2022).

## Project Proposal Optica Foundation 20th Anniversary Challenge

**Applicant: Dr. Carlos Doñate Buendía, University of Wuppertal, Germany**

**Category: Health**

**Anticipated total duration of the project: 24 months**

### **Stereolithography 3D printed bactericidal dental parts by laser generated $\text{Ag}_2\text{WO}_4$ nanoparticles additivation**

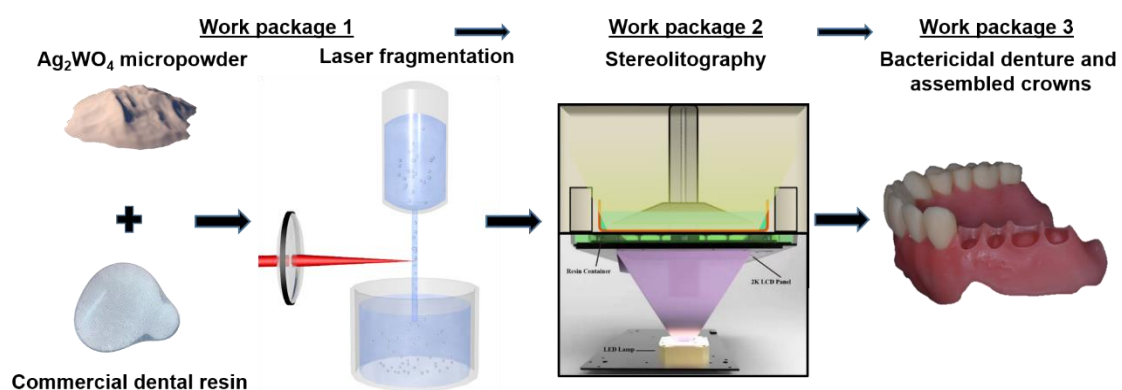
The proposed project addresses a fundamental problem in nowadays society, universal health access. Specifically, dental health costs limit its access to low-income population and countries, resulting in reduced well-being, sickness, and even death. Implants, crowns, and dentures costs still represent a barrier for their extended employment. One of the sources of the high costs comes from the necessity of fabricating custom dental prosthetics for each patient, not allowing serial production. To overcome this limit, a photonics-based 3D printing technique as stereolithography (SLA) is proposed to produce dentures and teeth crowns with complex custom geometries and low production costs.

Another problem linked to dental prosthetic is the proliferation of bacterias and the risk of infection. Dentures and crowns represent a reservoir of microorganisms that can derive into stomatitis or infections. In fact, 70% of dentures wearers suffer from denture stomatitis. To treat infection problematics, antibiotic protocols are developed. However, this solution is limited due to the emergence of antibiotic resistant superbugs. To address it, the employment of laser irradiated  $\text{Ag}_2\text{WO}_4$  particles exhibiting bactericidal properties is proposed.

Overall, in the current project a complete photonics based approach is proposed to produce dentures and crowns with bactericidal properties by the formulation and SLA printing of resins containing laser generated  $\text{Ag}_2\text{WO}_4$  particles with enhanced bactericidal properties.

The proposed methodology can be explained in three steps represented in the scheme below. First, the irradiation of  $\text{Ag}_2\text{WO}_4$  particles dispersed in two dental resins, a flexible one to produce dentures and a hard one to produce crowns. The irradiation is carried out by laser fragmentation in liquids (LFL), and it enhances the  $\text{Ag}_2\text{WO}_4$  bactericidal effects, as shown in preliminary work from the applicant. Then, the  $\text{Ag}_2\text{WO}_4$ -resin is employed for SLA after detailed characterization of the  $\text{Ag}_2\text{WO}_4$  particle stability in the resin, the viscosity and wettability. Finally, the produced dentures and crowns are characterized by tensile, hardness, bactericidal, and biocompatibility tests to evaluate their suitability for in-vivo applications.

The proposed approach aims to overcome the current main drawbacks of dental prosthetics. On the one side, high costs that difficult general population access to basic dental health treatments. On the other side, infection and bacteria proliferation and the subsequent loss of patient well-being and extra dental health treatment costs.



## **Project Proposal Optica Foundation 20th Anniversary Challenge**

**Applicant: Dr. Carlos Doñate Buendía, University of Wuppertal, Germany**

**Category: Health**

**Anticipated total duration of the project: 24 months**

### **Stereolithography 3D printed bactericidal dental parts by laser generated $\text{Ag}_2\text{WO}_4$ nanoparticles additivation**

#### **1 Literature Review and problem statement**

Oral diseases are considered by the World Health Organization (WHO) as a major health burden for many countries that affect people throughout their lifetime, causing pain, discomfort, disfigurement and even death [1]. Diseases as dental caries, periodontal, or dental trauma can lead to tooth loss or gums degradation, reducing the affected person wellbeing, and requiring the employment of prosthesis or implants. This worldwide problematic further affects low- and middle-income countries and society sectors [2] due to the costly access to dental care [3].

The impact of dental implants can be assessed in few numbers, its annual global market is estimated at around 12-18 million implants, with more than 200 million patients having received an implant in the last two decades [4]. However, implants, crowns, and dentures costs still represent a barrier for their extended employment in several countries and parts of society [3]. One of the sources of the high costs comes from the necessity of fabricating a custom implant for each patient, not allowing serial production. To overcome this limit, photonics-based 3D printing techniques have been employed to produce dentures and crowns for dental implants, achieving complex geometries and low-cost custom parts [5]. Within the broad spectrum of 3D printing techniques, stereolithography (SLA) provides key advantages for prosthetic manufacturing cost reduction. SLA is based on the photopolymerization of a liquid resin that turns into a solid under UV light illumination. The low energy photopolymerization threshold of the resins allows the employment of low cost UV sources such as LEDs. The light modulator used to spatially control the layer-by-layer photopolymerization of the resin can be a LCD display, reaching resolutions below 20  $\mu\text{m}$ . The employment of general consumer technology reduces the overall cost of standard SLA devices to hundreds of dollars. Besides, there already exist commercial dental resins suitable for denture base, crown, and dental implants surgical guides printing [6]. Overall SLA printing offers an excellent perspective to reduce production costs of dental parts, prospectively facilitating access to such essential goods to a broader worldwide population percentage.

Apart from the problem arising after implants surgery are the postoperative infections resulting in Peri-implantitis. It occurs in the 3% of the patients [7,8], which results in approximately 6 million people affected in the last two decades. Furthermore, the infection requires the implant removal and extra surgery in 65% of the cases [7]. Dentures and crowns also represent a reservoir of microorganisms that can derive into stomatitis. In fact, 70% of dentures wearers suffer from denture stomatitis [9]. To prevent infection problematics, antibiotic protocols are developed [8]. Nevertheless, this solution presents also limitations when the emergence of antibiotic resistant superbugs is considered. To address it, the employment of inorganic particles exhibiting bactericidal properties such as Ag or Cu has been proposed [10, p1]. However, when incorporated into crowns or dentures, the elemental metals can suffer from leaching, increasing their concentration in the media to toxicity levels where the health cells are affected [9]. To control the release of the bactericidal Ag, the employment of  $\text{Ag}_3\text{PO}_4$  is proposed, proving that the composite can be integrated in a scaffold providing bactericidal properties without cytotoxicity, and even allowing cell proliferation [11]. Hence, inorganic

particles have been shown effective as bactericidal agent in scaffolds [12]. However, the addition of bactericidal particles to SLA dental resins has been only recently tested for elemental metals, and oxides. Mostly focusing on the effect over the mechanical properties of the printed parts and not providing extra bactericidal properties [13]. Preliminary work from the applicant [p2,p3] confirmed that high intensity irradiation of  $\text{Ag}_2\text{WO}_4$  microparticles in air leads to the formation of Ag nanoparticles bonded to the original composite [14]. The Ag nanoparticles formed provide bactericidal, antifungal, and antitumor properties to the irradiated material, with specificity and biocompatibility with healthy human cells (BALB/3T3) [15]. Even SARS-CoV-2 deactivation has been demonstrated in a preliminary work from the applicant employing a laser irradiated chitosan/  $\text{Ag}_2\text{WO}_4$  composite [p2]. Consequently, laser irradiated  $\text{Ag}_2\text{WO}_4$  represents an interesting material to provide antiseptic properties to the dental resins employed in SLA for denture and crowns manufacturing.

Overall, a complete photonics based approach is proposed to produce dentures and crowns with bactericidal properties by the formulation and printing of new SLA resins containing laser generated  $\text{Ag}_2\text{WO}_4$ . This approach aims to overcome the current main drawbacks of dental parts. On the one side, high costs that difficult general population access to these dental health treatments. On the other side, infection and bacteria proliferation and the subsequent patient well-being and health treatment costs.

## 2 Objectives

The specific objectives are intended to provide broader worldwide access to dental parts by reducing production costs and to address human wellbeing and resources losses arising from bacteria development and infections in dentures and crowns. To achieve this, two main objectives are pursued within the current project:

- 1) **The production of bactericidal and biocompatible dentures and crowns** by the formulation of new  $\text{Ag}_2\text{WO}_4$ -resins printed by SLA.
- 2) **The adaptation of inorganic particle additivated resins as base materials in SLA**, allowing the production of **custom dentures and crowns with novel functionalities** at reduced costs, making them more accessible for low-income countries.

## 3 Work Plan

**Table 1.** Planned time flow for the work packages over the two-year project period.

Work packages	1st year				2nd year				
	Q1	Q2	Q3	Q4	Q1	Q2	Q3	Q4	
<b>WP1</b>	<b>Dental resin <math>\text{Ag}_2\text{WO}_4</math> additivation</b>								
WP 1.1: Laser fragmentation (LFL) of $\text{Ag}_2\text{WO}_4$ microparticles.	■				■				
WP 1.2: $\text{Ag}_2\text{WO}_4$ additivation of PMMA based dental resins.	■				■				
WP1.3: Optical and rheological characterization of additivated resins.			■			■			
<b>WP2</b>	<b>Stereolithography (SLA) 3D printing of additivated dental parts</b>								
WP 2.1: SLA printing of test samples for optimization and characterization.		■							
WP 2.2: SLA printing of additivated flexible dentures and dental crowns.			■						
<b>WP3</b>	<b>Bactericidal and mechanical characterization of the printed dental parts</b>								
WP 3.1: Hardness and tensile testing of the printed parts.			■					■	
WP 3.2: Antimicrobial and biocompatibility tests.			■				■		

The project is divided into 3 main work packages (WPs). The synergies and time flow are depicted in Table 1.

### **WP1 – Dental resin Ag<sub>2</sub>WO<sub>4</sub> additivation**

In WP1, a novel procedure to prepare Ag<sub>2</sub>WO<sub>4</sub> additivated dental resins will be studied. The process will be compared with direct mixing of the Ag<sub>2</sub>WO<sub>4</sub> micropowder with the SLA resins, and air irradiated Ag<sub>2</sub>WO<sub>4</sub> micropowder direct mixing with the SLA resins. This way the effect of direct laser fragmentation of Ag<sub>2</sub>WO<sub>4</sub> in the resin on the stability of the particles and their bactericidal performance will be highlighted.

#### **WP1.1 – Laser fragmentation (LFL) of Ag<sub>2</sub>WO<sub>4</sub> microparticles**

Direct addition of air irradiated Ag<sub>2</sub>WO<sub>4</sub> powders to the SLA resins could result in agglomeration of the material and sedimentation before printing. This would affect the homogeneous distribution of the particles in the printed part, generating local variations of the mechanical and bactericidal properties that can result in the fracture of the part or infection risk increase in specific areas. In order to avoid this problem, the novel procedure proposed in this project is based on the initial mixing of the Ag<sub>2</sub>WO<sub>4</sub> microparticles with the dental photopolymer resins employed, Fig. 1a. The mixture is ultrasonically dispersed, and irradiated in a liquid flow configuration, Fig. 1b. The irradiated particles with increased bactericidal properties will also gain stability in the resin due to the coverage of the particles' surface with the photopolymer functional groups. In order to avoid degradation of the resin during laser irradiation, the laser source employed will be a 1064 nm ps laser (4 MHz, 10 ps, 120 W). The resin, designed for printing at 405 nm, will consecutively be irradiated with an off-resonant wavelength far from its photopolymerization range.

#### **WP1.2 – Ag<sub>2</sub>WO<sub>4</sub> additivation of PMMA based dental resins**

The in-situ laser irradiated Ag<sub>2</sub>WO<sub>4</sub>-resins in WP1.1 will be compared in terms of particle stability, and viscosity (WP1.3), as well as mechanical, bactericidal, and biocompatibility properties (WP3), with **1) the base Ag<sub>2</sub>WO<sub>4</sub> added to the resins**, and **2) the Ag<sub>2</sub>WO<sub>4</sub> powder irradiated in air** (same laser parameters as in laser fragmentation) and mixed with the resins. Two different commercial dental resins will be employed in the project, since their base mechanical properties qualify each of them for the printing of flexible parts as dentures (DENTURE, Power Resins), or hard parts as crowns (TEMP, Power resins).

#### **WP1.3 – Optical and rheological characterization of additivated resins**

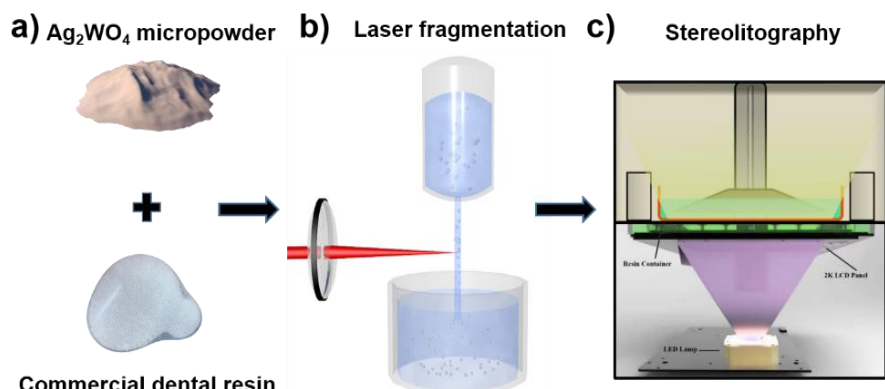
The effect of Ag<sub>2</sub>WO<sub>4</sub> particles addition to the resins will be evaluated by the influence on the resin optical and flow properties. The measurements described will be performed for the six Ag<sub>2</sub>WO<sub>4</sub>-resins prepared in WPs 1. 1) Flexible resin and base Ag<sub>2</sub>WO<sub>4</sub>; 2) Flexible resin and Ag<sub>2</sub>WO<sub>4</sub> irradiated in air; 3) LFL Flexible resin and Ag<sub>2</sub>WO<sub>4</sub>; 4) LFL hard resin and Ag<sub>2</sub>WO<sub>4</sub>; 5) Hard resin and base Ag<sub>2</sub>WO<sub>4</sub>; 6) Hard resin and Ag<sub>2</sub>WO<sub>4</sub> irradiated in air.

The optical properties will be characterized by UV-Vis spectrophotometry (StellarNet Inc.). The stability of the optical properties, absorption peaks wavelengths, and intensity provide information of the laser interaction effect over the resin and the dispersed Ag<sub>2</sub>WO<sub>4</sub> particles. The data collected will allow determining the mixing and laser irradiation methodology leading to the optimum dispersion of the Ag<sub>2</sub>WO<sub>4</sub> particles without resin degradation.

To evaluate the influence of the Ag<sub>2</sub>WO<sub>4</sub> particles and laser irradiation methodology on the flow properties of the resulting additivated resins, contact angle (sessile drop method) and viscosity measurements (rotational rheometry) will be conducted. These parameters are especially relevant for the processability of the resulting resins by SLA keeping the maximum spatial resolution and process reproducibility.

## WP2 – Stereolithography (SLA) 3D printing of additivated dental parts

Within this work package, the prepared  $\text{Ag}_2\text{WO}_4$  resins will be processed by SLA (Elegoo Mars 2) to produce test samples for characterization, WP 2.1. In WP 2.2, dentures and crowns from the  $\text{Ag}_2\text{WO}_4$ -resins will be produced with the optimum processing parameters, Fig. 1c.



**Figure 1.** a)  $\text{Ag}_2\text{WO}_4$  commercially available micropowder and dental resins mixed for laser irradiation in b). b) Laser fragmentation setup in a flow jet configuration to ensure uniform irradiation of the particles and promote a homogeneous bactericidal effect enhancement. c) Stereolithography (SLA)

Commercial dental resin

setup with a 405 nm LED and LCD employed to process the laser irradiated  $\text{Ag}_2\text{WO}_4$ -resins, bottom image reproduced from [16].

### WP 2.1: SLA printing of test samples for optimization and characterization

The influence of the 405 nm LED light employed in the SLA system on the  $\text{Ag}_2\text{WO}_4$ -resins will be evaluated in WP3.2 to confirm that bactericidal enhancement of the  $\text{Ag}_2\text{WO}_4$  particles can be achieved in-situ during SLA even if the material has not been previously irradiated. A strong synergy with WPs (WP 1.3 and WP3) will be required at this point to optimize the processing parameters and achieve simultaneously high printing spatial resolution, repeatability of the process, high mechanical properties of the printed part, and maximum bactericidal effect.

### WP 2.2: SLA printing of additivated flexible dentures and dental crowns

The flat geometries proposed in WP 2.1 will be replaced by the intended denture models for the additivated flexible resin, and the crown models for the additivated hard resin. Different complete and partial dentures and crowns will be printed to confirm the advantage that SLA provides for the production of custom parts with complex geometries.

### WP 3: Bactericidal and mechanical characterization of the printed dental parts

To quantify the effect of the  $\text{Ag}_2\text{WO}_4$  particles and the laser irradiation methodology over the performance of the printed dental parts, mechanical and bactericidal characterization of the printed objects is required.

#### WP 3.1: Hardness and tensile testing of the printed parts

Initially tensile test printed parts will be used for the characterization according to DIN 53504:2017-03, hardness tests will be performed according to DIN ISO 48-4:2021-02. The samples exhibiting a significant hardness or tensile stress values below the provider specified range will be discarded. The LFL processed samples are expected to exhibit the lower diminishing due to the size reduction of the  $\text{Ag}_2\text{WO}_4$  particles that will be better dispersed within the printed part contributing to a reduction of the part porosity and density increase.

#### WP 3.2: Antimicrobial and biocompatibility tests

The antimicrobial tests will be performed for *C. Albicans*, *E. Coli*, and MRSA, the most common bacteria present in dentures and crowns. Besides, to be able to prospectively qualify the produced parts for in-vivo employment, biocompatibility with the oral cells is required. Hence, alamarBlue™ assay and an MTT assay will be performed to ensure that the printed parts exhibit no toxicity that could damage the denture or crown host.

## Selected applicant's preliminary published work related to the project

[p1] **C. Doñate-Buendía**, A. Ingendoh-Tsakmakidis, ..., S. Barcikowski, B. Gökce, *Production of bactericidal powder suitable for Laser Powder Bed Fusion by silver nanoadditivation of polyamide*, Proc. CIRP 111 (2022).

[p2] P. Pereira, ..., **C. Doñate-Buendía**, G. Mínguez-Vega, J. Andrés, E. Longo, *Inactivation of SARS-CoV-2 by a chitosan/ $\alpha$ -Ag<sub>2</sub>WO<sub>4</sub> composite generated by femtosecond laser irradiation*, Sci. Rep. 12 (2022).

[p3] C. dos Santos, ..., **C. Doñate-Buendía**, J. Andres, E. Longo, *Proof-of-Concept Studies Directed toward the Formation of Metallic Ag Nanostructures from Ag<sub>3</sub>PO<sub>4</sub> Induced by Electron Beam and Femtosecond Laser*, Part. & Part. Syst. Char. 36 (2019).

## 4 Outcome and impact

The funds required to develop the project include the necessary Ag<sub>2</sub>WO<sub>4</sub> micropowders, the dental resins, and a SLA processing station including the washing and curing machines fully dedicated to the printing of dental resins (initially the available Elegoo Mars 2 will be employed). The UV-Vis, contact angle, viscosity, mechanical, bactericidal and biocompatibility tests can be performed with the already available devices in the group and close groups in the university of Wuppertal. The one year PhD student contract is envisioned to produce major evidences of the project outcomes, representing a fundamental advance in the applicant's current early career stage in order to start his independent career and apply for a 3year full-time proposal (in the scale of 400.000€) to the German Research Foundation (DFG) to continue the development of the topic and extend the PhD candidate position until graduation.

The expected outcomes of the project can be summed up as:

- 1) Qualification of the **laser fragmentation in liquid** approach for the **particle additivation of SLA resins** to provide them **bactericidal properties**.
- 2) Establishment of a photonics-driven printing protocol for the generation of **dentures and crowns with bactericidal properties and reduced cost**.

The project outcomes address a fundamental problem in nowadays society, universal health access. Specifically, dental health costs limit its access to low-income population and countries, resulting in reduced well-being, sickness, and even death. The photonics-driven qualification of lower cost approaches to generate dentures and teeth crowns offer a possibility to improve dental health for the general population. Furthermore, the bactericidal properties of the generated dentures and crowns further reduce health risks as infection, and bacteria proliferation. Representing a strong benefit for a situation that most of the population faces during their lives, the necessity of a dental replacement.

## 5 References

- [1] M.A. Peres, L.M.D. Macpherson, R.J. Weyant, et al., *Lancet*. 394 (2019) 249–260.
- [2] G.H. Gilbert, R. Paul duncan, B.J. Shelton, *Health Serv. Res.* 38 (2003) 1843–1862.
- [3] E. Bernabé, M. Masood, M. Vujcic, *BMC Public Health*. 17 (2017) 1–8.
- [4] B. Klinge, M. Lundström, M. Rosén, et al., *Clin. Oral Implants Res.* 29 (2018) 145–151.
- [5] L. Lin, Y. Fang, Y. Liao, et al., *Adv. Eng. Mater.* 21 (2019) 1801013.
- [6] A. Della Bona, V. Cantelli, V.T. Britto, et al., *Dent. Mater.* 37 (2021) 336–350.
- [7] O. Camps-Font, P. Martín-Fatás, A. Clé-Ovejero, et al., *J. Periodontol.* 89 (2018) 1165–1173.
- [8] R. Tabrizi, F. Mobin, M. Dehghanpour, et al., *J. Cranio-Maxillofacial Surg.* 50 (2022) 293–297.
- [9] P. Ramburrun, N.A. Pringle, A. Dube, et al., *Materials (Basel)*. 14 (2021) 3167.
- [10] M. Cao, S. Wang, J. Hu, et al., *Adv. Sci.* 9 (2022) 2103721.
- [11] K. Hayashi, M. Shimabukuro, K. Ishikawa, *ACS Appl. Mater. Interfaces*. 14 (2022) 3762–3772.
- [12] C. Zhao, W. Liu, M. Zhu, et al., *Bioact. Mater.* 18 (2022) 383–398.
- [13] M.M. Gad, A.M. Al-Thobity, *Jpn. Dent. Sci. Rev.* 57 (2021) 46–53.
- [14] N.G. Macedo, T.R. Machado, R.A. Roca, et al., *ACS Appl. Bio Mater.* 2 (2019) 824–837.
- [15] M. Assis, T. Robeldo, C.C. Foggi, et al., *Sci. Rep.* 9 (2019) 1–15.
- [16] A. Al Rashid, S.A. Khan, S. G. Al-Ghamdi, et al., *J. Mater. Res. Technol.* 14 (2021) 910–941.



# Hybrid Optoelectronic Memory for Dual Electronic and Photonic In-Memory Computing

PI: Carlos A. Rios Ocampo | University of Maryland College Park

## The Challenge (Category: Information)

In-memory computing has emerged as the optimum architecture for high-throughput matrix-vector multiplications. This approach breaks the processor-memory dichotomy in von Neumann computers by performing co-located computing and storage. In-memory computing on a photonic platform furthers the performance by enabling ultra-fast speeds and wavelength multiplexing, which has been demonstrated using optical pulses to write and perform scalar-scalar multiplications—work pioneered by the PI. However, this approach poses serious scalability challenges when considering architectures with thousands of memory elements due to the complexity of routing writing pulses on-chip. Optoelectronic memories that can be written electrically (i.e., leveraging standard electronic packaging) and read out optically are necessary to guarantee seamless scalability. However, such a memory remains a critical missing link. This proposal aims to fill this gap by creating an innovative optoelectronic memory based on photonic integrated circuits with embedded phase-change materials and a three-terminal electrical scheme. Furthermore, we aim to demonstrate the most versatile device that can be written and read with both optical and electrical signals. This way, we propose an in-memory computing paradigm that carries high-throughput parallel computation in both domains, thus avoiding electro-optical conversions, having continuous communication between parts, and mutually enhancing their performance. This proposal's scope matches OPTICA's interest in driving new scientific discoveries and breakthroughs to transform our world by enabling faster and more energy-efficient ways to compute large volumes of information.

## Overview and Objectives

The overall objective of this proposal is to develop a transformative hybrid optoelectronic memory (HOEM) based on phase-change materials (PCMs) for advanced photonic-electronic hardware accelerators. Our central hypothesis is that, unlike current PCM-based technology operating either optically or electrically, our HOEM will create innovative systems that integrate both into a single device, merging the best performance metrics from both domains. Photonic PCM architectures have advantages in bandwidth, throughput, heat dissipation, no drift, and multiplexing over their electronic counterpart. The latter benefits from mature, scalable CMOS fabrication and demonstrated memory architectures (exemplified by Micron/Intel's 3D Xpoint), enabling volume manufacturing and interfacing with ASIC logic units and DACs/ADCs – in-existent in the optical domain.

This project pursues a unique cross-disciplinary approach spanning optical material synthesis and processing, device design engineering, and scalable photonics manufacturing, which builds on our group's know-how and PI's accumulated experience in combinatorial PCM synthesis, photonic devices, foundry fabrication, and in-memory computing. The team will validate the central hypothesis by completing two main tasks: **1) optical materials innovation**: we hypothesize that Ge-Sb-Te PCMs alloyed with Sn, Ti, or Ag will achieve optimal optical and electrical performance. **2) device engineering, manufacturing, and testing**: we hypothesize that HOEM devices can be built using three electrical terminals on SOI waveguides with embedded PCMs for simultaneous optical and electrical signal processing. Developing a HOEM is the first step towards a long-term vision: a hybrid photonic-electronic in-memory computing processor.

## Expected outcomes

Our expectations for a one-year seed funding are ambitious, given our accumulated experience in this type of device and material. We anticipate: **1)** finding at least one optimum PCM alloy for simultaneous electrical and optical operation. **2)** demonstrate a high-yield device fabrication process for vertical vias in HOEM, including the crucial third electrode for electronic readout. **3)** experimentally demonstrate a HOEM using the alloy found in (1). We aim to achieve mixed-mode operation of the HOEM resulting from electrothermal Write and simultaneous optical and electrical read. **4)** demonstrate repeatable multilevel response in the optical domain, a crucial property for in-memory computing, and study the drift in both optical and electrical readout. Moreover, we expect insightful exchanges and fruitful collaborations from other scientists in the OPTICA network participating in the 20<sup>th</sup> Anniversary Challenge.

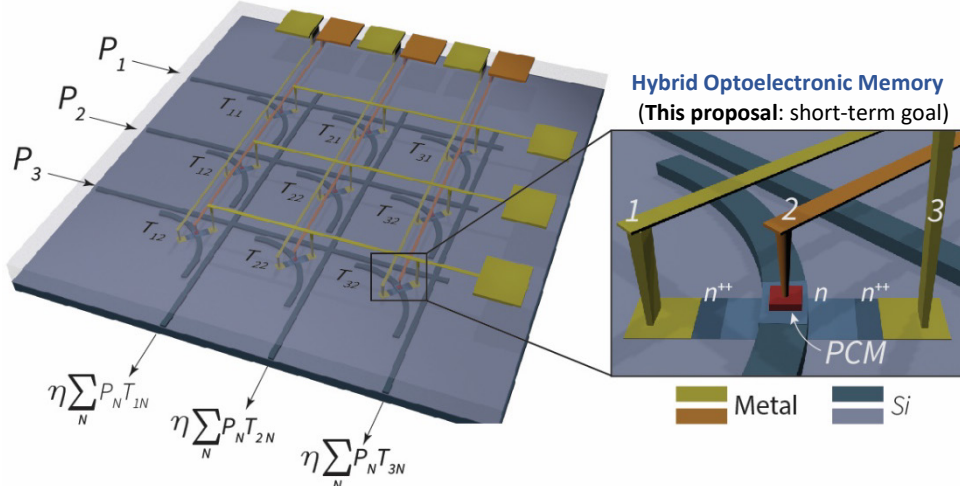
# Hybrid Optoelectronic Memory for Dual Electronic and Photonic In-Memory Computing

PI: Carlos A. Rios Ocampo | University of Maryland College Park

## Overview and Objectives

Today's prevailing von Neumann computing architecture is largely non-optimal when handling massive matrix-vector multiplications for machine learning.<sup>1</sup> This limitation has spurred tremendous efforts in developing advanced hardware accelerators capitalizing on the unique benefits of analog electronics<sup>2,3</sup> and optics<sup>4,5</sup> for ultrahigh-speed, low power consumption, and massive parallelism. In-memory computing has emerged as the most promising architecture for this task, given that it allows for performing scalar-scalar multiplications in a single time step and directly in the memory, i.e., breaking the processor and memory dichotomy and performing computing and storage in the same device.<sup>3</sup> Analog signals and multilevel memories are required to carry out such an efficient arithmetic operation—the scalars are mapped to the amplitude of an input optical/electrical signal and the amplitude-modulating multilevel memory. The signal at the output after simple propagation of an optical beam or an electrical current would then be equal to the product of both numbers. While several memristive platforms such as phase-change materials,<sup>6</sup> oxides,<sup>7</sup> and others have enabled analog electronic in-memory computing architectures, the optical counterpart is in its infancy. Photonic platforms for in-memory computing, although significantly less mature than the analog electronic version, allow for high-speed and multiplexing, which combined lead to unprecedented throughputs. This has been demonstrated with optically written and optically read phase-change materials on photonic integrated circuits.<sup>5,8</sup> However, optoelectronic memories that can be written electrically and read out optically are necessary to guarantee seamless scalability to architectures comprising hundreds or thousands of memories. Such a memory, especially if, in addition, offers simultaneous operation in both domains, remains a critical missing link. This is the challenge we aim to tackle in this project.

The *overall objective* of this proposal is to develop a transformative hybrid optoelectronic memory (HOEM) based on phase-change materials (PCMs) for advanced photonic-electronic hardware accelerators (**Fig. 1**). Our *central hypothesis* is that, unlike current PCM-based technology operating either optically or electrically, our device will create innovative systems that integrate both into a single device, merging the best performance metrics. Photonic PCM architectures have advantages in bandwidth, throughput, heat dissipation, no drift, and multiplexing over their electronic counterpart. The latter benefits from mature, scalable CMOS fabrication and demonstrated memory architectures (exemplified by Micron/Intel's 3D Xpoint<sup>9</sup>), enabling volume manufacturing and interfacing with ASIC logic units and DACs/ADCs – inexistent in the optical domain.



**Fig. 1.** Reconfigurable photonic matrix-vector multiplication and accumulation (MAC) processor based on HOEM. A nonvolatile matrix  $T_{MN}$  is codified in the PCM cells transmittance. An array of waveguide couplers is used to interconnect vertical and horizontal channels. Multiplication between the input pulses  $P_i$  takes place at each intersection. Each column waveguide collects the light from the multiplications. The result of each column is an entry for resulting vector. The PIC features doped-Si microheaters between the contacts 1 and 3. A PCM cell sits onto the waveguide and is connected to vias 2. The PCM can be switched using optical pulses, heating (1 & 3), or electrical pulses (2 & 3) and readout via optical transmission (waveguide) or conductivity (2 & 3) interrogation.

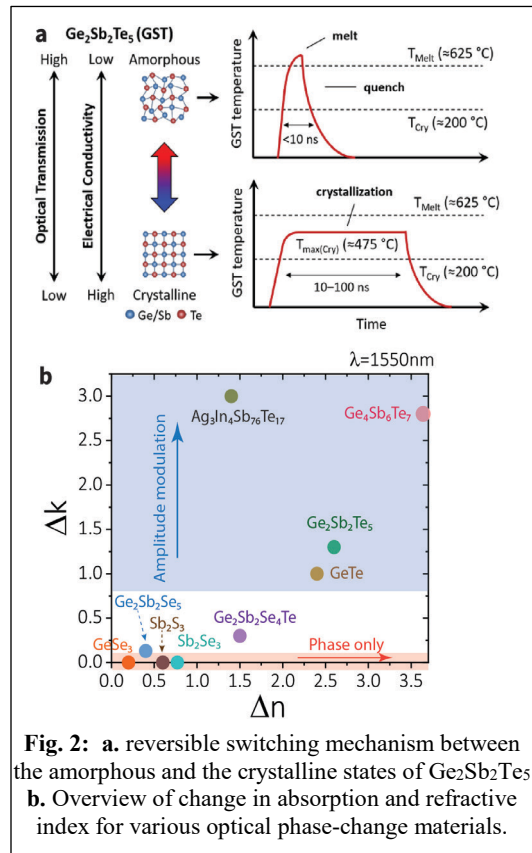
The proposed technology uses the remarkable bistable change in the optical and electrical properties of PCMs upon amorphization and crystallization, which enables nonvolatile reconfiguration of integrated electronic/photonic circuits. This material class succeeds as low-energy nonvolatile multilevel memories for on-chip photonic<sup>8</sup> and electronic<sup>6</sup> in-memory computing, demonstrating thus the fastest and most scalable way to perform matrix-vector multiplications. Moreover, the integration of PCMs with electronic ICs have been validated in Micron/Intel’s 3D Xpoint technology<sup>9</sup>. We will focus on identifying PCM compositions towards simultaneous electrical and optical properties optimization, the results of which then rationally guide combinatorial high-throughput material synthesis to expedite screening of new PCMs. On the device design front, we target silicon on Insulator (SOI) photonic integrated circuits (PIC) with doped-silicon microheaters, a PCM cell, and two metal layers with three vertical vias – all CMOS foundry processes.<sup>11,15</sup> The proposed architecture also closely parallels that of 3D Xpoint in the electronic domain and, therefore, can be scalable to large arrays with proven manufacturing and programming compatibility.

Developing a HOEM with seed funding is the first step towards a long-term vision: a photonic in-memory computing processor with dual optical and electrical readout, which we intend to pursue further through NSF funding. Moreover, this proposal’s scope perfectly matches OPTICA’s interest in driving new scientific discoveries and breakthroughs to transform our world in the information space by enabling faster and energy-efficient ways to compute large volumes of information.

### Work Plan

The project will support Ms. Chuanyu Lian, a PhD student in the PI’s group, to explore the transformative HOEM, leveraging our current efforts toward electrothermal control of PCMs on photonic integrated circuits. The two main thrusts areas that we will pursue in parallel during the first year of seed funding are 1) materials innovation: we will seek the best PCM with optimized optical and electrical performance, and 2) device engineering, manufacturing, and testing: we will fabricate devices based on vertical electrical vias for the three contacts (**Fig. 1**). The funding will be critical to supporting and enabling on-campus fabrication and characterization efforts while prototyping devices for future foundry tape out.

**Task 1: Optoelectronic material innovation:** Using phase-change chalcogenides (i.e.,  $\text{Ge}_2\text{Sb}_2\text{Te}_5$ ,  $\text{Sb}_2\text{Se}_3$ , etc.) to control optical properties on-chip is a particularly intriguing solution for photonic device tunability due to significant, reversible, and nonvolatile changes in refractive index and electrical conductivity when switched between their amorphous and crystalline states (**Fig. 2a**).<sup>10</sup> The large change in refractive index ( $\Delta n = n_{\text{cry}} - n_{\text{am}}$ ) significantly reduces the interaction length needed to achieve a  $\pi$ -phase shift, and thus reduces the device footprint by  $>10\times$  (e.g., a device length of  $\leq 10 \mu\text{m}$  for non-resonant  $\text{Sb}_2\text{Se}_3$  phase shifters demonstrated by the PI<sup>11</sup>). In addition, a large extinction coefficient ( $\Delta k = k_{\text{cry}} - k_{\text{am}}$ ) increases the amplitude modulation upon switching, which can be used to codify multiple transmission levels for data storage and computing, as demonstrated by the PI in the field’s pioneering work.<sup>5,8,12</sup> The optimization of either  $\Delta n$  or  $\Delta k$  leads to different photonic devices and applications, and with a growing library of optical PCMs, there are materials available for both phase and amplitude modulation (see **Fig. b**). In particular, the alloy  $\text{Ge}_4\text{Sb}_6\text{Te}_7$  with outstanding  $\Delta k$  and  $\Delta n$  was discovered at PI’s collaborator Prof. Ichiro Takeuchi’s group at UMD using machine learning in



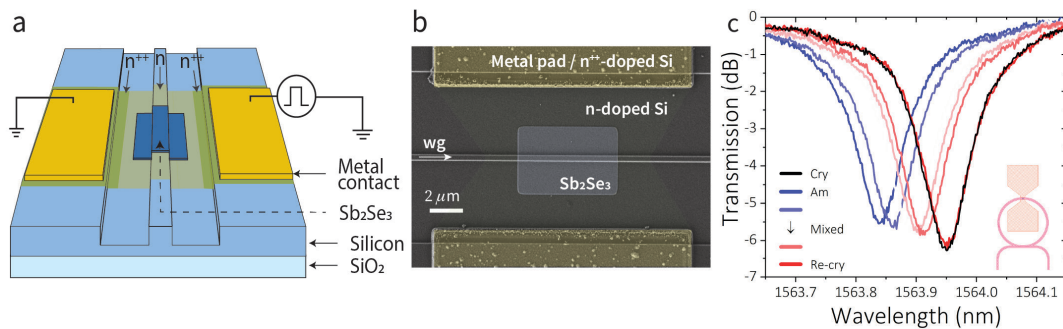
**Fig. 2:** a. reversible switching mechanism between the amorphous and the crystalline states of  $\text{Ge}_2\text{Sb}_2\text{Te}_5$  b. Overview of change in absorption and refractive index for various optical phase-change materials.

combinatorial material discovery techniques.<sup>13</sup> Another alloy of interest is  $\text{Ge}_2\text{Sb}_2\text{Se}_4\text{Te}_1$  or GSST, which offers broadband bi-state transparency.<sup>14</sup> This alloy was accomplished by the PI and colleagues at MIT through judicious engineering of the alloy’s resonant bonding configuration (to maximize optical contrast) as well as carrier localization (to suppress free-carrier absorption). Regarding electrical properties modulation, the community has focused on optimizing the contrast in resistivity: up to five orders of magnitude difference is achieved between insulating amorphous and conductive crystalline states.<sup>14</sup> However, achieving multilevel behavior has proved challenging. The resistivity of PCMs drifts in time, thus losing the stored information. Also, the switching mechanism in the electrical domain relies on a stochastic process that prevents the multilevel repeatability required in precise data storage – a task outstandingly done in the optical domain due to the stability of the refractive index.

The nonvolatility of PCMs also allows long-term reconfigurability and data storage (>10 years at 85 °C) without needing a continuous electric field or current. Additionally, these PCMs are glassy materials, making them substrate-blind. This provides a direct method to add optical tunability to photonic platforms other than silicon. The nature of these materials also opens many opportunities to engineer their physical properties by varying the atomic composition from a wide variety of possible elements. In this direction, finding a PCM simultaneously claiming significant optical and electrical contrast, fast switching kinetics, and large endurance is central to the project’s success.

We will leverage our GSST and  $\text{Ge}_4\text{Sb}_6\text{Te}_7$  success paradigms combining Machine Learning-enhanced material screening and high-throughput material characterization to facilitate rapid discovery and validation of new optoelectronic PCMs. We will capitalize on a wafer-scale platform we have recently pioneered, which is designed for combinatorial PCM synthesis and integrates device arrays encompassing waveguides, micro-heaters, and electrical probes for automated optical/thermal/electrical PCM characterizations. Since in-memory computing requires amplitude modulation, we will seek to optimize the  $\Delta k$  further. However, our HOEM also requires simultaneous electrical conductivity optimization, a multi-parameter optimization with no precedent. To do so, we will explore the combinatorial space of Ge-Sb-Se-Te alloys and metal-doped variations such as Sn/Ti/Ag-Ge-Sb-Te to enhance the electrical conductivity further while preserving a large optical modulation. With progress in device manufacturing, we will test the best alloys’ performance at attaining multilevel data in both domains.

**Task 2: Device engineering, manufacturing, and testing:** Through four years of extensive R&D collaborations with MIT Lincoln Laboratory (LL) as a postdoctoral associate at MIT, the PI successfully integrated PCMs as part of the standard LL’s Si photonics foundry process.<sup>11,15</sup> This important milestone means we can now manufacture PCM devices while enabling their seamless integration with mature Si photonic and electronic circuit components. We will leverage this unique capability, and our previous demonstrated electrothermal device in Fig. 3<sup>11</sup> to fabricate the proposed HOEM using UMD’s NanoCenter facilities. With devices shown in Fig. 3b as starting point (which already places us in an advantageous position), we propose fabricating the three metal terminals (see Fig. 4) following a deposition, lithography, etching, and electro-plating sequence. This process, however, comes with several challenges to be

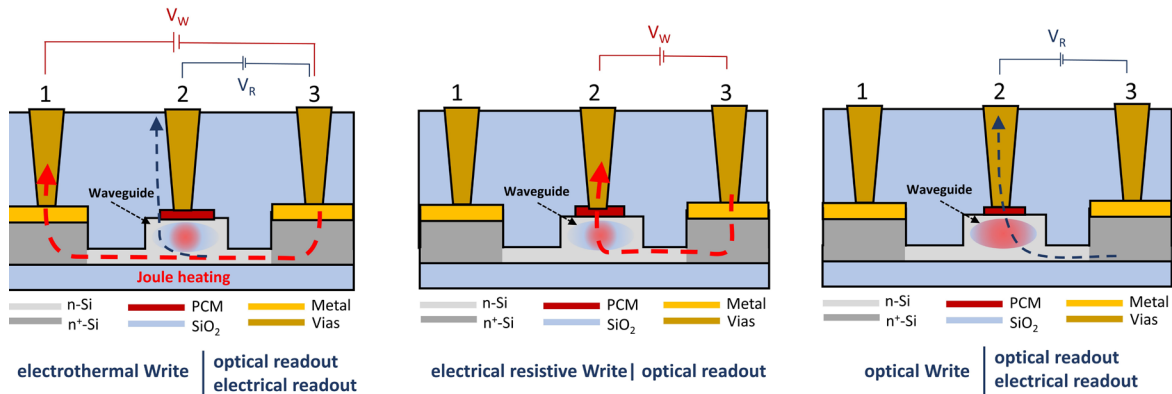


**Fig. 3:** **a** 3D sketched waveguide-integrated electrical heater used to switch  $\text{Sb}_2\text{Se}_3$  – this device is equivalent to that in Fig. 1, except for electrical terminal 2. **b** Colored SEM image of the actual device’ top view. **c** Experimental demonstration of  $\text{Sb}_2\text{Se}_3$  reversible switching in a ring resonator for optical readout with electrical switching.



addressed: 1) the contact area between the metal via and PCM needs to be carefully designed to display electrical conductivity with high SNR, yet low optical insertion loss – the larger the contact area, the more metal absorbs light from the waveguide. 2) Pattern a via terminal on top of the PCM cell without causing damage. 3) Optimum thickness of PCM capable of inducing high SNR measurement outputs in both the optical and electrical readouts. We will address these questions and design challenges using finite-element method (COMSOL) and finite differences in time domain (Lumerical) software. The result of the simulations will provide valuable information on the devices’ thermal, electrical, and optical properties and inform their fabrication.

We will use the PI’s customized automated electro-optical probe station to perform the on-chip photonic testing of our HOEMs. To control nonvolatile memory elements in the devices shown in **Fig. 3**, short pulses with high amplitude (e.g., 400 ns at 21V) were used to increase the heater’s temperature and melt-quench the PCM deposited onto the waveguide. A longer low amplitude (e.g., 0.1–1 ms at 3.2V) voltage pulse returns the PCM to its crystalline state to complete the reversible switching – see temperature evolution in **Fig. 2a**.<sup>11</sup> In this manner, high-contrast changes to the optical transmission can be achieved with electrothermal control of the PCM. Additional to this electrothermal write and optical-read measurement, we will pioneer a HOEM in which we also obtain electrical readout from contact 2 to verify the state of the PCM memory (**Fig. 4**). We expect high conductivity if the PCM is crystalline, unlike the insulating amorphous state. The electrical readout would enable us to interface the hybrid memory with external electronics (e.g., DAC, ADC, ASICs, etc.) and provide feedback to the system. A clear example of the potential of an electrical read is to measure the weight of each memory cell in real-time for processing in the digital domain, an otherwise difficult task since individual memory information is lost during accumulation. The electrical readout also avoids losing energy to an electro-optical conversion since we will not need photodetectors to convert from the analog optical to the electronic digital domain. Moreover, electrode 2 can induce filamentation through the PCM following a pulse excitation to either electrode 1 or 3, thus enabling electrical Write. A final degree of freedom is optical Write: use a strong optical pulse to switch a lossy (large  $\Delta k$ ) PCM, while having both electrical and optical readout. The unprecedented versatility of our HOEM will open avenues for inter-domain computing, where the choice of Write and Read operations will ultimately be determined by the nature of the application.



**Fig. 4:** Write and read possibilities with our Hybrid Optoelectronic Memory.  $V_w$  and  $V_r$  stand for voltage pulses to write and read, respectively, where  $V_w > V_r$ . Dashed lines represent electrical current. 1, 2, 3 denote the three vias. For optical write (right), a pump-probe scheme is necessary. A strong optical pump switches using the heat that results from material absorption and a subsequent lower power pulse reads out the state.<sup>12</sup>

### Expected outcomes

Our expectations for a one-year seed funding are ambitious, given our accumulated experience in this type of device. We anticipate:

1. finding at least one optimum PCM alloy for simultaneous electrical and optical operation.
2. demonstrate a high-yield device fabrication process for vertical via 2 (see Fig. 2) in HOEM, the crucial third electrode for electronic readout and biggest challenge.

3. experimentally demonstrate a functional HOEM using the alloy found in (1). As first step, we aim to achieve mixed-mode operation resulting from electrothermal Write and simultaneous optical and electrical read.
4. demonstrate repeatable multilevel response in the optical domain, a crucial property for in-memory computing, and study the drift in both optical and electrical readout.

Moreover, we expect insightful exchanges and fruitful collaborations from other scientists in the OPTICA network participating in the 20<sup>th</sup> Anniversary Challenge symposia.

### Impact

This project pursues a unique cross-disciplinary approach spanning optical material synthesis and processing, device design engineering, system architecture innovation, and scalable photonics manufacturing. Unlike existing PCM memories, our HOEM design allows cell programming and readout using both electrical and optical channels, which will boost the performance of the current in-memory processors by providing: **1)** active reconfiguration of the matrix using an optical or electrical signal to provide closed-loop control, which has been predicted to enable the array to perform arbitrary linear operations; **2)** enhanced optical matrix-vector computing by co-integrating with other ASIC carrying out operations, in parallel, that are not available in photonic circuitry such as nonlinear functions, logic, and DAC/ADC; **3)** use of electrical conductivity of the PCM matrix to retrieve the optical baseline and thus speed up the postprocessing and improve the precision of matrix-vector calculations<sup>8</sup>, and **4)** a scalable platform for a large volume of computing operations. Therefore, our approach adds unprecedented versatility to optoelectronic in-memory computing architectures for high-throughput data processing, thus enabling faster and more energy-efficient ways to compute large volumes of information. Furthermore, PCMs are a versatile family of materials enabling multiple technological innovations; these hybrid devices will find applications beyond computing, such as optical switching fabrics for data centers and reconfigurable optics for imaging<sup>16</sup> – areas in which the PI actively conducts research.

### References

1. Berggren, K. *et al.* Roadmap on emerging hardware and technology for machine learning. *Nanotechnology* **32**, 012002 (2020).
2. Traversa, F. L. & di Ventra, M. Universal Memcomputing Machines. *IEEE Trans Neural Netw Learn Syst* **26**, 2702–2715 (2015).
3. Sebastian, A., le Gallo, M., Khaddam-Aljameh, R. & Eleftheriou, E. Memory devices and applications for in-memory computing. *Nature Nanotechnology* **15**, 529–544 (2020)
4. Shen, Y. *et al.* Deep learning with coherent nanophotonic circuits. *Nat Photonics* **11**, 441–446 (2017).
5. Feldmann, J. *et al.* Parallel conv. processing using an integrated photonic tensor core. *Nature* **589**, 52–58 (2021).
6. le Gallo, M. *et al.* Mixed-precision in-memory computing. *Nat Electron* **1**, 246–253 (2018).
7. Li Jiancong and Li, Y. and Y. L. and M. X. Memristor-Based In-Memory Computing Architecture for Scientific Computing. in *Memristor Computing Systems* (ed. Chua Leon O. and Tetzlaff, R. and S. A.) 141–165 (Springer International Publishing, 2022)..
8. Ríos, C. *et al.* In-memory computing on a photonic platform. *Sci Adv* **5**, eaau5759 (2019).
9. Zhang, W., Mazzarello, R., Wuttig, M. & Ma, E. Designing crystallization in phase-change materials for universal memory and neuro-inspired computing. *Nat Rev Mater* **4**, 150–168 (2019).
10. Wuttig, M., Bhaskaran, H. & Taubner, T. Phase-change materials for non-volatile photonic applications. *Nat Photonics* **11**, 465–476 (2017).
11. Ríos, C. *et al.* Ultra-compact nonvolatile photonics based on electrically reprogrammable transparent phase change materials. *arXiv:2105.06010* (2021).
12. Ríos, C. *et al.* Integrated all-photonic non-volatile multi-level memory. *Nat Photonics* **9**, 725–732 (2015).
13. Kusne, A. G. *et al.* On-the-fly closed-loop materials discovery via Bayesian learning. *Nat Commun* **11**, (2020).
14. Zhang, Y. *et al.* Broadband transparent optical phase change materials for high-performance nonvolatile photonics. *Nat Commun* **10**, 2–3 (2019).
15. Hu, J. *et al.* Optical Devices with Phase-Change Materials. US Patent App. 17/183,267 (2021).
16. Zhang, Y. *et al.* Electrically reconfigurable non-volatile metasurface using low-loss optical phase-change material. *Nat Nanotechnol* **16**, 661–666 (2021).

Digital Holographic Microscopy (DHM) is a potential candidate to diagnose malaria without prior staining of the blood sample, thanks to its essential feature of visualizing and quantifying transparent samples. As a result, numerous applications of DHM in medicine and biology have been reported. One of the DHM versions, Digital lensless Holographic Microscopy (DLHM), is the simplest imaging method to recover information from microscopic samples. DLHM is instrumental in the point of care malaria diagnosis considering its portability-oriented developments. This technique allows the numerical retrieval of the complete optical complex wavefield scattered by the specimens, thus providing numerical refocusing of individual objects and phase information of transparent sample, as required in the malaria diagnosis scenario established before.

As with any other digital holography implementation, DLHM is a two-step technique: holograms of the studied sample are recorded in a digital camera, and further numerical processing allows the retrieval of its information in a plan-by-plane fashion. A simple instrument comprising a digital sensor and an illumination point source is required in the recording stage— notwithstanding its simplicity, significant efforts to enhance the technology in various aspects are continuously reported. Nevertheless, the implementation of portable devices with polarization sensitivity is required to extend the use of this imaging technique in point-of-care malaria diagnosis. Regarding portability, the main challenge is the development of new light sources that fulfill the requirements of DLHM but are cost-effective and mechanically stable. As for the polarization sensitivity of the technique, the challenge is to avoid using bulky setups that require computationally intensive reconstruction methods. In the literature can be found different proposals addressing the latter challenges, however, in practice, all these proposals are cumbersome, expensive, challenging to align, difficult to manufacture, or mechanically unstable. To solve these disadvantages, we have proposed a holographic point source to provide high spatial coherent illumination sources for DLHM without using micrometer pinholes. Moreover, we have reported the insertion of two linear polarizers in the typical DLHM system (LD-DLHM) to enhance disease diagnosis by quantifying the linear diattenuation response of the samples. As a result of our contributions, we have opened the path to portable devices without using bulky setups at a reduced cost and with high optical efficiency that also allows quantifying the polarization response of the studied samples. Nevertheless, in this proposal, we aim to develop specialized point of care platforms for the accurate in-situ diagnosis of the disease and its study. To do this, we propose three developments.

- (1) A mechanically stable, low-cost point source DLHM illumination with high spatial coherence using only off-the-shelf elements.
- (2) A full Muller-matrix polarization-sensitive DLHM system with a reduced number of polarizing elements and simple numerical processing that runs in affordable embedded computer systems.
- (3) A miniaturized DLHM 3D printing-based device comprising the first two developments.



**Name of Challenge Project:** Enhancing point of care malaria diagnosis with lensless holographic microscopy in Colombia.

## Literature Review

Early diagnosis and effective treatment are the basis for reducing malaria morbidity and mortality. Accurate quantification of parasitemia before antimalarial treatment allows the development of resistance by the parasite. Brightfield microscopy (BM) is a technique that allows direct visualization of *Plasmodium*, the malaria parasite. Thus, it is the most commonly used tool to diagnose and study the disease and to research antimalarial therapeutic efficacy. This is because BM is the only technique that allows recording the kinetics of the Plasmodium removal[1]. Despite these advantages, the sustainability of microscopy services is a challenge for most health systems in endemic areas, as they are usually regions with limited economic resources and qualified personnel. Other microscopy techniques, such as fluorescence microscopy[2], confocal[3], and phase contrast[4], have been used in the detection of *P. falciparum*; nonetheless, BM is the most affordable and relatively easy to use.

In the case of malaria diagnosis with BM, recognized as the "Gold Standard" [27], a blood sample, either in a thin spread or thick drop, is studied employing a microscope equipped with a 100X oil immersion objective. The sample, which has to be previously stained [30-34], is analyzed by a highly-trained microscopist to assess the various types of malaria and visually quantify its parasitemia[1]. Since BM is implemented in medium-complexity health centers, and the reagents required to perform the staining are limited, the possibility of achieving the diagnosis using the Gold Standard method is affected due to its costs and lack of portability. The latter is the case in some regions of our country. In addition to the difficulties associated with malaria diagnosis, the technical limitations of blood sample staining in any of its available methods[5] deserve special mention. Despite the relatively low cost, and high sensitivity and specificity, staining procedures require: (i) the use of highly contaminating reagents, (ii) personnel trained, and (iii) it can take up to 45 minutes to have the sample available for testing. Additionally, inadequate sample preparation facilitates the presence of fungi, artifacts, dye residues, dirt, and cell debris that can lead to a false-positive diagnosis. All the latter limitations invite the development of alternative diagnostic methodologies that eliminate the staining step of the blood sample.

To improve the accuracy of the diagnosis of this disease in unstained samples and to contribute with low-cost technology and simplicity of operation, there are several reports in the literature about the use of Digital Holographic microscopy (DHM) for Plasmodium detection[6,7]. Those supported by off-axis DHM architectures[8] provide information with high sensitivity; however, depending on their implementation, the development of portable and low-cost systems is limited.

Using the lensless DHM (DLHM) techniques, low-cost systems have been developed to inspect biological samples[9]. Different systems focused on the visualization of this type of sample have been reported previously[6]. In this proposal, the sample, placed directly on the digital sensor, is illuminated by a set of 23 point sources produced by 23 optical fibers. In relation to DLHM, this configuration has the advantage of providing a larger field of view and the disadvantages of requiring multiple point sources and a higher computational load. Its portability should be noted since it weighs only 95 grams; however, there is no exact

information on its cost, although according to the incorporated technology, it can be estimated to cost around USD 1000 per unit, which is a limiting factor for its implementation in some endemic zones. Although the detection of Plasmodium is provided by this method, (i) the microscope operates on samples stained by the Giemsa method, (ii) the sensitivity of the method is not reported, and (iii) the possibility of detection of mixed malaria is not explored. In summary, despite the advances reported in the literature on DHM-based Plasmodium detection, the state-of-the-art solution does not meet all the characteristics required for the specific problem in some regions of our country. Therefore, the accurate diagnosis of malaria with unstained blood samples is still open for research aiming at employing low-cost platforms supported by digital holographic microscopes with high sensitivity and usability as point of care diagnostic tools for this disease.

### **Problem Statement/Objective**

Digital Holographic Microscopy (DHM) is a potential candidate to diagnose malaria without prior staining of the blood sample, thanks to its essential feature of visualizing and quantifying transparent samples. As a result, numerous applications of DHM in medicine and biology have been reported[10][11,12][13]. One of the DHM versions, Digital lensless Holographic Microscopy (DLHM), is the simplest imaging method to recover information from microscopic samples[14–16]. DLHM is instrumental in the point of care malaria diagnosis considering its portability-oriented developments[17]. This technique allows the numerical retrieval of the complete optical complex wavefield scattered by the specimens, thus providing numerical refocusing of individual objects[18] and phase information of transparent samples[19], as required in the malaria diagnosis scenario established before.

As with any other digital holography implementation, DLHM is a two-step technique: holograms of the studied sample are recorded in a digital camera, and further numerical processing allows the retrieval of its information in a plan-by-plane fashion[20]. A simple instrument comprising a digital sensor and an illumination point source is required in the recording stage—notwithstanding its simplicity, significant efforts to enhance the technology in various aspects are continuously reported[7]. Nevertheless, the implementation of portable devices with polarization sensitivity is required to extend the use of this imaging technique in point-of-care malaria diagnosis. Regarding portability, the main challenge is the development of new light sources that fulfill the requirements of DLHM but are cost-effective and mechanically stable[21]. As for the polarization sensitivity of the technique, the challenge is to avoid using bulky setups that require computationally intensive reconstruction methods[22]. In the literature can be found different proposals addressing the latter challenges[23,24], however, in practice, all these proposals are cumbersome, expensive, challenging to align, difficult to manufacture, or mechanically unstable. To solve these disadvantages, we have proposed a holographic point source[25] to provide high spatial coherent illumination sources for DLHM without using micrometer pinholes. Moreover, we have reported the insertion of two linear polarizers in the typical DLHM system (LD-DLHM)[26] to enhance disease diagnosis by quantifying the linear diattenuation response of the samples. As a result of our contributions, we have opened the path to portable devices without using bulky setups at a reduced cost and with high optical efficiency that also allows quantifying the polarization response of the studied samples. Nevertheless, in this proposal, we aim to develop specialized point of care platforms for the accurate in-situ diagnosis of the disease and its study. To do this, we propose three developments.

- (1) A mechanically stable, low-cost point source DLHM illumination with high spatial coherence using only off-the-shelf elements.
- (2) A full Muller-matrix polarization-sensitive DLHM system with a reduced number of polarizing elements and simple numerical processing that runs in affordable embedded computer systems.
- (3) A miniaturized DLHM 3D printing-based device comprising the first two developments.

### Outline of tasks/Work Plan

The project is divided into four stages. For each stage, the activities, the required time, and the personnel in charge are reported.

- 1) Hardware implementation (first part).
  - a. In this first stage, we will perform the optical design of the full polarization-sensitive DLHM system and its experimental implementation in the laboratory[26]. To guarantee its proper functioning, known polarizing elements will be inserted into the system, and their known full-matrix parameters will be contrasted against the theoretical expectation. **(Months: 0-6). Physics engineer 1 + Professional with a master's degree in optics + Principal Investigator.**
  - b. Concurrently, we will develop holographic point sources with optimized optical diffraction efficiency to guarantee state-of-the-art imaging performance ( $<1\mu\text{m}$  lateral resolution,  $\lambda/10$  phase sensitivity)[25]. **(Month: 0-6). Physics engineer 2 + Professional with a master's degree in optics + Principal Investigator.**
- 2) Software implementation.
  - a. We will develop computationally simple numerical propagators to reconstruct the register DLHM holograms in affordable low-cost embedded systems[27]. These propagators will be implemented using computationally optimized versions of the already reported scalar diffraction-based well-known versions. **(Months: 6-11). Physics engineer 3 + Professional with a master's degree in computational science + Principal Investigator.**
  - b. Also, we will train learning-based methods for the pure end-to-end reconstruction of phase maps using datasets of images acquired with the instruments implemented in the project's first stage[28]. **(Months: 6-11). Physics engineer 4 + Professional with a master's degree in computational science + Principal Investigator.**
- 3) Hardware implementation (second part).
  - a. We will develop a miniaturized version of a DLHM platform[29] using dedicated CAD software, including polarization-sensitive elements[26] and the engineered illumination point source[30]. This platform will be enhanced up to the point where a  $10\text{cm}\times 10\text{cm}\times 10\text{cm}$  imaging device is attained. **(Months: 12-18). Physics engineer 1 + Physics engineer 2 + Principal Investigator.**
- 4) Validation with a medical expert.
  - a. Quality control will be carried out by a professional with expertise in malaria diagnosis to validate the platform and guarantee the reproducibility of its

measurements. The expert will make blind readings of the density and stages of the samples. The performance of the platform will be validated by considering the evaluations of the samples by two additional experts, via a concordance analysis. This procedure will be executed at the Malaria laboratory of the University of Antioquia in Medellin – Colombia (School of Medicine), which is regulated by the national guidelines for this purpose. **(Months: 16-24). Malaria Diagnosis experts (3)+ Principal Investigator.**

### **Outcome(s)**

- An affordable platform for the point of care diagnosis of malaria especially suited for its use in endemic zones of Colombia.
- Three (3) Q1 manuscripts accepted for publication (or published) in Optica open-access journals.
- Three (3) Q2 manuscripts accepted for publication (or published) in Optica open-access journals.
- Four (4) contributions to report project progress and results in Optica-organized symposiums.

### **Impact**

#### ***Short term***

- 1) Development of low-cost and simple-to-operate platforms for accurate and precise malaria diagnosis.
- 2) Specialized and high-level human capital training to carry out research and technological developments that improve the quality of life of the Colombian population.
- 3) Improvement of the installed capacities in the research infrastructure of the Universidad EAFIT

The contributions that will be developed in the project for the diagnosis of malaria and the corroboration of its performance will impact the national, institutional, and regional academic community. The latter by providing an innovative strategy for diagnosing malaria that could be applied as a model for manufacturing other platforms for use in fields such as medicine or industry. In addition, it will allow the region (Medellin, Colombia) to be at the level of the world's major innovation centers.

#### ***Long term***

The availability in malaria-endemic areas of the developments in this project will positively impact the quality of life of the people in these regions, reducing malaria morbidity and mortality and the associated costs.

### **References**

1. World Health Organization, 2nd ed. (World Health Organization, 2016).
2. C. J. Janse and P. H. Van Vianen, in *Flow Cytometry*, Z. Darzynkiewicz, J. P. Robinson,

- and H. A. B. T.-M. in C. B. Crissman, eds. (Academic Press, 1994), **42**, pp. 295–318.
3. A. Aroonsri, N. Posayapisit, J. Kongsee, O. Siripan, D. Vitsupakorn, S. Utaida, C. Uthaipibull, S. Kamchonwongpaisan, and P. J. Shaw, *PeerJ* **7**, e6713 (2019).
  4. C. Li, S. Chen, M. Klemba, and Y. Zhu, *J. Biomed. Opt.* **21**, 90501 (2016).
  5. B. K. Wilson, M. R. Behrend, M. P. Horning, and M. C. Hegg, *Opt. Express* **19**, 12190 (2011).
  6. S. Seo, T.-W. Su, D. K. Tseng, A. Erlinger, and A. Ozcan, *Lab Chip* **9**, 777 (2009).
  7. O. Mudanyali, D. Tseng, C. Oh, S. O. Isikman, I. Sencan, W. Bishara, C. Oztoprak, S. Seo, B. Khademhosseini, and A. Ozcan, *Lab Chip* **10**, 1417 (2010).
  8. A. Anand, V. K. Chhaniwal, N. R. Patel, and B. Javidi, *IEEE Photonics J.* **4**, 1456 (2012).
  9. C. A. Trujillo and J. Garcia-Sucerquia, *Opt. Lett.* Vol. 39, Issue 9, pp. 2569–2572 **39**, 2569 (2014).
  10. W. Xu, M. H. Jericho, I. A. Meinertzhagen, and H. J. Kreuzer, *Proc. Natl. Acad. Sci. U. S. A.* **98**, 11301 (2001).
  11. B. Sunarko, Djuniadi, M. Bottema, N. Iksan, K. A. N. Hudaya, and M. S. Hanif, in *Journal of Physics: Conference Series* (Institute of Physics Publishing, 2020), **1444**.
  12. B. Bai, H. Wang, T. Liu, Y. Rivenson, J. FitzGerald, and A. Ozcan, *J. Biophotonics* (2020).
  13. O. Mudanyali, C. Oztoprak, D. Tseng, A. Erlinger, and A. Ozcan, *Lab Chip* **10**, 2419 (2010).
  14. E. McLeod and A. Ozcan, *Reports Prog. Phys.* **79**, (2016).
  15. Y. Wu and A. Ozcan, *Methods* **136**, 4 (2018).
  16. J. Garcia-Sucerquia, W. Xu, S. K. Jericho, P. Klages, M. H. Jericho, and H. J. Kreuzer, *Appl. Opt.* **45**, 836 (2006).
  17. D. Tseng, O. Mudanyali, C. Oztoprak, S. O. Isikman, I. Sencan, O. Yaglidere, and A. Ozcan, *Lab Chip* **10**, 1787 (2010).
  18. P. Langehanenberg, G. Von Bally, and B. Kemper, *3D Res.* **2**, 1 (2011).
  19. C. Trujillo, R. Castañeda, P. Piedrahita-Quintero, and J. Garcia-Sucerquia, *Appl. Opt.* **55**, (2016).
  20. C. Trujillo and J. Garcia-Sucerquia, *Appl. Opt.* **56**, (2017).
  21. C. Buitrago-Duque, E. Zora-Guzmán, H. Tobon-Maya, J. Garcia-Sucerquia, and S. Zapata-Valencia, *Appl. Opt.* Vol. 60, Issue 4, pp. A205–A214 **60**, A205 (2021).
  22. Y. Zhang, S. Y. C. Lee, Y. Zhang, D. Furst, J. Fitzgerald, and A. Ozcan, *Sci. Rep.* **6**, 28793 (2016).
  23. M. Trusiak, M. Cywinska, V. Mico, J. A. Picazo-Bueno, C. Zuo, P. Zdankowski, and K. Patorski, *Sci. Rep.* **10**, 1 (2020).
  24. B. Patino-Jurado, J. F. Botero-Cadavid, and J. Garcia-Sucerquia, *J. Light. Technol.* **37**, 5660 (2019).
  25. M. J. Lopera and C. Trujillo, *Opt. Lett.* **47**, 2862 (2022).
  26. M. J. Lopera and C. Trujillo, *Appl. Opt.* **61**, B77 (2022).
  27. P. Piedrahita-Quintero, C. Trujillo, and J. Garcia-Sucerquia, *Comput. Phys. Commun.* (2017).
  28. R. Castaneda, C. Trujillo, and A. Doblas, *Sensors* **21**, 8021 (2021).
  29. C. Trujillo and M. J. Lopera, *Front. Opt. + Laser Sci.* 2021 (2021), Pap. JTh5A.14 JTh5A.14 (2021).
  30. M. J. Lopera, M. J. Lopera, C. Trujillo, and C. Trujillo, *Opt. Lett.* Vol. 47, Issue 11, pp. 2862–2865 **47**, 2862 (2022).

## Integrated Photonic Neuromorphic Processor Enabled Intelligent, Energy-Efficient Signal Processing for the Next-Generation Communication Systems

The Internet is vital in the modern society and global economy. In handling today's optical communication systems, digital signal processing (DSP) chips have adopted advanced CMOS technology nodes and approached the limits of semiconductor technologies in terms of power dissipation and density. Even so, DSP chips still must avoid using powerful but computationally expensive algorithms, in order to maintain their power dissipation below the thermal dissipation limit. In the coming decade, DSP needs to handle 10x more data traffic, and correspondingly, their energy per bit must be reduced by 10 times. However, as semiconductor technologies evolve at the end of Moore's law, DSP will find it increasingly difficult to satisfy future demand.

Therefore, to support continued internet traffic growth, it needs a paradigm shift in signal processing technology that can improve both energy efficiency and processing capability. This project proposes to develop such solutions by investigating a novel integrated photonic neuromorphic processor, which leverages the strengths of intrinsic properties of photonics, deep learning architectures, and integrated photonic technologies. Our approach promises to bring 10x higher energy efficiency and 1000x less processing latency. Meanwhile, the processor offers the capability of compensating for various transmission impairments, which DSP fails to achieve due to its limited bandwidth.

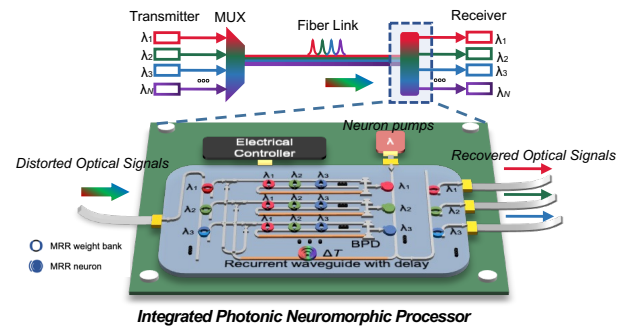


Figure: Proposed fiber communication link with photonic neuromorphic processor.

The proposed photonic neuromorphic processor is a system-on-chip that emulates the recurrent neural network (RNN) model using integrated photonic devices and waveguides. However, our neuromorphic processor is **NOT** simply a faster substitute of software RNN for the same operations (in contrast to some research on photonic AI accelerators). Instead, **our solution builds on our discovery of the strong analogies between the physics models of the proposed photonic neuromorphic processor and that of the fiber transmission systems.** By exploiting such analogies, our photonic neuromorphic processor, with only a small neural network, can advance signal processing beyond what is presently feasible by DSP. **The improvement lies in three aspects. First,** our photonic neuromorphic processor, with only  $N$  photonic neurons, can simultaneously process  $N$  channels, resolving dispersion, intra-, and inter-channel fiber nonlinearities in the transmission system. These capabilities are uniquely enabled by the wide bandwidth of photonics and, therefore, promise to break the nonlinear Shannon limit. **Second,** our photonic neuromorphic processor can process optical signals in their native form and photonic domain. This avoids prohibitive energy consumption and speed overhead in analog to digital converters (ADCs) and substantially reduces power consumption. **Third,** our photonic neuromorphic processor leverages photonic devices designed for optical communications and, thus, can always offer a processing speed matching the fiber communication line rate in the future.

This project will develop a practical and scalable photonic neuromorphic signal processor, built on our proposed architecture and prior research on integrated neuromorphic photonics. Three major tasks will be completed. (1) We will design a novel photonic system-on-chip that allows processing multi-dimensional communication signals in their native form and in the photonic domain. (2) We will explore the optimized photonic platform and photonic-electronic integration methods to realize practical and scalable photonic neuromorphic processors. This will be done by leveraging our prior research and cross-stack collaborations. (3) We will address a common concern in the optical signal processor: the reduced signal-to-noise ratio (SNR) caused by the device loss. To do that, we will conduct a novel joint design of the communication system and photonic neuromorphic processor at the system level. (4) We will experimentally demonstrate the optimized processor and communication link, showing that the photonic processor can address distortions across wide channels while offering energy advantages over DSP approaches. The success of our project will provide a fundamental solution for meeting the future communication demand by delivering faster, more energy-efficient, and more powerful signal processing technologies.

## Integrated Photonic Neuromorphic Processor Enabled Intelligent, Energy-Efficient Signal Processing for the Next-Generation Communication Systems

### Literature Review and Problem Statement

**1. Digital signal processing (DSP) for optical communications: current status and limits** Today's Internet traffic is growing 30% annually. In the next decade, optical network capacity needs to increase 10 times to sustain the operation of the Internet. Current optical communication systems have already strained the capacity of optical fibers, inevitably leading to increased channel imperfection and signal distortions. Currently, signal distortions are addressed by DSP implemented in high-speed custom application-specific integrated circuits (ASICs). As the digital ASIC/DSP is made with silicon, it is subject to the CMOS process node improvement cycle. Today, DSP chips for optical communications have approached the limits of semiconductor technologies in terms of power dissipation and density. The most advanced CMOS nodes are required to handle today's high-speed fiber communication systems. For example, 5nm CMOS PAM4 DSPs are used in 400G and 800G data center applications [1]. For next-generation 1.6T transceivers, the 3nm CMOS node will be required. The demand for advanced CMOS technology leads to excessively high costs in both R&D and manufacturing. As a result, the fabs that make the most advanced chips are becoming prohibitively pricey. The cost of a fab rises at around 13% a year and is expected to reach \$16 billion or more in 2022 [2].

Despite using state-of-the-art CMOS nodes, DSP chips still must avoid using powerful but computationally expensive algorithms to maintain their power dissipation below the maximum thermal dissipation capacity. For example, digital back-propagation, a powerful algorithm for fiber nonlinearity compensation, cannot be implemented on the DSP chips because its complexity and associated power consumption are too high. An even more challenging problem for DSP is to compensate for inter-channel crosstalk in a multi-dimensional communication system (for example, wavelength-division multiplexing (WDM) spatial-division multiplexing (SDM) systems). The reason is that these systems need to share and process a large volume of data from multiple high-speed channels between DSP chips. This is beyond the capability of today's semiconductor technology. As a result, the limited signal processing capability has resulted in the so-called nonlinear Shannon limit, describing that fiber nonlinearity-induced signal distortions currently limit the fiber transmission capacity. This limitation is still as valid today as it was first identified. In the coming ten years, DSP needs to deal with 10x more data traffic; correspondingly, their energy per bit must be reduced by 10. Unfortunately, as semiconductor technologies are evolving on probably the last bit of Moore's law, DSP will find it increasingly challenging to support the continued growth of internet traffic in the future.

**2. Photonic neuromorphic processors: opportunities and challenges** The bottleneck in DSP has motivated research in signal processing using photonics physics and in the photonic domain [3]. One emerging field that takes advantage of photonic physics is *neuromorphic photonics*, which attempts to physically mimic the massively distributed structure of brains with photonic devices and circuits [4]. In the neuromorphic photonic processor, photonic weighted addition, the analog photonic equivalent of a multiply-accumulate (MAC) operation, offers MAC energy consumption that does not tradeoff with MAC speed. As a result, photonic phenomena can be employed to implement analog weighted addition with unmatched speed and efficiency. Furthermore, photonic transport physics can support massively distributed interconnections with commensurate performance. Therefore, neuromorphic photonic hardware can potentially lead to faster and more energy-efficient intelligent information processing than its digital counterparts. In the meanwhile, integrated photonic fabrication and packaging technologies are advancing rapidly. For example, silicon photonics can already provide a mature and reliable platform to produce large-scale and low-cost optical systems. High-density integrated optoelectronic devices and interconnects make scalable information processing and computing possible.

There has been a surge of research interest in photonic neuromorphic processors in recent years [4–9]. Most research on neuromorphic photonics is interested in developing general-purpose artificial intelligence (AI) accelerators for conventional digital AI applications, such as image processing. However, a common problem of performing digital applications using photonics is that it requires the conversion of digital signals (e.g., image pixels) to photonic signals, which incurs high power consumption overheads and negates the promised energy savings.



In addition to general AI computing, neuromorphic photonics can also benefit wider areas in signal processing, particularly for optical communications [10–15], for the following reasons. First, many neuromorphic photonic systems leverage photonic devices initially designed for optical communications and thus can always offer a processing speed matching the fiber communication line rate. In contrast, DSP needs to rely on parallel computing to keep up with the data rate, which usually results in significant power consumption overhead. Second and more interestingly, in addition to potentially being faster and more energy efficient, photonic processors uniquely possess THz bandwidth resources, which can be leveraged to solve problems presently impossible by DSP, for example, inter-channel crosstalk.

Despite these potential advantages, many problems need to be engineered to fully utilize unique traits of photonic physics while minimizing overhead. To do that, an important design rule to follow is how to let the optical communication signals be processed directly in their native optical domain to avoid prohibitive energy consumption overhead and speed reduction in domain crossings (for example, digital-to-analog and analog-to-digital conversions, photonic-to-electrical conversions). Another design challenge is how to fully utilize the unique traits of photonics to address the signal processing problems currently inaccessible to DSP chips, such as inter-channel nonlinearity compensation. The third challenge is how to overcome the signal-to-noise degradation caused by the unavoidable insertion loss and noises in photonic processors.

### ***Project objectives, key innovations and expected outcomes***

The proposed project will respond to the above challenges and develop a high-speed, energy-efficient, integrated neuromorphic photonic processor for optical communication signal processing. We target to achieve the following objectives and innovations.

- The neuromorphic photonic processor will be able to simultaneously compensate for fiber dispersions, intra- and inter-channel nonlinearities, and other impairments in real-time across wide wavelength and spatial channels.
- The neuromorphic photonic processor will be able to directly interface and process the optical communication channels in the photonic domain without domain conversion overhead. We target to achieve energy efficiency and low latency at least one order of magnitude better than the state-of-the-art DSP and with a better scaling with the data rate, transmission distance, and channels.
- The neuromorphic photonic processor will have a small neural network size, and component counts ready to be handled by the current photonic-electronic packaging technologies. Only  $N$  photonic neurons are required to process  $N$  optical communication channels.
- The neuromorphic photonic processor can have minimum impact on the signal-to-noise ratio of the overall communication systems. This will be realized by co-designing the neuromorphic photonic processor and transmission link from the system level.

We will design, optimize, and fabricate the neuromorphic photonic processor by exploring different integrated photonic platform including hybrid silicon photonics and lithium-niobate-on-insulator (LNOI), and build an optical fiber communication testbed to characterize and test the processor with experiments. We will demonstrate enhanced functionalities for multichannel and multimode processing with up to 100 G speed, reduced power consumption and latency compared to the state-of-the-art in both theory and experiments. We expect the success of this project will deliver a solution to the challenges of maintaining long-term internet traffic growth while reducing energy consumption in the post-Moore's law era from a fundamentally different perspective.

### ***Technical Rationale and Approach***

***1. Architecture and system-on-chip design of the neuromorphic photonic processor:*** Architecture and system-on-chip design of the neuromorphic photonic processor: The conceptual schematic of the neuromorphic photonic processor shown in Figure 1(a) is modified from our prior work on the "Broadcast-and-weight" protocol [16] by adding a recurrent waveguide to form a photonic recurrent neural network (RNN). This architecture allows our processor to process optical communication signals directly in the photonic domain. The photonic RNN's input is an array of microring resonators (MRR) with  $N$  MRRs. They serve as the input layer of the photonic RNN to receive WDM signals from the transmission link and provide tunable weights of WDM signals at the optical domain. After the input

layer, the WDM signals are broadcast and weighted by an MRR weight bank consisting of  $N \times N$  MRRs and then summed by the following balanced photodetector.  $N$  is the number of WDM channels to be processed. The summed photocurrent modulates the transmission of the MRR modulator (that is, the photonic neuron). The MRR modulator exhibits nonlinear electrical-to-optical transfer functions, producing the nonlinear activation function in the photonic neural network. The outputs of the photonic neurons are partially connected back to the  $N \times N$  MRRs' inputs using a single feedback waveguide. The recurrent waveguide allow many Terabits information to exchange among many weight-and-summed channels, contributing to better compensation of inter-channel crosstalk. The MRR, photodetector, and modulators are mature and ubiquitous optical components for optical transceivers and other integrated photonic circuits. Thus these building blocks dramatically lower the program risk, and, meanwhile, ensure that the processing speed can always match the signal line rates and allow for the real-time processing of optical communication signals.

The photonic RNN can be modeled by a set of coupled ordinary differential equations describing how the  $N$  neuron states and the  $N$  outputs evolve with time [16]. After unfolding the mathematic model along time and then being discretized, the model is identical to a conventional software RNN. An RNN can behave as a universal approximator of dynamic systems, as theoretically demonstrated by several classic papers in machine learning. When the RNN is configured to approximate the "inverse model" of a fiber communication system, the RNN processor can flexibly undo all types of distortions (including distortions within both fibers and transceivers) and recover the transmitted signals. Therefore, an RNN can treat the fiber communication system as a black box for channel equalization and "learn" the inverse transmission channel from training data. This idea differs from conventional DSP techniques, which recover distorted signals by executing dedicated processing physics models to mitigate specific impairments sequentially. As a result, the photonic RNN, with only  $N$  neurons, can simultaneously resolve all types of distortions, including dispersion, fiber nonlinearities, and various kinds of distortions inside the transceivers in  $N$  channels.

**2. Photonic Hardware Compatible Training Method.** We then propose the following training method to train the photonic RNN. The task of training the photonic RNN is to learn the optimized weights and biases such that the outputs of the PNN are the recovered WDM signals. The procedures of training our photonic RNN are shown in Figure 1(b) and described as follows. The photonic RNN is first modeled by a set of coupled ordinary differential equations describing how the  $N$  neurons and  $N$  neural network outputs a response to the  $N$  inputs and evolve with time [16]. The input and output of the photonic RNN are the time series of the distorted and recovered signals, respectively, at a particular wavelength channel.  $N$  is the channel number of the WDM transmission system. To train the analog photonic RNN, we first discretize the Equation using the forward-Euler method. The discretized photonic RNN model can now be represented by a series of RNN cells similar to software-based RNNs, consisting of a series of photonic RNN cells. In this way, the photonic RNN can be constructed by Pytorch nn.module and trained using the backpropagation through time (BPTT) algorithm, similar to software-based RNNs [17]. Figure 1(c) shows the results of training our processor to process a 2-channel 56 GBaud PAM4 transmission system.

### 3. Preliminary results and hardware Implementation experiences

*(a) Preliminary results.* We first compare our proposed approach with other published transmission systems with a single-channel PAM4 signal. We have included both DSP (green dots) and photonic reservoir computing (blue dots) in the comparison. Our work can achieve a data rate-distance product

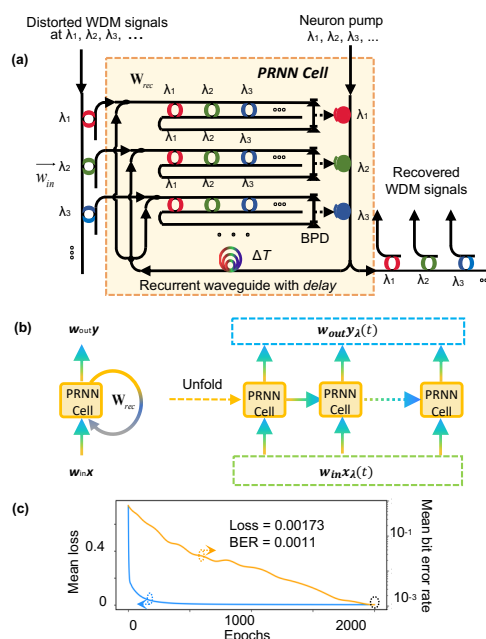


Figure 1: (a) Proposed photonic neuromorphic processor based on wavelength-division-multiplexing concept. The inputs of the processor are the distorted optical signals and the outputs are the recovered optical signals. (b) Training the photonic neural network using back propagation through time algorithm. (c) The mean training loss and mean BER for 56 GBaud PAM4 transmission system.

of 1200 GBaud·km when considering a single channel, outperforming most of the other published approaches. We then consider a multi-channel transmission link. In this case, we compare the photonic RNN with different DSP methods, including maximum likelihood sequence estimation (MLSE) and feed-forward neural network equalizer (FNN). It is worth noting that the DSP algorithms can only be implemented on a channel-by-channel basis, while the photonic RNN is able to process all WDM channels simultaneously. Figure 3 shows photonic RNN significantly outperforms all other DSP-based compensation algorithms due to its capability to process both intra- and inter-channel distortions.

**(b) Hardware Implementation experience.** MRRs, photodetectors, and modulators are building blocks in our photonic neuromorphic processor. These are standard components found in silicon photonic foundries' process design kits (PDK) (such as IMEC and AMF). Therefore, our approach can reduce risk by using mature, high-performance silicon photonic technology in the telecom bands. In our prior work, we optimized the key components (MRRs, photodetectors, and modulators) required for the proposed photonic RNN (Figure 3). We have also developed a series of technology stacks for implementing photonic neural network chips. First, we have developed an MRR control method for large-scale photonic integrated circuits, which achieved a record weights precision beyond 9 bits, which is comparable to digital AI hardware [18,19]. Second, for the photonic neuron, we have demonstrated the on-chip photonic neuron consisting of the silicon PN modulators and Ge-on-Si photodetectors [20]. To ensure the physical cascadability of photonic neurons, we integrated an electrical matching circuit that acts as a passive TIA to provide on-chip gain. With the photonic neuromorphic processor, we demonstrated the compensation for optical nonlinearities in a long-haul 16-QAM fiber transmission link [20]. This system demonstration proves our capability in designing, layout, and packaging large-scale photonic chips and testing the chip with optical communication systems. These developed building blocks and hardware implementation techniques will lay the foundations for this project.

### Outline of tasks

The project will be organized as three separate work packages:

**Work Package I. Expand the neuromorphic photonic processor for more complex multi-dimensional fiber communication systems.** Expand the neuromorphic photonic processor for more complex multi-dimensional fiber communication systems. The preliminary results show that the neuromorphic photonic processor can process WDM communications systems and compensate for intra- and inter-channel crosstalk. This project will further leverage the excessive bandwidth of photonics to extend the functions of the neuromorphic photonic processor for more complex multi-dimensional, such as polarization and mode multiplexed, communication systems. Following our prior work, the expanded neuromorphic photonic processor can be an array of photonic polarization/modal unscramblers, each unscrambling the polarization/modal coupling of individual wavelength in the optical domain. The unscrambler arrays are followed by the multi-wavelength photonic RNN. The photonic RNN will address the remaining dispersions (including chromatic and modal dispersion) and nonlinearities in the optical domain. A challenge of processing the polarization/modal crosstalks is that the crosstalk is time-varying. Thus an online and adaptive learning algorithm will be required. We will combine our

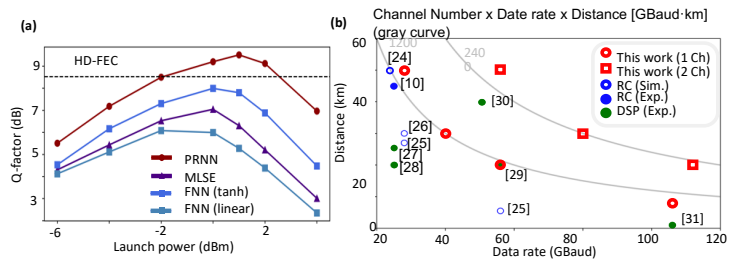


Figure 2: (a) Comparison of the proposed photonic processor and various DSP methods in 2-channel 56 GBaud/λ WDM PAM4 signals over 20 km transmission link. PRNN: photonic recurrent neural network; FNN: feed-forward neural network; MLSE: maximum likelihood sequence estimation. (b) Comparison of different PAM4 equalization systems with reservoir computing (RC) and DSP in terms of data rate and distance. Ch: channel; Sim: simulation; Exp: experiment.

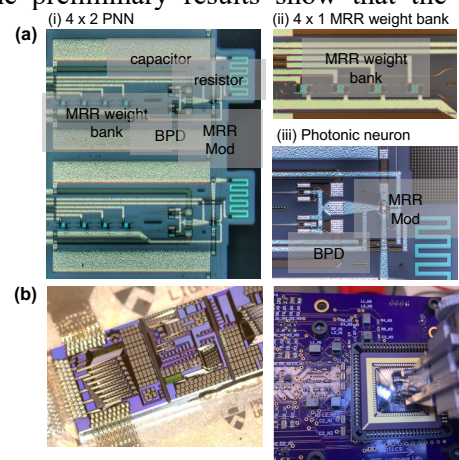


Figure 3. First-generation of photonic neuromorphic processor based on silicon photonic foundry technologies. (b) packaging and testing.

proven photonic blind source separation (BSS) algorithm [21], which allows the unscramblers to be automatically configured through unsupervised learning, with the current RNN training method. The combined learning method will be able to learn and compensate for both the dynamic and the static transmission impairments in real-time.

**Work Package II. Investigate pre-equalization to optimize transmission link performance .** Investigate pre-equalization to optimize transmission link performance. Photonic processors have a common limitation: the insertion losses and noises inside the processors reduce the optical SNR. To solve this problem, we have a vision that when the neuromorphic photonic processor is placed at the transmitter side before the transmission link as a pre-equalizer, the transmission should have a much better signal-to-noise ratio. We will validate the idea of applying the neuromorphic photonic processor as a pre-equalizer both theoretically and experimentally. A challenge of doing that is that, unlike the normal post-equalizer, which exactly knows the ground truth (i.e., the transmitted symbols), the target outputs from the neuromorphic processor are unknown. To solve this problem, we borrow the ideas from digital backpropagation and obtain the training data by solving inverse nonlinear Schrödinger equation (I-NLSE). The output of I-NLSE will be used as the target outputs of the our photonic neuromorphic processor.

**Work Package III. Optimize photonic device, platform, and packaging technologies** This work package will leverage the state-of-the-art photonic device, platform, and packaging technologies to make radical improvements to the power efficiency and speed of the proposed neuromorphic processor. To manage the project risk, we will first develop a proof-of-concept chip based on silicon photonic foundry technologies. The processing speed of our proposed processor is determined by the speed of the photonic neuron, which is essentially an on-chip optical-electrical-optical (OEO) link. The OEO link needs to provide a gain larger than unity, which means that the silicon modulator needs a large voltage swing to reach the nonlinear threshold in their nonlinear transfer function. To do that, we will bonding a TIA bridging between the photodetector and modulator. We need to simultaneously optimize the gain and the bandwidth of the OEO link. To do that, we will develop a link model that includes the equivalent circuit of the silicon photodetector and modulator bridging with the bond pads, bonding wires, and TIAs, and optimize the circuit design through simulations and experimental characterizations.

To further improve the energy efficiency and speed of our processor, we will also develop the advanced hybrid platforms by consolidating our established cross-stack collaborations. We will explore heterogeneous III–V silicon photonic integration for on-chip amplification and integrated laser pumps [21] with Prof. Chao Xiang from Hong Kong U and lithium niobate on silicon platforms for high-speed modulators [23] with Prof. Cheng Wang from City U of Hong Kong. In both stages, we will leverage on industry-level photonic-electronic packaging facilities by Ixiri Photonics Inc. in Suzhou, China to provide high-performance packaging service. We will build our fiber communication testbed using CUHK's high-speed characterization equipment and test our neuromorphic processor in the communication link. We will benchmark the performance with the state-of-the-art DSP.

### **Outcome and Impact**

Our new photonic neuromorphic processor should remove the bandwidth and power consumption bottlenecks that have held back existing DSP technologies and resolve the long-standing power consumption issues in communication systems. Our new photonic neuromorphic processor will have enhanced functionalities for multichannel and multimode processing with up to 100 G processing speed, reduced power consumption and latency enabled by the advance photonic platforms compared to the state-of-the-art digital processors. This will further increase the fiber transmission capacities and sustain the continued growth of the Internet and the uninterrupted provision of internet services despite the exponential increase in network traffic.

Meanwhile, our new hybrid photonic hardware platforms can generally apply to creating high-performance processors for deep learning and other applications. So the proposed research can further extend its applications to the broader context of power-efficient AI in diverse applications. This project also has a high educational impact, which rests on its multi-disciplinary nature. The proposed project requires collaborative multi-disciplinary work that crosses the boundaries of machine learning, electronic-photonic systems and devices, and optical communications and signal processing. Therefore, students and engineers working on this project will get comprehensive training on both algorithm and hardware development and wield different technical stacks for tackling new problems.



## References

1. "MaxLinear | OFC," <https://www.ofcconference.org/en-us/home/exhibition-and-show-floor-programs/2021/maxlinear/>.
2. "World Fab Forecast | SEMI," <https://www.semi.org/en/products-services/market-data/world-fab-forecast>.
3. A. E. Willner, S. Khaleghi, M. R. Chitgarha, and O. F. Yilmaz, "All-optical signal processing," *Journal of Lightwave Technology* **32**, 660–680 (2013).
4. B. J. Shastri, A. N. Tait, T. F. de Lima, W. H. Pernice, H. Bhaskaran, C. D. Wright, and P. R. Prucnal, "Photonics for artificial intelligence and neuromorphic computing," *Nature Photonics* **15**, 102–114 (2021).
5. Y. Shen, N. C. Harris, S. Skirlo, M. Prabhu, T. Baehr-Jones, M. Hochberg, X. Sun, S. Zhao, H. Larochelle, D. Englund, and M. Soljačić, "Deep learning with coherent nanophotonic circuits," *Nature Photonics* **11**, 441–446 (2017).
6. J. Feldmann, N. Youngblood, C. D. Wright, H. Bhaskaran, and W. H. P. Pernice, "All-optical spiking neurosynaptic networks with self-learning capabilities," *Nature* **569**, 208–214 (2019).
7. X. Xu, M. Tan, B. Corcoran, J. Wu, A. Boes, T. G. Nguyen, S. T. Chu, B. E. Little, D. G. Hicks, R. Morandotti, A. Mitchell, and D. J. Moss, "11 TOPS photonic convolutional accelerator for optical neural networks," *Nature* **589**, 44–51 (2021).
8. Lin Xing, Rivenson Yair, Yardimci Nezhil T., Veli Muhammed, Luo Yi, Jarrahi Mona, and Ozcan Aydogan, "All-optical machine learning using diffractive deep neural networks," *Science* **361**, 1004–1008 (2018).
9. A. N. Tait, T. F. de Lima, E. Zhou, A. X. Wu, M. A. Nahmias, B. J. Shastri, and P. R. Prucnal, "Neuromorphic photonic networks using silicon photonic weight banks," *Scientific Reports* **7**, 7430 (2017).
10. P. Antonik, F. Duport, M. Hermans, A. Smerieri, M. Haelterman, and S. Massar, "Online Training of an Opto-Electronic Reservoir Computer Applied to Real-Time Channel Equalization," *IEEE Transactions on Neural Networks and Learning Systems* **28**, 2686–2698 (2017).
11. A. Argyris, J. Bueno, and I. Fischer, "Photonic machine learning implementation for signal recovery in optical communications," *Scientific Reports* **8**, 8487 (2018).
12. F. D.-L. Coarer, M. Sciamanna, A. Katumba, M. Freiberger, J. Dambre, P. Bienstman, and D. Rontani, "All-Optical Reservoir Computing on a Photonic Chip Using Silicon-Based Ring Resonators," *IEEE Journal of Selected Topics in Quantum Electronics* **24**, 1–8 (2018).
13. A. Argyris, J. Cantero, M. Galletero, E. Pereda, C. R. Mirasso, I. Fischer, and M. C. Soriano, "Comparison of Photonic Reservoir Computing Systems for Fiber Transmission Equalization," *IEEE Journal of Selected Topics in Quantum Electronics* **26**, 1–9 (2020).
14. F. Da Ros, S. M. Ranzini, H. Bülow, and D. Zibar, "Reservoir-Computing Based Equalization With Optical Pre-Processing for Short-Reach Optical Transmission," *IEEE Journal of Selected Topics in Quantum Electronics* **26**, 1–12 (2020).
15. S. Sackesyn, S. Sackesyn, C. Ma, C. Ma, J. Dambre, P. Bienstman, and P. Bienstman, "Experimental realization of integrated photonic reservoir computing for nonlinear fiber distortion compensation," *Opt. Express*, OE **29**, 30991–30997 (2021).
16. A. N. Tait, M. A. Nahmias, B. J. Shastri, and P. R. Prucnal, "Broadcast and Weight: An Integrated Network For Scalable Photonic Spike Processing," *J. Lightwave Technol., JLT* **32**, 3427–3439 (2014).
17. H.-T. Peng, J. Lederman, L. Xu, T. F. de Lima, C. Huang, B. Shastri, D. Rosenbluth, and P. Prucnal, "A Photonic-Circuits-Inspired Compact Network: Toward Real-Time Wireless Signal Classification at the Edge," *arXiv:2106.13865 [cs, eess]* (2021).
18. C. Huang, S. Bilodeau, T. Ferreira de Lima, A. N. Tait, P. Y. Ma, E. C. Blow, A. Jha, H.-T. Peng, B. J. Shastri, and P. R. Prucnal, "Demonstration of scalable microring weight bank control for large-scale photonic integrated circuits," *APL Photonics* **5**, 040803 (2020).
19. W. Zhang, C. Huang, C. Huang, H.-T. Peng, S. Bilodeau, A. Jha, E. Blow, T. F. de Lima, T. F. de Lima, B. J. Shastri, B. J. Shastri, and P. Prucnal, "Silicon microring synapses enable photonic deep learning beyond 9-bit precision," *Optica*, OPTICA **9**, 579–584 (2022).

20. C. Huang, S. Fujisawa, T. F. de Lima, A. N. Tait, E. C. Blow, Y. Tian, S. Bilodeau, A. Jha, F. Yaman, H.-T. Peng, H. G. Batshon, B. J. Shastri, Y. Inada, T. Wang, and P. R. Prucnal, "A silicon photonic–electronic neural network for fibre nonlinearity compensation," *Nature Electronics* **4**, 837–844 (2021).
21. C. Huang, D. Wang, W. Zhang, B. Wang, A. N. Tait, T. F. de Lima, B. J. Shastri, and P. R. Prucnal, "High-Capacity Space-Division Multiplexing Communications With Silicon Photonic Blind Source Separation," *Journal of Lightwave Technology* **40**, 1617–1632 (2022).
22. C. Xiang, J. Liu, J. Guo, L. Chang, R. N. Wang, W. Weng, J. Peters, W. Xie, Z. Zhang, J. Riemensberger, J. Selvidge, T. J. Kippenberg, and J. E. Bowers, "Laser soliton microcombs heterogeneously integrated on silicon," *Science* **373**, 99–103 (2021).
23. C. Wang, M. Zhang, X. Chen, M. Bertrand, A. Shams-Ansari, S. Chandrasekhar, P. Winzer, and M. Lončar, "Integrated lithium niobate electro-optic modulators operating at CMOS-compatible voltages," *Nature* **562**, 101–104 (2018).
24. A. Bogris, C. Mesaritakis, S. Deligiannidis, and P. Li, "Fabry-perot lasers as enablers for parallel reservoir computing," *IEEE Journal of Selected Topics in Quantum Electronics*, vol. 27, no. 2, pp. 1–7, 2020.
25. A. Argyris, J. Bueno, and I. Fischer, "Pam-4 transmission at 1550 nm using photonic reservoir computing post-processing," *IEEE Access*, vol. 7, pp. 37 017–37 025, 2019.
26. X. Yu and F. Zhang, "Reservoir computing based signal recovery for 56 gb/s pam4 system," in *Optoelectronics and Communications Conference*. Optical Society of America, 2021, pp. S3A–5.
27. Z. Xu, C. Sun, J. H. Manton, and W. Shieh, "Joint equalization of linear and nonlinear impairments for pam4 short-reach direct detection systems," *IEEE Photonics Technology Letters*, vol. 33, no. 9, pp. 425–428, 2021.
28. Z. Xu, C. Sun, T. Ji, J. H. Manton, and W. Shieh, "Feedforward and recurrent neural network-based transfer learning for nonlinear equalization in short-reach optical links," *Journal of Lightwave Technology*, vol. 39, no. 2, pp. 475–480, 2020.
29. X. Tang, Y. Qiao, Y.-W. Chen, Y. Lu, and G.-K. Chang, "Digital pre- and post-equalization for c-band 112-gb/s pam4 short-reach transport systems," *Journal of Lightwave Technology*, vol. 38, no. 17, pp. 4683–4690, 2020.
30. Y. Yu, Y. Che, T. Bo, D. Kim, and H. Kim, "Reduced-state mlse for an im/dd system using pam modulation," *Optics Express*, vol. 28, no. 26, pp. 38 505–38 515, 2020.
31. B. Sang, J. Zhang, C. Wang, M. Kong, Y. Tan, L. Zhao, W. Zhou, D. Shang, Y. Zhu, H. Yi et al., "Multi-symbol output long short-term memory neural network equalizer for 200+ gbps im/dd system," in *2021 European Conference on Optical Communication (ECOC)*. IEEE, 2021, pp. 1–4.

## Executive Summary

**Dispersion engineering of light for new optical sensing and metrology technologies**

(Category: Information)

Dr. Chen-Ting Liao

Senior research associate, JILA, University of Colorado, Boulder, Colorado 80309, USA

Dispersion relationship engineering in materials and structures enables the desirable photonic properties, facilitating modern advances in metamaterials, plasmonics, and photonic slabs for optical sensing. Indeed, the design of coherent or optical transfer functions of materials and systems dictates the information and functionalities an exit optical field can carry. However, this is, in fact, an incomplete picture of a generic sensing principle that ignores the role of the optical illumination itself. As evidenced by the recent success of structured light for super-resolution imaging, enhanced sensing, and telecommunications, the holistic picture of optimized total dispersion relation must take optical illumination into account. In particular, exciting discoveries and creations of nontrivial, spatiotemporally sculptured light show that the nonlinear dispersion relations of light wave packets can elicit novel material properties. Over the past few years, the research has been primarily focused on the fundamental properties of such light, including its propagation, diffraction, refraction, and transmission. Little attention has been devoted to its great potential for parameter monitoring capabilities that can eventually corroborate with the material- and structure-based dispersion relation engineering for enhanced laser-based optical sensing.

By utilizing and optimizing the emerging field of space-time wave packets of light, this proposed project aims to address this knowledge gap and the demanding need to further enhance the existing parameter estimation and monitoring capabilities. Various novel space-time wave packets have been generated and studied recently, including toroidal pulses, baseband x-shaped space-time wave packets, time-varying and spatiotemporal orbital angular momentum of light. The goal of this project is to systematically investigate these space-time wave packets by theoretically and experimentally characterizing how the non-separable degrees of freedom of light can be utilized as a probe for parameter monitoring. Inspired by the analogous concept of dispersion engineering of materials, this project will design, develop, and test the sculptured dispersion relation of structured light pulses that reside on the light cone. The focus will be using sculptured laser pulses in a form that would further enhance nanomaterial, metastructure, or nanophotonic-based sensing applications.

The potential outcome of this project could be transformative as the spatiotemporal tailored illumination are largely under-exploited in laser-based sensing as of today. The potentially new optical sensing mechanisms could improve existing sensing capabilities for a broad range of applications in the future, ranging from materials and semiconductors research and development to environmental, biochemical, and biological sensing and monitoring.



## Dispersion engineering of light for new optical sensing and metrology technologies

*Category: Information*

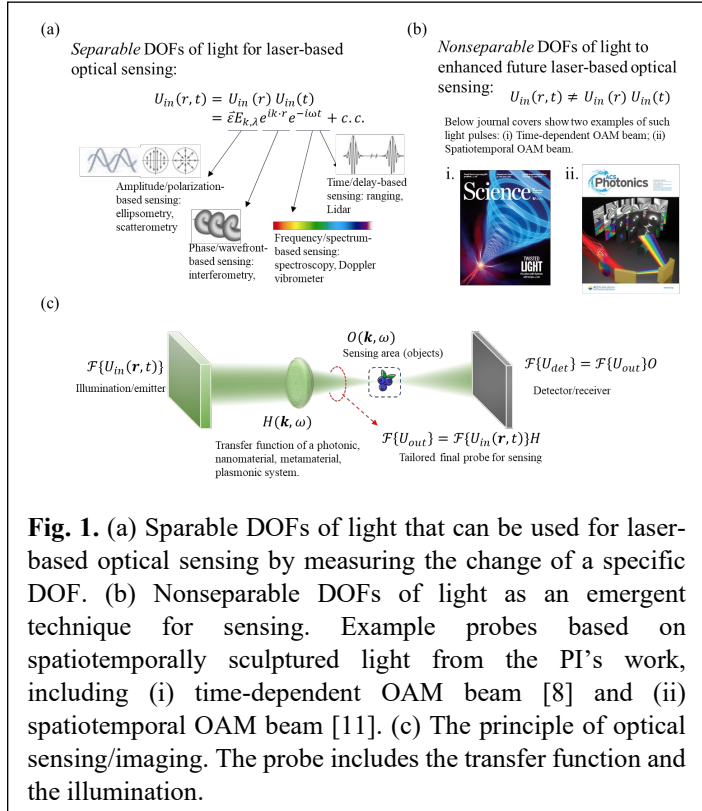
Dr. Chen-Ting Liao

Senior research associate, JILA, University of Colorado, Boulder, Colorado 80309, USA

**Literature Review.** Electronic bandgap (band diagram or dispersion relation) structure engineering in versatile materials allows for the creation of desirable electrical properties [1]. Similarly, photonic bandgap (band diagram or dispersion relation) engineering in dielectric structures allows for the creation of desirable photonic properties. Such dispersion-engineered photonic properties have enabled the emerging fields of metamaterials, metasurface, photonic crystal fibers, and plasmonics for optical sensing and metrologies [2-3]. With proper designs and engineering, such as introducing topological singularities in dispersion relation or phase space of a matter or structure, the nontrivial topologies could enable new discoveries and creations of nonreciprocal properties emerged in various systems and devices such as one-way optical diode and beam splitter, topological lasers [4]. However, most of the studies in dispersion engineering for photonics assume that the illumination is simply a plan wave or a Gaussian beam—without recognizing that spatiotemporally sculptured and coupled electromagnetic waves have their unique dispersion relation that is deviated from a simple linear dispersion relation property ( $\omega \propto k$ ) that could affect the desirable measurement outcomes.

Indeed, engineering and manipulating various degrees of freedom (DOFs) of light is of paramount importance in optical and information technologies. Utilizing the abundance of modern tools, versatile control of light's DOFs (Fig. 1(a)) such as wavevector, phase (wavefront), amplitude, and polarization became possible. As a result, the field of spatially, temporally, and spatiotemporal light fields (STLs) emerged subsequently [5]. Some of the spatially sculptured light fields and wavefronts have found crucial applications, ranging from super-resolution microscopy to telecommunications with multimode light shaping [6,7]. Contrarily, temporally sculptured or time-varying light fields or the temporal modes of photons are still in their infancy. This is especially the case for the STLs that have been attracting burgeoning interests over the past few years for its generation and characterization. Such spatiotemporal dependent DOFs, carrying non-separable (i.e., non-factorizable; (Fig. 1(b)) spatial and temporal parts of the wave equation solutions. Examples include light carrying self-torque (namely, time-varying spin and/or orbital angular momentum (SAM/OAM) [8], spatiotemporal optical vortices (STOVs) [9-11], toroidal light pulses, and space-time wave packets and light sheets [12,13]. The non-separable spatial and temporal modes of such pulsed waves provide a rich and under-exploited playground to engineer novel dispersion relations of light can further enhance or even exhibit new optical sensing capabilities beyond conventional illumination.

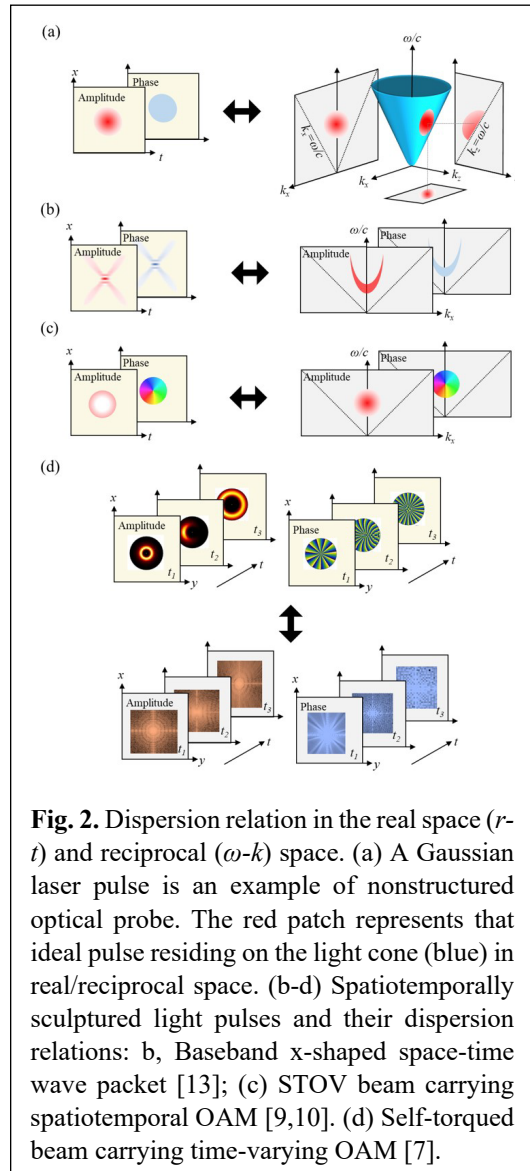
For instance, in a typical laser-based sensing and imaging system (Fig. 1(c)), the coherent imaging formula is  $\mathcal{F}\{U_{out}\} = \mathcal{F}\{U_{in}(\mathbf{r}, t)\}H(\mathbf{k}, \omega)$ , where



$H$  is a system matrix, coherent transfer function (including those stemming from bandgap/dispersion engineered materials and/or structures), and  $\mathcal{F}\{U_{in}(\mathbf{r}, t)\}$  is the Fourier transform of the illumination field  $U_{in}(\mathbf{r}, t)$ . For incoherent imaging,  $H$  is the optical transfer function and  $U_{in}$  is the illumination intensity. Despite its importance, paying attention to  $H$  alone would totally miss the opportunities that engineering the illumination  $U_{in}$  could bring us the final desired properties in  $\mathcal{F}\{U_{det}\}$  when probing objects  $O$ —enhanced optical sensing and imaging schemes. *Therefore, this proposal aims to address the other (half) largely missed opportunity that dispersion relation engineering of light could enable for optical sensing, metrology, and imaging for various enhanced parameter monitoring capabilities.* Unlike bandgap engineering for electronic and photonic properties of materials and structures, little attention to STLs focuses on similar perspectives—that is, to design and engineer the dispersion relation of STLs in its  $\omega$ - $k$  space for specific tasks and applications. Investigating nontrivial "structures" such as those with discontinuities or singularities in the  $\omega$ - $k$  space, one would be able to achieve the desired optical properties of light that are better for sensing.

**Problem Statement/Objective.** The development of new and improved optical sensing technologies for various parameter monitoring capabilities is of great importance. There are many advantages of optical sensing, including biocompatibility, capability to work in hazardous environments and media, immunity to electromagnetic interference, and low-SWaP (small size, weight, and power consumption), to name a few [14]. Dispersion relation engineering of light holds great promise to improve existing optical sensing capabilities further while enhancing and extending various parameter monitoring capabilities beyond the current state-of-the-art for future applications, including those in need in health and environment. The proposal aims (1) to understand better, (2) to improve and (3) to utilize coupled optical DOFs of STLs (e.g., time-varying OAM; STOVs; space-time wave packets, and their modified forms) to interact with the object under test (DUT) for enhanced laser-based sensing to improve various parameter monitoring capabilities.

Borrowing the language used in quantum information science, a measurement (sensing and imaging) indicates a projection of non-separable DOFs or states into one of their eigenstates. Implementing optimally designed strategies for making a measurement or parameter estimation is critical for eliciting novel advantages in optical metrology and sensing that conduct the statistical estimation of unknown physical parameters. The objective of the proposed work is to experimentally and theoretically investigate the fundamental aspects of STL-enabled optical sensing by studying the reciprocal space "structures" (Fig. 2) and how they perform in the most common metrological configurations of optical sensing using, for example, interferometry. To better optimize and exploit STLs interacting with DUT, we can treat the challenge as an inverse problem. That is, given a desirable interacting mechanism (for example, maximizing phase change detection through a scattering medium in a reflection geometry



**Fig. 2.** Dispersion relation in the real space ( $r$ - $t$ ) and reciprocal ( $\omega$ - $k$ ) space. (a) A Gaussian laser pulse is an example of nonstructured optical probe. The red patch represents that ideal pulse residing on the light cone (blue) in real/reciprocal space. (b-d) Spatiotemporally sculptured light pulses and their dispersion relations: b, Baseband x-shaped space-time wave packet [13]; (c) STOV beam carrying spatiotemporal OAM [9,10]. (d) Self-torqued beam carrying time-varying OAM [7].

used in laser ranging and optical coherence tomography), the objective is to find out the ideal wavefront, polarization, and/or other DOFs of light that we should engineer.

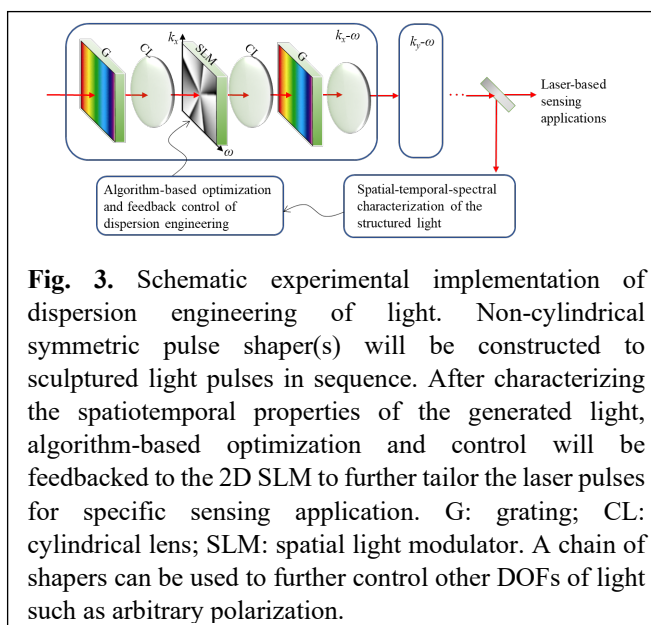
### Outline of tasks/Work Plan (for 2 years).

In **phase I**, the challenge to be tackled can be formulated as how do we extract the desirable information of a system by designing an optimized probe for the task. Novel STLs (e.g., time-varying OAM; STOVs; space-time wave packets, and their modified forms) will serve as foundations and starting points for further exploration, aiming for future laser-based sensing tasks and applications. Figure 3 shows a schematic experimental implementation of dispersion engineering of light. Non-cylindrical

symmetric pulse shaper(s) will be constructed to sculptured light pulses in sequence. After characterizing the spatiotemporal properties of the generated light, algorithm-based optimization and control will be feedbacked to the 2D spatial light modulator to further tailor the laser pulses for specific sensing applications. To provide a concrete sensing application example, the proposal will explore reflection-mode-based experimental configurations in **Phase II** as shown in Fig.4. In this case, instead of using only one STL pulse, two engineered STL pulses that carry anti-correlated, opposite properties of light such as opposite chirps or opposite spatial or spatiotemporal topological charges will be explored. It is worth mentioning that a subset of these STLs is also called classical entanglement of light in some literature. Classical entanglement has attracted increased attention, as well as controversies over the past decade. Classical entanglement may sound like an oxymoron, but it has been mostly clarified recently [15]: classical entanglement refers to correlations between non-separable DOFs of a system, and it is strictly local (absence of quantum nonlocality), a distinguishing feature from quantum entanglement. For example, one of the simplest forms of classically entangled light comes from the superimposing two optical beams that each carry two DOFs, such as SAM and OAM. Using classically entangled light, certain quantum-like advantages have been successfully demonstrated over the past few years in the fields of quantum communication, quantum metrology, and high-speed optical sensing [16].

The work plan in this proposal will build upon the principles similar or analogous to the classical entanglement through dispersion relation engineering of light, and then apply it to phase change-based sensing mechanism in a reflection measurement as is commonly used in optical sensing, laser ranging (or lidar), and optical coherence tomography. Detailed investigations, including theoretical calculations, numerical simulations, and experimental verification, are needed to understand better how different coherent combinations of dispersion engineered and optimized STLs could reach the best sensing performance. Prior studies of non-separable DOFs only focused on a stationary state basis, e.g., static OAM/SAM, and the research of spatial/temporal/spatiotemporal-varying state basis is still in its infancy and will be studied in this proposed work. The proposed theoretical studies include evaluating various known and hybrid structured light vector wave solutions and studying their basic properties such as transmission, reflection, diffraction, and especially backscattering. Understanding the backscattering properties of these beams in a scattering medium will lay out a foundation to enhance the performance of reflection-mode-based sensing and imaging.

In addition to some of the anticipated quantum-like advantages enabled by exploiting correlations, dispersion-engineered STLs could offer other highly sought-after properties for various biomedical and



**Fig. 3.** Schematic experimental implementation of dispersion engineering of light. Non-cylindrical symmetric pulse shaper(s) will be constructed to sculptured light pulses in sequence. After characterizing the spatiotemporal properties of the generated light, algorithm-based optimization and control will be feedbacked to the 2D spatial light modulator to further tailor the laser pulses for specific sensing application. G: grating; CL: cylindrical lens; SLM: spatial light modulator. A chain of shapers can be used to further control other DOFs of light such as arbitrary polarization.

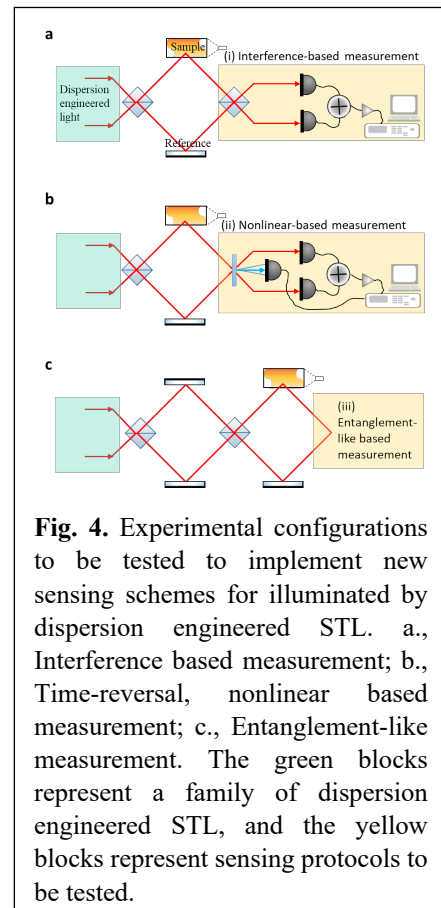
environmental sensing applications, such as enhanced transmission with less diffraction. In the past, non-diffracting waves have attracted many interests due to their practical application potential. Examples of such waves include the well-studied Bessel beams and Airy beams. Sensing and imaging through scattering turbid media are a longstanding challenge, and enhanced transmission is one of the highly demanded aspects of various applications. Scattering diffuses light fields and reduces the number of ballistic photons for final detection, leading to contrast reduction and degraded signal-to-noise ratio. These issues make sensing and imaging in a challenging environment very difficult. Over the past few years, some exciting proof-of-concept experimental results suggest some degrees of enhancement in optical transmission in biological tissues and turbid media and reduced scattering due to turbulence when using OAM and/or classically entangled light [17]. However, most prior studies have only explored the use of basic types of spatiotemporally coupled waveforms in attempt to create the so-called non-diffracting light waves with varying levels of success. How advanced or optimized forms of STLs could be exploited to facilitate high-resolution sensing and imaging through thick turbid media warrants further research.

After the creation of dispersion relation engineered STLs, the proposal will further investigate the optimized measurement (sensing) configurations that optimally utilize such light pulses. There are three different types of interferometric systems that could benefit from the STL pulse pairs (Fig. 4), representing different sensing and imaging protocols and multiparameter estimation strategies to be studied. As non-separable DOFs of dispersion engineered STLs are analogous to quantum states of particles, we seek to recapitulate super-performing traits of quantum sensing and imaging by configuring the interferometers and detection schemes such that the mathematical framework for quantum sensing/imaging can be applied.

In these configurations, we also aim to investigate the potential of using anti-correlated beams to attain focus spot sizes that surpass the classical diffraction limit, achieve better dispersion cancellation within scattering samples, reduction of noise floor by eliciting Hong-Ou-Mandel like interference effect, and amplification of the detection signals by creating analogous quantum-like photon states. To get depth-dependent information from the sample, we propose to adopt principles of spectral-domain optical coherence tomography to our sensing protocols. In spectral-domain optical coherence tomography, broadband light is used to illuminate the sample, and after the return light interferes with the reference, the signal goes to a spectrometer which represents the depth-dependent reflectivity profile of the sample in the Fourier domain. As the depth information is encoded spectrally, there is no need for mechanical scanning of the reference arm to modulate the optical path length. Similarly, the light pulses utilized in our study inherently carry a finite spectral bandwidth, and adapting them to such principles is a natural choice.

**Timeline and Milestone** – Due to the need to test and evaluate various related novel, untested concepts and theoretical applications for their feasibility, this proposal will have two overlapping phases. Phase I will study and further develop dispersion relation engineered STLs, and Phase II will test their corresponding sensing and imaging protocols and methods.

**Potential Outcome(s) and Impact.** Over the past two decades, quantum sensing and imaging using entangled photons promised better images—but has yet to deliver convincing results suitable for biological and environmental applications. This proposal could provide a novel quantum-like method with scalable and robust strategies that can truly translate and impact laser-based sensing and imaging



communities to achieve new optical sensing technologies for improved various parameter monitoring capabilities.

Similar to the success and impacts of bandgap engineering for electronic materials and photonic structures, the proposed research here could be transformative—by designing the optimal light fields that process advantageous properties for new optical sensing and metrology strategies. If this pilot study shows promising signs of success, namely, encouraging traits of enhancement of task-based sensing applications, one could imagine this new direction of research can benefit beyond optical sensing and metrology, to optical communications, optical ranging, and optical imaging, in which new, sculptured properties of light can carry more information of interests or perform the task better. One could also imagine that if this direction of pilot research works well, a better design(s) powered by artificial intelligence or machine learning could open a new avenue for searching for the ultimate *dream beams* that can perform the task on demand. Also, by combining the rapidly developing fields of bandgap engineering of electronic/molecular materials and photonic nano/meta-structures, one can achieve the integrated approach for the ultimate optical sensing—synergistically integrating designed light sources (the probe) and electronic/photonic apparatus (measurement apparatus) to accomplish the sensing application at will.

It is also important to note that while this proposal mainly addresses the "Information" category ("10. Exploring new optical sensing technologies to improve various parameter monitoring capabilities.") of the Optica Foundation 20th Anniversary Challenge, the potential results of the work can be easily adapted into the categories of "Health" and "Environment." This is simply because the dispersion relation between engineered and sculptured light sources also affects how light is used for such applications, especially for laser-based sensing, metrology, and imaging. Examples of future applications and impacts in the Health category include 1. Innovations in advanced photonic biosensors to detect and classify disease and to monitor and assess therapy responses. 2. Developing smart healthcare diagnostics technologies such as enhanced pathology technology using Raman, fluorescence, multispectral imaging, AI, etc. 3. Advancing biomedical imaging further to enable precision medicine, drug delivery and surgery. Example future applications and impacts in the Environment category include 1. Improving environmental monitoring capabilities using satellite, airborne imaging and measurement sensors, as well as ground-based measurement technologies (e.g., distributed optical fiber sensing, multispectral, thermal, and hyperspectral imaging, etc.). 2. Leveraging technology for active monitoring of water and air pollution.

## References

- [1] Chaves *et al.* "Bandgap engineering of two-dimensional semiconductor materials." *npj 2D Materials and Applications* 4, 1 (2020)
- [2] Poletti *et al.* "Hollow-core photonic bandgap fibers: technology and applications." *Nanophotonics* 2, 340 (2013).
- [3] Soukoulis., ed. *Photonic band gaps and localization*. Vol. 308. Springer Science & Business Media (2013).
- [4] Ozawa *et al.* "Topological photonics." *Reviews of Modern Physics* 91, 015006 (2019).
- [5] Shen *et al.* "Non-separable states of light: From quantum to classical." *Laser & Photonics Reviews* 2100533 (2022).
- [6] Padgett, M.J. "Orbital angular momentum 25 years on." *Optics express* 25.10 (2017): 11265-11274.
- [7] Willner *et al.* "Optical communications using orbital angular momentum beams." *Advances in optics and photonics* 7.1 (2015): 66-106.
- [8] Rego *et al.* "Generation of extreme-ultraviolet beams with time-varying orbital angular momentum." *Science* 364, eaaw9486 (2019).
- [9] Jhaji *et al.* "Spatiotemporal optical vortices." *Physical Review X* 6, 031037 (2016).
- [10] Gui *et al.* "Second-harmonic generation and the conservation of spatiotemporal orbital angular momentum of light." *Nature Photonics* 15, 608 (2021).
- [11] Gui *et al.* "Single-frame characterization of ultrafast pulses with spatiotemporal orbital angular momentum." *ACS photonics* 9, 2802 (2022).
- [12] Yessenov *et al.* "Space-time wave packets localized in all dimensions." *Nature Communications* 13, 1 (2022).
- [13] Kondakci *et al.* "Optical space-time wave packets having arbitrary group velocities in free space." *Nature Comm.* 10, 1 (2019).
- [14] Ferreira *et al.* "Roadmap on optical sensors." *Journal of Optics* 19.8, 083001 (2017).
- [15] Forbes *et al.* "Classically entangled light." *Progress in Optics*. Vol. 64. Elsevier 99-153 (2019).
- [16] Berg-Johansen *et al.* "Classically entangled optical beams for high-speed kinematic sensing." *Optica* 2, 864 (2015).
- [17] Cox *et al.* "On the resilience of scalar and vector vortex modes in turbulence." *Opt. Express*. 24, 18105 (2016).



## **Thermo-mechanical and chemical properties of cornea with hybrid Raman-Brillouin spectroscopy.**

**Introduction:** The mechanical and chemical properties of the cornea are linked to ocular diseases and therapeutic procedures. Brillouin microscopy is a novel and emerging non-contact spectroscopic sensing technology that enables the measurement of viscoelastic properties of a material. Raman micro-spectroscopy on the other hand is a powerful non-invasive optical tool for bio-photonics research and sensing applications targeting the chemical properties of tissues.

**Purpose and Impact:** Collagen cross-linking using combined riboflavin/UVA treatment has been shown to increase the biomechanical rigidity of the cornea and has been used successfully for the treatment of progressive keratoconus. From morphological and biochemical investigations, a different degree of cross-linking for the anterior and posterior stroma by the treatment is suggested. The present study will seek to better evaluate this effect by testing the thermomechanical behavior.

**Methods:** In this project, we will present a hybrid spectroscopic technique for cornea thermal-mechano-chemical properties and microstructure analysis that combines Brillouin and Raman spectroscopies with confocal microscopy into a single bio-imaging modality. This hybrid integrated approach to bio-sensing enables probing mechanical and chemical properties of the cornea simultaneously in a non-contact and non-invasive fashion with micrometer spatial resolution using a single laser probing source. Additionally, corneal anisotropy will be tested at different collagen orientations of the cornea. An automated data analysis technique will be developed for fitting the data which will allow fast and accurate spatial integrated mapping of Brillouin and Raman spectral peaks (position, linewidth, and intensity). Spectral images at different temperatures will be further analyzed using machine learning algorithms for extraction of correlated mechano-chemical information of diseased and healthy cornea with micron-scale spatial resolution.

# Thermo-mechanical and chemical properties of cornea with hybrid Raman-Brillouin spectroscopy.

## 1. Literature review

Noninvasive microscopic imaging of cornea biomechanical and chemical properties is an important clinical indicator in ophthalmology, in particular for diagnostics and risk assessment of several clinical conditions of an eye including glaucoma [1], keratoconus [2], and different corneal diseases. Here we will use non-invasive and non-contact hybrid use of Brillouin and Raman micro-spectroscopies to visualize and quantify corneal thermo-mechanical and chemical properties on a micrometer spatial scale using the same incident laser source. An automated algorithm will be developed and applied to automatically fit scans collected from motorized scan mapping of Brillouin and Raman micro-spectra to quantify corneal microscale mechano-chemical properties at different temperatures.

There are several ocular diseases in the human eyes. Here is a brief description of the most common eye diseases. (1) Glaucoma is a disease that leads to blindness irreversibly. It is the second leading cause of blindness globally that accounts for 14% of world blindness [3]. It is commonly accepted that high intra leads to glaucoma. It is estimated that over 4 million Americans have glaucoma. Approximately 120,000 are blind from glaucoma, accounting for 9% to 12% of all cases of blindness in the U.S. Nur-Sultan is expected to have similar statistics and other less-developed areas in Kazakhstan might have higher rates [4]. (2) Keratoconus is common corneal dystrophy characterized by the progressive thinning of central and para-central stroma and the subsequent conical ectasia. It leads to irregular astigmatism, corneal scarring, keratocytes apoptosis, and even blindness. The National Eye Institute reports that the keratoconus is the most common corneal dystrophy in the United States (affecting about one of every 2,000 Americans) [5]. (3) Hyperopia (long-sightedness) and myopia (short-sightedness) are two very common optic problems. Aggressive myopia is associated with severe, even blind, ocular morbidities such as retinal detachment, posterior staphyloma with retinal degenerative change, maculopathy, cataracts, and glaucoma. Myopia causes the distance vision to appear blurred, while hyperopia causes the near vision to be unclear [6].

Ocular biomechanics plays an important role in eye diseases in particular glaucoma, keratoconus, and myopia. Biological materials are viscoelastic in nature. Viscoelastic materials exhibit both viscous and elastic responses under deformation. These types of materials are strain-dependent. Biological soft tissues also consist of a network of visco-elastic collagen fibers which are responsible for anisotropic mechanical behavior. The vast majority of cornea contains a dense connective tissue called stroma that provides 90% of corneal mechanical strength. Stroma is composed of nanometer-thick collagen fibrils that usually follow a wavy course packed into strands [7]. A lot of efforts have been devoted to understanding corneal collagen structural organization, as the network of the collagen fibers directly determines stromal biomechanical properties [8]. Almost a third of the biomechanical strength of the stroma is concentrated on the anterior part of the stroma due to increased interweaving of lamellae [9]. Change in soft tissue mechanical anisotropy that resulted from fibrillar remodeling is often an indication of disease. For example, laser in situ keratomileusis (LASIK) may lead to cornea ectasia due to a change in mechanical properties [10]. Corneal biomechanical characterization is a sustained topic of interest in the pertinent research community since the cornea is exposed to various external forces (dehydration, eye rubbing, etc.) and internal forces including intraocular pressure (IOP). Therefore, corneal mechanical

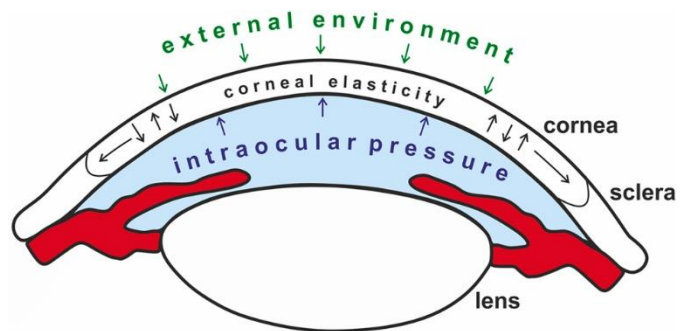


Figure 1. Scheme of relation between elasticity, external environment, and intraocular pressure.

Adapted from [11].



properties are manifested by tensile strength, elasticity, and the ability to maintain proper shape for stable visual perception (Figure 1) [11].

Conventional mechanical tests such as rheometry, nanoindentation, tension, and compression require forces to be applied to a material *in contact* with studied materials. Despite the comprehensiveness and high precision of such methods, they are not well suited for *in situ* noninvasive high-resolution measurements. Some evidence of corneal anisotropy, i.e. collagen orientation, has been applied using optical coherence elastography and tensile testing [12] but was limited to comparing elasticity in tangential directions [13]. Supersonic shear wave imaging has also been applied to quantify elastic anisotropy of the cornea but was limited with spatial resolution and sensitivity [14].

Laser-based Brillouin microscopy is an emerging imaging modality that allows non-contact and non-invasive direct readout of viscoelastic properties of cornea collagen fiber layers (lamellae) with high spatial resolution microscopy [15], [16]. This technique uses inelastic laser light scattering from stimulated or naturally occurring thermal acoustic waves (phonons) in the probed condensed medium. Brillouin spectral peak's position and linewidth represent the elastic and viscous response of probed medium, respectively. This enables measurements of spectral changes providing direct information on the mechanical properties which are related to GHz frequency viscoelastic properties of the material. Employing high resolution optical confocal microscope in conjunction with Brillouin spectroscopy and a focused laser beam, one can map viscoelastic properties with microscale spatial resolution. Brillouin microscopy has been used to map corneal elastic properties in normal and keratoconus patients [17] and quantify the change in corneal mechanical properties induced by corneal collagen crosslinking [18].

Laser-based Raman spectroscopy is another optical technique used to determine non-invasively vibrational modes of molecules in their native state. Over the last decades, several investigators utilized Raman spectroscopy to analyze the mechanical response of mechanically loaded bone [19]–[21]. Fourier Transform Raman spectroscopy was used to investigate the mechanical properties of collagen structure [22]. *In vitro*, axial tension of collagen fibers was examined with laser Raman spectroscopy [23]. These studies represent that changes in the chemical composition of collagen fibers can be changed due to strains and Raman spectroscopy can detect those changes.

Recently, there is an increasing interest in simultaneous Brillouin and Raman light scattering investigations as a diagnostic sensing tool for biomedical applications [24]–[31]. Hybrid Brillouin-Raman spectroscopy was applied for simultaneous assessment of bone biomechanics and biochemistry from the same laser-probed areas [32]. Figure 2 shows a typical 2D mapping of Brillouin frequency shift of human femoral diaphysis. The sole use of Brillouin scattering has shown anisotropic properties of plant stems, silks, and solid-state materials, but to the best of our knowledge, hybrid Brillouin-Raman micro-spectroscopy has never been employed to analyze therm-mechano-chemical properties on micron spatial scale.

## 2. Problem Statement

Collagen cross-linking using combined riboflavin/UVA treatment has been shown to increase the biomechanical rigidity of the cornea and has been used successfully for the treatment of progressive keratoconus. From morphological and biochemical investigations, a different degree of cross-linking for the anterior and posterior stroma by the treatment is suggested. We will evaluate this effect by testing the thermomechanical and chemical behavior from the same laser source. The goal of the project is to develop and validate the hybrid Brillouin-Raman micro-spectroscopy technique for simultaneous non-contact assessment of viscoelastic and chemical imaging of cornea at various temperatures and apply machine learning techniques to analyze biomechanical and chemical profiles of a diseased and healthy cornea.

## 3. Outline of tasks/Work Plan

To research the project goal, the following objectives are set, which are broken down into two financial years (FY):

- 1) **FY 2023:** Brillouin micro-spectroscopy: viscoelastic (including anisotropic) analysis of probed cornea tissues correlated at temperatures from 20-100 °C. Raman micro-spectroscopy: chemical analysis of probed cornea tissues at temperatures from 20-100 Celsius.
- 2) **FY 2024:** Hybrid Brillouin-Raman single point micro-spectroscopy and automated scan mapping of mechano-chemical spectra from cornea tissues at 20-100 °C. Correlation of viscoelastic and chemical properties with the results obtained from separate Brillouin and Raman micro-spectroscopies. Automated machine learning-based algorithm for the analysis of mechano-chemical data from cornea.

The proposed project will be an experimental and image/data analysis study including subsequently three following steps:

Stage I: Measurement validation and protocol development for Brillouin spectroscopy at temperatures 60-100°C.

Stage II: Development of a new automated method for mapping Raman spectroscopy at temperatures 60-100°C.

Stage III: Integrated Brillouin-Raman micro-spectroscopy and imaging of the healthy and diseased cornea at temperatures 60-100°C.

During stage I (3-4 months), Brillouin micro-spectroscopy system with the microscope will be tested against sheep cornea at temperatures 60-100°C. Sheep eye globes will be purchased from a local slaughterhouse and sealed in an ice container at most 4 hours postmortem before experiments. The eyes will be treated according to the Declaration of Helsinki standards. Viscoelastic properties extracted from Brillouin data will be extracted using Sandercock Tandem Fabry-Perot Interferometer (JRS instruments, Switzerland) and then cross-validated against viscoelastic values taken using virtually imaged phased array (VIPA)-based Brillouin spectrometer (Light Machinery, Canada); See section 6 for details. All experimental results will be protocolled for further evaluation of the cornea according to existing guidelines and protocols [28], [33], [34]. Our preliminary study of the cornea showed that eye viscoelastic material properties are an important factor affecting eye diseases [35]. These optical measurement techniques should be adjusted and validated to develop the best possible protocol for corneal anisotropy assessment.

During stage II (7 months) Raman micro-spectroscopy system will be used to test sheep corneas at temperatures 60-100°C. Raman spectroscopy technique provides chemical information with a high spatial resolution (<1µm) [36]. Surface-Enhanced Raman Scattering (SERS) will be performed to enhance Raman signals [37]. Sample maps will be obtained using a high-end Horiba Labram microscope/spectrometer with 785 and 633 nm laser excitation. Obtained results will be cross-validated with the SOL Instruments Raman spectrometer.

During the stage III (10-12 months) hybrid Brillouin-Raman single point micro-spectroscopy will be performed at temperatures 60-100°C. VIPA Brillouin spectroscopy will be integrated with Raman spectroscopy (SOL Instruments). An automated mapping algorithm of mechano-chemical spectra from cornea tissues will be developed that will allow a reliable way to extract the intensity of the Raman bands and the spectral peak position (elasticity) and spectral linewidth (viscosity) of the Brillouin peaks based on the calculation of spectral moments [38]. This method can be employed for simultaneous mapping to get 2D and 3D images of mechano-chemical properties of a diseased and healthy cornea. It will be helpful for an accurate fitting of the Raman-Brillouin data for mapping applications. The fitted imaging datasets of corneal mechano-chemical mapping will be further analyzed to automatically extract spectroscopic data using machine learning algorithms to characterize cornea biomechanics. In this stage, we will use various multivariate algorithms that can be employed to perform supervised and unsupervised image analysis applications, namely, segmentation, classification, unmixing, and image enhancement in the cornea to reveal collagen patterns. Image patterns of corneal biomechanics can be used for diagnostic applications of eye diseases described in Introduction section. Hybrid Brillouin-Raman experimental

measurement results will be cross-validated by separate Raman-Brillouin measurements from stage I and stage II.

**Ethics statement** – our project is strongly committed to complying with the ethical policy. We pledge that information presented in the framework of this project is unique and reliable. We confirm our devotion to research ethics, particularly avoiding any falsification and fabrication of research data resulting in fake authorship, inaccurate research data, and plagiarism. All work within the project will be operated in agreement with national and international ethical and legal standards. PI will follow health, ethical, and safety guidelines. The information obtained by this project will be entirely published via conventional academic channels such as national and international conference presentations and scientific publications. The results of the project will be published in reputable peer-reviewed scientific journals of international standing.

#### **4. Outcome and impact**

In this project, we will employ Brillouin spectroscopy to characterize the viscoelastic properties of the cornea, where measurement will be combined with Raman spectroscopy, both to be implemented on a micrometer spatial scale using the same focused laser light. We will also develop a new method for automated data fitting which will result in image maps of Raman and Brillouin spectral peaks (intensity, linewidth, and positions) for a comprehensive analysis of spectral features. This method will be suitable for 2D and 3D mapping applications for semi-transparent bio-tissues at different temperatures. The aim of the present study was to demonstrate the difference in the degree of cross-linking between the anterior and posterior stroma by investigating the thermomechanical shrinkage behavior because cross-linking results in less shrinkage after heat denaturation. The novelty of this project would be to develop a dual Brillouin-Raman spectroscopy method and apply it to characterize corneal thermal mechano-chemical denaturation. Another novelty is a new automated method for fitting which will result in 2D, and 3D mapping from the spectroscopic scans to get images of corneal thermos-mechanical and chemical profile which will demonstrate the crosslinking effect in the anterior stroma by the increased maximum shrinkage temperature of the cross-linked collagen in the anterior portion of the crosslinked cornea. The limitation of the cross-linking effect to the anterior stroma is advantageous for the treatment because the endothelium is spared and the stiffening effect is greater at the surface and in the anterior portion of the cornea, which is most important for stabilizing the corneal curvature.

#### **5. Project management**

The composition of the research group is drawn up according to table 1.

**PI – Dr. Chingis Kharmyssov** has received Ph.D. in Science, Engineering, and Technology with a focus on Biomedical Engineering from Nazarbayev University (NU), Kazakhstan in 2020. He has also a Master of Science in Medical Physics from the University of Aberdeen in the UK. During his Ph.D. studies, he has developed eye models for characterizing eye biomechanics. He has also experience in developing algorithms for medical image analysis.

**Scientific consultant – Dr. Zhandos Utegulov** is an Associate Professor in the Department of Physics at the School of Science & Technology of Nazarbayev University (NU) in Nur-Sultan, Kazakhstan. He earned his Ph.D. degree in Physics from Oklahoma State University, the USA in 2003. From 2003 to 2011, he has held R&D appointments at the University of Cincinnati, National Institute of Standards and Technology in Boulder -Colorado, University of Nebraska-Lincoln, and Idaho National Laboratory in the US. Since 2011 he has been directing Advanced Materials Research and Laser Technology (AMRELAT) Laboratory at NU. His R&D portfolio includes laser-optical sensing of materials (including biomaterials) with a focus on laser-matter interaction at various Spatio-temporal scales, laser-based materials characterization & development of fast and ultrafast time-resolved laser-acoustic and photo-thermal sensing techniques, Brillouin and Raman laser light scattering and surface plasmon-enhanced spectroscopies for diverse research & industrial applications. He has more than 60 publications and serves as a reviewer for the Journal of Biomedical Optics, Biomedical Optics Express, and other leading journals. He will perform advisory consultations with Brillouin micro-spectroscopy and

integrate Brillouin and Raman microscopy sensing platforms for monitoring of visco-elastic and chemical properties of the cornea.

## 6. Bibliography

- [1] R. Vinciguerra *et al.*, “Corneal biomechanics and biomechanically corrected intraocular pressure in primary open-angle glaucoma, ocular hypertension and controls,” *Br. J. Ophthalmol.*, vol. 104, no. 1, 2020, doi: 10.1136/bjophthalmol-2018-313493.
- [2] F. X. Crahay, G. Debellemanni re, S. Tobalem, W. Ghazal, S. Moran, and D. Gatinel, “Quantitative comparison of corneal surface areas in keratoconus and normal eyes,” *Sci. Rep.*, vol. 11, no. 1, 2021, doi: 10.1038/s41598-021-86185-3.
- [3] S. Kingman, “Glaucoma is second leading cause of blindness globally.,” *Bull. World Health Organ.*, 2004, doi: /S0042-96862004001100019.
- [4] L. Tashtitova and N. Aldasheva, “Study of the Prevalence of Glaucoma in Kazakhstan,” *Klin. Monbl. Augenheilkd.*, vol. 239, no. 2, 2022, doi: 10.1055/a-1327-3999.
- [5] NIH, “Facts About the Cornea and Corneal Disease | National Eye Institute,” <https://nei.nih.gov/health/cornealdisease>, 2016.
- [6] S. M. Saw, G. Gazzard, E. C. Shin-Yen, and W. H. Chua, “Myopia and associated pathological complications,” *Ophthalmic and Physiological Optics*, vol. 25, no. 5. 2005, doi: 10.1111/j.1475-1313.2005.00298.x.
- [7] T. Ushiki, “Collagen fibers, reticular fibers and elastic fibers. A comprehensive understanding from a morphological viewpoint,” *Archives of Histology and Cytology*, vol. 65, no. 2. 2002, doi: 10.1679/aohc.65.109.
- [8] K. M. Meek and C. Knupp, “Corneal structure and transparency,” *Progress in Retinal and Eye Research*, vol. 49. 2015, doi: 10.1016/j.preteyeres.2015.07.001.
- [9] S. J. Petsche, D. Chernyak, J. Martiz, M. E. Levenston, and P. M. Pinsky, “Depth-dependent transverse shear properties of the human corneal stroma,” *Investig. Ophthalmol. Vis. Sci.*, vol. 53, no. 2, 2012, doi: 10.1167/iovs.11-8611.
- [10] I. G. Pallikaris, G. D. Kymionis, and N. I. Astyrakakis, “Corneal ectasia induced by laser in situ keratomileusis,” *J. Cataract Refract. Surg.*, vol. 27, no. 11, 2001, doi: 10.1016/S0886-3350(01)01090-2.
- [11] P. Mlyniuk, E. Maczynska-Walkowiak, J. Rzeszewska-Zamiara, I. Grulkowski, and B. J. Kaluzny, “Probing biomechanical properties of the cornea with air-puff-based techniques - An overview,” *Advanced Optical Technologies*, vol. 10, no. 6. 2021, doi: 10.1515/aot-2021-0042.
- [12] A. Elsheikh, M. Brown, D. Alhasso, P. Rama, M. Campanelli, and D. Garway-Heath, “Experimental assessment of corneal anisotropy,” *J. Refract. Surg.*, vol. 24, no. 2, 2008, doi: 10.3928/1081597x-20080201-09.
- [13] M. Singh *et al.*, “Investigating elastic anisotropy of the porcine cornea as a function of intraocular pressure with optical coherence elastography,” *J. Refract. Surg.*, vol. 32, no. 8, 2016, doi: 10.3928/1081597X-20160520-01.
- [14] T. M. Nguyen, J. F. Aubry, M. Fink, J. Bercoff, and M. Tanter, “In vivo evidence of porcine cornea anisotropy using supersonic shear wave imaging,” *Investig. Ophthalmol. Vis. Sci.*, vol. 55, no. 11, 2014, doi: 10.1167/iovs.14-15127.
- [15] G. Scarcelli and S. H. Yun, “Confocal Brillouin microscopy for three-dimensional mechanical imaging,” *Nat. Photonics*, vol. 2, no. 1, 2008, doi: 10.1038/nphoton.2007.250.
- [16] A. M. Eltony, P. Shao, and S.-H. Yun, “Measuring mechanical anisotropy of the cornea with Brillouin microscopy,” 2021, doi: 10.1117/12.2584263.
- [17] G. Scarcelli, S. Besner, R. Pineda, P. Kalout, and S. H. Yun, “In Vivo Biomechanical Mapping of Normal and Keratoconus CorneasIn Vivo Biomechanical Mapping of CorneasLetters,” *JAMA*

*Ophthalmol.*, vol. 133, no. 4, 2015.

- [18] G. Scarcelli, S. Kling, E. Quijano, R. Pineda, S. Marcos, and S. H. Yun, "Brillouin microscopy of collagen crosslinking: Noncontact depth-dependent analysis of corneal elastic modulus," *Investig. Ophthalmol. Vis. Sci.*, vol. 54, no. 2, 2013, doi: 10.1167/iovs.12-11387.
- [19] M. Khalid, T. Bora, A. Al Ghaithi, S. Thukral, and J. Dutta, "Raman spectroscopy detects changes in bone mineral quality and collagen cross-linkage in staphylococcus infected human bone," *Sci. Rep.*, vol. 8, no. 1, 2018, doi: 10.1038/s41598-018-27752-z.
- [20] B. R. McCreadie *et al.*, "Bone tissue compositional differences in women with and without osteoporotic fracture," *Bone*, vol. 39, no. 6, 2006, doi: 10.1016/j.bone.2006.06.008.
- [21] S. Gamsjaeger, B. Buchinger, R. Zoehrer, R. Phipps, K. Klaushofer, and E. P. Paschalis, "Effects of one year daily teriparatide treatment on trabecular bone material properties in postmenopausal osteoporotic women previously treated with alendronate or risedronate," *Bone*, vol. 49, no. 6, 2011, doi: 10.1016/j.bone.2011.08.015.
- [22] M. Gasior-Głogowska *et al.*, "FT-Raman spectroscopic study of human skin subjected to uniaxial stress," *J. Mech. Behav. Biomed. Mater.*, vol. 18, 2013, doi: 10.1016/j.jmbbm.2012.11.023.
- [23] Y. N. Wang, C. Galiotis, and D. L. Bader, "Determination of molecular changes in soft tissues under strain using laser Raman microscopy," *J. Biomech.*, vol. 33, no. 4, 2000, doi: 10.1016/S0021-9290(99)00194-3.
- [24] S. Mattana *et al.*, "Non-contact mechanical and chemical analysis of single living cells by microspectroscopic techniques," *Light Sci. Appl.*, vol. 7, no. 2, 2018, doi: 10.1038/lsa.2017.139.
- [25] F. Scarponi *et al.*, "High-performance versatile setup for simultaneous Brillouin-Raman microspectroscopy," *Phys. Rev. X*, vol. 7, no. 3, 2017, doi: 10.1103/PhysRevX.7.031015.
- [26] Z. Meng, S. C. Bustamante Lopez, K. E. Meissner, and V. V. Yakovlev, "Subcellular measurements of mechanical and chemical properties using dual Raman-Brillouin microspectroscopy," *Journal of Biophotonics*, vol. 9, no. 3. 2016, doi: 10.1002/jbio.201500163.
- [27] S. Aitekenov *et al.*, "Raman, Infrared and Brillouin Spectroscopies of Biofluids for Medical Diagnostics and for Detection of Biomarkers," *Crit Rev Anal Chem .*, pp. 1–30, 2022.
- [28] A. Gaipov *et al.*, "Development and validation of hybrid Brillouin-Raman spectroscopy for non-contact assessment of mechano-chemical properties of urine proteins as biomarkers of kidney diseases," *BMC Nephrol.*, vol. 21, no. 1, 2020, doi: 10.1186/s12882-020-01890-x.
- [29] S. Aitekenov, A. Gaipov, and R. Bukasov, "Review: Detection and quantification of proteins in human urine," *Talanta*, vol. 223. 2021, doi: 10.1016/j.talanta.2020.121718.
- [30] A. Rakymzhan, T. Yakupov, Z. Yelemessova, R. Bukasov, V. V. Yakovlev, and Z. N. Utegulov, "Time-resolved assessment of drying plants by Brillouin and Raman spectroscopies," *J. Raman Spectrosc.*, vol. 50, no. 12, 2019, doi: 10.1002/jrs.5742.
- [31] D. Akilbekova *et al.*, "Brillouin spectroscopy and radiography for assessment of viscoelastic and regenerative properties of mammalian bones," *J. Biomed. Opt.*, 2018, doi: 10.1117/1.jbo.23.9.097004.
- [32] M. A. Cardinali, M. Govoni, D. Dallari, S. Caponi, D. Fioretto, and A. Morresi, "Mechano-chemistry of human femoral diaphysis revealed by correlative Brillouin–Raman microspectroscopy," *Sci. Rep.*, vol. 10, no. 1, 2020, doi: 10.1038/s41598-020-74330-3.
- [33] Z. Coker, M. Troyanova-Wood, A. J. Traverso, T. Yakupov, Z. N. **Utegulov**, and V. V. Yakovlev, "Assessing performance of modern Brillouin spectrometers," *Opt. Express*, vol. 26, no. 3, 2018, doi: 10.1364/oe.26.002400.
- [34] D. Akilbekova, T. Yakupov, V. Ogay, B. Umbayev, V. V. Yakovlev, and Z. N. **Utegulov**, "Brillouin light scattering spectroscopy for tissue engineering application," 2018, doi: 10.1117/12.2289923.
- [35] C. **Kharmyssov**, Y. G. Abdildin, and K. V. Kostas, "Optic nerve head damage relation to intracranial pressure and corneal properties of eye in glaucoma risk assessment," *Med. Biol. Eng. Comput.*, 2019, doi: 10.1007/s11517-019-01983-2.

- [36] M. Tanaka and R. J. Young, "Review Polarised Raman spectroscopy for the study of molecular orientation distributions in polymers," *Journal of Materials Science*, vol. 41, no. 3, 2006, doi: 10.1007/s10853-006-6595-7.
- [37] S. B. Ikramova *et al.*, "Surface-Enhanced Raman Scattering from Dye Molecules in Silicon Nanowire Structures Decorated by Gold Nanoparticles," *Int. J. Mol. Sci.*, vol. 23, no. 5, 2022, doi: 10.3390/ijms23052590.
- [38] H.-H. Chen, Y. She, and Y. Lin, "Spectral moment measures for the analysis of acoustic swallowing evaluation," *J. Acoust. Soc. Am.*, vol. 146, no. 4, 2019, doi: 10.1121/1.5137362.

## EXECUTIVE SUMMARY

Preeclampsia affects approximately 4.6% of pregnancies and is the second leading cause of maternal mortality. It is characterized by elevated blood pressure and evidence of end-organ dysfunction, and the majority of deaths are considered preventable with early diagnosis and treatment. Unfortunately, the signs and symptoms of preeclampsia (1) are not specific to preeclampsia, (2) often represent late-stage disease, and (3) require laboratory evaluation, which may not be readily available in rural and low-resource settings. Luckily, a few alternate cardiovascular parameters have been identified that can accurately diagnose preeclampsia. Preeclampsia patients have increased arterial stiffness measured via the augmentation index (Alx) compared to normal and chronic hypertensive patients. Alx effectively measures the speed of the reflected systolic pressure wave, which returns faster in stiffer arteries and results in an increased Alx. In addition, patients with early-onset preeclampsia, which has higher morbidity and mortality and requires distinct patient management, have higher systemic vascular resistance (SVR) than patients with late-onset preeclampsia. Current Alx and SVR measurement tools require either invasive catheterization or specialized equipment with a trained operator. A low-cost, non-invasive, point-of-care (POC) device for measuring Alx and SVR is needed to enable improved preeclampsia screening for earlier diagnosis and improved patient outcomes.

The light-based time varying measurement performed in pulse oximetry, photoplethysmography (PPG), has shown potential to measure Alx and SVR non-invasively. PPG sensors are small, wearable, and inexpensive, enabling widespread use and continuous monitoring. Furthermore, near infrared wavelengths can be used to minimize influence of skin color which has been shown to affect the accuracy of visible wavelength PPG data. Unfortunately, PPG suffers from poor signal-to-noise ratio (SNR) and thus is not used clinically for diagnosis of cardiovascular indicators beyond heart rate. The poor SNR of PPG may be overcome by using speckle plethysmography (SPG), which measures changes in blood velocity. SPG creates a similar periodic signal as PPG during the cardiac cycle but with significantly higher signal contrast. Preliminary data collected by our group in swine suggest that Alx and SVR may be extracted from SPG data with higher SNR than PPG, overcoming a key barrier for use as a POC diagnostic.

We developed a custom wearable SPG sensor and conducted a feasibility study in a swine model (n=2) of controlled volume hemorrhage. We compared our SPG-based SVR against an invasive gold standard SVR measure and achieved a correlation coefficient of 0.91. As PPG-based Alx has already been validated to show strong correlation, we compared our SPG-based Alx against PPG-based Alx from high SNR PPG waveforms and achieved a correlation coefficient of 0.8. Based on this preliminary data, we hypothesize that high fidelity Alx and SVR parameters can be non-invasively extracted from a miniaturized, high SNR design of our wearable SPG sensor for POC diagnosis of preeclampsia. We will test our hypothesis as follows:

**Aim 1: Validate the ability of a miniaturized wearable SPG sensor to extract accurate SVR and Alx values in patients.** Aim 1a: Construct miniaturized high SNR SPG sensor: The current SPG sensor will be redesigned to have a wristwatch footprint, 24 hour battery life, bluetooth data transfer, and a second camera to increase SNR. Aim 1b: Validate miniaturized SPG sensor's performance in patients with intra-arterial catheters: The newly miniaturized SPG sensor will be tested in 40 patients undergoing intra-arterial catheterization procedures from which gold standard SVR and Alx values will be extracted to compare against SPG-based SVR & Alx values.

Upon successful completion, we will launch testing of the device in pregnant patients in high and low resource settings. Our wearable SPG sensor will be the first device to provide non-invasive and operator independent POC assessment of Alx and SVR for early detection of preeclampsia and identification of early-onset preeclampsia. The sensor has been specifically designed to be a simple, quantitative, continuous monitoring tool, with the goal to reach underserved patients with the greatest preeclampsia burden.



## LITERATURE REVIEW:

### **Most preeclampsia deaths are preventable yet thousands of women die annually:**

Preeclampsia affects approximately 5% of pregnancies worldwide. It is a hypertensive disorder of pregnancy characterized by elevated blood pressure (BP) and evidence of end-organ dysfunction (1). Preeclampsia is responsible for 10-15% of maternal mortality (2), resulting in approximately 50,000 deaths annually. Furthermore, troubling racial disparities have been observed in which African American women are more likely to die from preeclampsia and have increased risk of intrauterine fetal death compared with white mothers (3). In the United States, approximately 60% of maternal deaths caused by preeclampsia are considered preventable (4) with timely and appropriate treatment (5). In low resource settings, significant barriers impede prenatal care delivery (6). Sadly, this results in significant global disparities in maternal mortality and morbidity in low resource settings compared to wealthy countries (7).

**Treatment of preeclampsia:** The only cure for preeclampsia is delivery of the fetus. Delivery timing is dictated by carefully weighing the gestation age of the fetus (and consequently the chances of fetal survival) against the likelihood of maternal and fetal complications caused by preeclampsia (8). Antihypertensive medications can be prescribed to prevent stroke in the mother, and magnesium sulfate may be prescribed to prevent seizures. If the decision to deliver the fetus is made, antenatal corticosteroids are prescribed to expedite fetal brain and lung development in fetuses that are less than 34 weeks gestation to improve their chances of survival and to reduce morbidity (8). The optimum timing of these interventions is of paramount importance, as is the monitoring that illuminates the time-sensitive treatment path.

**Clinical methods of detection and their limitations:** In the US, preeclampsia is diagnosed based on a combination of elevated BP and evidence of end-organ dysfunction. Unfortunately, the signs and symptoms of preeclampsia are (1) not specific to preeclampsia, (2) often represent late-stage disease, and (3) require laboratory evaluation for diagnosis of end-organ dysfunction, which may not be readily available in low-resource settings. BP measurements are used to screen patients for preeclampsia, however elevated BP in preeclampsia is often labile, resulting in delayed diagnosis until disease severity increases. In addition, preeclampsia diagnosis requires knowing a patient's BP prior to 20 weeks gestation to distinguish between chronic hypertension, and chronic hypertension superimposed with preeclampsia. Many patients enter prenatal care late (> 20 weeks), complicating diagnosis.

**Novel diagnostic tools for preeclampsia:** Due to the difficulties with preeclampsia diagnosis, alternate diagnostic strategies are being pursued. An ideal diagnostic tool would have point-of-care (POC) capabilities, use no consumables, be low-cost, non-invasive, and could be used and operated by a low-skilled worker. Researchers have pursued serum-based and urine based diagnostics (9), however these typically use consumables and many require high level lab facilities. In addition, a host of non-invasive BP monitors have been developed, however BP alone cannot be used to accurately diagnose preeclampsia (9).

Research has shown that preeclampsia patients have increased arterial stiffness compared to both normal and chronic hypertension patients as measured via the augmentation index (AIx) (10-12). AIx effectively measures the speed of the reflected systolic pressure wave, which returns faster in stiffer arteries and results in an increased AIx compared to normal and chronic hypertensive patients (13). AIx is typically performed using Applanation Tonometry which requires a skilled operator trained in using a tonometer (14). Despite its consistent findings in preeclampsia patients (10-13), AIx is not routinely performed during prenatal visits due to the added instrument complexity and requirement of a dedicated operator.

Clinical management of patients with early- and late-onset preeclampsia are distinct, thus distinguishing between these is important for optimum treatment and patient outcomes (11). Patients with early-onset preeclampsia, which is associated with higher morbidity and mortality,

have higher systemic vascular resistance (SVR), whereas patients with late-onset preeclampsia have normal or low SVR values (11). SVR is typically calculated by using invasive arterial catheters or echocardiography, however, invasive catheters are dangerous to insert during pregnancy for non-life threatening diagnostic reasons, and echocardiography requires a skilled operator, thus SVR is not routinely measured during pregnancy despite its consistent distinction between patients with and without preeclampsia.

Photoplethysmography (PPG) is a light-based technique that senses changes in blood volume throughout the cardiac cycle (15), and is the basis for optical heart rate monitors and pulse oximeters. Extensive research has been performed to mine PPG features for useful physiologic information beyond heart rate. Researchers have demonstrated that PPG can be used to measure Alx (systolic peak amplitude (y) divided by diastolic peak amplitude (x))(13), and SVR (width at half systolic peak height (W) (13)), (top right plot of **Figure 1**). Although these measures can provide accurate information under certain conditions (14), PPG has a number of limitations: 1) noisy PPG waveforms reduce accuracy of PPG-extracted features and necessitate extensive filtering which can introduce errors into the PPG waveforms (14, 15); 2) PPG has low signal-to-noise ratio (SNR) in instances of low perfusion (such as in patients with Raynaud's phenomenon which affects up to 16% of women (16)); 3) PPG is most often measured on a fingertip, an extremely peripheral location which can overwhelm the signal of the arterial vasculature and lead to inaccurate results (13); and 4) Pulse oximeters based on PPG signals have been shown to perform poorly in patients with highly pigmented skin which could further contribute to unacceptable maternal health racial disparities(17). Due to these limitations, PPG based devices are not clinically used beyond heart rate monitoring and pulse oximetry.

**PROBLEM STATEMENT: There is a critical unmet need for simple, inexpensive POC tools that enable early preeclampsia diagnosis and monitoring to guide timely treatment.**

**OBJECTIVE: Develop a wearable light-based sensor to measure and monitor Alx and SVR that overcomes the current PPG-based measurement limitations for early detection and monitoring of preeclampsia in high and low resource settings.**

### **OUTLINE OF TASKS/WORK PLAN**

**Proposed solution:** Our device uses a wearable form of laser speckle imaging. In this imaging method, interactions between coherent light and tissue result in constructive and destructive interference of coherent wave fronts that generate light and dark spots called "speckle." Moving particles have high speckle fluctuation, which causes the speckles to blur during data capture<sup>36</sup>. Laser speckle contrast ( $\kappa$ ) at a given pixel can be calculated by dividing the standard deviation of pixel intensity within a square window (e.g., 7 by 7 pixels) centered about that pixel by the mean intensity within the same window. This calculation is repeated for every pixel in the frame to provide a laser speckle contrast image. The inverse square of the laser speckle contrast image ( $1/\kappa^2$ ) defines the laser speckle flow index (LSFI), which is proportional to blood velocity and perfusion<sup>36-38</sup>. Determining LSFI at a rapid frame rate generates the speckle plethysmography (SPG) waveform that is sensitive to temporal changes in blood flow (15). Similar to PPG, SPG is information-rich and has features that can be extracted to quantify important physiologic parameters. The top right plot of **Figure 1** highlights example SPG features including Alx (ratio of systolic to diastolic peak amplitudes (y/x)) and SVR (pulse width of SPG waveform).

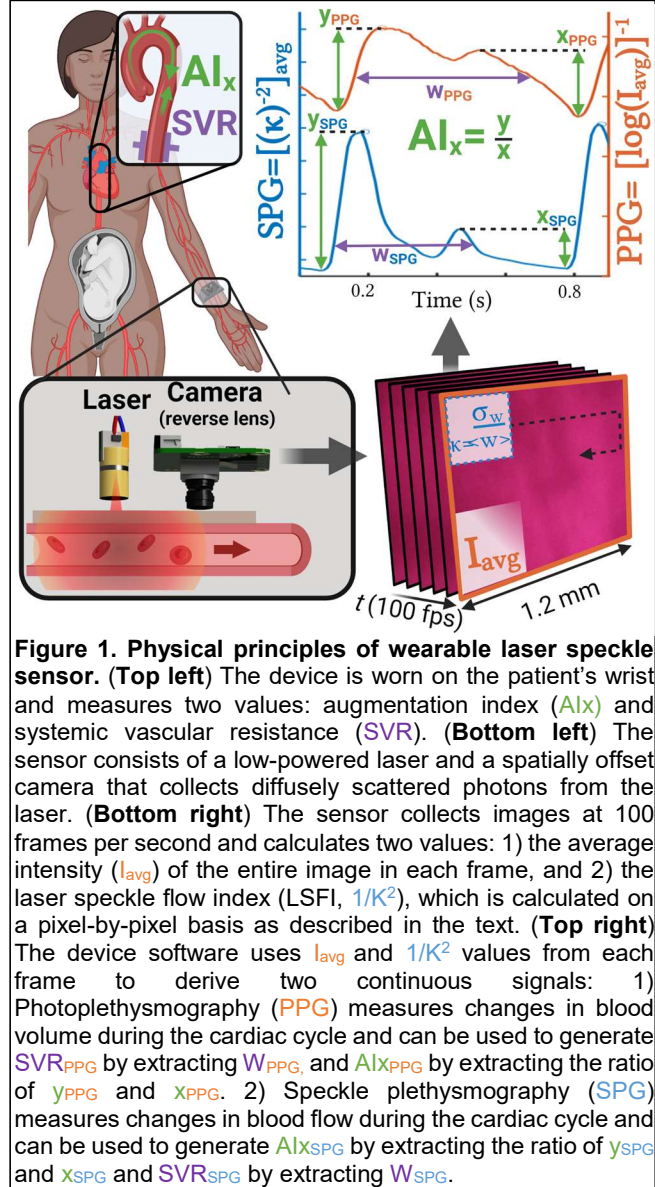
**Advantages over existing methodologies:** Limitations in current preeclampsia diagnostics include the use of consumables for serum and urine-based diagnostics, need for expensive equipment and skilled operators to extract diagnostic information, poor accuracy from non-invasive devices, and in the instance of PPG, noisy waveforms that lead to unreliable feature extraction that are further deteriorated by highly pigmented skin. Wearable SPG overcomes these limitations. Wearable SPG has significantly higher SNR than PPG and provides excellent signal quality, even in low perfusion states.(15) In addition, the physical principles of the laser speckle

phenomenon are minimally affected by skin pigmentation and we have chosen laser wavelengths ( $>750$  nm) that have minimal melanin absorption to further diminish any potential racial disparities. We have designed our wearable SPG sensor to measure the radial artery of the wrist, further reducing influence of extremely low perfusion often seen in the fingertips. Our wearable sensor is reusable and requires no consumables. Because it is completely external, the device can be wiped down with a sanitizing wipe between patients and then re-used. In parallel with hardware development, we are creating a user-friendly mobile app that a low-skilled healthcare worker can use to easily and accurately monitor for concerning SVR and AIx levels using our wearable SPG device. Finally, our device is low cost ( $< \$100$ ), extending use to low resource settings.

### Preliminary studies

**Wearable laser speckle sensor:** Our sensor uses a wearable form of laser speckle imaging. The SPG device is designed to be a low-cost, battery-powered sensor that mimics a wristwatch, and thus implements a reflectance-mode design. The current prototype consists of a 50 mW 780 nm laser diode module and a double-lens Raspberry-Pi camera sensor (**Figure 2**). Melanin absorption at 780 nm is minimal, thus we do not anticipate any difficulties in acquiring accurate data from patients with different levels of skin pigmentation. The laser module is incorporated into a custom circuit board that interfaces with a Raspberry Pi Zero 2W single board computer. The Raspberry Pi Zero 2W provides software-based control of the laser module and camera sensor, and performs real-time video capture and data processing. All components are powered by a rechargeable battery module that is connected to the computer board. The total device prototype costs less than \$100 and is designed to be lightweight and robust.

**Feasibility of AIx and SVR measurement:** We hypothesized that AIx and SVR could be extracted with high fidelity using SPG and demonstrated feasibility in a swine model of controlled volume hemorrhage ( $n=2$ ). For AIx, we performed correlation between the AIx values from high-quality PPG (signals had to meet a high SNR thresholds to be included for comparison) and SPG waveforms over paired time intervals. The correlation coefficient between the AIx values was  $R=0.8$ . For SVR, we calculated a gold standard SVR value by using an arterial and venous pressure catheter-based cardiac monitoring system and transthoracic echocardiography system. A correlation between our wearable SPG-derived SVR and the gold standard achieved an impressive correlation coefficient of  $R=0.91$ . These swine studies are ongoing, however, the AIx measures rely upon comparison against PPG (we do not have gold-standard AIx monitoring tools



**Figure 1. Physical principles of wearable laser speckle sensor.** (Top left) The device is worn on the patient's wrist and measures two values: augmentation index (AIx) and systemic vascular resistance (SVR). (Bottom left) The sensor consists of a low-powered laser and a spatially offset camera that collects diffusely scattered photons from the laser. (Bottom right) The sensor collects images at 100 frames per second and calculates two values: 1) the average intensity ( $I_{avg}$ ) of the entire image in each frame, and 2) the laser speckle flow index (LSFI,  $1/K^2$ ), which is calculated on a pixel-by-pixel basis as described in the text. (Top right) The device software uses  $I_{avg}$  and  $1/K^2$  values from each frame to derive two continuous signals: 1) Photoplethysmography (PPG) measures changes in blood volume during the cardiac cycle and can be used to generate  $SVR_{PPG}$  by extracting  $W_{PPG}$ , and  $AIx_{PPG}$  by extracting the ratio of  $y_{PPG}$  and  $x_{PPG}$ . 2) Speckle plethysmography (SPG) measures changes in blood flow during the cardiac cycle and can be used to generate  $AIx_{SPG}$  by extracting the ratio of  $y_{SPG}$  and  $x_{SPG}$  and  $SVR_{SPG}$  by extracting  $W_{SPG}$ .

in our swine facility), an imperfect measure of Alx.



Figure 2. CAD rendering and photos of wearable SPG prototype that was designed and built.

**Aim 1: Validate the ability of a miniaturized wearable SPG sensor to extract accurate SVR and Alx values in patients.**

**Aim 1a: Construct miniaturized high SNR SPG sensor:** The current wearable SPG sensor is bulky, has short battery life (2 hours), and does not have wireless data transfer capabilities, all of which limit clinical translation. Additionally, the hallmark feature of SPG is its high SNR, which can be increased with additional source-detector pairs.

**Miniaturized sensor development and benchmarking:** We will switch from using a Raspberry Pi-based microcontroller, camera, and battery, to a bluetooth-enabled ESP32 microcontroller, two ESP32 cameras, and a 400 mAh lithium-ion battery. To achieve a 24-hour battery life, we will reduce power consumption by 1) using shorter source-detector pair distances to increase photon capture, 2) using lower powered lasers, and 3) minimizing the amount of time that the laser is on. In addition, our current solderable perf board voltage regulator and laser driver circuits will be converted to surface mount PBCs. All components will be assembled into a 3D-printed housing with maximum dimensions of 30 mm width, 50 mm length, and 20 mm height. Bluetooth transfer of SPG waveforms will be established. Once fully assembled and operable, the device will measure static speckle from white cardstock paper, and the results will be compared against results from the existing SPG sensor and a bench-top laser speckle imaging system. The device will also be tested using a tissue-mimicking PDMS flow phantom that has a hollow channel connected to a syringe pump. The pump will push swine blood through the phantom at various flow rates to evaluate device sensitivity to known changes in blood flow, and performance will again be compared against a bench-top laser speckle imaging system. SPG SNR will be measured in a PDMS phantom with deep-seated channels to mimic low perfusion, and SPG SNR will be compared across the new sensor, the existing SPG sensor, and the benchtop system.

**Aim 1b: Validate miniaturized SPG sensor's performance in patients with intra-arterial catheters:**

Alx and SVR are significantly elevated in patients with preeclampsia and early-onset preeclampsia, respectively. Comparing SPG-based Alx and SVR against gold-standard values in patients will provide crucial data to inform future studies in pregnant subjects.

**Study population:** Patients scheduled for intra-arterial pressure catheter procedures will be recruited. We plan to exclude children (<18 years old) because the vast majority of catheterized patients are above 18 years of age, and less than 1% of pregnant subjects are < 18 years of age.

**Sample size estimation:** Assuming that the standard deviation of the difference is half of the mean difference, the study will have 80% statistical power at 0.1 alpha to detect a maximum allowed difference that is 2.35 times the mean difference with a sample size of 40. Washington University on average sees > 2 patients per week with the necessary intra-arterial catheters, thus we do not foresee difficulties in recruiting 40 patients over the course of 1-2 years.

**Study protocol:** IRB approval will be obtained prior to patient recruitment. Upon approval, patients will be enrolled using informed, written consent. Upon admission for catheter placement,



the miniaturized wearable SPG sensor will be placed on the patient's wrist. The SPG sensor and cardiac monitoring system will be synced in time to enable time-matched comparisons of SPG and gold standard Alx and SVR measurements. The sensor will acquire data for the duration of the procedure. Time-synced cardiac monitor data will be saved for subsequent analysis.

**Data processing and statistical analysis:** The SPG waveform will be extracted using our custom rapid-processing algorithm (patent pending). Alx (ratio of systolic to diastolic peak amplitudes (y/x) in SPG waveform) and SVR (pulse width of SPG waveform) will be extracted. Descriptive statistics will be generated to describe the study samples and data collected. The primary analysis for Aim 1b will include a comparison of Alx and SVR measurements using the SPG method as compared to the data collected by the gold standard method (Alx and SVR extracted from the intra-arterial pressure catheter waveform). Agreement between the two measurement methods will be quantified using a difference plot, the mean difference and the limits of agreement by Bland-Altman analysis.

Anticipated problems and alternate strategies: If Alx shows poor correlation with gold standard measures, we can instead use our SPG sensors to measure pulse wave velocity which has shown stronger correlation with arterial stiffness but requires measurement from two anatomic locations.

**OUTCOMES:** Upon completion, an ergonomic, miniaturized, high SNR wearable SPG sensor will have been developed to facilitate translation to patients. In addition, we will have characterized the accuracy of SPG-based Alx and SVR extraction from a gold standard patient study comparing against cardiac waveforms obtained from intra-arterial pressure catheters. This study will provide essential data to determine whether this device can be used for preeclampsia diagnosis. If high correlations are reached, these results will fuel investigation of the sensor in pregnant patients in both high and low resource settings, including partnership with existing collaborators in Nigeria where preeclampsia is the leading cause of severe maternal outcomes.

**IMPACT:** Our wearable SPG sensor is a highly innovative technology that has the potential to shift clinical practice during pregnancy, helping to save lives and reduce preventable maternal morbidity and mortality across the globe. Our sensor will serve to identify early features of preeclampsia and identify patients with early-onset preeclampsia who have the highest risk for morbidity and mortality and who are managed differently than late-onset preeclampsia. Wearable SPG has the potential to provide preeclampsia diagnosis in the absence of BP history and patient medical history, and without the need for lab assays for end-organ dysfunction, overcoming many of the current barriers to comprehensive preeclampsia screening/detection for pregnant patients. Our sensor will provide information that has not previously been obtainable in pregnant patients, with the potential to fundamentally change the standard of obstetric care. It can be worn throughout pregnancy or be thrown in a midwife's travel bag when visiting patients for antenatal care. In addition, it will open countless avenues for basic science research to help understand how and why preeclampsia happens and help to zero-in on mechanistic insights that can help explain the wide spectrum of pathophysiology and symptoms observed in preeclampsia patients.

**References:** **1)** O Erez et al., *AJOG* 226, (2022). **2)** B Sibai et al., *Lancet* 365, (2005). **3)** S Shahul et al., *Hypertens pregnancy* 34, (2015). **4)** EK Main et al., *Obstet & Gyn* 125, (2015). **5)** PS Bernstein et al., *Anesth Analg* 125, (2017). **6)** L Toledo-Jaldin et al., *Pregnancy Hypertens* 16, (2019). **7)** W Wang et al., *BMC Preg Childbirth* 21, (2021). **8)** ER Norwitz, *Preeclampsia: Antepartum management and timing of delivery*, UpToDate (2022). **9)** CE Majors et al., *Lab Chip* 17, (2017). **10)** MB Franz et al., *Acta Obstet Gynecol Scand* 92, (2013). **11)** G Masini et al., *AJOG* (2021). **12)** B Avni et al., *Blood Press* 19, (2010). **13)** M Elgendi, *Curr Cardiol Rev* 8, (2012). **14)** E von Wowern et al., *PLoS one* 10, (2015). **15)** M Ghijsen et al., *Biomed Opt Express* 9, (2018). **16)** R Garner et al., *BMJ open* 5, (2015). **17)** MW Sjoding et al., *NEJM* 383, (2020).

## **Germania Glass-based Optical Fiber and Light Source Technology for Green Photonics**

The broad objective of the proposal is to develop exceptionally novel optical fiber and light source technology for the mid-infrared wavelength region by integrating novel fiber design, material (Germania glass), and fabrication technology. The important chemical compounds such as CO<sub>2</sub>, NH<sub>4</sub>, CO, N<sub>2</sub>O, and CH<sub>4</sub> display strong absorptions in this wavelength region. Therefore, optical fibers and light sources operating in this wavelength region are critical tools for applications such as efficient high-power fiber lasers, high-power beam delivery, spectroscopy, imaging, material characterization, sensing (environmental, gas, and illicit drugs), monitoring (pollution, industrial, and food control), medical diagnostic, and security.

This proposal will establish novel outside vapor deposition (OVD) technology to fabricate optical-grade pure Germania and Germania-Silica glass rods and tubes. The Germania glass inherits the properties of the Silica glass such as good mechanical strength, lower susceptibility to moisture, lower reflection coefficients, higher power damage threshold, easy handling, and processing, therefore, outperforms the other competitive glasses such as ZBLAN and Chalcogenides.

The pure Germania and Germania-Silica glass rods and tubes will allow the fabrication of different kinds of fibers. For fiber lasers, a Silica-Germania cladding with a Silica core will allow a high number of rare-earth ions and other dopant ions such as phosphorus and aluminum. This combination will demonstrate large-core fiber lasers with low NA leading to high power, high efficiency, photodarkening resistance, and good beam quality with thermal stability. For passive fibers, a fluorine-doped layer between pure Germania core and cladding can offer effective single-mode operation for a large effective area. The development of these Germania fibers will lead to the demonstration of the fiber couplers, which are mandatory for an integrated (free from bulk optics) optical device. This project will also form the basis fabrication of the hollow-core negative-curvature fibers using fabricated Germania tubes. The Germania glass in cladding will increase the low-loss transmission window up to 6 μm, which is limited up to 4 μm for Silica glass.

These paths-breaking development will open doors for novel light sources in 2 to 3 μm which can be extremely useful for several applications such as early forest detection, medical diagnostics, pollution monitoring, gas sensing, etc. The project can dramatically scale the utility of fiber optics technology and can demonstrate products suitable for commercialization. On the scientific front, this project will provide a novel tool to researchers for advanced scientific discoveries and building new instruments.



# Germania-glass based optical fiber and light source technology for green photonics applications

## Problem Statement/Overview

Silica glass-based optical fibers and light sources have proved their tremendous importance in the last few decades for different applications such as communication, medical diagnostics & treatments, spectroscopy, imaging, and sensing, etc. However, the higher losses at longer wavelengths ( $>2 \mu\text{m}$ ) limit its functionality. The high absorption offered by water above  $2 \mu\text{m}$  makes this wavelength region eye-safe and suitable for medical-surgery and Light Detection and Ranging (LIDAR) applications. Moreover, the crucial chemical compounds such as  $\text{CO}_2$  (2, 2.7, and  $4.26 \mu\text{m}$ ),  $\text{NH}_4$  (2.2-2.3 and  $2.9 \mu\text{m}$  bands),  $\text{CO}$  (2.3-2.4 and  $4.4\text{-}5.2 \mu\text{m}$ ),  $\text{N}_2\text{O}$  (2.85-2.9 and  $8 \mu\text{m}$ ), and  $\text{CH}_4$  (2.4, 3.3 and  $8 \mu\text{m}$ ) display strong absorptions in this wavelength region. Therefore, this wavelength region is critical for several green photonics applications such as multi-tone spectroscopy, photoacoustic imaging, sensing (environmental and illicit drugs), and monitoring (pollution, industrial, and food control) [1].

Germania inherits the properties of silica glass, such as good mechanical strength, lower susceptibility to moisture, lower reflection coefficients, higher power damage threshold, and easy handling and processing. The germania ( $\text{GeO}_2$ ) glass-based fiber is an attractive option for exploiting the 2 to  $3 \mu\text{m}$  wavelength range thanks to the shift of the intrinsic IR absorption and the impurity of the Ge-OH absorption bands to longer wavelength, ensuring lower losses [2-3].

Moreover, Germania offers a higher refractive index than silica. Therefore, Germania-Silica or Germania glass cladding will allow the Silica glass core to accommodate enough refractive index-raising dopants such as  $\text{Yb}^{3+}/\text{Er}^{3+}/\text{Tm}^{3+}/\text{P}^{5+}/\text{Al}^{3+}$  while maintaining a low refractive index between core ( $n_c$ ) and cladding ( $n_{\text{cladd}}$ ). These refractive indices raising rare-earth ions ( $\text{Yb}^{3+}/\text{Er}^{3+}/\text{Tm}^{3+}$ ) and co-dopant ions ( $\text{P}^{5+}/\text{Al}^{3+}$ ) are essential for lasing. However, power scaling of fiber lasers with good beam quality strictly demands  $n_c \sim n_{\text{cladding}}$ . The required  $n_c \sim n_{\text{cladding}}$ , limits the number of required critical dopants in the core. The co-doping of fluorine can reduce the refractive index of the core, but its incorporation in silica is limited. The current state-of-the-art silica glass-based (both core and clad) fiber lasers at  $1 \mu\text{m}$  suffer from photodarkening and thermal modal instability due to the limited number of  $\text{P}^{5+}/\text{Al}^{3+}$  ions. Similarly, fiber lasers at  $2 \mu\text{m}$  suffer from poor slope efficiency ( $< 60\%$  with respect to  $79\text{X nm}$  pumping), as the limited number of thulium ions does not allow a 2 for 1 cross relaxation phenomenon.

*Unfortunately, optical-quality Germania glass tubes and rods are not available commercially. The objective of this proposal is to establish “Germania-glass based optical fiber and light source technology for green photonics applications”. The key aims are:*

A1: To develop and demonstrate the high-yield outside vapor deposition process for fabrication of optical-grade and low-loss ( $< 2 \text{ dB/km @ } 2 \mu\text{m}$ ,  $5 \text{ to } 10 \text{ dB/km @ } 2.4 \mu\text{m}$ , and  $< 100 \text{ dB/km @ } 2.8 \mu\text{m}$ ) pure Germania and Germania-silica rods and tubes. [**Now non-existing**].

A2: To demonstrate the world’s first  $2 \mu\text{m}$  laser with laser slope efficiency  $\sim 75$  to  $80\%$  using uniform Germania-Silica Cladding and Silica core with enough number of  $\text{Tm}^{3+}$  and  $\text{Al}^{3+}$  dopants. [**Now non-existing**].

Based on the early results obtained here using this seed grant, I will apply for large budget grants to further accelerate the technology with the following aims:

B1: To demonstrate Germania-glass based Anti-Resonant Negative-Curvature Hollow-Core (ARNC-HC) fibers for low-loss transmission in 2 to  $6 \mu\text{m}$  wavelength region. [**Now non-existing**].

B2: To exploit developed fibers and light sources (rare-earth doped  $\text{Er}^{3+}/\text{Tm}^{3+}/\text{Ho}^{3+}$  lasers and broadband light sources) in 2 to  $3 \mu\text{m}$  wavelength region for different applications such as early forest detection, breathe analyzer, gas sensors, mid-infrared single photon sources and long-wave mid-infrared supercontinuum sources in collaboration with partners. [**Now non-existing**].

## Literature

Initially, the Germanium-core and cladding fiber was fabricated with an aim to compete with Silica fibers to open a new communication channel of around 2  $\mu\text{m}$ . However, the lowest transmission losses remain around 4 dB/Km at 2  $\mu\text{m}$ , much larger than  $\sim 0.15$  dB/Km for a standard Silica fiber at 1.55  $\mu\text{m}$ . In the early 80s, Takahashi *et al.* demonstrated Antimony ( $\text{Sb}_2\text{O}_3$ ) doped Germanium preforms (Germanium Core with antimony doping and Germanium cladding) fabricated using Vapor Axial Deposition (VAD) process [4-6]. The lowest loss such as 4 dB/Km and 15 dB/Km at  $\sim 2$   $\mu\text{m}$  and  $\sim 2.4$   $\mu\text{m}$  wavelength respectively were achieved for a  $\sim 70$   $\mu\text{m}$  core diameter [4-6]. The losses were significantly high  $> 50$  dB/Km beyond 2.5  $\mu\text{m}$  due to the significant number of  $\text{OH}^-$  ions ( $\sim 500$  ppb) incorporated. Moreover, these fibers have a conventional step-index profile and offer multi-mode propagation (multi-mode propagation deteriorates the beam quality and dramatically reduces the utility of light beam exiting the fibers).

Afterward, there were very limited attempts to improve Germanium fiber fabrication process due to the availability of matured silica fiber fabrication process for communication. Since then, doping of Germanium in Silica core fibers with Silica cladding to lower the losses and exploit high nonlinearity due to Germanium (Germanium has three times higher  $n_2$  (nonlinear refractive index coefficient) than silica) has been demonstrated using modified chemical vapour deposition (MCVD) [7-10]. Such fibers are commercially available. However, the doping level of Germanium has been limited to lower than 30 to 40 mol % in most of these demonstrations. In the last decade, researchers at Fiber Optics Research Center, Russia fabricated several Germanium core fibers (where mol % of Germanium varied from 50 mol % to 97 mol %) with silica cladding and exploited them for non-linear applications such as broad-band supercontinuum source and Raman fiber lasers [2,11]. The losses were more than 100 dB/km at 2.2  $\mu\text{m}$ .

The alternative glasses to Germanium are ZBLAN and Chalcogenide glasses. The ZBLAN-based Er-doped fiber lasers have been demonstrated at around 2.9  $\mu\text{m}$  [12]. However, ZBLAN and Chalcogenide fiber suffer from poor damage threshold and higher nonlinearity than Germanium, therefore it is not suitable for high peak power transmissions in the pulsed regime. Moreover, ZBLAN and Chalcogenide fiber suffer from poor resistance to environmental factors (such as moisture, etc.) and poor handling (very difficult to cleave, splice, etc.). ZBLAN and Chalcogenide fiber's overall life is much lower than Silica and Germanium and does not pose a reliable candidate for long-term operations. On the contrary, Germanium fiber offers better mechanical strength, lower susceptibility to moisture, lower reflection coefficients, higher power damage threshold, easy handling, and good compatibility with current state-of-the-art fiber splicers and cleavers. Therefore, the Germanium fiber offers an attractive alternative to the soft glass fibers for applications.

The hollow-core fiber is an alternative approach, where more than 99.8% of the light is guided in the air-core of the fiber and cladding usually consists of a single material. This type of fiber offers numerous advantages such as no material dispersion, non-linear effects, and transmission losses. The transmission losses are mainly limited by the attenuation limit of the cladding material and waveguide design. Recently, Silica based anti-resonant negative-curvature hollow-core (ARNC-HC) fibers have been demonstrated with a  $\sim 40$  dB/km at 4  $\mu\text{m}$  wavelength and the same is expected to increase up to  $\sim 690$  dB/km at 5  $\mu\text{m}$  due to increasing material absorption of the silica glass [13]. However, the substantially lower losses of the Germanium glass than the Silica glass can ensure a low-loss transmission window up to 6  $\mu\text{m}$  wavelength region. Unfortunately, there has been no initiative to fabricate Germanium-glass-based hollow-core fiber yet. There is great potential for Germanium-glass-based ARNC-HC fibers for offering low-loss transmission in the mid-infrared wavelength region, in addition to tremendous glass-quality advantages over soft-glasses hollow-core fibers.

***The last decade has seen a tremendous surge in mid-infrared light sources and hollow-core fibers. Therefore, it is suitable time to put efforts to improve the Germanium glass-based fiber technology for 2 to 3  $\mu\text{m}$  wavelength. OVD and VAD processes are known to offer a much higher yield than the MCVD process. In this proposal, we will develop novel OVD fabrication process recipes for low-loss and high-yield Germanium glass tubes and rods. We aim to reduce the  $\text{OH}^-$  ions in Germanium glass to lower than 50 ppb.***

## Early Results and Work plan

Figure 1 (a) shows the calculated losses (material and waveguide) of Germania-glass and Silica-glass based ARNC-HC fibers for varying gaps between rings at 6  $\mu\text{m}$  wavelength for 1.5  $\mu\text{m}$  ring thickness, 60  $\mu\text{m}$  diameter, and 6 rings. The Germania-glass ARNC shows a lower loss by a factor of  $\sim 33$ , making Germania glass fiber fairly useful for many applications such as sensing, spectroscopy, gas-filled lasers, and beam delivery.

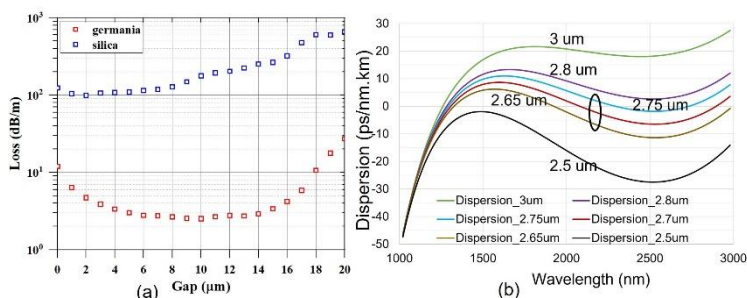


Figure 1(a) Calculated loss of Germania and Silica glass based ARNC fiber at 6  $\mu\text{m}$  wavelength (b) calculated dispersion for different germania-silica core and silica cladding fibers. [Author's group's result]

Figure 1(b) shows the calculated dispersion of a 70 mol % Germania and 30 mol% Silica core and  $\sim 100\%$  Silica cladding. For core diameter, varying from 2.65 to 2.7  $\mu\text{m}$ , fiber has three zero dispersion wavelengths leading to phase matching for four-wave mixing (FWM) to generate heralded single-photon sources between 2 to 3  $\mu\text{m}$ . To the best of the PI's knowledge, there has been no demonstration of a fiber-based mid-infrared single-photon source. The mid-infrared Single Photon sources can be useful for the long haul and secure optical communication through satellites at wavelengths that offer low atmospheric scattering and absorption. Other interesting applications include medical imaging at ultra-low light levels, quantum meteorology, quantum remote sensing, and quantum lidar.

Figure 2 shows a proposed large-core (large-mode-area), all-solid, pure-Germania core-cladding optical fibers for high-power beam delivery applications. Here, the core and cladding have the same refractive index, and both are pure-Germania glass separated by a Fluorine-doped Germania glass. The advantage of this proposed fiber over conventional step-index fiber is in terms of allowing an effectively single-mode operation ( $LP_{01}$  loss  $< 0.1$  dB/m and  $LP_{11}$  loss  $> 1$  dB/m) for a large-core diameter of 35 to 45  $\mu\text{m}$ , over 2 to 3  $\mu\text{m}$  wavelength region. This is the first proposal of an effectively single-mode, low-loss, large core diameter in this 2 to 3  $\mu\text{m}$  wavelength region respectively. The main motivation to propose this fiber design is the ease of fabrication, despite there being several other fiber designs for mode area scaling that can offer a better effective area. A layer of Fluorine-doped Germania can be deposited inside a Germania tube through a conventional modified chemical vapour deposition (MCVD) process using  $\text{GeCl}_4$  and  $\text{SF}_6/\text{SiF}_4$  as precursors. Afterward, a Germania rod can be inserted and collapsed (rod-in-tube technique) inside the tube after Fluorine-layer deposition. Once Germania fibers are available, the fused biconical tapering (FBT) technique can be used to make a coupler. Coupler brings flexibility, miniaturization, low-losses, immunity to external influences, and reliable alignment to an optical system.

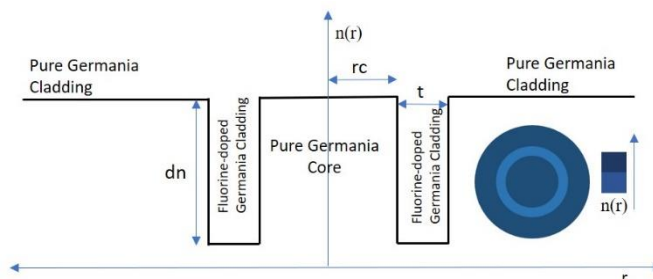


Figure 2 Large-mode, pure-Germania core-cladding, single-trench beam delivery fiber for 2 to 3  $\mu\text{m}$ .  $r_c$  is core radius,  $t$  is the thickness of the trench, and  $dn$  is the index difference between core and trench. Author's group's design.

These are novel results and designs and form the basis of this proposal. Once low-loss optical-grade Germania or Germania-Silica glass tubes and rods are ready, a wide range of fibers and light sources can be demonstrated for numerous green photonics applications.

The whole project will be divided into five work packages (WPs) as described below:

**Work Package (WP) 1: Numerical Modelling (0-24 Months):** The numerical simulations will be executed by running COMSOL Multiphysics software on a high-performance computer at IITB. I have

extensive experience in the numerical modelling of optical fibers. The detailed numerical study will determine the following objective:

**Milestone: M1, Deliverables: Two half-yearly reports (D1, D2).**

**WP2: Fabrication (0-24 Months):** The project aims to develop low-loss ( $< 2$  dB/km @  $2 \mu\text{m}$ , 5 to 10 dB/km@ $2.4 \mu\text{m}$ , and  $<100$  dB/km@ $2.8\mu\text{m}$ ) optical grade Germania glass rods and tubes using the OVD process. The fabrication will take place at the Optoelectronics Research Center (ORC), University of Southampton, UK. ORC has a current state-of-the-art OVD system (ref Fig 3). Preliminary work at ORC has demonstrated a 100 mol% Germania core and 100 mol% silica cladding fiber. However, the losses were significantly high ( $>100$  dB/km). There are the following challenges in the fabrication of high-volume and low-loss Germania glass using OVD: (a) thermal reduction of  $\text{GeO}_2$  to  $\text{GeO}$ , (b) formation of  $\text{GeO}_2$  crystalline phase in the soot body, (c) high  $\text{OH}^-$  incorporation due to unoptimized drying conditions, (d) halogenation of the  $\text{GeO}_2$  during the dehydration process.

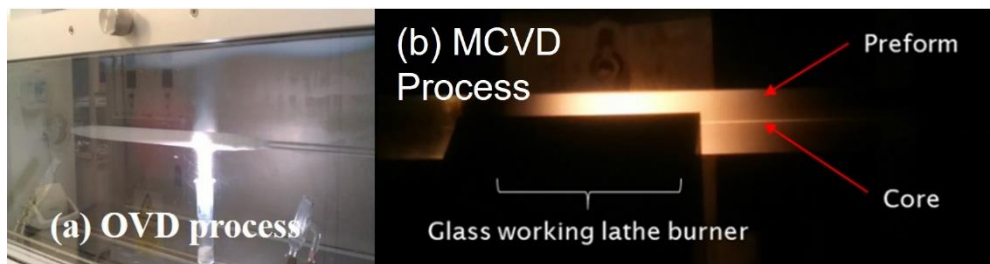


Figure 3(a) OVD process for 100% Germania (b) MCVD process for a 100% Germania core and 100% Silica Cladding. (Picture Source: ORC, Southampton, UK).

We will optimize the fabrication process by optimizing the deposition parameters (flow rate of  $\text{O}_2/\text{H}_2$ ,  $\text{SiCl}_4$ , and  $\text{GeCl}_4$ , soot deposition temperature, rotation speed of preform), and dehydration parameters ( $\text{He}/\text{Cl}_2/\text{O}_2$  atmosphere and temperature) to reduce  $\text{OH}^-$  incorporation in Germania (*lower than 50 ppb*), halogenation, and reduction of Germania glass, and consolidation parameters (temperature and He flow rate) to avoid devitrification. We will employ  $\text{O}_2$  rich atmosphere and low temperature during dehydration to avoid  $\text{GeO}_2$  halogenation. A low-temperature consolidation can mitigate the evaporation of  $\text{GeO}_2$ . *A collaboration letter from Prof. Jayanta Sahu is attached here.*

**Risk Mitigation Strategy:** The consumables budget to cover the multiple fabrication iterations is 18,750 USD. An additional budget of 10,000 USD has been reserved to cover more fabrication iterations in case required. *Dr. Peter Schultz (co-inventor of the first low-loss Silica glass fiber using the OVD process at Corning Corporation, USA) has also agreed to be a collaborator for this project and support letter is attached.*

**Milestones2: Demonstration of different Germania or Germania-Silica glass rods and tubes.**

**WP3: Characterization/testing (12-24 months):** Different material characterization techniques such as XRD, SEM, EDAX, and fiber refractive index profiles will be carried out to optimize the OVD process recipe. The simple step-index fiber will be drawn to measure the loss of Germania and Germania-silica cores. Once the low-loss Germania/Germania-Silica tubes will be ready, the Thulium-doped silica core fibers with silica-germania cladding will be fabricated using MCVD process and the solution doping process. Numerical simulations show that for a  $D_n \sim 0.001$  and core diameter  $\sim 46 \mu\text{m}$ , an effective-area  $\sim 1233 \mu\text{m}^2$  for the effective single-mode operation can be achieved at a coil diameter  $\sim 22$  cm for  $2 \mu\text{m}$  lasing. I was the key member of the team that first demonstrated the world's first highly thulium-doped silica (both core and clad) fibers to exploit the 2:1 cross-relaxation [14]. The laser slope laser efficiency of thulium doped fibers will be tested in a 4%-4% bulk optics laser cavity with respect to 790 nm pumping wavelength.

**Milestones: M3, Deliverables: Detailed characterization of different fabricated Germania glasses**

**Device, Application, and Future Exploration:** Applications for different grants will be applied based on early results obtained to construct devices and explore several green photonics applications over a



period of time. Based on approved funds, applications of fibers and amplifiers will be exploited in different domains such as beam delivery: testing of single-trench and ARNC-HC fibers to deliver high-peak-power laser beams (at 2 and 2.9  $\mu\text{m}$ ), gas-filled ARNC-HC fiber for broadband mid-infrared supercontinuum generation, gas sensors using quantum enhanced photo-acoustic spectroscopy (QEPAS), and breath-sensing device, and to pump different Chalcogenide fibers for long-wave mid-infrared supercontinuum sources in-house. An up-conversion mid-infrared detector can be used for detection.

### Impact and outcome

**New or advanced knowledge:** This project will establish the Germanium-glass-based optical fiber and light source technology to exploit the tremendous properties of the mid-infrared wavelength region such as “eye-safe”, “high-atmospheric transparency” and “molecular fingerprint”. The project will produce breakthroughs in developing next-generation “Outside Vapor Deposition” process matured enough to produce low-loss, Germanium core and cladding glass fibers, ARNC-HC Germanium glass fibers, and rare-earth doped highly-Germanium-Silica core and Silica cladding glass fibers.

This breakthrough in fiber fabrication technology will take the current mid-infrared optical fiber technology to the next generation level by offering low transmission losses, large bandwidth, a higher threshold for non-linear effects, good beam quality, outstanding chemical, thermal, and mechanical properties, low cost and suitability for industrial-scale production.

These matured Germanium fibers in mid-infrared wavelength will match the performance of the Silica fibers in the near-infrared wavelength region and will open pathways for high-peak-power pulsed beam delivery, ultra-high sensitivity for sensing and spectroscopy, and compact, high-power, efficient broadband mid-infrared light sources with unprecedented features for several green photonics applications such as early forest detection, breathe analysers, gas sensors, and long-wave mid-infrared supercontinuum sources.

**Economic, commercial, environmental, and health benefits for international communities:** The developed fibers and light sources will be of immediate interest to several companies in a billion-dollar laser applications industry, including TRUMPF (Germany), IPG Photonics (USA), Coherent Inc. (USA), nLight Inc. (USA), NKT Photonics (Denmark), and Lumentum (USA). The project is expected to lead to contracts with these global businesses for licensing of the proposed technology, as well as the potential for a start-up. The global market for the mid-infrared laser is expected to reach ~970 million USD by 2024 [15]. Additionally, potential commercialization pathways, including licensing and start-ups will be explored. The project will train students in optical fiber technology and contribute to the creation of a hi-tech workforce. Students and early researchers will be encouraged to join the project via several Govt. funding schemes. The joint work of the project team with different institutes and industries will result in significant technology and knowledge created in India, UK and other countries.

**Immediate Benefit to PI:** This project will help me to establish my group at IIT Bombay and convince the funding agencies to have a fiber fabrication facility here at IIT Bombay. All the attempts will be made to raise funds during and after the project through several schemes. The project is well aligned with the science and research priority of the Indian government’s Make in India mission.

### Reference

1. R. D. Maurer and **P. C. Schultz**, U. S. Patent 3884550 (1975).
2. E. M. Dianov *et al.*, “Germanium-based core optical fibers,” *J. Lightw. Technol.* 23, 3500-3508 (2005).
3. A. M. Stingel *et al.*, *J. Opt. Soc. Am. B* 34, 1163–1169 (2017).
4. H. Takahashi *et al.*, *Electron. Lett.* 18(10), 398-399 (1982).
5. H. Takahashi *et al.*, *Japanese Journal of Appl. Phys.* 22(3), L139-140 (1983).
6. H. Takahashi *et al.*, *JLT* 2(5), 613-616 (1984).
7. T. Okuno *et al.*, *IEEE J.S.T. Quantum Electron.* 5, 1385–1391, (1999)
8. J. W. Nicholson *et al.*, *Opt. Exp.*, vol. 12, pp. 3025–3034, 2004.
9. C. Xia *et al.*, *J. Sel. Top. Quantum Electron.* 13(3), 789–797 (2007).
10. LensLaser, Russia <https://lenlasers.com/>
11. E. A. Anashkina *et al.*, *IEEE Journal of Sel. Top. Quant. Electron.* 12, 7600608 (2014).
12. Fortin, V. *et al.*, *Opt. Lett.* 40, 2882-2885 (2015).
13. F. Yu *et al.*, *APL Photonics* 4, 080803 (2019).
14. P. C. Shardlow, **D. Jain**, R. Parker, J. Sahu, and W.A. Clarkson, *CJ* 14.3, in CLEO-Europe, Munich, Germany, June (2015).
15. Global Mid-Infrared Lasers Market 2019 by manufacturers, regions, type and application, forecast to 2024 SKU ID:GIR-13761522, published on 21-01-2019.

## EXECUTIVE SUMMARY

### DEVELOPMENT OF TUNABLE MULTI-COLOR LASER FOR SENSING: CASE STUDY FOR HYPERSPECTRAL DETECTION OF WATER CONTAMINANTS

Access to pollution free water is essential for humans and animals alike. It is from this point of view that photonic spectroscopic technologies have gained increased attention for water quality and environmental monitoring applications. The photonic technologies have the capability of detecting dissolved contaminants in clear water samples by way of inspecting optical water clarity. However, most of the well-established spectroscopic techniques such as spectrophotometry used in ongoing research at University of Eldoret require expensive instrumentation and are un-affordable. Therefore, the key motivating factor of this proposal lies in the ultrafast, sensitive optical detection of low levels of pollutants in clear water samples using a simple and cost-effective all-optical approach. Our long-term goal is to develop a multi-wavelength visible laser source generated through wavelength conversion for varied applications in water quality assessment, environmental monitoring and basic research. However, development of a tunable, multi-wavelength visible laser source remain unexplored and this proposal is an attempt to bridge the existing gap. We firmly believe that such a visible laser, once integrated in an optical communication system can find wide range of applications among them, water quality assessment. For instance, it is well known that the presence of contaminants in clear water sample causes optical absorption and/or fluoresces at certain wavelengths since most known substances have specific absorption spectra. Therefore, it is possible to tell the type of contaminant through their spectral ‘fingerprints’ because they can show strong absorption at particular wavelengths when a laser light interacts with the contaminated sample. Notably, some of the pollutants can be toxic even a low concentration and often difficult to detect.

The specific objectives are designed to provide a detailed design, fabrication and deployment of the multi-wavelength visible laser source for sensing applications. The specific objectives are to:

1. Design a step-chirped PPLN waveguide for tunable wavelength conversion in to the visible spectral range.
2. Investigate the tunability and wavelength broadening of the waveguide device.
3. Fabricate and characterize the compact monolithic multi-wavelength device.
4. Apply the generated wavelengths for detecting water contaminants in a laboratory set up.

Implementing this proposal will strengthen and broaden the applications of multiwavelength visible lasers to solve societal challenges such as in health and environmental monitoring just to name a few. For instance, an all-optical sensing system when used for water quality assessment can contribute to mitigation measures against water pollution, decrease waterborne illnesses and improve the quality of life. It is also expected that, upon completion of the project, the future career prospects of the participants will be enhanced. The project is expected to train two (2) MSc and one (1) PhD students. The research team will participate in scientific conferences, symposia and publish research findings in peer reviewed journals.



# Multi-core Polymeric Optical Fiber Sensors for Atraumatic Smart Cochlear Implantation

## Literature Review

Nearly 20% of the global population suffers from hearing loss [1,2]. It is considered the third most common chronic physical condition in the United States and is more prevalent than diabetes or cancer [3]. Rehabilitation of severe to profound hearing loss by means of cochlear implants (CIs) (Fig.1(a)) have substantially escalated since the introduction of these neuroprosthetics. Deploying an electrode array (EA) which is less than 1 mm in diameter through the round window (RW) and progressing down a 15-20 mm long tortuous cochlear lumen where the narrowest width is 2 mm, is challenging even for the most experienced surgeons. Any tactile sensation when in contact with the intracochlear membranes at this level requires force sensing capabilities which is beyond the limits of human tactile perception. The rupture force of the basilar membrane (BM) is 26-35 mN [4], but residual hearing is compromised even when the EA touches the membrane. Integration of a sensing device within the CI rather than external placement is vital due to the transmitted noise and the force attenuations caused by the flexible electrodes although, most studies have utilized external sensors in the measurements of tip or axial forces [5]. Furthermore, a single point measurement on the outside of the skull would not be able to isolate different forces (axial/lateral) experienced locally by the electrodes (at its tip or other specific localities on its sides). Hence, real-time assessment of insertion forces, position and shape of the CI are vital for atraumatic or minimally traumatic cochlear implantations and in the preservation of residual hearing.

Attempts to incorporate optical fibers in CIs for insertion measurements are rather sparse and the existing handful of studies have integrated silica-based fibers in CIs [6–8]. A fiber Bragg grating (FBG) inscribed in 125  $\mu\text{m}$  single mode fiber (SMF) has been utilized in a CI [6] where the tip force ranged from 75-225 mN which is far above the rupture force of the basilar membrane and exhibits a less force sensitivity. Furthermore, during CI insertions, the FBG based sensors are expected to navigate through critical bending radii due to the curvature of the cochlea, making the widely used 125  $\mu\text{m}$  SMF unsuitable due to its stiffness which increases the risk of trauma. Moreover, a uniaxial sensor [6], limits the information that can be retrieved in a complex 3-D geometry such as the cochlea which urges the need to develop specialty optical fibers capable of achieving shape sensing. By incorporating optical fibres in cochlear electrode arrays, measurements have been carried out to demonstrate the effect of buckling and deflection forces which affect the stiffness properties of the electrode arrays [9]. The study has been conducted on fibres with 125  $\mu\text{m}$ , 80  $\mu\text{m}$  and 50  $\mu\text{m}$  cladding diameters and concluded that 50  $\mu\text{m}$  fibres can be embedded inside an electrode array with the absence of significant changes in its stiffness properties. Furthermore, in the effort of evaluating the insertion forces of optical fibres in a cochlear model, [10] has reported that fibres with fibre diameters of 125  $\mu\text{m}$  experience breakage when inserted to depths of 7-15 mm in a scala tympani (ST) model.

In contrast to silica-based optical fibers, polymeric optical fibers (POFs) are increasingly popular among the research community due to their non brittle nature, biocompatibility, low Young's moduli with significantly low stiffness levels while possessing the same merits of silica-based fibers such as a light weight, immunity to electromagnetic interference and multiplexing capabilities [11]. Among the POFs, the recently revealed ZEONEX-based single core POFs (E48R core and 480R cladding) by the PI's research team permit FBG inscription in them within nanoseconds using a 248 nm UV laser [12]. These POFs are chemically inert, have low aptitude for moisture absorption and can survive temperatures of up to 132 °C [13] on the contrary to the widely used PMMA based POFs, which are prerequisites to be integrated within the CIs. The PI and her research team have a pending patent on this cutting-edge technology which overcomes stiffness complications of silica-based fibers with fiber sensors that are as soft and ductile as the CI and can aid in surgical navigation within the cochlear avoiding any potential trauma [14]. Hence, development of ZEONEX-based multi-core fibers (MCFs) inscribed with FBGs and integration of them in CIs can be considered as an appealing approach due to their myriad of benefits for real-time accurate measurements of the tip force, lateral forces, the position and orientation of the CI for atraumatic cochlear surgical interventions.

## Problem Statement/Objectives

1. Design and fabrication of low loss ZEONEX four-core single-mode MCFs with a diameter of

- 160  $\mu\text{m}$  and thinner.
2. Inscription and characterization of FBGs in ZEONEX MCFs and integration of them with CIs to evaluate tip force, lateral force, frictional force as well as curvature measurements.
  3. Develop a high precision optical fiber alignment setup to couple light from a single silica seven-core MCF to individual cores of the ZEONEX four-core MCF to detect reflection spectra of the inscribed FBGs in each core of it.
  4. Design and construct a measurement system using the optimized ZEONEX MCF inscribed with FBGs for real-time navigation experiments in a cochlear phantom.
  5. Develop algorithms to locate the CI position within the cochlear, and to aid surgeons to navigate the CI inside the cochlea during implantation.
  6. Perform trials on human temporal bones. This objective will be carried out at the Royal Victorian Eye and Ear Hospital, Melbourne and Dept. Otolaryngology, University of Melbourne.

### **Outline of tasks/Work Plan**

Positive results obtained from ZEONEX single core POFs integrated in experimental CIs (Fig.1(b-e)) motivates the development of low loss MCFs for cochlear implantation, permitting highly sensitive contact force measurements as well as shape sensing with increased accuracy. The fabrication of a CI, integrated with ZEONEX MCF, lies on meticulous adherence to technicalities which involves: (a) investigation of theoretical models and algorithms to calculate the contact forces (tip/lateral/frictional) and reconstruction of the shape for surgical navigation, (b) design and fabrication of ZEONEX MCFs with optimal core spacing configuration, low attenuation and small intrinsic twist, (c) development and characterization of the FBG sensors specifically inscribed for CIs, (d) construction and characterization of the CI (e) testing of the CI integrated with ZEONEX MCF to determine contact force and shape measurements in a cochlear phantom and human cadaveric cochleae (temporal bones).

#### **(a) Investigation of theoretical models and algorithms to calculate contact forces and shape reconstruction of the CI inside the cochlear [In parallel with parts (b)-(e)]**

Initially, a theoretical relationship between the measurands (i.e. tip force, shape) and the Bragg wavelength changes ( $\Delta\lambda_B$ ) in each core will be established. When the tip of the CI is in contact with the cochlear (Fig. 1(f)), force  $F$  is typically exerted from various directions, which consequently results in different degrees of compression in the fibre. Since the ZEONEX based MCF is fully embedded in the CI, any compression of the tip of the CI would induce strain (i.e. strain  $\epsilon_1, \epsilon_2, \epsilon_3, \epsilon_4$ ) on the MCF with a conversion coefficient  $\eta$  which will be experimentally calibrated. A model will be built to retrieve the tip force with respect to  $\Delta\lambda_B$  of all cores, and also to estimate the force angles  $\alpha$  and  $\beta$ , in 3D. With the advantage of multiple cores in ZEONEX MCF, the FBG arrays in it can detect strain along the CI from more than three degrees of freedom, which provides the necessary variables to reconstruct the shape of the CI in 3D. As opposed to conventional shape sensing realized using multiple fibres or MCFs where the shape of the entire fibre changes simultaneously, the CI during navigation typically starts to change its orientation in the segment that is being inserted. This means that the shape reconstruction model will change based on the inserted segment. The cochlear has a small bending radius varying from  $\sim 4$  mm to  $\sim 2$  mm [15], indicating that a large strain could be induced on the fiber. The theoretical analysis will account for the relationship between the spatial resolution, accuracy, grating separation and the insertion length. Shape of the MCF can be reconstructed using Frenet-Serret formulas by calculating the tangent ( $F_t$ ), normal ( $F_n$ ) and binormal ( $F_b$ ) vectors of the CI trace at each point of the FBG group (Fig.1(g)).

#### **(b) Design and fabrication of low loss, ZEONEX MCFs**

When approaching higher CI insertion depths ( $\sim 20$  mm), the bending loss of the fiber plays a vital role and will be investigated for the proposed MCF for bending radii as small as 2 mm. POFs have a much higher attenuation loss compared to their silica counter parts. The loss of PMMA-based POFs, especially doped PMMA POFs can have an attenuation loss as high as 100 dB/m which limits their usage in many practical applications. Preliminary analysis of bend spectral characteristics of ZEONEX-based single core FBGs have demonstrated an acceptable reflected peak power and a signal to noise ratio (SNR) with decreasing bending radii as shown in Fig.1(d). Nevertheless, to fabricate quality POFs to improve long-term reliability, certain alterations need to be carried out in the fabrication environment. One such modifications include purifying the raw ZEONEX material using an ionizer gas suspension

dedusting system together with N<sub>2</sub>. Oxygen present in the ZEONEX raw material reacts with it resulting in a high attenuation loss. This can be avoided by heating the raw material in a vacuum oven. Furthermore, the less stiff Teflon wire which is currently being used to create holes in the cladding preform which will subsequently be occupied with core canes, reduces the uniformity of the holes in the cladding preform. This will be optimized by using a rod with a higher stiffness (eg. ceramic rod) or by drilling the cladding preform. Spacing between the four cores of ZEONEX MCF will be matched to that of a seven-core silica MCF (eg. 36 μm or 42 μm) (Fig.1(h)) to be connected with a fan-out device.

**(c) Inscription and characterization of FBG sensors inscribed in ZEONEX MCFs**

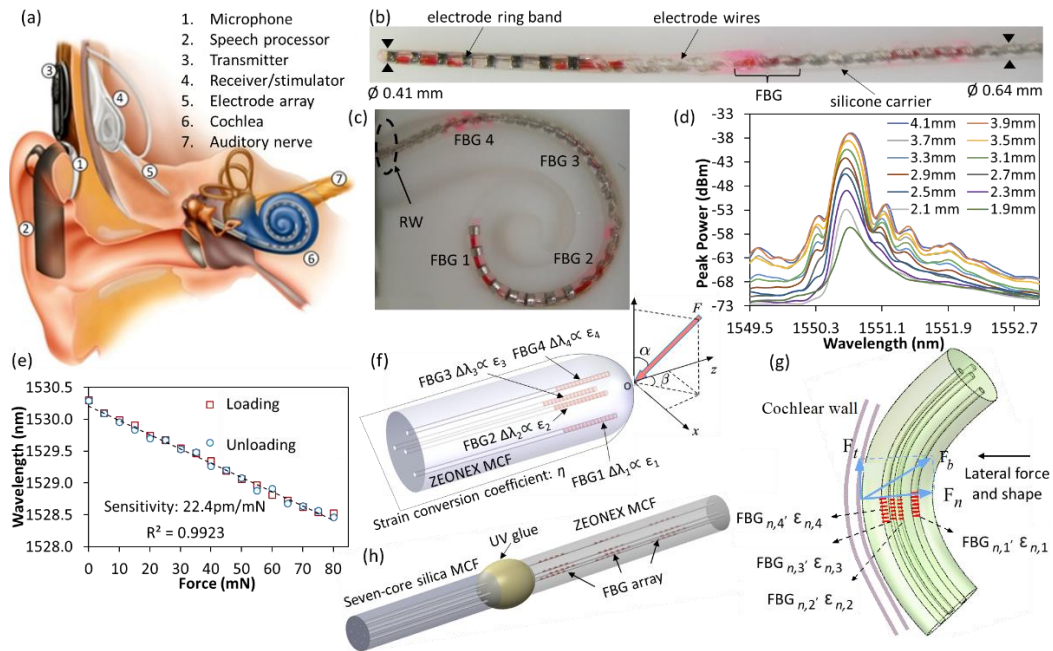
An array of FBGs with precise length, pitch as well as separation will be inscribed in the fabricated ZEONEX four-core MCFs with the aid of a 248 nm UV laser prior to integration with the CI. Since the length of the CI with electrodes is 20-30 mm, the number of groups of FBGs to be inscribed will be optimized to determine their optimal distribution along the fiber. Shorter grating lengths allow more FBGs to be inscribed in a fixed length of the fiber, which however, leads to a broader full width at half maximum (FWHM) of the reflection peak of the FBG, reducing the detection accuracy. Thus, there is a tradeoff between the number of FBGs to be integrated and the detection accuracy, which will be investigated in this project. To inscribe FBG arrays in all the cores of the fiber requires precise alignment of the laser beam. For example, after a group of FBGs at a certain position completes its inscription, the next group of FBGs at another position will commence its inscription process after switching to a phase mask with a different pitch compared to the one used to inscribe the former group. Separation between adjacent groups of FBGs is of utmost importance in this project, since it determines the spatial resolution of the reconstructed shape of the smart CI. A seven-core fiber fanout, will be incorporated to couple light to the four cores of the ZEONEX MCF in order to interrogate all the FBGs.

**(d) Construction and characterization of the smart cochlear implant**

A commercial CI with ~20 electrodes embedded in a silicone carrier with a diameter ranging from 0.4 mm to 0.6 mm is typically used in cochlear implantations. An experimental CI integrated with a ZEONEX single core POF fabricated by our collaborators in University of Melbourne, Australia is shown in Fig. 1(b). In this project, ZEONEX MCFs with FBG arrays will be integrated with the CI during the fabrication process. During CI fabrication, the first FBG will be placed exactly at the tip (within a 0.2 mm margin) of the implant. More electrodes tend to contribute to a larger stiffness increasing the rigidity of the CI, since each electrode is connected to a set of electrical wires to support frequency stimulation. The electrical wires can be arranged in a straight or spiral manner inside the silicone carrier, contributing towards a difference in the rigidity and flexibility of the CIs. Similarly, the introduction of ZEONEX MCFs with different diameters would change the mechanical properties of the CI, e.g. Young's modulus, which will be tested and analyzed in this project with respect to that of a bare CI. Furthermore, the stress profile of the CI integrated with ZEONEX MCF under various contact force values and deflections will also be simulated using COMSOL to investigate the impact of integrating the foreign element, ZEONEX MCF with the CI.

**(e) Evaluate tip, lateral force and shape in cochlear phantoms and human temporal bones**

This work can be divided into two parts: (1) force and shape measurement based on cochlear phantoms (Fig.1(c)) obtained from Cochlear Ltd (global CI manufacturer) using the smart CI; (2) conduct pre-clinical tests using the smart CI in human (cadaveric) temporal bones. To characterize the sensors, a high precision test rig with a multi-axis load cell will be constructed. The direction of the applied force should be distinguished with this test rig so that the FBGs at the CI tip can quantify force as well as the angle. During trials inside the cochlear phantoms (Part (1)), the insertions will be precisely controlled in terms of the insertion depth and speed, which require an additional test rig to be built. Various insertion speeds will be utilized to evaluate the relationship between the speed of insertion and the induced force. Real-time monitoring indicating the trajectory (position and shape) and force (tip, lateral and frictional forces) information will be realized to show visual feedback. Part (2), the clinical trials are expected to be conducted together with our much-experienced collaborators in the Department of Otolaryngology of The University of Melbourne, Australia. The investigators in Melbourne are recognized as world leaders in cochlear device technologies. Furthermore, their unique research relationship with the worldwide cochlear implant manufacturer, Cochlear Ltd places us in a crucial position to drive this field while ensuring rapid clinical translation.



**Fig. 1.** (a) Cochlear implant (Retrieved from <https://lmhofmeyr.co.za/conditions/conditions-we-specialise-in/cochlear-implant/cochlear-implant-website/>). (b) CI integrated with a single core POE fiber inscribed with an array of four FBGs, (c) in the cochlear lumen of a cochlear phantom, (d) reflection spectra of its first FBG (at the tip) during bending and (e) force calibration of its first FBG for a loading and unloading cycle. (f) Schematic illustration of the tip force based on ZEONEX MCF. (g) Coupling technique for interrogation of FBGs in ZEONEX MCF. (h) ZEONEX MCF when subjected to side forces.

## Outcomes

This funding will assist technological innovations in the treatment of hearing loss with the aid of fiber optics through the commencement of a research hub between researchers with expertise in photonics and otorhinolaryngology leveraging synergies from partner universities and organizations which will broadly benefit CI recipients.

- Fabrication of novel low loss ZEONEX-based polymeric MCFs inscribed with an array of FBGs integrated with CIs suitable for real-time assessment of insertion forces, position determination and shape retrieval during cochlear implantations.
- Development of a high precision optical alignment system for effective optical coupling between the proposed ZEONEX MCF and seven-core silica MCF.
- Improved clinical approaches for preservation of residual hearing, with immediate benefits for CI recipients with residual hearing. This will lead to better speech perception in background noise and improved music appreciation.
- The anticipated outcome of a complete system that integrates the smart CI to an interface that displays contact force, trajectory and position of the CI in real-time essential for the implementation of augmented reality assisted surgical navigation to improve the success rate of cochlear implantations.

## Impact

The success of current CI insertion surgical procedure relies largely on the experience of the surgeon to insert a fine, slender EA through a small opening in the cochlea. There is no visual feedback of the trajectory of the EA around the cochlear spiral or feedback of distal tip and lateral contact forces of the implant to help the clinician minimize structural damage to the cochlea. Damages to delicate cochlear structures are generally irreversible and usually result in the loss of any residual hearing. The latter is combined with electrical stimulation to improve performance in the presence of background noise. FBG sensors can be an attractive solution for this extremely sensitive surgical procedure. The CI experiences

axial, lateral and frictional forces during insertions. Hence, an array of FBG sensors inscribed in a novel ZEONEX four-core fiber can be integrated with the CI which can serve to carry out several measurements to detect tip force on multiple planes. The novel design of the ZEONEX MCF enables measurements of lateral force and navigation of the implant which is vital in providing feedback to the surgeon on the depth and orientation of the tip as well as the position of the EA within the cochlea. Thus, the predicted successful outcomes of this proposed project will immensely impact the surgical capability to minimize (even avoid) the damage to the inner ear structure during cochlear implantations. This would significantly improve the outcomes of the restored hearing to the patients with reliable and affordable implantations benefiting the hearing impaired across varying income groups. Furthermore, the proposed techniques can be further adhered in other medical related applications opening up a whole new level of sensing technology.

## References

1. World Health Organization, *World Report on Hearing* (2021).
2. L.M. Haile, K. Kamenov, P.S. Briant, A. U. Orji, J. D. Steinmetz, A. Abdoli, M. Abdollahi et al, "Hearing loss prevalence and years lived with disability, 1990–2019: findings from the Global Burden of Disease Study 2019," *The Lancet* **397**(10278), 996–1009 (2021).
3. E. A. Materson, P. T. Bushnell, C. L. Themann, and T. C. Morata, "Hearing Impairment Among Noise-Exposed Workers —United States, 2003–2012," *Morbidity and Mortality Weekly Report* **65**(15), 389–394 (2016).
4. T. Ishii, M. Takayama, and Y. Takahashi, "Mechanical Properties of Human Round Window, Basilar and Reissner's Membranes," *Acta Otolaryngol* **115**(sup519), 78–82 (1995).
5. E. Avci, T. Nauwelaers, V. Hamacher, and A. Kral, "Three-dimensional force profile during cochlear implantation depends on individual geometry and insertion trauma," *Ear Hear* **38**(3), e168–e179 (2017).
6. S. A. Wade, J. B. Fallon, A. K. Wise, R. K. Shepherd, N. L. James, and P. R. Stoddart, "Measurement of forces at the tip of a cochlear implant during insertion," *IEEE Trans Biomed Eng* **61**(4), 1177–1186 (2014).
7. E. Capcelea, P. Stoddart, S. Wade, and N. L. James, *U.S. Patent Application No. 13/231,957* (2013).
8. A. N. Vadivelu, Z. Liu, D. S. Gunawardena, B. Chen, H. Y. Tam, S. O'Leary, and D. Oetomo, "Integrated Force Sensor in a Cochlear Implant for Hearing Preservation Surgery," *Proceedings of the Annual International Conference of the IEEE Engineering in Medicine and Biology Society, EMBS* 3819–3822 (2019).
9. E. M. Carland, P. R. Stoddart, P. J. Cadusch, J. B. Fallon, and S. A. Wade, "Effect of embedded optical fibres on the mechanical properties of cochlear electrode arrays," *Med Eng Phys* **38**(2), 155–162 (2016).
10. S. Balster, G. I. Wenzel, A. Warnecke, M. Steffens, A. Rettenmaier, K. Zhang, T. Lenarz, and G. Reuter, "Optical cochlear implant: Evaluation of insertion forces of optical fibres in a cochlear model and of traumata in human temporal bones," *Biomedizinische Technik* **59**(1), 19–28 (2014).
11. C. Broadway, R. Min, A. G. Leal-Junior, C. Marques, and C. Caucheteur, "Toward Commercial Polymer Fiber Bragg Grating Sensors: Review and Applications," *Journal of Lightwave Technology* **37**(11), 2605–2615 (2019).
12. X. Cheng, D. S. Gunawardena, C.-F. J. Pun, J. Bonafacino, and H.-Y. Tam, "Single nanosecond-pulse production of polymeric fiber Bragg gratings for biomedical applications," *Opt Express* **28**(22), 33573 (2020).
13. D. S. Gunawardena, X. Cheng, J. Cui, G. Edbert, L. Lu, Y. T. Ho, and H.-Y. Tam, "Regenerated polymer optical fiber Bragg gratings with thermal treatment for high temperature measurements," *Photonics Res* **10**(4), 1011 (2022).
14. D. N. Oetomo, S. J. O'Leary, H. Y. Tam, Z. Liu, and D. S. Gunawardena, "Medical Device and System and Method for Guiding Positioning of Same, " *International Patent Application WO2021127738A1*, (2021), Status: Published
15. L. Leon, M. S. Cavilla, M. B. Doran, F. M. Warren, and J. J. Abbott, "Scala-tympani phantom with cochleostomy and round-window openings for cochlear-implant insertion experiments," *Journal of Medical Devices, Transactions of the ASME* **8**(4), (2014).

## **Multi-core Polymeric Optical Fiber Sensors for Atraumatic Smart Cochlear Implantation**

### **Category: Health**

Hearing loss is a growing global health issue which affects people of all ages. Latest statistics from the World Health Organization, affirms that globally, an estimated 1.5 billion people (1 in 5 people) suffer from hearing loss with a projected rise to 2.5 billion by 2050. It has downstream effects on speech recognition, cognitive development and leads to an increased risk of dementia. Surgical involvements such as cochlear implantations have the capacity to alleviate this burden. Cochlear implantation is the current well-established standard of care to treat the hearing-impaired suffering from severe to profound sensorineural hearing loss. A cochlear implant (CI) consisting of an electrode array (EA) is implanted into the inner ear (cochlea) bypassing the missing or defective sensory receptors by directly stimulating the auditory nerve and thereby, restoring hearing in deaf patients. This extremely delicate surgical procedure involves high precision and complex navigation. The quality of hearing restored to a deaf patient depends on accurate positioning of the EA while preserving the cochlear membranes. New bone formation that occurs inside the cochlea as a result of electrode insertion trauma, not only negatively impacts the hearing performance but also makes future explantations and re-implantations of CIs difficult. The typical lifetime of CIs is just over 20 years, so, replacement of old implanted CIs will be required several times over a young individual's life. Existing technological electrodes end up at an undesirable (traumatic) intracochlear location up to 50% of the time. Yet current approaches on cochlear implantation have significant shortcomings: lack of any visualization of the intracochlear structures during implantation which requires precise positioning in order to preserve the delicate cochlear structures and absence of feedback on insertion forces with blind insertions guided only by the clinician's tactile feedback.

With polymeric optical fibers (POFs) anticipated to revolutionize the biomedical sensing industry due to their intrinsically beneficial properties, in this project, we propose the application of a ZEONEX-based low loss multi-core polymeric fiber consisting of four cores inscribed with fibre Bragg grating (FBG) sensing arrays which can be integrated internally inside a CI. These smart CIs can provide real-time feedback to clinicians when navigating CIs during cochlear implantation surgical procedure with minimum insertion trauma thereby, promoting hearing preservation. Apart from extreme flexibility and low stiffness levels, ability to withstand temperatures exceeding 120 °C, absence of any risk of fiber breakage even under low bending radii, chemical inertness and insensitivity to humidity offered by these ZEONEX-based POFs which are fundamental requirements in the manufacturing process of cochlear implants emphasize their compelling candidacy. Feedback from the FBG arrays that will be inscribed in these proposed ZEONEX MCFs can be used to derive a multitude of forces (eg. tip force, lateral force, frictional force) experienced by the CI inside the constricted cochlea during insertions as well as its shape at specific localities. Insertion trials already carried out on CIs integrated with ZEONEX single core polymeric FBGs inside the cochlear phantoms permit contact force detections of these CIs in the scale of millinewtons with investigations inside human temporal bones anticipated to be conducted at the Royal Victorian Eye and Ear Hospital, Melbourne in late 2022.

Ongoing collaborative research with world leaders of cochlear implant technology places us in a unique position to pioneer the development of smart cochlear implants. Industrial collaborative experience brought in by the investigators paves the way for clinical translation of these research outcomes ensuring that new diagnostic approaches truly benefit the hearing impaired. Hence, adaptation of this technology provides a direct course to the next generation of CIs and we believe its virtues will complement lifetime implanted-hearing conditions.



# **Development of Tunable Multi-Colour Laser for Sensing: Case Study for Hyperspectral Detection of Water Contaminants**

## **1.0 Literature Review**

Safe and reliable supply of pollution free water is essential for human, animal and plant health. Thus, there has been growing global concern to search for mitigation measures that reduce the undesirable effects of water contaminants that may arise from pipeline leakages or environmental pollution among others. The World Health Organization (WHO) is well aware of this and through the United Nations water (UN water), it has set guidelines [1] on safe concentrations of water pollutants that can be exposed to human beings and animals without harmful effects. Some of these pollutants are heavy metals like lead, mercury and iron just to mention a few. It is from this point of view that various detection techniques have been developed ranging from atomic absorption spectroscopy [2], to atomic emission spectroscopy [3], and mass spectroscopy [4]. Albeit, these techniques require expensive instrumentation [5].

Even though there has been good progress with these techniques, other optical approaches that utilize lasers in the visible spectral region are fast becoming attractive for a variety of applications ranging from biomedicine [6], to spectroscopic [7], to fluorescent-based medical imaging [8], and more. However, existing visible laser sources, such as Raman lasers [9] [10], dye lasers [11] and optical parametric oscillators [12] are bulky, have poor beam quality or low efficiencies. Furthermore, there are still no commercial diode lasers with appropriate band gaps to cover this wavelength region [13]. Fortunately, sum frequency generation (SFG) based on the nonlinear crystals [12, 14-15], is an attractive way to generate visible lasers. Various techniques to generate red (R), green (G), blue (B), and even yellow (Y) colors have been previously reported. These techniques include utilizing several crystals each for different nonlinear process [16], self-frequency doubling and self-frequency mixing in Nd<sup>3+</sup>-doped bulk aperiodically poled lithium niobate [17], and cascaded nonlinear interactions in aperiodically poled lithium tantalate (LT) [18,19] or stoichiometric LT [20, 21]. In our previous work, we demonstrated a broadband yellow-orange laser, pumped with a C-band ASE laser source using a 20 mm periodically poled Magnesium oxide doped Lithium niobate crystal (PPMgLN) [22]. The yellow-orange spectrum was extended from 593 nm to 599 nm. We have also theoretically demonstrated a multi-wavelength laser generation in a single periodically poled lithium niobate (PPLN) crystal using two laser pumps in to the visible spectral range [23]. The relevance of our previous work in this proposal is the possibility to use a tunable C-band (1550 nm) and 980 nm pump laser sources to generate Blue-Green-Orange coherent outputs. A broadband (594 nm to 601 nm) yellow-orange laser was recently demonstrated based on a step chirped (SC) PPMgLN ridge waveguide [24]. Thus, it is of significance to develop a broadband laser source and utilize the waveguide-based SC-PPMgLN to improve the beam confinement. The merit of using a waveguide structure lies in the use of low pump power and becomes attractive for next generation optical detection techniques for water quality as well as environmental monitoring applications. For water quality analysis, the analyte (water) interacts 'quickly' with the emitted laser light and the shift in the spectra is detected using an Optical Spectrum Analyzer (OSA) as a deviation from that of clean water.

## **2.0 Problem statement and objective**

The key motivating factor of this proposal is the ongoing research at University of Eldoret in Environmental monitoring and in Agriculture that depends on expensive and un-affordable systems for sensing. Pollution is an important environmental issue that affects the quality of human life and there is need to seek solutions that can benefit from using multiple excitation wavelengths for mitigating against waterborne diseases. Specifically, we propose the ultrafast, sensitive optical detection of low levels of pollutants in drinkable water. Therefore, our long-term goal is to develop a multi-wavelength visible laser source generated through wavelength conversion that enables detection of different parameters and can benefit varied applications in sensing, environmental monitoring and basic research. However, development of a tunable, multi-wavelength visible laser source remains unexplored and this proposal is an attempt to bridge the existing gap. We firmly believe that such a visible laser once integrated in an optical communication system can find a wide range of applications among them, water quality assessment and environmental monitoring. The specific objectives are designed to provide a

detailed design, fabrication and deployment of the multi-wavelength visible laser source for simultaneous sensing applications:

- (i) **Design a step-chirped (SC) PPLN waveguide for tunable wavelength conversion into the visible spectral range.** The SC-PPLN device will perform sum frequency mixing and second harmonic generation accomplished in the different sections of the crystal simultaneously.
- (ii) **Investigate the tunability and wavelength broadening of the waveguide laser.** By tuning the input laser sources, it is possible to tune the multiple spectral outputs as well. We shall investigate the effect of temperature tuning as well as temperature gradient. We believe that temperature gradient technique will improve the bandwidth of the laser output which is beneficial for sensing.
- (iii) **Fabricate and characterize the compact multi-wavelength solid-state laser module.** The designed SC-PPLN waveguide will be fabricated at the Key Laboratory of Optoelectronic Materials Chemistry and Physics, Fujian Institute of Research on the Structure of Matter, Chinese Academy of Sciences, Fuzhou, China, (CTL Photonics Inc.).
- (iv) **Apply the generated wavelengths for detecting water contaminants in a laboratory set up.** Access to clean and pollution free water is crucial for human and animal health. It is vital to develop a highly sensitive, reliable, accurate and fast response all-optical system for fast and extensive water quality assessment. In most of the rural communities across the world, the main source of water for drinking and domestic purposes are wells, rivers and rain water. Any contaminants in water from such sources pose health risk to human and animal populations alike.

The schematic in Fig. 1 shows the proposed experimental set up. Two laser sources (1550 nm tunable telecom laser and 980 nm laser diode) will be used as input lights (signal and pump respectively) to generate multiple wavelengths (Blue, Green, Orange and Red) via frequency mixing in PPLN. The temperature controller will be used for wavelength tuning by adjusting the quasi-phase matching (QPM) condition of the PPLN waveguide device. The generated multiple wavelengths will pass through the water sample and the scattered is light collected and separated by bandpass filter before detection. An optical spectrum analyzer (OSA), having spectral response ranging from 400 to 1700 nm, will be used to detect the output.

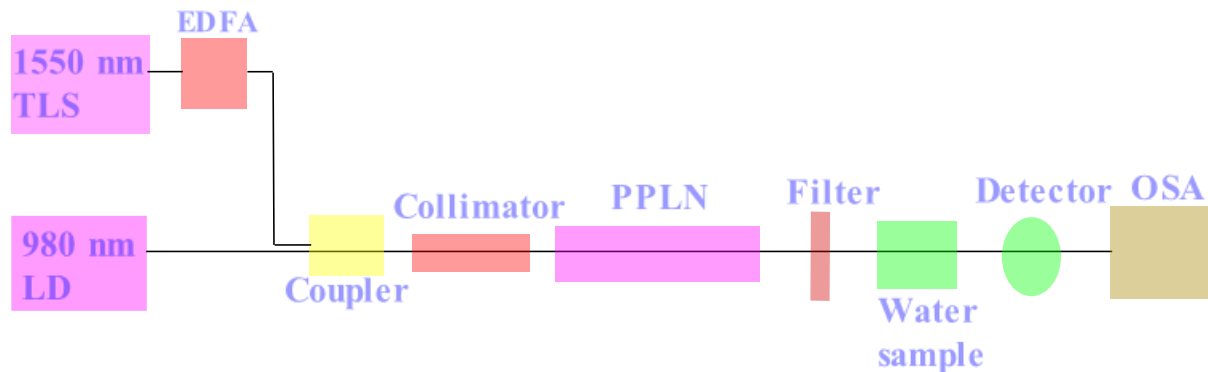


Figure 1: Proposed optical layout of the all-optical multi-wavelength generation for detection of water contaminants. TLS: Tuneable Laser Source; LD: Laser Diode; EDFA: Erbium-Doped Fibre Amplifier; PPLN: Periodically poled lithium niobate; OSA: Optical Spectrum Analyzer

### 3.0 Work Plan

A ridge waveguide will first be designed and optimized for single mode operation for a range of wavelengths within the visible region with a target wavelength around 600 nm. The optical modes and effective refractive indices will be simulated using COMSOL Multiphysics field solver based on finite element algorithm. The PPLN wavelength conversion device will be tested in a benchtop experimental setup to evaluate its performance. The project will run for three years as scheduled in Table 1.

Table 1: Scheduled research plan for the proposed project

Activity	Y1				Y2				Y3			
	Q1	Q2	Q3	Q4	Q5	Q6	Q7	Q8	Q9	Q10	Q11	Q12
1. Theoretical investigation of frequency conversion into the visible range	■	■										
2. PPLN device design & Simulation			■									
3. PPLN device fabrication & Performance evaluation				■	■	■						
4. Characterization of PPLN wavelength converter							■					
5. Device application set up for water quality assessment								■				
6. Data collection & Analysis									■	■		
7. Preparation & submission of manuscripts to peer-reviewed journals							■	■	■	■	■	■
8. Thesis writing & submission							■	■	■	■	■	■

#### 4.0 Outcomes

Multi-wavelength, tunable visible lasers are needed to pave way for broad and new areas of application. Such a laser source will improve access to multiple wavelengths that can be controlled simultaneously and become beneficial in the next generation of all-optical systems for water quality assessment as well as other areas of environmental monitoring.

The project is expected to train two (2) MSc and one (1) Ph.D. students. The research team will participate in scientific conferences, symposia and publish research findings in peer reviewed journals.

#### 5.0 Impact

The impact of the proposal will strengthen and broaden the applications of multi-wavelength visible lasers to solve a wide range of societal challenges such as in health and environmental monitoring. An all-optical sensing system when used for water quality assessment can provide a solution for mitigation against water pollution and decrease waterborne illnesses, consequently improving the well-being of the population. Successful implementation a compact multiwavelength visible laser will reduce costs as well unlock new application areas that can brighten the future of probing our environment further and enhance the quality of life. It is also expected that, upon completion of the project, the future career prospects of the participants will be enhanced and improve the skills of students in photonics.

## References

- [1] R. W. Herschy, *Water quality for drinking: WHO guidelines*. 2012.
- [2] C. H. Chiu, Y. H. Sung, and S. da Huang, "Simultaneous determination of manganese, iron and cobalt in copper with a multi-element graphite furnace atomic absorption spectrometer," *Spectrochim Acta Part B At Spectrosc*, vol. 58, no. 3, pp. 575–580, 2003.
- [3] C. Xiong, Z. Jiang, and B. Hu, "Speciation of dissolved Fe(II) and Fe(III) in environmental water samples by micro-column packed with N-benzoyl-N-phenylhydroxylamine loaded on microcrystalline naphthalene and determination by electrothermal vaporization inductively coupled plasma-optica," *Anal Chim Acta*, vol. 559, no. 1, pp. 113–119, 2006.
- [4] J. Wang, E. Harald Hansen, and B. Gammelgaard, "Flow injection on-line dilution for multi-element determination in human urine with detection by inductively coupled plasma mass spectrometry," *Talanta*, vol. 55, no. 1, pp. 117–126, 2001.
- [5] T. Liu, G. Li, N. Zhang, and Y. Chen, "An inorganic-organic hybrid optical sensor for heavy metal ion detection based on immobilizing 4-(2-pyridylazo)-resorcinol on functionalized HMS," *J Hazard Mater*, vol. 201–202, pp. 155–161, 2012.
- [6] S. Karrer, W. Bäumlner, C. Abels, U. Hohenleutner, M. Landthaler, and R. M. Szeimies, "Long-pulse dye laser for photodynamic therapy: Investigations in vitro and in vivo," *Lasers Surg Med*, vol. 25, no. 1, pp. 51–59, 1999.
- [7] V. Kapoor, F. v Subach, V. G. Kozlov, A. Grudinin, V. v Verkhusha, and W. G. Telford, "New lasers for flow cytometry: filling the gaps," *Nat Methods*, vol. 4, no. 9, pp. 678–679, 2007.
- [8] W. K. Chang, Y. H. Chen, and J. W. Chang, "Pulsed orange generation optimized in a diode-pumped Nd:YVO<sub>4</sub> laser using monolithic dual PPLN electro-optic Q switches," *Opt Lett*, vol. 35, no. 16, pp. 2687–2689, 2010.
- [9] H. M. Pask, P. Dekker, R. P. Mildren, D. J. Spence, and J. A. Piper, "Wavelength-versatile visible and UV sources based on crystalline Raman lasers," *Prog Quantum Electron*, vol. 32, no. 3–4, pp. 121–158, 2008.
- [10] Y. Sun *et al.*, "Second-harmonic generation of Nd:YAlO<sub>3</sub>/YVO<sub>4</sub> Raman laser optimization for orange emission," *Jpn J Appl Phys*, vol. 59, no. 4, pp. 042004, 2020.
- [11] M. Fukuda, K. Kodama, H. Yamamoto, and K. Mito, "Evaluation of new organic pigments as laser-active media for a solid-state dye laser," *Dyes and Pigments*, vol. 63, no. 2, pp. 115–125, 2004.
- [12] M. Ghotbi, A. Esteban-Martin, and M. Ebrahim-Zadeh, "BiB<sub>3</sub>O<sub>6</sub> femtosecond optical parametric oscillator," *Opt Lett*, vol. 31, no. 21, p. 3128, 2006.
- [13] A. Majid *et al.*, "First demonstration of InGaP/InAlGaP based orange laser emitting at 608 nm," *Electron Lett*, vol. 51, no. 14, pp. 1102, 2015.

- [14] G. Ma *et al.*, “Continuous-wave yellow laser generation at 578 nm by intracavity sum-frequency mixing of thin disk Yb:YAG laser and Nd:YAG laser,” *Opt Laser Technol*, vol. 92, no. July, pp. 32–35, 2017.
- [15] A. Kananovich, A. Demidovich, M. Danailov, A. Grabtchikov, and V. Orlovich, “All-solid-state quasi-CW yellow laser with intracavity self-Raman conversion and sum frequency generation,” *Laser Phys Lett*, vol. 7, no. 8, pp. 573–578, 2010.
- [16] F. Brunner *et al.*, “Powerful red-green-blue laser source pumped with a mode-locked thin disk laser,” *Opt Lett*, vol. 29, no. 16, pp. 1921–1923, 2004.
- [17] J. Capmany, “Simultaneous generation of red, green, and blue continuous-wave laser radiation in Nd<sup>3+</sup>-doped aperiodically poled lithium niobate,” *Appl Phys Lett*, vol. 78, no. 2, pp. 144–146, 2001.
- [18] J. Liao *et al.*, “Simultaneous generation of red, green, and blue quasi-continuous-wave coherent radiation based on multiple quasi-phase-matched interactions from a single, aperiodically-poled LiTaO<sub>3</sub>,” *Appl Phys Lett*, vol. 82, no. 19, pp. 3159–3161, 2003.
- [19] J. Liao *et al.*, “Red, yellow, green and blue - Four-color light from a single, aperiodically poled LiTaO<sub>3</sub> crystal,” *Appl Phys B*, vol. 78, no. 3–4, pp. 265–267, 2004.
- [20] Z. D. Gao, S. N. Zhu, S. Y. Tu, and A. H. Kung, “Monolithic red-green-blue laser light source based on cascaded wavelength conversion in periodically poled stoichiometric lithium tantalate,” *Appl Phys Lett*, vol. 89, no. 18, pp. 181101, 2006.
- [21] P. Xu *et al.*, “Compact high-power red-green-blue laser light source generation from a single lithium tantalate with cascaded domain modulation,” *Opt Express*, vol. 17, no. 12, pp. 9509, 2009.
- [22] D. K. Choge, H. Chen, Y. Xu, and G. Li, “Multi-peak tunable CW orange laser based on single-pass sum frequency generation in step-chirped MgO: PPLN,” *Opt Quantum Electron*, vol. 50, no. 5, pp. 1–7, 2018.
- [23] D. K. Choge, D. W. Waswa, K. M. Muguro, and W.-G. Liang, “Design of simultaneous multicolor coherent light generation in a single MgO:PPLN bulk crystal,” *Journal of the Optical Society of America B*, vol. 37, no. 11, pp. A304, 2020.
- [24] H. U. C. Hen *et al.*, “Broadband yellow-orange light generation based on a step-chirped PPMgLN ridge waveguide,” vol. 30, no. 18, pp. 32110–32118, 2022.

## **The Optica Foundation 20th Anniversary Challenge**

**Category:** Environment

**Title:** Spectral radiance mapping to characterize the ecological impacts of light pollution

**Name:** Dorukalp Durmus

**Affiliation:** Pennsylvania State University

### **Executive summary:**

#### The challenge

The accessibility and growing demand for electric lighting have a large-scale impact on natural habitats. Unfortunately, the electric light at night (LAN) can cause negative consequences, such as disrupting ecosystems, confusing migratory patterns, altering predatory-prey relations, causing stress, and interrupting the entrainment of circadian rhythms of many species. The negative effects of LAN (aka “light pollution”) is often quantified using photometric and colorimetric measures. Despite the complexity of spectral impact of light sources on the environment, research suggests that light source spectra influences arachnida, aves, insecta, mammalia, and reptiles in predictable manners. However, ecological research studies still use photometric (i.e., illuminance, luminance) and colorimetric (i.e., correlated color temperature) measures, which are based on human visual sensitivity. In addition, photometric and colorimetric measurements are performed using either spot measurements or satellite images. While these measurement methods have merits, they have limitations in accurately evaluating the ecological impacts of light pollution.

#### Proposed project

Characterizing the impacts of light pollution on several species requires a holistic measurement approach in spectral and spatial dimensions. The proposed research project aims to characterize optical radiation using a spectral imaging radiance colorimeter and assess the outcomes compared to spot (e.g., handheld spectroradiometer) and remote (satellite) measurements. A test field in central Pennsylvania will be identified, and light pollution of a large field of view will be characterized using radiance imaging colorimeter to simulate realistic field conditions. The variation between the traditional and proposed measurement methods will be evaluated, and a new metric for light pollution will be developed using the data generated in this project.

#### Intended outcomes

The results of this project will help characterize the unintended consequences of light pollution that captures the effects on the environment beyond just humans. New light pollution metric and measurement methods comparison will be disseminated to relevant bodies, such as the Council for Optical Radiation Measurements, the International Commission on Illumination, and International Dark-Sky Association. The project aims to reach a transformative impact on project development where designers and engineers can quantify the impact of lighting systems and mitigate any potential offence. The development of a holistic light pollution metric will also help ecological researchers find acceptability thresholds and guide outdoor lighting standards and recommendations, such as Model Lighting Ordinance (MLO), LEED Sustainable Sites program, the International Commission on Illumination (CIE) recommendations, and standards, such as the Australian New Zealand Standard AS/NZS 4282:2019 Control of the obtrusive effects of outdoor lighting.



## 1. Literature review

### 1.1 Negative impacts of light pollution

Light is imperative to achieve viable conditions for human activity at night, such as transportation, work, commerce, and leisure. The use of outdoor lighting is beneficial for commercial and cultural endeavours, especially in urban environments, but electric light at night (LAN) also reduces darkness which may be necessary for the ecology and some animals. For the outdoor lighting to be sustainable it should fulfil the functional needs of the users, be cost- and energy-efficient, and result in minimal environmental impact. The use of outdoor lighting during night-time can result in various unwanted and harmful side-effects (often collectively referred to as light pollution). The unwanted effects of the use of outdoor LAN include:

- Increase in human-made sky glow (the diffuse luminance of the night sky),<sup>1</sup>
- Degradation of ground-based astronomical observatories operating in the optical range and a decreased ability to observe the stars due to the brightening of the night sky,<sup>2</sup>
- Increase in obtrusive light causing nuisance and discomfort glare for humans,
- Adverse health outcomes, such as circadian disruption, mood effects, and increased breast cancer incidence risk in humans,<sup>3</sup>
- Disturbances and negative impacts on species, ecosystems, and wildlife.<sup>4</sup>

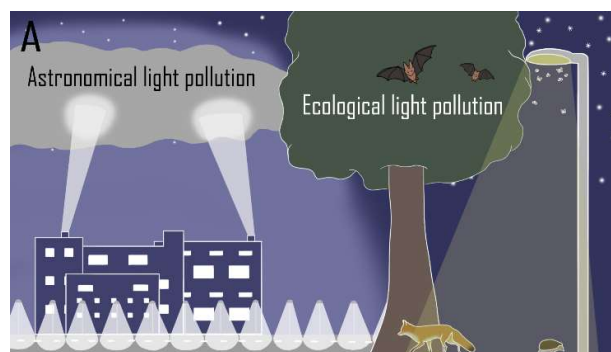


Fig. 1. Electric light at night can cause astronomical and ecological light pollution.<sup>5</sup>

The unwanted side-effects are measured through response variables and vary significantly depending on the research discipline and the study objects. In astronomy, the response variable can be sky brightness or upward emitted light. For impacts on human health, the response variable can be human behaviour or various health outcomes (e.g., sleep quality, melatonin suppression or risk of cancer). In ecology, the response variable is usually restricted to appropriate study variables for the specific species, the spatial scale or ecosystem of the investigation. Characterizing the ecological impacts of light pollution requires considering species' spectral sensitivity to optical radiation. The spectral sensitivities can help characterize

<sup>1</sup> Kyba, C., Tong, K. P., Bennie, J., Birriel, I., Birriel, J. J., Cool, A., ... & Gaston, K. J. (2015). Worldwide variations in artificial skyglow. *Scientific Reports*, 5(1), 1-7.

<sup>2</sup> Riegel, K. W. (1973). Light Pollution: Outdoor lighting is a growing threat to astronomy. *Science*, 179(4080), 1285-1291.

<sup>3</sup> Durmus D., Tengelin, M. N., & Jägerbrand, A. K. (2022) Investigating the methods and health outcomes of research studies on light pollution and human physiology and behaviour: a systematic review, 17th International Symposium on Science & Technology of Lighting, Toulouse, France.

<sup>4</sup> Sanders, D., Frago, E., Kehoe, R., Patterson, C., & Gaston, K. J. (2021). A meta-analysis of biological impacts of artificial light at night. *Nature Ecology & Evolution*, 5(1), 74-81.

<sup>5</sup> Jägerbrand, A. K., Tengelin, M. N., & Durmus, D. (2022) An overview of the adverse effects of outdoor light at night and the research methods used in different areas. 2022 Conference Proceedings of Lux Europa. Prague.

their visual response (i.e., brightness perception) to natural and electrical lighting. Some species may require darkness to hunt or hide from predators, find mating partners, or forage. Electric light at night with spectral distributions that are different than natural light sources (e.g., moonlight) may cause disruption to biological cycles of many species.

## 1.2 Light pollution measurement methods

Methods used in ecological light pollution studies are plentiful because of the large number of organisms that are studied. For example, LAN impact on birds have been studied through observational studies in the field that correlated bird responses (e.g., migration) to satellite-based light measurements or to ground-based measurements, but also through controlled indoor experiments or through experiments using bird enclosures outdoor. Biologgers attached on birds can help correlated exposure of LAN to movement patters. The effects of LAN on insects (or invertebrates) have been studied in observational studies, often by comparing the number of trapped insects, with and without lighting (often using light as a source of attraction for the insects), or by introducing different kinds of interventions in unlit or lit areas. Insect responses have also been studied by introducing LAN in previously unlit areas in manipulative field experiments and observing the responses.

Bats have only been studied through field experiments. Observational studies have been performed that compares bat movements and frequency of activity without any intervention. Field experiments varies much in their design, but some use already lit areas for introducing interventions (e.g., altered light sources, light intensity, or light distribution) and others use previously unlit areas to introduce LAN and study impacts on behaviour. Fish responses to LAN can be studied in field experiments, mesocosms, enclosures or in laboratory studies. Field experiments can be conducted to study both lit or unlit conditions with or without interventions. Use of mesocosms, enclosures or laboratory environments can improve the scientific reliability of the study since it is more controlled, and the influence of external factors can be minimized.

Responses of plants can be investigated through controlled field experiments manipulating various lighting conditions. Studies can also be performed as observations in unlit or lit areas with or without interventions. Tree phenology can be correlated with satellite-based measurements or with ground-based measurements. Similarly, turtles have mainly been studied in their natural habitats and in the field. Studies are often observations of behaviour before/after interventions have been introduced. Studies focuses on hatchlings, but adult turtles have also been under investigation. On the other hand, responses of rats, mice and rodents have been investigated in controlled laboratory studies where lighting manipulations can be fully controlled and measured. Field experiments of mice and rats in natural environments or in more controlled enclosures have also been performed. Response variables includes behaviour, ecological relevant variables and physiological measurements.

Many ecological studies are conducted without including data on environmental factors that may influence the results. Especially field experiments are very poor in reporting the lighting condition, for example light source, light intensity, and light distribution.<sup>5</sup> Only a few studies report enough information on light distribution to be able to repeat the study. Light sources are often mentioned but rarely with enough information to replicate the study. For example, the spectral power distribution (SPD) of the light sources are rarely reported. Even during controlled conditions, measurement details are not often clearly stated or reported. In addition, exposure levels for organisms are rarely reported.

These ecological studies often characterize the lighting conditions using photometric measures, such as illuminance (unit: lux). Illuminance, the total luminous flux incident on a surface per unit area, does not quantify the light reflected from surfaces and it is based on human visual sensitivity to optical radiation. The human spectral sensitivity to optical radiation is assessed using the photopic luminous efficiency function, which peaks at 555 nm. However,

most other animals (e.g., mammals except old and new world monkeys, insects, birds) have different photoreceptor spectral sensitivities due to evolutionary reasons, such as detecting flowers or fruits.<sup>6</sup> Some animals can even detect optical radiation beyond light, such as ultraviolet and infrared radiation. Therefore, the use of photometric measures (i.e., illuminance, luminance) is limited at best, and might mislead researchers, conservators, and lighting designers in their efforts in protecting natural habitats. In addition, the typical illuminance and luminance meters can only perform point measurements (a single point in time). A single point measurement does not fully characterize the visual scene in an outdoor setting but taking more measurements can be cumbersome and time intensive with these devices. Therefore, alternative methods should be used to characterize the lighting conditions of a field of view of a large area.

### 1.3 Satellite images

An alternative approach to photometric spot-measurements is extracting light exposure information from satellite images. Ground-based measurements include astronomical photometry and spectroscopy at large observatories, wide-field photometry using all-sky cameras with fish-eye lenses, narrow angle measurements (typically in only one band) using sky quality meters. Naked eye observations of stellar objects where citizen observations can be used to get large coverage of the observations. For light emitted through the earth atmosphere, remote sensing is carried out with radiance measurements by satellite-based sensors and photographs taken from NASA's International Space Station.

In earlier studies, mostly telescopes and naked eye observations were used in ecological research. From the year 2000 and onwards satellite-based radiometry has been used in the studies of light pollution, starting with the Defense Meteorological Satellite Program (DMSP) Operational Linescan System and later with the higher resolution of the monthly cloud-free night-time imagery from the Suomi National Polar-Orbiting Partnership (Suomi NPP), Visible Infrared Imaging Radiometer Suite (VIIRS) Day/Night Band, and most recently the Chinese satellite Jilin-1, claiming to have a spatial resolution below 1 m. With the development of wide-angle photometry, from 2010 and onwards the number of studies using camera-based measurements have increased.<sup>5</sup>

LAN measured by satellite is often correlated to urbanization, noise levels, and air pollution. In outdoors, it was found that satellite-based radiance measurements were useful when estimating the ground exposure, although luminance values from The New World Atlas had a better correlation with ground measurements considering the full sky. However, both the satellite image composites, and the estimated zenith brightness levels were found to smooth out local spatial variations as measurements performed on the ground have shown a much larger variation between high and low exposure sites when total exposure is considered.<sup>7</sup>

Although, satellite measurements of sky brightness can provide a broad analysis of a larger geographical area, it has limitations. For example, the process of sky glow and the measurement of the sky brightness is highly influenced by meteorological conditions. In astronomical studies, different units are used depending on the experimental technique. It is common to report the sky brightness in the astronomical magnitude system mag/arcsec<sup>2</sup>. This can be approximately compared to luminance in mcd/m<sup>2</sup>, but the different measurement techniques and bands used make it difficult to compare results from different studies. Another important limitation of the satellite images is the spectral sensitivity of the radiometers in the satellite (i.e., between 500 nm and 900 nm), which does not include a substantial portion of short wavelength energy that animals, including humans, are sensitive.

---

<sup>6</sup> Osorio, D., & Vorobyev, M. (2008). A review of the evolution of animal colour vision and visual communication signals. *Vision Research*, 48(20), 2042-2051.

<sup>7</sup> Simons, A. L., Yin, X., & Longcore, T. (2020). High correlation but high scale-dependent variance between satellite measured night lights and terrestrial exposure. *Environmental Research Communications*, 2(2), 021006.

## 1.4 Spectral radiance imaging

The limitations of photometric and satellite measures can be balanced by utilizing spectral radiance measurements captured through imaging systems. Spectral radiance imaging is the method of collecting radiometric data from a scene using a calibrated camera. Spectral radiance imaging is a subset of remote imaging, where electromagnetic radiation emitted or reflected from surfaces are measured. This method enables large field-of-view scanning and imaging for remote sensing and surveillance, with early applications focusing on the relationship between electromagnetic radiation and water,<sup>8</sup> complex vegetation,<sup>9</sup> and climate variability.<sup>10</sup> Today, spectral imaging cameras can be purchased to measure the radiometric quantities that are far more relevant for ecological and environmental research.

### 2. Problem statement / objective

The growing population and the increase in urbanization has rapidly expanded the human reach into the natural habitats. This increase comes at a price for the ecological environments and its inhabitants. Light, a key factor for human vision, can disrupt other species' biological cycles. Current methods of quantifying the negative impacts of light pollution is limited. The objective of this project is to evaluate the performance of spectral radiance imaging for a faster and accurate measurement of the lit night environment. The data collected in this study will be also used to develop new metrics to quantify the ecological impacts of light pollution.

### 3. Outline of tasks/work plan

The tasks of the proposed project is shown in Table 1.

Table 1. The outline of tasks for the proposed research project

<b>Task</b>	<b>Q1</b>	<b>Q2</b>	<b>Q3</b>	<b>Q4</b>
1. Identify test site				
2. Data collection from satellite images				
3. Field measurements with photometers and spectroradiometers				
4. Spectral characterization with spectral radiance colorimeter				
5. Data analysis				
6. Report, dissemination, outreach				

*Task 1.* Identifying a test site to conduct light pollution measurements: An outdoor area in central Pennsylvania (Centre County) will be identified to perform light pollution measurements. The outdoor area will include a rural access to a road, light installations (street lighting), and natural habitat to replicate a broad set of ecological research studies. The availability of the satellite images for this area will also be required before confirming the site.

*Task 2.* Data collection from satellite images: The lighting exposure in the test field will be evaluated using satellite information downloaded from DMSP Operational Line-Scan System (OLS) Nighttime Lights Time Series Version 4. For accurate satellite image analysis, World

<sup>8</sup> Curran, P. J., & Novo, E. M. M. (1988). The relationship between suspended sediment concentration and remotely sensed spectral radiance: a review. *Journal of Coastal Research*, 351-368.

<sup>9</sup> Goward, S. N., Cruickshanks, G. D., & Hope, A. S. (1985). Observed relation between thermal emission and reflected spectral radiance of a complex vegetated landscape. *Remote sensing of Environment*, 18(2), 137-146.

<sup>10</sup> Iacono, M. J., & Clough, S. A. (1996). Application of infrared interferometer spectrometer clear sky spectral radiance to investigations of climate variability. *Journal of Geophysical Research: Atmospheres*, 101(D23), 29439-29460.

Bank's Open Night Lights<sup>11</sup> tutorial will be utilized. Open Night-time Lights program offers open source tools (Python-based code) and basic operations for processing composite night-time images. A reference grid will be established, light sources will be identified and geolocated, and digital values will be established to the radiance scale.

*Task 3.* Field measurements with photometers and spectroradiometers: Photometric and radiometric measurements will be conducted in the field using calibrated Konica Minolta T-10A illuminance meter, LS-150 luminance meter, and Gigahertz BTS256 spectroradiometer. In addition, luminance maps will be created using state-of-art high-dynamic range (HDR) luminance mapping techniques<sup>12</sup> for an alternative fast and cost-effective measure.

*Task 4.* Spectral characterization with spectral radiance colorimeter: The spectral properties of the visual scenes of the test field will be characterized using a spectral imaging radiance colorimeter, which will be purchased with funds provided by this grant.

*Task 5.* Data analysis: The data points in each scene taken by imaging colorimeter will be matched with the data from the spectroradiometer and luminance meters. Radiometric quantities will be calculated for each pixel, and the variation between measurements methods will be quantified, and a regression model will be developed to use RGB values from a simple camera.

#### 4. Outcomes

The primary outcome of this project is the development and confirmation of novel method to accurately assess the impact of light pollution. A mathematical model will be developed that can best estimate radiometric quantities. In addition, a new light pollution metric will be develop considering light source spectra and irradiance of a visual scene. The data will be made available online for other researchers to develop their own approaches and evaluate the proposed metrics and measurement methods.

#### 5. Impact

The project outputs will directly impact the practice of lighting design and illumination engineering. There are currently several outdoor lighting standards that aim to limit the light exposure on unwanted areas to limit the negative consequences of light pollution. The International Commission on Illumination (CIE) "CIE 150:2017 Guide on the limitation of the effects of obtrusive light from outdoor lighting installations," the Model Lighting Ordinance (MLO) published jointly by the International Dark Sky Association and the Illuminating Engineering Society (IES), Leadership in Energy and Environmental Design (LEED) Light pollution reduction Sustainable Sites (SS8), and Australian and New Zealand Standards (AS/NZS) 4282:2019 Outdoor Lighting Obtrusive Effects are some of the most prominent examples. However, these standards still utilize photometric measures and are often limited to negative impacts on humans (e.g., glare). The PI Durmus has connections to many of these organizations and will work with the committees to improve the existing guideline to incorporate the metrics developed using outcomes of this research proposal. For example, Dr. Durmus is a member of two IES technical committees, was a member of CIE Australia and was a presentative, and worked in the AS/NZS standards committee previously. Through dedicated service work, the results will be metallized into reality to ensure immediate real-world impact.

---

<sup>11</sup> <https://worldbank.github.io/OpenNightLights/welcome.html>

<sup>12</sup> Pierson, C., Cauwerts, C., Bodart, M., & Wienold, J. (2021). Tutorial: luminance maps for daylighting studies from high dynamic range photography. *Leukos*, 17(2), 140-169.

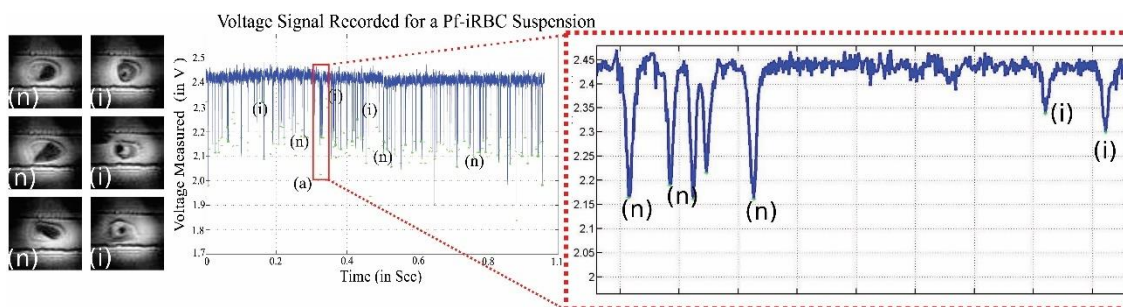
## 20th Anniversary Challenge (Optica Foundation)

**Name of Challenge Project:** Artificial Intelligence enabled smart Optical Absorption Point-of-Care device for Malaria screening

### Executive summary:

**Background:** For the larger interest of the needy design and development of Point-of-Care (PoC) diagnostics is the critical requirement of the health care industry. The requirement of rapid, sensitive detection and reliable solution with minimal human intervention is the front runner objectives of the research and innovation. The aim of the present research proposal is to develop an indigenous smart PoC instrument for screening/ detection of the malaria. The monitoring and screening of malaria transmission is possible with the advancement of the technology in view of malaria eradication.

**Scientific Rationale:** The microvascular system is responsible for the transfer of oxygen and nutrients and the removal of the waste products generated by the tissue it serves. Here, the main role of the erythrocyte/ Red Blood Cells (RBCs) is the transmission of hemoglobin (oxygenated) and nutrients through microvascular system. As we know that the malarial parasite targets RBCs such as infect inside the RBCs and reduce the hemoglobin concentration by degrading it as hemozome. As a result, there will be changes in the level of hemoglobin present in normal RBC and malarial infected RBCs. So, this information can be utilized to develop a point of-care device to differentiate between malarial infected and normal RBCs at single-cell high-throughput by differential light absorption in microfluidic channel as observed in any flow cytometry. The proof-of-concept and primary results shown briefly in the figure below.



**Novelty:** The present malaria diagnosis instruments including clinical microscopy, PoC, Rapid (**qualitative info.**) testing devices use standard signal/image processing algorithms. PoC devices integration with AI models for automatic malaria screening/ testing may give more promising results. Current proposal aims in development of an AI-enabled PoC device for Realtime analysis at single-cell high-throughput (**quantitative info.**). The primary objective of the study involves development of smart PoC device for malaria screening. The secondary objective of the study includes proper design of experiments for clinical validation and testing, Develop the novel AI based algorithm and comparison with state-of-the-art techniques

**Methods:** The major principle involved in development of device is to study the light (near UV) absorption properties of malaria infected and healthy/normal blood cells. Predominant features are automatically extracted from the output signal of the sensor using signal processing algorithms and trained with artificial intelligence algorithms for classifying malaria and non-malaria cells. Novel reinforcement learning techniques will be incorporated and further tested.

**Expected outcome:** Low cost and portable Smart point-of-care Instrument for malaria screening and research publications in high reputed journals along with patents. Custom design and developments of flow-focusing microfluidic devices which are used for identifying cell morphology, deformability, blood flow velocity. Development of GUI based algorithm for malarial parasite detections, finding the stages of infection, quantitative information of infected cells from overall assessed sample. Development of this type of product help in early screening of malaria endemic zone which help towards the eradication of malaria.



## 20th Anniversary Challenge (Optica Foundation)

**Name of Challenge Project:** Artificial Intelligence enabled smart Optical Absorption Point-of-Care device for Malaria screening

Malaria is one of the deadliest, sometimes it is fatal diseases caused by infection of red blood cells with a malarial parasite. Majorly, the transmission of malaria occurs through parasite that infects by female mosquitoes which feed the blood from human and animal. In the regular day by day basis, we are witness of spread of mosquitoes in all seasons. The seriousness of infection depends on the types of the parasite presences or injected in the body. The medical devices are the tools for screening/ detection of the malaria parasite present in the subject and take the necessary steps in the treatment. *The scheme of malaria eradication in developing and underdeveloped countries would be successful, if the more and more invention of novel, enhanced, and high-efficient screening and detection instruments are in practice.* Further, the success of these advanced instrument is screening, and detection should be robust, and could be reached to the remote location which is actual needy place. In the present three years research proposal I would like to bring novel high throughput single-cell detection Point-of-Care Device (PoCD) for screening of malaria. *The realization of PoCD is the synergetic integration of optics, microfluidics, and simple electronics.* The advancement of the AI will help in automate the PoCD to smart and real time point-of-care screening/ detection instrument. The current experience in design and development of point-of-care devices will help in the realization of the present novel work. My past work involves characterization of single cell in both the morphological and change of chemical composition presence in the malaria infected and normal red blood cells. I have extensively worked on finding the hemoglobin content present in normal single RBC and various stage malaria infected RBCs. This work can bring robust and smart PoC instrument bring for screening of malaria at single cell level. The work done so far in the realization of absorption flow-cytometer for point-of-care detection/ screening of malaria is reported in methodology. The significant features from the signal (output of optical device) will be extracted automatically and trained with different ML and AI models (SVM, Gradient boost, Decision Tree, ANN, etc.). Individual modules will be developed for each AI model with user friendly GUI to analyze the results.

**Literature Review:** Despite of Malaria severity like life threatening diseases transmitted and spread across by malaria infected female anopheles mosquitoes; the good sign is world progressively working towards the elimination of malaria. Every year the overall cases coming down as per the report of World Health Organization on Malaria (WHR2019) [1]. Worldwide, over 228 million cases were estimated in 89 countries and about 0.5 million death cases in 2018. As per the World Malaria Report (WMR) 2019, over a 3% of malaria cases were reported in India and it was around 49 % reduction compared to WMR-2018. However, the recent report of WMR 2021 shows the statistics of sudden raise of the estimated cases in parallel of COVID pandemic [2]. Globally over 258 million cases and death were 627000 estimated in 2020. It shows over 12% increased due to various reasons including COVID pandemic, neglecting measuring constraint, treatments and controlling Precautions. Specific to South-East-Asia over 82% cases were reported in India, these data shows that the effort we are putting towards malaria elimination needs to improve to success in the challenge of MERA-India by 2030. The necessary steps in eradication of the malaria involve precaution steps to avoid the spread/ transmission, screening of malaria within the transmission zone and detection/diagnosis followed by the treatment. Medical devices are the instruments for screening and detection/ diagnosis of any diseases [3]. The diagnosis of malaria involves the process of identifying the parasite or finding the protein content through antigens product test in the blood cells or blood sample. As it looks simple in view of visually, but the diagnosis of malaria efficacy relies on many factors which includes the form of malaria species, level of infections, immunity level of the infected individual, drug resistivity and region-based population density and mosquito's transmission within the location and many more parameters. The most conventional methods used for malaria diagnosis/ detection include clinical

diagnosis, which is the diagnosis process based on symptomatic signs of patients and physical findings of the pathologist. This method is more helpful in region specific and transmission of malaria in localities. The limitation includes the possibilities of misdiagnosed due to patients asymptomatic as well as symptomatic [4]. Laboratory diagnosis is the most effective method for diagnosis of malaria. These techniques help from over-treatment of symptomatic signs and effective diagnosis. Laboratory diagnosis comprises of “Gold-stranded” clinical microscopy, rapid diagnostic test (RDT), QBC, ParaScreen, Paracheck, Flow-Cytometry (FCM), Imaging FCM and molecular diagnostic methods like RT-PCR. Clinical microscopy is labor intensive method and RDT is used in inaccessible places of clinical microscopy. The accuracy of RDT is less than 70 % and it gives qualitative information only. The positive RDT test screening needs to perform the “gold stranded clinical microscopy” for the quantitative malaria diagnosis. Since RDTs is an antigen test, and provides qualitative information of malaria positive or negative, it requires clinical microscopy to reconfirm the severity of the infection [5-10]. Other techniques which are further sensitive like fluorescent microscopy and polymerase chain reaction (PCR) are useful for malaria detection but due to the limits of resources at ground settings inhibits the widespread usage of these techniques. Testing of RT-PCR, FCM and Imaging FCM is hardly performed in pathological laboratories due to expense and high expertise of manpower involved. In the recent past several attempts have been made for cost-effective, point-of-care instruments for malaria detection, such as magnetic resonance relaxometry, recording absorption spectrum has been reported. In addition, several optical detection techniques have been demonstrated (11-19). Overall, optics-based approaches have high sensitivity and single-cell level findings, microfluidics-based approaches provide high throughput and on-chip sample handling. The present advancement in the health care sector is smart move towards point-of-care Devices (PoCD) from proof-of-concept. There are some of the rapid and qualitative diagnostic devices are available for diagnosis of malaria and other diseases at point-of-care (POC) diagnosis [20-25]. *In the process of adopting new techniques, initial stage needs to address their own constraints and come up with advance and highly sensitive PoC diagnostics. Hence, there is a need to develop simple, user-friendly, battery operated, stand-alone device that can quick and quantitatively screen/ detection/ diagnose the patients and direct them towards proper medication.* Such advancement will increase the reach of diagnostic services to people living in rural, hilly, and remote location in both developing and underdeveloped countries.

This study proposes to develop a simple, indigenous, accurate, POC diagnostic device for screening of malaria. Further, the device is readily deployable to provide the diagnostic infrastructure facilities in the rural and semi-urban areas. The main working principle is based on the measurement of single-cell absorption/ transmittance properties. In the long run, the ultimate goal of the present device (POC) is a pathologist or primary health care operator would be able screen/ diagnose and communicate using this device whether the person is suffering from malaria/ viral fever at remote location.

**Problem Statement/Objectives:** The present research work aims to develop the indigenous single-cell high throughput microfluidic Absorption flow-cytometer for fast screening/ diagnosis of endemic diseases like malaria at Point-of-Care (POC). Integration with AI models for automatic malaria screening/testing may give more promising results. Current proposal targets in development of a smart (AI enabled) PoCD for real-time analysis at point-of-care detection/screening. To the best of Principle Investigator knowledge, malaria is an endemic disease, spread across half of the world and every year over 3.3 billion population undergoes screening/ testing of malaria and over 1.2 billion people are at a high-risk areas and India is one among those countries where the prevalence of malaria and dengue is high. Further, in region specific Odisha (PI institute home state) is one of the states which is having high-risk areas accounting over the 26 % malaria infection cases reported in India [26-28]. Moreover, as it evident that diseases effect the children under the age of 5 and pregnant woman’s, POC screening for early detection will help in prevention and control the transmission of malaria. The proposed device would be helpful in screening of epidemic disease like

malaria and help in addressing the global issue. Below are the objectives towards better way to address the problem

**The primary objectives of the study involve:**

- To develop a smart point of care instrument for malaria screening
- Development of AI based framework for high throughput analysis

**The secondary objectives of the study involve:**

- Design of experiments (DoE) for clinical validation of developed POC device
- Validation and comparison of developed AI based framework with the state-of-the-art techniques

**Outline of tasks/ Work Plan:** In the present research proposal aimed to develop a Point-of-Care Device for malaria screening. The diagnostic instrument would be working on the principle of absorption properties of malaria infected and uninfected blood cells. Initial study is the development of standalone system for the characterization of the chemical and morphological features of blood cells using both bulk as well as single-cell analysis at high throughput as shown figure 1. Though it has many applications like malaria, cancer cells, stem cells, DNA/ RNA analysis, drug discovery and drug screening but the implementation of single-cell technique is beset with problems. Ascertaining accurate information of single-cell from whole sample mean response is near-impossible. To address the single-cell characterization below experimental setup has been developed in my previous work.

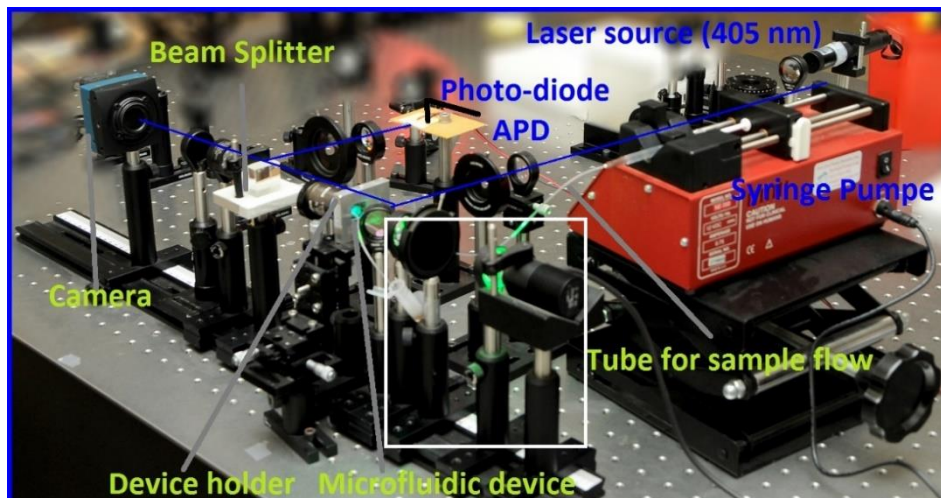


Figure 1 Experimental setup for characterization of malaria infected and healthy RBC high throughput microfluidic system

The experimental set-up developed in my preceding research work for simultaneously imaging and detection is shown in Figure 1. A laser diode (near-UV 405 nm, 10 mW used for a particular application), and 4-f lens system was used as the precisely illuminate tiny spot. In the beam path, collimated beam was focused as a tiny spot on the sample plane by using another biconvex lens. A polydimethylsiloxane (PDMS) microfluidic device was placed in the sample plane. The micro channel developed inside the microfluidic device was used as a sample-carrier to flow the sample, the design and development of which is discussed in the fabrication section. The micro-objective 40X is placed immediately after the microfluidic channel to collect the light transmitted through the sample. A beam splitter (BS, Thorlab) was placed in the same path in-between the micro-objective and the tube lens. The laser light coming from the microobjective was divided into two (transmitted and reflected) paths using the BS. The transmitted light path directly reaches the camera through the tube lens. The camera is connected to a personal computer to view and record the images. The reflected beam is at a right angle to the transmitted light path and is focused on to the photodetector. A condenser lens  $f = 40$  mm was used to focus a tiny spot on the active area of the detector. The photodetector is connected to

microcontroller which records the optical signal. The data recorded here is through the manual synchronization of camera and detector. In the present work, much valuable progress would be initial characterization and setting-up of absorption thresholds for malaria infected and uninfected blood cells. Moreover, the image and signal acquired would be analyzed with new AI algorithm (AI based framework). The exemplified threshold implemented in the redesigned user-friendly handheld device (Figure 2).

### **Project Implementation Plan: Smart Point-of-Care Device development for malaria screening**

This project proposal main aim is for the Re-design and fabrication of current lab-based absorption flow-cytometer (AFCM) that has been developed for malaria detection in the previous work as shown in figure. 2 with industrial component and incorporate additional features like AI enabled analysis in the current AFCM. It involves novel microfluidic design to perform sorting of blood cells automatically and enable single cell flow. As we knew, single-cell analysis (detection/ imaging) offers huge advantages over whole sample assays like single-cell analysis offers precise information of the molecular and optical properties of individual cells. More details of schematic and preceding work available in my research articles references 26-27. The overall cost of the present basic laboratory is around 1200 USD. However, the final prototype cost may reduce while mass production takes place. **Sample Size:** Sample collection will be taken from Ispat General Hospital, Rourkela. Sample size would be 200 (Normal and malaria infected sub.). Statistical analysis will be performed on the signal data received from PoC device.

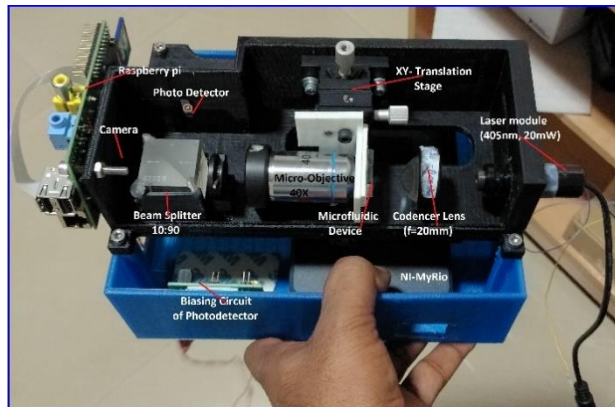


Figure 2: Developed Lab type prototype for same analysis using simple source, microfluidic device and simple electronics for malaria diagnosis at Point-of-Care (27)

### **AI based framework**

The focus of the work is to deploy the advancements in an optofluidic instrument to detect/ screen and classify malaria at point-of-care from a small drop (5 to 10  $\mu$ l) of whole blood. An automated algorithm would be developed using Artificial Intelligent (AI/ ML) algorithms for screening of malaria positive or negative quantitatively from the subject. This will facilitate the automated count of hundreds of thousands of normal and infected cells and the test case is *plasmodium falciparum* samples. More specifically, the goal is to introduce time-based denoising and drift removal techniques to enable better identification of cell-specific peaks in the signal. Mean-centering will be used for removing overall DC level and drift in the photodetector signal. Following this, the photodetector signal will be normalized, and peaks will be detected. The signal will be partitioned into small temporal windows which will be averaged and filtered to remove high-frequency noise. Handcrafted features will be automatically extracted from the filtered sample signal. These features will be fed to Machine learning models for classification.

### **Algorithm and technique involved**

In the current project we are interested to extensively use RL algorithms for automatic screening of malaria using **signal data**. This environment and agent interaction is considered as Markov Decision Process (MDP). Here we are going to study different Markov models and compare the results with the state-of-the-art machine learning and deep learning algorithms. Steps involved in implementation of policy gradient reinforcement algorithm is given below: Hand crafted feature extraction from the data is helpful for training.

Development of an Agent and creation of an objective function based on the influencing parameters. Strength of the algorithm depends on the optimal selection of Agent and the objective function (Policy).

- Assigning of formal work to Agent through a well-known framework known as Markov Decision Process (MDP) which helps in taking the decision to be made at each state. This gives rise to sequence of states, actions and rewards ( $S_0, A_0, R_0, S_1, A_1, R_1, \dots$ ), known as trajectory.
- The gradient of the rewards is determined such as derivative of expected reward is expectation of product of reward and gradient of log of policy
- The optimized path is determined using the policy gradient algorithm for automatic classification of malaria infected and uninfected cells.

#### Outcome(s):

The proposed work plan is for three years: based on the proposed system the vision and expected outcomes are portrayed as following:

- The work proposal brings a compact, battery-operated, Low-cost smart AI enabled PoCD instrument for malaria screening and this would be implemented for limited clinical trial.
- Development of GUI based algorithm for malarial parasite detections, stages of infection, quantitative information of infected cells from overall assessed sample.
- The vision of research will bring high impact factor publications on developed AI algorithms and developed device.
- Filing national and international Patents on the developed technology.
- The most important outcome is creating research and development platform at NIT Rourkela, in the department of Biotechnology and Medical Engineering.
- Of course, this work generates an employment and provides the necessary training to individual.
- The complete reports and user manual will be prepared for further use and commercial enhancement.

#### Impact of Research proposal/significance and clinical applications:

This research will be conducted on the custom developed hyper Imaging system where morphological and optical changes are characterized. The novel blood cells separation microfluidic channel design and development take place in the process of project execution. The characteristics This approach provides several advantages including: 1) Custom design and developments of flow-focusing microfluidic devices which are used for identifying cell morphology, deformability, blood flow velocity. 2) Ability to report the development of POC handheld device for malaria screening. 3) Innovative optical contrast techniques that enable exact measurement of passing single blood cell count through the microfluidic channels and validate. 4) Identify new ways to distinguish populations of blood cell counts, including various white blood cells, red blood cells, platelets based on morphology and signal spectra that are indicators of early blood-borne in addition to screening of malaria. 5) Development of this type of product help in early screening of malaria endemic zone which help towards the eradication of malaria in developing and underdeveloped countries.

#### References and Gantt chart kindly find in the Annexure-1

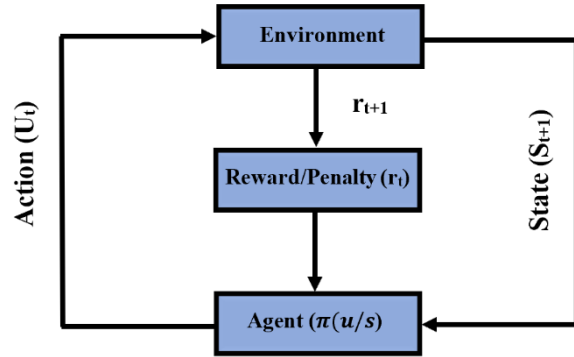


Figure 3: Figure 3 Flow diagram of Reinforcement Learning algorithm

# **Integrated NDIR gas sensor based on mid-infrared silicon photonics**

## **Executive summary**

*Floria Ottonello-Briano*

The technology that I developed in my PhD is currently in the technological “valley of death” and I want to lift it out of it. I successfully demonstrated the use of mid-infrared (mid-IR) Si photonic waveguides for optical gas sensing, as a path to dramatically reduce NDIR sensor size, power consumption, and cost. Miniaturizing optical gas sensors is crucial to enable the extensive and accurate measurement of greenhouse gases (GHGs), which negatively affect climate change and air quality. Optical gas sensors, which rely on the absorption of light by the analyte gas molecules, offer a superior performance in terms of selectivity, sensitivity, speed, stability, and lifetime, compared to other types of sensors. However, their widespread adoption is still limited due to high power consumption, size, and cost. In fact, despite the advantages, their development has been hindered by the lack of suitable optical components for the mid-IR spectral range, where the optical sensing of GHGs with a high selectivity and sensitivity is optimal. Nevertheless, recent advances in light sources, detectors, and integrated photonics for the mid-IR are now accelerating the development of on-chip optical gas sensors based on photonic waveguides.

In this project, I aim at demonstrating the first integrated mid-IR gas sensor based on silicon photonic waveguides and low-cost, low-power-consumption active components. The system will comprise a Si photonic chip and off-the-shelf mid-IR LED light source and photodiode detector with integrated optical filter. The main goal of the project is to show the compact integration of all components into a working gas sensor prototype for NDIR CO<sub>2</sub> detection. The main challenge of the project is to achieve a sufficiently efficient coupling from the light source to the photonic circuit and from the circuit to the detector.

Although the proposed prototype still uses discrete off-chip components, it is the crucial step towards a fully on-chip integrated system. Once demonstrated, the system will attract resources to be advanced further. The proposed technology will lead to a reduction in size and cost of one order of magnitude compared to current commercial NDIR sensors, enabling the adoption of optical gas sensors in an increasingly broad range of applications, in particular air quality monitoring for environmental, health, and safety purposes, with a positive impact of people’s and Earth’s well-being.



# Integrated NDIR gas sensor based on mid-infrared silicon photonics

Project proposal

*Floria Ottonello-Briano*

## Introduction and state-of-the-art

The Keeling curve [1] unequivocally shows us that we humans are dramatically changing the composition of Earth's atmosphere. Since the Industrial Revolution in the mid-18th century, the global concentration of carbon dioxide (CO<sub>2</sub>) increased at an alarming rate from a level of 280 ppm to the 422 ppm reached last June, the highest ever in the past 800 thousand years. CO<sub>2</sub> and the other main greenhouse gases (GHGs) – methane (CH<sub>4</sub>), nitrous oxide (N<sub>2</sub>O), fluorinated gases – produced by the combustion of fossil fuels or otherwise emitted by human activities, cause global warming and thus affect Earth's climate [2,3]. Moreover, elevated GHGs levels increase mortality due to air pollution [4,5] and gas leakages put people at risk of asphyxiation, intoxication, fire or explosion [6]. Indoors, even the common CO<sub>2</sub> levels can deteriorate human cognitive function and decision making [7–9], with consequences spanning from reduced attention and productivity in classrooms and offices [7,8] to an increased risk for car and airplane accidents [9]. A fundamental part of combating climate change, fighting air pollution, and improving people's health is therefore the extensive and accurate measurement of GHGs, to identify and quantify the emissions and to assess the outcomes of our interventions. Crucially, the monitoring at the global level and the measurements of a few far-apart environmental stations are not sufficient. They must be supported by a widespread monitoring at the local scale.

However, the implementation of distributed gas sensing with high spatial and temporal resolution remains a challenge due to technological and financial limitations. On one hand, some of the technologies used for environmental gas sensing, such as gas chromatography, mass spectrometry, FTIR spectroscopy, and IR laser spectroscopy, provide high-quality measurements, but consist in high-end, costly and bulky instrumentation. On the other hand, small and cheap consumable sensors, usually chemical sensors such as semiconductor and electrochemical sensors, have insufficient sensing performance and suffer from strong drift and degradation, resulting in a short lifespan. Additionally, both classes of sensors require frequent maintenance, which increases costs.

In this setting, low-cost miniaturized optical sensors are the prime candidates to accommodate the requirements of distributed gas sensing. In contrast to chemical sensors, optical sensors do not rely on the interaction between the analyte gas and the sensor material, but on the interaction between the gas and light. Thus, they offer a superior performance in terms of selectivity, sensitivity, speed, stability, and lifetime. However, their widespread adoption is still limited due to high power consumption, size, and high cost. Even the simplest optical gas sensors, non-dispersive infrared (NDIR) sensors, which are a mature technology, are still a few cubic centimetres big and come with a price tag in the order of 100 USD because they are not mass-production-friendly. A technological shift from the traditional free-space optics towards integrated photonics is required to achieve the miniaturization and low cost required for the pervasive adoption of optical gas sensor. Fully integrated photonic-based sensors will be suited for cost-efficient mass production and will enable integration in portable devices such as mobile phones thanks to their small size and low power consumption.

So far, the development of miniaturized optical gas sensors has been hindered by the lack of suitable optical components for the mid-infrared (mid-IR) spectral range. This, also called the fingerprint region, is the preferable range for high-performance gas sensing because for many chemical species, including GHGs, mid-IR wavelengths match the fundamental vibrational-rotational energy levels of the gas molecules, and are thus more strongly absorbed by the gas, providing a stronger optical response. Nevertheless, recent advances in technologies for the IR, such as integrated photonic components [10–12], IR lasers [13,14], integrated IR light

sources [10,11,15] and detectors [10,11] and their increased availability on the market [16–20] are stimulating new efforts towards integrated optical gas sensors.

A demonstration of an integrated, miniaturized photonic chip sensor for spectroscopy of  $\text{CH}_4$  is shown in [21], based on the silicon (Si) waveguide technology presented in [22] with the addition of an off-the-shelf external-cavity near-IR laser, photodiode, semiconductor optical amplifier, and filters. However, this sensor operates at near-IR wavelength, probing an overtone absorption band of  $\text{CH}_4$ , which is about two orders of magnitude weaker than the fundamental absorption band in the mid-IR. Although the Si photonics technology is mature at near-IR wavelengths, allowing for faster development, the physical properties of GHGs limit the applicability of near-IR gas sensors to high-concentration situations. In the mid-IR range, instead, various waveguide designs and materials have been explored, showing acceptable waveguide losses, but only using bulky, power-hungry, and costly external benchtop ICL and QCL sources [23–26]. Mid-IR laser sources, besides being incompatible with low-cost production, feature a narrow bandwidth and tuning range, which makes them unsuitable for relevant multi-gas detection. In [27], a broadband source was integrated with a Si waveguide and the detection of high  $\text{CO}_2$  concentrations was shown. However, optical detection was performed with laboratory instruments and the aspect of spectral filtering to ensure selectivity was not addressed. In conclusion, no fully integrated mid-IR gas sensing system has been demonstrated yet.

## Objective

In this project, I aim at demonstrating the first integrated mid-IR gas sensor based on Si photonic waveguides and low-cost, low-power-consumption mid-IR active components. The system will comprise a Si photonic sensing chip based on the technology that I developed in my PhD [26,28], and off-the-shelf mid-IR LED light source and photodiode detector with integrated optical filter. The main goal of the project is to show the compact integration of all components into a working gas sensor prototype for NDIR  $\text{CO}_2$  detection, as the crucial step towards a fully on-chip integrated system.

The main challenge of the project is to achieve a sufficiently efficient coupling from the light source to the photonic circuit and from the circuit to the detector.

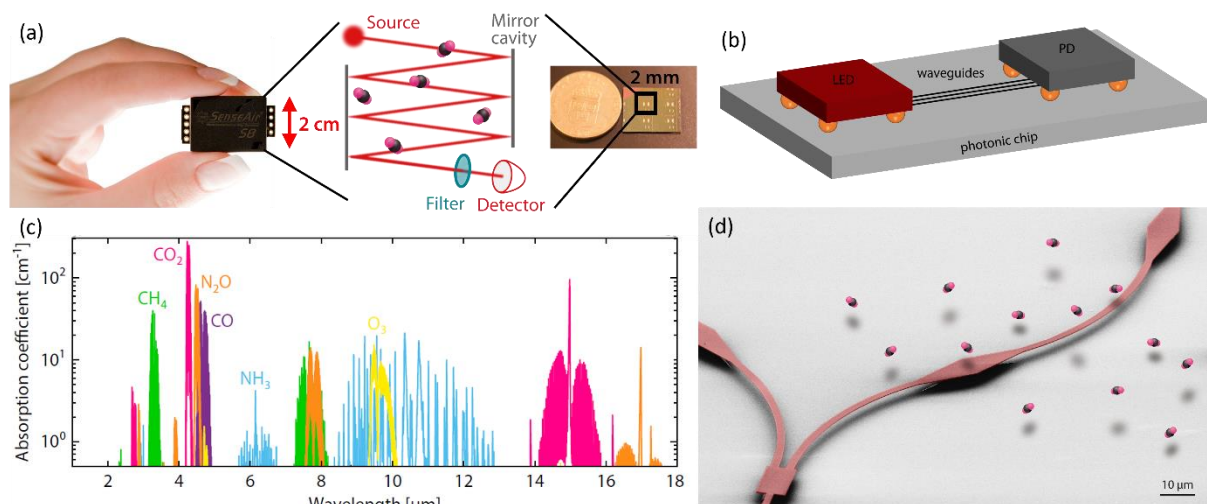


Figure 1: (a) Miniaturization of NDIR gas sensors by transitioning from the traditional free-space configuration to integrated photonic waveguides. (b) Illustration of the project objective: to integrate low-cost low-power-consumption discrete LED and photodiode on the photonic sensing chip. (c) The fingerprint region: wavelength-dependent absorption coefficient of the most abundant trace gases: carbon dioxide ( $\text{CO}_2$ ), methane ( $\text{CH}_4$ ), carbon monoxide ( $\text{CO}$ ), ammonia ( $\text{NH}_3$ ), ozone ( $\text{O}_3$ ), and nitrous oxide ( $\text{N}_2\text{O}$ ), as listed by the HITRAN database [29]. (d) Suspended silicon waveguide, false-color SEM image overlaid with an illustration of  $\text{CO}_2$  gas molecules [28].

## Work Plan

### Work package 1 (WP1): Design

#### Task 1.1: Evaluation and selection of mid-IR LED and photodiode

Different commercially available mid-IR LEDs and photodiodes for 4.2  $\mu\text{m}$  wavelength, such as [17–19], will be evaluated on performance, suitability for the intended integration, and cost. The investigation will rely on datasheet information and on existing characterization data previously collected in-house in Senseair. For the LEDs, the critical parameters are the emission power and the spatial distribution of the emission. For the photodiodes, noise-equivalent power (NEP), sensing area, and included optical filtering are the main discriminating factors.

#### Task 1.2: Investigation of discrete micro-optics components for improved efficiency

Achieving high coupling efficiency from an LED emitting area of about  $500 \times 500 \mu\text{m}^2$  to Si waveguides with cross-section of a few  $\mu\text{m}$  times a few hundred nm is extremely challenging. In this task, the possibility of interposing additional micro-optics components to improve the coupling efficiency will be investigated. The possible benefits of integrating traditional microlenses, Fresnel lenses, and metalenses will be evaluated with optical simulations. This task runs in parallel with Task 1.3.

#### Task 1.3: Optimization of photonic couplers

Starting from existing proprietary designs of diffractive grating couplers and in a feedback loop with Tasks 1.1 and 1.2, optimized mid-IR Si photonics grating couplers will be designed specifically for this application.

### Work package 2 (WP2): Fabrication and system integration

#### Task 2.1: Fabrication of Si photonic chip

The Si photonic chip, comprising the grating couplers designed in Task 1.3, will be fabricated, with a process analogous to that described in [26]. The process will be kept as simple as possible, preferably limited to a single lithography step. Existing research collaborations with universities and foundries will be leveraged to minimize the time effort and cost of this task, e.g. by seeking co-fabrication collaborations in a multi-project wafer scheme.

#### Task 2.2: Integration of source, detector, and possible additional micro-optics with photonic chip

Two main options will be considered for the integrating of the discrete components with the photonic chip: integration on the chip surface with physical contact and integration in the prototype package with spaced alignment to the chip. In the first case, the components will be flip-chip connected to the chip with solder bumps. In the second case, instead, the discrete components will be integrated in the package of the prototype, which will have to ensure adequate spacing and alignment.

#### Task 2.3: Design and fabrication of the prototype package

Based on the evaluation in Task 2.3, the prototype package, which must bring together all components, will be designed. If the discrete components are integrated in the package, the package design is particularly critical, as it plays a crucial role in positioning the active components with respect to the photonic circuit. The package may be of plastic material or metal, and fabricated in-house by 3D printing or, if higher precision is required, its micro-machining may be outsourced. The package must ensure the stability of the assembly and protection from external agents such as particles while being gas permeable.

### Work package 3: Characterization

#### Task 3.1: Optical characterization of the prototype

The optical performance of the prototype will be first characterized. Previously developed circuitry and instruments already present in-house will be leveraged to operate the active

components and apply suitable measurement schemes. However, dedicated electronics and software may be required.

### Task 3.2: Gas sensing demonstration

Finally, the prototype's gas sensing performance will be tested with CO<sub>2</sub> gas.

### **Outcome**

The outcome of the project will be the first fully integrated NDIR gas sensor based on photonic waveguide technology. The sensor will operate at 4.2 μm for CO<sub>2</sub> detection.

### **Impact**

During my PhD, I successfully demonstrated the use of Si photonic waveguides as the optical path for NDIR gas sensing as a way to dramatically reduce the sensor size. However, the technology I developed is currently in the technological "valley of death" because a demonstration of a fully integrated photonic-based sensor with low-cost potential is still missing. The prototype proposed in this project is key to attract attention and resources to advance the technology further.

The proposed technology, leading to a reduction in size and cost of one order of magnitude compared to current commercial NDIR sensors, has great scientific, societal, and commercial potential, in a global gas sensor market that was valued at 2.3 billion USD in 2020 [30]. In my work, I witness first-hand the need and wish for small, low-power, low-cost gas sensors by a broad range of stakeholders. Air quality monitoring for environmental, health, and safety related purposes is currently not performed at a satisfying level due to technological and economic limitations. Reliability, power consumption, mobility, and cost are the most critical aspects. The proposed technology targets precisely those aspects, by developing gas sensors that rely on optical absorption and thus have much better selectivity and lifetime than other types of gas sensors, that are miniaturized and integrated and can thus be installed in portable and mobile devices, and that can be mass produced in large batches for cost-effectiveness. Therefore, by meeting a clear existing need, the technology has a great potential for making a rapid societal impact through a broad range of applications.

Small low-cost gas sensors will become widespread in safety applications: they will be used in portable devices carried by personnel handling gases and will become essential components of equipment such as refrigerant and heating units that contain potentially hazardous or polluting gases. Moreover, increased public awareness about air pollution and new policies such as EU standards, the Green New Deal, the European Green Deal, and WHO guidelines, are driving the need for more and better measurements of polluting gases, in particular GHGs. Accurate and widespread measurements are urgent and crucial to progress towards the reduction of emissions, and the industrial and farming sectors, major contributors to GHGs emissions, are expressing the need for accessible sensing tools. The public is also increasingly aware of the effect of air quality on health. The growing understanding of the role of ventilation in the spread of infectious disease during the Covid-19 pandemic, and recent clinical studies of the role of air pollution in asthma [31], played an important role and result in demand for improved monitoring of both indoor and outdoor air quality, as well as in stricter guidelines. Hence, the demand for small low-cost low-power gas sensors is already great and will accelerate the impact of this technology.

### **References**

1. R. F. Keeling and C. D. Keeling, "Scripps CO<sub>2</sub> Program Data," <http://doi.org/10.6075/J0542KSG>.
2. A. A. Lacis, G. A. Schmidt, D. Rind, and R. A. Ruedy, "Atmospheric CO<sub>2</sub>: Principal Control Knob Governing Earth's Temperature," *Science* **330**, 356–359 (2010).
3. H. D. Matthews, N. P. Gillett, P. A. Stott, and K. Zickfeld, "The proportionality of global warming to cumulative carbon emissions," *Nature* **459**, 829–832 (2009).

4. T. A. Jacobson, J. S. Kler, M. T. Hernke, R. K. Braun, K. C. Meyer, and W. E. Funk, "Direct human health risks of increased atmospheric carbon dioxide," *Nature Sustainability* **2**, 691–701 (2019).
5. WHO, "Ambient (outdoor) air pollution," [https://www.who.int/news-room/fact-sheets/detail/ambient-\(outdoor\)-air-quality-and-health](https://www.who.int/news-room/fact-sheets/detail/ambient-(outdoor)-air-quality-and-health).
6. A. Guais, G. Brand, L. Jacquot, M. Karrer, S. Dukan, G. Grévilot, T. J. Molina, J. Bonte, M. Regnier, and L. Schwartz, "Toxicity of Carbon Dioxide: A Review," *Chem. Res. Toxicol.* **24**, 2061–2070 (2011).
7. U. Satish, M. J. Mendell, K. Shekhar, T. Hotchi, D. Sullivan, S. Streufert, and W. J. Fisk, "Is CO<sub>2</sub> an Indoor Pollutant? Direct Effects of Low-to-Moderate CO<sub>2</sub> Concentrations on Human Decision-Making Performance," *Environ. Health Perspect.* **120**, 1671–1677 (2012).
8. J. G. Allen, P. MacNaughton, U. Satish, S. Santanam, J. Vallarino, and J. D. Spengler, "Associations of Cognitive Function Scores with Carbon Dioxide, Ventilation, and Volatile Organic Compound Exposures in Office Workers: A Controlled Exposure Study of Green and Conventional Office Environments," *Environ. Health Perspect.* **124**, 805–812 (2016).
9. J. G. Allen, P. MacNaughton, J. G. Cedeno-Laurent, X. Cao, S. Flanigan, J. Vallarino, F. Rueda, D. Donnelly-McLay, and J. D. Spengler, "Airplane pilot flight performance on 21 maneuvers in a flight simulator under varying carbon dioxide concentrations," *J. Exposure Anal. Environ. Epidemiol.* **1** (2018).
10. H. Lin, Z. Luo, T. Gu, L. C. Kimerling, K. Wada, A. Agarwal, and J. Hu, "Mid-infrared integrated photonics on silicon: a perspective," *Nanophotonics* **7**, (2017).
11. J. Fedeli and S. Nicoletti, "Mid-Infrared (Mid-IR) Silicon-Based Photonics," *Proceedings of the IEEE* **106**, 1–11 (2018).
12. Y. Zou, S. Chakravarty, C.-J. Chung, X. Xu, and R. T. Chen, "Mid-infrared silicon photonic waveguides and devices [Invited]," *Photon. Res.* **6**, 254–276 (2018).
13. Y. Yao, A. J. Hoffman, and C. F. Gmachl, "Mid-infrared quantum cascade lasers," *Nat. Photon.* **6**, 432–439 (2012).
14. M. Razeghi, Q. Y. Lu, N. Bandyopadhyay, W. Zhou, D. Heydari, Y. Bai, and S. Slivken, "Quantum cascade lasers: from tool to product," *Opt. Express*, OE **23**, 8462–8475 (2015).
15. D. Jung, S. Bank, M. L. Lee, and D. Wasserman, "Next-generation mid-infrared sources," *J. Opt.* **19**, 123001 (2017).
16. "Thorlabs Turnkey MIR Laser Systems," [https://www.thorlabs.com/newgrouppage9.cfm?objectgroup\\_id=10097](https://www.thorlabs.com/newgrouppage9.cfm?objectgroup_id=10097).
17. Hamamatsu, "Characteristics and use of infrared detectors," [https://www.hamamatsu.com/resources/pdf/ssd/infrared\\_kird9001e.pdf](https://www.hamamatsu.com/resources/pdf/ssd/infrared_kird9001e.pdf).
18. "AKM Infrared LED Elements for NDIR Gas Sensor," <https://www.akm.com/content/www/akm/eu/en/products/gas-sensing/infrared-led-element-for-ndir-gas-sensor.html>.
19. "AKM Infrared Sensors for NDIR Gas Sensor," <https://www.akm.com/content/www/akm/eu/en/products/gas-sensing/infrared-sensor-for-ndir-gas-sensor.html>.
20. "Vigo Infrared Detectors," <https://vigo.com.pl/products-vigo/infrared-detectors/>.
21. W. M. J. Green, E. J. Zhang, C. Xiong, Y. Martin, J. Orcutt, M. Glodde, L. Schares, T. Barwicz, C. C. Teng, N. Marchack, E. Duch, S. Kamapurkar, S. Engelmann, N. Hinds, T. Picunco, R. Wilson, and G. Wysocki, "Silicon Photonic Gas Sensing," in *Optical Fiber Communication Conference (OFC) 2019 (2019), Paper M2J.5* (Optical Society of America, 2019), p. M2J.5.
22. L. Tombez, E. J. Zhang, J. S. Orcutt, S. Kamapurkar, and W. M. J. Green, "Methane absorption spectroscopy on a silicon photonic chip," *Optica* **4**, 1322–1325 (2017).
23. T. Jin, J. Zhou, P. T. Lin, P. T. Lin, and P. T. Lin, "Mid-Infrared Waveguides for Volatile Organic Compounds Detection," in *Optical Sensors and Sensing Congress (ES, FTS, HISE, Sensors) (2019), Paper EW2A.2* (Optical Society of America, 2019), p. EW2A.2.
24. P. Su, Z. Han, D. Kita, P. Becla, H. Lin, S. Deckoff-Jones, K. Richardson, L. C. Kimerling, J. Hu, and A. Agarwal, "Monolithic on-chip mid-IR methane gas sensor with waveguide-integrated detector," *Appl. Phys. Lett.* **114**, 051103 (2019).
25. C. Ranacher, C. Consani, N. Vollert, A. Tortschanoff, M. Bergmeister, T. Grille, and B. Jakoby, "Characterization of Evanescent Field Gas Sensor Structures Based on Silicon Photonics," *IEEE Photon. J* **10**, 1–14 (2018).
26. F. Ottonello-Briano, C. Errando-Herranz, H. Rödjegård, H. Martin, H. Sohlström, and K. B. Gylfason, "Carbon dioxide absorption spectroscopy with a mid-infrared silicon photonic waveguide," *Opt. Lett.*, OL **45**, 109–112 (2020).
27. C. Consani, C. Ranacher, A. Tortschanoff, T. Grille, P. Irsigler, and B. Jakoby, "Mid-infrared photonic gas sensing using a silicon waveguide and an integrated emitter," *Sens. Actuators B Chem.* (2018).
28. F. Ottonello Briano, "Mid-infrared photonic devices for on-chip optical gas sensing," (2019).
29. I. E. Gordon, L. S. Rothman, C. Hill, R. V. Kochanov, Y. Tan, P. F. Bernath, M. Birk, V. Boudon, A. Campargue, K. V. Chance, B. J. Drouin, J.-M. Flaud, R. R. Gamache, J. T. Hodges, D. Jacquemart, V. I. Perevalov, A. Perrin, K. P. Shine, M.-A. H. Smith, J. Tennyson, G. C. Toon, H. Tran, V. G. Tyuterev, A. Barbe, A. G. Császár, V. M. Devi, T. Furtenbacher, J. J. Harrison, J.-M. Hartmann, A. Jolly, T. J. Johnson, T. Karman, I. Kleiner, A. A. Kyuberis, J. Loos, O. M. Lyulin, S. T. Massie, S. N. Mikhailenko, N. Moazzen-Ahmadi, H. S. P. Müller, O. V. Naumenko, A. V. Nikitin, O. L. Polyansky, M. Rey, M. Rotger, S. W. Sharpe, K. Sung, E. Starikova, S. A. Tashkun, J. V. Auwera, G. Wagner, J. Wilzewski, P. Wcislo, S. Yu, and E. J. Zak, "The HITRAN2016 molecular spectroscopic database," *J. Quant. Spectrosc. Radiat. Transfer* **203**, 3–69 (2017).
30. Grand View Research, *Global Gas Sensor Market Size & Share Report, 2021-2028* (n.d.).
31. M. Ashworth, A. Analitis, D. Whitney, E. Samoli, S. Zafeiratos, R. Atkinson, K. Dimakopoulou, S. Beavers, J. Schwartz, K. Katsouyanni, and STEAM project research group, "Spatio-temporal associations of air pollutant concentrations, GP respiratory consultations and respiratory inhaler prescriptions: a 5-year study of primary care in the borough of Lambeth, South London," *Environ Health* **20**, 54 (2021).



Executive Summary for:  
**Noninvasive High-Resolution Imaging through Living Tissue  
with Single-Shot Synthetic Wavelength Holography**

Florian Willomitzer, Wyant College of Optical Sciences, University of Arizona, USA

**What is proposed?** This proposal seeks to develop a *computational camera* that can *image through dynamic scattering media* with *high resolution*. The camera is primarily proposed for medical imaging applications through living (moving) tissue. The proposed noninvasive technique only uses light in (or close to) the optical wave band and works with standard off-the-shelf camera technology – theoretically even with mobile phone camera sensors. The technique leverages the huge potential of carefully designed optical systems paired with sophisticated algorithms. If successful, the camera could become part of a new wave of computational imaging devices that will represent key technologies in our near future.

**Why is this important?** Over the last decades the field of medical imaging has spawned several seminal inventions which can be found in every hospital nowadays. Prominent examples include Optical Coherence Tomography (OCT), Computed Tomography (CT), Ultrasound, or Magnet Resonance Imaging (MRI). However, recent years have seen a growing interest in medical imaging techniques which enable to look inside the human body, *but are non-invasive* and can be facilitated in a *small form factor*, i.e., possibly even operated in a hand-guided fashion. In other words: Cameras that allow to image small structures (such as capillaries, lesions, tumors, etc.) through scattering media, such as tissue and bone.

**What is the problem?** The proposed plan to develop such a camera builds up on the recent publication of the PI's research group, which used "Synthetic Wavelength Holography" (SWH) to image through scattering media and around corners with a demonstrated resolution up to 800 $\mu$ m [1]. However, the current SWH approach relies on the *acquisition of sequentially captured images* (at different optical wavelength) and is *extremely susceptible to motion*. Even the slightest movement of object or scatterer between two captured images leads to a complete loss of information, which makes imaging through living (i.e., moving!) tissue impossible with the current method. Moreover, the current SWH technique relies on expensive modulation/imaging hardware, such as acousto optical modulators and specialized lock-in cameras.

**What is the solution?** This proposal outlines a solution for the aforementioned problems of the current SWH method. The solution draws inspiration from established optical metrology principles and allows for *single-shot (!)* SWH measurements with the same or similar quality as shown in [1]. This means that all required information can be captured *with one single camera image* in a very short exposure time (<1ms in our preliminary experiments). Moreover, the proposed approach allows to swap expensive and specialized imaging hardware with standard off-the-shelf camera technology that can be found in every smartphone nowadays.

**Who cares (impact)?** If successful, the proposed technique of "Single-Shot-SWH" could have immense impact on future academic research as well as today's billion-dollar industries. This impact goes far beyond potential applications in medical imaging (e.g., to noninvasively monitor the beating heart through the chest). Potential examples from other industries include self-driving cars that use the technique to analyze hidden scenes around corners or through fog, hand-guided industrial inspection devices that detect defects around corners in confined spaces, novel cameras for first responders that image through smoke or turbid water, or next generation VR/AR headsets that show the user obstacles or hazards which are hidden from his direct view.

**Why should this proposal be granted?** The proposed technique significantly advances the state-of-the-art and our fundamental understanding of limits. Moreover, the work represents a critical first step to put the PI's long-term research vision into practice and would eventually enable him to apply for follow up funding. Due to the risks involved in the initial "Single-Shot-SWH" demonstration (which would provide the basis for larger multi-year grants) the proposed project may be difficult to be funded from other sources.



# Noninvasive High-Resolution Imaging through Living Tissue with Single-Shot Synthetic Wavelength Holography

Florian Willomitzer, Wyant College of Optical Sciences, University of Arizona, USA

## 1) Introduction

Computational optical imaging techniques have been used in academia and industry for many years with great success. Fields of applications include industrial inspection, autonomous navigation, AR/VR, or forensics. Amongst the multitude of possibilities, one specific application of computational imaging has gained immense importance over the last decades and has contributed significantly to the advancement of our modern society: *Medical Imaging*. Medical Imaging devices and techniques are an impressive demonstration of the power and impact of carefully designed (optical) systems paired with sophisticated algorithms. Prominent examples include the invention and development of Optical Coherence Tomography (OCT), Computed Tomography (CT), Ultrasound, or Magnet Resonance Imaging (MRI) – all techniques that can be found in every hospital nowadays.

Recent years have seen a growing interest in medical imaging techniques which enable to look inside the human body, *but are non-invasive* and can be facilitated in a *small form factor*, i.e., possibly operated in a hand-guided fashion. In other words: Cameras that allow to image small structures (such as capillaries, lesions, tumors, etc.) through scattering media, such as tissue and bone.

This proposal seeks to develop such a new camera. Instead of, e.g., X-rays and X-ray detectors, the proposed technique uses optical light and conventional cameras to image the respective objects through scattering media. The method allows for a combination of capabilities that is, to the PI's knowledge, currently unmatched by the state of the art: Single-shot imaging, high spatial resolution, wide field of view, and small probing area (see Fig. 1 and Sec. 3 for explanation). This makes the proposed technique and device a perfect candidate for the next generation of medical imaging methods.

## 2) Problem Statement and Impact

The goal of this proposal is to develop a camera that can image through dynamic scattering media, such as living (moving) tissue, turbid fluids, or fog. The proposed method builds up on the recent publication of the PI's research group, which used "Synthetic Wavelength Holography" (SWH) to image around corners and through scattering media [1]. This technology has already proven that it can reconstruct objects behind scatterers with up to sub-mm resolution. However, each measurement required *at least 2 camera images* (at two slightly different wavelengths) captured in a *sequential* fashion. As the method relies on the correlation of speckle patterns (see Sec. 3.1), *even the slightest movement of object or scatterer between the two captured images leads to a complete loss of information*. This makes the current (multi-shot) method *highly susceptible to motion*, which makes imaging through living (i.e., moving!) tissue impossible.

A solution of this problem can potentially lead to a new (and relatively unexplored) wave of novel imaging techniques and devices. These techniques and devices can have immense impact on future academic research, but also on today's billion-dollar industries. For medical imaging, this could potentially lead to imagers that can noninvasively measure fast processes inside the human body, such as monitoring the beating heart through the chest (Fig. 1b). Application examples from other industries can be found in automotive (imaging around the corner or through fog, Fig. 1d), industrial inspection (defect detection, Fig. 1c), material science (image deeper through materials), or VR/AR (detect objects/persons in other rooms). Moreover, the proposed principle is universal and not restricted to optical wavelengths, which in turn will allow for an

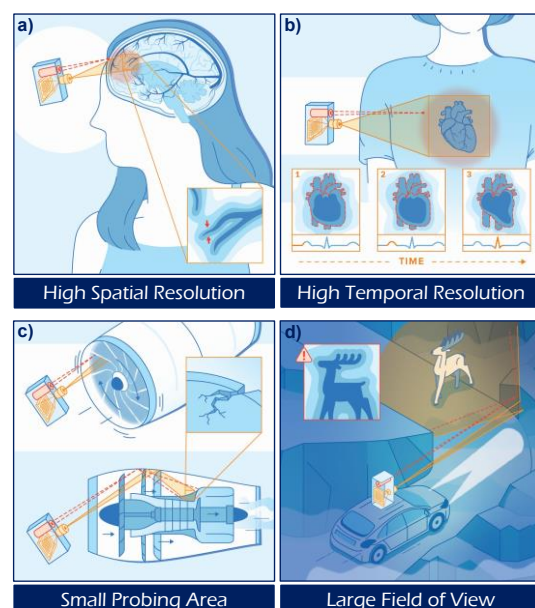


Fig. 1: Attributes of Synthetic Wavelength Holography and potential future applications.

even wider gamut of possible applications (e.g., in space exploration).

This proposal introduces a method that seeks to perform SWH measurements with the same or similar quality as shown in [1], *but in single-shot (!)*, meaning that all required information (from two different optical fields at two different wavelengths) can be captured *with one single camera image* within a very short exposure time (<1ms in our preliminary experiments). Prior to writing this proposal, the PI's team has already obtained preliminary results for the single-shot reconstruction of objects in "line of sight", i.e., not hidden in/behind a scattering medium. The preliminary results of this "single-shot high-precision ToF camera" are used in Fig. 2 to demonstrate the proposed method.

Demonstrating the proposed principle in "non-line-of-sight" at measurements through dynamic strongly scattering media (such as living tissue) would mark a significant step towards the PI's long term research goal and would eventually enable the PI to apply for follow up funding. Due to the risks involved in the initial "Single-Shot-SWH" demonstration (which would provide the basis for larger multi-year grants) the proposed project may be difficult to be funded from other sources.

### 3) State of the Art and Literature Review

#### 3.1) Synthetic Wavelength Holography (SWH) – the team's previous multi-shot solution

The presence of a scattering medium between an object and an observer severely limits the visual acuity of the imaging system. If a coherent light field undergoes multiple scattering (e.g., in tissue), the optical phase and intensity of the scattered light field is randomized. When imaging the backscattered field with a detector (camera), the resulting "speckle field" does seemingly not contain any information about the macroscopic optical path length anymore, which makes a reconstruction of the object hidden behind the scattering medium impossible with conventional imaging methods. Our previously published SWH approach [1]–[4] draws inspiration from multi-wavelength interferometry on rough surfaces, a technique that has been extensively researched by the PI's research group [5]–[9] and has been widely used in optical metrology [10]–[14]. The technique exploits spectral correlations in scattered light fields at optical wavelengths  $\lambda_1$  and  $\lambda_2$  to assemble a hologram of the obscured objects at a "synthetic wavelength"  $\Lambda = \frac{\lambda_1 \lambda_2}{|\lambda_1 - \lambda_2|}$ . The basic idea: By probing the scene with a second wavelength  $\lambda_2$ , slightly different from the initial wavelength  $\lambda_1$ , additional information can be exploited: If the illumination beams at the two wavelengths originate from the same source position (such as from a single fiber) *and the inhomogeneities in the scattering medium are quasi-static*, the speckle fields  $E(\lambda_1)$ ,  $E(\lambda_2)$  incident on the detector are highly spectrally correlated. This is because the light at the two wavelengths experiences nearly identical path length fluctuations. Hence, the residual changes in phase  $|\phi(\lambda_1) - \phi(\lambda_2)|$  encode the macroscopic structure of the obscured object [1], [2]. In [1], the team has exploited this fact to reconstruct obscured objects through *static* scattering media (see Figs. 3,4 in article [1] or Figs. 1.9, 1.10 in book chapter [2]). A complex valued hologram  $E(\Lambda)$  of the object at the synthetic wavelength  $\Lambda$  is obtained via computational mixing of the two sequentially acquired speckle fields

$$E(\Lambda) = E(\lambda_1) \cdot E^*(\lambda_2) = A_1 A_2 \cdot e^{i(\phi(\lambda_1) - \phi(\lambda_2))} = A_1 A_2 \cdot e^{i(\phi(\Lambda))} \quad , \quad (1)$$

with  $A_1, A_2$  being the respective amplitudes and  $\phi(\lambda_1), \phi(\lambda_2)$  the respective (speckled) phase maps at the given wavelengths  $\lambda_1, \lambda_2$ . For closely spaced optical wavelengths  $\lambda_1$  and  $\lambda_2$  the synthetic wavelength is orders of magnitudes larger than  $\lambda_1$  and  $\lambda_2$ . The synthetic phase  $\angle E(\Lambda) = \phi(\Lambda) = \phi(\lambda_1) - \phi(\lambda_2)$  becomes robust to the deleterious effects of scattering (see Fig. 1.1 in book chapter [2]). Eventually, an image of the hidden object can be retrieved by numerical backpropagation of  $E(\Lambda)$  at the synthetic wavelength  $\Lambda$  (Fig. 1a in article [1] or Fig. 1.7 in book chapter [2]). The team has demonstrated static measurements through weakly and strongly scattering scenes with holographic reconstructions of hidden objects of up to  $800 \mu\text{m}$  lateral resolution [1]. Related considerations and calculations of fundamental physical and information-theoretical limits performed in [1], [2] show that higher resolutions could be theoretically achieved as well (dependent on the scatterer).

#### 3.2) Competing methods for imaging through scattering media and comparison with SWH

Besides the introduced SWH technique, existing active methods to image through scattering scenes are either based on time-of-flight (ToF) cameras (pulsed or continuous wave) or exploit *spatial* correlations in the scattered speckle fields, sometimes called the spatial (or angular) "memory effect" [15], [16]. ToF-based techniques are commonly used for larger (human-sized) objects in larger hidden volumes.

Recent work has demonstrated results with lateral resolutions around  $\sim 5\text{cm}$  over a  $\sim 1\text{m} \times 1\text{m} \times 1\text{m}$  working volume, and in select cases providing near real-time reconstructions. However, many approaches rely on raster scanning large areas on the surface of the scatterer whose dimensions are comparable to the obscured volume [17]–[23]. The combination of *relatively low resolution* and *large probing area* makes the adaptation of ToF-based principles to medical applications impractical or even impossible, especially if the object should be measured with high resolution in a confined space. Spatial correlation-based techniques allow for the highest lateral resolution of object reconstructions ( $< 100\ \mu\text{m}$ ), sometimes even in single-shot. Moreover, the probing area imaged on the surface of the scatterer can be less than a few *cm*. These benefits, however, come at the expense of a *highly restricted angular field of view* ( $< 2^\circ$ , even for mild scattering), as determined by the angular decorrelation of scattered light. This “angular memory effect” does not only limit the field of view but also the maximal possible size of the measured object, which is not allowed to exceed the respective working volume [24]–[30]. Although those methods can be used (and are used with great success!) to analyze small samples with very high resolution, the limited angular field of view and restriction to small objects prevents them from being used for a generalized (possibly hand-guided) medical imager for the entire human body.

In contrast to both techniques described above, the SWH technique allows for a combination of capabilities that is, to the PI’s knowledge, currently unmatched by the state of the art [1]:

**Small Probing Area:** Many ToF-based schemes require large probing areas of  $\sim 1\text{m} \times 1\text{m}$  or larger, which limits their ability to detect hidden objects in confined spaces. SWH provides the ability to image obscured objects by simultaneously illuminating and observing a small area ( $58\text{mm} \times 58\text{mm}$  in [1]).

**Wide Angular Field of View:** Angular memory effect-based approaches are limited to highly restricted fields of view. As a holographic method, SWH provides the ability to recover obscured objects over a nearly hemispherical field of view that far exceeds the limited angular extent of the memory effect.

**High Spatial Resolution:** ToF camera-based approaches generally produce rather low spatial resolutions, due to the used intensity-modulated waves with long wavelengths [31], [32]. SWH allows for freely tunable synthetic wavelengths and provides the ability to resolve small features on obscured objects (below  $1\text{mm}$  for the experiments shown in [1]).

**High Temporal Resolution:** Many approaches rely on point-wise raster-scanning and/or the acquisition of a temporal image sequence. SWH can recover full field holograms of the obscured object using off-the-shelf camera technology, which makes the method already faster than many of its competitors. *However, it has been discussed above that the current SWH dual-shot solution is still not sufficient to image through dynamic scattering media, like living tissue or fog.*

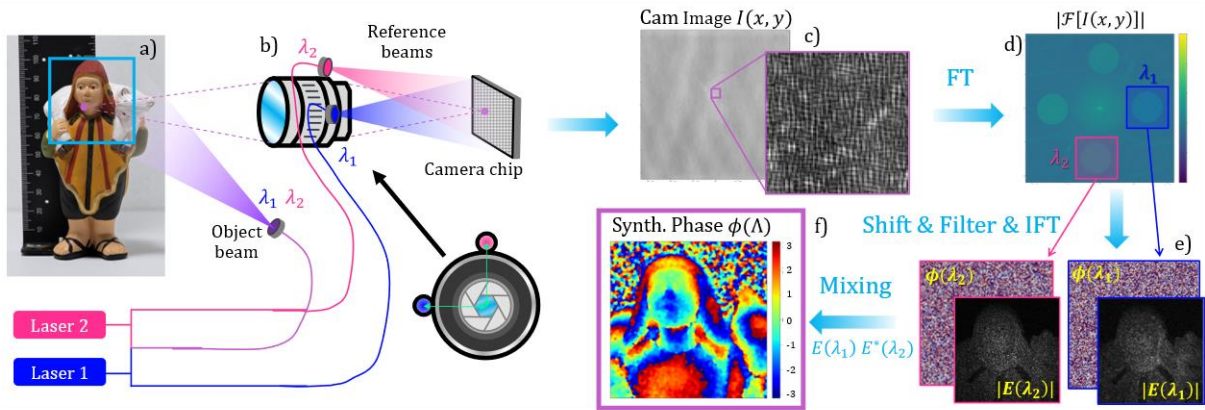
#### 4) Proposed Solution: Retrieving the Synth. Field in Single-Shot with Standard Camera Tech

The fact that two sequentially captured speckle patterns are prone to movement-induced decorrelation (which can happen even for the slightest movements of object or scatterer!) poses a *significant limitation* on the current SWH principle and has stimulated the idea for this proposal. The proposed idea draws inspiration from spatial heterodyning, off-axis holography, or single-sideband demodulation procedures (see e.g., [33], [34]). As mentioned above, the proposed method is now outlined with the help of preliminary results (Fig. 2) which have been captured in “line-of-sight” via synthetic wavelength interferometry [2], [5]. Of course, “line-of-sight” is a much easier problem than the proposed “non-line-of-sight” solution, but is still similar enough to demonstrate the principle.

*In the previous (multi-shot) SWH setup* both lasers at  $\lambda_1$  and  $\lambda_2$  were coupled together and incorporated in a common-path Michelson interferometer. For image acquisition, the lasers have been shuttered and the phase maps at each wavelength have been acquired sequentially via temporal heterodyning. This required additional acousto-optical modulators and specialized camera architectures, such as a focal-plane array lock-in camera (see Suppl. Fig. 4 in article [1] or article [5] for more information).

*In contrast, the new (proposed) setup configuration* only requires standard camera technology and works in *single-shot*. For this method, it is proposed to couple only one portion of both laser beams together, which forms the object beam. The other portions of both beams remain separated and form two separated reference beams at two different wavelengths at  $\lambda_1$  and  $\lambda_2$ . The two reference beams are arranged so that they directly illuminate the camera chip at an angle (Fig. 2). One reference beam (e.g.,  $\lambda_1$ ) encloses an angle with the horizontal x-axis, while the other reference beam (e.g.,  $\lambda_2$ ) encloses an





**Fig. 2:** Setup and algorithms for the proposed Single-Shot SWH solution (see sec. 4 for explanation). The method is explained with preliminary results which have been captured in line-of-sight via Synthetic Wavelength Interferometry. The SWH image formation is explained in Figs. 1.6 and 1.7 of book chapter [2].

angle with the vertical  $y$ -axis (see Fig. 2b). When reflected off or transmitted through a scattering scene, the object beam forms a speckle field at each wavelength  $\lambda_1$  and  $\lambda_2$ . These two speckle fields are incident on the detector and interfere with the reference beams. The speckle field at  $\lambda_1$  produces a static interference pattern with the  $\lambda_1$  - reference beam (vertical fringes), while the speckle field at  $\lambda_2$  produces a static interference pattern with the  $\lambda_2$  - reference beam (horizontal fringes). In other words: The camera image shows speckle which are overlaid by crossed fringes (Fig. 2c).

Eventually, the complex speckle fields (phase and amplitude)  $E(\lambda_1), E(\lambda_2)$  at both optical wavelengths are retrieved via computational demodulation in the Fourier domain as follows: The Fourier transform of the camera image shows five distinct regions (Fig. 2d). The center region, as well as the object spectra arranged around the respective carrier frequencies which are defined by the frequencies of vertical ( $\lambda_1$ ) and horizontal ( $\lambda_2$ ) fringes in the camera image.  $E(\lambda_1)$  (phase and amplitude) is retrieved by:

- Evaluating/finding the carrier frequency for the vertical fringe direction
- Shifting the Fourier spectrum to set the evaluated carrier frequency as new center frequency
- Applying a low pass filter (multiplication with Gaussian kernel or Hanning window) so that only the frequency band around the new center frequency remains

A Fourier back transform eventually delivers the speckled field  $E(\lambda_1)$  (Fig. 2e).  $E(\lambda_2)$  is retrieved in an analog fashion for the other fringe direction. Finally, the unspeckled synthetic field  $E(\Lambda)$  can be calculated, e.g., again via mixing (Fig. 2f), and the hidden object can be reconstructed via computational backpropagation at  $\Lambda$ , as described in [1], [2]. The whole process requires *only one* camera image.

## 5) Outline of Tasks, Workplan and Expected Outcomes

The proposed 1-year workplan is divided into four phases, each corresponding to 3 months.

Month 1-3	Complete proof of principle and limits analysis for “line-of-sight” measurements
Month 4-6	“Non-line-of-sight” imaging through static strongly scattering media
Month 7-9	“Non-line-of-sight” imaging through dynamic strongly scattering media
Month 10-12	Tradespace Exploration

### **Month 1-3: Complete proof of principle and limits analysis for “line-of-sight” measurements:**

During the first phase, our team will continue to refine and study the proposed single-shot method for the easier case of “line-of-sight” imaging, i.e., for the precise 3D measurement of macroscopic objects with rough surfaces (comparable to [5], but in single-shot). Besides the demonstration of single-shot measurement results, phase 1 also includes the analysis of physical and information-theoretical limits of the proposed idea, such as resolution, speed, space-bandwidth product, etc. [35].

**Expected outcome:** High-quality single-shot measurements of static objects (busts, etc.), as well as dynamic “3D videos” of moving and deforming objects, accompanied with a quantitative limits analysis which helps the team to make adjustments for the 2<sup>nd</sup> phase, if needed.

**Risk and mitigation:** Phase 1 involves relatively low risk, as initial results have been already demonstrated. However, method and apparatus still need to be refined and limits analysis will be of high value for phases 2-4.

#### **Month 4-6: “Non-line-of-sight” imaging through static strongly scattering media:**

In the second phase, our team will transfer the developed single-shot method to “non-line-of-sight”, i.e., image hidden objects through scattering media. For this phase, the team will predominantly limit itself to *static* scattering media, such as plastic slabs or “dead” tissue. However, in contrast to previous work [1] (which is again not single-shot!) experiments through *thick strongly scattering media* will be performed to further push the boundaries of the proposed principle.

**Expected outcome:** “Non-line-of-sight” measurements through thick strongly scattering media (beyond ~5-8 transport mean free paths). Possible examples include imaging through thick white plastic slabs, skull bone (not in-vivo), or chicken breast.

**Risk and mitigation:** Lasers: Preliminary experiments as well as phase 1 experiments will be/have been performed with lasers that are already present in the PI’s lab [36]. However, these lasers only have limited power (140mW) which will lead to signal-to-noise issues if used for strongly scattering media. Although the budget of this proposal does not allow for new lasers, the PI is in the process of purchasing new lasers from his startup funds. There is a small risk that these lasers will not arrive in time, due to the current shortages. In this case, the mitigation strategy is to perform the experiments through strongly scattering media *in simulation*. Although not part of the original workplan, a comprehensive and physically accurate simulation has merit, as it is a valuable tool for future developments.

#### **Month 7-9: “Non-line-of-sight” imaging through dynamic strongly scattering media:**

In the third phase the team will use the lessons learned in phases 1 and 2 together with the refined apparatus and evaluation methods to perform single-shot “non-line-of-sight” measurements through dynamic strongly scattering media, such as “living” tissue.

**Expected outcome:** “Non-line-of-sight” measurements through dynamic strongly scattering media. Examples include imaging the bone structure through the hand, imaging veins deep under the skin, or imaging through fog or turbid fluids (like blood).

**Risk and mitigation:** This task is very challenging and involves a moderate risk of failure. The mitigation strategy is “to make the problem easier”, i.e., image through *thin* or *weak* dynamic scatterers such as moving diffusers, “thin” fog, or thin layers of living tissue (ears, fingertips, ...). This would still warrant the demonstration of single-shot imaging through dynamic scattering media (as proposed) and would point towards a clear avenue for future research proposals (as intended).

#### **Month 10-12: Tradespace Exploration:**

The proposed method of single-shot SWH is not expected to work without limitations. The good news: Physical limits often come in the shape of uncertainty products! This makes it possible to optimize a technique towards a specific quantity (e.g., speed or resolution) by trading in information less critical for the targeted application. Phase 4 will devote effort towards studying the related tradeoffs (e.g., in size, weight, power and cost (SWaP-C)) for future implementations of single-shot SWH, with a focus on proposing an architecture that is principally suitable for deployment in possible commercial medical devices. The study will involve experiments and software simulations to compare the performance that can be achieved as a function of 1) wavelength of operation, 2) source/sensing technology and 3) image processing/enhancement algorithms. Additional considerations and modalities such as time-multiplexed gating of scattered photons will be explored to help determine the maximum possible performance that could be achieved for a SWH implementation.

**Expected outcome:** Comprehensive quantitative analysis of involved limits and tradeoffs. In the ideal case this analysis leads to a “concrete recipe” how to deploy single-shot SWH into medical devices. This will form the basis for future large scale research proposals and is considered as a crucial step in putting the PI’s research vision into practice.

**Risk and mitigation:** Depending on the explored modalities, this task might involve additional hardware (purchased from other funds), which might again not be delivered in time. The mitigation strategy is to wait for respective devices to be delivered and perform the necessary work later, e.g., within the framework of a no-cost-extension (NCE). As possible project periods for this call are 12-24 months and this proposal only plans with 12 months, an NCE is hopefully acceptable.

**6) Qualification of PI:** See “Short-Bio” in attached CV

**References** provided in additional document to meet proposal guidelines. [Click here to see References.](#)

**Foundation**

# 20th Anniversary Challenge

Use photonics. Find a solution. Change the world.

## Application Dates

07 Jul 2022 - 15 Sep 2022

Executive Summary of “hardware and software enablers for future optical access networks”

Contact: Gaël Simon, Philippe Chanclou

The access network recently witnessed an important increase, through the massive deployment of Fiber To The Home (FTTH). The industry is already working on the definition of the optical technologies which will replace the currently deployed technology, the G-PON (gigabit passive optical network) standard, offering higher than ever throughputs. Those future technologies will enable, beside the throughput increase, to answer the constantly evolving customers’ uses.

The success of G-PON and the coming XGS-PON technologies and similar permitted to imagine new use cases for those technologies, in taking advantage of their robustness, their low energy consumption, or their low-cost for mass production in other network segments. This is the objective of the “ETSI-F5G” organism, which aims to “extend the FTTH paradigm to a Fiber to Everywhere”.

In parallel, the rapid development of mobile networks (5G’s deployment started; 6G’s main directions emerge) requires the fiber infrastructure to evolve toward antenna sites. Mobile network transport and associated specifications induce important constraints on optical segments in terms of throughput (10x more in 6G than 5G), and latency (10x less in 6G than 5G). This is emphasized by the interest in solutions as “Cloud Radio Access Network”. The later splits the radio network functions and creates new interfaces, often requiring high bitrates, as the x-Haul.

The objective of this project is to identify technological solutions allowing to answer to previously presented stakes, and to identify their strength and weaknesses, while insuring interoperability of the future systems working at 100Gbit/s. The current optical transmission technologies for access network employ Non-return to Zero modulation format, for the sake of simplicity and cost. However, the need for high bitrate interface come at a price, which imposes to reevaluate the solutions and to assess the need for a technological rupture. It could mean to choose PAM4, coherent detection “regular” or simplified, the use of Frequency Division Multiplexing, Wavelength Division Multiplexing, NRZ at higher bitrate,... In any case, those solutions must adapt to the multiple access topology of the FTTH. The energy consumption must also be carefully monitored, and so must be the ability to maintain interface’s interoperability, avoid the dependency to a vendor, and make the optical fiber passive infrastructure viable.



Foundation

# 20th Anniversary Challenge

Use photonics. Find a solution. Change the world.

## Application Dates

07 Jul 2022 - 15 Sep 2022

Proposal “hardware and software enablers for future optical access networks”

Contact: Gaël Simon, Philippe Chanclou

### Literature review for Fiber to the Home:

The ITU-T has been preparing for several years the successor of Gigabit Passive Optical Networks (G-PON) and 10G Symmetrical (XGS-PON): Higher Speed PON (HS-PON). It already provides consolidated standards, even if several parameters remains for further study, particularly in upstream. It aims to provide 50Gb/s in downstream with a Non-Return to Zero (NRZ) modulation format. The upstream must be single wavelength and NRZ, and several bitrate options exist, namely 12.5Gb/s, 25Gb/s, or 50Gb/s, to enable wider applications than FTTH, such as high throughput gold offers for enterprises. HS-PON is the first PON standard to enable the use of Digital Signal Processing (DSP) in order to meet high bitrate performances. While DSP is more and more used in other network segments, it presents strong disadvantages, such as added costs and complexity and can be prohibitive for broadband applications. For example, solutions such as Feed-Forward Equalizers (FFE) present several “taps” to manage, which should be adapted to the different electro-optical path to be crossed by the signal: with different lasers or receivers with limited bandwidths, optical paths subject to chirp, radio frequency reflections, ... Also, the point-to-multipoint nature of HS-PON induces the use of various transceivers from many vendors and different generations, making the correct management of DSPs more complex.

Now in research, we have to define the next PON generation working at 100Gbit/s line rate supporting the existing fiber infrastructure and the coexistence with previous PON systems.

### Literature review for Fiber to the Antenna:

After the commercial deployment of the 5th generation of mobile network (5G), the work on the 6th generation (6G) has begun. To handle new usages unlocked by future 6G networks, the future optical access network needs to be capable to transport the great amount of data that 6G will lever. Mobile Back/Mid/Fronthaul optical links capable to transport 100 Gbit/s to up to 1 Tbit/s are required [1] on a point-to-point topology (PtP). New usages such as industry 4.0 and metaverse should also benefit from these future high bitrate fiber links. The current PtP standards [2] used for mobile X-haul use intensity modulation and direct detection (IM/DD) with the Non-Return to Zero On-Off Keying (NRZ-OOK) modulation format and provide up to 25 Gbit/s per wavelength. Coherent technologies intend to meet the requirements for such transmission systems [3] but the added complexity and cost compared to an IM/DD system remains a drawback. Standardisation bodies like the Institute of Electrical and Electronics Engineers (IEEE) have already edited specification on 100 Gbit/s links [4]. For these links, the targeted channel insertion losses must be above 15 dB and the optical budget (OB) must reach to 21.5 dB.

[1] N. Rajatheva, "White paper on broadband connectivity in 6G," 2020. Accessible online: <https://www.6gflagship.com/white-paper-on-broadband-connectivity-in-6g/>

[2] IEEE Standard for Ethernet -- Amendment 14: Bidirectional 10 Gb/s, 25 Gb/s, and 50 Gb/s Optical Access PHY, IEEE 802.3cp-2021, 2021.

[3] N. Suzuki, H. Miura, K. Mochizuki, and K. Matsuda, "Simplified digital coherent-based beyond-100G optical access systems for B5G/6G [Invited]," *Journal of Optical Communications and Networking*, vol. 14, no. 1, pp. A1–A10, Jan. 2022, doi: 10.1364/JOCN.438884.

**Problem Statement/Objective:**

The objective of this proposal is to identify technological solutions allowing to answer to previously presented stakes, and to identify their strength and weaknesses, while insuring interoperability of the future systems. The current optical transmission technologies for access network employ Non-return to Zero modulation format, for the sake of simplicity and cost.

However, the need for high bitrate interface come at a price, which imposes to reevaluate the solutions and to assess the need for a technological rupture. It could mean to choose PAM4, coherent detection "regular" or simplified, the use of Frequency Division Multiplexing, Wavelength Division Multiplexing, NRZ at higher bitrate,... In any case, those solutions must adapt to the multiple access topology of the FTTH. The energy consumption must also be carefully monitored, and so must be the ability to maintain interface's interoperability, avoid the dependency to a vendor, and make the optical fiber passive infrastructure viable.

**Outline of tasks/Work Plan:**

The main direct output of this proposal is to lead three PhD students towards their PhD defense during this three years project. Being part of a wider research team, the work in which the student will participate will include the following technical task:

- Assessment of 100Gbit/s or more based on NRZ modulation with DSP
- Evaluation of new optical access transmission supporting multiple access function
- Feasibility study to support existing optical fiber infrastructure and new fiber (multi-core and hollow core) and coexistence with legacy optical access solutions
- Feasibility to support interoperability (physical layer and MAC layer) to have open access systems

**Outcome(s):**

The expected outcomes are :

- Addressing disruptive research for complementary technologies enabling to support the full potential of future FTTH wired and 6G wireless communications and service infrastructure
- Availability of fixed xHaul networks with performance levels compatible with 6G KPI's in terms of bandwidth, capacity, latency, and flexibility
- Foster capabilities in key technologies and notably advanced signal processing for optical communications
- Trustworthy and energy-efficient network and infrastructures
- Offering increased network resilience, openness, and transparency

**Impact:**

Given the disruptive and ambitious nature of this proposal research and the potential of its ultimate deployment to break existing technological barriers enabling the sustainable growth of the internet into the 6G era, it can have a multi-dimensional, positive and long-lasting impact across many sectors.

The research proposal is primarily concerned with the generation of new high-quality knowledge that will play a central role in the development of next generation FTTH and 6G networks, and this will be created through practice, collaboration, interaction, and education, generated thanks to the complementary know-how provided by the scientific dissemination. In particular, this proposal is proposing a set of new advancements covering different scientific areas which are imperative for future optical access networks:

· High performance transceivers: Scientific impact here will be related to the development of proof-of-concept systems that can support up to Terabit/s capacity for short reach optical fiber communication. Additional impact in this area will be concerned with the development of components (photonic chips) for transceivers.

· Bespoke architectures for 6G services: Based on the novel optical transceiver, the research plan will design a truly converged and flexible mobile transport network architecture featuring ultra-high throughput, energy efficient and low latency optical communication, providing secure and reliable optical only pathways from remote antenna sites back to the network core. The establishment of a new network architecture offering unprecedented levels of network flexibility while ensuring the evolution to 6G connectively is a key scientific impact of the work.

This proposal will embrace the *Open Science practice*, sharing the knowledge and data generated in the RD&I process, through contributions in key scientific journals, conferences, and workshops, granting full and immediate Open Access to the project outcomes. This will increase the openness, quality and performance of the research, sharing with the scientific community and general public the new knowledge generated in the optical and 6G domain. The key results will be promoted also on social and popular science media to increase understanding and engagement of society in optical fiber capabilities and advantages.

# **Multi-contrast OCT + AI-based image processing supported by optical segmentation for minimally invasive assessment of bone quality (MOSOS)**

**Application for the Optica Foundation 20<sup>th</sup> Anniversary Challenge: Health category**

## **Executive summary**

Osteoporosis is a disease that causes progressive deterioration of the mechanical competence of bone resulting in an increased risk of fractures. Up to now, it is mostly characterized by the loss of bone mass or microstructural changes. However, changes in the material composition and properties of the bone tissue altogether lead to reduction in bone strength and increase in risk of fracture due to the more fragile skeleton. The methods currently used for clinical diagnosis of osteoporosis primarily consist of measurements of bone mass and density. However, changes in bone mass only account for approximately 15% of fracture risk, and in several diseases affecting the skeleton, such as type 2 diabetes (T2D) and glucocorticoid-induced osteoporosis, the correlation between bone mass and fracture risk is low. This fact makes it difficult to predict risk of fracture and thus determine when to initiate proper treatment to prevent future fragility fractures. Fractures put a strong burden on the health system, cause considerable risk for patients, and the prevalence is on the rise worldwide due to the aging population and the increase in associated disorders impacting bone quality such as T2D. Early fracture prevention is of paramount importance to reduce health care costs and prevent individual suffering. Hence, there is a high unmet need for new tools to assess bone quality in vivo.

The MOSOS project aims to provide proof of principle that optical coherence tomography (OCT) is such sought-after method for assessing early fracture risk in vivo. OCT is an imaging modality that uses infrared light to generate label-free cross-sectional images of tissue microstructure. Unlike existing diagnostic methods, OCT has sufficient spatial resolution necessary for segmentation of cortical or trabecular bone compartments. Additionally, OCT has the potential to assess bone quality directly through the modeling and extraction of optical properties, which are directly correlated with material properties and sub-resolution microstructure of the tissue. So-called multi-contrast OCT incorporating structural information and optical properties will aid in the identification of new optical biomarkers of fracture risk.

Until now, OCT imaging in hard tissues such as bone has been challenging due to the limited penetration depth of light in highly scattering tissues. We have recently developed a new embodiment of OCT, spatial offset OCT, which leverages the role of multiply scattered light to enhance contrast at depth in highly scattering tissues. As an added benefit, spatial offset OCT improves contrast between mesoscale tissue structures acting as “optical segmentation” to improve identification of regions of interest in tissue.

By combining the multi-contrast OCT and spatial offset OCT images as inputs to a deep learning algorithm, the MOSOS project will develop an innovative tool for assessing bone quality and fracture risk without the use of ionizing radiation. The MOSOS project holds promise to build a robust and cost-effective technique that can be used in a range of settings (outpatient clinics, general practitioners, etc.). If the hypothesis in this project is confirmed, MOSOS might disrupt the assessment of bone health.

# **Multi-contrast OCT + AI-based image processing supported by optical segmentation for minimally invasive assessment of bone quality (MOSOS)**

## **Background and literature review**

### *Osteoporosis: a growing healthcare challenge*

Bone fractures are on the rise worldwide due to aging of the population. The annual number of osteoporosis-related fractures in Europe is app. 4.3 million [1]. Consequently, fractures put a strong burden on the health system with enormous economic costs. In 2019, the annual fracture-related costs in the EU were € 57 billion with an expected cost increase of 27% from 2019 to 2030. Two-thirds of this cost was attributed to treating incident fractures, long-term care accounted for 29%, and pharmacological prevention just 5%. Therefore, early fracture prevention is of paramount importance to reduce health care costs and prevent individual suffering.

Osteoporosis and subsequent fragility fractures occur because of a progressive loss of bone and by deterioration of bone microarchitecture and quality [2]. Fractures most frequently associated with osteoporosis are hip fractures, vertebral fractures, and forearm fractures. Patients experiencing hip fractures are at considerable risk for subsequent osteoporotic fractures and premature death. Furthermore, recent studies suggest that long-term complications of type 2 diabetes (T2D) also include alterations of the bone, evident by a high coexistence rate of T2D with both osteoporosis and different fracture types [3–5].

### *An unmet need for a novel and innovative technique to measure bone quality in vivo*

When patients experience a fracture and are diagnosed with osteoporosis the disease is usually well established and severe. The most common method for diagnosing osteoporosis is measurement of bone mass by dual-energy X-ray absorptiometry (DXA) [2]. However, changes in bone mass only account for 15% of fracture risk, and in several diseases affecting the skeleton like T2D and glucocorticoid-induced osteoporosis, the correlation between bone mass and fracture risk is poor, making it difficult to predict risk of fracture and decide when to initiate treatment to prevent future fragility fractures. Other imaging-based techniques such as radiography, computerized tomography, and magnetic resonance imaging are used for diagnosis of fractures but cannot be used for determining bone microstructure and future fracture risk. There is a high unmet need for innovative techniques reflecting “bone quality” that can estimate risk of fracture quickly and affordably.

Osteoporosis and diabetic bone disease are characterized not only by the loss of bone mass but also by changes in the material composition and properties of the bone tissue leading to reduced bone strength. Several biological mechanisms for increased fracture risk have been proposed, which might provide opportunities to identify new optical biomarkers of early fracture risk. Several studies have reported lower material strength of diabetic bone [6,7], which renders the bone less flexible and reduces bone strength. Microstructural changes in cortical bone have been identified in more severe disease states [8,9], and one recent study has shown that diabetic bone has higher cortical porosity [10], which may weaken the bone. Finally, bone turnover is compromised in T2D, which impacts normal repair of microdamage [11]. None of these microstructural changes can be detected by DXA but could potentially be detected using optical imaging.

### *Multi-contrast optical coherence tomography for comprehensive characterization of bone*

OCT may be such sought-after method with the potential for assessing bone quality in vivo. Based on near-infrared light sources, OCT is a non-invasive, optical diagnostic imaging modality that provides cross-sectional tomographic, 3-D visualization of internal microstructure in biological systems at video-rate imaging speeds [12,13]. OCT images inherently contain information about how light is absorbed and scattered by tissue (optical properties), which is correlated with tissue material properties, structure, and composition [14]. These optical properties extracted from OCT images provide an additional contrast mechanism complementary to standard structural OCT images, thus multi-contrast OCT.

OCT is rapidly becoming a clinical standard in ophthalmology and dermatology but has infrequently been applied to hard tissue such as bone since the high optical scattering in bone limits the imaging depth of optical modalities [15–17]. An early attempt to investigate OCT and optical attenuation for bone demineralization was reported in 2008 [15]. Although their preliminary analysis showed promise, it also indicates improvements in OCT imaging and modeling are needed. Recent work in the area of optical attenuation has employed a new physical model of light propagation in tissue based on the extended Huygens-Fresnel (EHF) model modified to incorporate absorption [18]. This new model, which accounts for the role of multiply scattered light in OCT image formation, in conjunction with improved imaging depth, could provide new insight into sub-resolution structural changes in hard tissues such as bone.

*Spatial offset OCT: An innovative approach for improved image contrast deep in scattering tissue*

One of the biggest challenges for imaging in hard tissues is the low imaging depth caused by scattering. Spatial offset OCT is a new technique that leverages the role of multiply scattered light to enhance the contrast to noise ratio when imaging at large depths in highly scattering tissues [19]. Briefly, an offset is introduced between the illumination and collection paths in the OCT system such that ballistically scattered light from the surface is blocked and only multiply scattered light, which has traveled deeper into the sample, is collected. This allows the dynamic range of the detector to be optimized for the weaker multiply scattered signals. Through our preliminary results, we have demonstrated that spatial offset OCT is particularly useful for detecting boundaries between different tissue types, effectively acting as “optical segmentation” between different tissue layers. Such images could be incorporated into AI-based image analysis to improve segmentation and identification of different tissue types.

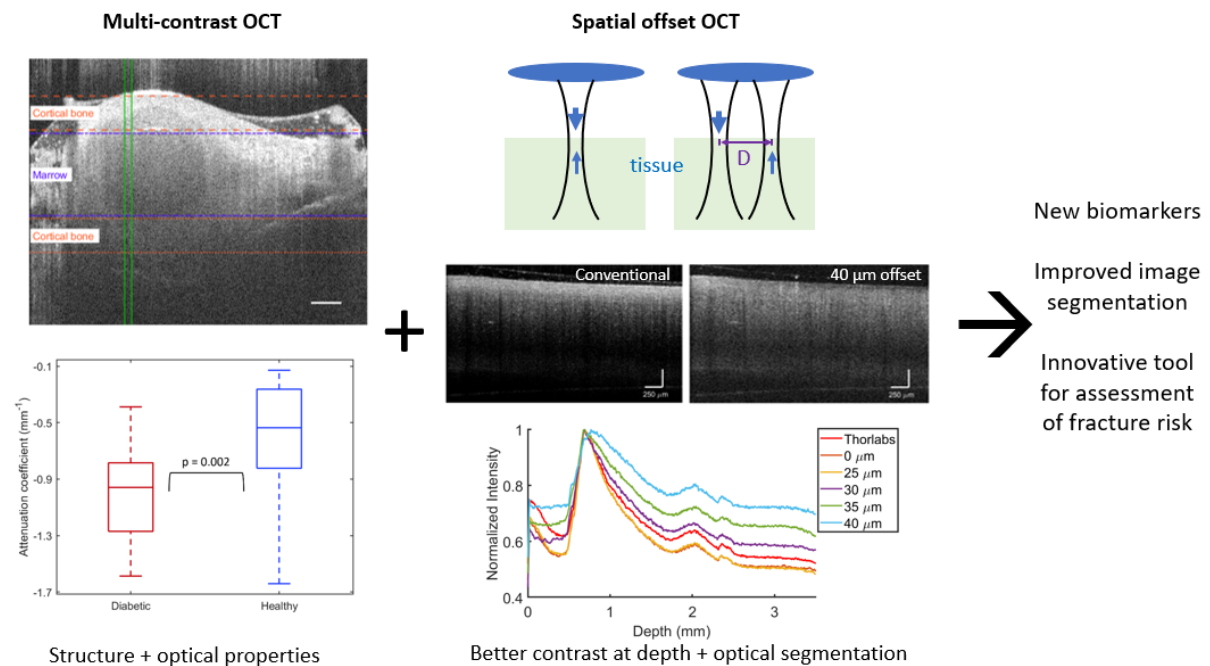


Figure 1 An overview of the MOSOS concept. Multi-contrast OCT comprising structural information and optical properties provides an initial input to deep learning systems to identify novel biomarkers of osteoporosis. Preliminary results demonstrate that optical attenuation can be used to distinguish between healthy and diabetic bone. Spatial offset OCT provides improved contrast-to-noise deeper in scattering tissue and enables optical segmentation to support AI-based segmentation algorithms. These two concepts combined will lead to an innovative tool for assessment of fracture risk.



## Problem statement and objective

**Overall aim:** to provide proof-of-principle of multi-contrast OCT as an innovative technique by which we can determine bone quality and fracture risk a) at earlier stages of osteoporosis than current assessment techniques and b) without the use of ionizing radiation.

### Objectives:

- To identify new optical biomarkers of bone quality that can be assessed in vivo in a minimally invasive manner
- To develop protocols for optical segmentation based on spatial offset OCT and demonstrate their advantage in assisting AI-based segmentation algorithms
- To develop a deep learning platform for assessing fracture risk based on multi-contrast OCT and spatial offset OCT.

## Work plan

The project will consist of three work packages (WP1-3). In WP1, I will use conventional and spatial offset OCT to collect morphological information about bone tissue and evaluate the correlation with gold-standard measurements. In WP2, I will further develop both OCT methods for the extraction of optical properties to obtain quantitative information from the OCT scans. Again, the correlation of the optical properties obtained from the bone tissue with data on bone strength. Finally, in WP3, I will apply deep learning techniques to develop classification schemes by which different disease states of osteoporosis can be detected. In all WPs we will use a well-established animal model of osteoporosis, the Zucker Diabetic Fatty (ZDF) rat model as diabetes is associated with several negative changes in the bone tissue. Bones will be used at age of 6 months. Wild-type animals will be used as controls. Ethical approval will be sought for all animal experiments before commencing research.

### *WP1: Correlation between OCT structural images and bone quality*

WP1 will comprise establishing the ground truth measurements and performing initial investigations with conventional and spatial offset OCT.

The biomechanical properties of bone (bone strength) will be assessed ex vivo using an Electropuls E1000 (Instron, United Kingdom) device. Bone mass and density will be determined using a PIXImus DXA densitometer (Lunar Corporation, Madison, WI) Bone microstructure will be determined using micro-computed tomography ( $\mu$ CT) (vivaCT 40, Scanco Medical, Switzerland) of the proximal tibiae to quantify 3D microarchitectural properties in both trabecular and cortical bone using standard histomorphometric parameters.

OCT imaging of the bones will be performed using conventional and spatial offset OCT. The performance of spatial offset OCT in bone will be assessed, and optical imaging parameters including the focal plane placement and range of relevant offsets will be determined. Qualitative and quantitative morphological parameters will be obtained and correlated with i) bone strength measurements, ii) number and nature of micro-damage in the cortical bone tissue, iii) microarchitecture (primarily cortical parameters), and iv) BMD.

### *WP2: Extraction of optical properties from OCT images and correlation with bone quality*

The overall objective of WP2 is to establish an algorithm for extracting optical properties from OCT images and to assess the correlation between the optical properties and the ground truth measurements established in WP1.

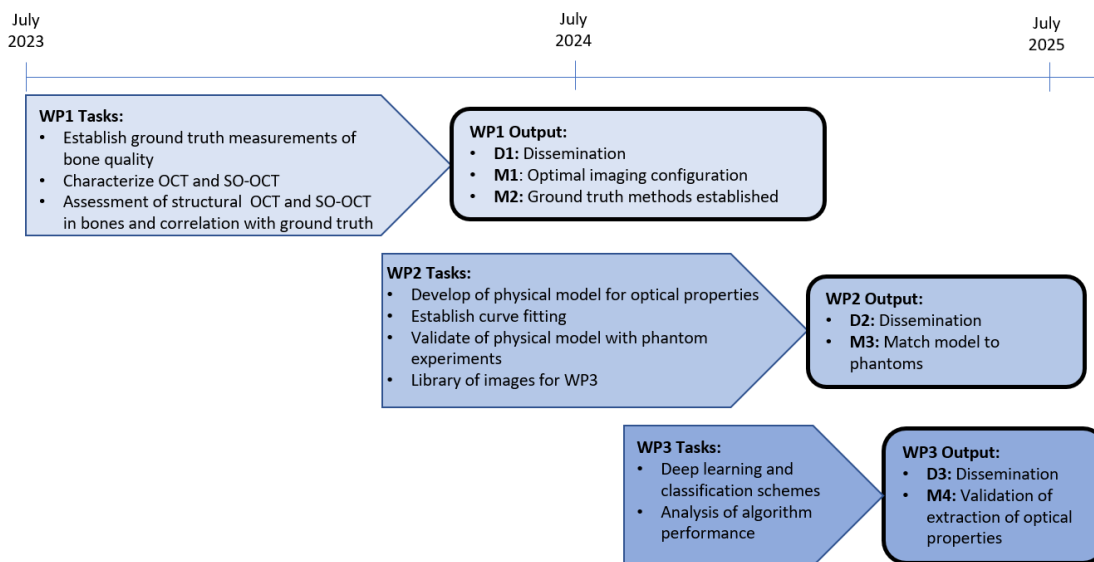
I will derive a model of the OCT signal for both conventional and spatial offset OCT based on the EHF model. Curve fitting routines will be used to extract the optical properties. The performance of the model and curve fitting will be validated in controlled phantoms. The protocol will be applied to the OCT images of the bones, and a library of multi-contrast OCT and spatial offset OCT images will be

established to feed into the development of the deep learning scheme in WP3. Finally, the correlation between optical properties and the ground truth measurements will be assessed.

### *WP3: Deep learning and classification schemes supported by optical segmentation*

The objective of WP3 is to demonstrate that by feeding the data from WP1-2 into a classification scheme, we can further develop and enhance algorithms for bone tissue condition detection beyond what is achievable with existing methods.

First, a segmentation algorithm based on spatial offset OCT images will be developed, and the performance improvement using optical segmentation will be evaluated. I will then develop a generative model classifying OCT images in their (disease) subcategories and will benefit from the low-dimensional nature of the problem to build tailor-made classifiers whose decision boundaries are easily visualized. To this end, I will pool the optical properties extracted from all ROIs across images of the category under consideration to estimate non-parametric distributions using kernel density estimation. The resulting category-specific distribution is then combined with prior information regarding the prevalence of each category to obtain a Bayesian classifier to predict the disease category from a given OCT image. Finally, the performance of the algorithm for classification of bone disease will be determined.



*Figure 2 An overview of the timeline for the MOSOS project. Dn: dissemination, including at least one publication in a peer-reviewed journal. Mn: milestone, representing a decision point in the project.*

### **Outcome and dissemination**

The overall end goal of the project is to provide proof of concept of OCT as a novel, innovative, non-invasive, non-ionizing tool to determine bone quality/strength *in vivo* with clinical applications. To achieve this goal, one outcome will be an AI-based classification scheme for assessing fracture risk that I expect will diagnose osteoporosis at an earlier stage than existing methods. A positive outcome will feed into *in vivo* validation in an animal model. I shall seek to publish at least one manuscript associated with each WP in a peer-reviewed journal within technical or clinical research domains. I will aim for high-impact, high-visibility journals such as Biomedical Optics Express, Optica, and Bone. I expect to present the results at renowned international conferences, as contributed and invited talks.

## Impact and outlook

Early detection of osteoporosis is essential for initiation of treatment of bone loss to prevent devastating fragility fractures. Current diagnostic tools only determine bone mass, but not bone quality. They clearly underestimate fracture risk in several conditions including T2D and glucocorticoid treatment. There is a high unmet medical need for novel and innovative non-invasive technologies which efficiently and precisely estimate fracture risk in patients. This project will provide proof of principle as to whether OCT can be used for diagnosing poor bone quality. OCT holds promise to be a robust and cost-effective technique that can be used in a range of settings (outpatient clinics, general practitioners, etc.). If the hypotheses in this project are confirmed, OCT might disrupt the assessment of bone health. The potential health economic benefits are enormous as the annual costs related to fragility fractures in the EU are € 57 billion and earlier and more precise diagnostics of bone diseases could reduce the number of fractures dramatically.

The technology and concepts developed as part of this project could have further applications in other medical fields. Segmentation between different tissue layers is a driving factor in medical diagnosis. Particularly in the fields of ophthalmology and dermatology, two of the largest applications for clinical OCT, diagnosis is highly reliant on accurate segmentation.

1. J. A. Kanis, N. Norton, N. C. Harvey, T. Jacobson, H. Johansson, M. Lorentzon, E. V. McCloskey, C. Willers, and F. Borgström, *Arch. Osteoporos.* **16**, 1 (2021).
2. R. Handa, *Clin. Rheumatol.* **177** (2021).
3. P. Vestergaard, *Osteoporos. Int.* **18**, 427 (2007).
4. V. V. Shanbhogue, S. Hansen, M. Frost, N. R. Jørgensen, A. P. Hermann, J. E. Henriksen, and K. Brixen, *Eur. J. Endocrinol.* **174**, 115 (2016).
5. Y. Fan, F. Wei, Y. Lang, and Y. Liu, *Osteoporos. Int.* **27**, 219 (2016).
6. J. N. Farr and S. Khosla, *Bone* **82**, 28 (2016).
7. J. R. Furst, L. C. Bandeira, W. W. Fan, S. Agarwal, K. K. Nishiyama, D. J. McMahon, E. Dworakowski, H. Jiang, S. J. Silverberg, and M. R. Rubin, *J. Clin. Endocrinol. Metab.* **101**, 2502 (2016).
8. E. A. C. de Waard, J. J. A. de Jong, A. Koster, H. H. C. M. Savelberg, T. A. van Geel, A. J. H. M. Houben, M. T. Schram, P. C. Dagnelie, C. J. van der Kallen, S. J. S. Sep, C. D. A. Stehouwer, N. C. Schaper, T. T. J. M. Berendschot, J. S. A. G. Schouten, P. P. M. M. Geusens, and J. P. W. van den Bergh, *Osteoporos. Int.* **29**, 2725 (2018).
9. J. M. Patsch, A. J. Burghardt, S. P. Yap, T. Baum, A. V. Schwartz, G. B. Joseph, and T. M. Link, *J. Bone Miner. Res.* **28**, 313 (2013).
10. A. Cirovic, J. Jadzic, D. Djukic, · Danijela Djonic, V. Zivkovic, S. Nikolic, M. Djuric, and · Petar Milovanovic, *Calcif. Tissue Int.* **2022** **1**, 1 (2022).
11. X. Liu, W. Li, J. Cai, Z. Yan, X. Shao, K. Xie, X. E. Guo, E. Luo, and D. Jing, *FASEB J.* **34**, 2579 (2020).
12. D. Huang, E. A. Swanson, C. P. Lin, J. S. Schuman, W. G. Stinson, W. Chang, M. R. Hee, T. Flotte, K. Gregory, C. A. Puliafito, and J. G. Fujimoto, *Science (80- )*. **254**, 1178 (1991).
13. S. Marschall, B. Sander, M. Mogensen, T. M. Jørgensen, and P. E. Andersen, *Anal. Bioanal. Chem.* **400**, 2699 (2011).
14. P. Gong, M. Almasian, G. van Soest, D. M. de Bruin, T. G. van Leeuwen, D. D. Sampson, and D. J. Faber, *J. Biomed. Opt.* **25**, 1 (2020).
15. N. Ugryumova, J. Stevens-Smith, A. Scutt, and S. J. Matcher, *Coherence Domain Opt. Methods Opt. Coherence Tomogr. Biomed. XII* **6847**, 684725 (2008).
16. M. Del-Valle, E. Lins, and P. Ana, *J. Biophotonics* **12**, e201900171 (2019).
17. C. Kasseck, M. Kratz, A. Torcasio, N. C. Gerhardt, G. H. van Lenthe, T. Gambichler, K. Hoffmann, D. B. Jones, and M. R. Hofmann, *J. Biomed. Opt.* **15**, 046019 (2010).
18. Z. Turani, E. Fatemizadeh, T. Blumetti, S. Daveluy, A. F. Moraes, W. Chen, D. Mehregan, P. E. Andersen, and M. Nasiriavanaki, *Cancer Res.* **79**, 2021 (2019).
19. M. Chen, J. Mas, and K. Dholakia, in *Conference on Lasers and Electro-Optics, OSA Technical Digest (Online)* (2018).

TITLE: Optimization of Windows for Energy Efficient Buildings: Non-imaging optics for ultra-cool surfaces

CATEGORY: Environment

#### OBJECTIVES:

The objective of the proposed project is to a) investigate efficient materials emitting in the atmospheric window and b) develop optical designs to direct this radiation towards space. Broadband directors of infrared radiation are required towards this end, and this project aims in investigating their designs based on suitable materials and windows exhibiting cooling at sub-ambient temperatures. Promising results reported multi-degree outdoors cooling by utilizing imaging optics. The throughput of several classes of non-imaging optics e.g. the compound parabolic, is superior compared to their imaging counterparts. The rational design of optics exhibited very efficient concentrators. By reciprocity, these thermodynamically ideal optics make for excellent directors. Many of these designs were inspired by nature and the bio-mimicking approach lead to many serendipitous discoveries. The advent of efficient evolutionary algorithms for the optimization of such designs can greatly speed up the development of efficient designs. Consequently, the core of the optimization based on advanced algorithms will be developed during this project. In this work dielectrics and polymer composites for radiative cooling will be investigated. On one hand, the extensive experience in one-dimensional deposition will enable wide-area cool surfaces. On the other hand, composite materials from recycled products can add value towards a circular economy of these much needed products.

#### INTENDED OUTCOMES:

The proposed research will develop advanced algorithms for optimization of one-dimensional filters and cool micro-structured materials for wide-area surfaces such as windows and buildings, based on non-imaging optics. In addition, benefits to industrial sectors such as building, windows, manufacturing, as well as automotive and space are expected via the transfer of the developments based on non-imaging optics and photonics. Training of personnel in developments of algorithms, film deposition and additive manufacturing during this project, will further aid the transfer of knowledge. Involving and training master's students during their final year projects will further expand the reach of optics and photonics, as well as arming them with skills for further professional development and job security. The results of the project will be published in reputable journals and disseminated in international conferences and workshops organized by Optica. 4 journal publications and 4 conferences presentations are expected during this project.

#### APPLICATION TO REAL-WORLD ISSUES:

The proposed research intends to progress the application of radiative cooling materials in wide-area surfaces to address the issue of urban heat island. This will be accomplished by replacing existing surface materials with these developed during this project, based on non-imaging optics and optimized one-dimensional structures. Real-world applications of the developed materials can take place in buildings, roofs or windows. In this way, the extensive experience of the industry in one-dimensional deposition, as well as the excellent radiative properties of non-imaging optics can be utilized towards enabling wide-area cool surfaces. Moreover, the use of recycled materials in the design will take some of the burden to the environment by the accumulation of leaching materials either escaping or buried underground in the absence of better alternative solutions.

# Optimization of Windows for Energy Efficient Buildings: Non-imaging optics for ultra-cool surfaces

## Problem Statement/Objective

Human activity is one of the main drivers of global warming and humanity can actively reverse it through smart, albeit urgent, consideration of such activities. Increased activity is observed in cities during the last 30 years [1], creating what is known in the literature as urban heat island. It is evident that the existing materials, contribute a great amount [2] to the heat stored in infrastructures. Recent advances in optical materials exhibit great promise towards reducing this heat content.

A wide list of optical materials and applications were reported towards this end. Smart windows utilizing photochromic [3] or thermochromic [4–6] materials either in glazing or opaque surfaces were reported. The absorption of these materials varies by light or temperature, thereby can operate as static louvers by switching sunlight on or off. Although these materials operate very well in the visible spectrum, the main contributor of heat, that is infrared, is still absorbed by the material.

A more promising solution of cooling surfaces below the ambient temperature is by radiative cooling. In this way, the infrared radiation is directed back towards space, enabling lower ambient temperatures. A window of low absorption exists in the atmosphere at 8–13  $\mu\text{m}$ , including the absorption of  $\text{O}_3$  at 9.5  $\mu\text{m}$  that breaks the continuity of this window [7]. It is, therefore, a promising approach to a) investigate efficient materials emitting in this windows and b) develop optical designs to direct this radiation towards space. Broadband directors of infrared radiation are required towards this end, and this project aims in investigating their designs with suitable materials.

## Literature Review

**Radiative coolers:** The recent literature exhibits promising results of geometrical concentrators in radiative cooling. According to Kirchhoff's law, the absorptivity of any material is proportional to its absorptivity [8,9]. The emissivity in planar materials utilized in buildings is isotropic. Consequently, a great fraction of this radiation remains trapped in the atmosphere or is reabsorbed by adjacent surfaces on earth. To further increase the reduction of emissivity on earth, it is therefore desirable to direct it towards space. It has been recently reported that concentrators can enhance radiative cooling of small-sized surfaces. Promising results reported outdoors cooling of 11°C by utilizing tapered reflectors [10], while similar designs reported advanced cooling CPV [11].

**Non-imaging optics:** The throughput of several classes of non-imaging optics e.g. the compound parabolic, is superior compared to their imaging counterparts. Several results were reported on their superior radiative coupling properties as integrated optics in direct comparisons with imaging optics [12,13], with compound parabolic concentrators exhibiting the best performance [14,15] for 3<sup>rd</sup> generation solar cells based on upconversion. The success of non-imaging concentrators for solar energy applications was widely demonstrated [16,17] and off-the-shelf products exist made of glass [18]. For a larger surface coverage and wider application, roll-to-roll printing [19] and rapid 3D printing [20]

are more suitable techniques. No reports on non-imaging optics in radiative cooling were found in the literature, to the best of the author's knowledge.

**Cooling materials:** The theoretical framework for nighttime operation was recently reported and confirmed by a demonstration with electroplated  $\text{Al}_2\text{O}_3$  emitters [21], while a plethora of polymeric and dielectric structures reported sub-ambient cooling [8,10]. The environment is burdened by the accumulation of leaching materials either escaping or buried underground in the absence of better alternative solutions. For the European zone, the amount of wind turbines to be recycled from 2020 to 2030 is estimated to 60.000 [22]. Composite materials from recycled products can add value towards a circular economy of these much needed products. Sorting plastic products made of PVC [23] and thermoplastic [24] is being developed, but not yet for composite materials the wind turbines are made of [25]. The recycled material will serve as lightweight raw material for 3D printing, as well as the radiative cooling materials. The latter can be developed by mean of a porous structure to utilize the high reflectance and high emittance of composites [26].

**Algorithms:** This rational design of optics exhibited very efficient concentrators. By reciprocity, these thermodynamically ideal optics make for excellent illuminators [27]. Many of these designs were inspired by nature [28,29]; a never ending inspiration for scientific endeavors. This bio-mimicking approach has lead to many serendipitous discoveries. Fortunately, the advent of efficient evolutionary algorithms for the optimization of such designs can greatly speed up the development of efficient designs. Recent results reported on optimized filter stacks with suitable matching of the atmospheric transmittance [30]. The present author recently reported on the optimization of concentrated solar energy systems [31] by the use of algorithms based on heuristic optimization [32]. This work will serve as a foundation for the modeling and optimization of efficient radiative cooling materials.

### **Outline of tasks/Work Plan**

The first step of this project is the development of the optimization algorithm. The foundation for this algorithm has been developed during the previous work of the author. Consequently, the core of the optimization based on mixed integer programming will be developed during the initial months of the project. In this work dielectrics and polymer composites will be investigated. The 3D designs of the non-imaging optics will be developed during these months as well. Ray-tracing will be used to verify the performance of the optics for radiative cooling.

After the design steps, the fabrication of testing specimen can take place. 3D printing of the designed models will be utilized in this fabrication step. Along with off-the-shelf 3D printing polymers, composites will be experimented as well. This approach will further focus on enhanced passive materials from recycled wind turbine blades. Their performance for structural integrity will be tested in the facilities of the university.

The 3D printed models will be used as the substrate for deposition of films. The investigated films include, but are not limited to, vanadium and titanium oxide. The structure optimized by the developed algorithms will be utilized in this step. Thin films will be deposited by plasma sputter, suitable for the deposition of the films during this project. Indoor and outdoor testing



of the thermal performance and spectral characteristics of the specimen will be conveyed based on the equipment purchased by the aid of this program.

The following work plan will be followed during this project.

#### Months 1-6

- Development of filter optimization algorithm
- 3D design of non-imaging optics

#### Months 6-12

- 3D printing of optimized optics
- Deposition of optimized filters

#### Months 12-24

- Indoor testing: transmittance, reflectance spectroscopy, thermal conductivity
- Outdoor testing at different locations and climate conditions

### **Outcomes**

The proposed research will have the following outcomes:

- Development of advanced algorithms for optimization of one-dimensional structures.
- Development of cool micro-structured materials for wide-area surfaces such as windows and building, based on non-imaging optics.
- Training of personnel in film deposition and additive manufacturing. There is also the possibility of training master's students during their final year project.
- All results of the project will be published in reputable journals and disseminated in international conferences and workshops organized by Optica. 4 journal publications and 4 conferences presentations are expected from this research.

### **Impact**

The proposed project will have the following impact:

- Transfer of developments based on non-imaging optics and photonics to industrial sectors such as building, windows, manufacturing, automotive.
- The developed materials with best performance can be the foundation for extending their application to wide-area surfaces and products for energy efficient cooling.
- Develop increased understanding of manufacturing processes from highly-sought recycled materials.
- Adding value and transferring knowledge to the expertise of the energy and manufacturing laboratories, while training students through a productive and creative work ethic, as well as arming them with skills for further professional development and job security.

## References

1. C. Tuholske, K. Caylor, C. Funk, A. Verdin, S. Sweeney, K. Grace, P. Peterson, and T. Evans, "Global urban population exposure to extreme heat," *Proceedings of the National Academy of Sciences* **118**, e2024792118 (2021).
2. N. Chrysoulakis, S. Grimmond, C. Feigenwinter, F. Lindberg, J.-P. Gastellu-Etchegorry, M. Marconcini, Z. Mitraka, S. Stagakis, B. Crawford, F. Olofson, L. Landier, W. Morrison, and E. Parlow, "Urban energy exchanges monitoring from space," *Scientific Reports* **8**, 11498 (2018).
3. G. H. Timmermans, B. W. H. Saes, and M. G. Debije, "Dual-responsive "smart" window and visually attractive coating based on a diarylethene photochromic dye," *Appl. Opt.*, **AO** **58**, 9823–9828 (2019).
4. B. Baloukas, R. Beaini, S. Loquai, O. Zabeida, J. E. Klemberg-Sapieha, and L. Martinu, "Thermochromic VO<sub>2</sub> Coatings for Energy Control," in *Optical Interference Coatings Conference (OIC) 2019 (2019)*, Paper MC.5 (Optica Publishing Group, 2019), p. MC.5.
5. G. E. Arnaoutakis and D. A. Katsaprakakis, "Energy Performance of Buildings with Thermochromic Windows in Mediterranean Climates," *Energies* **14**, 6977 (2021).
6. D. Vernardou, D. Louloudakis, E. Spanakis, N. Katsarakis, and E. Koudoumas, "Thermochromic amorphous VO<sub>2</sub> coatings grown by APCVD using a single-precursor," *Solar Energy Materials and Solar Cells* **128**, 36–40 (2014).
7. A. P. Raman, M. A. Anoma, L. Zhu, E. Rephaeli, and S. Fan, "Passive radiative cooling below ambient air temperature under direct sunlight," *Nature* **515**, 540–544 (2014).
8. B. Zhao, M. Hu, X. Ao, N. Chen, and G. Pei, "Radiative cooling: A review of fundamentals, materials, applications, and prospects," *Applied Energy* **236**, 489–513 (2019).
9. S. Jeon and J. Shin, "Ideal spectral emissivity for radiative cooling of earthbound objects," *Sci Rep* **10**, 13038 (2020).
10. L. Zhou, H. Song, J. Liang, M. Singer, M. Zhou, E. Stegenburgs, N. Zhang, C. Xu, T. Ng, Z. Yu, B. Ooi, and Q. Gan, "A polydimethylsiloxane-coated metal structure for all-day radiative cooling," *Nat Sustain* **2**, 718–724 (2019).
11. Z. Wang, D. Kortge, J. Zhu, Z. Zhou, H. Torsina, C. Lee, and P. Bermel, "Lightweight, Passive Radiative Cooling to Enhance Concentrating Photovoltaics," *Joule* **4**, 2702–2717 (2020).
12. G. E. Arnaoutakis, J. Marques-Hueso, A. Ivaturi, K. W. Krämer, S. Fischer, J. C. Goldschmidt, and B. S. Richards, "Enhanced up-conversion for photovoltaics via concentrating integrated optics," *Opt. Express*, **OE** **22**, A452–A464 (2014).
13. G. E. Arnaoutakis, E. Favilla, M. Tonelli, and B. S. Richards, "Single crystal monolithic upconverter solar cell device tandems with integrated optics," *J. Opt. Soc. Am. B*, **JOSAB** **39**, 239–247 (2022).
14. G. E. Arnaoutakis, J. Marques-Hueso, A. Ivaturi, S. Fischer, J. C. Goldschmidt, K. W. Krämer, and B. S. Richards, "Enhanced energy conversion of up-conversion solar cells by the integration of compound parabolic concentrating optics," *Solar Energy Materials and Solar Cells* **140**, 217–223 (2015).
15. G. E. Arnaoutakis and B. S. Richards, "Geometrical concentration for enhanced up-conversion: A review of recent results in energy and biomedical applications," *Optical Materials* **83**, 47–54 (2018).
16. J. M. Gordon and H. Ries, "Tailored edge-ray concentrators as ideal second stages for Fresnel reflectors," *Appl. Opt.*, **AO** **32**, 2243–2251 (1993).
17. R. Winston and J. M. Gordon, "Planar concentrators near the étendue limit," *Opt. Lett.*, **OL** **30**, 2617–2619 (2005).
18. R. Winston, "Thermodynamics illuminates solar optics," in *SPIE Newsroom* (2011).
19. H. Lee, H. Lim, S. Park, and D. Lee, "Low-concentration photovoltaic module with reflective compound parabolic concentrator fabricated by roll-to-roll slot-die coating and 3D printing," *Opt. Express*, **OE** **24**, A1571–A1579 (2016).

20. A. R. Gentle, A. Nuhoglu, M. D. Arnold, and G. B. Smith, "3D printable optical structures for sub-ambient sky cooling," in *Thermal Radiation Management for Energy Applications* (SPIE, 2017), Vol. 10369, pp. 16–24.
21. M. Dong, L. Zhu, B. Jiang, S. Fan, and Z. Chen, "Concentrated radiative cooling and its constraint from reciprocity," *Opt. Express*, OE **30**, 275–285 (2022).
22. V. Sommer and G. Walther, "Recycling and recovery infrastructures for glass and carbon fiber reinforced plastic waste from wind energy industry: A European case study," *Waste Management* **121**, 265–275 (2021).
23. G. Gao, A. Turshatov, I. A. Howard, D. Busko, R. Joseph, D. Hudry, and B. S. Richards, "Up-Conversion fluorescent labels for plastic recycling: a review," *Adv. Sustainable Syst.* **1**, 1600033 (2017).
24. J. Woidasky, J. Schmidt, M. Auer, I. Sander, A. Schau, J. Moesslein, P. Wendler, D. Kirchenbauer, D. Wacker, G. Gao, A. Turshatov, B. S. Richards, S. Wiethoff, and C. Lang-Koetz, "Photoluminescent Tracer Effects on Thermoplastic Polymer Recycling," in *Advances in Polymer Processing 2020*, C. Hopmann and R. Dahlmann, eds. (Springer, 2020), pp. 1–13.
25. D. A. Katsaprakakis, N. Papadakis, and I. Ntintakis, "A Comprehensive Analysis of Wind Turbine Blade Damage," *Energies* **14**, 5974 (2021).
26. J. Mandal, Y. Fu, A. C. Overvig, M. Jia, K. Sun, N. N. Shi, H. Zhou, X. Xiao, N. Yu, and Y. Yang, "Hierarchically porous polymer coatings for highly efficient passive daytime radiative cooling," *Science* **362**, 315–319 (2018).
27. J. Ferry, J. Ferry, L. Jiang, L. Jiang, R. Winston, and R. Winston, "Thermodynamics of ideal illumination: a novel figure of merit for characterizing illumination efficiency," *Opt. Express*, OE **28**, 1927–1935 (2020).
28. D.-E. Nilsson, "A new type of imaging optics in compound eyes," *Nature* **332**, 76–78 (1988).
29. G. E. Arnaoutakis, J. Marques-Hueso, T. K. Mallick, and B. S. Richards, "Coupling of sunlight into optical fibres and spectral dependence for solar energy applications," *Solar Energy* **93**, 235–243 (2013).
30. Y. Shi, W. Li, A. Raman, and S. Fan, "Optimization of Multilayer Optical Films with a Memetic Algorithm and Mixed Integer Programming," *ACS Photonics* **5**, 684–691 (2018).
31. G. E. Arnaoutakis, D. Al. Katsaprakakis, and D. G. Christakis, "Dynamic modeling of combined concentrating solar tower and parabolic trough for increased day-to-day performance," *Applied Energy* **323**, 119450 (2022).
32. G. E. Arnaoutakis, N. Papadakis, and D. Katsaprakakis, "CombiCSP: A python routine for dynamic modeling of concentrating solar power plants," *Software Impacts* **13**, (2022).

# DA VINCI: DISRUPTION & ADVANCEMENT OF VISIBLE IMAGING USING NANOPHOTONICS AND FREQUENCY COMB INTEGRATION

DR. GREGORY MOILLE - UNIV. OF MARYLAND/NIST

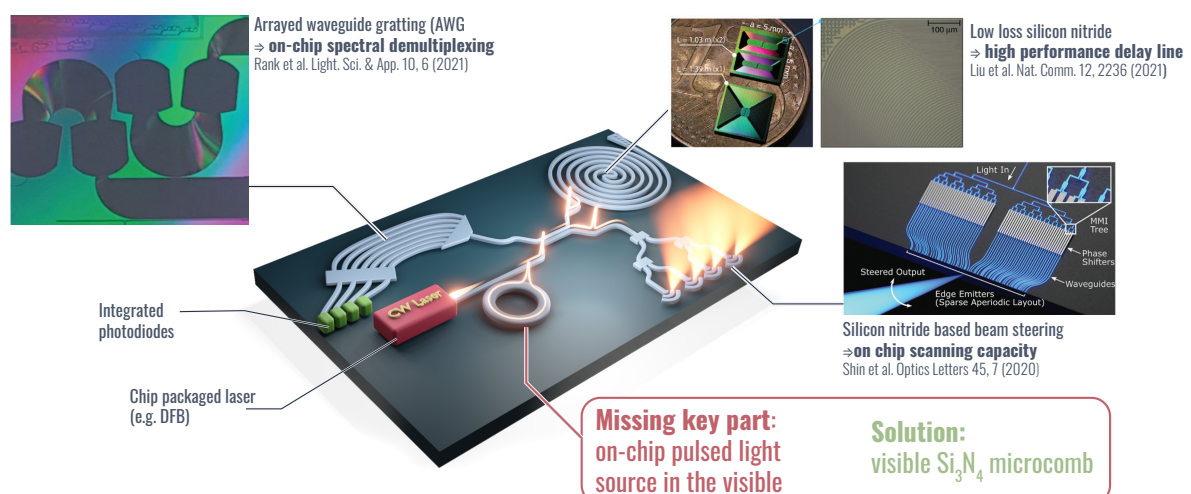
Optical Coherence Tomography (OCT) has revolutionized non-invasive *in-vivo* imaging thanks to its capacity to create a full three-dimensional image of a biological sample. OCT using visible wavelengths has shown dramatically improved resolution and promises breakthroughs in patient screening for gastrointestinal diseases and early brain stroke signs. However, the core technology for visible OCT, a visible pulsed light source, remains large and expensive, preventing low-cost OCT deployment in medical offices. In this project, we propose to develop an integrated visible pulsed source on chip by harnessing nonlinear optics in a microresonator. The perspective of integration would dramatically reduce the price of OCT systems, through low-cost mass-fabrication, and the small footprint would allow to fit systems in oral pills for complete non-invasive imaging.

## 1 | OPTICAL COHERENCE TOMOGRAPHY – WHY INTEGRATING IT?

Imaging techniques for medical purposes are at the very core of non-invasive disease diagnostics. Optical Coherence Tomography (OCT) is unique among the many imaging techniques, for example, through its three-dimensional (3D) imaging capabilities. It also allows for the possibility of *in-vivo*, high-resolution observation. The 3D properties of OCT are particularly attractive from a patient viewpoint. It allows to replace invasive biopsies that are complex and painful. These features explain the swift transition of this technique from research to medical offices in a matter of a decade (1, 2).

OCT is at its core an interferometric technique. It relies on the interference between the reflection or transmission through a biological sample and a reference path. A broad spectral light source is split into two paths. One shines on the sample and acquires a phase shift dependent on the sample properties. The other travels through a well-known path length. The recombination of these two signals creates an interference dependent on the delay acquired through the biological sample, which can be detected. A Fourier transform of the temporal intensity trace recreates the depth profile of the scanned area. This recreates a 3D image of the sample (1).

As with most imaging methods, OCT resolution is wavelength dependent: the shorter the wavelength, the higher the possible resolution. Therefore, shifting OCT toward visible wavelengths presents attractive properties for ultrahigh resolution imaging. In particular, visible OCT has been studied for



**Fig. 1 – Artist vision of the fully monolithic on-chip OCT system.** The pump, provided by a DFB laser, creates a cavity soliton through self-injection locking of a Kerr nonlinear resonator. The soliton is then extracted periodically using the same waveguide, forming a pulse train: this creates the frequency comb. The soliton pulse train is split, one part goes into a reference path made by a spiral and an end mirror and the other goes into a network of beam steering integrated grating that shine light onto the sample. In this project, we will develop the integrated microcomb that is used as the pulsed source light in the visible

retina imaging., which exhibits significant improvement over 1300 nm commercial OCT techniques (3–5).

Although OCT techniques have been swiftly adopted in retinal imaging, it remains mostly unused for other applications like oncology, where OCT could greatly benefit the patient. The elephant in the room which has been clearly identified remains the price tag of the systems (6). This hurdle is even exacerbated when considering visible sources for consumer grade systems (7). The first option is to use a super-luminescent photodiode. However, the gain bandwidth determined by the material limits it to a near-visible range, and the lack of temporal coherence decreases the OCT performance. Single wavelength swept laser sources allow for coherence, yet they present the same bandwidth issues as their superluminescent diode counterparts. Another possibility is to use a pulsed source with a temporal profile short enough to cover a large enough bandwidth. Along these lines, several works have demonstrated visible OCT using a supercontinuum source (3, 4) or Ti:sapphire laser (5). In this case, the lab-to-consumer barrier becomes cost, as such light sources cost from \$50K to more than \$100K.

Therefore, a solution must be provided to produce cheap visible pulsed light. Photonics integration throughout the past decade has enabled to bring on-chip many optical technologies, including lasers (8), delay lines(9), beam steering (10), interferometers (11) and spectral demultiplexing (12). Interestingly, all of these functions are needed for an OCT system to produce the interference pattern and process the phase shift acquired throughout the biological sample. In particular, all these key elements have been demonstrated in silicon nitride ( $\text{Si}_3\text{N}_4$ ), a material compatible with low-cost foundry fabrication, and therefore could be integrated on the same chip [fig. 1]. However, pulsed light generation on-chip remains the key element that so far has not been produced at the wavelength needed for visible OCT. Interestingly, if the light source can be integrated with the other elements, the fabrication price per chip – i.e. the price for a full OCT system – could fall below \$2,000<sup>1</sup>.

Nevertheless, on-chip pulsed light generation has seen tremendous effort and improvement since the realization of dissipative Kerr soliton (DKS) states in the early 2010s (13, 14). The DKS relies on a resonator - usually a microring – made of a nonlinear material. Once pumped with continuous wave light, which can be generated using an inexpensive on-chip laser (15, 16), under the right conditions where dissipation/driving and dispersion/nonlinear phase shift are balanced, mode locking occurs, resulting in the formation of a cavity soliton traveling throughout the ring (17). It is then extracted periodically at every round trip creating a pulse train at a fixed repetition rate. Such light sources are attractive for the OCT system as the repetition rate defined by the small resonator size increases the relative intensity noise (3), allowing for better detection of small reflective or absorption feature in a biological sample, and has been demonstrated at 1300 nm (18).

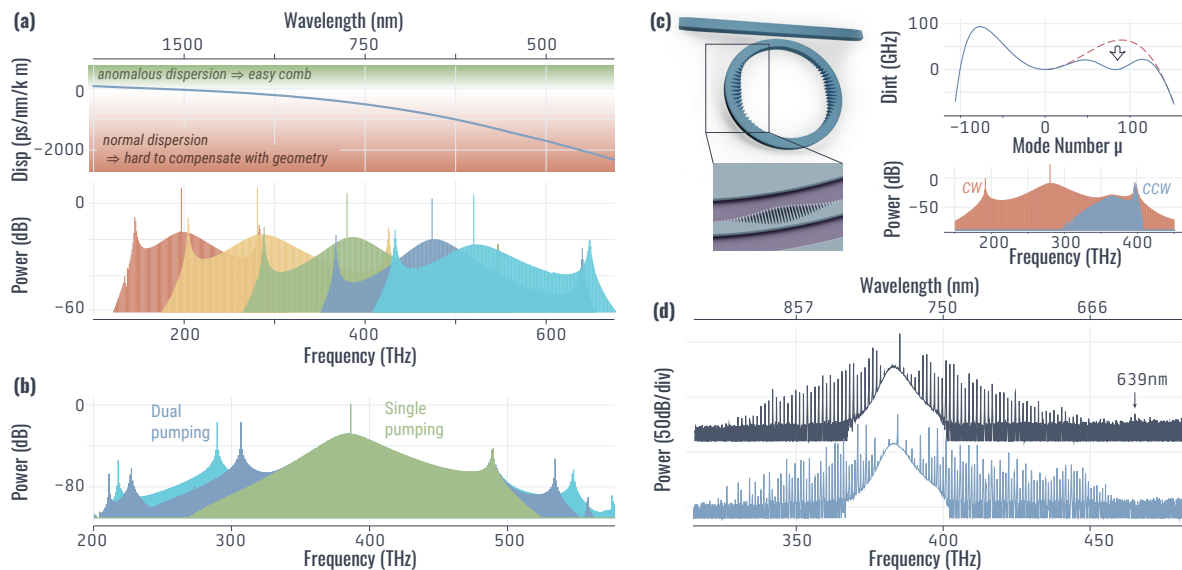
To produce a DKS in the visible, the dispersion of the resonator must be suited to compensate for the nonlinear Kerr effect, and hence needs to be in the so-called anomalous dispersion regime. However, most materials present increasingly normal chromatic dispersion the shorter the wavelength is, making the design of suitable ring resonators for visible DKS operation close to impossible until now.

In the project I am proposing for the 20<sup>th</sup> Anniversary OPTICA Challenge, I will develop an on-chip visible pulsed light source that can be monolithically integrated with the other silicon-nitride-based photonics elements to complete a full on-chip OCT system in the visible.

## 2 | DAVINCI OBJECTIVES – ON-CHIP PULSED VISIBLE SOURCE

The objective of this project is quite straightforward: creating an integrated pulsed source in the visible, which would dramatically reduce the cost and complexity of the OCT system. As pictured in fig. 1, many components that make an OCT imaging system have now been demonstrated on-chip, mainly through the advent of very low-loss silicon nitride photonics. This has allowed the creation of unprecedented long waveguides, bent and wrapped in spirals that can create meter-long delay lines on a tiny footprint (9), along with beam-steering grating photonics and broadband directional couplers. Wavelength demultiplexing, although demonstrated, remains to be implemented to process the frequency comb from aDKS and, therefore, will be part of the effort of this project. The objective of DAVINCI can be divided into the three following goals:

<sup>1</sup>Assuming a small-volume foundry such as Ligentec, AIM photonics or LETI, a cost of a 4 inch wafer fabrication of \$100K, and a chip size according to the footprint of each element. It is worth noting that mass production would drastically reduce the cost



**Fig. 2 – Preliminary results.** (a) Simulation of frequency combs using the simulated dispersion of different resonators. Our experience in different DARPA projects has given us insight into pushing frequency comb toward shorter wavelengths. Thanks to this experience, we can now design ring resonators that can potentially reach wavelengths below 500 nm. (b) Our team has recently unveiled new nonlinear pathways to expand the frequency comb bandwidth beyond its natural dispersion. Thanks to dual pumping, new light can be generated at a shorter wavelength (higher frequency), as demonstrated here in simulation. (c) We are also developing new systems that allow us to tune the resonance frequencies and tailor the dispersion as needed using photonic crystal-like ring resonators. A simple design rule allows for predictive experimental dispersion. (d) Preliminary experimental data show a visible frequency comb reaching as low as 639 nm using a single pumped simple ring resonator. We hope to push the limit of wavelengths accessible by integrated frequency combs using the different expertise presented here.

### Visible on-chip pulsed source

This is the most challenging - yet crucial - goal to make a fully integrated OCT system. In particular, this is due to the photonics materials presenting large normal dispersion at visible wavelengths, in contrast to bright DKS microcombs fundamentally requiring anomalous dispersion. Photonics systems present the advantage of confining light tightly and modifying the effective refractive index of the mode, which can differ significantly from the constituent materials. This allows the geometry to play a role in the dispersion and ultimately compensate for the material dispersion. At longer wavelengths, such as the region between 1060 nm and 1550 nm, this is well-known and has been demonstrated previously. In contrast and as noted above, the material presents such a large normal dispersion below 980 nm, and in particular, in the visible region, that geometrical dispersion compensation presents a considerable challenge, which to this day remains to be demonstrated.

Relying on multiple years of expertise in the integrated frequency comb field, my team and I will keep developing new designs that push the boundary of integrated microcombs toward the visible. During the past seven years, we have worked on multiple projects funded by the Defense Advanced Research Projects Agency (DODOS, ACES, APHI) with each project respectively moving from a microcomb at 1550 nm (reaching 1060 nm) (19, 20), to 1060 nm (reaching 780 nm) (21) to 980 nm (reaching 698 nm) (22) [see fig. 2(a)]. This led us to develop a unique expertise in the design and fabrication of microcombs for shorter and shorter wavelength applications, allowing us to tailor microring resonator dispersion that would theoretically allow pushing DKS to the visible in the  $\text{Si}_3\text{N}_4$  platform. To demonstrate the feasibility, we performed dispersion and frequency comb simulations through the Lugiato Lefever Equation, showcasing the possibility of pushing the frequency comb deep inside the visible region below 500 nm fig. 2(a).

In addition, in the past few years, we have developed new techniques to expand dramatically the bandwidth of an integrated frequency comb through dual-pumping operation (23). In conjunction with dispersion engineering allowing to push the comb to shorter wavelengths, dual pumping operation allows for another lever to generate shorter wavelength light, as shown in fig. 2(b)

Another unique tool we developed recently is the possibility to tailor the dispersion of the resonator beyond the simple dispersion of a ring geometry, through incorporation of a photonic crystal patterning (22, 24). In particular, we demonstrated that one could tailor at will the frequencies of resonance of the resonator by employing a simple Fourier transform design rule to determine the specific photonic



crystal pattern to apply to the microring [see fig. 2(c)]. This would allow the creation of an anomalous dispersion region – a prerequisite for bright DKS generation – far in the visible where otherwise regular dispersion engineering would not allow it.

Although this project is highly challenging, we are confident in our capacity to meet such a goal given preliminary experimental data that we recently obtained – from microrings fabricated in-house [fig. 2(d)] – which demonstrates a chaotic frequency comb (*i.e.* not in the DKS regime). In these results, we exhibit the shortest wavelength to date from a Si<sub>3</sub>N<sub>4</sub> integrated frequency comb [fig. 2(d)]. Using the three domains of expertise that we have: expertise in short wavelength frequency combs, new nonlinear interactions through multi-pumping, and novel dispersion engineering of microrings, demonstrating a visible on-chip pulsed source light thanks to the support of the OPTICA anniversary grant will be possible in the next three years.

### On chip comb processing

The demonstration of wavelength demultiplexing has been demonstrated in several works using the Si<sub>3</sub>N<sub>4</sub> platform, even in the wavelength of interest for this project. However, to this date, there is no demonstration of on-chip demultiplexing of the comb teeth. The demultiplexing of the comb teeth is crucial for the OCT system as this would allow retrieving spectral information of the biological sample, which has been demonstrated to be critical to differentiate between Chron's and ulcerative colitis diseases (25), and to retrieve information relative to brain stroke thanks to hemoglobin spectroscopy (26). Therefore, a cornerstone of this project would be to use existing technology (arrayed waveguide gratings, directional waveguides with grating) to demonstrate the possibility of on-chip processing of a visible microcomb.

### Monolithic integration

The final aim of the project is to demonstrate that the fundamental blocks for an on-chip OCT system can be integrated into a single monolithic chip. This is essential to allow for low-cost mass fabrication using microelectronics-like foundry facilities. To that end, we will demonstrate that the two previous goals can be made on the same chip and fabricated simultaneously, thanks to our end-to-end nanofabrication capacity, including material growth and nanolithography.

## 3 | WORK PLAN

The project targets a two-year duration, where each milestone is identified and addressed according to the following timeline.

### Year 1

Microcomb ring resonator	<ul style="list-style-type: none"> <li>• Design of integrated frequency comb centered around 780 nm with a 1 THz repetition rate</li> <li>• Generation of soliton microcomb reaching past 632 nm</li> <li>• Design of frequency comb pumped at 632 nm</li> <li>• Fabrication of optimal ring resonator</li> </ul>
On-chip WDM	<ul style="list-style-type: none"> <li>• Simulation and design of integrated grating</li> <li>• Decision for best technology for fabrication of integrated grating</li> <li>• Fabrication of integrated spectral grating to separate comb teeth of a microcomb pumped at 1060 nm</li> <li>• Design for short wavelength to address the 632 nm microcomb</li> </ul>

### Year 2

Microcomb ring resonator:	<ul style="list-style-type: none"> <li>• Test of microcomb around 632 nm pump</li> <li>• Soliton injection locking using on-chip laser at 780 nm</li> <li>• Packaging of soliton chip</li> </ul>
On-chip WDM: Integration:	<ul style="list-style-type: none"> <li>• Demonstration of 20 channel spectral separation of comb teeth</li> <li>• Mask and layout for mass fabrication in a foundry</li> </ul>
OCT system:	<ul style="list-style-type: none"> <li>• Frequency comb at 632 nm with spectral separation of teeth using the integrated grating. Demonstration with two chips.</li> <li>• OCT measurement of sample in the visible</li> </ul>

## 4 | IMPACT & OUTCOMES

### Technical and Scientific Impact

Optical coherence tomography has already created a revolution in how patients are treated and screened for a multitude of diseases, particularly retinal ones. However, this technique remains costly and, by extension, not accessible to a large portion of the population. In particular, OCT remains mostly inaccessible for routine checks such as colonoscopy, and colposcopy, which could help with the early detection of cancer, intestinal bowel disease (Crohn's, ulcerative colitis), or brain stroke. In particular, for routine tests involving biopsy, OCT presents a non-invasive alternative to the patient. The system's small footprint we propose, which can also be battery operated, presents a perspective to fit within an oral pill or endoscope for complete non-invasive 3D imaging.

The ability to demonstrate pulsed light generation on a chip addressing visible wavelengths will pave the way for mass industrialization of visible OCT systems that can find application in most medical offices. Alongside the clear technical impact, trying to reach visible wavelengths through nonlinear optics will allow for a better understanding of material properties (losses, dispersion, absorption) that could potentially hinder the formation of combs, alongside new ways of manipulating light on-chip either through dispersion engineering or new nonlinear pathways.

### Educational Impact

Our group has recently been actively engaged toward educational purpose, allowing undergraduate students at the University of Maryland and high-school students from Montgomery Blair High School to play a role in research. In particular, we are currently teaming up with a high-school student working on dispersion engineering as an avenue to learn about scientific research and to help us understand new simulation methodologies. In the project framework, part of the funding will be aimed at expanding our educational goal, including participating in science fairs in high school and allowing more undergraduate and high school students to join us and discover our research. As part of the budgeted funding, we are also committed to develop experimental setups dedicated to education, where our student partners can learn hands-on scientific methods.

## 5 | REFERENCES

1. D. Huang *et al.*, *Science* **254**, 1178–1181 (22, 1991).
2. A. F. Fercher *et al.*, *Reports on Progress in Physics* **66**, 239–303 (2003).
3. S. P. Chong *et al.*, *Biomedical Optics Express* **8**, 323–337 (1, 2017).
4. A. Lichtenegger *et al.*, *Biomedical Optics Express* **8**, 4007–4025 (1, 2017).
5. R. M. Werkmeister *et al.*, *Biomedical Optics Express* **8**, 1221–1239 (1, 2017).
6. V. C. Coffey, *Optics and Photonics News*, September 2016.
7. X. Shu, L. J. Beckmann, H. F. Zhang, *Journal of Biomedical Optics* **22**, 121707 (2017).
8. C. Xiang *et al.*, *Nature Communications* **12**, 6650 (1 17, 2021).
9. J. Liu *et al.*, *Nature Communications* **12**, 2236 (2021).
10. M. C. Shin *et al.*, *Optics Letters* **45**, 1934–1937 (1, 2020).
11. C. G. H. Roeloffzen *et al.*, *Optics Express* **21**, 22937–22961 (23, 2013).
12. E. A. Rank *et al.*, *Light: Science & Applications* **10**, 6 (2021).
13. T. Herr *et al.*, *Nature Photonics* **8**, 145–152 (2014).
14. F. Leo *et al.*, *Nature Photonics* **4**, 471–476 (2010).
15. B. Shen *et al.*, *Nature* **582**, 365–369 (7812 2020).
16. A. S. Voloshin *et al.*, *Nature Communications* **12**, 235 (1 11, 2021).
17. T. J. Kippenberg *et al.*, *Science* **361**, eaan8083 (10, 2018).
18. P. J. Marchand *et al.*, *Nature Communications* **12**, 427 (18, 2021).
19. Q. Li *et al.*, *Optica* **4**, 193 (20, 2017).
20. D. T. Spencer *et al.*, *Nature* **557**, 81–85 (2018).
21. S.-P. Yu *et al.*, *Physical Review Applied* **11**, 044017 (5, 2019).
22. G. Moille *et al.*, presented at the Conference on Lasers and Electro-Optics, CLEO: Science and Innovations, STh2E3, ISBN: 978-1-957171-05-0.
23. G. Moille *et al.*, *Nature Communications* **12**, 7275 (14, 2021).
24. X. Lu *et al.*, *Photonics Research* **8**, 1676 (1, 2020).
25. B. Shen *et al.*, *Clinical Gastroenterology and Hepatology* **2**, 1080–1087 (2004).
26. S. P. Chong *et al.*, *Biomedical Optics Express* **6**, 1429–1450 (1, 2015).

## Executive Summary of Proposal:

### Single-shot, Isotropic and Miniaturized Differential Interference Contrast (SIM-DIC) Microscopy Based on Computational Flat-Optics

Dr. Guangwei Hu ([guangwei@stanford.edu](mailto:guangwei@stanford.edu))  
Early-Career Member of Optica and SPIE  
Nanyang Assistant Professor (Starting Jan 2023)  
School of Electrical and Electronic Engineering  
Nanyang Technological University, Singapore

In our daily life, we care about our health and the environment on the earth. In the healthcare and biomedical technologies, we need to image the biological samples, including cells, tissue slices and many others; in many areas on this planet and in many working spaces, people and other living creatures are facing challenging problems such as air pollutions (due to PM<sub>2.5</sub> dust micro/nanoparticles), microplastics in the sea and others. It is important to image those tiny samples with optical microscopy, and to track their movements in real time and in three dimensions.

However, most of those matters are transparent in the visible spectrum, being hard to be seen in most microscopies based on the optical absorption variances. There are existing techniques such as differential interference contrast (DIC) microscopy to record the refractive index change and the associated phase difference for imaging purpose. DIC features the merits of high spatial resolutions, outstanding contrast, optical sectioning capability, cost effectiveness, and pseudo-3D relief type of image. However, the conventional system is bulky (use 4f system) and can only obtain the information in one dimension, not the others, which is known as problem of “orientation sensitivity”.

In this proposal, we will use the flat-optical elements, i.e. metasurfaces, to innovate the traditional DIC microscope and develop the *single-shot, isotropic and miniaturized* DIC (SIM-DIC) microscopy. Our single-layer metasurface is made of millions of *deeply subwavelength, thin* (~300 nm) and *COMS-compatible* Si nanostructures and can perform the multiple functionalities including the focusing phase, the polarization multiplexing, and the edge detection (i.e. the first-order derivative mathematic operations). Moreover, our system is a *2f* compact system and has the powerful capabilities of mapping the full and isotropic contours of moving transparent microparticles and bio-samples in three dimensions. Most importantly, it can be designed into a simple and flexible module as an add-on portable device for our daily consumer electronics such as cellphones and others.

Beyond those technological values, the proposed project will lead the innovation of conventional photonic technologies via fusing the emerging platforms such as computational flat-optics. Our designed important system is highly integrated, low-cost, portable, flat and multifunctional for various high-end applications, including bio-imaging microscopy, wearable healthcare devices, environmental monitoring (of air pollution, microplastic pollution and etc.) and others.

# Single-shot, Isotropic and Miniaturized Differential Interference Contrast (SIM-DIC) Microscopy Based on Computational Flat-Optics

Dr. Guangwei Hu ([guangwei@stanford.edu](mailto:guangwei@stanford.edu))

Early-Career Member of Optica and SPIE

Nanyang Assistant Professor, School of Electrical and Electronic Engineering  
Nanyang Technological University, Singapore

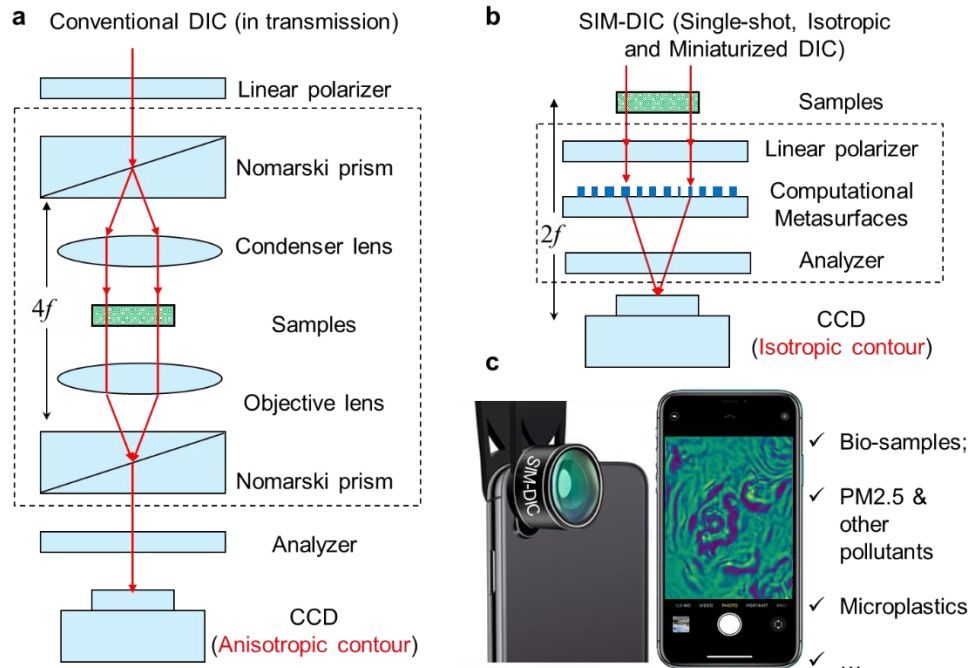
## 1. Background

Microscopy and imaging of biological samples (such as cancer cells, tissue slices and etc.), microplastics in the sea water, pollutant micro/nano-particles (such as PM<sub>2.5</sub> particles) in the air and many others is important in advancing the biological science, healthcare technologies and environmental monitoring. However, most of those samples are transparent in the visible spectrum. To create the image contrast in microscopies based on optical absorption variances, the staining and fluorescent labels are exploited (such as fluorescence microscopy), which however introduces problems of phototoxicity and photobleaching that limit the biological activity of living cells and is impossible for environmental monitoring. Instead of absorptions, one can use label-free microscopy, including phase-contrast microscopy and differential interference contrast (DIC) microscopy, via mapping the fine change of refractive index of transparent samples for imaging purpose. In DIC microscopy, the image is formed from the interference between two polarized waves with both phase shifts and lateral shears, thus rendering contours of transparent samples. DIC features the merits of high spatial resolutions, outstanding contrast, optical sectioning capability, cost effectiveness, and pseudo-3D relief type of images <sup>[1]</sup>.

Despite its great popularity, the regular DIC microscopy has significant limitations, including orientation sensitivity and bulk system. In a common DIC system (see **Figure 1a**), the lateral shear ( $2\Delta x$ ) is created by anisotropic crystals where two Nomarski prisms are used to split and combine two linearly polarized waves, respectively. Hence, the contrast will be created in a form of  $I_{aniso} = |O(x - \Delta x)e^{-i\Delta\phi} - O(x + \Delta x)e^{i\Delta\phi}|^2$ . However, only the information along  $x$  direction is obtained where the additional complicated operations are required to obtain the missing information. Moreover, two lens are required to construct a 4f system. These are against the modern requirements of single-shot imaging in a compact system.

Recent development of metasurfaces has realized the complete manipulation of light over an assembly of deeply subwavelength and thin nanostructures, stimulating an emerging field known as flat-optics and promising novel technologies such as multifunctional flat optical elements (metalens, phase plates etc.), holograms, integrated chips and others<sup>[2]</sup>. Particularly, computational metasurfaces can perform analog information processing such as mathematical integral, analog spatial differentiation for edge detections, imaging and others<sup>[2]</sup>. Moreover, as we recently showed, those platforms can significantly shrink the volume of the system from bulky 4f to 2f system<sup>[4]</sup>, very important for highly compact devices.

It is of great significance to combine emerging flat meta-optics with those innovative phase-sensitive microscopy techniques, which is the major motivation of this proposal. So far, limited demonstrations have been shown, including quantitative phase gradient microscope with multilayer metalens<sup>[5]</sup>, Fourier optical spin splitting microscopy with metasurfaces in 4f systems<sup>[6]</sup> and few others<sup>[7]</sup>. There are many unexplored possibilities of revolutionizing current microscopy technology based on flat-optics for integrated, low-cost and multifunctional imaging system, healthcare devices and environmental-monitoring technologies.



**Figure 1. Single-shot, isotropic and miniaturized differential interference contrast (SIM-DIC) microscopy.** **a**, The conventional DIC in transmission. The beam is split to two orthogonal linear polarization with lateral shift by Nomarski prism. Two lenses can create a  $4f$  system to image bio-samples. Another Nomarski prism can combine those two beams with different phase shift. **b**, the SIM-DIC that is  $2f$  system and can directly image the transparent samples. **c**, The add-on SIM-DIC module for consumer electronics such as cellphones, and other portable devices. This can be used for bio-imaging, the tracking of  $PM_{2.5}$  pollution for air quality monitoring, the detection of microplastic in the water and many other application scenarios.

## 2. Statement of problem, objectives, and method

The major problems that we aim to solve are the orientation sensitivity and bulky volume of DIC system. Scientifically, those problems are caused by the limited functionality of conventional optical elements. For example, Nomarski prism can only split the beam to two linearly polarized beam with a lateral shift (this shift is directional in a line). Hence, additional condenser and objective lens are required to modify the beam propagation in  $4f$  setup. Current methods to tackle the orientation-sensitivity problem have been mechanical rotations of either the specimen or the DIC prism<sup>[8]</sup>, which used four Nomarski prisms and two liquid-crystal variable retarders to switch the shear direction by  $90^\circ$  at high speed in at least two shots. This is time consuming and further adds the volume of the system.

Our objective is to develop highly compact microscopy (SIM-DIC) of  $2f$  system for isotropic image acquisition of bio-samples within a single shot and even in three dimensions (see **Figure 1b**). This will enable the real-time biomedical imaging and health monitoring, which could even be integrated in our cellphone and other portable/wearable devices (**Figure 1c**). Our results would also stimulate more scientific and cross-disciplinary endeavors of innovating the microscopy technology for ever increasing consumer-optoelectronic markets.

Our method is to use the recently developed computational flat-optics (i.e. metasurfaces, more precisely). The linear polarizer can split incident beam to  $x$  and  $y$  polarization and analyzer can



combine them (see **Figure 2a**). A single metasurface layer which is composed of thousands of nanostructures with few hundred nanometer thickness will be used to perform the mathematic computation of first-order derivative for our isotropic image acquisition. As illustrated in **Figure 2b** and for the intuitive understanding, this metasurface will create two images with one slightly larger than the other, instead of directional lateral shift in conventional DIC metasurface. Those two waves will interfere with each other, creating the image contrast in the focal point where CCD is.

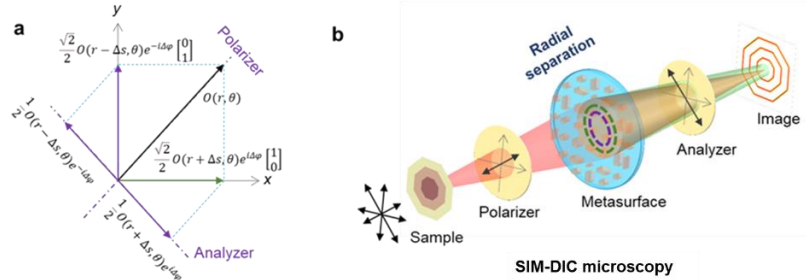


Figure 2. **Schematic of SIM-DIC microscopy and its operation principle.** **a**, The principle schematic diagram of DIC microscopy. **b**, The optical path schematic of SIM-DIC microscopy.

To perform this first-order derivative computation for contour recognition, we use the polarization-multiplexed multifunctional anisotropic metasurfaces. At the local unit cell (also known as meta-atom) of each metasurface denoted as  $(x_m, y_m)$ , the transmission phases can be

$$\phi_{x(y)}(x_m, y_m) = -\frac{\pi}{\lambda f} (x_m^2 + y_m^2) \pm \frac{2\pi\Delta s}{\lambda f} \sqrt{x_m^2 + y_m^2} \mp \Delta\varphi \quad (1)$$

where the subscript  $(x, y)$  denotes different polarization states and  $\Delta\varphi$  is the bias (the phase contrast due to the fine refractive index difference in spatial domain of bio-samples). With this phase profile, in the image plane, those two beams will have different magnification or the axial shift ( $\pm\Delta r$ ) and phase shift, which will interfere to create the image. The amplitude point spread function (APSF) in our system can be

$$h(r, \theta) = e^{-i\Delta\varphi} h_x(r - \Delta r, \theta) - e^{i\Delta\varphi} h_y(r + \Delta r, \theta) \quad (2)$$

where  $(r, \theta)$  is the coordinate in the CCD plane where  $h_{x,y}(r, \theta)$  is corresponding APSF for  $x$  and  $y$  polarization incidence. Note  $h(r, \theta) \approx dr \frac{\partial h}{\partial r}$  if the original input is a purely amplitude image, which bares the computational nature as this is essentially the first-order derivative in mathematics.

There are several advantages of our method. First, our method has contained all advantages of DIC microscopy. This includes 3D relief imaging, i.e. it is capable to obtain the 3D information of bio-samples, non-invasive, high contrast, and high resolution. [Note the resolution is still diffraction limited, but it would be important for various low- and middle-end technologies.] Second, there are increasing technological innovation to commercialize the metalens and metasurfaces, and it is possible to have the cost-efficient and massive production of those devices. Last, the system would be much integrated and simple. This can serve as the add-on module of various modern consumer electronics such as cellphones and others for real-time, portable, flat and cost-effective microscope and health-monitoring technologies.

### 3. Outline of Work Plan

#### 3.1 Design and fabrication of metasurfaces

In our design, for the CMOS compatibility of consumer electronics, we will choose the silicon as the composite material of thin nanostructures (thickness is  $\sim 300\text{nm}$ ) for our metasurfaces. We



use the full-wave numerical simulations with finite-difference time-domain (FDTD) techniques for the simulations. We will use the open-source algorithms such as MEEP<sup>[9]</sup>. It is important to note that the resolution of DIC is the diffraction limit, which is dependent on the numerical aperture (NA) of the design. In our case, we will design the high-NA metasurfaces. Note it is also nontrivial to consider both the phase profile (Eq. 1) and impedance matching, and our previous work<sup>[10]</sup> has demonstrated the efficiency near unitary by focusing. **Figure. 3a** shows one of our structures. **Figure 3b-c** shows the numerical analysis of obtained images. The designed NA=0.7 and the focusing efficiency is more than 80%. For the fabrication of the sample, Nanyang Technological University have the necessary facilities including electron-beam lithography (EBL) and others. In our previous work, we have accumulated and demonstrated those recipes for the fabrication<sup>[11]</sup>. For the demonstration of add-on module, we would seek the foundry fabrication and assembly.

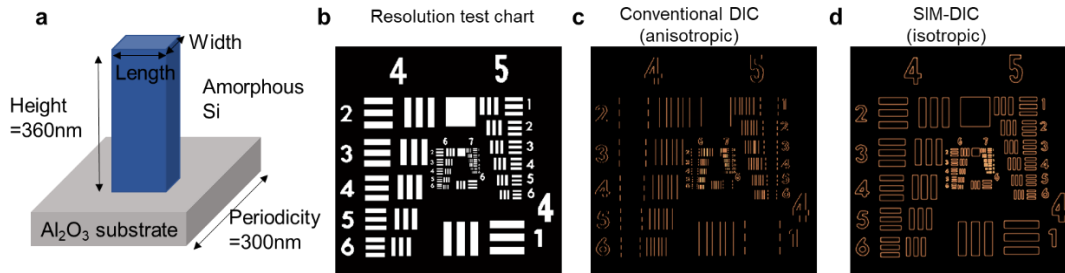


Figure 3 The design and simulation of SIM-DIC microscopy. **a**, The schematics of unit cell of designed computational metasurfaces. **b**, The input original 1951 USAF resolution test chart. **c-d**, The simulated obtained image with anisotropy using conventional DIC (panel **c**) and with isotropic contours in our proposed SIM-DIC microscope (panel **d**).

### 3.2 Bioimaging and 3D relief imaging of PM<sub>2.5</sub> particles with SIM-DIC microscopy

First, we will perform the imaging of 1951 USAF resolution test chart. After that, we plan to test the bio-sample and cancer cells. For this, we need to purchase the necessary optical setup and optical elements in our new lab. Moreover, we highlight that our SIM-DIC can perform the pseudo-3D relief image with isotropic edge detection in a single shot. For this demonstration, we will consider to imaging the moving micro- and nano-particles to track their 3D movements. This unique technique would be extremely important for living cell tracking and detection of plastic micro-particles and other PM<sub>2.5</sub> pollutants in the water or air and other fluids environments.

### 3.3 Exploration of add-on portable SIM-DIC module

In this part, we aim to seek the foundry fabrication and assembly of a SIM-DIC module which can be added on the available consumer electronics. We can use the cellphone as one possibility. The challenges are the assembly of those thin polarizers along with the fabricated metasurface. One possibility is to fabricate the multiple metasurfaces in the same sample, each with desired functionality<sup>[12]</sup>. The other one is to assembly commercial polarizer with the fabricated metasurfaces. We aim to use the first approach, since it offers more integration and the possible more update of functionality in the future for SIM-DIC.

### 3.4 Timeline of implementing this work

	2023 (by quarter)				2024 (by quarter)			
	1 <sup>st</sup>	2 <sup>nd</sup>	3 <sup>rd</sup>	4 <sup>th</sup>	1 <sup>st</sup>	2 <sup>nd</sup>	3 <sup>rd</sup>	4 <sup>th</sup>
Design and fabrication of metasurfaces	√	√	√	√				
Purchasing the setup and hiring	√	√	√	√				
In-lab demonstration of bio-imaging, tracking 3D movement of microplastics and other pollutants			√	√	√	√	√	√

Design the add-on module					√	√	√	√
Publication and finalization							√	√

#### 4. Outcome(s)

In this proposal, we will develop a novel and integrated phase-sensitive microscope and the specific outcome and deliverables include:

- (1). The SIM-DIC of 2f system with the capability of isotropic contour detection within a single shot imaging. The NA=0.7. The system can be assembled in a module to be added on available consumer electronics and can perform the pseudo-3D relief imaging of moving micro- and nano-particles in real time.
- (2). More than 2 high-impact publications (targeted in Optica and other journals).
- (3). One optical scientist to be trained

#### 5. Impact

Overall, this work would enable the fusion of emerging flat-optics with conventional photonic technologies exemplified by DIC microscope for new and paradigm-shift innovations. Specifically, our proposed work can develop the novel SIM-DIC module, which can be integrated in existing consumer electronics to benefit the human beings. The successful implementation of this technology could enable real-time, cost-effective, portable and highly efficient tools for bio-imaging, the water and air quality monitoring, the wearable health-monitoring and other high-end applications.

#### 6. Reference

1. R. D. Allen & G. B. David, *Zeitschrift fur wissenschaftliche Mikroskopie und mikroskopische Technik* 69, 193–221 (1969); C. Preza, D. L. Snyder. & J.-A. Conchello, *J. Opt. Soc. Am. A* 16, 2185–2199 (1999).
2. Yu, N. et al., *Science* 334, 333–337 (2011); Kildishev, A. V., Boltasseva, A. & Shalaev, V. M., *Science* 339, 1232009 (2013); A. Arbabi et al., *Nature Nanotech.* 10, 937–943 (2015).
3. Silva A et al., *Science* 343, 160–163 (2014); C. Guo et al., *Optica* 5, 251 (2018). M. M. Moeini & D. L. Sounas, *Optica* 7, 1325-1331 (2020); Y. Zhou et al., *Nat. Photon.* 14, 316–323 (2020). F. Zangeneh-Nejad et al., *Nat. Rev. Mater.* 6, 207–225 (2021).
4. Z. Wang et al., *Nat. Commun.* 13, 2188 (2022).
5. H. Kwon et al., *Nat. Photon.* 14, 109–114 (2020),
6. J. Zhou et al., *Phys. Rev. Lett.* 129, 020801 (2022)
7. Cordaro, A. et al., *Nano Lett.* 19, 8418–8423 (2019).
8. Danz, R. & Gretscher, P. *Thin Solid Films* 462–463, 257–262 (2004); Shribak, M. & Inoué, S. *Appl. Opt.* 45, 460–469 (2006); Shribak, M. *J. Opt. Soc. Am. A* 30, 769–782 (2013).
9. <https://meep.readthedocs.io/en/latest/>
10. J. Zhou et al., *ACS Nano* 12, 82-88 (2018)
11. T. Shi et al., *Nat. Commun.* 13, 4111 (2022); Z. Li et al., *Light: Sci. & Appl.* 7, 63 (2018).
12. A. Arbabi et al., *Nat. Commun.* 7, 13682 (2016); Y. Zhou et al., *Nano Lett.* 18, 7529–7537 (2018). G. Hu et al., *Trends in Chem.* 3, 342-358 (2021)

## Executive Summary

Coherent large bandwidth laser sources, e.g., supercontinuum sources, with a flat spectral profile are needed for a large plethora of optical devices. For example, they are used in sensing devices to detect substances, medical devices such as optical coherence tomography (OCT), and security devices like ones employed in airports or at events.

Wide-bandwidth low power coherent laser sources are also integral in telecommunications where the demand for more information channels – at lower powers is increasing as the size of global information exchange is ever increasing. Currently, all these devices need large pump powers for the coherent wide-bandwidth source used within them. This makes them expensive, bulky and large, which makes them expensive, not portable or robust and constrained to highly controlled environments such as laboratories.

We have an approach and prototype product that can significantly downscale the cost and size of supercontinuum laser sources, by significantly lowering these power requirements. Enabling these sources to be on microchips or in fibers while producing high-quality flat spectra relevant for applications. We plan to provide large bandwidth coherent sources on chip or fiber to device manufacturers that rely on this source technology, i.e. we want to make our technology practical to solve problems in all three categories: Health, Environment, and Information.

At the core of our approach, we rely on sign-alternating the waveguide dispersion, such that the supercontinuum process remains ongoing and thus highly efficient with pump power. By alternating between anomalous and normal dispersion segments, spectral clamping mechanisms are bypassed such as the shaping of the pump pulse to solitons that stagnate generation (in anomalous segments) or the loss of peak power that occurs in normal dispersion segments. The soliton profile is disrupted by the placing of the normal dispersion segments along the propagation and the anomalous dispersion segments recompress the temporally broadened pulses coming from the normal dispersion segments – thus, keeping spectral generation ongoing. Furthermore, the spectral bandwidth is generated primarily within the  $1/e$  range (achieving greater than 1000nm) instead of the -30 dB range found in conventional supercontinuum lasers.

Our approach is well suited for the integrated photonics setting such as in CMOS-compatible silicon nitride where the high-index contrast enables dispersion engineering simply by modulating the waveguide width. The reduction in pump power is now achieved with our technology, from the nanojoule pulse energy level to 9 picojoules ranges to a factor of thousands and can enable handheld or integrated wide-bandwidth lasers where the possibility did not exist. We have proven our technology through the construction of an integrated chip, described in a submitted publication and even in fiber waveguides. Furthermore, the output pulses from our devices are experimentally demonstrated to be non-linearly compressed by a factor of ten to approx. 20 fs. This makes our technology highly suitable for low-power pulse compression as well and can be used for timing distribution in optical networks.

We are at the TRL 5 technology level, with a functioning and demonstratable prototype. We have published in high-profile scientific magazines, participated in conferences (Laser and Photonics Reviews, Photonics, Optica Conferences) and our technology has been covered by popular science media outlets (e.g., Laser Focus World, AZO Optics, engineers online Netherlands, etc). With the grant, we would like to collaborate and offer a complete product to all major industries that would benefit.

## **Problem Statement and Objective**

Technologies such as Optical Coherence Tomography (OCT), spectrometry used to detect trace amounts of substances and high-resolution imaging (e.g., Light detection and ranging – LiDAR) are integral for new medical technologies and quality control in food and water processing for human consumption. These technologies rely on high-power lasers to generate wide bandwidths of light and coherent directed energy beams with high flux needed to increase the signal-to-noise ratio (for example, to detect trace gases in spectrometry). As such, the mobility of such technologies are currently limited to the laboratory setting, and are expensive, in particular because of the large space requirements and cost of the corresponding optical systems.

Current technologies that employ large bandwidth laser sources (supercontinuum laser sources) are expensive, not portable, and are delicate. These disadvantages are largely due to the high optical power demands of generating large bandwidth for the laser source itself. Thus, obtaining laser sources that do not need high powers to have a large bandwidth will drastically scale down the size and cost of these technologies and also make them function in out of the lab environments. In essence, this would unlock handheld medical or diagnostic devices that can quickly come to a result under fluctuating external and tough environmental conditions.

In addition to the high spatial footprint and cost of the drive lasers is that the spectra that they produce through nonlinear supercontinuum generation (SCG) is not smooth. While, the bandwidth below the -30dB level is large, potentially spanning multiple octaves the bandwidth at the 1/e level is narrow, usually limited to sub-100 nm. As most interferometric imaging technologies such as LiDAR and OCT require large 1/e bandwidth additional filters that smoothen the spectrum have to be employed, wasting available spectral energy and increasing cost and space requirements further.

The general problem of which the high power demand emerges from is that the bandwidth generation process, called “supercontinuum generation”, stops past a certain location in the optical waveguide of the source. Exceedingly large pump powers are then needed to overcome this saturation effect, for the large bandwidth generation to happen. Thus, the full length of the waveguide cannot be used for generation. By solving this problem, i.e. by keeping bandwidth increase ongoing across a large waveguide length, not only would the high-power demand be solved but sources could potentially generate more bandwidth than what is available on the market at lower optical power. This would pave the way for chip-based high bandwidth (at 1/e) supercontinuum integrated chip and fiber technologies that would lead to handheld diagnostic devices.

## **Objective and Impact**

We have a patented solution to drastically scale down the power requirements for supercontinuum generation while increasing the 1/e bandwidth. The reduced power requirements enables full SCG sources on chip or using small fiber lasers coupled to integrated chips for handheld devices.

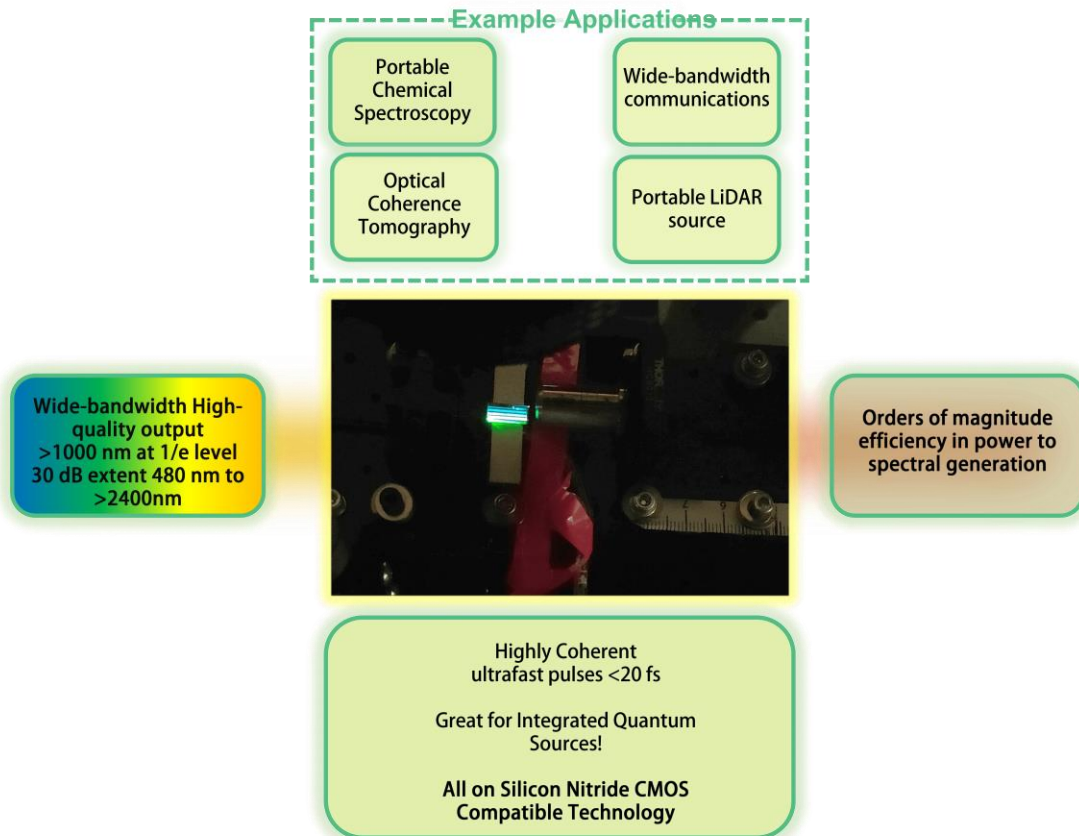
The main problem now that we seek to overcome is to incorporate our prototype technology into medical devices, such as handheld spectrometers, OCT devices or LiDAR devices to obtain valuable industry ready products. We choose to focus on handheld spectrometers and OCT devices in this proposal.

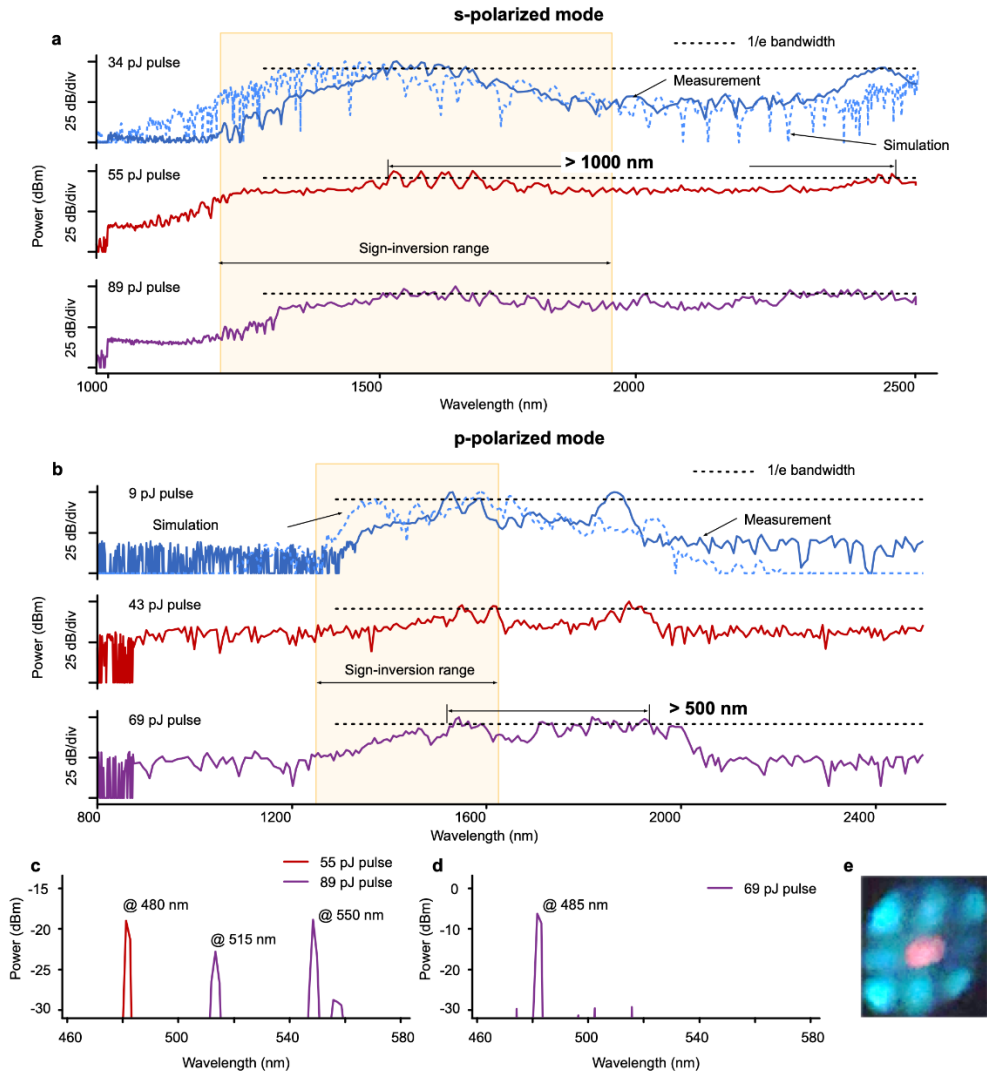
## Our prototype chipset in a nutshell

We have overcome the high-powered laser restrictions for wide-bandwidth sources by alternating the dispersion profile of the corresponding waveguide structure of the source. Our invention overcomes the stagnation that happens after a given length by removing the dispersion based mechanisms that cause this effect. Thus in this fashion we can generate substantial bandwidth at lower -by orders of magnitude- pump powers. Moreover, our concept maintains a smooth and flat spectral profile over the generated bandwidth, which is highly-beneficial for all of the above mentioned applications. [1–3] Figure 1 shows at the center a picture of our integrated chip whilst in operation (the supercontinuum is visible through scattered light from the waveguides) and also summarizes the main features and potential applications of our technology.

We have constructed a prototype of our concept in integrated Silicon Nitride chips that have demonstrated – sometimes orders of magnitude higher efficiency in spectral generation at unprecedented 1/e bandwidth (>500 nm) at pulse energies starting at 9 pJ. To compare typical integrated SCG requires nJ pulse energies with 1/e bandwidths less than 100 nm. [3]

For reference, figure 2a shows the output spectra of our chip devices (for S polarization) along with the corresponding pulse energy. The 1/e spectral bandwidth spans over > 1000 nm (detection is limited by our spectrometer) at a pulse energy of 34 pJ. Figure 2b shows the output spectra of the P-polarization. Here a bandwidth of 500 nm is obtained starting at a pulse energy of 9 pJ. Narrowband peaks are also generated in the visible portion of radiation that approach the 1/e level.





**Figure 2. Measured supercontinuum spectra from the silicon nitride waveguides.** a) Spectral power versus wavelength on a logarithmic scale for Structure 1's s-polarization mode, recorded at stepwise increased pulse energies as indicated in plots. Dispersive waves in the visible range are indicated in inset. b) Same plot as for a) for Structure 2's p-polarization mode. c) Real-color image of an example of higher order modes of the visible dispersive wave at 485 nm. The pink coloring in the center is due to the IR sensitivity of the camera. d) spectral power of the visible dispersive waves of Structure 1 at a pulse energy of 55 pJ and 89 pJ. e) spectral power of the visible dispersive waves of Structure 2 at a pulse energy of 69 pJ.

## Literature Review

The drive to lower power requirements for integrated SCG has been attempted by a plethora of different research groups worldwide. Solutions range from increasing the confinement of light by using high-contrast waveguide materials, to tapering waveguides to optimize soliton fission. Other solutions are simply to use high nonlinear materials in the construction of integrated waveguides such as Silicon on Insulator,[4] silicon rich nitride on oxide,[5] lithium niobate.[6]



However, while these technologies certainly do lower power requirements, they do not remove the fundamental stagnation mechanisms of SCG. As such, the increase in efficiency (i.e., bandwidth/input pulse energy) is intrinsically limited. In contrast, our technology does not have these limitations. To provide context of how are technology compares to past attempts, we have found the efficiency at the 1/e bandwidth of a large number of past works published in the past 5 years. In table 1, we show that our technology has an efficiency increase spanning several orders of magnitude.[3]

**Table 1. Efficiency comparison to previous state-of-the-art integrated SCG sources.**

Technology	Materials	Pump Pulse Input		SCG 1/e Bandwidth (nm)	Efficiency (nm/pJ)	Efficiency ratio of our work to cited work	
		FWHM (fs)	Energy (pJ)				
This work: s-pol. Optimized alternating waveguide	silicon nitride on oxide	190	34	950	28		
This work: p-pol. Optimized alternating waveguide	silicon nitride on oxide	190	9	375	42	s-pol. Optimized alternating waveguide	p-pol. Optimized alternating waveguide
two segment - either width or cladding removal - cascaded anomalous dispersion waveguide[7]	silicon nitride on oxide, 100 mm length	60	220	83	0.4	74	110
uniform-width anomalous waveguide [8]	silicon nitride on oxide	115	590	150	0.3	110	160
wide (1300 nm) uniform-width anomalous waveguide[9]	silicon nitride on oxide	120	1400	21	0.02	1900	2800
Bragg grating enhanced SCG[10]‡	silicon rich nitride on oxide (USRN)	1700	10	24	2.4	12	17
enhanced confinement and tapered anomalous waveguides[11]*	silicon on insulator (SOI)	250	27	400	15	2	3
Bragg grating and confinement enhanced SCG[12]*	silicon on insulator (SOI)	250	27	350	13	2	3
previous state of the art in efficiency SCG OCT source (operating at 1300 nm) [13]	silicon nitride on oxide	200	25	110	4.4	6	9

uncladded high confinement anomalous dispersion waveguide[14]	silicon nitride on oxide	78	300	1000	3.3	8	13
cross phase modulation intermodal SCG[15]	silicon nitride on oxide	88	250	100	0.4	70	100
Low pulse energy SCG [16]	Silicon nitride	70	18	5	0.3	101	150

The asterix refer to works with a waveguide nonlinear coefficient approx. a factor of around 3 times higher than what was used in our structures. The double cross refers to a work in silicon rich nitride (USRN) with a nonlinear refractive index and coefficient approx. an order of magnitude higher than our structures.

## Outline of Tasks and Work Plan

A brief and general outline of tasks is as follows:

1. Build or obtain compact fiber laser (1550nm, 20 mW, 160 fs pulses, 50 MHz), for example, from suppliers such as Menlo Systems.
2. Design and fabricate waveguides in silicon nitride especially suited for the input laser. Using intelligent algorithms that automatically solve the associated nonlinear Schroedinger Equation for SCG.
3. Meanwhile, we can directly use the available prototype to demonstrate functionality with compact fiber laser.
4. Combine our prototype with an integrated AgS detector for NIR spectroscopy.
5. Package the fiber laser and chip prototype system, along with detector in a compact package.
6. Market this as a product through a startup venture.
7. Obtain industrial partners, investors (parallel to the above steps).

## Outcome

The outcome of the workplan is to obtain a portable NIR highly sensitive spectrometer using our SCG chip and a small fiber laser source. We also plan to obtain a portable NIR OCT device, applicable for imaging organs in the human body such as skin. These devices should be close to a marketable product to generate profits for our startup spinoff company.

## Bibliography

1. H. Zia, N. M. Lüpken, T. Hellwig, C. Fallnich, and K. J. Boller, "Supercontinuum Generation in Media with Sign-Alternated Dispersion," *Laser Photonics Rev.* **14**(7), 1–11 (2020).
2. H. Zia, "Enhanced pulse compression within sign-alternating dispersion waveguides," *Photonics* **8**(2), 1–18 (2021).
3. H. Zia, K. Ye, Y. Klaver, D. Marpaung, and K.-J. Boller, "Ultra-Efficient On-Chip Supercontinuum Generation from Sign-Alternating-Dispersion Waveguides," (2022).
4. N. Singh, D. D. Hudson, Y. Yu, C. Grillet, S. D. Jackson, A. Casas-Bedoya, A. Read, P. Atanackovic, S. G. Duvall, S. Palomba, B. Luther-Davies, S. Madden, D. J. Moss, and B. J.

- Eggleton, "Midinfrared supercontinuum generation from 2 to 6  $\mu\text{m}$  in a silicon nanowire," *Optica* **2**(9), 797 (2015).
5. E. Sahin, A. Blanco-Redondo, P. Xing, D. K. T. Ng, C. E. Png, D. T. H. Tan, and B. J. Eggleton, "Bragg Soliton Compression and Fission on CMOS-Compatible Ultra-Silicon-Rich Nitride," *Laser Photonics Rev.* **13**(8), (2019).
  6. Y. Hu, M. Yu, B. Buscaino, N. Sinclair, D. Zhu, R. Cheng, A. Shams-Ansari, L. Shao, M. Zhang, J. M. Kahn, and M. Lončar, "High-efficiency and broadband on-chip electro-optic frequency comb generators," *Nat. Photonics* (2022).
  7. D. R. Carlson, P. Hutchison, D. D. Hickstein, and S. B. Papp, "Generating few-cycle pulses with integrated nonlinear photonics," *Opt. Express* **27**(26), 37374 (2019).
  8. J. P. Epping, T. Hellwig, M. Hoekman, R. Mateman, A. Leinse, R. G. Heideman, A. van Rees, P. J. M. van der Slot, C. J. Lee, C. Fallnich, and K.-J. Boller, "On-chip visible-to-infrared supercontinuum generation with more than 495 THz spectral bandwidth," *Opt. Express* **23**(15), 19596 (2015).
  9. M. A. G. Porcel, F. Schepers, J. P. Epping, T. Hellwig, M. Hoekman, R. G. Heideman, P. J. M. van der Slot, C. J. Lee, R. Schmidt, R. Bratschitsch, C. Fallnich, and K.-J. Boller, "Two-octave spanning supercontinuum generation in stoichiometric silicon nitride waveguides pumped at telecom wavelengths," *Opt. Express* **25**(2), 1542 (2017).
  10. E. Sahin, A. Blanco-Redondo, B.-U. Sohn, Y. Cao, G. F. R. Chen, D. K. T. Ng, B. J. Eggleton, and D. T. H. Tan, "Wideband Spectral Enhancement through On-Chip Bragg-Soliton Dynamics," *Adv. Photonics Res.* **2**(8), 2100107 (2021).
  11. N. Singh, D. Vermulen, A. Ruocco, N. Li, E. Ippen, F. X. Kärtner, and M. R. Watts, "Supercontinuum generation in varying dispersion and birefringent silicon waveguide," *Opt. Express* **27**(22), 31698 (2019).
  12. N. Singh, M. Raval, E. Ippen, M. R. Watts, and F. X. Kärtner, "Supercontinuum generation in silicon Bragg grating waveguide," *Appl. Phys. Lett.* **118**(7), (2021).
  13. X. Ji, D. Mojahed, Y. Okawachi, A. L. Gaeta, C. P. Hendon, and M. Lipson, "Millimeter-scale chip-based supercontinuum generation for optical coherence tomography," *Sci. Adv.* **7**(September), 1–7 (2021).
  14. E. Tagkoudi, C. G. Amiot, G. Genty, and C. S. Brès, "Extreme polarization dependent infrared supercontinuum generation in uncladded silicon nitride waveguide," *Opt. Express* **29**(14), 21348–21357 (2021).
  15. N. M. Lüpken, M. Timmerkamp, R. Scheibinger, K. Schaarschmidt, M. A. Schmidt, K. J. Boller, and C. Fallnich, "Numerical and Experimental Demonstration of Intermodal Dispersive Wave Generation," *Laser Photonics Rev.* **15**(9), 1–8 (2021).
  16. A. J. Metcalf, T. Anderson, C. F. Bender, S. Blakeslee, W. Brand, D. R. Carlson, W. D. Cochran, S. A. Diddams, M. Endl, C. Fredrick, S. Halverson, D. D. Hickstein, F. Hearty, J. Jennings, S. Kanodia, K. F. Kaplan, E. Levi, E. Lubar, S. Mahadevan, A. Monson, J. P. Ninan, C. Nitroy, S. Osterman, S. B. Papp, F. Quinlan, L. Ramsey, P. Robertson, A. Roy, C. Schwab, S. Sigurdsson, K. Srinivasan, G. Stefansson, D. A. Sterner, R. Terrien, A. Wolszczan, J. T. Wright, and G. Ycas, "Stellar spectroscopy in the near-infrared with a laser frequency comb," *Optica* **6**(2), 233 (2019).

# **Handheld MEMS-SOA Silicon Based Gas Analyzer for Real-time, Cumulative and Wide-Band Environmental Monitoring in Smart Cities**

**Assoc. Prof. Dr. Eng. Haitham Omran**

**OSA Early Career Professional**

**Laboratory of Micro Optics, Faculty of Information Engineering and Technology (IET), German University in Cairo, Egypt**

Human activities are the main cause of Earth's environmental changes [1]. Effects like global warming caused by increasing carbon dioxide (CO<sub>2</sub>) and methane (CH<sub>4</sub>) emission from fossil fuel, human waste and agricultural activities have disastrous effect on humankind [1, 2]. Rising sea levels and extreme weather triggered by environmental changes affects the existence of many communities and even nations across the globe [3, 4]. Limiting the global warming and pollution to the target levels requires continuous, wideband, cheap and accumulative monitoring solutions for CO<sub>2</sub>, CH<sub>4</sub> and other climate forcing emissions [1-4].

This proposal aims at contributing to achieve the global warming 2°C target limit implying a cumulative carbon emissions limit of the order of 500 GtC [1]. The target to be achieved by continuous, cumulative and smart monitoring of climate forcing gas emissions (e.g. CO<sub>2</sub>, CH<sub>4</sub>) using a flexible use case handheld micro-electro-mechanical-system semiconductor-optical-amplifier (MEMS-SOA) Silicon based gas analyzer with cloud connectivity for Internet of things (IoT) smart cities. The analyzer core engine is an experimentally verified MEMS-SOA swept laser connected to a small gas cell [5-7]. The MEMS is constructed from two deeply-etched Si/Air Bragg mirrors attached to an electrostatic comb actuator allowing the tuning of the swept laser over 100 nm bandwidth with up to 0.2nm resolution depending on sweep speed [6, 7]. The absorption spectrum of gases in the near-infrared is used for quantitative and qualitative monitoring of the environment climate forcing emissions [5]. The device smart IoT and cloud connectivity allow real-time and accumulative monitoring which is crucial for correct environmental assessment and decision-making. The device will have a flexible use case by working in two gas sampling modes; an in-device near gas cell mode and long-fiber far gas cell mode for difficult to access locations (e.g. factories, mining sites and gas pipelines) enabled by a detachable gas cell head.

At the end of the project, the team will demonstrate a working prototype of a packaged handheld MEMS-SOA gas analyzer in the near-infrared spectrum. The package is to include all functional parts including the MEMS-SOA swept laser core module, control electronics, power supply, gas flow control and detachable gas cell head. We will demonstrate practical sensing of climate forcing gas emissions (e.g. CO<sub>2</sub>, CH<sub>4</sub>) in the range (1500 nm – 1600 nm) with up to 0.2nm resolution. The device will have IoT connectivity for smart cities environmental monitoring. We will develop a mobile app with cloud connectivity allowing device control, real-time monitoring and cumulative data logging for fast and accurate analysis and long-term decision-making based on cumulative sensing in IoT smart cities.

# Handheld MEMS-SOA Silicon Based Gas Analyzer for Real-time, Cumulative and Wide-Band Environmental Monitoring in Smart Cities

Assoc. Prof. Dr. Eng. Haitham Omran

OSA Early Career Professional

Laboratory of Micro Optics, German University in Cairo

- **Literature Review**

Human induced climate changes are severely affecting and even threatening the existence of the humankind. Global warming is mainly attributed to increased carbon dioxide (CO<sub>2</sub>) emission from fossil fuels [1]. This emission have long lasting effects as they remain in the atmosphere for millennia affecting balanced eco systems [8]. A very dangerous consequence is the lock-in of these long lasting responses. European Union in 1996 proposed to limit global warming to 2°C [9] and the target was reaffirmed in the 2009 “Copenhagen Accord” [10]. Achieving the 2°C target converts to a fossil fuel emissions target using climate-carbon-cycle models. These models depends on cumulative emission data and not on temporal emission data [11]. Other human induced gas emissions like methane contribute to the global warming crisis [2]. Methane emission harms human and ecosystem health by contributing to the formation of ground-level ozone [2]. Thus limiting the global warming and pollution to the target levels requires multifold treatment with innovative systems enabling continuous, wideband, cumulative, cheap, and smart monitoring solutions for climate forcing gas emissions. CO<sub>2</sub> monitoring is also very important in the safety of natural gas pipelines [1] and in the quality control of agri-food industry [12].

Gas chromatography [13] and mass spectroscopy [14] are famous techniques for gas detection but are not suitable for real-time and low cost environmental monitoring. Gas chromatography cannot work in real-time while mass spectroscopy is very expensive and bulky.

Sensing mechanisms of CO<sub>2</sub>, methane and other climate forcing gases can be broadly classified as optical and electrochemical mechanisms [12]. The main optical mechanism depends on bulky and expensive mono-chromators and mid infrared optical detectors or high resolution but very expensive tunable laser sources [15, 16]. Optical MEMS based FT-IR spectrometers were demonstrated for gas sensing but they suffer from low resolution and low signal to noise ratio (SNR) attributed to the small travel range of the miniaturized MEMS interferometer [17]. On the other hand, electrochemical sensors depends on the chemical reactions that occur on the sensing surface. They have low cost and high sensitivity but suffer from limited measurement accuracy, problems of long-time stability, cross-response issues and limitation to individual type of gases [12, 16].

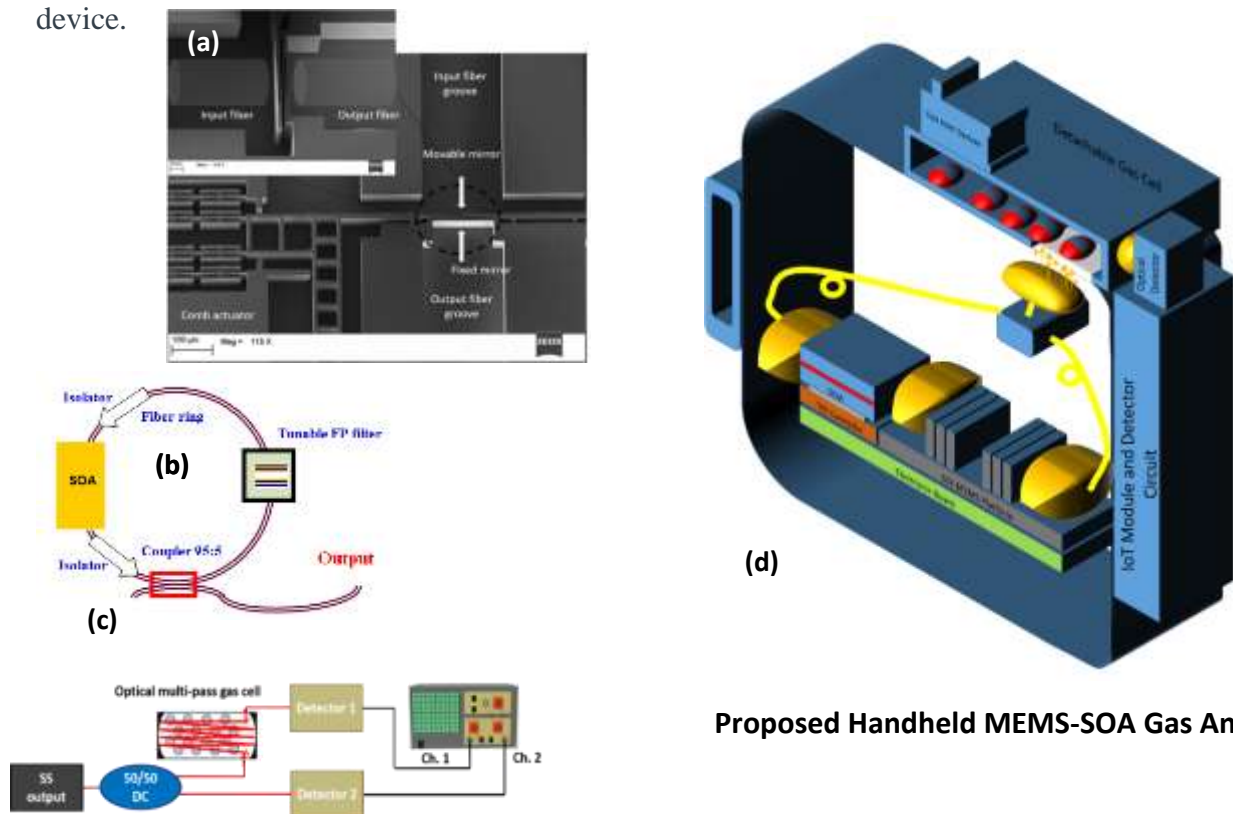
- **Problem Statement/Objective**

In this project, we propose a solution to real-time, cumulative, high resolution, high SNR and multiple gas environmental monitoring using a handheld MEMS-SOA Silicon based gas analyzer for IoT smart cities. A high-resolution optical MEMS-SOA based swept laser core module would combine both the merits of mass production; low cost and small size of silicon

integration technology compared to bulky expensive techniques, and overcome limitations of miniaturized structures in gas sensing. The handheld analyzer would contribute to achieving the 2°C target limit of global warming crisis and other industrial and environment monitoring requirements including agri-food industry.

The handheld MEMS-SOA gas analyzer is based on an experimental verified proof of concept of MEMS-SOA swept laser spectroscopic gas analyzer presented in [5-7]. The core engine of the analyzer is a micro-electro-mechanical system (MEMS) tunable optical filter and a semiconductor optical amplifier (SOA) in a MEMS-SOA swept laser configuration as shown in Fig. 1a, 1b and 1c. The MEMS filter is fabricated using deep reactive ion etching (DRIE) of silicon on insulator wafer (SOI). The MEMS filter consists of two deeply etched Si/Air Bragg mirrors and fiber grooves with 90  $\mu\text{m}$  depth on Silicon on Insulator wafer (SOI) as shown in figure.1. Light propagates in plane in the MEMS structure, which acts like a micro optical bench. One of the Bragg mirrors is movable and attached to an electrostatic comb actuator allowing tuning of the MEMS filter. The in-plane propagation allows hybrid integration of the MEMS with an SOA chip and micro collimation optics in a micro sized package. The MEMS-SOA is inserted in a swept ring fiber laser configuration, which can be tuned by the in-loop MEMS filter. A micro sized gas cell and a detector are further attached to the MEMS-SOA laser allowing absorption spectroscopy of gases over 100 nm tuning range with up to 0.2nm resolution depending on sweep speed.

The MEMS-SOA core engine is to packages together with electronic circuitry, micro gas cell, near and far sample collection heads and IoT cloud connectivity as a flexible use case handheld device.



**Proposed Handheld MEMS-SOA Gas Analyzer**



Fig. 1. (a) SEM photo of optical MEMS tunable filter. (b) Schematic of a basic MEMS-SOA swept laser. (c) Typical laboratory setup for swept source spectroscopic gas sensing. d) Proposed handheld MEMS-SOA gas analyzer

- **Outline of tasks/Work Plan**

	<b><u>Task</u></b>	<b><u>Description</u></b>	<b><u>Expected Duration</u></b>
1	MEMS design and Simulation	Design and FDTD simulation of a deeply-etched filter using Si/Air layers with 100 nm tuning range	2 months
2	MEMS-SOA coupling optics	Design and simulation of MEMS-SOA coupling optics	1 months
3	Swept laser core module	Design and simulation of the MEMS-SOA swept laser core module and system specs for achieving target detection limits.	3 months/In parallel
3	System control electronics	Includes MEMS electronic circuitry, temperature control circuit for SOA and system control	3 months/ In parallel
4	MEMS technology development and fabrication	MEMS Fabrication at ESIEE, Paris	3 months
	Control Boards Fabrication		
5	Assembly and testing of swept laser core module	Assembly and testing at GUC micro optics lab.	3 months
6	Design and implementation of gas sampling head	Includes gas sampling system, flow control and electronic control	4 months/In parallel
6	IoT and cloud connectivity	Design, simulation and implementation of cloud and IoT connectivity, Mobile app	4 months/ In parallel
7	Full system assembly and testing on use cases	Assembly of swept core module, electronic circuitry and gas sampling head	4 months
	<b>Total Duration</b>		<b>20 months</b>

- **Outcome(s)**

At the end of the project period, the project team will deliver a prototype of a novel handheld MEMS-SOA Silicon based gas analyzer for real-time, cumulative and wide-band environmental monitoring in IoT smart cities including the following subsystems:

- Wide bandwidth tunable optical MEMS filter
- MEMS-SOA swept laser core module
- Near and far gas sampling head
- Electronic control system
- Circuits for IoT connectivity.
- Mobile app for system control and cloud data logging.

- **Impact**

The implementation of a handheld MEMS-SOA gas analyzer is expected to have a multifold impact.

**Climate impact:** The device will contribute to achieve the 2°C target limit of global warming crisis by providing real-time and cumulative monitoring of pollution levels in IoT smart cities.

**Market impact:** The device will introduce a novel technology in the gas sensing market estimated to reach 2.1 USD billion by 2027.

**National impact:** The device will have a huge impact in Egypt. It would foster the idea of technological industries based economy. It will attract investors to new technological sectors. It will foster Egyptian researchers to address technological based solutions for demanding environment and economical problems.

- **References**

[1] Hansen, James, Pushker Kharecha, Makiko Sato, Valerie Masson-Delmotte, Frank Ackerman, David J. Beerling, Paul J. Hearty et al. "Assessing “dangerous climate change”: Required reduction of carbon emissions to protect young people, future generations and nature." PloS one 8, no. 12 (2013): e81648.

[2] United Nations Environment Programme and Climate and Clean Air Coalition (2021). Global Methane Assessment: Benefits and Costs of Mitigating Methane Emissions. Nairobi: United Nations Environment Programme.

[3] Zhang, Keqi, Bruce C. Douglas, and Stephen P. Leatherman. "Global warming and coastal erosion." Climatic change 64, no. 1 (2004): 41-58.

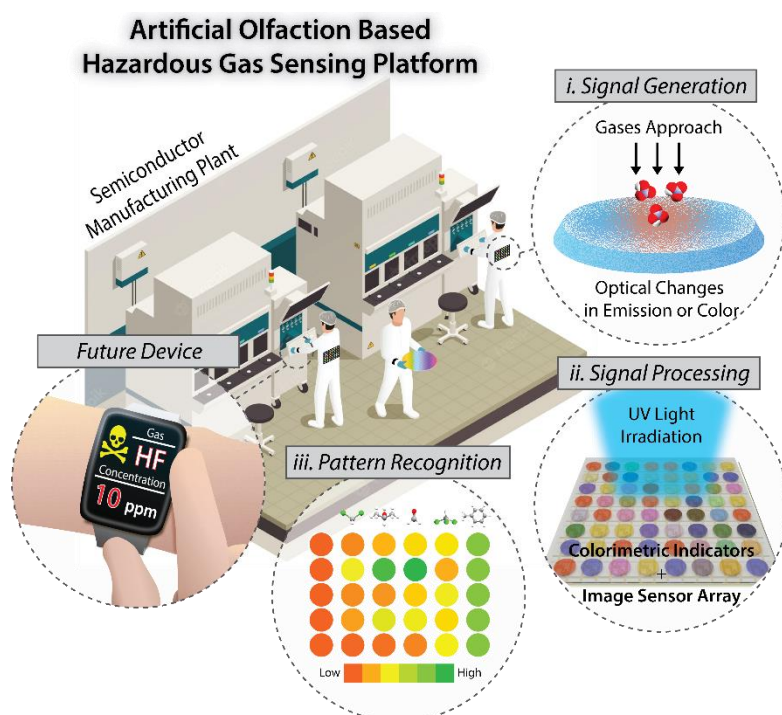
[4] DeConto, R.M., Pollard, D., Alley, R.B. et al. The Paris Climate Agreement and future sea-level rise from Antarctica. Nature 593, 83–89 (2021). <https://doi.org/10.1038/s41586-021-03427-0>

- [5] John O. Gerguis, Yasser M. Sabry, Haitham Omran, and Diao Khalil, "Spectroscopic Gas Sensing Based on a MEMS-SOA Swept Fiber Laser Source," *J. Lightwave Technol.* 37, 5354-5360 (2019).
- [6] Haitham Omran, Yasser M. Sabry, Mohamed Sadek, Khaled Hassan, and Diao Khalil, "Wideband Subwavelength Deeply Etched Multilayer Silicon Mirrors for Tunable Optical Filters and SS-OCT Applications", *IEEE Journal of Selected Topics in Quantum Electronics*, vol. 21, no. 4, July-Aug. 2015.
- [7] Haitham Omran, Yasser Sabry, Mohamed Sadek, Khaled Hasan, Mohamed Shalaby, and Diao Khalil, "Deeply-Etched Optical MEMS Tunable Filter for Swept Laser Source Applications", *IEEE Photonic Technology Letters PTL*, Vol. 26, No.1, pp37-39, January 1, 2014.
- [8] Archer, David. "Fate of fossil fuel CO<sub>2</sub> in geologic time." *Journal of geophysical research: Oceans* 110, no. C9 (2005).
- [9] Randalls, Samuel. "History of the 2 C climate target." *Wiley Interdisciplinary Reviews: Climate Change* 1, no. 4 (2010): 598-605.
- [10] Accord, Copenhagen. "United Nations Framework Convention on Climate Change, Draft decision 2/CP." (2009).
- [11] Matthews, H. Damon, Nathan P. Gillett, Peter A. Stott, and Kirsten Zickfeld. "The proportionality of global warming to cumulative carbon emissions." *Nature* 459, no. 7248 (2009): 829-832.
- [12] Neethirajan, Suresh, D. S. Jayas, and Shashikant Sadistap. "Carbon dioxide (CO<sub>2</sub>) sensors for the agri-food industry—a review." *Food and Bioprocess Technology* 2, no. 2 (2009): 115-121.
- [13] McNair, Harold M., James M. Miller, and Nicholas H. Snow. *Basic gas chromatography*. John Wiley & Sons, 2019.
- [14] Karasek, Francis W., and Ray E. Clement. *Basic gas chromatography-mass spectrometry: principles and techniques*. Elsevier, 2012.
- [15] Lee, Duk-Dong, and Dae-Sik Lee. "Environmental gas sensors." *IEEE sensors journal* 1, no. 3 (2001): 214-224.
- [16] Hodgkinson, Jane, and Ralph P. Tatam. "Optical gas sensing: a review." *Measurement science and technology* 24, no. 1 (2012): 012004.
- [17] Erfan, Mazen, Yasser M. Sabry, Mohammad Sakr, Bassem Mortada, Mostafa Medhat, and Diao Khalil. "On-chip micro-electro-mechanical system Fourier transform infrared (MEMS FT-IR) spectrometer-based gas sensing." *Applied spectroscopy* 70, no. 5 (2016): 897-904.

### A Colorimetric Optical Nose for Hazardous Gases

In this proposal, we would like to **develop a colorimetric optical nose for hazardous gases in industrial manufacturing environments**. Target gases include five volatile organic compounds (methylene chloride, isopropyl alcohol, formaldehyde, chloroform, and toluene) and five toxic industrial chemicals (ammonia, chlorine, hydrogen chloride, hydrogen fluoride, and nitric acid) with different concentration ranges of permissible exposure limit (PEL) and immediately dangerous to life or health (IDLH). This system consists of colorimetric indicator arrays as sensing components and image sensor arrays as signal conditioning components vertically assembled as an artificial olfaction system.

- In **signal generation**, **more than ten gas-reactive porous nanostructures**, including nanofibers and nanoparticles, will be developed to generate optical fingerprint-like patterns against individual gases. This can enhance the detectable concentration less than IDLH and PEL for multiple gases.
- In **signal processing**, gas-induced optical changes, e.g., emission wavelength, dyes' color, and transmitted light, are quantified and amplified in photocurrent signals, establishing **the data library on gas-fingerprint patterns** in terms of types and safety levels of hazard. In addition, the evaluation index of optoelectrical behaviors can be determined for post-processing.
- In **pattern recognition**, an unknown gas X can be determined by a newly defined pattern recognition algorithm based on a relative gas coefficient  $d_g = \sum_{n=1}^N |\log a_n / X_n|$ .
- The colorimetric optical nose separates sensing and signal conditioning components, allowing **quick, accurate identification of gases with thresholds** and amplifying the quantified current changes for **post-process and commercial viability on-site workplaces**.



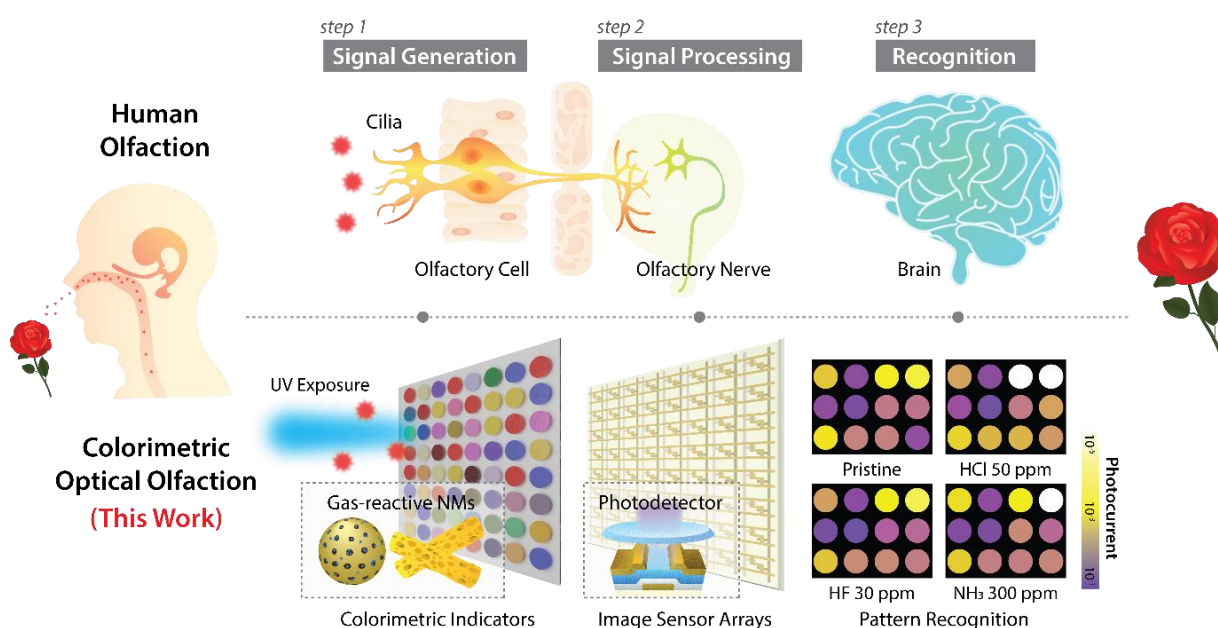
**Figure 1.** Schematic illustration of a colorimetric optical nose for hazardous gases.

## A Colorimetric Optical Nose for Hazardous Gases

### 1. Literature Review

Industrial gas detectors have been extensively developed since most chronic damage to the workplace is derived from a hazardous gas leak. Various technologies detect airborne compounds under different operating mechanisms, e.g., catalytic-based gas detectors, point infrared gas sensors, tunable laser diode spectroscopic gas sensors, and electrochemical gas detectors. However, it is highly challenging that a single gas detector can selectively sense multiple gases at a low concentration and discriminate against a particular substance. In this regard, artificial olfaction has received interest as a potential alternative to conventional gas detectors in the workplace.

Artificial olfaction is a sensor platform that mimics the human olfactory system to recognize odors<sup>1</sup>. The artificial olfaction utilizes sensor arrays to interact and react to gases and generates a unique pattern for each stimulus, identifying single or multiple airborne compounds<sup>2</sup>. To date, various sensing mechanisms have been proposed as a transducer to form a fingerprint gas pattern. For example, optical gas sensors are susceptible and selective to stimuli but difficult in miniaturization and field application possibility<sup>3</sup>. Chemoresistive sensors with multi-semiconductor materials facilitate quantifying signals and can be integrated with circuits for post-process. In this approach, sensors utilize a set of different semiconductor sensors to obtain output vectors, requiring a time-consuming and nonuniversal fabrication process<sup>4,5</sup>. In addition, it suffers from poor gas-sensing selectivity<sup>6</sup> and high operating temperature up to 200 °C<sup>7</sup>. Colorimetric sensors are utilized as preliminary data with multiple stimuli owing to rapid sensitivity and selectivity at thresholds of detection<sup>8</sup>. Although some studies have successfully identified chemical species, there is still much room for developing craft, sophisticated sensor formats to enable workplace safety innovation.



**Figure 1.** Schematics illustration of human olfaction and colorimetric optical olfaction (this work).

Herein, we propose “**A Colorimetric Optical Nose for Hazardous Gases**” to surpass existing artificial olfaction-based sensing platforms. We comprise the beauty of optical, chemiresistive, and colorimetric gas sensors and suggest a newly designed sensor format to immediately, sensitively sense and discriminate hazardous chemical species, including five volatile organic compounds (VOCs) and five toxic industrial chemicals (TICs) as single and multi-analytes. The colorimetric optical nose separates sensing and signal conditioning components, allowing quick, accurate identification of gases with thresholds and amplifying the quantified current changes for post-process and commercial viability on-site workplaces. This study contains three basic building blocks. In signal generation (step 1), colorimetric arrays react to analytes and form unique patterns. In signal processing (step 2), the phototransistor arrays extract the quantified current as readable digital signals derived from the optical changes of colorimetric arrays. Lastly, in recognition (step 3), we distinguish ten different toxic substances according to the accumulated data. This novel optical artificial olfaction will be able to provide unique, effective means to monitor industrial environments, realizing much safer, healthier workplaces.

## **2. Problem Statement/Objectives**

A complex, nonuniversal approach for lab-scale gas sensors is adequate; however, for highly olfactory systems in the workplace with possible various hazardous leaks, a compassionate, selective approach integrated with circuits is desirable. This proposal is primarily divided into three building blocks: **signal generation, signal processing, and pattern recognition**, and will address each problem and objective.

### **2.1 Highly selective, reversible optical signal generation to detect odors**

The olfactory response for airborne chemicals should be as highly selective and sensitive as possible, forming fingerprint patterns for each stimulus in early detection. In addition, it is demanded to determine a target substance under complex analytes with more than one gas. In general, colorimetric gas sensors show a susceptible reaction to some gases with thresholds of a low concentration. However, they could provide preliminary data but are not appropriate to incorporate as the transducer with circuits or systems since the outcome is presented in terms of color changes.

We would like **to develop porous nanostructures functionalized with gas-reactive dyes** to achieve sensitive, selective detection with processible output signals. Porous nanostructures, including nanofibers (1D) and nanoparticles (0D), have a high surface-to-volume ratio to have the advantage of responding to gases. In addition, we would like to functionalize nanostructures by fluorescent or color-indicating molecules. This way, colorimetric arrays show changes in optical features, such as photoluminescence or transmittance, under excitation light irradiation. In addition, they can improve their selectivity and sensitivity and be stable after gas exposures, possibly detectable multiple analytes, and reversible with repeated exposure. Then, **setting multiple indicators as a batch can form optical fingerprint-like patterns** against individual gas molecules.

### **2.2 Post-processible signal processing integrated with phototransistor arrays**

The artificial olfaction should convert input signals into quantified electrical signals after detection for post-process. However, fingerprint-like gas patterns from colorimetric indicator sets are shown in colors or emission light. **The indicator array would be vertically stacked between a light source to excite indicator layers and an image sensor array to convert them into electrical signals** for quantification. In addition, the image sensor array should include



multiple pixels with a pair of a switching transistor and a phototransistor, possibly suitable for IC integration and interface circuitry. This way, this optical nose system can generate random optical patterns with different analytes and extract output signals in a quantified manner.

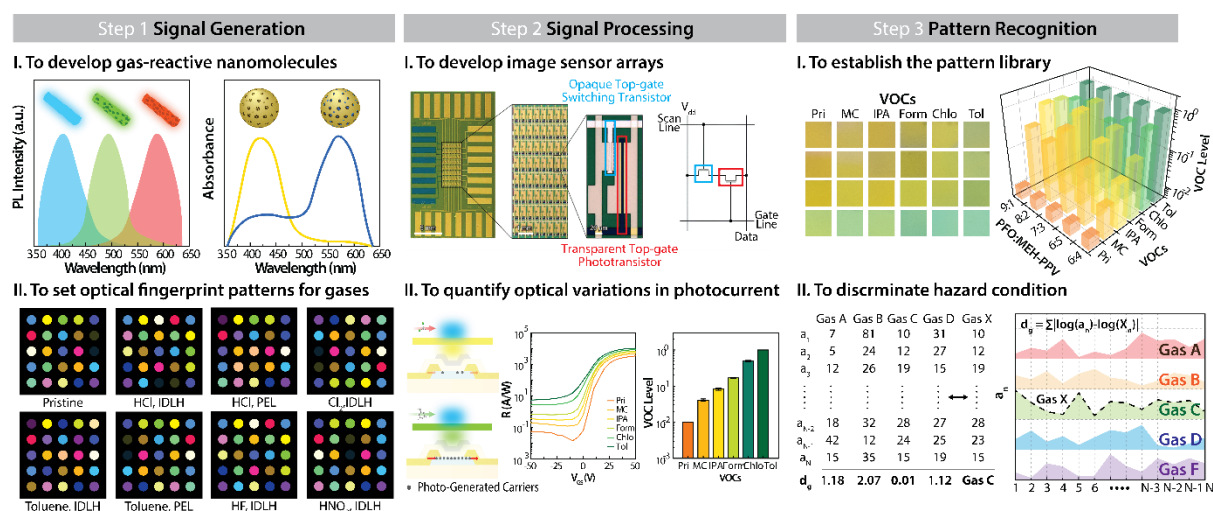
In this step, the data library on gas-fingerprint patterns will be set for more than ten gases in technical realms, including permissible exposure limit (PEL) and immediately dangerous to life or health (IDLH).

### 2.3 Straightforward pattern recognition based on the pattern library

For hazard discrimination, unknown gas X should be compared with the pattern library and matched as a particular gas. The matching algorithm for pattern recognition should estimate the variations for individual pixels and specify the hazard conditions, i.e., gas, concentration, and severity. This project will define a relative gas coefficient  $d_g$  as the following equation.

$$d_g = \sum_{n=1}^N \left| \log \frac{a_n}{X_n} \right|$$

$a_n$ ,  $X_n$ , and  $n$  represent a set value of the data library, an extracted value of unknown gas X, and a given coordinate for an individual indicator in the array. The program will calculate  $d_g$  for entire conditions and deduce the matching state with the minimum  $d_g$ .



**Figure 2.** Schematics of objectives for signal generation, signal processing, and recognition.

## 3. Outline of Tasks/Work Plan

### 3.1 Signal generation

#### 3.1.1 Development of Gas-reactive nanomaterials [3 months]

Synthesis and characterization of VOC-reactive porous nanofiber: (3.1.1.1) Electrospinning of solution precursors with various ratios in chloroform solvent. Solution precursors include organic donors and acceptors, possibly promoting fluorescence resonance energy transfer (FRET) to exhibit the gas-induced variations in emission properties under the excitation wavelength where donors are only absorbed. Possible donor-acceptor pairs for FRET would be PFO and MEH-PPV. (3.1.1.2) Conducting scanning electron microscope (SEM) and transmission electron microscopy (TEM) to understand geometrical features of nanofibers. (3.1.1.3) Photoluminescence (PL) and time-resolved photoluminescence (TRPL), fluorescence lifetime imaging (FLIM) characterize the optical properties of nanofibers and

exploit the optimal conditions.

Synthesis and characterization of TIC-reactive porous nanoparticles: (3.1.1.4) Solution-processing of zwitterionic-like porous silica nanoparticle (Si NPs) as carriers of gas-reactive dyes. TEOS as a silica precursor and APTES as an anchor are blended in ethanol and ammonium hydroxide solvent, undergoing hydrolysis via a polycondensation reaction. (3.1.1.5) Implementing SEM and TEM analyses to obtain geometrical features of Si NPs. (3.1.1.6) Doping Si NPs with various dyes via physical entrapment and covalent attachment. Possible dyes would include bromophenol blue, m-cresol purple, thymol blue, and so on. TEM-EDS mapping mainly characterizes the presence of dyes in Si NPs.

### 3.1.2 Development of indicator arrays [1 month]

Design and fabrication of colorimetric indicator batches: (3.1.2.1) Printing FRET nanofibers on flexible, transparent substrates and solution drop-casting of dye-doped Si NPs with the desired structures.

### 3.1.3. Demonstration of random optical patterns under gas exposures [3 months]

Generation of optical gas-fingerprint patterns: (3.1.3.1) Determining more than ten kinds of hazardous molecules and setting the lower limit of detection (LLOD) and detection limits (IDLH and PEL). (3.1.3.2) Setting a gas exposure system, including MFC, gas lines, and gas cabinets. (3.1.3.3.) Establishing gas exposure conditions to indicator batches, such as concentration, flow, and working temperatures. (3.1.3.4) Characterizing the changes in geometrical and optical properties of individual indicators using SEM, PL, absorbance, TRPL, and FLIM. (3.1.3.5) Establishing and archiving optical gas-fingerprint patterns as a color chart.

## **3.2 Signal processing**

### 3.2.1 Development and evaluation of image sensor arrays [2 months]

Fabrication and characterization of 4 x 4 image sensor arrays: (3.2.1.1) Designing a photolitho mask to image sensor arrays with a unit pixel including a phototransistor and a switching transistor. (3.2.1.2) Demonstrating a low-temperature process on the flexible substrate. Active matrix would be scalable IGZO. (3.2.1.3) Examining electrical and photoresponsive properties of each pixel under ultraviolet or blue laser irradiation. Photoresponsive characteristics are determined in photo responsivity ( $R_{ph}$ ), photosensitivity ( $S$ ), and rise/fall times.

### 3.2.2 Generation of the data library on gas-fingerprint patterns [3 months]

Quantitation and generation of gas-fingerprint pattern archive: (3.2.2.1) Assembling and aligning the image sensor and indicator arrays vertically. Quantifying and converting optical patterns of indicator arrays into photocurrent signals before and after gas exposures. Each phototransistor-indicator set is defined as coordinates for post-processing. (3.2.2.2) Calibrating the variations in photocurrent on the basis of pristine conditions and archiving the gas-fingerprint patterns based on the quantified outputs as the data library.

## **3.3 Pattern recognition**

### 3.3.1 Development of recognition algorithm for gas identification [2 months]

Definition of a relative gas coefficient  $d_g$ : (3.3.1.1) Establishing the equation and the relative gas coefficient  $d_g$  and comparing them with correlation coefficients to identify unknown gas X. (3.3.1.2) After several sequences of gas recognitions, correcting and revising the set-equation. (3.3.1.3) Estimating degree of accuracy in the algorithm to detect and discriminate unknown

gas X and its concentration.

#### 4. Outcome

In this project, we would like to develop highly sensitive, selective indicator patches with more than ten gas-reactive nanomaterials as indicator arrays. We can understand what optical reactions occur and how individual indicator interacts with hazardous gases. This would be helpful that the LLOD of the system is highly enhanced less than IDLH and PEL.

We also develop highly sensitive 4 x 4 image sensor arrays on the flexible substrate and assemble them with indicator arrays. Along with the hardware system, we would establish the evaluation index of optoelectrical behaviors on colorimetric optical noses. Moreover, pattern recognition algorithms are defined based on the gas-fingerprint pattern archive. This system can early detect and discriminate the types and concentrations of hazardous gases, highly applicable for industrial gas alarms.

#### 5. Impact

We propose “**A Colorimetric Optical Nose for Hazardous Gases**” to surpass existing artificial olfaction-based sensing platforms. It can be highly promising to determine possible industrial hazards by hybridizing colorimetric indicators and optoelectronic image sensors. The array quantifies the optical input and amplifies the differences into orders as the electrical output. The quantified signals were collected and statistically analyzed as the archive of gas-fingerprint patterns. We established the algorithm to calculate the relative coefficient  $d_g$  and determine the hazard conditions, including the types and concentration of airborne compounds, enabling the prohibition of fatal disasters for preventative health strategies in workplaces.

#### Reference

1. Turner, A. P. F. & Magan, N. Electronic noses and disease diagnostics. *Nat. Rev. Microbiol.* **2**, 161–166 (2004).
2. Gardner, J. W. & Bartlett, P. N. A brief history of electronic noses. *Sensors Actuators B Chem.* **18**, 210–211 (1994).
3. Rakow, N. A. & Suslick, K. S. A colorimetric sensor array for odour visualization. *Nature* **406**, 710–713 (2000).
4. Kang, H. *et al.* Multiarray Nanopattern Electronic Nose (E-Nose) by High-Resolution Top-Down Nanolithography. *Adv. Funct. Mater.* **30**, 2002486 (2020).
5. Hu, W. *et al.* Electronic Noses: From Advanced Materials to Sensors Aided with Data Processing. *Adv. Mater. Technol.* 1800488 (2018) doi:10.1002/admt.201800488.
6. Joshi, N. *et al.* A review on chemiresistive room temperature gas sensors based on metal oxide nanostructures, graphene and 2D transition metal dichalcogenides. *Microchim. Acta* **185**, 213 (2018).
7. Jeong, S., Kim, J. & Lee, J. Rational Design of Semiconductor-Based Chemiresistors and their Libraries for Next-Generation Artificial Olfaction. *Adv. Mater.* **32**, 2002075 (2020).
8. Lim, S. H., Feng, L., Kemling, J. W., Musto, C. J. & Suslick, K. S. An optoelectronic nose for the detection of toxic gases. *Nat. Chem.* **1**, 562–567 (2009).

**Title: Multimodal Imaging of Genetic Drug Delivery in Airway Cell Populations.****Category: Health**

Cystic fibrosis (CF) is a genetic disease caused by mutations of the cystic fibrosis transmembrane conductance regulator (CFTR) gene. CF patients experience dysregulated epithelial ion gating and severely impaired mucociliary clearance. The advent of highly effective CFTR modulator therapies has increased the expectancy of the CF patient population substantially. Nevertheless, there remain a portion of CF patients carrying mutations that are not treatable by the available CFTR modulators. Therefore, the field is moving towards alternative treatments based on genetic therapies that could benefit the entire CF patient population. Drug developers are seeking a mechanistic understanding of the drug's interaction with the microenvironment of CF airways and its subsequent impact on airway physiology.

This drug development process is fraught with numerous uncertainties, and there is an unmet need for optical imaging technologies to inform on the functional delivery (i.e., ability to both reach targeted cells and restore healthy physiological function) of investigational genetic therapeutics. Currently, the use of mRNA-based therapeutics to correct CFTR mutations is one of the most hotly pursued approaches, and they are tested on Cre reporter animal models. When CFTR mRNA enters the targeted cells of the reporter animal, Cre-mediated recombination occurs, and the cells express fluorescence proteins. Presently, the efficacy of genetic treatment is determined via fluorescence cell sorting and cell sequencing. Unfortunately, these methods provide little insight into the drug's effectiveness in restoring healthy airway physiology and how that evolves over different time points of the treatment. *The overall goal of this 2-year proposal is to overcome this drawback by developing a multimodal imaging platform based on micro-optical coherence tomography ( $\mu$ OCT), dynamic  $\mu$ OCT (D $\mu$ OCT), and confocal fluorescence microscopy (CFM).* The rationale is to leverage  $\mu$ OCT, D $\mu$ OCT, and CFM for co-localized *in situ* assessment of airway physiology via characterization of airway mucociliary transport system, identification of cell populations in the airway epithelium, and monitoring functional delivery of genetic therapeutics, respectively. This imaging platform will enable correlative studies that are particularly aimed at 1.) understanding which cell types the therapeutics have been delivered to, and 2.) if correction of the underlying CFTR defect is effective in modifying the course of CF disease, especially in the presence of epithelial damage.

While our lab has extensive experience in developing CFM and  $\mu$ OCT for investigating airway physiology, the development of D $\mu$ OCT for robustly identifying airway cell types is in its relatively early stages. Year 1 will be spent focusing efforts on developing multiple aspects of the D $\mu$ OCT technology for increasing accuracy in distinguishing airway cell types. We anticipate that the same hardware for performing D $\mu$ OCT will be capable of performing  $\mu$ OCT imaging of the airway physiology. Subsequently, we will integrate CFM imaging capabilities to the D $\mu$ OCT/ $\mu$ OCT system in year 2 and ramp up efforts to test investigational CF genetic therapeutics on Cre reporter cell models.

Although  $\mu$ OCT has subcellular optical resolutions that make it conducive for imaging airway functional microanatomy, it lacks cellular contrast due to minute differences in refractive indices between cells. To enhance contrast and, more importantly, to delineate cell types in the airway models in a label-free manner, we propose to advance a technology termed D $\mu$ OCT, which itself is an extension of  $\mu$ OCT. Instead of using information from a single snapshot image, the current form of D $\mu$ OCT utilizes temporal information extracted from  $\mu$ OCT videos of metabolically active cells to enhance the image contrast of cells. We will advance D $\mu$ OCT by developing methods to extract temporal signatures in  $\mu$ OCT that are specific to major cell types in the airway epithelium, thus enabling us to distinguish cell types in the airway without having to stain tissues. This capability will be critical for identifying which cell types the drug compounds have been delivered to via co-localized detection of fluorescence signals in Cre reporter mouse models.

The range of information that can be acquired in our proposed multimodal imaging platform will enable researchers to gain mechanistic insights into why certain investigational therapeutics work or not. Those insights are critical for understanding how to further optimize the efficacy of an investigational drug. For example, our imaging platform allows investigators to determine functional delivery across mucus barrier, characterize drug uptake by various cell types, and enable monitoring of long-term treatment effects on epithelial remodeling and restoration of healthy airway physiology. The ability to answer these questions will potentially improve the relevance of pre-clinical studies and allow for a more realistic assessment of the drug's clinical impact on CF patients' health.

## 1. BACKGROUND AND LITERATURE REVIEW

**1.1 The role of different cell types in airway physiology:** The human respiratory system is an intricately designed host defense system that protects the body from inhaled pathogens. The mucociliary transport bio-machinery found at the luminal surfaces of the respiratory tracts plays a critical role in the host defense (Fig. 1). Its healthy physiology relies on the coordination of various cell types that have distinct biological functions associated with them. For instance, goblet cells secrete mucinous liquid that lines and protects the airway epithelial surface against inhaled pathogens. Pathogen-laden mucus lining is continuously transported out of the body by micro-motors known as cilia. If foreign bodies manage to breach the protective mucus barrier, immune cells are recruited locally to resolve pathogenic action<sup>1</sup>. In the constant cell renewal process, basal cells ensure cell populations of various cell types needed for airway homeostasis is well maintained.<sup>2</sup>

**1.2 Abnormal airway physiology in Cystic Fibrosis (CF):** CF is a genetic disease caused by mutations of the cystic fibrosis transmembrane conductance regulator (CFTR) gene. CFTR gene mutations result in dysregulated epithelial ion gating and the generation of abnormally viscous mucus, which the mucociliary transport system is ill-equipped to expel. Moreover, people with CF exhibit abnormal epithelium phenotypes such as basal cell hyperplasia, goblet cell hyperplasia, and delayed ciliated cell differentiation.<sup>3</sup> Aberrations of the epithelium phenotype and mucus properties trigger a pathogenic cascade of pulmonary diseases in CF.<sup>4</sup> Although the advent of highly effective CFTR modulator therapies has increased the median expectancy of the CF patient population substantially<sup>5</sup>, there remain a portion of the CF patients carrying mutations that are not treatable by the modulators. Therefore, there is an increasing interest in developing alternative therapies based on genetic treatment<sup>6-9</sup> that could benefit the entire CF population. The development of such drugs is still in the nascent stages. A mechanistic understanding of a drug's interaction with the abnormal microenvironment of CF airways and its subsequent impact on airway physiology is often lacking, thus, the future of genetic treatment is shrouded in uncertainties.<sup>6,8,10,11</sup>

## 2. PROBLEM STATEMENT/OBJECTIVES

### Developing multimodal imaging tools for imaging functional delivery of genetic therapeutics

When faced with these gaps in knowledge, there is an unmet need for optical imaging technologies to inform on the *functional delivery* of investigational genetic therapeutics to facilitate the drug development process. Functional delivery of a drug is defined as the ability to both reach targeted cells and restore healthy physiological function. *The overall goal of this proposal is to address this unmet need by developing a multimodal imaging platform based on micro-optical coherence tomography ( $\mu$ OCT), dynamic  $\mu$ OCT (D $\mu$ OCT), and confocal fluorescence microscopy (CFM).* The rationale is to leverage complementary capabilities of  $\mu$ OCT, D $\mu$ OCT, and CFM for co-localized *in situ* characterization of airway physiology, identification of cell populations in the airway epithelium, and monitoring functional delivery of genetic therapeutics, respectively. This imaging platform will enable correlative studies that are particularly aimed at 1.) understanding which cell types the therapeutics have been delivered to, and 2.) if correction of the underlying CFTR defect is effective in modifying the course of CF disease, especially when there is tissue damage. Epithelial injury due to chronic inflammation is common in adult CF patients. It is unclear if correcting CFTR defects on remodeled airways with modified cell populations could promote the restoration of healthy airway physiology.

## 3. RATIONALE FOR DEVELOPING A CFM/ $\mu$ OCT/D $\mu$ OCT IMAGING PLATFORM

### 3.1 Confocal fluorescence microscopy enables molecular imaging of functional delivery of drugs

Currently, the use of mRNA-based treatments to correct CFTR mutations is one of the most promising approaches. The packaged therapeutics have to penetrate hyperviscous mucus with especially small mesh sizes<sup>11</sup> to reach the airway epithelium, avoid endocytosis, and unload its contents into the cytoplasm of cells. There is no guarantee that drugs could successfully enter cells, much less correct the underlying CFTR defect. It is common to test investigational therapeutics on Cre reporter animal

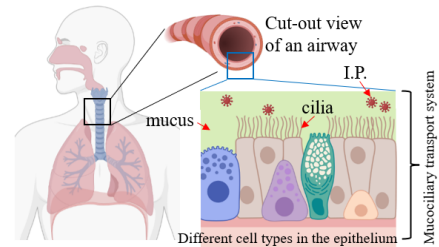


Fig 1. Illustration of the mucociliary transport system and major cell types in the airway epithelium. I.P.: Inhaled pathogens



models. Only when CFTR mRNA enters targeted cells of a reporter animal, resulting in Cre-mediated recombination, will the cells express fluorescence proteins (Fig. 2).<sup>8,12</sup> Presently, the efficacy of a genetic treatment is determined via terminal experiments that involve fluorescence cell sorting and cell sequencing.<sup>8</sup> Although these measurements provide valuable information about the biochemistry of the drugs at the cell level, they provide little insight into the drug's effectiveness in restoring healthy airway physiology and how the disease improve over time. CFM, on the other hand, is a molecular imaging method that is amendable to imaging living systems. Although CFM typically has ~100  $\mu\text{m}$  imaging depth, this will not be an issue in this application as the delivery of nebulized drugs is expected to be confined to cells that are several tens of microns below the epithelial surface.

**3.2  $\mu\text{OCT}$  is conducive to imaging airway function microanatomy** To complement the molecular imaging capabilities of CFM,  $\mu\text{OCT}$  will be utilized to perform structural imaging of the airway epithelium and characterization of mucociliary transport.  $\mu\text{OCT}$  has been well established to be an excellent imaging method for interrogating airway physiology of living systems *in situ*. The utilization of  $\mu\text{OCT}$  to elucidate CF pathophysiology using CF cell cultures, animal explants, and living human subjects has been demonstrated by the PI.<sup>13-15</sup> As a label-free, cross-sectional imaging method with subcellular optical resolutions (~ 1-2  $\mu\text{m}$  axially and laterally) over several hundreds of microns in depth,  $\mu\text{OCT}$  enables close examination of the airway epithelium's microanatomy and its functional characteristics (Fig. 3). Metrics that can be robustly and precisely determined include the thicknesses of the airway mucus layer, cilia beat frequency, mucociliary transport rate, the percentage of epithelial surface covered in motile cilia, and the number of inflammatory cells that have infiltrated the tissue.<sup>15-17</sup>

**3.3  $\text{D}\mu\text{OCT}$  is promising for discriminating cell types** Although  $\mu\text{OCT}$  has subcellular optical resolutions that make it conducive for imaging airway functional microanatomy, it lacks cellular contrast due to minute differences in refractive indices between cells. To overcome weak cellular contrast and, more importantly, to delineate cell types in the airway models in a label-free manner, we propose to advance a technology termed  $\text{D}\mu\text{OCT}$ <sup>18</sup>, which is an extension of  $\mu\text{OCT}$ . Instead of using snapshots,  $\text{D}\mu\text{OCT}$  utilizes temporal information extracted from  $\mu\text{OCT}$  videos of viable cells to generate image contrast (Fig. 4). This could be accomplished through signal autocorrelation<sup>19</sup> and/or Fourier analysis<sup>20,21</sup> on the time-dependent OCT fluctuations on a per-pixel basis. In our work, we have used Fourier analysis to determine the frequencies of the fluctuations. A color corresponding to the dominant frequency is then assigned to each pixel of an image.

To understand the basis of intracellular fluctuation, we must recognize that living cells utilize ATP-derived biochemistry<sup>22</sup> to orchestrate active diffusion<sup>23</sup> for cargo transportation necessary for specific biological functions. The directed diffusive transport of intracellular contents is different from thermal-driven Brownian motion.<sup>24</sup> Thermal-driven diffusion is described by the Stokes-Einstein equation, and the mean squared distance (MSD) traveled varies linearly with time. However, nonequilibrium cellular processes and aggregate biochemical forces in living cells give rise to either super- or sub-diffusive motion (fig. 5).<sup>25</sup> Since intracellular motion is governed by biological function,

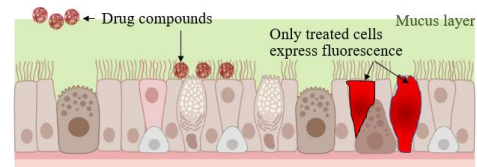


Fig 2. Drug compounds must traverse through the mucus layer, enter targeted cells, avoid endocytosis, before correcting the gene mutation. In Cre-reporter cell models, cells that have their gene mutation corrected will express fluorescence proteins.

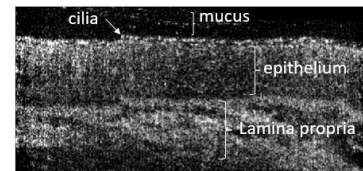


Fig 3. A  $\mu\text{OCT}$  image showing the microanatomy of the human airway epithelium. Structural metrics can be measured from a static  $\mu\text{OCT}$  image whereas dynamical function such as cilia beat frequencies and mucociliary transport rate are extracted from  $\mu\text{OCT}$  videos.

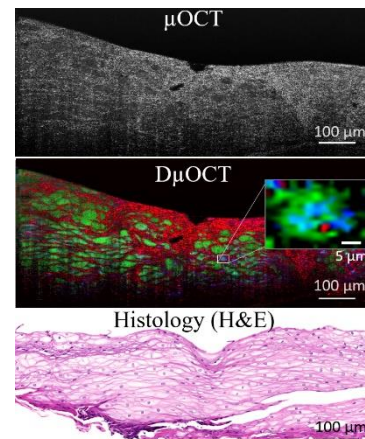


Fig 4. Comparison of  $\mu\text{OCT}$ ,  $\text{D}\mu\text{OCT}$ , and histology image of an esophageal biopsy. By detecting differences in intracellular motion within cells,  $\text{D}\mu\text{OCT}$  drastically enhances cellular contrast and enables visualization of intracellular contents in metabolically viable whole tissues. cytoplasm, nucleus, and perinuclear material appear as green, red, and blue respectively in the  $\text{D}\mu\text{OCT}$  image. The level of detail enabled by  $\text{D}\mu\text{OCT}$  is comparable to histological images.



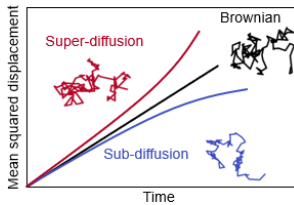


Fig 5. Biological activity in a cell dictates if intracellular motion occurs as super-diffusion, sub-diffusion, or Brownian motion.

we hypothesize that different cell types possess distinctive intracellular dynamics. Organelles in cells act as light scatterers, and when they undergo active diffusion, they impart signal fluctuations in OCT images. The ability to detect small displacements from a small ensemble of moving entities is highly desirable in D $\mu$ OCT, and the limit of detection is governed by the optical resolution. We have previously leveraged the high resolution of  $\mu$ OCT for high sensitivity optical measurements of intrinsic intracellular dynamics of whole tissues. We demonstrated that D $\mu$ OCT generates a tremendous amount of image contrast that is otherwise not achievable with conventional  $\mu$ OCT images (fig. 4), and it differentiates various cell types in the tissues.<sup>20,26</sup> However, how differences in intracellular motion is

linked to specific cell types is still unclear and will be addressed in this proposal. We aim to determine the distinctive signatures of intracellular dynamics of airway cell types, thereby enabling discrimination of cell types without having to extract and stain tissues. This advanced form of D $\mu$ OCT enable the identification of cell types that the drug compounds have been delivered to via co-localized fluorescence imaging in Cre reporter mouse models.

#### 4. OUTLINE OF TASKS / WORK PLAN

While the PI has extensive experience in building CFM and  $\mu$ OCT for airway studies, the development of D $\mu$ OCT for reliably identifying airway cell types is in its relatively early stages. Therefore, year 1 will be spent on improving multiple aspects of the D $\mu$ OCT technology to increase accuracy in distinguishing airway cell types. The same hardware for performing D $\mu$ OCT will be used for  $\mu$ OCT imaging of the airway physiology. In year 2, we will integrate CFM imaging capabilities into the D $\mu$ OCT/ $\mu$ OCT system and test investigational CF genetic therapeutics on Cre reporter cell models.

##### 4.1 Improve cell discriminating power by optimizing sampling frequency and imaging time of D $\mu$ OCT

Under active diffusion, intracellular entities exhibit trajectories that consist of a range of step sizes (Fig. 5), implying that the scatterers would diffuse in and out of the optical focus over a range of frequencies, creating signal fluctuations with finite bandwidth. The Nyquist–Shannon sampling theorem governs the necessary optical sampling rate and time required to capture the fluctuating signals accurately. Furthermore, the combined considerations of the optical focus size and MSD of the biological entities determine the suitable length of imaging time. In view of this, we will test a range of optical sampling rates, from a few Hz to kHz, and imaging times on human bronchial epithelial (HBE) cell cultures to determine the optimal parameters needed to distinguish airway epithelial cells. To cover the broad range of sampling rates, we will either adjust the scan rates of galvo mirrors (up to  $\sim$  100 Hz) or perform temporal gating with the  $\mu$ OCT detector (up to a few tens of kHz). Based on Nyquist's theorem, the highest fluctuation frequency that can be captured is half of the sampling rate, fs. If the sampling rate for D $\mu$ OCT is lower than what is required to detect fast diffusive motions that occur at smaller time scales, aliasing errors will negatively impact our ability to differentiate different motion patterns present in cells. To probe fluctuations at frequencies higher than what could be supported by galvo scanning, we will make use of the high line rates of our  $\mu$ OCT detector to temporally gate the data acquisition in the kHz range. In this method, the beam would not scan back and forth repeatedly. Instead, the beam would traverse across the sample in a stepwise fashion, stopping at equally spaced positions where multiple  $\mu$ OCT A-lines were recorded at the kHz line rate of the detector. While fs determines the highest fluctuation frequencies that D $\mu$ OCT is sensitive to, the inverse of  $\Delta T$  determines the spectral resolution and hence the lowest frequency that D $\mu$ OCT can detect. Although higher imaging times would allow the detection of low-frequency fluctuations, it has to stay within a period such that the MSD of organelles does not exceed the spatial dimension defined by the optical focus.

We will perform the D $\mu$ OCT studies on HBE cell cultures before advancing to tracheas excised from healthy and CF murine models.<sup>27</sup> All samples will be placed on DMEM-infused surfaces to maintain their viability during the imaging experiments. To validate D $\mu$ OCT, we will precisely mark the exact areas where D $\mu$ OCT was performed and compare the D $\mu$ OCT images against histology of the same regions (gold standard). Subsequently, histology will be performed on the tissues using H&E, AB-PAS stains, and immunohistochemistry. Cell markers to identify ciliated cells (Foxj1), basal cells (KRT5), and secretory cells (SCGB1A1) will be used to determine cell type distribution.

4.2 Develop phase-sensitive D $\mu$ OCT Without phase information, fluctuations in the brightness of  $\mu$ OCT images are generated by optical scatterers that have been displaced in and out of the optical focus. Therefore, motions smaller than the size of the optical focus will not be discernible with the current form of D $\mu$ OCT. We hypothesize that being sensitive to displacements below 1 $\mu$ m would improve our ability to analyze a broader range of organelle motions to better distinguish cells. Motivated by this need to detect nanometer-scale displacements (< focus size), we propose to include phase information in the  $\mu$ OCT interference patterns in our D $\mu$ OCT processing algorithms to implement phase-sensitive D $\mu$ OCT. In phase-sensitive methods, the smallest displacement that can be detected,  $\Delta z$ , is governed proportional to the minimal detectable phase change (i.e.,  $\Delta z = \Delta\phi/(4\pi n)$ )<sup>28</sup>, which is determined by the phase stability of the light source. With the performance of our current supercontinuum light source, we estimate that phase-sensitive methods would enable displacements as small as a few nanometers (<10 nm) to be detected. We note that although it is possible to increase the numerical aperture and, thus, decrease the focused spot size of the objective lens in the  $\mu$ OCT optical system, this approach will severely decrease the depth of field and limit our ability to image deep into the tissue. Therefore, the utilization of phase-sensitive methods is more advantageous.

4.3 Build a D $\mu$ OCT/ $\mu$ OCT/CFM multimodal imaging system Having optimized D $\mu$ OCT for distinguishing airway cell types, we will integrate CFM capabilities into the D $\mu$ OCT/ $\mu$ OCT hardware. This part of the proposal highly leverages a separate project in the lab, considerably reducing budgetary constraints. The CFM system will be optimized for delivering and collecting light in the wavelength ranges that coincide with the excitation and emission spectra of tdTomato (Ex/Em 561/581nm) and GFP (Ex/Em 488/510nm), fluorophores commonly used as CFTR mRNA-reporters. The confocal pinhole and NA of the objective lens will be designed to produce a lateral and axial resolution of approximately 3  $\mu$ m in 488-561nm excitation wavelengths. The high resolutions enable the delineation of fluorescence signals arising from individual cells treated with mRNA therapeutics. The excitation path of the CFM will be directed through the same optics as the  $\mu$ OCT system to facilitate co-localized imaging between the two modalities. A piezo-controlled stage will be used to translate the sample along the optical axis when performing CFM at multiple planes. Cross-sectional fluorescence images will then be generated to be co-registered with  $\mu$ OCT and D $\mu$ OCT images.

4.4 Characterize delivery of mRNA treatment to different cell types in airway epithelium and correlate functional delivery of therapeutics with performance metrics of the mucociliary transport system After the multimodal imaging system is fabricated, we will perform biological studies involving mRNA treatments applied to Cre-reporter cell and/or murine models. Our system will be used to determine the kinetics of drug delivery through mucus barriers. We will perform *ex vivo* studies and monitor the time from the application of nebulized drugs to the time fluorescence signals were observed in the cells.  $\mu$ OCT will also be used to assess the baseline, pre-treatment airway physiological status of the sample by quantifying cilia beat frequency, percentage of epithelial area with ciliated cells, mucociliary transport rate, and thicknesses of the airway mucus layer. In the same areas, the make up of cell populations before treatment will be determined by using D $\mu$ OCT. After establishing baseline measurements, cells will be treated. We will then use the system to sequentially perform D $\mu$ OCT,  $\mu$ OCT, and CFM to determine what cell types the investigational mRNA drug reached and what is the resultant impact on the airway physiological function. For longer terms studies aimed at understanding the efficacy of mRNA drugs in restoring healthy physiology in the injured epithelium, we will apply multi-dose treatments to healthy control animals and animals with advanced CF symptoms. After a course of treatment, the animals will be sacrificed, and their trachea excised for imaging experiments. By performing D $\mu$ OCT,  $\mu$ OCT, and CFM on samples from both groups, we will compare the differences in cell populations and airway physiology of both groups. The results will allow us to determine if the treatment brings about changes to the cell population and if that change correlates to a positive impact on the restoration of airway physiology in such cases.

## **5. POTENTIAL OUTCOMES AND IMPACT**

5.1 Facilitates screening of investigational genetic treatments Genetic treatments are gaining traction quickly in the CF field and beyond. There is a need to reliably screen and identify promising drugs before going into costly clinical trials. Moreover, improvements in a patient's clinical outcome, such as a reduction in pulmonary exacerbations and normalization of mucociliary clearance, are of most concern to physicians. It goes beyond simply determining if an investigational therapeutic can correct

the underlying gene mutation in cells. The proposed multimodal imaging tool provides valuable information about the drug's impact on physiological function, which cannot be obtained with the use of destructive, terminal measurements such as cell cytometry and single-cell sequencing.

**5.2 Gaining mechanistic insights into investigational genetic therapeutics for CF** Multiple aspects of a drug needs to be optimized to ensure high treatment efficacies in realistic clinical settings. The proposed multimodal imaging platform provides a wealth of information that potentially enables researchers to gain mechanistic insights into why certain investigational therapeutics work or not. Our imaging platform allows investigators to determine functional delivery of drugs across mucus barrier, characterize drug uptake by various cell types, and enable monitoring of long-term treatment effects on epithelial remodeling and restoration of healthy airway physiology. Not only could these information guide optimization of drug compounds, they could also improve the relevance of pre-clinical studies by providing a more realistic assessment of the drug's clinical impact on patient health.

**5.3 Paves the way for label-free *in situ* mapping of a broader range of cell types** Histology is the gold standard in pathology. However, because it requires tissue excision and staining, an alternative label-free method for non-destructive optical biopsy has been widely sought after. By developing methods to improve D $\mu$ OCT's ability to identify cell types while increasing cellular contrast, we are setting the foundation for a type of optical biopsy that could reveal how various cell types are organized in whole tissues. It is compatible with longitudinal and physiological studies of living systems. Although this proposal is focused on developing methods to discriminate cell types specific to the respiratory system, the results of our work could potentially shed light on ways to generalize D $\mu$ OCT for cell phenotyping in other tissue types, thus benefiting people beyond the CF and pulmonary research community.

## REFERENCES

1. Jones, H. R., Robb, C. T., Perretti, M. & Rossi, A. G. *Semin. Immunol.* **28**, 137–145 (2016).
2. Rock, J. R. *et al. Proc. Natl. Acad. Sci. U. S. A.* **106**, 12771–12775 (2009).
3. Adam, D. *et al. J. Pathol.* **235**, 408–419 (2015).
4. Saint-Criq, V. & Gray, M. A. *Cell. Mol. Life Sci.* **74**, 93–115 (2017).
5. © 2021 Cystic Fibrosis Foundation. *2020 Annual Data Report. Cystic Fibrosis Foundation Patient Registry* (2021).
6. Cooney, A. L., McCray, P. B. & Sinn, P. L. *Genes (Basel)*. **9**, (2018).
7. Vaidyanathan, S. *et al. Cell Stem Cell* **26**, 161-171.e4 (2020).
8. Da Silva Sanchez, A., Paunovska, K., Cristian, A. & Dahlman, J. E. *Hum. Gene Ther.* **31**, 940–955 (2020).
9. Christopher Boyd, A. *et al. J. Cyst. Fibros.* **19**, S54–S59 (2020).
10. Kim, N., Duncan, G. A., Hanes, J. & Suk, J. S. *J. Control Release* **240**, 465–488 (2016).
11. Suk, J. S. *et al. Biomaterials* **30**, 2591–2597 (2009).
12. Li, S. *et al. Anim. Model. Exp. Med.* **1**, 29–35 (2018).
13. Montoro, D. T. *et al. Nature* **560**, 319 (2018).
14. Fernandez-Petty, C. M. *et al. JCI Insight* **4**, (2019).
15. Leung, H. M. *et al. Sci. Transl. Med.* **11**, eaav3505 (2019).
16. Liu, L. *et al. PLoS One* **8**, e54473 (2013).
17. Chivukula, R. R. *et al. Nat. Med.* **26**, 244–251 (2020).
18. Leung, H. M. *et al. Biomed. Opt. Express* **11**, 2768–2778 (2020).
19. Leroux, C.-E., Bertillot, F., Thouvenin, O. & Boccarda, A.-C. *Biomed. Opt. Express* **7**, 4501 (2016).
20. Leung, H. M. *et al. Biomed. Opt. Express* **11**, 2768-2778 (2020).
21. Scholler, J. *et al. Biomed. Opt. Express* **10**, 731 (2019).
22. Weber, S. C., Spakowitz, A. J. & Theriot, J. A. *Proc. Natl. Acad. Sci.* **109**, 7338–7343 (2012).
23. Brangwynne, C. P., Koenderink, G. H., MacKintosh, F. C. & Weitz, D. A. *Trends Cell Biol.* **19**, 423–427 (2009).
24. Hacker, C. *et al. Nat. Commun.* **7**, 1–14 (2016).
25. Brangwynne, C. P., Koenderink, G. H., MacKintosh, F. C. & Weitz, D. A. *J. Cell Biol.* **183**, 583–587 (2008).
26. Oral Presentation. Applications of Dynamic Micro-Optical Coherence Tomography (D $\mu$ OCT). *SPIE Photonics West, San Fr. CA, USA* (2021).
27. Birket, S. E. *et al. Am. J. Respir. Crit. Care Med.* **202**, 1271–1282 (2020).
28. Larin, K. V & Sampson, D. D. *Biomed. Opt. Express* **8**, 1172–1202 (2017).

## Executive Summary

**Name of the proposal:** Mechanistic insight of ultrasound neuromodulation unveiled by local optoacoustic stimulation and super-resolved voltage imaging

**Category:** Health

Ultrasound neuromodulation is a next-generation technique for neural stimulation, but its real-world application such as the treatment of neurological disorders has been challenging due to the fundamental technical limitations and controversies on the molecular mechanism. Specifically, there is a critical need for improving the spatial resolution of the ultrasound neuromodulation and precision measurement of the ultrasound effects at the sub-cellular level.

The objective of the proposed study is to develop a panel of novel technologies to overcome these challenges in both stimulation and imaging. The specific aims are:

**Aim 1.** Demonstrate neuromodulation and membrane potential imaging with single-cell resolution.

**Aim 2.** Examine the mechanism of neuromodulation at the single-cell level.

By completing the proposed aims, we expect to develop a high-precision neuromodulation and membrane potential imaging platform and establish a systematic mechanism of the spatiotemporal profiles of ultrasound neuromodulation. Technically, we will develop an optoacoustic-based ultrasound stimulation device with sub-micron spatial resolution, which is capable of stimulating neurons at the single-cell level without any genetic modification. We will also develop a molecular fingerprint-based imaging system, namely stimulated Raman scattering voltage imaging, which allows quantitative mapping of membrane voltage at sub-cellular levels. With these technical innovations, we expect such a multi-modality platform will allow us to tackle the fundamental challenge in the ultrasound neuromodulation technique by providing a comprehensive mechanism. The new insight will be the *foundation for designing the next-generation neuromodulation device* for disease-specific applications in the clinical setting.

# Mechanistic insight of ultrasound neuromodulation unveiled by local optoacoustic stimulation and super-resolved voltage imaging

## Literature Review

Ultrasound neuromodulation is a promising technique for non-invasive neural stimulation. The capability to modulate nerves and muscles using high frequency ultrasound was demonstrated in 1920s [1]. More recently, the potential for treating various brain diseases has been demonstrated in preclinical models [2,3] and a few clinical studies [4-6]. Despite the long history, clinical translation is still difficult mainly because the specific mechanism of neural stimulation and inhibition remains unclear.

Mechanistically, direct neural stimulation by ultrasound has been observed in several *in vitro* studies [7]. Although it is generally believed that ultrasound can modulate neural networks through neural network integration [8], it is difficult to determine if the ultrasound effect is direct modulation of the membrane voltage or an indirect stimulation via synaptic or network pathways. Controversially, recent studies showed that ultrasound could activate the auditory system that subsequently generates brain-wide spread of neurostimulation [9,10], contradicting the *in vitro* studies where auditory activation is absent. Frequency-dependent effects of ultrasound neurostimulation on peripheral nerves and brain cells [11-13] could not be explained by these observations either. Other proposed mechanisms of ultrasound neuromodulation include the production of heat and tissue cavitation, transmembrane sonoporation, and activation of mechanosensitive channels [14, 15]. Among them, there is multiple evidence indicating sonoporation and mechanosensitive channels as the two main contributing factors. Several simulation and modeling studies have shown that the positive and negative pressures exerted by ultrasound on cells change membrane fluidity and lead to expansions and contraction of the lipid bilayer [16, 17]. This can cause membrane pore formation and ion exchange, which can lead to the accumulation of charge throughout tens of milliseconds until an action potential threshold is reached. Furthermore, the propagation of the mechanical waves can also cause the activation of mechanosensitive channels [14, 18], which leads to membrane depolarization, and subsequently, neuron activation.

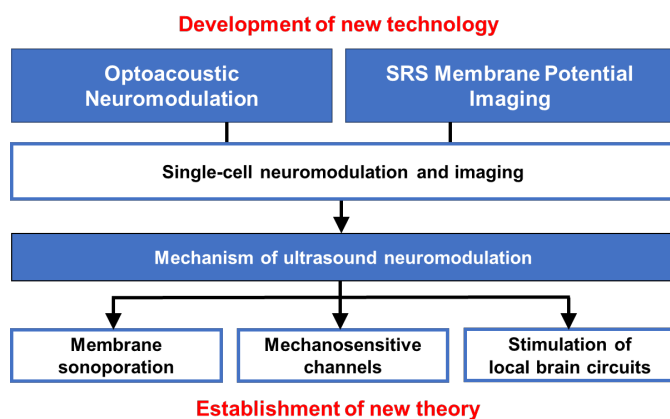
## Problem Statement/Objective

The challenges to studying the ultrasound neuromodulation effects, and thus promoting the clinical transformation of the technology, mainly come from a lack of techniques for a single-cell level ultrasound-mediated stimulation and quantitative subcellular mapping of transmembrane potential.

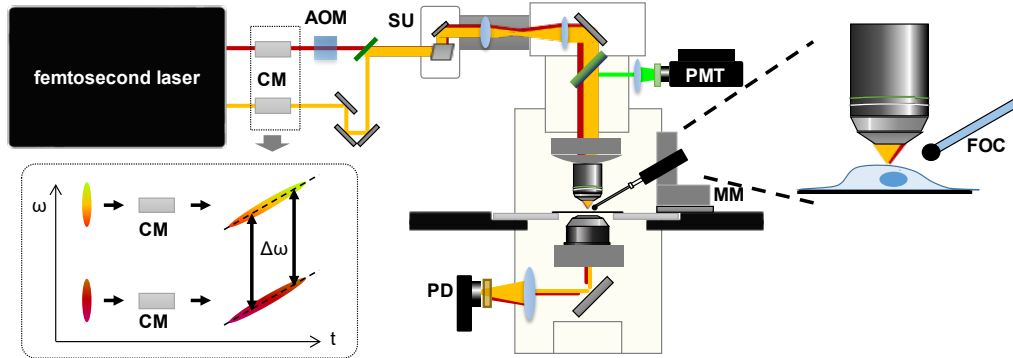
The objective of the proposed study is to **develop a panel of novel technologies to overcome these challenges** in both stimulation and imaging. On the stimulation side, a fiber optoacoustic converter (FOC) technique will be developed as a miniature ultrasound emitter, which can be positioned in the brain directly to allow unprecedented sub-millimeter spatial precision ultrasound neuromodulation without any genetic modifications. On the imaging side, a label-free stimulated Raman scattering (SRS) membrane imaging technique will be developed for quantitative mapping of membrane biophysical properties with subcellular resolution.

## Outline of tasks/Work Plan

Previously, our team designed and built a miniaturized ultrasound emitter, called FOC, based on the optoacoustic (OA) phenomenon. We also have developed a label-free SRS imaging method for mapping neuronal membrane potential at a subcellular level. The results from the preliminary studies have been published in *Nature Communications* [19] and *Journal of Physical Chemistry Letters* [20]. With these technological innovations as the foundations, we designed and planned the following work plan with two aims: **Aim 1. Demonstrate neuromodulation and membrane potential imaging with single-cell resolution; Aim 2. Examine the mechanism of neuromodulation at the single-cell level.**



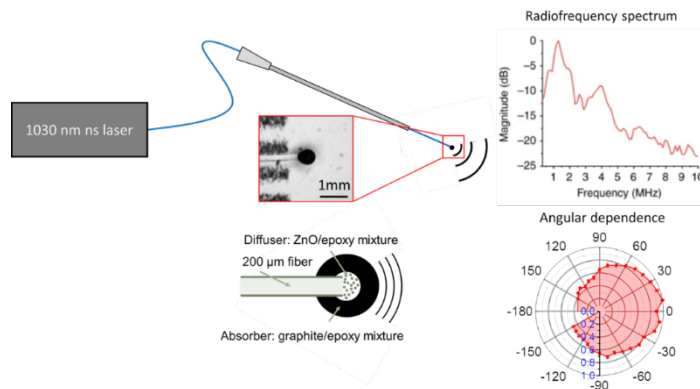
**Aim 1. Demonstrate neuromodulation and membrane potential imaging with single-cell resolution.** We will develop a FOC-mSRS system, where submillimeter neuromodulation is achieved by FOC and submicron membrane potential imaging is achieved by multi-modality stimulated Raman scattering (mSRS) voltage imaging (**Fig. 1**). The spatial resolution of neuromodulation by FOC will be validated by two-photon fluorescence  $\text{Ca}^{2+}$  imaging and SRS membrane potential imaging from the same mSRS microscope.



**Figure 1.** mSRS microscope integrated with FOC-based ultrasound emitter.

### 1.1: Build a FOC-mSRS system for OA neuromodulation and SRS voltage imaging.

FOC for micron-level ultrasound neuromodulation: The miniaturized FOC is a fiber-based ultrasound emitter with a nanocomposite coating at the distal end and has an overall diameter of  $\sim 400 \mu\text{m}$ . The nanocomposite contains two layers: an inner light-diffusing layer and an outer light-absorbing layer. The laser pulses ( $1030 \text{ nm}$ ,  $\sim 10 \text{ mJ}$ ,  $5\text{-ns}$  laser) delivered to the optical fiber are diffused by the light-diffusing layer, which consists of  $100 \text{ nm}$  diameter zinc oxide nanoparticles and epoxy (**Fig. 2**). The light-absorbing layer, a mixture of graphite and epoxy, absorbs the laser energy. Then, the light-absorbing layer converts the laser energy into heat, generating a local transient temperature increase, which is followed by a local pressure rise through thermoelastic expansion. The pressure travels in the form of ultrasonic waves, generating  $0.2\text{-}5 \text{ MHz}$  frequency ultrasound (center frequency  $\sim 2 \text{ MHz}$ ).



**Figure 2.** FOC for a localized ultrasound of micron-level spatial resolution. Adopted from [19].

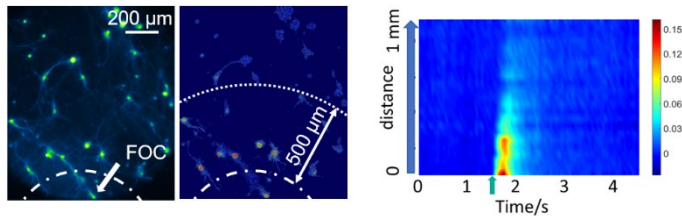
SRS for subcellular membrane voltage imaging: The SRS microscope is built following previous studies [20]. Previously, the spectroscopic signature of neuronal membrane potential was identified through hyperspectral SRS imaging of a single mammalian neuron under somatic voltage-clamp control. Because C-H bonds are the most abundant functional groups in cells, the high wavenumber C-H stretching region between  $2800 - 3000 \text{ cm}^{-1}$  was selected. We observed a significant decrease at  $2930 \text{ cm}^{-1}$ , mainly contributed by protein when the neuron is depolarized and established a correlation between SRS intensity at  $2930 \text{ cm}^{-1}$  and membrane potential, identifying the SRS peak at  $2930 \text{ cm}^{-1}$  as a vibrational signature of neuronal membrane potential.

### Preliminary studies

Using the OA effect, we have successfully demonstrated neuromodulation in cultured neurons *in vitro*

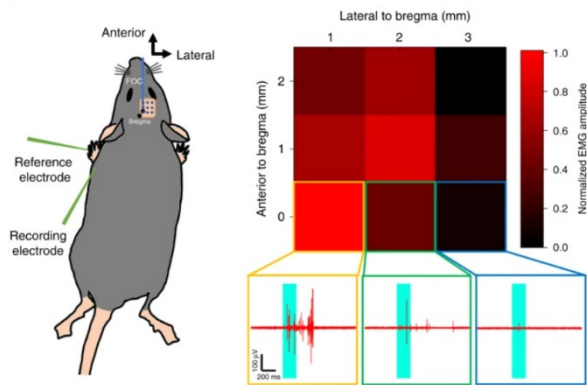


and mouse brains *in vivo*. By integrating FOC with fluorescence microscopy, we performed  $\text{Ca}^{2+}$  imaging in mouse primary cortical neurons under OA stimulation. With 200-ms OA stimulation, only the neurons within 500  $\mu\text{m}$  from FOC showed  $\text{Ca}^{2+}$  responses (Fig. 2), demonstrating unprecedented spatial resolution of ultrasound stimulation.



**Figure 2.** Spatially-confined stimulation by FOC. Adopted from [19].

To test whether FOC stimulation has a functional outcome, we placed the FOC on the motor cortex of the mouse brain and measured the changes in muscle responses by inserting EMG electrodes into the triceps of the mouse forelimb. We mapped the distribution of forelimb muscle responses in  $3 \times 3 \text{ mm}^2$  areas at 1-mm spacing in the mouse motor cortex, showing that stimulating different regions within the motor cortex elicits various muscle responses (Fig. 3). These preliminary data demonstrate the feasibility of using FOC as a miniaturized ultrasound source to locally modulate the neural activity.

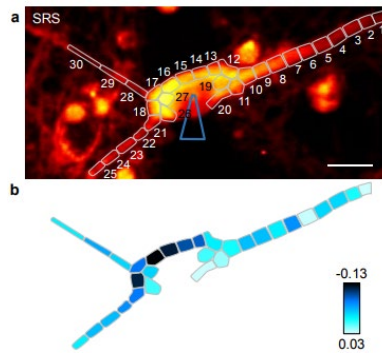


**Figure 3.** Modulation of motor activity by OA stimulation. Adopted from [19].

To demonstrate the capability of imaging membrane potential with subcellular resolution, we performed SRS imaging of a whole neuron during voltage clamping (Fig. 4). The SRS mapping shows a clear drop in the regions near the micropipette but smaller or no change in the regions further away from the micropipette, which provides visual evidence of the lack of space-clamp. Importantly, the sensitivity of this imaging technique allows us to image not only action potential but also threshold potential. Collectively, these data show the feasibility of detecting membrane potential based on the SRS spectral profile.

**1.2: Validate spatial resolution of neuromodulation by  $\text{Ca}^{2+}$  imaging and SRS imaging of cultured neurons.** We will perform  $\text{Ca}^{2+}$  imaging on cultured primary neurons to depict the spatial resolution of ultrasound stimulation by FOC. Ultrasound stimulation will be delivered with FOC, driven with lasers as described in preliminary results. FOC will be placed above GCaMP6-expressing neurons. The FOC will be pulsed at a variable repetition frequency (1.4 kHz) and pulse energy of 5  $\mu\text{J}$ . Each recording will consist of 5 s of baseline, 2 s of stimulation, and 12 s of post-stimulation periods. The membrane potential change upon FOC-induced ultrasound stimulation will be mapped by SRS membrane imaging. The laser beating frequency will be tuned to be resonant with  $\text{CH}_3$  vibration at  $2930 \text{ cm}^{-1}$ .

**Aim 2. Examine the mechanism of neuromodulation at the single-cell level.** We hypothesize that ultrasound induces transient membrane sonoporation and activation of mechanosensitive channels, which accumulatively lead to membrane depolarization and subsequently activates voltage-gated sodium channels to fire action potentials. To test this hypothesis, we will perform high spatial resolution mapping of ultrasound-induced change of membrane voltage across an entire neuron using SRS



**Figure 4.** Subcellular mapping of membrane potential in a mammalian neuron using SRS imaging. Adopted from [20].

microscopy. We will examine the impact of ultrasound on plasma membrane permeability. In parallel, the contribution of mechanosensitive channels and voltage-sensitive sodium channels in neuromodulation will be assessed by pharmacological inhibition of channel activity. The ultrasound-induced stimulation of the local brain circuit will be mapped by *in vivo* imaging.

**2.1: Examine the involvement of membrane deformation in ultrasound neuromodulation.** We hypothesize that acoustic waves from FOC induce membrane sonoporation, which makes the membrane permeable. To investigate this effect, we will measure the permeability of the plasma membrane by imaging propidium iodide influx or calcein efflux in neuron cultures upon ultrasound stimulation using FOC. The level of propidium iodide influx versus the intensity and duration of ultrasound stimulation will be compared. The membrane permeability will be plotted as a function of the intensity or duration of ultrasound stimulation. Calcein efflux will be used to monitor the membrane permeability to characterize the kinetics of this effect. Membrane fluidity will be assessed using the Membrane fluidity kit (ab189819), which allows quantitative real-time monitoring of membrane fluidity by ratio imaging of monomer to excimer fluorescence. We expect that membrane permeability will increase as the amplitude and duration of ultrasound stimulation increase, which will saturate at certain intensity. The membrane fluidity is expected to increase, which mediates membrane sonoporation upon ultrasound stimulation.

**2.2: Map the subcellular spatial distribution of threshold and action potential in ultrasound-stimulated neurons by SRS imaging.** We hypothesize that membrane sonoporation induced by ultrasound stimulation depolarizes neurons to reach threshold potential, which initiates firing at the axon hillock. To test this hypothesis, we will perform subcellular resolution SRS membrane potential mapping of neuron cultures simultaneously with ultrasound stimulation by FOC. We expect that immediately after the ultrasound stimulation, the membrane in soma will reach threshold potential, followed by axon hillock reaching action potential, leading to full activation of the neuron by showing the firings in the neurites.

Depolarization of membrane by ultrasound stimulation will consequently activate voltage-gated ion channels, which are essential for full activation of neuronal activity. Axon hillock is known to have a high concentration of voltage-gated sodium channels that are activated by the summation of sub-threshold potentials from soma. To study the potential role of voltage-gated sodium channels in the stimulation process by ultrasound, we will use loss of function pharmacological blockers of voltage-gated sodium channels, such as tetrodotoxin, and measure changes in membrane potential of ultrasound stimulation by SRS imaging. We expect that upon ultrasound stimulation, neurons are fully activated, showing a great decrease in the SRS signal intensity at  $2930\text{ cm}^{-1}$ . When voltage-gated sodium channels are blocked, ultrasound stimulation is expected to produce only sub-threshold potential in neurons, showing less decrease in the SRS signal intensity.

**2.3: Examine the involvement of mechanosensitive channels in ultrasound neuromodulation.** To investigate how mechanosensitive ion channels contribute to ultrasound neural modulation, we will use specific ion channel blockers to selectively inhibit the activity of different channels. ML 204 is a specific blocker of *trpc4*, and the activities of PIEZO channels are blocked by GsMTx-4. Sipatrigine, a neuroprotective drug blocks both TREK and TRAAK channels, while another drug, Chlorpromazine, will be used to block only TREK channels. To test for the contribution of channel activation, we will

integrate FOC and SRS voltage imaging with pharmacological inhibitions of specific mechanosensitive ion channel activity. To investigate the effect of membrane displacement upon channel activation, ultrasound intensity will be driven to 50, 200 and 750 mW/cm<sup>2</sup> by adjusting the optical power produced by the fiber laser.

**2.4: Map the spatial profile of ultrasound effects by stimulating the local brain circuit with FOC and *in vivo* Ca<sup>2+</sup> imaging.** Our working hypothesis is that localized ultrasound stimulation with FOC can activate neurons with high spatial precision, produce a distinct effect on cells at varying distances from the FOC, and influence behavior. To test this hypothesis, we will use FOC-mSRS system to perform *in vivo* Ca<sup>2+</sup> imaging. The FOC ultrasound effects on individual neurons will be plotted over their physical distance to the tip of the FOC fiber. We will calculate the latency and the amplitude of FOC-triggered Ca<sup>2+</sup> changes, and compare neural stimulation effects over distance to FOC.

**Statistical methods:** Repeated measurements will be represented as mean value ± SD. Statistical analysis will be performed with OriginPro or Matlab. Differences between individual groups will be analyzed by Mann-Whitney U test (which does not require the assumption of normal distributions).  $p < 0.05$  will be considered statistically significant.

**Potential pitfalls and alternatives:** One concern in membrane potential imaging is the weak SRS signal level when performing high-speed imaging. To address this challenge, we will apply dual-SRS balanced detection scheme [20]. In this imaging scheme, a small portion of the excitation lasers will be used to generate a reference SRS signal with a standard sample to monitor the stochastic noise of the system. We have shown that the overall standard deviation of the SRS signal trace can be improved from 2% to less than 0.5% of the average SRS intensity using this approach [20].

### **Outcome(s) and Impact**

Upon the completion of this study, we will deliver high-resolution imaging and modulation techniques for neuroscience research, and identify the causal role of membrane pore formation and mechanosensitive channels in contributing to the effects of neural modulation. The new insight will build a new foundation for the rational design of ultrasound neuro-stimulators and basic neuroscience research as well as the treatment of neurological disorders.

### **References:**

1. Harvey EN. Am J Physiol.91:284-90. (1929)
2. Yang Y, et al. Brain Stimulat. 14:790–800. (2021)
3. Li G, et al. IEEE Trans Biomed Eng. 66:217–224. (2018)
4. Elias W J, et al. N Engl J Med. 369(7):640-648. (2013)
5. Elias W J, et al. N Engl J Med. 375(8):730-9. (2016)
6. Legon W, et al. Nat Neurosci.17:322-9. (2014)
7. Baek H, Pahk K, and Kim H. Biomed Eng Lett. 7:135–142. (2017)
8. King RL, Brown JR, Newsome WT, Pauly KB. Ultrasound Med Biol.39:312-31. (2013)
9. Sato T, Shapiro MG, Tsao DY. Neuron.98;1031-1041.e5. (2018)
10. Guo H, et al. Neuron. 98;1020-1030.e4. (2018)
11. Tufail Y, et al. Neuron.66:681-94. (2010)
12. Tufail Y, Yoshihiro A, Pati S, Li MM, Tyler WJ. Nat Protoc. 6:1453-70. (2011)
13. Ye PP, Brown JR, Pauly KB. Ultrasound Med Biol. 42:1512-30. (2016)
14. Kubanek J, Shi J, Marsh J, Chen D, Deng C, Cui J. Sci Rep. 6:srep24170. (2016)
15. Fini M, Tyler WJ. Int Rev Psychiatry. 29:168-77. (2017)
16. Krasovitski B, Frenkel V, Shoham S, Kimmel E. Proc Natl Acad Sci U S A. 108:3258-63. (2011)
17. Plaksin M, Kimmel E, Shoham S. eNeuro. 3:ENEURO. 0136-15.2016. (2016)
18. Ibsen S, Tong A, Schutt C, Esener S, Chalasani SH. Nat Commun. 6:8264. (2015)
19. Jiang Y, Lee HJ, Lan L, Tseng H-A, Yang C, Man H, Han X, Cheng J-X. Nat Commun. 11:881. (2020)
20. Lee HJ, et al. J Phy Chem Lett. 2017;8:1932-36. (2017)

## **EXECUTIVE SUMMARY**

### **Design and fabrication of a fiber optic accelerometer based on surface plasmon resonance for environmental monitoring**

Accelerometers have several uses in the science and engineering fields. Fiber-based accelerometers largely employ various schemes based on Fiber Bragg grating (FBG) with cantilever beam structure, diaphragm or spring-mass structures. The main purpose of environmental monitoring is to manage the environment and minimize adverse impacts on it. To achieve this, effective environmental monitoring tools are needed. Photonic crystal fibers (PCFs) are a new class of optical fibers that allow their structural parameters and geometries to be tuned to realize tailored designs and properties [1]. Sensors based on PCFs are light in weight, very small in size, and immune to electromagnetic interference. In recent decades, the surface plasmon resonance (SPR) sensing technique has attracted tremendous research attention due to its real-time monitoring capabilities and high sensitivity [2]. SPR in PCF is currently well developed to achieve highly sensitive and robust sensors with high resolutions [5], [6], [7] for measuring parameters such as refractive indexes [8], temperature [9], and pressure. The response of the SPR in PCF can be controlled and improved through the variation of the geometrical structure and selective filling of the fiber cladding with plasmonic nanostructures such as nanowires, nanorods [10], etc.

The sensitivity and resolution levels of current accelerometers are not enough for several environmental monitoring applications. However, SPR in PCF technology can be applied to achieve higher accelerometer performance. Therefore, the main objective of this research is to design and fabricate a highly sensitive plasmonic fiber accelerometer based on surface plasmon resonance for environmental monitoring. The design methodology to be adopted in this research is based on the finite element method (FEM), which is well implemented in the Comsol Multiphysics® software. The plasmonic accelerometer will be fabricated via the stack-and-draw technology. The coating or infiltration of plasmonic materials will be accomplished by the plasma-enhanced chemical vapor deposition (PECVD) process using facilities at the University of Cambridge, UK.

The proposed plasmonic fiber optic accelerometer based on surface plasmon resonance is expected to be highly sensitive, compact, and low-cost. It can be integrated into existing environmental monitoring systems for acquiring seismic data and predicting hurricanes, volcanic eruptions, wind, and so on. It is also expected that the new plasmonic accelerometer will improve the efficiency of a wide variety of smart devices and equipment, including electronics, automobiles, robots, prosthetics, and so on.

# **Design and fabrication of a fiber optic accelerometer based on surface plasmon resonance for environmental monitoring**

## **1. Introduction**

Accelerometers belong to a category of sensors that measure proper acceleration, which is the rate of change of a body's velocity in its instantaneous rest frame. Accelerometers have several uses in the science and engineering fields. Several types of accelerometers exist, such as laser accelerometers, micromachined microelectromechanical systems (MEMS) accelerometers, piezoelectric, capacitive, and optical fiber accelerometers, and so on. Fiber-based accelerometers largely employ various schemes based on Fiber Bragg grating (FBG) with cantilever beam structure, diaphragm or spring-mass structures. Environmental monitoring identifies the processes and actions that are required to take place to characterize and manage the quality of the environment. Environmental monitoring is conducted during the development of environmental impact assessments as well as in many situations in which human activities pose a risk of detrimental impacts on the natural environment. The main purpose of environmental monitoring is to manage the environment and minimize adverse impacts on it. Effective environmental monitoring tools are needed to ensure national, regional, and global compliance with environmental laws and regulations.

## **2. Literature review**

Photonic crystal fibers (PCFs) are a new class of optical fibers that allow their structural parameters and geometries to be tuned to realize tailored designs and properties [1]. The PCF is typically made of fused quartz as the background material, with periodic array of tiny holes extending along the entire fiber length. Sensors based on PCFs are light in weight, very small in size, and immune to electromagnetic interference.

In recent decades, the surface plasmon resonance (SPR) sensing technique has attracted tremendous research attention due to its real-time monitoring capabilities and high sensitivity [2]. SPR occurs by the stimulation of surface electrons at metallic and dielectric interfaces when the frequency of incident light resonates with the frequency of the surface electrons, resulting in the generation of non-radiative surface waves known as surface plasmon polaritons (SPPs) [3], which are very sensitive to changes in surrounding conditions [4]. SPR in PCF has been well developed to achieve highly sensitive and robust

sensors with high resolutions [5], [6], [7] for measuring refractive indexes [8], temperature [9], pressure, and so on. The response of the SPR in PCF can be controlled and improved through the variation of the geometrical structure and selective filling of the fiber cladding with plasmonic nanostructures such as nanowires, nanorods [10], etc.

### **3. Problem Statement**

Accelerometers for environmental monitoring applications need to be highly sensitive and precise. For instance, some measurements of environmental changes, such as seismic waves, have low amplitude and low frequency [11], [12]. However, the sensitivity and resolution of current accelerometers are not enough for such applications [11]. Surface plasmon resonance detection is highly sensitive to environmental changes and is already successful in liquid and gas sensing applications. However, its deployment for acceleration measurement has not been well explored.

### **4. Objectives of the research**

The main objective of this research is to design and fabricate a plasmonic fiber accelerometer based on surface plasmon resonance for environmental monitoring. The specific objectives are:

- i.* To design a plasmonic fiber accelerometer based on the principles of surface plasmon resonance.
- ii.* To fabricate the designed plasmonic fiber accelerometer.

### **5. Methodology**

The methodology to be adopted in this research is explained as follow:

**The finite element method (FEM):** The design and analysis of the plasmonic fiber accelerometer are based on the finite element method (FEM). The FEM will be used to analyse the propagation characteristics and indexes of the fiber and plasmonic modes. FEM applies the division of the PCF cross-section into homogenous subspaces of meshes within which Maxwell's equations can be solved using applicable boundary conditions. The Maxwell's equations are a set of partial differential equations that work together to provide a mathematical basis for electrical, magnetic and optical behavior in various media. The FEM is well-implemented in the Comsol Multiphysics® software. The software runs the finite element analysis together with adaptive meshing and error control using a variety of techniques. Hence, the FEM will be used to investigate the propagation characteristics and indexes of the fiber modes.



**Perfectly matched layers:** The PML, which is available in the Comsol Multiphysics® software is commonly used to truncate computational regions in numerical techniques when simulating problems based on propagating waves.

**Fabrication method:** The accelerometer will be fabricated via the stack-and-draw technology. The coating or infiltration of plasmonic materials will be accomplished by the plasma-enhanced chemical vapor deposition (PECVD) process. The fabrication facilities are available at our partner institution- the University of Cambridge, UK.

## 6. Outcome

The proposed plasmonic fiber optic accelerometer based on surface plasmon resonance is expected to be highly sensitive, compact, and low-cost. It can be integrated into existing environmental monitoring systems for acquiring seismic data and predicting hurricanes, volcanic eruptions, and wind.

### WORK PLAN

Date	Task	Comments
15/01/2023	Modelling, simulation and optimization of the accelerometer	Comsol Multiphysics®
25/02/2023	Analysis of simulations and computation of sensor metrics	
29/03/2023	Preliminary arrangements towards accelerometer fabrication	Travel to the fabrication facility
15/04/2023	Fabrication of the plasmonic fiber accelerometer.	The fabrication will be done at the University of Cambridge
10/08/2023	Testing	

## 7. Impact

It is expected the impact of this research will be beneficial to several activities, such as the measurement of vibration and acceleration in boreholes, pressurized wells, and rotating machinery. In addition, the new plasmonic accelerometer will improve the efficiency of a wide variety of smart devices and equipment, including electronics, automobiles, robots, prosthetics, video recorders, and so on.

## 8. Budget

The budget for completing the project is outlined as follows:

	<b>Budget item</b>	<b>Description</b>	<b>Amount</b>	<b>Sub-Total</b>
<b>1</b>	<b><i>Personnel related expenses</i></b>			
	Remuneration for Project Team		\$20,000	
	<b>Total expenses on personnel</b>			<b>\$20,000</b>
<b>2</b>	<b>Capital Asset/Equipment</b>			
	Computers for PI and Co-PI	4 HP ENVY Laptops 17” Printer, Internet Subscription, Routers and other computing accessories.	\$ 14,000	
	Comsol Multiphysics® 6.0 software license	Cost of simulation software license	\$4,000	
	OriginPro® 2022b software	Cost of graphical and data analysis software license	\$2,000	
	Fabrication of multiparameter sensor	Cost of components and fabrication	\$20,000	
	<b>Total Capital Asset/Equipment cost</b>			<b>\$40,000</b>
<b>3</b>	<b><i>Travel</i></b>			
	Transportation, accommodation, and meals)	Travelling and related cost for two investigators	\$30,000	<b>\$30,000</b>
	Overhead @ 10%			<b>\$10,000</b>
	<b>GRAND TOTAL</b>			<b>\$100,000</b>

## **PROJECT PERSONNEL**

1. Ing. Dr. Iddrisu Danlard – Sunyani Technical University
2. Dr. Owusu Nyarko-Boateng - University of Energy and Natural Resources
3. Ing. Professor Emmanuel Kofi Akowuah – Kwame Nkrumah University of Science and Technology
4. Dr. Prince Bawuah – University of Cambridge
5. Dr. Benjamin Asubam Weyori - University of Energy and Natural Resources

## References

---

- [1] D. F. Santos, A. Guerreiro, and J. M. Baptista, "New SPR PCF D-type optical fiber sensor configuration for refractive index measurement," *IEEE Sens. J.*, vol. 15, no. 10, p. 96346Z, 2015.
- [2] X. Yan, B. Li, T. Cheng, and S. Li, "Analysis of High Sensitivity Photonic Crystal Fiber Sensor Based on Surface Plasmon Resonance of Refractive Indexes of Liquids," *Sensors*, vol. 18, no. 9, p. 2922, Sep. 2018.
- [3] M. S. Islam *et al.*, "Dual-polarized highly sensitive plasmonic sensor in the visible to near-IR spectrum," *Opt. Express*, vol. 26, no. 23, p. 30347, 2018.
- [4] X. Chen *et al.*, "Near-infrared long-range surface plasmon resonance in a D-shaped honeycomb microstructured optical fiber coated with Au film," *Opt. Express*, vol. 29, no. 11, p. 16455, May 2021.
- [5] Z. Rahman, W. Hassan, T. Rahman, N. Sakib, and S. Mahmud, "Highly sensitive tetra-slotted gold-coated spiral plasmonic biosensor with a large detection range," *OSA Contin.*, vol. 3, no. 12, p. 3445, Dec. 2020.
- [6] Q. Xie *et al.*, "Characteristics of D-shaped photonic crystal fiber surface plasmon resonance sensors with different side-polished lengths," *Appl. Opt.*, vol. 56, no. 5, p. 1550, 2017.
- [7] R. Otupiri, E. K. Akowuah, and S. Haxha, "Multi-channel SPR biosensor based on PCF for multi-analyte sensing applications," *Opt. Express*, vol. 23, no. 12, p. 15716, Jun. 2015.
- [8] J. Wang *et al.*, "Surface plasmon resonance sensor based on coupling effects of dual photonic crystal fibers for low refractive indexes detection," *Results Phys.*, vol. 18, no. July, p. 103240, Sep. 2020.
- [9] H. Liu, C. Chen, H. Wang, and W. Zhang, "Simultaneous measurement of magnetic field and temperature based on surface plasmon resonance in twin-core photonic crystal fiber," *Optik (Stuttg.)*, vol. 203, p. 164007, 2020.
- [10] B. D. Gupta and R. Kant, "Recent advances in surface plasmon resonance based fiber optic chemical and biosensors utilizing bulk and nanostructures," *Opt. Laser Technol.*, vol. 101, pp. 144–161, 2018.
- [11] S. Abozyd, A. Toraya, and N. Gaber, "Design and Modeling of Fiber-Free Optical MEMS Accelerometer Enabling 3D Measurements," *Micromachines*, vol. 13, no. 3, 2022.
- [12] P. Lu *et al.*, "Distributed optical fiber sensing: Review and perspective," *Appl. Phys. Rev.*, vol. 6, no. 4, 2019.

# DNA-assembled quantum-dot spatial barcodes with imaging flow cytometry for hundreds of analytes in liquid biopsy

## Research challenge

More than a quarter of people worldwide will ultimately be affected by cancer<sup>1</sup>, and cancer treatments are often more successful when the disease is detected early<sup>2</sup>. The analysis of blood for circulating tumor cells (CTC) or cell-free nucleic acids called “liquid biopsy” has opened new avenues for cancer diagnostics, including early detection of tumors, improved risk assessment and staging, as well as early detection of relapse and monitoring of tumor evolution in the context of cancer therapies<sup>3</sup>. However, the common detection methods for liquid biopsy can only process a few analytes simultaneously at a low throughput, making it challenging to find the optimal panel of biomarkers according to different objectives (e.g., accurately identify different tumors) due to the low detection efficiency. A massively parallel detection, high-throughput, and easy-to-operate liquid biopsy modality providing precise measurements of hundreds of specific circulating biomarkers will be a tremendously enabling tool for the researchers and doctors to comprehensively analyze the cancer development and further effectively discover the right panels for various objectives. This is the research challenge we propose to undertake here.

## Proposed project

This proposal is to combine DNA-assembled quantum-dot spatial barcodes and imaging flow cytometry for simultaneous detection of hundreds of analytes in liquid biopsy. The proposal has three aims.

- 1) To construct DNA-assembled quantum-dot spatial barcodes (QD barcodes). Quantum dot beads of different colors are connected in a line via DNA strands, which will offer a huge number of individual signatures (e.g., 5 colors <sup>5</sup> spatial positions = 3125 signatures) that can be exclusively allocated to single circulating biomarkers.
- 2) To establish imaging flow cytometer platform for visualizing QD barcodes. The imaging flow cytometer is aiming to offer a throughput of 5000 biomarkers per second, five fluorescence channels, and a spatial resolution of 1 $\mu$ m. In theory, with the QD barcode of 4/5 colors and 5 positions, it can offer a parallel detection up to 1024/3125 analytes.
- 3) To decorate the QD barcode with proper adapters for different circulating biomarkers in blood, including ctDNAs, CTCs, proteins, RNAs. We will first utilize this platform for detecting DNA mutations of lung cancer. Also, magnetic microbeads can be connected to QD barcodes for magnetic purification and reporter probes should be developed to prevent false positive result.

## Intended outcomes

Corresponding to the three aims, the outcomes include a fabrication method of QD spatial barcodes, a demo system of imaging flow cytometer for QD barcode detection, a high throughput and massive parallel detection platform for DNA, RNA, and proteins. We will publish at least one paper in Optica open-access journals and share progress and results in Optica-organized symposiums. If successful, the proposed platform will show, for the first time, hundreds of circulating biomarkers (potentially to be thousands) can be detected in a single assay at the throughput up to thousands of biomarkers per second, offering high - quality and high-content data of liquid biopsy for the researchers and doctors to detect and monitor multiple cancers at all stages. This platform will not only be a reliable and efficient tool for cancer research and therapy, but also pave the way for the practical application of personalized medicine.

<sup>1</sup> Siegel, R. L., Miller, K. D. & Jemal, A. Cancer statistics, 2015. CA: A Cancer Journal for Clinicians vol. 65 5–29 (2015).

<sup>2</sup> Lennon, A. M., ... & Papadopoulos, N. (2020). Feasibility of blood testing combined with PET-CT to screen for cancer and guide intervention. Science, 369(6499), eabb9601.

<sup>3</sup> Alix-Panabières, C., & Pantel, K. (2021). Liquid biopsy: from discovery to clinical application. Cancer discovery, 11(4), 858-873.

## **DNA-assembled quantum-dot spatial barcodes with imaging flow cytometry for hundreds of analytes in liquid biopsy**

### **1. Literature Review**

More than a quarter of people worldwide will ultimately be affected by cancer<sup>1</sup>, and cancer treatments are often more successful when the disease is detected early<sup>2</sup>. The analysis of blood or other body liquids for circulating tumor cells (CTC) or cell-free nucleic acids called “liquid biopsy” has opened new avenues for cancer diagnostics, including early detection of tumors, improved risk assessment and staging, as well as early detection of relapse and monitoring of tumor evolution in the context of cancer therapies<sup>3</sup>. Liquid biopsy owns the advantages over the traditional biopsy<sup>4</sup>, including minimal invasion, serial assessments, live monitoring, and access to tumor heterogeneity. In clinical applications, liquid biopsy not only can be independently used for the diagnosis, prediction, and prognosis of tumors, but also can be combined with imaging tools, like PET-CT, to safely detect and precisely localize several types of cancers in individuals not previously known to have cancer<sup>5</sup>.

CTC and circulating tumor DNA (ctDNA) are the two key components of liquid biopsy assays (others include cell-free RNA, extracellular vesicles, tumor-educated platelets, proteins, etc.). The common methods for CTC detection are epithelial ImmunoSPOT<sup>6</sup> (EPISPOT) assay for proteins and fluorescence in situ hybridization (FISH)<sup>7</sup> for DNA/RNA. They both are based on fluorescence microscopy with a low throughput and a few fluorescence channels. Currently, ctDNA detection is using next generation sequencing (NGS)<sup>8</sup> techniques. To increase the number of targets simultaneously detected, NGS utilizes fluorophore barcodes (fluorophores bounded together in a spatially discrete order) as unique signatures and each signature is exclusively allocated to one target<sup>8</sup>. In this way, NGS can detect hundreds of different analytes in parallel. However, it also relies on fluorescence microscopy imaging thus the throughput is still nonideal. Most NGS techniques require template enrichment and reverse transcription, giving a complicated operation procedure. Flow cytometry (FCM) is able to detect fluorescence or scattering lights emitting from cells or particles at an extremely high throughput of thousands to hundreds of thousands of particles per second<sup>9</sup>. With spectrum measurement<sup>10</sup> and dual-color fluorescence barcodes<sup>11</sup>, FCM may detect at most 50 different analytes simultaneously but is still insufficient for liquid biopsy. Imaging flow cytometry (iFCM) is emerging in recent ten years<sup>12</sup>, which is a combination of flow cytometer and fluorescence microscope, first enabling FCM with imaging ability.

Using hundreds of unique spatial barcodes to specifically mark various analytes and utilizing iFCM for detection, we will achieve a simultaneous high throughput and massive parallel detection. Since the illumination time for one particle in FCM is very limited (usually a few microseconds), the brightness of the fluorophores in barcodes should be strong enough. Thus, quantum dot (QD) is a good candidate with a brightness ten times brighter than that of organic dyes<sup>13</sup>. DNA assembling<sup>14</sup> is an approach to accurately control the order of different QD spheres in one barcode, creating hundreds of unique barcodes.

### **2. Problem Statement**

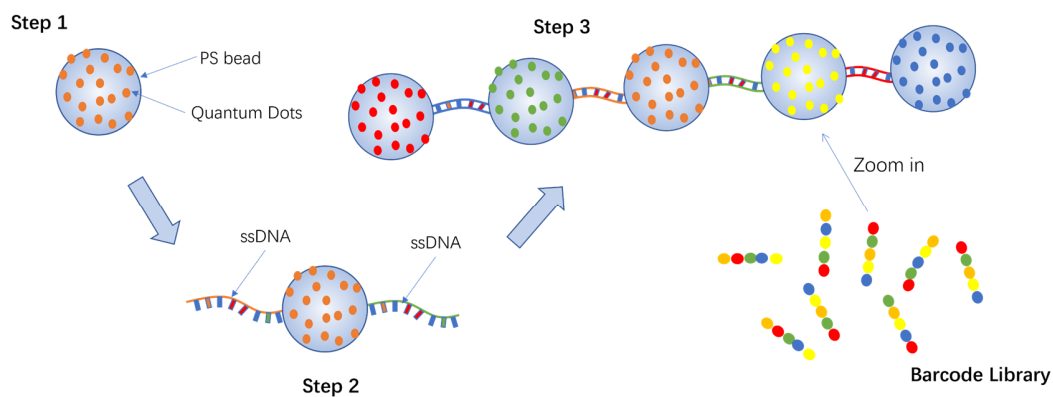
The existing detection methods for liquid biopsy cannot process numerous analytes simultaneously at a high throughput, making it challenging to find the optimal panel of biomarkers according to different objectives (e.g., accurately identify different tumors) due to low detection efficiency or lack of high content data. A massively parallel detection, high-throughput, and easy-to-operate liquid biopsy modality providing precise measurements of hundreds of specific circulating biomarkers will be a tremendously powerful tool for the researchers and doctors to comprehensively analyze tumors and further effectively discover the right panels for various objectives. This is the research challenge we propose to undertake.

### 3. Work Plan

To overcome this challenge, this proposal is to combine DNA-assembled quantum-dot spatial barcodes and imaging flow cytometry. By leveraging high throughput of imaging flow cytometry and plenty of unique signatures offered by barcodes, our solution is capable of simultaneous detection of hundreds of analytes in liquid biopsy. The proposal has three aims: 1) to fabricate quantum-dot (QD) spatial barcodes using DNA assembling, 2) to establish imaging flow cytometer as the platform to detect QD barcodes, 3) to decorate QD barcodes with proper adapters for different circulating biomarkers.

#### Aim 1. to fabricate quantum-dot spatial barcodes using DNA assembling

Our approach to construct QD spatial barcodes is to utilize specific DNA strands to connect QD beads of different colors in a discrete order, containing three main steps (**Figure 1**). Step 1, QD-labeled polystyrene (PS) beads: incorporate CdSe QDs with polymerisable ligands into PS beads via a suspension polymerisation reaction, making single PS bead contain thousands of the same QDs. Step 2, DNA-linked QD beads: functionalize QD beads with carboxyl groups and functionalize single-stranded DNA (ssDNA) fragments with amine groups, then link ssDNA fragments to QD beads via coupling of an amine with a carboxylic acid to form an amide bond, and each QD beads contains two different ssDNA fragments. Step 3, QD spatial barcodes: link one color QD bead with another color QD bead via the hybridization of the complementary ssDNA fragments on the surfaces of the two QD beads, then repeat this process to construct the final spatial barcodes. This approach will offer a huge number of individual signatures. For example, if we have four/five QD colors and the five positions in one barcode, then we will get  $4/5 \text{ colors}^5$  spatial positions = 1024/3125 signatures. Each signature can be exclusively allocated to one circulating biomarker. We will complete Aim 1 with the cooperations with Prof. Grigory Tikhomirov (UC Berkeley, an expert in DNA assembling<sup>14</sup>) and Prof. Adam de la Zerda (my postdoc mentor at Stanford University, an expert in nano reagents<sup>15</sup>).



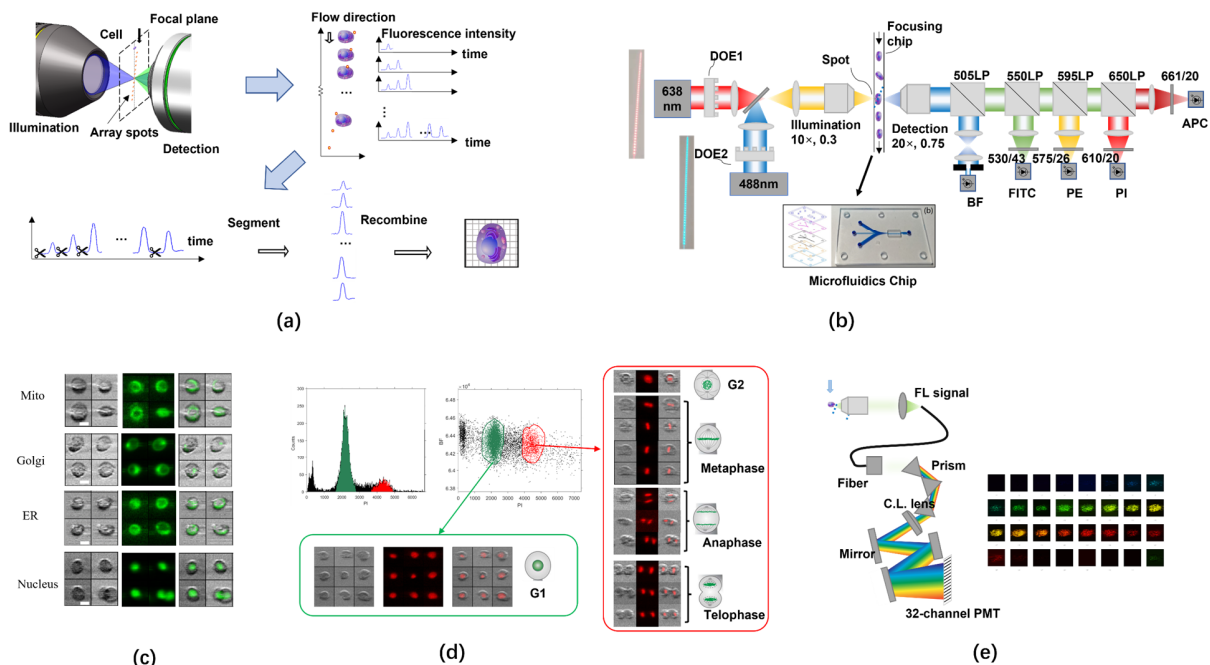
**Figure 1.** The synthetic process of QD spatial barcodes. QD, quantum dot; PS, polystyrene; ssDNA, single-stranded DNA.

#### Aim 2. to establish imaging flow cytometer platform for visualizing QD barcodes

We have invented a new method for high throughput and high content spectral imaging flow cytometer (iFCM) based on structured linear spot array excitation<sup>16</sup>. As illustrated in **Figure 2**, this method leverages equally spaced laser spots for illumination, scanning single cells by cell flowing, and the cell image is reconstructed by splitting and assembling photomultiplier tube (PMT) signals. We have tested this system with two lasers (488nm and 635nm) and five imaging channels (Bright-field, FITC, PE, PI, APC), or using a 32-channel array PMT for spectral detection across 480nm-750nm.



To visualize QD barcodes, we need to adjust our iFCM system, including: 1) since the ideal excitation wavelength range for QDs is 300-450nm, a 400nm laser should be added into the iFCM system; 2) design and fabricate new diffractive optical element (DOE) to shape the 400nm laser into the linear spot array, the DOE fabrication is based on lithography and reactive-ion etching using the process we developed<sup>17</sup>; 3) replace the current 10x illumination lens with 20x lens to increase the spatial resolution from 1.8 $\mu$ m to 1 $\mu$ m; 4) reconstruct the fluorescence detection channels to cover five QD emission peaks of 525nm, 565nm, 585nm, 625nm, 655nm, the fluorescence detection can be achieved using five independent PMTs with filters or the PMT array spectrometer, and we will test them both and choose the best for the following experiments. The updated iFCM can offer a flow velocity 5m/s and the detection throughput up to 5000 barcodes per second. In addition to the hardware updates, the imaging-based algorithm to distinguish various barcodes rapidly and accurately should be developed. If using PMT spectrometer for whole spectrum detection, we will also develop an algorithm for spectral unmixing.

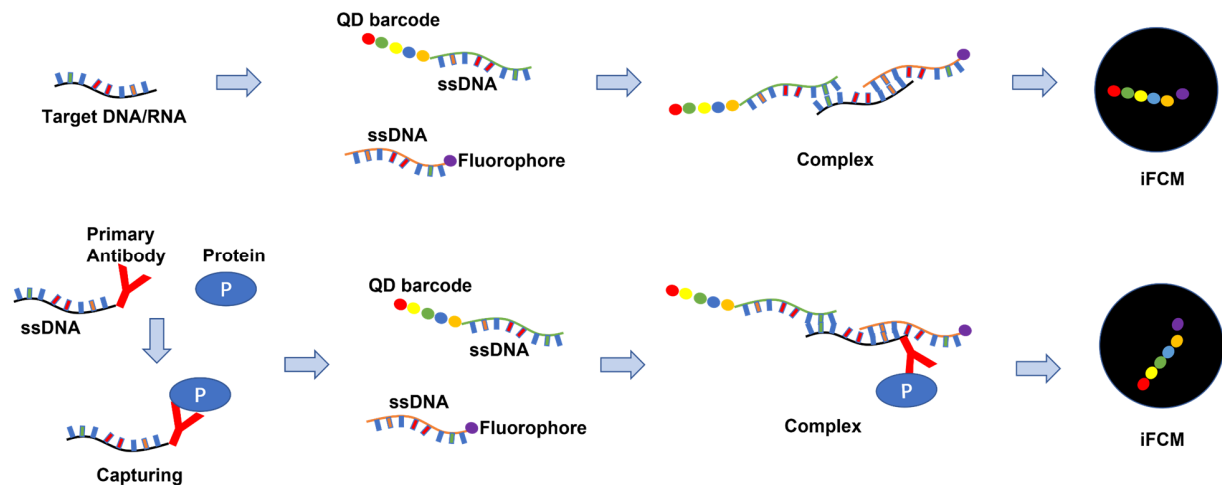


**Figure 2.** Imaging flow cytometer system<sup>16</sup>. (a) Imaging principle based on linear spot array. (b) Schematic. (c) Imaging of different organelles. (d) Imaging of cell cycle. (e) Spectrum detection.

### Aim 3. to decorate QD barcodes with proper adapters for different circulating biomarkers

The QD barcodes should be decorated with different adapters to specifically bond to different circulating biomarkers, such as ctDNAs, CTCs, proteins, cRNAs. The basic strategy is hybridization, as shown in **Figure 3**. QD barcode is connected to a ssDNA tag with the length 100 bases, and 50 bases of ssDNA tag is designed to be complementary to a target DNA/RNA fragment. A separate reporter probe composed of a 100-base ssDNA tag and a fluorophore (its fluorescence is different from that of QD barcodes) is used to prevent false positive results, and 50 bases in ssDNA tag is complementary to a target DNA/RNA fragment. For nucleic acid detection, a specific endogenous DNA or RNA (target) will be exclusively labeled with its complementary QD barcode and reporter probe. Different target DNA/RNA can be easily identified with the unique QD barcodes using imaging flow cytometer. To detect proteins, a probe combining a primary

antibody and a unique ssDNA tag is used to capture target proteins (circulating proteins or proteins on CTC surface) and specifically bind to its complementary QD barcode and reporter probe. Following this strategy, our platform will enable simultaneous quantification of DNA, RNA, and proteins in any combinations. In this proposal, we will first utilize this platform for detecting the DNA mutations of lung cancer. Also, magnetic microbeads can be connected to QD barcodes for efficient magnetic purification.



**Figure 3.** Detections of RNA/DNA and proteins. iFCM, imaging flow cytometer.

The timeline of this proposal is shown below.

	Months 1-5	Months 5-10	Months 11-14
<b>Aim 1</b>	QD barcodes		
<b>Aim 2</b>		iFCM for QD barcode detection	Algorithm for rapid identifying barcodes
<b>Aim 3</b>		QD barcodes + adapters Reporter probes	Comprehensive test

### Outcome(s)

Corresponding to the three aims, if successful, at the end of this project we will have a fabrication method of QD spatial barcodes, a demo system of imaging flow cytometer for QD barcode detection, a high throughput and massive parallel detection platform for DNA, RNA, and proteins. We will publish at least one paper in Optica open-access journals and share progress and results in Optica-organized symposiums.

### Impact

In the proposed research we will demonstrate the utility of the combination of DNA-assembled quantum-dot spatial barcodes and imaging flow cytometry for liquid biopsy arrays. If successful, the proposed platform will show, for the first time, hundreds of circulating biomarkers (potentially to be thousands) can be detected in a single assay at the throughput up to thousands of biomarkers per second, offering high-quality and high-content data of liquid biopsy for researchers and doctors to detect and monitor multiple cancers at all stages. This platform has prominent clinical values. For earlier cancer detection, this platform can help to identify the disease at a stage when it can be effectively treated, thereby offering the patient a better chance of long-term survival<sup>2</sup>. The liquid biopsy assays offered by this platform can be used to monitor minimal residual diseases, thereby aiding the discovery of new drugs that effectively eliminate or

control residual tumour cells in patients who have a high risk of disease relapse after primary therapy<sup>18</sup>. In summary, this platform will not only be a reliable and efficient tool for cancer research and therapy, but also pave the way for the practical application of personalized medicine. More generally, this platform will also serve as a common next generation sequencing tool with the advantages of high throughput and massive parallel detection.

## References

1. Siegel, R. L., Miller, K. D. & Jemal, A. Cancer statistics, 2015. *CA: A Cancer Journal for Clinicians* vol. 65 5–29 (2015).
2. Lennon, A. M., ... & Papadopoulos, N. (2020). Feasibility of blood testing combined with PET-CT to screen for cancer and guide intervention. *Science*, 369(6499), eabb9601.
3. Alix-Panabières, C., & Pantel, K. (2021). Liquid biopsy: from discovery to clinical application. *Cancer discovery*, 11(4), 858-873.
4. Poulet, G., ... & Taly, V. (2019). Liquid biopsy: general concepts. *Acta cytologica*, 63(6), 449-455.
5. Lennon, A. M., ... & Papadopoulos, N. (2020). Feasibility of blood testing combined with PET-CT to screen for cancer and guide intervention. *Science*, 369(6499), eabb9601.
6. Alix-Panabières, C., ... & Pantel, K. (2009). Full-length cytokeratin-19 is released by human tumor cells: a potential role in metastatic progression of breast cancer. *Breast cancer research*, 11(3), 1-10.
7. Grün, D., & van Oudenaarden, A. (2015). Design and analysis of single-cell sequencing experiments. *Cell*, 163(4), 799-810.
8. Goodwin, S., McPherson, J. D., & McCombie, W. R. (2016). Coming of age: ten years of next-generation sequencing technologies. *Nature Reviews Genetics*, 17(6), 333-351.
9. Adan, A., ... & Nalbant, A. (2017). Flow cytometry: basic principles and applications. *Critical reviews in biotechnology*, 37(2), 163-176.
10. Nolan, J. P., & Condello, D. (2013). Spectral flow cytometry. *Current protocols in cytometry*, 63(1), 1-27.
11. Krutzik, P. O., & Nolan, G. P. (2006). Fluorescent cell barcoding in flow cytometry allows high-throughput drug screening and signaling profiling. *Nature methods*, 3(5), 361-368.
12. Mikami, H., ... & Goda, K. (2018). High-speed imaging meets single-cell analysis. *Chem*, 4(10), 2278-2300.
13. Resch-Genger, U., Grabolle, M., Cavaliere-Jaricot, S., Nitschke, R., & Nann, T. (2008). Quantum dots versus organic dyes as fluorescent labels. *Nature methods*, 5(9), 763-775.
14. Tikhomirov, G., ... & Kelley, S. O. (2011). DNA-based programming of quantum dot valency, self-assembly and luminescence. *Nature nanotechnology*, 6(8), 485-490.
15. De La Zerda, ... & Gambhir, S. S. (2008). Carbon nanotubes as photoacoustic molecular imaging agents in living mice. *Nature nanotechnology*, 3(9), 557-562.
16. Han, Y.\*, Zhao, J.\*, ... & You, Z. (2022, March). Imaging flow cytometer based on linear array spot illumination generated by diffractive optical elements. *In Imaging, Manipulation, and Analysis of Biomolecules, Cells, and Tissues*. SPIE.
17. Zhao, J., ... & de la Zerda, A. (2022). Flexible method for generating needle-shaped beams and its application in optical coherence tomography. *Optica*, 9(8), 859-867.
18. Pantel, K., & Alix-Panabières, C. (2019). Liquid biopsy and minimal residual disease—latest advances and implications for cure. *Nature Reviews Clinical Oncology*, 16(7), 409-424.

**Name of the proposal:** Fabrication of semiconductor nanoparticles activated photocatalytic optical fiber for sustainable wastewater purification process

**Category:** Environment

In the 21<sup>st</sup> century, the sustainable and cost-effective wastewater treatment is a global challenging issue as the water pollution is increasing day by day due to rapid industrialization, expansion of population and unplanned urbanization. The photocatalysis is considered as most sustainable, eco-friendly and cost-effective process to purify wastewater. Thousands of research articles have been reported on preparation and photocatalytic wastewater purification performance of the photocatalyst nanoparticles, but there is no report in literature on industrial applications of these photocatalysts for wastewater treatment. The main problem with existing photocatalytic wastewater treatment process is that the powder nanophotocatalysts must be separated from water at the end of the purification process which is difficult and need special associated technique which will increase the cost of purification process. To address these challenging issues, I am proposing an innovative technique which will open new technological aspects for hassle-free sustainable wastewater purification in large scale. This technique can be implemented to built pilot reactor in company to clean wastewater in large scale or can be used directly to clean wastewater in nature like polluted ponds or lakes.

In the proposed project, special optical fibers called photocatalytic optical fibers will be fabricated using fiber drawing tower in COPL, Laval University. The various semiconductor nanoparticles like TiO<sub>2</sub>, ZnO etc will be incorporated in the plastic or glass optical fibers to optimize the efficiency of the photocatalysis process and to reduce the cost of purification process. The bundle of optical fibers can be put on the polluted ponds or lakes to degrade pollutants in presence of sunlight through photocatalysis process. The strong laser or LED can be used to inject light into the fibers to purify wastewater remotely. The bundle of fibers will be used to built pilot reactor coupled with UV or visible light source for industrial applications. This project will bring revolution in smart sustainable wastewater purification process.

# Fabrication of semiconductor nanoparticles activated photocatalytic optical fiber for sustainable wastewater purification process

Joy Sankar Roy

Center for Optics, Photonics, and Lasers

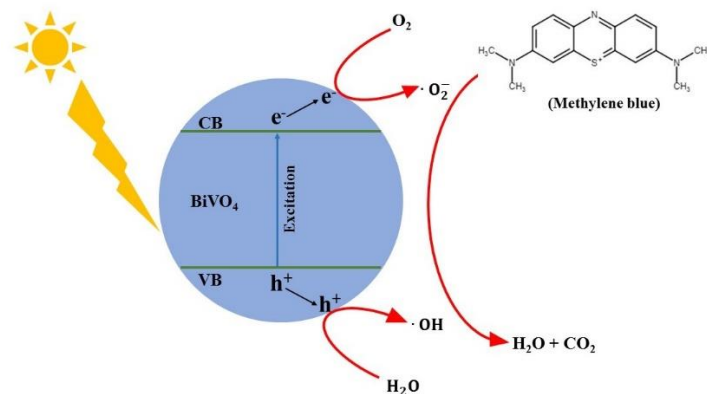
Laval University, 2375 rue de la Terrasse, Quebec, G1V 0A6, QC, Canada

Email: joy-sankar.roy.1@ulaval.ca

Ph: 4186562131 ext. 405926

## 1. Introduction and Justification:

Water is an essential constituent for the survival of human beings, although millions of people worldwide are suffering from lack of fresh and clean drinking water. The ground water and surface water have been polluted by rapid speed of industrialization, expansion of population, unplanned urbanization and environmental pollution. The discharge of untreated sanitary and toxic industrial wastes, dumping of industrial effluent, and run off from agricultural fields are the main sources of water pollution. The agriculture and pharmaceutical effluents release pesticides and other chemicals that are responsible for some chronic diseases. Various industries such as textiles, dyeing and printing discharge large amounts of synthetic organic dyes as effluents. In developing countries, almost 70 % of all the illness are related to water contamination. Therefore, it is the greatest challenges in 21<sup>st</sup> century to the researchers to develop an eco-friendly, cost-effective, and fast processing technology to remove the pollutants from wastewater in order to protect the environment and human beings. To address this serious issue, semiconductor photocatalysis has been believed as a low cost, sustainable and environmentally friendly process for wastewater purification process.



**Fig. 1: Mechanism of photocatalytic degradation of organic pollutants in wastewater**

The semiconductor photocatalysts have been studied extensively for purification of wastewater. Thousands of research articles have been reported on preparation and photocatalytic wastewater purification performance of the photocatalyst nanoparticles like titanium dioxide ( $\text{TiO}_2$ ), zinc oxide ( $\text{ZnO}$ ),  $\text{BiVO}_4$ ,  $\text{Bi}_2\text{WO}_6$ ,  $\text{AgTaO}_3$ ,  $\text{Ag}_3\text{VO}_4$ ,  $\text{AgNbO}_3$ ,  $\text{MoS}_2$  etc. The mechanism of photocatalytic methylene dye (a textile industry waste) degradation of  $\text{BiVO}_4$  nanoparticles under sunlight irradiation is presented in Fig. 1 to understand the sustainability of the process.

## **2. Objectives of the proposed project**

Thousands of research articles have been reported on preparation and photocatalytic wastewater purification performance of the photocatalyst nanoparticles, but there is no report in literature on industrial applications of these photocatalysts for wastewater treatment. The main problem with existing photocatalytic wastewater treatment process is that the powder nanophotocatalysts must be separated from water at the end of the purification process which is difficult and need special associated technique which will increase the cost of purification process. To address these challenging issues, I am proposing an innovative technique which will open new technological aspects for hassle-free sustainable wastewater purification in large scale. This technique can be implemented to built pilot reactor in company to clean wastewater in large scale or can be used directly to clean wastewater in nature like polluted ponds or lakes.

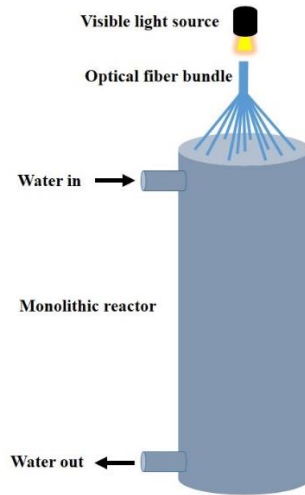
## **3. Work Plan**

The main objective of the proposed project is to fabricate the photocatalytic optical fibers using various semiconductor nanophotocatalysts such that it can be used for large scale industrial wastewater treatment as well as to clean polluted ponds or lakes. Two different methodologies will be implemented to fabricate photocatalytic fibers: type I-Nanophotocatalysts coated fiber and type II-nanoparticles embedded fibers. The objectives of the project can be summarized as follows:

1. Fabrication of type – I: Preforms of glass and polymer will be purchased to draw optical fibers. Various nanoparticles will be purchased and prepare nano-polymer composite to coat on the fiber during drawing process such that photocatalytic fibers can be made in large scale. The surface of the coating onto optical fiber will be investigated by SEM and AFM.
2. Fabrication of type – II: Nanoparticles embedded preforms will be prepared and then drawn and investigated by SEM/TEM.

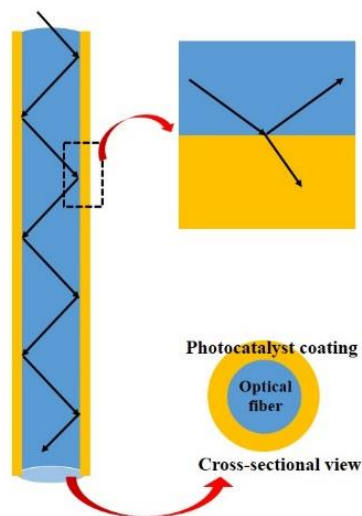


3. The photocatalytic activity of the coated fibers will be tested using tained wastewater under visible light irradiation. The fibers photocatalytic testing will be implemented using various light sources like UV/visible LED/halogen bulb/sunlight.
4. A bundle of fiber will be made coupled with LED/Laser to test remote wastewater treatment as shown in Fig. 2. The fiber bundle will be installed inside a metallic or plastic cylinder to build a reactor as shown in Fig. 2.
5. The performane of the reactor will be tested for photocatalytic wastewater treatment.



**Fig. 2: Schematic representation of the pilot reactor.**

6. The schematic of working principle of type I fiber under injection of light is shown in Fig. 3. Here, light will be transmitted to the coating as the refractive index of the coating is higher. The light transmission/ guidance for type II fiber is as usual because the nanoparticles will be inside the fiber.



**Fig. 3: Working principle of type I fiber**

#### **4. Expected outcomes and impact of the project**

The sustainable cost-effective wastewater treatment process is a global challenge. This project may bring revolution in sustainable wastewater purification process. This technique can be implemented to build pilot reactor in company to clean wastewater in large scale or can be used directly to clean wastewater in nature like polluted ponds or lakes.

The specific expected results are:

1. Fabrication of novel photocatalytic optical fiber.
2. Sustainable wastewater treatment using prepared photocatalytic optical fiber.
3. Development of pilot reactor for sustainable and cost-effective wastewater treatment.
4. Presentation of this new technology to international audience in conference and seminars.
5. Publications of patents and good research articles in reputed international journals.

#### **References:**

- [1] J.S. Roy, S. Morency, Y. Messaddeq; *Journal of Photochemistry and Photobiology* 2021, 7, 100037.
- [2] J.S. Roy, S. Morency, G. Dugas, Y. Messaddeq; *Solar Energy* 2021, 214, 93.
- [3] J. S. Roy, G. Bhattacharya, D. Chauhan, S. Deshmukh, R. K. Upadhyay, R. Priyadarshini, S. Sinha Roy; *SN Applied Sciences* 2020, 2, 796.
- [4] J.S. Roy, G. Dugas, S. Morency, Y. Messaddeq; *Physica E: Low-dimensional Systems and Nanostructures* 2020, 120, 114114.
- [5] J.S. Roy, G. Dugas, S. Morency, S.J.L. Ribeiro, Y. Messaddeq; *Applied Sciences* 2020, 2, 185.
- [6] A. Malathi, J. Madhavan, M. Ashokkumar, P. Arunachalam, *Appl. Catal. A: General* 555 (2018) 47.
- [7] A. García-Gil, E.G. Schneider, M. Mejías, D. Barceló, E. Vázquez-Suñé, S. Díaz-Cruz, *J. Hydrol.* 566 (2018) 629.
- [8] L. X. Henao-Herreño, A. M. López-Tamayo, J. P. Ramos-Bonilla, C. N. Haas, J. Husserl, *Risk Analysis*, 37 (2016) 733.
- [9] O. F. Lopes, K.T.G. Carvalho, A.E. Nogueira, W. Avansi Jr., C. Ribeiro, *Appl. Catal. B: Environ.* 188 (2016) 87.
- [10] S.M. Thalluri, S. Hernández, S. Bensaid, G. Saracco, N. Russo, *Appl. Catal. B: Environ.* 180 (2016) 630.

## Executive Summary

**Title:** A Novel Method for Scaling Manufacturing of Integrated Photonic Devices with Enhanced Connectivity

Category: Information

Objectives: Developing a novel method for enhancing the coupling between the optical fiber and the photonic chip by using a mode converter design. This design improves the performance by four folds. Secondly, developing a new device which can connect optical fibers to chips using laser fusion splicing technology in less than a minute.

Outcomes:

1. Industrial prototype of mode converter design chips: This industrial prototype will act as a proof of concept that we can manufacture a low-loss mode converter on foundry process lines without any difficulty. It will act as a stage for the creation of a process development kit that can be licensed by the company and will be used in optical transceiver chips. Due to the low loss advantage of the mode converter technology, this novel technology can then be used for quantum communications and sensing equipment.
2. Prototype of fiber to chip attach laser machine: The fiber attach laser machine will be the first-ever fiber attach machine which uses a laser to connect optical fibers to photonic integrated circuits. This one-of-a-kind machine will disrupt the current glue-based attach machines and will revolutionize the integrated photonics packaging industry. The prototype will be used at small research labs, and Universities initially as they can act as beta testers for the technology. We will then use the feedback from the customers to develop bigger machines that can be integrated into a process line or can be modified into an existing machine.

Applications:

The first part of the technology will help improve the device performance which is a key parameter for integrated photonic devices. The improved performance will help in reducing the link budget in an optical transceiver, thereby improving the overall yield of manufacturing. Application spaces like quantum computing, sensing, are very sensitive to low performance devices, using the mode converters can help them in achieving enhanced outputs and bits. In telecommunications, every dB of loss translates to the length over which the optical signal can travel before repeating it, making it an application field for the technology.

For the laser fusion technology, the entire data communication industry, telecommunication industry, LIDAR, quantum communications, and biological sensors all want to avoid the use of epoxies in the packaging and are driven by reducing the cost of manufacturing. The laser fusion machine can improve the manufacturing speed of packaging by 10X and will eliminate the use of epoxies.

The combination of the above mentioned technologies, helps in making integrated photonic devices future-ready and will help in keeping up with the increasing demand for data.

# A Novel Method for Scaling Manufacturing of Integrated Photonic Devices with Enhanced Connectivity

## Background and Literature Review

Integrated photonic devices are poised to enter high-volume markets such as data communications, telecommunications, biological sensing, and optical phased arrays. Nearly all our data communication over the internet, like, zoom calls, and online conferences use data centers to process and transmit the data. Optical transceivers are the heart and soul of a data center. Therefore, speed, performance, and low operating cost are very vital for the data centers. To make the field of information technology future-ready, we need solutions that are cost-effective and high-performance and can sustain the scalability of the technology. However, the optical packaging of integrated photonic devices with high optical efficiency and multiple I/O ports remains a slow and expensive process, while maintaining compatibility with CMOS processing without introducing changes to the fabrication process or consuming a significant area on the chip [1-4]. With the exponential increase in data traffic, enhanced and low-loss optical packaging will be a necessity. This problem will become more and more critical as the data-related market grows. An average large-scale data center requires 100,000 optical transceivers (Keysight blogs on "Keeping the Pulse on 400GE in the Data Center"). The time-consuming and inconsistent nature of the current fiber-to-chip connections is proving to be a major bottleneck for the widespread commercialization of photonic chips. The technology for packaging silicon photonic devices to optical fibers remains cost prohibitive, inefficient, and slow.

With the advent of co-packaged optics, optics onboard, [6–8] and pluggable high-speed optical transceivers, higher bandwidth density, integrated photonics has emerged as a gateway to achieving higher data rates with reduced manufacturing and thermal extraction costs. Optical transceivers with integrated photonics will become the norm as the parallelism between electronics and

optics grows. As integrated photonics devices become more complex, to suffice multiple I/O ports fiber arrays or ribbon fibers are also used in addition to a single optical fiber. As the number of I/O port counts keeps increasing, the number of optical fibers in an array keeps increasing, leading to increased packaging times and alignment complexities. Integrated photonic devices are helping us keep our information technology future ready.

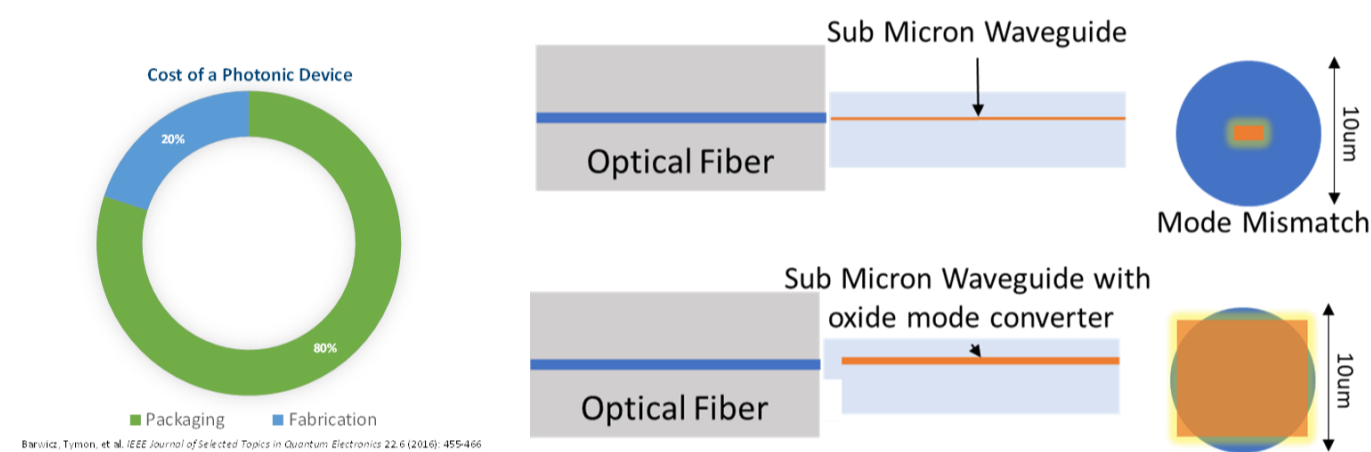


Figure 1 Distribution of cost of a packaging of a photonic device, mode mismatch between a SMF 28 fiber and a waveguide, vs mode match between a SMF28 fiber and a mode converter.

## Problem Statement and Objective

Currently, all optical fiber-to-chip attachment techniques rely on adhesives, which are inefficient and expensive. We aim to make the fiber-to-chip connection process more reliable, eliminating the use of adhesives, being highly efficient, and being cheaper than the current standards.

Almost all, of the current optical packaging, relies heavily on adhesives, a single optical fiber-to-chip connection can have stress relief adhesive, index matching epoxy, or thermal management epoxy. Curing adhesives in a process line while manufacturing is a bottleneck and increases the device cost significantly. For integrated photonics to be on par with electronics, we need to flip the amount of cost associated with packaging from 80% to 20% of the device cost as shown in figure 1. Adhesives are susceptible to environmental fluctuations and shrink during the curing process. On average curing of adhesives takes 5-10mins of tool time in a process line, this leads to increased production costs. These devices go in data centers which require high reliability and longer-life products. Using adhesives in harsh environments reduces the device's lifetime and increases failure in the field, further increasing the cost of the overall device. About 80% of the total cost of a photonic device is from packaging [3] and testing and approximately 40-60% of that is the fiber-attach process. The current industry standards are very rigid on the loss budget in an optical transceiver. As the fiber-attach process is the very last process in the production of transceivers, keeping the loss numbers low directly impacts the *yield* of the product.

During the process of aligning an optical fiber to a chip, the mode of the optical fiber needs to match the mode of the single mode fiber, as shown in figure 1. i. The overlap between the two modes needs to be as close as possible to achieve high optical coupling >90%. However, the current industry standard for optical coupling is only 50% or 3dB.

We developed a novel mode converter design to increase optical coupling between a fiber with a mode field diameter of 10.4um and an optical waveguide, here silicon nitride, with a mode field of 4umX3um [5]. To increase the optical coupling, we introduce a silicon dioxide mode converter which is carved out from the oxide cladding of the chip. This process forms an intermediary step for mode matching between the optical fiber and the waveguide and adiabatically increases the size of the waveguide mode to match that of the optical fiber. The introduction of the mode converter increases the optical coupling efficiency from 50% to 80% which is a 4X improvement in coupling and is state of the art. This coupling method can be used in fusing any device that has a cladding of silicon dioxide, including, for example, devices based on silicon, silicon nitride, and lithium niobate on the insulator. We isolate the oxide mode converter from the silicon substrate to prevent a loss of light to the substrate. To increase scalability, the oxide mode converter is permanently fused to the optical fiber using a CO2 laser via radiative energy. The fusion splice between the fiber and the chip forms a permanent bond and decreases coupling losses by eliminating the Fresnel reflections at both oxide-air interfaces

and the gap between the fiber and the oxide taper. This method is compatible with different types of inverse nanotapers (e.g., linear taper, metamaterial taper) [4,9].

Our objective is to develop a novel manufacturing machine that can attach optical fibers to photonic chips in *less than a minute* and uses laser fusion to form a permanent connection between them. Our goal and objectives are two folded:

1. We will develop a working prototype of the fiber attach process using a mode converter design from a CMOS foundry and determine its scalability.
2. We will develop a *new fusion technique* that can work for devices with a CMOS fabricated mode converter as well as devices without a mode converter.

Objective 1: Working prototype of mode converter technology

The work done by J. Nauriyal and J. Cardenas, on optical packaging of optical fiber to the chip using a mode converter has been licensed to the startup Photonect. Photonect will work on developing this technology so that it can be used in real life and create a larger impact on the information technology world. To scale this technology and bring it to market a crucial step is missing which is prototyping the design on a foundry run wafer at one of the big CMOS foundries like TowerJazz, or Global Foundries. This award will help the startup in validating the existing technology for commercial applications by doing a design run with one of the foundries and developing a new process development kit that can be used by the industry. Figure 2 shows the possibilities of the foundry-made PICs, that can achieve ultra-low loss useful for defense applications and quantum. This objective is split into a few parts:

- Designing of mode converters with design parameter limitations
- Addition of some mode converters specifically for quantum applications

These devices will act as a prototype for further testing using objective 2 stated below.

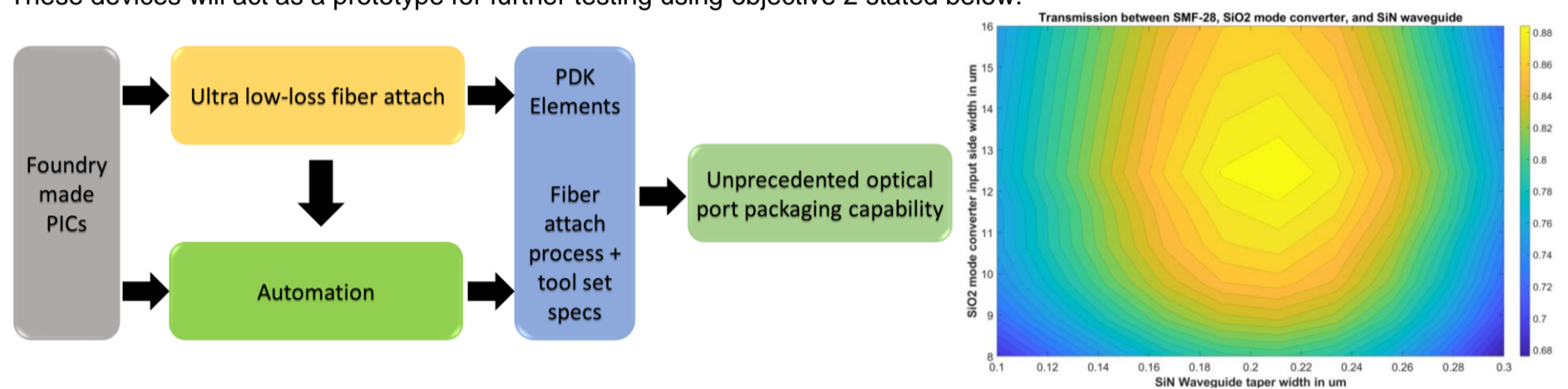


Figure 2 Objective 1: Prototyping of oxide mode converter devices at a foundry, ii) simulation results for an oxide mode converter to a SMF 28 fiber >90% coupling efficiency through the device.

From figure 2. ii, you can see eigen mode solutions for enhanced coupling between the optical fiber to oxide mode converter and the silicon nitride waveguide. We will implement this technology for ultra-low loss devices which can be used for quantum communications and at deep cryogenic temperatures. The plot provides results for different types of silicon dioxide total cladding thickness versus the size of the mode converter for different silicon nitride waveguide taper sizes. This shows the flexibility of this approach in that it can be used with a given set of parameters and still achieve enhanced optical performance.

Objective 2: Fusion splicing technique for attaching optical fibers to PICs

As mentioned in the previous papers [5], the introduction of a mode converter at the edge of the chip provides an interface for the optical fiber to attach to the chip during the splicing process. However, this technology has only been demonstrated on a benchtop setup and does not have any reliability data associated with it. Our objective for this setup will be to develop a compact fiber attach machine as shown in figure 3, side and top view, very similar to a fusion splicer which is automated and can fuse the optical fiber to the chip in merely a few seconds. We envision the machine to consist of a CO2 laser fusion splicing setup for both single fibers attach as well as multiple fibers attach by using a rotation mirror and changing the lenses between a spherical lens and a cylindrical lens.

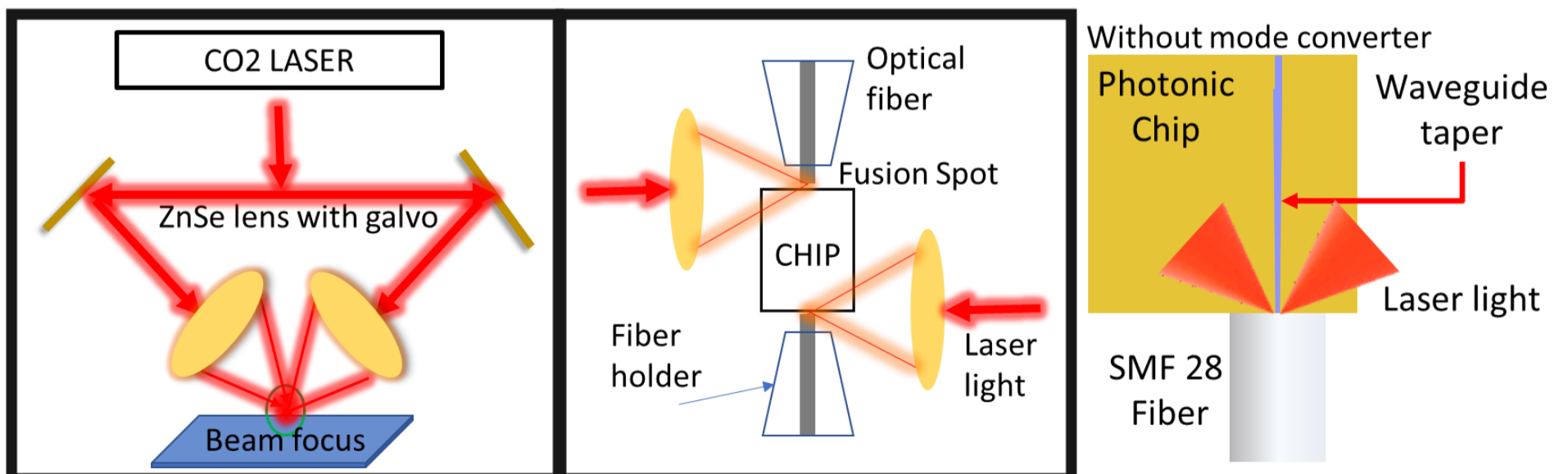


Figure 3 i) Side view of the proposed optical fiber to chip attach machine using two beams of laser at different angles to improve the reliability of the fusion splice, ii) Top view of the machine where two lenses will simultaneously fuse optical fibers on both sides of the chip, iii) zoomed in view of fusion splicing between an optical fiber and a chip without mode converters.

Previous work on optical fiber-to-chip fusion splicing has been performed on a lab scale with the use of mode converters [5] at the edge of the chip. However, introducing a design change in the mass manufacturing process line can lead to increased costs, hence, we also want to develop a technology that can attach any optical fiber to any photonic chip with an oxide cladding in less than a



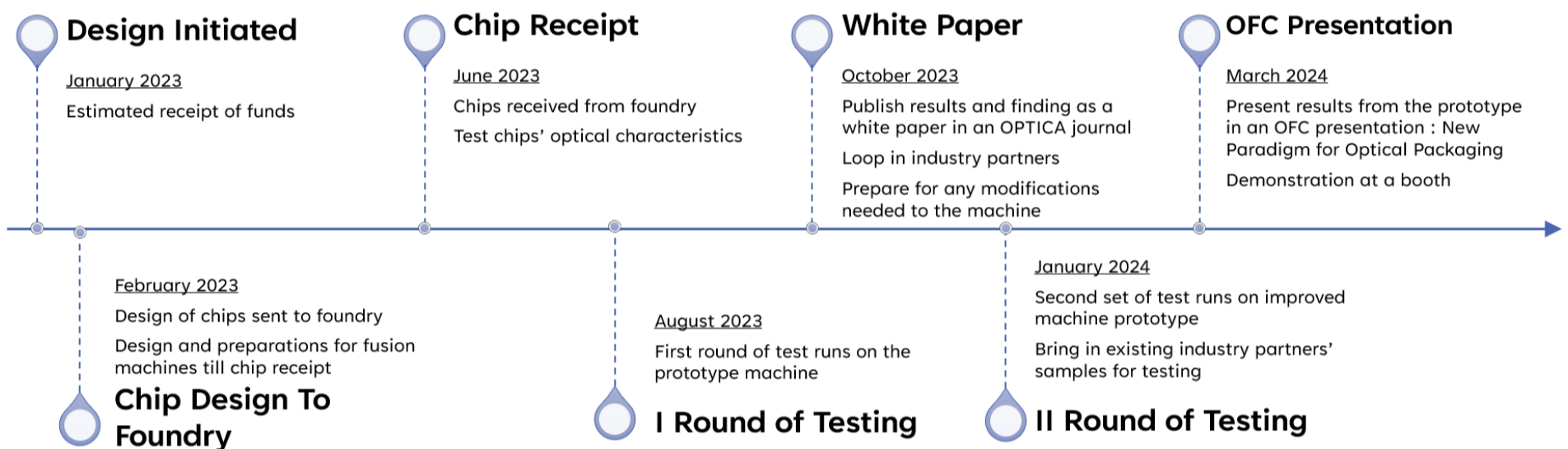
minute. This novel process will require multiple attachment points (figure 3. iii) between the optical fiber and the chip as we do not have the mode converter (waveguide made of glass) to act as an interface for the connection. As single fiber to chip attach was proven in the research lab, we envision we can develop a method and technology which can connect optical fibers to chips without the need for mode converters very similar to fusion splicing between two optical fibers. Using multiple splice points on the chip will also increase the overall reliability of the device and will help us in developing a process of attachment of fiber to the chip without the use of any adhesive.

Due to the low loss and robust nature of CO<sub>2</sub> laser fusion-based PIC packaging, and the elimination of adhesive from the system, this device will be a game changer for research in areas like quantum technologies, sensing, etc. Quantum communications, is an emerging area where each bit has value, decreasing the loss between a quantum photonic chip and the optical fiber is another field of application for the fiber-to-chip attach machine. Sensing devices that work in extreme environments like cryogenic temperatures cannot sustain adhesives over time, this device will help empower new research and development in the optics field.

### Outline of tasks and Work Plan

The project aims to develop a prototype of a laser fiber connection machine for enhancing the connectivity between an optical fiber and a photonic chip. This will make PIC packaging faster, more reliable, more sustainable environmentally, and more cost-efficient.

The first step in proving our low-loss fiber-to-chip coupling technology is to develop a prototype that can be mass manufactured in a CMOS foundry. We will work with established manufacturers of optical components and lasers to create a compact platform for fiber to the chip fusion process. Given the relatively lower power requirements, mature nature of CO<sub>2</sub> laser technology, and the variety of commercial CO<sub>2</sub>-based laser engravers available on the market. The compact and easy-to-use nature of the prototype is feasible. We will create a fiber-to-chip attach machine which uses a CO<sub>2</sub> laser beam for attachment and replaces the need for adhesives for the attachment process.



This initial prototype will be used in a small-scale settings like research labs, AIM TAP facilities, and national labs. Since these facilities are limited to low volume and are the hub for future inventions. These machines will then be developed for optical transceiver companies that need better technology for attaching optical fibers to chips.

The work plan is divided into two broad categories:

1. **Fabrication of devices** at a CMOS foundry like TowerJazz, or Global Foundry, to create a viable prototype of the mode converter chip design which will be used in the fiber-to-chip attach machine.
2. **Development of fiber-to-chip attach machine** and testing its compatibility with photonic chips with mode converters and without mode converters.

We envision working on the above-mentioned tasks over the next 15 months in the following timeline:

January 2023	Fund receipt anticipated. The design of the chips is initiated before this
January - February 2023	Design and planning of the fiber-fusion module begins
February - March 2023	Chip design is sent to the foundry partner Parts procurement for the fiber-fusion module initiated
April - June 2023	Fiber to chip fusion machine assembly initiated
June - July 2023	Chips received from the foundry. Optical characterization initiated
August - October 2023	The first round of test runs with the foundry chips on the assembled machine
October - November 2023	Results from the testing are submitted to an OPTICA journal/OFC as a company paper. Loop in industry partners (current customers) for compatibility checks and feedback
November - December 2023	Prepare for any modifications to the machine
January – February 2024	The second set of test runs on the improved machine Research with University and industry partners' chips for test runs
March – April 2024	Present results in OFC as company paper. Machine demonstration at OFC booth.



The work will be done by Photonect Interconnect Solutions at Nextcorps downtown Rochester NY. To achieve this, we will use the funds to buy equipment for the demo unit like alignment stages, CO2 laser, lenses, and optics, which will all go into the machine. This will create a demo unit for further research and development of the machine. The laser fusion attach machine will be able to do the optical fiber to chip attach within less than a minute including the alignment routine, improving **the speed of production by 10X**. We have allocated some funds to a foundry-based shuttle run so that we can test the feasibility of the mode converter design on a mass scale which will improve the **device performance by 4X** and can lead to up to 50% cost savings for the company.

Outcome(s)

The grant will help us in achieving two biggest outcomes:

1. Industrial prototype of mode converter design chips

This industrial prototype will act as a proof of concept that we can manufacture a low-loss mode converter on foundry process lines without any difficulty. It will act as a stage for the creation of a process development kit that can be licensed by the company and will be used in optical transceiver chips. Due to the low loss advantage of the mode converter technology, this novel technology can then be used for quantum communications and sensing equipment.

2. Prototype of fiber to chip attach laser machine

The fiber attach laser machine will be the first-ever fiber attach machine which uses a laser to connect optical fibers to photonic integrated circuits. This one-of-a-kind machine will disrupt the current glue-based attach machines and will revolutionize the integrated photonics packaging industry. The prototype will be used at small research labs, and Universities initially as they can act as beta testers for the technology. We will then use the feedback from the customers to develop bigger machines that can be integrated into a process line or can be modified into an existing machine.

Impact

This project will revolutionize the optical packaging of integrated photonic devices. With the use of the mode converter technology, the photonic chips can now be highly enhanced in performance, improved yields, reduced costs, high speed of manufacturing, and environmentally more sustainable. Here are the broad impacts this technology will bring to the industry:

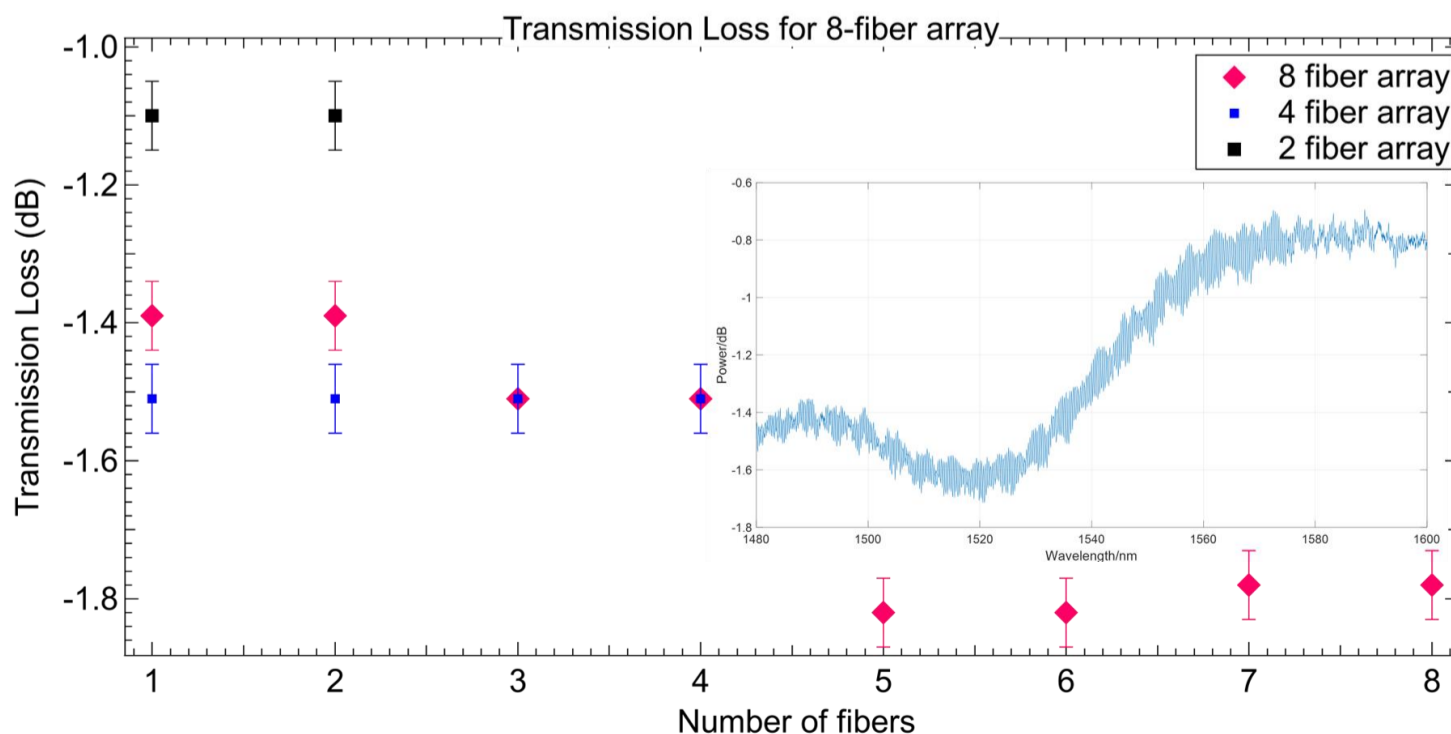
1. Economic impact

The fiber-to-chip fusion machine improves the speed of packaging by 10X. Currently, on average an optical transceiver manufacturing costs \$100, out of which \$30 is utilized in the optical fiber attachment process. The biggest cost factors are the labor time associated with the alignment of the fiber, monitoring of the power while curing the adhesive, and wait times while the adhesive cures. With our technology, we bring eliminate the cure time and instead use laser fusion splicing which takes <1 minute for attachment, independent of the number of fibers. This provides a 10X improvement in manufacturing, leading to reduced labor costs, energy costs, and increased production rates. This will help us in sustaining the need for the exponentially growing data demands for the next few years.

2. Environmental impact

Our mode converter technology provides a 4X enhancement of performance over industry standard because of the low loss coupling mechanism. There are 100,000 transceivers in a data center, and there are 2750 data centers in the US [10]. With the mode converter technology, we can save up to **0.5W per transceiver**. Hence, in each data center that has 100,000 optical transceivers, we can save 100MW of energy. This is the optical energy that we save per device, but because of the high-performance devices, now we don't need to run the lasers at higher power and further reduce energy consumption. As there is a transition from electronic circuits to more photonic integrated circuits, the heat extraction cost per data center also significantly reduces.

3. Performance



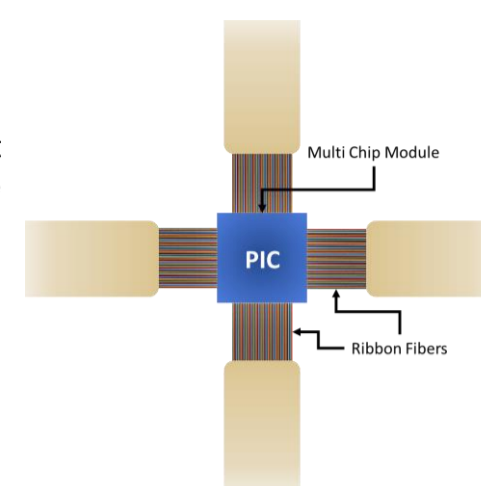
The mode converter technology can increase the coupling between an optical fiber and a chip from 50% to 90%. The measured results have shown consistent loss numbers of 1dB per facet for fiber-to-chip connection as shown in figure 4. The figure shows the transmission loss inset for a single fiber (0.8dB) and fiber arrays up to 8 fibers with a

Figure 4 Plot of transmission loss for multiple fibers to a chip connection

transmission loss of <2dB.

#### 4. Manufacturing yields

As the complexity of photonic devices increases due to the advent of co-packaged optics where a multi-chip module sits at the center with the ASIC and all the fibers are connected around it as shown in the figure on the right. With our technology, we can attach arrays of fibers in a single shot depending on the size of the laser beam. The current alignment system can do 12 fibers in a single shot because the beam size is 3mm. The size of the beam is limited by the focusing power of the ZnSe lens. The manufacturing yield will be increased because our mode converters can tolerate higher misalignments making them scaling to passive alignment a possibility for the future.



#### 5. Social impact

Our fiber-attach machine increases the production capacity of the fiber-attach machines from 40,000 units per year to 700,000 units per year leading to at least \$3.5M returns for the optical transceiver company. As the demand for the machines will increase, we will start a manufacturing facility in Rochester, creating jobs and opportunities for the optics and photonics community.

#### References

1. C. Kopp, S. Bernabé, B. B. Bakir, J. Fedeli, R. Orobtcouk, F. Schrank, H. Porte, L. Zimmermann, and T. Tekin, *IEEE J. Sel. Top. Quantum Electron.* 17, 498 (2011)
2. R. Soref, *IEEE J. Sel. Top. Quantum Electron.* 12, 1678 (2006).
3. I. M. Soganci, A. L. Porta, and B. J. Offrein, *Opt. Express* 21, 16075 (2013).
4. T. Barwicz, Y. Taira, T. W. Lichoulas, N. Boyer, Y. Martin, H. Numata, J.-W. Nah, S. Takenobu, A. Janta-Polczynski, E. L. Kimbrell, R. Leidy, M. H. Khater, S. Kamlapurkar, S. Engelmann, Y. A. Vlasov, and P. Fortier, *IEEE J. Sel. Top. Quantum Electron.* 22, 8200712 (2016)
5. L. Chen, C. R. Doerr, Y.-K. Chen, and T.-Y. Liow, *IEEE Photon. Technol. Lett.* 22, 1744 (2010)
6. Nauriyal, J., Song, M., Yu, R., & Cardenas, J. (2019). Fiber-to-chip fusion splicing for low-loss photonic packaging. *Optica*, 6(5), 549-552
7. M. Glick, L. C. Kimmerling, and R. C. Pfahl, "A Roadmap for Integrated Photonics," *Opt. Photonics News* **29**, 36–41 (2018).
8. R. Stone, R. Chen, J. Rahn, S. Venkataraman, X. Wang, K. Schmidtke, and J. Stewart, "Co-packaged Optics for Data Center Switching," in *2020 European Conference on Optical Communications (ECOC) (2020)*, pp. 1–3.
9. C. Scarcella, K. Gradkowski, L. Carroll, J.-S. Lee, M. Duperron, D. Fowler, and P. O'Brien, "Pluggable Single-Mode Fiber-Array-to-PIC Coupling Using Micro-Lenses," *IEEE Photonics Technol. Lett.* **29**, 1943–1946 (2017).
10. V. R. Almeida, R. R. Panepucci, and M. Lipson, *Opt. Lett.* 28, 1302 (2003)
10. <https://www.nature.com/articles/d41586-018-06610-y>

## **Kayn Forbes: Structured light photonics for next generation chiral nano-spectroscopy**

Chirality refers to an object which cannot be superimposed on to its mirror image, such as our left and right hands. The importance of studying and determining material chirality cannot be overstated. For example, the left-handed form of methamphetamine is a potent central nervous system stimulant, whereas the right-handed is a nasal decongestant found in supermarkets.

Light may also be chiral. The most well-known example of optical chirality is light with circular polarisation. Like the chiral discrimination present when you attempt to place a right-handed glove on your left hand, chiroptical spectroscopy exploits the differential interaction of chiral light with right- and left-handed types of materials. These techniques are critical to health as they provide a wealth of information about chiral materials, including the absolute configurations of chiral molecules, conformations and functionalities of biomolecules such as insulin, and molecular structure of viruses.

Until very recently, interrogating material chirality involved exclusively using circularly polarised plane waves. However, light can be chiral in more ways than its local state of polarisation. Structured light refers to optical fields which have inhomogeneous phase, polarisation, and amplitude. One very important type of structured light is the optical vortex. These beams travel in the shape of a tornado which may either twist to the left or the right. This chiral wavefront is characterised by the topological charge  $\ell = \pm 1, \pm 2, \dots, \pm \infty$  where the sign dictates the handedness; in contrast circular polarisation is described by the helicity  $\sigma = \pm 1$ .

In the last five years significant breakthroughs in the field of structured light chirality have occurred and research efforts have rocketed. In particular, the pivotal role of nano-optics and plasmonic confinement has been realised: when structured laser beams and electromagnetic fields are confined into nanoscale volumes, extremely novel interactions occur. This is because chirality is a scale-dependent phenomena. We cannot place our right-handed glove on our left hand due to the chirality of both objects, however we may place both gloves of a giant on either of our hands: our hands and the giant's gloves are chiral, but the size mismatch is so large they don't interact in a discriminatory fashion. Just like the giant's gloves, unless the light is shrunk down into tiny volumes of space, their chiral structures do not interact with small chiral materials in a discriminatory fashion.

The Key Objectives of this project are to:

- 1)** Develop the computational code to carry out the required numerical simulations to describe cutting-edge experiments in chiral nano-spectroscopies with structured light.
- 2)** Determination of optimal chiral light structures for specific methods in chiroptical spectroscopy of biomolecules and nanostructures.
- 3)** First experimental observation of nonlinear Rayleigh optical activity of optical vortices.

The immediate impact of this work will be the development of new ways to study chiral materials using novel types of light. These materials will range from nanostructures and metamaterials, to molecular matter including drugs and biomolecules which are key to pharmaceutical and medicinal advances. The techniques developed will also be applicable in the wider field of chiral photonics. Chiral light is central to many photonic technologies, including optical communication, computing, and information processing based on miniature integrated devices which possess the ability to sense and discriminate the chirality of the light. This work paves the way for the next generation of chiral photonic media based on structured light illumination.

# Structured light photonics for next generation chiral nano-spectroscopy

Kayn Forbes

## Introduction

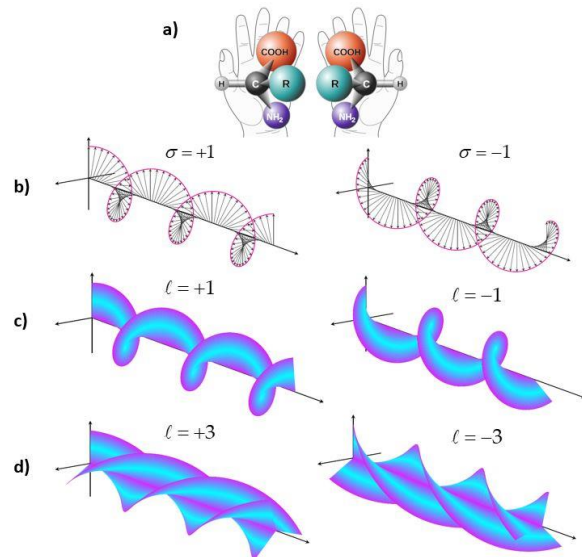
For most of history optical chirality has been associated with circularly polarised plane waves. Electric and magnetic fields trace out a helix structure on propagation, twisting either to the right or left, giving light its chirality (Fig 1). This optical chirality interacts differentially with chiral materials in a process known as optical activity [1]. There are many forms of optical activity, predominantly based on absorption or scattering of light, which are the fundamental mechanisms behind chiroptical spectroscopy [2].

Because essentially all drugs and biomolecules are chiral, chiroptical spectroscopy is critical to the pharmaceutical industry, the understanding and exploitation of biochemistry, and medicinal advances [3]. The techniques provide a wealth of information about chiral molecules, including absolute configurations, enantiomeric excesses, conformations and functionalities of biomolecules, and molecular structure of viruses [4,5]. When combined with plasmonic enhancement, hypersensitive characterisation of material chirality is possible [6].

Advances in photonics and laser technology allow exotic forms of light with complex structures to be readily generated in the laboratory [7]. Unlike the ubiquitous homogenous plane wave, these novel types of structured light possess spatially and temporally varying amplitude, phase, and polarisation. Importantly, these complex beams can possess chiral structures which are independent of the local state of polarisation. The most well-known type of structured chiral light is the optical vortex, whose wavefront is an integer number of intertwined helices which can twist to the left or right [8] (Fig 1). This chiral wavefront is characterised by the topological charge  $\ell = \pm 1, \pm 2, \dots, \pm \infty$  where the sign dictates the handedness; in contrast circular polarisation is described by the helicity  $\sigma = \pm 1$ .

Can vortex chirality be utilised in chiral spectroscopy in an analogous manner to circular polarisation? The motivation behind this question is twofold: firstly, it significantly expands the spectroscopic and photonics toolkit (e.g. in addition to circular dichroism we can get vortex dichroism); secondly, because  $\ell$  can increase in magnitude unlike  $\sigma$ , the use of vortex beams provide enhanced signals.

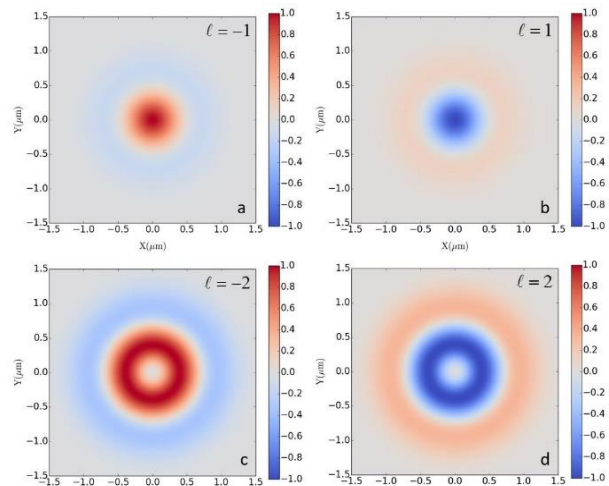
While original studies in this field suggested that it was not possible to engage the chirality of structured light in chiral spectroscopy, in the last five years significant breakthroughs in the field of structured light chirality have occurred [9]. In particular, the pivotal role of both nano-optics and plasmonic confinement has been realised: when structured laser beams and electromagnetic fields are confined into nanoscale volumes, extremely novel interactions occur. This is because chirality is a scale-dependent phenomena. We cannot place our right-



**Figure 1.** a) Material chirality with hands and molecules; b) optical chirality due to circular polarisation  $\sigma = \pm 1$  (positive sign corresponds to left-handed, negative sign right-handed); c) and d) optical vortex chirality due to the helical wavefront for  $\ell = \pm 1$  and  $\ell = \pm 3$ .

handed glove on our left hand due to the chirality of both objects, however we may place both gloves of a giant on either of our hands: our hands and the giant's gloves are chiral, but the size mismatch is so large they don't interact in a discriminatory fashion. Just like the giant's gloves, unless the laser beams and electromagnetic fields are shrunk down into tiny volumes, their chiral structures do not interact with small chiral materials in a discriminatory fashion.

Since around 2018, when breakthrough theoretical and experimental studies were published, the field of chiral spectroscopy with structured light has proliferated. Very recent start-of-the-art experiments include x-ray vortex dichroism in chiral organometallic complexes [10], vortex Raman optical activity of chiral molecular fluids [11,12]; vortex differential scattering in plasmonic-molecular hybrid systems [13]; and nonlinear vortex dichroism in chiral molecules as small as limonene and fenchone [14]. Exciting recent developments from the theoretical side include the discovery that unpolarised optical vortices are extremely unique in that they possess an optical chirality [15] (Fig 2), and therefore allow for chiral spectroscopies with unpolarised light.



**Fig 2.** Spatial distributions of optical chirality density at the focal plane of a source-unpolarised Laguerre Gaussian beam.  $p = 0$  in (a)-(d).

**Problem Statement and Objectives** The theoretical methods currently available to model and guide experiments in chiral spectroscopy with structured light are limited to general and qualitative analytical theory. Many such theories, which have stimulated the aforementioned experimental advances, stem from my own research over the last few years, e.g. [16–21]. However, it is well known that to quantitatively describe electromagnetic fields and light-matter interactions in nano-optics and photonics requires numerical methods. The number and complexity of new experimental techniques in the field is rapidly growing. For structured light chirality to fulfil its potential in applications within photonics and chiral spectroscopies, and for these techniques to transition from discovery science to widespread implementation outside academia and impact society, more sophisticated theoretical modelling is crucial. The Objectives of this project constitute the required developments which will allow structured light chirality to become a keystone in chiral photonics and chiroptical spectroscopy.

**Objectives 1)** Produce numerical theory which provides accurate simulations of Rayleigh optical activity of structured light in plasmonic nanostructures.

**2)** Develop numerical methods which provide accurate simulations and spectra of Raman optical activity of structured light in chiral molecular systems.

**3)** Experimental observation of nonlinear Rayleigh vortex optical activity in nano-helices.

**Methodology:** For **Objective 1** the most efficient method of producing numerical simulations involving plasmonic nanostructures interacting with arbitrary electromagnetic fields is to use the *complete* software package offered by the Wave Optics module in COMSOL Multiphysics. Using the near-to-far field transformation we can extract the relevant quantities (Stokes parameters) which correspond to the measurable observables in the scattering of chiral structured light off chiral nanostructures. We will focus specifically on Rayleigh and hyper-Rayleigh optical activity (i.e., a chiral material elastically scatters left-handed light at a different



rate to right-handed light, in both the linear and nonlinear regime), as these are the most important forms of chiroptical spectroscopy for nanostructures. We will explore extensively both the material and optical parameter space by studying the influence of material composition, orientation, shape, and dimensions, and the beam polarisation, degree of focusing, optical phase, and mode indices (e.g., topological charge, radial index), respectively. Exploration of the optical parameter space is particularly exciting: the future of structured light lays in understanding how to optimise the beam structure to achieve maximum benefits within a given application. Exotic chiral modes we would study include the spirally polarised, helical Mathieu, vector-vortex, and Poincaré beams.

For **Objective 2** involving chiral molecular systems a different approach will be implemented. This will involve the combination of vector-diffraction theory [22] and semi-classical optics [1] within MATLAB to write code which is tailored for purpose. In chiral (bio)molecular systems it is chiroptical spectroscopy based on Raman (vibrational) optical activity which gives the most useful structural information, and it is this form of optical activity which will be concentrated upon. Like in the methodology for **Objective 1**, we will calculate the relevant Stokes parameters which relate to the experimental observables [1]. We will once again explore the experimental parameter space, both optical and material. In the latter case, I will collaborate with computational chemists Dr Garth Jones and Dr Vasily Oganessian at UEA where they will provide the expertise in quantum chemical calculations (with the aid of the high-performance computer (HPC) cluster at UEA) to predict spectra for specific chiral molecules.

**Objective 3** will be carried out in collaboration with Professor Ventsislav Valev's MultiPhoton NanoPhotonics research group at the University of Bath. This group are leading experiments in nonlinear optical activity in nanostructures. They were the first group in the world to experimentally observe hyper-Rayleigh optical activity [23], and have recently discovered a new way to study material chirality through third-harmonic Mie scattering [24]. We will use an ultrafast laser (Ti:Sapphire, 70 fs pulses, 1 MHz, with tunable wavelength and group delay dispersion) directed through spiral phase plates  $\ell = \pm 1, \pm 2$  prior to illuminating a suspension of Ag nano-helices (size < 100 nm). After optically filtering out the fundamental wavelength, the nonlinear optical signal will be detected with a hand-picked, highly sensitive, ultra-low dark count photomultiplier tube. The numerical methods developed within **Objective 1** will provide the qualitative and quantitative theory to complement and aid the understanding of the experimental results.

**Outcomes** The main outcomes of this project can be described by Milestones (**MS**).

**MS1:** A systematic numerical description of Rayleigh optical activity (linear) spectroscopy of optical vortex beams in arbitrary chiral plasmonic nanostructures.

**MS2:** A numerical theory of hyper-Rayleigh optical activity (nonlinear) spectroscopy of optical vortex beams in arbitrary chiral plasmonic nanostructures.

**MS3:** Determination of the optimal chiral structured light for chiroptical Rayleigh spectroscopy of nanostructures.

**MS4:** Tailored for purpose numerical theory of Raman optical activity spectroscopy in chiral molecules using structured light.

**MS5:** First experimental observation of nonlinear Rayleigh optical activity of optical vortices.

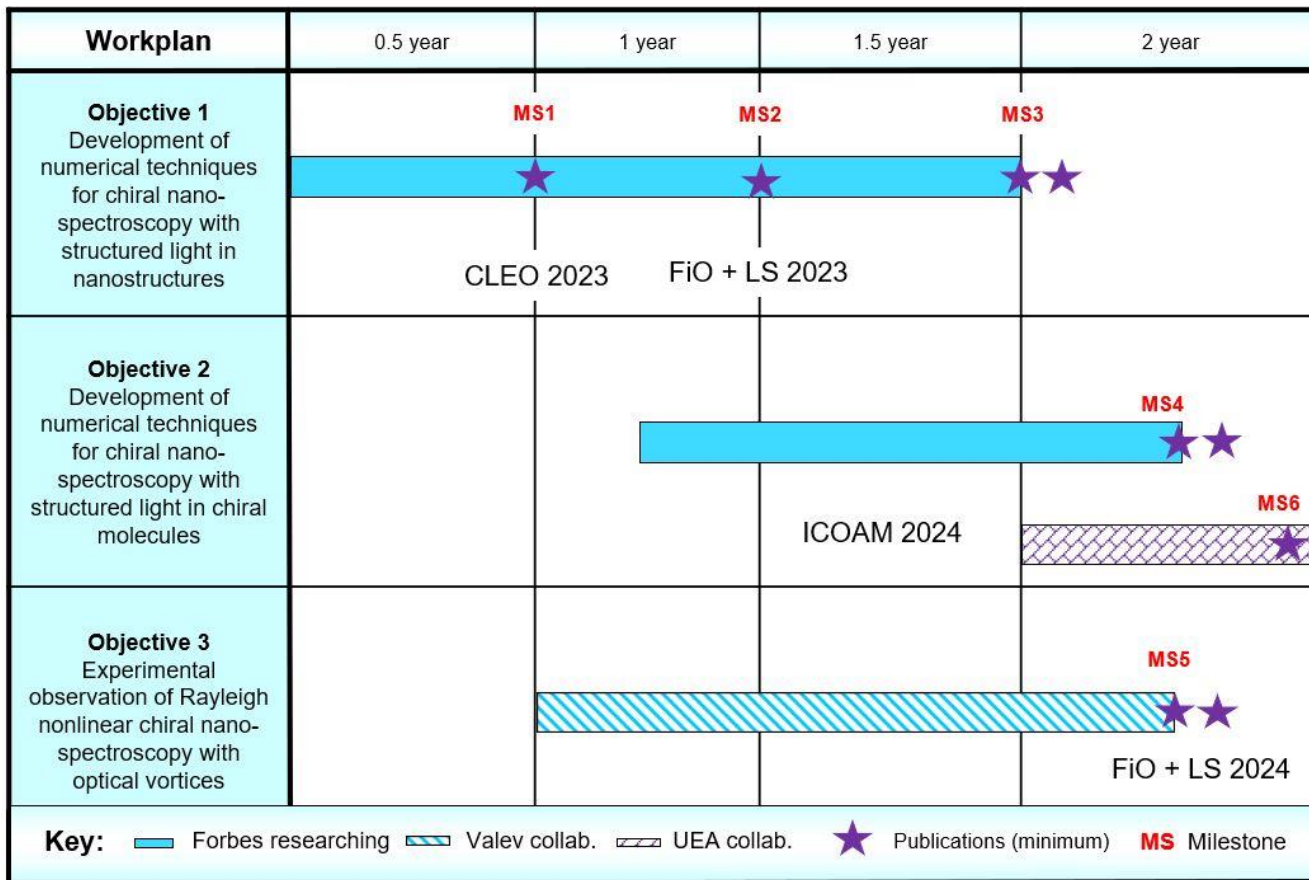
**MS6:** Predicted Raman optical activity spectra with optical vortex light for a specific chiral molecule, e.g., limonene.



**Impact** The immediate impact of this project will be the development of new ways to study chiral materials using light. These materials will range from nanostructures and metamaterials, to molecular matter including drugs and biomolecules which are key to pharmaceutical and medicinal advances. Beyond the new chiroptical spectroscopic developments, the principles that the numerical work establish will also be applicable to chirality-based biosensing [25]. The techniques developed will also be important in the wider field of chiral photonics. Chiral light is central to many photonic technologies, including optical communication, computing, and information processing based on miniature integrated devices which possess the ability to sense and discriminate the chirality of the light. A major impact of this work is paving the way for the next generation of chiral photonic media based on structured light illumination.

## References

1. L. D. Barron, (Cambridge University Press, 2009).
2. P. L. Polavarapu, (CRC Press, 2016).
3. M. Krupová, J. Kessler, and P. Bouř, *ChemPlusChem* **85**, 561 (2020).
4. E. Hendry, T. Carpy, J. Johnston, M. Popland, R. V. Mikhaylovskiy, A. J. Laphorn, S. M. Kelly, L. D. Barron, N. Gadegaard, and M. Kadodwala, *Nature nanotechnology* **5**, 783 (2010).
5. T. Kakkar, C. Keijzer, M. Rodier, T. Bukharova, M. Taliany, A. J. Love, J. J. Milner, A. S. Karimullah, L. D. Barron, N. Gadegaard, A. J. Laphorn, and M. Kadodwala, *Light Sci Appl* **9**, 195 (2020).
6. X.-T. Kong, L. V. Besteiro, Z. Wang, and A. O. Govorov, *Advanced Materials* **32**, 1801790 (2020).
7. A. Forbes, M. de Oliveira, and M. R. Dennis, *Nature Photonics* **15**, 253 (2021).
8. Y. Shen, X. Wang, Z. Xie, C. Min, X. Fu, Q. Liu, M. Gong, and X. Yuan, *Light: Science & Applications* **8**, 1 (2019).
9. K. A. Forbes and D. L. Andrews, *J. Phys. Photonics* **3**, 022007 (2021).
10. J. R. Rouxel, B. Rösner, D. Karpov, C. Bacellar, G. F. Mancini, F. Zinna, D. Kinschel, O. Cannelli, M. Oppermann, C. Svetina, A. Diaz, J. Lacour, C. David, and M. Chergui, *Nat. Photon.* **1** (2022).
11. F. Büscher, S. Müllner, D. Wulferding, Y. G. Pashkevich, V. Gnezdilov, A. A. Peshkov, A. Surzhykov, and P. Lemmens, *Low Temperature Physics* **47**, 959 (2021).
12. S. Müllner, F. Büscher, A. Möller, and P. Lemmens, *arXiv preprint arXiv:2208.03793* (2022).
13. J. Ni, S. Liu, D. Wu, Z. Lao, Z. Wang, K. Huang, S. Ji, J. Li, Z. Huang, Q. Xiong, Y. Hu, J. Chu, and C.-W. Qiu, *Proc Natl Acad Sci USA* **118**, e2020055118 (2021).
14. J.-L. Bégin, A. Jain, A. Parks, F. Hufnagel, P. Corkum, E. Karimi, T. Brabec, and R. Bhardwaj, (2022).
15. K. A. Forbes, *Physical Review A* **105**, 023524 (2022).
16. K. A. Forbes and D. L. Andrews, *Optics Letters* **43**, 435 (2018).
17. K. A. Forbes, *Physical Review Letters* **122**, 103201 (2019).
18. K. A. Forbes, *J. Opt.* **22**, 095401 (2020).
19. K. A. Forbes and G. A. Jones, *J. Opt.* **23**, 115401 (2021).
20. K. A. Forbes and G. A. Jones, *Phys. Rev. A* **103**, 053515 (2021).
21. K. A. Forbes and D. Green, *Optics Communications* **515**, 128197 (2022).
22. B. Richards and E. Wolf, *Proceedings of the Royal Society of London. Series A. Mathematical and Physical Sciences* **253**, 358 (1959).
23. J. T. Collins, K. R. Rusimova, D. C. Hooper, H.-H. Jeong, L. Ohnoutek, F. Pradaux-Caggiano, T. Verbiest, D. R. Carbery, P. Fischer, and V. K. Valev, *Physical Review X* **9**, 011024 (2019).
24. L. Ohnoutek, J.-Y. Kim, J. Lu, B. J. Olohan, D. M. Rășădean, G. Dan Pantoș, N. A. Kotov, and V. K. Valev, *Nature Photonics* **16**, 126 (2022).
25. W. Ma, L. Xu, L. Wang, C. Xu, and H. Kuang, *Advanced Functional Materials* **29**, 1805512 (2019).



## EXECUTIVE SUMMARY

Alzheimer's Disease (AD) is the most common form of dementia that results in cognitive deficit including loss of planning, personality, and memory. In the United States, AD is ranked as the third leading cause of death, and approximately 5 million Americans above 65 years of age suffer from dementia caused by AD. AD is generally attributed to the maladaptive accumulation of amyloid- $\beta$  protein (A $\beta$ ) extracellular plaques and intracellular neurofibrillary Tau tangles. These protein aggregates are thought to be the leading cause of neuronal cell loss and brain atrophy. An avenue of research that has attracted attention of many scientists is the role of Mitochondria in AD pathogenesis and progression. Mitochondria are pivotal metabolic and energetic machinery of cellular function crucial for energy homeostasis. Notably, **mitochondria dysfunction-mediated metabolic deficiencies are an early marker of pathogenesis of AD, however, the role of mitochondria in the disease progression is yet to be elucidated**, in particular regarding the rapid cascade of neuronal apoptosis. There is significant evidence that increased levels of A $\beta$  proteins interact with mitochondrial proteins, and cause disruption in fission and fusion processes, boost reactive oxygen species production, and deteriorate mitochondrial function. **Optical quantitative assessment of mitochondrial function and health can be done through several image-based bioenergetic parameters**, including their size, shape and their dynamic activities such as, membrane potential activity; all of which can be estimated using fluorescence imaging.

**A challenge in studying AD is the limitation of current optical microscopy technologies to image at organelle-level resolution deep inside of *in vivo* brain**, which has led many scientists to be reliant on *in vitro* studies. Multiphoton microscopy modalities leverage the long mean-free-path (MFP) of near-infrared light to penetrate deeper into biological tissue. However, the long wavelength of the excitation light negatively affects the resolution and makes imaging of sub-cellular features non-trivial, if not impossible. In this proposal, **we aim to address this problem by developing a novel 3-photon superresolution microscope that utilizes fluorescence excitation modulation and Adaptive Optics to achieve superresolution imaging at a depth of more than 0.5mm in the mouse brain**. This will allow to cover cortical layers III up to IV/V. The new microscope enables quantitative assessment of mitochondrial function and health through several bioenergetic parameters, including their size, shape and their dynamic activities such as, membrane potential activity *in vivo*, which facilitates studying their role in AD pathogenesis, and allows future exploration of potential therapies and drug discovery. In this proposal, we aim to address these problems by producing a novel microscope that is capable of deep tissue superresolution across multiple regions of the brain.

Imaging deeper requires longer wavelength light. However, longer wavelength increases the width of the point spread function (PSF), hence deteriorating the resolution. To improve the resolution, we aim to develop a novel microscope that takes advantage of an established technology called Coherent Control (CC), which enables modulation of fluorescence by phase modulation of broadband ultrafast beams. Ultimately based on stimulated emission depletion (STED) microscopy, we will develop a two-beam CC modulation of a Gaussian Excitation and a Vortex modulation beam, to decipher information from a restricted area close to the center of the focus. The two beams have different dispersion regimes and modulation frequencies which produce spatiotemporally varying wave-packets. Therefore, by solving for the frequency components assigned to the center of the PSF, imaging beyond the diffraction-limit becomes possible. This technique - called Modulated EXcitation IMaging (MEXIM) requires the ideal shape of the two PSFs deep inside of the tissue. Even with near-infrared light, beyond the MFP distortions can significantly distort the PSFs. This issue can be resolved by employing Adaptive Optics technology to restore the diffraction-limited imaging at high depth and enhance the fidelity of the beams. The MEXIM microscope is expected to achieve resolution of <150nm at a depth of >0.5mm inside of the *in-vivo* brain, at an imaging rate of 1 Hz. Since mitochondria have a size range of 200-500nm, this resolution would be ideal for imaging and analysis of their morphology.

This novel microscope provides an excellent tool which enables future therapeutic research and drug discovery.

## A. LITERATURE REVIEW

**A1. Alzheimer's Disease.** Approximately 5 million Americans above 65 years of age suffer from dementia caused by AD<sup>3</sup>. In the United States, AD is ranked as the third leading cause of death<sup>4</sup>. AD is the most common form of dementia and generally attributed to the maladaptive accumulation of amyloid- $\beta$  protein (A $\beta$ ) extracellular plaques and intracellular neurofibrillary Tau tangles. These protein aggregates are thought to be the leading cause to neuronal cell loss and brain atrophy, by rendering neuronal mitochondria dysfunctional. Mitochondria are pivotal metabolic and energetic machinery of

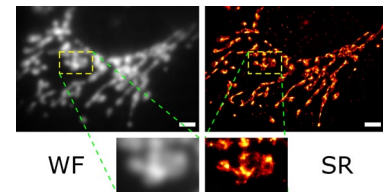


Figure 1 – Comparison of widefield (WF) and Super-resolution (SR) imaging of mitochondria. Several mitochondria that were not distinguishable are resolved in the SR image. Adapted from reference <sup>1</sup>.

cellular function. Notably, mitochondria dysfunction-mediated metabolic deficiencies are an early marker of pathogenesis of AD. However, the role of mitochondria in the disease progression and particularly in the rapid cascade of neuronal apoptosis, is yet to be elucidated<sup>5,6</sup>. **Quantitative assessment of mitochondrial function and health can be done through several bioenergetic parameters, including their size, shape and their dynamic activities such as, membrane potential activity<sup>7</sup>; all of which can be estimated using fluorescence imaging<sup>8</sup>.** There is significant evidence that increased soluble A $\beta$  levels as well as their clustered accumulation interact with mitochondrial proteins, and cause disruption in fission and fusion processes<sup>9-11</sup>, boost reactive oxygen species production<sup>12</sup>, and deteriorate mitochondrial function<sup>13</sup>. Most research on the etiology of AD, and the association of A $\beta$  toxicity with mitochondrial dysfunction, have been limited to *in vitro* studies<sup>7</sup>. The lack of *in vivo* studies is mainly due to a dearth of superresolution techniques successfully imaging deep into the brain, which restricts organelle-level-resolution imaging to regionally confined and superficial layers of the cerebral cortex. **In this proposal we aim to address this problem by using multi-photon excitation process microscopy to penetrate deeper inside of the brain and take a STED-like approach to improve the resolution. We will employ Adaptive Optics technology to minimize the optical aberrations and ensure the success of the method.**

**A2. Superresolution imaging of mitochondrial structures.** Mitochondria are the organelles responsible for energy generation of the cell in the form of adenosine triphosphate (ATP), which gives them a significant role in cellular metabolism regulation<sup>14</sup>. Mitochondrial structure and dynamic activity analyses are therefore of utmost significance to understand cell processes that occur throughout the brain and nervous system<sup>15,16</sup>. A cell's surrounding environment is known to have significant effect on the mitochondrial fission (separation), fusion (join together), and transport rates. Mitochondria of a cell in energy stress, show a higher rate of fission and lower rate of fusion<sup>17</sup>. They also go through elongation to boost ATP synthesis<sup>18</sup>. Given these characteristics, morphological features of mitochondria such as shape (e.g. circular or tubular), size, and their network structure, can produce significant insight to the metabolism and health of a cell or tissue. **In AD in particular, it has been shown that presence of A $\beta$  protein disrupts mitochondria transport, fission and fusion<sup>9-11</sup>.** Mitochondria, however, have a size range of 200~500 nm, they are abundant in the cell cytoplasm, and exist in close proximity of each other<sup>19,20</sup>. Therefore, conventional optical imaging modalities fail to image an individual mitochondrion within their contiguous layers (figure 1). With the advent of fluorescent superresolution microscopy modalities, visualizing the highly dynamic and regulated networks and processes of mitochondria entered a new era<sup>1,21,22</sup>. Methods including 3D structured illumination microscopy<sup>22</sup> with a 120nm lateral and 360nm axial resolution, TIRF-SIM<sup>23</sup>, and 2D stochastic optical reconstruction microscopy<sup>1,21</sup> (STORM) with 40nm lateral resolution, and stimulated emission depletion microscopy<sup>24,25</sup> (STED) with ~30nm resolution, enabled sub-diffraction-limit analysis of individual mitochondria. However, each of these methods perform extremely well on a monolayer of cells, when no significant optical aberration is present, yet fail in thick tissue<sup>2,26</sup>.

### **A3. Coherent Control of fluorescence**

Coherent control is a technique in ultrafast optics that leverages the phase of a laser source to control the efficiency of a light-dependent chemical process. In microscopy, this has been

used as a contrast mechanism to maximize the signal from a subset of fluorophores while minimizing the signal by spectral-interference within ultrafast pulses<sup>27</sup>. Myriads of pulse shape designs have been used, including sinusoidal phase shapes to modulate the peak wavelength for multiphoton absorption<sup>28</sup>, pseudorandomly-generated binary phase masks for selective excitation of narrow spectral bands for spectroscopy and cross-section measurements<sup>29-31</sup>, among other methods for controlling multiphoton processes. These same phase shaping techniques have been used to generate transform-limited optical pulses following system dispersion, group delay dispersion to linearly decrease the efficiency of an optical process, and third-order dispersion as well to shift fluorescence efficiency towards desired spectral bands<sup>32</sup>. Most recently, the principle has even been used to realize super resolution imaging<sup>33</sup>.

**A4. Adaptive Optics deep tissue imaging.** Biological tissues distort the optical wavefront even at moderate depths, hence an aberrated Point Spread Function reduces the resolution of microscopy<sup>34</sup>. Adaptive Optics (AO) is used in microscopy to correct both low<sup>35</sup> and high<sup>36</sup> order aberrations caused by a disordered transmission medium. AO has been implemented on many types of microscopy modalities including confocal<sup>37</sup>, 2-photon<sup>38</sup> and 3-photon<sup>39</sup> scanning microscopy modalities. We previously used AO for correcting aberrations and superresolution imaging in the brain of *drosophila*<sup>2,26</sup> using a deformable mirror (DM), and showed that without AO correction deep tissue superresolution imaging is unlikely to produce meaningful results. Compared to single-photon excitation, the improvement in the Strehl ratio of the 2 and 3 photon excitation point spread function (PSF), leads to a greater improvement in the signal due to their quadratic and cubic power dependence<sup>40</sup>. Therefore, **AO promises significant benefits in signal strength when combined with multi-photon microscopy, for deep tissue imaging inside of the brain.**

## **B. PROBLEM STATEMENT/OBJECTIVES**

In line with the Optica Foundation Challenge's vision to advance optical technologies in the medical arena, the current proposal will develop a technology to address a critical need for super-resolution microscopy of sub-cellular features deep inside of the murine brain to assess and evaluate the underlying mechanisms of AD progression. The technological advancements raised by this cutting-edge microscope help to answer critical questions in neuro-degenerative diseases, which gives the proposed work the potential to be transformative. There are several aspects of innovation within this proposal. We will:

- Develop the first multi-photon superresolution with the capability of imaging with <150nm resolution laterally, and <200nm axially. Exploiting the longer mean-free-path of multi-photon imaging and a spatiotemporal PSF modulation approach, we will demonstrate deep brain imaging with superresolution.
- First implementation of Coherent Control (CC) of laser pulses for multi-photon super-resolution microscopy. This novel technique, called modulated excitation imaging (MEXIM), leverages CC for modulation of multi-photon fluorescence excitation, and extract information from a restricted area at the center of the PSF.
- Adaptive Optics correction of optical aberration to restore diffraction-limited PSF and enable MEXIM imaging at a depth of more than 500µm.

## **C. WORK PLAN**

### **C1. Modulated Excitation Imaging (MEXIM) of mitochondria structure and metabolism.**

Near-Infrared (NIR) excitation wavelengths of multi-photon microscopy enables deep-tissue imaging with the sacrifice of the resolution. More recently 3PE process has attracted attentions due to the water absorption minima of 1300 and 1700 nm (GFP and RFP respectively)<sup>41-43</sup>. However, either 2PE or 3PE imaging of GFP (940nm and 1300nm) produce resolution >500nm<sup>44</sup> inside of the brain. While this resolution is sufficient for cell-level monitoring of neural activity, for imaging sub-cellular organelles it is extremely large. To overcome this issue, we propose to use a double-beam coherent control (DBCC) approach that surpasses the limitations of the traditional STED, to provide a true reduction in the multiphoton PSF. Previous efforts at multiphoton STED use single-photon depletion which limits the penetration depth, due to the mean-free-path length of the depletion light, and defeats the purpose of using a multiphoton process<sup>45-47</sup>. Coherent control method has shown a great promise in modulating



fluorescence emission<sup>27-33,48</sup> by adjusting the dispersion regimes of the ultrafast pulses. Our approach is to produce a transform-limited ultrafast pulse, and modulate it by super-imposing a second beam that detunes its perfect dispersion regime. Using this scheme we can intensity modulate the detuning beam and produce wave packets of fluorescence emission at our desired frequencies. The final signal will be demodulated using a lock-in-amplifier.

The realization of this technique will be using an ultrafast pulsed laser beam which will be split into two branches with different dispersion regimes. Each path is amplitude modulated at different frequencies - using a known temporal function such as  $\cos(\omega_i t)$ , where  $i$  is the beam frequency number - when combined colinearly on the sample, DBCC will produce a wave packet at a new frequency. **The produced wave packets are a function of DBCC spectral-phase modulation, and modulation frequency of the two beams.** The signal produced at the target molecules can be demodulated by precisely monitoring the temporal pulse envelopes. For instance, by using a Lock-in-Amplifier (LIA) approach, the acquired signals can be demodulated to produce information only on the exact frequency of interest. In this proposal we aim to use this previously proven technique, with the difference that in our implementation, one of the branches will also be spatially shaped to make a vortex PSF for the modulation (depletion beam in STED) of outer lobe of the Gaussian excitation PSF. We refer to these two beams as modulation (mod.) and excitation (ex.) beams, respectively. The Gaussian ex. beam is defined by  $a(r) = a_0 \exp(-r^2/2\sigma^2)$ , and the mod. beam has the form of a zero-center vortex given by  $b(r) = b_0 (J_2(krNA)/krNA)^2$ , where  $k$  is the wavenumber and  $NA$  is numerical aperture,  $a_0$  and  $b_0$  are the maximum intensities of their respective beams. The two beams together will produce spatially varying wavepacket with different frequencies, which can be categorized by their contribution to the effective PSF into 3 groups, 1) contribution from ex. beam only ( $f_1$ ), 2) contribution from mod. beam only ( $f_2$ ), and 3) dual contributions ( $f_1+f_2$  and  $f_1-f_2$ ). **Because these two beams have different spatial distributions, and at the center of the effective PSF only the excitation beam contributes, therefore solving for these contributions will result in extracting signal restricted to only the center of the PSF.** Our simulation of 3PE MEXIM shows a factor of 3 improvement in the effective resolution using MEXIM approach with final resolution of 117nm in ideal experimental situation (figure 2). We expect to achieve a resolution of <150nm in practice. We will base demodulation on measurement of both beam envelopes and extracting information from the multiphoton signal by using an LIA. The output signal used for image reconstruction will be determined by subtraction of dual beam

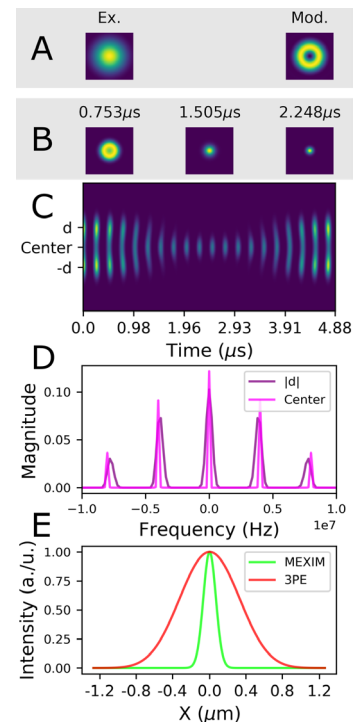


Figure 2 - Simulation of 3PE WPI,  $\lambda=1.3\mu\text{m}$ ,  $NA=1.05$ , (A) ex. and mod. beams. (B) effective PSF at different timepoints. (C) crosssection of effective PSF timeseries. (D) power spectrum of ex. and mod. (E) 3PE and MEXIM PSFs show 3x improvement in resolution. For presentation purpose only,

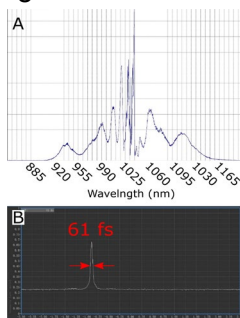


Figure 3 - Supercontinuum source will be optimized for 3P excitation. (A) current spectrum, (B) pulse duration.

contributions from the ex. beam only contribution. This allows deciphering of the signal from a restricted area close to the center of the two PSFs, to reconstruct a superresolution image.

**Experimental plan:** The proposed system consists of a LightConversion Flint ultrafast laser which produces 1040 nm. The output of the laser will be coupled into a Photonic Crystal Fiber to produce supercontinuum<sup>49</sup> from 920-1100nm (figure 3), which then will be launched into a Periodically Poled Lithium Niobate (PPLN) to produce 1300nm. In this project the neuronal mitochondria of **AD mouse model (5xFAD)** will be expressing 1) GFP for structural analysis, and 2) TMRE for MMP measurement and A $\beta$  plaques will be stained using Methoxy-XO<sub>4</sub>. We will perform regular 2PE imaging of A $\beta$  plaques and MMP<sup>50</sup> for precise localization of the center of the plaque, and metabolism respectively.



**MEXIM super-resolution imaging of GFP-tagged mitochondria for morphological analysis will be using the 3PE process.** It has been shown in the past that 3PE using 1320

nm is more power-efficient, and produces higher signal to background ratio than 920 nm 2PE of GFP<sup>51</sup>. For the 3PE process we will optimize our supercontinuum source to produce <50 fs pulses within the 3PE excitation spectrum of GFP to produce high SNR signal.

The two branches of the beam (excitation and modulation) go through amplitude modulation using Pockels cells to produce the wave-packets (figure 4). A Spatial light modulator (SLM) will be used for the generation and optimization of phase masks required for the vortex beam.

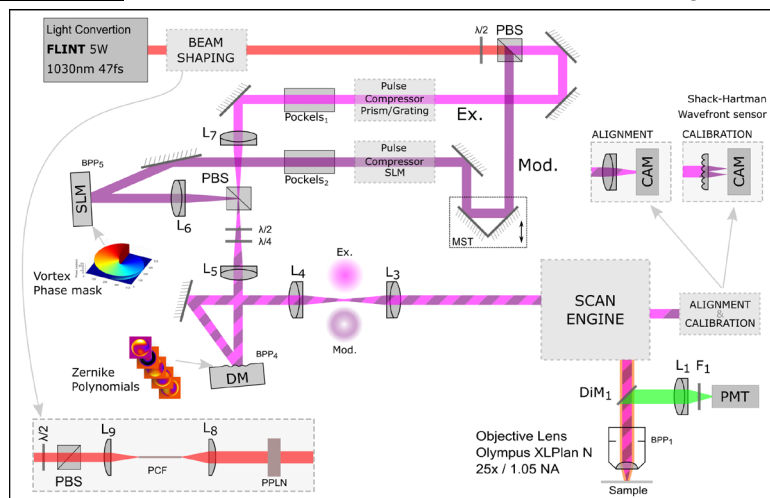


Figure 4 –MEXIM Microscope diagram. BPP: Back-pupil plane, BS: 1% Beam sampler, CAM: Camera, DiM: DiChroic mirror, DM: Deformable Mirror, F: Filter, IP: Image plane, L: Lens, MST: Motorized stage, PBS: Polarizing Beam Splitter, PCF: Photonic Crystal Fiber, PMT: Photon-Multiplier Tube, PPLN: Periodically Poled Lithium Niobate, SLM: Spatial Light Modulator. Excitation (Ex.) and Modulation (Mod.) beams are shown in bright and dark purple, respectively.

**C2. Adaptive Optics enhancement of beam fidelity at depth.** Since deep tissue imaging

requires correction of the wavefront distortions caused by the tissue, we will employ AO for depth enhancement. MEXIM microscopy requires maintenance of the precise shape of the ex. and mod. beams to achieve superresolution imaging. Although 2- and 3-photon excitation has shown an imaging depth range of 1-2 mm in brain<sup>42,52,53</sup> tissue, the mean-free-path of the near-IR light in brain is 170~200µm<sup>42,53</sup>. Beyond this depth, optical aberrations begin to degrade the PSF up to a point where the out-of-focus signal becomes more significant than in-focus signal<sup>54</sup>. To mitigate this problem, we will use sensor-less AO<sup>2,26,55</sup> technology with modal correction algorithm<sup>56</sup>. There is large body of literature which shows AO enables restoration of diffraction-limited PSF deep inside of the brain, as well as improving the maximum achievable depth<sup>57,58</sup>. We have previously shown that STORM superresolution microscopy inside of the central nervous system of *drosophila melanogaster* (figure 5), is only possible with AO. In this proposal we will use a model-based correction approach, which leverages Zernike polynomials (up to the 4<sup>th</sup> order) for modeling of the wavefront distortions. We expect the application of AO to MEXIM microscopy enables deep imaging up to 3 mean-free-paths from the brain surface, and achieve a depth of more than 500µm.

**Expected outcomes** Superresolution imaging of mitochondria with the resolution of 150nm, would give us a precise measure of mitochondria quantity, morphology, to gauge their metabolism with respect to their distance from the center of the plaque. This will result in an understanding of the mitochondrial morphology early-onset, mild, and severe AD. Combined with AO we expect to extend this resolution to planes deeper than 500 µm which enables imaging of layer III up to layer IV/V of the cortex, with an unprecedented superresolution at this depth. These datasets will be analyzed together to discover possible trends and correlation between these parameters and use it in potential future research on application of possible therapeutics.

**IMPACT** This novel microscope provides a window of opportunity for future therapeutic research and drug discovery. Success in this project enables many researchers to study therapeutic compounds, which reduce the burden of Aβ toxicity on the neuronal health, hence enhancing the quality of life of AD patients through optical methods.

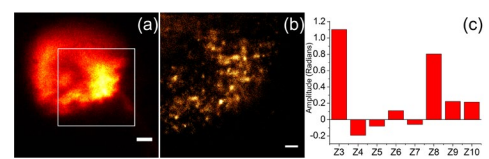


Figure 5 - AO correction enables super-resolution microscopy inside of the central nervous system of Drosophila. A widefield image (a), STORM image after aberration correction(b), and magnitude of Zernike modes corrected (c). Scale bar is 2 µm.<sup>2</sup>

## REFERENCES

1. Xu, J., et al., *ACS Nano* **2015**, 9 (3), 2917.
2. Tehrani, K. F., et al., *Optics Express* **2015**, 23 (10), 13677.
3. James, B. D., et al., *Neurology* **2014**, 82 (12), 1045.
4. Weuve, J., et al., *Alzheimer's & dementia : the journal of the Alzheimer's Association* **2014**, 10 (2).
5. Lopez Sanchez, M. I. G., et al., *British J. Pharmacology* **2019**, 176 (18), 3464.
6. Perez Ortiz, J. M., et al., *Br J Pharmacol* **2019**, 176 (18), 3489.
7. Xie, H., et al., *The Journal of Neuroscience* **2013**, 33 (43), 17042.
8. Bereiter-Hahn, J., et al., *Mitochondrial Dynamics*.
9. Wang, X., et al., *PNAS* **2008**, 105 (49), 19318.
10. Calkins, M. J., et al., *Human Molecular Genetics* **2011**, 20 (23), 4515.
11. Manczak, M., et al., *Human Molecular Genetics* **2011**, 20 (13), 2495.
12. Keller, J. N., et al., *J Neurochem* **1997**, 69 (1), 273.
13. Mattson, M. P., et al., *Brain Res* **1998**, 807 (1-2), 167.
14. Babbar, M., et al., *Mol Cell Pharmacol* **2013**, 5 (3), 109.
15. Li, Z., et al., *Cell* **2004**, 119 (6), 873.
16. Hollenbeck, P. J., et al., *Journal of Cell Science* **2005**, 118 (23), 5411.
17. Van Der Bliek, A. M., et al., *Cold Spring Harb Perspect Biol* **2013**, 5 (6).
18. Liesa, M., et al., *Cell Metab* **2013**, 17 (4), 491.
19. Betzig, E., et al., *Science* **2006**, 313 (5793), 1642.
20. Kennady, P. K., et al., *Cytometry* **2004**, 62A (2), 97.
21. Shim, S.-H., et al., *Proceedings of the National Academy of Sciences* **2012**, 109 (35), 13978.
22. Shao, L., et al., *Nat Meth* **2011**, 8 (12), 1044.
23. Brunstein, M., et al., *Optics Express* **2013**, 21 (22), 26162.
24. Schmidt, R., et al., *Nat Meth* **2008**, 5 (6), 539.
25. Schmidt, R., et al., *Nano Letters* **2009**, 9 (6), 2508.
26. Tehrani, K. F., et al., *Biomed Opt Express* **2017**, 8 (11), 5087.
27. Ogilvie, J. P., et al., *Optics Express* **2006**, 14 (2), 759.
28. Walowicz, K. A., et al., *The Journal of Physical Chemistry A* **2002**, 106 (41), 9369.
29. Lozovoy, V. V., et al., *Physical Review A* **2006**, 74 (4), 041805.
30. Xu, B., et al., *Applied Optics* **2010**, 49 (32), 6348.
31. Comstock, M., et al., *Optics Express* **2004**, 12 (6), 1061.
32. Labroille, G., et al., *Optics Letters* **2010**, 35 (20), 3444.
33. Liu, C., et al., *Science Advances* **2020**, 6 (16), eaaw6579.
34. Tehrani, K. F., et al., *Journal of Biomedical Optics* **2017**, 22 (3), 036012.
35. Kubby, J. A., *Adaptive Optics for Biological Imaging*. CRC Press: New York, NY, 2013; p 388.
36. Akbulut, D., et al., *Optics Express* **2011**, 19 (5), 4017.
37. Booth, M. J., et al., *Proc. Natl. Acad. Sci. USA* **2002**, 99 (9), 5788.
38. Ji, N., et al., *Nat Methods* **2010**, 7 (2), 141.
39. Tao, X., et al., *Biomed Opt Express* **2017**, 8 (3), 1277.
40. Hernández, F. E., et al., *Applied Optics* **2004**, 43 (28), 5394.
41. Guesmi, K., et al., *Light: Science & Applications* **2018**, 7 (1), 12.
42. Wang, T., et al., *Nat Meth* **2018**.
43. Rowlands, C. J., et al., *Light: Science & Applications* **2017**, 6, e16255.
44. Gu, M., *Optics Letters* **1996**, 21 (13), 988.
45. Takasaki, Kevin t., et al., *Biophysical Journal* **2013**, 104 (4), 770.
46. Otomo, K., et al., *Biomed Opt Express* **2018**, 9 (6), 2671.
47. Bianchini, P., et al., *Proceedings of the National Academy of Sciences* **2012**, 109 (17), 6390.
48. Dudovich, N., et al., *Nature* **2002**, 418 (6897), 512.
49. You, S., et al., *Nature Communications* **2018**, 9 (1), 2125.
50. Tehrani, K. F., et al., *Biomed Opt Express* **2018**, 9 (1), 254.
51. Wang, T., et al., *eLife* **2020**, 9, e53205.
52. Horton, N. G., et al., *Nat Photon* **2013**, 7 (3), 205.
53. Yildirim, M., et al., *Nature Communications* **2019**, 10 (1), 177.
54. Theer, P., et al., *J Opt Soc Am A Opt Image Sci Vis* **2006**, 23 (12), 3139.
55. Booth, M. J., *Optics Letters* **2007**, 32 (1), 5.
56. Booth, M. J., *Optics Express* **2006**, 14 (4), 1339.
57. Galwaduge, P. T., et al., *Biomed Opt Express* **2015**, 6 (8), 2997.
58. Kong, L., et al., *Optics Express* **2016**, 24 (2), 1214.

## Immune Cell Tracking with Adaptive Illumination

Highly motile immune cells actively migrate in various organs and tissues in normal and disease states to initiate efficient immune response. Understanding how the immune cells migrate in various organs under various conditions is important for finding disease treatments. The major technology used for immune cell tracking in intact, living tissue is multiphoton fluorescence microscopy. As a nonlinear process, however, multiphoton excitation generates an inherently weaker signal than one-photon excitation, and high excitation power is typically required for fast tracking deep within intact tissues. Because multiphoton microscopes typically operate at the photon shot-noise limit, the maximum number of cells that can be tracked at high spatial and temporal resolution is fundamentally limited by the number of signal photons, which in turn is determined by the maximum permissible average and peak power in biological specimens. Therefore, the fundamental limit for technologies aimed at measuring real-time immune cell migration in intact tissues is the photon budget: the number of signal photons obtainable from the sample within a given period of time. Simply scanning fast, while necessary, is not sufficient for high speed and large volume imaging. This proposal will create new imaging technologies to address this fundamental challenge in dynamic immune cell imaging.

To address the fundamental limit of the photon budget, we will develop adaptive cell tracking (ACT) that will illuminate only the ROIs. A one to two orders of magnitude gain in photon budget can be achieved by ACT because the ROIs usually only occupy a small fraction of the imaging volume (1-10%). This gain in photon budget can directly translate to an increase in imaging volume or imaging speed (or a combination of the two), without increasing the excitation power on the sample or sacrificing signal-to-noise ratio (SNR). (1) To demonstrate the concept of ACT, we will image T cell migration in a live mouse by using 3D ROI localization algorithms and direct modulation of the laser output to illuminate only the ROIs. This demonstration will show how much photon budget can be saved with ACT when compared to that without ACT. However, the direct modulation of the laser output wastes a large fraction of the laser output power and is impossible to achieve the optimum performance when imaging deep. (2) Next, we will combine the ACT with the adaptive excitation source (AES) that reduces the required output power of the excitation source and ensures every photon emitted from the laser is directed towards the ROIs. To do this, we will significantly reduce the time required for the gain equalization in the AES by obtaining a good initial guess of the input pulse train with a machine-learning approach. (3) In addition, we will develop photon efficient scanning and localization algorithms to further reduce the excitation and emission photons required for cell tracking.

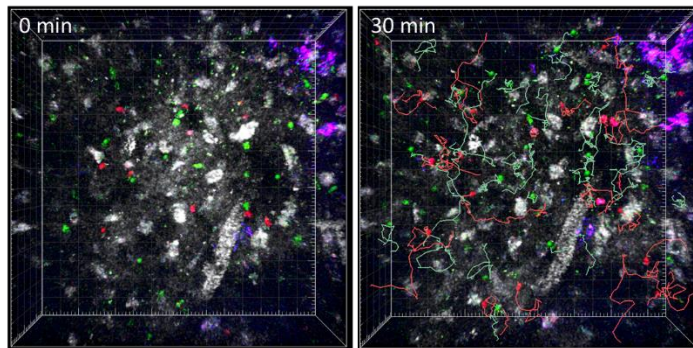
Through the development of imaging methods, lasers, photon efficient scanning and object localization algorithms, this work will increase the fluorescence signal by one to two orders of magnitude without increasing the excitation power in the specimen or the laser output power. While we will focus on immune cells, the technologies developed in this program are applicable for tracking any cells or molecules deep within intact tissues. The gain in photon budget will proportionally increase the tracking speed or volume (or a combination of speed, depth and volume), and ultimately enable dynamic, real-time tracking at the cellular and sub-cellular levels deep within intact tissues or organs that are completely beyond the reach of any existing techniques.

# Immune Cell Tracking with Adaptive Illumination

## Literature Review

Highly motile immune cells are actively recruited to the sites where infection or other diseases (autoimmune disease, tumor, etc.) occur to protect our body from invading pathogens (bacteria or virus) or to attack our body when they lose control. They are also continuously migrating even in normal state to search potential antigens in various organs and tissues for immune surveillance. The efficient recruitment or efficient antigen searching of immune cells is critical to initiate effective immune response at an early time of disease. Therefore, understanding how the immune cells migrate in various organs under various conditions is important for finding disease treatments. During the last 20 years, two-photon microscopy (2PM) have been utilized to visualize immune cell migration in various organs of live animal with sub-micron resolution and 4D resolution (x, y, z, and t)<sup>1</sup>. However, the imaging volume at sufficient temporal resolution to track the cells is limited, which makes it difficult to obtain long-term cell tracks (> 1 hour) because the cell can rapidly disappear from the imaging volume. In particular, thin volume imaging (e.g., 492x492x40  $\mu\text{m}^3$  with 20.3 s interval) due to slower scanning along z-axis than xy-axis can lead to skew the interpretation of the migration data<sup>2</sup>.

2PM technique has been improved for fast thicker imaging: simultaneous multiplane imaging<sup>3</sup> and fast z-scanning by remote focusing<sup>4</sup>. These techniques allow to visualize 690x675x600  $\mu\text{m}^3$  volume at 16.7 Hz with single-neuron resolution ( $\sim 5 \mu\text{m}$  for lateral,  $\sim 15 \mu\text{m}$  for axial) in a mouse brain cortex<sup>5</sup>. However, for more opaque organs than the brain cortex (e.g., lymph nodes densely packed with immune cells) the thick volume imaging has been challenging because conventional 2PM with 920nm excitation can penetrate only 300  $\mu\text{m}$  depth of lymph node. Recently, we demonstrated that three-photon microscopy (3PM) with 1300 nm excitation can visualize a mouse popliteal lymph node through its entire depth (600-900  $\mu\text{m}$ )<sup>6</sup>, but only a small volume ( $\sim 50$  cells within 300x300x100  $\mu\text{m}^3$ ) can be tracked at a low temporal resolution (30 s/volume) when imaging 500-600  $\mu\text{m}$  deep into the lymph node (Fig. 1)<sup>6</sup> because the maximum permissible average power (< 80 mW)<sup>6</sup> limits the rate of signal photons obtainable from the sample.



**Fig. 1** Intravital 3P imaging of immune cell migration at 500-600  $\mu\text{m}$  depth in a mouse lymph node. CD4+ T cell (green) and CD8+ T cell (red) were labeled with CFSE and CMRA fluorescent dyes, respectively. Green and red lines in right figure show tracks of the cells for 30 min. White and magenta are third-harmonic generation (THG) signal and eFluor615-labeled LYVE-1+ lymphatic sinuses, respectively. Imaging volume (300x300x100  $\mu\text{m}^3$ , 256x256 pixels and 25 planes) was acquired every 30 s with  $\sim 70$  mW of average laser power. The pulse repetition rate was 0.654 MHz.

## Problem Statement

A critical concern in large scale imaging for immune cell tracking is the photon budget. Because multiphoton microscopy typically operates at the photon shot-noise limit, the maximum volume where cells can be imaged and tracked at high spatial and temporal resolution is fundamentally limited by the rate of signal photons, which defines the signal-to-noise ratio (SNR), and in turn is determined by the maximum permissible average and peak power in biological specimens. For example, in multiphoton brain imaging over a large field of view<sup>7</sup> the SNR is currently limited by the total laser power that can be delivered to the mouse brain (< 250 mW)<sup>8</sup>. On the other hand, the regions of interest (ROIs), e.g., user defined cells and molecules, typically only occupy a small fraction of the volume. With standard raster scanning, a large fraction of excitation is therefore wasted on non-informative parts of the sample outside the ROIs. Therefore, there is an urgent need to create the most photon-efficient excitation scheme to enable dynamic

cell tracking with high spatial and temporal resolution over a large volume.

## **Objective**

The research proposed here directly addresses the challenges of large-scale, fast dynamic tracking at the cellular or sub-cellular level. To address the fundamental limit of the photon budget, we will develop adaptive cell tracking (ACT) that will illuminate only the ROIs. In principle, ACT is analogous to spotlight tracking of ballet dancers on a stage: each dancer is illuminated and tracked by one spotlight while the rest of the stage remains in the dark. ACT thereby dramatically improves the photon efficiency for dynamic cell tracking, i.e., every photon on the sample is used to record the cellular motion. A one to two orders of magnitude gain in photon budget can be achieved by ACT because the ROIs usually only occupy a small fraction of the imaging volume (e.g., the fluorescent-labeled T cells occupy < 1% of the volume imaged in Fig. 1). This gain in photon budget directly translates to an increase in imaging volume or imaging speed (or a combination of the two), without increasing the excitation power on the sample or sacrificing SNR.

While the concept of ACT can be demonstrated by direct modulation of the excitation source, direct modulation wastes a large fraction of the laser output power (e.g., >99% of the power will be wasted when imaging the T cells shown in Fig. 1) and is impractical to implement for imaging at the shallow depths and impossible to achieve the optimum performance when imaging deep. We will combine ACT with the concept of the adaptive excitation source (AES)<sup>9</sup>, which was developed recently by our group for imaging stationary ROIs (e.g., neurons in the mouse brain). AES reduces the required output power of the excitation source and ensures every photon emitted from the laser is directed towards the ROIs. The combination of ACT and AES will create the most photon efficient system for dynamic imaging: every photon from the laser which enters the specimen is used for dynamic tracking of the ROIs. The photon efficiency of AES and ACT will be further enhanced by exploring smart scanning patterns and object localization algorithms. The ultimate goal of this program is to create a new, readily deployable technology platform that uses the minimum number of excitation and/or emission photons for real-time tracking of cells or molecules in intact tissues.

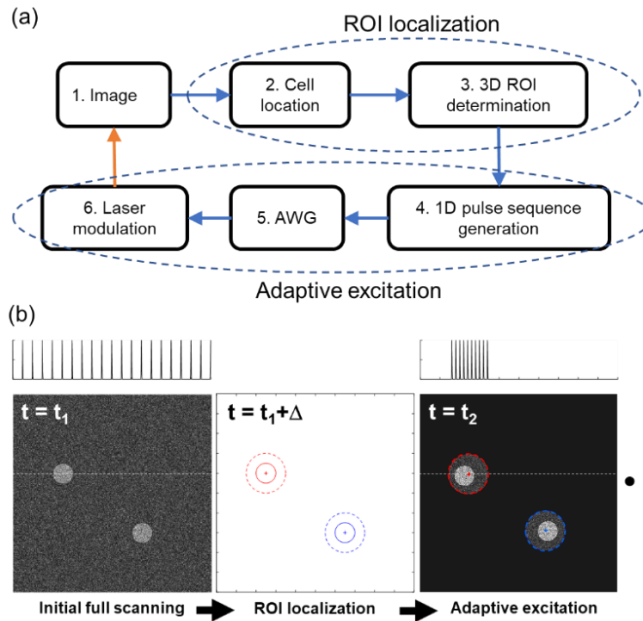
## **Work Plan**

### Aim 1: Demonstrating the concept of adaptive cell tracking (ACT).

The concept of ACT is schematically illustrated in Fig. 2. ACT starts with conventional raster scanning of a 3D volume capturing the cells to be tracked and their environment (e.g., using different colors to label the cells and their environment, such as shown in Fig. 1). Via real-time image processing, the ROIs will be defined by determining the cell boundaries and adding a user defined “guard region” to ensure that the cells will not move out of the ROIs before the next imaging volume is acquired. The ROIs define the pulse sequence of the excitation beam in the time domain (i.e., adaptive excitation). Synchronization of the pulse sequence and the beam scanner ensures that only the ROIs will be illuminated by the excitation beam. To track the new cells entering the imaging volume, the borders of the volume can be labeled as ROIs as well. Multiple cell types can be tracked simultaneously by labeling them with different colors and performing multiphoton multi-color imaging with a single excitation wavelength<sup>10,11</sup>. The 3D environment can be re-captured by imaging the entire volume as needed.

3D ROI localization and adaptive excitation generation (steps 2 to 6 in Fig. 2a) form an automatic adaptive loop to continuously image and track cells; however, the time required ( $\Delta$ ) to perform these steps represents a “dead time” between two image acquisitions. We will leverage the rapidly expanding field of computer vision that has created a plethora of image segmentation algorithms<sup>12,13</sup>. Determining ROIs is an image-specific task and therefore the best image segmentation technique can vary greatly depending on the cells imaged. For the T cells (Fig. 1), for example, we found an algorithm based on image erosion and Otsu’s method to be sufficient<sup>14</sup>. For other cell types, an extensive list of options utilizing state-of-the-art deep learning techniques





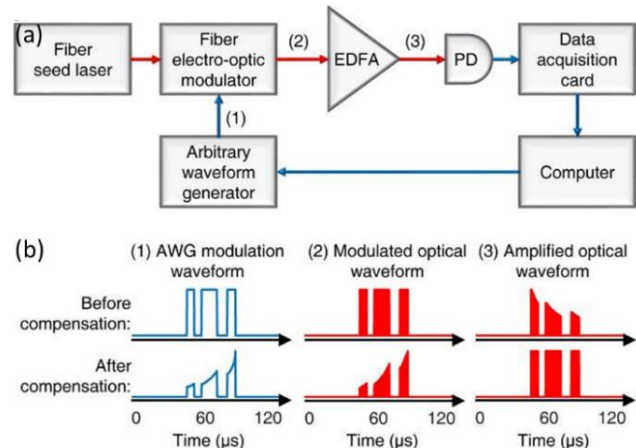
**Fig. 2** (a) Block diagram of ACT. The electrical path is shown in blue and the optical path is shown in orange. The dashed ovals show the two main steps for ACT: ROI localization and adaptive excitation generation. (b) Cartoon illustration of ACT. The top row shows the excitation pulse train along the scan line in the images below. Two cells and two ROIs are shown. The ROIs include the cell boundaries (solid circles) and the guard regions for each cell (dashed circles). The time required to complete the steps from 2 to 6 in (a) is  $\Delta$ . Inset on the right shows the real time trajectories of the two tracked cells.

exist<sup>13,15,16</sup>. Our current estimate is that  $\Delta < 70$  ms is achievable, which is sufficiently short for the concept demonstration.

We will directly modulate the laser output using an electro-optic modulator for 2PM and 3PM to demonstrate the ACT concept. To confirm if cell tracks obtained with ACT are same as that without ACT, we will image same T cell migration in a mouse lymph node simultaneously with and without ACT by simultaneous 2P and 3P imaging<sup>17</sup>. The CFP<sup>+</sup>DsRed<sup>+</sup> double-labeled T cells can be imaged by 2P excitation of CFP at 860 nm without ACT and 3P excitation of DsRed at 1650 nm with ACT.

### Aim 2: Combining ACT with an adaptive excitation source (AES).

We recently demonstrated an AES for imaging stationary ROIs (e.g., neurons in the mouse brain) for 2PM and 3PM<sup>9</sup>. Because the on-demand pulse train is not periodic in time, a key feature of the AES is pre-compensation of the gain transient from the fiber amplifiers<sup>9</sup>. Such gain transients are well-known in burst-mode amplification in fiber-optic telecommunications, and a closed-form solution of the inverse problem does not exist. Therefore, we used a feedback loop, which takes  $\sim 30$  iterations ( $\sim 15$  s) to equalize the gain for one frame (512x512 pixels)<sup>9</sup> (Fig. 3a and 3b). While such a time delay is inconsequential when imaging non-moving objects, it is incompatible for tracking fast moving cells. We propose to employ machine-learning to provide an intelligent initial guess of the pre-compensation for a given pulse sequence. Our aim is not to replace the feedback loop but to vastly reduce the number of iterations (e.g.  $< 10$ ). In addition, we will further reduce the time by increasing scanning speed and reducing pulse number

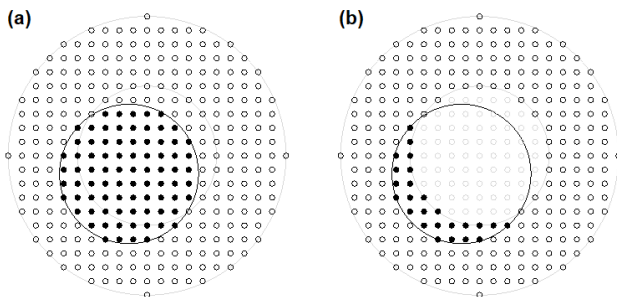




per pixel during the iterations so that the time required for gain equalization for one volume is smaller than a volume acquisition time (e.g., 1 to 10 s). We will then eliminate the dead time by using two AWGs to alternately drive the intensity modulator, with AWG1 for the odd imaging volumes (t1, t3, ..) and AWG2 for the even imaging volumes (t2, t4, ..).

**Aim 3: Developing photon efficient scanning and localization algorithms to improve ACT.**

Since for tracking applications it is only necessary to determine the cell location, it is possible to consider alternative scanning strategies that would use fewer excitation and/or emission photons, ultimately allowing for a further reduction in illumination power and an increased tracking time. We propose a strategy inspired by MINFLUX<sup>18,19</sup> for super-resolution microscopy. The MINFLUX technique tracks single emitters by using an intensity minimum. Intuitively, if one can exactly match the intensity minimum to the emitter location, then the emitter location is known without any photons being received. Similarly, we consider just illuminating the guard region (Fig. 4). Any cell that does not move can in principle be found without any emission photons. To test this idea, we have performed 1D simulations and back-of-the-envelope calculations for localizing a rigid 10  $\mu\text{m}$  cell which is allowed to move up to  $\pm 5 \mu\text{m}$  between two imaging frames. We then considered scanning the entire region and just the guard regions, while keeping the total number of received photons (on average) the same. Comparing the root-mean-squared error (RMSE) of both cases, we find that if the cell does not move much and the received photon number is low (which is likely the case for most practical applications), the RMSE is lower when scanning just the guard region, indicating a possible saving of emission photons. For example, if the cell takes random walk with a standard deviation of 0.5  $\mu\text{m}$ , with 16 received photons the guard region RMSE is better on average by a factor of 2. We also considered the same analysis but kept the total input power the same and found similar results. This preliminary analysis showed that for the same number of emission or excitation photons, scanning just the guard regions is a promising approach to further improve the photon efficiency. While generating arbitrary illumination patterns (e.g., generating an intensity minimum at the center of a point-spread function) in intact tissue is challenging in super-resolution microscopy, the various scanning patterns proposed here can be conveniently obtained from the AES by time-domain modulation. We will explore similar improvements in 3D volume by testing various scan patterns, e.g., a 3D shell around the cell instead of uniformly illuminate the entire ROI. We will further investigate the impact on cell localization by changes in cell morphology during the movement. Our ultimate goal is to use the minimum number of excitation and/or emission photons for real-time tracking of cells in intact tissues.



**Fig. 4** Illustrated is a cell (large dark grey circle) which has moved off center and is to be scanned by (a) full ROI scan, and (b) guard-region-only scan. The small black circles (both open and filled) indicate the voxels to be scanned, i.e., the laser is on at these locations, with open circles indicating no signal is produced and filled circles indicating signal is produced. The small grey open circles in (b) show voxels that the laser would be on in the full ROI scan but isn't for the guard-region-only scan.

**Outcomes & Impact**

ACT will improve the cell tracking speed or volume by 10 to 100x, which will enable T cell tracking over the entire volume of mouse popliteal lymph node ( $\sim 1000 \times 1000 \times 600 \mu\text{m}^3$ ). Although the entire volume is  $\sim 67x$  of the imaging volume in Fig.1, the required average power is well within the permissible range because the ROIs are  $\sim 1\%$  and the required power exponentially decreases as the depth approaches the surface. The T cell tracking in the entire volume will allow us to observe T cell migration in all directions over a long period of time ( $> 1$  hour), for the first

time. Our proposed imaging method will be powerful tool for uncovering many unresolved questions related fundamental physiology and dynamic cellular immune response to many diseases. In addition, the smart localization developed in Aim 3 represents a totally new direction for cell tracking that will provide the most photon-efficient tracking strategy. While we will focus on immune cells, the technologies developed in this program are applicable for tracking any cells or molecules deep within intact tissues. In addition, an important practical feature of the proposed imaging method is that it can be implemented with current multiphoton imaging systems without any modification of the microscope hardware.

## References

1. Germain, R. N., Robey, E. A. & Cahalan, M. D. A Decade of imaging cellular motility and interaction dynamics in the immune system. *Science (80-. )*. **336**, 1676–1681 (2012).
2. Textor, J. *et al.* Defining the quantitative limits of intravital two-photon lymphocyte tracking. *Proc. Natl. Acad. Sci. U. S. A.* **108**, 12401–12406 (2011).
3. Amir, W. *et al.* Simultaneous imaging of multiple focal planes using a two-photon scanning microscope. *Opt. Lett.* **32**, 1731 (2007).
4. Botcherby, E. J. *et al.* Aberration-free three-dimensional multiphoton imaging of neuronal activity at kHz rates. *Proc. Natl. Acad. Sci. U. S. A.* **109**, 2919–2924 (2012).
5. Weisenburger, S. *et al.* Volumetric Ca<sup>2+</sup> Imaging in the Mouse Brain Using Hybrid Multiplexed Sculpted Light Microscopy. *Cell* **177**, 1050–1066.e14 (2019).
6. Choe, K. *et al.* Intravital three-photon microscopy allows visualization over the entire depth of mouse lymph nodes. *Nat. Immunol.* **23**, 330–340 (2022).
7. Sofroniew, N. J., Flickinger, D., King, J. & Svoboda, K. A large field of view two-photon mesoscope with subcellular resolution for in vivo imaging. *Elife* **5**, 1–20 (2016).
8. Podgorski, K. & Ranganathan, G. Brain heating induced by near-infrared lasers during multiphoton microscopy. *J. Neurophysiol.* **116**, 1012–1023 (2016).
9. Li, B., Wu, C., Wang, M., Charan, K. & Xu, C. An adaptive excitation source for high-speed multiphoton microscopy. *Nat. Methods* **17**, 163–166 (2020).
10. Xu, C., Zipfel, W., Shear, J. B., Williams, R. M. & Webb, W. W. Multiphoton fluorescence excitation: new spectral windows for biological nonlinear microscopy. *Proc. Natl. Acad. Sci.* **93**, 10763–10768 (1996).
11. Hontani, Y., Xia, F. & Xu, C. Multicolor three-photon fluorescence imaging with single-wavelength excitation deep in mouse brain. *Sci. Adv.* **7**, eabf3531 (2021).
12. Zaitoun, N. M. & Aqel, M. J. Survey on Image Segmentation Techniques. *Procedia Comput. Sci.* **65**, 797–806 (2015).
13. Mary, S. P., Ankayarkanni, Nandini, U., Sathyabama & Aravindhan, S. A Survey on Image Segmentation Using Deep Learning. *J. Phys. Conf. Ser.* **1712**, (2020).
14. Otsu, N. A Threshold Selection Method from Gray-Level Histograms. *IEEE Trans. Syst. Man. Cybern.* **9**, 62–66 (1979).
15. Pachitariu, M. *et al.* Suite2p: beyond 10,000 neurons with standard two-photon microscopy. *Bioarxiv* **20**, 2017 (2017).
16. Upschulte, E., Harmeling, S., Amunts, K. & Dickscheid, T. Contour proposal networks for biomedical instance segmentation. *Med. Image Anal.* **77**, 102371 (2022).
17. Ouzounov, D. G. *et al.* In vivo three-photon imaging of activity of GCaMP6-labeled neurons deep in intact mouse brain. *Nat. Methods* **14**, 388–390 (2017).
18. Balzarotti, F. *et al.* Nanometer resolution imaging and tracking of fluorescent molecules with minimal photon fluxes. *Science (80-. )*. **355**, 606–612 (2017).
19. Gwosch, K. C. *et al.* MINFLUX nanoscopy delivers 3D multicolor nanometer resolution in cells. *Nat. Methods* **17**, 217–224 (2020).

**Summary:** Optical techniques are valuable for diagnosing and treating disease because optical spectroscopic interactions with molecules confer specificity with regard to target biochemical information and quite favorable spatial resolution. Yet, tissues strongly scatter light, making tissue opaque within tens to hundreds of  $\mu\text{ms}$  of propagation depth, moderating the success of optical biomedical imaging.

Some cancers are very difficult to detect with current technologies. As early detection leads to much better outcomes and lower mortality rates, new diagnostics technologies could profoundly impact our ability to detect and successfully treat disease. I am motivated by ovarian cancer, which is extremely difficult to detect and is usually detected at a late stage where treatments suffer from low efficacy.

I am focusing second harmonic generation (SHG) microscopy which is already established as a powerful tool for biological imaging. SHG has proven diagnostic and prognostic capabilities for a wide range of diseases. Of prominence is the use of SHG imaging to grade cancerous tumors by quantifying the type of organization of collagen around tumors. Moreover, cancers tend to reorganize collagen to present a spiral structure that aids in differentiating healthy tissues, benign tumors, and cancers. Despite this potential, SHG imaging is limited in imaging depth. As a result, non-invasive biological imaging (e.g., optical pathology without the need for surgery) is restricted to superficial tissues or through endoscopy and current SHG microscopy technology is extremely limited in its potential for use with *in-vivo* optical biopsies.

I propose a new approach to rendering opaque tissue effectively transparent using both advanced data science tools and wavefront control to sidestep the current limitations that restrict the SHG imaging depth. This is a radical departure from the conventional paradigm for nonlinear microscopy that relies on scanning a ballistic focus in the specimen and forming an image from the measured power from each focal point. Depth imaging is severely limited because the ballistic light intensity decays exponentially with depth.

This proposal seeks to remedy the deficiency in the limited imaging depth by posing the question: rather than throwing away multiply scattered (MS) light, can we redirect it into image formation? I will explore two methods of harnessing MS light for SHG imaging (e.g., collagen in the extracellular matrix around tumors) at unprecedented imaging depths in tissues. In Aim 1, I will unscramble the SHG light exiting the tissue to remap that information into an image deep within tissue. SHG fields exiting the tissue will be recorded with nonlinear holography. Since the SHG field propagates through tissue, the field is spatially randomized (exits as speckle). The speckle field is a distinct fingerprint of each SHG scattering source point. With a set of measurements that vary the SHG signal brightness spatially, the mapping between the SHG source points and the measured speckle will be uncovered. Armed with the random SHG speckle fingerprint for each point in the object field, the SHG image will be revealed by unscrambling the SHG light that was randomized with propagation through the tissue. Thus, I will break free from relying on image formation by scanning a ballistic focus. In Aim 2, the data will be used to estimate the transmission matrix for the fundamental field. This matrix operator describes the distortion of the input fundamental field at the image plane. This information will be used to focus the wave in the object plane through wavefront shaping to further improve the SHG image quality and enable deeper imaging depths.

This new approach to *in-situ* fundamental transmission matrix estimation opens new avenues of imaging by avoiding the need for a detector in the tissue (not possible) or relying on the accidental existence of a nonlinear guide star. Moreover, the wavefront reshaping increases the SHG signal power, and thus the image quality, and allows for increasing imaging depth. This could change the landscape for deep tissue imaging. Simulations will be employed to study the limits of imaging depth. Data from these experiments will be combined with simulation results to seek additional funding for pushing this new imaging approach to unprecedented imaging depths.

**Project outcomes:** A) Demonstrate unscrambling of measured SHG speckle fields to obtain an SHG image field deep in tissue. B) Demonstrate estimation of the transmission matrix of the fundamental field to the SHG image plane and use that transmission matrix to generate a brighter focus and a higher quality SHG image. C) Enable deeper imaging by pushing the depth where bright SHG imaging can be accomplished. D) Capture a set of data that will be used for papers, talks, and as preliminary data for future funding.

## Re-purposing multiply scattered light for early ovarian cancer diagnostic with deep tissue second harmonic generation

Annually, more than 200,000 women succumb to death by ovarian cancer, with nearly 13,000 of those deaths occurring in the United States alone. Ovarian cancer is the most lethal gynecological malignancy due in large part to a lack of methods for early-stage detection<sup>1</sup>. Typically, ovarian cancer is detected at a later stage where 5-year survival rates hover at  $\sim 39\%$  because, at the later stages, the tumor has metastasized and likely spread throughout the body. Early detection through routine screening is a potent tool in our arsenal to fight cancer. This benefit is evidenced by the fact that when detected in stage I, the 5-year survival rate jumps to 94%. Unfortunately, the early-stage diagnosis rate is below 16% due to the lack of effective screening methods. *We propose to pave the way for the use of second harmonic generation (SHG) microscopy as a minimally invasive early diagnostic tool for ovarian cancer (and other cancers in the future) by developing an approach to mitigate the fundamental barrier for deep nonlinear microscopy imaging.*

The two standard methods used in ovarian cancer screening provide early detection only in one out of six patients, accounting for the high mortality rate. The serum cancer antigen 125 levels assay has limited sensitivity, while transvaginal ultrasound provides limited resolution and contrast. Optical imaging has been recognized as an invaluable tool for observing and diagnosing diseases with higher sensitivity and resolution. Yet to date, optical diagnostic methods are not capable of detecting early ovarian cancers. Optical methods are limited by the fact that variations in the refractive index (RI) present in tissues scramble the propagation of light. This multiple scattering (MS) causes a loss of image information when light propagates through tissue.

Several standard imaging methods are impressively wielded to improve imaging depth by exploiting a mechanism that separates the light that has *only* interacted with the desired object (single scattering, SS, the events that carry image information) from the MS light that has completely scrambled image information. Confocal imaging isolates SS from MS light spatially with a pinhole, optical coherence tomography separates SS light through interference with a coherent reference, and nonlinear microscopy relies on intensity-dependent nonlinear excitation to preferentially probe the object with ballistic light and reject MS light. Until recently, these techniques represented the state-of-the-art.

We focus on SHG imaging, a form of nonlinear microscopy that can be used to take advantage of optical physics principles that remain unexplored for deep imaging in tissues. SHG imaging is powerful as a non-invasive, label-free screening method for ovarian cancer and diagnostic potential in general<sup>2,3</sup>. SHG imaging uses collagen, a structural network protein in the tissue extracellular matrix (ECM), as a biomarker. The lateral and axial resolution of ovarian cancer samples by SHG imaging can approach  $< 1 \mu\text{m}$  laterally and  $< 3 \mu\text{m}$  axially<sup>4</sup>. Imaging collagen using SHG could distinguish ovarian cells as normal, malignant, benign, or borderline<sup>5</sup>. A machine-learning-enabled polarimetric SHG microscopy method was reported to enable label-free diagnosis of breast cancer tissues with an accuracy  $> 90\%$ <sup>6</sup>. *Due to the limitations of optical scattering in state of the art in SHG microscopy, optical diagnostics based on SHG are restricted to invasive biopsies that study tissue removed from the patient.*

It is recognized that the tissue microenvironment – that is the milieu of cells, ECM, signaling molecules, nutrients, and vasculature surrounding cells within a cancerous tumor – drastically modulates the behavior of the cancer cells that one wishes to eliminate with treatments. While many studies and diagnostic tools avoid the issue of optical scattering by using cells or tissues extracted from patients, tissues and cells out of the body exist in a manifestly different environment than that within the host body. Access to optical

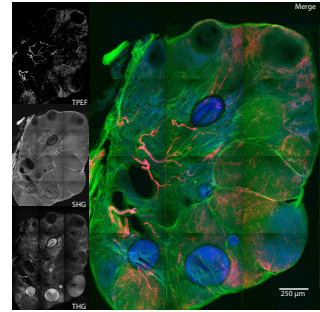


Figure 1: Two-photon excited fluorescence (TPEF), second- and third-harmonic generation (SHG, THG) images of fixed murine ovarian tissue, acquired in the Bartels laboratory circa 2012. Each image represents a maximal projection through  $250 \mu\text{m}$  of tissue.

biopsies inside of tissue is critical for both disease diagnosis and for the monitoring of treatment efficacy. As a consequence, there is a pressing need for *in-vivo* optical diagnostics of tumors. Although the infiltration depth of SHG imaging is  $200\ \mu\text{m}$ , MS renders tissue opaque for the imaging depths where subsurface stage I ovarian cancers arise within an inclusion cyst (usually detectable at the depth of a few millimeters).

**A. New strategies to exploit optical physics to push SHG microscopy deep into tissues.** In the past few years, new strategies have emerged to improve imaging depth. These strategies rely on the random variation of RI that causes scattering remaining stationary (i.e., not moving) on some timescale over which imaging is performed. Treating tissue as such a disordered system admits the ability to unscramble multiple scattering (MS) effects. Light propagation, even though a disordered system, is linear. As a result, the disordered medium can be characterized by a (very complicated) linear transfer matrix,  $\mathbf{T}$ . Many clever strategies have enabled the use of wavefront shaping of light incident on the disordered tissue to undo the multiple scattering<sup>7</sup>. Still, aside from a few cases, a detector must be placed behind the tissue through which imaging occurs. This requirement severely limits the usefulness of standard wavefront shaping strategies.

A few years ago new innovations emerged for exploiting the disorder of a random RI distribution while not requiring a detector to be placed behind the section of tissue that is to be imaged through. The idea is simple: in a thin object, transverse scattering vectors are preserved when the incident angle on the object is changed due to the single scattering (SS) angular memory effect (SAME)<sup>8,9</sup>. This scattering conservation can be retained when using a short longitudinal source (broad optical bandwidth) in holographic imaging. By measuring the output *field*, rather than the intensity, and noting that the input and output spatial frequencies can be related to the object spectrum with SAME, summation of the coherent scattered light is constructive. By contrast, summation of the MS field is characterized by a random walk, and the coherent sum averages to zero. The result is a new method to reject the MS field and preserve the SS field, improving image quality by a factor of  $N$  over the same number of intensity averages.

To date, only methods that exploit linear scattering for coherent field enhancement have been demonstrated. My postdoctoral research is aimed at exploiting the coherent field summation demonstrated for linear scattering (as described above) with coherent nonlinear scattering, e.g., SHG. This strategy isolates only the SS events – requiring that light be ballistic on the way in and on the way out of the tissue.

**Optical physics problem:** All of these methods for pushing imaging depth deep into tissues rely on a critical limitation: separating SS from MS light. This requirement suffers from a fundamental limitation that the SS light extracted for imaging also requires that the light used for imaging is unscattered (ballistic) both on the way into and out of the tissue.

**B. Proposed work: Coherent SHG imaging with MS light.** We propose to bypass the conventional depth limitations of nonlinear optical microscopy by harnessing, rather than suppressing MS light. To demonstrate this new paradigm, I will focus on coherent SHG imaging. The approach is broken into two Aims: 1 seeks to unscramble the SHG signal light as it exits the tissue, and 2 seeks to harness information obtained from 1a to use wavefront shaping to undo the scattering of fundamental light as it propagates into the tissue. The conceptual shift is illustrated in Fig. 2. I propose to explore new strategies that will redirect MS light for SHG imaging, rather than the standard approach of using ballistic light, which decays exponentially with propagation depth. Significant increases in imaging depth will be possible by using, rather than discarding, MS light. This task is complicated by the fact that I cannot place a detector on the distal side of the section of scattering tissue that I wish to image through. I propose two Aims:

**Aim 1. Direct SHG imaging in scattering media by unscrambling MS of the SHG field optically scattered as it exits the tissue.** Current nonlinear optical microscopy methods rely on the propagation of ballistic light into the tissue to produce an image. The ballistic focus is scanned in three dimensions to form an image (Fig. 1). Unfortunately, ballistic light intensity decays exponentially with propagation depth into the tissue. This decay is the primary limit on the imaging depth. A new strategy for imaging is proposed that will circumvent this limit. The idea is to unscramble the coherent nonlinear scattered light by developing a strategy inspired by the use of non-negative matrix factorization (NMF) for fluorescent imaging<sup>10</sup>.

The challenge in this approach is that NMF has not been developed for complex-valued matrices, which must be used to describe coherent light. To tackle this problem, I propose to measure the coherent SHG field with the epi-holography setup and then use the field to estimate the output speckle fields for each scattering point from the object that generates the SHG signal. The SLM in the system will be modulated to sweep through illumination field perturbations that will vary the excitation amplitude and thus the brightness of the SHG scattering spatially. With a suitably large set of measurements, i.e., larger than the number of independent spatial points that I wish to resolve, the measured field data matrix can be factored into a product of low-rank matrices. However, the data matrix will be complex and thus I require a strategy for separating the speckle patterns for the measured SHG field. This will be accomplished using emerging algorithms for complex NMF. Once the output speckle fields are obtained for each SHG image point, the images will be obtained by decorrelation with the speckle fields. In addition, I will be able to extract the illumination field transmission function, which will give us access to information needed for improved SHG signal generation and imaging depth with wavefront shaping.

This approach is inspired by a recent strategy for fluorescent microscopy that avoids the need for a detector behind the scattering medium. The key idea is that an image of a single-point fluorescent emitter will produce an intensity speckle pattern that is unique to that fluorescent source. Because of the spatial incoherence, the image intensity for multiple fluorescent sources is a sum of the speckle intensity patterns from each source. The recorded fluorescent image is a linear sum of the speckle intensity patterns weighted by the brightness of each source. The clever approach is to cycle through a sequence of random illumination patterns that vary the brightness of the fluorescent sources. Applying NMF to a large set of intensity images, the speckle patterns for each source, images, and the illumination transmission matrix can all be extracted.

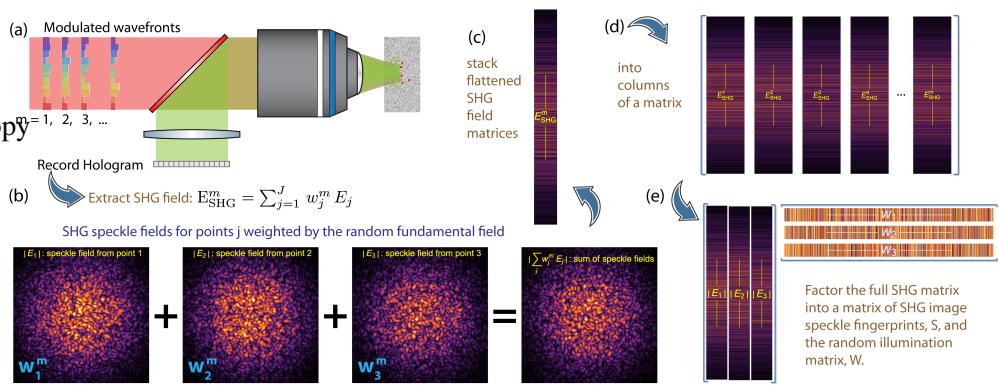


Figure 2: Concept for using MS light for SHG microscopy (described in text).

Because of the spatial incoherence, the image intensity for multiple fluorescent sources is a sum of the speckle intensity patterns from each source. The recorded fluorescent image is a linear sum of the speckle intensity patterns weighted by the brightness of each source. The clever approach is to cycle through a sequence of random illumination patterns that vary the brightness of the fluorescent sources. Applying NMF to a large set of intensity images, the speckle patterns for each source, images, and the illumination transmission matrix can all be extracted.

Figure 2 shows the concept for unscrambling MS SHG light exiting tissue. The approach revolves around epi-SHG holographic imaging of objects embedded in tissue. SHG holography allows for quantitative extraction of the SHG field. Because the SHG light generated by the object must pass through a large section of tissue, MS scrambles the image information. A single-point SHG scatterer will produce a speckle SHG field that is extracted from the hologram. The total recorded field is a sum over all SHG speckle patterns from each object point. The key observation is that each speckle field  $E_j$  does not change when the fundamental illumination light is changed.

However, for a given measurement, there is no way to disentangle the SHG image field produced by the object and the randomization of that field as it passes through the tissue before being captured in the hologram. While SHG scales nonlinearly with the illumination light, the propagation of the SHG field out of the can be modeled with a linear operator  $T_{\text{SHG}}$ , that maps the SHG field in the object plane  $E_{\text{obj}}$  to the camera plane  $E_{\text{SHG}} = T_{\text{SHG}} E_{\text{obj}}$ . Written as a matrix equation,  $E_{\text{obj}}$  and  $E_{\text{SHG}}$  are column vectors (flattened images) and  $T_{\text{SHG}}$  is a matrix. Our goal is to estimate  $T_{\text{SHG}}$  so that image information can be recovered.

To obtain the image, more information is needed. This can be accomplished by exploiting the fact that  $T_{\text{SHG}}$  remains unchanged while  $E_{\text{obj}}$  is varied. Additional information is injected by modulating the input fundamental beam wavefront (Fig. 2a). As the object field is modulated, a variation of a complex weight,  $w^m_j$ , for each SHG scattered point in the object is produced. The SHG field extracted from the hologram (for



the  $m^{\text{th}}$  modulation pattern) can be expressed as  $\mathbf{E}_{\text{SHG}}^m = \sum_j w_j^m \mathbf{E}_j$ , (Fig. 2b). To extract useful information, many modulated wavefronts are cycled through, leading to random variations of  $w_j^m$ . Each extracted SHG field,  $\mathbf{E}_{\text{SHG}}^m$ , is flattened (Fig. 2c) and stacked into columns of an SHG field matrix (Fig. 2d). Because of the limited information in this matrix (i.e., that speckle fields  $\mathbf{E}_j$  are invariant to the modulation variation of the fundamental illumination wave), the matrix is low-rank (rank is determined by the number of SHG image points in  $\mathbf{E}_{\text{obj}}$ ). Thus the matrix can be factored as:  $\mathbf{A}_{\text{SHG}} = \mathbf{T}_{\text{SHG}} \mathbf{W}^T$  (see Fig. 2e). Here  $\mathbf{T}_{\text{SHG}}$  is constructed from columns of the flattened speckle fields  $\mathbf{E}_j$  and  $\mathbf{W}$  is the set of columns given by the vector  $w_j^m$  that is formed from the sequence of modulated fundamental wavefronts at each point  $j$ . I hypothesize that the factorized matrix product to obtain  $\mathbf{S}$  and  $\mathbf{W}$  can be computed from a complex NMF (CNMF) of the data matrix  $\mathbf{A}_{\text{SHG}}$ . Note that CNMF is a generalization of NMF that is widely used in data science and has been demonstrated for extraction of speckle fingerprints for incoherent light scrambled by a scatterer.

The goal is then to use  $\mathbf{T}_{\text{SHG}}$  to estimate the object by inverting the equation  $\mathbf{E}_{\text{SHG}}^m = \mathbf{T}_{\text{SHG}} \mathbf{E}_{\text{obj}}$ . Although a direct inverse is not possible,  $\mathbf{E}_{\text{obj}}$  can be estimated using a regularized inverse problem approach. This approach will enable nonlinear imaging in tissue to break free from the limitation of requiring ballistic light to extract the coherent image. In addition, the set of  $M$  modulations can be used to coherently sum the SHG field measurements, resulting in a boost of  $M$  in the coherent sum of the SHG fields over simple averaging of image intensities.

**Aim 2. Increased SHG brightness and imaging depth using  $\mathbf{E}_{\text{obj}}$  obtained from Aim. 1.** As light propagates in tissue, scattering distorts the light, spreading out the beam spatially and stretching pulses in time. Both of these effects decrease the intensity of the beam in the sample. The drop in intensity decreases nonlinear scattering (such as SHG). While an increase in incident beam energy can compensate for the pulse broadening, even this standard tactic for imaging deep with nonlinear signals is severely limiting. Initial work has shown that by shaping the input wavefront, a beam focus in space and time can be attained by driving constructive interference between sets of scattering paths. Wavefront shaping can increase the beam intensity by orders of magnitude, thereby enabling nonlinear signal increases by orders of magnitude. Yet this strategy is limited because these methods largely rely on measurement of the transmission matrix, which has relied on the placement of a camera on the other side of the tissue.

The goal of Aim 2 is to boost the SHG signal and penetration depth by unscrambling the illumination (fundamental) light using the transmission matrix estimated in Aim 1. Shaping the wave entering tissue can produce a focused beam (in both space and time) deep inside the tissue that can boost nonlinear signal generation<sup>11</sup>. So far, this has only been accomplished with either a detector must be placed on the far side of the tissue or a nonlinear guide star (a bright, isolated point nonlinear object). Neither approach is practical in situations for non-invasive biomedical imaging. I propose to use the estimate of the transmission matrix  $\mathbf{T}_{\text{fund}}$  from Aim 1 to pre-compensate for the scrambling of incident fundamental beam by the tissue. The incident fundamental field at the object plane is given by the linear mapping  $\mathbf{E}_{\text{fund}} = \mathbf{T}_{\text{fund}} \mathbf{E}_{\text{in}}$ . Here,  $\mathbf{E}_{\text{in}}$  is the input fundamental field and  $\mathbf{T}_{\text{fund}}$  is the linear scattering transmission matrix for the incident field. The object SHG field is then generated by  $\mathbf{E}_{\text{obj}} = \chi^{(2)} \mathbf{E}_{\text{fund}}^{\odot 2}$ . The operator  $\odot$  in the square of the fundamental field is an element-wise squaring operation. Observing that the weight in the SHG field at an image point  $j$  is simply given by  $w_j^m = \chi^{(2)} \mathbf{E}_{\text{fund}}^{\odot 2}$ , one may use the  $\mathbf{W}$  matrix obtained from the CNMF algorithm to solve for the input transmission matrix by solving the equation  $\mathbf{W} = (\mathbf{T}_{\text{fund}} \mathbf{E}_{\text{in}})^{\odot 2}$ . Again, this will be treated as an inverse problem from which I will obtain an estimate of  $\mathbf{T}_{\text{fund}}$ . Armed with  $\mathbf{T}_{\text{fund}}$ , a spatial frequency phase mask that is applied to the SLM can be used to focus the fundamental field onto the object, producing a brighter SHG field that is extracted from the hologram. Using the estimate of the  $\mathbf{T}_{\text{SHG}}$ , the SHG object field can be extracted from the complex field obtained from the SHG hologram.

**Going deeper:** This strategy for deeper imaging will be pursued iteratively. Confidence in the iterative approach is high because I have observed in simulations that a wavefront correction persists over some range of optical depth in the tissue. Thus, I can shift to deeper imaging depths by controlling the arrival

time of the reference beam on the camera, which determines the depth from which  $\mathbf{E}_{\text{obj}}$  is extracted. Aims 1 and 2 can be repeated deeper into the tissue to iteratively push to deeper imaging depths. This strategy will be explored more extensively theoretically using scattering propagation codes developed in the Bartels laboratory.

**C. Tasks and work plan.** All of the major equipment required for the proposed project exists in the Bartels laboratory, which will be at my disposal. These resources include scattering models and a full nonlinear SHG epi-holographic imaging system equipped with a high pixel density spatial light modulator (SLM), which was constructed for the aforementioned CZI project (ends June 2023).

**Aim. 1a (months 1-2):** Develop simulations for CNMF of SHG field data to yield  $T_{\text{SHG}}$  and  $W$  matrices and obtain an SHG object field. **Aim. 1b (months 3-6):** Take data for a variety of samples (SHG-active objects) and scattering media (diffusers, tissue simulating phantoms, tissues) and process them to extract images with CNMF. **Aim. 2a (months 4-6):** Develop simulation for extracting  $T_{\text{fund}}$  from  $W$ . **Aim. 2b (months 7-12):** Take additional data and use those data to control the focused fundamental wavefront to improve the SHG image field brightness by using a wavefront-shaped field and image estimation from the previously obtain  $T_{\text{SHG}}$ .

**D. Outcomes.** A new approach to deep imaging by harnessing, rather than rejecting, MS light. Simulations that study the limits of imaging depth and validated with data. Preliminary results will use used to seek additional funding for pushing SHG imaging to unprecedented imaging depths, for clinical ovarian cancer screening.

**E. Impact.** By making use of physics of optical scattering, we will open new avenues for deep tissue imaging. This work will prove the principles and feasibility of an imaging method that may allow for minimally invasive imaging of the ECM around tumors for expanded early screening of cancers, with a particularly high possible impact of detecting ovarian and possibly pancreatic cancers at early stages, which could save the lives of a majority of patients who now succumb to these diseases.

## References

1. Huang J, et al., Worldwide Burden, Risk Factors, and Temporal Trends of Ovarian Cancer: A Global Study, *Cancers* 29, 2230 (2022).
2. Qian, S., et al., Identification of human ovarian cancer relying on collagen fiber coverage features by quantitative second harmonic generation imaging. *Optics Express* 30(14), 25718, 7 (2022).
3. Campagnola, P. J. and Dong, C. Y. Second harmonic generation microscopy: Principles and applications to disease diagnosis. *Laser and Phot. Rev.* 5(1), 13–26, 1 (2011).
4. Gant, K.L., et al., Evaluation of collagen alterations in early precursor lesions of high grade serous ovarian cancer by second harmonic generation microscopy and mass spectrometry. *Cancers* 13(11), 2794, 6 (2021).
5. Huttunen, M. J., et al., Automated classification of multiphoton microscopy images of ovarian tissue using deep learning. *Journal of Biomedical Optics* 23(06), 1, 6 (2018).
6. Mirsanaye, et al., Machine learning-enabled cancer diagnostics with widefield polarimetric second-harmonic generation microscopy. *Scientific Reports* 12(1), 1–14, 6 (2022).
7. Rotter, S. and Gigan, S. Light fields in complex media: Mesoscopic scattering meets wave control. *Reviews of Modern Physics* 89(1), 015005, 3 (2017).
8. Kang, S., Kang, P., Jeong, S. et al., High-resolution adaptive optical imaging within thick scattering media using closed-loop accumulation of single scattering. *Nat. Commun.* 8, 2157 (2017).
9. Badon, A., et al., Smart optical coherence tomography for ultra-deep imaging through highly scattering media. *Science Advances* 2, 1600370, (2016).
10. Zhu, L., Soldevila, F., Moretti, C. et al. Large field-of-view non-invasive imaging through scattering layers using fluctuating random illumination. *Nat. Commun.* 13, 1447 (2022).
11. de Aguiar, Hilton B., et al., Enhanced nonlinear imaging through scattering media using transmission-matrix-based wave-front shaping, *Phys. Rev. A*, 94 043830 (2016).

# LOGIC: Logic Optical Gates for Integrated Computing

Category: Information

This project aims to provide a stepping stone toward digital optical computing by developing integrated digital optical components such as logic gates, adders, and counters.

**Applications to real-world issues** Electronic data processing is ubiquitous and has a problem. The increasing difficulties in shrinking the fabrication process and increasing the clock speed led the industry to rely on parallelization with the drawback of increasing power consumption. The dream I am pursuing with my company Akhetonics is to realize the first photonic digital processor. A more grounded goal is to target the bottlenecks of electronic computing, that are easy to replace optically.

Data centers provide two basic functions that are perfect candidates. Packet routing and packet filtering. These can be performed by tens, maybe a few hundred, of logic gates and would benefit from the superior speed and latency of photonic processing at a reduced power footprint.

The emerging analog optical computing and quantum computing would benefit too. Both of these fields require some processing of the optical information before and after the core computing, and an interface with the system where they will be embedded. Let's say that they need a "janitor", and a digital photonic processor plays a crucial support role for these technologies.

**Capabilities** My company Akhetonics GmbH has an internal lab with an optical and electrical probing station equipped with all the required tools and instruments to characterize photonic integrated circuits (PIC). We follow a fabless approach, with a strong network of partners for fabrication. We are collaborating with the Max Planck Institute for the Science of Light, which provides a clean room with very flexible and rapid prototyping but low volumes. We have a contract with IHP that is capable of medium volume  $\text{Si}_3\text{N}_4$  fabrication and graphene deposition. We already scheduled a run with them. For mass production, we are in contact with Ligentec and Paragraf.

I have experience in  $\text{Si}_3\text{N}_4$  fabrication in the MPL clean room where I worked for the last two years. Also, I worked in nonlinear optics since 2013. In recent years my work focused on the realization of all-optical switches, memories, and logic gates in microresonators. However, those devices were only proof-of-principle. Here is where my co-founder, Michael Kissner, comes into play. He has a background in chip security, chip hacking, and architecture design as a researcher for the German military. Michael is an invaluable source of knowledge on device integration and interfaces. He designed an architecture for optics instead of adapting one for electronics.

**Intended outcomes** The most immediate outcome of this project will be patent publishing on the researched technologies, which will be immediately followed by publication in peer-reviewed journals and presentation at international conferences, such as CLEO, ECOC, and graphene week.

This dissemination will promote the research of 2D materials for optics. Currently, most of the research is in electronics despite the intriguing optical properties of graphene and friends.

As a company, we will release the first products such as PIC logic gates, adders, and counters that will function all optically at unprecedented speed. Finally, the technology will be available and easy to integrate for researchers and industry for real, not only as a proof-of-principle.

As a result of the above, I expect to establish myself and my company as one of the reference points in digital optical computing. Also, the success of this project would allow us to attract more funding, public and private, to continue on the road to optical digital processors.

# LOGIC: Logic Optical Gates for Integrated Computing

## 1 Literature review

Photonic digital computing is not a new idea, it was investigated by Bell Labs around 1990. But the times were not mature. In the original proposal by the group of Alan Huang [1] light was transmitted in free space. The programming of logic gates was done with the optical equivalent of punch-cards steering light to the appropriate path. After that attempt digital photonic computing was almost forgotten for 30 years while electronic computing was growing at an astonishing rate becoming what it is today.

In recent years several works regarding individual all-optical components started to emerge again. I investigated Kerr bi-stability in ring resonators [2, 3], together with other groups, e.g. [4]. Kerr effect can be used for both memory and logic gates, and provides robust logic states in a passive device. However, resonant structures are inherently slow. Logic gates have been theorized in several configurations and demonstrated in silicon photonic integrated circuits (PIC) with carrier generation [5] and four-wave mixing [6]. Active micro-ring lasers seem promising as optical memories [7]. However, active devices require complex fabrication of multi-layer structures and power distribution in the chip. Alternatives are the use of phase-changing materials [8], photonic crystals or semiconductor optical amplifier Mach-Zehnder interferometer (SOA-MZI) [9].

All the aforementioned research has been demonstrated at the proof-of-principle level of a single logic gate or a single bit of memory (except [9]). Most of the devices described above work great individually but they are bulky, unstable, and difficult to integrate on a single platform. Little research has been made in terms of memory addressing, logic gate cascading, and architecture.

Times are now mature for this kind of research. All information is now traveling in fiber and the PIC technology was barely available in the 90s. Nowadays instead, there is a problem to solve with electronic computing (more on this in the Problem statement section) and integrated photonic is developing quickly.

The most diffused platform is silicon since it benefits from about 70 years of research, technological progress, and process optimization in the field of electronics microfabrication which can mostly be translated to the field of optics. The problem with silicon is the high absorption of light, on the order of dB/cm. This limit comes mostly from two-photon absorption and it is, therefore, a physical limit. Silicon is more transparent in the mid-IR, but unfortunately, it starts absorbing strongly below the wavelength of 3.5  $\mu\text{m}$  where the telecom band is.

Silicon Nitride ( $\text{Si}_3\text{N}_4$ ) is a promising alternative to silicon. It is much more transparent than silicon, with losses as low as 0.13 dB/m [10], especially in the telecom frequency band. The fabrication process had to be developed from scratch, however, there is a clear indication that this material has reached maturity for mass production. High yield has been demonstrated [11], and some of the highest Q-factors in integrated optics [12] have been reached, proving the quality of the process. Furthermore, techniques to bond different platforms, such as wire bonding, allow combining the benefits of both worlds and include even more materials in the mix.

## 2 Problem statement / Objectives

How not to cite one of the most iconic laws that even the laymen know: *the number of transistors in an integrated circuit will double every 2 years*. In the 90s Moore law was [13] driving the electronic industry, and the limit of computing speed was not in sight, even if it was already studied [14]. At first sight, computing power is still increasing to fulfill the requirements of emerging technologies, such as machine learning. At a closer look, however, it is clear how

the computing industry is struggling to keep pace with the Moore law. We haven't seen any significant clock speed improvement in the last 15 years and we are stuck at 5 GHz after years of literally exponential increase. All major manufacturers are forced to rely on parallelization to keep increasing CPU performances. An AMD Ryzen EPYC CPU now contains 64 cores, has a thermal design power of 280 W, and has the size of a credit card. This poses a two-fold problem. Not only does heat dissipation in data centers require additional energy for the temperature control system, but, with the current energy crisis, power is a precious resource both in economical and environmental terms.

Digital optical computing is the most promising solution to these problems. While in an electronic computer the information is only encoded in the voltage level of a signal, light has a much greater potential. The corresponding quantity for electronic voltage could be optical power. But on top of that phase, polarization, wavelength, and sometimes spatial modes can be used to store and encode additional information. It is not surprising that the whole field of telecommunication was forced to change from copper wires to optical fibers, the advantages were too conspicuous to be ignored. Regarding the clock speed, photonics is again the solution to break the few-GHz barrier. As an example, microresonators are used to produce frequency combs, corresponding to a train of pulses in the time domain, with repetition rates up to the THz region. Most of the optical nonlinearities proposed for information processing, such as the Kerr effect or saturable absorption, can easily respond at that frequency.

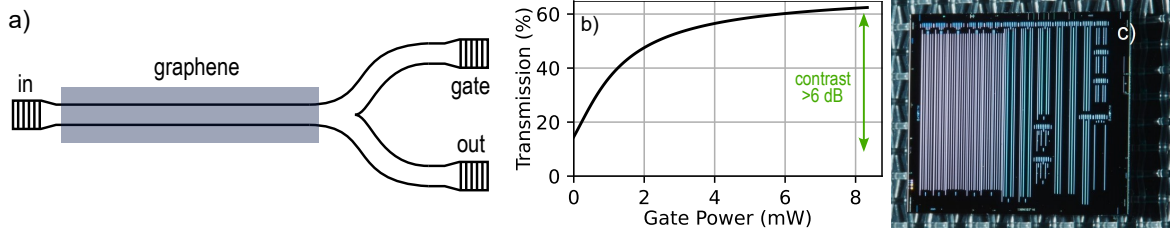
Most information is nowadays transmitted optically, especially when the transmission distance is over 1 m. But all the processing is electrical. Despite the conversion from optical to electrical and back requires fast lasers and photodiodes to be implemented, the bandwidth of optical communication makes it beneficial. So much advantageous that Nvidia and Intel are planning to use photonics interconnects even for smaller distances: board-to-board and chip-to-chip communication. The natural continuation of this trend would be avoiding the conversion back and forth to electric. Bringing also some of the processing, such as the one necessary for the routing of signals, into the photonic design would further reduce latency in the data centers. Not to mention the second-order benefit of reducing the complexity. A device made of fewer components, all integrated into the same platform, would reduce both the cost of and the power consumption.

The "old" classical computing will not be the only field affected by digital optical computing. The emerging analog optical computing and quantum computing would benefit too. Both of these fields require some processing of the optical information before and after the core computing, and an interface with the system where they will be embedded. Let's say that they need a "janitor", and a digital photonic processor plays a crucial support role for these technologies.

You may ask, if there are all these advantages, then why this "optical computing revolution" did not happen already? The reasons are multiple. The investment required to build a silicon foundry is estimated at over 10 B\$ and the foundry requires several years to become operational. Hence, semiconductor companies are not agile "garage" start-ups anymore. Making such an important pivot is not easy for them and they could be dealing with a sunk cost fallacy. The other reason is that, until now, the material technology was not ready for implementation. Only now clean rooms facilities are appearing that provide photonic integrated circuits (PIC) manufacturing. Some of our collaborators like Ligentech and IHP are an example.

The goal of Akhetonics is to fabricate the first integrated optical digital processor. We realize that building an all-optical digital processor is a complex task and will require time. That is why we are initially focusing on telecommunication and data center applications where simple operations, such as routing and packet inspection, must be performed repeatedly at a very high speed. Our approach is unique in combining the common physicist approach from the bottom-up with a top-down approach typical of architecture design. On one side, we are studying the technology to realize the individual components and how to combine them into more and

more complex devices. On the other, we are working on the high-level architecture designing the whole chip starting from the desired functionality. These two approaches provide valuable feedback to each other, in terms of identifying key specs and directing the development. As an example, we found out that a simple instruction set that can be performed at high speed with fewer components is better for photonic computers, instead of the current electronic approach of complex instruction that requires billions of transistors to be executed.



**Fig. 1.** a) Simplified schematic of the transistor. b) Simulated performances of the transistor. c) Test chip.

The current funding situation of Akhetonics does not allow testing the transistor design. The focus is mostly on optical design software development. Securing the Optica 20th anniversary challenge grant would allow me to realize designs that I have only simulated so far. My goal is to fabricate and test optical logic gates based on the saturable absorption of graphene in  $\text{Si}_3\text{N}_4$  waveguides and combine them to realize digital components such as digital adders and counters. On the road to this goal, I will first characterize the saturable absorption of graphene on  $\text{Si}_3\text{N}_4$  waveguides to realize an optical transistor. I already experimented with side polished optical fibers and transferable graphene and with  $\text{Si}_3\text{N}_4$  chips without graphene (Fig. 1c) with promising results. Simulations show that an integrated waveguide with better mode confinement performs significantly better (Fig. 1b).

I already developed an all-optical transistor design based on the saturable absorption of graphene (Fig. 1a). Using the language typical of MOSFET transistors, a gate beam would saturate the graphene absorption making the waveguide transparent for a source/drain beam.

I can then combine the transistors to implement logic gates, from the simple AND to the more challenging XOR or NAND. In particular, the NAND gate is a universal logic gate that would allow the realization of any other logical port. Of course, it is possible to implement better designs than just a combination of NAND gates to realize the other logic gates. Compared to the previous realization of logic gates described in the literature review section, this one would have significantly better performance. First, graphene saturation is broadband, so the device would be wavelength agnostic, removing the need for laser tuning or locking. Also, the graphene saturation and relaxation have a timescale of the order of picoseconds, much faster than resonant devices or effects based on thermal tuning.

Finally, I will combine logic gates to realize either a full- or half-adder. This is one of the key components for optical computing since it is at the foundation of counters, multipliers, and almost any component of a CPU. For more complex devices I would need to implement optical gain in the chip. This has been demonstrated in materials such as InP and is being explored in GaN, but unfortunately, the fabrication would be over the budget of this grant. Nevertheless, the demonstration of a working platform would allow me to attract funding for further research on the topic. Another benefit of the industrial setting of my research is that there are already clients interested in devices such as adders or simple logic. The revenues from these devices would be also invested in further research.

### 3 Outline of tasks / Work Plan

For the fabrication, I will follow the fabless approach. I already have contacts and agreements in place with Ligentech and IHP for the fabrication of state-of-the-art SiN waveguides and



components. Also, I have an ongoing collaboration with IHP and Paragraf for the deposition of Graphene as a saturable absorber on the waveguides. Akhetonics is a member of the graphene flagship, an invaluable source of networking and insight. Furthermore, we are discussing a collaboration with the cleanroom at Max Planck Institute for the Science of Light (MPL), where I previously worked. MPL cleanroom is equipped to fabricate silicon nitride PICs via electron beam lithography, which allows for very quick prototyping and iteration.

This project will proceed by realizing incrementally more complex devices based on the results of the previous steps. This allows us to easily identify possible problems and pin them to a specific item, instead of resulting in complex troubleshooting. The task list for each step consists of a classic development cycle with the typical timescale reported in parenthesis. Initially, I will simulate the device with Ansys Lumerical and custom code and design the GDS file for fabrication with Nazca and Klayout (1.5 months). GDS is a standard file format used in microfabrication that contains all the instructions and the geometry of the device. The file will then be sent to a cleanroom to be fabricated (1 month) and once ready will be tested in-house (1 month). The characterization will provide both the ground basis for the next step and material for scientific publication in peer-reviewed journals and conference talks (1 month). The dead time provided by fabrication will be used for the dissemination phase. The steps are described in the previous section. The timeline for their realization follows:

1. **Graphene on  $\text{Si}_3\text{N}_4$ .** Simulations and GSD files are completed. (December 2022)
2. **Transistor.** The device is already simulated. (March 2023)
3. **Logic gate.** An initial design is available. (September 2023)
4. **Adder.** (Q1 2024)

## 4 Outcome(s)

I will demonstrate all-optical logic gates and transistors integrated on a chip. Given the industrial environment of the project, it will not be a simple proof of principle but a fully implemented and interfaced system.

Intermediate results will be published and/or presented at conferences. Specifically, I plan to write a paper on all-optical transistors based on this technology including the characterization of the underlying physics of graphene on  $\text{Si}_3\text{N}_4$ . A second paper will disseminate the results on logic gates based on this technology. This work will be presented at international conferences such as ECOC, CLEO, and graphene week.

A product will be realized making this technology available to industry and academia

## 5 Impact

The impact of digital photonic computing is so vast that it is difficult to quantify. Removing the current barrier to energy-efficient computation power may lead to performing some of the tasks relegated to servers on portable devices. Our long-term approach is to scale up the number of gates to realize a full processor. We already have the architecture for a 4-bit processor that we call ANKH4. We also developed a compiler so that the processor can run general-purpose code.

On a shorter timescale, the implementation of photonic-based RISC in data centers and communication hubs, where the infrastructure is already optical, will significantly reduce the power consumption and boost the speed, first in key areas and devices and then replacing the whole technology used in the data center. All-optical devices in data centers also drastically reduce the latency and increase the bandwidth of network traffic. These two factors have been the showstoppers for network-wide adoption of encryption and security. The most obvious and direct impact will be the greatly reduced power consumption by our CPUs compared to electronic CPUs. As an example, our ANKH4-Prototype is expected to have the same or

better computing performance metrics as a modern Intel Core i9 9900K running at 249W. But our ANKH4 has a great advantage: it only uses approximately 1W of power. Data centers currently account for more than 200 TWh per year or 1 % of global electricity consumption and this number is doomed to rise if we do not change something [15]. Of course, we do not want to stop at the data center. Our vision is to bring these reductions to all digital devices, potentially saving over 800 TWh per year.

But the impact will not only be economical. Participating in conferences about photonics and 2D materials, I realized how the two fields are still separated. Deepening the knowledge in the use of graphene for optics could boost fields beyond computing since it provides a form of nonlinearity that is very broadband and can be accessed at low input power. I am convinced that producing the first results in a combined field would spark ideas in many research groups. We have very close collaborations with academia such as MPL (Erlangen, Germany) and WinPhos (Thessaloniki, Greece), and both of them are curious about the result of this research.

## References

- [1] A. Huang. “Architectural considerations involved in the design of an optical digital computer”. In: *Proceedings of the IEEE* 72.7 (1984), pp. 780–786.
- [2] Leonardo Del Bino, Niall Moroney, and Pascal Del’Haye. “Optical memories and switching dynamics of counterpropagating light states in microresonators”. In: *Opt Express* 29.2 (Jan. 2021), pp. 2193–2203.
- [3] Niall Moroney et al. “Logic Gates Based on Interaction of Counterpropagating Light in Microresonators”. In: *Journal of Lightwave Technology* 38.6 (Mar. 2020), pp. 1414–1419.
- [4] Wataru Yoshiki and Takasumi Tanabe. “Analysis of bistable memory in silica toroid microcavity”. In: *Journal of the Optical Society of America B* 29.12 (2012), p. 3335.
- [5] Qianfan Xu and Michal Lipson. “All-optical logic based on silicon micro-ring resonators”. In: *Optics Express* 15.3 (2007), p. 924.
- [6] Meng Xiong et al. “All-optical 10 Gb/s AND logic gate in a silicon microring resonator”. In: *Opt. Express* 21.22 (Nov. 2013), pp. 25772–25779.
- [7] Martin T. Hill et al. “A fast low-power optical memory based on coupled micro-ring lasers”. In: *Nature* 432.7014 (Nov. 2004), pp. 206–209.
- [8] Carlos Rios et al. “Integrated all-photonics non-volatile multi-level memory”. In: *Nature Photonics* 9.11 (Sept. 2015), pp. 725–732.
- [9] Christos Vagionas et al. “Integrated Optical Content Addressable Memories (CAM) and Optical Random Access Memories (RAM) for Ultra-Fast Address Look-Up Operations”. In: *Applied Sciences* 7.7 (2017). ISSN: 2076-3417.
- [10] Xingchen Ji et al. “Ultra-low-loss on-chip resonators with sub-milliwatt parametric oscillation threshold”. In: *Optica* 4.6 (June 2017), p. 619.
- [11] Junqiu Liu et al. “High-yield, wafer-scale fabrication of ultralow-loss, dispersion-engineered silicon nitride photonic circuits”. In: *Nature Communications* 12.1 (Apr. 2021).
- [12] Xingchen Ji et al. “Methods to achieve ultra-high quality factor silicon nitride resonators”. In: *APL Photonics* 6.7 (July 2021), p. 071101.
- [13] Gordon E. Moore. “Cramming more components onto integrated circuits”. In: *Electronics* 38.8 (Apr. 1965).
- [14] R.W. Keyes. “Physical limits in digital electronics”. In: *Proceedings of the IEEE* 63.5 (1975), pp. 740–767.
- [15] Eric Masanet et al. “Recalibrating global data center energy-use estimates”. In: *Science* 367.6481 (Feb. 2020), pp. 984–986.

# **Dielectric nonlinear metamaterials for generation of Radiation at THz frequencies**

## **DART**

### **Executive summary**

The THz spectral band, between the far-infrared and microwave bands, has been for many years unexplored due to technological challenges. New applications in several areas such as medicine, astronomy, material science, communications, and security have galvanized interest in THz systems. The high bandwidth availability makes the use of THz signals with ad-hoc orbital angular momentum (OAM) a promising approach to accommodate the demand for ever-increasing wireless capacity with ultra-secure links. However, the lack of efficient, compact, and controllable THz sources has held back progress in this sector.

I propose to lead a potential breakthrough in this field by developing a new family of THz-photonics transceivers with unmatched functionalities based on a disruptive platform founded on novel artificial nonlinear optical materials. The approach is based on difference frequency generation (DFG) in dielectric metasurfaces (DM) – large-area two-dimensional metamaterials – for optical-to-THz conversion with an efficiency that is comparable to the best nonlinear materials in nature. This will mark a paradigm shift reducing the device dimensions by a factor of 1000 and enabling the generation of light in the THz-gap where existing sources cannot provide an exploitable signal.

We will design novel dielectric metasurfaces that efficiently emit THz beams with a generation efficiency that is enhanced by more than three orders of magnitude compared to the state-of-the-art and build the foundations for the development of ultracompact THz-photonics transceivers for seamless data conversion with unmatched functionalities compared to existing technologies.

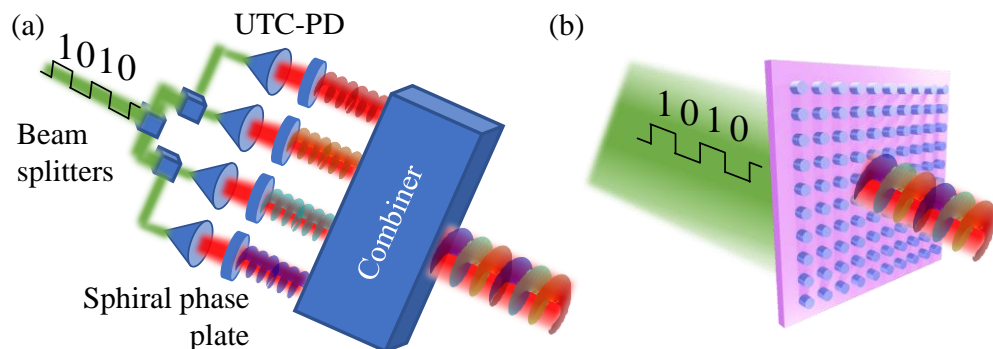
The research approach is based, first, on the development of analytical and numerical models of NIR-to-THz DFG in isolated dielectric nanoresonators. Since the dimensions of the nanoresonators (1 micrometer) are comparable to the NIR signals (1.55 micrometer) but much smaller than the wavelength of the THz radiation (30-300 micrometers) this multi-physical modeling is challenging. I will consider AlGaAs and LiNbO<sub>3</sub> as constituent materials due to their high nonlinear response in the THz band. The crystal orientation and modal engineering (e.g. bound states in the continuum) will be used to enhance conversion efficiency and control the emission properties. These models will be validated in DFG experiments. Once the modeling is established, I will move to metasurface and arrayed structures. Exploiting the huge dimensional difference between NIR and THz physics, I will study nanoparticle arrangements that are individually optically resonant in the NIR and collectively form a cavity (e.g. dipole antenna) in the THz band.

I expect that the outcome of this research will be the development of a unique THz generation technology that will lead to the, long sought, leap in the THz gap and will seed new THz short-range wireless communications standards for Tbps wireless interconnects in data centers, broadcasting of HDTV channels for real-time conversations, kiosk downloading, wireless cognition, and intersystem (card-to-card, device-to-device) communication. The results will also benefit other applications requiring on-demand coherent THz light as sensing, imaging, and holography.

➤ **General context and key-points**

The recent spreading of *cloud services*, *big data centers*, and the emergence of new applications such as *virtual/augmented reality*, *Internet of Things*, *autonomous driving*, and *information shower*, are posing an increasing demand for additional capacity and reduced latency for distributed computation and faster bandwidth provisioning. While fiber-linked optical communication is successfully growing, the data rate of wireless links remains relatively poor and needs to rapidly approach Tbps rates. The only feasible solution is to increase the carrier frequency beyond the Microwave region of the electromagnetic (EM) spectrum. Radiation at THz frequencies (1 – 10 THz) is nonionizing and currently unregulated by telecom agencies. For these reasons, **THz photonics-wireless** or “**wireless over fiber**” communication systems could provide a solution fit for future wireless networks and applications [1,2]. The key element of this framework is a **THz-photonics transceiver (THz-PT)**: an all-optical device capable to convert the information signal from optical frequencies (typically in the near-infrared, NIR) to THz frequencies without corruptions (i.e., conserving amplitude and phase modulation). Extreme data rates can be obtained by boosting spectral efficiency with special multiplexing techniques such as the one based on the **orbital angular momentum (OAM)** state of EM beams [3]. A representation of THz-PT implementing OAM multiplexing using current technological solutions is shown in Fig. 1a. Operating in the full THz band (above 1 THz) and increasing the number of channels requires radically new technological solutions.

I will introduce a novel key point that will be the cornerstone of a new scientific exploration: **THz-PT based on dielectric metasurfaces (DMs)**. My idea is to develop a *novel class of artificial nonlinear optical materials (metamaterials)* for the generation and manipulation of THz beams (Fig. 1b).



**Figure 1.** Schematics of THz-PT implementing OAM multiplexing schemes based on (a) uni-traveling-carrier photodiodes (UTC-PDs) and (b) Difference frequency generation in a DM. The signal carrying the digital information at NIR frequencies (green) is converted to the THz band (red) with a controlled OAM state (different colors represent different OAM states – communication channels).

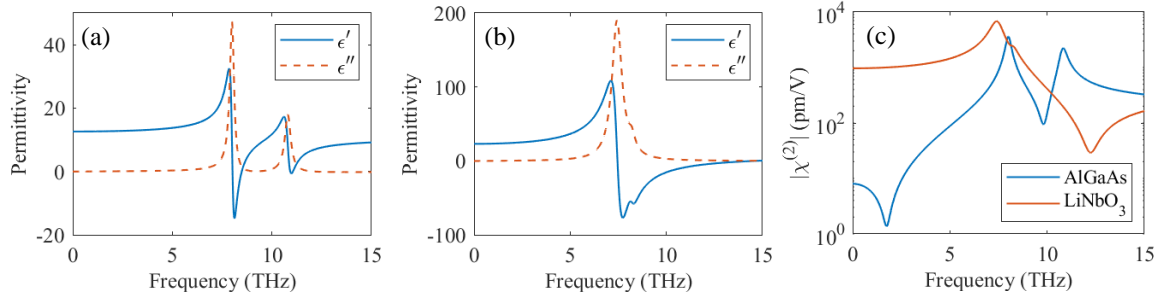
➤ **Challenges and objectives**

The DART project faces different aspects and challenges of light-matter interaction at the nanoscale that are among the hot topics in current scientific research in optics.

**Nanoscale THz light sources.** Nonlinear optical phenomena have been widely used to access new spectral regions. For example, in difference frequency generation (DFG) a photon at frequency  $\omega_1$  and one at  $\omega_2$  are converted into a photon at frequency  $\omega_3 = \omega_1 - \omega_2$ . If  $\omega_1$  and  $\omega_2$  are in the NIR band (around a wavelength of 1550 nm) and separated by less than 10 THz ( $\leq 85$  nm), then the DFG photons are in the THz band. However, achieving high conversion efficiency requires strong EM fields and/or bulky components due to the low nonlinear optical response of natural materials. Recently, a new approach based on the extraordinary electric field enhancement in nanoscale volumes exhibited by dielectric nanoparticles supporting Mie resonances has emerged [4,5]. In 2015, I have been the first to demonstrate their potential for **second-harmonic generation**, a second-order nonlinear process as DFG, in **AlGaAs nanoantennas in theory** [6] and **experiment** [7]. In 2018, I have shown that **high Q-factor**

*modes* inspired by the bound states in the continuum (BIC) physics can yield higher conversion efficiencies [8,9]. DFG for THz generation has been recently demonstrated in plasmonic metasurfaces [10,11] with conversion efficiencies comparable to a 0.2 mm thick ZnTe crystals. However, plasmonic structures are limited by ohmic loss and the use of only surface nonlinearity. Instead, DFG in nanostructured polar dielectric materials (like AlGaAs and LiNbO<sub>3</sub>) has a stronger potential: in the THz band, these materials support lattice vibrational modes (phonons) that can strongly couple to EM fields originating phonon-polaritons (PhPs) [12]. This results, from one side, in negative permittivity in the PhP band (Fig. 2a-b) that originate localized modes – *local surface phonon-polaritons* (LSPPhPs) – with extreme subwavelength field enhancement and, from the other side, in an enhancement of the second-order nonlinear permittivity,  $\chi^{(2)}$ , by a factor  $\sim 10^2$  with respect to the NIR band (Fig. 2c). Our preliminary studies, [13], indicate that these effects are fundamental for enhancing DFG in dielectric nanoresonators by several orders of magnitude compared to plasmonic nanostructures.

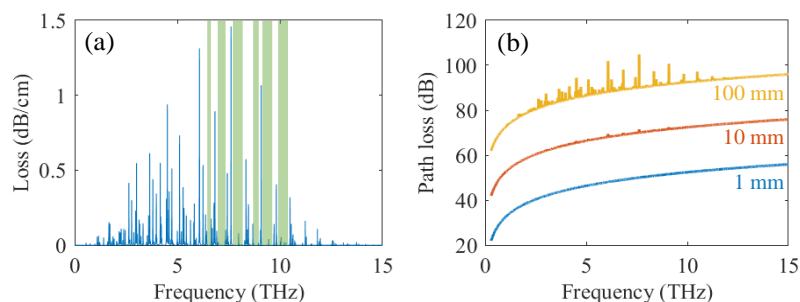
**Objective: enhanced THz generation in DMs.** I will exploit high Q-factor modes and Mie-LSPPhP coupling to enhance the *conversion efficiency of DFG up to  $10^{-5}$*  demonstrating efficient optical-to-THz conversion in an ultrathin ( $\sim 1\mu\text{m}$ ) DM, i.e., large area two-dimensional arrangements of resonant nanostructures (meta-atoms). This will be at least three orders of magnitude larger than plasmonic metasurfaces.



**Figure 2.** Complex permittivity ( $\epsilon = \epsilon' + i\epsilon''$ ) of AlGaAs (a), and LiNbO<sub>3</sub> (b) in the THz band. (c) Magnitude of  $\chi^{(2)}$  for optical-to-THz DFG.

### ➤ Impact

The technological approaches to THz communications currently rely on principle demonstrations that are several decades old [2,14–16]. The use of DMs for optical-to-THz converters will bring them a step forward toward the hoped-for industrial devices. Typical system architectures to generate and manipulate THz light (Fig. 1a) are of difficult integration. Although first demonstrations of integrated systems are emerging, [17,18], my technology based on nonlinear DMs will mark a paradigm shift reducing the device dimensions by a factor of 1000 with improved functionalities. Optical metasurfaces have demonstrated unprecedented capabilities for the manipulation and steering of light and the dynamic control of the optical response up to GHz modulation rates. This entails the possibility to overcome the current limitation of components that are used to manipulate the light properties (e.g., polarization state, focusing, steering) in the THz band. Furthermore, DFG enables the generation of light in the **THz-gap** where existing sources cannot provide an exploitable signal [2]. *Photomixers* (pin diodes and UTC-PDs) and *photoconductive mixers* suffer from a decrease in THz power as the frequency increases [2]. DFG in *nonlinear crystals* results in bulky setups [19,20]. *Quantum cascade lasers* (QCL) operate only at cryogenic temperatures. Despite a promising approach at room temperature based on DFG inside QCL that has been reported [21], QCLs are limited to sub-6-THz emission. Finally, *vacuum and solid-state electronic devices* are limited to sub-THz bands [22]. The approach that I propose here based on DMs will overcome these hurdles and enable access to available low-loss telecom windows ( $>50$  GHz) in the THz-gap where path losses are minimized (Fig. 3).



**Figure 3.** (a) Absorption loss due to water vapor in air. Green bars show low-loss telecoms windows in the 5 – 10 THz spectral range. (b) Path loss for links of different lengths over the THz spectral range.

DART envisions a new paradigm for THz short-range wireless communications for Tbps wireless interconnects in data centers, broadcasting of uncompressed HDTV channels for real-time conversations, kiosk downloading, wireless cognition, and intersystem (card-to-card, device-to-device) communication in complex electronic apparatus. The results of DART research will also benefit other applications requiring on-demand structured THz light beams such as sensing, imaging, and holography.

### ➤ Research methodology and Outcomes

The purpose of DART is efficient *generation of THz beams* by mastering nonlinear optical interactions in DMs. I envisage four working packages (WP), each of them bringing several advances and novelties compared to the state-of-the-art.

#### **WP1: DFG in isolated nanoresonators**

Objective: new models to describe DFG from NIR to THz bands in dielectric nanoresonators.

Methodology: rational design tools based on accurate and predictive models are fundamental to engineer miniaturized photonic devices such as nanoantennas and metasurfaces for specific applications [6]. DFG in polar crystals like AlGaAs and LiNbO<sub>3</sub> will be driven by Mie and LSPHP resonances. This coupling has never been modeled. I will adopt three different approaches. (1) Finite-element-method (FEM) simulations based on commercial software. The challenge is to manage computational resources to couple physical models where the wavelength of light is extremely different. (2) Analytical model based on quasi-static approximation (QST). Since the dimensions of the nanoresonators (<1μm) are much smaller than the wavelength of the THz radiation (30 – 300μm), their optical response can be modeled using QST [13]. (3) Semi-analytical model based on quasi-normal modes (QNM) [23]. I will extend this framework to the THz band and DFG. These models will be used to enhance DFG, by designing high-Q modes like BIC in the NIR band, different crystalline orientations ([110] AlGaAs), and materials (LiNbO<sub>3</sub>).

In DART I will go beyond a purely theoretical approach. The strong active collaborations with the Université Paris-Diderot (AlGaAs) and the Italian Institute of Technology (LiNbO<sub>3</sub>) will be an asset for the fabrication of the most promising designs. DFG conversion efficiency will be estimated in nonlinear microscopy experiments performed at the host institution. The experimental setup is based on an optical parametric amplifier (OPA) delivering two femtosecond pulses with a tunable central wavelength between 640–940 nm ( $\omega_s$ ) and 1150–2600 nm ( $\omega_i$ ) that is already present at the host institution.

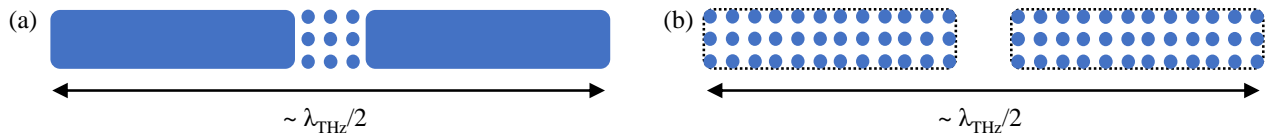
Risk and Backup: WP1 is moderate risk because DFG has never been modeled in these systems, but our preliminary results are encouraging [13]. The risk mitigation strategy is based on diversification of the approaches each presenting strengths and weaknesses: FEM requires a high computational load but can fully describe the nonlinear process, QST and QNM models provide fast and useful physical insights, but conversion efficiency estimations are more difficult. The payoff (**M1**) will be models that are parametric, predictive, and generalizable to large classes of engineered materials and geometries.

#### **WP2: From a single element to a metasurface**

Objective: NIR-to-THz DFG in DMs.



**Methodology:** The large dimensional difference between the NIR and THz wavelengths will be exploited to design meta-atoms arrangements to form resonant THz structures (Fig. 5). This will allow to enhance THz emission and locally control the light properties with sub-wavelength resolution. Different systems inspired by radio-frequency antennas will be designed such as dipole antenna or bow-tie antenna. I envision two approaches: 1) use DFG in nanodisks to feed the THz antenna based on LSPnP (Fig. 5a); 2) arrange the nanodisk to form the layout of a resonant antenna (Fig. 5b). Both techniques require a non-trivial evaluation of modal overlap between the DFG sources and the resonant THz field. These approaches enable designs with high-Q modes in the NIR and THz bands since the problems are separated. The most promising designs will be fabricated. The THz response will be inferred from micro-Raman and Fourier-transform infrared (FTIR) spectroscopy; DFG will be characterized by adapting the setup shown in Fig. 4 for metasurface excitation.



**Figure 5.** Top view of devised structures. (a) Centre fed THz dipole antenna. (b) THz dipole antenna constituted by NIR metasurfaces.

**Risk and Backup:** WP2 is high-risk/high-gain due to the difficulty of simultaneously modeling and designing devices that exploit physical phenomena that act at such different dimensional scales. However, our preliminary results and previous experience support these expectations [6,8,24,25]. The high payoff is in the importance of the achievement of M2 that will open to efficient THz-PTs based on ultrathin metasurfaces.

### Milestones

**M1: Models for optical-to-THz DFG in dielectric meta-structures.**

**M2: Efficient DM-based THz-PT. *Conversion efficiency*  $\geq 10^{-5}$**  using a femtosecond pulse of a few GW/cm<sup>2</sup>.

The WPs and the timelining of DART are shown in the Gantt-chart table below:

ID	Action name	Year 1		Year 2	
		I	II	I	II
WP1	Modeling DFG in isolated nanoresonators	[Bar]			
M1	Models for optical-to-THz DFG in dielectric meta-structures			[Diamond]	
WP2	From a single element to a metasurface			[Bar]	
M2	Efficient DM-based THz-photonics transceiver				[Diamond]

### References

1. H. Shams and A. Seeds, "THz Wireless," Opt. Photonics News **28**, 24–31 (2017).
2. M. Tonouchi, "Cutting-edge terahertz technology," Nat. Photonics **1**, 97–105 (2007).
3. L. Allen, M. W. Beijersbergen, R. J. C. Spreeuw, and J. P. Woerdman, "Orbital angular momentum of light and the transformation of Laguerre-Gaussian laser modes," Phys. Rev. A **45**, 8185–8189 (1992).
4. A. Krasnok, M. Tymchenko, and A. Alù, "Nonlinear metasurfaces: a paradigm shift in nonlinear optics," Mater. Today **21**, 8–21 (2018).
5. V. Zubyuk, L. Carletti, M. Shcherbakov, and S. Kruk, "Resonant dielectric metasurfaces in strong optical fields," APL Mater. **9**, 060701 (2021).
6. L. Carletti, A. Locatelli, O. Stepanenko, G. Leo, and C. De Angelis, "Enhanced second-harmonic generation from magnetic resonance in AlGaAs nanoantennas," Opt. Express **23**, 26544–50 (2015).
7. V. F. Gili, L. Carletti, A. Locatelli, D. Rocco, M. Finazzi, L. Ghirardini, I. Favero, C. Gomez,

- A. Lemaître, M. Celebrano, C. De Angelis, and G. Leo, "Monolithic AlGaAs second-harmonic nanoantennas," *Opt. Express* **24**, 15965–15971 (2016).
8. L. Carletti, K. Koshelev, C. De Angelis, and Y. Kivshar, "Giant Nonlinear Response at the Nanoscale Driven by Bound States in the Continuum," *Phys. Rev. Lett.* **121**, 033903 (2018).
  9. K. Koshelev, S. Kruk, E. Melik-Gaykazyan, J. H. Choi, A. Bogdanov, H. G. Park, and Y. Kivshar, "Subwavelength dielectric resonators for nonlinear nanophotonics," *Science* **367**, 288–292 (2020).
  10. M. Tal, S. Keren-Zur, and T. Ellenbogen, "Nonlinear Plasmonic Metasurface Terahertz Emitters for Compact Terahertz Spectroscopy Systems," *ACS Photonics* **7**, 3286–3290 (2020).
  11. Y. Lu, X. Feng, Q. Wang, X. Zhang, M. Fang, W. E. I. Sha, Z. Huang, Q. Xu, L. Niu, X. Chen, C. Ouyang, Y. Yang, X. Zhang, E. Plum, S. Zhang, J. Han, and W. Zhang, "Integrated Terahertz Generator-Manipulators Using Epsilon-near-Zero-Hybrid Nonlinear Metasurfaces," *Nano Lett.* **21**, 7699–7707 (2021).
  12. S. Foteinopoulou, G. C. R. Devarapu, G. S. Subramania, S. Krishna, and D. Wasserman, "Phonon-polaritonics: enabling powerful capabilities for infrared photonics," *Nanophotonics* **8**, 2129–2175 (2019).
  13. U. Arregui Leon, D. Rocco, L. Carletti, M. Peccianti, S. Maci, G. Della Valle, and C. De Angelis, "THz-Photonics Transceivers By All-Dielectric Phonon-Polariton Nonlinear Nanoantennas," *Sci. Rep.* (n.d.).
  14. G. Ducournau, P. Szriftgiser, A. Beck, D. Bacquet, F. Pavanello, E. Peytavit, M. Zaknoune, T. Akalin, and J.-F. Lampin, "Ultrawide-Bandwidth Single-Channel 0.4-THz Wireless Link Combining Broadband Quasi-Optic Photomixer and Coherent Detection," *IEEE Trans. Terahertz Sci. Technol.* **4**, 328–337 (2014).
  15. X. Yu, S. Jia, H. Hu, M. Galili, T. Morioka, P. U. Jepsen, and L. K. Oxenløwe, "160 Gbit/s photonics wireless transmission in the 300-500 GHz band," *APL Photonics* **1**, (2016).
  16. H. Shams, M. J. Fice, L. Gonzalez-Guerrero, C. C. Renaud, F. Van Dijk, and A. J. Seeds, "Sub-THz wireless over fiber for frequency band 220-280 GHz," *J. Light. Technol.* **34**, 4786–4793 (2016).
  17. Z. Xie, X. Wang, J. Ye, S. Feng, W. Sun, T. Akalin, and Y. Zhang, "Spatial Terahertz Modulator," *Sci. Rep.* **3**, 3347 (2013).
  18. S. Lepeshov, A. Gorodetsky, A. Krasnok, E. Rafailov, and P. Belov, "Enhancement of terahertz photoconductive antenna operation by optical nanoantennas," *Laser Photon. Rev.* **11**, 1600199 (2017).
  19. P. Shumyatsky and R. R. Alfano, "Terahertz sources," *J. Biomed. Opt.* **16**, 033001 (2011).
  20. K. Kawase, J. Shikata, and H. Ito, "Terahertz wave parametric source," *J. Phys. D: Appl. Phys.* **35**, R1–R14 (2002).
  21. Q. Lu, D. Wu, S. Sengupta, S. Slivken, and M. Razeghi, "Room temperature continuous wave, monolithic tunable THz sources based on highly efficient mid-infrared quantum cascade lasers," *Sci. Rep.* **6**, 23595 (2016).
  22. J. H. Booske, R. J. Dobbs, C. D. Joye, C. L. Kory, G. R. Neil, G.-S. Park, J. Park, and R. J. Temkin, "Vacuum Electronic High Power Terahertz Sources," *IEEE Trans. Terahertz Sci. Technol.* **1**, 54–75 (2011).
  23. C. Gigli, T. Wu, G. Marino, A. Borne, G. Leo, and P. Lalanne, "Quasinormal-Mode Non-Hermitian Modeling and Design in Nonlinear Nano-Optics," *ACS Photonics* **7**, 1197–1205 (2020).
  24. G. Marino, A. S. Solntsev, L. Xu, V. Gili, L. Carletti, A. N. Poddubny, D. Smirnova, H. Chen, G. Zhang, A. Zayats, C. De Angelis, G. Leo, Y. S. Kivshar, A. A. Sukhorukov, and D. N. Neshev, "Sum-Frequency Generation and Photon-Pair Creation in AlGaAs Nano-Scale Resonators," in *2017 Conference on Lasers and Electro-Optics (CLEO)* (2017), p. FTu4D.2.
  25. L. Carletti, A. Locatelli, D. Neshev, and C. De Angelis, "Shaping the Radiation Pattern of Second-Harmonic Generation from AlGaAs Dielectric Nanoantennas," *ACS Photonics* **3**, 1500–1507 (2016).

# **Integrated optical phased array-enabled ultrafast multiphoton lightsheet lensless microscopy + AI-based compressed sensing (Opa-fast-sheet)**

**Application for the Optica Foundation 20<sup>th</sup> Anniversary Challenge: Health category**

## **Executive summary**

Optical imaging is an important tool for biologists and doctors to understand fundamental biology and diagnose diseases. One emerging approach to this end is multiphoton lightsheet fluorescence microscopy (LSFM), which can capture images with subcellular resolution in real-time in a minimally invasive manner and generate images comparable to histopathology circumventing the need for tissue excision, enabling optical biopsy. Recently, lensless microscopy has been proposed to adapt LSFM to an optical fiber platform as an important step towards clinical translation. Lensless microscopy employs wavefront shaping to replace lenses at the distal end of the fiber leading to improved miniaturization. In order to correctly shape and steer the beam at the distal end of the fiber, the wavefront shaping must compensate for the so-called transmission matrix, which describes how the wavefront changes as it propagates through the fiber. The transmission matrix is highly variable as the fiber conformation changes, so the transmission through the fiber must be actively monitored and compensated for imaging in real world applications. Ultimately, wavefront shaping for lensless and lightsheet microscopy is inherently limited by the slow refresh rate of SLMs and camera-based wavefront sensors.

The Opa-fast-sheet project aims to revolutionize multiphoton lightsheet lensless microscopy with radically improved speed and wavefront correction by using an integrated silicon nitride optical phase array. We propose a new approach of beam shaping for lensless imaging and LSFM based on a novel integrated silicon-nitride optical phased array. Replacing current wavefront shaping techniques with an optical phased array has the potential to improve the imaging speed of light sheet microscopy by more than two orders of magnitude. In combination with compressive sensing-based wavefront monitoring, all speed bottlenecks for multiphoton lightsheet lensless microscopy will be removed. Once the Opa-fast-sheet hypothesis is confirmed, the final implementation of the technology will enable a new suite of biological studies and diagnostic methods based on minimally invasive fast volumetric image acquisitions.

# **Integrated optical phased array-enabled ultrafast multiphoton lightsheet lensless microscopy + AI-based compressed sensing (Opa-fast-sheet)**

## Background and literature review

### *Multiphoton lightsheet fluorescence microscopy for fast volumetric imaging*

Optical imaging is an important tool for biologists and doctors to understand fundamental biology and diagnose disease, but many challenges exist including the need for high resolution imaging fast enough to characterize highly dynamic biological processes in vivo. One emerging approach is multiphoton excited fluorescence microscopy (MPM), which can capture images with subcellular-resolution in real-time in a minimally invasive manner and generate images comparable to histopathology without the need to excise tissue. Compared with 1-photon fluorescence microscopy, MPM uses longer wavelengths of light and can image deeper in tissue. MPM imaging of the autofluorescence signal produced by endogenous metabolic substrates and structural proteins enables the analysis of tissue morphology and metabolism [1]. Utilizing exogenous fluorophores such as green fluorescent protein can provide additional specificity in images [2].

While MPM has many advantages over 1-photon fluorescence microscopy, MPM is limited by the low probability of a multiphoton fluorescence excitation event. As such, the signal-to-noise ratio in MPM is limited [3], and 3D volumetric scans are limited to low speeds such as 1 Hz [4]. Additionally, the high power and long acquisition times required for MPM risk photobleaching and photodamage of the sample. Recently, lightsheet fluorescence microscopy (LSFM) has been proposed as an alternative technique to reduce the risk of photodamage. LSFM employs selective illumination in the imaging plane to reduce the overall light exposure in the sample. Additionally, since LSFM uses a planar instead of point scanning, it can acquire images 100 – 1000 times faster than point-scanning methods. For fast 3D volumetric image acquisition and reduced laser irradiation to the specimen, LSFM must replace conventional point-scanning laser microscopy.

### *Miniaturizing fiber optic endoscopes using lensless microscopy*

For the clinical translation of multiphoton LSFM, miniaturization of bulky benchtop microscopes to endoscope prototypes is necessary and is often realized using optical fibers. Most endoscopes in current clinical use require lenses at the distal end to focus the beam, which limits the ability to miniaturize them. One recent development accelerating the miniaturization of micro-endoscopes is lensless microscopy, which uses wavefront shaping at the proximal end of the fiber instead of optical elements at the distal end, thus reducing its overall size to that of an optical fiber (a few hundred  $\mu\text{m}$ ) [5,6]. While single mode fibers lack the degrees of freedom for beam shaping due to the lack of multiple supported modes and hence are not suitable for lensless microscopy, multimode and multicore fibers are excellent candidates [7,8]. Through appropriate wavefront shaping techniques, one could generate a focal point or a lightsheet at the fiber distal facet and scan the beam.

### *Changing transmission matrix impedes lensless microscopy*

To fully utilize such beam-shaping techniques, one must have a thorough understanding of how a shaped beam propagates through a given fiber and how optical scattering in the sample impacts the wavefront. The so-called transmission matrix can be measured to determine optical propagation through a fiber and scattering material [9,10], but this experimental transmission matrix is only accurate if the fiber conformation and sample structure stays unchanged; if there is a significant change in the fiber's bending or twisting, the transmission matrix must be redetermined. The transmission matrix is typically measured by imaging the wavefront on a 2D pixel array or camera. This process is time consuming, limited by the acquisition rate of the camera (typically around 100 Hz), and thus limits the application of lensless microscopy in a real-world setting. One approach which could improve the speed of wavefront sensing is compressive sensing. Compressive sensing is an image processing protocol where size of the acquired datasets could be reduced by under-sampling images revoking the Nyquist criterion

[11]. Compressive sensing therefore demonstrates interesting potential for high-speed measurement of the transmission matrix since slow camera arrays could be replaced by fast photodetectors.

### *State of the art wavefront shaping tools*

To generate a lightsheet or to perform lensless microscopy, wavefront shaping tools must be employed. Deformable mirror devices [12], optical phase conjugation [13], micro-electro-mechanical system-based mirror arrays [14], and spatial light modulators (SLMs) [15] are the state-of-the-art techniques for wavefront shaping. All these approaches share the same significant limitation: speed. Of these approaches, the SLM stands out as the most promising so far. SLM is a display device with several liquid-crystal-filled cells or pixels whose spatial orientations are independently controlled to modulate the phase of the interacted light, creating the desired beam shape [16]. Although the SLM provides dynamic beam-shaping, the speed is limited by the refresh rate of the pixels, typically around 100 Hz. Moreover, the pixelated display introduces diffraction of light forming undesired orders, side lobes, and reduced power/intensity in the desired (modulated) order. The unmodulated component (undiffracted light) could take away 5-20% of the incident power which could add artifacts and noise, impeding contrast.

**Ultimately, wavefront shaping for lensless and lightsheet microscopy is inherently limited by the slow refresh rate of SLMs and camera-based wavefront sensors.**

### *Optical phased array: a new approach for ultrafast beam shaping*

Optical phased array (OPA), the optical counterpart to phased array radar, can electronically control the phase of light emitters, and allow for very stable, rapid and precise beam steering and shaping without any mechanical moving parts [17]. Due to the unique features of compact size, fast scanning (>10 kHz based on thermal-optic effect and >MHz based on electro-optic effect) and low cost, integrated OPA is becoming a transformative technology for optical beam steering [18]. These features are not available in any state-of-the-art SLM but will enable scientific breakthroughs in terms of applications enabled by high speed and compact size, and technological breakthroughs in terms of low cost.

**Replacing the SLM with an OPA has the potential to improve the imaging speed of lightsheet microscopy by more than two orders of magnitude.**

**In combination with compressive sensing-based wavefront monitoring, all speed bottlenecks for multiphoton lightsheet lensless microscopy will be removed.**

### *Problem statement and objective*

**Overall aim:** To revolutionize multiphoton lightsheet lensless microscopy with radically improved speed and wavefront correction by using an integrated silicon nitride optical phase array.

#### **Objectives:**

- To revolutionize lightsheet lensless microscopy using a fast, robust system, enabling imaging of dynamic biological processes with low phototoxicity
- To develop a new, fast integrated optical phased array combined with compressive sensing that will provide the necessary increase in terms of speed and performance
- To demonstrate two-photon and three-photon excited fluorescence lightsheet lensless microscopy enabled by the silicon nitride optical phased array

### *Work plan*

The three interrelated work packages (WP1-3) aim at a truly integrated approach to assess the feasibility of using an OPA to enable ultrafast multiphoton lightsheet lensless microscopy. The work plan involves a close collaboration between the two research groups and will include continuous and intensive knowledge sharing and data exchange, as the progression relies heavily on the synergy between the

highly different expertise of the collaborating groups: Integrated Photonics, Department of Electrical and Photonics Engineering at DTU (Dr. Hao Hu) and Biophotonic Imaging Group, Department of Health Technology at DTU (Dr. Peter E. Andersen). An overview of the project is presented in Fig. 1, and a project timeline in Fig. 2.

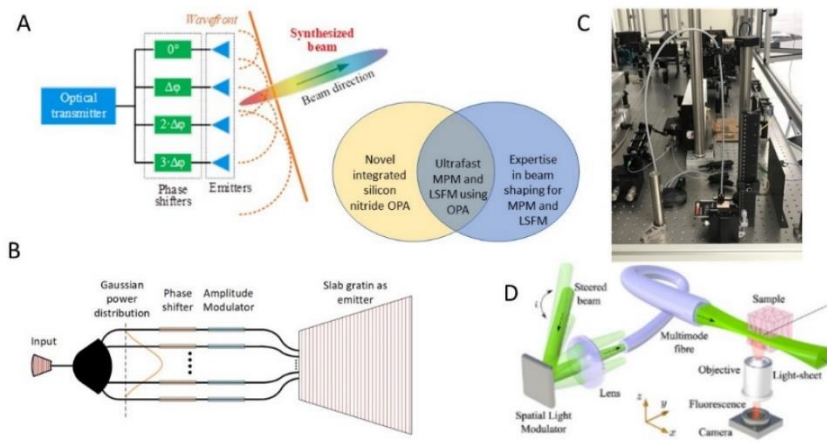


Figure 1: Opa-fast-sheet project overview. The project consists of a close collaboration between two groups, one with expertise in the fabrication of novel integrated optical phased array (OPA) devices, and one with expertise in multiphoton microscopy (MPM) and lightsheet fluorescence microscopy (LSFM). A) Working principle of an OPA, which can dynamically steer and shape a beam. B) Schematic of integrated OPA, consisting of grating coupler, star coupler, phase shifter, amplitude modulator, and a slab grating emitter. C) An endoscope for MPM developed by the Biophotonic Imaging Group, DTU. D) A schematic of lightsheet formation through a multimode fiber using a spatial light modulator (adapted from Ploschner et al. [10]).

Using the existing silicon-on-insulator OPA, we will develop a protocol for beam steering for LSFM (in free space, and through both multicore and multimode optical fibers) and investigate opportunities for compressive sensing-based dynamic, high-speed compensation of the transmission matrix through both fiber types (WP1). Concurrently, we will develop a new silicon nitride OPA, which will have lower loss and higher maximum power to fulfil the large power throughput required for MPM (WP2). Building on WP1 and WP2, we will demonstrate multiphoton lightsheet microscopy using the new silicon-nitride OPA, both in free space and through optical fiber (WP3).

#### WP1: Wavefront shaping and sensing with multicore and multimode fibers

I will investigate different scanning patterns proposed for lightsheet microscopy and develop a protocol for wavefront shaping and beam steering. I will characterize the performance of the OPA, including the modulation speed, efficiency, and presence of side lobes for the different scanning patterns proposed.

I will investigate the ability to perform wavefront shaping using OPA through two different types of optical fibers, multicore and multimode fibers. Multicore fiber is generally easier to work; each core is independent, which means that each channel of the OPA can be coupled directly into one of the fiber cores for wavefront shaping with low cross talk. Additionally, multicore fibers are less sensitive to conformational changes, which means that dynamic sensing of the transmission matrix is less crucial for their implementation. I have recently shown numerical results that could potentially improve the power in the main lightsheet through tapering the end of a multicore fiber [19]. Multimode fibers, although inexpensive, are highly sensitive to conformational changes, and active sensing of the transmission matrix is a crucial step towards implementing them in a translatable platform. I will demonstrate the ability to implement the selected scanning pattern through both fiber types in a controlled laboratory setting. Additionally, I will investigate the opportunity for compressive sensing for dynamic correction of fiber transmission matrix using a fast CMOS camera (HiCAM Fluo) to find the minimum number of pixels required for efficient wavefront sensing.

#### WP2: Developing silicon nitride optical phased array for beam steering and shaping



We aim to develop an integrated optical phased array on the new platform of silicon nitride with high speed, large field of view, low loss, and high-power handling. One of the key components for OPA is phase tuning elements, which are electronically controlled to dynamically tune the angle of the beam and shape the wavefront. Thermo-optic phase shifter [20] features simple fabrication and small footprint, with the tuning speed on the order of  $\sim$ ms. However, silicon nitride has a weak thermo-optic effect with a thermo-optic coefficient much smaller than that of silicon [21]. To lower the power consumption and footprint, we will design thermo-optic phase shifters based on densely distributed spiral waveguides with introduced phase mismatching between neighbouring waveguides to reduce inter-waveguide crosstalk [20].

To avoid crosstalk between adjacent emitters, conventional OPAs have an emitter pitch much larger than half-wavelength, resulting in a field of view much smaller than  $180^\circ$ . To overcome this limitation, we will explore a new regime of integrated OPA which can avoid the crosstalk issue by near-field interference and far-field emission. The integrated silicon nitride OPA will be fabricated at the DTU Nanolab cleanroom. We will establish a free-space optical setup to characterize the integrated silicon nitride OPA in terms of field of view, tuning speed, side lobes level, and beam size. Full-complex wavefront control (including both phase and amplitude) will be used to achieve significantly better performance than the phase-only or amplitude-only method. By having both phase shifter and amplitude modulator in each channel of the OPA (Fig. 1B), the full-complex wavefront control can be achieved. The wavefront shaping speed will also be characterized.

### *WP3: Lensless Lightsheet microscopy with silicon nitride optical phased array*

Using the protocols developed in WP1 and the OPA developed in WP2, I will implement the dynamic wavefront shaping and sensing through optical fiber. I will investigate the efficiency and wavefront shaping performance and evaluate the speed and performance of the dynamic wavefront sensing. Next, I will demonstrate 2-photon lightsheet microscopy with our new integrated device. The fluorescence signal will be collected at the distal end of the fiber using the HiCAM Fluo camera. Finally, I will image the highly dynamic embryonic development of zebrafish to demonstrate the advantages of the high-speed wavefront shaping, scanning, and acquisition. As a final step, I will demonstrate three-photon fluorescence lightsheet lensless microscopy through our integrated device.



Figure 2: An overview of the timeline for the Opa-fast-sheet project.

### Outcome and dissemination

By harnessing the synergy of the two advanced technologies, at the end of this project, we will demonstrate the feasibility of using integrated OPA- based wavefront shaping in multiphoton lightsheet

lensless microscopy. The final implementation of the technology with compressive sensing could aid longitudinal studies of highly dynamic biological processes without motion artifacts with adaptive correction to fiber transmission matrix. We aim to design, fabricate, and validate a prototype optical fiber probe delivering multiphoton virtual lightsheet. To enhance the impact of our research, we will publish our findings jointly in high-impact journals such as *Biomedical Optics Express* and *Optica* and present our results jointly at national and leading international conferences. We will also develop a project-specific website and social media platforms, and actively participate in conferences, workshops, and courses, to communicate the project's objectives and ongoing work. Besides publications, we will also identify valuable innovations and apply for IP protection.

## Impact and outlook

The high-speed wavefront shaping and the reduced cost of OPA will assist the easier clinical translation of multiphoton lightsheet endoscopy. The device developed in this grant will lead to a prototype endoscope that could be employed *in vivo* for a range of diagnostic applications including (but not limited to) early cancer detection and screening.

As a continuation of this project, we intend to further develop the technology with ultrashort pulsed fiber laser with tunable wavelength range. The advantages of utilization of such a source are two-fold. First, the tunability in wavelength will help us identify the multiphoton excitation spectrum of relevant endogenous fluorophores for estimating the rate of metabolism of various cancer tissues. Second, the fiber coupled compact laser source could potentially reduce the fiber coupling losses into the endoscope and enhance the photon budget available whilst reducing the system footprint for easier mobility in the clinic.

1. Borile, G. et al., *Int. J. Mol. Sci.*, 2021. **22**(5): 1-20.
2. Veetikazhy, M. et al., *Sc. Rep.*, 2020. **10**: 8090.
3. Maioli, V. et al., *Biomed. Opt. Express*, 2020. **11**(10): 6012.
4. Wolf, S. et al., *Nat. Methods*, 2015. **12**(5): 379-380.
5. Papadopoulos, I. N., et al., *Biomed. Opt. Express*, 2013. **6**: 260–270.
6. Cizmar T. et al., *Nat. Commun*, 2012. **3**: 1027.
7. Psaltis D. et al., *OPN*, 2016. **27**(1): 24-31.
8. Andresen, E. R. et al., *J. Biomed. Opt.*, 2016. **21**(12): 121506.
9. Plöschner, M. et al., *Sc. Rep.*, 2012. **5**: 18050.
10. Popoff, S. M. et al., *Phys. Rev. Lett.*, 2010. **104**: 100601.
11. Laue, H. E. A. et al., *IEEE Signal Process. Mag.*, 2017. **34**(4): 171-176.
12. Conkey, D. B. et al., *Opt. Express*, 2012. **20**: 1733-1740.
13. Wang, D. et al., *Optica*, 2015. **2**: 728-735.
14. Blochet, B. et al., *Opt. Lett.*, 2017. **42**: 4994-4997.
15. Liu, Y. et al., *Optica*, 2017. **4**: 280-288.
16. Rosales-Guzmán, C. et al., *SPIE PRESS*, 2017.
17. Heck, M. J. R., *Nanophotonics*, 2017. **6**(1): 93–107.
18. Poulton, C. V. et al., *Opt. Lett.*, 2017. **42**(20): 4091.
19. [Veetikazhy, M., DTU Health Tech PhD Thesis, 2021](#). Ch. 7: 121-130.
20. Qiu, H. et al., *Opt. Lett.* **45**(17), 4806 (2020).
21. Arbabi, A. et al., *Opt. Lett.*, 2013. **38**(19): 3878–3881.

## NANOEYE | A novel non-destructive quantitative multimodal plasmonic nanoscopy approach to stop Myopia progression

Myopia is growing around the world. On average, 30% of the world is currently myopic and by 2050, it will be 50%, 5 billion people. Almost 1 billion of high myopes predicted by 2050 makes Myopia the leading cause of permanent blindness worldwide with significant implications for planning comprehensive eye care services globally, and vision loss among people with high myopia. But also with great global economic consequences, where the global cost of myopia from lost productivity due to vision impairment from uncorrected myopia and myopic macular degeneration was estimated to be USD 244 billion in 2015, and significant impact on learning and education. However, refractive correction remains the only option, and the causes of the increasing risk, and furthermore even the underlying structural and physiological mechanisms of Myopia are not fully understood, which is frustrating the efforts of developing treatments and lowering the Myopia-induced risks in potentially sight-threatening eye diseases.

Myopia research is a very active area due to the lack of consensus on its etiology and moderate success of interventions to stop its progression: the topic has raised interest in the scientific, clinical and industrial communities for many years. Since 1980, >10k papers address Myopia etiology/treatment. However, a general weakness is technology-oriented groups have not tackled Myopia as a research question, therefore there is a lack of state-of-the-art 3D biometry tools, high resolution imaging techniques and visual simulators, which would allow a more accurate assessment and understanding.

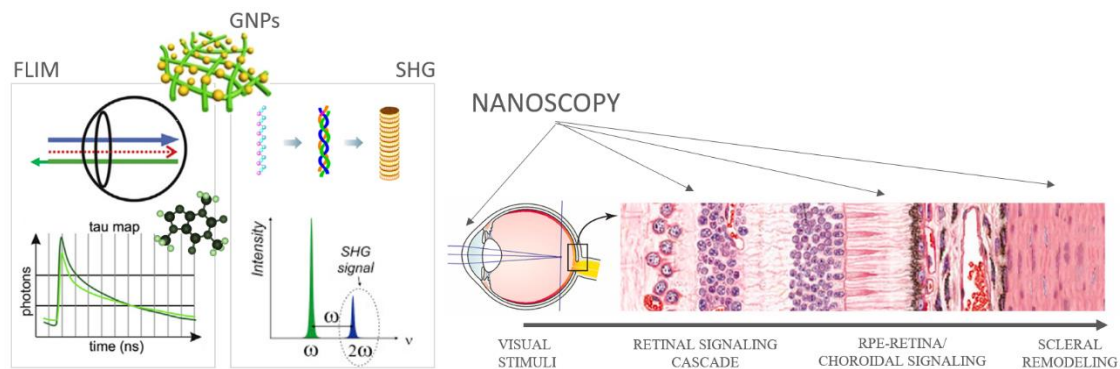


Figure. Overview of the scope of the novel non-destructive quantitative multimodal plasmonic nanoscopy approach to investigate the multilayered signaling cascade disruptions leading to Myopia development.

The goal of this project is to advance our understanding of Myopia, and help to develop new treatments. As an important step, I propose to develop new innovative optical techniques to characterize myopic eyes in unprecedented details to gain novel insights, and to enhance treatment effects. The experimental approach is highly interdisciplinary as it brings together fundamental nanophotonics and clinical human eye research, to develop new imaging technologies in ophthalmology, following a multidisciplinary approach (3 researchers and 2 institutions), involving optics, physics, bioengineering, visual sciences, ocular biology and clinical ophthalmology. The development of a SHG-FLIM microscope in combination with plasmonic methods (multimodal plasmonic nanoscopy) will have a significant impact in the way we study molecular/structural changes in ocular tissues, and consequently Myopia development, are studied. Also, gold nanoparticles are the first FDA-approved nanomaterials so our techniques could be readily translated from bench to bedside to impact clinical eye study. The expected results from the project have great innovation potential. Moreover, the development of safe *in vivo* imaging and crosslinking techniques for procedures *in vivo* will significantly impact the clinical treatment of Myopia, therefore helping 30% of the world's current population. Using light to see light.

Research on emerging solutions for Myopia prevention will help to assess their potential and propose improved interventions, potentially reaching millions. In particular,

1. A novel innovative imaging method, quantitative multimodal plasmonic nanoscopy, combining a 2P-SHG-FLIM microscope and nanophotonics methods for ocular applications.
2. Greater understanding of the molecular/structural changes during emmetropization leading to Myopia development, using novel strategies for multimodal microscopy *ex vivo* to quantify collagen crosslinks and endogenous fluorophores distortions in ocular tissues of special interest for emmetropization.
3. Strategies for multimodal plasmonic nanoscopy *in vivo* in human eyes
4. Nanoscopy enhanced treatments in corneal and scleral crosslinking therapeutical approaches.

## **NANOEYE | A novel non-destructive quantitative multimodal plasmonic nanoscopy approach to stop Myopia progression**

Myopia is growing around the world. Almost 1 billion of high myopes predicted by 2050 makes Myopia the leading cause of permanent blindness worldwide[1] with significant implications for planning comprehensive eye care services globally, and vision loss among people with high myopia. However, refractive correction remains the only option, and the causes of the increasing risk, and furthermore even the underlying structural and physiological mechanisms of Myopia are not fully understood, which is frustrating the efforts of developing treatments and lowering the Myopia-induced risks in sight-threatening eye diseases.

The goal of this project is to advance our understanding of Myopia, and help to develop new treatments. As an important step, I propose to develop new innovative optical techniques to characterize myopic eyes in unprecedented details to gain novel insights, and to enhance treatment effects. Specifically, I aim to accomplish the following: (a) substantial advances in the understanding of molecular/structural changes underlying Myopia thanks to the development of novel multimodal plasmonic nanoscopy approaches, (b) quantitative assessment of optical, structural, and molecular properties of the eye during Myopia, to widen our knowledge of the emmetropization process, and (c) anatomical- & structural-level assessment of novel interventions to stop Myopia progression.

### **Introduction. Literature Review. State of the art**

---

The eye grows in a coordinated manner during normal development so that the ocular optics projects focused images on the retinal plane. However, in myopic eyes, the eye grows excessively in the axial direction, causing images to be focused in front of the retina, resulting in blurred images and poor vision. Currently, refractive correction remains the only option to compensate for blurred retinal images, but do not reverse the excessive eye growth, nor the increased risk for potentially sight threatening diseases in high myopia. Thus, a variety of interventions has been proposed to halt myopia progression: optical treatments based on the rationale that retinal blur is the visual signal that drives refractive error development, chemical retardation of myopia progression in children or the light-activated tissue remodeling (scleral crosslinking)[2] to stop the excessive eye growth in Myopia. However, none of them is proved yet. Recent advances in eye biometry, physiological optics and systems genetics of refractive error have significantly advanced our understanding of the biological processes involved in refractive eye development and provided a framework for the development of new treatment options, but many key questions remain unanswered.

Refractive eye development is a tightly coordinated developmental process. The general layout of the eye and its various components are established during embryonic development, which involves a complex cross-tissue signaling[3]. The eye then undergoes a refinement process during the postnatal emmetropization process, which relies heavily on the integration of environmental and genetic factors and is controlled by an elaborate genetic network. This genetic network encodes a multilayered signaling cascade, which converts visual stimuli into molecular signals that guide the postnatal growth of the eye, triggered by visual feedback driven probably by optical defocus[4]. This cascade begins in the retina, continues through the retinal pigment epithelium (RPE) and choroid, and ultimately acts on the sclera causing changes in the scleral extracellular matrix, which manifest in axial elongation[3]. The feedback control mechanisms of refractive error is triggered when defocused objects induce an error signal (image blur)[5]. A decisive factor is that the retina recognizes the sign of optical defocus and generates molecular signals specific to it, which modulate postnatal eye growth and determine its refractive state [5]. The signaling cascade underlying refractive eye development spans across all ocular tissues, from cornea to sclera, through retina, and comprises multiple signaling pathways. Notably, tissue-tissue interaction, following molecular changes, plays a key role in both, embryonic eye development and postnatal eye emmetropization. Understanding how these molecular changes are linked to the different structural and mechanical tissue-tissue interactions is essential to unravel the feedback control mechanisms of refractive error, therefore opening the path for novel effective treatments.

To investigate the links between structural and molecular changes in the emmetropization process, a multidisciplinary approach is required. Very recently, different light-based technologies have allowed to partially understand structural and molecular[6] changes in the ocular tissues. In particular, Second harmonic generation (SHG) imaging microscopy has proven to be particularly suitable to investigate collagen fibrils[7]. SHG from collagen is an intrinsic and a coherence process, so that samples can be investigated under physiological conditions. Coherent constructive or destructive interference of SHG provides extra



hints to the ultra-structure of collagen fibrils and their organizations in ocular tissues[8, 9]. However, scleral fibril distribution in myopic eyes has never been quantified to the level of relating macroscopic inherent mechanical properties of scleral tissue with the microscopic underlying structure of collagen fibers. On the other hand, fluorescence lifetime imaging microscopy (FLIM) has proven very useful as a noninvasive technique to measure and quantify lifetimes of endogenous retinal autofluorescence[6, 10]. When endogenous fluorophores are excited by photons derived from a monochromatic light source, they gain a higher level of energy before returning to their ground state by emitting photons of longer wavelengths than the exciting light. The average time between excitation and reaching the ground state again can be quantified as the fluorescence lifetime. Every fluorophore is characterized by its own excitation and emission wavelength spectrum and exhibits an individual fluorescence lifetime, which depend on the molecular environment but are largely independent of the fluorophore's concentration. Therefore, fluorescence lifetime measurement can be applied to detect weakly fluorescing fluorophores if they differ in terms of their lifetime. Additionally, lifetimes can be used as indicator for specific metabolic conditions of changes within the molecular micro-environment. A common drawback for both techniques is the damage threshold for *in vivo* application in the human eye, which forces to work at very low radiation levels, where either the SHG or the fluorescence signals are not well captured.

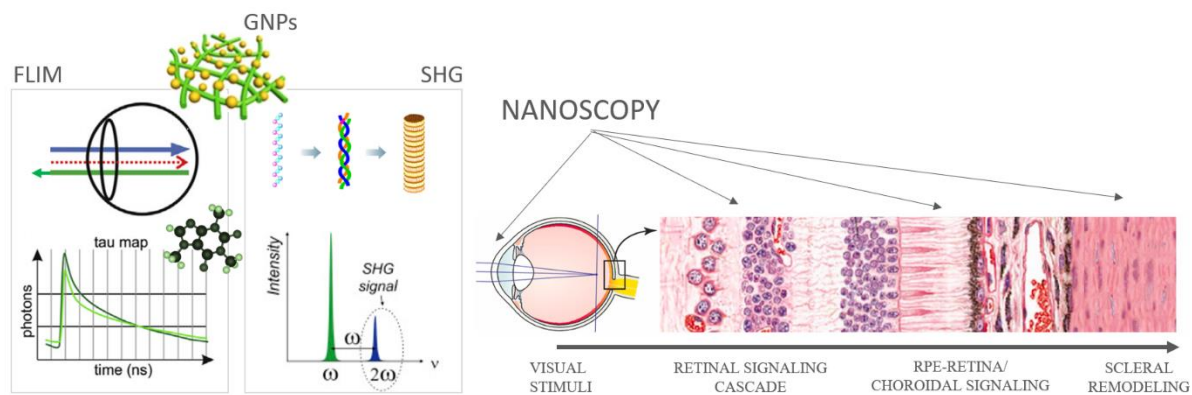


Figure. Overview of the non-destructive quantitative multimodal plasmonic nanoscopy scope on the multilayered signaling cascade of emmetropization to understand the structural and molecular disruptions leading to Myopia development.

Functionalized gold nanoparticles (GNPs) with controlled geometrical and optical properties are the subject of intensive studies and biomedical applications, including genomics, biosensorics, immunoassays, clinical chemistry, laser phototherapy of cancer cells and tumors, the targeted delivery of drugs, DNA and antigens, optical bioimaging and the monitoring of cells and tissues with the use of state-of-the-art detection systems. In particular, GNPs allow individual enhancement of the fluorophores signals[11], therefore enhancing our access to low intensity endogenous fluorophores. Moreover, collagen-GNPs hybrid hydrogels[12] can be used for local delivery of therapeutic agents, showing enhanced antitumor efficacy. Therefore, coupling GNPs with different ocular tissues might help enhance different ocular treatments (i.e. crosslinking of collagen fibers of cornea (Keratoconus) and sclera (Myopia), 2P corneal crosslinking). A proof of concept using this novel approach, combining SHG and FLIM microscopy with different GNPs strategies (multimodal plasmonic nanoscopy), was demonstrated using porcine scleral and retinal tissue (in preparation Vinas-Pena & Cho, 2022).

1. B. A. Holden, T. R. Fricke, D. A. Wilson, M. Jong, K. S. Naidoo, P. Sankaridurg, T. Y. Wong, T. J. Naduvilath, and S. Resnikoff, "Global Prevalence of Myopia and High Myopia and Temporal Trends from 2000 through 2050," *Ophthalmology* **123**, 1036-1042 (2016).
2. M. Vinas-Pena, X. Feng, G. Li, and S. Yun, "In situ measurement of stiffness increase in posterior sclera after UV-riboflavin crosslinking by optical coherence elastography," *Biomedical Optics Express* **13**(2022).
3. J. A. Summers, F. Schaeffel, S. Marcos, H. Wu, and A. V. Tkatchenko, "Functional integration of eye tissues and refractive eye development: Mechanisms and pathways," *Exp Eye Res* **209**, 108693 (2021).
4. R. Chakraborty, L. A. Ostrin, A. Benavente-Perez, and P. K. Verkicharla, "Optical mechanisms regulating emmetropisation and refractive errors: evidence from animal models," *Clin Exp Optom* **103**, 55-67 (2020).
5. J. Wallman and J. Winawer, "Homeostasis of eye growth and the question of myopia," *Neuron* **43**, 447-468 (2004).
6. C. Dysli, S. Wolf, M. Y. Berezin, L. Sauer, M. Hammer, and M. S. Zinkernagel, "Fluorescence lifetime imaging ophthalmoscopy," *Prog Retin Eye Res* **60**, 120-143 (2017).
7. X. Chen, O. Nadiarynkh, S. Plotnikov, and P. J. Campagnola, "Second harmonic generation microscopy for quantitative analysis of collagen fibrillar structure," *Nature Protocols* **7**, 654-669 (2012).

8. M. Han, G. Giese, and J. F. Bille, "Second harmonic generation imaging of collagen fibrils in cornea and sclera," *Optics Express* **13**, 5791-5797 (2005).
9. J. A. Germann, E. Martinez-Enriquez, and S. Marcos, "Quantization of collagen organization in the stroma with a new order coefficient," *Biomed Opt Express* **9**, 173-189 (2018).
10. J. A. H. Tang, C. E. Granger, K. Kunala, K. Parkins, K. T. Huynh, K. Bowles-Johnson, Q. Yang, and J. J. Hunter, "Adaptive optics fluorescence lifetime imaging ophthalmoscopy of in vivo human retinal pigment epithelium," *Biomed Opt Express* **13**, 1737-1754 (2022).
11. G.-C. Li, D. Lei, M. Qiu, W. Jin, S. Lan, and A. V. Zayats, "Light-induced symmetry breaking for enhancing second-harmonic generation from an ultrathin plasmonic nanocavity," *Nature Communications* **12**, 4326 (2021).
12. R. Xing, K. Liu, T. Jiao, N. Zhang, K. Ma, R. Zhang, Q. Zou, G. Ma, and X. Yan, "An Injectable Self-Assembling Collagen-Gold Hybrid Hydrogel for Combinatorial Antitumor Photothermal/Photodynamic Therapy," *Advanced materials* **28**, 3669-3676 (2016).

## Problem Statement/Specific objectives and overview of the project

In summary, despite the high prevalence of Myopia, several key questions remain, in part because of the unavailability of quantitative techniques to characterize optical/morphological properties of the myopic eye, and structural changes produced by intervention. The primary **research questions** are: (1) How does the ocular tissues (cornea, sclera and retina) change at the molecular/microstructural level when Myopia develops? (2) Can a novel combination of fluorescence life time imaging microscopy and nanoparticles approach (nanoscopy) enhance the signal of endogenous fluorophores so the technique can evolve towards *in vivo* applications? (3) Can nanoscopy allow improvements in tissue modifying ocular procedures? This project will answer these questions via four **specific research objectives (ROs)** as follows:

**RO1:** Development of innovative imaging methods for the quantitative assessment of optical, structural and molecular properties of ocular tissues in Myopia development.

**RO2:** Understanding the changes in molecular/structural properties in Myopia development.

**RO3:** Development of novel in vivo imaging techniques.

**RO4:** Development of novel ocular treatments based on the tissue-nanoparticles interactions.

## Outline of tasks/Team/Work Plan

We will develop novel non-destructive quantitative methods to image the ocular tissues involved in myopia development and to develop novel ocular treatments. The key idea behind our novel plasmonic nanoscopy method is to enhance fundamental light-matter interaction with ocular tissue using plasmonic nanomaterials.

A general overview of the project is summarized here:

- **Experimental developments:** The project will develop a set of complementary novel imaging technologies (multimodal plasmonic nanoscopy) to study Myopia and its treatment, providing powerful capabilities for the development of new paradigms for diagnostics/treatments of Myopia.
- **Towards in vivo paradigms:** The use of novel imaging technology will shed light into the structural/molecular changes occurring in Myopia, and clarify the role of scleral/retinal events in the development of Myopia. The final goal of the project is to develop the bases for future safe *in vivo* imaging methods, and significant advances in tissue remodeling approaches to stop myopia progression.
- **International multidisciplinary team:** The proposal follows a highly multidisciplinary approach involving researchers in the fields of optics, physics, optical engineering, bioengineering, visual sciences, ocular biology and clinical ophthalmology and different research institutions (1) Institute of Optics, Spanish National Research Council (IO-CSIC) (Spain) & (2) Wellman Center for Photomedicine-Massachusetts General Hospital & Harvard Medical School (WCPM) (USA).

### The team

<b>(PI) Dr. Maria Vinas-Pena. Marie Skłodowska Curie ERC independent fellow.</b> OPTICA Ambassador 2019. Dr. Vinas research focuses on the study of the physics of vision and novel ocular treatments through the use of different biophotonics technologies.	IO-CSIC WCPM& Harvard Medical School
<b>(Co-PI) Dr. Sangyeon Cho. 2022 ECOR FMD research fellow.</b> OPTICA Ambassador 2021. Dr. Cho focuses on the study of nanolasers for biomedical imaging and plasmonics	WCPM & Harvard Medical School
<b>(Co-PI) Dr. James Germann. Researcher.</b> Dr. Germann interests lies on multiphoton imaging for ocular applications	IO-CSIC U. Rochester

## Research methodology and approach

The following describes the methodological approaches that will define the 4 research objectives (RO1-4):

**WPI(RO1): Development of innovative imaging methods for the quantitative assessment of optical, structural and molecular properties of ocular tissues in Myopia development.** The development of custom



FLIM-nanoscopy techniques for the ocular tissues, by modifying already existing custom-developed systems, will allow significant advances in the current knowledge of the emmetropization process and Myopia development. In *WP1.1*, a dedicated FLIM channel will be developed and incorporated to a custom developed SHG microscope for ocular applications (cornea and sclera) previously developed at the Institute of Optics (IO-CSIC), where fundamental differences in endogenous fluorophores and structural features of the tissues will require optimization of spectral ranges and current backward and forward scattering modes. In *WP1.2*, FLIM imaging techniques in combination with nanoparticles shining will expand the knowledge of myopic corneal, scleral and retinal properties, and possible treatments.

**WP2(RO2): Understanding the changes in molecular/structural properties in Myopia development.** We will study endogenous fluorescence changes in normal/myopic eyes along the tissues involved in the retinal signaling cascade, the RPE/choroid signaling and the sclera, thus new optical models will be developed. Nanoscopy technologies developed in *WP1.1-2* will be applied to unravel the links between molecular and structural features in Myopia, studying endogenous fluorescence changes in normal/myopic eyes along the tissues involved in the retinal signaling cascade, the RPE/choroid signaling and the sclera.

**WP3(RO3): Development of novel in vivo imaging techniques.** An ultimate goal of the action is to develop the bases for future safe *in vivo* ocular imaging to address molecular changes following different visual stimulation to understand the processes underlying the visual cascade, and possible disruptions leading to Myopia progression, so that a significant impact will be made on clinical treatment of Myopia.

**WP4(RO4): Development of novel ocular treatments based on the tissue-nanoparticles interactions.** Knowledge acquired in WP2 will allow to revolutionize the different collagen-based tissue remodeling ocular treatments. Particularly, corneal 2P crosslinking and scleral UV crosslinking, where the endogenous fluorescence from scleral/corneal collagen fibers will change after plasmonic interactions between GNPs and the collagen fibers after UV light treatment. Increasing the number of crosslinks between the fibers, reducing treatment time and increasing the *in vivo* applications for both treatments, with a significant impact in the management of Myopia and other blinding diseases.

<b>WP1 Development of innovative imaging methods</b>		
<b>WP1.1</b>	<b>Structural and molecular ocular FLIM-SHG imaging</b>	<b>6 months</b>
<i>Target</i>	A dedicated fluorescence life time imaging (FLIM) channel will be developed and coupled to a previously built ocular 2P-SHG microscope (IO-CSIC) for sectioned imaging in the eye (cornea, sclera and retina)	
<b>WP1.2</b>	<b>Nanoscopy strategies for ocular imaging</b>	<b>6 months</b>
<i>Target</i>	Different experimental methods using gold nanoparticles (GNPs) will be implemented (1) to enhance collagen fibers imaging in cornea and sclera allowing to allow linking structural & molecular changes after Myopia development, (2) to enhance retinal fluorophores (retinoic acid, rhodopsin) signal allowing <i>in vivo</i> detection (3) to improve cornea/sclera crosslinking treatments, since as the nanoparticles are incorporated into the fiber network, the SHG process in the collagen fibers and the fluorescence process in the riboflavin used in the CXL will be accelerated. We will use this enhancement as a marker to quantify fiber reorganization after myopia development. Also, GNPs are the first FDA-approved nanomaterials so our techniques could be readily translated from bench to bedside to impact eye research.	
<i>Milest.</i>	<b>M1.1</b> (1) 2P-SHG-FLIM microscope for ocular applications (2) Detection & image analysis routines <b>M1.2</b> (1) GNPs strategies for cornea, sclera and retinal imaging, and ocular treatment enhancement	
<b>WP2 Multimodal nanoscopy as a novel imaging tool to understand Myopia development</b>		
<b>WP2.1</b>	<b>2P-SHG-FLIM microscopy to link molecular and structural changes in scleral crosslinked tissues</b>	<b>8 months</b>
<i>Target</i>	Nanoscopy technologies developed in WP1.1-2 will be applied to unravel the links between molecular and structural collagen features in an animal model (porcine eye) after SCXL, targeting the quantification of the number of crosslinks between the collagen fibers.	
<b>WP2.2</b>	<b>2P-SHG-FLIM microscopy to study endogenous fluorophores changes in myopic retinas</b>	<b>8 months</b>
<i>Target</i>	Multimodal nanoscopy to investigate endogenous fluorescence changes in normal/myopic eyes along the tissues involved in the retinal signaling cascade, the RPE/choroid signaling and the sclera.	
<i>Milest.</i>	<b>M2.1</b> (1) Strategies for multimodal microscopy ex vivo on crosslinked scleral tissues (2) Number of scleral collagen fiber crosslinks after treatment (3) Endogenous fluorescence changes in the ECM of normal/myopic scleras <b>M2.2</b> (1) Endogenous fluorescence changes in retinal fluorophores of special interest for emmetropization (retinoid acid & rhodopsin) in normal/myopic retinas	
<i>Dissem</i>	<b>D2.1</b> Publication on molecular and structural changes in scleral crosslinked tissues to stop myopia progression <b>D2.2</b> Publication on endogenous fluorophores changes in myopic retinas	
<b>WP3 In vivo nanoscopy developments</b>		
<b>WP3.1</b>	<b>From animal model to human eye</b>	<b>8 months</b>
<i>Target</i>	Results from WP2 in a porcine eye animal model will be transferred to the human eye. Myopia-induced biochemical, structural, and mechanical changes in 5 human eyes (2 emmetropes/3 myopes) thanks to the <b>EyeFind Research Grant 2022-Round1 (ARVO &amp; Bright Focus Foundation) awarded to Dr. Vinas-Pena &amp; Dr. Cho</b> . Measurements ex vivo will be performed in the retina, cornea, sclera, and lens.	

<b>WP3.2</b>	<b>Development of novel in vivo imaging techniques</b>	<b>8 months</b>
<b>Target</b>	Information gathered on WP2.1-2, about endogenous fluorescence changes in normal/myopic eyes, in both sclera and retina, as well as in WP1.2, about GNPs strategies for retinal imaging, will be used to develop novel <i>in vivo</i> nanoscopy developments, which will provide invaluable information about the emmetropization process in the human eye.	
<b>Milest.</b>	<b>M3.1</b> (1) Strategies for multimodal microscopy in human eyes <b>M3.2</b> (1) Strategies for multimodal microscopy in vivo on myopic/normal scleras <b>M3.2</b> (2) In vivo multimodal microscopy approaches for myopic/normal retinas	
<b>Dissem</b>	<b>D3.1</b> Publication on multimodal microscopy on human eyes <b>D3.2</b> Publication on molecular and structural changes during the emmetropization process in the human eye.	
<b>WP4 Nanoscopy enhanced treatments</b>		
<b>WP4.1</b>	<b>GNP enhanced crosslinking</b>	<b>8 months</b>
<b>Target</b>	Endogenous fluorescence from scleral/corneal collagen fibers will change after plasmonic interactions between GNPs and the collagen fibers after UV light treatment. Increasing the number of crosslinks between the fibers, reducing treatment time and increasing the <i>in vivo</i> applications for both treatments.	
<b>Milest.</b>	<b>M4.1</b> (1) Changes in collagen crosslinks (cornea and sclera) after GNPs-UV treatment	
<b>Dissem</b>	<b>D4.1</b> Publication on nanoscopy enhanced treatments for collagen crosslinking	
<b>WP5 Communication &amp; Dissemination of results</b>		
<i>Manuscript writing &amp; submission, Organisation of scientific workshops, Outreach activities, Conferences and meetings</i>		
<b>WP6 Management &amp; transversal tasks</b>		
<i>Research and financial management; Entrepreneurship &amp; patent applications; IPR, responsible research &amp; open science</i>		

Month	1-2	3-4	5-6	7-8	9-10	11-12	13-14	15-16	17-18	19-20	21-22	23-24
WP1	WP1.1-1.2											
WP2						WP2.1-2.2						
WP3									WP3.1-3.2			
WP4												WP4.1
WP5								WP5				
WP6	WP6											

## Outcome(s)

The proposal aims to develop new imaging technologies in ophthalmology, following a multidisciplinary approach (3 researchers and 2 institutions), involving optics, physics, bioengineering, visual sciences, ocular biology and clinical ophthalmology. Research on emerging solutions for Myopia prevention will help to assess their potential and propose improved interventions, potentially reaching millions. In particular,

**01.**A novel innovative imaging method, quantitative multimodal plasmonic nanoscopy, combining a 2P-SHG-FLIM microscope and nanophotonics methods for ocular applications.

**02.**Greater understanding of the molecular/structural changes during emmetropization leading to Myopia development, using novel strategies for multimodal microscopy *ex vivo* to quantify collagen crosslinks and endogenous fluorophores distortions in ocular tissues of special interest for emmetropization.

**03.**Strategies for multimodal plasmonic nanoscopy *in vivo* in human eyes

**04.**Nanoscopy enhanced treatments in corneal and scleral crosslinking therapeutical approaches.

## Impact

Myopia is a very active research area, due to the lack of consensus on its etiology and moderate success of interventions to stop its progression. With high prevalence of Myopia in developed countries and increasing dramatically, and high economic and social costs associated to Myopia, the topic has raised interest in the scientific, clinical and industrial communities for many years. Since 1980, >10k papers address Myopia etiology/treatment. However, a general weakness is that technology-oriented groups have not tackled Myopia as a research question, therefore there is a lack of state-of-the art 3D biometry tools, high resolution imaging techniques and visual simulators, which would allow a more accurate assessment and understanding.

In this project, the experimental approach is highly interdisciplinary as it brings together fundamental nanophotonics and clinical human eye research. The expected results from the project have great innovation potential. The development of an ocular 2P-FLIM microscope in combination with plasmonic methods will have a significant impact in the way we study molecular/structural changes in ocular tissues, and consequently Myopia development, are studied. Also, gold nanoparticles are the first FDA-approved nanomaterials so our techniques could be readily translated from bench to bedside to impact clinical eye study. Moreover, the development of safe *in vivo* imaging and crosslinking techniques for procedures *in vivo* would significantly impact the clinical treatment of Myopia, therefore helping 30% of the world's current population. Using light to see light.

## **Executive Summary, “Integrated Photonic Polarimeter Circuit for portable Fiber-optic Stress Sensor”**

### **Optica Foundation 20<sup>th</sup> Anniversary Challenge**

#### **Principal Investigator: Mark C. Harrison, Ph.D.**

Studies have shown that the stiffness of biological tissue can be correlated with the onset of various diseases, including cancer. In fact, the stiffness of cancerous tissue has been linked to the likelihood of metastasis. Although pathologists tend to be self-consistent in grading the likelihood of metastasis in biopsied tissue, there is still variation between individuals and the entire process is error-prone. Therefore, monitoring the stiffness of tissues in organs such as the heart and lungs can help evaluate the severity of cancer and can aid in the early detection of other diseases as well. However, methods for characterizing the mechanical behavior of living tissue samples often suffer from poor spatial resolution, are destructive to the sample being tested, or are too large to be practical in most settings. This makes tissue stiffness monitoring a method of untapped diagnostic potential. Recently, we developed a polarimetric optical fiber stress sensor based on the photo-elastic effect which addresses these issues. A portable and easy-to-use technology like the fiber stress sensor could have large benefits in a variety of settings, including in developing nations where resources for medical diagnostic equipment may be more limited. Although the sensor has demonstrated high sensitivity and resolution, it comprises several large and complex pieces of optical equipment which reduce the device portability and make it difficult to use in settings where it would be most useful.

In the past few decades, large strides have been made in the world of silicon photonics, and there are now several commercial foundries that will manufacture reliable photonic integrated circuit (PIC) designs for hire. These foundries often require use of a process design kit (PDK) which standardizes commonly-used photonic components. By standardizing processes, these foundries serve as a key link between small-scale research and large-scale commercial fabrication of integrated photonic devices. Recently, several groups have demonstrated integrated polarimetry. A polarimeter is one of the largest and most complex components of the fiber stress sensor, and is a prime candidate for miniaturization into a PIC. By leveraging the PDKs and reliability of foundries, we can design a polarimeter PIC that meets the precise needs of the stress sensor. Doing so will also make the fiber stress sensor much easier to operate.

The research funded by this grant will focus on developing integrated photonic circuits that can replace the large, expensive benchtop polarimeter used in the fiber stress sensor. Replacing it with a PIC will also allow us to make other improvements to the fiber stress sensor to reduce its overall size and the complexity of its operation. Once these improvements have been made, we will enhance the performance of the sensor by developing the capability to take parallel measurements on a single sample simultaneously. These system improvements will result in a device that is truly portable and can be used to characterize a variety of tissue samples in a variety of locations. The resulting enhanced device will be a flexible, quantitative diagnostic tool useful in a variety of healthcare settings worldwide.

# Proposal, “Integrated Photonic Polarimeter Circuit for portable Fiber-optic Stress Sensor”

## Optica Foundation 20<sup>th</sup> Anniversary Challenge

### 1. Literature Review

Studies have shown that the stiffness of tissue can be correlated with the onset and severity of various diseases, including cancer [1–3]. Therefore, measuring the stiffness of tissues in organs such as the heart and lungs can aid in the early detection of diseases [4,5]. However, methods for characterizing the mechanical behavior of living tissue often suffer from poor spatial resolution, are destructive to the sample being tested, or are too large to be practical in most settings [6–8]. The deficiency of quantitative tools for characterizing resected and biopsied tissues forces physicians to rely on more qualitative methods, reducing the quality of care for patients. Recently, we developed a polarimetric optical fiber stress sensor based on the photo-elastic effect which addresses these issues [9,10]. Although the sensor has demonstrated high sensitivity and resolution, it comprises several large and complex pieces of optical equipment which make it difficult to use in many settings where it would be most useful.

Large strides have been made in the world of silicon photonics, and there are now several commercial foundries that will manufacture reliable photonic integrated circuit (PIC) designs for hire. These foundries often require use of a process design kit (PDK) which standardizes commonly-used photonic components. These foundries are key to miniaturizing and integrating all sorts of photonic tools. Recently, several groups have demonstrated integrated polarimetry [11,12]. A polarimeter is one of the largest and most complex components of the fiber stress sensor, and is a prime candidate for miniaturization into a PIC. By leveraging the PDKs of foundries, a design that meets the precise needs of the stress sensor can be realized. Furthermore, developing a PIC in a foundry will demonstrate the ability to manufacture the design at scale, which is essential for the resulting device to be affordable and to have a global impact.

The research funded by this grant will focus on developing integrated photonic circuits and printed circuit boards (PCB) that replicate the behavior of the large pieces optical equipment, primarily the polarimeter. We will also make other improvements to the fiber stress sensor to reduce its overall size and the complexity of its operation. Once these improvements have been made, we will enhance the performance of the sensor by developing the capability to take parallel measurements on a single sample simultaneously. This enhancement will directly improve the performance of the device, as well as increasing its usefulness in diagnosing a wide variety of diseases in a wide variety of settings. These system improvements will result in a device that is truly portable and has the potential to be commercialized in an affordable manner. The resulting fiber stress sensor can then be used to characterize a variety of tissue samples in a variety of locations all over the world, having a truly global impact on health.

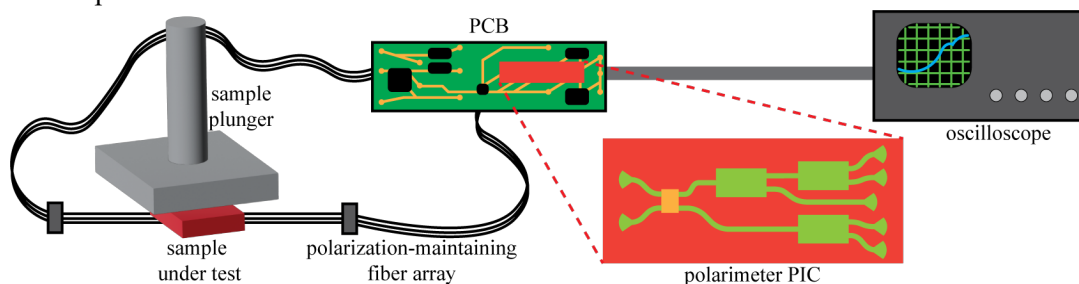


Fig. 1. Conceptual diagram of fiber stress sensor with polarimeter PIC designed by this project. From left to right, a motorized plunger compresses a sample under test over an array of polarization-maintaining optical fiber. An optical signal, generated on the PCB, is sent through the fiber array and analyzed by the polarimeter PIC. The PIC signal is measured electronically and the output is sent to an oscilloscope to be read.

## 2. Problem Statement/Objectives

The polarimetric fiber stress sensor is a robust platform that would be improved by increasing its portability. Increasing the portability via a polarimeter PIC would also allow simultaneous parallel measurements of samples, further increasing the utility of the device in characterizing a wide variety of tissue samples and detecting various diseases in early stages. To address these issues, we propose to fully miniaturize the photonic detection equipment by completing the following three objectives: manufacture a polarimeter PIC, manufacture a PCB to handle electrical control of the PIC, and test and characterize the PIC independently and as an element of the PCB containing both the light generation circuit (laser) and light characterization circuit.

### 2.1 Manufacture polarimeter photonic integrated circuit

As previously mentioned, integrated polarimeters have been reported in the literature [13,14], but they often have complicated designs or analysis required. Our goal in designing our own polarimeter circuit is to reduce the complexity of the design and analysis by optimizing it specifically for the fiber stress sensor application. Optimizing the design for the particular application will allow us to collect only the information about the polarization state of light required for proper detection of stress, and ignore the information that is not necessary for robust stress sensing. This will have a downstream effect of making the stress sensor even more robust and easier to use, as the data being read from the polarimeter PIC can be closer to the post-processed data when the fiber stress sensor uses a full polarimeter for measurement.

There are several photonic foundries that can manufacture reliable PICs for research or industrial applications, including AIM Photonics administered by the State University of New York. These foundries often have tightly controlled procedures and long manufacturing timelines to ensure that they can reliably manufacture a large number of projects in a manageable way. Therefore, we will engage with one of these foundries early to make sure we can secure a spot for a multi-project wafer (MPW) run to get our polarimeter PIC design manufactured and packaged in a way that will allow us to test it with our fiber stress sensor.

### 2.2 Manufacture accompanying printed circuit board

It is expected that the design and manufacture of the PIC will take some time, and there will be a period of downtime while the photonic foundry is manufacturing the PIC. During that downtime, we will design a simple, custom PCB to appropriately control and read the PIC. The PCB will also be used to power a laser module that will serve as a signal source for the fiber stress sensor. The output of the optical fiber from the sensor will be read by the PIC. The PCB will include supporting hardware to power and read the integrated photodetectors for either datalogging or display on an oscilloscope or other electronic test and measurement equipment. By using a custom design, the PCB can be optimized for the PIC designed in the previous objective.

### 2.3 Test, characterize, and validate the polarimeter PIC design

Once we receive manufactured PICs with the polarimeter design, we will test and characterize them. This will begin with the PICs as standalone circuits, in a controlled test bed to understand their behavior and limitations compared to the simulations used to design them. Once the manufactured polarimeter PICs are characterized, we will move on to installing them in the PCB circuits and using them as part of the fiber stress sensor. This will allow us to validate the improved fiber stress sensor with polarimeter PIC as a whole.

## 3. Outline of tasks/Work Plan

Task	Jan	Feb	March	April	May	June	July	Aug	Sept	Oct	Nov	Dec
1. Design and manufacture polarimeter PIC												

2. Design and manufacture PCB												
3. Test, characterize, and validate designs												

The work for this project will consist of three phases corresponding to each of the three objectives, as outlined in the chart above.

**3.1 Design and manufacture polarimeter photonic integrated circuit**

The first task, to design and manufacture polarimeter PIC, will take approximately 8 months. We expect about 5 months to be spent on the design of the PIC, and 3 months to be spent manufacturing the PIC. We will first need to identify a foundry partner to manufacture the polarimeter PIC, as that will determine some design constraints. We already have a design kit license agreement in place with AIM Photonics and have access to their PDK, making them our first choice for a photonic foundry partner. Although the design of an element such as a polarimeter has many engineering tradeoffs to consider, we will work with the PDK from our chosen foundry to simplify the process. These PDKs will allow us to engage in designing the complicated polarimeter PIC with confidence that our design will be manufacturable. Using a PDK will allow us to design with realistic performance and loss values for the individual elements, which is essential when designing a large PIC with the intent manufacturing and potential commercialization. We will take time to familiarize ourselves with the foundry PDK, making sure we properly understand foundry fabrication constraints, and designing and optimizing a polarimeter PIC. In addition, we will work to simplify the design constraints of the PIC in a way that is optimized for the fiber stress sensor.

Many MPW runs at foundries have an approximately 3-month lead time between design submission and delivery. This leadtime is built into the timeline for the first task. Although we will not be actively working on the task while the foundry is manufacturing our PIC designs, it is important to account for that time in the overall scope of the project. The result of this task will be a polarimeter PIC design that meets the needs of the fiber stress sensor and is subsequently manufactured by our chosen photonics foundry.

**3.2 Design and manufacture accompanying printed circuit board**

The second task, designing and manufacturing the PCB, overlaps with the first task and will last approximately 4 months. This is due to the downtime expected with the photonic foundry manufacturing process. While the foundry is fabricating our designs, we will work on designing and manufacturing the supporting PCB circuit. This PCB will control a laser source as well as electronically read out measured light from photodiodes on the PIC. The PCB will be custom-designed to interface with the PIC designed in the first task, making overall operation of the fiber stress sensor more streamlined. We have PCB manufacturing and prototyping equipment available at Chapman University, so we will be able to engage in a rapid prototyping process to design and improve the PCB, even before the PIC has been manufactured. Through the process of iterative design and prototyping, we expect that we will be able to quickly design a PCB that meets all the needs of the polarimeter PIC and fiber stress sensor. That way, once we receive our PICs, we will be able to immediately move on to the third task. The result of this task will be prototype PCBs that meet the needs of the fiber stress sensor and are ready for testing with the polarimeter PICs.

**3.3 Test, characterize, and validate the polarimeter PIC design**

The final task, testing and validating our designs, is expected to last approximately 5 months. Although we should be well-situated to begin testing rapidly, we may make adjustments to the PCB design based on the final PIC devices we receive from the photonic foundry. Planning for 5 months of testing will allow us to fully characterize not only the polarimeter PICs, but the capability of the fiber stress sensor system while using the PICs. We will begin by testing the manufactured PICs by



themselves in a test bed to validate their behavior. The next round of testing will be to validate the polarimeter PICs as useful detection elements in the fiber stress sensor. We will characterize their performance compared to a benchtop polarimeter, including an analysis of the limit of detection and noise in the system. This comparison will serve as proof of feasibility for the polarimeter PIC, and therefore a validation of a truly portable fiber stress sensor. In addition, we will explore the possibility of parallel measurements using multiple PICs, which will entail understanding the performance variation between individual manufactured polarimeter PICs. The outcome of this task is to fully understand manufactured PIC performance, allowing us to set a development roadmap for further enhancements of the fiber stress sensor and to begin planning for further studies using actual tissue samples.

Although this project will represent a substantial improvement for the fiber stress sensor system, the individual tasks fit reasonably within a yearlong timeline.

#### **4. Outcome**

The immediate outcome of the proposed work is an integrated polarimeter PIC that can be used to miniaturize and optimize the fiber stress sensor. We expect that we will be able to operate the polarimeter PIC using benchtop electronic equipment along with the PCB designed to support it. A follow-on outcome of the polarimeter PIC is the improvements it will make to the fiber stress sensor itself. Not only will the sensor design be miniaturized, but we expect that the use of the polarimeter PIC will make overall operation simpler as well. This is because the polarimeter component is large and collects data that requires substantial analysis before it is useful. The design of the polarimeter PIC and PCB will reduce the size and provide an output that requires no or minimal analysis, allowing the fiber stress sensor to operate and provide a meaningful output in real-time.

In addition to the general performance and ease-of-use improvements, we also expect that the polarimeter PIC will provide new capabilities for the fiber stress sensor. Specifically, the miniaturization of the polarization measurement will enable the fiber stress sensor to take simultaneous measurements from multiple fibers. This is theoretically possible with a benchtop polarimeter, but is space- and cost-prohibitive, and has not been demonstrated. Enabling multiple simultaneous measurements will allow us to use an array of fiber sensing elements under a single sample, which will allow us to measure sample stiffness variations across an entire sample in one dimension. We may also be able to explore more complicated measurement schemes that allow mapping the stiffness variations of the sample in two dimensions. This will represent a significant improvement for the fiber stress sensor and its capabilities, which will allow it to have a larger impact in the arena of cancer diagnostics, for which it was originally designed. We expect that this improvement in detection will make the fiber stress sensor more useful in diagnosing other diseases as well.

#### **5. Impact**

The results of the proposed research project have the potential for broad impact in the area of healthcare via improvements made to the fiber stress sensor. The polarimetric fiber stress sensor addresses critical existing issues in the practice of diagnosing biopsied and resected cancer tissue. In particular, it has the potential to make prognoses more consistent between different pathologists who are grading the severity of the disease, such as the likelihood for metastasis. Finally, it can make examination of biopsied and resected tissue quicker, even moving it in to the operating room so that the timing of sample examination is no longer a factor.

Despite this potential, in its current form the fiber stress sensor has serious shortcomings. These are mostly related to the size and ease of operation of the device. By addressing these issues directly and creating a polarimeter PIC to interrogate the sensor output, we will offer substantial improvements to the device. A consistently working polarimeter PIC component might be sufficient

to experiment with the fiber stress sensor in a clinical setting. It will certainly be a large step towards making sure the device can be operated by someone without specific training in optics. Furthermore, the potential for parallel measurements will not only improve the quality of data from the stress sensor, but will likely open it up for new applications. For example, a pathologist might be able to measure the extent of tumorous tissue in a surgically-removed sample without relying on sight alone, thereby confirming that all cancerous tissue has been removed immediately in the operating room. Additionally, there may be applications for use in other disease diagnostics, such as diseases which affect the heart and lungs, many of which have also been correlated with tissue stiffness.

The realization of the polarimeter PIC for the fiber stress sensor will be a massive step towards bringing the sensor itself to a commercially viable state. Because of its unique portability and sensitivity, the fiber stress sensor has the potential to provide great benefit in a variety of healthcare settings all over the world. Thus, the completion of the proposed work has potential for a vast impact in the arena of human health.

## 6. References

1. A. M. Handorf, Y. Zhou, M. A. Halanski, and W.-J. Li, "Tissue Stiffness Dictates Development, Homeostasis, and Disease Progression," *Organogenesis* **11**(1), 1–15 (2015).
2. L. Martinez-Vidal, V. Murdica, C. Venegoni, F. Pederzoli, M. Bandini, A. Necchi, A. Salonia, and M. Alfano, "Causal contributors to tissue stiffness and clinical relevance in urology," *Commun Biol* **4**(1), 1011 (2021).
3. L. Huang, M. Ma, Z. Du, Z. Liu, and X. Gong, "Quantitative evaluation of tissue stiffness around lesion by sound touch elastography in the diagnosis of benign and malignant breast lesions," *PLoS One* **14**(7), e0219943 (2019).
4. X. Ma, L. Wang, H. Wu, Y. Feng, X. Han, H. Bu, and Q. Zhu, "Spleen Stiffness Is Superior to Liver Stiffness for Predicting Esophageal Varices in Chronic Liver Disease: A Meta-Analysis," *PLoS ONE* **11**(11), e0165786 (2016).
5. I. Mozos, C. Malainer, J. Horbańczuk, C. Gug, D. Stoian, C. T. Luca, and A. G. Atanasov, "Inflammatory Markers for Arterial Stiffness in Cardiovascular Diseases," *Front. Immunol.* **8**, 1058 (2017).
6. Q. Li, F. Qu, B. Han, C. Wang, H. Li, R. L. Mauck, and L. Han, "Micromechanical Anisotropy and Heterogeneity of the Meniscus Extracellular Matrix," *Acta Biomater* **54**, 356–366 (2017).
7. F. Malekipour, C. Whitton, D. Oetomo, and P. V. S. Lee, "Shock absorbing ability of articular cartilage and subchondral bone under impact compression," *Journal of the Mechanical Behavior of Biomedical Materials* **26**, 127–135 (2013).
8. A. Abdelgaied, M. Stanley, M. Galfe, H. Berry, E. Ingham, and J. Fisher, "Comparison of the biomechanical tensile and compressive properties of decellularised and natural porcine meniscus," *Journal of Biomechanics* **48**(8), 1389–1396 (2015).
9. M. C. Harrison and A. M. Armani, "Portable polarimetric fiber stress sensor system for visco-elastic and biomimetic material analysis," *Appl. Phys. Lett.* **106**(19), 191105 (2015).
10. A. W. Hudnut and A. M. Armani, "High-resolution analysis of the mechanical behavior of tissue," *Appl. Phys. Lett.* **110**(24), 243701 (2017).
11. L. Fang, S. Zheng, and J. Wang, "Design of on-chip polarimetry with Stokes-determined silicon photonic circuits," *Opt. Express* **29**(20), 31026 (2021).
12. J. Dong and H. Zhou, "Polarimeters from bulky optics to integrated optics: A review," *Optics Communications* **465**, 125598 (2020).
13. Z. Lin, L. A. Rusch, Y. Chen, and W. Shi, "Optimal ultra-miniature polarimeters in silicon photonic integrated circuits," *APL Photonics* **4**(10), 100806 (2019).
14. W. Liu, J. Liao, Y. Yu, and X. Zhang, "High-efficient and high-accurate integrated division-of-time polarimeter," *APL Photonics* **6**(7), 071302 (2021).

With the age of zetta-scale computing rapidly approaching, humanity's thirst for high-speed digital communication shows no sign of slowing. Increased bandwidth is needed on all scales, whether to cope with exponential growth in internet traffic flowing through data centers, to increase global equity by providing broadband internet access to remote or under-developed regions or provide higher cloud connectivity to ever smaller consumer electronic devices. Free-space optical telecommunication offers a unique opportunity to address these challenges, as highlighted by forecasts suggesting that this market will be worth \$2 billion by 2027. Not only is the density of free-space information channels much greater than in optical fibers, but the topology of a free-space optical information network need not be fixed. A network that can adapt to changing patterns of data traffic can reduce congestion without needing to boost the capacity of any single channel. In data centers, for example, where resources utilized at any moment can drop as low as 15%, power consumption could be drastically reduced simply by spreading out that load. Even when data traffic patterns are stable, reconfiguration is vital in environments with fast moving agents, such as fleets of autonomous vehicles or surveillance drones and crowds of people sporting wearable devices. Of course, as bandwidth is always tied to the transmitted signal to noise ratio, the benefit of any reconfiguration strategy is constrained by the cost incurred in term of power consumption. ***Targeting the Optica 20th Anniversary Challenge in information, here, we propose to solve a key bottle neck towards realizing dynamic free-space optical systems by building extremely energy-efficient infrared wave shaping technology that can update on microsecond timescales and with spatial resolution approaching the diffraction limit.***

Two established solutions exist for reconfiguring free-space optical networks: liquid crystal spatial light modulators and micro-electro-mechanical mirror arrays. While both have been deployed in specialized applications, material constraints limit their widespread use. Liquid crystal only allows switching on millisecond timescales and micromechanical devices require large drive voltages which hinders efficient tuning. Emerging platforms based on carrier injection or phase change materials look promising for producing high speed modulation with modest electrical biases. However, to be suitable for communication, the vanishingly weak signal strengths, often <1% of the input, must be drastically improved.

This proposal will focus on the design, fabrication, and testing of nanoscale silicon antennas that by virtue of being highly resonant exhibit a strong response to very small changes to their refractive indices. Based on high quality factor-dipolar-guided-mode-resonances (DGMRs) - the nanoantennas will not only be highly responsive but will also couple efficiently to free-space with point dipole radiation patterns, leading to very low insertion loss. To capitalize on the extreme sensitivity, the subtle temperature dependence of silicon's refractive index will be used to dynamically and precisely tune the resonant frequencies and therefore scattered phases of each element. Temperature control will be delivered by nanoscale resistive heating elements which can be very efficient due to their small size. By developing nanofabrication procedures that optimize both the optical and electrical properties of the nanoantennas, we seek to demonstrate dynamic light wave shaping with speeds at the limit of thermal tuning, ~100kHz, and with low power operation <1mW/pixel. Importantly, sub- $\lambda$  pixel pitch will unlock an unprecedented number of modes.

While ~100kHz wave shaping will open many exciting doors for free-space optical communication, the proposed project is the first step towards operation at much higher speeds. The key enabling concept is subwavelength pixels that are nevertheless highly sensitive. Mechanisms such as carrier injection in 2D materials and the Pockels effect produce index modulation 1-2 orders of magnitude smaller than for thermo-optic tuning in silicon. With further refinements to our nanofabrication procedure which will unlock even higher Q factors, steering rates at 10s to 100s of GHz should be possible. Such performance would allow for network reconfiguration at the scale of a single data packet.

## Fast, low-power, and high-resolution meta-reflect-arrays for massive space-division multiplexing

**Problem statement/Objective:** Given the vast number of modes available in empty space for light to propagate, wireless optical communication represents a largely untapped resource for dealing with the ever-increasing demand for higher communication bandwidth. Without the need to physically define information channels, as with fiber optics, free-space optics offers not just increased capacity but also tremendous flexibility to steer bandwidth where it is needed. ***Here we seek to break down a key technological barrier to realizing this potential – rapid and extremely efficient light wave shaping. Specifically, by developing dynamic reflect-arrays made from nanoscale antennas that are highly electro-thermally responsive, we will demonstrate beam-steering, dynamic focusing and dot-projection at ~100 kHz speeds, over an unprecedented field of view (>60°) and with <1mW/pixel tuning power.*** These devices will lay the foundations for a host of programmable optical communication applications, from switch fabrics in datacenters to light-based WiFi, or LiFi, and even connecting robotic agents in dynamic autonomous networks. In each case, the ability to scale to large systems and to adapt to sudden changes in data traffic patterns or network topology while consuming very little of the overall energy budget, is vitally important.

**Motivation and literature review:** Dynamic wave-shaping devices, or spatial light modulator (SLM)s, typically involve an array of pixels each of which can be electrically tuned to exhibit variable transmission or reflection. In its simplest form, such a pixel consists of a transparent film whose refractive index can be electrically adjusted. Liquid crystal (LC) is a natural choice because index changes as large as ~0.4 can result from applying a weak electric field. This allows SLMs made from LC to be just a few micrometers thick, which is not only useful for maintaining a compact device footprint but also permits micrometer scale pixelation, which is typically constrained by fringing fields between closely spaced electrodes causing crosstalk. Unfortunately, the molecular rotation that LC relies upon takes milliseconds to occur, limiting wavefront modulation rates to a few hundred Hz. SLMs have been developed using mechanisms with a much faster response, kHz to 10s of MHz, including ferro-electric-LC (FC-LC), digital-micro-mirror-devices (DMD), and galvanic-light-valves (GLV)<sup>1,2</sup>. Although these come with limited spatial and/or angular resolution, along with other drawbacks. FC-LC and DMD systems, for example, operate in a binary fashion and, more importantly, all demand large drive voltages, often 10s if not 100s of volts.

Recently, resonant nanoscale structures have attracted attention for their ability to mimic long optical paths while maintaining a subwavelength footprint<sup>3</sup>. This also means they can be arranged into dense arrays, often called metasurfaces. It is important that the objects be resonant as the extended time over which light is trapped within a resonance helps to compensate for the tiny interaction distances or volumes. As well as improving the resolution of transmissive LC SLMs<sup>4</sup>, while of course still inheriting the LC speed limitation, nanoantenna phase tuning via mechanisms capable of operating at MHz speeds has been realized, including carrier injection<sup>5,6</sup>, the Pockels effect<sup>7,8</sup> and the quantum-confined stark effect<sup>9</sup>. Unfortunately, these devices exhibit incredibly weak diffraction efficiencies, a few percent at most and often less than 1%. This is either because the modulation is itself dissipative, or the index modulation is so weak that absorbing configurations were used to amplify the phase response. Amplitude modulation of a few ten percent has been shown using phase change materials<sup>10,11</sup>, for which reversible transitions can be electrically or electro-thermally induced between crystalline and amorphous phases. But continuous phase tuning has yet to be realized with these materials, let alone individually addressable phased arrays. Approaching atomic scale SLMs, beam steering on nanosecond timescales has been

demonstrated via exciton resonances in 2D semiconductors<sup>12</sup>. While compelling, reasonable signal strengths were only observed at cryogenic temperatures, which is necessary to extend the exciton lifetime. An overriding challenge here is that while all these devices are resonant, the reduction in optical path length far outstrips the degree of resonant enhancement achieved.

Extreme resonant enhancement, characterized by the presence of a high quality factor (Q-factor) resonance, has been observed in integrated photonic systems. Micro-ring and photonic crystal defect cavities boast Q-factors from  $10^3$  to  $10^7$ . Due to the ultra-narrow linewidths these represent, both platforms have been employed to realize high contrast electro-optic modulators operating at speeds of up to 40GHz and requiring an electrical bias of just a few volts<sup>13,14</sup>. In contrast, the nanoantennas typically used in free-space metasurfaces have Q of order 10. The question remains whether high-Q nanoantennas can be developed to bring the benefits of extreme electro-optic sensitivity to SLMs. Recently, collective resonances, often referred to as lattice, guided mode, or quasi bound state in continuum, resonances, have attracted attention due to their ability to also support high Q-factors with strong coupling to free-space light by leveraging destructive plane-wave interference. Free-space electro-optic amplitude modulators have been demonstrated based on this principle, operating at speeds of up to a few GHz<sup>15</sup>. Unfortunately, the extended nature of these modes has constrained pixel sizes to  $>50\mu\text{m}^2$ . Not only does this severely limit wave shaping resolution, but, because electrical performance scales inversely with gate size, high voltages were needed. Efficient free-space phase modulation has been observed with subwavelength gratings, all be it again with very low spatial resolution<sup>16</sup>.

### High quality factor phase gradient metasurfaces:

To generate extremely responsive optical pixels, we will build on our recent development of a new class of silicon nanoantennas which support dipolar guided mode resonances (DGMRs)<sup>17,18</sup>. Unlike traditional Mie resonances, guided mode standing waves that, in principle, remain perfectly trapped inside the dielectric structure, form the foundation of DGMRs. As seen in Fig.1a-b, subtly breaking specific symmetries, by introducing dissimilar widths for neighboring nano-bricks for example, opens a small amount of leakage, turning the bound mode into a resonance. Importantly, while the symmetry breaking strength controls the leakage rate, as revealed in Fig.1c, it has no bearing on the shape of the leaked wave. Instead, the shape of the bound mode in question dictates the corresponding radiation pattern. If dielectric materials with negligible absorption are patterned with processes that minimize scattering loss, it is therefore possible to produce extremely high quality factor (Q-factor) resonances with dipole radiation patterns, or high-Q DGMRs. Calculated by taking the ratio of the resonant frequency to the linewidth, the Q-

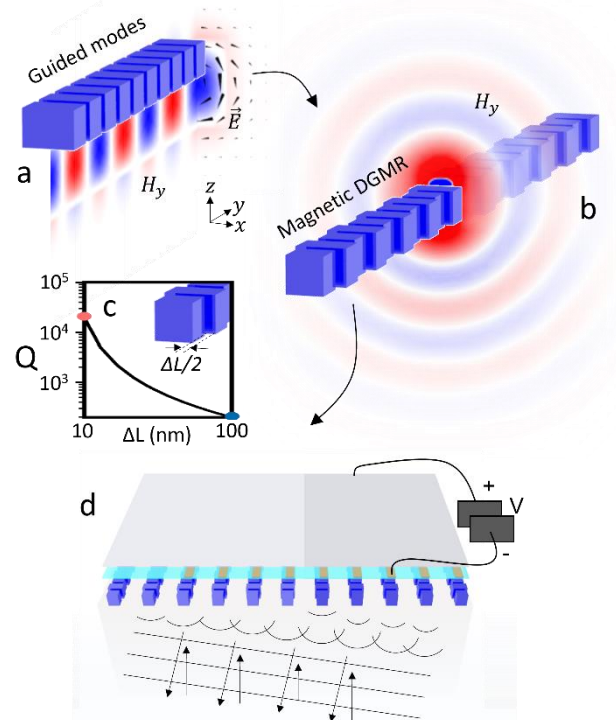


Figure 1. Dynamic meta-reflect-arrays from high Q nanoantennas. a) Bound guided mode in silicon nano-brick array. b) Symmetry breaking induces dipolar guided mode resonance. c) Q scales inversely with symmetry breaking. d) Schematic for SLM made from high Q nanoantennas.

factor is relevant to the pursuit of efficient modulation because the narrower the linewidth the larger the scattered amplitude or phase change will be for a given spectral shift. As drawn schematically in Fig.1d, by electrically driving subtle red-shifts we plan here to build dynamic infrared wave-shaping devices.

Highly resonant dipole scatterers become sensitive phase modulators when placed above a mirror. Combining the forward scattering from the nanoantennas with the reverse scattering, virtually all of the wavelength dependence is removed from the reflectance, while a steep resonant slope in the reflected phase remains. The phase also spans the full range of  $2\pi$ . As seen in Fig.2a, modifying the nanoantenna shape causes a redshift of the DGMR, translating

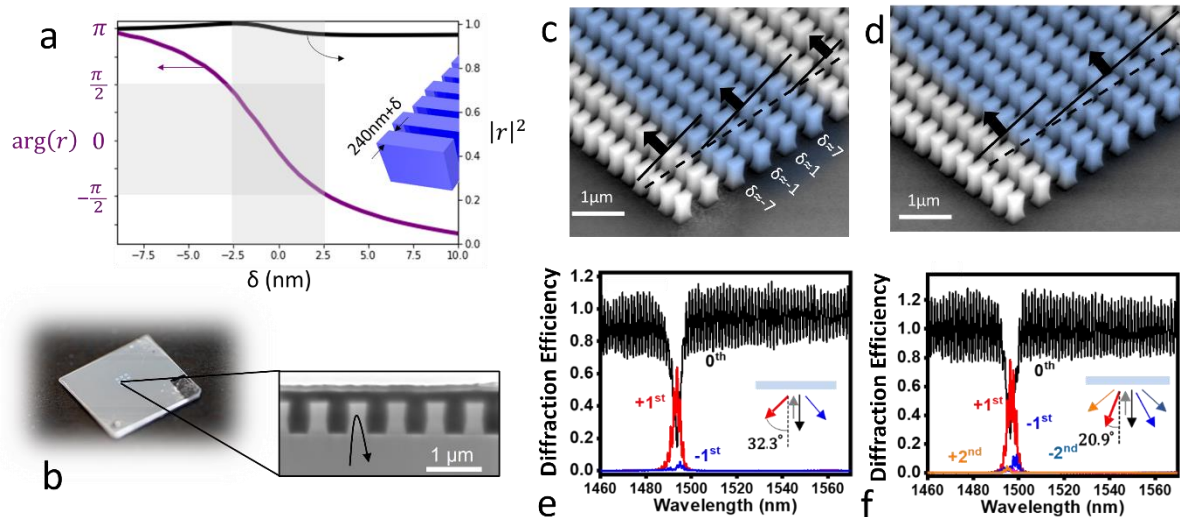


Figure 2. Passive high Q meta-reflect-array. a) Reflected phase and intensity for metal backed DGMR nanoantenna with varying nano-block width. b) Photograph and side-on SEM image of meta-reflect-array sample. c and d) SEM images of beam steering metasurfaces, prior to metal backing, corresponding to diffraction spectra in e and f, respectively.

the phase dependence on the wavelength into a structure dependent response at a fixed operating wavelength, chosen to be  $1495.5\text{nm}$ . Specifically, the width of the smaller nano-block is adjusted by the amount  $\delta$ , as shown in the inset of Fig.2a. Phase coverage of  $\pi$  and almost  $2\pi$  can be accessed with  $\delta$  varying between  $-2.5\text{nm}$  to  $2.5\text{nm}$  and  $-15\ \text{nm}$  to  $+15\text{nm}$ , respectively. These equate to volume fractions of only 0.9%, for  $\pi$ , and 5.6%, for  $2\pi$ . Such a strong response to weak structural tuning is a direct consequence of working with a high Q-factor. If each nanoantenna within the metasurface can be treated as an independent element, Fig.2a can be thought of as a menu of possible phase levels to combine spatially for producing different wavefronts. To prove that this is the case, we have fabricated metal backed metasurfaces, an example of which can be seen in Fig.2b, with the parameter  $\delta$  varying from nanoantenna to nanoantenna. Specifically, two devices are presented, pictured in Fig.2c-d, both designed to impart linear phase gradients on the reflected light but with different phase slopes. For example, in Fig.2c the structure repeats every four nanoantennas with  $\delta$  values  $-7, -1, 1$  and  $7\text{nm}$ . From the corresponding diffraction measurements in Fig.2e-f, clearly the desired phase profiles have been successfully produced as efficient beam steering is seen in the direction normal to the designed phase fronts. As well as confirming that DGMR nanoantennas can act as independent high-Q pixels, the fact that they facilitate beam-steering with a maximum change in volume fraction across the array of just 2.6%, supports the notion that this platform is well suited to dynamic manipulation. Weak structural tuning essentially acts as a proxy for weak refractive index modulation.

**Electro-thermo-optic meta-reflect-arrays (Proposed research):** The key advantage of DGMR nano-pixels is the fact that their cross-sectional size and Q-factor are decoupled,



meaning that we can realize subwavelength pixels with, in-principle, arbitrarily large  $Q$ . However, the minimum pixel pitch also depends on the strength of near field coupling. Neighboring nanoantennas will only respond approximately independent from one another if the coupling time between them, the reciprocal of the coupling rate, is smaller than the shortest individual lifetime. Although the physics of nearfield coupling applies equally to all dielectric resonators, as lifetime scales inversely with  $Q$ -factor, the high- $Q$  DGMRs we will develop will require very low coupling rates. We will explore three different strategies for reducing coupling and therefore maximizing the  $Q$  achievable with subwavelength pixel pitch. 1) Including anisotropic fin structures between nanoantennas to decrease the evanescent decay lengths 2) Combining nanoantennas with incommensurate translational symmetry so that coupling is suppressed via destructive interference, and 3) Combining modes with opposite out-of-plane parity, such as electric and magnetic DGMRs, leading to similar interference-based suppression. Ultimately, we will target  $Q > 10^4$ .

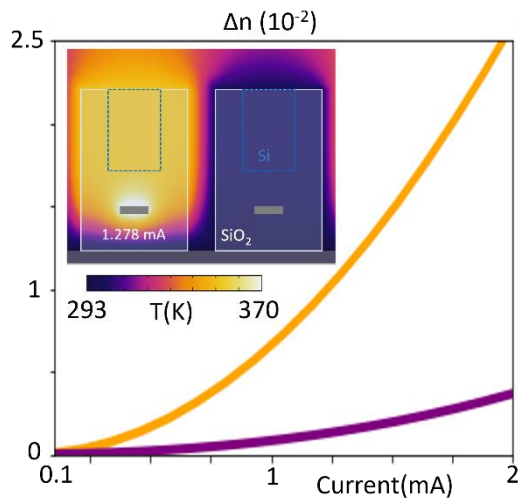


Figure 3. Joule heating simulations showing average temperature increase within  $\text{SiO}_2$  encapsulated Si nanowires as a function of current through Ti nanowires.

Inspired by developments in integrated photonics, thermal changes to the refractive index of silicon will be driven by resistive nanowire heaters placed in the vicinity of each nanoantenna. The thermo-optic coefficient of silicon is small ( $1.83 \times 10^{-4} \text{ K}^{-1}$ ), but sufficient to red-shift a DGMR having  $Q > 10^4$  by a full linewidth with a temperature increase of just a few degrees. For a Titanium wire a few hundred nanometers wide and a few micrometers long placed close to a nanoantenna,  $\mu\text{A}$  currents will produce the necessary temperature increase, corresponding to a few microwatts. Thermal modelling will be used to design electro-optic nanoantennas with minimal electrical tuning power while keeping optical absorption in the metal low. Those simulations will also be employed to reduce thermal crosstalk.

In Fig.3 for example, mA currents are seen to give a temperature rise sufficient for reproducing the beam steering in Fig.2. Low crosstalk in Fig.3 results from nanoscale air trenches acting as thermal shields – a feature that will be explored in more detail throughout the project. Fabrication procedures will be developed to realize the multilayer designs, involving a multistep process incorporating, electron-beam lithography with reactive ion etching, electron-beam and photolithography with metal evaporation and lift-off, PECVD of silicon dioxide and wet etching. After testing single channel operation to determine the threshold current, the meta-reflect-array will be connected to a high-density analog output module to demonstrate independent pixel control and spatial light modulation. A home-built Fourier-plane imaging spectrometer will allow the far field diffraction to be measured.

### Schedule

- Design meta-reflect-array binary phase grating to determine the minimum pixel density corresponding to  $Q > 10^4$  (Month 1)
- Fabricate and test optimized meta-reflect-array binary phase grating with structural tuning (Month 1-2)
- Design thermal bias structure for meta-reflect-array using coupled heat transport and optical simulations (Month 2)
- Develop multistep fabrication procedure for thermal bias structure (Month 3-5)
- Test thermal bias with simultaneous current control of every other element within meta-

- reflect-array binary phase grating to electrically switch diffraction on and off (Month 5-7)
- Build independent multi-element tuning system by driving meta-reflect-array with multi-in/out microcontroller (Month 8-10)
- Demonstrate dynamic beam steering and focusing and measure limits of tuning speed and tuning energy (Month 11-12)

**Outcomes and impact:** By producing a compact and efficient dynamic wave shaping prototype, capable of subwavelength resolution and high speed, this project will bring reconfigurable optical communication to a whole new technological class, including consumer electronics and even wearables. Although here we will focus on electro-thermal control, which limits the tuning speed to the kHz domain, the platform we will experimentally introduce can be extended to faster mechanisms such as carrier injection and the Pockels effect. As such we are charting a course towards spatiotemporal light modulation on unexplored length and time scales.

## References

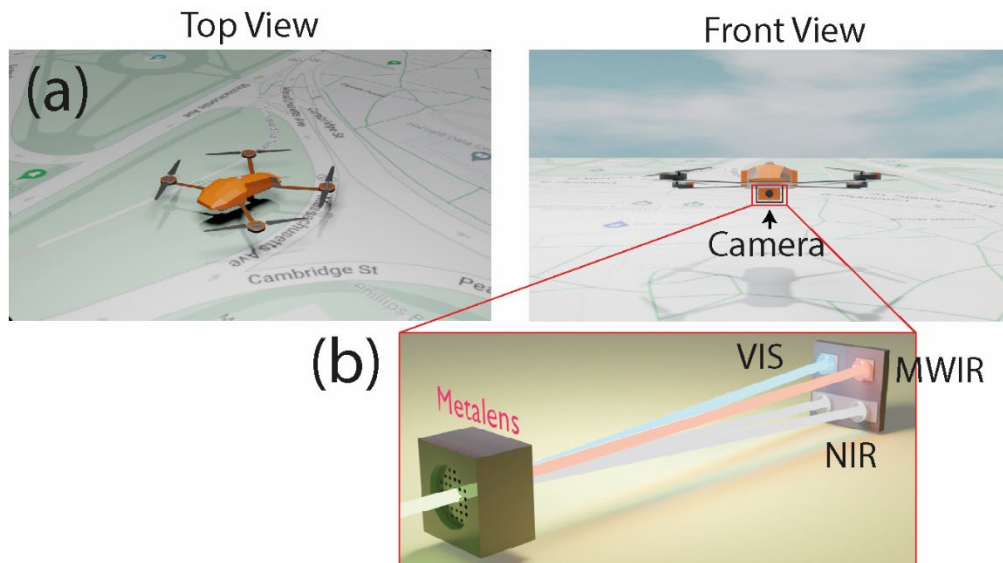
1. Bloom, D. M. *et al.* Deformable grating optical modulator. *Opt. Lett. Vol. 17, Issue 9, pp. 688-690* **17**, 688–690 (1992).
2. Yano, M. *et al.* Optical MEMS for photonic switching - Compact and stable optical crossconnect switches for simple, fast, and flexible wavelength applications in recent photonic networks. *IEEE J. Sel. Top. Quantum Electron.* **11**, 383–394 (2005).
3. Kim, I. *et al.* Nanophotonics for light detection and ranging technology. *Nat. Nanotechnol.* **16**, 508–524 (2021).
4. Li, S. Q. *et al.* Phase-only transmissive spatial light modulator based on tunable dielectric metasurface. *Science (80-. )*. **364**, 1087–1090 (2019).
5. Huang, Y. W. *et al.* Gate-Tunable Conducting Oxide Metasurfaces. *Nano Lett.* **16**, 5319–5325 (2016).
6. Shirmanesh, G. K. *et al.* Electro-optically Tunable Multifunctional Metasurfaces. *ACS Nano* **14**, 6912–6920 (2020).
7. Weiss, A. *et al.* Tunable Metasurface Using Thin-Film Lithium Niobate in the Telecom Regime. *ACS Photonics* **9**, 605–612 (2022).
8. Smolyaninov, A. *et al.* Programmable plasmonic phase modulation of free-space wavefronts at gigahertz rates. *Nat. Photonics* **13**, 431–435 (2019).
9. Wu, P. C. *et al.* Dynamic beam steering with all-dielectric electro-optic III–V multiple-quantum-well metasurfaces. *Nat. Commun.* **10**, 1–9 (2019).
10. Zhang, Y. *et al.* Electrically reconfigurable non-volatile metasurface using low-loss optical phase-change material. *Nat. Nanotechnol.* **16**, 661–666 (2021).
11. Wang, Y. *et al.* Electrical tuning of phase-change antennas and metasurfaces. *Nat. Nanotechnol.* **16**, 667–672 (2021).
12. Andersen, T. I. *et al.* Beam steering at the nanosecond time scale with an atomically thin reflector. *Nat. Commun.* **13**, 1–7 (2022).
13. Shakoov, A. *et al.* Compact 1D-silicon photonic crystal electro-optic modulator operating with ultra-low switching voltage and energy. *Opt. Express* **22**, 28623 (2014).
14. Xu, Q., Schmidt, B., Pradhan, S. & Lipson, M. Micrometre-scale silicon electro-optic modulator. *Nature* **435**, 325–327 (2005).
15. Benea-Chelms, I. C. *et al.* Electro-optic spatial light modulator from an engineered organic layer. *Nat. Commun.* **2021 121** **12**, 1–10 (2021).
16. Horie, Y. *et al.* High-Speed, Phase-Dominant Spatial Light Modulation with Silicon-Based Active Resonant Antennas. *ACS Photonics* **5**, 1711–1717 (2018).
17. Lawrence, M. *et al.* High quality factor phase gradient metasurfaces. *Nat. Nanotechnol.* **15**, 956–961 (2020).
18. Lawrence, M., Barton, D. R. & Dionne, J. A. Nonreciprocal Flat Optics with Silicon Metasurfaces. *Nano Lett.* **18**, 1104–1109 (2018).

**Title:** Airborne Gas Detection Metalens (AGDM) Camera

**Category:** Environment (Improving or creating tools to measure, monitor and mitigate climate change.)

**Introduction**

Global warming is one of the central challenges that humanity is facing, and it is signified by the increase in the average temperature on Earth. It leads to heat waves, hurricanes, droughts, raised sea levels, and altering ecosystems. The primary reason for these effects is connected to human activities, which include deforestation and burning fossil fuels that release greenhouse gases. Carbon dioxide accounts for 79% of all greenhouse gasses emitted due to human activity in the USA in 2020 (following worldwide trends). Therefore, its monitoring is essential for predicting Earth's average temperature growth rate.



**Figure 1.** (a) Concept art of a drone equipped with a gas detection metalens camera monitoring the area. (b) Schematic of a gas detection metalens camera.

**Objective**

Artificial satellites provide an excellent platform for remote CO<sub>2</sub> monitoring, but this technology is very expensive and provides limited abilities to modify the mission objectives after the launch. In addition, a substantial volume and mass of the satellite are required to accommodate optical components of the monitoring instrument that further increase the mission's price. This project aims to minimize and simplify CO<sub>2</sub> detection optical instruments. Microsatellites, weather balloons, or drones could be used to deploy proposed gas detection optical instruments, expanding accessibility of the CO<sub>2</sub> monitoring projects to the broad scientific community. Moreover, drones can monitor CO<sub>2</sub> at any time of the day, unlike satellite-based optical instruments, leading to the generation of new scientific data.

**Outcome**

The proposed gas detection metalens camera will operate similarly to optical CO<sub>2</sub> monitoring instruments currently used in space. The operation principle comprises image acquisition at three different wavelengths, including 0.75 μm (O<sub>2</sub> band), 1.61 μm (weak CO<sub>2</sub> band), and 2.01 μm (strong CO<sub>2</sub> band). Additionally, images at 4.8 μm (MWIR CO<sub>2</sub> absorption band) will be acquired (see Fig. 1(b)). Adding this wavelength will allow for the detection of point sources of CO<sub>2</sub> emission, like, biomass burning events, lava flow events, or industrial emissions. Furthermore, a proposed expansion of functionality will not require any extra optical elements.

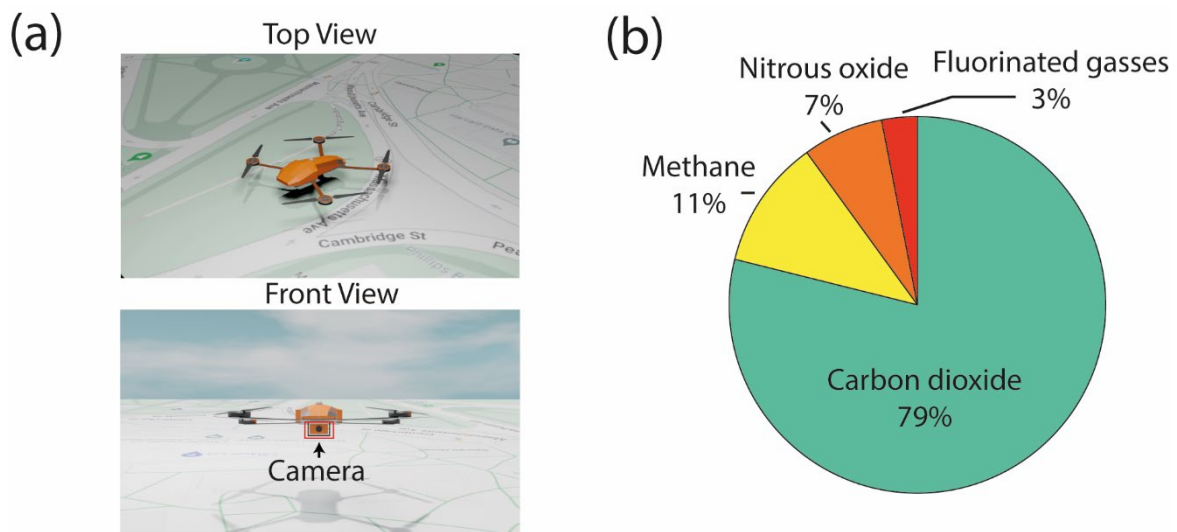
The form factor of the CO<sub>2</sub> detection instrument will be minimized by employing metalens technology. Single metalens will replace multiple optical components of a traditional detection camera. Recently developed unique holey metalens technology will be used to achieve guiding of light at a visible (VIS), near-infrared (NIR), and mid-infrared (MWIR) parts of the spectrum covering three octaves.

To demonstrate the performance of the proposed camera, it will be mounted on the drone, and CO<sub>2</sub> detection will be performed over the streets of Cambridge in Massachusetts, USA.

## Airborne Gas Detection Metalens (AGDM) Camera

### Proposal summary

Greenhouse gases, including carbon dioxide and methane, released in excess due to human activities, are the leading causes of global warming. Monitoring the spatial and temporal evolution of such gases allows for real-time evaluation and prediction of temperature and climate dynamics as a result of radiative forcing on Earth. I propose the development of a compact and lightweight gas-detection metalens-camera system for remote sensing of CO<sub>2</sub> concentrations. It will simultaneously collect images at four different wavelengths over three octaves to quantitatively measure CO<sub>2</sub> levels at high specificity: in the visible (VIS), near-infrared (NIR), and mid-infrared (MWIR) parts of the electromagnetic spectrum. This unique low-component-number functionality will be achieved using the recently developed holey metalens platform. The imaging system will be deployed to monitor the CO<sub>2</sub> concentration of the selected areas above the city of Cambridge, Massachusetts using a drone (Fig.1(a)).



**Figure 1.** (a) Concept art of a drone equipped with a gas detection metalens camera monitoring the area. (b) U.S. greenhouse gas emissions in 2020<sup>1</sup>

### Detection of CO<sub>2</sub> concentration in the atmosphere

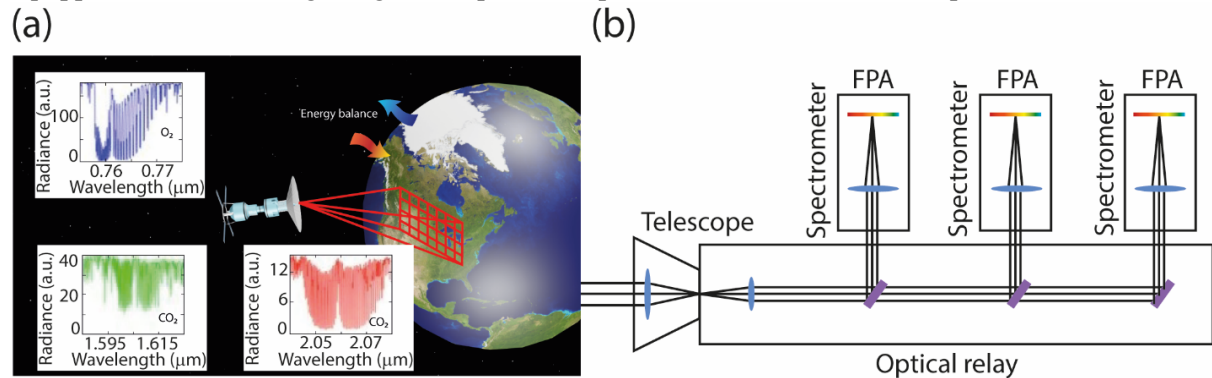
Global warming is one of the central challenges that humanity is facing, leading to increased frequency of heat waves, hurricanes, droughts, elevated sea levels and altered ecosystems<sup>2</sup>. The primary reason for these effects is human activities which include deforestation and burning of fossil fuels that release greenhouse gases<sup>1</sup>. Carbon dioxide accounts for 79% of all greenhouse gases emitted due to human activity in the USA in 2020, which aligns with worldwide trends (see Fig. 1(b))<sup>1</sup>.

Many tools, including ground-based and airborne missions, have been developed to monitor the spatial concentration of CO<sub>2</sub> in the atmosphere. Several satellite instruments measure column-averaged dry-air molar fractions of CO<sub>2</sub>, including TANOS-FTS-2 on board the GOSAT-2 satellite<sup>3</sup>, OCO-2<sup>4</sup>, TanSat<sup>5</sup>, and OCO-3<sup>6</sup> onboard the International Space Station (ISS). The principle of operation for these instruments relies on the measurement of reflected light from the Earth's surface at specific wavelengths (see Fig. 2(a)). The choice of wavelength depends on the type of gas to be detected. When light travels through the atmosphere, it is partially absorbed by gas molecules at specific wavelengths. The amount of absorbed light is directly linked to the concentration of gas in the atmosphere.

### The optical module of OCO-2

I will consider the operation principle of the OCO-2 instrument as a representative example<sup>4</sup>. This instrument measures spectrum of reflected light in the vicinity of three wavelengths (see inset in Fig. 2(a)). The first channel acquires a signal in the O<sub>2</sub> A-band at 0.76  $\mu\text{m}$ . The concentration of O<sub>2</sub> in the atmosphere is a well-known value and is used as a reference measurement for this instrument. The reflection spectrum at this wavelength provides information about the presence of clouds and aerosols that disturb CO<sub>2</sub> concentration measurements. Furthermore, the total atmospheric pressure and light path length through the atmosphere are inferred from these measurements.

The second channel is a weak CO<sub>2</sub> band in the vicinity of 1.61 μm. This wavelength band is the most sensitive to the CO<sub>2</sub> concentration near the surface, as other gases only weakly absorb in this band. Finally, the third channel is a strong CO<sub>2</sub> band in the vicinity of 2.06 μm. This channel provides an entirely independent concentration measurement which improves the overall measurement accuracy. The simplified schematic of the optical module of OCO-2 is shown in Fig. 2(b). A telescope is used to collect light reflected from Earth. The collected light is redistributed over three different channels equipped with dedicated gratings. The spectral response is recorded with the help of cooled detectors.

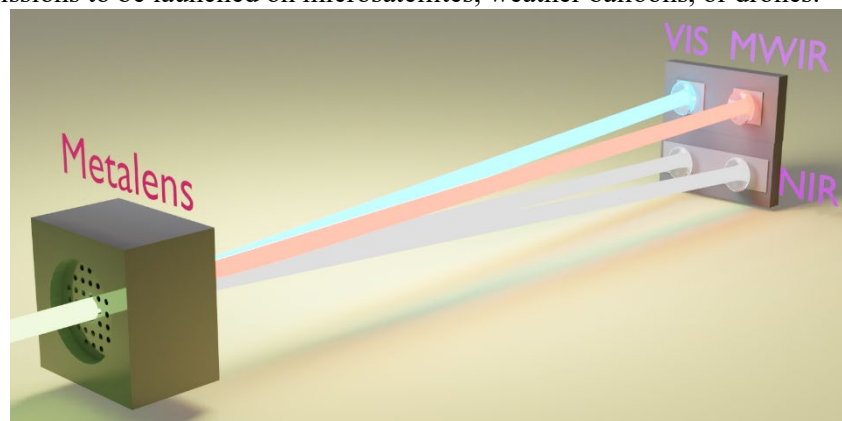


**Figure 2.** (a) The satellite measures reflected light at three different wavelength bands to detect CO<sub>2</sub> concentration. Insets show detection wavelength bands of O<sub>2</sub> and CO<sub>2</sub>. (b) Simplified schematic of OCO-2 optical module. The proposed project aims to reduce the size of the optical relay of this instrument by replacing it with single metalens with engineered passive chromatic behavior. Certain optical elements are omitted in the scheme.

### Problem statement

Orbital satellites provide an excellent platform for CO<sub>2</sub> remote sensing, but these projects are costly and have only limited flexibility to modify the mission objectives after launch. In addition, a substantial fraction of the satellite mass is dedicated to accommodating the optical components of the instrument, further increasing the mission price.

To resolve the current problems that remote sensing devices face, I propose to create a lightweight and compact CO<sub>2</sub> monitoring instrument using recently developed holey metalens technology. Minimizing and simplifying optical instruments will make airborne CO<sub>2</sub> monitoring missions accessible even for student-led projects. In addition, it will help intensify global climate change studies, allowing smaller and cheaper missions to be launched on microsatellites, weather balloons, or drones.



**Figure 3.** Schematic of the optical module of gas detection metalens camera. Holey metalens focuses incident light to four different spatial positions depending on the wavelength of the incident light.

### Gas detection metalens camera

I propose the creation of a gas detection metalens camera that can record images required for CO<sub>2</sub> concentration detection in the atmosphere. By multiplexing optical functions using metalens technology, the proposed camera will possess a small form factor and reduce the weight of the airborne optical instrument, significantly reducing the costs required for satellite operation. The target



wavelengths will include 0.75  $\mu\text{m}$  ( $\text{O}_2$  band), 1.61  $\mu\text{m}$  (weak  $\text{CO}_2$  band), 2.01  $\mu\text{m}$  (strong  $\text{CO}_2$  band), and 4.8  $\mu\text{m}$  (MWIR  $\text{CO}_2$  absorption band), covering three octaves. To my knowledge, a single-layer metalens that can guide light at a visible, NIR, and MWIR part of the spectrum simultaneously has not been demonstrated.

Images acquired at a wavelength of 4.8  $\mu\text{m}$  are not currently used for  $\text{CO}_2$  detection. However, it has been shown that the information at this wavelength can be used to detect and characterize point sources of  $\text{CO}_2$  emission, for example, in quantifying biomass burning events<sup>7</sup>, forecasting lava flow events<sup>8</sup>, monitoring industrial emission, or characterizing hot spots of Jupiter's moon Io<sup>9</sup>. The observations at this wavelength can be done continuously throughout the day and night. Imaging of point source emissions of  $\text{CO}_2$  can provide vital information about natural disasters or be used for regulatory and law enforcement purposes.

The proposed camera design is shown in Fig. 3. It consists of a metalens that will focus light into four distinct spatial positions and direct it towards the appropriate sensor. Metalens will replace the optical relay shown in Fig. 2(b) with a simplified, more compact architecture. It is followed by a set of optical bandpass filters (not shown in the schematic) that filters out background light for an enhanced signal-to-noise ratio. Finally, the image is recorded by photosensors in the lens focal plane.

For  $\text{CO}_2$  observation, the OCO-2 instrument collects the spectra in the vicinity of the specified wavelengths using a set of gratings. Given this project's budget and timeline, this spectroscopic capability will not be demonstrated here. I will demonstrate imaging at four distinct wavelengths instead. Further research can integrate the demonstrated camera with compact metalens spectrometers<sup>10</sup>, creating an integrated all-metasurface device with minimal footprint and launch mass.

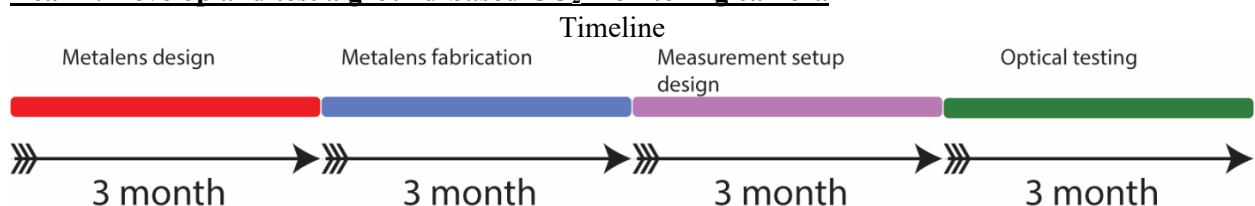
### **Metasurface technology**

Recently the holey metalens platform<sup>11</sup> enabled the creation of an ultra-high aspect ratio metalens for the infrared part of the electromagnetic spectrum. The holey metalens consists of a 5.7  $\mu\text{m}$  thick suspended Si membrane that contains nanoholes with varying diameter and can focus light at a central wavelength of 1550 nm. This platform provides a unique advantage that is not available to other metalens platforms; it can operate in the spectral bandwidth spanning from the visible to MWIR parts of the spectrum. Despite silicon being a lossy material in the visible spectrum, the micron-scale thickness of the silicon membrane reduces losses in this spectral range. Furthermore, the holey metalens platform employs a CMOS-compatible fabrication process, which allows for the mass production of optical components using modern semiconductor foundry capabilities. One of the advantages of the holey metalens platform is that the nanostructures comprise a rigid monolithic structure that is robust against the substantial vibrations that can occur in deployable payloads during lift-off.

### **Work Plan**

Two years will be dedicated to developing an airborne  $\text{CO}_2$  monitoring metalens camera.

#### **Year 1: Develop and test a ground-based $\text{CO}_2$ monitoring camera**



#### **Milestone 1: Metalens design**

A holey metalens will be designed to focus four wavelengths required for  $\text{CO}_2$  detection to different spatial positions using the holey metalens platform. This platform is an excellent candidate to realize the required functionality, as it can operate in the VIS, NIR, and MWIR spectral ranges. A library of meta-atoms used for the metalens design will be generated using a broad parameter sweep of nanostructure geometries (~1 000 000 meta-atoms) using the Harvard University supercomputing Cannon cluster. An SQL server will be used to store and retrieve generated data and electromagnetic



simulations efficiently. Silicon possesses relatively small but noticeable absorption at the wavelength of 0.75  $\mu\text{m}$ . It will be compensated in design by normalizing the measurement data.

### **Milestone 2: Metalens fabrication**

A 1 cm diameter holey metalens will be fabricated using a CMOS compatible recipe outlined in our recent publication<sup>11</sup>. In the first step, using rapid e-beam lithography prototyping available at Harvard nanofabrication facilities (Center for Nanoscale Systems, CNS) a silicon-on-insulator (SOI) wafer will be patterned. Next, the wafer will be etched using the deep reactive ion etching – Bosch process. The leftover resist will be removed by submerging the fabricated device into Piranha solution.

### **Milestone 3: Measurement setup design**

Two setups will be used to characterize the proposed metalens' point spread functions (PSF). First, the industry-grade LensCheck tool, which is available at the Capasso lab, will be used to characterize the focusing behavior of the metalens in the visible and infrared parts of the spectrum. A new setup will be built using expertise that is present in the group to characterize a focal spot at the MWIR part of the spectrum. This setup is analogous to one described in a previous publication<sup>11</sup>. The only difference is that a commercially available thermopile infrared array will be used to record the spatial distribution of light intensity at the focal plane of the device. A tabletop model of a street enclosed in an airtight transparent container with the CO<sub>2</sub> source will be created. This model will be used to test the camera's imaging capabilities in Milestone 4.

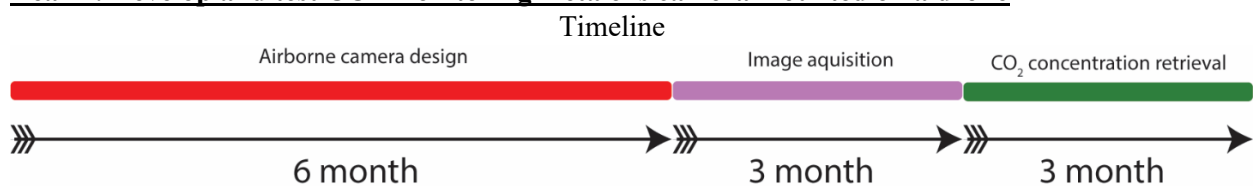
### **Milestone 4: Optical testing**

A fabricated holey metalens will be optically tested using the setups described in Milestone 3. In the first step, for each wavelength a PSF will be measured. In the second step, a metalens will be mounted in the imaging setup, and the scene with the distinct gas sources will be imaged.

#### **Outcomes:**

- A holey metalens that can focus light at four different wavelengths, including 0.75  $\mu\text{m}$  (O<sub>2</sub> band), 1.61  $\mu\text{m}$  (weak CO<sub>2</sub> band), 2.01  $\mu\text{m}$  (strong CO<sub>2</sub> band), and 4.8  $\mu\text{m}$  (MWIR CO<sub>2</sub> absorption band).
- The PSF measurement setups that can operate in VIS, NIR, and MWIR parts of the spectrum.
- A model of the street for a testing of imaging capabilities of the gas detection metalens camera.
- Images of the model street with distinct CO<sub>2</sub> sources.

## **Year 2: Develop and test CO<sub>2</sub> monitoring metalens camera mounted on a drone**



### **Milestone 1: Airborne camera design**

Develop a compact camera that can be mounted on the drone. This camera will have three separate sensors required to detect the image at four wavelengths (see schematic in Fig. 3). A Si sensor array will be used for imaging at the 0.75  $\mu\text{m}$  wavelength range. A InGaAs sensor array will be used for the infrared part of the spectrum. Its surface will be divided into two parts, and each part will detect images at 1.61 and 2.01  $\mu\text{m}$  wavelengths, respectively. Finally, a thermopile array will be used to perform imaging at a wavelength of 4.8  $\mu\text{m}$ . Three detectors can be replaced with an HgCdTe detector that can obtain images at all four wavelengths and is used for airborne applications, but the purchase of such a sensor is outside the budget of this proposal.

### **Milestone 2: Image acquisition**

The developed camera will be mounted on the drone, and an imaging of the testing sites will be performed. The testing site will include parts of the city of Cambridge, including local sources of CO<sub>2</sub> emission.

### Milestone 3: CO<sub>2</sub> concentration retrieval

Extraction of the CO<sub>2</sub> concentration will be performed using MODTRAN (MODerate resolution atmospheric TRANsmission) software package. This is a commercially available package that is developed in collaboration between the Spectral Sciences, Inc and the Air Force Research Laboratory (AFRL), and it is used for the analysis of optical measurements through an atmosphere. It uses the radiative transfer equations to compute spectral transmittances and radiance.

#### Outcomes:

- Compact gas detection metalens camera mounted on the drone.
- Images of the streets with CO<sub>2</sub> point sources in the city of Cambridge.
- Analysis of the airborne images for CO<sub>2</sub> concentration detection.

#### Impact:

*Customization:* The proposed project opens great possibilities for creating optical instruments for monitoring greenhouse gases. The suggested metalens platform can be easily customized to detect various greenhouse gasses and not be limited to only CO<sub>2</sub> gas.

*Redundancy:* Multiple compact imaging devices can be incorporated as redundant backups, increasing the operation's robustness and the mission's lifetime.

*Accessibility:* Cheap, lightweight monitoring tools will allow CO<sub>2</sub> measurements to be performed at a broader range of times of day and more costly polar orbital inclinations. In addition, this flexibility expands the observation parameter space compared to current missions.

1. Overview of Greenhouse Gases | US EPA. <https://www.epa.gov/ghgemissions/overview-greenhouse-gases>.
2. Schultz, J. A. *et al.* DIEGO: A Multispectral Thermal Mission for Earth Observation on the International Space Station. <https://doi.org/10.1080/22797254.2019.1698318> **53**, 28–38 (2019).
3. Kuze, A., Suto, H., Nakajima, M. & Hamazaki, T. Thermal and near infrared sensor for carbon observation Fourier-transform spectrometer on the Greenhouse Gases Observing Satellite for greenhouse gases monitoring. *Applied Optics*, Vol. 48, Issue 35, pp. 6716–6733 **48**, 6716–6733 (2009).
4. Orbiting Carbon Observatory-2: Home. <https://ocov2.jpl.nasa.gov/>.
5. Yang, D. *et al.* First Global Carbon Dioxide Maps Produced from TanSat Measurements. *Advances in Atmospheric Sciences* 2018 35:6 **35**, 621–623 (2018).
6. Orbiting Carbon Observatory-3: Home. <https://ocov3.jpl.nasa.gov/>.
7. Wooster, M. J., Zhukov, B. & Oertel, D. Fire radiative energy for quantitative study of biomass burning: derivation from the BIRD experimental satellite and comparison to MODIS fire products. *Remote Sens Environ* **86**, 83–107 (2003).
8. Wright, R. & Flynn, L. P. Space-based estimate of the volcanic heat flux into the atmosphere during 2001 and 2002. *Geology* **32**, 189–192 (2004).
9. Howell, R. R. Thermal Emission from Lava Flows on Io. *Icarus* **127**, 394–407 (1997).
10. Zhu, A. Y. *et al.* Compact Aberration-Corrected Spectrometers in the Visible Using Dispersion-Tailored Metasurfaces. *Adv Opt Mater* **7**, 1801144 (2019).
11. Lim, S. W. D., Meretska, M. L. & Capasso, F. A High Aspect Ratio Inverse-Designed Holey Metalens. *Nano Lett* **21**, 8642–8649 (2021).

**The Optica Foundation 20<sup>th</sup> Anniversary Challenge Proposal (Category: “Information”)**  
**Efficient and broadband THz spin wave photodetectors (TeraSpin)**  
**Executive Summary**

Terahertz (THz) bands contain rich physics (nonlinear optics, phonon modes, fingerprints of chemical bonds) and offers many opportunities for applications such as sensing, imaging, and 6G telecommunication. Many phonon modes lie in THz, thus, highly molecule-specific signatures in the THz bands may be detected for many organic molecules. Consequently, THz time-domain spectroscopy (THz-TDS) arose as one of the most promising THz probing techniques for analytical chemistry and nondestructive testing.

Previous studies investigated GaAs/AlGaAs quantum wells with low doping and subband transitions for detecting excitations with energies below 20 meV (J. Phys. D: Appl. Phys. 55 (2022) 193001), double or single-walled carbon nanotubes (Optics Express 23, 13349 (2015)), graphene (Nat. Mater. 11, 865–871 (2012)), reduced graphene oxide-silicon nanowire array heterojunctions (Small 10, 2345–2351 (2014)) and antenna-coupled transistors (Optics Express 22, 19252 (2014)). Multiple THz detection mechanisms have been explored with these materials, including (photo)thermoelectricity of nanotubes, subband transitions within quantum wells, photoconductivity, and photovoltaic effects. While quantum confinement and doping allowed energy level tuning for higher sensitivity to THz frequencies, the signal-to-noise ratio (SNR) of the device needs to be improved by limiting the thermally excited electrons.

Despite the development of THz-TDS and the new functional materials mentioned above, THz bands are not fully utilized for applications due to the lack of low noise and high SNR THz detectors. Although hot carrier assisted transport in graphene (Science 334, 648-652 (2011)) or graphene/WS<sub>2</sub> heterostructure (Sci. Adv. 2019; 5:eaax9958) has been proposed to be used for broadband and tunable THz detection, simultaneous enhancements in efficiency, broadband and tunable responsivity, noise reduction and simplified device structures are necessary for practical THz applications.

Here, we propose to experimentally demonstrate our previous theoretical prediction (Sci. Rep. 11, 15976 (2021)) that THz spin waves can be triggered by fs laser pulses on ultrathin magnetic metallic detectors with near unity photon-to-spin wave power conversion efficiency. In the extreme quantum confinement limit (thickness < 5 nm), magnetic metallic layers such as nickel have significantly lower density of phonon states than for bulk. When a femtosecond laser pulse impinges on a magnetic metallic nanofilm, the absorbed pulse energy is predicted to scatter from far fewer phonons, leading to much more efficient conversion to spin polarized charge currents (provided that the magnetic nanolayer is embedded within a cavity). Thus, broadband THz spin waves might be triggered efficiently for on chip probes or spin Hall voltage readout.

To further improve upon the ultrathin metallic THz detection, we have the second aim to grow heterostructures of magnetic topological insulators (TI) (heterostructures of FeTe or GeTe on Bi<sub>2</sub>Te<sub>3</sub>, i.e. [FeTe/Bi<sub>2</sub>Te<sub>3</sub>]<sub>n</sub> on a magnetic insulator Tm<sub>3</sub>Fe<sub>5</sub>O<sub>12</sub>) where (1) quarter wave and absorptive cavity effects due to the thickness of the heterostructure can absorb all of the fs laser pulse, (2) convert all the energy into unidirectional spin waves due to the time-reversal symmetry breaking coming from the magnetic insulating underlayer (Sci. Adv. 3, e1700307 (2017)) and (3) only the top/bottom surface of the TI layers conduct with spin selective Dirac electrons while the bulk of the TI does not. Hence, phonon scattering rates are expected to be reduced further. These advantages might minimize THz detection noise and improve the SNR to help achieve room temperature, broadband, voltage-gated and near-unity quantum efficiency THz detection.

Using our molecular beam epitaxy, pulsed laser deposition, sputtering systems and clean room facilities, these functional nickel nanolayers and magnetic TI heterostructures are going to be grown and fabricated into devices. Using the Ti:sapphire laser in our lab, we aim to investigate the time domain THz response of the devices using THz-TDS, responsivity and the noise spectra using fs optical parametric oscillator setup. We expect the project to yield 4 papers, a patent, 2 PhD trainings and a THz-TDS setup as its outcomes.

**The Optica Foundation 20th Anniversary Challenge Proposal (Category: “Information”)**  
**Principal Investigator: Assist. Prof. Dr. Mehmet Cengiz Onbaşlı**

**Efficient and broadband THz spin wave photodetectors (TeraSpin)**

Terahertz (THz) bands contain rich physics (nonlinear optics, phonon modes, fingerprints of chemical bonds) and offer many opportunities for applications such as sensing, imaging, and 6G telecommunication. Many phonon modes lie in THz, thus, highly molecule-specific signatures in the THz bands may be detected for many organic molecules. Consequently, THz time-domain spectroscopy (THz-TDS) arose as one of the most promising THz probing techniques for analytical chemistry and nondestructive testing.

**Literature Review:**

Previous studies investigated GaAs/AlGaAs quantum wells with low doping and subband transitions for detecting excitations with energies below 20 meV<sup>1</sup>, double or single-walled carbon nanotubes<sup>2</sup>, graphene<sup>3</sup>, reduced graphene oxide-silicon nanowire array heterojunctions<sup>4</sup> and antenna-coupled transistors<sup>5</sup>. Multiple THz detection mechanisms have been explored with these materials, including (photo)thermoelectricity of nanotubes, subband transitions within quantum wells, photoconductivity, and photovoltaic effects. While quantum confinement and doping allowed energy level tuning for higher sensitivity to THz frequencies, the signal-to-noise ratio (SNR) of the device needs to be improved by limiting the thermally excited electrons.

**Problem Statement/Objective**

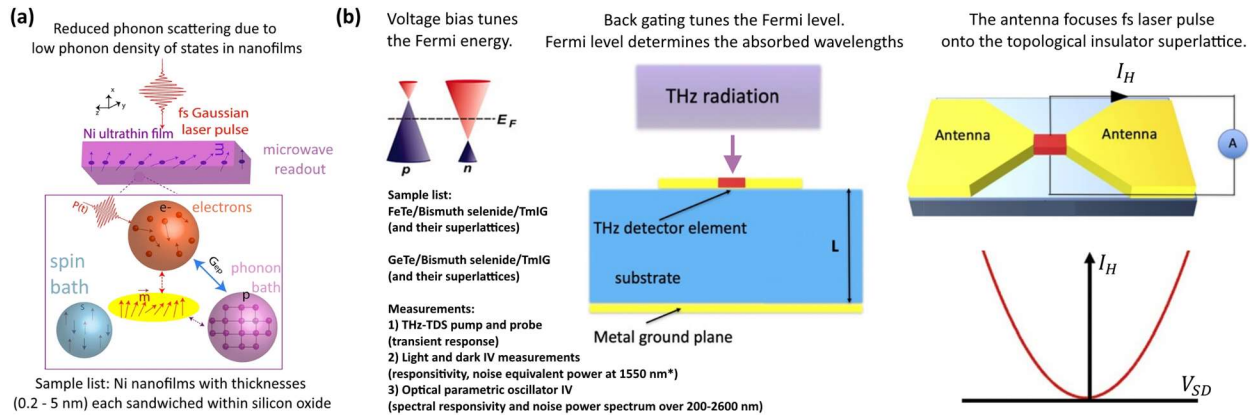
Despite the development of THz-TDS and the new functional materials mentioned above, THz bands are not fully utilized for applications due to the lack of low noise and high SNR THz detectors. Although hot carrier assisted transport in graphene<sup>6</sup> and graphene/WS<sub>2</sub> heterostructure<sup>7</sup> have been proposed to be used for broadband and tunable THz detection, simultaneous enhancements in efficiency, broadband and tunable responsivity, noise reduction and simplified device structures are necessary for practical THz applications.

**Proposed solution in the project:** In this project, we propose a two-step breakthrough in the THz detection schemes which could potentially help achieve broadband THz detection with high SNR at room temperature. First, we propose to experimentally demonstrate our previous theoretical prediction<sup>8</sup> that THz spin waves can be triggered by fs laser pulses on ultrathin magnetic metallic detectors with near unity photon-to-spin wave power conversion efficiency. In the extreme quantum confinement limit (thickness < 5 nm), magnetic metallic layers such as nickel have significantly lower density of phonon states than for bulk. When a femtosecond laser pulse impinges on a magnetic metallic nanofilm, the absorbed pulse energy is predicted to scatter from far fewer phonons, leading to much more efficient conversion to spin polarized charge currents (the magnetic nanolayer is embedded within a cavity such as a SiO<sub>2</sub>/Ni/SiO<sub>2</sub> rib waveguide cavity with small mode volume). Thus, broadband THz spin waves might be triggered and detected efficiently.

Second, to further improve upon the ultrathin metallic THz detection, we aim to epitaxially grow heterostructures of magnetic topological insulators (TI) (heterostructures of FeTe or GeTe on Bi<sub>2</sub>Te<sub>3</sub>, i.e. [FeTe/Bi<sub>2</sub>Te<sub>3</sub>]<sub>n</sub> on a magnetic insulator Tm<sub>3</sub>Fe<sub>5</sub>O<sub>12</sub>) where (1) quarter wave and absorptive cavity effects due to the thickness of the heterostructure can absorb all of the fs laser pulse, (2) convert all the energy into unidirectional spin waves due to the time-reversal symmetry breaking coming from the magnetic insulating underlayer<sup>9</sup> and (3) only the top/bottom surface of the TI layers conduct with spin selective Dirac electrons while the bulk of the TI does not. Hence, phonon scattering rates are expected to be reduced further. As TI's allow for giant spin-orbit coupling and Fermi level tuning by lattice strain, chemical substitution, proximity effects, external magnetic field or voltage bias, THz sensitivity can be maximized<sup>10</sup> in these materials.

These advantages might minimize THz detection noise and improve the SNR to help achieve room temperature, broadband, voltage-gated and near-unity quantum efficiency THz detection (Figure 1).

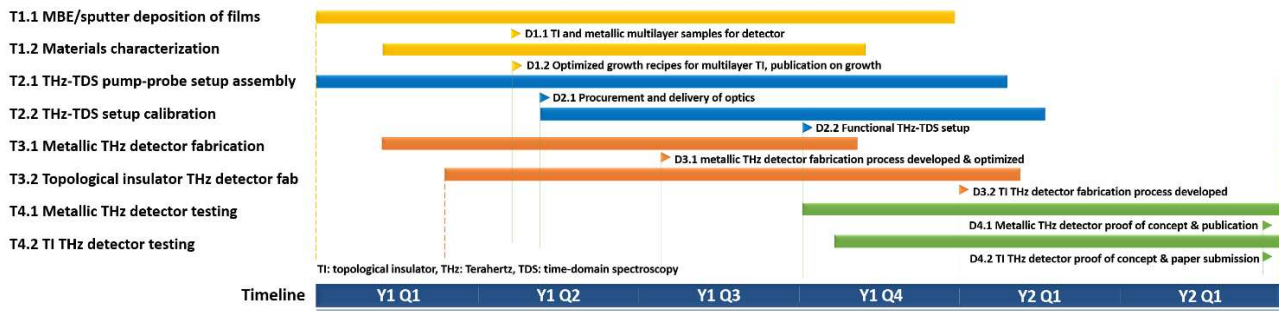
Using our molecular beam epitaxy, pulsed laser deposition, sputtering systems and clean room facilities, these functional nickel nanolayers and magnetic TI heterostructures are going to be grown and fabricated into devices. Using the Ti:sapphire laser in our lab, we aim to investigate the time domain THz response of the devices using THz-TDS, responsivity and the noise spectra using fs optical parametric oscillator setup.



**Figure 1. Mechanism & device concept for (a) metallic<sup>8</sup> and (b) semimetallic TI THz detectors<sup>20</sup>.**

### Outline of tasks/Work Plan:

This project consists of four work packages (or tasks): T1 (materials deposition), T2 (THz-TDS setup assembly), T3 (device fabrication) and T4 (detector testing) over 18 months as shown in Figure 2 below.



**Figure 2. Gantt chart shows the project timeline (Y: year, Q: quarter), the tasks and the deliverables.**

**Task 1 (Materials deposition):** Here, we prepare two categories of samples using DC magnetron sputtering (for ultrathin magnetic metals) and molecular beam epitaxy (for heterostructures of ultrathin topological insulator films) (T1.1). Our theoretical model<sup>8</sup> showed that the significantly reduced phonon density of states of magnetized nickel nanofilms scatter less with electrons than for thicker nickel films ( $t > 5$  nm).

**Nickel deposition:** To test this hypothesis, we sputter nickel films under argon gas with 5 mTorr pressure, 150 mm working distance, 300 W power at room temperature ( $P_{\text{base}} \sim \text{low } 10^{-9}$  Torr). Substrate is going to be held under -10 to -90 V bias to assist in the formation of larger and continuous grains free from voids<sup>11</sup>.

**Magnetic topological insulator heterostructure growth:** We first deposit magnetic insulators thin film  $\text{Tm}_3\text{Fe}_5\text{O}_{12}$  (TmIG) using pulsed laser deposition (PLD) as we described previously<sup>12,13</sup>. This layer breaks the time-reversal symmetry in the above TI multilayers<sup>9</sup> which would be grown subsequently and could allow for unidirectional on chip THz spin wave propagation. We grow the TI multilayers on insulating single-crystal c- $\text{Al}_2\text{O}_3(0001)$  substrates (hexagonal surfaces) ( $P_{\text{base}} = 1 \times 10^{-10}$  Torr). The initial growth of  $\text{Bi}_2\text{Te}_3$  are done using high-purity (5N) Bi and Te constituents thermally co-evaporated from separate Knudsen cells adjusted to obtain a 2:3 Bi:Te deposition ratio as determined by an in situ crystal monitor during growth<sup>14</sup>. The growth rates are confirmed by ex situ X-ray reflectivity measurements. For FeTe and

GeTe<sup>15</sup>, the samples are heated to 600 °C (3 h), followed by 700 °C (30 min) then to 350°C for FeTe and 230-250°C for GeTe<sup>16</sup>. Iron (germanium) and tellurium fluxes generated by an e-beam evaporator and an effusion cell are codeposited onto the substrates at  $T_{\text{substrate}} = 350 \text{ }^\circ\text{C}$ .  $P_{\text{max}}$  during growth =  $5 \times 10^{-9}$  mbar, the Te:Fe flux ratio is kept at  $\sim 15$  (growth rate:  $\sim 0.1$  nm/min). For heterostructures, we repeat an alternating flux protocol using the above steps for repetitions of the bilayers. The growth is followed by a postdeposition in situ anneal at 600°C for 10 min with the chalcogen flux on. During our process optimization, we plan to test the growth recipe by ref.<sup>17</sup>, which uses 50 nm ZnSe buffer layer first on the GaAs (001) substrate and on TmIG (001) (Tm<sub>3</sub>Fe<sub>5</sub>O<sub>12</sub>) before growing FeTe. The structure and crystallinity (phase purity, crystal orientations, grain sizes, thickness, lattice parameters, strain state) are going to be characterized using high-resolution x-ray diffraction ( $\omega$ -2 $\theta$ , rocking curve, pole figures, x-ray reflectometry, reciprocal space maps). Cross-section transmission electron microscopy imaging will reveal layer thicknesses and elemental interdiffusion along TI superlattice interfaces. Refractive index and extinction coefficients of the films will be extracted from ellipsometry.

Task 2 (THz-TDS setup assembly/calibration): A custom THz pump-probe setup as shown in Fig. 1 of ref.<sup>18</sup> is going to be assembled. A Ti:sapphire fs laser (Spectra Physics Mai-Tai) with 84 MHz pulse repetition rate that is tunable between 780-820 nm ( $P_{\text{out}} = 400$  mW) and for other wavelengths (200-2600 nm), Spectra Physics TOPAS OPA (1 kHz optical parametric amplifier) will be used. For setup calibration, parts of the study by Fang et al.<sup>19</sup> will be reproduced. For both TI and nickel samples, THz-TDS and magneto-transport properties (spin Hall voltage,  $S_{21}$  transmission spectra, back-gated I-V measurements<sup>20</sup>) will be measured.

Task 3 (Device fabrication): The functional layers are going to be first grown using the PLD/MBE. Next, the metal contact (gold/copper adhesion) is going to be blanket sputtered or evaporated on these layers without breaking the vacuum. Electron beam lithography is going to be used to pattern antennas and metal contacts of different sizes under a dose matrix (e-beam currents and times). After e-beam resist development, the bowtie antenna and the probe contacts are going to be obtained by reactive ion etching of gold.

Task 4 (Detector testing): The photodetector devices will be tested in 3 different ways: (1) THz-TDS for 1550 nm is going to be used as in ref.<sup>18,19</sup> to test the time domain THz response of the devices. (2) Light and dark IV response, responsivity and noise equivalent power will be measured under different pump laser powers and back gate voltages<sup>20</sup>. (3) Using optical parametric oscillator (Spectra Physics TOPAS OPA), spectral responsivity of the photodetectors between 200-2600 nm are going to be measured and the spectral quantum efficiency of the detectors are going to be calculated. TI doping type and carrier concentrations will be measured using temperature dependent longitudinal and transverse Hall conductivity measurements. All the major equipment are available and functional on campus at Koç University (DC sputter system, molecular beam epitaxy, characterization setups, Spectra Physics Mai-Tai Ti:sapphire fs laser, clean room facilities, vector network analyzer). Optics, sample stage, RF electronics will be purchased with this project.

### **Risk mitigation:**

Task 1 (materials growth): Risks exist in the reproducibility of the film quality, thickness, grain size or defect density. For *in situ* thickness monitoring and control, we use quartz crystal microbalance (sputter) and RHEED (reflection high-energy electron diffraction for MBE). We calibrate, revise or optimize the MBE recipes by systematic checks: (1) MBE power/partial pressure/temperature controls for the electron guns, cracker, effusion cells, sensor calibration, (2) systematic process parameter optimization over the phase diagrams of the TI's<sup>21,22</sup>, and (3) MBE diagnostics by growing/reproducing a well-known topological insulator (Bi<sub>2</sub>Se<sub>3</sub>)<sup>14</sup>, (4) evaluation of the effect of different capping/cavity claddings on the TI surfaces<sup>23</sup>.

Task 2 (THz-TDS setup): Setup risks are minimized by reproducing the results of a previous THz-TDS study<sup>18</sup>. Since the TI and the magnetic insulator layer are exchange coupled, their joint THz response need to be deconvoluted by first doing THz-TDS (both in reflection and transmission modes) on TmIG without the TI. Next, the THz response of the full stack with the TI heterostructure should be measured and compared



with the THz-TDS of TmIG layer. Setup calibration with control samples could verify the functional operation and noise levels as well.

Task 3 (device fabrication): During etching, the functional TI layers could be damaged. This damaging can be prevented by spin coating an etch barrier resist that is hard baked and patterned to have the appropriate device geometry. After this layer serves as a mask and the device and its contacts are patterned, this layer could be removed by using an asher and gentle rinsing step.

Task 4 (device testing): If the laser spot and the device sizes significantly differ from each other, the signal to noise ratio (SNR) of the detector might be low. By coinciding the laser spot exactly on the detector area, the maximum SNR should be obtained. All setups are going to be first calibrated using reference samples with no or known responsivity.

**Outcome(s):**

This project aims to deliver 4 high-impact publications (D1.2: 2 papers on new topological insulator growth/characterization; D4.1 and D4.2: 2 papers on THz detectors), 1 device patent (D4.3), 2 conference presentations, and online video training series mainly for students (D4.4) as summarized with Table 1.

We plan to train 2 new PhD students on optics, THz photonics, measurement techniques, control hardware and software, academic writing, and presentation skills. We plan to publicly share our setup and control code for the THz pump-probe system (D1.2, D4.1 and D4.2). We plan to prepare and post educational videos/animations (D4.4) on a new Youtube channel on how to build optical setups, THz photonics/devices, molecular beam epitaxy, characterization, nanofabrication, and this project’s results.

**Table 1. Project deliverables (M: month, T: task)**

Task #	Deliverable and estimated time	Description
T1 (Materials deposition)	D1.1 (M4) Optimized magnetic metal deposition recipe, characterization results and samples	Magnetic metallic samples and magnetic TI multilayer samples are going to be deposited with the optimized sputtering/evaporation recipe for excellent crystal quality and thickness control.
	D1.2 (M4-7) Optimized TI deposition recipe, characterization data, samples, 2 papers	
T2 (THz-TDS setup assembly)	D2.1 (M9) THz-time domain spectroscopy (TDS) setup (hardware), control software and calibration data	The THz-TDS setup is going to be assembled. Its control software is going to calibrate the setup and sweep the laser fluence, pulse width, sample position and spot size control.
T3 (Device fabrication)	D3.1 (M7) Optimized magnetic metallic detector fabrication recipe & devices	Optimized magnetic metallic layer passivation, patterning, and etching recipes, samples ready for testing with THz-TDS
	D3.2 (M12) Optimized magnetic TI patterning, etching, and passivation recipe, samples	Optimized magnetic multilayer TI capping, exposure and etching recipes, device samples ready for testing with THz-TDS
T4 (Detector testing)	D4.1 (M18) Metallic THz detector proof of concept and publication	Efficient THz spin wave generation and detection by testing the devices from D3.1
	D4.2 (M18) Magnetic multilayer TI THz detector demonstration, 2 papers	THz spin wave generation and detection by testing the devices from D3.2
	D4.3 (M18) Photodetector device patent	The patent application covers the new materials, growth, and operation principles
	D4.4 (M17) Educational outreach on THz photonics	Educational animations, short and fun videos for training students on photonics

**Impact:** To maximize the impact of this project, several breakthroughs and new projects are planned:

1. **Materials breakthroughs:** epitaxial growth of ultrathin topological insulators and their superlattices would enable the scientific exploration of the effects of surface Dirac modes and the hybridization of top and bottom surface Dirac modes on phonon transport, thermoelectricity, nonlocal anisotropic mobility, or spin transport properties.
2. **Device breakthroughs:** Achieving highly efficient room temperature THz detectors requires harvesting polarized charge carriers efficiently through cavity effects and appropriate laser energy, cavity design, surface passivation, defect-free TI surfaces and metallic contacts. These challenges need to be resolved with optimal THz photonic cavity models, precise control and optimization of MBE growth processes and doping concentrations, and nanofabrication process refinement.
3. **Demonstrators:** Topological insulator heterostructures and their collection of polarized charge carriers (Dirac electrons) might achieve highly efficient THz detector demonstrations.
4. **New applications:** This project might enable new THz detectors to measure a range of new THz modes in especially emerging quantum materials and their interactions with chemical defects, broken symmetries (time reversal, space inversion, charge polarity) and external bias (voltage, magnetic field, acoustic or phonon probes, or thermal gradients). Coherent excitation of THz spins or chirality-selective excitations of phonons could enable new on-chip quantum state generators. For spintronic devices, voltage-controlled generation of coherent modes triggered with external laser pulses might allow for ultrafast magnetoelastic or piezoelectric logic devices and their fast electronic readout.
5. **Patent:** The patent for the device design might enable commercialization and protection of the technology when the proposed aims of this project are realized.
6. **Education:** The free, short, and visually appealing Youtube video series, lectures, setup design and code are going to accelerate the motivation and trainings of the new generation of scientists and engineers.

## References

- 1) Yachmenev, A. E. et al. *Journal of Physics D: Applied Physics* **55**, 193001 (2022).
- 2) Wang, Y. et al. *Optics Express* **23**, 13348-13357 (2015).
- 3) Vicarelli, L. et al. *Nature Materials* **11**, 865-871 (2012).
- 4) Cao, Y. et al. *Small* **10**, 2345-2351 (2014).
- 5) Bauer, M. et al. *Optics Express* **22**, 19235-19241 (2014).
- 6) Gabor, N. M. et al. *Science* **334**, 648-652 (2011).
- 7) Chen, Y. et al. *Science Advances* **5**, eaax9958 (2019).
- 8) Zanjani, S. M. et al. *Scientific Reports* **11**, 15976 (2021).
- 9) Tang, C. et al. *Science Advances* **3**, e1700307 (2017).
- 10) Sheng, X.-L. et al. *Physical Review B* **90** (2014).
- 11) Geetha Priyadarshini, B. et al. *Journal of Materials Science* **46**, 2860-2873 (2011).
- 12) Avci, C. O. et al. *Nature Materials* **16**, 309-314 (2017).
- 13) Quindeau, A. et al. *Advanced Electronic Materials* **3**, 1600376 (2017).
- 14) Katmis, F. et al. *Nature* **533**, 513-516 (2016).
- 15) Boschker, J. E. et al. *AIP Advances* **7**, 015106 (2017).
- 16) Wang, R. et al. *Crystal Growth & Design* **16**, 3596-3601 (2016).
- 17) He, Q. L. et al. *Nature Communications* **5** (2014).
- 18) Neu, J. & Schmuttenmaer, C. A. *Journal of Applied Physics* **124**, 231101 (2018).
- 19) Fang, Z. et al. *Applied Physics Letters* **115**, 191102 (2019).
- 20) Zhang, Y. & Fu, L. *Proceedings of the National Academy of Sciences* **118**, e2100736118 (2021).
- 21) Shibayev, P. P. et al. *Nano Letters* **19**, 716-721 (2019).
- 22) Gu, M. et al. *Nature Communications* **12**, 3524 (2021).
- 23) Salehi, M. et al. *APL Materials* **3**, 091101 (2015).

## **Integrated high-speed mid-infrared electro-optic modulator for free space optical communication**

Optica 20<sup>th</sup> Anniversary Challenge: Information

PI: Mengjie Yu, University of Southern California, 3737 Watt Way, PHE 612, Los Angeles, CA 90089, USA, 917-847-0825; [mengjiey@usc.edu](mailto:mengjiey@usc.edu)

Mid-infrared (Mid-IR) spectral regime from 3-5  $\mu\text{m}$  is well-known as robust optical carriers for free space optical communications due to the low absorption atmosphere window and the higher tolerance to scattering than the near-infrared. However to produce high data rate optical link, direct current modulation of a quantum cascade laser is often deployed either at cryogenic temperatures up to 20 GHz modulation speed or at room temperature up to a few GHz speed. It is because that the high-speed low-loss electro-optic modulator is lacking in the mid-IR due to the material absorption and lack of individual control of both microwave and optical properties. We propose to overcome this limitation by using the integrated photonic technology where the tightly confined nanophotonic waveguide can be used to tailor the optical property via dispersion engineering and the microwave field can be tuned via electrode design.

Thin film lithium niobate (LN) technology has recently attracted significant interest in data center applications due to its excellent electro-optic performance in terms of low insertion loss ( $< 0.5$  dB), high EO bandwidth ( $> 100$  GHz) as well as low  $V_{\text{pi}}L$  ( $2$  V $\cdot$ cm) demonstrated at telecommunication wavelengths near 1.5  $\mu\text{m}$ . In addition, LN is a long-sought-after integrated photonic material due to its wide transparency window from 400 nm to 5  $\mu\text{m}$ , large second order and third order nonlinearities as well as large piezoelectric response. It has superior advantages for reconfigurable mid-IR photonics, as compared to silicon-based photonics which intrinsically lacks EO response and different frequency generation. We propose to design and develop a low-loss integrated EO modulator on thin film LN in the mid-IR from 3-4.5  $\mu\text{m}$  with  $> 50$  GHz EO bandwidth and  $10$  V $\cdot$ cm  $V_{\text{pi}}L$ . The operating bandwidth and power consumption for switching is an order of magnitude beyond the state-of-art mid IR modulators (of a few GHz, 20-50 V $\cdot$ cm). We will explore two potential geometries including suspended LN and LN on sapphire platforms to overcome the absorption-induced loss of silicon dioxide. Furthermore, we propose to develop a flat-top optical frequency comb (OFC) driven by cascaded EO modulators for wavelength division multiplexing (WDM). The device consists of an amplitude modulator and a phase modulator, where the amplitude modulator carves a flat-top temporal pulse and phase modulator imposes a quadratic temporal phase. The system transfers the flat-top profile from time to frequency. This approach would enable a high and uniform signal to noise ratio across the optical bandwidth, featuring a high pump-to-comb conversion efficiency of up to 50%. Such approach overcomes the low conversion efficiency and the exponentially decaying intensity profile of the integrated microcombs technology, and could be a highly desired WDM source for mid-IR optical communication. Together with the compatibility of high speed EO modulators, we envision a fully integrated EO-comb-driven optical data link with the potential for aggregate transmission rates of tens of Tb/s. The mid-IR nanophotonic technology will also have profound impact in areas including precision spectroscopy and imaging.

Optica 20<sup>th</sup> Anniversary Challenge: Information

## **Integrated high-speed mid-infrared electro-optic modulator for free space optical communication**

PI: Mengjie Yu, University of Southern California, [mengjiey@usc.edu](mailto:mengjiey@usc.edu)

### **Literature Review/Introduction**

As Google just launched a high-speed free space laser communication project- Aalyria, it aims to manage hyper fast ultra-secure, and highly complex communication network that span land, sea, air and space for better connectivity around the world at ultrafast speed. Needless to say, free space optical communication is an emerging technology as there is the ever-increasing demand of large-volume data transfer to remote assets through atmospheric communication channels, driven by heavy broadband internet traffic nowadays. Optical signals offer tremendous advantages over radio-frequency carriers due to its high bandwidth, immunity to electromagnetic interferences, low latency, low power consumption, and multiplexing features<sup>1</sup>, making it particularly attractive (and practical) to address the broadband connectivity bottlenecks created in high-speed internet as well as the security problems in military defense applications.

The mid-infrared (mid-IR) spectrum range from 3 – 5  $\mu\text{m}$  is well-known as a robust transmission window as compared to the visible and near-infrared as the optical attenuation is drastically reduced in atmosphere<sup>2,3</sup>. In addition, beam with longer wavelength would penetrate through fog, haze, rain and snow due to its larger Rayleigh length. Since the health of free space optical communication links are affected by the atmospheric attenuation and turbulence, optoelectronic devices in the mid-IR ensures better system reliability especially in adverse weather conditions with low visibility. However, there is a huge technological gap between the conventional telecommunication wavelengths and the mid-IR in terms of device development including lasers, modulators, and detectors. In particular, to produce high data rate optical link, direct current modulation of a quantum cascade laser (QCL) is probably the only practical solution since the high-speed low-loss electro-optic modulator is lacking in the mid-IR<sup>2</sup>. And most of the high speed direct modulation of QCL are done at cryogenic temperatures. State of art performance is up to 23.5 GHz modulation of a 4.5- $\mu\text{m}$  single mode emitting distributed feedback QCL at 250K temperature (3-dB cut off at 6.6 GHz)<sup>4</sup>. At room temperature, the modulation bandwidth is limited to a few GHz<sup>5</sup>. Alternatively, different frequency generation can be utilized to convert the data stream at 1.5  $\mu\text{m}$  to the mid-IR using a periodically poled lithium niobate (LN) crystal<sup>6</sup>. This method suffers from the limited nonlinear frequency conversion efficiency and bandwidth as well as the demand of an external high power laser pump. Electro-optic (EO) material could be used to modulate the refractive index or optical absorption via external voltages. The mid-IR EO modulators have been demonstrated in silicon<sup>7</sup>, silicon on lithium niobate<sup>8</sup>, black phosphorus on silicon<sup>9</sup>, germanium on silicon<sup>10</sup>, aluminum nitride<sup>11</sup>, GeSn/SiGeSn<sup>12</sup>, and barium titanate<sup>13</sup>. However, none of the material platform offers beyond a few GHz modulation speed. In addition, silicon-based modulator suffers from high optical losses due to the free carrier absorption, AlN has a relatively low EO coefficient and hybrid platform has poor mode overlap with EO layers. Therefore, a compact, high speed, efficient and low loss EO modulator in the mid-IR is still missing.

Thin film LN technology has recently attracted significant interest in data center applications due to its excellent electro-optic performance in terms of low insertion loss ( $< 0.5$  dB), high EO bandwidth ( $> 100$  GHz), as well as low  $V_{\text{pi}} \times L$  (2 V·cm) demonstrated at telecommunication wavelengths near 1.5  $\mu\text{m}$ <sup>14</sup>. In addition, LN is a long-sought-after integrated photonic material due to its wide transparency window from 400 nm to 5  $\mu\text{m}$ , large second order and third order nonlinearities as well as large piezo-electric response. It has superior advantages for reconfigurable mid-IR photonics, as compared to silicon-based photonics which intrinsically lacks EO response.

## Problem Statement/Objective

To address the free-space communication requirement in terms of device size, weight, power and cost (SWAP-C), we propose to use the integrated LN photonic technology to build an EO modulator in the mid-IR. The tightly confined and low-loss nanophotonic waveguide can be used to tailor the optical and microwave properties for velocity-matching beyond 60 GHz.

Objectives of this proposal include:

1. Development of a low loss mid-IR photonic platform based on thin film LN on insulator at 3.5  $\mu\text{m}$ .
2. Design and fabrication of a mid-IR EO modulator with  $V_{\pi} \times L$  (10 V $\cdot$ cm), < 3 dB insertion loss and 50 GHz EO bandwidth.
3. Generation of a mid-IR EO frequency comb with > 40 comb lines at 30 GHz line spacing for wavelength division multiplexing (WDM).

## Outline of tasks/Work Plan

Prof. Yu has already demonstrated mid-infrared microcombs and spectroscopy at 3  $\mu\text{m}$  using silicon photonics<sup>15,16</sup>, high speed EO modulators and EO frequency combs at 1.5  $\mu\text{m}$  using integrated LN devices<sup>17,18,19</sup>.

## Low loss mid-IR photonic platform based on thin film LN

To overcome the absorption loss of silicon dioxide (cut off at 3  $\mu\text{m}$ ), we will consider two main platforms: suspended LN and LN on sapphire. Sapphire has a wide transparency window from 150 nm to 6  $\mu\text{m}$ . The linear loss can be extracted from the quality factor of microresonators. Our initial results in Fig. 1 shows a measured Q of 2.2 million and 15 k at 1.5  $\mu\text{m}$  and 3.5  $\mu\text{m}$ , respectively, on a X-cut 800-nm LN wafer. This still corresponds to a large propagation loss of 20 dB/cm, and it is likely due to the redeposition product on the waveguide sidewall. It is also well-known that annealing could further reduce the loss induced by OH bonds. The fabrication process is plotted in Fig.2. The LN waveguide is patterned using HSQ ebeam resist and followed by Ar ion etching. Arrays of openings adjacent to the waveguides are patterned using photolithography and reactive ion etching (RIE). A second photolithography is used to define the metal layers for Au electrodes, followed by a liftoff process. Finally a wet etch process is used to remove the thermal oxide underneath the LN using BOE. There are several key design principles: 1) the dimension of the holes size needs to be carefully designed so that the waveguide can be supported

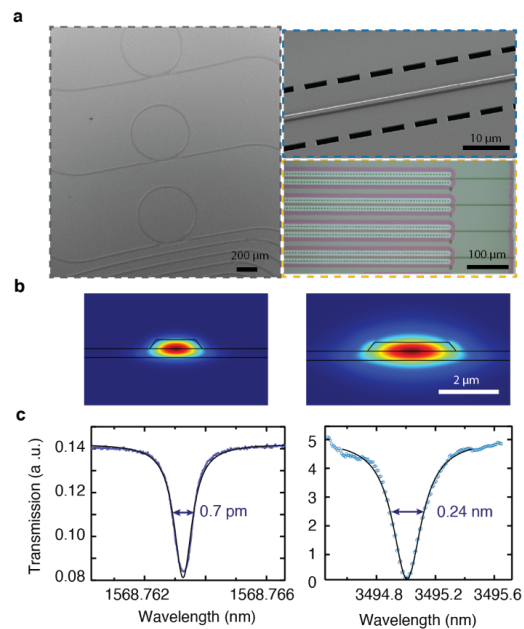


Figure 1| **Suspended LN microresonators** a) The optical graph and scanning electron micrograph of the suspended LN platform. The holes are patterned for wet etching silicon dioxide underneath LN. b) The simulated optical mode profile at 1.5  $\mu\text{m}$  and 3.5  $\mu\text{m}$ , respectively. c) The cavity resonance measurement reveals a cavity linewidth of 0.7 pm at 1.5  $\mu\text{m}$  and 0.24 nm at 3.5  $\mu\text{m}$ .

stably at facets for optical coupling. 2) due to the large optical mode volume at mid IR, the oxide thickness needs to be larger than  $4\ \mu\text{m}$  to avoid overlapping with high index silicon substrate. 3) the microwave index needs to be tuned to match the group index of the optical mode therefore oxide thickness, metal thickness as well as metal gaps need to be designed. Overall, the final structure needs to satisfy the required optical and microwave performance under a reliable nanofabrication protocol. Annealing and chemical mechanical polishing could be used to further reduce the material absorption and sidewall roughness. We expect a linear insertion loss of 1-3dB/cm can be reached at  $3.5\ \mu\text{m}$ .

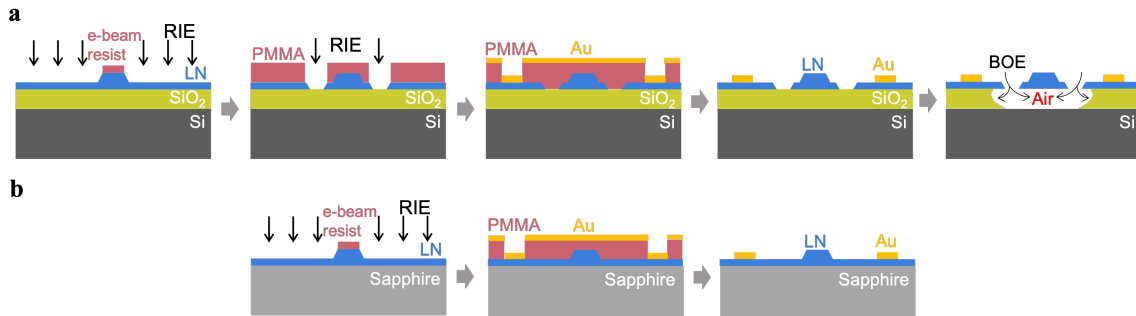


Figure 2| **Nanofabrication process.** a) Suspended LN. The optical waveguide is patterned and formed using reactive ion etching (RIE), followed by photolithography and RIE to open the holes. The electrodes are formed via metal deposition and liftoff process. At last, the LN film is suspended via BOE wet etching. b) LN on sapphire. The optical waveguide is patterned and formed using RIE, followed by photolithography and metal life off.

### High-speed mid-IR EO modulator

Integrated photonics offers a unique and powerful advantage over the bulky discrete components, because the tightly confined optical waveguide can be used to tailor the optical property (refractive index, group velocity dispersion, etc) with a large degree of freedom. Figure 3 shows a dispersion engineered suspended LN waveguide with different top widths from 1900 to 2500 nm, which is used to generate mid-IR spectrum via supercontinuum generation pumped at  $1.5\ \mu\text{m}$ . Fig. 3c shows the dispersive wave generation from 2.5 to  $3.5\ \mu\text{m}$ , the spectral intensity of which is more than an order magnitude stronger than the emission spectrum from a fully cladded LN waveguide, indicating significant reduction of the linear loss in the mid IR. Moreover, the refractive index of LN waveguide needs to be engineered to match the refractive index of the guided microwave modes to minimize the temporal walk off between the optical signal and the RF signal. This velocity matching ensures the high EO bandwidth in a travelling wave modulator configuration.

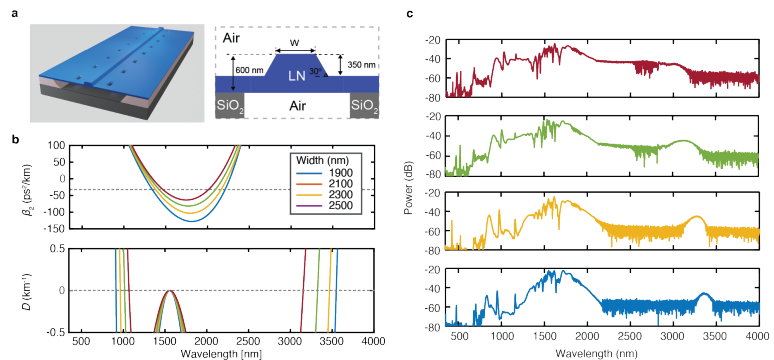


Figure 3| **Dispersion engineering of suspended LN waveguide and mid-IR spectrum enhancement.** a) Suspended LN on 600 nm thin film with an etch depth of 350 nm. b) Dispersion engineering via varying the waveguide top widths. c) The supercontinuum spectra of different waveguide dimensions showing mid-IR spectral generation from 2.5 to  $3.5\ \mu\text{m}$ , the power density of which are significantly higher as compared to the results of a fully cladded waveguide.



The tuning of the microwave index can be done via changing the parameters of the film stack such as the thickness of the oxide, air and metal layer as well as the choice of substrate material. In addition, the impedance and the microwave loss of the electrodes could impact the EO efficiency. So is the mode overlap between the optical mode and microwave mode. We simulate the half wave voltage  $V_{\pi}$  and the EO response as a function of RF frequency, shown in Fig. 4. The optimized geometry is an 800-nm LN thin film with a top width of 2.5  $\mu\text{m}$  and an etch depth of 400 nm. Underneath the 1.6  $\mu\text{m}$  gold electrode is 6  $\mu\text{m}$  thick silicon dioxide while keeping the LN waveguide suspended. The entire structure is sitting on a 500  $\mu\text{m}$  silicon substrate. We achieve an impedance of 37 ohm at 50 GHz. The simulated 3-dB EO bandwidth reaches 50 GHz, and the  $V_{\pi}$  is 5V at 2 cm electrode length.

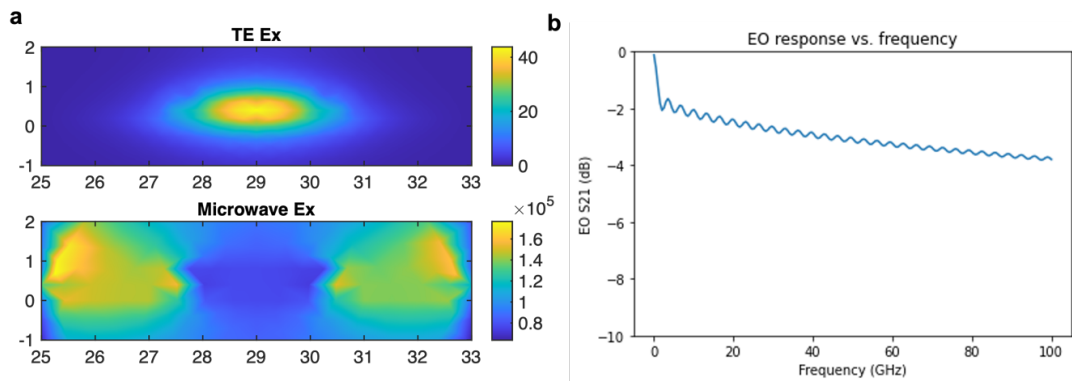


Figure 4| **Simulation of a LN mid-IR EO modulator performance.** a) the optical field (at 3.5  $\mu\text{m}$ ) and microwave field distribution in a X-cut 800 nm suspended LN waveguide with an etch depth of 400 nm. The metal gap is set to be 8 $\mu\text{m}$  and the signal metal width is 50  $\mu\text{m}$ . b) the simulated EO response showing a 3-dB EO bandwidth of 50 GHz.

### Mid-IR modulator-based flat-top EO optical frequency combs

Integrated EO frequency combs offer the prospect of generating many single-frequency components that are evenly spaced to ultrahigh precision. Such a source is ideal for WDM applications since the spacing of all the frequency components can easily be fixed to a specified microwave frequency. We propose to build an integrated time-lens platform based on the high speed modulators, allows for optical frequency comb generation with microwave line spacings and offers compelling advantages in frequency agility, robust operation and comb efficiency. Fig.5 shows the scheme of the device which consists of one amplitude modulator and a double-pass phase modulator. Fig. 5b shows the simulated EO comb spectrum driven at 30 GHz RF frequency with a flat-top intensity profile, offering a uniform SNR across channels for a WDM optical communication system.

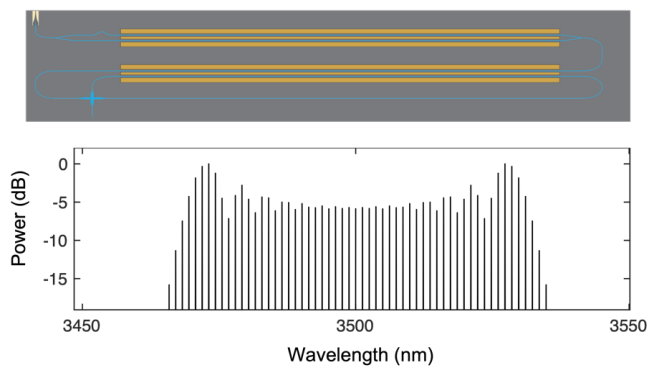


Figure 5| **Simulation of a flat-top mid-IR EO comb.** a) the schematic of the device which consists of an amplitude modulator and a double-pass phase modulator. b) the simulated EO frequency combs driven by a microwave source at 30 GHz. It shows a uniform comb intensity profile (central part) with 50-nm optical bandwidth at 3.5  $\mu\text{m}$ .

## Outcomes

The outcome of the project is the first mid-IR electro-optic nanophotonic platform based on thin film LN. Advanced nanofabrication protocol will be used for manufacturing suspended LN or LN on sapphire waveguides to achieve  $< 3\text{dB/cm}$  loss at  $3.5\ \mu\text{m}$ . Based on that, an EO modulator at  $3.5\ \mu\text{m}$  will be demonstrated with metrics of  $> 50\ \text{GHz}$  EO bandwidth,  $10\ \text{V}\cdot\text{cm}$   $V_{\pi}L$  and  $> 20\ \text{dB}$  extinction ratio. The targeted bandwidth and the power consumption are an order of magnitude better than the state-of-art mid IR modulators based on AlN, Si or III-V material or direct modulation of a QCL at room temperature. In addition, a frequency-agile EO optical frequency comb source will be generated via cascading an amplitude modulator with a phase modulator, as a system-level demonstration.

## Impact

As the next generation of internet growth will continued to push the infrastructure to support high speed video streaming and multimedia, free space optical links would play an essential role in addressing the connectivity bottlenecks. The success of this project will have a profound impact in miniaturized high-speed and low-power-consumption optoelectronic circuits for free space optical communication links. We believe that the proposed integrated technology will provide a unique solution to the greater challenge of information demand, enabled by optics. In addition, the suspended LN platform is an excellent acousto-electro-optic device suitable for microwave to optical conversion<sup>20</sup> for quantum communication. Finally, the mid-IR spectral regime is a gold mine for precision spectroscopy and imaging. The molecule absorption is orders of magnitude stronger than the absorption strength in the near infrared. Our proposed work of a frequency-agile broadband EO combs will address a wide range of applications in biological and chemical analysis, medical diagnostics and environmental sciences.

## References

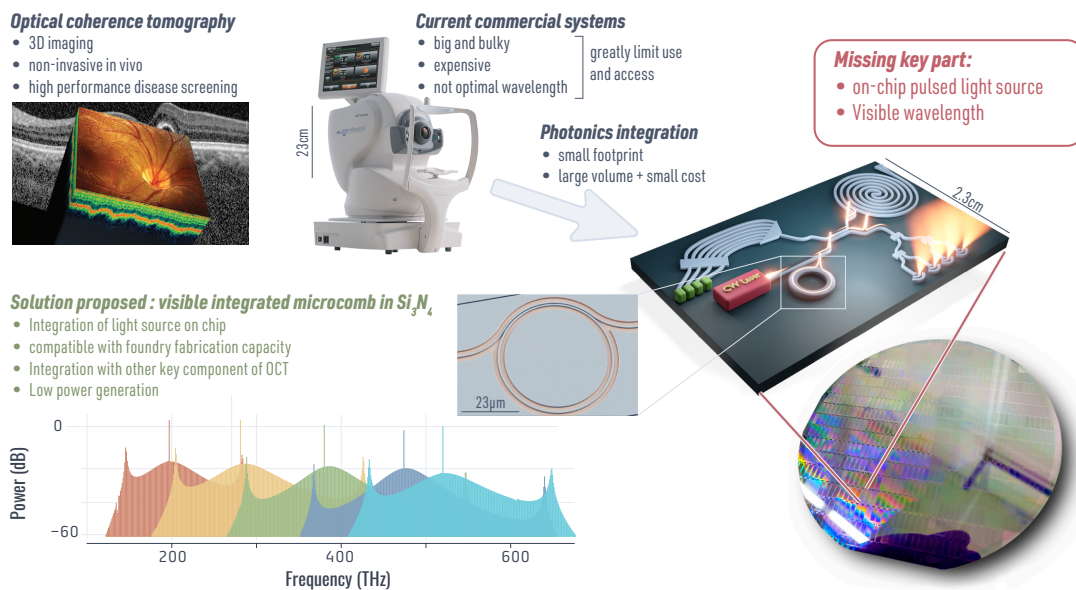
1. Willner, A. E. *et al. Philosophical Transactions of the Royal Society A: Mathematical, Physical and Engineering Sciences* vol. 375 (2017).
2. Liu, J. J., *et al.*, <https://doi.org/10.1117/12.2530969> vol. 11133 1 (SPIE, 2019).
3. Corrigan, P., *et al. Opt. Express* **17**, 4355 (2009).
4. Hinkov, B., Hugi, A., Beck, M. & Faist, J. *Opt. Express* **24**, 3294 (2016).
5. Pang, X. *et al. Opt. Lett.* **42**, 3646 (2017).
6. Zou, K. *et al. Optics InfoBase Conference Papers W7E.5* (Optica Publishing Group, 2021). doi:10.1364/ofc.2021.w7e.5.
7. Becker, R. A., Rediker, R. H. & Lind, T. A. *Appl. Phys. Lett.* **46**, 809 (1998).
8. Chiles, J. & Fathpour, S. *Optica* **1**, 350–355 (2014).
9. Peng, R. *et al. Nano Lett.* **17**, 6315–6320 (2017).
10. Shen, L. *et al. Opt. Lett.* **40**, 268 (2015).
11. Liu, S., Xu, K., Song, Q., Cheng, Z. & Tsang, H. K. *J. Light. Technol.* **34**, 3837–3842 (2016).
12. Akie, M., *et al.*, *IEEE J. Sel. Top. Quantum Electron.* **24**, (2018).
13. Jin, T. & Lin, P. T. *IEEE J. Sel. Top. Quantum Electron.* **26**, (2020).
14. Wang, C. *et al. Nature* **562**, 101–104 (2018).
15. Yu, M., Okawachi, Y., Griffith, A. G., Lipson, M. & Gaeta, A. L. *Optica* **3**, 854 (2016).
16. Yu, M. *et al. Nat. Commun.* **9**, 1869 (2018).
17. Yu, M. *et al.* doi:10.48550/arxiv.2112.09204 (2021). (accepted in *Nature*)
18. Hu, Y., Yu, M., *et al. Nature* **599**, 587–593 (2021).
19. Hu, Y. \*, Yu, M. \*, *et al. Nat. Photonics* 1–7 (2022) doi:10.1038/s41566-022-01059-y.
20. Shao, L., Yu, M., *et al. Optica* **6**, 1498–1505 (2019).

## DA VINCI: DISRUPTION &amp; ADVANCEMENT OF VISIBLE IMAGING USING NANOPHOTONICS AND FREQUENCY COMB INTEGRATION

DR. GREGORY MOILLE - UNIV. OF MARYLAND/NIST

Imaging techniques for medical purposes are at the core of non-invasive diagnosis, helping countless patients get screened to provide life-saving treatments. Optical Coherence Tomography (OCT) is a unique imaging technique based on interference, allowing for 3D reconstruction of tissues without taking a biopsy. It is desirable from both the doctor's and patient's viewpoint as this limits pain and provides instantaneous results. Although OCT techniques have swiftly transitioned from laboratory to commercial use, their presence in medical offices remains sporadic. The steep price and the system bulkiness prevent a mainstream use (1). In parallel, research has demonstrated that shortening the OCT wavelength presents many advantages, from resolution to penetration depth (2). Yet the price of such a light source is even larger, doubling down on the commercial challenge.

Photonics integration has drastically reduced countless optical systems' footprints, resulting in a considerable cost drop through mass-producing fabrication. Silicon nitride ( $\text{Si}_3\text{N}_4$ ), which has recently been incorporated in foundry industries (3) allows for integrating most key photonics components and is a material of choice for its large transparency window and its nonlinear properties. The latter allows power-efficient parametric generation of new colors, including frequency combs (4). However, frequency combs fundamentally rely on the system's dispersion property, accounting for both material and geometrical dispersion of the  $\text{Si}_3\text{N}_4$  microresonator – which must be anomalous for bright soliton pulses (inverse Fourier transform of the frequency comb) to exist. However,  $\text{Si}_3\text{N}_4$  presents a more significant normal dispersion regime the shorter the wavelength is (larger the frequency is), which has to this day made impossible the realization of short wavelength frequency combs in this platform.



In this *Optica 20<sup>th</sup> Anniversary Challenge*, I propose to create an on-chip pulsed light source harnessing the progress made over the past five years in our group. Leveraging our unique experience in dispersion engineering of microring resonators (5), I aim to create a frequency comb in the visible domain. Preliminary results demonstrate the possibility through different novel dispersion engineering techniques to reach blue wavelengths with a  $\text{Si}_3\text{N}_4$ -based frequency comb. Beyond the demonstration of an on-chip, visible OCT light source, I aim to demonstrate monolithic integration of the different components to create a fully on-chip OCT system. Such a demonstration would reduce the cost by several orders of magnitude while making its use much more accessible to the many medical applications through which OCT could help patients. Visible OCT has been reported to help early screening of brain stroke and better diagnose gastrointestinal diseases such as Crohn's and ulcerative colitis. The success of this project could potentially revolutionize everyday patient care in many medical offices.

1. V. C. Coffey, *Optics and Photonics News*, September 2016.
2. X. Shu, L. J. Beckmann, H. F. Zhang, *Journal of Biomedical Optics* **22**, 121707 (2017).
3. J. Liu *et al.*, *Nature Communications* **12**, 2236 (2021).
4. G. Moille *et al.*, *Nature Communications* **12**, 7275 (14, 2021).
5. G. Moille *et al.*, presented at the CLEO 2022, SW4H.6.

## THUNDER - THERmal UNpolarized radiation Design for Energy Recycling

The ever-growing requirement of energy is one of the most challenging problems that us scientists, together with policy makers, are called to solve in a timely, effective manner. We need research to face the threat of climate change and ensure a smooth transition to cleaner industries and economies, while providing for the energy needs of the world population, currently reaching the terawatt-scale<sup>1</sup>. The European Commission has set an ambitious target, via the European Green Deal<sup>2</sup>: to reduce net greenhouse gas emissions by at least 55% by 2030, compared to 1990 levels. The estimate presented in the Green Deal shows that the production and use of energy alone account for more than 75% of the EU's greenhouse gas emissions. Nonetheless, a striking amount of the energy we produce is rejected into the environment as low-grade waste heat. This is the unwanted product of industrial processes, and it's deemed low-grade because its temperature is below 900 K. For example, in the USA both in 2020 and 2021, waste heat amounted to over 67% of the total energy consumption<sup>3</sup>. This makes it an abundant energy resource, the potential of which is not fully capitalized.

Energy production schemes based on light harvesting are very efficient heat engines. Recent research has shown record-high results for both photovoltaic<sup>4</sup> and thermophotovoltaic<sup>5</sup> systems. Particularly, the use of **thermophotovoltaics**, is proving promising, due to the possibility of spectrally engineering the thermal sources, finely tailoring the design of the thermal emitter<sup>6,7</sup>. Solar photovoltaic devices are based on the collection of the radiation emitted by the sun, followed by the straightforward conversion of the absorbed part of the radiation into electrical energy. On the other hand, solar **thermophotovoltaic** schemes present an intermediate step: the sun's radiation is used to heat up a designed thermal emitter. When comparing efficiencies, this results in a striking advantage of solar thermophotovoltaics over traditional solar photovoltaics, the former presenting a theoretical efficiency limit of 54%, compared to the standard Shockley-Queisser limit for solar photovoltaics which is roughly 30%<sup>8,9</sup>. Aside from direct solar energy conversion, thermophotovoltaic systems hold additional potential for converting low-grade waste heat into electricity<sup>10,11</sup>. This constitutes an outstanding opportunity to recycle the heat generated locally, in any industrial process, and use it or feed it back to the grid once it is converted to electricity.

Current heat-to-electricity conversion approaches are either fluid-based heat engines or thermoelectric materials. The former are quite bulk and involve moving and fluid components, whereas the latter suffer from low conversion efficiency, low power density, and low melting points. The reason why low-grade waste heat is hard to recycle is clear from a thermodynamic analysis of a heat engine: Carnot's theorem provides an upper bound for conversion efficiency, given by  $\eta=1-T_{\text{cold}}/T_{\text{hot}}$ , where  $T_{\text{hot}}$  and  $T_{\text{cold}}$  are the temperatures of the hot and cold bodies exchanging heat, respectively. Carnot suggests that achieving high conversion efficiency generally requires a high temperature of the thermal emitter. However, thermophotovoltaic systems represent a viable potential alternative to standard approaches, with high efficiencies possible even at low emitter temperatures, thanks to clever photonic engineering of the thermal emitters<sup>12,13</sup>.

Photonic engineering of thermal emitters has also been extensively used for **radiative cooling**. The concept of daytime radiative cooling is surprisingly counterintuitive and yet so simple: a device that cools down if placed in direct sunlight. It consists of the combination of a very broadband mirror which reflects most incident sunlight and a very narrowband emitter. When engineered properly, the emission wavelength range overlaps with the transparency window of the Earth's lower atmosphere, so that the emitted radiation escapes Earth's premises<sup>14,15</sup>. The net energy balance *inside* the atmosphere is negative: the Earth is cooler, and the heat escaped thermalizes with the outer space which has an average temperature of 3K<sup>16</sup>. Designing a device to be an almost ideal mirror for the entire solar spectrum *and* a narrowband emitter in a specific frequency window is challenging, particularly because it is complex to accommodate for all the weather and cloud coverage conditions that the solar spectrum might be subject to. This difficulty, however, is worth the potential gain, as this technology promises immediate applicability. Devices for passive daytime radiative cooling could be installed simply on any building's rooftop. Such a cooling system, working in broad daylight and requiring no external energy, could help minimize the current energy expenditure necessary for inside cooling. In the USA, in 2021, this amounted to approximately 10% of the total electricity consumption<sup>17</sup>.

Thermophotovoltaics and radiative cooling are technologies based on harvesting thermal radiation. The emitter can either be the sun, another independent heat reservoir or an emitter that absorbs sunlight and re-emits thermally. The performance of these devices depends on how well the spectrum of the thermal emitter matches what can be absorbed and converted by the photovoltaic cell or reflected by the radiative cooler. Aside from being spectrally tailored to the desired application, the optimal thermal emitters must also be easy to fabricate on a large scale, cheap, robust, and long lasting if we want to harvest the power of thermal radiation effectively. A recipe to design and optimize these spectra will give the push needed for the technology to become attainable, and valuable at the industrial level.

This is what my project will achieve: a design of novel types of thermal emitters. My goal is for these new emitters not to be technically improved versions of the current solutions. On the other hand, I will design emitters that rely on physical mechanisms which are currently unexploited in thermal photonics. These phenomena can benefit and enhance the harvesting and conversion of thermal energy. The mission of project **THUNDER** (**T**HERMAL **U**Npolarized radiation **D**esign for **E**nergy **R**ecycling) is to spectrally engineer simple emitters with well-defined characteristics to identify, classify and isolate each phenomenon that can enhance heat transfer and conversion.

Let me now clarify what makes thermal radiation so interesting, which phenomena I am planning to uncover and how they will be beneficial for heat transfer. Thermal emission from macroscopic objects is limited by Planck's law for the blackbody, an idealized emitter whose emissivity is unitary. Radiation from a blackbody is unpolarized, polychromatic and omnidirectional. Furthermore, at low temperatures (300 K - 800 K) it peaks in the mid-IR, a range where optical elements and instrumentations are limited. Thus, it is a complex type of radiation to engineer and manipulate, much more so than, for example, coherent, polarized, visible light from a laser source. Nonetheless, examples of directional thermal emission, both spectrally narrowband<sup>18</sup> and broadband<sup>19</sup>, have been realized by means of photonics engineering of the thermal emitter. Analogously, circularly polarized thermal emission has been observed, nanopatterning the emitter with a chiral metasurface<sup>20</sup>. There is room for tailoring thermal radiation at a fundamental level, engineering intrinsic degrees of freedom of light such as polarization, coherence length or directionality. **Directionality** is fundamental for radiative cooling, as the light emitted by the device must be radiated away from the object it is cooling, towards the open sky. It would also benefit heat transfer and, consequently, thermophotovoltaics, as a directed flow of energy will reduce the amount of light that doesn't reach the photovoltaic cell. Similarly, a control on **polarization** and **chirality** would benefit devices harvesting thermal radiation. Tailoring the polarization of the emitter can allow for more channels to be excited in the absorber, increasing the capacity of the device and the heat flux. Chirality, angular momenta and helicity could all be exploited to design devices with **nonreciprocal** responses, a promising pathway for a feasible technological advancement in the field of radiative cooling<sup>21</sup>.

Via project THUNDER, I will design simple thermal emitters to investigate the tunability of specific degrees of freedom of thermal radiation independently. This is particularly suited to me, as my research experience pertains to the study of light's degrees of freedom<sup>22</sup> and the optimization of structures to observe desired spectral features, signatures of light possessing specific nonzero values of a given degree of freedom<sup>23,24,25</sup>. I have designed and optimised nanostructures to engineer the spectra of their scattered fields, and verified my theoretical findings experimentally<sup>26,27</sup>, validating the design methods and hypothesis. Specifically, I have investigated the properties of sources with a defined value of **transverse spin** and **time averaged power flow** (the real part of the Poynting vector). I have shown that both are locked with linear momentum: light from a source which has a defined nonzero spin or time averaged power flow will, under certain conditions, propagate directionally. It has recently been shown that this phenomenon still holds for unpolarized light<sup>28</sup>. This mechanism, often referred to as spin-momentum locking, can be exploited to achieve topologically protected directional thermal emission. Via project thunder I plan to explore spin-momentum locked thermal emitters. I have also investigated the properties of sources with a nonzero **reactive power** (the imaginary part of the Poynting

vector), such as the **Janus dipole**, whose existence we unveiled during my PhD<sup>23</sup>. Such sources are near-to far field directional emitters when excited via evanescent fields<sup>29</sup>, an important property to exploit for **near-field radiative heat transfer**. Near-field radiative heat transfer is the key mechanism behind the record-high efficiencies of near-field thermophotovoltaics<sup>30,31</sup>. Very recently, chiral emission from a metasurface excited via a laser pulse has been observed<sup>32,33</sup>. It will be crucial to determine the physics that comes into play when designing a similar device for thermal emission. This field is rich of potential discoveries that will enhance our understanding and lead to better solutions to suit our energy needs.

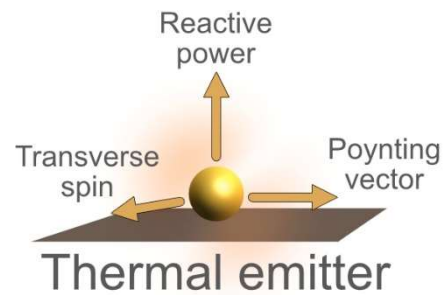


Figure 1: Schematics of a triad of orthogonal degrees of freedom of light which can be identified on a surface.

Project THUNDER will be developed via two work packages, one tackling the formalism to describe the fields and the degrees of freedom of thermal radiation and another one developing an open-source computational package for the design and optimization of the thermal emitters.

**WP1: Fluctuational Electrodynamics.** In this work package I will develop the fluctuational electrodynamics calculations necessary to define the degrees of freedom of thermally emitted light. First, I will employ the Thermal Discrete Dipole Approximation (TDDA)<sup>34</sup>, which consists of describing the emitting 3D structure as the superposition of infinitesimal sub-volumes, each behaving as point dipoles. The fields generated by the oscillations of these point dipoles will be calculated via the dyadic Green's function. Furthermore, the fluctuation-dissipation theorem will have to be imposed on the current density inside the emitter to ensure its statistical correlation function. I have extensive experience with these methods as I have utilized them routinely in my research. Moreover, I will develop this work package leveraging on the strong expertise in the topic which is here at ICFO. First, my current mentor Prof. Papadakis, group leader of the *Thermal Photonics* group and leading expert in the field of thermal radiation and radiative heat transfer; second, Prof. García de Abajo, group leader of the *Nanophotonics Theory* group and close collaborator of Prof. Papadakis. From the generated fields I will write expressions to describe the degrees of freedom of light that we want to isolate. For this as well, I can benefit of my previous experience in describing light's angular momenta, helicity, Poynting vector and other degrees of freedom<sup>22,23</sup>, together with a network of collaborators who are world-class experts in the topic, such as Dr Bliokh from Riken Center Tokyo and Dr Rodríguez-Fortuño and Prof. Zayats from King's College London. My knowledge of the field, together with the rich network of experts I collaborate with will be the key to achieve project THUNDER's ambitious outcomes.

**WP2: Computational package for numerical simulations.** After the theoretical framework for the degrees of freedom definition has been set, I will implement a computational package to calculate the angular spectrum of the thermal emitters and identify the signature of each degree of freedom. The structures will be optimized numerically to achieve the desired spectra. Once the thermal emitters are fully spectrally characterized, I will evaluate their performance metrics when applied to a device, such as a thermophotovoltaic cell or a radiative cooler. In this way, I will numerically estimate and maximize heat transfer, conversion efficiency and extracted electrical power density (defined as the product of current and voltage for a photovoltaic cell). This computational package will be open-source and available to the photonics community with an extensive documentation. I will use computational resources, a powerful machine for numerical simulations and, if needed, usage time on a cluster.

The outcomes of project THUNDER will be simple thermal emitters characterized by a nonzero value of a given degree of freedom of light. Each of them will serve as a toy model for a given phenomenon aimed at the enhancement of performance metrics for thermal energy recycling. The final optimized quantities will be heat transfer, conversion efficiency and extracted electrical power density, depending on each application.



Project THUNDER has two twin aims: 1) to develop a novel theoretical framework and computational package to investigate the science of thermal radiation for energy applications; and 2) apply it to enable the fabrication of ground-breaking devices. This will build the basis to make an impact at a scale that is unattainable using current state of the art technology. Achieving these aims will have a profound impact at a scientific, societal, and economic level. Firstly, it will have a transformational scientific impact, as its success will advance our knowledge of thermal radiation and its manipulation. It will also advance our understanding of mechanisms that favour radiative heat transfer, heat to electricity conversion and radiative cooling. THUNDER will unveil, distinguish, and classify phenomena that contribute to enhanced performance in devices which rely on thermal radiation, an improvement which is technical and will become economical once top-performing devices are realized. Finally, the societal impact of this project is the most valuable. Low grade waste heat takes up the vast majority of the energy produced and in the current catastrophic climate situation it is crucial to invest in solutions that minimise energy waste. Thermophotovoltaics and radiative cooling are two of the few fields where the heat generated in industrial processes can be converted into a resource. Thermophotovoltaic devices pose themselves as a greener way to produce and use energy, compared to carbon or gas-based solutions. Until recently, thermophotovoltaics was a largely academic concern. However, the latest developments clearly show that it is on the cusp of making a major industrial breakthrough, which would be coupled with significant job creation and concomitant benefits throughout the supply chain. In February 2022, Antora, the first start-up in the USA to work on solar thermophotovoltaic devices, received funding for over 50 million dollars, demonstrating the potential of this emerging technology. The field is bustling with possibilities for important applications, discoveries and technological developments; industrial stakeholders are investing, making it the ideal time to work on it, before the technology is fully established. Similarly, novel mechanisms to boost the performance of radiative cooling will benefit a technology which is becoming a real-life application. A few days ago, in September 2022, a patent for a radiative cooling device was filed<sup>35</sup>, showing how timely and relevant this line of research is. Research on harvesting and manipulating of thermal radiation, will provide industries and policy makers with effective tools to make a sharp change from our current energy industry and economy.

As an early career scientist, I consider project THUNDER the seed from which my own group will grow. It is an ambitious project, as it aims at unveiling unexplored phenomena in thermal radiation. The few very recent publications showing the capabilities of engineering emission's degrees of freedom are a solid ground on which to build, even though the field is new and full of unknowns. While being ambitious, THUNDER's goals are achievable, as the designed emitters will only need to be proof of concept simple designs, optimized geometrically to visualize each phenomenon. Project THUNDER will deliver an insight into the capabilities associated with the manipulation and engineering of the degrees of freedom of thermal radiation. It will be the topic of future proposals to define the optimal design tailored for applications, which will be possible with the knowledge that this project will provide.

After THUNDER, an effective solution for the optimal design of thermal emitters will likely be found via machine learning or deep learning algorithms. Building and training a neural network to design the ideal emitters for a specific application is bound to be the most effective way to handle the optimization in such a large parameter space. The results ought to achieve higher performance metrics, since the algorithm does not rely on three-dimensional geometrical thinking to optimize the structures, but it is capable of hyperdimensional visualizations. This has been proven to work excellently to optimize existing solutions<sup>36,37,38</sup>, boosting performance metrics and computational times by orders of magnitude.

However, due to the size of the parameter space available in the framework of thermal emission, a blind application of neural networks would lead to a surprisingly long and expensive training. Moreover, setting up and training complex neural networks to optimize a device does not automatically guarantee the *existing* solution will be optimized. Deep learning algorithms get to the optimized result through minimization of parameters which do not necessarily have a physical significance, particularly when trained without any *a priori* knowledge. The enhanced performance of the optimized design is due to

known physical mechanisms or novel phenomena which must be untangled and interpreted afterwards. The limit of this approach is that, for complex optimizations, many channels might simultaneously contribute to an effect and discriminating between them might not be feasible or easy. This is where the results from Project THUNDER will make a difference, as we will bank on the knowledge of mechanisms and phenomena already unveiled. Project THUNDER is the first, necessary step to identify how light's intrinsic properties influence its potential to transfer heat effectively. Building on the results of project THUNDER, I will establish my group and start a career as an independent researcher.

---

<sup>1</sup> Global energy transformation: A roadmap to 2050, International Renewable Energy Agency, 2018

<sup>2</sup> European Green Deal - [https://ec.europa.eu/info/strategy/priorities-2019-2024/european-green-deal\\_en](https://ec.europa.eu/info/strategy/priorities-2019-2024/european-green-deal_en)

<sup>3</sup> Lawrence Livermore National Laboratory, Estimated U.S. Energy Use <https://flowcharts.llnl.gov/commodities/energy>

<sup>4</sup> Nayak, P.K., Mahesh, S., Snaith, H.J. *et al.* Photovoltaic solar cell technologies: analysing the state of the art. *Nat. Rev. Mater.* **4**, 269–285 (2019).

<sup>5</sup> Fan, S. Thermal Photonics and Energy Applications, *Joule* **1**, 2 (2017).

<sup>6</sup> Baranov, D.G., Xiao, Y., Nechepurenko, I.A. *et al.* Nanophotonic engineering of far-field thermal emitters. *Nat. Mater.* **18**, 920–930 (2019).

<sup>7</sup> LaPotin, A., Schulte, K.L., Steiner, M.A. *et al.* Thermophotovoltaic efficiency of 40%. *Nature* **604**, 287–291 (2022).

<sup>8</sup> Shockley, W. and Queisser, H.J. Detailed Balance Limit of Efficiency of p-n Junction Solar Cells, *J. Appl. Phys.* **32**, 510 (1961).

<sup>9</sup> Harder, N.P. and Wurfel, P. Theoretical limits of thermophotovoltaic solar energy conversion, *Semiconductor Science and Technology* **18**, 151–157 (2003).

<sup>10</sup> Fan, D., Burger, T., McSherry, S. *et al.* Near-perfect photon utilization in an air-bridge thermophotovoltaic cell. *Nature* **586**, 237–241 (2020).

<sup>11</sup> Inoue, T., Koyama, T., Kang, D. D., *et al.* One-Chip Near-Field Thermophotovoltaic Device Integrating a Thin-Film Thermal Emitter and Photovoltaic Cell, *Nano Lett.* **19**, 3948–3952 (2019).

<sup>12</sup> Papadakis, G. T., Orenstein, M., Yablonovitch, E. and Fan, S. Thermodynamics of light management in near-field thermophotovoltaics, *Phys. Rev. Applied* **16**, 064063 (2021).

<sup>13</sup> Omair, Z., Scranton, G., Pazos-Outón, L. M., *et al.* Ultraefficient thermophotovoltaic power conversion by band-edge spectral filtering, *Proc. Natl. Acad. Sci.* **116**, 31 (2019).

<sup>14</sup> Rephaeli, E., Raman, A. and Fan, S. Ultrabroadband Photonic Structures To Achieve High-Performance Daytime Radiative Cooling, *Nano Lett.*, **13**, 1457–1461 (2013).

<sup>15</sup> Raman, A., Anoma, M., Zhu, L. *et al.* Passive radiative cooling below ambient air temperature under direct sunlight. *Nature* **515**, 540–544 (2014).

<sup>16</sup> Fan, S., Li, W. Photonics and thermodynamics concepts in radiative cooling. *Nat. Photon.* **16**, 182–190 (2022).

<sup>17</sup> Annual Energy Outlook 2022 - <https://www.eia.gov/tools/faqs/faq.php?id=1174>

<sup>18</sup> Greffet, J. J., Carminati, R., Joulain, K., Mulet, J. P., Mainguy, S. and Chen, Y. Coherent emission of light by thermal sources, *Nature* **416**, 61–64 (2002).

<sup>19</sup> Xu, J., Mandal, J. and Raman, A. P. Broadband directional control of thermal emission, *Science* **372**, 393–397 (2021).

<sup>20</sup> Dyakov, S. A., Semenenko, V. A., Gippius, N. A. and Tikhodeev S. G. Magnetic field free circularly polarized thermal emission from a chiral metasurface, *Phys. Rev. B* **98**, 235416 (2018).

<sup>21</sup> Zhang, Z. and Zhu, L. Nonreciprocal Thermal Photonics for Energy Conversion and Radiative Heat Transfer, *Phys. Rev. Applied* **18**, 027001 (2022).

<sup>22</sup> Picardi, M. F., Bliokh, K. Y., Rodríguez-Fortuño, F. J., Alpegiani, F. and Nori, F. Angular momenta, helicity, and other properties of dielectric-fiber and metallic-wire modes, *Optica* **5**, 1016–1026 (2018).

<sup>23</sup> Picardi, M.F., Zayats, A.V. and Rodríguez-Fortuño, F.J. Janus and Huygens dipoles: Near-field directionality beyond spin-momentum locking, *Phys. Rev. Lett.* **120**, 11 (2018).

<sup>24</sup> Picardi, M.F., Zayats, A.V. and Rodríguez-Fortuño, F.J. Unidirectional evanescent-wave coupling from circularly polarized electric and magnetic dipoles: An angular spectrum approach, *Phys. Rev. B* **95**, 245416 (2017).

<sup>25</sup> Picardi, M.F., Zayats, A.V. and Rodríguez-Fortuño, F.J. Amplitude and Phase Control of Guided Modes Excitation from a Single Dipole Source: Engineering Far-and Near-Field Directionality, *Laser & Photonics Reviews* **13**, 1900250 (2019).

<sup>26</sup> Picardi, M.F., Neugebauer, M., Eismann, J.S. *et al.* Experimental demonstration of linear and spinning Janus dipoles for polarisation- and wavelength-selective near-field coupling, *Light: Science & Applications* **8**, 52 (2019).

<sup>27</sup> Picardi, M. F., McPolin, C.P.T., Kingsley-Smith J.J. *et al.* Integrated Janus dipole source for selective coupling to silicon waveguide networks, *Applied Physics Reviews* **9**, 021410 (2022).

<sup>28</sup> Eismann, J.S., Nicholls, L.H., Roth, D.J. *et al.* Transverse spinning of unpolarized light. *Nat. Photonics* **15**, 156–161 (2021).

<sup>29</sup> Wei, L., Picardi, M. F., Kingsley-Smith, J. J., Zayats, A. V., & Rodríguez-Fortuño, F. J. Directional scattering from particles under evanescent wave illumination: the role of reactive power, *Optics Letters* **43**, 3393 (2018).

<sup>30</sup> Iizuka, H. and Fan, S. Significant Enhancement of Near-Field Electromagnetic Heat Transfer in a Multilayer Structure through Multiple Surface-States Coupling, *Phys. Rev. Lett.* **120**, 6 (2018).

<sup>31</sup> Fernández-Hurtado, V., García-Vidal, F. J., Fan, S. and Cuevas, J. C. Enhancing Near-Field Radiative Heat Transfer with Si-based Metasurfaces, *Phys. Rev. Lett.* **118**, 20 (2017).

<sup>32</sup> Forbes, A. Chiral light sources get a helping hand, *Science* **377**, 6611 (2022).

<sup>33</sup> Zhang, X., Liu, Y., Han, J., Kivshar, Y. and Song, Q. Chiral emission from resonant metasurfaces, *Science* **377**, 1215–1218 (2022).

<sup>34</sup> Edalatpour, S. and Francoeur, M. The Thermal Discrete Dipole Approximation (T-DDA) for near-field radiative heat transfer simulations in three-dimensional arbitrary geometries, *J. Quant. Spectrosc. Radiat. Transf.* **133**, 364–373 (2013).

<sup>35</sup> Raman, A., Goldstein, E. A. and Fan, S. *United States Patent Application 20220275973*, 01 September 2022.

<sup>36</sup> Kudyshev, Z. A., Kildishev, A.V., Shalaev, V. M. and Boltasseva, A. Machine-learning-assisted metasurface design for high-efficiency thermal emitter optimization, *Applied Physics Reviews* **7**, 021407 (2020).

<sup>37</sup> Sullivan, J., Mirhashemi, A. and Lee, J. Deep learning based analysis of microstructured materials for thermal radiation control. *Sci Rep* **12**, 9785 (2022).

<sup>38</sup> Garcia-Esteban, J.J., Bravo-Abad, J. and Cuevas J.C. Deep Learning for the Modeling and Inverse Design of Radiative Heat Transfer, *Phys. Rev. Applied* **16**, 064006 (2021).

## **Probing and perturbing the oligomerization of membrane protein utilizing nanoparticle plasmon coupling and Deep learning**

**Dr. Abu S. M. Mohsin, Associate Professor**  
**BracU,EEE, 66 Mohakhali,Dhaka-1212,Bangladesh**

**Challenges:** Membrane proteins are the first line of communication between the extracellular environment and the cell interior. This communication in cellular systems is largely under the control of complex spatial and temporal networks of macromolecular interactions called signaling pathways [1]. Traditional biochemical tools such as yeast-two-hybrid [2], co-immunoprecipitation [3] together with gene [4] and protein arrays [5] provides critical information on the constituents of interaction networks. Recently it has been known that the activation of epidermal growth factor receptor (EGFR) occurs via dimerization [6,7,8] or higher order oligomerization however the precise geometry, stoichiometry, and relevance to signaling pathways is not known at this time [9].

More recently several state-of-the-art fluorescence based non-destructive, non-invasive super resolution imaging techniques has been used in lateral micrometer and sub-wavelength range to track and analyse the biological molecules, interaction and oligomerization. However, due to the photo blinking and photo bleaching property of fluorophore and destructive nature of imaging these techniques cannot be utilized in live-cell imaging or to examine dynamic information about the uptake or aggregation. In order to investigate the oligomerization of membrane protein and subsequent activation pathway we proposed to use plasmonic nanoparticle and deep learning-based image segmentation technique in human cervical carcinoma (HeLa) cells. Plasmonic nanoparticle will be used as multifunctional probes and nano-spacers in a model cell system to investigate the organization of membrane proteins and to determine how receptor spatial arrangement influences cell behavior. The findings of this study will be helpful in spatial structuring, receptor organization and cellular function and drug delivery. Most importantly, the novelty of our work lies in the presentation of a pioneering technique that allows in-vitro cellular studies of membrane protein interaction in a non-destructive setting under the diffraction limit.

**Proposed Project:** The aim of the project is to determine the role of spatial organization on the function of membrane proteins. The objective of the project is as follows: **(a)** Investigate the light matter interaction of nanoparticle & structure using analytical models (Mathematica/Matlab) & numerical methods (Lumerical-FDTD). **(b)** Probe the spatial organization of membrane proteins (EGFR). **(c)** Control the spatial organization of membrane proteins. **(d)** Determine how receptor spatial arrangement influences cell behaviour.

**Expected Outcome: Expected outcome from aim 1:** Investigate the light matter interaction of single particle and cluster on the 10-100 nm scale. We will provide evidence how the shape, size and geometry of the particle influence the plasmonic property. **Likely Impact from aim 1:** The results will be useful for understanding the fundamental properties of plasmonic nanoparticles and structures and employ them in several applications. This will help to investigate monomer-dimer transitions at the molecular scale. We expect to have one peer reviewed paper from these findings.

**Expected outcome from aim 2:** We will probe the spatial organization of membrane proteins (EGFR) using nanoparticle as a probe or nanospacer. We will demonstrate perturbation of spatial organization through the creation of clusters of different size, spatial extent and geometry. **Likely impact from aims 2:** The impact from this study will be high because it will address the issues of creating clusters with defined size and geometry directly. We expect to have one peer reviewed paper from these findings.

**Expected outcome from aim 3:** We will determine how cellular function is linked to spatial organization of membrane proteins. **Likely impact from aims 3:** The concept of spatial organization appears to be important for polyvalent ligand-receptor interactions where ligand-mediated receptor cross-linking brings components into molecular contact. However being able to ascertain the role of different sizes and geometries has been challenging because of the numerous species on the cell surface. Our novel approach will provide the link between spatial structuring, receptor organization and cellular function. We expect to have one peer reviewed paper from these findings.

The proposed project will help to address SDG 3-Good Health and Wellbeing, SDG4 Quality education and SDG 9 Industry, Innovation, and Infrastructure and help to create skilled workforce for Industry 4.0.

## **Executive summary for “Ultrafast dynamic contrast optical coherence microscopy enabled by a microcomb photonic flywheel”**

Imaging the dynamics of cells by the non-invasive optical coherence microscopy (OCM) is an effective way to test their response to drugs or pathogens and monitor health. Here we propose a method to overcome the bottleneck of data acquisition in dynamic OCM imaging and improve both the imaging speed and dynamic range.

### **Problem statement**

- (1) Commercial electronic analog-to-digital converters (ADCs) limit the performance of ultrafast dynamic contrast OCM due to the compromise between the high sampling rate and large effective number of bits (ENOB).
- (2) Although photonic ADCs (PADCs) can help to improve the performance of electrical ADCs by overcoming the bottleneck of electrical jitter, there is no demonstration of improving dynamic medical imaging such as OCM based on PADCs.
- (3) Laser sources for PADCs with ultralow jitter and high repetition rate  $> 1$  GHz is challenging for conventional mode-locked lasers.

### **Objectives**

- (1) PADC with sampling rate of 8 GSa/s and ENOB of  $>10$  based on Brillouin-Kerr microcombs at 1 GHz.
- (2) Demonstrate the first ultrafast dynamic contrast OCM imaging with the improved PADC.

### **Intended outcomes**

- (1) A PADC prototype with 8 GSa/s sampling rate and  $>10$  ENOB, which can be used in universal applications not limited in ultrafast dynamic contrast OCM.
- (2) Demonstration of ultrafast dynamic contrast 3D OCM imaging.
- (3) Publish one or two articles in high-impact journals such as Optica.

### **Impact**

The PADCs enabled by microcomb photonic flywheel can overcome the bottleneck of electrical jitter for electrical ADCs and improve the performance of more than 1 bit at 8 GSa/s. They can be applied to the critical applications such as radar systems, software radio, medical imaging and next-generation communication systems. In addition, it is feasible to integrate all the components onto a chip to realize a compact, power efficient and high-performance chip-scale PADC. The application in dynamic OCM imaging can not only increase the imaging speed, but also the dynamic range, providing a better tool for scientific research and health monitoring.

# Ultrafast dynamic contrast optical coherence microscopy enabled by a microcomb photonic flywheel

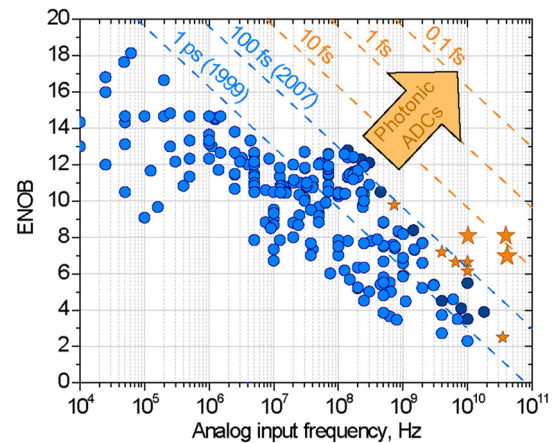
## 1. Literature Review

As a microscopic incarnation of optical coherence tomography (OCT), optical coherence microscopy (OCM) can provide 3D reconstructions of a cell based on intrinsic contrast of back-scattered coherent light [1,2]. The non-invasive OCM is an alternative imaging approach to live fluorescence microscopy and is widely applicable in medicine as the primary method for 3D structural and functional imaging *in vivo* with micrometer resolution [3] and a sampling frequency of up to tens of megahertz [4]. By leveraging the full-field OCT/OCM and dynamic micro-OCT technique [5,6], intracellular structure imaging has been achieved to reveal subcellular metabolic contrast and subcellular compartments motion, which are important markers of health [7]. In addition, imaging the dynamics of cells is an effective way to test their response to drugs or pathogens.

However, it is challenging that imaging the dynamics of cells by OCM requires both high speed with sampling rate  $> 1$  GHz and high-quality. A major limiting factor is the analog-to-digital converter (ADC) in the data acquisition systems. The sampling rate of the ADCs limits the imaging speed, while the resolution defined by effective number of bits (ENOB) limits the dynamic range and contrast [8,9]. Although the radio frequency (RF) electrical ADCs can now run at unprecedented sampling rates up to 128 GSa/s, their performance is not improved commensurately with 5 ENOB due to the bottleneck from the aperture jitter [10]. As reviewed by Walden [11,12] (Figure 1), the jitter-limited ENOB linearly decreases with the analog input frequency, leading to the compromise between the high speed and high resolution. The best electronic ADCs now can deliver jitter levels of  $\sim 50$  fs in the 5–10 GHz frequency range with ENOB of 8.8 (ADC12DJ5200-EP, Texas Instruments). Nevertheless, reducing the jitter of electrical ADCs results after 2007. At multi-GHz frequencies is increasingly difficult if not possible [12].

Photonic ADCs (PADCs) provide another simple route to overcome the bottleneck of electrical jitter and achieve high speed and high resolution at the same time, resulting from the ultralow jitter from ultra-stable and ultrashort pulses with mode-locked lasers at tens of megahertz [12–14]. By accomplishing the sampling process in optical domain, the sampling ambiguity can be significantly reduced. Moreover, optical multiplexing in temporal and frequency (wavelength) domain can be leveraged to increase the sampling rate without sacrificing the resolution. The state-of-art PADCs at tens of GHz level are realized by optical down-sampling of narrowband RF signals, demonstrating 8.0 ENOB at 10 GHz and  $\sim 8.0$  ENOB at 40 GHz [15,16]. Although PADCs have been applied to radar systems and software radio [17,18], there is no demonstration of medical imaging based on PADCs. In addition, to achieve better PADC performance, it requires laser sources with higher repetition rate  $> 1$  GHz and lower jitter, which are challenging for conventional mode-locked lasers.

Kerr soliton microcombs, realized by coherently pumping a high-Q microresonator, can provide easy access to  $> 1$  GHz soliton pulses with low-power consumption and miniaturized chip-scale size. The demonstration of integrated turnkey soliton microcombs in 2020 represents a milestone towards mass production of optical frequency combs [19,20] for applications out of the lab. Moreover, by combining



**Figure 1.** “Walden plot”: ENOB of existing ADCs as a function of analog input frequency. Shadow blue circles: electrical ADC results before 2007; dark blue circles: electrical ADC results after 2007. dashed lines: aperture jitter. orange stars: results from PADCs.

the Brillouin effect [21,22] and the microresonator-filtered laser cavity configuration [23], our group recently proposed another method to achieve turnkey soliton microcombs at 10 GHz with record ultralow jitter less than 1 fs from 20 kHz to 1 MHz [24]. It is believed that the robust phase-independent turnkey operation, high long-term stability and ability to be integrated on a chip of our Brillouin-Kerr soliton microcomb can significantly improve the performance of PADC.

## 2. Problem Statement/Objective

According to the literature review, problems for the existing OCM and PADCs are:

- (1) Commercial electronic ADCs limit the performance of ultrafast dynamic contrast OCM due to the compromise between the high sampling rate and large ENOB.
- (2) Although PADCs can help to improve the performance of electrical ADCs by overcoming the bottleneck of electrical jitter, there is no demonstration of improving dynamic medical imaging such as OCM based on PADCs.
- (3) Laser sources for PADCs with ultralow jitter and high repetition rate  $> 1$  GHz is challenging for conventional mode-locked lasers.

Here we aim to demonstrate the first ultrafast dynamic contrast optical coherence microscopy enabled by a microcomb photonic flywheel, which can provide improved performance for both PADC and OCM imaging:

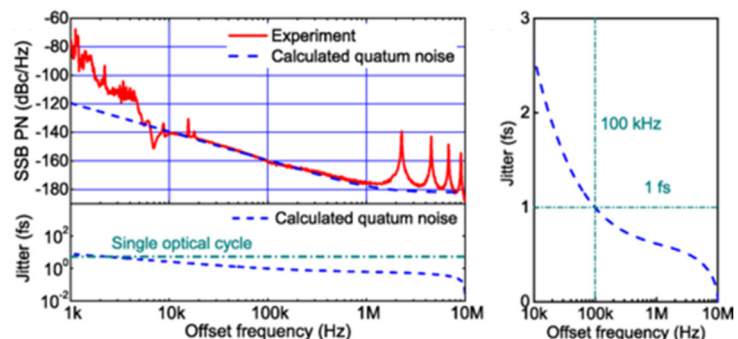
- (1) PADC with sampling rate of 8 GSa/s and ENOB of  $>10$  based on low-jitter Brillouin-Kerr microcombs at 1 GHz.
- (2) Demonstrate the first ultrafast dynamic contrast 3D OCM imaging with the improved PADC.

## 3. Outline of tasks/Work Plan

To increase the sampling rate while keeping the resolution of PADCs at the same time, two (de)multiplexing methods are proposed to lower the requirement of electrical ADCs for digitization: time division demultiplexing (TDD) and wavelength division multiplexing (WDM). For example, to achieve a 10-GSa/s sampling rate PADC, the first method is to sample with 10-GHz Brillouin-Kerr soliton. A high-speed optical switch matrix (OSM) with high extinction ratio should be introduced for time division by  $N$ . The sampling rate for each channel is  $10/N$  GSa/s, where electrical ADCs with high resolution can be applied. The other method is to utilize wavelength-time interleaving. The spectrum of 1-GHz Brillouin-Kerr soliton microcombs can be divided into 10 channels through WDM. The combination of 10 channels can form a 10-GHz pulse train, equivalently aggregating the sampling rate. Despite the potential of fully integrated system on a chip, the PADC based on microcomb and TDD method is limited by the high-speed OSM, which is not commercially available. Therefore, we plan to build the PADC based on WDM method.

### Task 1: Feedback control of ultralow jitter Brillouin-Kerr soliton microcombs at low offset frequencies

Recently, our group demonstrated a photonic flywheel based on Brillouin-Kerr soliton microcomb with repetition rate of 0.945 GHz and bandwidth of 1.5 THz [21]. The soliton phase noise is -140 dBc/Hz at 10 kHz, -160 dBc/Hz at 100 kHz and -178 dBc/Hz at 1 MHz (Fig. 2). The integrated jitter is less than 3 fs from 10 kHz to 10 MHz, which is suitable for high-performance PADC. To implement the PADC application



**Figure 2.** Phase noise (left) and corresponding integrated jitter (right) of 1-GHz Brillouin-Kerr soliton microcomb.

for a long period, soliton phase noise and jitter below 10 kHz offset frequencies will be suppressed by locking the repetition rate to a commercial low-noise oven controlled crystal oscillator (OCXO).



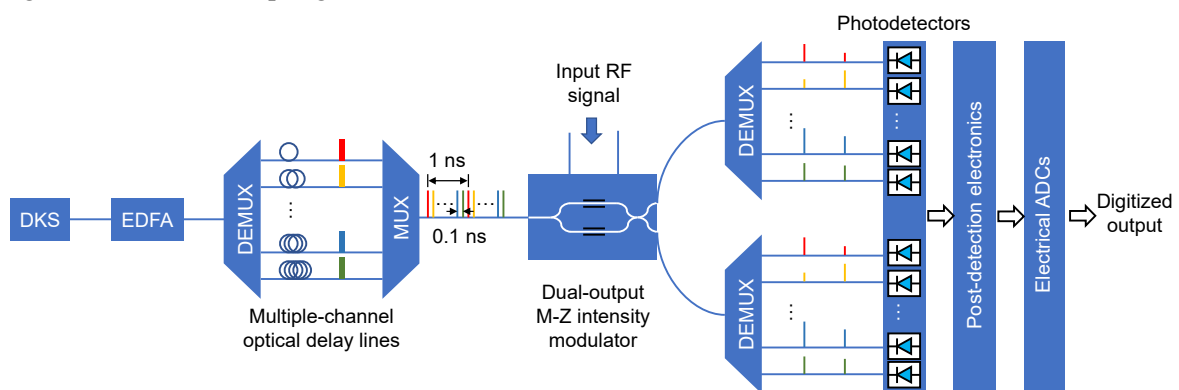
## Task 2: PADC at 8 GSa/s with ENOB >10 through wavelength interleaving

Our PADC is a 8-channel ADC, realized by wavelength-time interleaving (Fig. 3). The Brillouin-Kerr soliton microcomb with repetition rate of  $\sim 1$  GHz is first amplified and split into 8 trains, each centered at a different wavelength by a 1-to-8 wavelength demultiplexer with 200 GHz channel spacing and 150 GHz bandwidth. The wavelength-interleaved pulse trains pass through different optical delay lines and then be recombined with a multiplexer to create a pulse train with repetition rate of  $\sim 8$  GHz, resulting in discrete time-to-wavelength mapping within the pulse train. The pulse trains are then injected to the RF signal modulated dual-output Mach-Zehnder intensity modulator (20 GHz bandwidth), accomplishing the optical sampling process. The modulated pulse train is then split into 8 channels by a wavelength demultiplexer, detected by balanced photodetectors, amplified in RF domain and digitized with commercial electrical ADCs with 1 GSa/s and ENOB of 11.5 (Texas Instruments, ADS54J60). For each channel, two outputs from the dual-output intensity modulator are injected to a balanced photodetector, which enables the differential detection and increases the SNR by rejecting the common mode noise and cancelling quadratic nonlinearity. The ADCs are synchronized with the unmodulated DKS pulse rains and precisely convert the pulse peak intensity to electrical voltages. Variable optical and RF delay lines should be used to precisely align the modulated pulse train with the ADC sampling clock to ensure that pulses are sampled at their peaks.

We will first build a two-channel ADC with discrete components and test its performance to find out the limiting factor for the SNR and the method to compensate the channel mismatch, including the timing skew, gain mismatch and offset mismatch. The timing skew and offset mismatch can be digitally compensated by minimizing spurious frequency components in the interleaved data [25]. Gain and offset mismatch between the two channels were digitally compensated as well. The gain mismatch can be calibrated by the same response from the same ADC input for both channels. The nonlinearity of the sinusoidal transfer function of the MZ modulator can be compensated by taking arcsine of the data points multiplied by a factor to minimize harmonic distortions in the resulting data.

To test the PADC performance, the modulator will be driven with a single-tone RF probe (sinusoid) at various frequencies from 0-1 GHz. The ENOB can be derived from the spectra of the compensated digitized data according to the ADC test standard [26]. The 2-channel ADC is targeted at 2 GSa/s sampling rate and >10 ENOB.

After gaining experience from the two-channel PADC, we will move further to the 8-channel ADC with integrated optical delay lines to minimize the channel mismatch. Performance test will be done by using a 5-GHz repetition rate and 1 GHz bandwidth from a RF synthesizer. The 8-channel ADC is targeted at 8 GSa/s sampling rate and >10 ENOB.

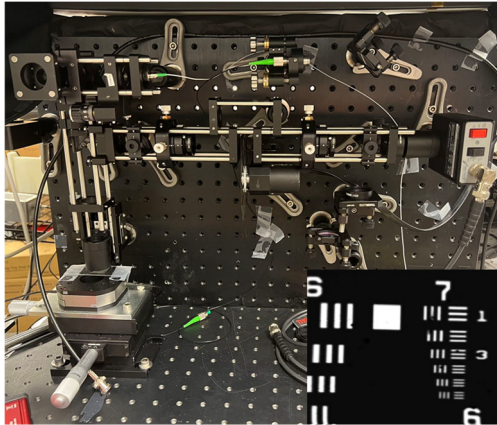


**Figure 3.** Layout of wavelength-interleaved photonic ADC.

## Task 3: Demonstration of ultrafast dynamic contrast OCM imaging

Figure 4 shows the schematic of the homebuilt OCM that will be combined with the PADC to enable the first dynamic contrast 3D OCM. Together with the 1- $\mu\text{m}$  30-MHz time-stretched mode-locked laser

and the 2-axis MEMS scanner, the dynamic contrast 3D OCM can generate a 1-Gvoxel volumetric image at a rate of 60 Hz with a 2- $\mu\text{m}$  transverse resolution and an 8- $\mu\text{m}$  axial resolution.



**Figure 4.** Homebuilt OCM with a 2- $\mu\text{m}$  transverse resolution (inset).

First, 3D-structured silicone tissue-mimicking phantoms will be fabricated as test samples for benchmarking the imaging parameters of the dynamic contrast 3D OCM. Sensitivity, dynamic range, resolution, speed, and depth are the key parameters that will be quantitatively characterized. Silicone is the preferred material for 3D-structured phantoms as it is compatible with a highly flexible soft lithography technique known as replica molding. Minimum feature size of 2  $\mu\text{m}$  can be achieved with the photolithography tools in the Colorado Shared Instrumentation in Nanofabrication and Characterization (COSINC). To fine tune the optical properties of the 3D-structured phantom, a variety of inorganic scatterers and absorbers can be selected and

dispersed in the silicone matrix. Silica microsphere is an especially suitable scatterer as its scattering coefficient and anisotropy factor can both be finely adjusted and accurately calculated using Mie and continuum theory. However, strong electrostatic force between microspheres results in significant aggregation and it is rather challenging to obtain homogeneous distribution of silica microspheres in silicone matrix. To mitigate such aggregation problem, we will adopt a recently developed manufacturing recipe that effectively reduces silicone viscosity and facilitates the uniform dispersion of silica microspheres.

Next, we will perform *ex vivo* imaging studies on porcine retina, an easily accessible tissue model that resembles human except for the lack of macula. All porcine eyes will be obtained from a local slaughterhouse immediately after slaughter and stored in Dulbecco's modified Eagle's medium at 6  $^{\circ}\text{C}$  until use within an hour postmortem. An incision will be made 3 mm posterior to the pars plana to make a circumferential cut. Then the anterior part of the eye will be removed, and the vitreous will be peeled off before a sample segment is cut out from the eye cup. A time series of OCM images over 10 seconds will be acquired, and an estimated power spectrum for each pixel in the OCM dataset will be obtained by employing a short-time Fourier transform with Welch's method. To enable direct visualization of the intracellular dynamics within the tissue, the estimated power spectrum for each pixel will be binned into three frequency ranges (0-0.3 Hz, 0.3-3 Hz, and 3-30 Hz) and each frequency bin will be assigned a color channel within the RGB color model to create the final dynamic contrast 3D OCM representation. The goal of this *ex vivo* study is to establish the imaging protocols for future *in vivo* experiments.

#### 4. Outcomes

- (1) A PADC prototype with 8 GSa/s sampling rate and  $>10$  ENOB, which can be used in universal applications not limited in ultrafast dynamic contrast OCM.
- (2) Demonstration of the first ultrafast dynamic contrast 3D OCM imaging.
- (3) Publish one or two articles in high-impact journals such as Optica.

#### 5. Impact

The PADCs enabled by microcomb photonic flywheel can overcome the bottleneck of electrical jitter for electrical ADCs and improve the performance of more than 1 bit at 8 GSa/s. They can be applied to the critical applications such as radar systems, software radio, medical imaging and next-generation communication systems. In addition, it is feasible to integrate all the components onto a chip to realize a compact, power efficient and high-performance chip-scale PADC. The application in dynamic OCM imaging can not only increase the imaging speed, but also the dynamic range, providing a better tool for scientific research and health monitoring.

## Reference

1. D. Huang, E. A. Swanson, C. P. Lin, J. S. Schuman, W. G. Stinson, W. Chang, M. R. Hee, T. Flotte, K. Gregory, C. A. Puliafito, and others, *science* **254**, 1178 (1991).
2. A. F. Fercher, C. K. Hitzenberger, G. Kamp, and S. Y. El-Zaiat, *Opt. Commun.* **117**, 43 (1995).
3. L. Liu, J. A. Gardecki, S. K. Nadkarni, J. D. Toussaint, Y. Yagi, B. E. Bouma, and G. J. Tearney, *Nat. Med.* **17**, 1010 (2011).
4. M. Wojtkowski, *Appl. Opt.* **49**, D30 (2010).
5. C. Apelian, F. Harms, O. Thouvenin, and A. C. Boccara, *Biomed. Opt. Express* **7**, 1511 (2016).
6. H. M. Leung, M. L. Wang, H. Osman, E. Abouei, C. MacAulay, M. Follen, J. A. Gardecki, and G. J. Tearney, *Biomed. Opt. Express* **11**, 2768 (2020).
7. M. Guo, A. J. Ehrlicher, M. H. Jensen, M. Renz, J. R. Moore, R. D. Goldman, J. Lippincott-Schwartz, F. C. Mackintosh, and D. A. Weitz, *Cell* **158**, 822 (2014).
8. W. A. Ling and A. K. Ellerbee, *Opt. Express* **20**, 15654 (2012).
9. B. D. Goldberg, B. J. Vakoc, W.-Y. Oh, M. J. Suter, S. Waxman, M. I. Freilich, B. E. Bouma, and G. J. Tearney, *Opt. Express* **17**, 16957 (2009).
10. A. Zandieh, P. Schvan, and S. P. Voinigescu, in *2018 IEEE BiCMOS and Compound Semiconductor Integrated Circuits and Technology Symposium (BCICTS)* (IEEE, 2018), pp. 52–55.
11. R. H. Walden, *Wiley Encycl. Comput. Sci. Eng.* 1 (2007).
12. A. Khilo, S. J. Spector, M. E. Grein, A. H. Nejadmalayeri, C. W. Holzwarth, M. Y. Sander, M. S. Dahlem, M. Y. Peng, M. W. Geis, N. A. DiLello, and others, *Opt. Express* **20**, 4454 (2012).
13. J. Chou, J. A. Conway, G. A. Seffler, G. C. Valley, and B. Jalali, *J. Light. Technol.* **27**, 5073 (2009).
14. P. W. Juodawlkis, J. J. Hargreaves, R. D. Younger, G. W. Titi, and J. C. Twichell, *J. Light. Technol.* **21**, 3116 (2003).
15. A. O. Wiberg, L. Liu, Z. Tong, E. Myslivets, V. Ataie, B. P.-P. Kuo, N. Alic, and S. Radic, *Opt. Express* **20**, B419 (2012).
16. D. J. Esman, A. O. Wiberg, N. Alic, and S. Radic, *J. Light. Technol.* **33**, 2256 (2015).
17. P. Ghelfi, F. Laghezza, F. Scotti, G. Serafino, A. Capria, S. Pinna, D. Onori, C. Porzi, M. Scaffardi, A. Malacarne, and others, *Nature* **507**, 341 (2014).
18. S. S. S. Panda, T. Panigrahi, S. R. Parne, S. L. Sabat, and L. R. Cenkeramaddi, *IEEE Sens. J.* (2021).
19. B. Shen, L. Chang, J. Liu, H. Wang, Q.-F. Yang, C. Xiang, R. N. Wang, J. He, T. Liu, W. Xie, and others, *Nature* **582**, 365 (2020).
20. C. Xiang, J. Liu, J. Guo, L. Chang, R. N. Wang, W. Weng, J. Peters, W. Xie, Z. Zhang, J. Riemensberger, and others, *Science* **373**, 99 (2021).
21. K. Jia, X. Wang, D. Kwon, J. Wang, E. Tsao, H. Liu, X. Ni, J. Guo, M. Yang, X. Jiang, and others, *Phys. Rev. Lett.* **125**, 143902 (2020).
22. S.-W. Huang, M. Nie, K. Jia, Y. Xie, S. Zhu, and Z. Xie, "Spatiotemporal mode-locking and photonic flywheel in multimode microresonators"(2022).
23. H. Bao, A. Cooper, M. Rowley, L. Di Lauro, J. S. T. Gongora, S. T. Chu, B. E. Little, G.-L. Oppo, R. Morandotti, D. J. Moss, and others, *Nat. Photonics* **13**, 384 (2019).
24. M. Nie and S.-W. Huang, in *CLEO: Science and Innovations* (Optica Publishing Group, 2022), pp. SS1B-5.
25. G. Yang, W. Zou, L. Yu, K. Wu, and J. Chen, *Opt. Express* **24**, 24061 (2016).
26. J. Márkus and I. Kollár, in *IMTC 2001. Proceedings of the 18th IEEE Instrumentation and Measurement Technology Conference. Rediscovering Measurement in the Age of Informatics (Cat. No. 01CH 37188)* (IEEE, 2001), **3**, pp. 1847–1852.
27. J. Kang, P. Feng, X. Wei, E. Y. Lam, K. K. Tsia, and K. K. Wong, *Opt. Express* **26**, 4370 (2018).
28. D. Huang, F. Li, Z. He, Z. Cheng, C. Shang, and P. Wai, *Opt. Lett.* **45**, 6675 (2020).

# **THUNDER - THERmal UNpolarized radiation Design for Energy Recycling**

## **Executive Summary – Environment Challenge**

The world's consumption and production of energy are ever-growing and predicted to continue doing so. It has become of vital importance to find efficient and carbon-free solutions that will allow us to harvest and store energy produced from industrial processes, in order to reduce our emissions and impact on the planet. Among heat-harvesting energy technologies, thermophotovoltaics promises excellent performance. Indeed, theory predicts that thermophotovoltaics could approach the thermodynamic limit for the conversion of heat into electricity. Similarly, daytime radiative cooling promises to be a clean way to lower the internal temperature of buildings without any external energy input, other than, of course, sunlight. Recent breakthroughs in both of these topics have been made possible by developments in the field of nanophotonics, where designing subwavelength structures has resulted in unprecedented capabilities to control light over very broad wavelength ranges.

In this framework, the possibility of engineering the spectrum of thermal radiation to tailor it for specific applications is exciting, as it can dramatically boost the performance of these devices. If thermal emission possessed properties such as, directionality, a high degree of polarization and chirality, applications would benefit from it massively. Directionality, for example, is important for radiative cooling, as the light emitted by the device must not be radiated towards the object it is cooling, but needs to travel away from it. Directional emission would also benefit heat transfer and, consequently, thermophotovoltaics, providing a directed flow of energy from the emitter to the cell. In addition to this, a control on polarization and chirality could have several interesting consequences. Designing the polarization profile of the emitter can allow for more channels to be excited in the absorber, increasing the capacity of the device and the heat flux. Furthermore, chirality could be exploited to design devices with nonreciprocal responses. These properties and degrees of freedom of light have been extensively studied for coherent, monochromatic light. However, interest towards the study of these quantities in the framework of thermal radiation has not been transversal yet. This is because the magnitude of the performance achievable with radiative heat-harvesting devices has only recently been fully understood. However, recent promising results have shown that the manipulation of thermal radiation can drive devices with unprecedented efficiencies and a clean footprint.

Via project **THUNDER** (**THERmal UNpolarized radiation Design for Energy Recycling**), I plan to design thermal emitters to harvest the power of thermal radiation leveraging on phenomena which are robust and due to the intrinsic nature of light. For example, I plan on designing directional emitters that rely on spin-momentum locking or on a large reactive power, a task I have previously successfully achieved with coherent nanophotonic designs. Other degrees of freedom such as Poynting vector, chirality and angular momentum will also be examined. I will develop a theoretical framework that allows for the description of thermal fields and a formalism to calculate their degrees of freedom. Via this, I will be able to evaluate their magnitudes and the possibility of engineering them to attain specific values. The devices realized with this method will serve as a model to estimate the effect that the manipulation of each degree of freedom can have on thermally emitted spectra. Once the phenomena that can enhance radiative heat transfer have been identified, they can be combined to explore their joint effects.

This is a very exciting moment to work on these topics, as devices based on thermal emission are becoming the state-of-the-art for energy conversion right in front of our eyes. Recent scientific advances are showing us the possibility for the waste heat generated in industrial processes to be exploited as an abundant energy resource. It is time to give thermal radiation the same attention that has been given to coherent, directional and monochromatic light, as the potential for discoveries in this field is vast. Discoveries in this field could be the solutions that will empower us to face climate change and pull the break on the disastrous damages we have done to the planet.

**Title:** Smart PHOTOvoltaic module for bidirectional Visible Light Communication (PHOTOVLC)

**Category:** Environment

### Executive summary

Mobile devices are ubiquitous and their number has been continuously and considerably increasing. However, the exponential rise in data volumes over the next decade will make it increasingly challenging to provide sufficient RF resources. A novel alternative to RF communications is the so-called Visible Light Communication (VLC). Solar cells represent a relevant alternative to PDs for detecting information from a light source. Compared to PDs, the use of solar cells as a receiver has the advantages of easy alignment between transmitter and receiver, a combination of data transmission and energy harvesting, and optimization for outdoor application. However, scholars have not adequately addressed the alternative use of solar cells as receivers because they have focused on increasing efficiency in terms of energy harvesting.

The overall objective of PHOTOVLC is to develop the **first-ever** Photovoltaic module for bidirectional Visible Light Communication. Such a PHOTOVLC module allows to receive and transmit information thanks to the joint adoption of solar cells and LEDs or LDs, combined into the same device, while still producing usable electrical power. During the project, different intermediate outcomes will be generated in order to finally realize the PHOTOVLC demonstrator. Specifically: (1) a novel methodology to study different solar cell technologies in the frequency domain using various light sources as transmitters will be developed and the related testbench realized; (2) custom solar cells, including perovskite devices, will be fabricated and characterized to identify the physical parameters that play a major role on their dynamic performance. From this study, guidelines for the realization of PV cells that are optimized for VLC application, i.e. with improved frequency response (for larger data bandwidth) will represent another important outcome of the project; (3) in-depth solar cell models that take into account the dynamic behavior of the PV devices and can be used to study and design PV-based receivers for VLC applications will be developed; (4) both commercially available and custom-designed solar cells will be characterized in terms of bandwidth (to quantify performance as information receivers) and efficiency (to quantify performance as generators); (5) a new parameters' estimation method for both conventional and advanced solar cell's model will be developed; (6) novel electronic circuits able to divide the DC and AC signal for transceiver and power generator, to realize a self-powered device that can be combined with a DC-DC converter with MPPT, will be designed; and (7) different options for the integration of on-module transmitters – to enable bidirectional communication – will be studied, characterized and designed.

The research will be carried out at the Photovoltaic Materials and Devices (PVMD) group of Delft University of Technology (TU Delft). The realization of the testbench and the characterization of the different components of a PHOTOVLC module will be carried out in the Photovoltaics Laboratory of TU Delft, whereas the characterization of the large-area demonstrator will be performed partly in the Photovoltaic Laboratory of TU Delft (indoor), and partly at the PVMD monitoring station (outdoor). Furthermore, custom c-Si and perovskite PV cells will be fabricated in collaboration with different specialists in the PVMD group and using the Else Kooi Laboratory (EKL) facilities of TU Delft.

The outcome of the project will impact important United Nations (UN) initiatives focusing on the transition towards a secure, clean, and efficient energy policy. “Sustainable Cities and Communities”, “Grow Affordable and Clean Energy” and “Industry, Innovation and Infrastructure” are the three focus areas of the *17 Sustainable Development Goals* of the UN mostly affected by PHOTOVLC. Innovative PV module technologies, such as the PHOTOVLC module in this proposal, are needed in order to reach the UN's goal to significantly increase access to information and communication technologies. The use of the PHOTOVLC module represents a significant advancement in the field of optical transmission and for new 5G technologies. Integrating VLC into 5G enables the achievement of challenging targets such as lower power consumption, reduced latency, and increased number of connected devices.

# Smart Photovoltaic Module for Bidirectional Visible Light Communication (PHOTOVLC)

## 1. Literature Review

Mobile devices are ubiquitous and their number has been continuously and considerably increasing. Next to these ever-connected devices, also Internet of Things (IoT) devices need connectivity. TVs, washing machines, home automation systems, vehicles and monitoring systems, are and will be increasingly connected. By 2025, the number of connected IoT devices is forecasted to be 41.6 billion, generating 79.4 zettabytes (ZB) of data<sup>1</sup>. However, connecting anything through the internet will require much more infrastructural resources. Indeed, most IoT devices use wireless communications in the Radio Frequency (RF) spectrum, demanding for more bandwidth. As a result, the radio spectrum below 10 GHz has become insufficient. Thus, frequencies above 10 GHz and up to 300 GHz (the so-called *millimeter waves*) will be used, with the major drawback of increased propagation losses<sup>2</sup> with respect to those obtainable at low frequencies.

The exponential rise in data volumes over the next decade will make it increasingly challenging to provide sufficient RF resources. A novel alternative to RF communications is the so-called *Visible Light Communication* (VLC), standardized in December 2011<sup>3</sup>. VLC is a data communication technology that uses visible light between 430 and 790 THz (700 - 380 nm). The use of VLC for indoor applications has been rapidly growing during the last years, especially in Europe. An example of VLC application is the Light Fidelity (LiFi) technology, first introduced in 2011 at the University of Edinburgh<sup>4</sup>. This new technology complements the WiFi (Wireless Fidelity) technology: it reuses existing lighting infrastructure to overcome the lack of RF channels. The principle of operation of VLC is based on the use of the visible light to transmit information, e.g. to provide internet connection or exchange IoT data. It typically uses light-emitting diodes (LEDs) or Laser for sending data to a receiver made of photodiodes (PDs). The photodiodes convert the high-frequency variations of the light intensity, that are the transmitted signal, into an electric signal. The main advantages of VLC compared to RF communications are the following<sup>5</sup>: **(1) VLC can be integrated in existing infrastructures.** Indeed, the extensive use of LEDs allows this technology to be quickly deployed in large scale. For example, street/house lights can be used to transmit information. **(2) The spectrum of VLC is much larger than RF.** As explained above, allocation of frequencies is very narrow in RF, and it is coordinated by international telecommunications institutions and regulated by each country. **(3) VLC spectrum is totally free** and not licensed for now, and the devices can use all frequencies. **(4) VLC has a much lower energy cost than RF**, making it a green communication technology. Indeed, the energy used for communication is close to zero because the light sources acting as transmitters, e.g. street/house/car lights, are turned on most of the time. Even when the lighting is turned off, energy-efficient intensity modulation (IM) techniques would enable data communication<sup>6</sup>. **(5) VLC has a high wave frequency** (THz), which allows for very high data rates. Currently, the highest data rate achieved by Wifi is close to 7 Gbps (WiGig standard<sup>7</sup>). Thanks to the high frequency of light waves, scientific research on VLC has reached speeds up to 100 Gbps<sup>8</sup>.

The main components that make a VLC system are the transmitter, the receiver, and the electronic circuit used to process the signal and to extract the information. Significant attention has been given to transmitters able to generate light for data transmission in an optical system. Currently, GaN-based LEDs are considered as the most suitable devices for combining lighting and communication applications. However, commercial GaN-based LEDs have low bandwidth, about 10-20 MHz, due to the large resistance-capacitance time constant of the p-n junction<sup>9</sup>. For indoor applications, LEDs are enough to cover all the space and can be used for both illumination and data transmission. Furthermore, light bulbs based on light amplification by stimulated emission of radiation (LASER) diodes (LDs) increase the range of transmission compared to LEDs and are a good solution for outdoor communication owing to their illumination range and reduced path loss<sup>10</sup>.

Concerning the VLC receiver, solar cells represent a relevant alternative to PDs for the detection of the information from a light source (PV-VLC). Compared to PDs, the use of solar cells as receiver has the following advantages:

---

<sup>1</sup> Worldwide Global DataSphere IoT Device and Data Forecast, 2019-2023, Forecast from International Data Corporation (IDC)

<sup>2</sup> C. Cheng, et al., 2017 11th European Conference on Antennas and Propagation (EUCAP), 2017.

<sup>3</sup> Part 15.7: Short-Range Wireless Optical Communication Using Visible Light, IEEE Standard for Local and Metropolitan Area Networks, IEEE Standard 802.15.7, 2011

<sup>4</sup> H. Haas, "Wireless data from every light bulb," TEDGlobal, 2011

<sup>5</sup> L. Matheus, et al., IEEE Communications Surveys & Tutorials, vol. 21, no. 4, pp. 3204-3237, 2019.

<sup>6</sup> D. Tsonev, et al., SPIE OPTO, Int'l. Society for Optics and Photonics, 2013, pp. 702-900.

<sup>7</sup> "Wi-Fi Alliance rebrands 802.11ac as Wi-Fi 5, picks 802.11ax as Wi-Fi 6". 3 October 2018.

<sup>8</sup> A. Gomez et al., IEEE Photon. Technol. Lett., vol. 27, no. 4, pp. 367-370, Feb. 2015.

<sup>9</sup> J. Grubor et al., in Proc. 33rd Eur. Conf. Exhib. Opt. Commun.-Post-Deadline Papers, 2008, pp. 1-2

<sup>10</sup> A. Ndjiongue and K. Ouahada, 2019 International Symposium on Networks, Computers and Communications (ISNCC), 2019.



- Easy alignment between transmitter and receiver, due to the large area of solar cells and/or photovoltaic (PV) modules compared to conventional receivers. Indeed, a system with PDs requires a highly complex apparatus to align the beam due to the tiny receiver's dimensions<sup>12</sup>.
- The solar cells are already optimized for outdoor application compared to PD-based solutions, since PDs suffer from strong performance degradation under sunlight<sup>11</sup>.
- The solar cells are able to combine data transmission and energy harvesting, whereas PDs need an external power supply to work and detect the data from the transmitter<sup>12</sup>.

Over the years, solar cell technology has undergone several developments for improving performance and/or reducing production cost. This is especially the case of PV technologies based on monocrystalline or polycrystalline silicon (Si)<sup>13</sup>, that is the most used absorber material to manufacture PV modules. Other absorber materials, such as amorphous silicon (a-Si), CdTe and CIGS, can be used for alternative, thin-film, multi-junction, and possibly-flexible PV modules for terrestrial applications<sup>14</sup>, as opposed to III-V semiconductors, that are mostly used for PV space applications<sup>15</sup>. Besides, organic materials and perovskite absorbers materials are constituting examples of latest PV technologies, which can potentially exhibit in the future cheaper production process than silicon-based cells<sup>16</sup>.

Many PV-VLC systems have been developed over the years<sup>12</sup>. However, solar cells are not designed to receive information in the form of a modulated light signal as their bandwidth is not considered during their design and manufacturing process<sup>17</sup>. To increase the performance of a VLC system that uses solar cells as receiver, both light source optimization combined with modulation and custom design of the solar cells should be employed. For example, using a Triple-cation perovskite solar cell optimized for VLC application with a custom active layer thickness, it has been possible to achieve a data rate of 56 Mbps<sup>18</sup>. Whereas, using a GaAs photovoltaic cell combined with optical orthogonal frequency-division multiplexing (OFDM) modulation, the record data rate of 0.5 Gb/s has been reached<sup>19</sup>. Nevertheless, these speeds were achieved indoor without the interference of ambient light. Also, these systems do not provide bidirectional communication, which is an essential feature. An alternative approach based on the use of 5W a-Si solar panel and external 940 nm laser has been presented in literature<sup>17</sup>, where an example of internet communication through VLC has been reported. This solution is optimized for outdoor application and is able to reach a maximum data rate of 8 Mb/s with a distance of 30 m between transmitter and receiver and bidirectional communication. However, this system has been designed only for VLC and the solar panel cannot be used to also generate energy to power utilities.

## 2. Problem Statement/Objective

The innovative solution proposed in this project is based on the joint adoption of solar cells, light transmission elements, and an ad-hoc electronic circuit for signal modulation/demodulation, combined in a single large-scale device, called **PHOTOVLC module**, the *first of its kind*. An example of possible layout for a PHOTOVLC module is shown in Figure 1. Transmitters and electronic circuit are integrated into the module to create a bidirectional VLC device. To the best of the applicant knowledge, the design of a PHOTOVLC module that incorporates both transmission and reception on high power (large area) PV panels has not yet been realized. Location and dimensions of the transmitters must be designed so that they do not shade the surrounding cells, whereas the number of transmitters and their position on the panel must be defined as to ensure proper and stable bidirectional communication. The applicant will investigate the mounting position of the transmitters (on glass, laminated under glass, in the PV module frame, etc.) and their correct angle of installation to find out the best solution for fabrication.

The solar cell technology allowing for the best trade-off between performance as AC receiver (high data rate and high Signal-to-Noise Ratio (SNR)) and maximum power generation must be identified. The designed electronic circuit will be able to (1) separate DC and AC components to extract the information and (2) drive the transmitter for sending data. The design of such a driving circuit will strongly depend on the type of transmitter (LEDs or LDs). Data will be processed by a microcontroller, which will manage all the components

<sup>11</sup> N. Lorriere et al., Journal of Lightwave Technology, pp. 1-1, 2020.

<sup>12</sup> Z. Wang et al., IEEE Journal on Selected Areas in Communications, vol. 33, no. 8, pp. 1612-1623, 2015.

<sup>13</sup> D. Yan et al., Applied Physics Letters, vol. 113, no. 6, p. 061603, 2018.

<sup>14</sup> T. Lee and A. Ebong, Renewable and Sustainable Energy Reviews, vol. 70, pp. 1286-1297, 2017.

<sup>15</sup> F. Si et al., Solar RRL, vol. 1, no. 3-4, p. 1700036, 2017.

<sup>16</sup> J. Connolly et al., 36th European Photovoltaic Solar Energy Conference and Exhibition, WIP, Sep 2019, Marseille, France. pp.779,

<sup>17</sup> S. Das et al., Energies, vol. 12, no. 19, p. 3772, 2019.

<sup>18</sup> N. Mica et al., "Triple-cation perovskite solar cells for visible light communications", Photonics Research, vol. 8, no. 8, p. A16, 2020.

<sup>19</sup> J. Fakidis et al., IEEE Photonics Technology Letters, vol. 30, no. 9, pp. 841-844, 2018.

of the electronic circuit. An additional module-level converter can be used to locally implement a maximum power point tracking (MPPT) algorithm. Figure 2 shows the block diagram for a PHOTOVLC module.

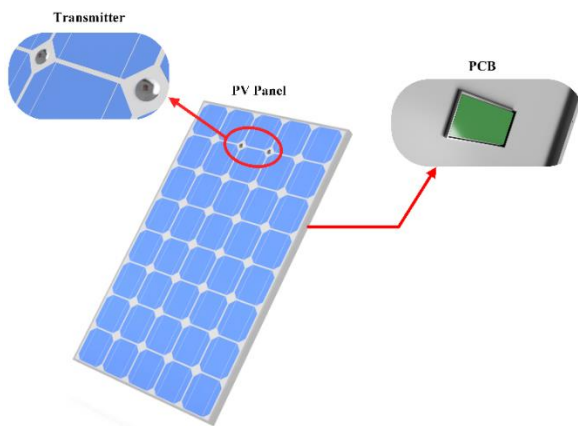


Figure 1: Possible final demonstrator of the proposal.

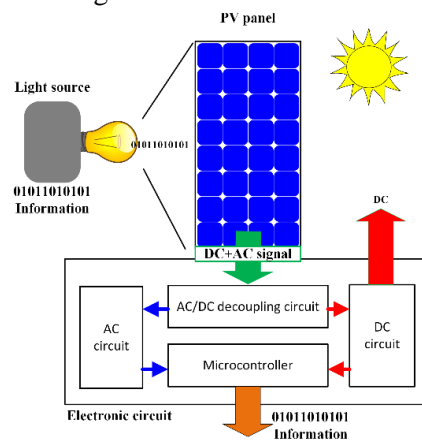


Figure 2: Block diagram of a PHOTOVLC module..

**The main objective of this proposal is to design and realize a first demonstrator of a photovoltaic module combining bidirectional visible light communication and generation of electricity.** The electronic circuit will be designed for a specific photovoltaic module which has integrated LEDs or LDs for data transmission. The choice of the solar cell and the transmitter element will be performed combining simulations and experiments. Concerning the solar cells, a characterization of conventional technologies in high-frequency domain will be performed. Besides, the design of custom solar cells to improve the performance in AC domain will also be considered. Furthermore, for the design of the electronic system, both classic analog and microwave approaches will be employed. The applicant needs to realize the following sub-objectives to achieve the main research objective:

- O1: **Study and characterization of transmitter devices (LED or LD)**, to identify their advantages and drawbacks for the given application and select the most suited one.
- O2: **Analysis and characterization of conventional solar cells**, i.e. commercially available PV cells, in the frequency domain and development of an AC equivalent model.
- O3: **Analysis and characterization** in the frequency domain **of innovative/advanced solar cells**, i.e. solar cells fabricated in the cleanrooms of TU Delft, to identify which parameters can be tuned to increase the bandwidth and the overall performance of the whole system.
- O4: **Design and realization of the electronic circuit.**
- O5: **Realization of the PHOTOVLC demonstrator**, integrating the solar cells, the transmitters, and the electronic circuit.
- O6: **Analysis of modulation techniques** that are typically used in VLC applications and **selection of the one that better fits with the whole system.**
- O7: **Outdoor characterization of the final Demonstrator**, to validate the SNR and the maximum reachable data rate and communication distance.

### 3. Outline of tasks/Work Plan

This project combines theoretical study, simulations, design and fabrication of both solar cells and electronic circuits, as well as the realization of a physical demonstrator. To achieve all objectives, a research methodology that links all these different activities and optimally combines theoretical and experimental approaches will be employed. The work is organized in different intertwined work packages (WPs), that will lead to the achievement of the research (sub-)objectives previously described.

The first work package (WP1) will focus on the **characterization of the main components of the PHOTOVLC demonstrator**, namely the transmitter and receiver devices. To study such devices and their interaction, the **applicant will realize a testbench** to recreate the expected indoor and outdoor operating conditions, allowing proper characterization of both transmitters and receivers. For the transmitter, different light sources, LEDs and LDs, must be tested to understand their advantages and drawbacks in VLC applications, and to quantify their performance at different wavelengths (objective O1). For the receiver, Si-based solar cells, thin-film solar cells, or III-V solar cells and perovskite solar cells will be considered. These solar cells will be characterized in frequency domain through excitation with a modulated light signal coming from the transmitter and generated using a constant current driver system, in order to study their dynamic behavior and their ability to act as VLC receivers. On the one hand, commercially available PV cells will be

characterized (objective O2). On the other hand, custom c-Si and perovskite PV cells will be fabricated in collaboration with different specialists in the PVMD group and the Else Kooi Laboratory (EKL) of TU Delft and characterized with the developed testbench (objective O3). Different iterations will be performed on the custom designed devices to identify the physical parameters that play a major role on their dynamic performance, and to come up with guidelines for the realization of PV cells that are optimized for VLC application, that is PV cells showing better performance in terms of achievable communication distance, SNR and bandwidth.

**WP2** aims at the **development of the solar cell model**. The applicant will develop an AC small-signal equivalent circuit complementing the well-known solar cell's DC equivalent circuit. The solar cell characterization performed in WP1 (for both conventional and custom solar cells) will be used to calibrate the model for different PV technologies and validate it (objectives O2 and O3). If necessary, different models will be created to describe the dynamic behavior of the various technologies. Finally, a non-linear model of the solar cell, usable for Simulation Program with Integrated Circuit Emphasis (SPICE) simulations<sup>20</sup>, will be worked out. The SPICE model will enable accurate design of the electronic circuit in WP4.

**WP3** will focus on the **analysis of modulation techniques** for VLC applications, in order to select the one to be used in the demonstrator (objective O6). First of all, software simulations will be done to assess the performance of various modulation techniques using the solar cell model developed in WP2. To finalize this work package, the applicant will test the different modulation techniques using the testbench developed in WP1, in order to assess the performance of the complete system and decide which technique perform the best in terms of data losses<sup>21</sup>. Results from WP1 and WP2 will be used as input for the evaluation and implementation of the various modulation techniques.

**WP4** will focus on the **design and realization of the electronic circuit** (objective O4). The electronic circuit will be able to separate the DC component – to realize a self-powered device and to combine it with a DC-DC converter with MPPT functionality – from the AC signal, that is the transmitted information. Moreover, since the PHOTOVLC module also embeds a transmitter, a driving circuit for such transmitter will be designed. The solar cell SPICE model developed in WP2 will be used to run SPICE simulations during the electronic circuit design phase. Different PV module topologies will be simulated to identify the best module layout (number of cells and their interconnection) in terms of static (energy) and dynamic (information) behavior. Also, an optical design and analysis software will be used to identify the optimal number of light sources and their optimal position within the PHOTOVLC module. Finally, a PCB will be realized and the electronics board assembled. The transmitter and receiver circuits will be characterized in term of noise, gain, sensitivity, and bandwidth using measuring instruments available in the Photovoltatronics Laboratory of the PVMD group.

**WP5** aims at the **realization and testing of the final PHOTOVLC module prototype**. The characteristics of such a demonstrator (number of solar cells, electrical interconnection of the solar cells, number of LEDs/LDs, location of LEDs/LDs) and the electronic circuit will be as designed in WP4 (objective O5). The physical integration of the transmitters within the PHOTOVLC module (on glass, laminated under glass, etc.) will be also investigated. The performance of the PHOTOVLC demonstrator in terms of maximum communication distance, SNR and maximum achievable data rate will be at first evaluated indoor using the facilities of the PV Laboratory of TU Delft and the workbench developed in WP1, and then validated through outdoor experiments (objective O7).

#### 4. Outcome(s)

The main outcome of the project is the design and realization of the first prototype of what we call a PHOTOVLC module, that is a PV module that allows to receive and transmit information thanks to the joint adoption of solar cells and LEDs or LDs, combined into the same device, while still producing usable electrical power. Other original and innovative outcomes of the project are enlisted below:

- Development of a methodology and a testbench to study different solar cell technologies in frequency domain using various light sources as transmitters.
- Design and realization of custom solar cells, including perovskite devices, to identify the physical parameters that play a major role on their dynamic performance. From this study, guidelines for the realization of PV cells that are optimized for VLC application, i.e. with improved frequency response (for larger data bandwidth) will represent another important outcome of the project.
- Development of in-depth solar cell models that take into account the dynamic behavior of the PV devices and can be used to study and design PV-based receivers for VLC applications.

---

<sup>20</sup> M. Muttillio et al., Lecture Notes in Electrical Engineering, pp. 425-431, 2020.

<sup>21</sup> J. Wu et al., Optics Communications, vol. 392, pp. 119-122, 2017.

- Characterization of both commercially available and custom-designed solar cells in terms of bandwidth (to quantify performance as information receivers) and efficiency (to quantify performance as generators).
- Development of a new parameters' estimation method for both conventional and advanced solar cell's model.
- Design of a new kind of electronic circuits able to divide the DC and AC signal for transceiver and power generator, to realize a self-powered device and to combine it with a DC-DC converter with MPPT.
- Design and characterization of a new on-module transmitter for bidirectional communication.

These aspects pave the way toward the optimal use of solar cell technology as signal receivers for outdoor VLC applications, without hindering the primary purpose of PV technology, that is generation of usable electrical power.

## 5. Impact

The use of the photovoltaic panel for bidirectional VLC represents a significant advancement in the field of optical transmission and for new 5G technologies. Integrating VLC into 5G enables achievement of challenging targets such as lower power consumption, reduced latency, and increased number of connected devices<sup>22</sup>. Furthermore, the PHOTOVLC module represents a first example of PV-based intelligent energy agent<sup>23</sup>: it does not only work as a power generator, but also integrates functionalities that go beyond pure power production; in this specific case, it embeds visible light communication capabilities. The outcome of the project will impact important United Nations (UN) initiatives focusing on the transition towards a secure, clean, and efficient energy policy. “Sustainable Cities and Communities”, “Grow Affordable and Clean Energy” and “Industry, Innovation and Infrastructure” are the three focus areas of the *17 Sustainable Development Goals* of the UN mostly affected by the PHOTOVLC project.

The major results expected from the proposal will be: (1) the characterization of the ability of the solar cell to receive information, (2) the design of an electronic circuit capable of being used in VLC and power generator applications, (3) integration of the transmitter on the module for bidirectional communication. The dissemination of the project results to the scientific community and the industrial sector will be carried out by publication in renowned scientific journals in the field of photovoltaics such as *IEEE Journal of Photovoltaics*, and *Progress in Photovoltaics*, among the others. Some research results will be published in journals focusing on electronics and communication such as *IEEE Transactions on Communications* and *IEEE Transactions on Signal Processing*. The on-module light transmitter results combined with the whole system performance will be published on *Optica Publishing Group's* journals such as *Applied Optics*, and in the open-access *Energy and Environmental Optics Express* dedicated section of *Optics Express*. The research results will be presented at conferences focusing on photovoltaic technology, such as *IEEE Photovoltaic Specialists Conference* (IEEE PVSC). Furthermore, Electronics and Communication-oriented research results will also be presented at conferences with a broader focus on sustainable technologies as well as conferences focused on optical communications and in the Optica-organized symposium. The progress and results of the project will be shared in at least two meetings with the Challenge Committee for advice and guidance. The host institution has an Open Access policy and its Library offers the possibility to store the applicant's scientific publication for the accessibility to others (OpenAIRE-compliant online repository). The host institute's nature to promote interaction between university and society is an important driving force for technological, educational, and societal progress. The activities promotion, such as social posts on Twitter, Facebook, Youtube, and LinkedIn, are already being used at TU Delft. These social media will be used to communicate the results of this project. Furthermore, specific magazine articles such as PV magazine and Optics and Photonics News will be prepared to increase the impact and reach a larger audience.

Outside the Challenge, the project results obtained will be used for further future research activities. The results obtained will be discussed and a strategy will be evaluated to use them both in research and industrial areas. Possible industrial applications could be in vehicle-to-vehicle or street light-to-vehicle communication for solar cars. The results of both the photovoltaic and electronic research activities could lead to innovative PV-based intelligent energy agents and smart PV modules. Industrial collaborations, spin-off creations and licensing of research results will be considered.

<sup>22</sup> I. Kurbatska et al., 2019 IEEE 2nd 5G World Forum (5GWF), 2019.

<sup>23</sup> H. Ziar et al., Energy & Environmental Science, vol. 14, pp. 106-126, 2021

# Bridging the peri-urban digital divide with “fibre,” before the fibre

Mitchell A. Cox<sup>\*1</sup> and Abderrahmen Trichili<sup>2</sup>

<sup>1</sup>School of Electrical and Information Engineering, University of the Witwatersrand, Johannesburg, South Africa; <sup>2</sup>King Abdullah University of Science and Technology, Saudi Arabia; \*PI / Applicant: mitchell.cox@wits.ac.za

## Executive Summary

Eventually, most of the world’s population is expected to live in an urban environment. Rapid urbanisation occurs across many developing nations, where informal settlements have little or no infrastructure for electricity, water, or communications. South Africa is one such nation. While there is a constitutional mandate to provide infrastructure in these rapidly evolving areas and informal settlements, the inevitable timescales for conventional infrastructure roll-out leaves an unmet need in the interim. These settlements are often within a few kilometres (and sometimes just across the road) of areas with excellent infrastructure.

Can we bridge this peri-urban digital divide using free-space (wireless) optical communications while balancing the need for resilience and performance with the cost? Typical, lower-cost optical wireless communication systems often use fibre Ethernet-like technologies that provide no resilience to the adverse effects of atmospheric propagation and thus have a limited range of several hundred meters.

The primary objective of this project is to leverage and combine robust, high data-rate WiFi hardware with radio over optical techniques to develop and test a low-cost, high-speed, and potentially very long-range (i.e., more than one kilometre) free-space optical communication system. We will then field test the system in a real-life application in collaboration with a local startup company that typically deploys wireless links in nearby informal settlements. At the end of the project, we plan to open-source the designs for this device for maximum social benefit. We hope to enable people to solve their own unique issues using our system but also hope that others will contribute improvements with time, creating a sustainable and evolving solution.

Our proposed low-cost, high-speed, long-range internet connectivity solution presents a unique opportunity. We can extract and use the internal WiFi channel state information (CSI) to perform environmental sensing. However, this is through the “proxy” laser beam that carries the WiFi signal. While conventional WiFi CSI-based sensing targets would no longer be applicable, as we do not use radio, we believe that we will be able to sense new and otherwise “un-sensable” (with this particular technique) environmental parameters based on perturbations of the carrier laser beams’ intensity, phase, and polarisation. Our approach will likely be more affordable than conventional optical sensing techniques because we do not require optical amplification, special optical fibre components, or expensive digitisation equipment. Instead, we “simply” make use of the very high-performance hardware that exists in consumer-grade WiFi hardware, and couple it with sophisticated deep learning that we will research and develop.

Thus, for the second objective of this project, we will focus on demonstrating this new sensing approach and then applying it to the unique and interesting application of lightning detection and positioning. Global lightning detection networks are heavily relied upon to monitor climate change, determine where lightning strikes happened (usually for insurance claims), and for early-warning systems. Unfortunately, in South Africa lightning kills about 250 people annually – many of whom live in informal settlements. Perhaps this could be alleviated with better detection networks, or indirectly through the educational opportunities afforded by a good internet connection?

We believe that the ability to provide low-cost, fast, reliable, and long-range internet connectivity with an open-source platform will help to connect the unconnected. Additionally, our system may also be used to optically sense environmental parameters, with lightning as a specific goal. Will this open up novel avenues to fund the deployment and operation of the system and help bridge the digital divide? We hope to take the first step toward this future with the generous support of the Optica Foundation’s 20<sup>th</sup> Anniversary Challenge.



# Bridging the peri-urban digital divide with “fibre,” before the fibre

Mitchell A. Cox<sup>\*1</sup> and Abderrahmen Trichili<sup>2</sup>

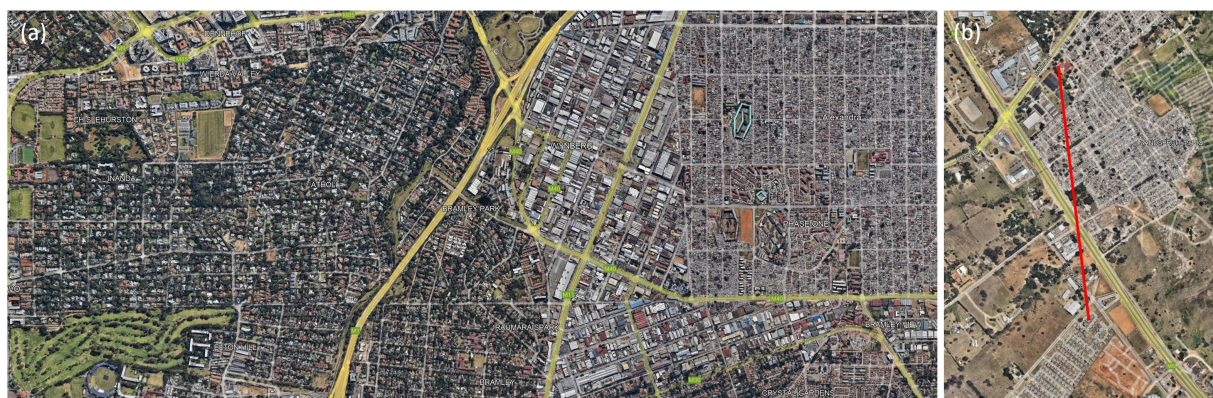
<sup>1</sup>School of Electrical and Information Engineering, University of the Witwatersrand, Johannesburg, South Africa; <sup>2</sup>King Abdullah University of Science and Technology, Saudi Arabia; \*PI / Applicant: mitchell.cox@wits.ac.za

## 1. Introduction

By 2050, two-thirds of the world’s population is expected to live in an urban environment (1). This rapid urban growth, if well planned, has the potential to improve peoples’ access to education, infrastructure, and health care. Unfortunately, rapid urbanisation presents several formidable challenges, especially in developing nations. Settlements are often informal, with little or no prior infrastructure for electricity, water, or communications. South Africa is one such nation. While the South African government (and indeed many others around the world with similar challenges) is constitutionally mandated to provide infrastructure in these rapidly evolving settlements, the inevitable timescales for conventional infrastructure roll-out leave an unmet need in the interim

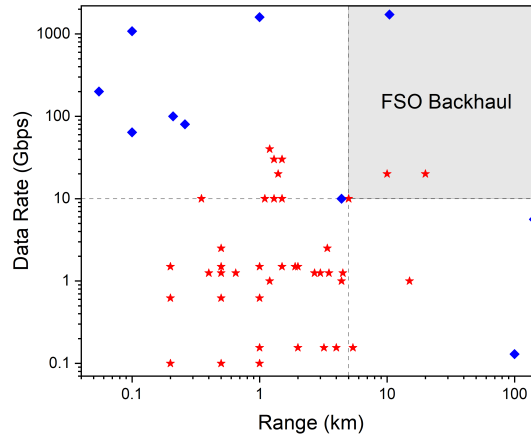
Informal settlements and low-income “suburbs” are often within a few kilometres (and sometimes just across the road) of areas with excellent infrastructure: for an example, see Fig. 1. How can we begin to bridge this peri-urban digital divide? Bringing digital inclusion to the people living in these areas could have a significant impact in terms of education, and work opportunities (2). A possible solution that can be rapidly deployed in the interim – while these communities wait for conventional infrastructure such as fibre – is free-space optical communications (FSO) or simply wireless optical communications, which is also expected to be a significant part of future 6G deployments (3). There are several issues with existing commercial FSO solutions in this context, most obviously their affordability. There is a delicate and challenging balance between the data rate, range, and cost of an FSO system, and commercial systems are not tailored with the peri-urban digital divide in mind. The first and foremost objective of this project is to develop a low-cost, “do it yourself” FSO solution that can be used to deliver internet to peri-urban, disconnected communities: for example, to schools and community centres that are within about a kilometre of existing fibre infrastructure. At the end of the project, we plan to release the designs for our system as open source.

Typical wireless optical communication systems make use of fibre-Ethernet-like technologies – almost literally “fibre without the fibre”, which provides no resilience to the adverse effects of atmospheric propagation. This helps keep costs down but limits the range of most commercial systems to a few kilometers at gigabit speeds, shown in Fig. 2 (4). It is indeed possible to build a very low-cost FSO system



**Fig. 1.** Satellite photos where the peri-urban digital divide is clear. In (a), the left of the photo is one of the wealthiest suburbs on the African continent (Sandton), and across the road to the right is Alexandra: an “informal” settlement built with corrugated-iron dwellings and very little infrastructure besides roads. (b) is an example of an informal settlement with a school (top) that is within a kilometre of a large block of middle-class flats that have fibre to the home. A possible FSO link is illustrated in red.





**Fig. 2.** Range versus data rate of commercial FSO systems (red stars) and some noteworthy experimental systems. Note that these are typically under favourable atmospheric conditions.

using off-the-shelf fibre hardware, and the PI is currently finalising a demonstrator based on this concept. For this Optica Anniversary Challenge project, we want to take this work to the next level, but a further explanation of *how* and *why* is obviously necessary.

One of the target links for the PI’s ongoing project is shown in Fig. 1 (b), where the goal is to connect a school in an informal settlement to the nearest fibre-to-the-home. Our prototype system is affordable and costs about \$500 US (we have not yet made it weather-proof or user-friendly, which would no doubt add to the cost), as it uses all off-the-shelf components such as fibre SFP’s, standard lenses, etc. Unfortunately, its range is limited to less than half a kilometre at 1 Gbps (tested to 400 m thus far). We are continuing to develop the system with a more sophisticated 3D printed mechanism and some other (as yet unpublished) techniques, but we believe 500 m to be the limit of this approach. Extending the range using conventional approaches (such as optical amplification) would dramatically increase the system cost, making it unfeasible. There is a similar commercially available system called Koruza, which is capable of 150 m (an older version could do 300 m) at 1 Gbps and costs about \$1500 (5). Our system is superior due to a better choice of wavelength for atmospheric propagation and larger apertures.

The ability of low-cost FSO systems such as these to help bridge the peri-urban digital divide is hindered primarily by their limited range, which, as mentioned before, is mainly constrained by atmospheric turbulence. Some of the only ways to effectively deal with turbulence-induced errors are by using forward error correction (FEC), signal processing techniques like multi-input multi-output (MIMO), some form of adaptive optics, or by significantly increasing the transmit power (4, 6, 7). None of these solutions are possible within the minimal cost envelope required for a system that can help bridge the peri-urban digital divide – but is there a way?

We believe that the answer is YES, but some design, experimentation, and research are required for us to confirm our ideas, which are described in more detail in Sec. 2. As an extension of our core idea, we believe that environmental sensing will be possible using our hardware as-is. Only special software is required for this, some of which is already open source. As such, the second part of the proposed project is to investigate this potential in the context of lightning strike detection (lightning kills many people annually in informal settlements (8)), using a federated deep learning approach on the already present channel state information. The impact of the proposed project is described in Sec. 3, outputs and deliverables in Sec. 4, and a brief project plan in Sec. 5. The attachments contain financial details for travel, equipment, consumables, and student funding

## 2. Project Objectives and Activities

**A. Primary Objective: The WiFo System (WiFi over FSO).** Modern WiFi hardware (IEEE 802.11n/ac/ax) is able to sustain hundreds of megabits to gigabit data rates in a challenging wireless environment. Strong

forward error correction, robust MIMO (for multiple antennas, used for higher speed and robustness), and diverse modulation schemes are standard. If we remove the usual sources of radio interference and instead transmit WiFi over a wireless optical link, can we harness gigabit (i.e., fibre to the home-like) speeds with higher resilience to turbulence than typical “fibre without the fibre”-based approaches and thus increase the range to over a kilometre?

Since we would still (mostly) be using off-the-shelf hardware, this could be done in an affordable manner, especially since we would leverage our experience building a low-cost fibre-based FSO system, as well as in the alignment of such systems (9). A naive approach would be to directly modulate the 2.4 GHz WiFi signal onto an optical carrier. This would require expensive optical intensity modulators and high-speed photodiode receivers to be effective. In our approach, we will down-convert the WiFi signal to a much lower frequency which can easily and affordably be optically modulated, received, and then up-converted again (i.e., effectively creating a transparent optical interconnect). This subsystem requires some custom electronic development. Fortunately, we have recently begun fostering a partnership with a local South African startup company that has up and down-conversion components in their radio-based products. They are willing to share the relevant components with us as their company vision aligns with bridging the digital divide.

Several research questions arise from this approach, which are divided into the following activities:

1. We are currently developing a minimum viable prototype as a final year honours project. The first activity of the project will be to refine this, add polarisation channels and make it more robust and flexible.
2. How well does the system work through real turbulence (i.e., between two buildings on campus: our usual test-bed) in terms of the possible data rates and optical link range? In the presence of atmospheric turbulence and other “real life” impairments, what are the capabilities of such a system? How does this approach compare to typical OOK-modulated “fibre without the fibre” systems (i.e., our previous work)?
3. WiFi is capable of operating with various different modulation, error correction formats, and MIMO: what is the optimal configuration, given that WiFi protocols are designed for a channel quite different to FSO?

**Students Involved:** MSc(Eng) A, 2x BSc(Eng) Honours

**Collaborators:** RIOT.network Pty(Ltd) (A local startup focused on connecting informal settlements)

**B. Secondary Objective: Harnessing “WiFo” CSI for Sensing.** A WiFi-over-Optical approach has a useful added benefit: internally, WiFi maintains accurate channel state information (CSI), which can be conveniently extracted with some driver hacking and has been demonstrated to be usable for environmental sensing (10). While simultaneously providing high-speed internet connectivity, can we “appropriate” this information, process it with federated deep learning and perform environmental sensing along the path of the laser beam to help others investigate the living conditions in these areas?

South Africa, particularly the Johannesburg area, has a high incidence of lightning. There are many lightning-related injuries and deaths on an annual basis, especially in informal settlements (where our system is intended to be installed) and rural areas (8). If our system is able to detect lightning strikes (due to the Faraday Effect, which would cause a rotation in polarisation detectable by the WiFi MIMO CSI), perhaps it could be used as an early warning system or for other lightning location services (11)?

1. The first activity to fulfill this objective is to implement the WiFi CSI extraction software (we will use available, open-source software as a basis for this). We will then measure some laser beam perturbations to test the basic system operation.
2. Thoroughly characterise the system in the university high voltage lab (through our collaborator) to determine the accuracy in terms of measurement accuracy and time precision.
3. Deploy two systems outdoors in time for the lightning season, which is from November. The systems will be separated, and we will attempt to detect actual lightning strikes by correlating the data with the Johannesburg Lightning Research Lab’s lightning detection capabilities.

We expect the sensing research within this objective to continue for several years following this project. This is an exciting opportunity for the investigators to gain novel optical sensing experience while leveraging one of the core research fields (lightning) in the PI's department.

**Students Involved:** MSc(Eng) A, MSc(Eng) B, 2x BSc(Eng) Honours

**Collaborators:** Dr Hugh Hunt (Johannesburg Lightning Research Lab, South Africa)

### 3. Project Impact

Inequality in South Africa is a major challenge. As many as 13% of South African households are situated in informal settlements. Unfortunately, these settlements are usually underserved and do not have adequate water, electricity, and communications infrastructure. The cost of providing this infrastructure is formidable, and the inevitable timescales for conventional infrastructure roll-out leave an unmet need in the interim.

It is pertinent to note that informal settlements have arisen due to the apartheid era spatial mismatch in which African communities were located far away from business centres and employment opportunities. Informality is characterised by “poor living conditions as well as social and economic exclusion”, with the government reporting in 2014 that “over two million children live in backyard dwellings or shacks in informal settlements”, with over 40% in the vulnerable 0-5 year age group, with a “serious divide in access to basic services on the basis of race, geography and economic status.” The scale of the challenge is both clear and daunting.

Officially, 99.9% of the South African population was covered by 3G mobile signal, and 97.7% had LTE/4G coverage in 2021. Smartphone penetration is also quite high, at 81.7% in 2018 and, presumably, higher now. Unfortunately, simply being “covered” is not enough to guarantee good quality of service, which is required to be a part of the “big data society” or so-called “total human experience”. Backhaul links to mobile base stations are often best-effort and sometimes capacity limited, and there is not always a strong economic incentive for operators to upgrade these links to low-income areas. This is a factor in both the peri-urban digital divide as well as the more conventional rural digital divide.

We have discussed previously (2) that bridging the digital divide brings with it social, economic, and health advances. How can one connect the unconnected and, at the same time, lay the foundation for service delivery and social impact? In this project, we hope to demonstrate that it is viable with low-cost technology.

Our proposed system is a stepping stone towards a longer-range device that may be used in rural areas. According to Markets&Markets, the global market for long-range wireless optical technology is growing at a rate of 38% and is projected to be worth almost \$2B by 2025. A successful business would therefore lead to significant economic benefits and employment opportunities.

The potential for a high social impact of the project will enable us to create awareness, both directly and indirectly, for the work that we do. This is particularly important for early-career researchers. My lab is relatively new and building momentum, which this project will enhance. Through student chapter outreach, where we can demonstrate elements related to the system and our work in general, perhaps we can inspire more students to consider STEM careers. Additionally, Wits is a research-intensive university, so increasing the number of postgraduate students and publications is essential.

Finally, the opportunities afforded by this grant to communicate our research at local and international conferences will allow us to meet leading experts, discuss ideas and develop new collaborations with researchers in similar fields.

### 4. Research Outputs and Outcomes

**Journal Papers (2).** We plan to publish at least one paper per objective but more are likely. Preliminary titles: “Characterising the performance of low cost, long-range WiFi over FSO”, *Applied Optics*; “Detecting lightning using a free-space optical communication system”, *Optics Express*.

**Conference Presentations (6).** We will present our work at both local and international conferences. Locally, the students working on the project will present at SAIP 2023, 2024 (a physics conference) and SATNAC 2023, 2024 (a telecommunications conference). Internationally, the PI and CoI will each partake in one project-funded conference, probably OFC 2024. The topics to be presented will relate to the objective in that year, specifically the WiFi over optical in year one (and for OFC 2024) and the lightning sensing in year two.

**Artefacts.** We will deliver an open-source design on GitHub for the WiFi over the optical system at the end of the project. This will include the CAD files for the 3D printable components and custom electronics, as well as firmware and software required for the control and monitoring of the system.

**Outreach Activities.** We will be engaged in several educational and general-public outreach activities to benefit next-generation scientists and engineers. Jointly with the Wits Optics student chapter, we will organise demos for high-school and undergraduate students. We will also endeavour to release a series of videos to explain the basic principles behind the developed tool and its mode of operation.

## 5. Project Planning

The project is based around the objectives and activities above, which are also in chronological order, as shown in the Gantt chart in Fig. 3.

Objective	Activity	Description	Year		2023		2024		People Involved
			Semester		1	2	1	2	
A	<b>The WiFo System</b>								
	1	Refine and add pol. MIMO (prototype already in development in 2022)							MSc A
	2	How well does it work through real turbulence?							MSc A, 2x Honours
	3	What is the optimal configuration?							MSc A
B	<b>Harnessing "WiFo" CSI for Sensing</b>								
	1	Implement WiFi CSI extraction and basic testing							MSc B
	2	Characterise detection of emulated lightning (in the Wits high voltage lab)							MSc B
	3	Deploy outdoors for testing during the lightning season							MSc B, 2x Honours
	<b>In-person Lab Collaboration</b>								MC, AT, MSc
	<b>Local Conferences</b>				SAIP + SATNAC		SAIP + SATNAC		
	<b>International Conferences</b>						OFC		

Fig. 3. Gantt chart showing the order of the various project activities as well as intended students involved (the PI and CoI with both be involved in all activities).

In terms of risk mitigation, the experimental setup (i.e. hardware) for the sensing objective is not necessarily the final WiFo system. We are able to create a suitable setup independently in the lab for initial work in the second year.

**A. Finances.** The project finances/budget are given separately on the requested template.

## References

1. United Nations, Concise Report on the World Population Situation in 2014. *Dep. Econ. Soc. Aff. Popul. Div.* pp. 1–38 (2014).
2. MPJ Lavery, et al., Tackling Africa's digital divide. *Nat. Photonics* **12**, 249–252 (2018).
3. S Dang, O Amin, B Shihada, MS Alouini, What should 6g be? *Nat. Electron.* **3**, 20–29 (2020).
4. A Trichili, MA Cox, BS Ooi, MS Alouini, Roadmap to free space optics. *J. Opt. Soc. Am. B* **37**, A184 (2020).
5. IRNAS, Koruza – Light-speed networking (2022).
6. A Jahid, MH Alsharif, TJ Hall, A contemporary survey on free space optical communication: Potentials, technical challenges, recent advances and research direction. *J. Netw. Comput. Appl.* **200**, 103311 (2022).
7. AE Willner, et al., Perspectives on advances in high-capacity, free-space communications using multiplexing of orbital-angular-momentum beams. *APL Photonics* **6**, 030901 (2021).
8. HG Hunt, R Blumenthal, KJ Nixon, C Gomes, A multidisciplinary forensic analysis of two lightning deaths observed in south africa. *Int. J. Disaster Risk Reduct.* **51**, 101814 (2020).
9. MM Abadi, et al., A space division multiplexed free-space-optical communication system that can auto-locate and fully self align with a remote transceiver. *Sci. Reports* **9**, 1–8 (2019).
10. Y Ma, G Zhou, S Wang, WiFi sensing with channel state information: A survey. *ACM Comput. Surv.* **52** (2019).
11. M Mahomed, AD Clulow, S Strydom, MJ Savage, T Mabhaudhi, Lightning monitoring and detection techniques: Progress and challenges in south africa. *South Afr. J. Sci.* **117**, 1–7 (2021).

**Project Title:** Compact and Scalable Platforms for Optical Analog Computing

**Category:** Information

**PI:** Nasim Mohammadi Estakhri, Assistant Professor, Chapman University

## 1. PROJECT DESCRIPTION

### a. Summary of the Objectives of the Proposed Project

The overall objective of this project is to employ powerful *computational inverse-design* approaches to create **fully integrable and scalable optical analog computing platforms** through leveraging *the inherent compactness of multimode waveguides* compared to their single-mode counterparts. The compactness and scalability of the proposed structures distinguishes this approach from previous devices (see “1.b Background and Literature Review”) where increasing input size would linearly increase the [physical] footprint of the device, thus limiting the practicality of optical analog processors and possibility of their integration with electronic circuitry.

### b. Background and Literature Review

Analog computing refers to a wide class of “computing” devices that perform some form of mathematical operation on an analog input signal [electric, mechanical, acoustic, etc.]. Indeed, before the era of “digital computers” as we know them today, majority of computing devices have been performing a form of analog computation [1-3]. With the fast advancement of digital computers, possibility of automated design of digital circuits, increasingly small footprints of CMOS transistors, standardized foundry fabrication, straightforward error correction stemming from quantization in digital signals, and readily available signal amplification using CMOS transistors, digital computing have become the mainstream approach to analyze and process data for different applications [4,5]. Indeed, digital computation offers so many advantages (as listed above) that it has been believed to be the ultimate solution for any application.

The advent of lasers in 1960, however, gradually initiated another paradigm in computing (and signal processing). With the availability of a stable coherent source, two relevant research ideas have emerged. First, to replace electronic computers with their optical counterparts (i.e., optical computers using optical transistors) to exploit their potential advantages in terms of speed, bandwidth, and low loss. The idea has been widely explored, particularly thanks to profound advances in the fields of fiber optics and silicon photonics [6,7], and while fully optical computers are not yet realistic [8], the scientific exploration have resulted in many breakthroughs in designing optical interconnects and modulators, complementing and enhancing the operation of current electronic computers [9,10].

The second line of research exploiting the potentials of “light” for computations, aims at utilizing the inherent *parallel processing* that is attainable through propagation of light in a suitably designed optical element [linearity]. The simplest example of such operation is an optical lens. A lens “*computes*” the Fourier transform of an input image, which is then displayed on its focal plane almost instantly (by which we mean at the speed of light). To



perform the same operation using an electronic computer, one must first convert the input analog image into a digital signal, apply a two-dimensional Fourier transformation algorithm, and again convert the digital output back into a 2D image. Indeed, depending on the specific application and how many times a specific computation process needs to be repeated, analog computing using light can offer several advantages in terms of speed and power consumption, however, it naturally does not provide the accuracy and error correction available by digital computers.

In addition to the simple example of a lens, several platforms for optical analog computing have been proposed, each aiming to implement a specific mathematical operation. Some notable examples include: Free-space optical setups to perform differentiation and equation solving [11,12], Mach-Zehnder arrays with dielectric integrated waveguides for matrix multiplication [13], metasurfaces for differentiation and edge detection [14], photonic crystals to implement Laplace transform [15], inverse-designed equation solvers [16], fiber-optics network for matrix-inversion [17], and nonlocal scatterers for compact free-space computing [18], among several other important proposals.

### c. Problem Statement and Objectives

Investigating the examples discussed above, and the state-of-the-art approaches for integrated optical computing [13,16], the common denominator in these approaches is to use multiple integrated optical waveguides to carry the information. In such setups, the amplitude and phase of the propagating mode in each waveguide represents *one input data point*. For instance, to implement an optical device to inverse a 10x10 matrix, ten separate single-mode waveguides are required to carry the information along the device path (where the computation occurs). Similarly, when solving an integral or differential equation, the waveguides represent spatial sampling of the input (i.e., discretization). If one is interested in a higher resolution or when dealing with more complex signals, the number of these single-mode waveguides must be increased accordingly, in order to meet the required resolution. This is illustrated through an example borrowed from a recent paper published in 2022 [19], as shown in Fig. 1. In this special example an angular resolution of 15 degrees (7 points across 0-90 degrees) is achieved by using seven outgoing single-mode waveguides (shown on the right side). Similarly, the design of the core operator (left side) also relies on combination of several single-mode waveguides which are arranged to form coupled interferometers.

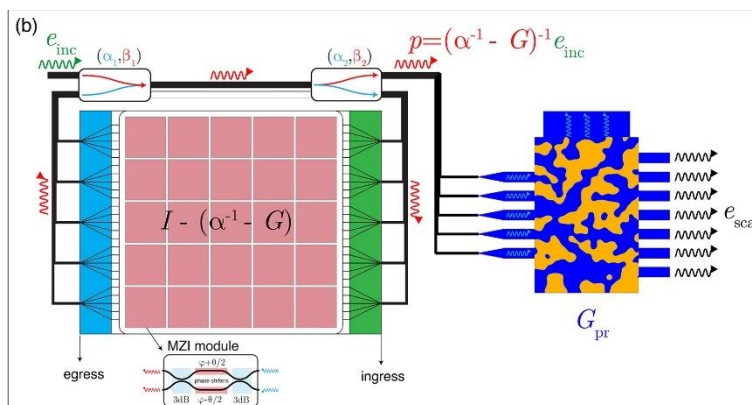


Fig. 1: An example borrowed from [19], where an optical analog computing device is designed to compute the scattered field in electromagnetic forward scattering problems (equivalent to matrix inversion). As it can be seen, the physical footprint of the device is significantly dependent on the number of data points (i.e., number of waveguides). See also [16]



This approach (and all similar proposals) is intrinsically limited for practical applications, due to the *significant increase in the physical footprint of the structure when high resolution is needed*. Indeed, even simple dielectric photonic elements are typically much larger compared to electronic elements [20], and such additional increase in the physical size is highly undesirable for electronic/photonic integration. In addition, when working with few data points, the parallel processing features offered through light-based devices are no longer beneficial and electronic processors can easily outperform their optical counterparts. **The key advantages of optical analog computing can only be unlocked through realizing real scalability in such devices.**

The main objective of the current proposal is to put forward a new approach to implement integrable optical analog computing elements that allow for realistic scalability of the device (i.e., when increasing the number of input data points), without detrimental impact on the physical footprint of the structure. For this purpose, we propose to employ multimode silicon waveguides, where the *data is carried through the amplitude and phase of multiple overlapping modes, occupying the same physical space*. A single multimode silicon waveguide (operating as an analog data bus) carries the information throughout the device, and the desired operator such as matrix inversion, differentiation, integration, etc. is implemented via a compact inverse-designed integrated structure. As an example, let us consider the simple case of a 2x2 matrix inversion. To implement the kernel operator a 2-input, 2-output photonic system is required to satisfy a pre-defined desired scattering matrix [S-Matrix]. By using 2 separate single-mode waveguides, a minimum size limit is automatically imposed on the structure to avoid mutual coupling between these waveguides (for example see [21]). However, same information can be carried using the first two modes of a properly chosen waveguide (see Fig. 2), with no intrinsic limit on the physical size of the kernel. Indeed, as it can be seen in Fig. 2, using a standard inverse optimization technique [22], the overall size of the kernel can be progressively pushed down, understandably depending on the complexity of the chosen kernel.

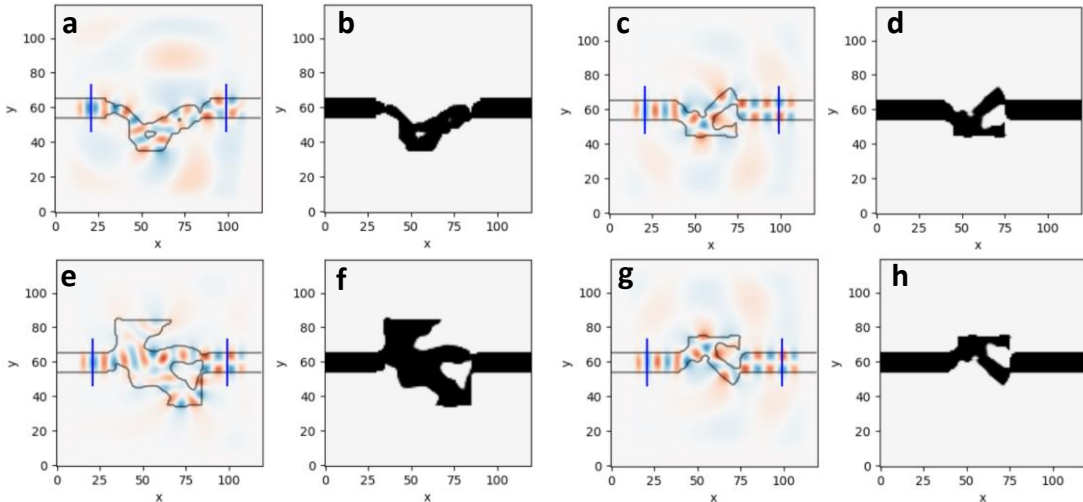


Fig. 2: (a,c,e,g) Field distribution and (b,d,f,h) permittivity distribution of four sample structures, each representing a 2x2 transmission matrix for  $TE_0$  and  $TE_1$  modes in two-dimensional silicon waveguides at wavelength of 1.5[ $\mu\text{m}$ ]. The inverse designed region is a square with side lengths of (b,f) 2.4[ $\mu\text{m}$ ] and (d,h) 1.6[ $\mu\text{m}$ ]. In all cases the input  $TE_0$  mode is converted to  $TE_1$  mode with different phases. Simulations are performed using a slightly modified version of Ceviche code [22].

## 2. RESEARCH PLAN and OUTCOMES

Our research plan for this proposal is based on 5 sequential steps, as summarized in Fig. 3. In the following, we provide a summary of the important aspects and steps of each task and the anticipated timeline (a total of 24 months period).

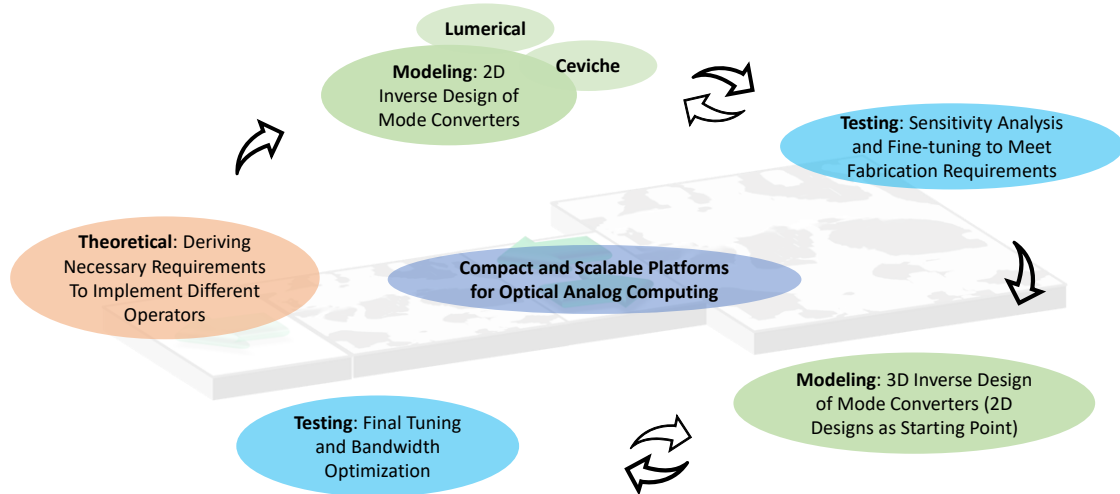


Fig. 3: Summary of the research plan and different tasks in the proposal

**Task 1 [Months 1-6]:** In the first step, we will adapt the current approaches to solving matrix equations (i.e., a closed-loop system) and implementing operators such as integration and differentiation (i.e., an open-loop system), to be realized in our multimode setup. The second part of our theoretical study will be focused on understanding and estimating the capacity of inverse-designed photonic integrated structures to implement a general multi-mode kernel. To the best of our knowledge, it is not currently possible to pre-determine the minimum physical size which can guarantee successful completion of an inverse design task. We will investigate this problem both theoretically and through establishing some empirical data.

**Task 2 [Months 3-9]:** Next, we will employ two inverse-design tools (Ceviche [22] and Lumerical [23]), to design two-dimensional multimode kernels (operators), as well as multimode couplers (please see [16, 19] for details on the necessity of using couplers to access the output in equation solvers). Two-dimensional structures are chosen to allow for first-step proof of principle designs to test our idea. In addition, these designs will be used as the starting points for the three-dimensional structures in “Task 4”.

**Task 3 [Months 8-12]:** To ensure practically and foundry-friendly design, we will perform series of sensitivity analysis (physical parameters, bandwidth, mode cross-coupling, etc.) to fine-tune our designs. The two-dimensional operators will be finalized at this stage (first publication/presentation).

**Task 4 [Months 13-18]:** Using the two-dimensional structures in “Task 2”, the designs will be pushed toward fully realistic, three-dimensional integrated elements. New rounds of optimization using Lumerical will be performed at this stage. For three-dimensional waveguides, we will study symmetric and asymmetric integrated waveguides, decide on the best option between using hybrid or purely TE modes.

**Task 5 [Months 19-24]:** Finally, each three-dimensional design is fine-tuned to satisfy fabrication requirements (such as minimum feature size). Series of sensitivity analysis on physical parameters and bandwidth will be performed (second publication/presentation).

Accomplishing the above tasks, the important **outcome of this project** is to design integrated optical analog computing elements with *significantly smaller physical footprint compared to the current state-of-the-art structures*.

### 3. RESEARCH IMPACT

In addition to the scientific impact of this project in advancing the *applications of light for parallel and low-power information processing*, we believe that this project will have several broader impacts, as listed below:

- (i) **Scientific impacts:** Designing scalable and compact integrated analog computing, paving the way toward hybrid/electronic processors exploiting the parallel processing and speed of light-based analog computation.
- (ii) **Educational impact:** Training undergraduate students in electrical engineering and computer science. This is especially valuable for Chapman University as a PUI. Training and mentoring include research planning and execution, presentation and dissemination of results, preparation for next career stage.
- (iii) **Community impact:** Organizing workshops for senior high school students and local undergraduate students to broaden their perspective of applications of light in state-of-the-art information and computing applications.

### 4. REFERENCES

1. Thomson, W., Proc. R. Soc. Lond. 24, no. 164-170 (1876): 269-271.
2. Bush, V., J Franklin Inst. 212, no. 4 (1931): 447-488.
3. Price, D., IEEE Micro 4, no. 1 (1984): 22-52.
4. Gill, S., Math. Proc. Camb. Philos. Soc., vol. 47, no. 1, pp. 96-108. Cambridge Univ. Press, 1951.
5. Atanasoff, JV., IEEE Ann. Hist. Comput 6, no. 03 (1984): 229-282.
6. Ghatak, A., and K. Thyagarajan. An introduction to fiber optics. Cambridge Univ. Press, 1998.
7. Lipson, M., J. Light. Technol. 23, no. 12 (2005): 4222-4238.
8. Miller, DAB., Nat. Photonics 4, no. 1 (2010): 3-5.
9. Subbaraman, H., X. Xu, A. Hosseini, X. Zhang, Y. Zhang, D. Kwong, and R. T. Chen, Opt. Express 23, no. 3 (2015): 2487-2511.
10. Sorger, VJ., ND. Lanzillotti-Kimura, R. Ma, and X. Zhang, Nanophotonics 1, no. 1 (2012): 17-22.
11. Cederquist, J., JOSA 71, no. 6 (1981): 651-655.
12. Rajbenbach, H., Y. Fainman, and S. H. Lee, Appl. Optics 26, no. 6 (1987): 1024-1031.
13. Bogaerts, W., D. Pérez, J. Capmany, DAB. Miller, J. Poon, D. Englund, F. Morichetti, and A. Melloni, Nature 586, no. 7828 (2020): 207-216.
14. Silva, A., F. Monticone, G. Castaldi, V. Galdi, A. Alù, and N. Engheta, Science 343, no. 6167 (2014): 160-163.
15. Guo, C., M. Xiao, M. Minkov, Y. Shi, and S. Fan, Optica 5, no. 3 (2018): 251-256.
16. Mohammadi Estakhri, N., B. Edwards, and N. Engheta, Science 363, no. 6433 (2019): 1333-1338.
17. Wu, K., C. Soci, P. P. Shum, and NI. Zheludev, Opt. Express 22, no. 1 (2014): 295-304.
18. Goh, H., and A. Alù, Phys. Rev. Lett. 128, no. 7 (2022): 073201.
19. Nikkhah, V., DC. Tzarouchis, A. Hoorfar, and N. Engheta, ACS Photonics (2022).
20. Ozbay, E., Science 311, no. 5758 (2006): 189-193.
21. Qu, Y., H. Zhu, Y. Shen, J. Zhang, C. Tao, P. Ghosh, and M. Qiu, Science Bulletin 65, no. 14 (2020): 1177-1183.
22. Hughes, TW., IAD. Williamson, M. Minkov, and S. Fan, ACS Photonics 6, no. 11 (2019): 3010-3016.
23. <https://www.lumerical.com/>

## **Monitoring Dysfunctions of the Arousal Response with Biometric Ocular Photometry**

*N. Pégard, UNC Chapel Hill - 20th Anniversary Challenge: Health - Executive Summary*

Nearly one in five U.S. adults currently live with a mental illness, yet only few people have access to adequate mental healthcare. Even with ample financial resources, diagnosis, treatment, and support for these chronic and intermittent conditions are particularly difficult to provide outside inpatient facilities. For instance, dysfunctional arousal responses are common components of many neuropsychiatric disorders, yet these signs are routinely ignored because arousal cannot be simply measured with a sensor. The ability to detect dysfunctions of the arousal response with practical, inexpensive, and minimally invasive technology would revolutionize mental healthcare. Tracking arousal in real time would enable currently infeasible personalized medicine, with tailored treatment strategies for mental illnesses, where counseling, advice, or even fast-acting drugs could be provided to patients exactly at the time and place where they would be most beneficial.

The current state of the art technology for arousal studies is pupillometry, with bulky cameras placed near the eye that monitor the changes in pupil size that correlate with arousal. Pupillometry alone is often insufficient to reliably assess arousal states and a preferred strategy also includes heart and breathing rates measurements with additional monitoring devices. This approach is impractical and limits arousal studies to laboratory settings. Round the clock tracking of arousal in humans remains currently impossible.

We propose to tackle this challenge with a new technology, Biometric Ocular Photometers (BOPs) that can simultaneously record several biometric data that encode arousal with a single device. BOPs operate with invisible infrared light to illuminate the back of the eye, and with photodetectors to measure the flow of diffused infrared photons through the pupil. Our team has already developed a BOP device for animal studies (small rodents) and demonstrated that it can simultaneously record pupil size, heart, and breathing rates.

With the support of the Optica 20<sup>th</sup> Anniversary Challenge, we will leverage our successful proof of concept for animal research, and we will develop a wearable optical technology to monitor arousal in humans. For this, we will integrate BOPs in a modified pair of glasses with infrared LEDs that will illuminate the surface of the skin in the periphery of the eye, and with several photodetectors pointed towards the eye that will quantify diffused light through the pupil from multiple perspectives. We anticipate that the technology we propose will simultaneously capture pupil size, eye motion, heart, and breathing rate at multi-kilohertz sampling speeds. A Bluetooth connection will stream all these biometric data to the user's cell phone where unsupervised deep learning algorithms will infer arousal states in real time. Our interdisciplinary team with experts in optics, electronics, and computer science, and an established collaboration with the laboratory of Prof Jose Rodriguez Romaguera (UNC Psychiatry dpt.), brings all the expertise that is needed to develop and validate the hardware and the software for this project, and to tailor their design for medical applications.

We will first validate our prototype by comparing our capabilities against the current state of the art (commercial pupillometry and eye tracking devices, heart and breathing monitors) in controlled tests. Our team will commit to publish all the results, data, and design files in open-access journals to facilitate the replication of our systems in not-for-profit applications. We will also explore potential commercial applications of the technology.

We expect that the prototype we intend to deliver within the timeline of this award to first be of interest to medical researchers for the study of neurological disorders and open new research directions through traditional funding opportunities. Our long-term goal is to provide a wireless device for patients suffering from PTSD, anxiety or depression, that will be programmed to detect early symptoms of distress in real-time and enable new personalized medicine solutions for these patients.

# Monitoring Dysfunctions of the Arousal Response with Biometric Ocular Photometry

*N. Pégard, UNC Chapel Hill - 20th Anniversary Challenge: Health - Proposal*

## 1. Literature Review

Dysfunctional arousal responses are a core component of many neuropsychiatric disorders. For instance, depression and anxiety disorders are commonly defined by atypical arousal responses to motivational stimuli<sup>1-3</sup>. Also, atypical sensory reactivity and physiological arousal are reported by parents in pre-symptomatic infants that go on to develop neurodevelopmental disorders<sup>4</sup> and are predictive of the later severity of adverse symptomatology<sup>5</sup>. Despite its high clinical significance, arousal cannot be measured directly with a sensor, and arousal dysfunctions remain underexplored. Neuroscientists currently assess arousal qualitatively by subjective reporting or indirectly by interpreting multiple biometric data that have a known correlation with the response dynamics to specific events, such as pupil size, eye gaze, heart, and respiration changes. Any of these biometric measurements alone is insufficient to confirm changes in the arousal response because their recorded values may fluctuate for many other reasons unrelated to arousal. However, arousal responses and dynamics can be more reliably confirmed when changes are detected synchronously across multiple biometrics.

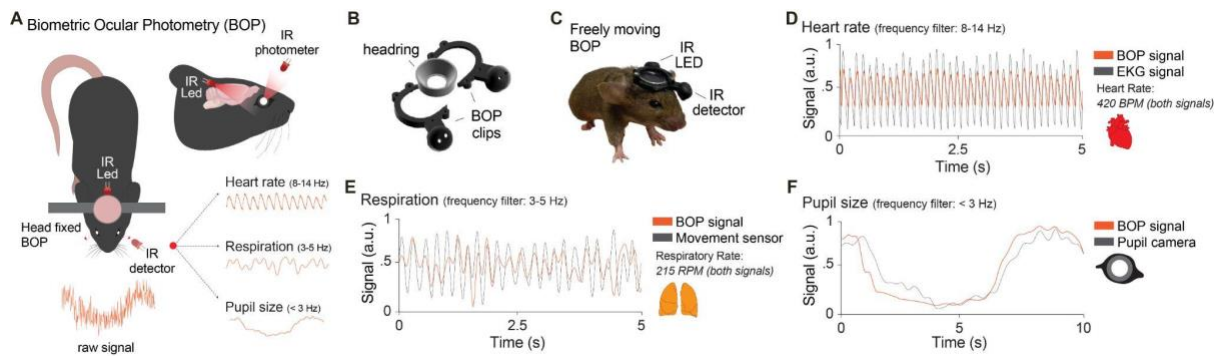
The current state-of-the-art for arousal studies combines heart and breathing rate monitors with pupillometry. Camera-based systems capture videos of the pupil illuminated externally with infrared (IR) light<sup>6-8</sup>. Pupillometry requires bulky cameras placed near the eye that occlude the field of view, and the video data must be post-processed with complex segmentation algorithms to extract pupil size and eye motion from each frame. Sampling rates are limited by the camera frame rate, typically at or below 100 fps, preventing the capture of high-speed physiological events, and real-time operation is computationally challenging. Certain gaze tracking and pupillometry systems replace the camera in favor of infrared emitters and sensors placed in front of the eyes<sup>9</sup>, however, these systems do not segregate pupillary responses that come from arousal changes and pupillary responses caused by fluctuations in ambient light. Additionally, the pupillary light reflex is an important metric of autonomic nervous system function that has been exploited for a wide range of clinical applications across multiple neurological disorders<sup>10</sup>. However, these measurements are only taken across brief periods of time (seconds) and longitudinal tracking of pupillary light responses across longer periods of time (minutes, hours, days, months) is not yet feasible.

By lack of adequate technology, the study of arousal responses in neuropsychiatric and neurodevelopmental disorders has been historically limited to preclinical models with experiments in restrained animals with neck collars that are stress inducing<sup>11</sup> or invasive methods that require surgical implantation of a device inside the body<sup>12</sup>, and the full repertoire of natural behaviors<sup>13</sup> cannot be observed. With human subjects, only a few clinical studies have been performed<sup>14</sup>, with subjects tested in unfamiliar and often stressful experimental laboratory settings, which imposes substantial limitations on the scope of potential findings.

## 2. Problem Statement / Objective

We propose to develop, validate, and disseminate a wearable device that will address all the issues of current technology and enable real-time tracking of arousal states in human subjects for extended periods of time. To achieve this goal, we propose to implement Biometric Ocular Photometers (BOPs) in a modified pair of glasses. BOPs are a technology that our team recently developed and successfully tested to perform arousal studies in freely moving mice. The principle of BOPs and preliminary experimental results are shown in **Figure 1**.





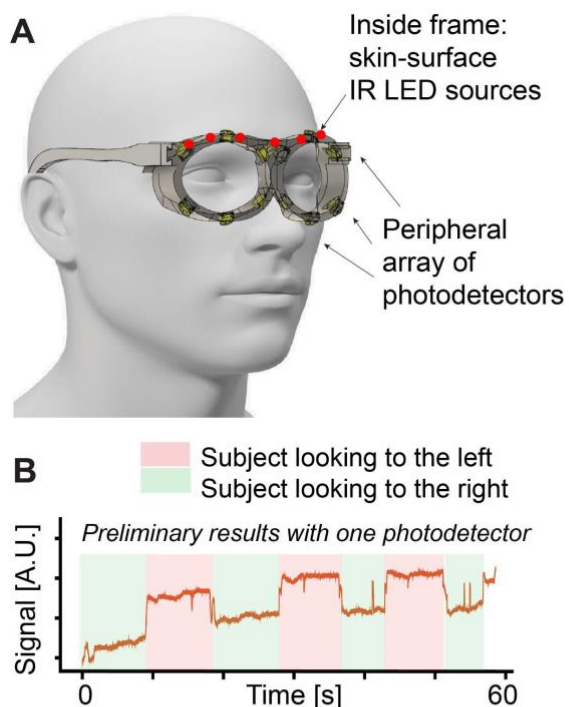
**Figure 1:** Proof of concept results demonstrating Biometric Ocular Photometry (BOP) in (A) head-fixed and (B-C) freely moving mice. (D-F) Validation of BOP with traditional techniques acquiring biometric data responses using EKG electrodes in the skin (heart rate), a piezo movement sensor in the chest (respiration), and a camera aimed at the eye (pupil size) of the mouse. Unpublished data.

Our novel method relies on low-power invisible infrared light diffusing through tissue (**Figure 1A**) to illuminate the retina internally, while infrared detectors placed in the periphery of the eye measure the amount of light exiting the pupil. Since changes in pupil size, respiratory motions, and blood flow all modulate the propagation of light through tissue and the pupil, all these arousal biometrics can be easily retrieved in real time with minimal computation. We performed validation experiments by comparing data obtained with our BOP technology to simultaneous recordings of heart rate EKGs (**Figure 1D**), piezo sensors for respiratory motions (**Figure 1E**), and camera-based pupillometry (**Figure 1F**).

With the support of Optica's 20th-anniversary challenge, our goal is to leverage this proof of concept and early results in mice to develop a wearable device for arousal tracking in humans that will address the previously described limitations of current experimental techniques.

The device that we envision is shown in **Figure 2A**. A modified pair of glasses will be fitted with several low-power infrared LEDs to evenly illuminate tissue in the periphery of the eyes from the surface of the skin. In front of the frame, we will place a peripheral array of directional photodetectors oriented towards the center of the eye that will measure the amount of diffused infrared light passing primarily through the pupil from multiple perspectives.

Preliminary results with a single photodetector placed near the eye (**Figure 2B**), indicate that the technology we propose can reliably identify eye motion. We observed that the photodetector collects more infrared light when the pupil



**Figure 2 :** A) Proposed eyewear design for arousal monitoring in human subjects featuring skin-contact infrared illumination and six photodetectors in the periphery of each eye. B) preliminary data showing signal collected by one photodetector in response to voluntary eye motions towards and away from the sensor.



is oriented towards it than when it is oriented away from it. The technology we propose will scale this concept with six calibrated detectors placed around each eye. We hypothesize that differential measurement from multiple perspectives will be sufficient to reliably estimate eye motion, in both horizontal and vertical directions, in addition to other biometric information that can already be obtained in animal models.

Our secondary objective will be to integrate all electronics within the frame to enable arousal measurements with a practical, discrete, and comfortable device that human study participants, and later patients, could wear for extended periods of time without experiencing discomfort. A wireless (Bluetooth) connection will stream the raw data to a cell phone where it will be processed to infer arousal states in real-time. In future applications, we envision that the phone app could use this data to alert the user in real-time when arousal dysfunctions are observed. Our technology would enable personalized medicine strategies, for instance by recommending actions before the detected adverse situation gets a chance to worsen. (e.g. the app could recommend stepping away from an ongoing activity, alerting a clinician or contacting a friend or family member, or even taking a fast-acting prescribed medication at the precise moment when it's effects would be most beneficial).

### **3. Outline of tasks/Work Plan**

A manuscript is currently in preparation and will disseminate our BOP technology for arousal studies in mice to the scientific community. Should this project receive funding support, our team will lead the proposed project in collaboration with the laboratory of Prof. Jose Rodriguez-Romaguera, a translational neuroscientist that works with both human subjects and mouse models and a co-inventor of the BOP technology. My laboratory will lead the prototype design with 3D printing, optics, electronics, and signal processing skills, and our collaborator will provide additional expertise in computational analysis of biometric data, and in translational neurosciences.

In addition, we also have an already established pipeline to test our device in ongoing studies in both human adults and infants. Together, our goal is to design, build, and validate a working prototype by the end of year 1, as illustrated in **Figure 2A**, with six photodetectors around each eye.

Our interdisciplinary expertise will allow our teams to progress fast, by simultaneously exploring the design of optical hardware, electronic systems, and computational methods. We will leverage the joint design of hardware and software to maximize performance. Ongoing animal studies currently being led by our collaborator will allow our team to perform validation experiments in mice before attempting any work with human subjects. Since the illumination technology we propose, with diffused infrared light sources, is already used safely in pulse oximeters and in fNIRS systems (functional near-infrared spectroscopy), we do not anticipate any issue in securing permission to perform human studies once our prototype is ready for testing.

In year 2 of the project, our team will develop a second-generation technology tailored for measurements across extended periods of time, with onboard electronics and a wireless connection that will stream the data directly to the user's cell phone. We will create a phone application to analyze the data and detect arousal dysfunctions in real-time. To achieve this goal, we will leverage ongoing work in raw BOP data analysis that we are currently performing for animal studies. Our approach will rely on unsupervised deep learning models that will identify arousal encoding patterns across multiple biometric data streams. We will then test our devices in ongoing clinical studies that aim to understand arousal responses in two separate studies with subjects suffering from either anxiety disorders or neurodevelopmental disorders. This will allow us to seek further funding to initiate studies to test our device across clinical samples.

#### **4. Outcome(s)**

We will validate our first prototype with a series of controlled experiments like those performed on mice in **Figure 1**. We will compare eye tracking and pupillometry data obtained by our device with simultaneously recorded images of the pupil analyzed using conventional commercially available pupillometry techniques. We will also compare simultaneous inferences of heart and respiratory rates to the reference data obtained with heart and breathing rate monitors commonly used in hospital settings.

We will then evaluate our ability to predict arousal variations in healthy subjects with additional validation experiments in controlled environments where we will track arousal with our device while stimuli are presented to them. The success of these validation experiments will be a deciding criterion for our teams to begin the dissemination of the technology to collaborators, and to seek additional funding for the next steps of this project.

We will disseminate our inexpensive technology by sharing data analysis software, parts list, assembly instructions, and 3D models for all hardware and software associated with the project on open access platforms. We anticipate that our technology will be rapidly and widely adopted by the broader community of neuroscientists and clinicians who strongly value the ability to track arousal biometrics in minimally invasive experimental, and clinical settings with practical and cost-effective technology. Our team has a solid track record of open-software and open-hardware research practices and will make all the technology we develop available and easy to replicate for not-for-profit applications. We have nonetheless filed provisional patents to protect commercial applications of our technology.

#### **5. Impact**

The ability to monitor arousal states in humans has many applications ranging from basic neuroscience discovery to medicine, and consumer electronics.

Basic neuroscience research will be the first field to benefit from our technology. The device we propose will enable neuroscientists to revisit any previously performed behavioral study by integrating the acquisition of previously inaccessible experimental arousal tracking data. Our device will provide new insight into how humans interact with their environments, in familiar and unfamiliar situations without any of the bias currently observed in laboratory settings.

The ability to detect dysfunctions of the arousal response will revolutionize the diagnosis, and treatment of many neuropsychiatric and neurodevelopmental disorders. Our device will be able to alert patients if they detect atypical arousal dynamics and/or states that stimuli in their surrounding environment cannot explain. Simply being able to alert patients of a distressing event, especially in the early stages, will enable more efficient strategies to manage neuropsychiatric disorders (e.g. calling a friend, a therapist, or simply advice to step aside from an ongoing activity) and help reduce the need for default options like drug-based treatments with notorious side effects.

Our device is also inexpensive to manufacture which will have the added benefit of easily expanding mental health treatment opportunities toward remote and underserved areas that do not benefit from easy access to mental health services, or inpatient facilities.

Finally, our technology will find applications in consumer electronics. Near-eye BOPs for arousal tracking can be integrated into safety equipment to alert users of fatigue or attention deficit when they perform critical tasks. They are also suitable to improve the perception of computed-rendered scenes in virtual reality headsets, by providing perceptual feedback and allow image synthesis to be dramatically improved to render more immersive environments.

## References

1. Craske, M. G. *et al.* Anxiety disorders. *Nat. Rev. Dis. Primer* **3**, 17024 (2017).
2. Lang, P. J. & McTeague, L. M. The anxiety disorder spectrum: fear imagery, physiological reactivity, and differential diagnosis. *Anxiety Stress Coping* **22**, 5–25 (2009).
3. Wilhelm, F. H. & Roth, W. T. The somatic symptom paradox in DSM-IV anxiety disorders: suggestions for a clinical focus in psychophysiology. *Biol. Psychol.* **57**, 105–140 (2001).
4. Sacrey, L.-A. R. *et al.* Can parents' concerns predict autism spectrum disorder? A prospective study of high-risk siblings from 6 to 36 months of age. *J. Am. Acad. Child Adolesc. Psychiatry* **54**, 470–478 (2015).
5. Grzadzinski, R. *et al.* Sensory Reactivity at 1 and 2 Years Old is Associated with ASD Severity During the Preschool Years. *J. Autism Dev. Disord.* **50**, 3895–3904 (2020).
6. Rodriguez-Romaguera, J. *et al.* Prepronociceptin-Expressing Neurons in the Extended Amygdala Encode and Promote Rapid Arousal Responses to Motivationally Salient Stimuli. *Cell Rep.* **33**, 108362 (2020).
7. Reimer, J. *et al.* Pupil fluctuations track fast switching of cortical states during quiet wakefulness. *Neuron* **84**, 355–362 (2014).
8. Privitera, M. *et al.* A complete pupillometry toolbox for real-time monitoring of locus coeruleus activity in rodents. *Nat. Protoc.* **15**, 2301–2320 (2020).
9. Roth, N. Automatic Optometer for Use with the Undrugged Human Eye. *Rev. Sci. Instrum.* **36**, 1636–1641 (1965).
10. Hall, C. A. & Chilcott, R. P. Eyeing up the Future of the Pupillary Light Reflex in Neurodiagnostics. *Diagnostics* **8**, 19 (2018).
11. Kim, S.-Y. *et al.* Diverging neural pathways assemble a behavioural state from separable features in anxiety. *Nature* **496**, 219–223 (2013).
12. Stiedl, O. & Spiess, J. Effect of tone-dependent fear conditioning on heart rate and behavior of C57BL/6N mice. *Behav. Neurosci.* **111**, 703–711 (1997).
13. Meyer, A. F., Poort, J., O'Keefe, J., Sahani, M. & Linden, J. F. A Head-Mounted Camera System Integrates Detailed Behavioral Monitoring with Multichannel Electrophysiology in Freely Moving Mice. *Neuron* **100**, 46-60.e7 (2018).
14. Hazlett, H. C. *et al.* Early brain development in infants at high risk for autism spectrum disorder. *Nature* **542**, 348–351 (2017).
15. Ortiz-Juza, M. M., Alghorazi, R. A. & Rodriguez-Romaguera, J. Cell-type diversity in the bed nucleus of the stria terminalis to regulate motivated behaviors. *Behav. Brain Res.* **411**, 113401 (2021).
16. Pegard, N. *et al.* Holographic Temporal Focusing for 3D Photo-activation With Single Neuron Resolution. **2017**, 3–5 (2017).
17. Mardinly, A. R. *et al.* Precise multimodal optical control of neural ensemble activity. *Nat. Neurosci.* (2018) doi:10.1038/s41593-018-0139-8.
18. Eybposh, M., Caira, N., Atisa, M., Chakravarthula, P. & Pegard, N. DeepCGH: 3D Computer-Generated Holography Using Deep Learning. *Opt. Express* (2020) doi:10.1364/oe.399624.

**Project Title:** Compact and Scalable Platforms for Optical Analog Computing

**Category:** Information

**PI:** Nasim Mohammadi Estakhri, Assistant Professor, Chapman University

## EXECUTIVE SUMMARY

**Overview:** In this project we propose a fully integrated platform to realize all-optical analog computation using *compact* and *scalable* mode converters. The scalable operation of the proposed structures distinguishes this design from previous devices presented in the literature, where increasing the input size would linearly increase the physical footprint of the device, thus hindering their practicality when large amount of data needs to be parallel processed. The outcome of this project are low-power and integrable devices that can impart linear mathematical operations on the input signal and solve the associated integral equations. In the proposed design, the output signals can be easily accessed through a single multimode coupler placed in the signal path. The compact nature of these inverse-designed optical structures leads toward realistically scalable optical analog computers, enabling futuristic high-resolution parallel computations.

**Detailed Objective, Outcomes, and Impact:** The overall objective of this project is to employ powerful *computational inverse-design* approaches to create **fully integrable and scalable optical analog computing platforms** through leveraging *the inherent compactness of multimode waveguides* compared to their single-mode counterparts. This allows for realistic scalability of the device (i.e., when increasing the number of input data points), without detrimental impact on the physical footprint of the structure. For this purpose, we propose to employ multimode silicon waveguides, where the *data is carried through the amplitude and phase of multiple overlapping modes, occupying the same physical space*. Indeed, the key advantages of optical analog computing can only be unlocked through realizing real scalability in such devices, so the important **outcome of this project** is to implement scalable integrated optical analog computing elements with *significantly smaller physical footprint compared to the current state-of-the-art structures*. The single multimode silicon waveguide (operating as an analog data bus) carries the information throughout the device, and the desired operator such as matrix inversion, differentiation, integration, etc. is fully implemented via a compact inverse-designed integrated structure.

Given the nature of the project which can be appealing to both engineering and computer science community, we envision several meaningful impacts, including **(i) Scientific impacts:** Designing scalable and compact integrated analog computing, paving the way toward hybrid/electronic processors exploiting the parallel processing and inherently high computation speed of the light-based analog computation. **(ii) Educational impact:** Training undergraduate students in electrical engineering and computer science. This is especially valuable for Chapman University as a PUI. Mentorship will include research planning and execution, as well as presentation and dissemination of research results, and preparation for next career stage. **(iii) Community impact:** Organizing workshops for senior high school students and local undergraduate students to broaden their perspective of applications of light in state-of-the-art information and computing applications. Chapman University is located in Orange County, a technology hub in US, which will allow us to plan a strong collaboration with the local industry.



# Design of an Optical Brain Interface: **Bio-Neural Dust**

## CHALLENGE

The field of optogenetics has undergone significant development in recent years. One of its applications is stimulation of neurons with light. However, when coming to stimulating the actual brain, using optical fiber inserted through the skull is not practical. To achieve neural stimulation wirelessly, the concept of neural dust was introduced. Neural dust is a type of brain-computer interface, which uses devices the size of a millimeter as wireless nerve sensors to remotely monitor neural activity. However, despite of their small size, these devices are still very large compared to the size of a neuron, making it impossible to achieve stimulation and monitoring at the granularity level of a single neuron; it is also impossible to achieve very localized brain stimulation/monitoring. In addition, CMOS technology is reaching its limits in terms of miniaturization due to quantum phenomena, making the control of CMOS sensors at the nano level very challenging. The brain stimulation at a single neuron precision level is faced with two problems; size miniaturization and biocompatibility. In the optogenetics literature, we either find miniaturized systems with no biocompatibility, or biocompatible systems but very large compared to the size of neurons.

## PROPOSED PROJECT

One promising solution in designing wireless nanosensors is to use bioluminescence and biological agents such as bacteria and viruses. Besides their biocompatibility inside the human body, bio-inspired systems are stable, inexpensively manageable, their tiny size allows them to be injected noninvasively inside the brain and they are easily controlled with genes and enzymes. The goal of this project is to design and implement bio-nanosensors that can monitor and stimulate neurons at nano level by using optogenetics. The proposed bio-nanosensor contains two biosystems. The first uses the piezoelectric properties of M13 virus to harvest the mechanical energy of ultrasonic waves, converting it to electricity. The second biosystem uses a photo-protein called *Aequorin*, which generates bioluminescent blue light in the presence of  $\text{Ca}^{2+}$  ions. Both biosystems will be placed inside a transparent nanosphere creating a bio-nanosensor, which detects ultrasonic waves, converts them to electricity, which triggers release of  $\text{Ca}^{2+}$  ions in the pool where *Aequorin* is located. The reaction generates blue light emission. A network of these bio-nanosensors creates the Bio-Neural Dust that will be used as an optical brain interface to stimulate neurons *in vitro* by using optogenetics.

## INTENDED OUTCOMES

The project is divided into an analytical study and an experimental study. The intended outcomes of the analytical study are journals, conference publications and a patent of the designed bio-nanosensor. The intended outcomes of the experimental study are testbed, in vitro prototype and a patent of the constructed bio-optical brain interface. The project will involve 4 graduate students (2 PhD and 2 Master), who will acquire multidisciplinary expertise and research training. We have secured use the laboratories required for our research. This project will have a significant scientific and technological impact, especially in the field of medical applications and neuroscience.



# Design of an Optical Brain Interface: **Bio-Neural Dust**

## RESEARCH CONTEXT AND LITERATURE REVIEW

The rapid and impressive advancements in nanotechnology have paved the way for new emerging applications in medicine, biosensing and nanonetwork design, which were previously impossible. One of these new emerging applications is the use of light to communicate at the nanoscale. Compared to radio-frequency radiation, light is characterized by high photon energy, very high frequency and very small wavelength, which makes nanoscale interactions feasible. The design of a nanonetwork that can broadcast information optically can lead to very interesting applications, especially in neuroscience by using optogenetics. Optogenetics has the potential not only to realize the dream of understanding neural circuits at single-cell precision level, but also to provide insights into new regenerative medicine protocols, new molecular targets for drug development and other strategies targeting the repair of the brain [1].

Size miniaturization of optical technologies has been one of the current trends in the photonics field. Recent fabricated micro-/nanofibers (MNFs) have aroused great interest. Intensive work has been published related to the design and evaluation of these tiny fibers that are having diameters close to or below the wavelength of the guided light [2]. However, despite the very attractive properties of MNFs, their precision and sensitivity need to be improved and they still have significant challenges to resolve related to both theoretical research and their use in practical applications. Environmental contamination is another challenge that needs to be tackled, because ultrasensitive sensors require extreme cleanness, especially when designed for long-term operations [3]. These remaining challenges make use of these tiny fibers impractical, especially *in vivo* (inside the body) medical applications and for neuro-stimulation. The design of beamforming optical antenna arrays for use in nano-bio sensing was proposed recently [4]. The authors designed a bow-tie optical antenna that uses plasmonic waves and active phase control to allow dynamic beamforming. Nonetheless, the materials used to fabricate such antenna arrays are not biocompatible, which limits their use *in vivo* applications. In addition, the antenna array is fixed in space, which makes it more suitable for usage for *in vitro* than *in vivo*.

Neural dust is a promising technology for achieving wireless neuro-stimulation at single neuron precision level. It is called dust because it contains thousands of independent, floating, small-scale sensor nodes that detect and report local extracellular data. The neural dust system proposed in [5] consists of three communication layers: an external transceiver with a long-range transmitter inserted from the outside, an ultrasound sub-dural transceiver implanted under the skull and independent neural dust sensing nodes dispersed throughout the brain. However, this system is only limited to monitoring neurons and transmitting reports to the sub-dural transceiver via backscattering. The study in [6] proposed an enhancement to the system proposed in [5] by integrating the wireless optogenetic component to the neural dust. The wi-opt neural dust in [6] added a Light Emitting Diode (LED) unit and piezoelectric nanowires allowing the system to stimulate neurons with light and harvest energy generated by ultrasound waves. Nevertheless, despite their small size, these devices are still very large compared to the





size of a neuron (they are at millimeter level vs the nanometer/micrometer level of cells), which makes their use in monitoring and stimulation at single-neuron precision level or placement within the brain at very high granularity level practically impossible. In addition, CMOS technology is reaching its limits in terms of miniaturization due to quantum phenomena, making the control of CMOS sensors at the nano level very challenging.

## PROBLEM STATEMENT AND OBJECTIVES

The brain stimulation at single neuron precision level faces two problems; size miniaturization and biocompatibility. In the optogenetics literature, we either find systems with no biocompatibility [5], [6], or biocompatible systems but with size considerably larger compared to the size of neurons [7].

Aim of this project is to design, evaluate and implement an optogenetics-based bio-optical brain interface at the nano level, which can be used non-invasively inside the human body and is capable of monitoring and stimulating neurons at single cell precision level. The proposed optical brain interface can be very useful to many medical applications such as treating Parkinson's disease and neutralizing epileptic seizures as well as offering a new way to kill pain rapidly at specific and very localized areas of the body, without use of drugs. The project will follow the objectives below:

- Design and evaluate a single nanosensor capable of emitting light, receiving light and be powered using ultrasonic waves.
- Study the optical connection between two nanosensors, a source and an actor.
- Study and evaluate a network of optical nanosensors, which will construct the optical brain interface.
- Implement simulators, testbeds, and produce a prototype of the proposed bio-optical brain interface.

Outcomes will be published in patents and academic research papers published in highly reputable journals and conferences.

## OUTLINES OF TASKS

### Analytical Study:

- First, we will design a biosystem capable of harvesting mechanical energy, converting it into electricity using the piezoelectric properties of M13 virus. Initially we will implement a 3D model of the virus in order to study its mechanical and piezoelectric parameters. We will convert the mechanical process to an equivalent circuit and approximate the values of its components based on the simulation results.
- Second, we will design a biosystem that uses photoproteins, which generate bioluminescent blue light in the presence of  $\text{Ca}^{2+}$  ions. The  $\text{Ca}^{2+}$  ions release is triggered by electrical inputs. We will model the system with an equivalent circuit and derive the expressions for the circuit's components. We will analyze the circuit and calculate the intensity of the emitted light that is necessary to stimulate a neuron. This



analysis will allow us to make accurate estimates for the bio-components involved in the implementation of the prototype.

- Third, we will merge the two proposed equivalent circuits into a single one, which models the proposed bio-nanosensor. We will study the equivalent circuit analytically and numerically as well as study the output response and behavior of the bio-nanosensor for a variety of different inputs. We will then use the resulting output as input to a neuron model and study the generated action potential.
- Fourth, after studying the response and behavior of a single bio-nanosensor with a single neuron, we will increase the complexity of the system and study the interaction between multiple bio-nanosensors in order to understand its behavior when stimulating multiple neurons. We will also study the behavior of the system in three scenarios; 1) wired stimulation of neurons by using actin filaments as nanowires between nanosensors, 2) wireless stimulation with optogenetics and 3) a combination of wired and wireless stimulations.

### Construction of the system and Experimental Study

- First, we will construct bacteriophage M13 in the laboratory with its PVIII coat major proteins. We attach the constructed M13 with electrodes using gold coated flexible substrates. Then, we will test the piezoelectric properties of M13 *in vitro*. We will measure the obtained current when stimulating M13 mechanically with ultrasound waves. If the constructed bacteriophage uses malign substances, a toxicity test will be conducted and the results will be made public.
- Second, we will construct a transparent nanosphere using polymers and inject calcium ions and photo-proteins into it to generate a bioluminescent reaction. We will place an endoplasmic reticulum (ER) inside the nanosphere, which functions as storage space for calcium ions as shown in Fig. 1. We will measure *in vitro* the light intensity emitted by the engineered transparent nanosphere.
- Third, we will connect the constructed M13 and ER with a nano-wire (materialized using actin filaments) inside the engineered nanosphere. We will generate an ultrasonic signal which will be converted to electricity by M13 and stimulate the ER. The stimulated ER secretes calcium ions triggering the bioluminescent reaction between calcium ions and photoproteins. We will measure the intensity of emitted light for different ultrasonic intensities. Finally, we will stimulate a neuron *in vitro* using optogenetics and the emitted light by the transparent nanosphere (bio-nanosensor), then, several neurons will be stimulated by a network of bio-nanosensors and we will study the behavior of the group.

### WORK PLAN AND OUTCOMES

The proposed research is divided into 4 work packages (WPs). WPs will be completed within the following time intervals. WP1: Jan. to April 2023. WP2: May to Aug. 2023. WP3 Sept. to Dec. 2023. WP4: Jan. to Nov. 2024.

- **WP1:** Design and evaluate a single nanosensor by modeling it as an equivalent circuit. The designed nanosensor contains a piezoelectric part that harvests the energy of ultrasonic waves and a bioluminescent part that receives electricity and emits light.



**Outcomes:** Patent, journal and conference papers reporting on the designed bio-nanosensor.

- **WP2:** Study the optical connection between two nanosensors by deriving the expression of the energy transfer rate, which is influenced by the calcium concentrations inside/outside the nanosensors, the number of photoproteins inside the nanosensor and bound to its membrane. Derive the expression of the energy transfer efficiency of the optical connection, which is influenced by the distance between the two nanosensors, the refractive index of the medium and the absorption of ChR2.

**Outcomes:** Journal and conference papers reporting on the optical connection between two designed nanosensors and its rate and efficiency.

- **WP3:** Design the structure and evaluate the performance of a network formed by the proposed optical bio-nanosensors. The transmission of information between sources and actors in the proposed system is a birth-death process, which can be modeled by a Markov chain. We will also derive a closed form expression for the probability of successful triggering of light emission throughout the whole entire optogenetics nanonetwork.

**Outcomes:** Journal and conference papers reporting on the optical nanonetwork, its behavior and performance.

- **WP4:** Implement a laboratory testbed and produce an actual prototype of the proposed system. Produce a bio-nanosensor (containing both its piezoelectric and optical parts). Then, test the connection between two nanosensors *in vitro* in a Lab-On-a-Chip and extend the system to become a network of these bio-nanosensors. We will genetically modify a neuron by adding opsins to its membrane, extract it and stimulate it *in vitro* with one bio-nanosensor. Then, we will stimulate several neurons with the extended network of bio-nanosensors (Bio-Neural Dust). We will also implement a wired network with self-assembled actin filaments, which we proposed in our recent studies, and evaluate the performance of a combination between wired and optical nanonetworks.

**Outcomes:** Patent, journal and conference papers reporting on the experimental study. Testbed and a prototype of the optical brain interface.

## IMPACT

Optogenetics has a critical place in neuroscience and brain related medicine. The development of optics and molecular genetics has provided breakthroughs in our ability to detect and manipulate neural activity and has enhanced immensely our understanding of brain operation. Claiming that optogenetics has the potential to revolutionize neuroscience and brain medicine is far from an overstatement.

The outcomes of this project will lead to the development of new diagnostics techniques and treatments. The proposed optical brain interface will be useful to the treatment of several medical conditions such as Parkinson's disease and epilepsy as well as fast, localized, drugs free pain relief. The project will involve 2 PhD and 2 Master graduate

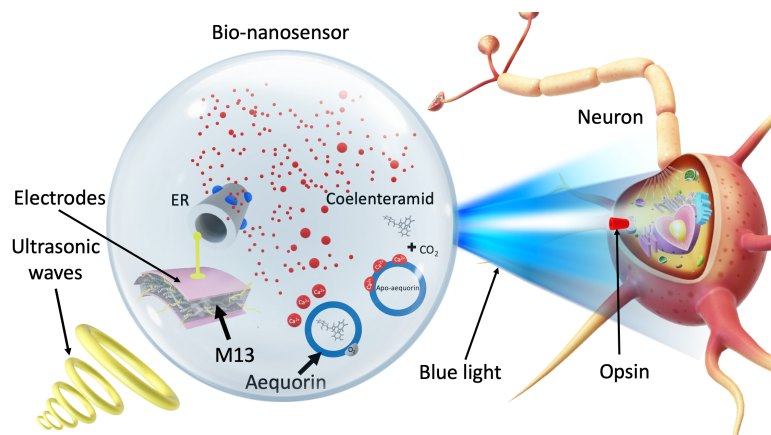


Fig. 1. Design of a bio-nanosensor in the proposed optical brain interface.

students. The PhD students will be funded from the project. The project's nature is multidisciplinary. It requires skills from the electrical and computer engineering, biology and neuroscience. The applicants' graduate and undergraduate studies enable them to have skills in the mentioned areas. We have already secured the right to use the electrical/electronic and biology laboratories we need to carry out our research. It should be noted that the multidisciplinary nature of the project will provide the students with multidisciplinary training, thus enhancing their marketability in all sectors of the high-tech work market; academia, private and public sectors. Therefore, this project will have a significant scientific and technological impact, especially for medical applications in the field of neuroscience. We will also provide several graduate students to acquire unique multidisciplinary knowledge and research skills. Journals and conference publications are anticipated. Also, as mentioned earlier, patents (to secure intellectual property) are expected as well.

## REFERENCES

- [1] Boyden, Edward S. "Optogenetics and the future of neuroscience." *Nature Neuroscience* 18 (2015): 1200-1201.
- [2] Hironaga Maruya, Yasuko Oe, Hideaki Takashima, Azusa N. Hattori, Hidekazu Tanaka, and Shigeki Takeuchi, "Non-contact detection of nanoscale structures using optical nanofiber," *Opt. Express* 27, 367-376 (2019).
- [3] Lei Zhang, Yao Tang, Limin Tong, "Micro-/Nanofiber Optics: Merging Photonics and Material Science on Nanoscale for Advanced Sensing Technology", *iScience*, Volume 23, Issue 1, 2020.
- [4] Amit Sangwan, Josep M. Jornet, "Beamforming optical antenna arrays for nano-bio sensing and actuation applications," *Nano Communication Networks*, Volume 29, 2021.
- [5] Seo, Dongjin et al. "Neural Dust: An Ultrasonic, Low Power Solution for Chronic Brain-Machine Interfaces." *arXiv: Neurons and Cognition* (2013).
- [6] Wirdatmadja, Stefanus A. et al. "Wireless optogenetic neural dust for deep brain stimulation." *2016 IEEE 18th International Conference on e-Health Networking, Applications and Services (Healthcom)* (2016): 1-6.
- [7] K. Laursen, A. Rashidi, S. Hosseini, T. Mondal, B. Corbett and F. Moradi, "Ultrasonically Powered Compact Implantable Dust for Optogenetics," in *IEEE Transactions on Biomedical Circuits and Systems* 14 (2020): 583-594.

# **Design and fabrication of a plasmonic photonic crystal fiber multiparameter sensor for refractive index, temperature, magnetic fields, and strain for lab-on-a-fiber applications**

## **1. Introduction**

Conventionally, medical, biochemical, and related analyses are conducted in centralized laboratories. This is because the centralized labs require skilled personnel and specialized equipment. However, in recent decades, because of the need to move closer to the users, points-of-care devices such as lab-on-fibers are in high demand. The lab-on-a-fiber platforms offer several benefits. Firstly, because of their very small feature sizes, extremely small sample volumes are required for analysis. Secondly, lab-on-a-fiber devices are low-cost, generate less waste, and consume less energy. Lastly, the platform can be integrated into micrototal analysis systems to automate several laboratory processes. This would allow for fast analysis and eliminate the need for skilled personnel for operation. Meanwhile, refractive index, temperature, magnetic fields, and strain are frequently measured during medical, biochemical sample analysis.

## **2. Challenges**

Current techniques for detecting multiple parameters in plasmonic PCF sensors mostly employ multi-peak tracking on confinement loss spectrographs. However, during multiple peak monitoring, some peaks on confinement loss spectrographs are frequently not well defined, leading to confusion during the monitoring process. Additionally, this technique slows down the measurement process when the resonance peaks are separated by several wavelengths. Additionally, potential errors are likely when using large wavelength steps in tracking the phase-matching points. On the other hand, it was recently suggested that individual plasmon modes can be hybridized into cooperative plasmonic modes to allow strongly guided modes to couple to several localized plasmonic modes for multiple parameter sensing.

## **3. Objectives of the research**

The main objective of this research is to design and fabricate a plasmonic PCF multiparameter sensor for determining refractive index, temperature, magnetic fields, and strain for lab-on-a-fiber applications. The specific objectives are:

- i.* To design a plasmonic PCF multiparameter sensor for measuring refractive index, temperature, magnetic fields, and strain. The modal characteristics, wavelength, and amplitude sensitivities, as well as sensor resolutions will be computed. The concept of cooperative plasmons will be explored as part of this objective.
- ii.* To fabricate the designed plasmonic PCF multiparameter sensor for determining refractive index, temperature, magnetic fields, and strain variations.

## **4. Outcome**

A plasmonic photonic crystal fiber multiparameter sensor for refractive index, temperature, magnetic fields, and strain for lab-on-a-fiber applications potentially presents the following advantages: increased portability, ease of operation, low sample consumption, fast assaying time, label-free platform, high sensitivity and high resolution, remote sensing capabilities, robustness and compactness, low-cost, multi-analyte detection capability, and a means for providing real-time results. At the same time, the sensor is not susceptible to electromagnetic interference and has high biocompatibility. Ultimately, sensor has a broad application range and will be relevant to the health sector, food industry, pharmaceutical industry, research in life sciences and related industries.

# **Design and fabrication of a plasmonic photonic crystal fiber multiparameter sensor for refractive index, temperature, magnetic fields, and strain for lab-on-a-fiber applications**

## **1. Introduction**

Conventionally, medical, biochemical, and related analyses are conducted in centralized laboratories. This is because the centralized labs require skilled personnel and specialized equipment [1]. However, in recent decades, because of the need to move closer to the users, points-of-care devices such as lab-on-fibers are in high demand. The lab-on-a-fiber platforms offer several benefits. Firstly, because of their very small feature sizes, extremely small sample volumes are required for analysis. Secondly, lab-on-a-fiber devices are low-cost, generate less waste, and consume less energy [1], [2]. Lastly, the platform can be integrated into micrototal analysis systems to automate several laboratory processes. This would allow for fast analysis and eliminate the need for skilled personnel for operation. Meanwhile, refractive index, temperature, magnetic fields, and strain are frequently measured during medical, biochemical sample analysis.

## **2. Literature review**

Photonic crystal fibers (PCFs) are a new class of optical fibers that allow their structural parameters and geometries to be tuned to realize tailored designs and properties [3]. Sensors based on PCFs provide several degrees of freedom for developing new multiparameter sensors. At the same time, advances in plasmonic science present several paradigms for extending the sensitivity limits of PCF-based multiparameters in real-time [4]. The implementation of plasmonic resonance detection on PCFs for multiparameter sensing can be achieved in several ways. It can be achieved, for example, by selectively coating metallic thin films on the inner walls of air-holes and infiltrating them with analyte, by partially removing fiber cladding [3], [5] and coating the interior of its air-holes, or by coating the surface of the PCF so that the analyte can be poured directly on top.

The operating principles of PCF-based plasmonic multiparameter sensors for refractive index, temperature, magnetic fields, and strain are premised on two major mechanisms, the first of which is based on the principle of direct RI sensing [6]. Usually, a calculated portion of the fiber's cladding is removed from a section of the fiber and a plasmonic film is sputtered onto the exposed segment of the core. The plasmonic excitation may take place within the cladding capillaries [7] or around [8] the fiber to give rise to the SPP modes. The propagation of the SPP modes at the metallo-dielectric interfacial boundary is described by the Helmholtz equation [9].



The second scenario is based on the principle of transduction, where additional quantities such as temperature, and magnetic field, are sensed via a functional or smart material. In this arrangement, one or several air holes in the PCF cladding are infiltrated with a functional or smart material such as toluene, chloroform, benzene, carbon disulfide, hydrogel, or other organic liquid mixtures [10] for sensing additional parameters.

### **3. Problem Statement**

Current techniques for detecting multiple parameters in plasmonic PCF sensors mostly employ multi-peak tracking on confinement loss spectrographs [11]. However, during multiple peak monitoring, some peaks on confinement loss spectrographs are frequently not well defined [12], [13], leading to confusion during the monitoring process. Additionally, this technique slows down the measurement process when the resonance peaks are separated by several wavelengths. Additionally, potential errors are likely when using large wavelength steps in tracking the phase-matching points. On the other hand, it was recently suggested that individual plasmon modes can be hybridized into cooperative plasmonic [14] modes to allow strongly guided modes to couple to several localized plasmonic modes for multiple parameter sensing.

### **4. Objectives of the research**

The main objective of this research is to design and fabricate a plasmonic PCF multiparameter sensor for determining refractive index, temperature, magnetic fields, and strain for lab-on-a-fiber applications. The specific objectives are:

- i.* To design a plasmonic PCF multiparameter sensor for measuring refractive index, temperature, magnetic fields, and strain. The modal characteristics, wavelength, and amplitude sensitivities, as well as sensor resolutions will be computed. The concept of cooperative plasmons will be explored as part of this objective.
- ii.* To fabricate the designed plasmonic PCF multiparameter sensor for determining refractive index, temperature, magnetic fields, and strain variations.

### **5. Methodology**

The methodology to be adopted in this research is explained as follow:

**The finite element method (FEM):** The design and numerical analysis are based on the finite element method (FEM). The FEM will be used to investigate the propagation characteristics and indexes of the core-guided and plasmonic modes. FEM applies the division of the PCF cross-section into homogenous subspaces of meshes within which Maxwell's equations are solved using applicable boundary conditions.

The Maxwell's equations are a set of coupled partial differential equations that work together to provide a mathematical model for electrical magnetic and optical behavior in various waveguiding domains. The FEM is well-implemented in the Comsol Multiphysics® software. The software runs the finite element analysis together with adaptive meshing and error control using a variety of techniques. Hence, the FEM will be used to investigate the propagation characteristics and indexes of the fiber modes.

**Perfectly matched layers:** The PML, which is available in the Comsol Multiphysics® software is commonly used to truncate computational areas in numerical methods when simulating problems based on propagating waves.

**Fabrication method:** The PCF for the sensors will be fabricated via the stack-and-draw technology. The coating of plasmonic materials will be accomplished by the plasma-enhanced chemical vapor deposition (PECVD) process, while the infiltration of the transduction materials will be achieved by micro pumping, or capillary motion. The fabrication facilities are available at our partner institution- the University of Cambridge, UK.

## 6. Outcome

A plasmonic photonic crystal fiber multiparameter sensor for refractive index, temperature, magnetic fields, and strain for lab-on-a-fiber applications potentially presents the following advantages: increased portability, ease of operation, low sample consumption, fast assaying time, label-free platform, high sensitivity and high resolution, remote sensing capabilities, robustness and compactness, low-cost, multi-analyte detection capability, and a means for providing real-time results [15]. At the same time, the sensor is not susceptible to electromagnetic interference and has high biocompatibility. Ultimately, sensor has a broad application range and will be relevant to the health sector, food industry, pharmaceutical industry, research in life sciences and related industries.

## WORK PLAN

Date	Task	Comments
01/12/2022	Model, design and perform simulation and optimization	Comsol Multiphysics® will be used
15/01/2023	Analysis of simulation results and calculation of theoretical sensing metrics	
15/2/2023	Preliminary arrangements towards sensor fabrication	Travel to fabrication facility
01/03/2023	Fabrication of the plasmonic PCF multiparameter sensor	
29/06/2023	Testing sensor and benchmarking with simulated results	

## 7. Impact

Plasmonic PCF multiparameter sensors are preferred over conventional, multiplexed, and cascaded sensors for medical, biochemical, and related analysis [16]. This is because plasmonic PCF multiparameter sensors combine low-cost, compactness, high sensitivity for real-time parallel and distributed sensing capabilities [17]. Additionally, plasmonic PCF multiparameter sensors are in high demand for lab-on-a-fiber and similar applications [2], [4]. The outcome of this research can potentially advance the functionality and performance of lab-on-a-fiber and micro total analysis devices. Furthermore, the outcome of this research can be applied to develop multiparameter sensors for different applications for structural health monitoring, environmental engineering, embedded systems, consumer electronics, and so on.

## 8. Budget

The budget for completing the project is outlined as follows:

	<b>Budget item</b>	<b>Description</b>	<b>Amount</b>	<b>Sub-Total</b>
<b>1</b>	<b><i>Personnel related expenses</i></b>			
	Remuneration for Project Team		\$20,000	
	<b>Total expenses on personnel</b>			<b>\$20,000</b>
<b>2</b>	<b>Capital Asset/Equipment</b>			
	Computers for PI and Co-PI	4 HP ENVY Laptops 17” Printer, Internet Subscription, Routers and other computing accessories.	\$ 14,000	
	Comsol Multiphysics® 6.0 software license	Cost of simulation software license	\$4,000	
	OriginPro® 2022b software	Cost of graphical and data analysis software license	\$2,000	
	Fabrication of multiparameter sensor	Cost of components and fabrication	\$20,000	
	<b>Total Capital Asset/Equipment cost</b>			<b>\$40,000</b>
<b>3</b>	<b>Travel</b>			
	Transportation, accommodation, and meals)	Travelling and related cost for two investigators	\$30,000	<b>\$30,000</b>
	Overhead @ 10%			<b>\$10,000</b>
	<b>GRAND TOTAL</b>			<b>\$100,000</b>

## PROJECT PERSONNEL

1. Dr. Owusu Nyarko-Boateng (PI) - University of Energy and Natural Resources
2. Ing. Dr. Iddrisu Danlard (Co-PI) – Sunyani Technical University
3. Ing. Professor Emmanuel Kofi Akowuah – Kwame Nkrumah University of Science and Technology
4. Dr. Prince Bawuah – University of Cambridge

## 5. Dr. Benjamin Asubam Weyori - University of Energy and Natural Resources

### References

---

- [1] A. D. Sheehan, J. Quinn, S. Daly, P. Dillon, and R. O’Kennedy, “The development of novel miniaturized immuno-sensing devices: A review of a small technology with a large future,” *Anal. Lett.*, vol. 36, no. 3, pp. 511–537, 2003.
- [2] R. Keçili, S. Büyüktiryaki, and C. M. Hussain, “Micro total analysis systems with nanomaterials,” *Handb. Nanomater. Anal. Chem. Mod. Trends Anal.*, pp. 185–198, 2019.
- [3] D. F. Santos, A. Guerreiro, and J. M. Baptista, “New SPR PCF D-type optical fiber sensor configuration for refractive index measurement,” *IEEE Sens. J.*, vol. 15, no. 10, p. 96346Z, 2015.
- [4] A. J. Qavi, A. L. Washburn, J. Byeon, and R. C. Bailey, “Label-free technologies for quantitative multiparameter biological analysis,” *Anal. Bioanal. Chem.*, vol. 394, no. 1, pp. 121–135, May 2009.
- [5] A. A. Rifat *et al.*, “Photonic crystal fiber based plasmonic sensors,” *Sensors Actuators, B Chem.*, vol. 243, pp. 311–325, May 2017.
- [6] G. An, X. Hao, S. Li, X. Yan, and X. Zhang, “D-shaped photonic crystal fiber refractive index sensor based on surface plasmon resonance,” *Appl. Opt.*, vol. 56, no. 24, pp. 6988–6992, 2017.
- [7] S. Silva, P. Roriz, and O. Frazão, “Refractive Index Measurement of Liquids Based on Microstructured Optical Fibers,” *Photonics*, vol. 1, no. 4, pp. 516–529, 2014.
- [8] S. Wang, X. Sun, and G. Peng, “Surface plasmon resonance sensor based on D-shaped dual-core photonic crystal fiber,” in *Advanced Photonics 2018 (BGPP, IPR, NP, NOMA, Sensors, Networks, SPPCom, SOF)*, 2018, no. Optical Society of America, p. JTu2A.56.
- [9] L. Rindorf and O. Bang, “Sensitivity of photonic crystal fiber grating sensors: biosensing, refractive index, strain, and temperature sensing,” *J. Opt. Soc. Am. B*, vol. 25, no. 3, p. 310, 2008.
- [10] Y. Peng, J. Hou, Z. Huang, and Q. Lu, “Temperature sensor based on surface plasmon resonance within selectively coated photonic crystal fiber,” *Appl. Opt.*, vol. 51, no. 26, pp. 6361–6367, 2012.
- [11] C. Lin *et al.*, “Liquid modified photonic crystal fiber for simultaneous temperature and strain measurement,” *Photonics Res.*, vol. 5, no. 2, p. 129, Apr. 2017.

## **EXECUTIVE SUMMARY**

### **Reducing and Preventing Airborne Diseases Transmission in Healthcare, Educational and occupational environments.**

Dr. Ing. Pablo Fredes Donoso <sup>1</sup>

One of the Sustainable Development Goals declared by the UN currently in force is to guarantee a healthy life and promote well-being for all at all ages. An innovative, effective and multidisciplinary project, for the reduction and prevention of airborne disease transmission, based mainly on implementation of Ultraviolet Germicidal Radiation (UV-C) air disinfection devices is presented. This project have a key focus on Hospital Acquired Infections (HAIs)<sup>2</sup> and will be extended to other fields such as occupational, educational and other public indoor places, where a large number of persons congregates. The outcomes are the reductions of the number of infection diseases in the people, with high potential to save lives.

Today it is clear that reducing or preventing the Hospital Acquired Infections (HAIs), specifically airborne diseases transmission including SARS-CoV-2, is a critical and unprecedented global challenge. The U.S. Centers for Disease Control and Prevention (CDC) and the World Health Organization (WHO) continuously monitor and work to prevent HAIs because they are a critical threat to patient safety and global health security<sup>3</sup>. While previous studies by healthcare providers have estimated an economic burden of approximately \$10 billion annually for HAIs, a more contemporary examination of the impact of societal costs included the economic value of mortality risk reductions, thereby giving an estimate for the total economic burden to society in excess of \$200 billion annually.

An innovative and effective preventive action is the application of UV-C to the air flowing through UV-C Devices. Considering that a great offer in the global market of many types of UV-C air disinfection devices is available today, it becomes necessary to define clear evidence and scientific information that may contribute to a generalized, effective and secure use of the proposed solution.

The objective is the development and implementation of the Big Multidisciplinary Project to obtain real and empirical evidence of the impact of the correct use of the UV-C disinfection technologies. The enormous task includes actualization of protocols, i.e. cleaning and disinfection, a rigorous tracing of epidemiological statistics and an interdisciplinary basis following the coordination of a correct execution of the required task to complete the goals.

This evidence will be obtained from different interconnected fields, as epidemiological analysis, air treatment engineering, physical and radiometric analysis, biosecurity and healthcare considerations and microbiologist analysis. This methodology will allow implementing the best option according to the physical characteristics of the space, number of persons, the ventilation situation and specific disinfection levels required.

---

<sup>1</sup> CEO and founder of Hydraluvx Spa, [www.HYDRALUVX.com](http://www.HYDRALUVX.com), Staff member of the Optics and Semiconductors Laboratory, Physics Department, Universidad de Santiago de Chile.

<sup>2</sup> <https://www.usach.cl/news/grupo-estudiantes-osa-usach-dona-dispositivos-medicos-desinfeccion-uv-al-hospital-sotero-del>

<sup>3</sup> Poster DL, Miller CC, Martinello RA, et al. Ultraviolet radiation technologies and healthcare-associated infections: Standards and metrology needs. J Res Natl Inst Stand Technol. 2021;126(126014):1-33. doi:10.6028/JRES.126.014

# Reducing and Preventing Airborne Diseases Transmission in Healthcare, Educational and occupational environments

Dr. Ing. Pablo Fredes Donoso <sup>i</sup>

## Abstract

An innovative, effective and multidisciplinary project, for the reduction and prevention of airborne disease transmission, based mainly on implementation of UV-C air disinfection devices is presented. This project have a key focus on Hospital Acquired infections (HAIs) and will be extended to other fields such as occupational, educational and other public indoor places, where a large number of persons congregates. The outcomes are the reductions of the number of infection diseases in the people, with high potential to save lives.

## Introduction

One of the Sustainable Development Goals declared by the UN currently in force is to guarantee a healthy life and promote well-being for all at all ages<sup>1</sup>.

Today it is clear that reducing or preventing the Hospital Acquired Infections (HAIs), specifically airborne diseases transmission including SARS-CoV-2, is a critical and unprecedented global challenge. This challenge is extended to other fields such as occupational, educational and other public indoor places, where a large number of persons congregates<sup>2,3,4</sup>. The public outbreak of SARS-CoV-2 and the efficiency of transmission for any respiratory virus have important implications for containment and mitigation strategies<sup>5</sup>. COVID-19 is not only a new biological concern<sup>6</sup>, it has substantially impacted traditional HAIs surveillance and prevention efforts<sup>7</sup>. The U.S. Centers for Disease Control and Prevention (CDC) and the World Health Organization (WHO) continuously monitor and work to prevent HAIs because they are a critical threat to patient safety and global health security<sup>3</sup>.

This placed HAIs as the eighth leading cause of death in the United States, just after diabetes (79,535 deaths)<sup>8</sup>. While previous studies by healthcare providers have estimated an economic burden of approximately \$10 billion annually for HAIs, a more contemporary examination of the impact of societal costs included the economic value of mortality risk reductions, thereby giving an estimate for the total economic burden to society in excess of \$200 billion annually<sup>3,9,10</sup>.

## Problem: Airborne transmission diseases

According to the work of Wang et al. entitled “Airborne transmission of respiratory viruses”, which has been published by *Science* in August of 2021. Airborne transmission of pathogens has been vastly underappreciated, we must acknowledge that airborne transmission is much more prevalent than previously recognized and eventually understood. Given all that we have learned about SARS-CoV-2 infection, the aerosol transmission pathway needs to be reevaluated for **all respiratory infectious diseases** implying long and complex experimental procedures. Additional precautionary measures must be recognized and implemented for mitigating aerosol transmission, with particular attention inter alia, to ventilation, airflows, air filtration and UV-C disinfection. The interventions with UV-C air disinfection devices are critical tools for ending the current pandemic and preventing future outbreaks<sup>11</sup>.

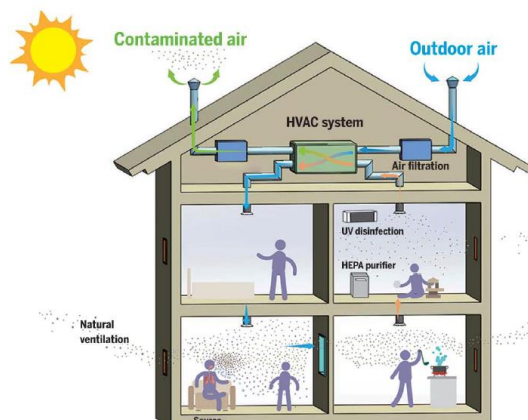
The current global pandemic shows that the high levels of SARS-CoV-2 transmission have overwhelmed national healthcare systems resulting in millions of deaths and caused long term health problems. Meanwhile, the impact on the global economy has been, and will continue to be,

---

<sup>i</sup> CEO and founder of Hydraluvx Spa, [www.HYDRALUVX.com](http://www.HYDRALUVX.com), Staff member of the Optics and Semiconductors Laboratory, Physics Department, Universidad de Santiago de Chile.



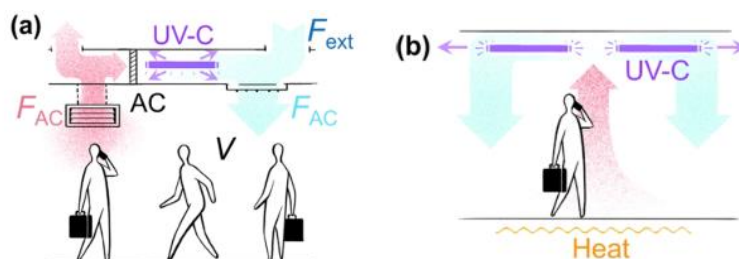
devastating, which in turn has resulted in further welfare and public health issues<sup>4</sup>. Figure 1 shows that the risk of airborne transmission increases in indoor environments where large groups of people congregate, especially when the environment is poorly ventilated.



**Figure 1**, Factors affecting indoor airborne transmission. Whereas the motion of large droplets is predominantly governed by gravity, the movement of aerosols is more strongly influenced by airflow direction and pattern, type of ventilation, and air filtration and disinfection. (Source: Wang et al., Science 373, eabd9149 (2021).)

### UV-C Technologies

The adoption of additional measures to reduce airborne diseases propagation in different levels according to specific needs and places is an urgent task. An innovative and effective preventive action is the application of Ultraviolet Germicidal Radiation (UV-C) to the air flowing through specific UV-C devices. The correct implementation is based on a rigorous methodology that considers, optical and geometrical features of the UV-C sources and the lethal UV-C Dose required for every microbiological target (microbiological threats). The applied UV-C dose refers to the germicidal energy applied to a sample with a specific wavelength  $\lambda$  in the ultraviolet range. The unit for the UV-C dose (i.e., the UV radiant exposure) is Joules per square meter ( $J/m^2$ ), but millijoules per square centimeter ( $mJ/cm^2$ ) is commonly used.



**Figure 2**, Reduction of viral spread through UV-C light. (a) UV-C sources placed inside air-conditioning (AC) ducts. (b) UV-C collimated wallpaper ceiling illumination combined with temperature-driven air circulation. (Source: ACS Nano 2020, 14, 7704–7713)

### How is UV-C produced?

Artificial UV light is produced primarily from plasma discharge lamps and UV-C light-emitting diodes (UV-C LEDs), as well as unintentional emissions from activities such as welding. Plasma discharge lamps contain a gas mixture enclosed inside a glass tube. As a voltage is applied to the lamp filament, electrons within the enclosed gas are excited to a higher energy state; as they fall back to the ‘ground’ state, they release that extra energy as a photon. Common plasma discharge

lamps include mercury vapor lamps, metal halide lamps, xenon lamps (pulsed UV-C), excimer, and other gas-based lamps.

On the other hand, the Ultraviolet light emitting diodes (UV-C LEDs) are solid-state semiconductor devices. With an applied voltage, electrons are 'pushed' across an energy barrier (band gap) separating differently charged layers within the LED crystal structure. Once across the barrier, these electrons can lose the energy gained in the transition and emit a photon. Commercial UV LEDs are formed with thin crystalline aluminum gallium nitride (AlGaN) layers deposited onto a substrate (sapphire or aluminum nitride); while the ratio of aluminum to gallium in the thin layers determines the band gap and therefore the emission spectrum emitted by the LED<sup>12,13</sup>.

### **How UV-C disinfect?**

Ultraviolet radiation in the range 225–302 nm is lethal to microorganisms and is referred to as ultraviolet germicidal irradiation OR UV-C. Germicidal radiation has been applied in sterilization for over a century, including in the treatment of the disease lupus vulgaris<sup>14</sup>, for which Niels Ryberg Finsen received the Nobel Prize in Medicine in 1903. Each wavelength (225-302 nm) can alter the DNA structure of microorganism and is referred to as a biophotochemical reaction<sup>15</sup>. If the amount of radiation and the exposition time is adequate (germicidal dose) then it becomes possible to break the DNA structure which in turn then implies that the microorganism cannot be replicated and cannot cause further damage<sup>16</sup>.

### **UV-C air disinfection devices**

Early studies (1942) had already shown the benefits of using UV-C irradiation to prevent the spread of measles in rural schools<sup>17</sup>. Air disinfection with UV-C are proven and reliable technologies, but airstream disinfection systems have had varying and unpredictable performance in applications<sup>18</sup>. In spite of the widespread use of UV-C today for air disinfection and microbial growth control, design information about the effects of UV-C on airborne pathogens lacks the detail necessary to guarantee predictable performance. In addition, few airborne rate constants are known with certainty due to the inherent difficulties of setting up an experiment and accurately interpreting test results<sup>19</sup>.

### **Objectives**

Considering that a great and variable offer of disinfection models of air disinfection devices based on UV-C is available today, it becomes necessary to define clear evidence and scientific information that may contribute to a generalized use of the solution. The objective is the development and implementation of the Big Multidisciplinary Project to obtain real and empirical evidence of the impact of the correct use of the UV-C disinfection technologies. This evidence will be obtained from different but interconnected focus, as epidemiological analysis, air treatment engineering, physical and radiometric analysis, biosecurity and healthcare considerations and microbiologist analysis. This methodology will allow implementing the best option according to the physical characteristics of the space and number of participating individuals depending all on the ventilation situation, which will define the parameters of the present research.

### **Methodology**

Leading investigations will establish the intervention of UV-C Technology supported by an increasing number of medical environments allowing the decrease of infections. The enormous task includes actualization of protocols, i.e. cleaning and disinfection, a rigorous tracing of epidemiological statistics and an interdisciplinary basis following the coordination of a correct execution of the required study.

### **Previous stage**

Acquisition of various air disinfection devices offered in the market based on three types of UV-C sources, discharge lamps, UV-C LEDs and far UV LEDs.

### **Stage 1**

1. Identification of the number of closed spaces, which satisfy the necessary conditions for the study.
2. A methodology satisfying the inclusion and exclusion criteria referring to the spaces, considering the ventilation level, volume capacity etc. Finally, the amount of disinfection levels required for each selected space.

### **Stage 2**

1. Installation of air disinfection devices based on UV-C, In the specific environment places selected.
2. Verification of the Photo biological safety of the systems based on IEC 62471:2006 and other related normative.

### **Stage 3**

1. Estimation of effectiveness with bio aerosols samples.
2. Developing of Reports to publish in an appropriate journal of the area.

### **Final Stage**

Original design of optimal devices, effectiveness and reliability for air disinfection. The goal is to promote the massive use in critically and risk environments referring to air disinfection, which will reduce infections and hence potential death rate in a medium and long term.

### **References**

1. Lauren Barredo, Irene Agyepong, Gordon Liu SR. Goal 3—The SDGs and a Healthier 2030. Beyond 2015. Published 2015. <https://www.un.org/en/chronicle/article/goal-3-sdgs-and-healthier-2030>
2. Poster DL, Martinello RA, Miller CC, Obeng Y, Postek MT, Cowan TE. Innovative approaches to combat healthcare-associated infections using efficacy standards developed through industry and federal collaboration. *Proceeding SPIE Int Soc Opt Eng 2018*. Published online 2018:55. doi:10.1117/12.2500431
3. Poster DL, Miller CC, Martinello RA, et al. Ultraviolet radiation technologies and healthcare-associated infections: Standards and metrology needs. *J Res Natl Inst Stand Technol*. 2021;126(126014):1-33. doi:10.6028/JRES.126.014
4. Eadie E, et al. Far-UVC (222 nm) efficiently inactivates an airborne pathogen in a room-sized chamber. *Sci Rep*. 2022;12(1):1-9. doi:10.1038/s41598-022-08462-z
5. Fauci AS, Lane HC, Redfield RR. Covid-19 — Navigating the Uncharted. *N Engl J Med*. 2020;382(13):1268-1269. doi:10.1056/nejme2002387
6. Hartnett KP, Kite-Powell A, DeVies J, et al. Impact of the COVID-19 pandemic on emergency department boarding. *Acad Emerg Med*. 2021;28(SUPPL 1):S218-S219. <http://ovidsp.ovid.com/ovidweb.cgi?T=JS&PAGE=reference&D=emed22&NEWS=N&AN=635077588>
7. Stevens MP, Doll M, Pryor R, Godbout E, Cooper K, Bearman G. Impact of COVID-19 on traditional healthcare-associated infection prevention efforts. *Infect Control Hosp Epidemiol*. 2020;41(8):946-947. doi:10.1017/ice.2020.141

8. Murphy SL, Xu J, Kochanek KD, Curtin SC, Arias E. Deaths: Final data for 2015. *Natl Vital Stat Reports*. 2017;66(6). doi:10.1136/vr.h753
9. Scott RD, Culler SD, Rask KJ. Understanding the economic impact of health care-associated infections: A cost perspective analysis. *J Infus Nurs*. 2019;42(2):61-69. doi:10.1097/NAN.0000000000000313
10. Poster DL, Postek MT, Obeng YS, et al. Models for an Ultraviolet-C Research and Development Consortium. *J Res Natl Inst Stand Technol*. 2021;126(126055):1-33. doi:10.6028/jres.126.055
11. Wang CC, Prather KA, Sznitman J, et al. Airborne transmission of respiratory viruses. *Science (80- )*. 2021;373(6558). doi:10.1126/science.abd9149
12. Shur MS, Gaska R, Member S. Deep-Ultraviolet Light-Emitting Diodes. *IEEE Trans Electron Devices*. 2010;57(1):12-25.
13. Shatalov M, Sun W, Jain R, et al. High power AlGaIn ultraviolet light emitters. *Semicond Sci Technol*. 2014;29(8):8-13. doi:10.1088/0268-1242/29/8/084007
14. Finsen N. *Phototherapy*. (Royal College of Physicians Edinburgh, ed.). Wellcome Collection UK; 1904. <https://wellcomecollection.org/works/ju88nrgq>
15. Schreier WJ, Schrader TE, Koller FO, et al. Thymine dimerization in DNA is an ultrafast photoreaction. *Science (80- )*. 2007;315(5812):625-629. doi:10.1126/science.1135428
16. Bolton JR, Mayor-Smith I, Linden KG. Rethinking the Concepts of Fluence (UV Dose) and Fluence Rate: The Importance of Photon-based Units - A Systemic Review. *Photochem Photobiol*. 2015;91(6):1252-1262. doi:10.1111/php.12512
17. Wells WF, Wellsi MW, Wilder TS. The environmental control of epidemic contagion: I. An epidemiologic study of radiant disinfection of air in day schools. *Am J Epidemiol*. 1942;35(1):97-121. doi:10.1093/oxfordjournals.aje.a118789
18. Reed NG. The history of ultraviolet germicidal irradiation for air disinfection. *Public Health Rep*. 2010;125(1):15-27. doi:10.1177/003335491012500105
19. Kowalski WJ, Bahnfleth WP, Witham DL, Severin BF, Whittam TS. Mathematical modeling of ultraviolet germicidal irradiation for air disinfection. *Quant Microbiol*. 2000;2(3):249-270. doi:10.1023/A:1013951313398

**Executive summary of the proposal titled  
“Transfer to circular economy by fiber optic sensor monitoring of waste containers”  
for the Optica Foundation 20th Anniversary Challenge**

Rapidly increasing generation of the municipal solid waste (MSW) is an environmental problem, which can be observed for at least 50 years. The MSW is considered as waste that comes from households, but also businesses, schools and institutions. It is caused by multitude of factors, including improper waste management, urbanization and population growth, economic development and many others. Globally, the MSW amounts to over 2 billion tons per year.

Proper disposal of the MSW includes keeping it in the secure areas, preventing the leakage and spreading of waste, limiting concentration of gases. Limited space in the residential areas force the development of various techniques of waste collection and treatments. One of such solution was implementation of underground and semi-underground waste containers, which help limit the odors, make public spaces cleaner and make easier to collect and transport the waste. However, it does not solve the main issue related to the circular economy, such as reduction of waste, limitation of gas emission, waste management efficiency and possibility of spontaneous combustion.

Therefore, the aim of this project is to design the fiber-optic sensor system and embed it in the aforementioned containers to allow for real-time monitoring. The task of the sensor system will serve as:

- monitoring the level of collected waste inside the container,
- detection of the container leakage,
- detection of the emission of volatile organic compound (VOC),
- monitoring the temperature and humidity inside the containers,
- monitoring the proper closure of the container lid.

The sensors will be functionalized to increase their specificity and ensure proper operation (e.g., ZnO coating for temperature monitoring, microsphere structure as a probe).

Application of the presented fiber-optic sensor system will reduce the dangers to the environment immensely. The outcome fiber-optic sensor system will help transfer to circular economy by improving in the monitoring capabilities of the waste containers and in turn the environment and reduction of the release of dangerous byproducts resultant from waste decomposition and energy necessary for waste management, therefore improving its safety and quality.

**Proposal titled**  
***“Transfer to circular economy by fiber optic sensor monitoring of waste containers”***  
**for the Optica Foundation 20<sup>th</sup> Anniversary Challenge**

1. Problem Statement/Objective

Rapidly increasing generation of the municipal solid waste (MSW) is an environmental problem, which can be observed for at least 50 years. The MSW is considered as waste that comes from households, but also businesses, schools and institutions. It is caused by multitude of factors, including improper waste management [1], urbanization [2] and population growth [3], economic development [4] and many others. According to the United States Environmental Protection Agency (EPA) in 2018, the United States generated over 250 million tons of the MSW, of which only about a third was recycled or composted [5]. Furthermore, in 2020 European Union generated 225 million tones [6], while the Association of Southeast Asia recorded over 150 million tons [7]. Globally, the MSW amounts to over 2 billion tons per year [8]. The problem was not helped by an ongoing COVID-19 pandemic, which in the last two and a half years caused generation of additional 87000 tons of waste just from personal protective equipment, according to the WHO.

Unfortunately, regardless of the source, the accumulation of the solid waste also brings drastic effects and consequences to the environment. Starting with air pollution and the effect on the atmosphere, the decaying waste produces toxic gases during the chemical and biological processes [9,10]. Those gases are released to the air, impacting its quality and trapping solar radiation. Another way, in which the environment is impacted is by spoilage of ground [11] and contaminating the groundwaters [12,13]. During the decomposition of the waste, the emerging substances are leaking and seeping into the ground, firstly saturating it with potentially poisonous chemicals, rendering it unusable followed by carrying it into underground water and providing the incubation for various bacteria [14] and allowing the spread of diseases . A consequence of the previously mentioned gas release is also increased risk of a fire [15,16]. Depending on the temperature and humidity of the accumulated waste, the amount of the gas, pressure can lead to easy ignition of the flame. Once it starts burning, the waste itself act as a kindling, making it difficult to put out.

Proper disposal of the MSW includes keeping it in the secure areas, preventing the leakage and spreading of waste, limiting concentration of gases. Limited space in the residential areas force the development of various techniques of waste collection and treatments. One of such solution was implementation of underground and semi-underground waste containers, which help limit the odors, make public spaces cleaner and make easier to collect and transport the waste. However, it does not solve the main issue related to the circular economy, such as reduction of waste, limitation of gas emission, waste management efficiency and possibility of spontaneous combustion.

Therefore, the aim of this project is to design the fiber-optic sensor system and embed it in the aforementioned containers to allow for real-time monitoring. The task of the sensor system will serve as:

- monitoring the level of collected waste inside the container,
- detection of the container leakage,
- detection of the emission of volatile organic compound (VOC),
- monitoring the temperature and humidity inside the containers,
- monitoring the proper closure of the container lid.



The sensors will be functionalized to increase their specificity and ensure proper operation (e.g., ZnO coating for temperature monitoring, microsphere structure as a probe).

## 2. Outline of tasks/Work Plan

The research project is planned to be executed over the duration of 2 years. To achieve the objective of the project, research and engineering tasks have been established. There are three primary parts of the research plan, i.e., the development and optimization of the fiber-optic sensor system; the establishment of the research methods and instruments; analysis and interpretation of obtained data. Each part is further divided into detailed tasks, which must be completed:

- A. Design of the fiber-optic sensors
- B. Fabrication of the fiber-optic sensors
- C. Validation of the fiber-optic sensors
- D. Consolidation of the sensors into one system
- E. Validation of the sensor system
- F. Design of the data acquisition and analysis method
- G. Optimization of the sensor system
- H. Embedding the fiber-optic sensor system into the waste containers
- I. Execution of measurements in real-life conditions
- J. Verification of the proper operation of the sensor system
- K. Analysis of the data obtained from the measurements

The estimated schedule is presented in the Gantt chart in table 2.

Table 1. Gantt chart

	Month																							
	1	2	3	4	5	6	7	8	9	10	11	12	13	14	15	16	17	18	19	20	21	22	23	24
A	█	█	█	█	█	█	█																	
B					█	█	█	█	█															
C						█	█	█	█	█	█													
D										█	█	█	█	█										
E												█	█	█	█									
F															█	█								
G													█	█	█	█	█	█	█	█	█			
H																█	█	█	█	█				
I																		█	█	█	█	█	█	
J																							█	█
K							█	█	█	█	█	█	█	█	█	█	█	█	█	█	█	█	█	█

Progression of the research conducted so far, allows to assume low risk of failure onward. Possible delays are the result of systematic risk and will be resolved if they occur. Potential risks were assessed and presented in table 2.

Table 2. Risk assessment

Risk	Risk	Possible solutions
------	------	--------------------

	level	
Troubles with cooperation due to unforeseen world events	medium	<ul style="list-style-type: none"> <li>• Change in cooperation methods depending on available possibilities</li> </ul>
Damage of the equipment used during the research	low	<ul style="list-style-type: none"> <li>• Reconfiguration of the system, using substitute equipment</li> <li>• Equipment replacement</li> </ul>
Sample damage or loss in transportation	low	<ul style="list-style-type: none"> <li>• Proper safeguarding the samples during transportation</li> <li>• Production of new samples</li> <li>• Posting samples in several, separate batches</li> </ul>
Proper integration of the samples with waste containers	medium	<ul style="list-style-type: none"> <li>• Selection of different method of integration the fiber-optic sensor within waste containers</li> <li>• Selection of another type of a waste container to integrate with the fiber-optic sensor</li> <li>• Optimization of the sensor</li> </ul>
Proper application of selected functionalization materials as a coating on the surface of an optical structure	low	<ul style="list-style-type: none"> <li>• Selection of another material</li> <li>• Application of the coating by a different method</li> </ul>

### 3. Outcomes and Impact

Application of the presented fiber-optic sensor system will reduce the dangers to the environment immensely.

Firstly, the monitoring of the filling levels will result in preventing the overflowing of the waste outside the container, reducing transfer of the harmful substances into the environment. Furthermore, it will optimize waste pickup and facilitate dynamic collection, therefore allowing to determine optimal collection routes, which in turn will limit the pollution and energy related to transferring of the waste.

Secondly, the detection of the container leakage will ensure no dangerous substances and chemicals would be able to spill into the ground surrounding nor the underground water, which will preserve the aquatic and terrestrial wildlife.

Moreover, the detection of the emission of volatile organic compound (VOC) will allow to take steps in order to prevent the buildup of the excessive amounts. In this case, the probability of the combustion will be limited, preserving the potential damage to the surrounding area, including residential buildings as well as air quality.

The monitoring of the heat and humidity on one hand will signal the accumulation of the heat, which is also conducive to ignition of the fire, on the other hand it will indicate possible freezing. Freezing inside the container can lead to inability to empty it. By monitoring subzero temperatures, it will reduce energy required on waste collection.

Lastly, the monitoring of lid closure, would ensure the container is tightly sealed after each use and prevent the gases from being released into the environment, therefore improving air quality and minimizing the odors related to the decaying waste.

Overall, the impact of the proposed system will be improvement in the monitoring capabilities of the waste containers and in turn the environment and reduction of the release of dangerous byproducts resultant from

waste decomposition and energy necessary for waste management, therefore improving its safety and quality.

The properly operating fiber-optic sensor system for monitoring of the waste containers has also a lot of promise for future development and modification by automatizing it and making it fully self-sufficient. It also has a potential for easy commercial implementation. It is especially true, because the European Parliament intends to introduce environmentally sustainable, toxic-free fully circular economy by 2050, based on Ecodesign Directive. The system, which will be the result of this project will help to achieve those goals and will bring the society closer to the healthy and clean environment [17].

Furthermore, the MSW accounts for about tenth of the entire global waste, therefore successful execution of the project will provide possibility to apply the system to other types of waste, for example: hazardous waste, medical waste, combustible waste, which would give the society the tools needed to switch to circular economy even more.

#### 4. References

- [1] A. Singh, Solid waste management through the applications of mathematical models, *Resources, Conservation and Recycling*. 151 (2019) 104503. <https://doi.org/10.1016/j.resconrec.2019.104503>.
- [2] Y.-C. Chen, Effects of urbanization on municipal solid waste composition, *Waste Management*. 79 (2018) 828–836. <https://doi.org/10.1016/j.wasman.2018.04.017>.
- [3] Y. Ding, J. Zhao, J.-W. Liu, J. Zhou, L. Cheng, J. Zhao, Z. Shao, Ç. Iris, B. Pan, X. Li, Z.-T. Hu, A review of China's municipal solid waste (MSW) and comparison with international regions: Management and technologies in treatment and resource utilization, *Journal of Cleaner Production*. 293 (2021) 126144. <https://doi.org/10.1016/j.jclepro.2021.126144>.
- [4] Y.V. Vazquez, F. Barragán, L.A. Castillo, S.E. Barbosa, Analysis of the relationship between the amount and type of MSW and population socioeconomic level: Bahía Blanca case study, Argentina, *Heliyon*. 6 (2020) e04343. <https://doi.org/10.1016/j.heliyon.2020.e04343>.
- [5] O. US EPA, National Overview: Facts and Figures on Materials, Wastes and Recycling, (2017). <https://www.epa.gov/facts-and-figures-about-materials-waste-and-recycling/national-overview-facts-and-figures-materials> (accessed September 12, 2022).
- [6] Municipal waste statistics, (2021). [https://ec.europa.eu/eurostat/statistics-explained/index.php?title=Municipal\\_waste\\_statistics](https://ec.europa.eu/eurostat/statistics-explained/index.php?title=Municipal_waste_statistics) (accessed September 13, 2022).
- [7] Waste Management in ASEAN Countries. Summary Report, (2017). [https://wedocs.unep.org/bitstream/handle/20.500.11822/21134/waste\\_mgt\\_asean\\_summary.pdf?sequence=1&isAllowed=](https://wedocs.unep.org/bitstream/handle/20.500.11822/21134/waste_mgt_asean_summary.pdf?sequence=1&isAllowed=) (accessed September 13, 2022).
- [8] Trends in Solid Waste Management, (n.d.). [https://datatopics.worldbank.org/what-a-waste/trends\\_in\\_solid\\_waste\\_management.html](https://datatopics.worldbank.org/what-a-waste/trends_in_solid_waste_management.html) (accessed September 13, 2022).
- [9] D. Majumdar, S. Ganguly, Air Pollution from Municipal Solid Waste Management Techniques, in: S.K. Ghosh (Ed.), *Waste Management and Resource Efficiency*, Springer, Singapore, 2019: pp. 1115–1132. [https://doi.org/10.1007/978-981-10-7290-1\\_92](https://doi.org/10.1007/978-981-10-7290-1_92).
- [10] Q. Zhou, J. Yang, M. Liu, Y. Liu, S. Sarnat, J. Bi, Toxicological Risk by Inhalation Exposure of Air Pollution Emitted from China's Municipal Solid Waste Incineration, *Environ. Sci. Technol.* 52 (2018) 11490–11499. <https://doi.org/10.1021/acs.est.8b03352>.
- [11] H.I. Abdel-Shafy, M.S.M. Mansour, Solid waste issue: Sources, composition, disposal, recycling, and valorization, *Egyptian Journal of Petroleum*. 27 (2018) 1275–1290. <https://doi.org/10.1016/j.ejpe.2018.07.003>.
- [12] D. Zeng, G. Chen, P. Zhou, H. Xu, A. Qiong, B. Duo, X. Lu, Z. Wang, Z. Han, Factors influencing groundwater contamination near municipal solid waste landfill sites in the Qinghai-Tibetan plateau,

Ecotoxicology and Environmental Safety. 211 (2021) 111913.  
<https://doi.org/10.1016/j.ecoenv.2021.111913>.

- [13] S. Chakraborty, R.N. Kumar, Assessment of groundwater quality at a MSW landfill site using standard and AHP based water quality index: a case study from Ranchi, Jharkhand, India, *Environ Monit Assess.* 188 (2016) 1–18. <https://doi.org/10.1007/s10661-016-5336-x>.
- [14] U. Anand, B. Reddy, V.K. Singh, A.K. Singh, K.K. Kesari, P. Tripathi, P. Kumar, V. Tripathi, J. Simal-Gandara, Potential Environmental and Human Health Risks Caused by Antibiotic-Resistant Bacteria (ARB), Antibiotic Resistance Genes (ARGs) and Emerging Contaminants (ECs) from Municipal Solid Waste (MSW) Landfill, *Antibiotics (Basel)*. 10 (2021) 374. <https://doi.org/10.3390/antibiotics10040374>.
- [15] M. Yan, Antoni, J. Wang, D. Hantoko, E. Kanchanatip, Numerical investigation of MSW combustion influenced by air preheating in a full-scale moving grate incinerator, *Fuel*. 285 (2021) 119193. <https://doi.org/10.1016/j.fuel.2020.119193>.
- [16] D. Chavan, P. Lakshmikanthan, P. Mondal, S. Kumar, R. Kumar, Determination of ignition temperature of municipal solid waste for understanding surface and sub-surface landfill fire, *Waste Management*. 97 (2019) 123–130. <https://doi.org/10.1016/j.wasman.2019.08.002>.
- [17] EU waste management: infographic with facts and figures | News | European Parliament, (2018). <https://www.europarl.europa.eu/news/en/headlines/society/20180328STO00751/eu-waste-management-infographic-with-facts-and-figures> (accessed September 13, 2022).

### Executive Summary - Reduction Techniques for Dissipative Systems

Dissipative systems or dissipative solitons are complex dynamics that exist in physical and biological nature. Much of the rich dynamics exists beyond traditional mathematics. This dissipative soliton research discipline has been developed by world-leading Professors Nail Akhmediev and Adrian Ankiewicz, at the Australian National University (ANU). This makes the ANU the priority research facility to develop and drive this proposed research challenge.

Contemporary mathematical & scientific studies focus on conserved system models which can also have stochastic or statistical frameworks, and where the meaning of experimental data is determined empirically. These modeling frameworks are subject to entropy constraints. Entropy constraints are brought into focus by conserved system self-preserving dynamic objects called solitons. The self-preserving soliton dynamics in light-wave fiber communications have been seen to prolong the effects of entropy.

A deeper study of entropy constraints and their ‘elasticity’ may be explored deterministically with Prigogine’s ideas of reversibility and irreversibility on dissipative solitons and dissipative system models, which are self-organizing. *This is a crucial area of research that needs to be developed, not just across physics, but also in biophysics modeling for improved precision health medicines. This research may also assist in utilizing self-organizing quantitative economic frameworks to optimally deliver global clean climate environment initiatives*, in a symphony of support of key industry sectors, inclusive of OPTICA commercialization research projects.

**INFORMATION:** My dissertation on ‘extreme waves in dissipative systems’ is a fundamental road map focused on new laser signal developments with the master laser equation. This is an engineered technology described by a dissipative soliton equation. It borrows from the pattern dynamics of nature. In my PhD research studies, the ‘spiny solitons’ discovery holds applications to super-continuum generation and can be a serious attraction for commercialization. Analytical insights into the high-power ultra-short pulse characteristics of spiny solitons can advance technological laser limits and represent a fundamental challenge of importance in improving reduction technique methodologies. The significance of these techniques applied to the laser master equation is that it is based on the Ginzburg-Landau superconductivity formulations, applicable across general physics and that it can be adapted to numerous modified research and laser models. The application of new laser signal technologies is crucial across a plethora of industry commercialization sectors from laser research developments, data and storage information, industrial cutting, emerging augmented and holographic technologies, and also medical diagnostic tools and precision tools for non-invasive laser surgery.

**HEALTH:** Dissipative soliton system dynamics of nature can model biological processes that inherit self-organizing properties. Healthy biological processes maintain stable properties that may be ideally identified with analytical reduction techniques. Health complications can emerge when a biological process deviates from stability. Analytical dynamical insights to aid understanding of deterministic reversibility of the deviation path from order to disorder and vice versa are crucial to improving medical research. These reduction techniques may assist us to foster cross-disciplinary research discoveries, beyond current medical linear techniques and methodologies. To better guide precision medicine research. This may present to OPTICA new cross-disciplinary synergies, alongside medical laser research developments, especially to address recently-observed mortality concerns.

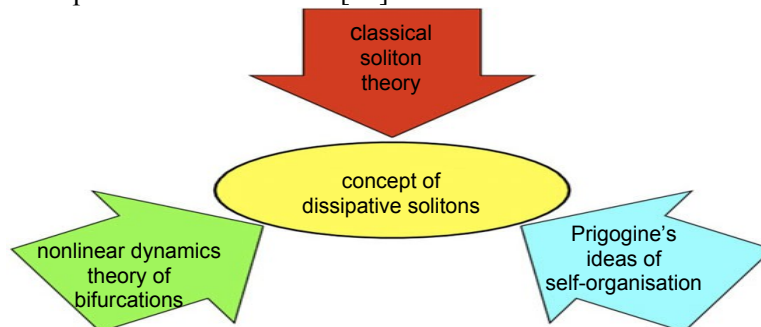
**ENVIRONMENT:** A stable climate offers health and longevity benefits. This challenge may *only* be achieved if the ‘accommodation’ of lasting co-operation between China and the United States is maintained. The need for this ‘accommodation’ is seriously expressed by professional politicians and strategists for geopolitical order. As a complex geopolitical dynamical system, the two existing superpowers, as the primary driving parameters, can maintain the most influential stabilizing geopolitical ‘soliton-type’ behaviors to best guarantee long-term financial investment and commercialization initiatives. My deep belief is that this ultimate challenge is of the highest importance, so that this must be secured. The international OPTICA community may play an important role by using fundamental research developments to strengthen national economies across the globe. This requires insightful initiatives of ‘accommodation’ for organized geopolitical financial security. In evolving financial market regimes, requires developing and extending new financial engineering models to better stabilize and secure investment strategies for global preservation of the environment and stable climate. These reduction techniques may aid in establishing new optimal financially engineered models for evolving market regimes.

*20th Anniversary Challenge Proposal applying to a) Information, b) Health and the c) Environment.*

This research task *may also* be linked to the Australian Research Council Discovery Early Career Award (DECRA23101101) ‘Applications of self-organizing dynamics’ *a pending* proposal.

*Proposal part a) Information : Reduction Techniques for Dissipative Systems*

**Literature Review:** Contemporary mathematics today is limited by a Partial Differential Equation (PDE) non-integrability ‘barrier’. The dissertation [1], essentially a didactic manuscript, demonstrates an efficient conceptual methodology investigating the Complex Ginzburg-Landau Equation (CGLE) / PDEs. It aligns 3.5 centuries of accumulated advancements concisely to aid investigations of PDE behaviors beyond non-integrable barriers. It is based on fundamental and theoretical foundations from Newton onwards. Which delivers numerical precision for a dissipative soliton or a dissipative system. An extensive chapter review [1] highlights the laser signal advancements and applications across physics and cross-disciplinary research fields. A conceptual framework (see Figure 1) establishes and defines the field of ‘dissipative solitons’ [13,14], especially for mode-locked lasers [1,16], which evolved from the concept of classical solitons [15].



**Figure 1:** Three sources and constituent parts of the concept of dissipative solitons [1,13,14]. Classic solitons are self-preserving phenomena of a conserved system. Non-linear dynamics theory explains the process into bifurcation, and into chaos. Prigogine's ideas of self-organisation balance energy and mass inflows with the localised surrounding environment. They describe systems that ‘live’, including living organisms.

The master laser equation can be revealed [1,15] as the well-known [17] cubic-quintic CGLE where it is used to define the self-preserving properties of dissipative solitons [1-12,13-16]. In essence, it may be viewed as the generalized cubic-quintic nonlinear Schrödinger wave equation with dissipative effects. Phenomenologically, the CGLE was developed in superconductivity [18] and has applications in modeling water-wave and light-wave dynamics across general physics [19].

A major advantage is that certain solution structures of complex self-organizing models can be explored mathematically with reduction techniques. One of my optical sciences group's research articles [20] received spotlight attention from *OPTICA for a journal article* using Lagrange methodologies to study dissipative systems. Lagrange methodologies, including the ‘method of moments’ [21], have been applied to the CGLE [22-26]. Both the Lagrange and ‘method of moments’ methodologies for the CGLE have been compared. They are identified to be in general agreement but do differ slightly with higher-order chirps [30]. The ‘method of moments’ technique has also been applied to the CGLE Dissipative Soliton Resonance (DSR) phenomena with success [25,26]. DSR can exist in both the anomalous [25-29] and normal [1ch3,10,25,26,29] dispersion regimes. From the guided analysis [25-29], experimental confirmations were revealed [31-34]. The DSR phenomenon, in a short time from theoretical discovery, developed into commercial applications with much attention.

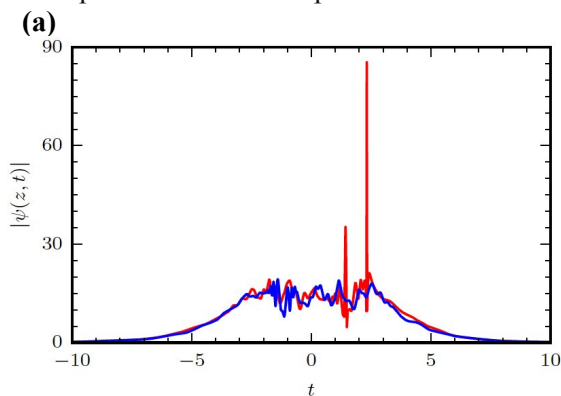
The Australian DECRA-230101106 initiative signifies the importance of an intensive catalog and classification of dissipative soliton solutions of the CGLE. It is evident that the numerical discoveries can be verified with the reduction techniques and their insights [20,22-26,30]. Both the proposed *OPTICA* reduction techniques and Australia's DECRA-230101106 project initiative, hold important implications related to early numerical nonlinear dynamic research conducted at Los Alamos research [35], where the embedding of the important properties of a class of solitary waves were later revealed [36].

This initial scientific inquiry led to establishing integrable non-linear techniques [37-39] as an evolved discipline. This discipline permitted theoretical frameworks across general and important areas of physics [40-43] to develop soliton fiber-optics and nonlinear laser technologies for commercialization opportunities. The goal is to persevere to pioneer discoveries of new non-

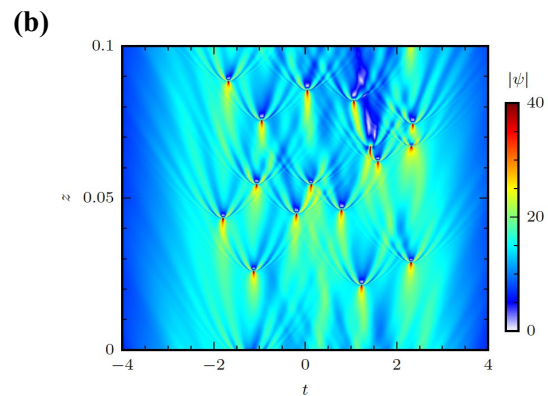


integrable PDE dissipative physics and improve on current techniques. The most inspiring insight that has emerged from my doctoral studies in self-organizing systems is a scope to develop a theoretical understanding of the emergence of order from an unstable far-from-equilibrium process. This direction [1-12] of scientific inquiry holds much potential as a theoretical framework in further expanding fundamental concepts with classical physics.

**Problem Statement/Objective:** An important factor for the DSR phenomena [1,25-29], as with the Raman delay rogue [20] is that they are well-defined and stable wave structure signals. As such, reduction techniques can be of benefit when dissipative systems maintain stable and longer-duration characteristics. However, applying the reduction methods with high-amplitude short-lived pulses appearing in chaotic formations such as spiny solitons (of the CGLE) can be challenging. These are short-lived ultra-short high pulses that appear chaotically on top of a base soliton pulse. See **Figure 2a,b**. The discovery of their unique characteristics has received much attention, evident by many citations. This attention to commercial applications is significant, but also as a road-map to advance current limits of laser precision technology research. The theoretical insights with reduction techniques would be an important and valuable contribution.



**Figure 2a**, Spiny solitons profile in red occurring on top of base blue soliton at different times [1,5,7].



**Figure 2b** False colour plot or red spiny solitons appearing chaotically on top of base soliton[1,5,7].

Applying such reduction techniques to investigate spiny solitons is challenging because of these rapid and chaotic characteristics (see Figure 2a,b). Here the attempt would be to model an infinite degree of freedom system with a finite degree of freedom one. However, identifying even the primary characteristic of spiny solitons and extreme pulses [1-12], across both normal and anomalous regimes using reduction techniques would be significant, to aid in their experimental detection.

The current difficulty is that there is no systematic method to seek desired solutions for dissipative systems like the GGLE. Seeking such solutions relies on ‘needle in a haystack’ numerical investigations. The aim here is to also improve reduction techniques, e.g. ‘method of moments’ and Lagrange methodologies, with the aid of symbolic programming languages, e.g. Mathematica or Maple. This approach may be utilized to firstly seek out new parameter regions of dissipative systems that are potentially identifiable by their solution profile characteristics: - identifiable by the reduction techniques. This would aid the proposed project initiative to catalog database solutions of dissipative systems. The challenge is that dissipative systems like the CGLE are riddled with chaos, instabilities, and singularities. The conceptual methodology in **Figure 1** remains the proven approach to guiding the development of non-integrable CGLE/PDE of this research initiative.

**Outline of tasks/Work Plan:** Any imagined profile shape may be explored for the dissipative systems. The challenge is to seek out an appropriate trial function that mimics or encapsulates profiles that match the extreme wave characteristics demonstrated in [1-12], and to seek out profile solutions that are integrable to at least fifth order. A theoretical verification may utilize the characteristics of solution profiles to seek out new regions of the master laser equation or similar dissipative models.

**Outcome(s):** The advantage of reduction techniques, once solutions are determined, may be used, to explore their immediate localized solution regions with ease and less numerical computation. The research process would be documented as preparations for future advanced coursework in dissipative systems. This research may be linked to supporting Australia’s DE-230101106 initiative.

**Impact:** To establish new theoretical insights of [1-12,44] that support current laser frontier research. Seeking out extreme wave pulses [1-12] remains a *current* road map for next-generation

lasers. This incentive in conjunction seeks to evolve these techniques for exploring non-integrable systems. Advanced coursework on these reduction techniques may also stimulate cross-disciplinary research, especially in biological modeling, towards new commercialization opportunities. New insights of laser signals [1-12,44], include applications for super-continuum generation.

#### *Proposal part b) Health : Reduction Techniques of Dissipative Systems*

One inherent behavior of biological processes is that they are fundamentally self-organizing. It is a natural autonomous process that sustains life. Thus, Prigogine's biological ideas in self-organization with established concepts (**Figure 1**) may be explored. The biological ideas of Prigogine may be utilized as principles for road-maps toward precision medicines from the numerous PDEs of such a nature. This research differs from the main historical approaches like Prigogine's thermodynamic views of systems far from equilibrium. Cells and organs are usually seen as growing structures, while this new approach stresses them as ongoing structures that maintain their forms due to energy and nutrient inputs/outputs. Evidently, sect.1.5 of 'Solitons in biology' [1] includes the CGLE to stimulate cross-disciplinary collaborations. The aim is to establish new fundamental foundations in exploring the biophysical frontier. Here the advantage is that the desired solution characteristics are required to be stable; thus, the fundamental building blocks for living organisms [45] hold self-organizing biological dynamics which can further be explored and developed.

Biological processes of self-organization are primarily and naturally homogenous, as they may appear in their function, and also adhere to a behavioral continuity when stable. These guiding characteristics are essential, extremely crucial, and inherent in the fundamental mathematical foundational principles of dissipative soliton models, when modeling biological behavior, i.e., behaviour that sustains 'stable' life. The similarities between physics and biology in exploring physical and biological theory are evident, but the approaches may differ. An important note is that advancing biology may not be the same as advancing physics [46]. The approach to using reduction techniques for biological self-organizing models [1 ch1.6, 45] is a synergy benefit, that embraces common insights of scientific inquiry in seeking to better advance both disciplines.

An issue that remains in theoretical biology is that dynamics is commonly limited primarily to a single and simple dispersion-diffusion parameter control. Therefore, the insights prevalent to advances in dissipative physics hold a wide scope for a collaborative scientific inquiry into theoretical biology, where biological dynamics can become highly complex. For example a biological process that is failing, and unable to return to its original stable state, may be directed to another localized solution region within its dissipative model. This is because the variability of any one or more parameter paths in what may seem a simple diffusion process may be dynamically controlled from a complex dissipative system model. This is something linear approaches may not detect in their methodologies. This alternative approach may be a preferable option to replacing a biological organ with a transplanted one. This could even decrease the need to seek donors, and avoid issues of donor matching, and even the demands of the illegal organ trade which fuels human trafficking.

Any health epidemic is a serious concern. These reduction techniques to be developed may be delivered as cross-disciplinary skill-sets to biological and medical science research and development institutions and organizations. The pending prospect for the DE-230101106 initiative is for an Optical and Biophysical Sciences Group at the Australian National University. If there is *demand* for these skills-sets to evolve medical science beyond linear methodologies for deterministic precision medicine, then a contingency to expedite and train up current and emerging sciences may exist for an online course; to be deliverable globally. Such dissipative science skill-sets are also required at a policy level, where a process for new commercialization opportunities is needed to direct benefits to health insurance and pharmaceutical industries, including longevity care and home facilities.

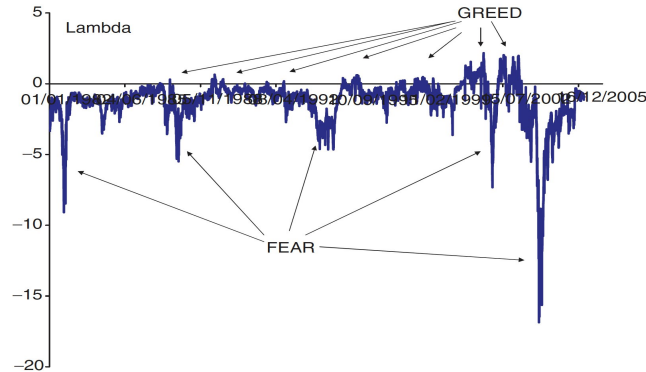
#### *Proposal part c) Environment : Reduction Techniques of Dissipative Systems*

**Literature Review:** *Global Financial Markets to protect our Environment and Stable Climate*

The financial market price of risk, a market indicator used in financial engineering, is driven by the psychological factors of greed and fear (Figure 1). This makes financial markets unpredictable. Yet a deep study into the complex dynamics of the market behaviors, may permit us to direct them (via insights from dissipative solitons) to protect our environment and obtain a stable climate.

In finance, option pricing models and credit derivative instruments are driven by the applications of the Black-Scholes equation (BSE) [47]. This mathematical model can be transformed

into the heat/diffusion equation and so standard convolution methods can be used for solving it. Correspondingly, the BSE borrows some principles from the physics of the heat transfer equation. These BSE models dynamically evolve into play through a diffusion process. This BSE is a dominant model utilized in assessing the numerous financial instruments and continually emerging highly-leveraged financial instruments. Since the introduction of BSE, global markets have been ‘deeply shaped’ by embedded ‘BSE diffusion’ properties. These processes over decades, are likely to remain.



**Figure 1:** Market price of risk (MPOR) interest rate  $\lambda$  vs. date, from [48].

Therefore it is reasonable to consider a self-organizing ‘calibrating thermostat’ in the global financial market. The self-organizing ‘calibrating thermostat’ can be used to ‘*optimally calibrate*’ investment incentives to companies that initiate the correct ‘transition policy initiatives’ towards ‘science policy approved’ energy technologies that are safe for our environment. For this ‘calibrating thermostat’ to be practically effective, it needs to be placed in the financial micro market structure as an international financial policy. Numerous world expert economists [48-51] have always supported new directions for markets to evolve, but these ideas were not explored as the big stakeholders could not anticipate the benefits. Perhaps as evolved ideas, and with Australia’s DE230101106, also briefly mentioned here, it may be possible to better protect our environment and a stable climate.

**Problem Statement/Objective:** My inspired idea is to use models and solutions found in nonlinear dissipative formations in physics, and apply them to world economics. These models, based on PDEs, are successful in explaining single pulse and rogue events in optics and ocean wave studies.

Financial Engineering models though linear stochastic PDEs, attempt investment strategies in highly complex markets that are excessively and surprisingly dissipative. The BSE models utilize the Gaussian profile which is suitable to protect investment portfolio and may assess credit default derivative instruments of an investment industry or basket of instruments. These modeling activities in turn, are based on the term structure interest rate models. That is, the variance of short-term interest rates is also modeled with the BSE. This suffices when the global markets are ‘well-behaved’. This is because the Gaussian may encapsulate up to 5 standard deviations of risk tolerance within a modeling time frame. When 5 standard deviations is exceeded, jump diffusion models can be used to improve risk tolerance. But there is uncertainty when applying jump diffusion, and they involve a premium.

The interest rate term structure frameworks also have issues with calibration, and these introduce challenges when evaluating portfolio investments over long time frames, especially as the market regime behavior changes or evolves. Market behaviors are also shaped by higher leverage financial instruments that do not always pertain to real productivity. Non-productivity, together with defaults, can make the economy increasingly dissipative. Hence, traditional fiscal policy parameters can be challenged, with uncertainty on whether or not to act, and by what amount.

New initiatives to regulate the micro-economic consumption of national economies, without addressing concerns that impact sovereign security, make the complex financial market system highly unpredictable; increasing exposure to extreme events. Conversion to digital regulated currencies without an applied ‘calibrating thermostat’ at the financial market micro-structure will perpetuate the ‘fear and greed’ and diminish long-term innovations of research and civilization infrastructures.

**Outline of tasks/Work Plan:** Financial models may be developed with new trial functions that are integrable, like a Gaussian, but with ‘fat’ tails that may better encapsulate risk tolerance beyond 5 standard deviations. For example, with a dissipative soliton model, an indefinitely widening pulse dissipative soliton resonance (DSR) profile is possible [25-29]. With a stochastic financial

model, a profile beyond 5 standard deviations may be possible. Financially engineering capabilities with self-widening profiles beyond 5 standard deviations may be commercialized for improved risk assessment and investment portfolio strategies. The interest rate term structure modeling with a self-widening profile may better mitigate financial modeling risk across global markets.

However, to anticipate the risk tolerance from the disruptive dissipative market effects, a ‘calibrating thermostat’ may be applied to the micro market structure. This incentive may likely introduce the ‘parameter operators’ that could be incorporated into new models to assist mitigate around, or in phase with, the volatility impacts of large weighted highly-leveraged instruments. Introducing this ‘calibrating thermostat’ requires a compelling community behind the (Australian DECRA-230101106) incentive, to emphasize the interests and benefits to significant stakeholders.

**Outcome(s):** Cross-disciplinary insights from extreme events in dissipative systems may make it possible to apply new Partial Derivative Equations (PDEs) to economics/finance to create a new paradigm that greatly differs from the existing analysis in this area. ‘Reduction techniques’ may be utilized to adapt to any evolving financial market regime. For instance, this proposal also could be linked with the Australian DECRA-230101106 one. Predesignated option pricing stochastic models could be developed with new parameters of market behaviors, or they could adapt to market regime behaviors of ‘self-organizing’ international financial policy investment incentives. Correctly executed, new extensions of democratic quantitative financial economic theories, are likely to develop.

**Impact:** The crucial ‘accommodation’ between China and the United States may be achievable with *an international financial market policy initiative* presented in Australia’s DE230101106 initiative. Here national economies may ‘timely calibrate’ their investments for the improving the environment and constant climate industry initiatives, without carbon credits or emission trading schemes. The larger the debt of a national economy, and the more investments one nation invests in another – the better new benefits exist for national governments. These new benefits would better assist the inherit issues of nations who may accept *a new international financial policy*.

As the United States and China are the dominant bearers of the greatest credit default debt instruments, here lay the terms of interlocking positive international engagements. In this way, nations build towards global long-term stability. These may also be supported by collaborating industry sector initiatives with well-aided civilization-preserving long-term (fundamental) research and developments to realizable commercialization. Evolving financial market regimes require new financial engineering models to better stabilize and secure investment strategies. These reduction techniques may assist in establishing new optimum financially-engineered models for evolving market regimes.

### Bibliography

- [ 1 - 12 ] author bib. in CV. [13] Akhmediev, N. & Ankiewicz, A., ed. (2005), p 1–17. Spr. Berl. Heid. [doi:10.1007/10928028\\_1](https://doi.org/10.1007/10928028_1). [14] Akhmediev, N. and Ankiewicz, A., ed. (2008). Vol. 741. Spr., Berl. Heid., [doi:10.1007/978-3-540-78217-9](https://doi.org/10.1007/978-3-540-78217-9). [15] Akhmediev, N. & Ankiewicz, A. (1997). Solitons. Chap. & Hall. ISBN: 978-0-412-75450-0. [16] Grelu, P., & Akhmediev, N. (2012). *Nat. phot.* 6(2), 84–92, [doi:10.1038/nphoton.2011.345](https://doi.org/10.1038/nphoton.2011.345). [17] Haus, H. A. (1975). *J. App. Phys.*, 46(7):3049–3058, [doi:10.1063/1.321997](https://doi.org/10.1063/1.321997). [18] Ginzburg V.L., Landau L.D. (2009) On Superconductivity & Superfluidity. Spr. Berl., [doi:10.1007/978-3-540-68008-6\\_4](https://doi.org/10.1007/978-3-540-68008-6_4). [19] Aranson, I. S. and Kramer, L. (2002). *Rev. Mod. Phys.*, 74:99–143m [doi:10.1103/RevModPhys.74.99](https://doi.org/10.1103/RevModPhys.74.99). [20] Ankiewicz, A., et al (2018). *J. Opt. Soc. of Am. B*, pp. 899–908, [doi:10.1364/JOSAB.35.000899](https://doi.org/10.1364/JOSAB.35.000899). [21] Maimistov, A. I. (1993). *J. Exp. and Theo. Phys.*, 77 (5):727–731. *Zh. Eksp. Teor. Fiz.* 104, 3620–3629. [22] Ankiewicz, A., et al. (2007). *Opt. Fib. Tech.*, 13(2):91–97, [doi:10.1016/j.yofie.2006.12.001](https://doi.org/10.1016/j.yofie.2006.12.001). [23] E. N. Tsoy, A., et al *Phys. Rev. E* 73, 036621 2006, [doi:10.1103/PhysRevE.73.036621](https://doi.org/10.1103/PhysRevE.73.036621). [24] Chang, W., et al (2007). *Phys. Lett. A*, 362(1), pp.31–36, [doi:10.1016/j.physleta.2006.10.003](https://doi.org/10.1016/j.physleta.2006.10.003). [25] Chang, W., et al (2008). *Phys. Rev. A*, 78(2), 023830, [doi:10.1103/PhysRevA.78.023830](https://doi.org/10.1103/PhysRevA.78.023830). [26] Chang, W., et al (2009). *Phys. Rev. A*, 79:033840, [doi:10.1103/PhysRevA.79.033840](https://doi.org/10.1103/PhysRevA.79.033840). [27] Chang, W., et al (2008) *J. Opt. Soc. Am. B*, 25 (12) 1972–1977, [doi:10.1364/JOSAB.25.001972](https://doi.org/10.1364/JOSAB.25.001972). [28] Chang, W., et al (2009). *Phys. Rev. A*, 79, 033840, [doi:10.1103/PhysRevA.79.033840](https://doi.org/10.1103/PhysRevA.79.033840). [29] Grelu, P. et al. (2010). *J. Opt. Soc. of Am. B*, 27 (11): 2336–2341, [doi:10.1364/JOSAB.27.002336](https://doi.org/10.1364/JOSAB.27.002336). [30] Ankiewicz & Akhmediev (2008). *Chaos: An Interdisc. Jour. of Nonlin. Sci.*, 18(3):033129, [doi:10.1063/1.2976628](https://doi.org/10.1063/1.2976628). [31] Wu, X. et al. (2009). *Opt. Exp.*, 17(7):5580–5584, [doi:10.1364/OE.17.005580](https://doi.org/10.1364/OE.17.005580). [32] Liu, X. (2009). *Opt. Exp.*, 17(25):22401–22416, [doi:10.1364/OE.17.022401](https://doi.org/10.1364/OE.17.022401). [22] Xu, Z. W. and Zhang, Z. X. (2013). *Opt. & Las. Tech.*, 48:67–71, [doi:10.1016/j.optlastec.2012.09.020](https://doi.org/10.1016/j.optlastec.2012.09.020). [34] Liu, L. et al. (2013). *Opt. Exp.*, 21(22):27087–27092, [doi:10.1364/OE.21.027087](https://doi.org/10.1364/OE.21.027087). [35] Fermi, E., et al. (1955). *Studies in Nonlinear Problems*. Los Alamos Sci. Lab., [doi:10.2172/4376203](https://doi.org/10.2172/4376203). [36] Zabusky, N. J. & Kruskal, M. D. (1965). *Phys. Rev. Lett.* ,15, [doi:10.1103/PhysRevLett.15.240](https://doi.org/10.1103/PhysRevLett.15.240). [37] Lax, P. D. (1968). *Com. Pure & App. Math.*, 21(5):467–490, [doi:10.1002/cpa.3160210503](https://doi.org/10.1002/cpa.3160210503). [38] Lax, P. D. and Phillips, R. S. (1976). (AM-87). Princeton Uni. Press.:240-243 <https://www.jstor.org/stable/j.ctt1bc5419>. [39] Lax, P. D. & Phillips, R. S. (1980). *Bull. Amer. Math. Soc. (N.S.)*, 2(2):261–295. [40] Zakharov, V. E. (1968). *J of Appl. Mech. and Tech. Phys.*, 9(2):190–194, [doi:10.1007/BF00913182](https://doi.org/10.1007/BF00913182). [41] Zakharov, V. E. & Shabat, A. B. (1972). *Soviet Physics JETP*, 34:62–69. [Russian original: *Zh. Eksp. Teor. Fiz.* 61, 118–134 (1971)]. [42] Peregrine, D. H. (1983). *J. Aust. Math Soc. B. App. Math*, 25(1):16–43, [doi:10.1017/S0334270000003891](https://doi.org/10.1017/S0334270000003891). [43] Akhmediev, N. & Korneev, V. (1986). *Theo. and Math. Phys.*, 69:1089, [doi:10.1007/BF01037866](https://doi.org/10.1007/BF01037866). [44] Chang, W. & Akhmediev, N. (2015). *In Nonl. Opt. Cav. Dyn.* p.263–276. John Wiley & Sons, L., [doi:10.1002/9783527686476.ch11](https://doi.org/10.1002/9783527686476.ch11). [45] Akhmediev, N., et al (2013). *Phys. Lett. A*, 377(13): 968 – 974, [doi:10.1016/j.physleta.2013.02.015](https://doi.org/10.1016/j.physleta.2013.02.015). [46] Schulten K, et al. (1997) In: Flyvbjerg H., et al, (eds) *Phy. of Biol. Syst. Lect. Notes in Phys.*, vol 480. Spr., Berl., Heid., [doi:10.1007/978-3-540-49733-2\\_6](https://doi.org/10.1007/978-3-540-49733-2_6). [47] Black, F. & Scholes, M. (1973). *J. of Pol. Econ.*, 81 (3): 637– 654, [doi:10.1086/260062](https://doi.org/10.1086/260062). [47] Ahmad, R. & Wilmott, P. (2006). *Wilmott*, 2006 (58):64–70. [48] Tobin, J. (1978) *Eastern Economic Journal*, 4(3– 4):153–159. [49] O’Grady, S. (2010). *The Independent*, 15th Feburary. [50] Stiglitz, J. E. (2012). *J. W. W. Norton & Company*, 1 edition. ISBN:0393345068. [51] Atkinson, A. & Stiglitz, J. (2015). Princeton Uni. Press. ISBN:9780691166414.



## Executive Summary

### High-Speed and Efficient Quantum Light Generation with Semiconductor Quantum Emitters Embedded in Integrated Photonic Structures

**Impact:** In this project, we propose to use semiconductor artificial atoms in nanofabricated optical cavities to generate single and entangled photons efficiently and at gigahertz rates. The project will use semiconductor quantum dots (QDs), the most efficient on-demand quantum light sources to date, which emit photons with near-unity efficiency upon excitation. These QDs will be integrated with high-quality-factor optical cavities fabricated by photo- and electron-beam-lithography to efficiently couple the emitted photons into optical fiber networks. Based on quantum light traveling through these networks, our QD-cavity source offers a high-speed solution for secure quantum networking applications such as *unbreakable encryption for data storage and transmission* via *certified random number generation*, *quantum key distribution*, and *entanglement swapping*. These applications are based on entanglement distribution and measurement with end-to-end efficiencies higher than 75%, a threshold for a *loophole-free Bell-test*. This test will result in private or shared encryption keys with *unprecedented low bias*, with a *quantum privacy signature* which alerts the user(s) if adversaries try to tamper with the keys to obtain their information. Therefore, this signature is the ultimate form of security, ensuring that the encryption keys are known only by the target users.

**Objectives:** The focus of this project is to design and fabricate optical cavities that can efficiently extract quantum light from QDs and into optical fiber. Our novel cavity design will extract photons more efficiently compared to other state-of-the-art solutions, surpassing the threshold for generation of unbreakable encryption keys. Our system is based on a novel dual-structure cavity: circular trenches in the shape of a bullseye, and a vertical top-down cavity consisting of planar mirrors at the bottom and a concave mirror on top (Fig. 1). We have already fabricated and characterized bullseye cavities, and during this program, will design and fabricate vertical cavities that are compatible with the bullseye cavities. During the 1-year period of this project, we will:

- (1) Design and simulate the dual-structure cavity to result in record-high photon collection efficiencies ( $> 75\%$ ).
- (2) Fabricate these cavities using molecular-beam epitaxy and nanofabrication.
- (3) Characterize cavity performance with classical light (quality factor  $Q > 20,000$ ).

**Team:** This project will be led by Poolad Imany, who is a postdoctoral associate in Quantum Nanophotonics Group (QNG) at the National Institute of Standards and Technology (NIST) and University of Colorado Boulder, Colorado. Imany is also the Founder and CEO of Icarus Quantum Inc, the only company in the United States that works on commercializing quantum emitters for the purpose of quantum networking technologies. Imany has more than nine years of experience in quantum light generation and quantum networking, and will leverage decades of expertise from the QNG group in QD wafer growth and nanofabrication.

**Facilities:** For Multiphysics simulations, we will use NIST's multicore, gpu-equipped workstations. For nanofabrication, we will use NIST's world-class cleanroom facilities. Finally, we will characterize our devices at NIST and University of Colorado Boulder's laboratories equipped with tunable lasers and superconducting nanowire single-photon detectors. Although Icarus Quantum is the institution leading this effort, the NIST and University of Colorado Boulder facilities will be used through a cooperative research and development agreement (CRADA) between Icarus and these institutions.

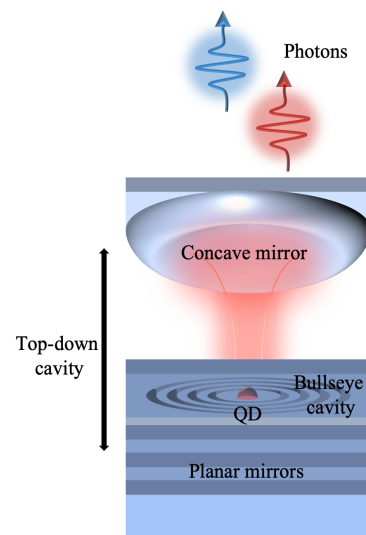


Fig. 1. A quantum dot embedded in a dual-structure optical cavity.

# High-Speed and Efficient Quantum Light Generation with Semiconductor Quantum Emitters Embedded in Integrated Photonic Structures

## 1. Literature Review

We propose to use semiconductor quantum dots (QDs) embedded in nanofabricated high-quality-factor photonic cavities to generate single and entangled photons efficiently and at gigahertz rates. These photons can then be coupled into optical fiber networks to enable *secure and high-rate quantum communications protocols* such as *generation of unbreakable encryption keys with the ability of tampering detection (certified random number generation)* [1], and *generation of shared keys between two parties with the capability of detecting eavesdropping attacks (quantum key distribution)* [2,3]. Our ultimate goal is to fabricate a QD-cavity system with the ability to generate entangled photon pairs on-demand, a scalable solution for long-range entanglement distribution, and the backbone of a secure quantum network. As quantum networking testbeds are being developed around the world, the timing is right to tackle this challenge from leveraging partnerships between industry, government agencies, and academia. We will use the expertise of all these institutions through the PI's affiliation with Icarus Quantum Inc, National Institute of Standards and Technology (NIST), and University of Colorado Boulder.

For quantum light generation, two main avenues have been explored: spontaneous down conversion (or four-wave mixing) in optical nonlinear materials and spontaneous emission from atomic systems. The first avenue uses nonlinear processes to generate single photons [4,5]. It is based on the simple concept that a higher frequency photon (referred to as the pump photon) has some chance to be converted to two lower frequency photons (referred to as signal and idler photons) upon going through an optical nonlinear material. A single signal photon is thus generated conditioned on the detection of an idler photon. The main problem with this approach is that the nonlinear conversion process is fundamentally probabilistic, leading to a fundamental tradeoff between photon generation rate and single-photon purity. While multiplexing can be used to overcome this challenge, it requires fast and highly-efficient optical switches, which are not available today.

A more plausible avenue, which we make use of, is spontaneous emission from a two-level system, for example a single atom [6]. Since a single atom can only emit one photon at a time, this process naturally suppresses multi-photon events, resulting in high single-photon purity. The generation rate of single photons is decided by how fast the atom can emit a photon, and how fast one can repopulate the atom into the excited state, hence the generation rate is no longer coupled with the single-photon purity. Therefore, single-photon sources based on single atoms are fundamentally deterministic.

Nearly all atomic systems can emit single photons on-demand, but few are suitable for realizing a single-photon source that is useful in real-world applications. For atoms and ions, sophisticated trapping apparatus is required to isolate single atoms or ions in vacuum [6,7]. Such devices are bulky in nature and also suffer from poor photon extraction efficiency. One can also create single atomic defects, impurities, or dopants in a solid-state material and use them as single-photon emitters [8–11]. These atomic systems naturally live inside a semiconductor chip and therefore do not require any bulky traps. However, they will inevitably interact with phonons (crystal lattice vibrations) and random defects/charges in their host material, limiting the quantum efficiency and coherence of the emitted photons.

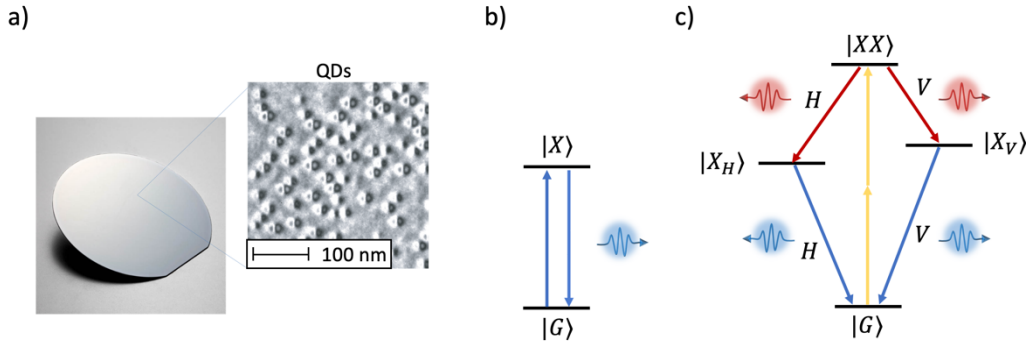
**Our choice of quantum emitter is an artificial atom made of an InAs QD inside a GaAs crystal (Fig. 1a).** Icarus Quantum Inc. and the Quantum Nanophotonics Group at NIST Boulder (institutions the PI is affiliated with) have extensive experience in high-quality molecular-beam epitaxially (MBE)-grown InAs QDs on GaAs substrates and their nanofabrication [12,13]. Optical excitation of these QDs create a single electron-hole pair (exciton) inside the dot, which can recombine and emit a single photon (Fig. 1b). This system offers unique advantages as a single-photon source:

- i. QDs naturally live inside a semiconductor material, eliminating the need for complex atomic traps.
- ii. QDs are  $\sim 1000$  times larger than single atoms. This property leads to a much larger optical dipole moment and an intrinsic insensitivity to high-frequency acoustic phonons.



- iii. The host material of the QDs can be grown with high quality to eliminate material defects. They can also be doped to form p-i-n diode structures for charge control.

Due to these unique advantages, QDs have shown the best performance among all single-photon sources to date, with >99.96% single-photon purity [14], >93% photon indistinguishability [15], and >96% quantum efficiency [16].

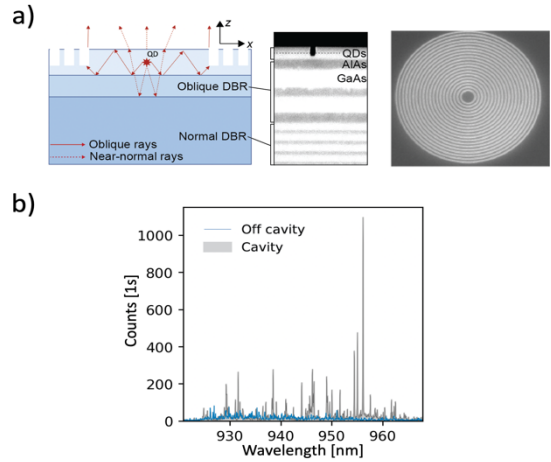


**Fig. 1. a)** A GaAs wafer with self-assembled InAs QDs grown by molecular-beam epitaxy (MBE). A transmission electron microscope (TEM) picture of the QDs is shown in the magnified sub-figure. **b)** The exciton state of the QD, which upon excitation emits a single photon.  $|G\rangle$  is the ground state, and  $|X\rangle$  is the exciton state. **c)** Two-photon excitation of a QD (yellow arrows) to the biexciton level ( $|XX\rangle$ ). The biexciton state can decay through two different channels, emitting two horizontally- or vertically-polarized photons, resulting in an on-demand polarization-entangled two-photon state of  $|\psi\rangle = 1/\sqrt{2}(|HH\rangle + |VV\rangle)$ . The slight difference between energy levels of  $|X_H\rangle$  and  $|X_V\rangle$  is due to fine structure splitting.

Another important feature of QDs is that they can directly generate entangled photon pairs [8,9] or even more complex photonic graph states [17,18] on-demand, due to their rich energy levels. For example, entangled photon pair generation can be achieved via two-photon excitation into the biexciton state. The two possible decay channels of the biexciton state will lead to a polarization-entangled two-photon state (Fig. 1c). An entangled photon pair with a fidelity of 0.98 has been demonstrated using this approach (although with low efficiency), with a clear path to surpass 0.99 using optical cavities [19]. The capability for on-demand generation of entangled photons is crucial for quantum communication and scalable quantum networks [20,21].

## 2. Problem Statement/Objective

Our goal in this project is to design and fabricate optical cavities that can efficiently extract the photons emitted from a QD into a single-mode optical fiber. For this purpose, micropillars [22], photonic crystals [23], bullseye cavities [24], and top-down cavities with a concave mirror on top and planar mirrors on the bottom [16] have been proposed. The top-down cavities have shown great promise in that (1) they don't need any nanofabrication on the QD wafer, hence the QD performance does not suffer from the defects created by fabrication, (2) they have the highest quality factors ( $>10^6$ ) [25], and (3) the output mode can be coupled to a single-mode fiber efficiently. All these properties have contributed to these cavities to demonstrate record-high single-photon efficiencies up to 57% coupled into fiber [16].



**Fig. 2. a)** The bullseye cavity structure fabricated on a set of DBRs. The side- and top-view image from a scanning electron microscope (SEM) are shown in the center and right figures, respectively. **b)** The photoluminescence spectrum of a QD ensemble on and off the bullseye cavity, showing more than  $10\times$  enhancement in counts for the QDs inside the cavity. The counts are on a CCD camera and not on an SNSPD.

A drawback of top-down cavities is the possibility of the photons escaping horizontally. In [16], 14% of the emitted photons are lost due to this effect. Here, we propose to combine a top-down cavity with circular trenches etched into the surface of GaAs around the QD to prevent the QD from emitting horizontally, namely a bullseye cavity. Based on our simulations, these trenches can be microns away from the QD, minimizing the effect of defects on the QD performance. We have already fabricated bullseye cavities around QDs with MBE-grown distributed Bragg reflector (DBR) layers under the QD layer, which have enhanced the photons collected into fiber by more than  $10\times$  (Fig. 2a,b) [26]. We propose to combine the bullseye and top-down cavity structures to further increase the photon extraction efficiency (Fig. 3), surpassing the threshold for device-independent random number generation and quantum key distribution (75%). In this project, we will design, fabricate, and characterize these dual-structure cavities and infer their photon extraction efficiency from a QD based on their quality factor.

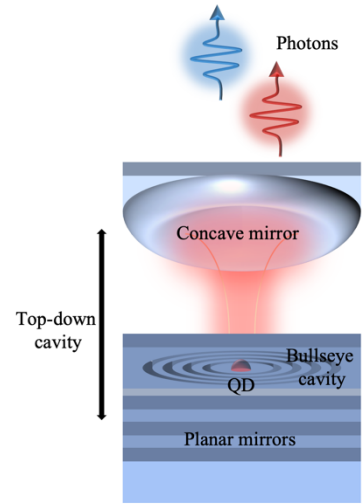
### 3. Outline of Tasks and Outcomes

Our tasks divide into three major areas focused on dual-structure optical cavities: simulations, fabrication, and characterization. We have already started simulations of top-down and bullseye cavities individually (Fig. 4a). In this project, we will combine the simulations of the two optical structures and an optical dipole (the QD) inside them in the Multiphysics simulator Lumerical. The desired outcome for these simulations is to find the right parameters for *mirror curvature*, *DBR structure*, *mirror reflectivity*, and *bullseye radius*, *trench depth*, and *trench period* to extract polarization-entangled photons with  $>75\%$  efficiency from the QD and into fiber.

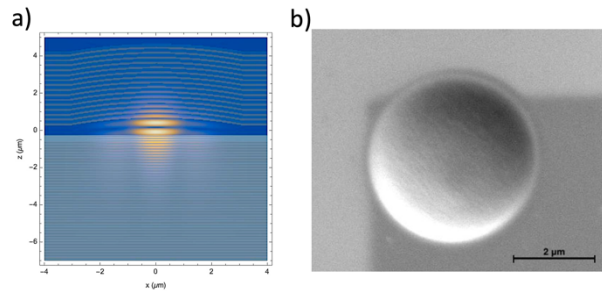
In the meantime, will fabricate the concave mirrors on a fused silica substrate using three different approaches: (1) Focused ion-beam (FIB) milling, (2)  $\text{CO}_2$  laser ablation [16], and (3) photoresist reflow [27]. We have already fabricated mirrors with  $5\ \mu\text{m}$  radii of curvature using FIB (Fig. 4b). While this technique offers high-precision control of the mirror shape, it is not suitable for scalable manufacturing since ion beam milling is slow and expensive. Therefore, we will consider the two other approaches to find the most suitable and scalable method for making the concave mirror in this project. Based on simulations, the desired outcome is to fabricate mirrors with radius of curvature  $\sim 10\ \mu\text{m}$  [16]. We will then coat the mirrors with DBR layers with desired reflectivity at the emission wavelength of our QDs ( $\sim 950\ \text{nm}$ ), using the local vendor FiveNine Optics.

After extracting the correct parameters for a bullseye structure compatible with the top-down cavity from simulations, we will fabricate these structures on wafers with MBE-grown DBRs. We will then glue these samples to the fused silica substrate to form the complete dual-structure cavity.

Finally, we will build a room-temperature optical setup to characterize these cavities. We will measure the transmission and reflection from these cavities across different wavelengths using a tunable continuous wave laser and extract the cavity quality factor ( $Q$ ) from these measurements. We will perform these measurements for both the top-down cavities and the dual-structure cavities. Our milestone for these measurements is to show  $Q$ 's above 20,000, limited by the concave mirror reflectivity, which will ensure



**Fig. 3.** A quantum dot embedded in a dual-structure optical cavity.


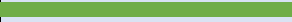
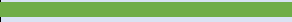
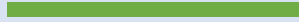
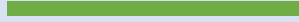

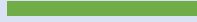
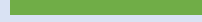


**Fig. 4.** **a)** Simulated mode profile of the designed top-down cavity. **b)** Scanning electron microscope (SEM) image of the concave mirror fabricated by focused FIB milling.

We will then coat the mirrors with DBR layers with desired reflectivity at the emission wavelength of our QDs ( $\sim 950\ \text{nm}$ ), using the local vendor FiveNine Optics.

efficient photon extraction from a QD inside this cavity. These areas, tasks, outcomes, and their timeline is summarized in Table 1.

Table 1. Breakdown of objective areas, tasks, outcomes, and timeline

	Area	Task, Outcome	Timeline (1 Year)			
			M3	M6	M9	M12
1	Simulations	<ul style="list-style-type: none"> <li>Dual-cavity simulations, Photon extraction &gt;75%</li> </ul>				
2	Fabrication	<ul style="list-style-type: none"> <li>Concave mirror fabrication</li> </ul>				
		<ul style="list-style-type: none"> <li>Bullseye cavity fabrication</li> </ul>				
		<ul style="list-style-type: none"> <li>Dual-cavity fabrication</li> </ul>				
		<ul style="list-style-type: none"> <li>Concave mirror coating</li> </ul>				
3	Characterization	<ul style="list-style-type: none"> <li>Build cavity characterization setup</li> </ul>				
		<ul style="list-style-type: none"> <li>Characterize Top-down cavity</li> </ul>				
		<ul style="list-style-type: none"> <li>Characterize dual cavity, Q &gt; 20,000</li> </ul>				

The challenging steps of this project are threefold, and we discuss our risk mitigation measures for each of them below:

- 1) **Concave mirror fabrication:** we have not yet fabricated concave mirrors with the desired radii of curvature, surface roughness, and scalability. We propose to take three different routes to mitigate the risk in accomplishing this task: FIB milling, CO<sub>2</sub> laser ablation, and photoresist reflow.
- 2) **Multimode support:** the polarization-entangled photon pairs generated by the QDs have slightly different wavelengths due to the biexciton binding energy (~2 nm). Therefore, to develop an efficient entangled photon source, the cavity should be able to support two frequency modes in each polarization. For this purpose, we will first start with low-*Q* cavities that can support the two frequencies in the same cavity mode. We will then move to high-*Q* cavities with more complex DBR structures, capable to support two modes with ~2 nm spacing in each polarization.
- 3) **Tunability:** For efficient photon extraction, the modes of the QD and cavity must match perfectly. Although outside of the scope of this project, we will explore strain-tuning methods for both the cavities and QDs to match these modes, and to eliminate the fine-structure splitting of the QD which is the main source of entanglement degradation [19]. We will also explore charge-tuning of the QD with a vertical electric field.

#### 4. Impact

By the end of this project, we will show the feasibility of a QD-cavity system to generate entangled photon pairs efficiently, with high quality, and at gigahertz rates. Such an efficient source of quantum light is the backbone of quantum communications protocols, all of which require high-rate entanglement distribution over long distances. An on-demand source of entangled photons leads to scalable quantum repeaters, which act as an alternative to classical amplifiers for quantum states to battle loss in quantum networks, enabling entanglement distribution over even intercontinental distances. Efficient entanglement distribution enables loophole-free Bell tests at dramatically higher rates compared to spontaneous sources, allowing for secure quantum networking applications such as certified random number generation [1] and device-independent quantum key distribution [2,3]. These applications ensure data encryption and transmission with ultimate privacy, with the ability to detect adversarial attacks on the keys.

#### 5. References

1. P. Bierhorst, E. Knill, S. Glancy, Y. Zhang, A. Mink, S. Jordan, A. Rommal, Y. K. Liu, B. Christensen, S. W. Nam, M. J. Stevens, and L. K. Shalm, "Experimentally generated randomness certified by the impossibility of superluminal signals," *Nature* **556**, 223–226 (2018).
2. D. P. Nadlinger, P. Drmota, B. C. Nichol, G. Araneda, D. Main, R. Srinivas, D. M. Lucas, C. J. Ballance, K. Ivanov, E. Y.-Z. Tan, P. Sekatski, R. L. Urbanke, R. Renner, N. Sangouard, and J.-D. Bancal, "Experimental quantum key distribution certified by Bell's theorem," *Nature* **607**, 682–686 (2022).
3. W. Zhang, T. van Leent, K. Redeker, R. Garthoff, R. Schwonnek, F. Fertig, S. Eppelt, W. Rosenfeld, V. Scarani, C. C.-W. Lim, and H. Weinfurter, "A device-independent quantum key distribution system for distant users," *Nature* **607**, 687–691 (2022).

4. P. G. Kwiat, K. Mattle, H. Weinfurter, A. Zeilinger, A. v. Sergienko, and Y. Shih, "New High-Intensity Source of Polarization-Entangled Photon Pairs," *Phys Rev Lett* **75**, 4337 (1995).
5. F. Kaneda and P. G. Kwiat, "High-efficiency single-photon generation via large-scale active time multiplexing," *Sci Adv* **5**, (2019).
6. F. Ripka, H. Kübler, R. Löw, and T. Pfau, "A room-temperature single-photon source based on strongly interacting Rydberg atoms," *Science* (1979) **362**, 446–449 (2018).
7. H. G. Barros, A. Stute, T. E. Northup, C. Russo, P. O. Schmidt, and R. Blatt, "Deterministic single-photon source from a single ion," *New J Phys* **11**, 103004 (2009).
8. E. N. Knall, C. M. Knaut, R. Bekenstein, D. R. Assumpcao, P. L. Stroganov, W. Gong, Y. Q. Huan, P.-J. Stas, B. Machielse, M. Chalupnik, D. Levonian, A. Suleymanzade, R. Riedinger, H. Park, M. Lončar, M. K. Bhaskar, and M. D. Lukin, "Efficient Source of Shaped Single Photons Based on an Integrated Diamond Nanophotonic System," arXiv preprint arXiv: 2201.02731 (2022).
9. S. Castelletto, "Silicon carbide single-photon sources: challenges and prospects," *Materials for Quantum Technology* **1**, 023001 (2021).
10. A. Alizadehkhaledi, A. L. Frencken, F. C. J. M. van Veggel, and R. Gordon, "Isolating Nanocrystals with an Individual Erbium Emitter: A Route to a Stable Single-Photon Source at 1550 nm Wavelength," *Nano Lett* **20**, 1018–1022 (2020).
11. A. Ajoy, D. Englund, D. L. Perry, E. S. Bielejec, F. Jelezko, J. L. Pacheco, K. Saha, L. Marseglia, P. Cappellaro, R. Walsworth, and T. Schröder, "Bright nanowire single photon source based on SiV centers in diamond," *Opt Express* **26**, 80–89 (2018).
12. P. Imany, Z. Wang, R. A. Decrescent, R. C. Boutelle, C. A. McDonald, T. Autry, S. Berweger, P. Kabos, S. W. Nam, R. P. Mirin, and K. L. Silverman, "Quantum phase modulation with acoustic cavities and quantum dots," *Optica* **9**, 501–504 (2022).
13. R. A. DeCrescent, Z. Wang, P. Imany, R. C. Boutelle, C. A. McDonald, T. Autry, J. D. Teufel, S. W. Nam, R. P. Mirin, and K. L. Silverman, "Tightly Confined Surface Acoustic Waves as Microwave-to-Optical Transduction Platforms in the Quantum Regime," arXiv preprint arXiv:2205.01277 (2022).
14. F. Sbresny, L. Hanschke, E. Schöll, W. Rauhaus, B. Scaparra, K. Boos, E. Zubizarreta Casalengua, H. Riedl, E. del Valle, J. J. Finley, K. D. Jöns, and K. Müller, "Stimulated Generation of Indistinguishable Single Photons from a Quantum Ladder System," *Phys Rev Lett* **128**, 093603 (2022).
15. P. Senellart, G. Solomon, and A. White, "High-performance semiconductor quantum-dot single-photon sources," *Nat Nanotechnol* **12**, 1026–1039 (2017).
16. N. Tomm, A. Javadi, N. O. Antoniadis, D. Najer, M. C. Löbl, A. R. Korsch, R. Schott, S. R. Valentin, A. D. Wieck, A. Ludwig, and R. J. Warburton, "A bright and fast source of coherent single photons," *Nat Nanotechnol* **16**, 399–403 (2021).
17. S. C. Wein, J. C. Loredó, M. Maffei, P. Hilaire, A. Harouri, N. Somaschi, A. Lemaître, I. Sagnes, L. Lanco, O. Krebs, A. Auffèves, C. Simon, P. Senellart, and C. Antón-Solanas, "Photon-number entanglement generated by sequential excitation of a two-level atom," *Nat Photonics* **16**, 374–379 (2022).
18. Y. Zhan and S. Sun, "Deterministic Generation of Loss-Tolerant Photonic Cluster States with a Single Quantum Emitter," *Phys Rev Lett* **125**, 223601 (2020).
19. D. Huber, M. Reindl, S. F. Covre Da Silva, C. Schimpf, J. Martín-Sánchez, H. Huang, G. Piredda, J. Edlinger, A. Rastelli, and R. Trotta, "Strain-Tunable GaAs Quantum Dot: A Nearly Dephasing-Free Source of Entangled Photon Pairs on Demand," *Phys Rev Lett* **121**, 033902 (2018).
20. M. Zopf, R. Keil, Y. Chen, J. Yang, D. Chen, F. Ding, and O. G. Schmidt, "Entanglement Swapping with Semiconductor-Generated Photons Violates Bell's Inequality," *Phys Rev Lett* **123**, 160502 (2019).
21. F. Basso Basset, M. B. Rota, C. Schimpf, D. Tedeschi, K. D. Zeuner, S. F. Covre Da Silva, M. Reindl, V. Zwiller, K. D. Jöns, A. Rastelli, and R. Trotta, "Entanglement Swapping with Photons Generated on Demand by a Quantum Dot," *Phys Rev Lett* **123**, 160501 (2019).
22. P. Senellart, G. Solomon, and A. White, "High-performance semiconductor quantum-dot single-photon sources," *Nat Nanotechnol* **12**, 1026–1039 (2017).
23. R. Uppu, L. Midolo, X. Zhou, J. Carolan, and P. Lodahl, "Quantum-dot-based deterministic photon-emitter interfaces for scalable photonic quantum technology," *Nat Nanotechnol* **16**, 1308–1317 (2021).
24. L. Sapienza, M. Davanço, A. Badolato, and K. Srinivasan, "Nanoscale optical positioning of single quantum dots for bright and pure single-photon emission," *Nat Commun* **6**, 1–8 (2015).
25. D. Najer, I. Söllner, P. Sekatski, V. Dolique, M. C. Löbl, D. Riedel, R. Schott, S. Starosielec, S. R. Valentin, A. D. Wieck, N. Sangouard, A. Ludwig, and R. J. Warburton, "A gated quantum dot strongly coupled to an optical microcavity," *Nature* **575**, 622–627 (2019).
26. R. A. DeCrescent, Z. Wang, P. Imany, R. C. Boutelle, R. P. Mirin, and K. L. Silverman, "Semicircular dielectric gratings for strongly polarized and enhanced emission from GaAs/InAs quantum dots," in *Conference on Lasers and Electro-Optics (CLEO)* (2022).
27. N. Jin, C. A. McLemore, D. Mason, J. P. Hendrie, Y. Luo, M. L. Kelleher, P. Kharel, F. Quinlan, S. A. Diddams, and P. T. Rakich, "Scalable fabrication of ultrahigh-finesse micromirrors with variable geometry," arXiv Preprint arXiv: 2203.15931 (2022).

## EXECUTIVE SUMMARY

Silicon photonics and printable photonic ink LEDs for a new affordable medical sensor platform  
Optica Foundation 20<sup>th</sup> Anniversary Challenge Category: Health

**The Challenge:** Traditional medical sensors consisting of discrete optics cannot keep pace with patient need. This limitation was highlighted during the COVID-19 pandemic, when the standard pulse oximeters used to measure blood oxygen levels yielded incorrect diagnoses for people with darker skin pigmentation, thicker skin, or lower blood flow rate. These standard oximeters used discrete optics, including LEDs (660 nm and 940 nm), filters, and photodetectors from that must be sourced from separate supply chains, assembled, and packaged into a single device. Accurate devices that can compensate for skin pigmentation require four or more LEDs of different wavelengths. However, adding additional discrete optical components increases the complexity of packaging, resulting in poor adoption due to their high cost. This illustrative example, pulse oximetry, is not alone in suffering the challenges imposed by discrete optics. Existing medical sensor products, such as carbon monoxide poison detectors, require eight or more LEDs and are niche as a result. Looking to the future, the \$20 billion noninvasive medical sensor industry needs a way to achieve accuracy, complexity, and versatility while maintaining a low cost to expand global access to healthcare.

**Proposed Project:** *This Optica Foundation 20<sup>th</sup> Anniversary Challenge will provide critical seed funding for demonstrating the world's first affordable noninvasive medical sensors based on silicon photonic chips.* The promise of silicon photonics is that it will enable integrated optics to replace discrete optics in the same way that integrated circuits replaced discrete electronics. Our company's vision is to print LEDs of different wavelengths directly onto a silicon photonic chip to avoid the costs associated with discrete optics and their packaging. We are pioneering a new class of printed photonic inks for light sources and detectors (actives) based on nanoscale black phosphorus (BP), a material that exhibits desirable opto-electronic properties including direct-gap light emission and high conductivity. BP is a 2D semiconductor that can be tuned to emit over a broad spectrum from visible to infrared based on the number of atomic layers. **In this project, we will separate a multi-layer (polydisperse) BP solution by layer number to achieve inks that emit at specific wavelengths relevant to medical devices. We will then demonstrate printed BP LEDs fashioned from these inks on silicon chips. This project will leverage key results from our company's work on BP over the last several years.**

**Intended Outcomes:** The final outcome of this project will be LEDs fashioned from monolayer BP (emission at 600-900 nm) and bilayer BP (emission at 800-1200 nm) that we print on a silicon photonics chip. To achieve this result, we will use density gradient ultracentrifugation (DGU) to separate monolayer and bilayer BP from a multi-layer (polydisperse) solution. We will engineer this process specifically for BP to achieve maximum yield using a combination of surfactants and centrifugation parameters. This technique has been commercialized for graphene, giving confidence in the approach. Next, we will characterize the opto-electronic properties of inks of both BP (native p-type) and doped-BP (n-type) with optical emission bands at 660 nm and 940 nm wavelengths required to discriminate between oxygenated and deoxygenated blood. Electrical transport meeting sheet and contact resistance metrics in line with existing commercial devices will be targeted. The final prototype LED devices will be printed onto a silicon photonics chip using aerosol jet printing. **This advance will represent the first ink-printed BP LEDs on silicon chips.**

**New Capabilities:** The success of this project will illustrate how printed photonic inks can enable silicon photonics to reach its full potential as a transformative technology. An integrated pulse oximeter will be a major step toward sophisticated medical, non-invasive devices that will improve patient outcomes and provide more relevant health data per dollar. At scale, our new photonic chip medical sensor platform will enable access to affordable, state-of-the-art medical care for people all over the world. This advances here have the potential to be used in the broadest terms and across industries. Printable photonic inks solve one of the most important outstanding problems in silicon photonics platform. Namely, the need for an on-chip gain medium applications requiring multi-wavelength operations including environmental monitoring, communications, and quantum photonics. Finally, the photonic inks expand the reach of additive manufacturing and open the way for printed opto-electronics.



**Objective:**

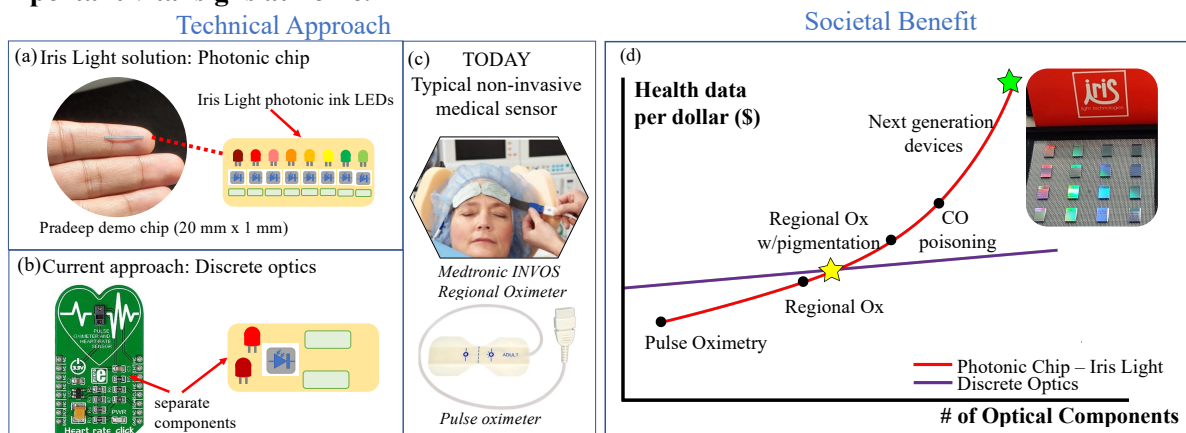
This Optica Foundation 20<sup>th</sup> Anniversary Challenge will provide critical seed funding to demonstrate *the world's first affordable non-invasive medical sensors based on silicon photonic chips*. The overall objective of the proposal is to develop a new class of printed photonic inks for LED light sources. **Figure 1(a)** shows a vision of the approach with high-density multi-colored LEDs on a single chip. These devices will be based on nanoscale black phosphorus (BP), a material that exhibits desirable opto-electronic properties including direct-gap light emission and high conductivity. The specific technical objectives are:

- (1) Purification of nanomaterial inks based on monolayer (1L) & bilayer (2L) black phosphorus,
- (2) Characterization of the opto-electronic properties of the 1L & 2L inks, and
- (3) Fabrication of printed LEDs at 640 nm and 940 nm that are needed for pulse oximetry.

This advance will be the first printed BP photonic ink LEDs on silicon photonic chips. **Silicon photonics has the potential to revolutionize the medical industry with sophisticated monitoring devices that collect more health data per dollar for improved patient outcomes.** In brief, the low-cost, on-chip light sources developed here will open up the possibility of entire new class of non-invasive medical devices and drastically expand the reach beyond today's medical sensors.

**Problem Statement:**

To illustrate the broader nature of the challenge, we first consider a well-known medical application that uses discrete optics, the pulse oximeter. Using this baseline to identify the shortcomings of the current approach will provide a clearer picture of the future of wearable medical sensors enabled by silicon photonics. Pulse oximetry has reached the level of 'standard of care' and is one of the five vital signs measured at every doctor's visit [1]. Before this invention, patients had to endure a blood draw to measure their blood oxygen saturation levels (SpO<sub>2</sub>) [2]. Currently, diabetic patients still have to poke themselves multiple times a day to track their glucose levels. Beyond diabetes, there are a significant number of additional health issues that require invasive monitoring today. **In contrast, new non-invasive medical sensors promise to avoid painful poking and allow patients to measure their own important vital signs at home.**



**Figure 1: Illustrating advantage of silicon photonics over discrete optics with example of pulse oximeters.** (a) Iris Light approach to ink-printed LEDs on silicon chips. Image: model chip on Pradeep Subedi's hand. (b) Multiple large discrete components are required for conventional pulse oximeters. (c) Typical commercial non-invasive medical sensors today: oximeter and regional oximeter on a patient. (d) Societal benefits enabled by a new silicon photonic chips non-invasive sensor platform.

**Figure 1(b)** shows a schematic of the current discrete optics approach for oximetry. These devices consist of two LEDs, photodiodes, filters, and packaging. Light absorption is used to measure patient physiological data. Signal processing takes place using off-chip electronics, posing additional signal-to-noise issues beyond the scope of this proposal. A major drawback of the current approach based on two LEDs is that these devices cannot be used for patients with different skin pigmentations and skin thickness. At least four LEDs are needed to overcome these limitations. There are two related commercial applications that require up to eight LEDs: (1) carbon monoxide poisoning and (2) regional oximetry for improved surgical outcomes. **However, each additional LED increases the packaging cost of current devices and in turn makes them more expensive and unaffordable to the general**



**populace.** The economics simply do not work for the traditional, discrete optics solution. These specific examples are a direct illustration of a broader challenge for the entire medical sensor industry: **we need solutions for more medical data at a lower price point to expand access to healthcare.**

It is likely that many emerging applications in human health monitoring have not even been conceived of yet because of the limitations imposed by discrete optics. Quite simply, the traditional discrete optics platform that has been used to date cannot scale to meet the present and future needs of the \$20 billion non-invasive medical sensor industry. To overcome this challenge, we are introducing silicon photonics chips with printed photonic ink to the non-invasive medical device industry.

**Proposed Solution:** With the Iris Light solution, we can easily print more than four LEDs on a single photonic chip reducing the packaging cost compared to the discrete optics approach. Although myriad industries (e.g. optical communications, LIDAR, immunoassays, quantum) recognize the revolutionary potential of silicon photonics, a major obstacle hampering its growth is the lack of a suitable gain material for silicon. The main current method for coupling light into silicon is to bond a separate laser chip to the surface of the photonic integrated circuit (PIC), which is cumbersome and expensive (>20% of packaging cost). Moreover, current gain media have limited spectral bands unsuitable for medical sensing. Iris Light Technologies is solving this problem by developing a photonic ink that can be simply printed onto the surface of a pre-patterned PIC chip. The ink is based on the two-dimensional (2D) nanomaterial black phosphorus (BP). BP is a semiconductor that emits light covering 550-4000 nm (visible to near-infrared) based on tuning the number of atomic layers. We have already demonstrated proof-of-concept hybrid light sources that couple BP gain material with silicon resonators [3]. The low-cost photonic ink can be printed on-chip using commercially available, wafer-scale printing techniques including inkjet printing (IJP) and aerosol jet printing (AJP).

**Figure 1(c)** illustrates how silicon photonics will enable the medical sensor industry to grow. As devices become more complex, photonic chips rapidly overtake discrete optics in terms of health data per dollar. This transition point, marked by a yellow star in **Figure 1 (c)**, occurs when devices consist of four or more LEDs. At this point, additional LEDs can simply be printed onto a photonic chip to compensate for skin pigmentation, blood flow, and to detect CO poisoning which adds nominal device cost to the photonic chip compared to the discrete optics approach. Photonic chips leverage semiconductor wafer manufacturing and are suited to large volume production.

#### **Literature Review – medical non-invasives for oximetry**

**Commercial pulse oximetry (two wavelengths):** Since its first development by Japanese bioengineers in 1972 (Ear Oximeter OLV-5100), pulse oximeters have been used to measure blood oxygen saturation (SpO<sub>2</sub>) in patients. SpO<sub>2</sub> is determined by illuminating the skin and measuring light absorption. Two wavelengths of light, 660 nm (red) and 940 nm (near-infrared), are emitted using two different LEDs through translucent skin in the fingertips or earlobe to measure oxygenated blood and deoxygenated blood, respectively. The device calculates the ratio of absorption and translates this data into SpO<sub>2</sub> [2].

#### **Commercial medical devices (four or more wavelengths):**

Regional oximetry is a related application in which oxygen in tissue is measured in different regions of the body during surgery and improves patient outcomes. Commercial devices such as Nonin Equanox, Medtronic INVOS™, and Edwards ForeSight feature between two and five LEDs. A third non-invasive application is carbon monoxide (CO) poisoning for which Nonin recently released CO-Pilot™. This solution requires eight LEDs to perform. As a fourth example, the COVID pandemic brought the shortcomings of the current two LED pulse oximeter to light after people with different skin pigmentation received incorrect diagnoses [4]. Edwards has shown that more wavelengths are required to compensate for skin pigmentation. There is a clear need for a scalable solution like silicon photonics that incorporates more light sources into a single sensor.

#### **Emerging efforts in medical non-invasive sensing:**

The big players of the non-invasive medical industry (Medtronic, Edwards, Nonin) are still using discrete optics technology and are only beginning to learn about photonic chips. Medtronic appears to be the early leader with their involvement in the EU project CARDIS (R&D) and their investment in Rockley Photonics in 2021. However, they have not released a product using silicon photonics. In

addition, the product being worked on by Rockley targets smart watches, not medical sensors. This approach is expensive, and consequently not affordable to everyone, especially people from developing countries. Emerging companies like SiPhox (US) and AntelopeDX (Belgium) are working on introducing photonics to point-of-need and at-home diagnostic sensors. However, their approach relies on two separate pieces, a consumable test, and a reader unit containing the light source and additional components. This is only *partial* integration and limited in potential reach. It is worth mentioning that non-invasive optical glucose and blood pressure monitoring are also of significant interest for both the research and commercialization sectors and would additionally benefit from photonic integration.

**Black Phosphorus Photonic Devices and Inks:** Although first synthesized in 1914, BP was reintroduced as a 2D layered material at the beginning of 2014 [5]. Semiconductor BP exhibits desirable opto-electronic properties including direct-band gap light emission and high conductivity. The optical properties of BP *can be engineered* because its bandgap can be tuned *by the number of 2D layers* that are stacked together in a flake [5]. This makes BP highly tunable to achieve emission at broad range of wavelengths from visible 550 nm (1L) to 4000 nm infrared (bulk). Other 2D materials like graphene and transition metal dichalcogenides (TMD) are not suitable for these applications. Graphene lacks a band gap, does not exhibit optical gain, and is too noisy for detectors. TMDs are only direct band gap in the monolayer and are also not efficient light emitters for many wavelengths of interest.

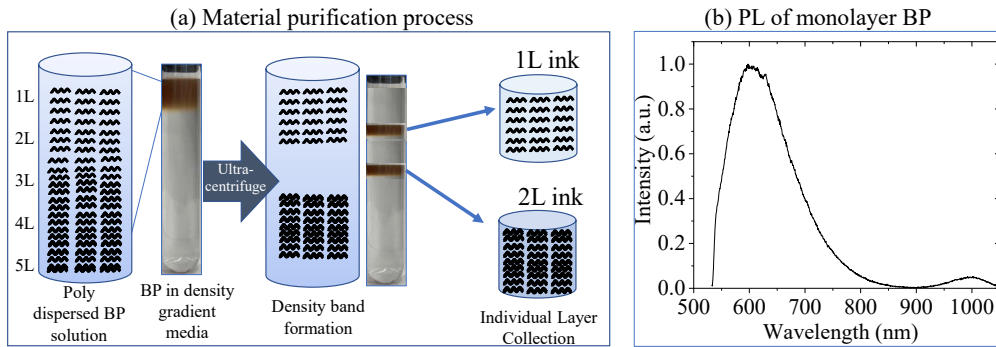
In recent years, the research community has demonstrated several examples of opto-electronic devices using BP that demonstrate the immense potential of this material. Examples of creating opto-electronic devices such as LEDs and detectors with BP have been shown [6,7]. Bulk BP (no nanomaterial) was used to show electroluminescence with limited efficiency (<0.01%) since the material was not electrically doped. Literature p-n junctions involving BP have required different partner 2D materials and metal contacts for the n-type. In contrast, n-type doped BP materials are the best route towards reaching efficiencies of greater than 1% and our motivation to pursue the approach. To date, *no commercial deployment of BP has been achieved*, likely due to the lack of scalable approaches. We are developing BP photonic ink using a method that was previously commercialized for graphene, highlighting a scalable path forward [8]. Note that the process needs to be engineered specifically for each material, which is the subject of this proposal. Additive manufacturing is a relatively young field and most inks in this industry are metallic (silver). To our knowledge, there is only one commercial graphene ink for R&D scale [9]. BP inks have only been demonstrated recently for *undoped, multi-layered* materials with unoptimized parameters [10]. Overall, there is a need for doped, single-layer BP inks to target specific optical properties. Beyond the immediate impact here, our success will fulfill a key need for semiconductor inks for emerging additive manufacturing of printed opto-electronics.

**Outline of tasks/Work plan**

OBJECTIVE	TASK	PROJECT MONTH											
		1	2	3	4	5	6	7	8	9	10	11	12
Purification of 1L & 2L nanomaterial inks based on 2D black phosphorus (BP)	1	M1											
Achieve desirable opto-electronic properties of 1L and 2L photonic inks	2			M2									
Demonstrate on chip printed LEDs with response at 660 nm and 940 nm.	3						M3						
Project reporting with Optica							**					**	

In terms of background achievements to date, we have achieved the following milestones:

- BP-Silicon light emitters - proof of concept:** first demonstration of hybrid Si-BP light source [11].
- Demonstrated scalability of photonic chips:** Designed, taped out, and optically characterized custom silicon photonics Bragg grating chips using the 300 mm silicon line at AIM Photonics [12].
- Demonstrated scalability of printed nanomaterial inks:** Developed a polydisperse ink (BP flakes with range of layers) and printed on AIM Photonics chips using aerosol jet printing. Demonstrated 550-2200 nm light emission and electrical conduction.
- Opto-electronic devices:** We achieved chip-scale passivation [11], demonstrated electrical contacts with numerous metals and characterized their properties [unpublished]. Currently, we are working on characterization of Schottky photodiodes using unpurified (polydisperse) ink.



**Figure 2: Separation of layers using DGU.** (a) Material purification process for 1L and 2L photonic inks using density gradient ultracentrifugation (DGU). The technique has been commercialized for graphene. (b) Photoluminescence data obtained for DGU separated monolayer BP at Iris Light.

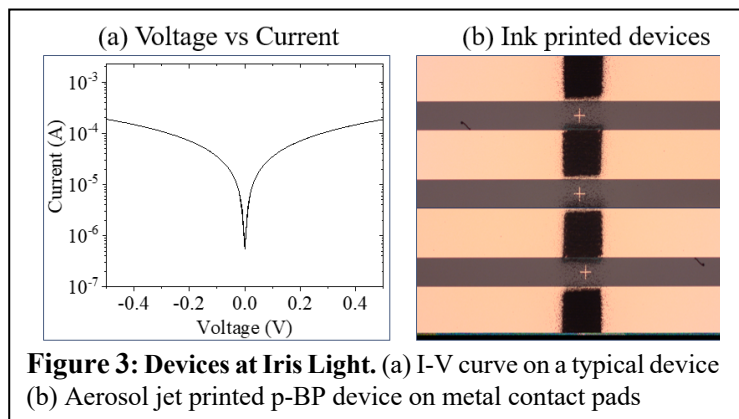
The overall technical goal of this proposal is to demonstrate printed opto-electronics (LEDs) based on novel photonic inks created from monolayer (1L) and bilayer (2L). Specific technical objectives include: (1) Purification of nanomaterial inks based on monolayer (1L) & bilayer (2L) black phosphorus, (2) Characterization of the opto-electronic properties of the 1L & 2L inks, and (3) Fabrication of printed LEDs at 640 nm and 940 nm that are needed for pulse oximetry. These objectives will be achieved through the following tasks:

**Task 1: Density gradient ultracentrifugation (DGU) separation of 1L and 2L BP.**

**Figure 2 (a)** shows the first critical step using DGU to separate BP by layer number. Layer purification of exfoliated BP is necessary to achieve wavelengths relevant for specific devices. DGU has successfully been used to separate layers of graphene [8,13]. Iris Light has already begun testing DGU for BP. **Figure 2 (b)** shows our preliminary data on successful separation of 1L BP from the exfoliated mixture using unoptimized DGU media. In particular, the photoluminescence (PL) matches isolated 1L material from the literature. Despite this initial success, there are several variables required to improve the material yield to a point where it is sufficient for printing on chips. A combination of surfactants and centrifugation parameters will be investigated to separate the 1L and 2L BP with maximum yield. **Milestone/Success metrics:** Photoluminescence spectra of the separated layers will show emission peaking at 620 nm for 1L and 1000 nm for 2L. Material yield of 10% or more.

**Task 2: Opto-electronics characterization of purified 1L and 2L n-type and p-type BP inks.**

BP is a native p-type material. We are currently developing an n-type photonic ink to make a complete p-n junction (funded by NSF). Iris Light has established the measurement protocol for electrical transport including current vs. voltage (I-V), transmission line measurements (TLM), and photo measurements. **Figure 3(a)** shows an I-V curve for a typical device with multilayer BP on metallic contacts with contact resistivity of  $10^{-2}$  ( $\Omega\text{-cm}^2$ ). The resistivity of these film is already more than two orders of magnitude lower than other printed BP films in the literature [10].



**Figure 3: Devices at Iris Light.** (a) I-V curve on a typical device (b) Aerosol jet printed p-BP device on metal contact pads

**Milestone/Success metrics:** Contact resistivity of  $10^{-3}$  ( $\Omega\text{-cm}^2$ ) and sheet resistance of 5,000 ( $\Omega\text{-sq}$ ) will be achieved. Commercial contact resistivity ranges from  $10^{-3}$  to  $10^{-8}$  ( $\Omega\text{-cm}^2$ ), and sheet resistance  $\sim 1,000$  ( $\Omega\text{-sq}$ ).

**Task 3: Demonstrate prototype LEDs at 660 nm and 940 nm suitable for pulse oximetry.**

After preparing the ink from 1L and 2L we will print on-chip LEDs in our foundry produced silicon photonic chips. LEDs capable of emitting wavelength of 660 nm and 940 nm will be achieved for measuring oxygenated and deoxygenated blood. **Figure 3(b)** shows an ink-printed photodiode device using polydisperse ink by the Iris Light team. **Milestone/Success metrics:** Measurements of LED

optical spectra with emission at 660 nm and 940 nm. Target external quantum efficiency (EQE) of 1% (current literature value is ~0.01% for undoped BP).

### **Outcome(s)**

The ultimate outcome for the project is the development of a new silicon-photonics approach for non-invasive medical sensors. Our initial devices will be ink-printed LEDs operating at 660 nm and 940 nm wavelengths and suitable for pulse oximetry. Along the way to reaching the final device, we will achieve additional key objectives. We will produce the first semiconductor photonic inks made from BP. Despite the rise of additive manufacturing, today most inks in this industry are metallic. Iris Light is filling a core need for semiconductor inks for advanced printed opto-electronics. In the long term, we will create a platform with an unprecedented number of distinct wavelengths in a single chip. Customer discovery interviews have revealed the need for collecting more relevant health information by non-invasive means. By combining our inks with silicon photonics, we will be able to achieve that objective, producing sensors capable of generating more relevant health data at an affordable price point. This advance will be achieved by printing multiple LEDs on a single photonic chip.

### **Impact**

**At scale, our solution developed with support from the 20<sup>th</sup> Anniversary Challenge offers the potential for broad societal and economic benefit shared globally.** The on-chip medical sensor platform will enable access to state-of-the-art medical care for people all over the world. Reduction of packaging costs compared to legacy optics will facilitate affordability so that people from all over the world will benefit from accurate, non-invasive devices. While the initial applications cited here are oximetry related, there is a vast range of applications that will benefit including cardiovascular diseases, continuous glucose monitoring for diabetes patients, diagnostic assays, and breath analysis. In terms of photonic innovation, the demonstration of low-cost integration of a novel gain medium based on printed photonic inks into silicon chips would mark a major path forward for the field. Indeed, getting light into silicon chips has been a long-standing issue and continues to inspire R&D and commercial efforts (see Integrated Photonic Systems Roadmap – IPSR). Our techno-economic analysis of the ink-based approach demonstrates the potential to be orders of magnitude lower cost compared to current and emerging approaches and offers a fresh perspective to the challenge.

### **References:**

1. W. R. Mower, G. Myers, E. L. Nicklin, K. T. Kearin, L. J. Baraff, and C. Sachs, "Pulse Oximetry as a Fifth Vital Sign in Emergency Geriatric Assessment," *Acad. Emerg. Med.* **5**, 858–865 (1998).
2. J. W. Severinghaus and Y. Honda, "History of blood gas analysis. VII. Pulse oximetry," *J. Clin. Monit.* **3**, 135–138 (1987).
3. C. Husko et al, "Silicon-Phosphorene Nanocavity-Enhanced Optical Emission at Telecommunications Wavelengths," *Nano Lett.* **18**, 6515–6520 (2018).
4. E. R. Gottlieb et al., "Assessment of Racial and Ethnic Differences in Oxygen Supplementation Among Patients in the Intensive Care Unit," *JAMA Intern. Med.* **182**, 849 (2022).
5. H. Liu, Y. Du, Y. Deng, and P. D. Ye, "Semiconducting black phosphorus: Synthesis, transport properties and electronic applications," *Chem. Soc. Rev.* **44**, 2732–2743 (2015).
6. N. Youngblood, C. Chen, S. J. Koester, and M. Li, "Waveguide-integrated black phosphorus photodetector with high responsivity and low dark current," *Nat. Photonics* **9**, 247–252 (2015).
7. J. Wang, A. Rousseau, M. Yang, T. Low, S. Francoeur, and S. Kéna-Cohen, "Mid-infrared Polarized Emission from Black Phosphorus Light-Emitting Diodes," *Nano Lett.* **20**, 3651–3655 (2020).
8. A. A. Green and M. C. Hersam, "Solution Phase Production of Graphene with Controlled Thickness via Density Differentiation," *Nano Lett.* **9**, 4031–4036 (2009).
9. E. B. Secor, P. L. Prabhurashi, K. Puntambekar, M. L. Geier, and M. C. Hersam, "Inkjet Printing of High Conductivity, Flexible Graphene Patterns," *J. Phys. Chem. Lett.* **4**, 1347–1351 (2013).
10. H. Y. Junet et al. "Inkjet Printing of Few-Layer Enriched Black Phosphorus Nanosheets for Electronic Devices," *Adv. Electron. Mater.* **7**, 2100577 (2021).
11. J. Kang, S. A. Wells, J. D. Wood, J.-H. Lee, X. Liu, C. R. Ryder, J. Zhu, J. R. Guest, C. A. Husko, and M. C. Hersam, "Stable aqueous dispersions of optically and electronically active phosphorene," *Proc. Natl. Acad. Sci.* **113**, 11688–11693 (2016).
12. C. Husko, A. Ducharme, N. M. Fahrenkopf, and J. R. Guest, "Phase-shifted Bragg gratings in a foundry silicon nitride platform," *OSA Contin.* **4**, 933 (2021).
13. X. Sun, D. Luo, J. Liu, and D. G. Evans, "Monodisperse Chemically Modified Graphene Obtained by Density Gradient Ultracentrifugal Rate Separation," *ACS Nano* **4**, 3381–3389 (2010).

**Name of the proposal:**

Ultra-low loss, all-fiber, acousto-optic isolators and circulators (LowLoCircl)

**Category:** Information

**Applicant:** Riccardo Pennetta, Humboldt University of Berlin

**Executive summary**

The introduction of low-loss optical fibers probably represents the single most important advance in the growth of our current global telecommunication system, which, in turn, fostered the rapid development of all kind of novel and more efficient fiber-based optical components. To meet our growing demand for secure communication and to interconnect future quantum computers, it is likely that our “classical network” will soon operate side by side of a so-called “quantum network”, which, extremely sensitive to loss, poses new constraints and challenges to the performance of existing fiber devices. In particular, already demonstrated quantum networks prototypes explicitly pointed out a surprising flaw in our current fiber technology, namely the absence of low-loss non-reciprocal fiber components (i.e., isolators and circulators). To date, the best commercially available fiber-coupled circulators rely on free-space optics and feature high insertion-loss of approximately 1 dB at telecom wavelengths, which only increases for NIR and visible light.

**Proposed project**

In this project, I propose a solution to this pressing technological challenge by designing and fabricating novel all-fiber non-reciprocal devices based on acousto-optic interaction. These devices will combine ultra-low insertion loss ( $<0.1$  dB), large extinction ratio (at least 20 dB), polarization independent operations and no frequency shift of the transmitted light. They will be built from standard single-mode fiber and therefore could be readily integrated into existing fiber networks. Furthermore, they will be electrically switchable and reconfigurable within a response-time smaller than 100  $\mu$ s.

The elementary units of my proposal are so-called fiber null-couplers. In brief these are fiber couplers, whose splitting ratio can be controlled via acoustic waves traveling along the coupler waist. It is well known that the acousto-optic effect breaks Lorentz reciprocity if the acoustic frequency is large enough, i.e., of the order of 1-10 GHz for fiber-based devices. However, in practice, it is really challenging (and not yet demonstrated) to excite such high frequency waves in optical fibers via electrical actuation, an imperative requirement for any technologically relevant device. In this proposal, I show that, some unique and, so far, unexplored properties of null-couplers allow to break Lorentz non-reciprocity with acoustic waves of any frequency. As a consequence, I demonstrate how this concept can be applied to the design of novel electrically-actuated all-fiber isolators and circulators with ultra-low loss.

**Intended outcomes**

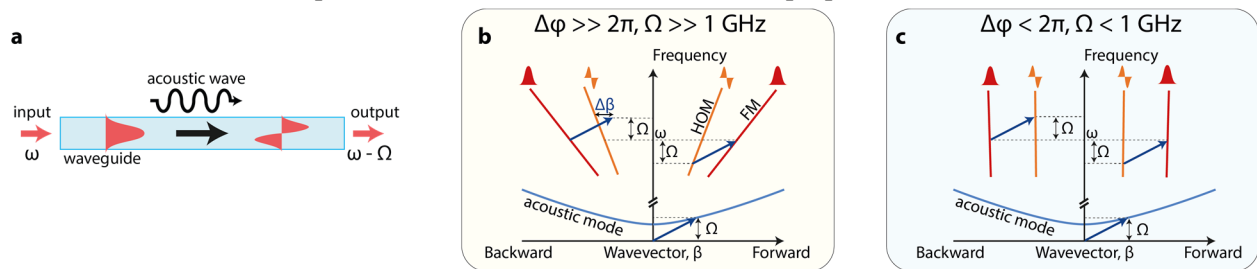
The most striking feature of the proposed devices is their ultra-low insertion loss, which is comparable to the one of standard fused couplers ( $< 0.1$  dB). For this reason, these non-reciprocal devices could become a new technological standard for all optical systems in which low-loss are key, as in particular for current and future quantum networks. Indeed, after an initial phase of careful design and parameters optimization, the future of these devices could go beyond the pure research environment, due to the relatively simple and potentially low-cost fabrication procedure.

# Proposal - Ultra-low loss, all-fiber, acousto-optic isolators and circulators

## Literature review

Non-reciprocal devices, such as isolators and circulators, constitute an important part of any optical setup and find application in simple tasks such as protecting a laser from back-reflections to more demanding operations as signal routing and processing in optical networks. Most off-the-shelf devices rely on the Faraday effect, an approach not easy to implement in integrated devices, may they be based on fiber-optics or photonic circuits, due to fabrication complexity, large material losses and difficulty in handling magnetic fields. For these reasons, extensive effort has been devoted to identify alternative ways to break Lorentz reciprocity, as for instance using non-linear optics [1], electro-optics [2], chirally coupled atoms [3] and acousto-optics. The latter has been particularly successful because of the strong coupling between light and acoustic vibration that can be achieved, when both waves are confined to small volumes, as for instance in tapered [4] and photonic-crystal fibers [5] or in photonic circuits [6-8] and whispering gallery mode resonators [9]. From a practical perspective, to date this approach is certainly the most promising for the next generation of magnetic-field-free non-reciprocal devices as it potentially allows low insertion loss, electrical actuation and linear input-output operations.

The best acousto-optic non-reciprocal devices in the literature roughly all rely on the same working principle, which is briefly explained in the following. Let us consider the configuration in Fig. 1(a), in which light (frequency  $\omega$  and wavevector  $\beta_{FM}$ ) propagates along a waveguide in its fundamental optical mode (FM). Let us now assume that an acoustic wave of frequency  $\Omega$  also co-propagates along the waveguide, causing a periodic modulation of its refractive-index. If phase-matching occurs, i.e., if the acoustic wavelength matches the beat-length between the FM and the first higher order mode (HOM), an energy transfer occurs between the two optical modes (see Fig. 1(a,b)). Interestingly, trying to use the same acoustic wave to couple backward propagating light fields (left-hand side of Fig.1(b)) results in a total phase mismatch [10]:  $\Delta\phi = \Delta\beta L = (\beta_{FM} + \beta_{HOM}) L \Omega/\omega$ , where  $L$  indicates the waveguide length. Non-reciprocal acousto-optic interaction occurs if  $\Delta\phi \gg 2\pi$  and, since for most experimental systems  $L < 10$  cm, it is only possible if the acoustic frequency  $\Omega$  is large enough (e.g.,  $\Omega \gg 1$  GHz). For a long time, exciting such high frequency waves required the use of auxiliary intense laser fields, which made the resulting devices unsuited for further applications [5, 10]. In the field of photonic circuits, electrical actuation of GHz acoustic waves has been reported only very recently [6-8], however, due to large in- and out-coupling loss, these state-of-the-art devices are not suited for low-loss fiber networks. To the best of my knowledge, no electrically-actuated all-fiber non-reciprocal device has been demonstrated or proposed so far.



**Fig. 1** (a) Diagram of acousto-optic interaction in optical waveguides:  $\omega$  is the light frequency and  $\Omega$  the acoustic frequency. (b,c) Dispersion diagram for optoacoustic intermodal coupling. (b) For large acoustic frequencies:  $\Delta\phi \gg 2\pi$ . The acoustic mode only phase-matches intermodal coupling in the forward direction ( $\beta > 0$ ). The wavevector mismatch in the backward direction is indicated with  $\Delta\beta$ . (c) In state-of-the-art electrically actuated all-fiber devices the achievable mechanical frequencies are usually small (1-50 MHz), therefore  $\Delta\phi \approx 0$ . The same acoustic can mediate intermodal coupling both in forward and backward direction. The resulting device are completely reciprocal.

## Problem Statement/Objective

Among the motivations behind the broad interest in non-reciprocal light propagation, one of the most startling and long-standing deficiencies of our current optical networks clearly stands out: the absence of fiber-coupled and low-loss isolators and circulators. Despite the great efforts and recent remarkable

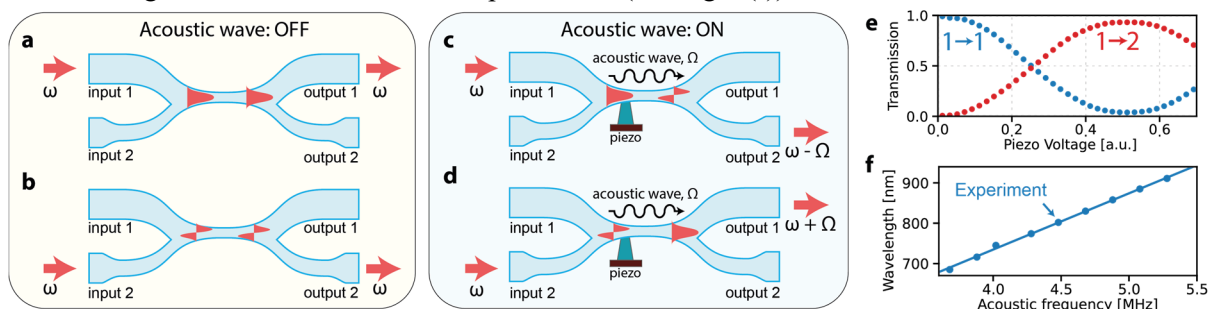


advances, this issue endures and is soon expected to become a substantial obstacle for the development of future quantum networks [11, 12], for which loss represents a highly undesired additional source of decoherence.

The main objective of this project is to provide a concrete and robust solution to this issue by the proof-of-principle demonstration of all-fiber non-reciprocal devices (both isolators and circulators) with ultra-low loss ( $<0.1$  dB) and high extinction ratios ( $>20$  dB). In addition, they will feature linearity (i.e., no frequency shift of the transmitted light) and polarization independent operations. Fabricated with standard single-mode fiber, these devices will be compatible with any existing or future optical network.

The key ingredient of this proposal is a particular type of fiber coupler known as null-coupler, first introduced by Birks et al. [4]. A standard fiber coupler is fabricated by heating and fusing together two identical fibers. Controlling the coupler length and degree of fusion allows any coupling ratio between 0% and 100%. However, if the fibers have different starting diameters, the maximum achievable coupling is less than 100%. A null-coupler is a fiber coupler made with fibers so dissimilar that the maximum coupling is approximately zero. In this case, adiabatic propagation along the coupler ensures that light launched into the larger fiber excites the FM of the coupler waist, eventually emerging from the same fiber at the other end of the coupler. The same occurs for light launched into the thinner fiber, which, instead, excites the HOM of the coupler waist (see Fig. 2(a,b)).

Acousto-optic interaction can transform a null-coupler in an arbitrary splitting-ratio coupler [4]. Let us consider the configuration in Fig. 2(c), in which a piezo transducer is employed to excite along the coupler waist acoustic waves, whose frequency and wavevector fulfills phase-matching between the FM and the HOM. As a result, light will couple from the FM to the HOM in an amount given by amplitude of the acoustic wave (see Fig. 2(c,d)). Figure 2(e) shows a preliminary measurement of this process for a null-coupler fabricated in our self-built fiber post-processing/tapering setup, based on a scanning hydrogen-oxygen flame. For a fixed acoustic frequency  $\Omega$ , the phase-matching condition is fulfilled over an optical bandwidth of a few nm, but by changing  $\Omega$ , phase-matching can be achieved for any frequency over the entire working bandwidth of the selected optical fiber (see Fig. 2(f)).

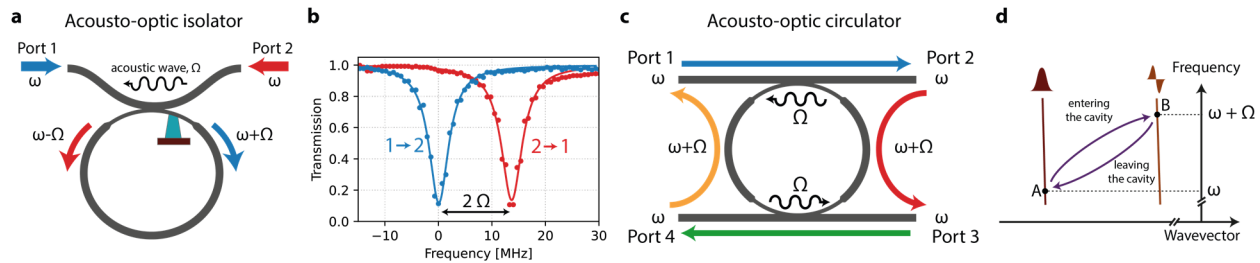


**Fig. 2** (a-d) Schematic representation of the working principle of a null-coupler. (e) Measured coupling ratio between the input and output port of a null-coupler as a function of the amplitude of the voltage applied to the piezo transducer ( $\Omega \approx 4.9$  MHz). The blue and red dots refers to the transmission measured from input 1 to output 1 and from input 1 to output 2, respectively. (f) Measured phase-matching wavelength as a function of the acoustic frequency,  $\Omega$ . The device was fabricated with standard SM800 optical fiber.

Light propagation in all null-coupler devices demonstrated so far was completely reciprocal. However, a more careful analysis of the system reveals that the acousto-optic effect actually causes a non-reciprocal frequency shift of the output light, whose sign depends on the relative direction of propagation of the light and acoustic wave. This equals  $-\Omega$  if the light and acoustic wave are co-propagating and  $+\Omega$  in the opposite case (see Fig. 1(c)). To use this to our advantage, let us consider the configuration in Fig. 3(a), in which the two ends of a null-coupler (input 2 and output 2 in Fig. 2) have been spliced together, in order to create a fiber ring-cavity. In this configuration, light traveling along the cavity has a different frequency depending on whether it was launched from port 1 or from port 2 (see Fig. 3(a)). Therefore, the cavity transmission spectra for  $1 \rightarrow 2$  and  $2 \rightarrow 1$  propagation will be shifted compared to each other by  $2\Omega$  (see Fig. 3(b) for some

preliminary measurement). **Optical isolation** can be achieved if the amplitude of the acoustic wave is set so that the ring-cavity operates at **critical coupling**, for which the transmission on resonance is zero.

This physical intuition can be extended to an **all-fiber circulator** considering the configuration depicted in Fig. 3(c), in which two null-couplers have been spliced together to form a ring-cavity with 4 input/output ports. By adjusting the amplitude of the acoustic wave, the cavity is operated in the so-called **add-drop** configuration, meaning that the coupling rate to the cavity is the same for both null-couplers and is much larger than the intrinsic cavity loss rate. In this case, light entering the cavity from the first null-coupler completely leaves through the second one. Optical circulation can be obtained by tuning the ring-cavity via, e.g., a piezo-stretcher [13, 14], so that light launched from port 1 and 3 is not resonant to the cavity and therefore completely transmitted to ports 2 and 4, respectively. At the same time, light launched from ports 2 and 4 enters the cavity and then emerges from ports 3 and 1, respectively (see Fig. 3(c)). Light transmission in any other direction is forbidden by the cavity resonance condition. To ensure operations with **no frequency shift**, the direction of propagation of the acoustic waves must be chosen, so that the shift imprinted when light enters the cavity is perfectly canceled when leaving it (see Fig. 3(d)). It is also necessary that both null-couplers operate at same the acoustic frequency. In practice this can be easily achieved using almost any two null-couplers, as the phase-matching acoustic frequency can be widely tuned by stretching the waist using, e.g., an additional piezo actuator [4].



**Fig. 3** (a) Schematic diagram of an acousto-optic isolator. (b) Preliminary measurement of optical isolation. The measured splitting of the cavity resonance of 13.62 MHz compares very well with the expected value of  $2\Omega = 13.58$  MHz. Already in this completely un-optimized device an extinction ratio of  $\approx 10$  dB could be obtained with total insertion loss of approximately 0.15 dB. (c) Schematic diagram of a 4-ports acousto-optic circulator, consisting of two null-couplers in an add-drop configuration. (d) Corresponding dispersion diagram: every time light enters the ring-cavity it is frequency up-shifted (A → B) and then again down-shifted to the original frequency, when leaving the cavity (B → A). In any configuration, the input and output light fields always have the same frequency.

## Outline of tasks/Work Plan

The route to the fabrication of technologically relevant non-reciprocal devices will require to address a number of challenges, which are schematically listed below in work points (WP).

### WP 1: Fabrication of polarization independent null-couplers

Optical components based on fused fiber-couplers are known to exhibit strong birefringence and polarization dependent operation, an issue that needs to be addressed for any meaningful isolator/circulator. Remarkably, the fabrication of polarization independent null-couplers has been demonstrated [15] and requires precise control of the degree of fusion of the coupler waist. This is currently beyond the capabilities of our post-processing setup, which was originally designed for the fabrication of optical nanofibers. For this project it will be necessary to: **WP1.1:** update the fabrication algorithm to improve the control over the shape and uniformity of the fabricated devices; **WP1.2:** equip the setup with a high-resolution optical microscope for real time inspection of the coupler shape and degree of fusion; **WP 1.3:** build an optical setup to measure the polarization properties of the produced null-couplers directly after fabrication **WP 1.4:** systematically characterize of the shape of the fabricated devices for all parameters of the tapering process and minimize the polarization dependence of their optical response.

### WP 2: Operations with large optical bandwidth

Non-reciprocal devices for applications in quantum networks and quantum technologies demand a bandwidth of the order of 100 MHz, as recently achieved in electrically-driven state-of-the-art photonic-

circuits [7]. Since in the proposed devices the bandwidth is approximately given by the acoustic frequency  $\Omega$  (see Fig. 3(b)), it is important to design the null-couplers such that  $\Omega \approx 100$  MHz. By changing the diameter of the coupler waist, the phase-matching acoustic frequency can be easily tuned from few MHz up to the GHz range, with the only limiting factor being availability of efficient actuators and drivers. So far, values up to only 40 MHz have been demonstrated [16], but given the significant technological advances in the field of RF amplifiers and piezoelectric materials, extending the bandwidth to the 100-200 MHz range seems within reach. This will require: **WP2.1:** careful selection and testing of new piezo actuators and relative drivers; **WP2.2:** more in-depth understanding of the transfer of acoustic energy between the piezo and the fiber waist; **WP2.3:** consequent design of new holders/clamps which allow efficient transfer of acoustic energy.

### WP 3: Fabrication and characterization of optical circulators

This is the key WP of this proposal. The fabrication of two high-quality null-couplers, in which phase matching occurs at the same acoustic frequency, will require to: **WP 3.1:** characterize the tuning of the phase-matching condition via piezo-controlled stretching of the coupler waist; **WP 3.2:** assembly an optical setup for the characterization of 4-ports optical circulators; **WP 3.3:** systematic study of the properties the circulator.

### WP 4: Packaging for long-lifetime

In a null-coupler light is guided at the interface between glass and air, making the device sensitive to pollutants that might be deposited on its surface over time. To ensure a long lifetime (of several years), we plan to: **WP 4.1:** design an air-tight mount that allows operation in low pressure. Lifetime of >10 years has been demonstrated for optical nanofibers using this approach. **WP 4.2:** as more elegant alternative, one could surround the coupler waist by a fluorine-doped low-index cladding during the fabrication process. This would allow to maintain guidance of light, while protecting the device from pollution. This approach will require a careful optimization of the null-coupler parameters due to the different refractive index step, but it was already proven to be successful in the field of photonic lanterns [17].

### Working team and duration of the project

This project has an expected duration of **1 year** and relies on the extensive background in the **fabrication and post-processing of glass fibers**, that I acquired during my education [18, 19]. From the beginning, I will be assisted by a **PhD student**, who will work with me on all WPs and whose salary will be covered by the project budget. At the end of the project, the student will continue their studies, partially under my supervision, in the group of **Prof. Arno Rauschenbeutel** (Humboldt University of Berlin, Germany), with the long term goal of integrating one of the realized circulators into a cold atoms experiment [14, 20] in order to build a quantum network prototype.

Month:	1	2	3	4	5	6	7	8	9	10	11	12
<b>WP 1: Fabrication of polarization independent null-couplers</b>												
<b>WP 2: Operations with large optical bandwidth</b>												
<b>WP 3: Fabrication and characterization of optical circulators</b>												
<b>WP 4: Packaging for long-lifetime</b>												

### Outcomes

The major outcome of this project will be the **demonstration of all-fiber ultra-low loss optical isolators and circulators**. After checking that the **intellectual property** is secure, the working principle, the fabrication technique and the experimental results will be **published** in an open access journal. Being able to fabricate such a unique device will be a splendid opportunity to **establish scientific collaborations:** we will partner with several research groups to discuss design constraints and possible use cases.

For instance, **Prof. Gerhard Rempe** (Max Planck Institute for Quantum Optics, Munich, Germany) already exhibited interest in integrating an ultra-low loss fiber circulator in his quantum networks prototypes. We

are also in contact with **Dr. Andreas Wicht** of the Ferdinand Braun Institute (FBH) in Berlin, who is currently considering alternative solutions to on-chip acousto-optics isolators due to their extremely large power consumption (few orders of magnitude larger than what required for a standard null-coupler [7, 4]). The FBH is one of the world leading institution in the fabrication of integrated quantum photonics components and its collaboration would be highly beneficial for us. Furthermore, **Prof. Nicolas Joly** of the Max Planck Institute for the Science of Light (Erlangen, Germany) would be interested in collaborating with us, as null-couplers represent an ideal platform for the long-sought-after generation of photon triplets in the field of quantum optics [21] and we are one of the few groups in the world able to fabricate them.

Last but not least, succeeding in this proposal would represent **a major step in my scientific career** and a unique opportunity to establish myself as a leader in my research field.

## Impact

Currently, the lack of all-fiber low-loss non-reciprocal devices represents the most striking flaw in existing fiber networks and one important ingredient still missing in the processing of quantum information stored in optical photons [11]. Succeeding in this project will represent a substantial and concrete step in solving this issue. From a more fundamental perspective, the proposed scheme demonstrates an additional and advantageous way to break Lorentz reciprocity, which could be easily extended to other platforms (e.g., photonic circuits). In addition, I would like to mention that, beyond non-reciprocity, this technology could be employed for the fabrication of ultra-narrow, low-loss and electronically reconfigurable filters, with linewidth from hundreds of GHz down to several hundred kHz, an ideal too for a large number of applications in quantum optics and quantum technologies.

Finally, given their compact size (few tens of  $\text{cm}^3$ ) and relatively simple and low-cost fabrication procedure, I believe that there is a concrete possibility that, in a time-span of few years, the proposed devices can become a commercially available tool for experiments in optics and phonics and set new standards in terms of low-loss in optical non-reciprocity.

## References:

- [1] L. Del Bino et al., “Microresonator isolators and circulators based on the intrinsic nonreciprocity of the Kerr effect”, *Optica*, 5, 279 (2018)
- [2] H. Lira, “Electrically Driven Nonreciprocity Induced by Interband Photonic Transition on a Silicon Chip”, *Phys. Rev. Lett.*, 109, 033901 (2012)
- [3] M. Scheucher et al., “Quantum optical circulator controlled by a single chirally coupled atom”, *Science*, 354 (2016)
- [4] T. Birks et al., “The acousto-optic effect in single-mode fiber tapers and couplers”, *J. Light. Technol.*, 14 (1996)
- [5] M. S. Kang, “Reconfigurable light-driven opto-acoustic isolators in photonic crystal fibre”, *Nat. Photonics*, 5 (2011)
- [6] E. A. Kittlaus et al., “Electrically driven acousto-optics and broadband non-reciprocity in silicon photonics”, *Nat. Photonics*, 15 (2021)
- [7] D. B. Sohn et al., “Electrically driven optical isolation through phonon-mediated photonic Autler–Townes splitting”, *Nat. Photonics*, 15 (2021)
- [8] H. Tian et al., “Magnetic-free silicon nitride integrated optical isolator”, *Nat. Photonics*, 15 (2021)
- [9] J. Kim, S. Kim and G. Bahl, “Complete linear optical isolation at the microscale with ultralow loss”, *Scientific Reports*, 7 (2017)
- [10] E. A. Kittlaus et al., “Non-reciprocal interband Brillouin modulation”, *Nat. Photonics*, 12 (2018)
- [11] D. Niemietz et al., “Nondestructive detection of photonic qubits”, *Nature*, 591 (2021)
- [12] D. Witthaut et al., “Photon sorters and QND detectors using single photon emitters”, *Europhysics Letters*, 97, 50007 (2012)
- [13] A. Johnson et al., “Observation of Collective Superstrong Coupling of Cold Atoms to a 30-m Long Optical Resonator”, *Phys. Rev. Lett.*, 123, 243602 (2019)
- [14] R. Pennetta et al., “Collective Radiative Dynamics of an Ensemble of Cold Atoms Coupled to an Optical Waveguide”, *Phys. Rev. Lett.*, 128, 073601 (2022)
- [15] S. Farwell, “2x2 fused fiber null couplers with asymmetric waist cross sections for polarization independent (<0.01 dB) switching”, *J. Light. Technol.*, 16 (1998)
- [16] D. Culverhouse et al., “40-MHz all-fiber acoustooptic frequency shifter”, *IEEE Photon. Technol. Lett.*, 8 (1996)
- [17] A. M. Velazquez-Benitez et al., “Six mode selective fiber optic spatial multiplexer”, *Opt. Lett.*, 40 (2015)
- [18] R. Pennetta et al., “Tapered Glass-Fiber Microspike: High-Q Flexural Wave Resonator and Optically Driven Knudsen Pump”, *Phys. Rev. Lett.*, 117, 273901 (2016)
- [19] Xie et al., “Self-alignment of glass fiber nanospike by optomechanical back-action in hollow-core photonic crystal fiber”, *Optica*, 3, 3 (2016)
- [20] R. Pennetta et al., “Observation of Coherent Coupling between Super- and Subradiant States of an Ensemble of Cold Atoms Collectively Coupled to a Single Propagating Optical Mode”, *Phys. Rev. Lett.*, 128, 203601 (2022)
- [21] Cavanna et al, “Progress toward third-order parametric down-conversion in optical fibers”, *Phys. Rev. A*, 101, 033840 (2020)

## **Executive summary**

- **Challenge**

Portable diagnostic or therapeutic devices based on purely microwave or optical analysis have proved their importance in health monitoring and remote health care services. But these devices lack versatility of applications and their range of operation is restricted by the inherent limitations of each technology. None of these devices are useful to monitor the condition of inner organs like kidney, liver, lung, bone, muscle, brain etc. Integration of the microwave and optical technologies can bridge this gap and can expand the scope of remote health care for a plethora of medical issues. This integration requires measuring the frequency of the microwave signal with high precision. Photonic measurement of microwave signal is a well-known research field and progressed a lot in recent years. But none of the reported techniques meet the three main criteria such as low fabrication cost, high precision and possibility to realize on an integrated photonic circuit platform simultaneously to translate this technique for our vision in healthcare applications. The challenge is to optimize the photonic technology, satisfying all these prerequisites such that the technology can be utilized to provide a personal diagnostic or therapeutic healthcare device which is presently unavailable.

- **Proposed project**

Our proposal is to integrate microwave and photonic technology to design a low cost portable diagnostic or therapeutic device to monitor different health conditions which is otherwise impossible with conventional personal healthcare machines. We shall use a microwave wearable antenna to probe the target. Any change happening in the target will be manifested by a change in dielectric property of the target. Hence the received microwave signal will be frequency shifted. Our previous simulations predict this shift may range from tens to hundreds of KHz. Such small frequency shifts cannot be tracked by any available RF measurement technology. On the other hand, an optical signal modulated by RF signal can be utilized to track the frequency change of the modulating RF signal. We shall utilize this property to design a photonic arrangement to measure the RF signal frequency with required precision. First we shall produce a proof of concept photonic arrangement. Next the proof of concept design will be tested with known microwave signal inputs. After this the design will be tested with real time data available from the microwave wearable device placed on human phantoms with specific conditions. Finally, the design will be fabricated on an integrated circuit platform and will be tested for validation.

- **Outcome**

The outcomes of the project can be divided in short term and long term outputs.

**Short term outcome:**

1. An integrated cost effective photonic device for measuring instantaneous RF signal frequency in a limited bandwidth with very high precision.

**Long term outcome:**

2. A portable, cost effective photonic-microwave device for self-assessment of health disorder to facilitate self-monitoring and remote diagnosis.
3. A low cost device for frequency measurement of RF signal which may be utilized in various other applications like communication engineering, military applications etc.

## Optica 20<sup>th</sup> Anniversary Challenge

Project Name: **Hybrid Photonic-Microwave diagnostic device for remote health care services**

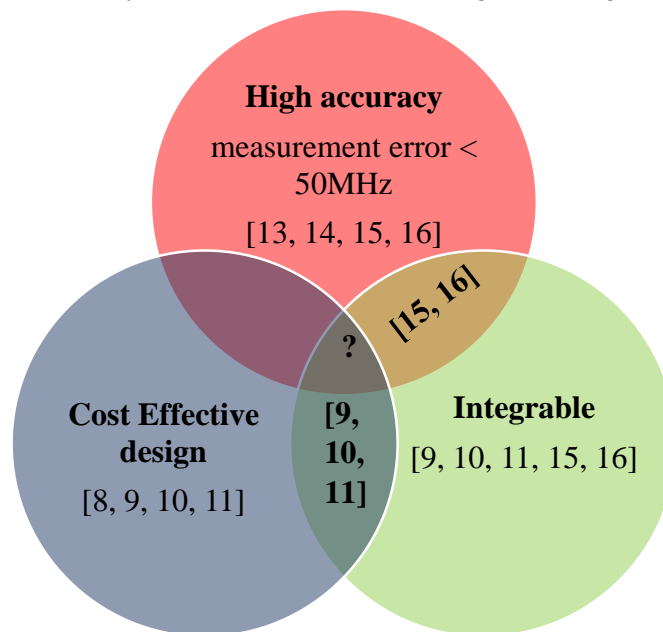
We are observing a huge demand in portable diagnostic or therapeutic devices. The modern life style has created a necessity to manage health related issues by constant monitoring at home without any supervision and this in turn opens an opportunity to bring health care services remotely. The recent pandemic also showed us the necessity of building such health care infrastructure. Though such self-care devices for monitoring of several health vitals like blood pressure, blood sugar etc. are available but monitoring the conditions of internal organs like lung or liver, bone and muscle condition, brain monitoring etc. are still dependant on imaging techniques like MRI, CT scan, X ray imaging etc., which requires professionals to operate. If a portable self-operating low cost device for such needs can be realized, then the remote health care services can be expanded to a large range of medical issues. Light-based diagnostic and therapeutic devices for different health care services are already available [1]. But these sensors cannot be used in for internal organs, since the penetration depth of the light signal depends on the operating wavelength [2]. Therefore, to reach the inner organs we need to use a large optical wavelength which may not be safe for human physiology. Implantable photonic therapeutic devices has emerged in recent times as a suitable option which can be used to monitor internal organs but they require surgical interventions and is not a general purpose solution [2]. On the other hand wearable microwave sensors emerged as a potential candidate for different disease detection like breast cancer, brain tumour, glucose measurements etc. [3] [4]. But the major problem of these microwave sensors is that a large change in signal is required to be detected by present radio frequency (RF) measurement technologies. This limits the use of such sensors for precise monitoring of human health condition since most of the times the change is very marginal and cannot be detected by present RF measurement devices. A new branch of research is developing in last few decades i.e. instantaneous frequency measurement (IFM) of radio frequency (RF) signals using photonic set up [5]. The integration of this technology with wearable microwave sensor technology can open up the possibility to achieve our goal i.e. a microwave sensor backed by a photonic analysis system can make it possible to detect or monitor the condition of internal organs with precision. The challenge is to produce a cost effective compatible optical system for this purpose.

### 1. Literature review

Many photonic IFMs have been conceived and demonstrated [6] [7] which can be classified on the basis of optical processes used to perform the frequency measurement. These various techniques can be broadly categorized into optical interferometry, polarization based responses, optical filtering, frequency to time mapping, optical mixing and Stimulated Brillouin Scattering (SBS). A recent study reported a photonic assisted IFM of RF signal which is scalable and can be implemented on integrated platform [8]. The reported scheme can measure the frequency of a RF signal within the frequency range DC to 20GHz with an error of 0.1GHz. A Sagnac interferometer based scheme is reported [9] to measure the frequency of RF signal between 0.01 to 40 GHz with a measurement error of less than 5% i.e. 250 MHz for 5GHz signal for RF power as low as -30dBm. Further improvement on measurement error can be achieved by using polarization based IFM. This approach utilizes the optical State of Polarization (SOP) to measure the unknown RF frequencies [10] [11]. This method was demonstrated to be accurate within the frequency range from 2 to 11 GHz with an error of ~50 MHz. The drawbacks of this technique include the need to calibrate the system, a small useable dynamic range and a reduced bandwidth in comparison with other methods. A modification of these scheme is experimentally demonstrated [12] where the bandwidth of the operation is increased from 2 to 23 GHz but at the expense of the measurement resolution of 200 MHz. In recent times few works were reported [13] [14] [15] where the measurement error can be brought down to few tens of MHz. All these works are based on utilizing the Brillouin scattering gain bandwidth to filter out the optical sideband generated from the modulation of an optical carrier by the RF signal. Since Brillouin scattering of an optical fiber has a very narrow bandwidth hence the photonic system can be tuned in such a way that the optical carrier experience peak gain during the scattering process while the modulated side band is shifted from the peak gain. Hence a difference in amplitude can be observed between the carrier and the sideband after the



scattering. The difference becomes dependent on the central frequency of the side band and therefore on the RF signal frequency and thus an amplitude comparison function can be defined. Measurement error upto 1 MHz has been reported [13]. But these systems require an optical fibre of length ~22km to produce sufficient amount of ACF. Hence they cannot be implemented on integrated platform. In 2015 [15] a work was reported which suggested a chip based architecture using the same mechanism for instantaneous determination of RF frequency with a measurement error of 1 MHz. But this requires multiple Mach Zehnder modulator which may not be a cost effective design. The frequency range is also between 9-38 GHz which may be outside the body safe radiation spectrum. Hence this scheme cannot be used for the specified purpose of this project. In 2021 Y. Wan et. al. experimentally demonstrated microwave frequency measurement from 1-20 GHz range with a measurement error of 40 KHz [16]. This system utilizes excitation of whispering gallery mode in a micro ring for detection of RF frequency. This shows that such measurement scheme can be implemented on an integrated platform. But the system requires recalibration if the ambient temperature changes. This makes the scheme unfit for ready to use devices. All these studies shows that IFM of microwave signal can be done through photonic arrangements and some of these schemes can be implemented on an integrated platform. The entire scenario may be described in the following Venn diagram



So it is evident that none of these technologies fulfil all the criteria like high resolution, cost effective and feasibility of implementation on an integrated circuit platform. Hence these area needs further attention to translate this technology for health care and other potential applications.

## Bibliography

- [1] S. H. Yun and S. Kwok, "Light in diagnosis, therapy and surgery," *Nat. Biomed. Eng*, p. 0008, 2017.
- [2] G.-H. Lee, H. Moon, H. Kim, G. H. Lee, W. Kwon, S. Yoo, D. Myung, S. H. Yun, Z. Bao and S. K. Hahn, "Multifunctional materials for implantable and wearable photonic healthcare devices," *Nat Rev Mater*, vol. 5, no. 2, pp. 149-165, 2020.
- [3] L. Wang, "Microwave sensors for breast cancer detection," *Sensors*, vol. 18, p. 655, 2018.
- [4] A. E. Omer, G. Shaker, S. Safavi-Naeini, H. Kokabi, G. Alquié, F. Deshours and R. M. Shubair, "Low-cost portable microwave sensor for non-invasive monitoring of blood glucose level: Novel design utilizing a four-cell CSRR hexagonal configuration," *Sci. Rep.*, vol. 10, p. 15200, 2020.
- [5] L. A. Bui, "Recent advances in microwave photonics instantaneous," *Progress in Quantum Electronics*, vol. 69, p. 100237, 2020.

- [6] S. Pan and J. Yao, "Photonics-based broadband microwave measurement," *J. Light. Technol.*, vol. 35, no. 16, pp. 3498-3513, 2016.
- [7] R. Maram, S. Kaushal, J. Azana and L. Chen, "Recent trends and advances of silicon-based integrated microwave photonics," *Photonics*, vol. 6, p. 13, 2019.
- [8] C. Yang, L. Wang and J. Liu, "Photonic-assisted instantaneous frequency measurement system based on a scalable structure," *IEEE Photonics*, vol. 11, no. 3, pp. 1-11, 2019.
- [9] H. Emami, M. Hajihashemi, S. Alavi, A. Supaat and L. Bui, "Microwave photonics instantaneous frequency measurement receiver based on a Sagnac loop," *Opt. Lett.*, vol. 43, no. 10, pp. 2233-2236, 2018.
- [10] T. Mengual, B. Vidal and J. Marti, "Photonic RF frequency measurement combining SSB-SC modulation and birefringence," *Opt. Commun.*, vol. 283, no. 13, pp. 2673-2680, 2010.
- [11] Y. Li, L. Pei, J. Li, J. Zheng, Y. Wang, J. Yuan and Y. Tang, "Instantaneous microwave frequency measurement with improved resolution," *Opt. Commun.*, vol. 354, pp. 140-147, 2015.
- [12] C. Yang, W. Yu and J. Liu, "Reconfigurable instantaneous frequency measurement system based on a polarization multiplexing modulator," *IEEE Photonics*, vol. 11, no. 1, pp. 1-11, 2019.
- [13] T. Shi and Y. Chen, "Multiple radio frequency measurements with an Improved frequency resolution based on stimulated Brillouin scattering with a reduced gain bandwidth," *Opt. Lett.*, vol. 46, no. 14, pp. 3460-3463, 2021.
- [14] D. Wang, L. Pan, Y. Wang, Q. Zhang, C. Du, K. Wang, W. Dong and X. Zhang, "Instantaneous microwave frequency measurement with high-resolution based on stimulated Brillouin scattering," *Optics and Laser Tech.*, vol. 113, pp. 171-176, 2021.
- [15] H. Jian, D. Marpaung, M. Pagani, K. Vu, D.-Y. Choi, S. J. Madden, L. Yan and B. J. Eggleton, "Wide-range, high-precision multiple microwave frequency measurement using a chip-based photonic Brillouin filter," *Optica*, vol. 3, no. 1, pp. 30-34, 2016.
- [16] Y. Wan, X. Fan, B. Xu and Z. He, "Microwave frequency measurement with high accuracy and wide bandwidth based on whispering-gallery mode barcode," *Opt. Lett.*, vol. 46, no. 19, pp. 5008-5011, 2021.

## 2. Problem statement/ Objective

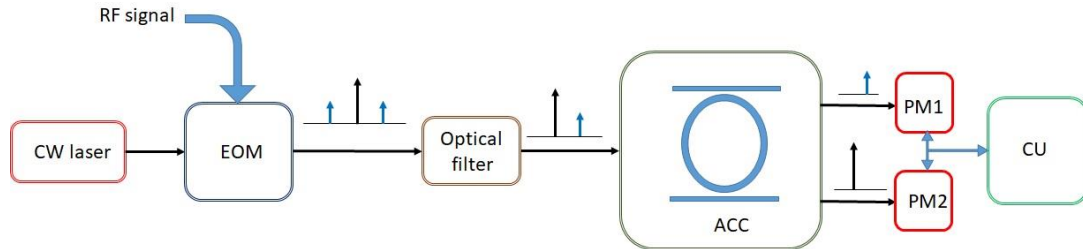
The overall objective of the project is to build a hybrid microwave-photonic sensor to detect and categorize changes in human bone, muscle and other internal organs condition which may lack in detailing than conventional imaging technique but will give an estimation with acceptable accuracy and can be implemented to build a portable health care device for therapeutic and diagnostic purpose. The microwave sensor will probe the target with a RF signal and will receive the reflected/transmitted signal. The photonic device will measure the change in frequency between the transmitted and received microwave signal. Afterwards these measurements will be linked with the appropriate health issues we intend to diagnose. The present scope of the project is to develop a low cost integrated photonic setup for determining the frequency of a microwave signal with desirable resolution, typically ~ 8-20 KHz.

## 3. Outline of task/ Work plan

### • Methodology

In the proposed project microwave antennas will be placed on different part of human body to collect the data of different physiological processes. The data will be in the form of RF signals. Whenever any change in the target region occurs the received RF signal from the target area will change its frequency and amplitude. Our study showed that the change in frequency is more consistent than the amplitude, but it is very small to be detected by any conventional RF measurement method. So we shall use an electro optic modulator to modulate an optical carrier signal with the received RF signal. The frequency of the sidebands of the modulated signal will be directly related to the RF signal frequency. Therefore, any change in frequency of the RF signal will be reflected as a frequency shift in the modulated optical sideband. We shall then develop an optical filtering process based on integrated micro-ring resonator to determine the frequency shift of the side band. Our experience

shows that in most of the cases the shift in RF signal is  $\sim 20\text{-}100\text{ KHz}$  with an input RF frequency of  $2.3\text{ GHz}$ . So our photonic design must have a measurement precision less than  $20\text{ KHz}$ . First we shall simulate the design of the integrated optical filter response through FEM (Finite Element Method) or FDTD (Finite Difference Time Domain) based simulator to optimize the design. Next we shall design the experiment to validate our results and finally some real time testing shall be performed to validate the proof of the concept. The schematic of the proposed scheme is shown in Fig. 1.



**Fig. 1:** Schematic of the proposed scheme. The spectrum at each output node is shown by the arrow diagram. The optical filter will suppress one of the side bands. ACC will compare the power available in the carrier and in the sideband. EOM: electro optic modulator, ACC: amplitude comparator circuit, PM: power meter, CU: computational unit.

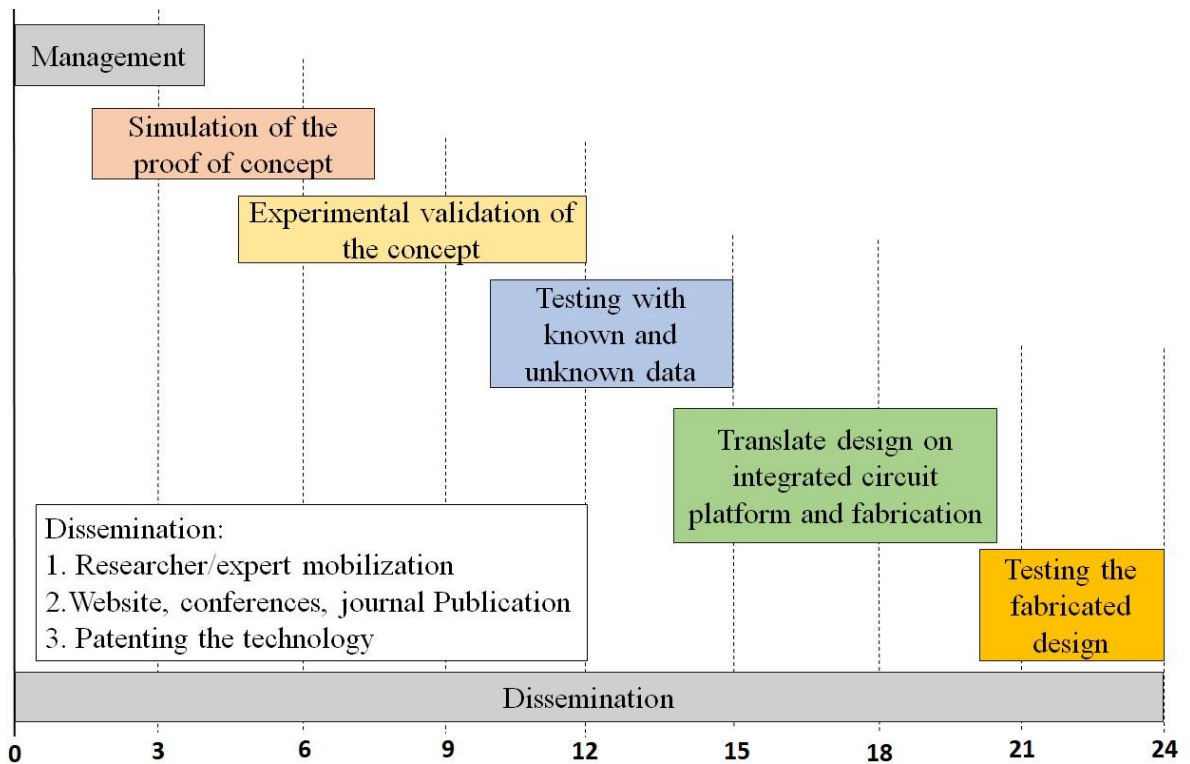
**A probable list of required equipment is as follows:**

1. Electro Optic Phase modulator
2. Laser diode with TEC driver
3. Power sensor
4. Power and energy meter
5. Power meter interfaces
6. Fiber polarization controller
7. PM fiber (100 m)
8. Single mode fiber (500 m)
9. Fiber accessories
10. Gain flattening fiber
11. Fiber interferometric setup
12. Tunable fiber optic bandpass filter
13. Tunable Laser source

• **The detailed work plans are as follows:**

Work Plan	Description
WP1: Project management	Allocating resources (e.g. equipment purchase and man power allocation) and coordinate with existing/potential collaborators about the deliverables of the project
WP2: Simulation design	Development of simulation environment to optimize the design of the proposed scheme
WP3: Dissemination Exploitation and Communication	Publication /workshops &conferences / mutual research visits
WP4: Experiment design	<ul style="list-style-type: none"> <li>• Design the experimental set up (at IEST)</li> <li>• Testing the system with known data (at IEST with intra department collaboration with Dr. Debasis Mitra)</li> <li>• Testing the system with microwave sensor input (at IEST with intra department collaboration with Dr. Debasis Mitra)</li> <li>• Validation of the scheme using human phantoms (in probable collaboration with Dr. Robin Augustine, Uppsala University)</li> </ul>
WP5: System integration and Demonstrators for application	Putting the devices together such that the analysis and detection can be done in real-time.
WP6: Dissemination Exploitation and Communication	Patenting of the product/publication

- The time frame of the work plans is provided as:



#### 4. Outcomes

The outcomes of the project can be divided in short term and long term outputs.

##### Short term outcome:

1. An integrated cost effective photonic device for measuring instantaneous RF signal frequency in a limited bandwidth with very high precision.

##### Long term outcome:

2. A portable, cost effective photonic-microwave device for self-assessment of health disorder to facilitate self-monitoring and remote diagnosis.
3. A low cost device for frequency measurement of RF signal which may be utilized in various other applications like communication engineering, military applications etc.

#### 5. Impact

The proposed project focuses on developing and integrating more than one technology to realize some health care devices which can be used at home by the user himself/herself for the health issues where no such scheme is present till date. The integration requires invention of a low cost integrated optical arrangement to measure RF signal frequency with utmost precision. This invention will not only impact health care industry, but this technology can be utilized for applications in the fields of military application, communication industry etc. The objective of this project focuses on but no limited to improving health care services. In turn the project will impact on uplifting the quality of light of the global population in various ways.

## Executive Summary

### **Nanophotonic scintillators for low-dosage X-ray imaging of sensitive materials and particularly its medical application in PET-CT scanners**

The purpose of our research is to develop a new kind of scintillators that are based on novel concepts in nanophotonics. Such scintillators will be orders of magnitude more efficient than those available today in medical imaging, particularly for CT and PET-CT scanners. Such a breakthrough will lower the dose rate of X-ray radiation inflicted on patients, which is especially critical for leukemia patients during diagnostics. Scintillators convert X-rays to easier detectable light, usually in the visible domain. The efficiency of this conversion is a bottleneck limiting most of the technology in this field. Our approach can increase brightness, sharpness, and conversion time, which is very important for the medical application of PET-CT scanners. The Optica award will enable us to participate in the 10-ps international challenge, aiming to shorten the scintillators conversion time to a regime that will revolutionize PET scans and all applications of time-of-flight detectors. We propose to achieve this goal by introducing the phenomenon of superfluorescence to the field of scintillators. This concept has been proposed in theory by our group, but has not been shown experimentally so far. Being based on fundamental science, our project is high-risk–high-gain, hard to finance by conventional means, yet having the potential for a major advance in medical imaging.

To achieve this ambitious goal, we will use the award as a stepping stone that will help us establish a new collaboration between international academic groups and health care industrial partners such as the PET-CT scanner division of the GE corporation. A very broad range of testing instrumentation and material production methods are available at Technion's inhouse facilities. The X-ray testing environment has been conceptualised and built by the applicant of this proposal in our own laboratory. The central tool of the project is a proprietary X-ray imaging microscope that is specially designed to characterise the performance of scintillation materials, which will be tested in real PET-CT scanners. With this instrumentation, we have recently achieved the first demonstration of the enhancement of the conversion efficiency by means of the Purcell effect in nanophotonics – showing the feasibility of the high-risk ideas of this proposal. The grant support will enable us to purchase a sensitive EM-CCD and an X-ray tube equipped with a polycapillary half-lens for parallel X-ray beam collimation. This equipment will enable us to achieve **superfluorescence-based scintillation**.

## **Nanophotonic scintillators for low-dosage X-ray imaging of sensitive materials and particularly its medical application in PET-CT scanners**

### **Literature review**

**Context / medical application:** The interactions of X-rays with matter are at the heart of many important imaging and characterization technologies. Perhaps one of the most high-profile applications is in medicine, where X-rays are used in various modalities (2D imaging in dental X-rays, or 3D imaging, as in computed tomography (CT) scans and PET scanners). Computed tomography plays an outsized role in modern medicine, serving as a “workhorse” imaging modality, deployed over a large range of tasks from the routine imaging of acute injuries to the early diagnosis of cancers. This central role stems from its unique capability of accessing three-dimensional (3D) voxel information with sub-micron resolution and highest efficiency to lower down the x-ray dose rate applied to patients.

CT, while being a mature technology, suffers from major limitations. One such limitation is a compromise between image quality and X-ray dose exposure. Eliminating this compromise would unlock the potential of CT scanner, **making X-ray imaging technologies a safe, fast, and high-resolution tool for the early detection of multiple pathologies, including tumors.** For instance, this would enable the imaging of tumors in their earliest stages of development, with very low and effectively riskless X-ray doses, enabling universal periodic screenings of various recurrent diseases and their efficient treatment. This could save up to 20,000 additional lives per year [1] just considering breast cancer in the US alone. More broadly, for cancers with limited screening rates due to the potential risk of X-ray exposure, the wide deployment of low-dose screening could save millions of lives over the next decade.

There are two main avenues to address these limitations: (1) the development of more sensitive and efficient X-ray detectors (e.g., more efficient *scintillators*, which convert X-rays into detectable visible photons) [2-5], (2) the development of more robust image-reconstruction algorithms that convert the X-ray detector signals into a human-interpretable image [6-7] (e.g., based on new sparsity-based reconstruction algorithms like compressed sensing and neural networks). Thus far, these two approaches have been considered separately. However, as shown by Roques-Carmes et al. [8], our close collaboration partner within the frame of this proposed project, by leveraging explicit information about the detection process in the reconstruction algorithms, the result can be far greater than the sum of the parts, offering potentially orders-of-magnitude dose reduction at the same quality. Whereas, the focus of this proposed project concentrates on the first approach: developing new generation efficient scintillators using new concepts of material design, such as Super-fluorescence, Purcell-effect-based directional enhancement in structured photonic crystals, and the controlled polarization by means of 3d printing technology [9-10]. Our approach can increase brightness, sharpness, and conversion time, which is very important for the medical application of PET-CT scanners. The Optica award will enable us to participate in the 10-ps international challenge [21], aiming to shorten the scintillators conversion time to a regime that will revolutionize PET scans and all applications of time-of-flight detectors. We propose to achieve this goal by introducing the phenomenon of superfluorescence to the field of scintillators. This concept has been proposed in theory by our group, but has not been shown experimentally so far. Being based on fundamental science, our project is high-risk–high-gain, hard to finance by conventional means, yet having the potential for a major advance in medical imaging. To achieve this ambitious goal, we will use the award as a stepping stone that will help us establish a new collaboration between international academic groups and health care industrial partners such as the PET-CT scanner division of the GE corporation.

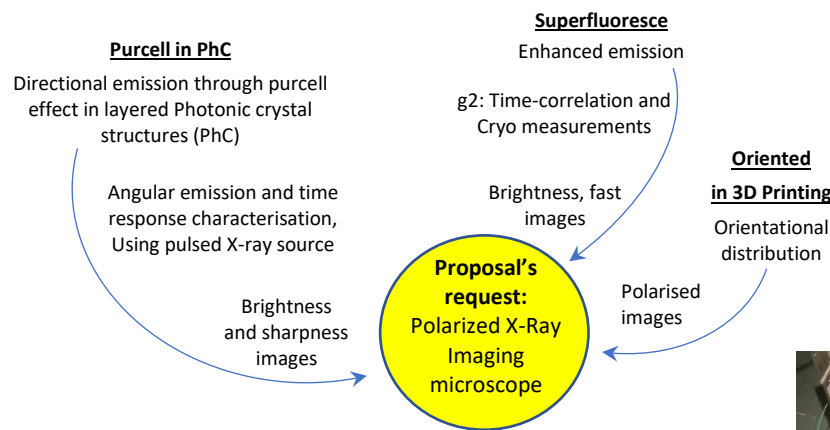
### **X-Ray testing facility:**

A very broad range of testing instrumentation and material production methods are available at Technion's inhouse facilities. The X-ray testing environment, though, has been conceptualised and built by the applicant of this proposal in our own laboratory. On the excitation side it comprises CW X-ray tubes as well as laser driven pulsed x-ray sources in order to achieve the development of 10-50ps

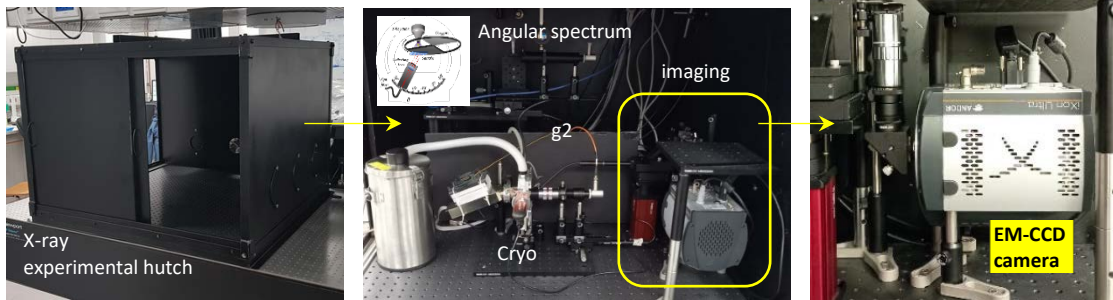


emission time scintillators. On the characterisation side, the experimental hutch has been equipped with an external spectrometer and with fibre optics based experimental stations for 1. angular emission measurements, 2. time correlation second order coherence ( $g_2$ ), 3. temperature dependant cryo stage, 4. preliminary imaging microscope setup. Fig. 1. Whereas, the central tool of the project is a proprietary X-ray imaging microscope that is specially designed to characterise the performance of scintillation materials, which will be tested in real PET-CT scanners. For the proof of concept, we have been using a borrowed CCD camera but for further research continuation we do require our own camera and collimated x-ray source, which will continue the successful progress of the project. With this instrumentation, we have recently achieved the first demonstration of the enhancement of the conversion efficiency by means of the Purcell effect in nanophotonics – showing the feasibility of the high-risk ideas of this proposal. The results are in the submissions stage for publication and are presented in the next paragraph. The grant support will enable us to purchase a sensitive EM-CCD and an X-ray tube equipped with a polycapillary half-lens for parallel X-ray beam collimation. This equipment will enable us to achieve the next step: **superfluorescence**-based scintillation.

**Development of advanced new generation scintillators with increased efficiency:  
Super-fluorescent, directional, faster, sharper and polarised emission**



**Application in medical PET-CT scanners to significantly lower down the radiation dose to patients**



**Fig. 1: Scheme of the research overview. The photographs show the experimental hutch and set-ups.**

**Recent achievements: Purcell effect-based emission enhancement in PhC structures:**

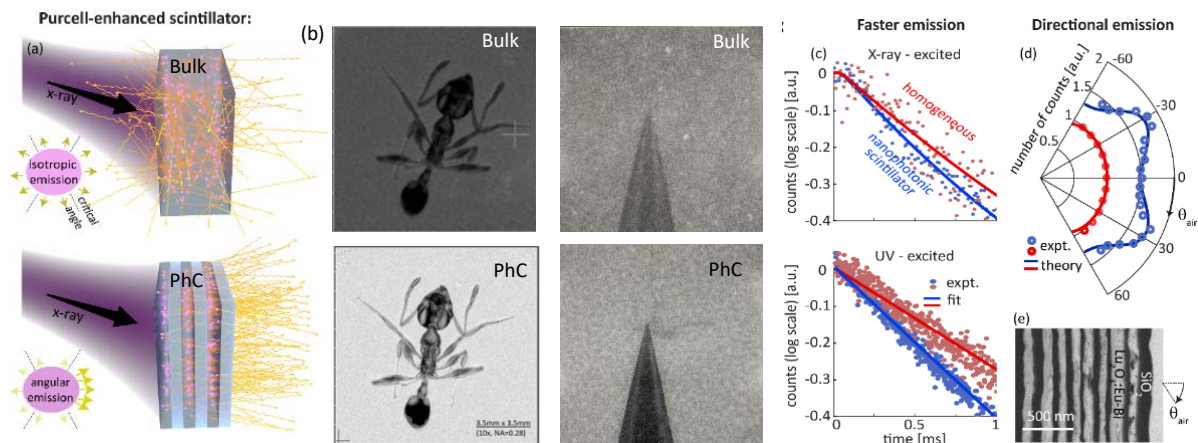
The concept of Purcell-enhanced scintillators has been recently proposed by our group [5], wherein the predetermined nanoscale geometry of the scintillator volume controls its intrinsic spontaneous emission properties. Such novel nanophotonic scintillators are bulk materials structured on the nanoscale with alternating index of refraction (in one, two, or three dimensions). Yaniv Kurman, our former PhD candidate working on this project, predicted that a precise nanostructure design could increase the emission rate and shape the angular distribution of spontaneous emission in scintillators, resulting in greater directionality and faster emission, via an angle-dependent Purcell effect. Our approach is

completely material agnostic and can be applied to both well-established and new scintillator material platforms, as long as their nanoscale geometry can be controlled.

We have demonstrated enhanced emission rate and yield following an X-ray excitation of a thin nanophotonic scintillator (paper in submission process). These enhanced capabilities arise from a specially designed nanophotonic structure prepared by alternating layers of a conventional scintillator (europium- and bismuth-doped lutecia,  $\text{Lu}_2\text{O}_3:\text{Eu-Bi}$ ) and a conventional dielectric (silica,  $\text{SiO}_2$ ).  $\text{Lu}_2\text{O}_3$  is selected for its combination of high atomic number and relative transparency in the relevant optical window (even when doped by Eu-Bi). We use a sol-gel method that enables the fabrication of exceptionally thin  $\text{Lu}_2\text{O}_3$  layers (under 100 nm), while being a scalable and inexpensive process for growing relatively homogeneous crystalline films [13]. More standard thin layer deposition techniques are challenging to adapt for scintillating oxides like  $\text{Lu}_2\text{O}_3$ , especially when large crystalline domains are required. Absorption of X-rays and energetic excitation of  $\text{Lu}_2\text{O}_3$ , is propagated to a Bi level that acts as a sensitizer when coupled to the Eu level. Radiative recombination in the Eu finally results in emissions of visible photons.

This designed multilayer structure enabled us to demonstrate the angle-dependent Purcell enhancement for both UV excitation (photoluminescence) and X-ray excitation (scintillation). The effect is reflected in enhanced spontaneous emission rates into desired directions and inhibited emission into undesired directions. Instead of being emitted isotropically (Fig. 2a, top panel), the generated photons are emitted to useful angles upon creation (Fig. 2a, bottom panel).

Our nanophotonic scintillator increases the overall scintillated light yield, showing brighter and sharper X-ray images (Fig. 2b) compared to a homogeneous scintillator film of the same material and thickness. Moreover, the Purcell effect enhances the scintillation rate of emission (Fig. 2c) – a result that has never been achieved for X-ray-induced processes. This is especially intriguing because the scintillation emission rate is often regarded as an intrinsic property of the material and is now shown to be modified by the geometry. Most intriguingly, our design shows tolerance to fabrication imperfections which we also explain theoretically. We stress that the same concept could be implemented with any scintillator material and could be generalized to additional geometries.



**Fig. 2 Comparison between bulk and PhC scintillator. Bulk emits isotropically whereas, PhC directional.**

Although shown successfully, several limiting factors of the sol-gel method hamper the fabrication of multilayered nanostructures and cause the deviation from our original design. These limiting factors include stress build-up between dissimilar layers that leads to sample non-uniformities in thickness and composition (i.e, the intermediate silicate phase). Thanks to the low quality-factor of the photonic design, the Purcell-enhanced scintillators are robust to such imperfections, as evident from matching the predicted enhanced X-ray scintillation to the measured data. It is currently unknown whether this robustness will persist for much thicker structures, where thickness variations may reduce out-coupling [5] (due to Anderson localization of the emitted light). Nevertheless, the sol-gel process may be further optimized to result in improved layer homogeneity, which enables scaling of the Purcell scintillator both laterally and in the number of layers.

## **Objective: Superfluorescence**

We propose a novel concept – of superfluorescent (SF) scintillators – to speed up the spontaneous emission time of scintillators and thus improve the ToF (time of flight) resolution of scintillator-based detectors, particularly in PET-CT detectors. To the best of our knowledge, the idea of superfluorescence scintillators, or any related effect of superradiance, has never been demonstrated or even proposed in scintillators. We will demonstrate the first measurement of superfluorescence excited by an X/ $\gamma$ -ray.

There are three aspects of quantum science that take place this research. (1) Using quantum optical measurements such as  $g(2)$  and Hong–Ou–Mandel to characterize the effect. (2) The use of novel quantum materials such as perovskite quantum dots. (3) The exploration of the superfluorescence [14–15] quantum effect. In SF, a number ( $N$ ) of emitters that fill a volume much smaller than the emitted wavelength ( $V \ll \lambda^3$ ) are excited simultaneously, and through an interaction with the quantized electromagnetic field, develop quantum correlations. The correlations cause the entire ensemble of emitters in the volume to emit at a much faster rate ( $\tau_{SF} = \tau_{spontaneous}/N$ ), preserving certain coherence that is not usually found in events of spontaneous emission from individual emitters. The result is a short intense light pulse with an intensity proportional to  $N^2$ .

Since this idea relies on demonstrating a fundamental concept – spontaneous emission – that appears at the core of many technologies, its implications go beyond medical imaging and can help improving other usages of ToF detection and other applications of scintillators.

We propose to develop scintillator samples with the physical requirements for SF. The requirements are long coherence times (which benefit from our measurements in cryo conditions), and large atomic numbers (to enable higher absorption cross-sections of X/ $\gamma$ -rays). Our two main candidates for such samples are single crystal LYSO doped with Ce and CsPbBr<sub>3</sub> quantum dots. LYSO(Ce) is a standard scintillator that is currently used for PET scans [16]. By combining nanophotonic techniques in the design and fabrication of such a sample, we hope to achieve an emission that passes the threshold of the SF regime. In comparison, CsPbBr<sub>3</sub> is a highly researched perovskite that is finding many novel usages, especially in recent years (such as is solar cells [17]). Recent research has shown that a large single crystal made from this material is a fast X-ray scintillator ( $\tau_{spontaneous} \approx 1$  ns) [18]; while other research has shown the SF effect under UV excitation at low temperatures from quantum dot clusters [15,19]. These recent experiments show the feasibility of the experiment we proposed. We hope to be the first to observe superfluorescent scintillation. This concept in fundamental science has only recently been proposed by our group (not published yet) and has never been observed.

In order to observe such an effect, we first need to develop an experimental system for measuring the SF effect from an X-ray excitation. We plan to perform spectroscopy measurements and second order coherence ( $g(2)$ ) [20] measurements at room temperatures and in liquid nitrogen (77K) temperatures, which according to literature should be low enough to enable SF5.

By applying  $g(2)$  measurements to X-ray-driven SF, we recently extracted the emission lifetime ( $\tau_{spontaneous}$ ) of a scintillator. This is the first time that  $g(2)$  measurements are applied for the process of scintillation, which enables measuring the scintillation lifetime without using a pulsed source.

## **Work plan: experimental milestones**

Milestone 1-6 months: assembling the system, alignment and fine-tuning. Theoretical background

Milestone 2-12 months: preliminary results for wide variety of materials. Choosing the most promising from them. Getting interesting photon statistics from them. Start design a PhC and 3D printed scintillators.

Milestone 3-18 months: collaboration with industry players such as GE, implementing the device and measuring coincidence under gamma radiation.

Milestone 4-24 months: achieving superfluorescence in scintillators under X/gamma radiation. Imaging SF and CT of SF, spectrum and  $g(2)$  as well.

## **Outcomes and Impacts (final remarks)**

The implications of better light yield and reduced decay times can have an impact on a wide range of scintillator technologies. Applications requiring relatively low-thickness scintillators such as free-electron cameras or night-vision devices could already benefit from multilayered structures of few-to-tens of microns, which are within reach of our current fabrication capabilities (from sol-gel to III-V quantum well growth [12]). The sensitivity of such technologies may be improved by the better light yield. In a different direction, the repetition rate of scintillation-based detectors could be enhanced by inhibiting afterglow with adequate spectral shaping via the Purcell effect. Many more applications may become feasible in the longer term, depending on breakthroughs in scaling the fabrication to larger volumes, as required for thick scintillators used in medical imaging and nuclear medicine. There, nanophotonic Purcell-enhanced scintillators could enable faster and better resolution scans, reducing the radiation exposure for patients. Therefore, our research and material design will continue to elaborate further on the Purcell effect together with our other approaches, such as the super-fluorescence and polarisation control in 3D printing.

In particular the fast reaction factor as well in parcel structures as in superfluorescence will play a role beyond applications to CT scans, as already pointed out, the scintillators developed in this project will find applications in other detection and imaging modalities involving high-energy particles, such as gamma-rays in PET scanners for molecular imaging, and detectors in high-energy physics. In the PET-CT scans, the patient is injected with a slightly radioactive substance, that tends to concentrate on cancerous tumours. Due to positron-electron annihilation in this material, a pair of photons (each with an energy of 511 keV, i.e., in the  $\gamma$  radiation regime) are emitted at the same time in opposite directions [11]. By placing the patient inside an array of detectors, one can currently roughly pinpoint the exact position and shape of the tumour. These detectors are comprised of  $\gamma$ -ray scintillators and photomultiplier tubes (PMT). The function of the scintillator material is to convert the  $\gamma$ /X-rays to visible light that in turn can be measured by conventional light detectors such as the PMT. The key limiting factor in these detectors today is the light emission time inside the scintillators. The shorter the conversion/ emission time of the scintillator, the less uncertainty we have in ToF measurements and therefore higher spatial resolution we are able to achieve. The emission time is fundamentally tied to the rate of spontaneous emission inside the scintillator and our scintillators provide the answer to those challenges.

## **References**

- [1] Cancer Prevention & Early Detection Facts & Figures 2021 - 2022, American Cancer Society
- [2] Gektin, Korzhik, et al., Inorganic scintillators for detector systems. Springer (2017)
- [3] Cherry, Sorenson, Phelps, Physics in Nuclear Medicine, Wiley (2012)
- [4] Chen et al., Nature (2018)
- [5] Kurman et al., Physical Review Letters (2020)
- [6] Graff et al., Applied Optics (2015)
- [7] Shen et al., Scientific Reports (2019)
- [8] Roques-Carmes† C. et al. A framework for scintillation in nanophotonics, Science 375 (2022)
- [9] Shilpa N. et al. ACS Applied Materials & Interfaces 8 (51), 35523-35533 (2016)
- [10] Zhou N, et al. Sci Adv. eaav8141 (2019)
- [11] Schmitz, R. E., Alessio, A. M. & Kinahan, P. E. The Physics of PET/CT scanners (2013)
- [12] Hospodková, A. et al. Radioluminescence and photoluminescence. Nanotech.25, (2014)
- [13] Nedelec, J. M. Sol-gel processing of nanostructured inorganic scintillating J. Nanomater, (2007).
- [14] Bonifacio, R. & Lugiato, L. A. Superfluorescence. II. Phys. Rev. A 12, 587–598 (1975).
- [15] Zhou, C. et al. Nat. Commun. 11, 329 (2020).
- [16] Schmitz, R. E., Alessio, A. M. & Kinahan, P. E. The Physics of PET/CT scanners (2013).
- [17] Zhou, C. et al.. Nat. Commun. 11, 329 (2020).
- [18] Mykhaylyk, V. B. et al. Sci. Rep. 10, 8601 (2020).
- [19] Rainò, G. et al. Nature 563, 671–675 (2018).
- [20] Lubin, G. et al. Opt. Express 27, 32863 (2019).
- [21] <https://the10ps-challenge.org/>

## Executive Summary

As an all-solid laser device, fiber lasers play a pivotal role in advanced manufacturing industry especially in the fields of space science, earth and environment science, medical and life science, due to the intrinsic advantages such as good beam quality, high lasing efficiency, compact structure and low energy consumption. The modernization of advanced fiber laser would become a powerful technical tool for mankind to further understand and transform the world. On the other hand, for free space science technology, such as space laser communication and remote sensing, light passing through a long-distance transmission would inevitably encounter the atmospheric turbulence, the cloud and the smoke which would cause strongly loss for the beam power and the interference for the information carried by the light wavefront due to the scattering effect induced by the inhomogeneous media. Therefore, it is of great importance for the free space science technology to further study the long-distance free space transmission based on the novel fiber laser light source which could mitigate the above limitations to some extent.

In the past decade, random fiber lasers (RFLs), featuring as an open-cavity structure, have attracted considerable attention due to the unique properties. In typical RFL configuration, random distributed Rayleigh scattering provides the optical feedback, while the stimulated Raman scattering (SRS) or active gain mechanism in rear-earth doped optical fiber provides the gain amplification. Therefore, no resonant cavity is needed in RFL, since the fiber itself bears with the three crucial components (i.e., the gain medium, the feedback mechanism and the optical confinement) for the lasing process. Thanks to the release of constraints from the conventional resonant cavity, various applications based on the concept of RFL have been innovated such as the generation of special lasing wavelength, high power/efficiency output, low noise lasing and remote distributed amplification. It is worth noting that by combining the high power/high spectral density and the low coherence features RFLs have been revitalized recently in the fields of high-power low coherence light source, speckle-free imaging, temporal ghost imaging and speckle correlated imaging.

In view of the above background, here in this proposal we focus on the research of digital fiber laser propagating through long distance free space transmission. The RFL based seed light source and possible modulation techniques could be integrated deeply by optimizing the wavelength, linewidth, power and polarization features of the lasing output, along with introducing the wavefront shaping and spatial coherence modulation techniques in order to realize high power low spatial coherence lasing light source that is preferable for long distance space transmission. Meanwhile, the retention characteristics of both the average beam power and the carried wavefront information passing through inhomogeneous medium would be considered comprehensively. We aim to provide alternative option of digital fiber laser light source that enables long distance transmission in the atmosphere for the development of space science such as free space laser communication and remote sensing.

# Digital random fiber laser for transmitting through atmospheric scatterings

## —Research Proposal

### 1. Literature Review

Laser light source is a powerful technique tool in advanced applications. For most practical applications, the laser light could be employed directly in near field or delivered across long distance within the confinement of waveguide such as optical fiber. However, for space science such as free space laser communication and remote sensing, light propagating through long distance would inevitably encounter atmospheric turbulence, the cloud which could be regarded as inhomogeneous media and would bring strong light scattering. Even for relatively shorter transmission distance in lidar, the capability of detection under strong smoke and fog is also a major restriction for its application. In those scenarios, it would not only reduce the average beam power of the emitted laser signal but also deteriorate the carried information on the wavefront. Therefore, it is of great importance to further study laser transmission through atmospheric scattering based on the novel fiber laser light source which could mitigate the above limitations to some extent.

To cope with the topic that light passing through strong scattering in atmospheric environment, we turn to a recently widely studied laser, the random fiber lasers (RFLs) [1]. As a special optical fiber laser, RFLs have been investigated extensively in the past decades due to the unique structure and the attractive lasing performance in contrast to conventional lasers. In typical incoherent feedback RFLs, random distributed Rayleigh scattering is directly employed to provide the optical feedback, while the nonlinear gain mechanism, such as the stimulated Raman scattering (SRS) or active gain in rear-earth doped fibers, provides the optical amplification. The open cavity structure (completely open or half open), i.e., without resonant oscillations, is the major feature of an incoherent feedback RFL, which nourishes its successful research branches in high efficiency/power output [2], agile lasing wavelength [3], narrow linewidth [4][5] or supercontinuum generation [6]. More importantly, in the past several years, the RFL has been innovated in the fields of speckle-free imaging [7], speckle correlated imaging [8], temporal ghost imaging [9]. These researches all consist of light transmitting through strong scattering medium such as ground glass or biological tissue, which is similar to the considered light signal propagating through atmospheric scatterings in space science scenarios. Therefore, utilizing the RFL as an effective laser light source may provide an attractive solution in dealing with laser transmission through atmospheric scatterings.

It is explicit that the direct use of previously reported RFL is still far away from the requirement to achieve high performance laser transmitting through atmospheric scatterings. The intrinsic lasing features such as the lasing wavelength and linewidth, the polarization and output power should be optimized firstly. For example, since the scattering strength is inversely proportional to the light wavelength, a longer wavelength is preferred when choosing the lasing wavelength of the RFL. After that, advanced wavefront shaping technique based on light field modulation [10] (e.g., the super pixel based optical field modulation using a digital micromirror device), along with spatial coherence modulation [7] (e.g., extra-large mode area multimode fiber) would be combined accordingly to further tailor the performances of the light beam. For example, it has been investigated that a partially coherent Gaussian beam could reduce intensity scintillations at the receiver in atmospheric turbulence [11]. Partially coherent vortex beams even show the property of



self-reconstruction which is attracting when considering laser transmission through atmospheric scatterings[12][13]. Therefore, by combining these advanced wavefront shaping techniques with the RFL, it is promising to develop a digital fiber laser that is suitable for laser beam transmission through atmospheric scatterings and serves the versatile applications in space science.

## Reference

- [1] S. K. Turitsyn, S. A. Babin, A. E. El-Taher, P. Harper, D. V. Churkin, S. I. Kablukov, J. D. Ania-Castañón, V. Karalekas, E. V. Podivilov, "Random distributed feedback fiber laser," *Nature Photon.*, 4, 231-235 (2010).
- [2] H. Zhang, L. Huang, J. Song, H. Wu, P. Zhou, X. Wang, J. Wu, J. Xu, Z. Wang, X. Xu, and Y. Rao, "Quasi-kilowatt random fiber laser," *Opt. Lett.* 44(11), 2613-2616 (2019).
- [3] L. Zhang, H. Jiang, X. Yang, W. Pan, S. Cui, and Y. Feng, "Nearly-octave wavelength tuning of a continuous wave fiber laser," *Sci. Rep.* 7, 42611 (2017).
- [4] S. Sugavanam, N. Tarasov, X. Shu, and D. V. Churkin, "Narrow-band generation in random distributed feedback fiber laser," *Opt. Express* 21(14), 16466-16472 (2013).
- [5] L. Zhang, C. Wang, Z. Li, Y. Xu, B. Saxena, S. Gao, L. Chen, and X. Bao, "High-efficiency Brillouin random fiber laser using all-polarization maintaining ring cavity," *Opt. Express* 25(10), 11306-11314 (2017).
- [6] R. Ma, Y. J. Rao, W. L. Zhang, X. Zeng, X. Dong, H. Wu, Z. N. Wang, and X. P. Zeng, "Backward supercontinuum generation excited by random lasing," *IEEE J. Sel. Topics Quantum Electron.* 24(3), 0901105 (2018).
- [7] R. Ma, Y. J. Rao, W. L. Zhang, and B. Hu, "Multimode random fiber laser for speckle-free imaging," *IEEE J. Sel. Top. Quantum Electron.* 25(1), 0900106 (2019).
- [8] R. Ma, Z. Wang, H. H. Zhang, W. L. Zhang, and Y. J. Rao, "Imaging through opacity using a near-infrared low-spatial-coherence fiber light source," *Opt. Lett.* 45(13), 3816-3819 (2020).
- [9] H. Wu, B. Han, Z. Wang, G. Genty, G. Feng, H. Liang, "Temporal ghost imaging with random fiber lasers," *Opt. Express* 28 (7), 9957-9964 (2020).
- [10] S. A. Goorden, J. Bertolotti, A. P. Mosk. "Superpixel-based spatial amplitude and phase modulation using a digital micromirror device," *Opt. Express* 22(15), 17999-18009 (2014).
- [11] J. C. Ricklin and F. M. Davidson, "Atmospheric turbulence effects on a partially coherent Gaussian beam: implications for free-space laser communication," *J. Opt. Soc. Am. A* 19(9), 1794-1802 (2002).
- [12] B. Perez-Garcia, A. Yepiz, R. I. Hernandez-Aranda, A. Forbes, and G. A. Swartzlander, "Digital generation of partially coherent vortex beams," *Opt. Lett.* 41(15), 3471-3474 (2016).
- [13] J. Zeng, R. Lin, X. Liu, C. Zhao, Y. Cai, "Review on partially coherent vortex beams," *Front. Optoelectron.* 12, 229-248 (2019).

## 2. Problem Statement/Objective

### 2.1 Problem Statement:

(i). The optimization of RFL to meet the requirement of propagating through atmospheric scatterings.

The basic features of RFL, i.e., wavelength, linewidth, polarization and output power, need to be comprehensively optimized firstly. The lasing wavelength is preferable at  $\sim 1.6 \mu\text{m}$  which shows a lower scattering effect and a relatively high output power that could be obtained. In free space laser communication or lidar, coherent detection is generally employed which requires the laser light

source to have a narrow linewidth. Polarized lasing would greatly enhance the signal detection capability when light transmitting through scattering medium. Therefore, all these features should be optimized firstly and further combined with the high average power of RFL.

(ii) Optimization transverse mode in terms of spatial coherence and wavefront shaping.

The transverse mode features of the emitted laser light source play an important role in propagating through long distance especially when confronts with atmospheric scatterings. It has been demonstrated that partially spatial coherence is optimal for free space laser communication since the intensity scintillations at the receiver could be greatly reduced. Therefore, the spatial coherence of the emitted RFL should be modulated based on mode composition theory and the decoherence when employing multimode fiber. After that, the wavefront of the obtained partially coherent lasing should be further modulated in combination with super-pixel based optical field modulation using a digital micromirror device to realize a partially coherent vortex beam which has the self-reconstruction feature in the propagation. At last, the retention characteristics of both the intensity and the wavefront should be monitored at long distance accompanied by atmospheric scattering.

## 2.2 Objective

To realize a partially coherent random vortex beam that is capable for long distance free space propagating especially through atmospheric scattering. The characteristics of the random laser light source (i.e., the wavelength, the linewidth, the polarization, the output power), the transverse mode features (i.e., spatially decoherence and wavefront shaping) and the propagating through atmospheric are all considered to meet the requirement of the above objective.

## 3. Outline of tasks/Work Plan

### 3.1 Outline of tasks

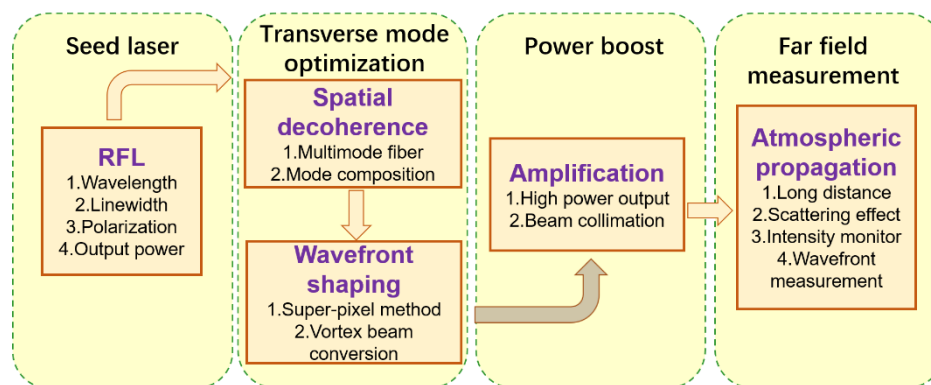


Fig.1 the outline of tasks

As shown in the above diagram, the proposed task could be divided into four major parts:

(i). The seed laser, that is to achieve a 1.6  $\mu\text{m}$  band RFL with narrow linewidth ( $\sim 100$  MHz) and polarized output with an appropriate output power for the following steps.

(ii). Transverse mode optimization, that is to achieve a partially coherent RFL through multimode fiber based decoherence and further convert it into a partially coherent vortex beam through wavefront shaping technique.

(iii). Power boost, that is to amplify the modulated laser beam to a relatively high average power ( $>10$  W) for long distance propagating.

(iv). Far field measurement, that is to characterize the intensity and wavefront feature of the laser beam after transmitting through long distance atmospheric scattering.

### 3.2 Work plan

Based on the above outline of tasks, we plan to proceed this project in the next two years. The work plan also follows the outline as listed above.

#### (i) Polarized narrow linewidth RFL

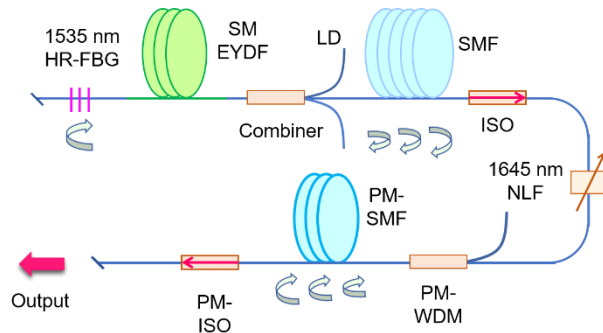


Fig.2 Schematic diagram of the RFL seed

The 1645 nm RFL seed is a half-open cavity structure composed of all-polarization-maintaining (PM) fiber and 1645 nm narrow linewidth filter (NLF), as shown in Fig. 2. The pump source here is a 1535 nm RFL which is also excited in a half-open cavity using EYDF as the initiated gain. The relationship between the linewidth of the NLF and the final output needs to be carefully investigated to mitigate the spectral broadening effect. This procedure is going to be carried out during Jan. 2023~May. 2023.

#### (ii) Transverse mode optimization of the polarized RFL

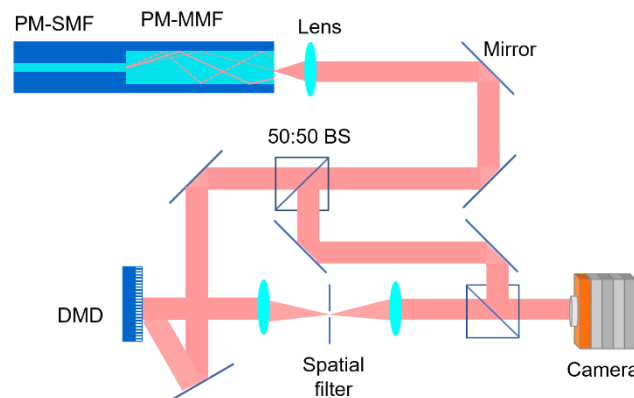


Fig.3 Decoherence using multimode fiber and wavefront shaping using super-pixel based method

Partially spatial coherent laser could be obtained by injecting the single mode laser into a piece of multimode fiber (MMF). The length and coupling condition would be detailedly investigated. After that, super-pixel based optical field modulation using a digital micromirror device (DMD) is employed to convert the Gaussian mode into a partially coherent vortex beam. Both the intensity and the phase distribution need to be optimized here. The characteristics of the modulated laser beam would be investigated using the off-axis digital holography as shown in Fig. 3. This procedure is going to be carried out during Jun. 2023~Dec. 2023.

#### (iii) Laser beam amplification

Although the DMD could bear relatively high input power, after the wavefront shaping the power of the final output beam would be greatly restricted. Therefore, laser beam amplification based on Er:YAG or other available solid crystal would be considered to boost the average power to at least

~10 W. This procedure is going to be carried out during Jan. 2024~May. 2023.

(iv) Far field measurement under atmospheric scattering

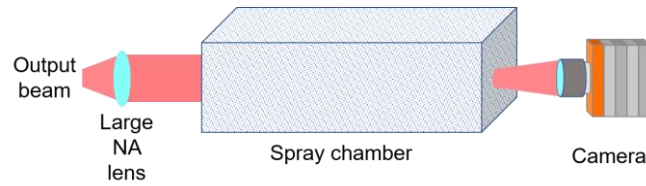


Fig.4 Spray chamber based transmitting through atmospheric scattering

Far field measurement using both the experimental spray chamber (Fig. 4) and the real outfield test would be considered to characterize the features of the obtained partially coherent random vortex beam in transmitting through atmospheric scattering. The scattering strength would be modulated to investigate the limitation of the transmitting capability. Both the intensity and wavefront feature of the laser beam needs to be characterized. This procedure is going to be carried out during Jun. 2024~Dec. 2023.

#### 4. Outcome(s)

- (i) Realize a partially coherent random vortex laser beam based on digitally modulated fiber laser.
- (ii) Characterize the capability of transmitting through atmospheric scattering of the proposed laser beam.
- (iii) Publish 2~3 journal articles in the field of optoelectronics. Participate in international conference 1~2 times for academical interaction.

#### 5. Impact

This proposal would combine laser beam propagation through atmospheric scattering, RFL and advanced wavefront shaping technique together. The flexible lasing wavelength and available output power of the RFL seed, and the partially coherent vortex beam would both contribute to laser beam transmitting through long distance in free space. The proposed digital laser would benefit the space science such as free space communication, lidar and remote sensing.

## **Executive Summary**

Stress is a unique individualized experience that can both cause a disease and exacerbate existing neuropsychiatric diseases such as mood-, substance use-, and eating disorders. The global COVID-19 pandemic has caused affective disorder prevalence to balloon, and it is expected that numbers will continue to rise at alarming rates in the coming years. Despite this clear urgency, neuroscience research has shown painstakingly little progress when it comes to diagnoses, prevention, and prognosis of stress-related disorders. Sophisticated optical approaches must be adopted to understand how- and which- dysfunctional brain circuits drive affective disorders. Light sheet microscopy has emerged as a powerful tool to image large intact samples with high resolution. Used in conjunction with optogenetic and genetic manipulation strategies, light sheet microscopy provides a unique opportunity to perform large scale functional and structural circuit mapping with single cell resolution.

*Why are certain individuals susceptible to stress disorders, while others appear to be resilient?* Early detection of stress effects on the brain can help predict affective disorder vulnerability and improve precision of interventional strategies. Using targeted functional brain imaging to characterize an individual as being 'high risk' for developing an affective disorder or stress-induced relapse in a patient with a substance use disorder can dramatically impact individualized treatment strategies, reducing the cost burden of treating affective disorders *after* they manifest. Achieving this goal begins with robust preclinical models that are conducive for innovative optical imaging approaches with novel viral labelling and biosensor technologies. These studies are optimally designed for using holistic, environmentally controlled approaches to unbiasedly characterize brain networks regulating the larger stress response. To this end, our goals are to 1) elucidate unique brain circuit biomarkers impacted by stress, 2) characterize distinct stress-specific neuronal ensembles within these circuits, 3) identifying potential key sex differences in stress response brain circuitry, and 4) isolate circuit- and ensemble-specific biomarkers that can predict- and be targeted to prevent or mitigate- stress disorders.

**This project will use whole brain light sheet microscopy and neuronal ensemble-specific optogenetics to identify and manipulate stress ensembles in the mouse brain. We will gain unparalleled insight into the mechanism underlying stress disorders, paving the way for improved prevention, diagnosis, and treatments.**

**Aim 1: Identify whole brain stress-activated ensemble circuitry using light sheet microscopy with automated high-resolution single-cell brain atlas registration.** We will use a genetic mouse line, FosTRAP2, that facilitates permeant access to transiently active neurons to isolate and fluorescently-tag stress-activated neurons in the mouse brain. Once tagged, these brains will undergo delipidation (i.e., "clearing"), whole brain imaging with light sheet microscopy, and automated machine learning-based single cell detection, quantification, and atlas registration. Accordingly, we will develop and provide a comprehensive database containing the location of all stress activated neurons in the male and female mouse brain.

**Aim 2: Use optogenetic inhibition of the insula to assess the effects of "removing" this network hub on anxiety-like behavior.** We and others have identified the insular cortex (insula), a cortical area intimately involved in emotional regulation, sensory processing, valence, decision making, and many other behaviors, as an affective network hub that regulates amygdalar circuitry. Aim 2 will zero in on insula stress ensembles to determine if optogenetically inhibiting this population of cells can prevent the emergence of negative affect in mice.

This highly translational and reverse-translational approach has the potential to shift how affective disorders are diagnosed and treated by defining biomarkers early in disease progression. Understanding how stress impacts the brain at a molecular and circuit level *before* affective disorders manifest can vastly improve strategies to mitigate the long-term impacts of stress and identify those at risk for developing affective disorders.

## **Literature Review and Problem Statement/ Objective**

Stress regularly impacts our lives to some degree, yet we still do not fully understand the wide range with which it can alter normal brain function. Stress is a unique individualized experience that can both cause a disease and exacerbate existing neuropsychiatric diseases such as mood-, substance use-, and eating disorders. A strikingly strong correlation exists between stress and depression and anxiety, of which close to 50 million adults in the US are diagnosed, but only ~40% are successfully treated. The global COVID-19 pandemic has caused these numbers to balloon, and it is expected that stress-related disorders will continue to rise at alarming rates in the coming years (Öngür et al., 2020 *JAMA*, Turközer et al., 2020 *Mol Psychiatry*). Despite this clear urgency, neuroscience research has shown painstakingly little progress when it comes to diagnoses, prevention, and prognosis of stress-related disorders. Much of this failure can be attributed to the foundation that neuroscience research is based on- hypothesis driven studies that examine brain regions in isolation or single-synapse circuits (e.g., Penfield, Hodgkins & Huxley, etc.). While these foundational studies laid the groundwork for modern neuroscience, technical limitations thwarted continued progress. Imaging or recording synaptic activity in the whole brain is extremely cumbersome with traditional technologies. Sophisticated optical approaches must be adopted to understand how- and which- dysfunctional brain circuits drive affective disorders. Light sheet microscopy has emerged as a powerful tool to image large intact samples with high resolution. The decoupling of the detector from the illumination source facilitates optimized numerical aperture that minimizes photobleaching and allows for high magnification imaging with large working distance. Rapid advancements in tissue delipidation approaches to increase light penetration while minimizing scattering underscore the vast potential for this technique. Advanced optics with circuit-specific optogenetic manipulation and novel genetic and viral tracing strategies in preclinical models can significantly impact the speed and accuracy with which functional brain network activity can be characterized.

*Why are certain individuals susceptible to stress disorders, while others appear to be resilient?* Answering this question begins with robust preclinical models that are conducive for innovative optical imaging approaches with novel viral labelling and biosensor technologies. These studies are optimally designed for using holistic, environmentally controlled approaches to unbiasedly characterize brain networks regulating the larger stress response. Using targeted functional brain imaging to characterize an individual's risk of developing an affective disorder or stress-induced relapse can have a dramatic impact on individualized treatment strategies and reducing the cost burden of treating affective disorders *after* they manifest. To this end, our goals are 1) elucidate unique brain circuit biomarkers impacted by stress, 2) characterize distinct stress-specific neuronal ensembles within these circuits, 3) identifying potential key sex differences in stress response brain circuitry, and 4) isolate circuit- and ensemble-specific biomarkers that can predict- and be targeted to prevent or mitigate- stress disorders.

**This project will use advanced whole brain light sheet microscopy and neuronal ensemble-specific optogenetics to identify and manipulate stress ensembles in the brain. This strategy will provide unparalleled in-depth insight into the regulatory mechanisms underlying stress disorders, paving the way for improved prevention, diagnosis, and treatments for affective disorders.**

Collectively, we predict that larger yet-to-be-defined brain networks and unique ensembles within these networks represent key targets for mitigating the long-term effects of stress exposure. This proposal will address the following key questions: *Are there distinct mechanistic circuit signatures that dictate stress-induced hyperactivity? What are the larger holistic circuit biomarkers driving sustained changes in activity during stress that can lead to prolonged dysfunction and the development of affective disorders?* We will use novel preclinical genetic mouse models to “tag” stress-activated neuronal ensembles in the whole



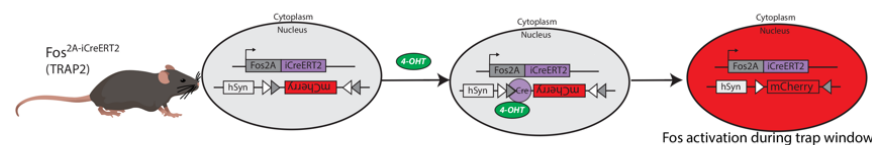
brain and combine this approach with whole intact brain light sheet microscopy, creating a comprehensive preclinical database for stress active brain areas in male and female mice. This database can inform future preclinical and clinical studies focused on stress-related disorders. Early detection of stress effects on the brain can 1) help predict affective disorder vulnerability and 2) improve precision of interventional strategies. In addition, based on our previous work outlined below, we will optogenetically mitigate activity in stress ensembles in a specific insular cortical brain circuit implicated by our group and others to be a network hub for stress integration.

## Outline of Tasks/ Work Plan

### Aim 1: Identify whole brain stress-activated ensemble circuitry using light sheet microscopy with automated high-resolution single-cell brain atlas registration.

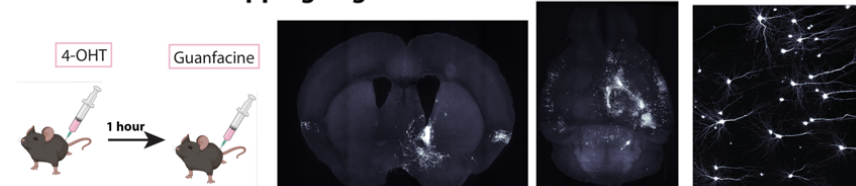
*Rationale:* We propose to map all stress-activated cells in the brain and provide a unique database to serve as a valuable resource for future stress studies. The combination of whole-brain light sheet imaging with sophisticated genetic mouse models provides unparalleled insight into individual cell activity in the entire brain during behavior- something that can only be achieved in preclinical models with advanced optical techniques. We will

#### A Isolation of activity-dependent neurons using FosTRAP2 Mouse Line



isolate and gain genetic access to stress ensembles with the new FosTRAP2 mouse line described in figure 1.

#### B Whole brain mapping of guanfacine-activated neurons in the brain



This window will be opened prior to stress to 'trap' stress-activated cells.

In addition, we propose to zero in on a specific network hub for stress response. Evidence from our group and others suggests the source of affective disorders is centered around dysregulated activity in the extended amygdala brain regions. However, the upstream

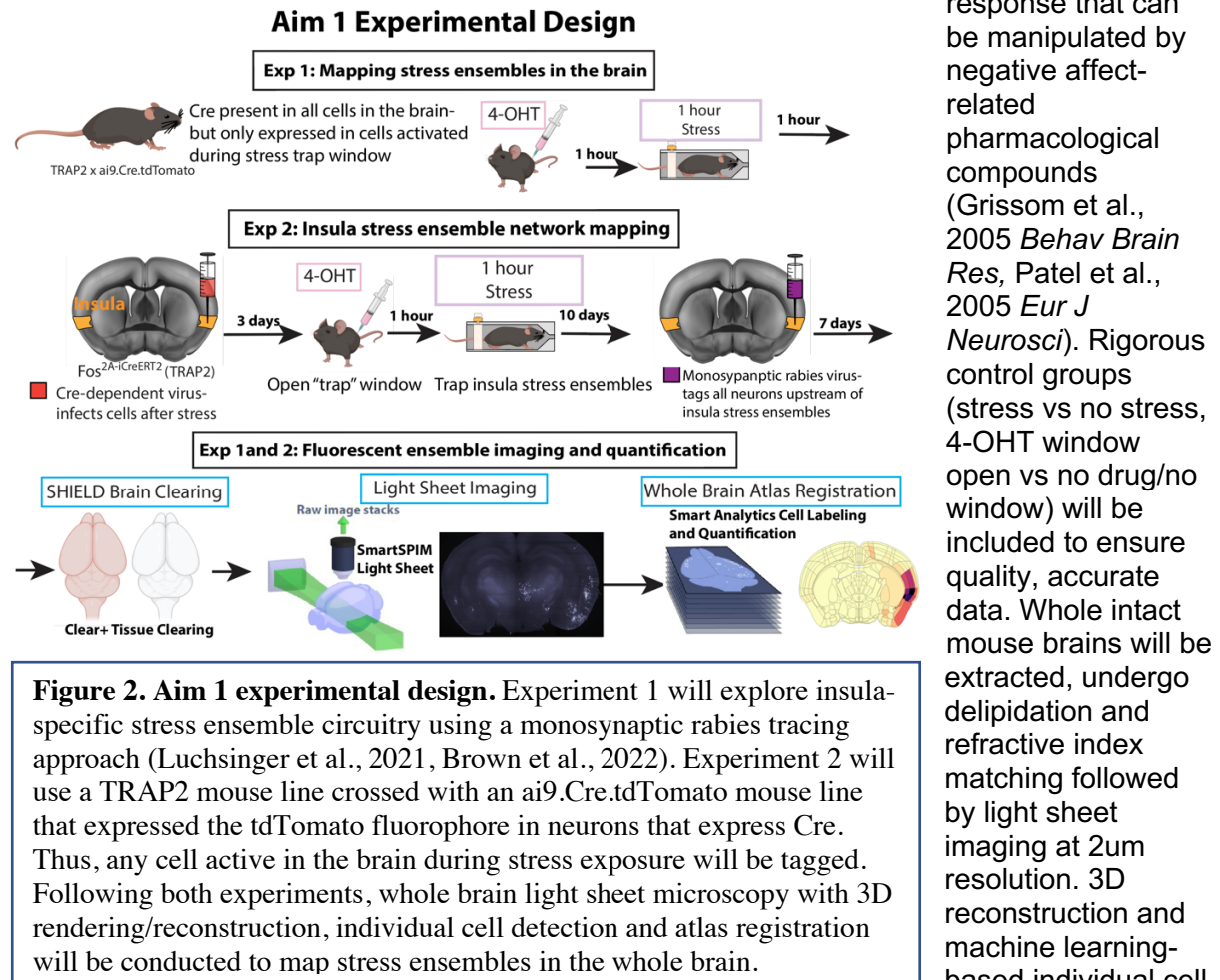
### Figure 1. FosTRAP2 mouse model to isolate behavior ensembles.

A) Fos2AiCreER<sup>T2</sup> mice (Guenther et al., 2013 *Neuron*, DeNardo et al., 2019 *Nat Neurosci*) express a tamoxifen (4-OHT)-inducible Cre knock-in allele driven by the immediate early gene *c-fos*, a proxy for neuronal activity. The 4-OHT window is open for 1h. B) Data from our group showing trapping of BNST cells activated by the adrenergic receptor agonist guanfacine. Monosynaptic tracing with light sheet mapped all upstream inputs onto these cells (Brown et al., 2022 *NPP*).

cortical circuits controlling these areas are not well characterized. We identified the insular cortex (insula), a cortical area intimately involved in emotional regulation, sensory processing, valence, decision making, and many other behaviors (for review see Centanni et al., 2021 *Neuropharmacology*), as an affective network hub that regulates amygdalar circuitry (Flook et al., 2020 *Neuroimage*). Interestingly, resting state functional connectivity in the insula-amygdala pathways is low in healthy controls; however, patients diagnosed with PTSD show higher connectivity (Torrissi et al., 2018 *Transl Psychiatry*), suggesting this pathway is recruited for emotional regulation and stress response. Using translationally validated mouse models, we established a role for this pathway in regulating alcohol abstinence-induced negative affect (Centanni et al., 2019, *NPP*) and coping strategy choice during a stressor (Luchsinger et al., 2021, *Nat Commun*). Using light sheet microscopy and optogenetic circuit manipulation strategies, we identified a unique upstream motor cortical control network into the insula. This circuit not only drives the initiation of escape behavior during a stressor but receives feedback from affective circuitry indicating success or failure of the escape attempt. Thus, the insula network could serve as a circuit biomarker for stress responsivity in humans. *We hypothesize that insula stress ensembles are network hubs that*

receive dense input from upstream cortical areas involved in cognition and decision making (e.g., prefrontal cortex, anterior cingulate) and memory (hippocampus, amygdala). Given the insula's downstream connectivity to brain areas involved in negative affective states, this would support an integral role for the insula as a central network hub of stress response.

**Experimental Design:** Male and female FosTRAP2 mice crossed with a Cre-reporter mouse line (ai9.Cre.tdTomato) that expresses the tdTomato fluorophore only in cells that are active when the trap window is open (i.e., during the stressor). We will use a mouse model of restraint stress, which has been validated by our group and others to induce a robust stress



**Figure 2. Aim 1 experimental design.** Experiment 1 will explore insula-specific stress ensemble circuitry using a monosynaptic rabies tracing approach (Luchsinger et al., 2021, Brown et al., 2022). Experiment 2 will use a TRAP2 mouse line crossed with an ai9.Cre.tdTomato mouse line that expressed the tdTomato fluorophore in neurons that express Cre. Thus, any cell active in the brain during stress exposure will be tagged. Following both experiments, whole brain light sheet microscopy with 3D rendering/reconstruction, individual cell detection and atlas registration will be conducted to map stress ensembles in the whole brain.

response that can be manipulated by negative affect-related pharmacological compounds (Grissom et al., 2005 *Behav Brain Res*, Patel et al., 2005 *Eur J Neurosci*). Rigorous control groups (stress vs no stress, 4-OHT window open vs no drug/no window) will be included to ensure quality, accurate data. Whole intact mouse brains will be extracted, undergo delipidation and refractive index matching followed by light sheet imaging at 2um resolution. 3D reconstruction and machine learning-based individual cell

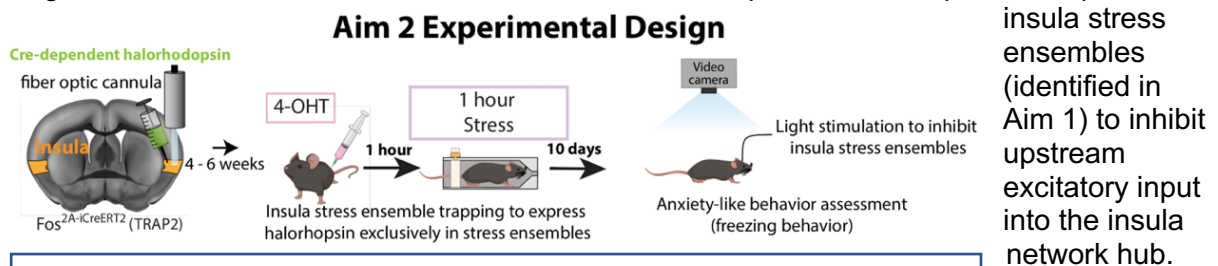
detection will register cells to each brain regions outlined by the Allen Mouse Brain Atlas. This data will be made publicly available through Optica Publishing Groups journals, serving as a valuable resource for preclinical and clinical stress researchers.

As a direct comparator focusing in on a specific circuit, we will use this same strategy to map upstream inputs specifically regulating insula stress ensembles. A separate cohort of FosTRAP2 only mice will receive a viral cocktail injection into the middle to posterior insular cortex. These viruses will only express in cells active during the specific genetic access window which will be opened at the time of the stressor. In all, this will not only determine the larger role of the insula in the stress response system but will provide an unprecedented, detailed map of all cells in the mouse brain activated by acute exposure to stress.

**Aim 2: Use optogenetic inhibition of the insula to assess the effects of “removing” this network hub on anxiety-like behavior.**

**Rationale:** We hypothesize that insula stress ensembles are a key integrator of the stress response that drives negative affective disorders. To test this, we will isolate insula stress ensembles and virally express a Halorhodopsin which will allow us to directly inhibit insula

stress ensembles during anxiety-invoking behavioral tasks in mice. The ability to directly measure a relationship between stress-activated neurons and subsequent anxiety-like behavior in male and female mice will significantly impact larger studies aimed at developing novel pharmacological targets to mitigate negative affect and prevent the emergence of a negative affective disorder. In addition, we will isolate a specific dense upstream input onto



**Figure 3. Aim 2 experimental design.** Insula stress ensembles will express the inhibitory opsin Halorhodopsin, allowing for light-activated inhibition of insula stress ensembles. Ensembles will be inhibited just prior to exposure to a novel stressor that induces freezing in mice. On separate days mice will receive either an air puff, a loud sound (acoustic startle), or a mild foot shock.

insula stress ensembles (identified in Aim 1) to inhibit upstream excitatory input into the insula network hub.

*Experimental Design:* Male and female FosTRAP2 mice will be

used as described above to isolate and gain genetic access to insula neurons active during acute exposure to a stressor. Halorhodopsin, a light-activated inhibitory chloride channel, will be stereotaxically injected into the middle-posterior insula along with a fiberoptic to deliver light. Negative affect-like behavior will be assessed using an acoustic startle test, a validated model for inducing anxiety-like behavior in the form of freezing (Börchers et al., 2022 *Psychoneuroendocrinology*). Light will be delivered five seconds prior to the start of each trial to inhibit stress-activated insula neurons. Freezing behavior will be quantified and statistically compared to control groups (no virus/light stimulation, no stress ensemble/light stimulation, stress ensemble/no light stimulation).

### **Outcomes**

On its surface, this proposal will reveal a detailed map of all stress activated neurons in the mouse brain- data that can be used as a reference for future clinical and preclinical studies. On a more granular level, we will identify unique network signatures of insula-centric stress circuitry. We predict insula stress ensembles will receive dense projections from cortical and hippocampal brain areas. Moreover, inputs identified in Aim 1- either with the whole brain approach or insula-centric approach- have the potential to spawn larger NIH-funded studies. A key component of these experiments is to examine sex differences in stress circuitry. Given that females have a higher susceptibility to develop a stress disorder, we predict female mice will have a greater overall number of *c-fos* activated neurons in the insula and other brain regions identified in Aim 1 compared to males. Although the literature is somewhat mixed, coping strategies are thought to differ between males and females, with males tending to choose problem-focused coping strategies and females use more maladaptive emotion-focused coping strategies (Howerton et al., 2009 *Int J Stress*, Moret-Taytay et al., 2016 *Social Behav and Personality*). While we predict general overlap in cortical and limbic projections, an intriguing outcome would be the observation of more upstream projection neurons originating from prefrontal cortical areas and areas regulating impulsivity in males and greater connectivity in sensory and emotional cortical areas in females. In both sexes, we predict inhibiting neuronal activity in stress ensembles will reduce stress-induced affective behavior. In all, the inconclusive clinical data in this area further underscores the importance of environmentally controlled preclinical studies using optic-based strategies.

*Alternative Approaches.* While we have confidence in the FosTRAP2 mouse line and have published its use for whole brain mapping, activity recording with fiber photometry, and optogenetic manipulation (Figure 3, Brown et al., 2022 *NPP*), other activity-dependent cellular trapping strategies are available including an ArcTRAP mouse line as well as viral

constructs that can be directly injected into the insula. Traditional immunohistochemistry with activity-related protein antibody staining in whole mouse brains can also be implemented as an alternative. If aim 2 produces null results, we can pivot to other inhibitory opsins such as archaerhodopsins or inhibitory channelrhodopsins. Additionally, we can *increase* the stress response with excitatory opsins. An exciting future direction involves multi-site simultaneous optogenetic inhibition of upstream brain regions identified in aim 1. In all, we are confident that any outcome will yield high impact results, impacting both neuroscience and optics field.

### **Impact**

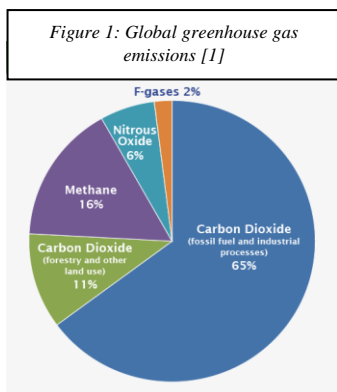
This project is designed to push the field of neuroscience towards adopting cutting-edge optical-based technologies to characterize neuronal circuitry rapidly and unbiasedly. We will utilize whole intact mouse brain light sheet microscopy, sophisticated high resolution neuronal tracing, and *in vivo* optogenetic manipulation of stress ensembles to isolate and map the holistic stress circuitry with a focus on an intriguing, understudied brain network hub, the insular cortex. To this end, we hope to shift how affective disorders are diagnosed and treated by defining biomarkers early in disease progression. Understanding how stress impacts the brain at a molecular and circuit level *before* affective disorders manifest can vastly improve interventional strategies to mitigate the long-term impacts of stress and identify those at risk for developing affective disorders. The proposal has high translational value with the goal of impacting human imaging studies in the short term and serving as the foundation for more in-depth pharmacological, behavioral, and imaging studies to delineate how stress ensembles guide emotion. Our preclinical whole brain studies can then *inform* better targeted studies in humans, alleviating issues with limited resources and directions for big data analysis in clinical studies. Indeed, this approach has already seen translational success in our hands. Our studies sparked a fruitful collaboration with Jennifer Blackford's clinical lab which led to characterizing structural connectivity of the insula-BNST pathway in humans (Flook et al., 2020 *Neuroimage*). They recently identified altered connectivity in this same pathway in patients with an alcohol use disorder in abstinence (Flook et al., 2021, *ACER*). **The high throughput approach in preclinical models is critical for overcoming the bottlenecks that slow progress in clinical imaging studies. Identifying circuit biomarkers in preclinical models is an essential step towards providing rapid diagnoses of dysfunctional brain circuitry in patients suffering from an affective disorder.** Furthermore, this strategy has *reverse* translational value. Circuits and networks identified in clinical studies can be incorporated into preclinical whole brain optical imaging and manipulation approaches, providing rapid, high throughput elucidation of circuitry impacted by stress. Bi-directional translation is essential for making progress in this area.

Emerging evidence continues to elucidate drastic differences in how males and females respond to stress including the development of an affective disorder, rate of progression, and coping mechanisms. A strength of this proposal is the ability to directly measure sex differences in brain circuit activity in an environmentally controlled preclinical model. Stress response/ coping strategies, and affective disorder prevalence differ widely between males and females (Bangasser et al., 2014 *Front Neuroendocrinol*, Grigoriadis et al., 2007 *Ann Clin Psychiatry*, Peltier et al., 2019 *Neurobiol Stress*), which impacts disease progression and severity. Many foundational affective circuitry and stress response studies were conducted in males only, underscoring a need for more research to understand potential critical sex differences. Observable sex differences could have a major impact on diagnostic accuracy and provide sex-specific imaging targets. Lastly, the experiments mapping stress-induced neuronal activation in the entire mouse brain during stress will significantly impact the larger neuroscience field, serving as a resource that could spawn many parallel lines of research. Support from the Optica Foundation is critically needed to convey the impact optically based technologies can have on the biomedical neuroscience and psychiatry fields. This funding will serve as a springboard for larger funding through the NIH BRAIN Initiative and NIMH. In sum, this work can change clinical diagnoses and treatment strategies for negative affective disorders and related diseases.



## Low-cost and miniaturized mid-infrared photonic chemical sensing platform for continuous ecosystem monitoring

Samuel Serna (Bridgewater State University)



- **Climate challenge problem:** Based on Environmental Protection Agency (EPA) studies (Fig. 1), Green House Gases (GHGs) like carbon dioxide (CO<sub>2</sub> at 76%) and methane (CH<sub>4</sub> at 16%) are the highest polluters of the environment today [1], contributing significantly to our current climate crisis. Since “*we need to measure to define policies for effective change*”, this project emphasizes sensing technology and readout analytics to “monitor” as well as “predict” when GHG emissions exceed threshold values. Real time detection of “above-threshold” GHG emissions is more actionable than historical, slowly varying data. In addition, the determination of GHG type, its concentration and geographical site will enable efficient mitigation strategies. However, such a comprehensive distributed and networked GHG monitoring and predictive detection system does not exist today.

- **Solution:** We propose to build low cost mega-distributed and networked monitoring and predictive sensor arrays for real time detection of GHGs, providing information on chemical specificity, concentration, and geographical site, with data accessible on cellphones via integrated photonic circuits fully integrated with the source, detector and read-out electronic system, designed to work in the mid-infrared region, where GHG have their characteristic fingerprints.

- **Impact:** With real time and site-specific detection of “above-threshold” GHG emissions, leaks can be fixed in a timely fashion. Farmers can modify their cattle fodder in real-time to reduce methane gas emissions. Massive deployment at low-cost is possible due to foundry manufacturing of sensor arrays and will enable continuous monitoring of the soundness of our environmental ecosystem. For example, for methane, this project can lead to redesign of human intervention in the carbon cycle ecosystem by providing real time on-site emissions data for both fossil methane (20%) and methanogens (80%) based on chemical flow data, industrial practice as well as governmental policy and regulation.

- **Vision:** We envision a system of mega-distributed and networked planar sensor arrays based on miniaturized Photonic Integrated Circuit - Chemical Environment Mapping (PIC-ChEM) technology to detect site-specific GHG emission concentrations in real time, for both monitoring and prediction. The use of PICs and integrated detectors will allow the implementation on mobile devices.

- **Technology:** Photonic integrated circuit sensors (PIC sensors) monitor changes in the optical properties (refractive index, phase, polarization, intensity, wavelength) of photons transmitted through on-chip waveguides [2]. With each sensor we can measure changes in intensity at specific wavelengths (also called on-chip absorption spectroscopy), providing information on a specific GHG and its concentration. With large, low cost, manufacturable planar arrays of such miniaturized sensors, we can perform simultaneous multi-species detection. Distributed and networked sensor arrays can allow us to gather data from multiple locations simultaneously. Prototypes will be fabricated with dies from a commercial foundry, showing the potential for massive distribution. Machine Learning (ML) algorithms can be leveraged to recognize patterns for different gases and provide real time site-specific concentration data on each GHG [3]. Our envisioned sensing system can be placed on an Unmanned Aerial Vehicle or a drone, both desirable due to their low Size, Weight, Power and Cost (SWAP-C).

- **Prior established art:** Integrated photonic gas sensor that can detect 200 ppm of methane gas at room temperature using on-chip absorption spectroscopy has been demonstrated with the proposed technology [4]. Near-infrared (NIR) on-chip digital Fourier transform spectrometry (dFT) [5] and large scale foundry manufacturability have also been demonstrated. The principal obstacles that will need to be overcome to accomplish our method at scale include the development of on-chip integrated light sources, Read Out Integrated Circuits (ROICs) [6], ML/Neural network algorithms, implementation of mega-distribution, and creation of networked sensors with data accessible by cellphones.

### References:

- [1] <https://www.epa.gov/ghgemissions/global-greenhouse-gas-emissions-data>
- [2] Marris-Morini, et al (2018). Nanophotonics, 7(11), 1781-1793.
- [3] Tânia F. G. G. Cova and Alberto A. C. C. Pais, Front. Chem., 26 November 2019
- [4] Su, Peter. MIT PhD Thesis, DMSE, May 2020
- [5] Kita, Derek et al (2018). Nature Communications 9:4405.
- [6] Guglielmi, E., et al (2021) Journal of Lightwave Tech, 39(22), 7326-7333.

# Low-cost and miniaturized mid-infrared photonic chemical sensing platform for continuous ecosystem monitoring

Samuel Serna (Bridgewater State University)

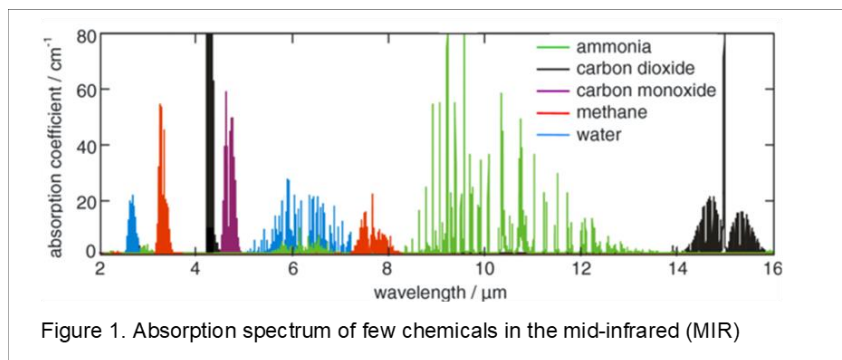
## Abstract:

By integrating a chemical sensor chip into a smartphone, the proposed technology will enable a mobile distributed sensor network across the globe.

In this work we propose to design and build a low-cost and miniaturized mid-infrared photonic *chemical sensor technology* for *continuous ecosystem monitoring*. Our technology features (i) a CMOS-compatible broadband sensing element, (ii) a mid-infrared photodetector, and (iii) a read-out integrated circuit for data processing, all integrated onto the same chip. *The “lab-on-a-chip” technology will be a key enabler in the field of integrated mid-infrared sensing, for building a network of smartphone-connected sensors, and will lead to a “Chemical IoT” for ecosystem monitoring.* Smartphones will provide continuous information about air, food and water quality at any destination. Our work on this project will be adapted to enable rapid, qualitative and quantitative detection of chemical molecules of greenhouse gases. In particular, I will be working on a prototype to sense methane, present in chemical concentrations as low as 100 ppm, to provide proof of principle.

## Significance and Background

Chemical sensing benefits from photonics, because changes in the real and imaginary parts of the complex refractive index can be used to *rapidly, specifically and sensitively* detect the presence of chemical molecules. The mid-infrared (MIR) wave band (2 to 12  $\mu\text{m}$ ) is a strategically important spectral regime for photonic chemical sensing, because characteristic vibrations of most molecules occur here, leading to absorption “fingerprinting” [1], as shown in Fig. 1. MIR spectral analysis such as Fourier transform infrared spectroscopy (FTIR), can provide accurate qualitative and quantitative detection of chemical molecules, but typically requires *expensive and cumbersome equipment* which is not conducive to point-of-use testing. To overcome this challenge, portability must be enhanced at a lower cost while retaining sensor performance.



Today a single smartphone typically contains more than 10 sensors. *A mobile distributed chemical sensor network across the globe can be envisioned with a miniaturized “lab-on-a-chip” in every smartphone.* The possibilities are endless. Forewarning about the presence of trace levels of toxic chemicals such as CO can avert tragedies within the home and the workplace. Asthmatics can determine the suitability of outdoor conditions from local air pollution data. Scientists can monitor the evolution of pollution patterns in different cities using a massive database of crowd-sourced air quality data. Regional authorities can identify terrorist chemical attacks early enough to issue timely public warnings, saving lives.

## Challenges and Solution

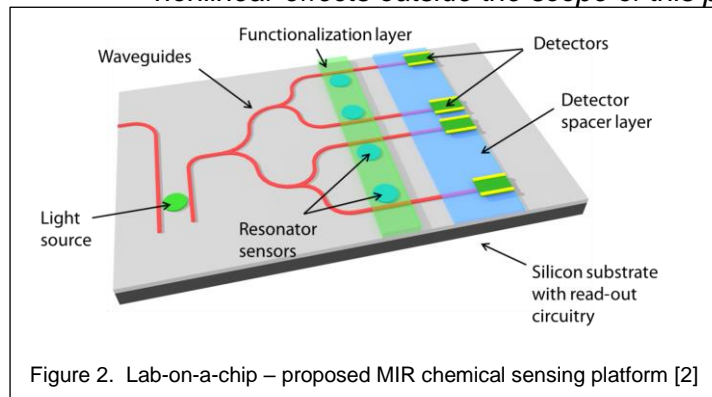
Photonic devices are already widely used in communication and personal electronics, so the technology is very mature, covering a wide range of wavelengths from the ultraviolet to the infrared. Although sensitive and specific FTIRs exist, they are bulky.

Our vision is to integrate *the entire sensing platform onto a single chip* (See Figure 2) [2]. Individual components required to build such a MIR system have been identified as light



sources, sensors, functionalized layers, photodetectors, and data-processing readout electronics. Component integration poses materials, processing and device design challenges. *Our project will build a miniaturized MIR chemical sensing platform. In doing so, we will tackle challenges in integration of the following components:*

- A quantum cascade laser (QCL) or interband cascade laser (ICL) can be used as a MIR light source
  - *We are exploring a broadband on-chip integrated light source solution based on nonlinear effects outside the scope of this project*



- To increase the interaction between chemical molecules and light, waveguide sensors need to provide a long path length which can be obtained either using resonators (highly sensitive narrowband structures), or spirals (less sensitive but broadband structures)

◦ *We will use broadband spirals [3] and run a fabrication process with AIM Photonics in silicon nitride on insulator (SiNOI) as specified in the*

*budget. We will also collaborate with MIT (Prof. Kimerling, Prof. Hu and Dr. Agarwal), University of Paris Saclay (Dr. Vivien and Prof. Marris-Morini) and CEA-LETI (Dr. Reboud) to design and test germanium, silicon, chalcogenides and other less standard platforms as demonstrated with previous publications [4]*

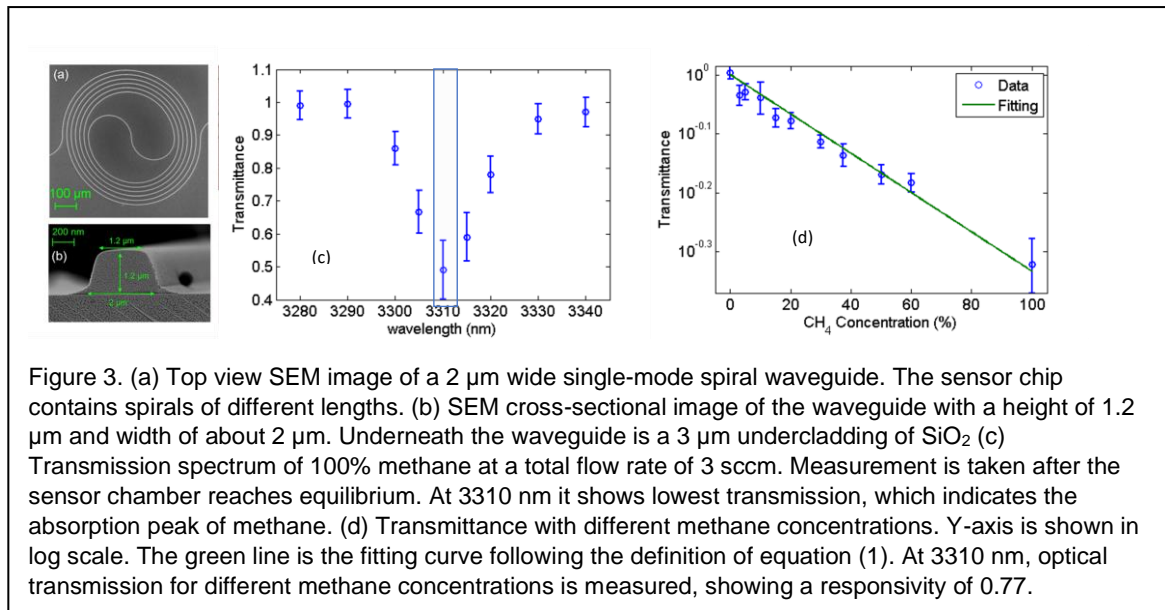
- To improve specificity and/or sensitivity, sensor surfaces can be modified by chemically functionalized layers
  - *We will employ characteristic absorption sensing for high specificity, and the MIR regime for high absorption sensitivity, so we do not need functionalized layers*
- A photodetector relying on carrier generation induced by infrared photons, offering better speed and sensitivity compared to a thermal IR detector, can be chosen
  - *We will choose a PbTe photoconductor [5]*
- A ROIC which improves signal to noise, computes, processes data, communicates remotely, and manages power can be implemented. Large volume production using CMOS processes can ensure low cost ROICs that enable a *portable, smart and remotely-accessible sensing platform*
  - *We will custom-build the ROIC in collaboration with Prof. Sampietro at Politecnico di Milano as demonstrated with previous publications [6]*
  - *We will also use our packaging expertise in this project to properly integrate the electro-optical components in the sensor as described in the patent from the PI.*

*To enable our vision of a MIR lab-on-a-chip, we propose to overcome design, fabrication and on-chip integration barriers faced by three important sensing system components: (i) sensor, (ii) detector, and (iii) ROIC:*

### **(i) Integrated MIR Waveguide Sensor**

Waveguide design and fabrication is the foundation of an integrated sensing system. Based on our collaborator's previous success using chalcogenide glass (ChG) spirals for methane gas sensing [3] at 3.3  $\mu\text{m}$  wavelength (Figure 3), we will choose a spiral as the sensing element.

However, due to greater *CMOS-process-compatibility of silicon nitride (SiN) like at AIM Photonics, we will build a broadband MIR SiN spiral* instead of a ChG spiral. Also, since SiN is transparent from the visible up to 6  $\mu\text{m}$ , we can detect methane gas, which absorbs light at 3.3  $\mu\text{m}$ , as we benchmark SiN spiral sensors against our ChG spiral sensors, and against bulkier methane gas sensors available in the market today.



Photonic waveguide sensing follows the standard Beer-Lambert law given by:

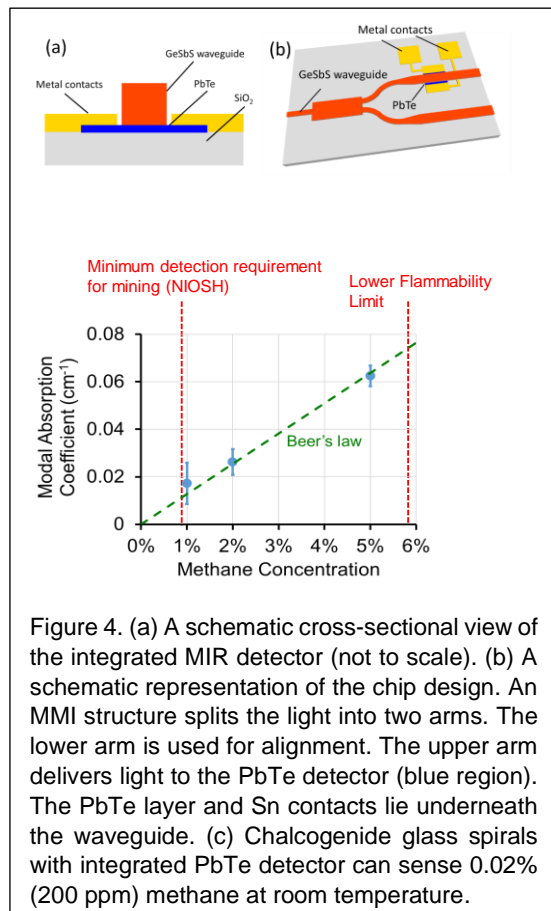
$$T = \exp(-\alpha C \Gamma L) \quad (1)$$

where T is the transmittance which is defined as the optical intensity transmitted through the waveguide immersed in the gas mixture normalized by the intensity with pure nitrogen gas.  $\alpha$

is the absorption coefficient of 100% methane (partial pressure 1 atm), C is the volume concentration of methane,  $\Gamma$  is the confinement factor which indicates the overlap between the gas analyte and the optical mode (evanescent field), and L is the total length of the waveguide. We will address questions such as: What limits sensor performance? How can it be optimized for on-chip ppm methane gas sensing in the MIR?

### (ii) Integrated MIR photodetector

PbTe is a photoconductive detector and has successfully been integrated monolithically (Figure 4(a)) to work at room temperature, with the ChG waveguide [7]. Using a ChG spiral integrated with a PbTe detector (Figure 4(b)), on-chip methane gas sensing has been demonstrated (Figure 4(c)) [5]. The material properties and fabrication techniques for PbTe have previously been well established by my PhD student's collaborating group [4,5]. In this work we will leverage that know-how to optimize *the design, fabrication and testing of a SiN spiral methane gas sensor, integrated with an on-chip MIR PbTe detector*. In addition to a monolithic solution using our photo-conducting PbTe film, we will investigate a hybrid-integrated solution using a *novel high performance MIR detector from our collaborating partner, Analog Devices*.



### (iii) On-chip Read Out Integrated Circuit

A readout circuit designed and built on a PCB, and wire-bonded to the on-chip PbTe MIR detector, (Figure 5) demonstrated that electrical noise in the sensing system can be

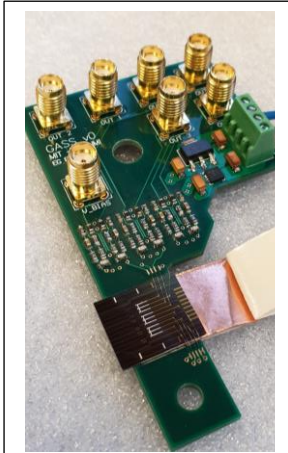


Figure 5. PbTe detector integrated with a ROIC on a PCB.

significantly reduced with integration. *In the proposed work, we will integrate such a ROIC with the sensor system, to boost overall performance.*

To work towards the development of a “Chemical IoT” device, a prototype can include a USB connection and networking functionality, such as a bluetooth or wireless transceiver, allowing data visualization on a smartphone. A custom ROIC design in 0.35  $\mu\text{m}$  CMOS technology to further miniaturize the measurement front-end can boost sensor system performance even further.

With our team’s experience in low-noise impedance measurements and systems design, we expect to improve the sensitivity of chemical detection in applications that span industrial and environmental pollution monitoring, food monitoring, medical diagnostics and drug delivery.

Our goal is to enable a low-cost and miniaturized mid-infrared photonic chemical sensor technology for ecosystem monitoring.

Finally, after the establishment of the sensors, we will develop artificial intelligence software to analyze the different data and train the neural networks to recognize different gases and their concentrations in different areas.

the neural networks to recognize different gases and their concentrations in different areas.

### Student participation

We will use part of these funds to support one assistant research student from BSU throughout the two years of the project, this includes the four academic semesters and the two summers. Also, the PI is the co-supervisor of PhD student Katherine Stoll, who is working towards a degree from the Department of Material Science and Engineering (DMSE) at MIT. BSU provides other internal grants that will be used to have another student involved in the project.

### Collaborations

The PI will collaborate with EMAT (Electronic Materials) and PMAT (Photonics Materials) groups at MIT consisting of Dr. Anu Agarwal, Prof. L.C. Kimerling, Prof. Juejun Hu and Prof. Kazumi Wada. They have expertise in the design, fabrication, test and packaging of on-chip integrated photonic systems using SiN and PbTe. We will leverage our past successes and know-how in this field to enable a novel “Chemical IoT”. *Analog Devices is actively enabling our sensing solution platform with the integration of their own novel commercial MIR detector.* The PI will also collaborate with the Silicon Photonics Group at the University of Paris Saclay (France) as well as the microelectronics group at the Politecnico di Milano (Italy).

### Prior relevant work by the PI

The PI has relevant experience in integrated photonics, particularly in nonlinear and sensing applications in the telecom wavelengths. Here some few publications relevant to the presented proposal:

Guglielmi, E., et al. (2021). 1/f Noise Characteristics of Waveguide-Integrated PbTe MIR Detectors and Impact on Limit of Detection. *Journal of Lightwave Technology*, 39(22), 7326-7333.

Kimerling, L. C., Michel, J., Agarwal, A. M., Wada, K., Weninger, D. M., & Serna, S. (2021). *U.S. Patent No. 11,067,754*. Washington, DC: U.S. Patent and Trademark Office.

Marris-Morini, D., et al (2018). Germanium-based integrated photonics from near-to mid-infrared applications. *Nanophotonics*, 7(11), 1781-1793.

Serna, S. et al (2016). Experimental investigation of top cladding on properties of silicon slotted photonic crystal waveguides. *IEEE Journal of Selected Topics in Quantum Electronics*, 22(6), 305-311.

### Equipment and capabilities

**Laboratories and equipment:** The PI has a new laboratory space in BSU’s Science and Mathematics Center called Photonics and Optics Engineering Laboratory. The space has 4 optical tables and a fume hood with diverse equipment, including a MapleLeaf probe station, tunable lasers in all the telecom bands, photodetectors and powermeters in different ranges, optical amplifiers, mechanical and optical pieces for different wavelength ranges (Fig. 6).



Specialty equipment for photonics was purchased in the last 2 years from previous grants obtained through the Commonwealth of Massachusetts [SEMA-LEAP, Mass-Tech Collaborative], through MIT for the Massachusetts Engineering Education Program [MEEP; through the Office of Naval Research] and through the Capital Skills Grant. Examples of major instrumentation available for the PI includes a set of sources in different regimes: Chromacity few-ps OPO 100 MHz repetition rate (pump- 1064 nm, tunable signal – 1.4  $\mu\text{m}$ -2  $\mu\text{m}$ , tunable idler – 2 $\mu\text{m}$ -4 $\mu\text{m}$ ) (Fig. 6). Menlo systems <150 fs erbium amplified laser. Tunable CW Toptica TOPO X-IR laser (pump- 1550 nm, tunable signal – 1.9  $\mu\text{m}$ -2  $\mu\text{m}$ , tunable idler – 4.5 $\mu\text{m}$ -8 $\mu\text{m}$ , >100mW (Signal), >100mW (Idler), Linewidth: < 2MHz). Thermal power meter up to 12  $\mu\text{m}$  wavelength - Thorlabs S470C; wavemeters - High Finesse HF-ANGS WS/6-200-IR3 Wavelength Meter, Solid State, High Precision, IR3 - measurement range: 1400-11000 nm - absolute accuracy:  $\pm$  200 MHz; mid-IR collimators, fiber CIR- 1.5-6 $\mu\text{m}$ ; fiber PIR- 4-18 $\mu\text{m}$ ; APE Spectrum Analyzer; Optical Spectrum Analyzer Yokogawa 1200 nm - 2400 nm; beam quality  $M^2$  up to 5  $\mu\text{m}$ . DIC and Fluorescence Microscopes; NMR, mass and optical spectroscopy equipment for chemical analysis; a robotics and digital electronics lab; an x-ray diffraction lab; a Raman/PL Horiba system - imaging spectrometer, iHR320; a magneto-optical trap (MOT) lab; quantum optics basic equipment for entangled pair generation and detection, single photon and HOM interferometry; a machine shop and a Think Tank with 3D printers.

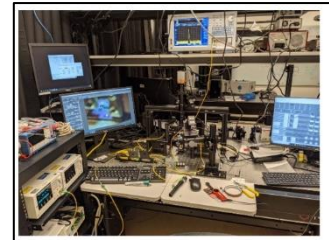


Figure 6. PI BSU's facilities. Up: Electro-optical characterization set-up. Down: Chromacity tunable OPO system.

**Computer/IT:** Two high-end computers of exclusive use for the photonics research spaces will serve the project's simulation tasks. The PI has licenses for LabView, Matlab and Comsol as part of previous grants. The university has all the tools to keep a cloud back-up of all the data as well as create shareable documents for reporting and publications.

### Project Sustainability

Several commercial entities whose products span diverse applications (oil, gas, mining, automotive, environment, medical), are interested in incorporating our *on-chip integrated and networked chemical sensing systems*, into their products. Government laboratories like Draper Lab and Lincoln Lab have expressed an interest in collaborating with our team through federal DARPA and DTRA contracts to build out this technology. Finally, defense contractors such as United Technologies Research Center and Raytheon are eager customers as they seek to bolster homeland security. The focus of the project on photonic fabrication and integration also aligns well with the objective of AIM Photonics, the federal-private partnership to support photonic manufacturing in the US, in particular the CHIPS Act and a potential funding source of follow-on efforts.

### References

- [1] "Optical gas sensing: a review", *Measurement Science and Technology* 2013, 24, 012004
- [2] "Mid-infrared materials and devices on a Si platform for optical sensing", *J. Science and Technology of Advanced Materials* 2014, 15, 014603
- [3] "On-chip mid-infrared gas detection using chalcogenide glass waveguide", *Applied Physics Letters* 108, 141106 (2016)
- [4] "Enhancing SiN waveguide optical nonlinearity via hybrid GaS integration", *Journal of Optics*, 23(2), 025802 (2021)
- [5] "Monolithic on-chip mid-IR methane gas sensor with waveguide-integrated detector", *Applied Physics Letters* 114, 051103 (2019)
- [6] "1/f Noise Characteristics of Waveguide-Integrated PbTe MIR Detectors and Impact on Limit of Detection", *Journal of Lightwave Technology*, 39(22), 7326-7333 (2021)
- [7] "On-chip chalcogenide glass waveguide-integrated mid-infrared PbTe detectors", *Applied Physics Letters* 109, 071111 (2016)

**Summary.** With the OPTICA 20th anniversary challenge, we will demonstrate *the world-smallest laser particle operating in human physiological conditions*. Such virus-sized nanolaser will be delivered into the cytoplasm of the living cells and emit ultranarrow laser emission for a unique spectral nametag. This new optical probe resolves the color limitation of fluorescent probes and opens new avenues in multiplexed biomedical studies for drug development, disease diagnostics, and high-resolution tissue imaging.

Fluorescent probes are ubiquitous for bio-labeling and spectrum-based assays. Despite the easy usage, their broadband emission due to the intrinsic quantum nature (spectral linewidth 50~100 nm) limits the multiplexing ability to only a handful of resolvable colors. This small color palette often restricts the number of unambiguous color tagging and comprehensive understanding of the single-cell state characterized by various biomarkers. To address this issue, my lab colleagues and I have worked on intracellular microlasers, which are tiny enough to go inside the cells and generate ultranarrow laser emissions with a linewidth of 100 to 1000 times narrower than fluorescence following optical excitation. Thick silica surface coating made color tags insensitive to surroundings. Therefore, we could track the movement of thousands of living single cells tagged with microdisk lasers within the breast cancer organoid using hyperspectral microscopy.

Reducing the size of laser particles to the nanoscale is highly desirable because it will minimize the perturbation of homeostasis and allow more probes to be tagged to a single cell. The nanosized particle will prevent any obstructions in microvessels while it is traveling in the bloodstream. Delivering multiple nanolasers in a single cell will dramatically increase the number of spectral nametags. This strong motivation in biomedical application shares same goal of laser miniaturization with fundamental nanophotonic research and industrial application in on-chip integration, display, and photonic computing.

My early postdoctoral work in plasmonic-assisted laser miniaturization laid the foundation for this unique idea. Plasmonics is considered one of the promising ways for subdiffraction-limit laser. The evanescent light on the metal surface can be amplified to generate an ultrasharp laser emission. Nevertheless, almost all the plasmonic lasers demonstrated to date have needed the gain medium to be  $>1 \mu\text{m}$  because of the large cavity loss. Recently, we demonstrated the smallest plasmonic laser in volume by placing a perovskite semiconductor nanocube on the gold substrate. The size was equivalent to the emitted wavelength of light. We also found so-called beneficial plasmonic effect, in which strong light and matter interaction in plasmonic nanocavity boots up the brightness of the gain material to continue the miniaturization.

Here, we propose the 1-2 year period project to make exciting innovations on nanolasers for biomedical study. The experimental approach is highly interdisciplinary as it brings together the knowledge and the tool from both plasmonic physics, nanochemistry, and cell biology. Our project has one specific aim below.

***Aim 1: Demonstrate biocompatible plasmonic nanolaser particle.*** The plasmonic laser devices have been prevented from stand-alone usage because of the necessity of the metal substrate and metal sputtering on the semiconductor structure on the substrate. In addition, the perovskite material we used in the previous demonstration is limited for the biological environment due to water solubility and toxic lead ions. In this aim, we will develop a three-dimensional (3D) plasmonic nanolaser particle by coating optically thin gold on the surface of the water-insoluble III-V semiconductor nanodisk. This new material combination between near-infrared gain and plasmonic metal is expected to maximize the beneficial plasmonic effect. Pico-second optical pumping will help accumulate as many as Purcell-accelerated carriers in population inversion states to lower the threshold. Therefore, we will break our previous record to achieve a sub-400 nm scaled stand-alone laser whose volume is reduced by  $\sim 30$  folds from the state-of-the-art substrate-supported plasmonic laser. We will evaluate the biocompatibility of the plasmonic nanolaser and conduct proof-of-concept experiments for tagging developed tiny lasers into sub-micron-sized immune Jurkat T cells and functionalizing the nanolaser surface with biological molecules.

## Title. “Plasmonic nanolaser particle for multiplexed biomedical study”

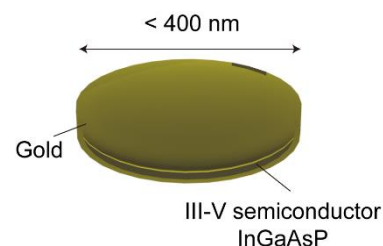
**Literature Review.** In 1873, Ernst Abbe, a German physicist, discovered a ‘diffraction-limit’ [1]: that is, light confinement is fundamentally limited by the wavelength of light. Since then, nanolasers smaller than the size of emitted light have long remained one major challenge in modern photonics. Continuous efforts by many physicists allowed various micro-scale high-quality (Q) lasers to be fabricated with a dielectric semiconductor, including vertical-cavity surface-emitting laser (VCSEL) [2] and microdisk laser [3].

Freestanding micro- and submicron-sized lasers have been proving their usefulness in biomedical applications, including cell tracking [4,5], high-speed flow cytometry [6], tissue imaging [7,8], and cellular mechanics sensing [9]. Their narrow spectral emission not only creates a larger number of unique colors compared to conventional fluorescent probes but also enables to detection of small optical changes in the dielectric environment. Such newly emerged probes can be engineered in different directions for better performance. For instance, sub-micrometer-sized laser probes will minimize perturbations on homeostasis when they are incorporated into the few-micron-sized biological cells. This technical interest in laser miniaturization largely overlaps with the need in applications for optical computing [10], and display [11].

Plasmonics is considered one of the most promising ways to make a miniaturized laser on a nanoscale. Surface plasmon (SP) waves can be confined into sub-diffraction volume and amplified to generate laser light if the supplied optical gain is large enough to overcome the loss. Plasmonic laser has different scaling laws in the threshold-device size relationship compared to the dielectric counterpart due to strong light-matter interaction in the metallic cavity. Since its early demonstration, plasmonic lasers made of the different gain materials and plasmonic device structures, including nanowire, cylinder, and microplate, have been studied for room-temperature operations and exotic laser physics ranging from thresholdless behavior and strongly coupled plasmon-exciton [12]. Recently, we demonstrated submicron plasmonic nanolasers operated at room temperature using a recently emerged lead halide perovskite (LHP) material and gold [13]. The smallest device has a size of 580 nm, which is comparable to the emission wavelength of 540 nm.

**Problem Statement/Objective.** Despite their outperformed compactness, most plasmonic laser devices have been fabricated on metal substrates [12]. Conventional epitaxial or sputtering processes need the semiconductor structure on the substrate so that they cannot coat the metal three-dimensionally. This technical problem prevents plasmonic lasers from stand-alone applications. In addition, the perovskite materials we used in the previous study are limited for biomedical study because it is dissolvable in water and contains heavy atom ions.

This study aims to demonstrate the first biocompatible plasmonic laser particle for massively multiplexed studies. The particles are made of water-insoluble III-V semiconductor laser coated with optically thin gold. The gold nanoparticle is the first and only FDA-approved metallic nanomaterials for in vivo study and chemically robust in a water environment and easily functionalized by biomolecules. We will devise solution-based, self-assembly technology, which is scalable to high volume and can be realized in a lab flask at a low cost. Therefore, we could envision fabricating many nanolaser particles in the order of millions or more demanded in their anticipated multiplexed biological cell studies. Based on our theoretical study, a high refractive index of III-V semiconductors shifts the gold’s plasmonic mode asymptote to the far-red and infrared region so that the beneficial plasmonic effect on laser miniaturization can be maximized and accessible by III-V gain. Therefore, it is possible to break our previous record on the smallest size of the plasmonic laser and be the

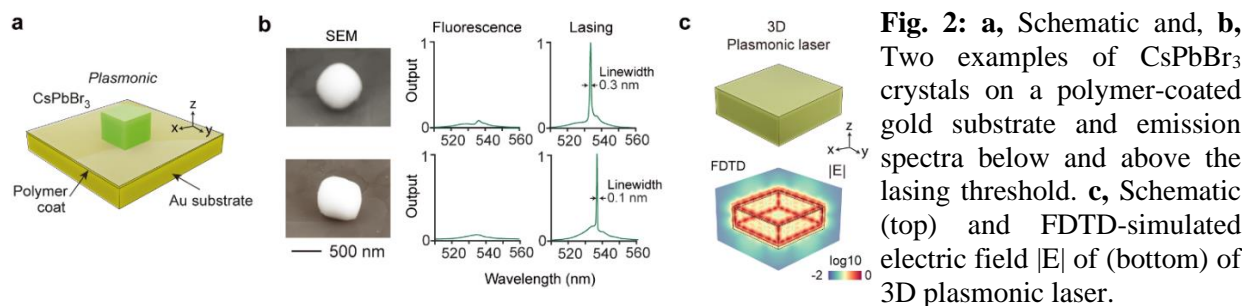


**Fig. 1.** Schematic of full-gold coated plasmonic III-V semiconductor nanolaser

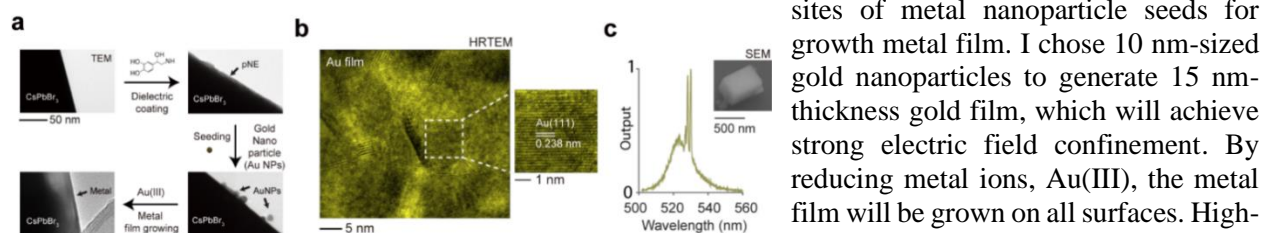


first demonstration of a stand-alone plasmonic laser. Additional biocompatible coating and surface attachment of biomolecules transforms the nanolaser into functional bioimaging probe.

**Outline of tasks/Work Plan.** *Recent progress in plasmonic laser (Fig.2).* Recently, we demonstrated plasmonic lasing with submicron cesium lead bromide perovskite ( $\text{CsPbBr}_3$ ) crystals atop polymer-coated gold substrates (Fig.2a). It represents the smallest plasmonic laser ever demonstrated on a substrate (Fig.2b). The size of the particle is about 580 nm, comparable to the wavelength size of 530 nm. Above the threshold energy, narrow emission peaks with a linewidth of about 0.1~0.3 nm appeared. Our main finding from observing more than 100 devices is that attaching metal next to a semiconductor nano-cube can greatly enhance laser amplification by confining the electric field in the small volume. We called this phenomenon as ‘Beneficial plasmonic effect’. After this work, the next question readily arises: would full metal-coating on the particle may present the similar effect? Considering the probe application for biomedical study, nanolasers should have free-standing particle form. Based on the finite-difference time-domain (FDTD) simulation result, such three-dimensional (3D) plasmonic laser can have the strong electric field ( $|E|$ ) confinement especially when the thickness of metal becomes around the half of the skin depth of the surface plasmon (about 15 nm in the case of wavelength of 530 nm). This 3D plasmonic laser can achieve high Purcell enhancement by the help of the small mode volume and be tolerant to environmental perturbation. In addition, thin metal coating allows for optical excitation of the core material because of the transparency.



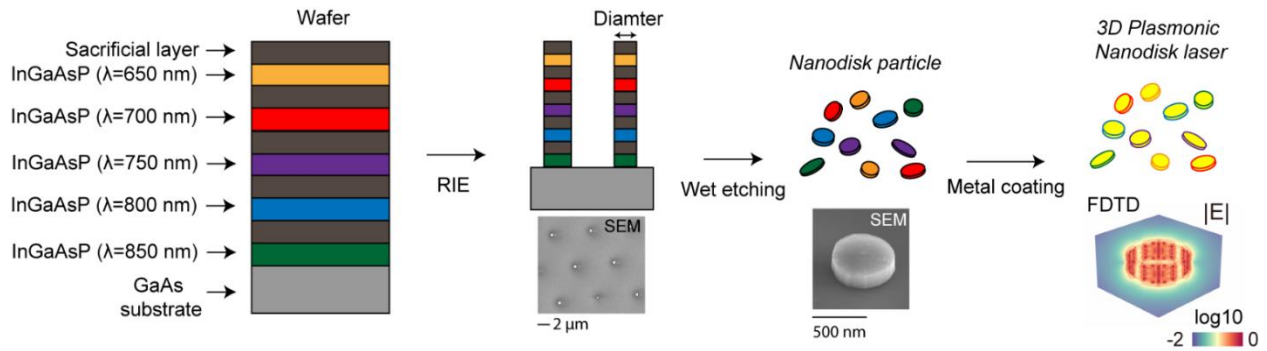
*Thin gold surface coating (Fig. 3a & 3b).* To make 3D plasmonic perovskite nanolaser, I devised the novel wet chemistry method for thin gold coating. This technique is based on poly-norepinephrine (pNE) encapsulation method developed in our previous study for improving perovskite’s water stability and biofunctionalization [14]. The strategy consists for three sequential steps: (i) pNE coating, (ii) metal seeding, and (iii) metal ion reduction (Fig. 3a). First,  $\text{CsPbBr}_3$  submicron particles are coated with 5 nm-thickness pNE in saturated dimethyl formaldehyde (DMF). Transmission electron micrograph (TEM) confirmed that the ultrasmooth conformal layer with 5 nm thickness was formed on the surface of the  $\text{CsPbBr}_3$  after 5 min reactions at 50 celsius. The pNE coating provides organic functional groups, such as the amine and the catechol and indole ring, on the surface of the inorganic  $\text{CsPbBr}_3$ . These functional groups offer attaching sites of metal nanoparticle seeds for growth metal film. I chose 10 nm-sized gold nanoparticles to generate 15 nm-thickness gold film, which will achieve strong electric field confinement. By reducing metal ions, Au(III), the metal film will be grown on all surfaces. High-resolution TEM presents typical Au (111) lattice in the film, confirming polycrystalline gold with high quality and gold purity in the submicron-sized area.



**Fig. 3:** a, Strategy for the synthesis of 3D plasmonic perovskite nanolaser and TEM images of each processing steps. b, HRTEM characterization of the polycrystalline gold film (left) and zoomed-in gold (111) lattice image (right). c, Emission spectra and SEM image of 620 nm-sized gold-coated  $\text{CsPbBr}_3$  particle.

3D plasmonic perovskite nanolaser (Fig. 3c). We demonstrated lasing from 620 nm-size thin gold coated CsPbBr<sub>3</sub> particle. Similar to the substrate-supported plasmonic laser, the critical element to this efficient lasing is the improvement in the quantum yield, the ability to produce photons at given excitation energy.

3D plasmonic InGaAsP nanodisk laser for biomedical application. The major limitation in using perovskite materials for biomedical applications are water-solubility and potential toxicity by releasing lead ions. This is the key motivation that makes me turn to III-V InGaAsP semiconductor. Dr. Yun's lab has been working on InGaAsP microdisk particle emitting near-infrared-II (NIR-II) lasers for multiplexed barcoding of the biological cells [4]. The previous study confirmed that III-V microdisk is robust inside the living cells and did not alter cell viability and proliferation rates. In this proposed study, we will use same InGaAsP material but different composition for near-infra-red-I (NIR-I) wavelength, ranging from 600 nm to 900 nm. Due to the higher refractive index ( $n=3.4$ ) compared to CsPbBr<sub>3</sub> perovskite ( $n=2.3$ ), the plasmonic supremacy effect becomes red-shifted from green (530 nm) to the NIR-I window. Given the color window, laser wavelength can be tuned by varying alloy compositions of InGaAsP and controlling the disk's diameter.

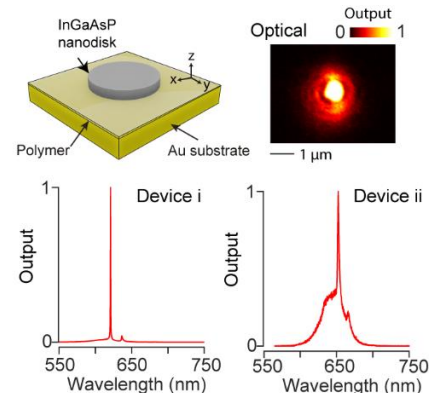


**Fig. 4:** A schematic of fabrication of plasmonic nanodisks with five different compositions covering 600-900 nm. SEM images of the multi-layer wafer after RIE and bare nanodisk particle after wet etching are shown (middle bottom). FDTD simulation of the electric field ( $|E|$ ) in gold-coated nanodisk (right bottom).

Fabrication (Fig. 4) A semiconductor wafer with five active layers separated by sacrificial layers was used to fabricate the NIR1 nanodisk. Lithography and reactive ion etching (RIE) produce the differently sized pre-release disks, and wet-etching selectively dissolves the sacrificial layers for producing stand-alone nanodisk particles. The gold-coating method for CsPbBr<sub>3</sub> will be applied to transform nanodisk into 3D plasmonic nanolasers. FDTD calculation result presents that the electric field is strongly confined in the vicinity of the circumference of the nanodisk, representing plasmonic mode in the beneficial regime.

Plasmonic effect in III-V InGaAsP nanodisk (Fig. 5) It is not straightforward to expect a similar plasmonic effect in CsPbBr<sub>3</sub> to InGaAsP nanodisk because of different properties, including unity quantum yield and faster carrier decay. We experimentally tested whether the nanodisks can be lased on a polymer-coated gold substrate. Under nano-seconds optical pumping at 532 nm, single nanodisk with a diameter of about 380 nm emit spectrally narrow stimulated emission above the threshold energy. Optical imaging presents the ring-like interference pattern surrounding the disk particle, evidencing the spatially coherent laser emission.

Confocal LASE microscopy. Confocal scanning laser-particle stimulated emission (LASE) microscopy [4,7] will be used to record the nanolaser emission. We built this microscopy by adding visible spectrometer to the conventional confocal microscope. For this project, the pico-second pump laser will be installed to excite and



**Fig. 5:** Plasmonic lasing from InGaAsP nanodisks on the polymeric coated gold substrate

accumulate the Purcell accelerated carrier to lower the threshold energy.

*Intracellular delivery and Biocompatibility.* In this step, we will evaluate the biocompatibility of developed plasmonic nanolaser particle. For intracellular delivery, plasmonic nanolasers will be uniformly mixed and loaded into a few micron-sized liposomes made of DOPE/DOTAP [14]. My previous study confirmed that liposome delivery minimizes the water damage of CsPbBr<sub>3</sub> perovskite laser particles and evades endosomal escape during the internalization process. After delivery, we will use conventional live and dead assay for quantifying the cell viability. Phototoxicity of long-term monitoring, toxicity induced by potential arsenic-release, toxicity related to the number of cytosolic nanolasers will be also addressed.

*Potential pitfall and alternative approaches in Aim 1:* (i) Reducing agents for gold coating may damage the InGaAsP material. Alternatively, I will try gold reduction using active electrons generated directly from laser particles by UV illumination. (ii) Thermodynamic instability of a particular combination of InGaAsP quaternary may cause indirect bandgap or poor light emission properties. In this case, I will try to make different color batches within the available material by only controlling the diameter. (iii) Unity quantum yield of InGaAsP may prevent further miniaturization toward sub 500 nm because faster radiative decay can no longer be beneficial. In this case, I will try to excite the nanodisk using picoseconds or femtoseconds laser. (iv) Diameter control and circularity of the nanodisk may become poorer because of the limitation of the resolution of the lithography apparatus. In this case, I will first fabricate large-sized disks and then decrease the size smoothly and isotropically by using wet-based etching chemistry.

<b>Aims</b>	<b>Sub-aims</b>	<b>1~3 months</b>	<b>3~6 months</b>	<b>6~9 months</b>	<b>9~12 months</b>
1. Nanolaser development	Nanodisk lithography				
	Building optical setup				
	Gold coating				
	Biocompatibility evaluation				

**Outcome(s).** Upon the successful completion of the project, we will accomplish the first free-standing, biocompatible 3D plasmonic nanolaser particles. The expected size of the laser is sub 400 nm in diameter and sub 200 nm in thickness, which will be the smallest volume among room-temperature operating lasers, also equivalent to 0.001% volume of the single cancer Hela cell. Therefore, increased multiplexity and volume-associated biocompatibility are expected. Developed solution-based and self-assembly technology for the gold coating will be applicable to the different nanophotonic devices. Combining top-down lithography, the production of the plasmonic laser particle could be scalable up to high volume at a low cost to meet the anticipated applications in tagging millions of cells in the tissue; for example, we may envision a vial containing billion nano-laser particles for labeling numerous cells in the cancer tissue.

**Impact.** The novelty of our challenge is considered significantly high as the project will open avenues for medical diagnostics and developing personalized medicine. This new technology visualizes the real-time expressions of biomolecules such as signaling proteins, which has been never achieved before. The concept of high-precision molecular sensing is not new, however, it was demonstrated only in the extracellular space. It is based on passive optical microresonators or plasmonic nanoparticles, equivalent to the micro- and nanolaser without light-emitting material. As analytes bind to the resonator, the optical field circulating inside the cavity is perturbed, resulting in a resonance shift. Previously, whispering gallery mode (WGM) microcavity succeeded in single virus and single mRNA detection with three-sigma accuracy in vitro. However, due to the tapered fiber and the tunable laser coupling to the read-out spectral changes, applications to intracellular bio-sensing are not possible. Regarding the plasmonic nanoparticles, intracellular applications were demonstrated to mRNA by using remote coupling of a broadband source.

However, because of the same reason for the case of fluorescence, low-quality resonance due to the nanosize and gold's intrinsic light absorbance generate a broad scattering response, limiting two-color sensing. In addition, free-space coupling generates the signal that has low contrast to the background and misled by intrinsic scattering of the biological sample.

The proposed plasmonic nanolaser will have high sensitivity due to the surface-confined electric field on the metal and background-free signals. At the same time, narrow stimulated emissions allow us to unprecedented precision in intracellular sensing and multiplexed detection. Therefore, intracellular application will make significant advances in single-cell evaluation and later for the assessment of patient-derived tumor samples and a commercial drug response assessment platform. Therefore, pure nanophotonic device will be translated from bench-to-bedside.

Besides technical innovations in biomedicine, the proposed research will advance our ability to improve the optical and material properties of semiconductors by Purcell enhancement. The gained knowledge will provide insights into design strategies for even smaller—sub 100 nm—semiconductor-based laser particles. From the perspective of applications, mass-producible, low-cost, nano-laser particles may find a wide range of applications beyond cancer cell study including on-chip communications, and laser display.

## References

1. E. Abbe, "Beiträge zur Theorie des Mikroskops und der mikroskopischen Wahrnehmung," *Arch. für mikroskopische Anat.* **9**, 413–418 (1873).
2. K. Iga, F. Koyama, and S. Kinoshita, "Surface emitting semiconductor lasers," *IEEE J. Quantum Electron.* **24**, 1845–1855 (1988).
3. Z. Zhang, L. Yang, V. Liu, T. Hong, K. Vahala, and A. Scherer, "Visible submicron microdisk lasers," *Appl. Phys. Lett.* **90**, 111119 (2007).
4. N. Martino, S. J. J. Kwok, A. C. Liapis, S. Forward, H. Jang, H.-M. Kim, S. J. Wu, J. Wu, P. H. Dannenberg, S.-J. Jang, Y.-H. Lee, and S.-H. Yun, "Wavelength-encoded laser particles for massively-multiplexed cell tagging," *Nat. Photonics* **13**, 720–727 (2019).
5. A. H. Fikouras, M. Schubert, M. Karl, J. D. Kumar, S. J. Powis, A. Di Falco, and M. C. Gather, "Non-obstructive intracellular nanolasers," *Nat. Commun.* **9**, 4817 (2018).
6. S. J. J. Kwok, S. Forward, M. D. Fahlberg, S. Cosgriff, S. H. Lee, G. Abbott, H. Zhu, N. H. Minasian, A. S. Vote, and N. Martino, "Laser particle barcoding for multi-pass high-dimensional flow cytometry," *bioRxiv* (2022).
7. S. Cho, M. Humar, N. Martino, and S. H. Yun, "Laser particle stimulated emission microscopy," *Phys. Rev. Lett.* **117**, 193902 (2016).
8. A. Kavčič, M. Garvas, M. Marinčič, K. Unger, A. M. Coclite, B. Majaron, and M. Humar, "Deep tissue localization and sensing using optical microcavity probes," *Nat. Commun.* **13**, 1–10 (2022).
9. M. Schubert, L. Woolfson, I. R. M. Barnard, A. M. Dorward, B. Casement, A. Morton, G. B. Robertson, P. L. Appleton, G. B. Miles, and C. S. Tucker, "Monitoring contractility in cardiac tissue with cellular resolution using biointegrated microlasers," *Nat. Photonics* **14**, 452–458 (2020).
10. H. H. Zhu, J. Zou, H. Zhang, Y. Z. Shi, S. B. Luo, N. Wang, H. Cai, L. X. Wan, B. Wang, and X. D. Jiang, "Space-efficient optical computing with an integrated chip diffractive neural network," *Nat. Commun.* **13**, 1–9 (2022).
11. J. Roh, Y.-S. Park, J. Lim, and V. I. Klimov, "Optically pumped colloidal-quantum-dot lasing in LED-like devices with an integrated optical cavity," *Nat. Commun.* **11**, 1–10 (2020).
12. R.-M. Ma and R. F. Oulton, "Applications of nanolasers," *Nat. Nanotechnol* **14**, 12–22 (2019).
13. S. Cho, Y. Yang, M. Soljačić, and S. H. Yun, "Submicrometer perovskite plasmonic lasers at room temperature," *Sci. Adv.* **7**, eabf3362 (2021).
14. S. Cho and S. H. Yun, "Poly (catecholamine) coated CsPbBr<sub>3</sub> perovskite microlasers: lasing in water and biofunctionalization," *Adv. Funct. Mater.* 2101902 (2021).

## Executive Summary

### Human Breath Analysis: Frequency Comb-based Non-Invasive Biomedical Diagnostics

The exhaled human breath contains a remarkably complex mixture of gases and is an unparalleled window into the health of the individual. If harnessed, medical breath analysis promises to be a powerful and inherently non-invasive diagnostic tool. A portable device capable of quantitatively detecting molecular species characteristic to certain disease states (biomarkers) within the exhaled breath would have the potential to transform medical care: allowing the early detection of disease, easier screening, and faster medical intervention in a variety of contexts - ultimately improving the health and prognosis of patients worldwide. However, there is currently no compact, low-cost, deployable breath analysis device with the molecular sensitivity and selectivity to provide medically relevant information across multiple disease states for point-of-care use by clinicians in real time. This project aims take a critical step towards this ideal, creating a prototype optical sensor with the required molecular sensitivity and selectivity for medical breath analysis, while remaining compatible with future compactification efforts.

There is currently a great push to develop and apply photonic technologies to medical breath analysis measurements. However, it is a challenging task to achieve the required selectivity, sensitivity, and broad use cases while maintaining a small device size. This project will explore the use of a near-ideal optical interrogation source for molecular spectroscopy dual near-infrared electro-optic frequency combs. Previous experience in the design, construction, and utilisation of near-infrared optical frequency combs for molecular spectroscopy - and their application to medical breath analysis - has demonstrated that the near-infrared absorption features of important biomarkers are too weak without optical enhancement. Instead, these electro optic combs in the near-infrared will be converted to the 1000x more spectroscopically sensitive mid-infrared spectral region with a nonlinear crystal, removing the need for an optical enhancement cell that traditionally hampers the compactification efforts of optical breath analysis devices. In addition, the use of two combs allows for the performance of dual-comb spectroscopy, replacing another traditionally bulky (and difficult in the mid-IR) component - the spectrometer responsible for unravelling the absorption of the interrogating light at each frequency - with a simple photodiode and radio-frequency components. This project will allow us to demonstrate the first proof-of-principle of a device that can deliver on the long-term dream to create a photonic non-invasive, affordable, portable quantitative diagnostic tool.

This technology has the promise to provide a future low-cost, compact, deployable device with sufficient molecular sensitivity, accuracy, and selectivity to provide medically relevant information to the clinician in a variety of contexts.

At the completion of the project, we will have advanced the frontier in precision spectral analysis and created a compact prototype breath analysis system in the mid-IR that is 1000x more sensitive than its near-infrared counterparts. Additionally, the proposed methodology is compatible with future photonic chip integration, opening the doorway for the development of a robust, compact, low-cost and lightweight breath analysis device suitable for rapid breath analysis for clinical use. This has the potential to have a transformative impact on applications ranging from pre-symptomatic disease detection and diagnosis, critical patient monitoring, measurement of human fitness, performance and compliance testing, breath fingerprinting, and other gaseous measurement applications beyond breath analysis.



## Proposal: Human Breath Analysis: Frequency Comb-based Non-Invasive Biomedical Diagnostics

### Literature Review

The exhaled human breath contains a complex mixture of gases including nitrogen, oxygen, carbon dioxide, hydrogen and over 2000 different volatile organic compounds (VOCs) [1]. The composition of the breath and its change over time is a potential goldmine for applications including: pre-symptomatic disease diagnosis, critical and paediatric patient monitoring; measurement of human fitness, performance and drug compliance; as well as breath fingerprinting [2, 3, 4, 5]. Many diseases (e.g. COVID, lung cancer, diabetes, oesophageal cancer, Chronic Obstructive Pulmonary Disorder (COPD), asthma, hypoxia and heart conditions) are only caught late in the disease progression, when patient outcomes are less positive than they might otherwise be with earlier intervention [6, 7].

Furthermore, breath analysis is a safe and non-intrusive diagnostic tool with the potential for providing a deployable photonic biosensor and screening tool for the clinician. Breath analysis offers the opportunity for early diagnosis and screening for numerous disease conditions, in a low cost, rapid, and low-intervention point-of-care device, the need for which has only become more apparent with the rise of COVID [8, 9]. The current gold-standard for medical breath analysis – mass spectrometry (MS) – is large, costly, slow and requires specialist technicians to perform the testing [10]. Due to these reasons, the identification of new biomarkers for diseases is slow [11]. Other approaches include E-noses and electrochemical sensors, but these devices are highly selective and are unlikely to become broad-spectrum diagnostic devices [10].

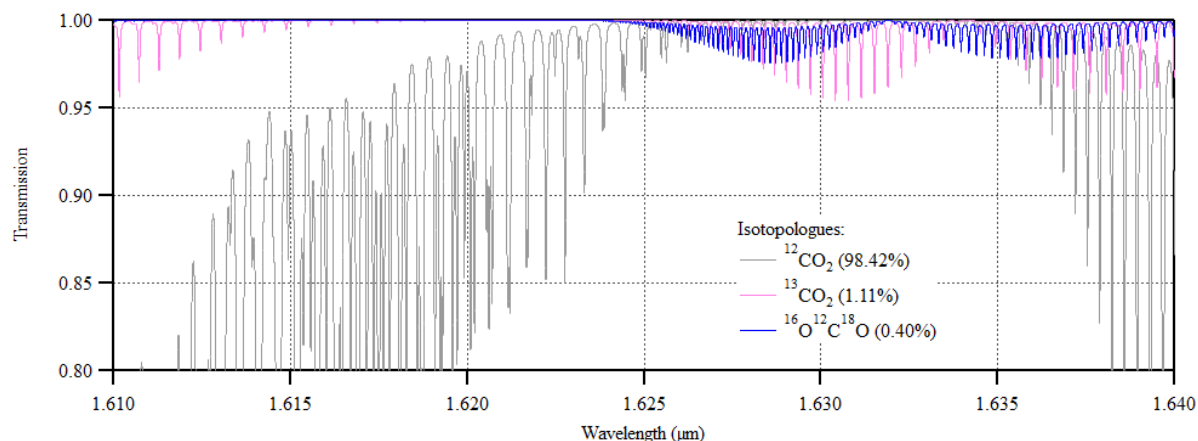


Figure 1: A simulated 30nm carbon dioxide absorption profile breakdown for the three most common isotopologues in the near-IR. Note this simulation was performed with a path length of 60m - the commonly achievable path length by use of a non-resonant optical enhancement cell. Carbon dioxide is one of over 2000 different VOCs found in the human breath.

There is currently a great interest in applying photonics to breath measurements. Each molecule, including isotopologues of the same species, possess a characteristic, broad-spanning, and unique absorption signature (see Figure 1) [12]. Furthermore, there are often more than one species of molecule in the breath whose presence and relative concentration correlate to each specific disease state [13]. These molecules are known as 'biomarkers', and the need to measure the presence and concentration of multiple biomarkers simultaneously makes breath analysis a true challenge [14]. When a breath sample is illuminated with a suitable light source, the absorbed frequencies of light form a complex spectrogram from which we can identify the specific molecules that are present along with their concentration [15]. In tandem, the development and recent proliferation of optical frequency combs (OFCs) in the near-infrared (near-IR) has provided a near-ideal laser source for molecular spectroscopy, combining a broad frequency bandwidth and dense spectral sampling with the optical enhancement opportunities only a coherent source can afford [12]. An OFC's broad



spectral coverage is advantageous, in that can interrogate multiple chemical species in parallel. This avoids the misidentification that can occur when the spectrum is examined at a single frequency.

While the use of OFCs as the interrogation source for optical spectroscopy has been a step-change, the challenges of using OFCs in this way has been apparent from the beginning: one needs to individually resolve each comb 'tooth'. This provides a real challenge as the comb tooth spacing is often finer than the resolution of most conventional spectrometers, resulting in the loss of the benefits of using an OFC [16]. Certain spectrometers do possess sufficiently high resolution for comb use, such as dispersive spectrometers based on Virtually Imaged Phased Arrays (VIPAs), cavity vernier techniques, and high-resolution Fourier Transform Infrared (FTIR) spectrometers, though each have certain downsides [17]. However, the simplest way of retaining the benefits of the OFC as an interrogation source is to dispense with the spectrometer element altogether, which is possible with *dual-comb spectroscopy* (DCS), in which two combs with slightly differing comb tooth spacing are transmitted through the sample, encoding the absorption features onto the comb light, before the two combs are optically interfered on a photodiode. This generates a radiofrequency (RF) comb that is easily measured with RF electronics and can be disentangled to produce the same absorption spectra as achieved with physical spectrometers.

This DCS technique has allowed a number of spectroscopic measurements to be performed, including some early work on human breath [18] with promising results. Unfortunately, the near-IR spectral regime targets only the harmonics of most fundamental molecular absorption features, resulting in the absorption signatures being more than 1000 times less sensitive than the fundamental absorptions, which lie in the mid-infrared (mid-IR) [19]. This means that optical enhancement methods are required, including the use of optical enhancement cavities and multi-pass cells. This decrease in sensitivity places a fundamental limitation on the ultimate sensitivity of breath analysis in the near-IR, along with limiting the compactness of any device based on this technology.

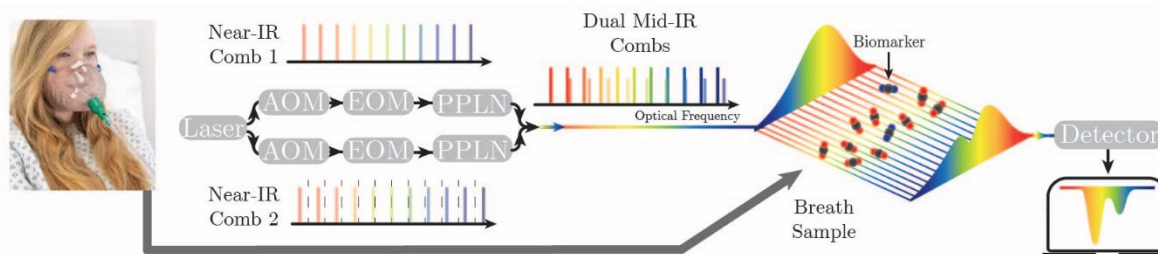


Figure 2: Proposed scheme for a compact mid-IR dual-comb breath analysis device. The characteristic absorption profile of the biomarker(s) are imprinted onto the transmitted light. AOM: Acousto-optic modulator; EOM: Electro-optic modulator; PPLN: periodically poled lithium niobate (crystal).

The obvious solution is to move to the more spectroscopically sensitive mid-IR region. However, this produces new challenges: the generation of mid-IR OFCs is difficult but not impossible [20], and the detection of light in this region is challenging. To combat these challenges, we propose the generation of two flexible electro-optic (EO) combs in the near-IR, which are transformed into the mid-IR with periodically poled lithium niobate (PPLN) crystals as shown in Figure 2. With the two mid-IR combs of slightly differing comb line spacings, we will perform dual-comb spectroscopy in the more spectroscopically sensitive mid-IR regime, removing the need for optical enhancement cells, compactifying the device, and translating the spectral signal into electrical signals that can easily be measured, generating a rapid breath analysis capability [21]. While this proposal utilises bulk components, it is important to note that each of these components has been realised with photonic chip technology and is the ultimate future of photonic breath analysis devices [22].

This proposal builds on previous experience of designing, constructing, and utilising optical frequency combs for molecular spectroscopy, and their application to medical breath analysis. While

currently funded to perform experimental medical breath analysis using near-IR combs, this project would allow us to extend this pioneering breath analysis research into the promising and spectroscopically-rich mid-IR region. This technology has the promise to provide a future low-cost, compact, deployable device with sufficient molecular sensitivity, accuracy, and selectivity to provide medically relevant information to the clinician in a variety of contexts.

### Problem Statement/Objectives

**Problem statement:** *There is currently no compact, deployable breath analysis devices with the molecular sensitivity and selectivity to provide medically relevant information for clinicians in real time. This project aims to create a prototype sensor in the mid-IR with the required molecular sensitivity and selectivity, compatible with future compactification efforts to address this gap.*

The solution to this problem can be divided into three related objectives:

- **Objective 1:** *Develop architecture for creation of a dual-comb mid-IR breath analysis device that addresses the problem statement.* The prototype device will be developed using bulk connectorized components, with a goal of optimising the system for size, performance, sensitivity, and spectral selectivity.
- **Objective 2:** *Benchmarking the prototype device against known molecular samples.* The prototype device will be tested and optimised using known molecular samples of interest without an enhancement cell, to ensure that the final device is compatible with future portability and the considerations above.
- **Objective 3:** *Apply the prototype device to breath samples.* The existing device and the new prototype mid-IR device will be applied to real breath samples.

### Outline of tasks/Work Plan

This project will explore a new compact instrument that leverages the Nobel Prize winning technology of the optical frequency comb to provide rapid breath analysis to measure the concentration of biomarkers in the human breath. By translating the optical frequency combs to the mid-infrared (mid-IR) in combination with the dual comb spectroscopy technique, we will translate the spectral signal into electrical signals that can easily be measured and analysed, generating a rapid breath analysis capability. This technology has the promise to provide low-cost, compact, deployable devices with sufficient molecular sensitivity, accuracy, and selectivity to provide medically relevant information rapidly. As a stretch goal, we will upgrade our current analysis algorithms to employ machine learning and apply it to the complex spectrographs. This will complement the current research efforts to perform similar tasks in the near-IR, for which a clinical trial is approved and funded. To achieve accurate and deployable breath analysis devices, the project is structured into the following tasks:

- **Task 1:** Apply previously developed spectral modelling algorithms to the mid-IR and determine the exact spectral region of interest, avoiding the plentiful water vapour absorptions. (*3 months*)
- **Task 2:** Identify and acquire the components for the creation of a compact mid-IR dual-comb spectral analysis system: Assembly of an electro-optic dual comb system operating in the near-IR (using mature and low-cost telecom equipment) and use nonlinear optical frequency mixing to convert the dual near-IR combs into the sensitive mid-IR regime (Figure 2). (*~12 months*)
- **Task 3:** Benchmarking & data analysis of pure samples of interest. We will in the first instance apply our existing spectral analysis code to replicate the high accuracy, selectivity, and sensitivity of molecular detection previously demonstrated with our near-IR approach. (*~6 month*)
- **Task 4:** Perform a measurement on a breath sample with the system. This will utilise the existing breath analysis infrastructure within the lab, and integrate it with the new system. (*~3 months*)
- **Task 5 (stretch goal):** Apply machine learning algorithms to spectrograms of the pure sample tests, and comparison to the existing analysis algorithm. Machine learning algorithms for

identification of the complex spectroscopy patterns will be developed with the expertise and assistance of current collaborator Dr Johan Verjans (Australian Institute for Machine Learning).

I am an ECR working in labs of the Precision Measurement Group headed and mentored by Professor Andre Luiten, within the Institute for Photonics and Advanced Sensing as part of the University of Adelaide, Australia. The wider Precision Measurement Group (PMG), and myself, have extensive experience in the creation and utilisation of optical frequency combs, and the successful translation of fundamental research into out-of-lab photonic devices.

### Outcome(s)

At the completion of the project, we will have advanced the frontier in precision spectral analysis and created a prototype breath analysis system in the mid-IR. This will be achieved using the more flexible bulk components, paving the way for optical breath printing in the mid-IR. Additionally, this project would form the basis for the next phase of development, being the jump into photonic chip technologies (in alignment with the expertise and future direction of the PMG), and further the development of a robust, compact, and lightweight breath analysis device, suitable for rapid breath analysis for clinical use. Moreover, the first comb I built was in collaboration with visiting international researchers from the National Institute of Standards and Technology (NIST). This project would enable me to take up their invitation for a research visit to their dual-comb spectroscopy labs and comb-construction facilities in Boulder, Colorado.

The outcomes will be the deeper understanding of medical breath analysis, combined with a suite of new technologies capable of monitoring the composition of the breath and able to provide quantitative information about the human breath and the links to disease. This has the potential to have a transformative effect on applications ranging from pre-symptomatic disease detection and diagnosis, critical patient monitoring, measurement of human fitness, performance and compliance testing, breath fingerprinting, and other gaseous measurement applications beyond breath analysis.

### Impact

The optical frequency comb offers the first avenue to provide low-cost deployable breath analysis technology with sufficient molecular sensitivity, accuracy and selectivity to be medically relevant. Breath analysis itself has the potential to provide a rapid, simple, non-invasive method for the detection, monitoring and prognosis of a spectrum of diseases, using breath biomarkers at eventually, very low cost. This project will allow us to demonstrate the first proof-of-principle of a device that can deliver on the long-term dream to have a non-invasive, affordable, portable quantitative diagnostic tool. The outcomes will be the deeper understanding of medical breath analysis, combined with a suite of new technologies capable of monitoring the composition of the breath able to provide quantitative information about the human breath and the links to disease. This has the potential to have a transformative impact on applications of critical health importance now and into the future, including pre-symptomatic disease detection and diagnosis, critical patient monitoring, and beyond.

## References

- [1] M. Karunakaran, P. Ramani, S. Gheena, R. Abilasha and R. Hannah, "Volatile Organic Compounds in Human Breath," *Indian Journal of Dental Research*, vol. 33, no. 1, pp. 100-104, 2022.
- [2] A. G. Dent, T. G. Sutedja and P. V. Zimmerman, "Exhaled breath analysis for lung cancer," *Journal of thoracic disease*, no. 5, p. S540–S550, 2013.
- [3] A. T. Popov, "Human exhaled breath analysis," *Annals of allergy, asthma & immunology : official publication of the American College of Allergy, Asthma, & Immunology*, vol. 106, no. 6, p. 451–457, 2011.
- [4] Z. -C. Yuan and B. Hu, "Mass Spectrometry-Based Human Breath Analysis: Towards COVID-19 Diagnosis and Research," *Journal of Analysis and Testing*, vol. 5, p. 287–297, 2021.
- [5] K. -H. Kim, S. A. Jahan and E. Kabir, "A review of breath analysis for diagnosis of human health," *TrAC Trends in Analytical Chemistry*, vol. 33, pp. 1-8, 2012.
- [6] I. Nardi Agmon, Y. Y. Broza, G. Alaa, A. Eisen, A. Hamdan, R. Kornowski and H. Haick, "Detecting Coronary Artery Disease using Exhaled Breath Analysis," *Cardiology*, p. (Advance publication), 2022.
- [7] F. S. J. Cikach and R. A. Dweik, "Cardiovascular biomarkers in exhaled breath," *Progress in cardiovascular diseases*, vol. 55, no. 1, pp. 34-43, 2012.
- [8] M. Abumeeiz, L. Elliott and P. Olla, "Use of Breath Analysis for Diagnosing COVID-19: Opportunities, Challenges, and Considerations for Future Pandemic Responses," *Disaster medicine and public health preparedness*, vol. (Advance online publication), pp. 1-4, 2021.
- [9] N. V. R., A. K. Mohapatra, V. K. Unnikrishnan, J. Lukose, V. B. Kartha and S. Chidangil, "Post-COVID syndrome screening through breath analysis using electronic nose technology," *Analytical and Bioanalytical Chemistry*, vol. 414, p. 3617–3624, 2022.
- [10] B. Behera, R. Joshi, G. K. A. Vishnu, S. Bhalerao and H. J. Pandya, "Electronic nose: a non-invasive technology for breath analysis of diabetes and lung cancer patients," *Journal of Breath Research*, vol. 13, p. 024001, 2019.
- [11] O. Lawal, W. M. Ahmed, T. M. E. Nijsen, R. Goodacre and S. J. Fowler, "Exhaled breath analysis: a review of 'breath-taking' methods for off-line analysis," *Metabolomics*, p. 110, 2017.
- [12] S. K. Scholten, C. Perrella, J. D. Anstie, R. T. White and A. N. Luiten, "Accurate optical number density measurement of  $^{12}\text{CO}_2$  and  $^{13}\text{CO}_2$  with direct frequency comb spectroscopy," *Physical Review Applied*, vol. 12, p. 034045, 2019.
- [13] J. H. Shorter, D. D. Nelson, J. B. McManus, M. S. Zahniser, S. R. Sama and D. K. Milton, "Clinical study of multiple breath biomarkers of asthma and COPD ( $\text{NO}$ ,  $\text{CO}_2$ ,  $\text{CO}$  and  $\text{N}_2\text{O}$ ) by infrared laser spectroscopy," *Journal of Breath Research*, vol. 5, p. 037108, 2011.
- [14] D. Smith and P. Spanel, "The challenge of breath analysis for clinical diagnosis and therapeutic monitoring," *Analyst*, vol. 132, no. 5, p. 390–396, 2007.
- [15] S. K. Scholten, C. Perrella, J. D. Anstie, R. T. White, W. Al-Ashwal, N. B. Hébert, J. Genest and A. N. Luiten, "Number-density measurements of  $\text{CO}_2$  in real time with an optical frequency comb for high accuracy and precision," *Physical Review Applied*, vol. 9, p. 054043, 2018.
- [16] N. Picqué and T. W. Hänsch, "Frequency comb spectroscopy," *Nature*, vol. 13, pp. 146-157, 2019.
- [17] N. Coluccelli, M. Cassinerio, B. Redding, H. Cao, P. Laporta and G. Galzerano, "The optical frequency comb fibre spectrometer," *Nature Communications*, vol. 7, p. 12995, 2016.
- [18] J. Xia, F. Zhu, J. Bounds, E. Aluauee, A. Kolomenskii, Q. Dong, J. He, C. Meadows, S. Zhang and H. Schuessler, "Spectroscopic trace gas detection in air-based gas mixtures: Some methods and applications for breath analysis and environmental monitoring," *Journal of Applied Physics*, vol. 131, no. 22, p. 220901, 2022.
- [19] M. Ebrahim-Zadeh and I. T. Sorokina, *Mid-Infrared Coherent Sources and Applications*, Springer, 2007.
- [20] B. Henderson, A. Khodabakhsh, M. Metsälä, I. Ventrillard, F. M. Schmidt, D. Romanini, G. Ritchie, S. Te Lintel Hekkert, R. Briot, T. Risby, N. Marczin, F. Harren and S. M. Cristescu, "Laser spectroscopy for breath analysis: towards clinical implementation," *Applied physics. B, Lasers and optics*, vol. 124, no. 8, p. 161, 2018.
- [21] I. Coddington, N. Newbury and W. Swann, "Dual-comb spectroscopy," *Optica*, vol. 3, no. 4, pp. 414-426, 2016.
- [22] M. Li, J. Ling, Y. He, U. A. Javid, S. Xue and Q. Lin, "Lithium niobate photonic-crystal electro-optic modulator," *Nature Communications*, vol. 11, p. 4123, 2020.

### **Executive Summary**

The focus area of NECTO is *information*, with a specific challenge of development of a new integrated photonic device to protect the digital-infrastructure from the anticipated data-traffic congestion crisis of the Internet-of-Things (IoT) era. There will be more than 29 billion IoT devices in 2030, more than double the 2021 figure. These devices will drive an exponential increase of data-traffic. Ericsson predicts a 4-fold increase of global data traffic from 2021 to 2027 with a significant portion of such traffic for the purpose of performing Artificial Intelligence (AI) tasks, like pattern recognition, in the cloud. To date, there is no compact digital-computing platform which can perform AI tasks on a high-throughput massively parallel data stream in real time – this is the main reason why data must be transferred to the cloud.

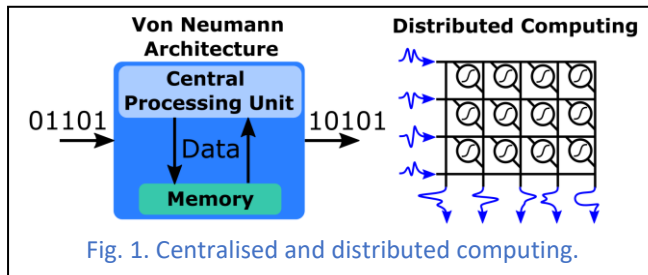
To overcome such a Challenge, NECTO will develop a new truly compact photonic chip to perform AI tasks on a high-throughput massively parallel data stream at the ‘edge’ of the data infrastructure landscape – *edge*, here, means at the point of data collection. Thus, by performing AI directly at the point of collection, demand for cloud computing services will be reduced. The proposed photonic computing chip is inspired by how humans process and infer information, i.e., neuromorphic. It will be developed on all-passive components exploiting chaotic light dynamics, whereas other reported chips are based on heat-generating active nonlinear components. Thus, the new chip will be a truly compact system. The new chip is envisaged to impact other technological areas, for example, micro-satellite computing – it will be immune to space radiation, not heat-generating, low-size, low-weight, low-power and low-error rate.

To realize such a chip, a high-quality factor cavity exhibiting chaotic wave dynamics is central. Therefore, minimizing loss is key, and it has shaped the workplan of this project. The chip will be developed on a silicon-on-insulator platform, capitalizing on the well-established integrated photonic fabrication processes. To suppress radiation loss and maintain light confinement, a symmetric (z-direction) cavity will be developed on a photonic crystal platform. Insertion loss will be minimized by developing a new impedance matched mode-converter between the photonic crystal and silicon strip waveguides using the recently reported inverse design technique. High-quality fabrication of the chip will be performed in world-class partner imec, Belgium. It will be packaged and fixed with a high-coupling input/output interface in the world-class packaging facility, National Tyndall Institute, Ireland. The prototype will be demonstrated for two key AI applications, namely nonlinear wireless communication signal equalization and pattern-recognition of sensors’ signals. In my previous research, pattern-recognition of sensors’ signals has been performed using a ‘bulky’ version of neuromorphic computing system in the lab; the compact neuromorphic chip will underpin the realization of an *offline* wearable sensor.

The 20th Anniversary Challenge from Optica will enable Dr Phang, an early career researcher, to embark on a novel and adventurous journey marrying chaos wave optics with photonic neuromorphic computing. Dr Phang has developed his career on cross-disciplinary research encompassing computational photonics, information photonics, chaotic electrodynamics, wireless communication, machine learning and photonic neuromorphic computing. Optica Challenge funding will enable Dr Phang to conduct frontier research in collaboration with world-class international partners, imec and the Tyndall Institute. Dr Phang will capitalize on his involvement in complementary research projects like the flagship [H2020-Rise6G](#) wireless communication and a British Council project on photonic sensing for environmental monitoring to demonstrate the photonic neuromorphic technology as a key-enabler in the areas of information-and-communication and environmental monitoring. He will be supported by an advisory group to help him engage with academia and industry, bring photonic neuromorphic computing through the technological development process, and extend the impact of the neuromorphic photonics in other areas, like light-matter interaction and hyperspectral imaging.



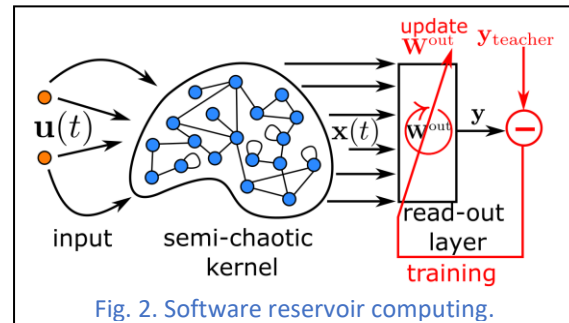
**LITERATURE REVIEW:** There is a clear unmet need for an innovative computing platform to process information beyond what current digital computers can do, especially to perform Artificial Intelligence (AI) tasks. These include optimization, discrimination, forecasting and pattern recognition tasks, on a high-throughput massively parallel data stream. It stimulates a new line of research of brain-inspired computing, for example neuromorphic computing. In fact, the human nervous system is an efficient and powerful ‘computer’<sup>[1,2]</sup>. For comparison, the data center which runs Google’s AlphaGo AI uses 50,000 times more energy than a human’s nervous system<sup>[1-3]</sup>. No digital computer can emulate the computing power of the human brain, more than 20 billion RIKEN-Fugaku (current top supercomputer) are required to fully emulate the computational capacity of humans<sup>[4]</sup>. Neurophysiology shows that the key to the vast capability of humans’ computing ability lies in how and where such information is processed<sup>[5]</sup>.



A digital computer processes information at a centralized processing unit (von Neumann architecture) with a separate memory device, see Fig. 1. The human nervous system is, however, based on a distributed processing architecture in which each neuron “remembers and processes” a stream of (electro-chemical)

signals as it travels to the brain for “inferring”. Inspired by the distributed computing architecture of the human nervous system, several neuromorphic computing architectures have been developed<sup>[5]</sup>. The central aim of a neuromorphic computing system is to realize the distributed computing architecture of the human nervous system as hardware, enabling a hardware-level integration of AI. Realization of neuromorphic computing as a photonic system promises a computing system which is 6-8 orders of magnitude faster and 4-8 orders of magnitude more efficient than digital electronics<sup>[5]</sup>.

Photonic reservoir computing (PhRC) is a relatively new member of the physical neuromorphic computing system; it is implemented in a photonic system based on software reservoir computing<sup>[6]</sup>, see Fig. 2. Implementing reservoir computing in photonics leads to a design for very high-speed processing exploiting the availability of ultrawide bandwidth optical telecommunication components. It offers a fundamentally different approach to other neuromorphic photonic systems, in terms of both architecture and how the system is trained (or optimized)<sup>[6]</sup>. PhRC only trains the Read-Out layer. The kernel of the PhRC is not trained/optimized, thus retaining the characteristic of the kernel as a random and chaotic system, i.e., mimicking the chaotic behavior of the human nervous network. Other neuromorphic systems<sup>[7-13]</sup> require full system optimization. Thus, the PhRC offers practical benefits for two reasons: a physical implementation is now practically feasible and task-specific training will be done exclusively at the Read-Out layer, which offers a significant simpler optimization mechanism compared to the whole system optimization in other neuromorphic systems. Examples of PhRC implementations include a swirl configuration of semiconductor amplifiers<sup>[14,15]</sup>, fiber delay lines with an electro-optical system<sup>[16-19]</sup> and others<sup>[6]</sup>.

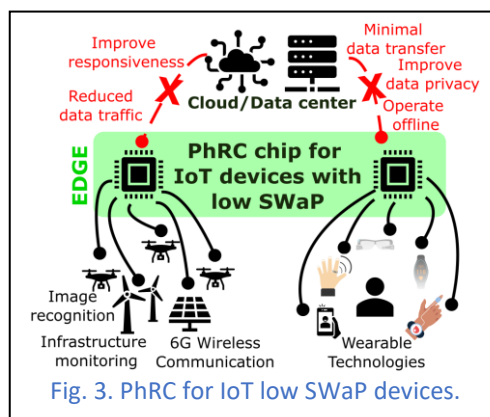


**PROBLEM STATEMENT AND OBJECTIVES:** The focus area of NECTO is *information*, with a specific challenge of developing a new integrated photonic device to protect the digital-infrastructure from the anticipated data-traffic congestion crisis of the Internet-of-Things (IoT) era. Statista predicts<sup>[20]</sup> that the number of IoT devices will surpass 29 billion devices in 2030, more than double from 11 billion devices in 2021. Most of these IoTs will be wearable sensors to monitor vital indicators, like heart rate, blood oxygenation, blood pressure, temperature,

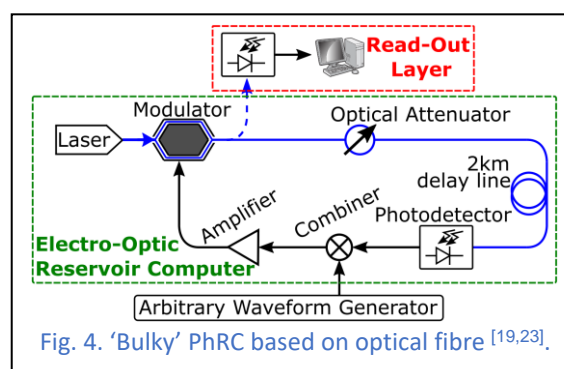


perspiration, and glucose, for real time healthcare monitoring, >5 sensors/person<sup>[21]</sup>. Such devices will be essential in future healthcare with an increasing number of chronic diseases, an ageing population and limited healthcare resources. These wearable IoT devices perform AI, including pattern recognition, data fitting, and forecasting. However, to date, there is no *compact* digital-computing platform suitable for IoT devices which can perform AI tasks on a high-throughput massively parallel data stream in real time. This is the main reason why data must be transferred to the cloud. Ericsson predicts a 4-fold increase of global data traffic from 2021 to 2027 with a significant portion of such traffic being for the purpose of performing AI in the cloud<sup>[22]</sup>. For non-IoT applications, currently AI is commonly performed in a personal computer and field programmable gate array (FPGA) for time-critical applications, like finance forecasting and early warning systems. Such computing platforms are big, heavy, and power consuming – and so not suitable for IoT wearable devices.

To address the challenge, NECTO will develop a new PhRC which will be on an integrated photonic platform to perform AI on a high-throughput massively parallel data stream at the edge of the data-infrastructure landscape, offline and operate under low Size, Weight, and Power (SWaP) suitable for IoT wearable devices. ‘At the edge’ here refers to a new technology concept in which the operation applications and related processes happen close to the users. By performing AI at the edge, demand for cloud computing service will be reduced or eliminated. Thus data-traffic will be reduced, improving IoT devices’ responsiveness and users’ data privacy, see Fig 3.



In my previous research<sup>[19,23]</sup>, a PhRC based on ‘bulky’ 2 km of fiber delay lines and electro-optic components, see Fig. 4, has been developed on an optical bench. I demonstrated, for the first-time, AI-on-hardware to perform data-interpolation and regression for multi-channels sensors’ signal recognition. NECTO will realize a PhRC at chip scale. There are implementations of PhRC on chip reported, to date, by the Bienstman group<sup>[15,24]</sup>. Note that the chip in<sup>[24]</sup> uses active components of amplifiers and modulators, and in<sup>[15]</sup> uses several long spiral waveguides and splitters/couplers. A problem with an active PhRC chip is *robustness and scalability*. It needs stringent packaging with temperature management of complex hybrid photonic-electronic integrated circuits – active components radiate heat due to ohmic-loss which consequently perturb the system response – thus hindering the realization of a truly compact PhRC on chip. The PhRC chip to be developed in NECTO will be *all passive components* which will be based on a completely different concept to previously reported PhRCs<sup>[15,24]</sup>. In the new PhRC chip to be developed in NECTO, the nonlinear-like effect arises from the chaotic optical dynamics, not from active components<sup>[24]</sup> nor photodiodes<sup>[15]</sup>. To generate the chaotic dynamics, a new topology of PhRC will be developed, fabricated, tested, and benchmarked to perform classification and prediction tasks. Numerical studies by me and others<sup>[25-27]</sup> have recently shown that a D-shaped cavity, in Fig. 5, due to its geometry, exhibits chaotic dynamics. Although from simulation, a 60  $\mu\text{m}$  x 30  $\mu\text{m}$  D-shaped photonic crystal cavity based on Silicon-on-Insulator (SOI) is shown to exhibit a high Q-factor 15000, decay time  $\sim 10\text{ps}$  and can perform an XOR task with low error ( $\sim 30\text{ dB}$ ), previous attempts of fabrication realization have, so far, failed to achieve the minimum  $\sim 40\text{dB}$



transmission threshold for high-speed measurement. The low transmission is due to asymmetry in the refractive index below (SiO<sub>2</sub>) and above (air) the photonic crystal which breaks the confinement of the light and high mismatch loss due to the poor impedance matching between the strip and photonic crystal waveguides. In NECTO, my team and I will develop a symmetrical (z-direction) D-shaped photonic crystal cavity and innovate a new impedance matched interface between the photonic crystal and stripe waveguides. The impedance matched interface will be developed using the recently reported inverse design method<sup>[28,29]</sup>, performing mode conversion between the strip and photonic crystal waveguide modes. The PhRC chip will be developed on SOI to

operate at telecom wavelength, capitalizing on the availability of well-established integrated photonic fabrication processes, packaging, and low-noise ultra-fast detectors.

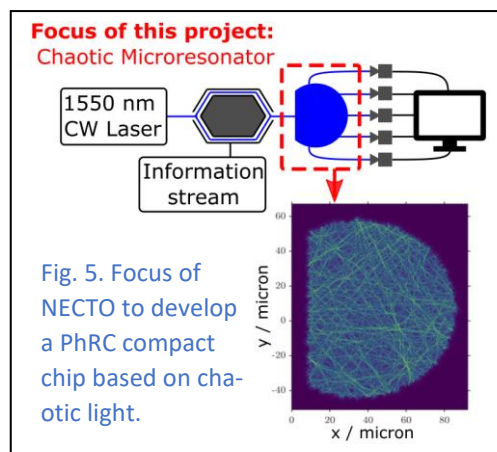
**AIM:** NECTO will for the first time realize an innovative neuromorphic computing platform in a photonic chip to enable photonic-hardware-level integration of artificial intelligence for IoT wearable devices. The key **OBJECTIVES** (O is an objective) of NECTO are:

- O1.** To design a symmetric D-shaped high-Q factor chaotic cavity,
- O2.** To develop a new impedance matched mode converter and undertake whole system simulation,
- O3.** To fabricate the PhRC chip in partner facility imec,
- O4.** To test and package the PhRC chip in partner facility Tyndall Institute,
- O5.** To experimentally benchmark and provide demonstrator applications of the PhRC chip.

**IMPACT:** NECTO will develop a novel design and hardware demonstrator. The new PhRC chip, as an adaptable low-SWaP and low-error all-optical signal processor, will be a key-enabling-technology in the realization of applications which require fast operation of AI, including pattern recognition, data-fitting, forecasting and optimization, under strict SWaP demand. IoT wearable devices are the primary application for the new PhRC chip. As mentioned, it will enable edge computing on IoT devices, allowing computational offloading from the cloud to the device directly. Immediate impact of such computation offloading includes reducing the energy consumption and carbon footprint of datacenters. Conservatively, assume the PhRC enables 1% global reduction of cloud computing utilization in 2030, it yields to saving of ~100 TWh of energy<sup>[30]</sup> – equivalent to 1 months energy consumption of the New York district in 2020<sup>[31]</sup>. As data are processed locally, it will improve the data-privacy of IoT wearable devices.

The new chip is envisaged to impact on other technological areas. For example, it will be a suitable computing platform for micro-satellites as the new PhRC will be immune to space radiation, not heat-generating and low SWaP. It will enable a rapid response reconfigurable intelligent surface (RIS) for 6G wireless communication. RISs are man-made surfaces with thousands of reconfigurable elements, which are used to dynamically control radio-wave multipath propagation for localization, mitigate obstructions, and to extend radio coverage in dead-zones. Experimental demonstration of RIS has been reported under an ideal, conditioned, laboratory environment, i.e., static and few obstacles. The PhRC will allow operation of RIS in a realistic environment. It will enable edge computing close to the end-users and therefore increase the responsiveness of RIS by predicting the optimum configuration of RIS from the outset; currently it is done by means of slow and energy inefficient heuristic optimization<sup>[32]</sup>.

NECTO will be a 2-year research project led by the Principal Investigator, Dr Phang, assisted by a post-doctoral researcher (costed to the grant) and Dr Phang's on-going PhD students (at



no-cost to the project). **THE WORK PLAN (WP)**, see Fig. 6, **map onto the Objectives** (D is a Deliverable):

**WP1. Design of symmetric D-shaped high-Q factor chaotic cavity. [Months 1-3]** To maintain the confinement of Transverse Electric (TE) polarized light, a symmetric (z-direction) photonic crystal cavity will be designed using commercial finite-difference time-domain (FDTD), Lumerical software. The initial design will be based on my previous numerical investigations<sup>[19,23]</sup> from which the dimension will be optimized to provide at least Q-factor 15000 and signal decay time 10 ps.

Such a cavity will have an extended-time signal propagation and sensitive. A realistic model will be developed taking account material dispersion. Previous simulations show that a hexagonal lattice photonic crystal with cylindrical holes of 200 nm diameter and 400 nm pitch distance has a bandgap centered at the operational wavelength 1550 nm, ideal to confine the TE mode. The D-cavity will be equipped with one input and seven output ports, each connected to a grating coupler with single mode TE waveguides for light input/output between the integrated circuit to fiber arrays. The simulation will provide information on source requirement (temporal profile, width, and repetition rate) and power requirement (scattering-parameter and radiation losses). **D1: Design of a high-Q factor D-shape chaotic photonic crystal cavity.**

**WP2. Design of new impedance matched interface & full-system model. [Months 2-20]** To minimize loss due to poor impedance matching between the strip and photonic crystal waveguide, a new impedance-matched interface between photonic crystal cavity and strip waveguides will be designed using<sup>[28,29]</sup>. It is aimed to achieve <-40 dB of insertion loss. Then, a full PhRC system will be simulated, integrating the highly optimized grating couplers design from the iMEC process design kit (PDK), the D-shaped cavity (from WP1) and the impedance matched interface. Full wave FDTD simulation will be performed to numerically characterize the device. Iterate design (WP1-2) to achieve maximum overall loss of -30dB. Noise will be introduced to the FDTD simulation to investigate the impact of noise to the performance of the PhRC in performing benchmark tests, e.g., Nonlinear Auto-Regressive Moving Averages test (NARMA)<sup>[16,17]</sup> and memory capacity tests. **D2: Full wave numerical characterization of the whole PhRC system including supporting components, including grating couplers, impedance-matched mode-converter, and bent waveguides.**

**WP3. Fabrication of the PhRC chip in partner facility iMEC. [Months 7-20]**

The design developed in WP2 will be fabricated in partner facility iMEC, Belgium, using a multi-project-wafer (MPW) 220nm SOI process (ISiPP50G) and e-beam lithography (EBL). Several chips, differing in cavity size, will be fabricated to validate the impact of size on the temporal memory and investigate the correlations between output ports (measuring the chaotic behavior of the cavity). **D3: PhRC chip fabricated.**

**WP4. Packaging of the PhRC chip in partner facility Tyndall Institute. [Months 14-20]**

The fabricated chip will be first optically characterized. WP1-4 will be iterated to achieve the minimum Q-factor of 15000 and decay time of 10 ps. and then assembled into a semi-permanent package in partner facility National Tyndall Institute, Ireland. Optical characterization will be performed by the nano-aligner system available in Tyndall. For a robust configuration, quasi planar integration between the grating couplers and the fiber array will be achieved by using a 40° polished facet with total internal reflection allowing the fiber array to lie flat on the chip. Optimum coupling will be achieved via automatic alignment process, capable of correcting for misalignment with 6 degrees of freedom. **D4: Packaged, fixed, and assembled PhRC chip.**

**WP5. Experimental benchmark of the PhRC system. [Months 18-24]** In the University of Nottingham (UoN), an optical rig will be constructed integrating the Mach–Zehnder modulator, to encode information stream to the PhRC chip (D4). High speed and high-bandwidth 10 GHz InGaAs photodetector will be used to monitor the outputs from the PhRC chip. The following characteristic will be measured by exciting a short pulse via the fiber array in UoN including,

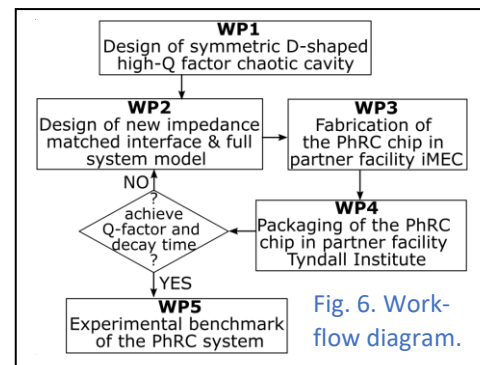


Fig. 6. Work-flow diagram.

the echo state characteristic, fading memory. The PhRC will be experimentally benchmarked in terms its memory capacity and error in performing NARMA test<sup>[16,17]</sup>. To pass the benchmark tests, the PhRC should achieve at least total memory capacity of 90% (of nodal number) and NARMA with error -10dB, i.e., comparable to<sup>[16-18]</sup>. After passing the benchmark tests, the PhRC will be used to demonstrate key applications of AI in wireless communication, namely, to perform header recognition and multi-fading nonlinear channel equalization problems. This demonstrator will evaluate the nonlinear memory reconstruction ability of the PhRC. Another demonstrator will be developed to test other AI application of the PhRC to perform multi-channels sensor pattern recognition, regression and fitting application, similar to our previous publications<sup>[19,23]</sup> but here it will be performed in a chip. **D5: Optical demonstrator rig. D6: PhRC demonstrator to perform AI for wireless communication. D7: PhRC demonstrator for multichannel sensor AI applications.**

**OUTCOMES:** NECTO will develop a novel concept and hardware demonstrator of PhRC on chip based on chaotic optical dynamics unlike previously reported system. The PhRC developed in NECTO will be an adaptable all-optical signal processing and be a key-enabling-technology in the realization of compact edge devices. Two kinds of prototype will be developed in WP5, namely for wireless communication and on-sensors AI. Two technology disclosures will be made based on the novel impedance-matched interface system (developed in WP2) and the demonstration platform in WP5. A new kind of PhRC based on chaotic wave dynamic concept will be generated. Exploitation of chaos for photonic reservoir computing is novel and be ground-breaking. To support the investigator through technological development pathway of the PhRC, I will establish an oversight group with confirmed members from academia (Prof Trevor Benson, Fellow of the Royal Academy, UK, and Prof John Dudley, Université de Bourgogne-Franche-Comté, France) and industry (Prof Mark Farries, chief technological adviser of the Gooch & Housego plc., UK, and Prof Peter O'Brien, National Tyndall Institute, Ireland). The group, which will also take role in the advisory role in the project management, will support the PI in engaging with industrial stakeholders and publish a road-mapping whitepaper laying out the role of photonic reservoir computing in the IoT era. At least, three technical publications in Optica journals will be submitted for D2, D6 and D7. The investigator will attend and disseminate results at Optica conferences, including European Conference on Optical Communication (ECOC) and Conference on Lasers and Electro-Optics (CLEO). The project will provide the necessary seed fund for the early career investigator (Dr Phang) to establish his laboratory and generate key results further establishing his track record in integrated neuromorphic photonics. It will enable Dr Phang to further enhance collaboration with external partners, imec, University of Ghent, Belgium, and National Tyndall Institute, Ireland.

**REFERENCES:** <sup>[1]</sup>Levy, *et al.* BioRxiv:2020.04.23.057927, 2020. <sup>[2]</sup>Harnett, *et al.* *Cell*, 175, 3, 2018. <sup>[3]</sup>Eleftheriou, *et al.* *J Appl Phys*, 124, 11, 2018. <sup>[4]</sup>D'Angelo, *et al.* *Trend Neurosci*, 2022. <sup>[5]</sup>Lima, *et al.* *Nanophotonics*, 6, 3, 2017. <sup>[6]</sup>G. Tanaka, *et al.* *Neural Netw*, 115, 2019. <sup>[7]</sup>Srouji, *et al.* *APL Photonics*, 7, 5, 2022. <sup>[8]</sup>Christensen, *et al.* *Neuromorphic Comp. Eng.*, 2, 2, 2022. <sup>[9]</sup>Prucnal, *et al.* DOI: 10.1201/9781315370590, 2017. <sup>[10]</sup>Capmany, *et al.* DOI: 10.1093/oso/9780198844402.001.0001, 2020. <sup>[11]</sup>Shen, *et al.*, *Nat Photonics*, 11, 7, 2017. <sup>[12]</sup>Tait, *et al.* *IEEE JSTQE*, 22, 6, 2016. <sup>[13]</sup>Shi, *et al.* *IEEE JSTQE*, 26, 1, 2019. <sup>[14]</sup>Bienstman, *et al.* *IEEE Trans Neural Netw*, 22, 9, 2011. <sup>[15]</sup>Bienstman, *et al.* *Nat Comm*, 5, 1, 2014. <sup>[16]</sup>Massar, *et al.* *Sci Rep*, 2, 1, 2012. <sup>[17]</sup>Fischer, *et al.* *Nat Comm*, 2, 1, 2011. <sup>[18]</sup>Massar, *et al.* *Opt Exp*, 20, 20, 2012. <sup>[19]</sup>Phang, *et al.* *Opt. Mat. Exp.*, 12, 5, 2022. <sup>[20]</sup>Statista [weblink](#). <sup>[21]</sup>Deloitte [weblink](#). <sup>[22]</sup>Ericsson [weblink](#). <sup>[23]</sup>Phang, *et al.* "A neuromorphic sensory system," in Photon 2022, Institute of Physics, 2022. <sup>[24]</sup>Bienstman, *et al.* *Opt Exp*, 28, 3, 2020. <sup>[25]</sup>Phang, *et al.* DOI:10.1049/pbcs077g\_ch12, 2019. <sup>[26]</sup>Phang, *et al.* DOI: 10.1117/12.2584187, 2021. <sup>[27]</sup>Bienstman, *et al.* *Opt Exp*, 26, 7, 2018. <sup>[28]</sup>Yablonovitch, *et al.* *Opt Exp*, 21, 18, 2013. <sup>[29]</sup>Vuckovic, *et al.* *Nat Photonics*, 12, 11, 2018. <sup>[30]</sup>N. Jones, *et al.* *Nature*, 561, 7722, 2018. <sup>[31]</sup>EIA [weblink](#). <sup>[32]</sup>Fink, *et al.* *Sci Rep*, 4, 1, 2014.



# Nanoscale nonreciprocal photonic components

**CATEGORY:** Information

The project aims to develop new ways to control light in *nonreciprocal* [1] ways, similar to ways we control electricity with modern semiconductor technology. Nonreciprocal behaviour of light is difficult to achieve, and it is currently limited to relatively large systems, representing a roadblock for making light-based information technologies and devices smaller, cheaper and more energy efficient. Expected outcomes of this project include first demonstrations of nonreciprocal control of light by tiny devices made with nanotechnology. The outcomes should progress the development of vital next-gen information and communication technologies (ICT).

Nonreciprocal components, including isolators and circulators are indispensable components for communication systems. Although, free-space nonreciprocal components are currently available commercially, their miniaturisation and on-chip integration has proven to be a challenge. 21st century information and communication technologies might depend on nonreciprocal optical isolators and circulators as much as 20th century ICT developments depended on nonreciprocal semiconductor diodes and transistors.

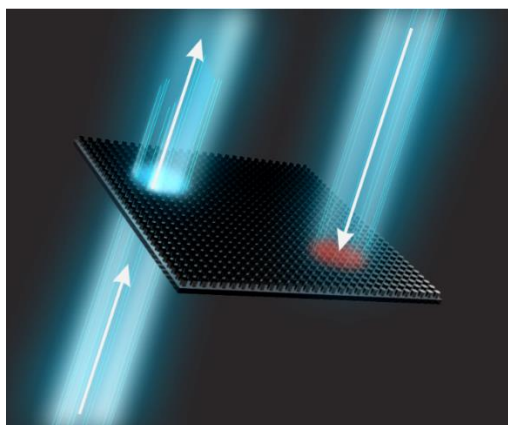


Fig. 1. Concept image of nonreciprocal transmission of light through a metasurface.

The project proposes to miniaturise nonreciprocal optics with metasurfaces made of novel emerging material platforms for nonlinear optics. Recently, metasurfaces, often 100 times thinner than a human hair, made a tremendous progress from fundamental concepts [2] to mass-fabricated consumer products [3]. Today, new frontiers in metasurfaces research are being actively explored is nonlinear optics which changes the basic principles of interaction between light and matter, including reciprocity breaking. I recently demonstrated nonlinear metasurfaces with asymmetric generation of optical harmonics [4]. With this project, I aim to build upon this progress to achieve nonreciprocal self-action. For this I will incorporate into the design novel photonic material platforms of two categories: epsilon-near-zero materials and phase-change materials – both

of which offer giant nonlinear self-action effects compared to more standard Kerr-type nonlinearities of dielectrics. I will deliver laboratory demonstrations of first nanoscale nonreciprocal metasurfaces and will perform their characterization.

**INTENDED OUTCOMES:** The project aims to fill knowledge gaps enabling manufacturing of sub-micrometre small nonreciprocal optics, such as optical isolators and circulators. The project will deliver isolators operating at low intensities (mW) of continuous-wave (CW) light sources. The isolator designs will be compatible with standard nanofabrication technologies. The research outputs will be disseminated via peer-reviewed publications in premier journals and presentations at reputable conferences and congresses.

**APPLICATIONS TO REAL-WORLD ISSUES:** The developed nonreciprocal components based on nonlinearity will be fully passive and self-biased, which makes them ideal in applications for pulsed or periodic operations, such as in optically controlled transmission switches, directional filters and power limiters, as well as chip-scale LiDARs.

[1] C. Caloz et al., “Electromagnetic Nonreciprocity” *Phys. Rev. Applied* 10, 047001 (2018).

[2] S. Kruk and Y. S. Kivshar, “Functional meta-optics and nanophotonics governed by Mie resonances,” *ACS Photon.*, 4, 2638 (2017).

[3] Products - Metalenz <https://www.metalenz.com/products/>

[4] S. Kruk et al., “Asymmetric parametric generation of images with nonlinear dielectric metasurfaces” *Nature Photon.* 16, 561–565 (2022).

# Nanoscale nonreciprocal photonic components

## LITERATURE REVIEW

Photonics in the 21<sup>st</sup> century is undergoing revolutionary transformations driven by nanotechnology. Today we can nanofabricate functional optical components hundreds of times thinner than a human hair that match the performance or even outperform conventional bulky optics<sup>1-4</sup>, including holograms<sup>5</sup> and wave retarders<sup>6</sup> as was demonstrated in my co-authored publications. An important problem yet to be addressed is *nonreciprocal optical response at the nanoscale*. The 21<sup>st</sup> century photonics might depend on nonreciprocal optical components as much as the 20<sup>th</sup> century electronics depended on nonreciprocal semiconductor diodes.

A nonreciprocal system exhibits different received-transmitted field ratios when their sources and detectors are exchanged. How can we envision a nonreciprocal optical component? Imagine holding a translucent slide, such as a frame from a film strip or a camera roll. We shine light through the slide and see an image on a wall. Then we flip the translucent slide and see a completely different image (Fig. 1). This uncommon behaviour of light would require breaking the Lorentz reciprocity theorem. I aim to demonstrate such a slide within the lifetime of this project. Nonreciprocal traffic control is the necessary property for many key photonic components such as isolators and circulators.

The vast majority of optical processes obey reciprocity<sup>7</sup>, including refraction, diffraction, mode conversion, polarization conversion, etc. There are only few conceptual pathways for breaking optical reciprocity:

- materials with asymmetric permittivity/permeability tensors,
- time-varying systems,
- nonlinear optics.

The dominant approach is based on *materials with asymmetric tensors*, such as ferrites<sup>8,9</sup>. However, ferrite-based systems are not compatible with nanotechnology as they rely on rather large permanent magnets or resistive/superconductive coils. A second approach based on *time-varying systems*<sup>10,11</sup> imposes major technological challenges for a radical nanoscaling in optical spectral range due to the ultra-high oscillation frequencies of light. *Nonlinear optical interactions* have been used in classical, relatively large optical systems to induce nonreciprocity, albeit with significant limitations<sup>12</sup>. Nonlinearity-induced nonreciprocity is regarded as weak and difficult to achieve. As a result, currently there exists no pathway towards a nanoscale nonreciprocal optical system. This creates a roadblock preventing further nanoscaling and integration of many photonic devices and systems.

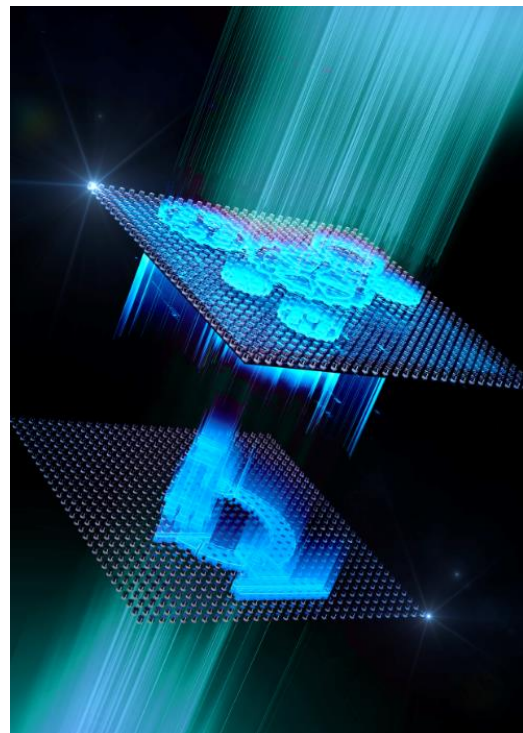


Figure. 1. Illustrative example of a nonreciprocal optical element. Opposite directions of light illumination produce different results in transmission.



## PROBLEM STATEMENT AND OBJECTIVES

**The project aims to fill the gap in knowledge** on how to bring nonreciprocal optics to the realm of nanoscience.

**The project aims to demonstrate first laboratory prototypes** of nanoscale optical isolators.

The project proposes a new take on the third conceptual pathway towards nonreciprocity: *nonlinear optics*. Traditionally, nonlinearity-based nonreciprocal photonics is associated with bulky optical components<sup>13-15</sup>. Relatively more compact photonic chips with coupled waveguide resonators<sup>16</sup> were demonstrated to enable asymmetric control of light. Recently, there has been an interest in theoretical investigations of various nonlinear nanophotonics platforms for asymmetric and nonreciprocal light control<sup>17-21</sup>. A plasmonic metasurface with asymmetries in nonlinear light generation was demonstrated experimentally<sup>22</sup>. However, the approaches demonstrated to date rely on optical components that are substantially larger than the wavelength of light in at least two spatial dimensions, including demonstrated systems of optical waveguides and phase gradient metasurfaces. This hinders dense integration of large quantities of such photonic components into compact systems analogous to integration of large quantities of electronic components into semiconductor chips.

In my recent work, I demonstrated asymmetric parametric generation of light at the level of individual subwavelength resonators in metasurfaces<sup>23</sup>. By design, these nonlinear metasurfaces produced different and completely independent images for the reversed directions of illumination, that is when the positions of the infrared transmitter and the visible light receiver are exchanged. Nonlinearity-enabled asymmetric control of light at the level of individual subwavelength resonators opens the way to nonlinear self-induced nonreciprocity with an untapped potential for developing novel nanophotonic components via dense integration of large quantities of nonlinear resonators into compact metasurfaces.

### OBJECTIVE 1. THEORETICAL DESIGN.

To develop a new avenue towards nonreciprocal control of photons at the nanoscale for optical isolation. There exist several pathways to reach nonreciprocity with classical, bulky optical components. None of these approaches are directly suitable for miniaturisation down to the nanoscale. The objective is to develop an approach towards nanoscale nonreciprocity. In particular, to achieve a 100 times transmission contrast between the "forward" and "backward" light propagation in a sub-micrometer component with excitation powers in the milli-Watt (mW) range.

### OBJECTIVE 2. NANOFABRICATION.

To demonstrate design frameworks and fabrication approaches for nanoscale nonreciprocal components. Nanofabrication techniques, such as electron beam lithography, will be used to fabricate layouts of nanoresonators (100-600 nm in size) using dielectric and semiconductor materials as well as emerging epsilon near-zero materials and phase-change materials.

### OBJECTIVE 3. OPTICAL DIAGNOSTICS.

To evaluate experimentally characteristics of the nanoscale nonreciprocal components. Characterisation of the designed and fabricated nonreciprocal optical elements will be conducted experimentally. It will include measurements of isolation levels, spectral bandwidth and suitable excitation regimes. The aim of the objective is to transfer the project towards applied science and engineering.

## OUTLINE OF TASKS/WORK PLAN

**Theoretical component.** Nonlinearity-induced nonreciprocity is regarded as weak and difficult to achieve. The project puts forward two hypotheses to achieve strong and practical nonreciprocity via nonlinear light-matter interactions.

■ **Meta-photonics and artificial magnetism.** One of the key advantages of nanoscale optics in contrast to its bulky counterpart is the ability to engineer interactions beyond the electric dipole type, in particular to mimic strong *artificial magnetic response*<sup>6,24</sup>. I propose to employ artificial magnetism for an efficient scenario for nonreciprocal response via *magneto-electric coupling* – an effect that was not readily available in classical bulky optics. In the presence of the magneto-electric coupling the excitation of the electric and the magnetic dipole modes can be written as<sup>23</sup>:

$$\begin{aligned} p_x &= \alpha_{ee}^{xx} E_x \pm \alpha_{me}^{xy} H_y \\ m_y &= \pm \alpha_{mm}^{yy} H_y - \alpha_{me}^{xy} E_x \end{aligned} \quad (1)$$

where we assume x-polarized light,  $E_x$  and  $H_y$  are local fields,  $\alpha_{ee}^{xx}$ ,  $\alpha_{mm}^{yy}$ ,  $\alpha_{me}^{xy}$ , and  $\alpha_{me}^{yx}$  components of the electric/magnetic/ magneto-electric polarizability tensors. The “±” sign in front of the “ $H_y$ ” terms accounts for the cases of forward/backward illumination thus making the multipolar composition direction dependent despite the fact that the total scattering remains independent on the direction of incidence. The nonlinear response of a nanoresonator depends strongly on the multipolar composition of its resonances, which translates direction-dependent composition of electric and magnetic dipoles into nonreciprocal nonlinear self-action.

■ **Novel material platform for nonlinear photonics.** Two highly promising group of materials are proposed to be used in this project: media with near-zero dielectric constant such as ITO and PEDOT<sup>25</sup> and phase-change materials such as VO<sub>2</sub><sup>26</sup> and GST<sup>27</sup>. Recent research of these material platforms include reports of giant nonlinear optical responses that are much stronger than more standard Kerr-type nonlinearities of conventional photonic material platform, such as silicon. The implementation of such materials to nanophotonics might dramatically increase the efficiency of nonlinear light-matter interactions, and thus nonlinearity-based nonreciprocity.

The central theoretical question of this research project is: can engineered *magneto-electric coupling* in nanoresonators made of *novel material platforms* bring nonlinearity-induced nonreciprocal self-action to applications?

Work plan: complimentary analytical and numerical techniques will be employed to perform modelling of the nanostructures. Analytical approaches based on Mie theory will be used to formulate solutions of nonlinear problems. These solutions will then be analysed numerically using finite-element software, such as COMSOL.

**Nanofabrication.** The designed nanoresonators and their 1D and 2D layouts will be nanofabricated. A portion of nanofabrication will rely on standard processes using conventional photonic materials such as Si, Ge, GaAs etc. New fabrication protocols will be developed for emerging and highly promising epsilon-near-zero materials and phase-change

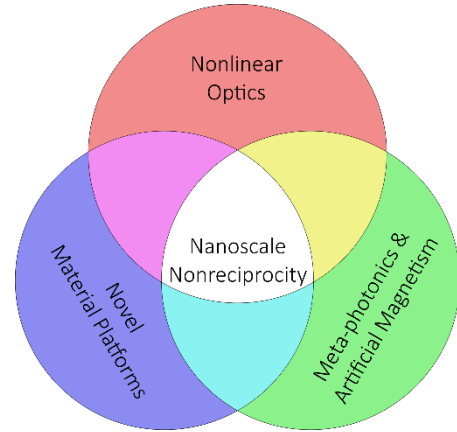


Figure. 2. Key elements for nanoscale nonreciprocal optics.

materials which will be incorporated into the design. The nanofabrication will rely on major nanotechnology infrastructure available at the ANFF. Fabrication of semiconductor materials will benefit from my lasting collaborations with nanofabrication centres at Oak Ridge National Laboratory (TN, USA) and at Centre for Integrated Nanotechnologies (CINT), Sandia National Laboratory (NM, USA). Fabrication of VO<sub>2</sub>-based nanostructures will benefit from my collaboration with Vanderbilt University, TN, group of Prof. Jason Valentine<sup>26</sup>. Fabrication of PEDOT-based nanostructures will benefit from my collaboration with Stuttgart University, Germany, group of Prof. Harald Giessen<sup>25</sup>.

*Work plan:* thin-films of materials will be grown by chemical vapour deposition (materials such as silicon and silicon nitride), epitaxially (materials such as III-V semiconductor, e.g. GaAs) or via spin-coating (polymers such as PEDOT). Electron beam lithography (EBL) will be the main tool to define nanoscale geometries. The nanoscale geometry defined by the EBL will be translated into the thin films by the existing reactive ion etching processes. The required fabrication facilities are available at my institution, and are backed by research facilities of my collaborators.

**Optical diagnostics.** Experimental observations will rely on photonics laboratory at the ANU which I established under my DECRA Fellowship. New optical diagnostics setups will be developed at the ANU to specific needs of the project in delivering first experimental demonstrations of nanoscale optical nonreciprocity. The Fellowship will benefit from my links with Prof. Thomas Zentgraf, leader of the Ultrafast Nanophotonics group and the host of my former European Fellowships at Paderborn, Germany.

*Work plan:* optical measurements will rely on tunable laser systems at my institution. The signal measurements will be performed with sensitive Peltier-cooled cameras (such as Trius-694 by Starlight Xpress) and spectrometers with Si detectors for vis-NIR spectral range, and InGaAs detectors for NIR spectral range (such as QEPro and NIR Quest by Ocean Optics). The experimental methods will be built up on those described in my publications in Refs.<sup>28</sup> and <sup>29</sup>.

## OUTCOMES

The project will deliver early-stage research on design and manufacturing of optical components structured at the nanoscale that possess the unique property of nonreciprocity. The proposed research aims to develop manufacturing approaches for the novel type of components for nanoscale photonic applications starting from basic principles and progressing to experimental proofs-of-concept demonstrations and measurements of operational parameters within the lifetime of the project.

**Peer-review publications.** It is envisaged that the results of the project will deliver top-level research outcomes, producing publications in highly ranked journals. My previous track record includes publications in top journals in my field as detailed in the CV.

**Conferences.** Publicity of the results will be achieved by presentations at the major national and international conferences such as Conference on Lasers and Electro-Optics (CLEO), Frontiers in Optics, and topical meetings hosted in Australia and overseas. My previous experience includes invited and keynote presentations as detailed in the CV.

**Press-releases and media engagement.** A broader community will be communicated via media press-releases. In the past I have had a positive experience with reaching a broad audience via media engagement, including internet platforms, TV news, radio, Australian newspapers, such as Canberra Times, Sydney Morning Herald, etc. I will dedicate efforts to media engagement aiming to explain how the discoveries of this project might impact lives in

the future striving to promote Optica and to encourage young people to pursue careers in STEM.

**Technology transfer.** The applied outcomes of the project will be assessed together with the ANU Technology Transfer Office and our industry partners to identify opportunities for transfer of knowledge. My previous experience includes a provisional patent application “Metasurface optical spatial mode modulator and method 2017903177”.

## IMPACT

The project is inspired by the tremendous social changes brought about by our advancements in information and communication technologies and the challenges that these technologies are now facing. We live in an information-driven society. Our exponentially growing data exchange has well-surpassed a zetta-byte per year, that’s a number with 21 zeros. The pathway to cope with the increasing demand for data transfer is to deploy novel photonics technologies. Next envisioned technological steps include incorporating photonics inside devices, their individual integrated circuits, and ultimately inside microchips. This creates an ever-increasing demand for miniaturisation of photonic elements.

Nonreciprocal components are among the most challenging to miniaturise. This project proposes to tackle this problem putting forward a hypothesis that our recent advancements in novel material platforms and in artificially engineered magnetic-like resonances in metasurfaces may serve as the enabling knowledge for nanoscale nonreciprocal photonics. The project proposes to develop this hypothesis from basic concepts to laboratory prototypes for demonstrations and testing.

Nanoscale nonreciprocal components based on nonlinear self-action will be fully passive and self-biased which makes them ideal for applications in optically controlled transmission switches, directional filters, LiDARs, directional power limiters and ultrathin protective layers for sensitive optical components.

1. Kruk, S. S. & Kivshar, Y. S. *ACS Photonics* 4, 2638–2649 (2017).
2. Schonbrun, E., Seo, K. & Crozier, K. B. *Nano Lett.* 11, 4299–4303 (2011).
3. Chong, Y. D., Ge, L., Cao, H. & Stone, A. D. *Phys. Rev. Lett.* 105, 053901 (2010).
4. Lin, H. et al. *Nat. Photonics* 13, 270–276 (2019).
5. Wang, L. et al. *Optica* 3, 1504–1505 (2016).
6. Kruk, S. et al. *APL Photonics* 1, 030801 (2016).
7. Caloz, C. et al. *Phys. Rev. Applied* 10, 047001 (2018).
8. Wang, Z., Chong, Y., Joannopoulos, J. D. & Soljačić, Nature 461, 772–775 (2009).
9. Bahari, B. et al. *Science* 358, 636–640 (2017).
10. Kang, M. S., Butsch, A. & Russell, P. S. J. *Nat. Photonics* 5, 549–553 (2011).
11. Estep, N. A., Sounas, D. L., Soric, J. & Alù, A. *Nat. Phys.* 10, 923–927 (2014).
12. Shi, Y., Yu, Z. & Fan, S. *Nat. Photonics* 9, 388–392 (2015).
13. Gallo, K., Assanto, G., Parameswaran, K. R. & Fejer, M. M. *Appl. Phys. Lett.* 79, 314–316 (2001).
14. Lepri, S. & Casati, G. *Phys. Rev. Lett.* 106, (2011).
15. Biancalana, F. J. *Appl. Phys.* 104, 93113 (2008).
16. Bender, N. et al. *Phys. Rev. Lett.* 110, (2013).
17. Poutrina, E. & Urbas, A. *Sci. Rep.* 6, 25113 (2016).
18. Kim, K. H. *Plasmonics* 16, 77–82 (2021).
19. Lawrence, M., Barton, D. R. & Dionne, J. A. *Nano Lett.* 18, 1104–1109 (2018).
20. Jin, B. & Argyropoulos, C. *Phys. Rev. Appl.* 13, 054056 (2020).
21. Cheng, L. et al. *ACS Photon.* 8, 2, 585–591 (2021).
22. Shitrit, N. et al. *Phys. Rev. Lett.* 121, 046101 (2018).
23. Kruk, S. et al., *Nat. Photon.* 16, 561–565 (2022).
24. Kruk, S. S. et al. *Nat. Commun.* 7, 11329 (2016).
25. Karst, J. et al. *Science* 374, 612–616 (2021).
26. Zhu, Z., Evans, P. G., Haglund, R. F. & Valentine, J. *Nano Lett.* 0, null (2017).
27. Wang, Y. et al. *Nat. Nanotechnol.* 2021 166 16, 667–672 (2021).
28. Kruk, S. et al. *Nat. Nanotechnol.* 14, 126–130 (2019).
29. Kruk, S. et al. *Nano Lett.* 17, 3914–3918 (2017).

## EXECUTIVE SUMMARY

Project Title: **X-ray Quantum Nano-Tomography for Medical Imaging**

Sergio Carbajo, Assistant Professor  
UCLA, Electrical & Computer Engineering  
UCLA, Physics & Astronomy  
Stanford University, SLAC Photon Science

The science of X-rays is over 125 years old, starting with Wilhelm Röntgen's discovery of X-rays in 1895 rendering the first Nobel Prize in Physics. X-rays have fundamentally impacted humankind in many scientific and technological areas and have so far been responsible for over 25 Nobel Prizes in Physics, Chemistry, and Medicine-Physiology.

The ubiquitous use of X-ray technology in commercial applications, airports, and hospitals may seem to declare that there's little left to discover regarding the fundamentals of X-ray science and its applications in medical imaging and therapies. But recent work in quantum electrodynamical (QED) theory has revived interest in studying new, non-intuitive regimes to record X-ray images as a means to revolutionize coherent tomographic (CT) imaging, one of the most powerful imaging techniques today known as CT scans recognized with saving hundreds of thousands lives from cancer screening in the US alone. Through the Optica Foundation 20th Anniversary Challenge, we aim to demonstrate a novel nanoscale quantum tomographic X-ray technique to disrupt the current X-ray medical imaging paradigm and expand to emerging applications in life sciences and beneficial cost-accessibility tradeoffs relative to comparable commercial and medical instrumentation.

This project presents two specific near-term objectives for future nanoscale, high-brightness X-ray imaging techniques based on tomographic QED:

- First, we will experimentally demonstrate that X-ray emission through quantum interference of electrons is possible from a quantum electrodynamical standpoint for the first time. This foundational physical demonstration will confirm that it is possible to tune the X-ray emission wavelength up to 10s of keV as well as the emission monochromaticity and directionality by shaping electron wavepackets interacting with nanoscale materials.
- Second, we will extend this demonstration to the interference of two coherent near-field X-ray tomographic images by arising from an electron wave packet shaped to produce multiple distinct, coherent X-ray pulses. Exploiting the quantum interference produced by the wavepackets, we will obtain and reconstruct tomographic images with nm-scale resolution and element specificity with a far lower dosage compared to state-of-the-art CT scans.

Our approach constitutes a novel electron-photon quantum interference method that will become an important tool not only for nanoscale X-ray imaging devices but also for operando diagnostics and endoscopic radiation therapies. Technologically, we anticipate a novel, ultrabright X-ray source that dramatically reduces the cost and size, is fully integrable and portable, and offers a power and energy scalable architecture to enable on-chip and integrable hyperspectral X-ray frequency combs. Our aims may also open the door to the engineering of quantum-level controlled X-ray sources and their real-world applications including ultrafast microscopy, quantum simulation, compact XFELs, quantum-level semiconductor lithography, atom-by-atom matter assembly, and a plethora of new and old theorized nanoscale radiation sources.

## 1. INTRODUCTION AND STATE-OF-THE-ART REVIEW

The science of X-rays is over 125 years old, starting with Wilhelm Röntgen's discovery of X-rays in 1895 rendering the first Nobel Prize in Physics. X-rays have fundamentally impacted humankind in many scientific and technological areas and have so far been responsible for over 25 Nobel Prizes in Physics, Chemistry, and Medicine-Physiology. The ubiquitous, commercial use of X-ray technology may signal there's little left to discover regarding the fundamentals of X-ray science. But recent work in QED theory<sup>1</sup> has awakened newfound interest from a new generation of scientists to study uncharted frontiers in emerging X-ray production regimes. In this proposal, we will focus on one specific frontier henceforth referred to as “quantum” X-ray emission which can have a profound impact on basic life and energy sciences, and ultracompact and ultrabright X-ray radiation sources for national security and medicine.

Free electrons can be readily controlled via light-electron or electron-matter interactions, as manifested by semi-classical physics including stochastic heating<sup>2</sup> and free-space acceleration<sup>3,4</sup> – which includes prior work by the PI – as well as other quantum phenomena such as the Kapitza–Dirac effect and two-slit single-electron interference. In the same way that optical waveshaping has unveiled a host of intriguing electromagnetic semi-classical and quantum phenomena, shaping electronic wavepackets promises to enrich exciting physics driven by electrons, which encompasses unique secondary radiation characteristics, namely X-ray radiation. In this context, we would like to focus on the **fundamental question of whether QED interactions, such as X-ray photon emission, can be transmuted to control and enhance its properties by precisely shaping an electronic wavepacket.**

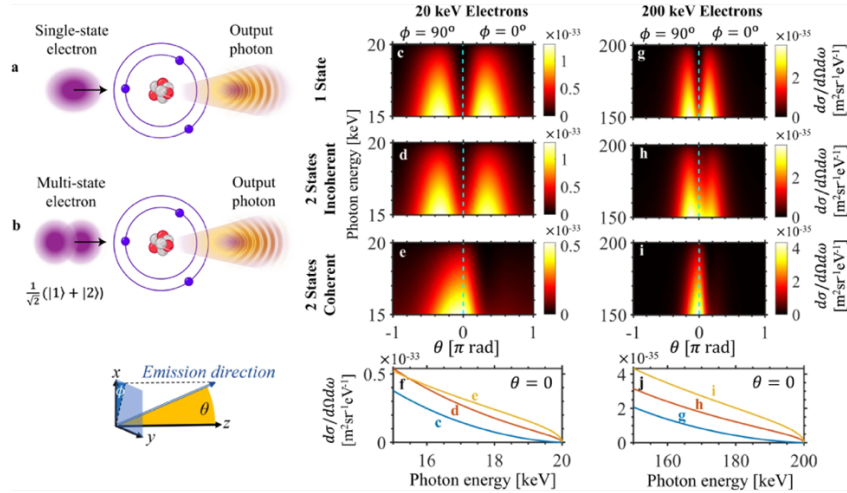


Fig. 1: QED depiction of (a) single-state v. (b) multi-state electron wavepacket interaction with a quantum system (e.g. ion) to emit X-rays, courtesy of collaborators Wong et al.<sup>5</sup> The QED theory predicts higher monochromaticity, brightness, and directionality from the quantum interference between two coherent states relative to a single-state electron beam. Off-axis emission is suppressed to enhance on-axis emission monochromaticity and intensity with the coherent superposition of 2-state emission.

Fundamental QED processes, such as spontaneous emission and electron-photon scattering, involve phenomena that underlie much of modern science and technology. A recent study by collaborators Wong et al.<sup>5</sup> shows that in the typical atomic bremsstrahlung scenario depicted in Fig. 1.a, a single momentum state electron scatters off a carbon atom – as a simplified model for a quantum Coulombic potential – to emit X-ray electromagnetic radiation. Conversely, if not a single electron momentum state but multiple coherent states are used instead with the same Carbon atom, the X-ray output emission properties can be transformed through the superposition of these different electron wavepacket states, for example, in momentum or energy space. To take the example shown in Fig. 1.b, the output X-ray photon properties are a result of two superposed states  $|1\rangle$  and  $|2\rangle$  of an electron wavepacket, which is born out of the interference between the processes associated with each electron state  $|1\rangle$  and  $|2\rangle$ . This multi-state superposition-enabled interference is what we call “quantum X-ray emission,” which can be exploited to dramatically enhance the properties of traditional (i.e., classical) X-ray emitters and enable **emerging frontiers in nanoscale X-ray**



**instrumentation in medicine.** To exemplify new capabilities enabled by quantum X-ray emission not possible classically, Fig. 1.c–e show the differential cross-section  $d\sigma/d\Omega$  of the X-ray emission solid angle for 20 keV electrons, with a single z-directed input electron state in **c**, and two input electron states ( $|1\rangle + |2\rangle$ ) of opposite phase with respect to the z-axis in **d** and **e**. Unintuitively, quantum interference between the constituent processes in Fig. 1.e strongly suppresses off-axis emission, resulting in a highly-directional emission pattern. Cross-section emission patterns at  $\theta = 0$  are compared in **f**. The enhanced directionality also holds at other choices of electron energies, as shown in **g–j**, which presents the emission spectra corresponding to the scenarios in **c–f**, respectively, but for 200 keV electrons. That is, **electronic quantum interference permits the production of high-brightness, monochromatic, and highly directional ultrashort X-rays bursts** using few-keV electrons, which are readily produced in scientific and commercial instruments

Compared to current state-of-the-art medical X-ray instrumentation, quantum X-ray emission can not only dramatically enhance the X-ray properties – brightness, spatial directionality, and wavelength – but it exhibits **unparalleled portability, integrability, and dramatic cost reduction**. By and large current X-ray devices are present in well-established scientific, medical, and inspection technologies today, such as synchrotrons, cyclotrons, and X-ray tubes, used in a plethora of X-ray imaging and spectroscopy applications. Small medical cyclotrons, for instance, are common in dental X-ray imaging, while X-ray scanners in airports or hospitals, to name other popular examples, also rely on classical X-ray emission – in addition to characteristic X-ray lines depending on the anode – using (quasi)-continuous wave (CW) thermionic electron emitters and solid-state anodes. Specifically, X-ray coherent tomography (CT)-based imaging is well-established in the medical community with over 75 million CT scans per year<sup>6</sup>. CT scans generate nondestructive 3D representations of human body structure with mm-range resolution and moderate radiation doses. The dosage ranges from 10-20 mSv depending on the area of the body, bringing to the fore concerns about adverse effects of cumulative radiation in the human population globally. Conversely, quantum X-ray emitters are nanoscale in nature produced by non-relativistic electrons that are well confined and do not require high driving voltages, which translates into reduced need for shielding, further reducing cost and size paving the path to future integrated on-chip devices (*c.f.* Section 5. Impact).

## 2. RESEARCH OBJECTIVES

**OBJECTIVE 1: Experimentally demonstrate that 2-state electron waveshaping controls spatial and spectral characteristics of X-ray emission, i.e., first-time quantum X-ray emission.**

We will demonstrate that it is possible to control the emission of X-ray photons – specifically, to tailor their spatial and spectral distributions – from non-relativistic free electrons by shaping the electron wavefunction. Specifically, electron waveshaping gives rise to quantum interference which can then be used to control spontaneously emitted X-ray photons, just as quantum interference between multiple atomic transitions can be used to control spontaneous emission from an atom. **The resulting X-ray photons will possess enhanced directionality, monochromaticity, and versatility compared to bremsstrahlung from an unshaped electron wavefunction.** The electron energies will range from a few keV to a few tens of keV, which is readily available using a 100-keV electron DC gun owned by the PI. This DC gun has a proven track record of high-impact demonstrations and applications of on-chip accelerators. Nominally, the gun produces <1 ps to few-ps duration, 0.1-0.5 mm radius electron beams at few 10s of fC-level charges (i.e., 1000s  $e^-$ /event), although higher pC-level charges are possible with longer pulses. Electron photoemission will be fired by harmonic up-conversion of a high-power femtosecond Yb-based lasers amplifier system (LightConversion PHAROS-20, owned by the PI) in the ultraviolet (UV) with  $\sim$ 200-fs pulse duration. The maximum repetition rate of this system is 1 MHz, thereby producing up to  $\sim$ 200 nA average current, i.e., over a trillion  $e^-$ /second. After generation and static acceleration, a solenoid will be used to focus the electron beam into a  $\sim$ 10  $\mu$ m spot on the W sample. Waveshaping of electrons can be accomplished through a variety of methods. For our objective of demonstrating waveshaping involving 2 electron states, the baseline approach in our research involves producing two coherently interfering beams using an electron biprism.

**OBJECTIVE 2: obtain and reconstruct tomographic images with nanoscale resolution and element specificity with a far lower dosage compared to state-of-the-art CT scans.**

Motivated by the medical relevance of CT scans, our second objective will leverage our prior work under Objective 1 to bring about a dramatic leap in the performance of CT scans and demonstrate that (i) nanometer-scale resolution, (ii) element specificity, and (iii) shorter exposure times relative to current CT scans are possible using quantum X-ray technologies. This is achievable due to (i) a near-field imaging modality relying on the interference between the generated X-ray pulses, (ii) higher monochromaticity and tunable X-ray emission frequency peak, and (iii) increased emission directionality, respectively. To meet this objective in near-field modality, we will employ our quantum X-ray emitter in a scanning mode, where it will be used as a nanoprobe to raster-scan the sample. We will employ a 2D solid-state heterostructure (e.g. hBN flakes on a TEM grid) to best demonstrate these new capabilities. Specifically, in the **scanning mode, fluorescence- (for elemental distribution), diffraction- (for strain mapping in crystals), and transmission signals (for morphology) will all be collected simultaneously at each specific position.** This will enable a **multimodal imaging capability** that provides a comprehensive characterization of the sample in one experiment. Specifically, tomography will be carried out by collecting 2D images, or projections, taken from different perspectives as the stage rotates. Images will be recorded using the TIMEPIX3 detector, a versatile, state-of-the-art hybrid 256 x 256 pixels semiconductor detector readout chip (Pixel size 55 $\mu$ m x 55 $\mu$ m) ideal for X-ray imaging and electron tracking reconstruction owned by the PI. The detector's high sensitivity combined with its time-stamping precision (< 1.56 ns) enables both single-event and averaged measurements at 1 MHz repetition rate. For the reconstruction, we will resort to existing algorithms – e.g., algebraic reconstruction technique algorithm (ART) in real-space or the filtered back projection algorithm (FBP) in the Fourier domain – all of which allow 3D reconstruction employing existing projection data. Advanced algorithms may be considered at a later stage of the project in conjunction with deep-learning image reconstruction methodologies.

### 3. TASKS AND TIMELINE OF ACTIVITIES

Our technical approach and methods are itemized by activity as follows:

**Task 1 – laser-electron synchronization and electron beam generation:** generate and deliver UV photoemission pulses to the DC cathode with ~200 fs duration, sub- $\mu$ J energy at 1 MHz to produce 10-30 keV, fC-level electron wavepackets with ~ps duration.

**Task 2 – electron beam characterization and optimization, and classical X-ray production:** an interaction chamber and interfaces with diagnostics will be designed and constructed. The electron beam duration and charge level will be characterized and optimized via acceleration gradient and UV laser tuning using the TIMEPIX3 detector. Using a thin-film W target, unshaped-electron X-ray emission will be measured to test the X-ray detection scheme, i.e., EDX/WDX with Si(440) analyzers, and benchmark unshaped emission characteristics.

**Task 3 – construction and testing of electron biprism:** parallel to Task 2, we will design and fabricate a vacuum-compatible sub-micrometer suspended nanowire consisting of two parallel grounded plates with a positively-biased and bias-tunable filament using well-established peel-off nanofabrication techniques. We will also incorporate high-precision positioning stages to measure 2-state electron waveshaping via electron interference on the Timepix3.

**Task 4 – quantum X-ray production and characterization:** first-time demonstration of quantum X-ray production using the instrumentation in Task 2 and Task 3. The measurable X-ray properties via EDX will consist of spectral and spatial emission distributions as a function of 2-state shaping (e.g., filament bias voltage) and electron beam energy via electron energy loss spectroscopy (EELS) using a dipole magnet. We will also quantify the brightness of quantum X-ray production vis-à-vis unshaped emission (c.f. milestones and expected outcomes below).

**Task 5 – tomographic image captures and reconstruction:** acquiring diffractive and transmissive X-ray images of 2D solid-state heterostructure in a rotational stage using X-ray emission probe in scanning mode, and subsequent tomographic reconstruction to render nanoscale 3D images with element specificity.

Table 1: timeline of activities per year (divided into 8 quarters totals)

R&D Task	Year 1				Year 2			
	1	2	3	4	5	6	7	8
Task 1								
Task 2								
Task 3								
Task 4					M1			
Task 5								M2

**M1:** first-time demo of quantum X-ray emission is completed, and emission properties are characterized i.e. spectral and spatial distribution enhancement

**M2:** first tomographic images are reconstructed using nanoscale quantum X-ray emitters.

#### 4. ANTICIPATED OUTCOMES

From our first milestone – M1 under Objective 1 – we will have produced a reliable testbench for coherent production of modulated electrons to open the door to the engineering of quantum-level controlled X-ray sources and their real-world applications beyond medicine, including but not limited to microscopy, quantum simulation, compact XFELs, quantum-level semiconductor lithography, atom-by-atom matter assembly, and a plethora of new and old theorized nanoscale radiation sources. Deriving from our second milestone – M2 under Objective 2 –we expect to demonstrate for the first time a different regime of nanoscale quantum X-ray CT that demonstrates nm-level resolution, element specificity, and orders of magnitude lower dosage relative to conventional CT scans. The instrument built by the end of the program will be fully operational to conduct experiments in **ultrafast molecular dynamics** and study unique states of **nonequilibrium structural and dynamical properties of matter**.

#### 5. IMPACT

Concerning advanced X-ray emission properties, the 2-momentum state’s coherent interference radiation is much more monochromatic as the synchrotron-radiation-like tail in the low-photon-energy regime is greatly suppressed by destructive interference, whereas the undulator radiation peak remains relatively unaffected. This off-peak suppression is expected to be reduced by about two to five orders of magnitude<sup>7</sup> relative to the unshaped electron depending on the free-electron velocity and optimization of the 2-momenta states. From this foundational demonstration, **controlling directionality and intensity of X-ray emission with multi-state (> 2 states) electron beams in a crystalline solid (e.g. graphene flake) will enable the engineering with higher control over directionality, intensity, monochromaticity**, as predicted by our simulations shown in Fig. 2. At the heart of our proposal lies a novel concept for tunable-wavelength and monochromatic, high brightness ultracompact (X-ray) light sources not previously accessible under semi-classical physics. In this context, the prospect of quantum X-ray technologies opens a plethora of opportunities. *Technologically*, compared to the state-of-the-art, the technological advantages described above will dramatically **reduce the cost and size**. The energy transfer between a photoemitting laser field and the electron beam, although requiring very precise control both spatially and temporally, is also a very efficient process that can be readily manufactured on a chip via integrated photonics, thereby producing a **fully integrable and portable X-ray source in medicine. The nanoscale nature of the probe may enable future endoscopic single-cell level imaging techniques or laparoscopic radiation therapy devices**. The electron bunches can be readily produced at up to 100s of MHz repetition rates and high (>30%) wall-plug efficiencies to increase their competitiveness in terms of average radiation power, thereby presenting a readily **scalable X-ray architecture**. The low requirements on the shielding of electrical voltage, secondary radiation, and laser power allow operators to work in contact or near the accelerator instrumentation. Moreover, GHz repetition rate scalability is far more accessible in on-chip and compact accelerators<sup>8</sup> compared to state-of-the-art MHz repetition-rate ultra-relativistic XFELs, such as LCLS-II and the European XFEL, thereby presenting a prospective increase of at least 3 orders of magnitude in average brightness. *Scientifically*, the novel electron-photon QED explored in this proposal has the potential to become an important tool in **quantum information science** as it has been theoretically shown that electron beams modulated at optical frequencies can drive quantum-system – e.g., driving and entangling solid-state color centers – transitions that correspond to the optical frequencies and its harmonics. The emission of X-ray photons from bremsstrahlung radiation can be entangled with incoming and outgoing electron states and similarly, shaping Cherenkov radiation through orbital angular momenta beams can change the power

spectrum via carefully selected electron states. In the realm of **X-ray science**, future work promises to revolutionize ultrafast measurement science by enabling **electron diffraction and electron microscopy and *operando* attosecond X-ray diffraction and crystallography** with a temporal resolution better than 100 attoseconds, thereby leading to a unique tool for **multi-modal ultrafast imaging** which does not exist today. In conjunction with optional light-excitation mechanisms, this will constitute a novel pump-probe method to investigate interactions with systems ranging from isolated atoms and molecules, **physical and biochemistry, and soft and hard condensed matter systems**, bypassing the need to use large-scale billion-dollar cost-level synchrotrons and XFEL sources. Quantum X-ray instruments could enable film molecular movies in action, one of the PI's expertise, to understand foundational energy processes, such as photosynthetic reactions to mimic photosynthesis in green-energy production or atmospheric aerosol characterization molecular dissociation. It would also support the study of attosecond pulse propagation and new fundamental interpretations of **attosecond measurements** for the characterization of thin films and 2D materials that are important for the next generation of **quantum electronics**. Last, novel QED approaches and the subsequent control over the X-ray spectral emission could enable future ultrastable hard X-ray frequency combs for the first time by invoking cavity-free XFEL mode-locking.

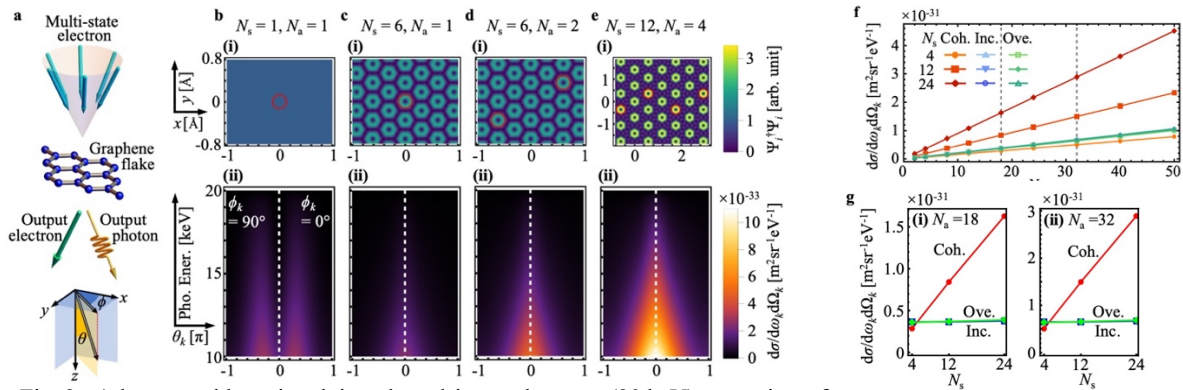


Fig. 2: a) bremsstrahlung involving shaped input electrons (20 keV) scattering off a graphene monolayer; b-e show (i) the electron population density distribution (atom locations denoted by red circles) and (ii) the coherent differential cross-section  $d\sigma/d\omega_k d\Omega_k$  of X-ray emission, respectively, for increasing the number of discrete electron momentum eigenstates ( $N_s$ ) and the number of atoms in the graphene lattice ( $N_a$ ); f) and g) comparing the actual (coherent) differential cross-section with its incoherent counterpart X-ray emission. Note that scaling with  $N_a$  and  $N_s$  occurs in a very different way – which can be tailored through the shape of the electron wavepacket.

## Bibliography

1. Garcia de Abajo, F. J. & Di Giulio, V. Optical excitations with electron beams: Challenges and opportunities. *ACS Photonics* **8**, 945–974 (2021).
2. Jingyi, T. *et al.* Laguerre-Gaussian Mode Laser Heater for Microbunching Instability Suppression in Free Electron Lasers. *Phys. Rev. Lett.* accepted.
3. Wong, L. J. & Kärtner, F. X. Direct acceleration of an electron in infinite vacuum by a pulsed radially-polarized laser beam. *Opt Express* **18**, 25035–25051 (2010).
4. Carbajo, S. *et al.* Direct longitudinal laser acceleration of electrons in free space. *Physical Review Accelerators and Beams* **19**, 21303 (2016).
5. Wong, L. J. *et al.* Control of quantum electrodynamical processes by shaping electron wavepackets. *Nat Commun* **12**, 1–10 (2021).
6. Rehani, M. M. *et al.* Patients undergoing recurrent CT scans: assessing the magnitude. *Eur Radiol* **30**, 1828–1836 (2020).
7. Ben Hayun, A. *et al.* Shaping quantum photonic states using free electrons. *Sci Adv* **7**, (2021).
8. Toonen, W. F., Stragier, X. F. D., Mutsaers, P. H. A. & Luiten, O. J. Gigahertz repetition rate thermionic electron gun concept. *Physical Review Accelerators and Beams* **22**, 123401 (2019).

## Asymmetric Pharmaceutical Synthesis with Molecular Hall Effect

Shoufeng Lan, Texas A&M Engineering Experiment Station, Texas A&M University

**Overview:** More than 80% of U.S. Food and Drug Administration or FDA-approved commonplace pharmaceuticals such as ibuprofen carry an inherent flaw, pairing the active and beneficial ingredient with an ineffective or toxic counterpart. The underline mechanism is chirality, which discerns the dissimilarities between objects and mirror images. One prominent example is human hands because the left hand is the mirror image of the right hand, but they are not superimposable. Each handedness or so-called enantiomer of chiral objects should have the same probability of occurring, like the left hand and right hand always appearing in a pair. Unfortunately, the pairing of left- and right-handed chiral materials might not be favorable or often detrimental in the pharmaceutical industry, for example, the thalidomide tragedy that led to more than 10,000 birth deformities in the 1960s. Therefore, asymmetric synthesis, or selecting/sorting one enantiomeric handedness over the other, is a pressing need yet a grand challenge for human health and the pharmaceutical industry. According to the symmetry principle, the asymmetric synthesis should have a fundamental force (i.e., electromagnetic, gravitational, strong, and weak) to break the symmetry. The only one that breaks the parity-inversion symmetry is weak interaction. That is why all atoms are slightly left-handed, and indeed it results in enantiomeric excess, however, on the level of thermal fluctuation. Emulating the weak interaction using light and magnetism, we found a new magneto-chiral effect (MChE) that is several orders of magnitude stronger. Although the MChE could lead to enantiomeric excess in principle, implementing it for practical applications in asymmetric synthesis is a daunting task, which is also the challenge we will address. To that end, we have three specific objectives based on our recently published works on the MChE. (1) Electromagnetically induce enantiomeric excess by developing a plasmonic magneto-chiral system. (2) Dramatically enhance the plasmonic MChE with nanostructures to achieve an unprecedented spatial separation of chiral pharmaceuticals, which we named the molecular Hall effect. (3) Obtain enantiopure pharmaceutical molecules with on-demand handedness fully controlled by light and magnetism. Like the electronic Hall effect that lays the foundation of modern electronics, the molecular Hall effect could contribute to asymmetric synthesis, hence the pharmaceutical industry and human health.

**Outcomes and Unique Aspects:** Our proposed research will produce a universal physical means to separate chiral objects for asymmetric synthesis – in stark contrast to current techniques that use existing chiral objects (e.g., catalysis for the 2001 and 2021 Nobel prizes in Chemistry) to biologically and chemically transfer handedness. These chemical and biological methods are expensive, may only apply to specific molecules near the asymmetric center (proximity effect), or may damage more complex molecules with multiple chiral centers. Due to its physical rather than chemical or biological nature, our proposed method can enable all chiral species to be selectively sorted by their inherent handedness, potentially achieving absolute enantioselectivity. Also, the research will generate a molecular Hall effect from our proposed plasmonic magneto-chiral technique, providing the elusive spatial separation of chiral molecules favorable for asymmetric synthesis in pharmaceutical manufacturing.

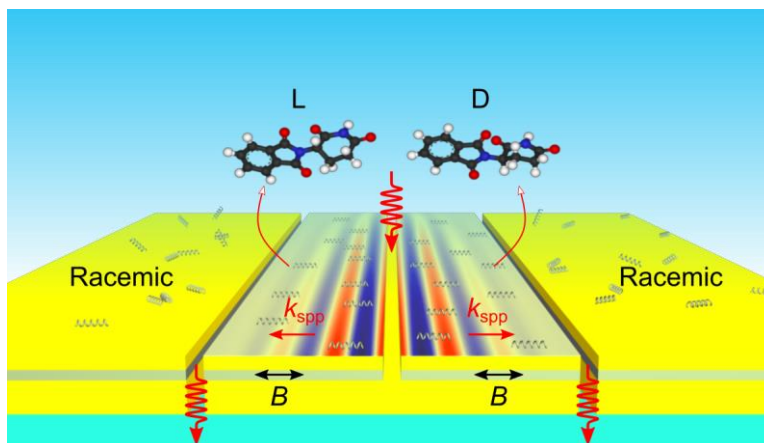
**Potential Impact:** To the scientific community, the proposed research will introduce a relatively unknown phenomenon called plasmonic MChE, enhanced by momentum matching and directionally controlled by the polarization of light. With broader impacts, it can also lead to the cost-effective production of a wide range of enantiopure drugs. As 80% of FDA-approved drugs are chiral, our technique can play a role in the pharmaceutical industry and human health in general. Also, since the predicted global market for asymmetric synthesis is ~133 billion dollars by 2030, our research can contribute to the U.S. and the world economy.



# Asymmetric Pharmaceutical Synthesis with Molecular Hall Effect

Shoufeng Lan, Texas A&M Engineering Experiment Station, Texas A&M University

**1. Literature Review:** One of the most fundamental mysteries is the homochirality of life, in which all living organisms on the Earth contain exclusively left-handed amino acids and right-handed sugars, not their mirrored counterparts. Scientists have spent endless efforts understanding the origin of such absolute enantiomeric excess ever since Louis Pasteur's great discovery of the molecular asymmetry of tartrates in the 1840s. From a physical point of view, a result of asymmetry (i.e., homochirality) must have a physical force to break



**Figure 1.** Schematic of a plasmonically induced universal asymmetric synthesis with electromagnetic control for selectively separating left- and right-handed (L and D) chiral objects from racemic mixtures. The layers of the structure are gold/cobalt/gold/glass. **B**: magnetic field,  $\mathbf{k}_{\text{SPP}}$ : wavevector of the excited surface plasmon polariton (SPP).

the symmetry, according to Pierre Curie's fundamental symmetry principle. In 1956 [*Phys. Rev.* 104, 254–258 (1956)], Tsung-Dao Lee and Chen Ning Yang discovered that weak interaction, albeit small, is the only one that breaks parity-inversion symmetry among the four fundamental forces (i.e., electromagnetic, gravitational, strong, and weak interactions). Four decades later, Rikken *et al.* found an optical analogous of weak interactions named the magneto-chiral effect (MChE) that is several orders of magnitude stronger [*Nature* 390, 493–494 (1997)]. Indeed, the same group observed an enantiomeric excess of  $\sim 0.01\%$  induced by the MChE in chemical reactions under a strong external magnetic field ( $\sim 10$  Tesla or about 100,000 times of the Earth's magnetic field) [*Nature* 405, 932–935 (2000)]. Recently, we obtained a record-strong MChE ( $\sim 40$  times Rikken's work) with the spontaneous magnetic moment of a ferromagnetic substrate while eliminating the need for an external magnetic field [*Nature Communications* 12, 2088 (2021)]. Despite the excellent work on the enantiomeric excess generation, scholars have not addressed the grand challenge of spatially separating chiral objects by physical means, which hampers applications in asymmetric synthesis with desired electromagnetic control. We propose to tackle the problem by combining the MChE with surface plasmon polariton (SPP) so that the left- and right-handed chiral objects experience different forces depending on the propagation direction of the SPP (**Figure 1**).

**2. Background and Technical Methodology:** A phenomenological description of electro- and magneto-optical effects is the expansion of the natural dielectric susceptibility,  $\epsilon_{\text{N}}$ , with vectors and tensors that characterize either the wave itself or an external force. With the terms related to this work, the expansion is the following:  $\epsilon_{\pm}(\omega, \mathbf{B}, \mathbf{k}) = \epsilon_{\text{N}}(\omega) \pm \epsilon_{\text{M}}(\mathbf{B}) \pm \epsilon_{\text{Ch}}(\mathbf{k}) + \epsilon_{\text{MCh}}(\mathbf{B}, \mathbf{k})$ , where  $\omega$  is the angular frequency of the right (+) and left (–) circularly polarized light,  $\mathbf{B}$  is a magnetic field, and  $\mathbf{k}$  is a wavevector; the subscription of M, Ch, and MCh are the magnetically induced rotation, chirality, and magneto-chiral effect, respectively. For a general isotropic medium, the well-known magnetically induced rotation, Faraday or magnetic Kerr effect, results from a Larmor precession of electrons with the angular velocity  $\Omega_L = -e\mathbf{B}/2mc$ , where  $e$  is the negative electron charge,  $m$  is the mass, and  $\mathbf{c}$  is the velocity of light



in vacuum. Therefore, the right and left circularly polarized light experiences the dielectric susceptibility, not at the frequency of  $\omega$  but a shifted frequency of  $\omega_{\pm} = \omega \pm \Omega_L$ . And hence, the dielectric susceptibility for the magneto-optical effect writes as:

$$\varepsilon_{\pm}(\omega \pm \Omega_L) = \varepsilon_N(\omega) \pm \frac{|e|}{2mc} \cdot \frac{\partial \varepsilon_N}{\partial \omega} \mathbf{B} \quad (1)$$

On the other hand, the dielectric susceptibility of a chiral medium is described by  $\varepsilon_{\pm}(\omega) = \varepsilon_N(\omega) \pm \alpha_{\text{Ch}}(\omega)\mathbf{k}$ . Similarly, light waves in a chiral medium under an externally applied magnetic field experience a new dielectric susceptibility:

$$\varepsilon_{\pm}(\omega, \mathbf{B}, \mathbf{k}) = \varepsilon_N \pm \frac{|e|}{2mc} \cdot \frac{\partial \varepsilon_N}{\partial \omega} \mathbf{B} \pm \alpha_{\text{Ch}}\mathbf{k} + \frac{|e|}{2mc} \cdot \frac{\partial \alpha_{\text{Ch}}}{\partial \omega} (\mathbf{B} \cdot \mathbf{k}) \quad (2)$$

where the last term signifies the MChE that depends on the inner product of the magnetic field and wavevector together with the derivative of the chirality-induced dielectric susceptibility.

We can understand the underline mechanism of physically induced asymmetric synthesis by the fundamental symmetry principle. Although the theory of Nobel Prize-awarded weak interactions by Lee and Yang is particularly complicated, we can use a simplified equation, possibly oversimplified but not losing physical picture, to illustrate the violation of parity conservation.  $S(\boldsymbol{\sigma} \cdot \mathbf{p}) = S(\boldsymbol{\sigma}) \cdot S(\mathbf{p}) = -\boldsymbol{\sigma} \cdot \mathbf{p}$ , where the parity symmetry operator  $S$  operates on the weak interaction proportional to  $\boldsymbol{\sigma} \cdot \mathbf{p}$ , and the parity symmetry is no longer conserved ( $-\boldsymbol{\sigma} \cdot \mathbf{p}$ ). The key is the time-even pseudoscalar or the inner product between an axial vector (i.e., the spin  $\boldsymbol{\sigma}$ ) and a linear vector (i.e., the momentum  $\mathbf{p}$ ), both being either time-even or time-odd. Similarly, the MChE is proportional to  $\mathbf{B} \cdot \mathbf{k}$ , in which  $\mathbf{B}$  and  $\mathbf{k}$  are the magnetic field (axial vector) and wavevector (linear vector), both time-odd. As  $\mathbf{B} \cdot \mathbf{k}$  is a pseudoscalar, mimicking weak interactions, the MChE must violate the parity symmetry conservation or  $S(\mathbf{B} \cdot \mathbf{k}) = -\mathbf{B} \cdot \mathbf{k}$ . Following Pierre Curie's symmetry principle, it should also lead to absolute enantiomeric excess with the handedness depending on the relative direction between  $\mathbf{B}$  and  $\mathbf{k}$ .

**3. Problem Statement and Objectives:** Although the MChE could lead to enantiomeric excess in principle, it is a daunting task to implement for practical applications in asymmetric synthesis. The first challenge we have to address is that the MChE is relatively weak, even if it is already several orders stronger than the weak interaction. We plan to follow our previous strategy to replace the external magnetic field with a spontaneous magnetic moment from a widely accessible ferromagnetic material - cobalt. Furthermore, we will dramatically increase the optical length for light-matter interaction using SPPs propagating along the in-plane direction. Also, SPPs have a strongly enhanced density of states and Purcell factor by confining light at the metal-dielectric interface, further elevated by purposely designed surface structures. With all these aspects in mind, we expect to obtain an enantiomeric excess of ~99%. The second challenge for asymmetric synthesis is the electromagnetic control, which we automatically solve by adopting the MChE proportional to a magnetic field and light. The third challenge is the spatial separation of chiral objects, which we will achieve by the excitation of SPPs because the sign of the plasmonic MChE is opposite on the two sides of the groove (**Figure 1**). Such physically induced asymmetric synthesis and spatial separation of chiral objects with built-in electromagnetic control have been long looked for but are still elusive. The long-term goal is to develop a physically induced asymmetric synthesis that is universal and cost-effective. To that end, we have three specific objectives based on our recently published works on the MChE. (1) Electromagnetically induce enantiomeric excess by developing a plasmonic magneto-chiral system. (2) Dramatically enhance the plasmonic MChE with nanostructures to obtain the molecular Hall effect. (3) Obtain enantiopure pharmaceutical molecules with on-demand handedness fully controlled by light and magnetism.

**4. Outline of Tasks and Work Plan:** Due to the nature of universality, physically induced spatial separation of chiral objects or the molecular Hall effect holds strong potential for cost-effective asymmetric synthesis. For unlocking its full potential, the foremost and essential step

is to find a physical force to induce enantiomeric excess. To do that, we will implement the MChE, emulating weak interactions, to violate the conservation of parity-inversion symmetry. We then plan to leverage the MChE by coupling it to SPPs to achieve a desirable yet challenging task of enantiomeric spatial separation (**Figure 1**). We will further enhance the plasmonic molecular Hall effect using grating couplers to provide the necessary momentum mismatched between free-space light and SPPs (**Figure 2**). We then plan to obtain enantiopure molecules through the polarization-controlled unidirectional excitation of SPPs (**Figure 3**).

#### 4.1 A new plasmonic magneto-chiral system for enantioselective separation (Months 1-8)

We found a new path for MChE with record-high magneto-chiral anisotropy in atomic crystals that sustain excitons [*Nature Communications* 12, 2088 (2021)]. However, the atomic-scale thickness inevitably only affords a short distance for photons to interact with matter in the out-of-plane direction. We thus propose a plasmonic magneto-chiral system (**Figure 1**), in which photons interact with electrons forming SPPs that propagate along the surface in the in-plane direction. Also, instead of the previous thulium iron garnet (TIG,  $\text{Tm}_3\text{Fe}_5\text{O}_{12}$ ), we plan to use cobalt as the ferromagnet with an in-plane magnetic moment. The schematic of the structure that contains layers of gold-cobalt-gold on a glass substrate is in **Figure 1**. In stark contrast to the well-studied magneto-plasmonic applications that use similar devices with a perpendicular magnetic field [*Nature Photonics* 4, 107–111 (2010)], our magnetic field is in-parallel to SPPs, leading to a relatively unknown phenomenon of plasmonic MChE.

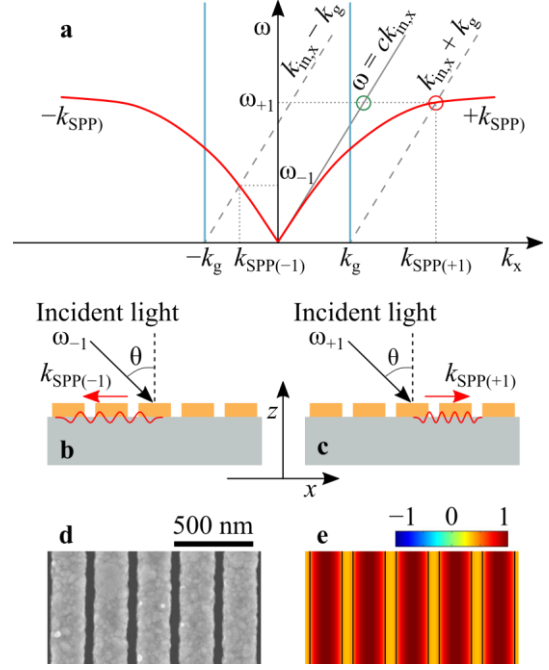
As an initial step, we will use nanogroove (~100 nm) for free-space light in water to couple to SPPs (middle nanogroove) and back to water (left and right nanoslits) through the glass substrate. On the two sides of the middle nanogroove, the wavevectors of the SPPs ( $k_{\text{spp}}$ ) are opposite. Because the MChE is proportional to the inner product between the magnetic field and wavevector, the generated force by the plasmonic MChE is also the opposite, provided with a fixed magnetic field. From the magneto-chiral theorem, a positive (negative) MChE preferably interact with the right- (left-) handed or D- (L-) enantiomer. As a result, the handedness of the chiral materials adsorbed on the two sides must also be different, achieving the molecular Hall effect. Another outstanding feature of the proposed plasmonic magneto-chiral system is that we can detect the chirality of the materials by analyzing the left/right circular polarization (LCP/RCP) of the out-coupling SPPs in the device. This effect is because the chirality will lead to different responses to LCP and RCP light or the so-called circular dichroism. Meanwhile, since only a tiny part of the scattered light by the groove can couple to SPPs, we expect the plasmonic MChE to be relatively weak at this stage.

#### 4.2 Significant enhancement of plasmonic MChE using nanostructures (Months 9-16)

To enhance the plasmonic MChE, we will use grating couplers instead of a single groove for more light to couple to SPPs while keeping the magnetic field constant. Specifically, we will design gratings to provide the necessary momentum for efficient coupling between free-space light and SPPs, as shown in **Figure 2a**. Light shining on a metal surface at an angle of  $\theta$  will have an in-plane wavevector component  $k_{\text{in},x} = k_{\text{in}} \sin \theta$ , manifesting in the light line (solid gray). Similarly, SPPs propagate at the metal-dielectric interface have a wavevector of  $k_{\text{SPP}}$ . For light to couple to SPPs, the two in-plane momenta must be the same. At the specific frequency, for example,  $\omega_{+1}$ , the in-plane wavevectors  $k_{\text{in},x}$  and  $k_{\text{SPP}}$  at the green and red circles are, unfortunately, not equal. This wavevector or momentum-mismatch prevents an efficient coupling between free-space light and SPPs. The scattering of light from a nanogroove in Section 4.1 enables part of the input light to match the momentum with SPPs, which can partially address the problem but with relatively low efficiency.

We plan to use grating couplers because their periodic structures provide an extra wavevector  $k_g$  in the reciprocal space. As a result, the light line shifts with a total wavevector

of  $k_{\text{in},x} + k_g$  (dotted line) that matches  $k_{\text{SPP}(+1)}$  at the red circle. Since the  $k_g$  can be in the opposite direction ( $-1$  order), the total wavevector can also be  $k_{\text{in},x} - k_g$  or  $k_{\text{SPP}(-1)}$  at a different frequency of  $\omega_{-1}$ . **Figures 2b** and **2c** clearly show the excited first-order SPPs propagating in positive and negative directions, accordingly. There will be higher orders of waves but with much lower efficiency. In addition, the analysis uses an oblique input light, but it also works for gratings under normal incidence (blue lines). As part of the preliminary results, we show in **Figure 2d** a scanning electron microscopy (SEM) image of the fabricated grating sample. We also provide the simulated electric field distribution (**Figure 2e**) using a full-wave simulation software of COMSOL for the grating at normal incidence. We should note that the current preliminary results are silver gratings on the glass in the air. We will optimize the operating conditions with gold, cobalt, water, and an extended nonpatterned area. Nevertheless, the wavevector of SPPs on the two sides of the grating will be opposite, leading to opposite plasmonic MChE selecting the handedness.



**Figure 2.** Grating coupler to enhance the plasmonic magneto-chiral effect. (a) The mechanism of grating coupler to excite backward (b) and forward (c) propagating SPPs. (d) SEM image of a grating coupler. (e) The simulated electric field under normal incidence using COMSOL.

#### Unidirectional excitation of plasmonic MChE for enantiopure molecules (Months 17-24)

The enantiomeric spatial separation of chiral molecules from racemic mixtures that contain an equal amount of L- and D-molecules could contribute to cost-effective asymmetric pharmaceutical synthesis. A higher-level challenge is to produce enantiopure molecules, not their enantiomeric counterparts. To do that, we will continue to use SPPs but only excite them in one direction under normal incidence. It is not an easy task because, under normal incidence, a plasmonic structure, including nanogroove and gratings, will excite an equal amount of SPPs in both directions. With oblique incidence at a specific frequency, on the other hand, plasmonic gratings can partially excite directional SPPs, as shown in **Figure 2a**. However, there will always be some scattering of the incident light, albeit small, to excite SPPs in the opposite direction, not to mention that the oblique incidence is not favorable for practical applications.

To eliminate the SPPs in the undesirable direction, we plan to manipulate the resonant scattering of nanostructures under the interference mechanism. In this context, Capasso's group at Harvard University demonstrated fantastic and inspiring work using plasmonic metasurfaces that contain an array of double-column apertures (**Figure 3**). When  $W \ll L < \lambda_{\text{SPP}}$ , where  $\lambda_{\text{SPP}}$  is the wavelength of SPP, each one of the apertures selectively scatters incident light with polarization perpendicular to the elongated direction, giving rise to SPPs. We can treat the excited SPPs by a column of such apertures as a plane wave with electric fields  $E_1$  and  $E_2$ . With the arrangement of the two columns shown in **Figure 3a**, i.e.,  $\theta_1 = 45^\circ$ ,  $\theta_2 = 135^\circ$ , separated by a distance of  $S = \lambda_{\text{SPP}}/2$ , they will excite SPPs in the + and - directions as the following:

$$I_{\pm} \propto C[(E_1^2 + E_2^2) \pm 2E_1E_2 \sin(\delta)] \quad (3)$$

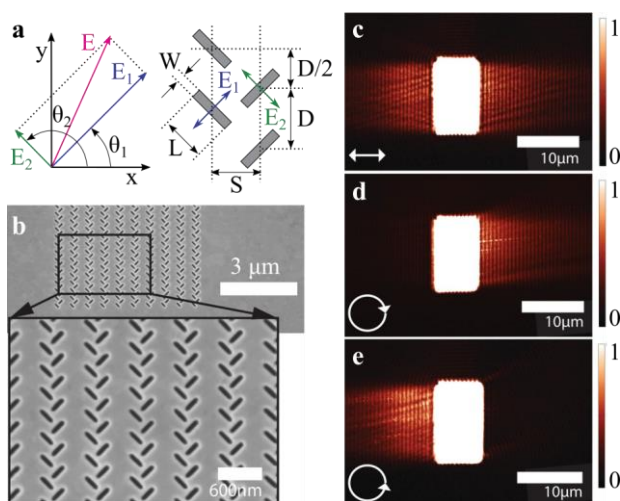
where  $\delta$  is the relative phase difference between  $E_1$  and  $E_2$  by the coupling process and transferred to the SPPs. Unidirectional excitation of SPPs occurs when the incident light has a

circular polarization ( $E_1 = E_2$ ), with the direction determined by the handedness ( $I_- = 0$ ,  $\delta = \pi/2$  for LCP and  $I_+ = 0$ ,  $\delta = -\pi/2$  for RCP), as shown in **Figures 3c to 3e** for the structures in **3b**. In this project, we will leverage the unidirectional SPPs by coupling them to the magnetic field of cobalt so that the plasmonic MChE will also happen in one direction. We note that the use of polarization for unidirectional SPPs is by no means contradictory to the fact that MChE is independent of polarization.

**5. Outcomes:** The proposed research will produce a universal physical means to create/sort chiral seeds for asymmetric synthesis – in stark contrast to current techniques that use existing chiral objects to biologically and chemically transfer handedness (e.g., the 2001 and 2021 Nobel Prizes). These chemical/biological methods are expensive, may only apply to specific molecules near the asymmetric center (proximity effect), or may damage more complex molecules with multiple chiral centers. Due to its physical rather than chemical or biological nature, the proposed method can enable all chiral species to be selectively sorted by their inherent handedness, achieving absolute enantioselectivity with electromagnetic control. The research will also generate the first spatial separation of chiral molecules depending on the handedness (molecular Hall effect) using the plasmonic MChE, further enhanced by grating couplers with momentum matching. Moreover, the research will create a unidirectional plasmonic MChE that only interacts with one handedness of chiral molecules, not the other.

**6. Impact:** While magneto-plasmonics has a magnetic field perpendicular to SPPs, our magnetic moment from a ferromagnetic substrate is in- or anti-parallel to the SPPs, leading to a relatively unknown phenomenon called plasmonic MChE. By providing the necessary momentum mismatched between free-space light and SPPs, our research will also introduce a general technique of grating coupling for enhancing plasmonic MChE. Moreover, our research will develop a unidirectional plasmonic MChE, leveraging the unidirectional SPPs. Beyond the scientific importance to the community, the proposed project can also have much broader impacts. The successful execution of this research can lead to the cost-effective production of a wide range of enantiopure drugs and bio/chemical products. As 80% of small-molecule drugs approved by the U.S. Food and Drug Administration or FDA were chiral, and 75% were enantiopure, our technique can play a role in the biomedical, pharmaceutical industries, and human health in general. Also, since the predicted global market for asymmetric synthesis is ~133 billion dollars by 2030, our research can contribute to the U.S. and the world economy.

**7. The PI's Qualifications:** The PI has in-depth experience in light-matter interactions, including plasmonics, chirality, and metamaterials. His research has consistently contributed to advancing the field with solid results in well-regarded journals, such as 4 in *Nature*-sister journals, 4 in *Advanced Materials*, and 4 in *Nano Letters*. Recognizing his accomplishments, he has received many awards, such as the SPIE Lovell scholarship. He also shows significant leadership by organizing conferences, serving on reviewer panels, and as an Associate Editor.



**Figure 3.** Polarization-controlled directional coupling of SPPs. **(a)** Illustration of the coupling of waves from two columns of apertures. **(b)** SEM images of the samples. **(c to e)** Near-field images with illumination by linear polarization **(c)**, RCP **(d)**, and LCP **(e)**. Figure modified from [*Science* 340, 331-334 (2013)].

## Executive summary

**Title:** Mid-infrared laser correction of photonic chips fabrication errors to improve manufacturing yield and reduce energy consumption.

**Challenge category:** Information

### **Project summary:**

Data consumption is increasing at an exponential pace (2X every 3 years). Standard electronic chips are reaching their fundamental bandwidth limits and the energy consumption of these devices is too important to keep up with the data growth. Over the past years, photonic chips have proven to be a scalable technology that promises higher bandwidth and lower power consumption. Photonic chips are now widely used for transceiver applications in datacenters. However, due to the inherent sensitivity of light, process variations affect the phase of photonic components inside the chip. This problem reduces the manufacturing yield and achievable performances of these devices, slowing down the adoption of the technology. Active thermal tuning techniques must be added to the chip, increasing the power consumption and diminishing the potential energy saving.

Simon Duval, co-founder and VP R&D at Femtum, wants to tackle this challenge with his R&D team by proposing a new mid-infrared fiber laser solution that permanently corrects photonic chips after their fabrication. By exploiting nonlinear refractive index change in silicon waveguides with the proprietary short pulsed mid-infrared lasers developed at Femtum, Simon aims at demonstrating the first resonance tuning of a microring resonator across its whole free-spectral range.

This first demonstration will serve as a building block for correcting various phase sensitive components in photonic chips to reduce power consumption, increase manufacturing yield and enable new, simplified designs. The current project will convince Femtum, its investors and its clients in photonic chips manufacturing to invest more into the development of an automated solution that could be commercialized at scale and that could accelerate the deployment of photonic chip technologies in datacom as well as in quantum computing, lidar and biosensor applications.

### **About Simon Duval and Femtum:**

Before creating Femtum with its partner Louis-Rafaël Robichaud, Simon demonstrated the first mid-infrared femtosecond fiber laser at 2800 nm during its PhD studies at Laval University. While being an industrial post-doctoral fellow at Femtum and Laval University, Simon built an R&D team of 6 people and acquired managing skills. He and his team also developed and matured an industrial nanosecond fiber laser and an application lab that will be used in the framework of this project.

Femtum inc. is a deeptech Canadian startup now incubated at the National Institute of optics (INO). Now 4 years old, the company is the world's first manufacturer of short pulse 3  $\mu\text{m}$  fiber lasers. Femtum technology platform comes out of several decades of research at the Center for Optics, Photonics and Lasers and is currently used for scientific and industrial applications. The company is proud to offer its support to this bold project by allocating human resources and user time in its application lab and for its lasers.

# Project Proposal

## Title

Mid-infrared laser correction of photonic chips fabrication errors to improve manufacturing yield and reduce energy consumption.

## Overview

The photonic chips market is expected to grow at a very fast pace ( $> 20.5\%$  compound annual growth rate) over the next years. The main driver for the adoption of this technology is the datacom area (datacenter), where current electronic chips require increasing, unsustainable power consumption and bandwidth to keep up with the data requirements. Datacom is driving the rise of photonic chips for transceiver applications, but other massive emerging markets are also adopting this enabling technology. Photonics chips are now being developed in research centers and companies for quantum computing (e.g. Xanadu), consumer biosensors (e.g. Rockley Photonics) and Lidar applications (e.g. Huawei).

However, photonic chips are much more sensitive to manufacturing variations than electronic chips. They are made of several tens of components based on tiny ( $< 1 \mu\text{m}$ ) semiconductor waveguides (most likely silicon) that guide light into the chip to transmit information or perform computing tasks. The smallest variations in the waveguide structure (few nanometers) during its fabrication causes phase variations along the key components of the chip, affecting their performance. When a chip contains components that are out of specification, it is discarded at the testing phase, causing a lot of waste and poor yield along the supply chain.

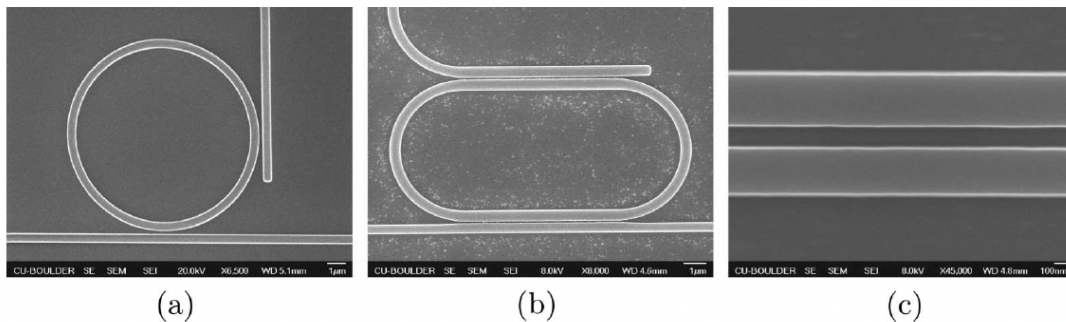


Figure 1: Microscopic image of a) and b) microring resonators and c) a section of the coupling region of a directional coupler <sup>1</sup>.

Examples of key components that suffer from manufacturing variations are modulators, lasers or couplers. Microring resonators (MRR) are used as efficient and compact modulators, but they are highly sensitive to manufacturing processes due to their resonant nature. Process variations (width, height, surface roughness, etc.) affect the waveguide effective refractive index (the phase) along the ring. Since the optical performance (resonance wavelength, losses, etc.) highly depend on the cumulative phase along the ring, even the smallest process variations lead to random optical



performances that limit their use in real world applications. Figure 2 shows a typical photonics chip wafer containing 58 photonics chips with ring resonators <sup>2</sup>. After the wafer fabrication, the resonance wavelengths of the ring resonators are randomly distributed across the wafer.

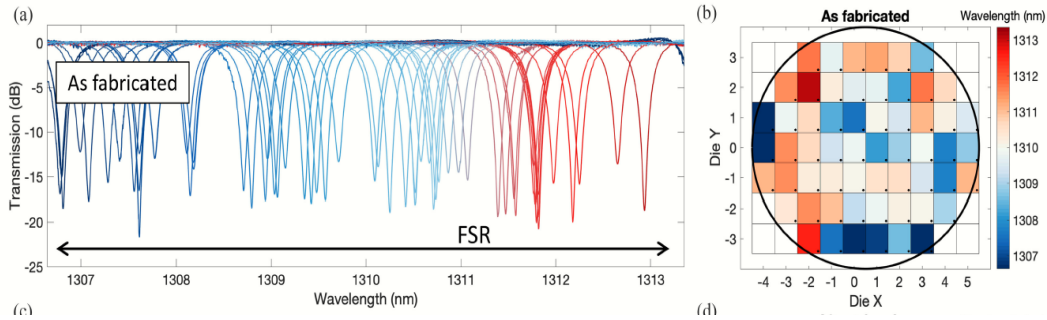


Figure 2: Process variations leading to randomly varying resonances of ring resonators across the same wafer.

The current method for correcting the phase of these components is the use of active tuning techniques (e.g. thermal tuners), which add to the complexity and the power consumption of the chip. Low power consumption is a critical specification in datacenters; the total energy consumption used for datacom could be an important fraction of the world's energy in a decade <sup>3</sup>.

To solve this important challenge, Intel corporation has recently developed a post-fabrication correction method based on Germanium implant at specific locations on the component <sup>2</sup>. The germanium is implanted through a photoresist mask and a heater is formed at the top of the microring. A heating sequence is performed to anneal the germanium layer, changing the refractive index on a portion of the ring. The resonance frequency of the ring can then be permanently tuned to the targeted wavelength. Although this technique can change the resonance wavelength across the whole free-spectral range (FSR) of the ring, the required time to correct the ring is currently around 4 minutes, which is hardly scalable at a production scale on a chip with several microrings (8 or 16 modulators/chip and even more in the future). Moreover, this technique induces very large losses inside the component, it requires extra fabrication steps and it can cause thermal crosstalk that affects the surrounding components since the annealing temperature is around 650 °C.

Post-fabrication laser tuning using pulsed lasers is a very promising technique to correct for phase errors inside photonic chip because 1) of its inherent high-speed nature, 2) its potential compatibility with the already existing photonic chip testing machine and because 3) it involves no extra steps during fabrication. Bachman et al. <sup>4</sup> and several research groups have already demonstrated the phase tuning of silicon photonics chip using femtosecond lasers at 400 nm and 800 nm. The pulses are directed at different points on the ring to modify and amorphize the top surface of the waveguide. However, these methods only showed a weak compensation for phase error (tunability limited to 3 nm, while FSR can reach 15 to 20 nm), a critical requirement for implementation in the real world, where the MRR resonance can be randomly distributed across the FSR.

Recently, the modification of silicon in volume based on novel multi-photon interaction with mid-infrared pulsed laser has generated a lot of interest <sup>5,6</sup>. Short pulsed mid-infrared lasers (wavelength above 2.5  $\mu\text{m}$ ) allows for precise modification in the

semiconductor bulk while avoiding nonlinear distortion and plasma screening in the pre-focal volume. Garcia-Lechuga et al.<sup>7</sup> recently demonstrated that the amorphization of silicon under the surface is deeper at longer wavelengths and especially around 3  $\mu\text{m}$ . Deeper refractive index change through multiphoton process is thus a promising approach to modify silicon waveguides on photonic chip in a more uniform way. Using this approach, the phase error of the ring resonator has the potential to be varied across the whole FSR without causing significant losses. Other phase sensitive components in photonic chips, like Mach-Zehnder interferometers, distributed-feedback (DFB) lasers and even couplers could also be corrected using a similar approach. Finally, this approach could be implemented in other semiconductor platforms that are commercially deployed, like Indium Phosphide (InP) or Silicon Nitride (SiN).

## Project description

In this project, Simon Duval (Vice-president R&D) and the R&D team of Femtum aim to develop a new laser process to change the refractive index of key components inside photonic chips. The process is based on the use of pulsed fiber lasers above the bandgap of silicon ( $> 800 \text{ nm}$ ), and more specifically around 3  $\mu\text{m}$  with the nanosecond and femtosecond fiber laser technologies already commercialized by Femtum<sup>7</sup> as well as the newly developed application lab (see figure 3).

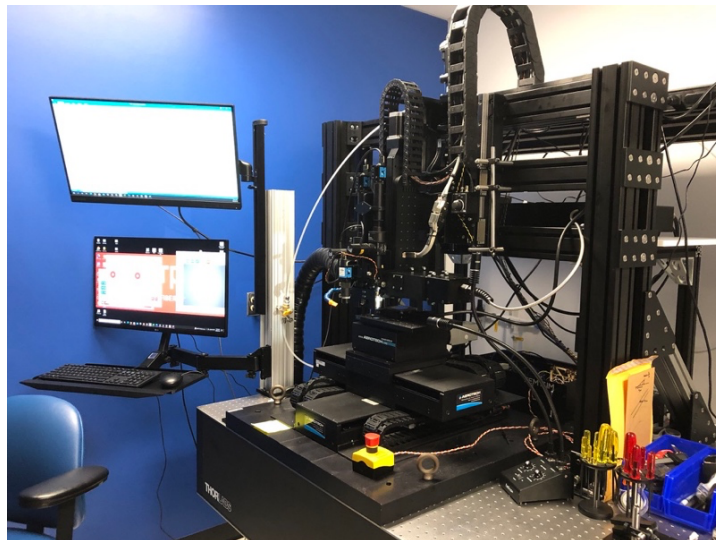


Figure 3: Femtum application lab

The main objective is to demonstrate the permanent wavelength tuning of microring resonators across their whole FSR (5-15 nm) using Femtum nanosecond and femtosecond lasers. The microring resonator was chosen because the refractive change modification inside the ring resonator directly impacts the resonance wavelength, which can be easily measured by an optical spectrum analyzer. Microring resonators also have a simple geometry, which will simplify the analysis. The project will be separated in three phases:

### 1. Design and fabrication of a photonic chip holder and an inline monitoring setup compatible with the laser platform (3 months)

In this phase, a suction holder that must hold the chip perfectly straight and flat along the laser processing area will be developed. The test bench will include

electronics as well as optical fiber probes that must be precisely positioned for inline monitoring of the photonic chip performances during the laser process. A broadband fiber laser is side coupled to the photonic chip by buttcoupling the input fiber into the silicon waveguide with micro-positioning stages. The light coming out of the chip will also be sent to an optical fiber connected to an optical spectrum analyzer for monitoring the spectrum in real time. This test bench will be solitary fixed on the motorized x,y & z stages to keep the monitoring setup aligned when positioning/moving the photonic chips before/during the laser process.

**2. Study of the impact of the Femtum Nano 2800 on the refractive index modification inside the ring resonator (6 months)**

In this phase, a nanosecond (30-100 ns) fiber laser emitting 0.5 to 150  $\mu\text{J}$  pulses around 2800 nm will be focused tightly on various points in the ring resonator using precise positioning stages and a vision system on the application lab that was developed by Femtum. The laser parameters (spot size, pulse energy, pulse duration, repetition rate, number of incident pulses) will be varied to study the effect of mid-infrared laser interaction with the silicon waveguide. Objectives with different focal lenses will be tested to vary the overlap of the laser spot with the waveguide. The laser will be scanned at different locations along the ring to evaluate the influence on the wavelength change. The ring resonance (central wavelength, and linewidth) will be characterized after each laser process to validate the performance of this technique. These results will be indicative of the maximal tuning range and the induced loss inside the ring resonator.

**3. Study of the impact of a sub-nanosecond fiber laser at 2800 nm on the refractive index modification inside the ring resonator (6 months)**

The results obtained in phase 2 will provide a guideline for improving the refractive index change with a laser with shorter pulse duration. As compared with nanosecond pulses, refractive index tuning of silicon by ultrafast laser involves other nonlinear physical mechanisms (e.g. amorphization). The parameters (pulse duration, energy, rep. rate) of a femtosecond or a picosecond fiber laser at 2800 nm will be adjusted in order to demonstrate modification inside Silicon. Then, the same process study as in phase 2 for the modification of micro-ring resonator will be realized. Results will be compared to those using the nanosecond laser. Preliminary long term and thermal cycling/annealing tests of the corrected the ring resonators will be performed to evaluate the commercial viability of this approach.

The outcome of this project is to determine the best laser solution that can be provided by Femtum to induce a permanent, low loss correction in microring resonators across the largest possible tuning range (ideally the whole FSR). This study will provide the building blocks and the lasers parameters required for the correction of other important components inside a photonics chip.

By proposing a post-fabrication laser correction platform to the photonic chip industry, Simon and his team aim at increasing the manufacturing yield while reducing the energy consumption of these chips by a significant factor. This approach can limit the use of active phase tuners or greatly reduce their power consumption, which can

represent around 30% of the total chip energy consumption. It will also enable the use of smaller components that are normally discarded due to manufacturing errors to increase the chip density. For instance, microring modulators can be more than 100 times smaller in size than Mach-Zehnder modulators. Finally, knowing that the chips could be corrected for manufacturing errors, it can help chip designers and manufacturers around the world to think of new energy-efficient chip designs and accelerate their speed-to-market for a massive adoption of their photonic chips globally.

## Reference

1. Chen et al., “Process variation in silicon photonic devices”, *Applied optics* 52 (2013).
2. Jayatilleka, Hasitha, et al., “Post-fabrication trimming of silicon photonic ring resonators at wafer-scale.” *Journal of Lightwave Technology* 39 (2021).
3. Nicolas Jones, “How to stop data centres from gobbling up the world’s electricity”, *Nature* 561 (2018).
4. Bachman, Daniel, et al., “Postfabrication phase error correction of silicon photonic circuits by single femtosecond laser pulses”, *Journal of Lightwave Technology* 35 (2009).
5. Werner et al., “Single-shot multi-stage damage and ablation of silicon by Femtosecond mid-infrared laser pulses”, *Scientific Reports* 9 (2019).
6. Mareez et al., “Single-shot femtosecond bulk micromachining of silicon with mid-IR tightly focused beams”, *Scientific reports* 12 (2022)
7. Garcia-Lechuga et al., “Deep silicon amorphization induced by femtosecond laser pulses up to the mid-infrared”, *Advanced optical materials* 9 (2021).
8. [www.femtum.com/products/](http://www.femtum.com/products/)

## **Early detection and monitoring of neurodegeneration via advanced ophthalmic imaging**

Neurodegenerative diseases constitute a severe health problem worldwide. Parkinson's and Alzheimer's, alone affect the lives of hundreds of millions of people globally. They impose significant stress on healthcare system costs and limit the level of activity of patients and their family members in the work market, which in turn has long-term financial consequences. Neurodegenerative diseases are progressive and currently not curable, efforts towards their early detection, management and progression prediction are thus crucial.

Recently, our research group has managed to design and build a new fast and precise scanning laser ophthalmoscope capable of recording the fast, delicate motions of the human eyeball with an unprecedented level of accuracy. Our goal is to push the limits of our current understanding of the connection between eye motion (also known as saccadic motion) and the early detection of neurodegenerative diseases and their gradual progression.

Our main objective is to create a clinical-use device based on our laboratory prototype along with protocols that will ultimately result in the pathway towards the popular clinical use of eye motion as diagnostics for early-stage detection of neurodegeneration. We have the proven technical and clinical expertise as evidenced by our group's current and past work on biomedical ophthalmic devices design, construction and clinical use. Goals include the design and deployment of data acquisition protocols, visual tasks, data analysis and synthesis methods for extraction of features characteristic for various neurodegenerative diseases. We plan to undertake exploratory studies with normal controls and patients in currently collaborating medical clinics. Our clinical efforts will initially focus on data analysis with the goal of extracting collections of candidates for biomarkers of neurodegeneration.

## **Early detection and monitoring of neurodegeneration via advanced ophthalmic imaging**

Neurodegeneration is the progressive loss of structure or function of neurons. This process is naturally associated with aging and is the underlying cause of neurodegenerative diseases. Examples of neurodegenerative diseases include: Alzheimer's disease, Parkinson's disease, Schizophrenia, Macular degeneration, rheumatoid arthritis and multiple sclerosis. For many of these diseases, genetic mutations are also a risk factor. Currently there is no known treatment capable of reversing neurodegeneration, thus neurodegenerative diseases are considered to be incurable.

Neurodegenerative diseases constitute a severe health problem worldwide. Parkinson's and Alzheimer's, alone affect the lives of hundreds of millions of people globally. They impose significant stress on healthcare system costs and limit the level of activity of patients and their family members in the work market, which in turn has long-term financial consequences.

Given that neurodegenerative diseases are progressive and not curable, efforts towards their early detection, management and progression prediction are crucial. Recently, the connection between the continuous, delicate movements of the eyeball – also known as saccadic motion and neurodegenerative disease has attracted the interest of biomedical researchers worldwide [1-15]. In particular, subtle differences in the statistics of the saccadic motion of diseased subjects differ significantly from those of control group subjects. Analyzing the statistical moments of the frequency, lateral and angular excursion as well as the velocity of individual displacements has been part of routine protocols for ophthalmology for decades.

The dynamics of saccadic motion are often studied with scanning laser ophthalmoscopes (SLOs) [16], fast instruments capable of producing reflectivity maps of the fundus of the eye using a scanning laser spot. Progress in SLOs or saccades promises the long-sought level of detail to find the link between saccadic motion statistics and the early onset of neurodegenerative diseases. Due to their widespread use in ophthalmic science, SLOs are a powerful, convenient probe into the inner workings of saccadic motion.

On the other hand, the main drawback of SLOs has been their inherently limited degree of precision to pinpoint the spatial location of the reflected signal, which in turn imposes bounds on the level of detail that they can effectively resolved. Several sources of noise contribute to the limited spatial resolution of SLOs. Mainly the electromechanical nature of the state-of-the-art scanners most commonly used for SLOs and the coherent nature of the optical source are of most concern. The former issue results in spatially heterogeneous sampling frequency, which in turn produces spatially varying resolution. The latter is a more delicate problem, in which the coherence of the scanning laser produces interference and thus coherent modulation of the signal and light scattered throughout diverse loci in the sample.

Recently, our research group has achieved two major milestones. Namely, we have managed to build a fast and precise retinal tracker [17] based on the narrow field SLO and furthermore, to effectively suppress the levels of signal noise in SLOs using applied statistical analysis and methods [18]. Specifically, we have improved the accuracy of SLO so that we can now locate the coordinates of points in the trajectory of scanning laser with accuracy greater than the optical resolution of the scanning imaging system. This crucial milestone allows collecting the delicate details of saccades in more detail than ever before. Being able to record the fast, fine motions of the eyeball with this unprecedented level of accuracy paves the way to our main aim: monitoring and characterizing saccadic motion statistics to find reliable, useful biomarkers for the early detection of neurodegeneration and its gradual progression.

In particular, our main objective is to create a clinical-use device based on our laboratory prototype along with protocols that will ultimately result in the pathway towards the popular clinical use of eye motion as diagnostics for early-stage detection of neurodegeneration. We have the proven technical and clinical expertise as evidenced by our group's current and past work on biomedical ophthalmic devices design, construction and clinical use.



We plan to improve on our current data acquisition protocols and visual tasks as well as data analysis and synthesis methods for extraction of features characteristic for various neurodegenerative diseases, given the newly achieved capabilities of our SLO. We also plan to undertake exploratory studies with normal controls and patients in currently collaborating medical clinics. Our clinical efforts will initially focus on data analysis with the goal of extracting collections of candidates for biomarkers of neurodegeneration.

In addition, given the significant proportion of patients with neurodegenerative diseases with disabilities, we aim to optimize and adapt our protocols and hardware in order to facilitate the examination of patients with disabilities in a clinical environment. This includes device optomechanical configuration and ease of software operation. Our design will focus on ensuring that reliable data can be obtained in a clinical environment regardless of patient disability status.

We are grateful for Optica's welcoming of proposals exploring innovative, groundbreaking research or technology developments. We are convinced that our newly developed ophthalmic technology will provide the medical community with a game-changing tool which will forever improve neurodegeneration detection, diagnostics and prognosis. While our SLO is now far from a clinical reality, its main obstacle remains lack of funding. We believe our goals are perfectly inline with Optica's 20<sup>th</sup> Anniversary Challenge of "Increasing the availability of optics-based treatments for common diseases and new optics-based treatments for diseases without cures and treatment options."

- [1] C.-C. Wu, B. Cao, V. Dali, C. Gagliardi, O.J. Barthelemy, R.D. Salazar, M. Pomplun, A. Cronin-Golomb, A. Yazdanbakhsh, Eye movement control during visual pursuit in Parkinson's disease, *PeerJ*. 6 (2018) e5442–e5442. <https://doi.org/10.7717/peerj.5442>.
- [2] I.M. Pavisic, N.C. Firth, S. Parsons, D.M. Rego, T.J. Shakespeare, K.X.X. Yong, C.F. Slattery, R.W. Paterson, A.J.M. Foulkes, K. Macpherson, A.M. Carton, D.C. Alexander, J. Shawe-Taylor, N.C. Fox, J.M. Schott, S.J. Crutch, S. Primativo, Eyetracking Metrics in Young Onset Alzheimer's Disease: A Window into Cognitive Visual Functions, *Front. Neurol.* 8 (2017) 377. <https://www.frontiersin.org/article/10.3389/fneur.2017.00377>.
- [3] R. Molitor, P. Ko, B. Ally, Eye Movements in Alzheimer's Disease, *J. Alzheimers. Dis.* 44 (2014). <https://doi.org/10.3233/JAD-141173>.
- [4] M.L.G. de F. Pereira, M. Villa, D.H. Koh, M. von Z. de A. Camargo, A.F. Belan, M. Radanovic, M. Pomplun, O.V. Forlenza, Saccadic eye movements associated with executive function decline in mild cognitive impairment and Alzheimer's disease, *Alzheimer's Dement.* 16 (2020) e040036. <https://doi.org/10.1002/alz.040036>.
- [5] K. Morita et al. "Eye movement as a biomarker of schizophrenia: Using an integrated eye movement score," *Psychiatry Clin. Neurosci.* 71 (2017) , 104–114. <https://doi.org/10.1111/pcn.12460>.
- [6] J. Fielding, T. Kilpatrick, L. Millist, O. White, Antisaccade performance in patients with multiple sclerosis, *Cortex*. 45 (2009) 900–903. <https://doi.org/10.1016/j.cortex.2009.02.016>.
- [7] C.K. Sheehy, E.S. Bensinger, A. Romeo, L. Rani, N. Stepien-Bernabe, B. Shi, Z. Helft, N. Putnam, C. Cordano, J.M. Gelfand, R. Bove, S.B. Stevenson, A.J. Green, Fixational microsaccades: A quantitative and objective measure of disability in multiple sclerosis, *Mult. Scler. J.* 26 (2020) 343–353. <https://doi.org/10.1177/1352458519894712>.
- [8] H.D.-M. MA McDonald, CH Stevenson, HM Kersten, Eye Movement Abnormalities in Glaucoma Patients: A Review, *Eye Brain*. 14 (2022) 83–114.
- [9] S.C. Kolbe, T.J. Kilpatrick, P.J. Mitchell, O. White, G.F. Egan, J. Fielding, Inhibitory saccadic dysfunction is associated with cerebellar injury in multiple sclerosis, *Hum. Brain Mapp.* 35 (2014) 2310–2319. <https://doi.org/10.1002/hbm.22329>.
- [10] T. Rempe, N. Dastgheyb, A. Miner, M. Palomino, R. Kinkel, D. Liston, J.S. Graves, Quantification of Smooth Pursuit Dysfunction in Multiple Sclerosis, *Mult. Scler. Relat. Disord.* (2021). <https://doi.org/10.1016/j.msard.2021.103073>.
- [11] A. Serra, C.G. Chisari, M. Matta, Eye movement abnormalities in multiple sclerosis: Pathogenesis, modeling, and treatment, *Front. Neurol.* 9 (2018). <https://doi.org/10.3389/fneur.2018.00031>.
- [12] Y. Backner, P. Petrou, H. Glick-Shames, N. Raz, H. Zimmermann, R. Jost, M. Scheel, F. Paul, D. Karussis, N. Levin, Vision and vision-related measures in progressive multiple sclerosis, *Front. Neurol.* 10 (2019). <https://doi.org/10.3389/fneur.2019.00455>.
- [13] E.M. Frohman, T.C. Frohman, D.S. Zee, R. McColl, S. Galetta, The neuro-ophthalmology of multiple sclerosis, *Lancet Neurol.* 4 (2005) 111–121. [https://doi.org/10.1016/S1474-4422\(05\)00992-0](https://doi.org/10.1016/S1474-4422(05)00992-0).
- [14] M.R. MacAskill, T.J. Anderson, Eye movements in neurodegenerative diseases, *Curr. Opin. Neurol.* 29 (2016) 61–68.
- [15] T. Anderson, M. MacAskill, Eye movements in patients with neurodegenerative disorders, *Nat. Rev. Neurol.* 9 (2013). <https://doi.org/10.1038/nrneuro.2012.273>.
- [16] C.K. Sheehy *et al.*, "High-speed, image-based eye tracking with a scanning laser ophthalmoscope," *Biomed. Opt. Express*. 3 (2012) 2611. <https://doi.org/10.1364/boe.3.002611>.
- [17] M. M. Bartuzel *et al.* "High-resolution, ultrafast, wide-field retinal eye-tracking for enhanced quantification of fixational and saccadic motion," *Biomed Opt Express* 11, 3164-3180(2020). High-resolution, ultrafast, wide-field retinal eye-tracking for enhanced quantification of fixational and saccadic motion
- [18] Michał Meina *et al.* "Accurate calibration of beam trajectories in scanning optical imaging systems," *Opt Lett.* Nov 1; 46(21), 5377-5380. <https://doi.org/10.1364/OL.431577>.

Title: Fiber tip-based surface-enhanced Raman simultaneous pathogen detection in cerebrospinal fluid samples

Category: Health

In-vivo rapid detection and identification of pathogens, such as bacteria, viruses, fungi, and parasites, in patients' cerebrospinal fluid (CSF) samples continue to be a challenge for clinical diagnostics. Bacterial infections can cause death in a couple of hours. According to the latest reports from the World Health Organization, antimicrobial resistance is of major growing public health concern. Resistant bacterial infections alone are associated with nearly 4.95 million deaths per year, with 1.27 million deaths directly attributed to AMR. The latter occurs when bacteria, viruses, fungi, and parasites change over time and no longer respond to medicines. Hence, it is crucial to directly identify and distinguish pathogens' origin and to monitor the treatment response to their resistance. Current detection methods typically require in-vitro sample monitoring. The most commonly used technique that gives a fully reliable result is polymerase chain reaction (PCR). However, the test is ready within up to four hours and is an expensive bacterial monitoring procedure. On the other hand, bacterial resistance tests and identification are performed through CSF culture examination, which can last up to four days whereas bacterial infections can cause irreversible health damage if the right treatment is not applied. To the best of our knowledge, there is a lack of a rapid, cheap, in-vivo detection method that can immediately distinguish between bacteria and viruses, between types of bacterial infections and meanwhile serve as a tool to monitor a real-time response to treatment. Hence, we propose a label-free and highly specific optical sensor based on Raman spectroscopy. It has recently been tested in our laboratory the possibility to distinguish E-coli and Staphylococcus aureus in the same sample by implementing machine-learning algorithms on the obtained Raman spectra. Nevertheless, to further enhance the signal and precisely detect more variants of pathogens within the same sample, surface-enhanced Raman Spectroscopy (SERS) can be applied. The use of SERS substrates in the identification between N. meningitides, S. pneumonia, and H. influenza bacteria has already been demonstrated. Yet, the mentioned study has been performed in in-vitro conditions. To overcome this problem, we go a step further in this proposal and suggest fiber tip-based SERS substrates that can be placed inside the lower spine through the lumbar puncture and give real-time information on different pathogens present in the CSF as well as show the dynamics of the treatment. The possibility to fabricate SERS substrates on the glass fiber tip using two-photon polymerization (2PP) has already been reported. Therefore, to further bring this technology closer to clinical implementation, in this project we will fabricate SERS substrates on a biocompatible polymer fiber, which can stay in a body without causing additional discomfort. The fiber-based SERS system will be connected to the illumination and collection parts, which will be fully integrated on a polymer platform. A commercially available 785nm laser diode will be used as an illumination light source with up to 50mW output power. The light from the laser to the fiber will be coupled through 2PP printed microlens. On the detection side, the collected signal from the SERS substrate through the fiber will be coupled to the commercial spectrum analyzer. Obtained spectral data will be proceeded with ML algorithms to precisely identify a present pathogen.

This research is possible to realize since Brussels Photonics at Vrije Universiteit Brussel, where I am a postdoctoral researcher, has longstanding experience in fiber and plasmonic sensing, micro- and nanofabrication and biophotonics. The Photonics Innovation Center at VUB has facilities for in-house [two-photon polymerization fabrication, micro- and nanostructure metrology and Raman measurements](#). Moreover, we collaborate with the [UZ-Brussel hospital](#), which provides us with clinical samples from patients. This project will result in a proof-of-concept demonstration that can play a revolutionary role in pathogens detection in CSF saving lives. Finally, through outreach events, the knowledge on bacterial infections and damage to our health will be spread helping to prevent the overlooked pandemic of antimicrobial resistance.

**Title:** Fiber tip-based surface-enhanced Raman simultaneous pathogen detection in cerebrospinal fluid samples

**Category:** Health

### State-of-the-art

In-vivo rapid detection and identification of pathogens, such as bacteria, viruses, fungi, and parasites, in patients' cerebrospinal fluid (CSF) samples continue to be a challenge for clinical diagnostics. Remember, that CSF is the fluid that flows in and around our brain and spinal cord. Any pathogen present in CSF is direct damage to our neural system controlling all that a human does. Bacterial infections can cause sudden death or sepsis in a couple of hours [1]. However, bigger damage can cause unawareness of the effective treatment of bacterial infections caused by antimicrobial resistance (AMR). According to recent reports from the World Health Organization, AMR is of major growing public health concern. Resistant bacterial infections alone are associated with nearly **4.95 million deaths per year**, with **1.27 million deaths** directly attributed to AMR [2]. The high death rate due to bacterial infections and AMR is a global problem. In the same report, for 2019, six main pathogens: **E-coli**, **Staphylococcus aureus**, **K pneumoniae**, **S pneumoniae**, **Acinetobacter baumannii**, and **Pseudomonas aeruginosa**, were each responsible for more than 250 000 deaths associated with AMR (see Fig.1). Mentioned pathogens caused 95% of death attributable to AMR. AMR occurs when bacteria, viruses, fungi, and parasites change over time and no longer respond to medicines.

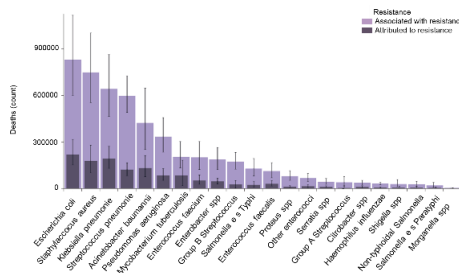


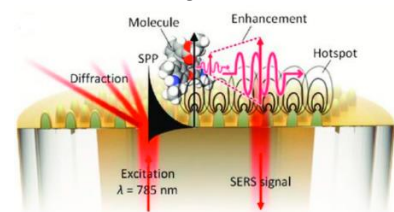
Fig.1 Global deaths attributable to and associated with bacterial antimicrobial resistance by the pathogen by 2019. Estimates were aggregated across drugs, accounting for the co-occurrence of resistance to multiple drugs. Error bars show 95% uncertainty intervals [2].

Hence, it is crucial to directly identify and distinguish pathogens' origin and real-time monitor the treatment response to their resistance. Current detection methods typically require in-vitro sample monitoring. The most

commonly used technique that gives a fully reliable result is polymerase chain reaction (PCR). In 2009 the development of a multiplex PCR array system has been reported which enabled the detection of the 9 most important bacterial and viral pathogens found in Danish meningitis patients. The assay showed high sensitivity and selectivity for target pathogens. Moreover, the method provides a valuable supplement to the traditional techniques, such as microscopy and culture of cerebrospinal fluid (CSF) samples in a routine diagnostic setting, and results can be available within 1 workday [3]. In another work, a method based on a modified broad-range PCR and an oligonucleotide microarray for the simultaneous detection and identification of 12 bacterial pathogens at the species level has been reported [4]. The total assay took only three hours, including all the steps from the DNA extraction to PCR and microarray sequence. Although the latter method increased the speed of the test, it still requires hours to provide reliable results. In addition, PCR is an expensive bacterial monitoring procedure. On the other hand, bacterial resistance tests and identification performed through CSF culture examination are still required for a complete image. This can last up to four days whereas bacterial infections can cause irreversible health damage if the right treatment is not applied. Optical biosensors are being developed based on various detection techniques for bacteria and virus monitoring in CSF to improve the duration while keeping the precision of the tests. One of the most used detection

techniques that shows the highest sensitivity among optical biosensing mechanisms is surface plasmon resonance (SPR). Employing the Kretschmann configuration, detection of *N. meningitidis* DNA has been demonstrated using the ZnO matrix. The developed biosensor exhibits a low limit of detection (5 ng/μl) and high specificity over a wide concentration range of DNA (10–180 ng/μl) [5]. Moreover, SPR-based biosensors are widely used in virus detection [6]. Despite its high sensitivity and selectivity, the SPR sensor has the disadvantage of being dependent on surface functionalization and is capable to detect only a single target molecule that will specifically bind the immobilized ligand. Therefore, using the plasmonic enhancement phenomenon, label-free and more general detection methods such as surface-enhanced Raman spectroscopy (SERS) analysis of biological molecules can provide rich structural information as well as quantitative and qualitative analysis, with the ability to simultaneously detect multiple analytes. More importantly, **SERS can be applied to samples under physiological conditions in a non-destructive way**. It has been successfully demonstrated that SERS spectroscopy combined with multivariate analysis (PCA) can be applied with high accuracy to label-free, simultaneous, and rapid identification of all three meningitis pathogens: *Neisseria meningitidis*, *Haemophilus influenzae*, and *Streptococcus pneumoniae* in clinical CSF samples [7]. In this work, the authors have, however, tested ex-vivo samples treated in the laboratory upfront. Moreover, they used Au/Ag-coated polycarbonate membranes with different pore sizes. Nevertheless, it is reported that the **most sensitive SERS substrates are those with a periodical distribution of metallic nanostructures** [8]. To further increase the importance and application domain of the SERS technique it is often combined with another popular player in the field of optical biosensors such as fibers. Essentially, lab-on-fiber technology envisions a noble class of fiber devices arising from the integration of the micro- and nanoscale functional materials achieving fibers' new functionalities but, more importantly, the capability to outperform miniaturization performance, power consumption, etc. Fabrication of SERS substrates on a fiber tip has recently been achieved by using two-photon polymerization (2PP) technology (see Fig.2). In addition, the final device has been tested for E-coli detection in suspension [9]. The results are promising as characteristic Raman peaks of the bacteria in suspension have been possible to distinguish from the background signal, yet, only a single bacteria in ex-vivo condition has been studied. The measurements are performed with integration times as small as 2.5ms (10 averages). Moreover, the fabricated SERS substrates' minimum dimension was 300nm.

Fig.2 Schematic illustration of the excitation of the hotspots (nanopillars) fabricated on the fiber tip through 2PP technology [2].



## Objectives

Combining all the expertise in design, fabrication, metrology of SERS substrates and optical fibers, moreover considering the existing gaps between technologies and clinical requirements for pathogen monitoring, in this project we propose a **unique solution for rapid, in-vivo detection capable of the immediate differentiation between types of bacteria and viruses**. We go a step further in this proposal and suggest fiber tip-based SERS substrates that can be placed inside the lower spine through the lumbar puncture (see Fig.3) and give **real-time information on different pathogens present in the CSF**.

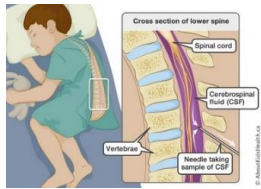


Fig.3 Local anaesthetic lumbar puncture

It is important to note, that **after 2 years the project will pave the way for further development** through the online monitoring of the treatment dynamics through the fiber sensor left inside the body for a long period. **The novelty of this project will be the implementation of the fiber-tip SERS sensor in clinical diagnostics with real samples directly in the human body. Moreover, to the best of our knowledge, a biocompatible polymer fiber for the first time will be used to fabricate a SERS substrate on the tip. The fiber will be inserted and kept inside the body through a needle for the whole duration of the test. Therefore faster detection and analysis duration is crucial. Finally, the data acquisition and processing methods will allow for simultaneous detection of various types of pathogens without additional steps in between.**

As already mentioned, SERS substrates can be fabricated on the fiber tip using 2PP. Nevertheless, in the reported work the smallest nanostructures had 300nm dimensions. However typical SERS substrates have dimensions lower than 100nm. Hence, to achieve high enhancement factors (EF) for SERS substrates and consequently reduce the integration time during Raman spectra acquisition, one needs to push the limits of 2PP nanofabrication. **During my research, I have recently obtained 2PP conditions to fabricate nanostructures smaller than 200nm** (see Fig.4, left). Scanning Electron Microscope (SEM) image shows that the diameter of the conical nanostructures at the bottom is around 300nm while the brightest cycle corresponding to the top of the structures is less than 200nm. The fabrication is reproducible and guarantees good periodic structures (see Fig.4, right).

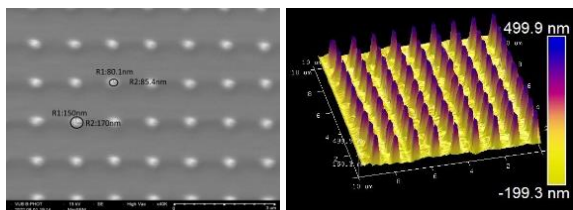


Fig.4 SEM image (top) of a 2PP fabricated conical nanostructures and Atomic Force Microscope (AFM) 3D image (bottom) of periodic nanostructures.

Note, the preliminary results have been presented during Advanced Photonics Congress 2022 [10].

The proposed research is possible to realize since Brussels Photonics at Vrije Universiteit Brussel, where I am a postdoctoral researcher, has longstanding experience in fiber and plasmonic sensing, micro- and nanofabrication and biophotonics. The Photonics Innovation Center at VUB has facilities for in-house [two-photon polymerization fabrication, micro- and nanostructure metrology and Raman measurements](#).

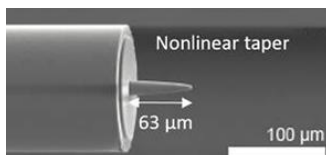


Fig.5 Microstructured down-taper with internal air channels.

To translate these nanostructures on the fiber tip, in this project the expertise of B-PHOT in fabricating structures on a fiber tip (see Fig.5) will be used [11]. Moreover, the group has also extensive experience in fiber design, fabrication and sensing. Recently the development of a biodegradable and biocompatible fiber has been reported [12].

In addition to this expertise, in collaboration with [UZ-Brussel hospital](#), we have recently performed preliminary Raman measurements on E-coli and Staphylococcus aureus samples both separately as well as together in the same suspension. The obtained Raman signal is later studied with PCA (see Fig.6). The PCA plot shows a clear separation between two bacteria. The classifiers confirm this: Support Vector Machine (SVM) classification test accuracy is 93%, while Multi-layer Perceptron (MLP) classification gives 100% accuracy.



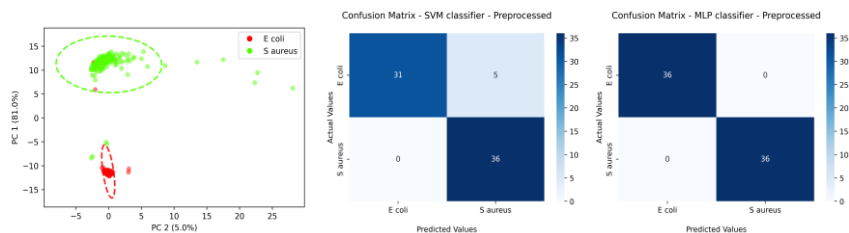


Fig.6 Summarizing the spectra into two dimensions based on the datapoints' variance clusters the classes. The ellipses show the classes' 95% confidence level. SVM and MLP classifiers give 93% and 100% accuracy, respectively.

The measurements are performed with a Renishaw Raman confocal InVia microscope. Although the results are good, the used **integration time is currently up to 10 minutes. This will be reduced by applying SERS substrates. A polymer fiber, as well as SERS fabricated with 2PP will reduce the price of the sensor.** To further decrease the cost of the final device, **2PP fabricated polymer microlenses will realize light coupling to and from the fiber.** The fiber-based SERS system will be connected to the illumination and collection parts, which will be fully integrated on a polymer platform. A commercially available 785nm laser diode will be used as an illumination light source with up to 50mW output power. The light from the laser to the fiber will be coupled through a 2PP printed microlens. On the detection side, the collected signal from the SERS substrate through the fiber will be coupled to a commercial spectrum analyzer.

### Outcome and Impact

This project will result in a **proof-of-concept demonstration for clinical monitoring** as well as in the **research domain to study various pathogens and their resistance to drugs.** On-time detection and identification of bacterial infections can save lives. Finally, through outreach events, the knowledge on bacterial infections and damage to our health will be spread helping to prevent the overlooked pandemic of antimicrobial resistance. Moreover, the master's students who will work on the project will gain experience in the life-important research topic and get involved with fibers, SERS, lasers and detectors. This project fits into the 17 sustainable development goals (SDGs) of the UN to transform our world. In particular, it is devoted to good Health and Well-being ensuring healthy lives and promoting well-being for all at all ages.

### Ethical approval

This project will be carried out in collaboration with UZ-Brussel hospital. The partners from the hospital will submit an amendment to the Ethics Committee for using test samples from patients.

### Work packages

**WP1 (0-6 months)** - Different samples obtained from the hospital and benchmarked with commercial devices will be tested at B-PHOT using our Renishaw Raman confocal InVia microscope. Based on the obtained data, machine learning (ML) algorithms will be developed for the correct identification of many pathogens. In parallel, simulations on COMSOL multiphysics will be carried out to design SERS substrates.

**WP2 (6-12 months)** - After the optimal design, the SERS substrates will be fabricated with 2PP technology using a Nanoscribe Professional GT. Initially, the substrates will be fabricated on a flat borosilicate piece. Next, these substrates will be characterized through AFM and SEM images. Finally, sensitivity, EF and limit of detection (LOD) will be measured and compared with the simulations. In parallel, the CAD design of SERS on the fiber tip will be prepared for simulations on COMSOL. The optimal coupling and collection conditions will be defined for the fabrication. By

August 2023, initial results will be obtained and presented at the Optical Sensors and Sensing Congress in Munich.

**WP3 (12-18 months)** - The SERS substrates fabricated on the flat borosilicate piece will next be tested with the samples from the hospital. The obtained data will be verified by the ML algorithms developed in WP1. Modifications will be performed if required. In parallel, the fabrication of SERS on the fiber tip will be carried out with 2PP technology, as well as the microlens fabrication. The fabricated device's characterisation will be done with continuous AFM and SEM measurements. A master thesis will be carried out within WP2 and WP3

**WP4 (18-24 months)** - In the final quarter of the project, the fibre tip SERS sensor will be placed inside a needle and integrated on the polymer-based platform for light coupling and collection. First clinical tests will be performed. Feedback and data will be collected for the further optimization of the device. Moreover, results will be presented at FiO+LS 2024.

### Risk & Mitigation

Risk	Related task	Level	Impact	Solution
Sample delay from the hospital	WP1-WP4	High	Delay in measurements	We could also obtain commercial samples.
Metrology devices' limited availability	WP1-WP4	Middle	Delay in measurements	As part of the PhotonHub EU project, I can use devices from the project partners.
Unknown pathogens	WP1, WP4	Middle	Misinterpretation of results	Discussion with medical doctors and microbiologists.
Too low sensitivity	WP2-WP4	High	Too long measurement time	Additional optics, external to the polymer platform, will be added to increase sensitivity.

### References

1. Sudden Natural Death|Infectious Diseases; M.A.Dada, et.al. (2005).
2. Global burden of bacterial antimicrobial resistance in 2019: a systematic analysis; C.JL. Murray et.al. (2022).
3. Eight-Plex PCR and Liquid-Array Detection of Bacterial and Viral Pathogens in Cerebrospinal Fluid from Patients with Suspected Meningitis; M. K. Bøving, et.al. (2009).
4. Rapid identification of bacterial pathogens using a PCR- and microarray-based assay; A. K. Järvinen et.al. (2009).
5. Detection of Neisseria meningitidis using surface plasmon resonance based DNA biosensor; G. Kaur et.al. (2016).
6. A comprehensive review on plasmonic-based biosensors used in viral diagnostics; A. M. Shrivastav et.al. (2021).
7. Rapid detection and identification of bacterial meningitis pathogens in ex vivo clinical samples by SERS method and principal component analysis; A. Kamińska, et.al. (2016).
8. Highly sensitive, reproducible and uniform SERS substrates with a high density of three-dimensionally distributed hotspots: gyroid-structured Au periodic metallic materials; L. Wu, et.al. (2018).
9. Fiber-Optic SERS Probes Fabricated Using 2PP For Rapid Detection of Bacteria; J. A. Kim, et.al. (2020).
10. Two-Photon Polymerization based fabrication of SERS substrates for biosensing applications; T. Chalyan. (2022).
11. Two-Photon Polymerization-based Laser Direct Writing of Mode Conversion Down-tapers for Physical Contact Fiber-to-Chip Coupling; K. Vanmol, et.al. (2021).
12. Microstructured Optical Fiber made from Biodegradable and Biocompatible Poly (D, L-Lactic Acid)(PDLLA); A. Gierzej, et.al. (2022).

# EXECUTIVE SUMMARY

Name of Proposal: SpheroScan: WGM-Enabled Microbial Sensor

Category Addressed: 20th Anniversary Challenge (Optica Foundation)

The physical effect of Whispering Gallery Modes (WGM) changes the way how pathogens can be detected in agriculture and food production. It allows inline monitoring of production processes at any stage of the supply chain, thus establishing an unprecedented level of efficiency, quality, and safety.

SpheroScan, an WGM-enabled sensor system, features capabilities that none of the existing analytical technologies can match, namely:

- very short time to result (< 3 min.)
- on-site process integration
- automated operation independent from a laboratory

The sensor data is immediately actionable to control the production process. Continuous monitoring provides mass data which is a valuable source for process improvements.

This is made possible by an innovative optical technology in combination with microbiological methods. Micro beads from polystyrene are brought to produce the WGM effect when excited with laser light. Such beads with a biologically functionalized surface are added to the liquid analyte and work as highly specific probes. Once the target organism or molecule binds to a bead, its WGM light signature (Fluorescent Resonance Signature – FRS) changes thus giving an immediate indication of the target's presence.

Current quality control methods for pathogens are slow, laborious and give only spotlight data depending on the intervals of probing and the availability of laboratory capacity. It can take up to four days to detect Salmonella in animal products using standard lab-based methods. This means that quality control results typically are only available after production or even after shipping. In case of a contamination, entire lots must be disposed of and the loss absorbed by the manufacturer. If shipped already, consumers can be harmed with more negative consequences for the manufacturer. At this stage, it also becomes a matter of public health. Salmonella infestations alone cause medical costs of about \$4.1 billion each year in the USA with over one million cases and close to 400 deaths (USDA: “Cost Estimates for Foodborne Illnesses”, 2018).

SpheroScan allows the producer to take action while a process is running (Advanced Process Control). Thus, major savings in raw materials, time and energy can be achieved. It will also make visible the sources and drivers of contaminations (e.g. in the supply chain) and help to reduce . This will raise the awareness for quality and provide the basis for proactive quality management in agriculture and food processing. Hence, we envision food production on a new level of efficiency and quality that will bring food on the consumers' table that is fresh, unadulterated and save at the same time.

Currently, a lab version of the sensor is available to refine the FRS-technology and test it with varying target organisms. Within the Project, a first field demonstrator of an inline measuring FRS system will be built and tested in a first field application, namely Legionella contaminations in fresh water supply. The results of the study will be published in a scientific journal and presented at an international scientific conference.



# PROPOSAL

## Problem Statement/Objectives

The overarching objective of the SpheroScan sensor is to put microbial analysis “ahead of the curve”. Today, this is generally not the case for the processing of organic substances (whether in batches or continuously). Test results from the laboratory only come back after the point where the process and its results can be influenced. Pausing the process to wait for test results is not an option.

Hence, the shortcomings of current analytical methods, namely that they are time-consuming, depending on the availability of qualified staff, and performed in a laboratory remote from the production process, leave no other option than to run such processes “blind-folded”. As the real nature of the food product and its ingredients cannot be known at the time of processing, past experience takes the place of evidence, trial and error the one of data-based optimization. This describes the current situation in many bio-process industries.

The negative consequences of the current predicament are plenty. *Manufacturers and farmers* can only react to contaminations after the fact. For them, the economic damage from an adverse event is the primary concern. It can mean a total loss of product or life stock, treatment costs, lower output, and less business. In the USA alone, the economic damage in the fields of agriculture and food processing is estimated at USD 18 bn each year (2018). According to the Worldbank, lost productivity and medical expenses due to food-borne illnesses amount to USD 110 bn annually in low- and middle-income countries (2018).<sup>1</sup>

For *consumers*, it means that food is a source of health hazards, one way or the other. Since inline quality monitoring is not feasible, contaminated food does get into the market from time to time. Preventative measures instead of monitoring do not always make things better. The excessive use of antibiotics in farming that leads to multi-resistant bacteria (MRSA) in our food is just one example for this. Heavy processing (e.g. heating) of foodstuffs or the adding of preservatives does not improve food quality either.

Finally, food contaminations are also a concern for *public health*. Salmonella infestations alone cause medical costs of about \$4.1 billion each year in the USA with over one million cases and close to 400 deaths (USDA: “Cost Estimates for Foodborne Illnesses”, 2018).

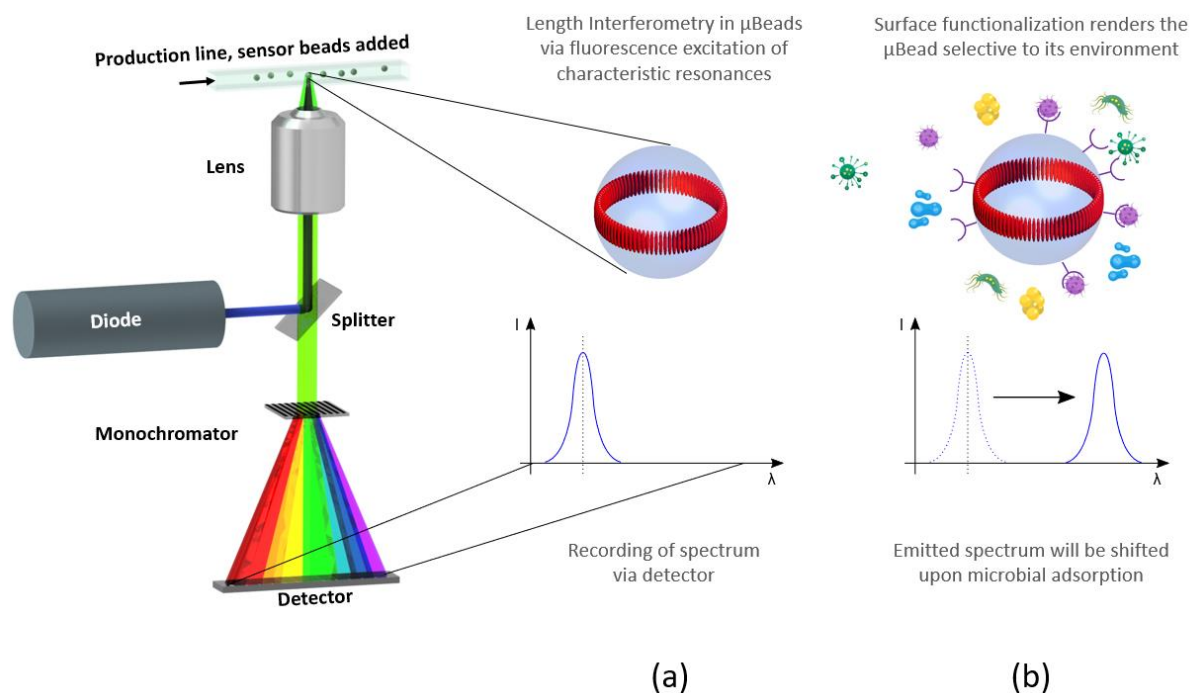
With the Fluorescent Resonator Signature (FRS) technology, we strive for a novel approach to label-free bacterial and fungal detection. The idea is based on fluorescent, specifically functionalized polymer microbeads, which bind to their target organism while freely floating in the analyte. Current label-free biosensors are mostly designed as microfluidic devices with the bio-functionalized surface formed on one of the channel walls. In contrast to this, microbeads roam the analyte and thus raise the chance of hitting their specific targets. Figure 1 shows a schematic of a basic implementation of the sensor. Sensor beads are added to a reactor line containing the analyte to be screened for microbes. When the microbeads pass the measuring channel, the organic dye embedded in the polymer is excited by laser. Due to the effect of Whispering Gallery Modes formed inside the beads by their fluorescent radiation, they start to glow at a characteristic wavelength which can be read out optically (Fig. 1a). A numeric algorithm based on the Mie theory is then applied to the fluorescence spectra for the assessment of potential binding events on the sensor surface. Depending on the particles’ specific surface functionalization, only selected microbes bind to the microbeads, thereby causing changes in the FRS of the respective sensor particle (Fig. 1b). Since the sensors are microscopic particles, their number can

---

<sup>1</sup> <https://www.worldbank.org/en/news/press-release/2018/10/23/food-borne-illnesses-cost-us-110-billion-per-year-in-low-and-middle-income-countries>

be made sufficiently high to allow for reliable statistics on the concentration of the targeted microbe in the monitored bioreactor system. Also, this sensor scheme can be expanded easily to the simultaneous detection of more than a single type of microbe by variation in the specific bio-functionalization of the microbeads and their dye.

Currently, a lab device of the sensor is being operated to demonstrate the potential of this FRS-technology. Within the Project, a first field demonstrator of an inline measuring FRS system will be built and tested with an application under relevant ambient conditions. As a first application, legionella contamination in fresh water supply shall be tested.



**Fig. 1:** Schematic of Fluorescent Resonator Signature (FRS) sensing: (a) optical set-up for excitation and read-out of FRS from the free-floating sensor beads; (b) illustration of the change in FRS by specific binding of targeted microbes to the microbead surface.

## Outline of tasks/Work plan

The operating principle of a possible demonstrator is shown in Fig. 2. For building the demonstrator, the following work packages are needed:

**System design and component selection:** Based on the existing findings and the design of the laboratory setup, a system will be conceived that is adapted to the actual environment including a degree of automation. At this stage, standard components will be used for the most part. Customized parts will be avoided if possible.

**Microbead functionalization:** Specific surface-functionalized  $\mu$ Beads must be fabricated for the application. For this purpose, standard micorbeads will be functionalized with off-the-shelf antigens and tested for their sensitivity and specificity in the respective medium.

**Software development:** A device software based on Matlab has to be developed which controls all the components of the setup and thus ensures an automated test procedure. For this purpose, a simple user interface must be created which is suitable for measurements in the field.





**Assembly and alignment:** The supplied components, in particular the optical components of the spectrometer, must be mounted and adjusted. The entire system must be put into operation.

**System lab test:** In a first laboratory test, the demonstrator must be checked for its function. Any errors that occur must be corrected.

**Field test:** Together with a cooperation partner who runs a relevant application, a field test will be carried out. The purpose is to obtain data that allow to draw conclusions about the suitability of the system for the respective application.

**Data analysis:** Evaluation of the collected data and preparation of a publication and a presentation.

**Documentation:** Documentation of the project will be carried out during the entire project period.

**Publication:** The results of the project will be published at a relevant international conference.

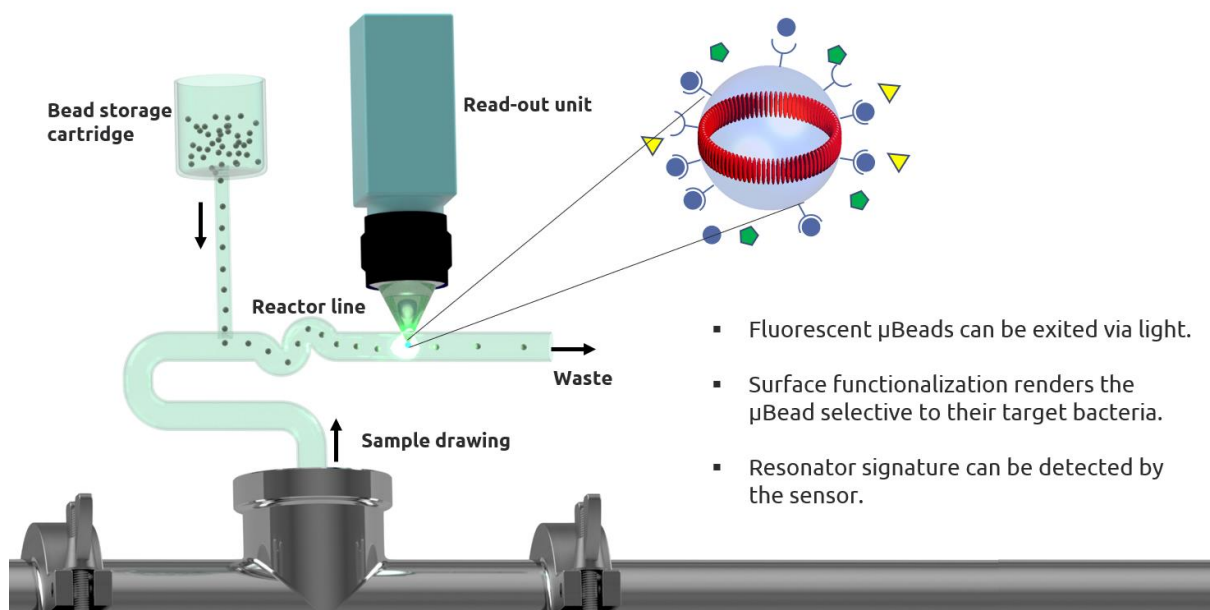


Fig. 2: Schematic of a possible functional demonstrator for field deployment of FRS technology. Small samples of the liquid analyte are taken from a pipeline or a bioreactor and brought into reaction with the specifically surface-functionalized  $\mu$ Beads. The  $\mu$ Beads can then be read optically.

## Timeline

Work Package	Personnel	M1	M2	M3	M4	M5	M6	M7	M8	M9
System design and component selection	price winner	█	█							
Delivery time of the components	price winner		█	█	█					
Microbead functionalization	laboratory assistant		█	█	█					
Software development	price winner			█	█	█	█			
Assembly and alignment	price winner					█	█			
System lab tests	laboratory assistant						█	█		
Field test	price winner							█	█	
Data analysis	laboratory assistant / price winner						█	█	█	
Documentation	laboratory assistant / price winner		█	█	█	█	█	█		
Publication	price winner									█



As a result of the project, an automated demonstrator based on the FRS technology will be available. This will be used to test drinking water for Legionella and Salmonella in a field trial at a water supply utility. The device must be able to withstand the harsh ambient conditions of a production plant and be easy to operate. At the same time, robust and reliable test results are expected. At the end of the field test, the recorded data will be evaluated and conclusions drawn as to the suitability of the FRS technology for the seamless monitoring of liquid foodstuffs. The results of the study will be published in a scientific journal and presented at an international scientific conference.

### **Outcome**

With the SpheroScan sensor, bio-processes can be monitored 24/7 with a cycle rate of 3-5 minutes. Its capabilities include both qualitative and quantitative testing as well as multiplex testing for the simultaneous identification of different targets. The sensor can be placed at critical steps in the production process, take probes automatically, and feed test results into the data network of the plant. These basic features, namely continuous monitoring, low time-to-result and automated analysis set the SpheroScan apart from lab-based methods.

These properties make the sensor suitable to operate inline and to provide near-real-time data. The data can be used in closed-loop applications to control ongoing processes (Advanced Process Control) and to react immediately to adverse events. This will have significant consequences for producers: they can take countermeasures during production to save their output or to minimize the damage, and they can safely avoid that contaminated product is released to the market. Moreover, they can effectively barr contaminated raw product from entering their plant based on results from incoming inspection within minutes.

In addition, the sensor delivers process data on biological substances continuously and in large numbers. With advanced statistical and AI methods, this data can be used to drive process improvements (e.g. yield, energy consumption or cycle time) and to inform new product development. Preventative maintenance (e.g. cleaning cycles) is another application which is enabled by mass data.

What adds further to the utility of the SpheroScan sensor is the fact that it does not require a laboratory or operator attendance. This means further cost savings, and it allows to free up qualified personnel for working with the sensor data and getting a better understanding of their processes.

For consumers and for public health, this new sensor will reduce health hazards because it allows producers and manufacturers to monitor the quality of their products in a reliable, timely, and seamless fashion. Questional regulatory standards, like total cell count, can be augmented (if not replaced) by the accurate identification of specific contaminants. This will help to reduce health system costs significantly. It will also help to improve the quality of food because producers can be confident to get a good product even with less (or without) antibiotics or preservatives.

### **Impact and Outlook**

The major impact of inline microbial analytics with the SpheroScan sensor will be a new and wholesome concept of “quality” in the entire food supply chain. This is made possible by the data that the new sensor provides, immediately and at the point of presence, about specific microbial targets. This puts manufacturers, wholesalers and regulatory authorities in a position to do their job before a food product is released and passed on. It will allow to identify and trace back to its source any product issues and, thus, to establish real accountability at every stage of food production. Only evidence-based quality control can do this.

This change will be driven primarily by the economic advantages of inline quality control. Producers will be able to reduce their cost and production risk once they can control and optimize their processes

based on real data and scientific principles. It will also give them more leverage on their suppliers. SpheroScan will allow them to specify and rate the quality of their inputs, e. g. raw milk delivered to a dairy plant. The quality level of the milk will have an impact on the price paid to the farmer.

This, in turn, will have an impact on the farmer and the way cows are kept, fed, and treated. Farmers may take a closer look at their suppliers of feed or of livestock. The concept of One Health stresses the connection between animal health and human health and highlights the importance of seamless quality control along the entire food supply chain. The SpheroScan sensor provides a key component for this approach to work, namely the ability to connect the dots and to trace back cause and effect along the supply chain.

It is, therefore, a stepping stone for improved public health, animal health, and food safety in the 21. century. SpheroScan can contribute in a meaningful way to improve both the efficiency and quality of food production. This will not only benefit people in the industrialized world but also offer the prospect of improving the availability of affordable and wholesome food in low-resource countries.

### **Literature Review**

As thoroughly worked out in the recent review of Prada et al., “Technique Evolutions for Microorganism Detection in Complex Samples: A Review” (1), the development of fast, sensitive and reliable techniques for microbial detection is still in its infant stage. The most promising approaches rely on cytometry, Raman spectroscopy, and Surface Plasmon Resonance, but either lack reliability or are still significantly above the required detection limits, e.g. 1 CFU/mL for Legionella in drinking water (2). The method applied by FluIDect is based on the real-time analysis of the Fluorescence Resonance Signature (FRS) of fluorescent microbeads (3). This approach is sensitive even to the detection level of single bacteria (4) and, most importantly, can be applied in a high-throughput, statistical fashion (5), thus improving performance and reliability at low microbe concentrations as typical, e.g., for drinking water. Therefore, at the moment, it appears as the only technique suitable for in-line detection of microbes at the required level of accuracy (6).

- 1) Pierre Prada et al., Technique Evolutions for Microorganism Detection in Complex Samples: A Review, *Appl. Sci.* 2022, 12, 5892. <https://doi.org/10.3390/app12125892>
- 2) For example: 100 CFU/mL in S Nair et al., Rapid label-free detection of intact pathogenic bacteria in situ via surface plasmon resonance imaging enabled by crossed surface relief gratings - *Analyst*, 2020 - [pubs.rsc.org](https://pubs.rsc.org)
- 3) M. Himmelhaus, Microsensors on the Fly, *Optik & Photonik*, Vol. 11(1), pp. 43-47, (2016)
- 4) Hai-Cang Ren et al., High-Q microsphere biosensor - analysis for adsorption of rodlike bacteria, *Vol. 15, No. 25 / OPTICS EXPRESS*, 2007
- 5) M. Charlebois et al., Toward Automatic Label-Free Whispering Gallery Modes Biodetection with a Quantum Dot-Coated Microsphere Population, *Nanoscale Res Lett* (2010) 5:524–532 DOI 10.1007/s11671-010-9541-1
- 6) S. Rentschler, Emerging Options for the Diagnosis of Bacterial Infections and the Characterization of Antimicrobial Resistance, *Int. J. Mol. Sci.* 2021, 22(1), 456; <https://doi.org/10.3390/ijms22010456>



## LIGHTING RESEARCH SOLUTIONS LLC

Research • Education • Design • Development • Verification  
www.LightingResearchSolutions.com | Philadelphia, PA 19122 USA

# The Earth and its inhabitants deserve darkness

September 12, 2022

### *Executive Summary*

Humans use electric light at night to illuminate our homes, our streets, sidewalks, outdoor sporting events, buildings, facades, landmarks, bridges, parks, parking lots, and commercial and industrial properties. Nearly everything we interact with at night is illuminated. Light at night has become essential to our feeling of security and to our ability to extend our activities into the evening.

But this is not without cost. Outdoor electric light sources placed by humans to illuminate the night—often called *artificial* or *anthropogenic* (i.e., “human generated”) light at night (ALAN)—is seriously eroding natural light-dark cycles across the planet, having marked impacts on the biological functions and rhythms of humans, plants, and animals. This includes impacts on mortality (through light attraction or aversion), disruption of migratory and diurnal patterns, increasing or decreasing population size, altering natural competition, disturbing inter-species communication, and negative impacts on human health and well-being.

A significant portion of the Earth’s population—especially in Europe and the Americas—now experiences light-polluted nights, which creates a sky glow that limits or eliminates our view of the night sky, poses significant problems for amateur and professional astronomical observations, negatively impacts animals that use the night sky for navigation, and wastes a significant amount of energy at great financial cost. The estimated cost of this wasted energy exceeds USD \$7 Billion.

Without serious intervention, the problem is projected to get worse.

The objective of this project is to advance the science in architectural lighting with the goal of developing strategies to reduce the negative impacts of ALAN, to disseminate research findings to spread awareness of these negative impacts, and to develop a lighting standard to minimize the negative impacts of ALAN (especially sky glow).

Corresponding to these objectives, the project will constitute three tasks.

**Task 1 | advance research:** the goal of this task is to advance research in the field of architectural engineering to provide actionable guidance for the lighting professionals that design and install lighting systems. The outcome of task 1 is a journal-quality research paper that will be submitted to an Optica journal, likely Optics Express. The impact of the work is two-fold: 1. It addresses the problem closer to the source (i.e., the lighting professionals installing lighting systems), and 2. It sends a message to the non-lighting researchers of the world that lighting researchers are interested in protecting darkness for the Earth and its creatures.

**Task 2 | disseminate and advocate:** to goal of task 2 is to spread awareness of the negative impacts of light at night by participating in up to 5 industry and industry-adjacent events. This will be done by presenting current and future research findings and recommendations. The outcome of this task is a series of educational presentations and scientific reports. The impact of this work is an increased awareness and sensitivity to the impacts of the lighting systems that our industry installs.

**Task 3 | reduce sky glow:** the goal of this task is to develop a joint standard of the American National Standard Institute (ANSI) and the Illuminating Engineering Society (IES) through my role as Co-Chair of the Color Committee of the IES. The outcome of this task is a lighting standard that provides recommendations for reducing the negative impacts of ALAN, especially sky glow. The potential impact of this work is large. IES standards are influential, and this will be the first standard of its kind for an industry that is dealing with the problem directly.

Thank you for your time and consideration. I am grateful for this potential opportunity. Thank you.



# The Earth and its inhabitants deserve darkness

September 12, 2022

## *Proposal*

### **Background (and literature review)**

Humans use electric light at night to illuminate our homes, our streets, sidewalks, outdoor sporting events, buildings, facades, landmarks, bridges, parks, parking lots, and commercial and industrial properties. Nearly everything we interact with at night is illuminated. Light at night has become essential to our feeling of security and to our ability to extend our activities into the evening.

But this is not without cost. Outdoor electric light sources placed by humans to illuminate the night—often called artificial or anthropogenic (i.e., “human generated”) light at night (ALAN)—is seriously eroding natural light-dark cycles across the planet [Sanders 2020; Kyba et al 2017]. The negative impacts of ALAN are endless and have marked impacts on the biological functions and rhythms of living organism [Jagerbrand and Bouroussis 2021]. Here are some examples:

- It disrupts circadian rhythms (e.g., in humans [Tahkamo et al 2018])
- It suppresses melatonin—the “hormone of darkness”—in humans (e.g., Brainard 2001; Thapan 2001) and other vertebrates (e.g., Grubisic et al 2019)
- Decreases survivability and growth (e.g., in coral reef fish [Schligler et al 2021])
- Impacts hormone levels of animals, alters daily onset of activity in diurnal species and life history traits (e.g., number of offspring, predation, and cognition [Sanders et al 2020])
- It impacts cognition and sea finding in sea turtles [Berry et al 2013], a disorientation that causes them to wander significant distances from the ocean, leaving them susceptible to predators and accidental death by humans<sup>1</sup>
- Alters the balance of species, biodiversity, and predation in entire ecosystems [Spoelstra et al 2015]
- Produces physiological responses in plants, which impacts their seasonality, growth, and resource allocation [Bennie et al 2016]
- Disrupts visual signaling between flowers, pollinators, and predators (e.g., hawkmoths [Briolat et al 2021])
- Light attracts some organisms (moths, frogs, sea turtles), concentrating them as a food source to be preyed upon (or creating a trap which exhausts and kills them). Light repels some organisms, pushing them out of their habitat. Light alters the day/night patterns, resulting in insufficient sleep and associated consequences.<sup>2</sup>
- And many, many more.

ALAN is also a significant contributor to sky glow, which is described as “the brightening of the night sky that results from the scattering and reflection of light from the constituents of the atmosphere [of Earth]...in the direction of the observer” [IES 2021]. Sky glow limits or eliminates our view of space and the stars, poses significant problems for professional and amateur astronomy, has negative impacts on animal behavior patterns (e.g., on migratory species [UN 2021]), and wastes a significant amount of energy at great financial cost (estimates exceed USD \$7 Billion [Gallaway et al. 2010]).

---

<sup>1</sup> <https://myfwc.com/wildlifehabitats/wildlife/sea-turtle/lighting/disorientations/>

<sup>2</sup> Paraphrased from: <https://myfwc.com/conservation/you-observe/lighting/criteria/>

This problem will not fix itself. Instead, the problem is getting worse. Most of the world's population now experiences light polluted nights. Here, I will quote some of the world's experts to illustrate the severity and dire nature of the situation:

“About two-thirds of the World population and 99 per cent of the population in the United States (excluding Alaska and Hawaii) and European Union live in areas where the night sky is above the threshold set for polluted status. ...about one-fifth of the World population, more than two-thirds of the United States population and more than one half of the European Union population have already lost naked eye visibility of the MilkyWay.” [Cinzano et al 2001]

“...more than 80% of the world and more than 99% of the U.S. and European populations live under light-polluted skies. The Milky Way is hidden from more than one-third of humanity, including 60% of Europeans and nearly 80% of North Americans. Moreover, 23% of the world's land surfaces between 75°N and 60°S, 88% of Europe, and almost half of the United States experience light polluted nights.” [Falchi et al 2016]

Without serious intervention, light pollution will get worse, wasting a significant amount of energy and increasing the negative impacts of ALAN on humans, plants, and animals.

## Problem Statement/Objective

Humans light up the nighttime environment generating light pollution that wastes a significant amount of energy and causes a suite of deleterious impacts on humans, plants, and animals. This includes [Jagerbrand and Bouroussis 2021], but it not limited to, the following:

- **Mortality rates of species:** species attracted to light may be killed. As a concentrated food source for their predator(s), this may lead to an imbalance in the ecosystem
- **Migratory patterns:** light disrupts natural migratory patterns and disorients animals. This kills a significant number of migratory birds each year.
- **Increasing or decreases population size:** light can increase or decrease foraging of various species
- **Alters natural competition:** light may benefit some species at the expense of others
- **Communication:** light can disturb species-specific communication
- **Health and circadian rhythm:** ALAN impacts various physiological processes, such as hormone production and maintaining a normal circadian rhythm, which impacts human health and well-being.

Without serious intervention, the problem is expected to worsen. The objective of this project is to advance research in architectural lighting with the goal of developing strategies to reduce the negative impacts of anthropogenic light at night, to disseminate research findings to spread awareness of these negative impacts, and to develop a lighting standard to minimize the negative impacts of ALAN (especially sky glow).

## Outline of Tasks/Work Plan

**Task 1 | advance research:** I recently co-authored a journal article that has been accepted to LEUKOS, the journal of the Illuminating Engineering Society. It is currently in the typesetting phase. In that work, my co-author and I detail how light source spectral power distribution—i.e., the specific combination of wavelengths of radiation that a light source emits—impacts sky glow. We then provide a specification framework for architectural lighting practitioners to consider the impact of light sources on sky glow during the design phase of their lighting projects and provide actionable recommendations.

With additional funds, I will perform a research project that evaluates the impact of light sources on outcome measures other than sky glow and attempt to extend actionable recommendations for the design of architectural lighting systems and products to other negative impacts of light at night. This

is important because many studies in this area—for example, those referenced above—are performed by ecologists, biologists, environmentalists, and the like, and *not* by applied lighting scientists (like myself), whom have direct knowledge and experience with the design and construction of lighting systems. The negative impacts of ALAN are vast, and the problems are complex; solutions require cross-disciplinary input that include applied lighting scientists. This funding will help immensely in that effort.

I am favorable to publishing this work in one of Optica’s journals. Optics Express is frequently used by authors in my industry. I have previously published there as well [see Esposito and others 2022].

**Task 2 | disseminate and advocate:** To spread awareness of the negative impacts that light at night has on humans, plants, and animals, my current and future research findings will be presented at industry and industry-adjacent conferences and events. An estimated five (5) events will be attended over the course of the project period. The goal is to be a speaker at each event. Note that this requires a submission to each event and is not a guaranteed outcome.

**Task 3 | develop lighting standards:** In the lighting industry, there are currently no lighting standards that attempt to reduce the negative impacts of light at night. Without lighting standards, lighting manufacturers, lighting designers, and building owners are left to figure it out on their own.

In the co-authored work I described in Task 1, my co-author and I call for lighting standards organization, such as the Illuminating Engineering Society (IES) or the International Commission on Illumination (CIE) to seriously consider developing standards around these ideas. I am an influential member of the IES Color Committee, a committee that may partially or entirely host this work. Importantly, however, this is a substantial undertaking and will be most successful with a dedicated front-person, developer, and advocate. I am positioned to lead this, and financial support for this project would allow me to focus my time and attention here.

## Outcomes

- **Outcome of Task 1:** This task will produce a research paper that advances the science of the negative impacts of anthropogenic light at night with a focus on actionable advice for mitigating the problem.
- **Outcome of Task 2:** The outcomes of Task 2 will include either or both of the following: when accepted to speak at an industry or industry-adjacent event, I will produce presentation materials used to educate, spread awareness, and disseminate research findings; when not accepted to speak at such an event, research papers will be submitted for paper presentations to be included in the conference proceedings
- **Outcome of Task 3:** The goal of Task 3 is to develop a lighting standard that provides a framework for architectural lighting professionals to design and specify light sources to reduce negative impacts of ALAN, especially sky glow. With funding support, I will be able to lead the development of this standard in my role as co-chair of the Color Committee of the Illuminating Engineering Society. The desired outcome for Task 3 is a lighting standard from the IES in support of reducing the negative impacts of ALAN.

## Impact

- **Impacts of Task 1 | knowledge and lighting recommendations:** additional research and recommendations provided through the lens of the architectural lighting industry has the potential to have broad impact since lighting professionals are closer to the source of the problem (i.e., the implementation of electric light at night). A secondary effect of this work is that it sends a message to the non-lighting researchers of the world that lighting research scientists are interested in preserving darkness to reduce humanity’s impact on the environment.
- **Impacts of Task 2 | awareness:** awareness inside and outside of the lighting industry is necessary to create broad change. Spreading awareness within the lighting industry, which has



the potential to significantly reduce the amount of light spilled into the nighttime environment, is necessary for measurable change.

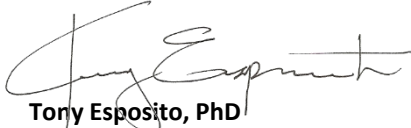
- **Impacts of Task 3 | reduced impact on sky glow:** The lighting industry is currently missing lighting standards developed on sound science that provide actionable guidance. Developing such a standard has the potential to profoundly reduce the negative impacts of light at night and drastically reduce sky glow.

The negative impacts of human-generated light at night are vast and getting worse. There are currently no lighting standards intended to reduce these negative impacts and not enough actionable guidance exists for members of the lighting industry to attempt to do so on their own. Funding this project has the potential to set in motion a cascade of lighting standards development activity intended to darken our planet and minimize our impact on Earth's creatures.

## Acknowledgement

I want to thank Optica for this funding opportunity for work that is important, but otherwise difficult to secure funding for. I am grateful for the potential opportunity to fight for nighttime darkness for Earth's creatures. I look forward to hearing the outcome of your decisions.

Thank you,



**Tony Esposito, PhD**

Founder and Head Research Scientist  
Lighting Research Solutions LLC  
tesposito@LightingResearchSolutions.com

## Bibliography

Berry, M., Booth, D. T. & Limpus, C. J. Artificial lighting and disrupted sea-finding behaviour in hatchling loggerhead turtles (*Caretta caretta*) on the Woongarra coast, south-east Queensland, Australia. *Aust. J. Zool.* 61, 137–145 (2013).

Briolat, E.S., Gaston, K.J., Bennie, J. et al. Artificial nighttime lighting impacts visual ecology links between flowers, pollinators and predators. *Nat Commun* 12, 4163 (2021).  
<https://doi.org/10.1038/s41467-021-24394-0>

Brainard GC, Hanifin JP, Greeson JM, Byrne B, Glickman G, Gerner E, Rollag MD. Action spectrum for melatonin regulation in humans: evidence for a novel circadian photoreceptor. *J Neurosci.* 2001 Aug 15;21(16):6405-12. doi: 10.1523/JNEUROSCI.21-16-06405.2001. PMID: 11487664; PMCID: PMC6763155.

Conservation of migratory species (CMS). 2021. Impact of light pollution on different taxa of migratory species. Convention on the Conservation of Migratory Species of Wild Animals

Esposito T, Royer MP, Houser KW, "Measures of illuminant-induced metameric mismatch: theory, comparative analysis, and implications for application," *Opt. Express* 30, 14686-14708 (2022)

Gallaway T, Olsen RN, Mitchell DM. 2010. The economics of global light pollution. *Ecol Econ.* 69(3):658–665. <https://doi.org/10.1016/j.ecolecon.2009.10.003>

Grubisic, M.; Haim, A.; Bhusal, P.; Dominoni, D.M.; Gabriel, K.M.A.; Jechow, A.; Kupprat, F.; Lerner, A.; Marchant, P.; Riley, W.; Stebelova, K.; van Grunsven, R.H.A.; Zeman, M.; Zubidat, A.E.; Höölker, F. Light Pollution, Circadian Photoreception, and Melatonin in Vertebrates. *Sustainability* 2019, 11, 6400. <https://doi.org/10.3390/su11226400>

IES. 2021. ANSI/IES LS-1-21, Lighting Science: Nomenclature and Definitions for Illuminating Engineering. Illum Eng Soc [Internet]. <https://www.ies.org/standards/definitions/>

Kyba CCM, Kuester T, Sánchez de Miguel A, Baugh K, Jechow A, Hölker F, Bennie J, Elvidge CD, Gaston KJ, Guanter L. 2017. Artificially lit surface of Earth at night increasing in radiance and extent. *Sci Adv.* 3(11):e1701528. <https://doi.org/10.1126/sciadv.1701528>

Leena Tähkämö, Timo Partonen & Anu-Katriina Pesonen (2019) Systematic review of light exposure impact on human circadian rhythm, *Chronobiology International*, 36:2, 151-170, DOI: 10.1080/07420528.2018.1527773`

Sanders D, Frago E, Kehoe R, Patterson C, Gaston KJ. 2021. A meta-analysis of biological impacts of artificial light at night. *Nat Ecol Evol.* 5(1):74–81. <https://doi.org/10.1038/s41559-020-01322-x>

Schligler J, Cortese D, Beldade R, Swearer SE, Mills SC. Long-term exposure to artificial light at night in the wild decreases survival and growth of a coral reef fish. *Proc Biol Sci.* 2021 Jun 9;288(1952):20210454. doi: 10.1098/rspb.2021.0454. Epub 2021 Jun 9. PMID: 34102892; PMCID: PMC8187998.

Spoelstra, K., van Grunsven, R.H.A., Donners, M., et al. (2015) Experimental illumination of natural habitat – an experimental set-up to assess the direct and indirect ecological consequences of artificial light of different spectral composition. *Philosophical Transactions Royal Society B.* 370: 20140129. doi: 10.1098/rstb.2014.0129

Thapan K, Arendt J, Skene DJ. An action spectrum for melatonin suppression: evidence for a novel non-rod, non-cone photoreceptor system in humans. *J Physiol.* 2001 Aug 15;535(Pt 1):261-7. doi: 10.1111/j.1469-7793.2001.t01-1-00261.x. PMID: 11507175; PMCID: PMC2278766.

Jägerbrand, A.K.; Bouroussis, C.A. Ecological Impact of Artificial Light at Night: Effective Strategies and Measures to Deal with Protected Species and Habitats. *Sustainability* 2021, 13, 5991. <https://doi.org/10.3390/su13115991>

**Name:** Enabling wide accessibility of Optical Coherence Tomography (OCT) through the development of cost competitive systems based on low-cost, low-intensity noise supercontinuum (SC) sources. **Category:** Health.

**Intended Outcomes:** 1) Development of high-power, low-intensity noise SC sources based on cascaded Raman fiber lasers. 2) Development of compact OCT system using the novel SC source. 3) Experiments with animal models using the developed OCT system

Optical Coherence Tomography (OCT) is a life transformation technology that revolutionized health care industry. At the heart of OCT system contains a broadband optical source which enables low-coherence interferometry in the spectral domain (SD) and hence it is also called as SD OCT. Latest developments in optical sources having more than octave spanning bandwidth, and in high-speed optical scanning elements, enabled OCT in obtaining ultra-high resolution (few  $\mu\text{m}$ ) 2D and 3D images at high speeds and sensitivities that provide powerful monitoring and diagnostics capabilities of many diseases like Glaucoma, Skin cancer, Diabetic retinopathy, Coronary artery stenosis etc. Further, due to non-invasive nature, OCT provides highly comfortable and hygienic (without having to add any biomarkers) method of imaging biological systems and therefore, it was heralded as the most important technological development in ophthalmology. However, OCT technology is still very expensive and as per the latest (2021) Nature journal's review article, OCT systems cost around £30,000 to £100,000 and the systems are limited to typical clinical settings. This has significantly limited the access of OCT to only high-income developed countries. However, there are billions of people with the same healthcare needs from low-income and developing countries. For example, being from a remote village in developing country such as India I have seen many elderly people losing eyesight due to non-accessibility of OCT. As per 2021 statistics, there are about 80 million Indians having severe visual impairment out of which 8 million are blind. Given that current pace at which the OCT is advancing, these numbers are worrying, and millions of people would have been saved from blindness if only this technology is easily accessible and affordable. Motivated by this, the goal of this project is to enable accessibility of OCT technology to billions of underserved populations across the world through the development of cost competitive systems. The major contributor to the cost of the latest OCT systems is the broad-bandwidth optical source itself. This is because, the need for obtaining ultra-high axial resolution OCT images with higher speeds and sensitivities requires advanced broadband (multiple octaves spanning bandwidth) optical sources. Supercontinuum (SC) sources perfectly satisfy these requirements. SC is defined as broad bandwidth optical spectrum generation through nonlinear frequency conversion of an input pump laser which is focused to high intensities in a dielectric medium. The most useful form of SC is generated in optical fibers and has greater than octave spanning bandwidth ranging from visible to far infrared ( $2.5\mu\text{m}$ ), with average power spectral densities (PSDs) of  $>50\text{mW/nm}$ . In optical fibers, the entire bandwidth of SC is generated within the single waveguide mode and hence preserves the spatial coherence properties of the input laser. Such SC possesses brightness and focusing properties like a laser while having broad bandwidth like an incandescent white-light bulb. These characteristics make SC sources unique, and they have revolutionized many applications including OCT. High-peak power pulsed lasers are typically used as pumps for SC generation. However, costly nature of sophisticated pulsed lasers, low-average PSDs and significant amplified intensity noise in SC generated due to high peak powers used for SC generation makes them not only costly, but unsuitable for latest OCT requirements such as high SNR and high contrast images. Continuous wave (CW) SC, providing higher PSDs, are best suited and cost competent sources for OCT. However, their higher intensity noise levels (in demonstrated SCs so far) and the use of expensive specialty Photonic Crystal fibers (PCFs) make them not suitable for satisfying the latest requirements of OCT images and expensive. This is where I want to leverage my research expertise on wavelength agile, cascaded Raman fiber lasers (CRFLs) and low-intensity noise, high-coherence fiber lasers. Our latest work demonstrated, the best method to achieve CW low-intensity noise CRFLs over a wide wavelength tuning range ( $1\mu\text{m}$  to  $1.5\mu\text{m}$ ). It won the best student paper award at SPIE photonics west Fiber Lasers conference and was accepted for post-deadline presentation at Advanced Solid State Lasers conference. Such CRFLs can naturally be used as pump sources for low-noise SC generation using low-cost commercially available standard Telcom fibers (instead of PCFs). Inspired by this, the current proposal achieves the goal of much needed low-cost OCT technology, without compromising on the performance requirements, through the development of low-cost, low-intensity noise SC sources.

# Enabling wide accessibility of Optical Coherence Tomography through the development of cost competitive systems based on low-cost, low-intensity noise supercontinuum sources

## 1. Motivation - Optical Coherence Tomography and its importance

Optical Coherence Tomography (OCT) is a life transformation technology that has revolutionized health care industry by providing powerful medical diagnostic tools. It uses low-coherence light interferometry technique for obtaining high quality 2D and 3D images which are widely used for diagnosis of many diseases such as Glaucoma, Skin cancer, Diabetic retinopathy, Coronary artery stenosis etc. [1,2] A typical OCT system in the simplest form is shown in figure 1. It consists of a broad-bandwidth or low-coherence length optical source, and a Michelson interferometer with a reference mirror and a scanning optical element in the sample path of the light beam. The scanning optics in the sample path scans the sample under test (typically biological samples) laterally and the Fourier transform of the spectral interference detected using spectrometer and detector gives the axial (or depth) information. At the heart of the OCT system contains a broadband optical light source which enables low-coherence interferometry in the spectral domain (SD) and hence it also called as SD OCT. Latest developments in the optical sources having more than octave spanning bandwidth (called Supercontinuum) and the high-speed scanning optical elements, enable OCT in obtaining ultra-high resolution (typically of few  $\mu\text{m}$ ) 2D and 3D images at high speeds and high sensitivities which provide rich monitoring and diagnostic capabilities [1,3,4]. Further, due to its non-invasive nature, OCT provides highly comfortable and hygienic (without having to add any biomarkers) method of imaging biological samples and currently, it has been heralded as the most important technological development in ophthalmology.

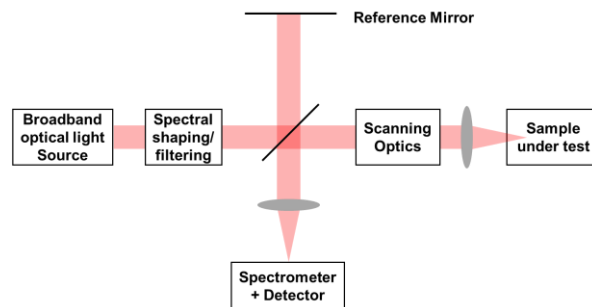


Fig. 1. Schematic of general OCT system based on low-coherence interferometer

## 2. Problem Statement and Objective

However, the technology of OCT is still very expensive and as per the latest review article published in Nature journal, OCT systems cost around £30,000 to £100,000 and the systems are limited to typical clinical settings [5]. This has significantly limited the access of OCT technology to only high-income developed countries. However, there are billions of people with the same healthcare needs from low-income and developing countries. For example, being from a remote village in developing country such as India I have seen many elder people losing eyesight due to non-accessibility of OCT technology. As per global estimates, India ranks 2<sup>nd</sup> having tens of millions of people with Diabetes Retinopathy (DR) which is the primary reason for vision loss. Currently, there are about 80 million Indians having severe visual impairment out of which 8 million are blind [6-8]. Given the current pace at which OCT is advancing, these statistics are worrying, and millions of people would have been saved from blindness if only they had access to affordable OCT technology. Motivated by this, the goal of this project is to

enable accessibility of OCT technology to billions of underserved populations across the world through the development of cost competitive systems as described in the following sections.

### 3. Reasons for high cost of the OCT systems and the limitations of existing cost-competitive solutions

The major contributor to the cost of latest OCT systems is the broad-bandwidth optical source itself. This is because, the need for obtaining ultra-high-resolution images with higher speeds and sensitivities has made the OCT to advance from conventional time domain (TD-OCT) systems to Fourier domain (FD-OCT) systems [4]. In FD-OCT systems, spectral interference waveform is used to get the axial/depth information of the sample under test in a single shot. This eliminates the scanning reference mirror that is needed in TD-OCT systems and therefore substantially increases the speed of image acquisition. Also, due to independent detection of spectral components, FD-OCT provides significant increase in sensitivities [4]. However, typical superluminescent laser diodes (SLDs) (SD OCT) and the wavelength swept sources (SS) (called as SS OCT) used in FD-OCT systems doesn't satisfy the requirement of ultra-high-resolution due to their limited spectral bandwidths (few 10s of nm) and wavelength tunability. This requires an optical source which has more than octave spanning bandwidth and was met partially by multiplexing multiple SLDs or SSs operating at different spectral regions. However, such an approach significantly increases the overall complexity and cost of OCT systems. Supercontinuum (SC) sources perfectly satisfy the large bandwidth requirements of OCT. SC is defined as broad bandwidth optical spectrum generation through nonlinear frequency conversion of an input laser which is focused to high intensities in a dielectric medium. The most useful form of SC is generated in optical fibers and has greater than octave spanning bandwidth ranging from visible to far infrared ( $\sim 2.5\mu\text{m}$ ) with average power spectral densities (PSDs)  $>50\text{mW/nm}$  [9]. Figure 2(a) shows the schematic of SC generation set-up in optical fibers. It consists of a narrow-bandwidth pump source and an optical fiber acting as a nonlinear medium which outputs more than octave spanning bandwidth SC light. Typically, input pump laser wavelength chosen should be in the anomalous dispersion region (but close to zero-dispersion wavelength (ZDW)) of the optical fiber being used for efficient SC generation [10]. In optical fibers, the entire bandwidth of the supercontinuum is generated within a single waveguide mode and therefore the generated SC preserves the spatial coherence properties of the input laser. Such SC possesses the brightness and focusing properties like a laser while having broad bandwidth like an incandescent white-light bulb. These characteristics make the SC source unique, and it has revolutionized many applications like OCT, microscopy, chemical sensing, optical metrology in manufacturing industries by enabling advanced monitoring and diagnostic features [10,11]. In 2008, SC based confocal microscope has been listed in top ten innovations [12].

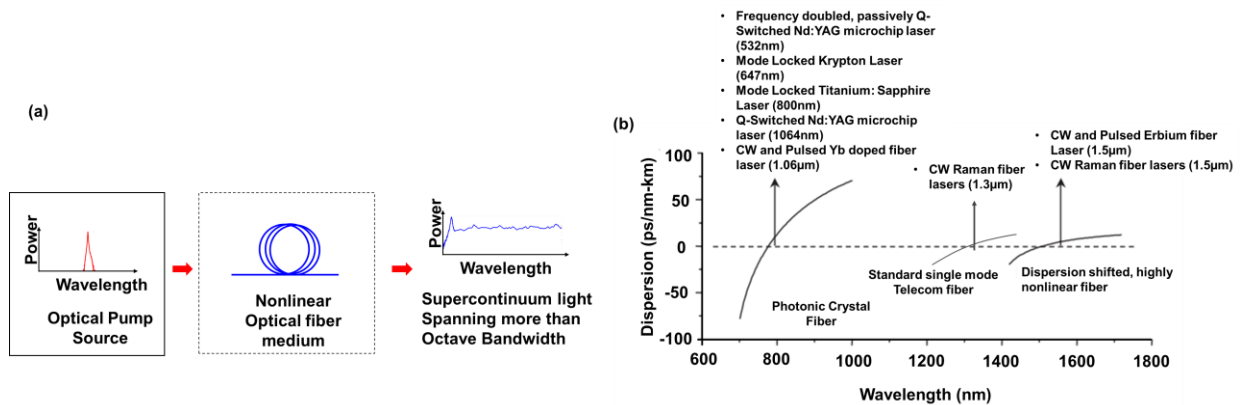


Fig. 2. (a) Schematic of Supercontinuum generation in optical fibers; (b) Dispersion profiles of different fibers and different pump lasers used for Sc generation

Typically, high-peak power (few kilowatts), femtosecond and picosecond bulk solid state pulsed pump sources operating in visible or near infrared spectral region are used to pump a photonic crystal fiber (PCF) for SC generation (see figure 2(b)). High-peak powers provides the advantage of efficient nonlinear processes generation inside PCF, which evolve into multiple octaves spanning SC. However, costly nature of sophisticated pulsed lasers, difficulties in free-space coupling of bulk pump lasers into PCF, very-low average PSDs of the generated SC (few  $\mu\text{W}/\text{nm}$ ), significant amplified intensity noise in SC generated due to high peak powers used to generate it, technological challenges associated with PCFs such as high scattering losses, difficulty in splicing to standard single mode fibers (SMFs), and the expensive specialty PCFs make such SC sources unsuitable for low-cost OCT systems [13]. On the other hand, continuous wave (CW) SC sources are attractive options for OCT systems due to their smooth spectral profile, high average PSDs ( $>50\text{mW}/\text{nm}$ ), relatively low intensity noise in the frequency range of interest of OCT (upto few MHz RF frequencies), all fiber configuration of the SC source (no free-space alignment hassles) [13]. Further, low-cost nature of CW pumps compared to pulsed pumps make CW SC more suitable towards the development of cost competitive OCT systems. Different types of optical fibers are used for CW SC generation depending on the pump's wavelength. Figure 2(b) shows the different fiber and corresponding different pump lasers used for SC generation. Due to their superior dispersion engineerable characteristics, PCFs are fabricated with zero-dispersion wavelengths (ZDW) around  $1\mu\text{m}$  where standard commercially available Ytterbium (Yb) doped fiber lasers can be used for CW SC generation. However, for all the reasons mentioned above, using PCFs for SC generation increases the overall cost of the OCT system. Dispersion shifted, highly nonlinear step index fibers (HNLFs) pumped with Erbium (Er) doped fiber lasers or Raman fiber lasers can also be used for SC generation [14-16]. Even though these fibers are easy to manufacture, easy to splice to standard SMFs and less costly compared to PCFs, because of the longer ZDW ( $1.5\mu\text{m}$ ), the short-wavelength extension of generated SC is limited which in turn limits the overall bandwidth of SC thereby limiting the resolution OCT. As of now, commercially available Telecom fibers are the best choice due to their lowest cost (lower than HNLFs), easy to manufacture, easy to splice, shorter ZDW (compared to HNLFs,  $1.3\mu\text{m}$ ) etc. However, there are no standard rare-earth doped fiber lasers available at  $1.3\mu\text{m}$  and by using our research expertise in development of wavelength agile cascaded Raman fiber lasers [17-19], we have demonstrated a high efficiency, high average PSD SC in standard Telecom fiber [20]. Even though the demonstrated system is the most cost-effective method of SC generation so far, however, the SC generated has higher intensity noise levels that it cannot meet the high SNR, high contrast requirements of OCT. Temporally stable, amplified spontaneous emission based (ASE) based pump sources are proposed to reduce the intensity noise SC in both PCFs [13] and Telecom fibers [9]. However, ASE sources are inherently noisy, and therefore might not be the optimal pump sources for nonlinear process like SC generation.

#### **4. Proposed approach to achieve low-cost OCT systems without compromising the performance**

This is where I want to contribute by leveraging my research expertise on CRFLs and low intensity noise, high-coherence fiber lasers. During my PhD, I have demonstrated advanced CRFLs which can produce power scalable high power fiber laser with ultra-wide wavelength tunability [19] and high spectral purity [22]. The work on high spectral purity CRFLs was accepted for post-deadline presentation at prestigious Advanced Solid-State Lasers (ASSL) conference in 2018. Recently, I demonstrated a best method (so far) to achieve CW low-intensity noise CRFLs over a wide wavelength tuning range ( $1\mu\text{m}$  to  $1.5\mu\text{m}$ ) [24]. Rather than using ASE sources as pump, which are inherently noisy, using low-intensity noise, phase modulated single frequency fiber sources in master oscillator and power amplifier configuration (MOPA) achieves very-low-intensity noise (compared to ASE pumping and conventional cavity-based laser pumping cases) cascaded Raman conversion [24]. Our results showed that greater than 36dB on intensity noise reduction can be achieved compared to cavity-based pump sources [24]. This work has won the best student paper award at prestigious SPIE Photonics West Fiber Lasers conference. Naturally, such low-intensity noise, CW CRFLs operating at  $1.3\mu\text{m}$  region, suit themselves to be the optimal pump sources for low-intensity noise CW SC generation in standard Telecom fibers. Inspired by this, figure 3 shows the detailed schematic of the proposed system. It follows our key idea in [24] where, we use low-intensity,



phase modulated single frequency fiber MOPA source for nonlinear frequency conversion instead of conventional cavity based and ASE based fiber sources.

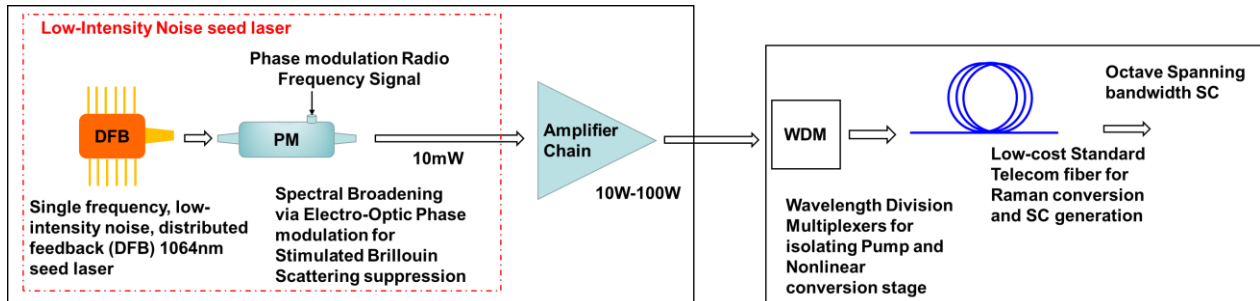


Fig. 3. (a) Proposed Schematic for low-intensity Supercontinuum generation using low-cost Telecom optical fibers

This is very crucial, as any nonlinear processes including SC exponentially amplifies the intensity noise present in the pump source. Therefore, the best way to achieve low-intensity noise nonlinear frequency conversion is to start with very low intensity noise (ideally zero) pump source.

## 5. Work Plan and Tasks

All the key tasks anticipated for the above proposed research work are outlined below with timelines:

Task	0-4 mos.	4-8 mos.	8-12 mos.	12-16 mos.	16-20 mos.	20-24 mos.
1. Assembly of 100W class high-power, low-intensity noise Yb fiber source at 1064nm						
2. Investigation of relative intensity noise (RIN) performance of high-power, single fiber lasers broadened to different optical bandwidths using multiple phase modulation schemes						
3. Assembly of highly efficient, stable, and reliable combined Cascaded Raman conversion and SC generation module.						
4. Study of impact of the above pump source's RIN on SC generation at various power and optical bandwidths and compare it with SC source generated using conventional Ytterbium fiber lasers Development of compact OCT system using this novel SC source						
5. Experiments with animal models using the developed OCT system						
6. Numerical analysis and performance evaluation in terms of SNR and contrast of the obtained images from the above OCT system						

## 6. Intended Outcomes

- 1) Development of high-power, low-intensity noise SC sources based on cascaded Raman fiber lasers
- 2) Development of compact OCT system using the novel SC source
- 3) Experiments with animal models using the developed OCT system

## 7. Impact

The impact of this work will be significant as it enables reduced cost OCT systems while not compromising on the performance in terms of intensity noise, image quality and speed. Such a system

will naturally enable wide accessibility of OCT systems to billions of underserved populations in low-income and developing countries across the globe.

## 8. References

1. <https://www.hamamatsu.com/eu/en/applications/medical-imaging/oct.html>
2. J. M. Schmitt, "Optical coherence tomography (OCT): a review," in *IEEE Journal of Selected Topics in Quantum Electronics*, vol. 5, no. 4, pp. 1205-1215, July-Aug. 1999, doi: 10.1109/2944.796348.
3. Ali S, Gilani SBS, Shabbir J et al. Optical coherence tomography's current clinical medical and dental applications: a review, *F1000Research* 2021, 10:310 (<https://doi.org/10.12688/f1000research.52031.1>)
4. Johannes F. de Boer, Rainer Leitgeb, and Maciej Wojtkowski, "Twenty-five years of optical coherence tomography: the paradigm shift in sensitivity and speed provided by Fourier domain OCT [Invited]," *Biomed. Opt. Express* 8, 3248-3280 (2017).
5. Chopra, R., Wagner, S.K. & Keane, P.A. Optical coherence tomography in the 2020s—outside the eye clinic. *Eye* 35, 236–243 (2021). (<https://doi.org/10.1038/s41433-020-01263-6>)
6. <https://www.who.int/en/news-room/fact-sheets/detail/blindness-and-visual-impairment>
7. <https://idronline.org/the-link-between-blindness-and-poverty/>
8. Praveena, A.K., Barik, R.R. and Tiwari, P.K., 2020. Prevalence of visual impairment and associated vision related quality of life among older adults in an urbanized village in Delhi. *International Journal of Community Medicine and Public Health*, 7(12), p.5068.
9. Xin Cheng, Jinyan Dong, Xin Zeng, Jiaqi Zhou, Shuzhen Cui, Weiao Qi, Zhiqian Lin, Huawei Jiang, Yan Feng, 130 W continuous-wave supercontinuum generation within a random Raman fiber laser, *Optical Fiber Technology*, Volume 68, 2022, 102825, ISSN 1068-5200, <https://doi.org/10.1016/j.yofte.2022.102825>.
10. Dudley, John M., and James Roy Taylor, eds. *Supercontinuum generation in optical fibers*. Cambridge University Press, 2010.
11. Nicolai Granzow, "Supercontinuum white light lasers: a review on technology and applications," *Proc. SPIE* 11144, Photonics and Education in Measurement Science 2019, 1114408 (17 September 2019); <https://doi.org/10.1117/12.2533094>
12. The Scientist: Top Innovations of 2008. Accessed 18 Mar 2020. <https://www.the-scientist.com/uncategorized/the-scientist-top-innovations-of-2008-44572>.
13. C. J. S. de Matos, S. V. Popov, and J. R. Taylor, "Temporal and noise characteristics of continuous-wave-pumped continuum generation in holey fibers around 1300nm", *Appl. Phys. Lett.* 85, 2706-2708 (2004) <https://doi.org/10.1063/1.1801175>
14. J.W. Nicholson, A.K. Abeeluck, C. Headley, M.F. Yan, C.G. Jorgensen Pulsed and continuous-wave supercontinuum generation in highly nonlinear, dispersion-shifted fibers *Appl. Phys. B*, 77 (2-3) (2003), pp. 211-218
15. V. Choudhury, S. Arun, R. Prakash, V.R. Supradeepa High-power continuous-wave supercontinuum generation in highly nonlinear fibers pumped with high-order cascaded Raman fiber amplifiers *Appl. Opt.*, 57 (21) (2018), pp. 5978-5982.
16. R. Prakash, V. Choudhury, S. Arun, V.R. Supradeepa Pump wavelength flexible, continuous-wave fiber supercontinuum using two-stage spectral broadening *IEEE Photonics Technol. Lett.*, 33 (1) (2021), pp. 31-34
17. V. R. Supradeepa, Y. Feng, and J. W. Nicholson, "Raman fiber lasers," *J. Opt.* 19, 023001 (2017).
18. Y. Feng and L. Zhang, "High power Raman fiber lasers" in *Raman Fiber Lasers*, Berlin, Germany:Springer, 2017.
19. V. Balaswamy, Santosh Aparanji, S. Arun, Siddharth Ramachandran, and V. R. Supradeepa, "High-power, widely wavelength tunable, grating-free Raman fiber laser based on filtered feedback," *Opt. Lett.* 44, 279-282 (2019)
20. S. Arun, Vishal Choudhury, V. Balaswamy, and V. R. Supradeepa, "Octave-spanning, continuous-wave supercontinuum generation with record power using standard telecom fibers pumped with power-combined fiber lasers," *Opt. Lett.* 45, 1172-1175 (2020).
21. V. Balaswamy, S. Ramachandran and V. R. Supradeepa, "High-power cascaded random Raman fiber laser with near complete conversion over wide wavelength and power tuning", *Opt. Exp.*, vol. 27, no. 7, pp. 9725, Apr. 2019.
22. J. Dong, L. Zhang, H. Jiang, X. Yang, W. Pan, S. Cui, X. Gu, and Y. Feng, "High order cascaded Raman random fiber laser with high spectral purity," *Opt. Express* 26, 5275 (2018).
23. Chu Qihui, Guo Chao, Yan Donglin, et al. Recent progress of high-power narrow linewidth fiber laser[J]. *High Power Laser and Particle Beams*, 2020, 32: 121004. doi: 10.11884/HPLPB202032.200144
24. Rashmita Deheri, Sarthak Dash, V. R. Supradeepa, and V. Balaswamy, "Cascaded Raman fiber lasers with ultrahigh spectral purity," *Opt. Lett.* 47, 3499-3502 (2022).

**Name of the project: MODular system for the MEasurement of the electric field by E-FISH technique (MOMEFISH)**

**Category: ENVIRONMENT**

**Highlights:**

- **Construction of a modular system for the effective measurement of the electric field. It has the advantage of adapting to different types of experiments, thus facilitating the diagnosis of this type of devices.**
- **It is of particular interest for the characterization of devices applied to fusion, such as plasma reactors, the new source of clean energy that is currently being developed.**

Plasma physics has become a field in its own right in recent decades. The many applications that have been developed in fields as diverse as medicine, industry, etc., clearly show the strategic importance of this field, which involves multiple lines of current and future development.

A project is presented for the design and construction of a modular system to measure the electric field in plasmas, using the Electric Field Induced Second Harmonic (E-FISH) technique. This technique allows the generation of a radiation with a wavelength equal to half of the original one (second harmonic). This project arises from the importance of measuring the electric field, and the difficulty of carrying out non-intrusive measurements in the discharge itself. Laser spectroscopy has been a widely used tool, but it is usually designed for a single experiment. The possibility of designing a diagnostic that fits multiple plasma physics devices represents an important advance in the field.

In this project we plan and design such a diagnostic, which will be tested in an air plasma generated with different geometrical conditions and different spatial resolutions. The laser system to be used for spectroscopy is a nanosecond NIR laser, which is a more economical option than other lasers of shorter time duration. Finally, this system will be tested in real plasma experiments located in different laboratories to check its reliability.

These preliminary measures will be used to study their application to devices such as fusion reactors, which are key to the energy and ecological transition that the world is currently undergoing.

**MODular system for the MEasurement of the electric field by E-FISH technique (MOMEFISH)**

**1. Background and state of the art**

Plasma physics has become a field in its own right in recent decades. The many applications that have been developed in fields as diverse as fusion, medicine, industry, etc., clearly show the strategic importance of this field, which involves multiple lines of current and future development<sup>1,2</sup>. The world of plasma physics is extraordinarily diverse, and plasmas with very different characteristics can be found: continuous discharges<sup>3</sup>, radio-frequency<sup>4</sup>, high-pressure<sup>5</sup>, atmospheric pressure<sup>6</sup>, different geometries<sup>7</sup>, etc.

Among the many parameters that characterize a plasma, the distribution of the electric field present in it is of vital importance for the complete study of the same. Knowing the distribution of the electric field within a plasma allows access to important parameters of the plasma, since it determines the flows of charged particles, their energy distributions and charge densities, as well as conditioning to a large extent the structure of the discharge itself<sup>8</sup>.

Despite the enormous interest in this parameter, it is extremely difficult to obtain quality experimental measurements of it, always claimed by the plasma physics community. Over the years, several strategies have been developed to measure the electric field in different types of plasmas. The first ones were through Langmuir probes, evolving to devices such as Pockels cells; both with good results, but very perturbative for the plasma at the local level, which makes a good spatial resolution impossible. Optical diagnostics soon emerged as a powerful technique for characterizing plasmas. The advent of lasers allowed direct access to the interior of plasmas, in addition to providing a spatial resolution hitherto non-existent in this class of experiments<sup>9</sup>. Over the years, different strategies for measuring the electric field have been developed with excellent results, but in many cases with complex experimental systems<sup>10-14</sup>.

In the 1970s, the technique known as E-FISH (Electric Field Induced Second Harmonic) was discovered, based on the generation of the second harmonic of an original radiation when it passed through a region in which there is an electric field<sup>15,16</sup>. The success of this technique is since it is independent of the gas to which it is applied, since the generation of the second harmonic does not depend on the medium through which the radiation passes, but only on the electric field it encounters in its path. This means that it can also be used to measure electric fields in vacuum, and even in air at atmospheric pressure<sup>17</sup>. In recent years this technique has been successfully applied to the measurement of the electric field in different types of plasmas<sup>18-21</sup>, as a powerful tool for this type of measures.

Despite all the advantages described so far, this kind of diagnostic setups often suffer from being extremely bulky and difficult to adapt from one experiment to another. Given the multitude of existing experimental systems, each with its own particularities, it would be very advantageous to have an electric field measurement system that could be installed in different experiments. This project proposes the creation of a modular system to advance in this direction. This project may have direct applications in systems such as fusion oriented devices, surgical scalpels, welding flames, thin film growth systems; all of them leading in their respective areas, both academic and industrial.

To conclude this section, it should be noted that the proponent has extensive experience in plasma physics and the experimental measurement of the electric field by means of

different optical techniques. Her doctoral thesis dealt with the measurement of the electric field distribution in hydrogen and deuterium discharges by laser spectroscopy<sup>22-25</sup>, and the subject of his postdoc was the characterization of an argon plasma column by spectro-tomography<sup>26</sup>. She is currently collaborating in the development of a system for the measurement of electric field distribution by induced fluorescence. Her experience in the area and necessary to tackle this project is duly demonstrated.

## **2. Objectives. Methodology and work plan**

The main objectives (indicated as GO) and specific objectives of the project (indicated as SO) will be detailed below, detailing how to proceed to achieve each of them.

### GO1. Simulation and preliminary study of electric fields in air at atmospheric pressure.

#### *SO1.1. Simulation of the expected electric field distribution for different geometrical distributions of the electrodes*

To know in advance, the distribution of the electric field that will be generated between the electrodes, it is proposed to simulate it using programs such as Quickfield. In this way, it will be possible to test different configurations, and to proceed to the tests in the most favorable conditions.

#### *SO1.2. Simulation of expected second harmonic generation in each configuration*

Since the second harmonic generation follows a quadratic dependence, it is straightforward to be able to estimate the amount of second harmonic radiation that will be generated at each geometrical condition of the discharge. This will be done by Matlab calculations in conjunction with Quickfield simulations.

### GO2. Construction of a flat electrode discharge for electric field generation in air at atmospheric pressure.

#### *SO2.1. Discharge installation*

The first step will be the installation of all the elements that constitute the discharge (power supplies, resistors, etc.) together with the electrodes. All the safety elements (grounding, insulating screens, etc.) will be checked.

#### *SO2.2. Testing of the discharge in different geometries and study of performances*

For this system to be a diagnostic prototype for different discharges, it is necessary to be able to test different spatial resolution needs; for which the simplest way is to modify the geometry of the discharge. For this, the installed discharge must allow to modify, at least, the distance between both electrodes. Based on the previous simulations (objective OE1.2), the resulting discharge will be characterized on the basis of the voltage-intensity characteristic curves.

### GO3. Tuning of a nanosecond laser system for second harmonic generation

Among the different options for measuring the electric field by E-FISH, femtosecond and picosecond lasers are usually used because, having a higher peak power in each of their pulses, they favor the generation of the second harmonic. However, nanosecond lasers also allow these measurements to be carried out and are a much more economical alternative to lasers with shorter temporal durations.

#### *SO3.1. Laser characterization with different focusing lenses*

The idea of a modular system is based on the possibility of having different beam focuses depending on the discharge to be studied, in order to adapt the laser focus to the required spatial resolution. For this purpose, lenses of different focal lengths will be available to be able to adapt to the distances implied by the sizes of different plasma experiments, which can range from a few millimeters or centimeters to the order of meters. A characterization of the focusing on each configuration, in terms of time and beam shape

(by means of a beam analyzer or camera) and energy (by means of photomultipliers) will be performed.

GO4. Electric field measurements

The final objective of the present project will be the experimental testing of the modular system under different conditions. Ideally, we will try to generate electric field conditions that have already been measured experimentally before in order to be able to consult with existing data in the literature.

*SO4.1. Electric field characterization at different spatial resolutions.*

Once the different geometrical configurations and the optimal optical designs for each of them have been studied, the electric field distribution in each of them will be measured exhaustively, with the optical configuration that best suits them.

*SO4.2. Testing of the experimental system in a real experiment*

As has already been indicated, the objective of this project is to serve as a starting point for the design of an experimental device for the measurement of the electric field that is easily adaptable to different plasma generation devices. In order to test the performance of this system, it is planned to test it in two experiments already in progress, with different characteristics:

- **MISTRAL:** magnetized plasma column about one meter long and 20 cm in diameter. Plasmas can be generated at different pressures and from different gases (argon, helium). This experiment is in the [PIIM](#) laboratory (Aix-Marseille Université - CNRS), in which the proposer has been working for about two years and with which the collaboration continues.
- **Jet-type plasma for substrate deposition.** In its simplest version, this device generates an argon jet, which involves measuring in a plasma with a size around centimeters. However, this experiment is easily convertible into a hollow cathode micro-discharge, with different orifices, so that in the same device we can propose different configurations, with experimental resolution needs in the order of millimeters. This system is in the laboratory [LSPM](#) (Université Sorbonne Paris Nord). The proponent maintains an active collaboration with this group and is involved in other projects with them.

**3. Scientific equipment and facilities**

Although, as mentioned above, the proponent has a long experience in the field of plasma physics, this work was developed in institutions different from the present one. This project represents the opening of a new line of research in the field of plasma physics into the [Applied Optics Complutense Group](#). This group specializes in the development of sensors and different optical characterizations, so this project represents an extension of the current horizons of the group. In the Faculty of Optics and Optometry of the Complutense University of Madrid, where this project will be carried out, there is space available for the installation of the new experimental device, in addition to being able to take advantage of various materials, such as power supplies, oscilloscopes, monochromator, various optomechanical material and common tools.

**4. Timeline**

The project is intended to be developed over 18 months. The following schedule details the different phases of work over the duration of the project. The work blocks into which the schedule is divided are detailed below and have been matched to the objectives described in section 2. The general objectives are summarized here for a better understanding of the schedule:



B0. Management. Project reports and documents related to the economic and scientific progress of the project. Publications of the results.

B1. Simulation of electric fields

B3. Laser system set-up

B2. Discharge construction

B4. Electric field measurement

Objectives	MONTH																	
	1	2	3	4	5	6	7	8	9	10	11	12	13	14	15	16	17	18
B0																		
B1																		
B1.1																		
B1.2																		
B2																		
B2.1																		
B2.2																		
B3																		
B3.1																		
B4																		
B4.1																		
B4.2																		

**5. Expected impact of the results**

The applications and objectives of the present project coincide with some of the pillars of the Horizon Europe agenda. Specifically with the global challenges labeled as "Climate, Energy and Mobility". Photonics is identified as a key technology in the objectives of Horizon2030; as well as the need to promote new safe and eco-responsible forms of energy, within which fusion is one of the main strategies to be pursued.

This project is defined as exploratory, with the aim of creating for the first time an accurate and modular system for measuring the electric field in plasmas or discharges in air. It is a research with a strong experimental character, which can be oriented to the realization of laboratory devices from which commercial applications can be derived. Therefore, the activity developed within the framework of the project could produce positive economic consequences. On the other hand, the project offers a very remarkable basic research aspect, so that, from the point of view of scientific knowledge in general, it is to be expected that this project will serve as a starting point for future research.

The results obtained from this research will be published in journals of impact in the field such as *Plasma Sources Sciences and Technologies*, *Spectrochimica Acta B*, *Journal of Applied Physics*, etc. It is expected that this project will generate at least two publications in quality scientific journals. In addition, the possible commercial interest of the developed technology justifies the possibility of exporting these results in the form of a patent.

The work developed will be presented in specific congresses of the area such as *International Symposium on Laser-Aided Plasma Diagnostics*, *Frontiers in Low Temperature Plasma Diagnostics*.

From an educational point of view, the Complutense Group of Applied Optics regularly welcomes students from both the Physics and Optics and Optometry undergraduate and master's degrees. Dr. González-Fernández has previous experience supervising undergraduate and master's degree theses. The project presented here is an excellent opportunity for recent graduates to have a first contact with an experimental laboratory and how to proceed to build and operate a real system. In addition, the opening of this new line of research represents an excellent opportunity for the development of doctoral theses.

**6. Future perspectives**

To conclude the report of this project, we include some of the possible future lines that this proposal opens up:

- Modification of the discharge, including cylindrical electrodes, widely used in plasma discharges.
- Inclusion in the experiment of a vacuum chamber to generate low-pressure discharges. Purchase of gases, e.g. argon, for the generation of gas plasmas.

**7. References**

- |   |   |
|---|---|
| <p><b>1</b> Samukawa, S. <i>et al. J. Phys. D Appl. Phys.</i> 45, 253001 (2012)</p> <p><b>2</b> Adamovich, I. <i>et al. J. Phys. D Appl. Phys.</i> 50, (2017)</p> <p><b>3</b> Ivanović, N. V <i>et al. J. Phys. D Appl. Phys.</i> 50, 125201 (2017)</p> <p><b>4</b> Lisovskiy, V. <i>et al. J. Phys. D Appl. Phys.</i> 39, 660 (2006)</p> <p><b>5</b> Chen, F. F. <i>Introduction to Plasma Physics and Controlled Fusion</i> (2016)</p> <p><b>6</b> Talsky, A. <i>et al. J. Spectrosc.</i> 2017, (2017)</p> <p><b>7</b> Hirose, C. <i>et al. Appl. Spectrosc.</i> 42, 815–819 (1988)</p> <p><b>8</b> Bogaerts, A. <i>et al. Appl. Phys. B Lasers Opt.</i> 75, 731–738 (2002)</p> <p><b>9</b> Gavrilenko, V. P. <i>Instruments Exp. Tech.</i> 49, 149–156 (2006)</p> <p><b>10</b> Lawler, J. E. <i>et al. Adv. At., Mol., Opt. Phys.</i> 34, 171–206 (1994)</p> <p><b>11</b> Czarnetzki, U. <i>et al. Phys. Rev. Lett.</i> 81, 4592 (1998)</p> <p><b>12</b> Booth, J. P. <i>et al. Appl. Phys. Lett.</i> 65, 819–821 (1994)</p> <p><b>13</b> Hebner, G. A. <i>et al. J. Appl. Phys.</i> 76, 4036–4044 (1994)</p> <p><b>14</b> Spasojević, D. <i>et al. J. Appl. Phys.</i> 119, 53301 (2016)</p> | <p><b>15</b> Godefroy, P. <i>et al. Appl. Phys. Lett.</i> 68, 1981–1983 (1996)</p> <p><b>16</b> Ward, F. <i>et al. Phys. Rev. Lett.</i> 26, 285–289 (1970)</p> <p><b>17</b> Cui, Y. <i>et al. 7th IEEE Int. Conf. High Volt. Eng. Appl. ICHVE 2020 - Proc.</i> (2020)</p> <p><b>18</b> Chng, T. L. <i>et al. Opt. Lett.</i> 45, 1942 (2020)</p> <p><b>19</b> Goldberg, B. M. <i>et al. Appl. Phys. Lett.</i> 112, (2018)</p> <p><b>20</b> Fujii, T. <i>et al. Opt. Lett.</i> 46, 238 (2021)</p> <p><b>21</b> Cui, Y. <i>et al. IEEE Trans. Dielectr. Electr. Insul.</i> 27, 2071–2077 (2020)</p> <p><b>22</b> Gonzalez-Fernandez, V. <i>et al. Plasma Sources Sci. Technol.</i> 26, 105004 (2017)</p> <p><b>23</b> Gonzalez-Fernandez, V. <i>et al. J. Appl. Phys.</i> 124, (2018)</p> <p><b>24</b> Gonzalez-Fernandez, V. <i>et al. Spectrochim. Acta Part B At. Spectrosc.</i> 105972 (2020)</p> <p><b>25</b> Gonzalez-Fernandez, V. <i>et al. Spectrochim. Acta - Part B At. Spectrosc.</i> 180, 106194 (2021)</p> <p><b>26</b> Gonzalez-Fernandez, V. <i>et al. Sci. Rep.</i> 10, 1–12 (2020)</p> |
|---|---|

## Project summary

### Title: Volumetric light modulation and measurement using virtual array imaging

#### Challenge category: Health

Our challenge is to enable volumetric imaging at high spatiotemporal resolution, using simple commercially available components. This is, lower complexity and higher spatiotemporal resolution than the many existing volumetric microscopy methods.

This problem is motivated by the study of neuroscience, where such volumetric imaging is needed to measure fast neuronal activity reporters with the goal to study, for example, information storage in the form of persistent neuronal activity.

To address limitations in spatiotemporal resolution of current volumetric microscopy, we propose to develop a new class of volumetric imaging method to enable fast, localized optical neurophysiology of live behaving zebrafish. We aim to enable record neuronal activity at 50 Hz bandwidth from a 700x500x110  $\mu\text{m}^3$  volume with cellular resolution. Unlike existing cell-resolved volumetric microscopes that only resolve up to  $\sim 10$  Hz, or existing fast volumetric microscopes that compromise cell resolution, our original approach to volumetric recording is multi-focal virtual image formation with a single camera. Each frame captures an array of virtual images focused at different depths of the sample, generated by reflections inside an optical cavity made with off-the-shelf components. The virtual array imposes different path lengths onto sections of the imaging aperture, thereby allowing simultaneous focusing at multiple depths on a volumetric sample while maintaining a diffraction-limited resolution.

Our hypothesis is that virtual array microscopy would enable high-speed volumetric activity recordings with cellular resolution, and that its implementation would allow probing fast dynamics of excitatory synaptic release during persistent activation in the whole zebrafish brain. The long-term goal of this project is to understand neuronal circuit function during animal behaviors by enabling high-resolution, high-speed volumetric optical neurophysiology for larval zebrafish.

**Specific Aim 1. Investigate volumetric image formation using a virtual array.** This Aim will test whether multifocal imaging generated by a reflective light cavity can be used to capture three-dimensional data with high resolution and will characterize performance of custom image reconstruction algorithms.

1.1 Implement prototype volumetric microscope. A mirror arrangement will be designed to simultaneously focus an array of virtual images onto the camera of a standard epifluorescence microscope.

These advances have the potential to enable fast, localized, wide volumetric microscopy for study of neurophysiology and thus to expand knowledge about neural mechanisms of behaviors and of psychiatric disorders.

Moreover, our proposed solution using virtual arrays of multifocal images is widely applicable to any volumetric or multiplane optical measurements. For example, virtual array imaging could be combined with off-axis holography to record 3D light fields for transmission matrix characterization of complex scattering systems. Virtual array imaging would be also applicable to measure multiple images of an object in an ultrafast sequence, due to the differential delay in path length incurred by each virtual image. The same design principles could even also enable 3D light projection by creating multiplane patterns in a sample at multiple depths from different areas of a projection device.

## A. Background

**Behavior and neurophysiology measurement.** One central goal in neuroscience is to understand how behavior including learning and cognition arise from brain activity patterns. Measurements of neuronal activity allow establishing correlations among sensory inputs, neuronal activations, and behavioral outputs. Fluorescent activity indicators are measured in live model animal systems<sup>1</sup> using optical microscopy, including scanning two-photon (2P) microscopy that can be used to record  $\text{Ca}^{2+}$  transients in ~12k neurons of a live behaving mouse brain<sup>2</sup>. Zebrafish maintain their location in a familiar territory even in the presence of flowing waters<sup>3</sup>. Previous work has uncovered that zebrafish larvae remember visual motion information over many seconds to guide their choice on tail movement direction<sup>4</sup>. However, it is unclear whether the persistence of information is mediated by an intrinsic slow biophysical response<sup>5</sup>, or if it is mediated by a fast excitation-inhibition balance<sup>6</sup>. Fast molecular reporters of neuronal activity<sup>7</sup> including excitatory synaptic release<sup>8</sup> and membrane voltage<sup>9</sup> in principle allow optical measurement of these transients during behavior with enough time resolution to discriminate sustained recurrent activity from intrinsic slow responses.

**State-of-the-art volumetric brain imaging.** The motivation to capture intracellular  $\text{Ca}^{2+}$  dynamics from neuronal volumes has driven many fluorescent microscopy innovations, recently reviewed by Weisenburger and Vaziri<sup>1</sup>. The main differences among these approaches rest on the nature and distribution of fluorescence excitation and of image formation. Linear single-photon (1P) fluorescence excitation can be applied to a whole plane or volume concurrently at low illumination power, thereby facilitating high frame rates when images are captured by a camera. Nonlinear 2P excitation using ultrafast pulsed lasers must cover the volume sequentially or with some degree of parallelism, which can be discriminated by multiplexed recording or computational unmixing. To record cell-resolved  $\text{Ca}^{2+}$  dynamics, a significant milestone was achieved with whole brain recording in zebrafish, initially up to 5 Hz using light-sheet microscopy<sup>2,3</sup>, and later increased to 12 Hz by using extended depth of field (SPED) light-sheet microscopy<sup>4</sup>. At similar time resolution, combination of structured illumination and fast axial piezo scanning allowed volumetric brain imaging during active tracking of freely swimming zebrafish<sup>5</sup>. Recent advances in molecular reporters demand faster time resolution to register dynamics of neurotransmitter release and membrane voltage<sup>6</sup>. Methods that capture the whole volume of interest with each frame of a camera result in the fastest time resolution and are scalable to large volumes. One approach using multifocal diffraction optics allows volumetric microscopy at high magnifications, but requires complex custom components that hinder adoption and scalability to large areas<sup>7</sup>; this method is being extended to enable whole-worm (*c. elegans*) volumetric imaging when paired with an array of 25 cameras. Another efficient approach to volumetric imaging is SCAPE and similar methods, wherein oblique light-sheet illumination and detection are performed through the same objective<sup>8</sup>. This family of methods can access a large volume at high volumetric framerate and resolution by acquiring frames focused at different oblique depths sequentially with rotation of a galvanometric mirror as the only mechanical scanning. The mechanical scanning limitation of SCAPE is like that of SPED<sup>4</sup>. Limitations of SCAPE for application to neuronal activity recordings are the decreased sensitivity due to shared NA split between illumination and detection, and increased hardware complexity including at least 3 high-NA objectives in the imaging path. This approach has not been applied to neuronal activity recording in whole zebrafish brain.

Among readout-limited methods that capture whole volumes with single camera frames, computational microscopy has gained notoriety for its hardware simplicity: A representative example is light-field microscopy using lenslet arrays, that captures many small views of the sample on each frame, from where sample tomography can be computed<sup>9</sup>.

**Limitations of existing light-field microscopy (LFM).** LFM was demonstrated in whole zebrafish brain at 30 Hz bandwidth, at the expense of cellular resolution<sup>10,11</sup>. An alternative method to capture light fields in a single camera frame is based on placing attenuation masks in an intermediate plane, enabling miniature lensless implementations<sup>12</sup>. Random diffuser elements have also been proposed to generalize lenslet arrays and attenuation masks for single-shot light field imaging. Volumetric methods based on computational tomography result in dramatically lower resolution, limited by the individual numerical aperture (NA) of lenslets in the array<sup>10,13</sup>, or limited to sparse sample fluorescence

distributions<sup>14</sup>, especially when using a diffuser or mask<sup>15,16</sup>. This causes the LFM point spread function to be typically  $\sim 100$ -fold larger in volume than the one allowed by the diffraction limit of the objective<sup>10,13</sup>. Multi-focal lens placement, specialized sample mounting, and correlated imaging have also been applied to LFM, ameliorating image artifacts while increasing hardware complexity<sup>17</sup>. Attenuation masks additionally result in decreased light throughput and sensitivity. Diffuser based methods further require sparse samples to survive the unavoidable noise associated with background fluorescence detection<sup>15</sup>. Substantial improvement in light field resolution closer to the diffraction limit was achieved by incorporating wave-optic effects into the image reconstruction model<sup>13</sup>, but only when the sample is restricted to a single plane. Similarly, accounting for tissue scattering improved volumetric resolution, but constrained to sparse samples<sup>18</sup>.

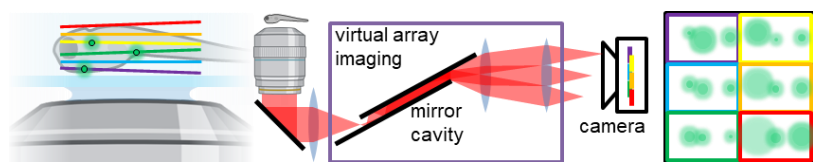
## B. Innovation in this proposal

Many microscopy techniques have been tailored to image zebrafish neuronal activity, including whole-brain approaches. Our approach to volumetric imaging differs entirely from previous efforts. This proposal introduces the use of a reverberating light cavity to generate optical “echoes” or virtual images with different optical path lengths. Virtual images are then focused on the plane of a camera detector resulting in simultaneous non-overlapping multiple-depth widefield imaging. This innovation permits a novel type of volumetric image formation at diffraction limited resolution, where the diffraction limit is set by the full numerical aperture (NA) of virtual images.

Recent progress in spectroscopy<sup>19</sup> and kHz-bandwidth multiphoton scanning<sup>20,21</sup> have used repeated reflections to create arrays of virtual point foci, attaining parallelism advantages. A parallel mirror configuration has also been used to increase the lateral resolution of a point image<sup>22</sup>. Here we propose to extend these concepts from points to complete sample volumes. When applied to the imaging path of a widefield epifluorescence microscope, we expect to enable high-resolution volumetric microscopy while avoiding high complexity in optics, thus representing a substantial advance compared to previous lenslet- and lensless-based volumetric imaging modalities.

The microscope and algorithm we propose will overcome current limitations of volumetric microscopy to enable fast, localized whole brain zebrafish neurophysiology. Our new approach to volumetric recording is direct multi-focal image formation with a single camera by focusing an array of virtual images generated by an optical cavity, as shown in Figure 1. This innovation will enable brain wide volumetric samples at diffraction-limited resolution with each camera frame, while significantly reducing complexity in data processing and hardware implementation.

**Figure 1.** Schematic representation of virtual array multifocal imaging. Multiple sample focal planes are imaged concurrently in a camera by a mirror cavity (only 1D depicted).



**Summary.** To capture fast dynamics of neurotransmitter release and transmembrane voltage in whole zebrafish brains, there is a need for sensitive high-resolution volumetric imaging that can resolve single cells and subcellular compartments with  $>50$  Hz temporal bandwidth. Here we propose an original approach that would enable fast neurophysiological recordings at high spatial resolution within the microscope focal volume. This project has the potential to advance understanding of how neuronal activity leads to behavior and cognitive functions and thus our understanding of neurological and psychiatric mechanisms and disorders.

## C. Problem and objectives

Zebrafish larvae swim against flowing water to maintain their location in familiar territory, for which they remember their visual environment over several seconds. Their memory and its localization in the brain have been studied by imaging persistent neuronal Calcium transients upon patterned visual stimulation. The limited time resolution of current cell-resolved volumetric neuronal activity recordings, and limited resolution or sensitivity of fast volumetric recording methods, do not allow

resolving whether zebrafish persistent neuronal activation is sustained by an intrinsically slow activation or by a fast-recurrent network, even though faster fluorescent reporters are available. This limitation extends to many other questions requiring measurement of fast transient dynamics such as neurotransmitter release and optical membrane electrophysiology.

To address this problem, we propose to develop a new class of microscope and algorithms to enable fast, localized optical neurophysiology of live behaving zebrafish. We aim to record neuronal activity at 50 Hz bandwidth from a  $700 \times 500 \times 110 \mu\text{m}^3$  volume with cellular resolution. Unlike existing cell-resolved light-sheet microscopes that only resolve up to 5 Hz<sup>2,3</sup>, or existing fast volumetric microscopes that compromise sensitivity<sup>8</sup> or cell resolution<sup>10</sup>, our original approach to volumetric recording is multi-focal virtual image formation with a single camera. Each frame captures an array of virtual images focused at different depths of the sample, generated by reflections inside an optical cavity. The virtual array imposes different path lengths onto sections of the imaging aperture, thereby allowing simultaneous focusing at multiple depths on a volumetric sample while maintaining a diffraction-limited resolution.

Our hypothesis is that virtual array microscopy would provide high-speed volumetric activity recordings with cellular resolution, and that its implementation would allow probing fast dynamics of excitatory synaptic release during persistent activation in the whole zebrafish brain.

The long-term goal of this proposal is to understand neuronal circuit function during animal behaviors by enabling high-resolution, high-speed volumetric optical neurophysiology for larval zebrafish. Here we propose a new class of microscope to enable fast optical neurophysiology of live behaving zebrafish. In the scope of this proposal, we will design and characterize the general principles of volumetric imaging using virtual arrays, which will be applicable to any 3D measurement situation.

**Specific Aim 1. Investigate volumetric image formation using a virtual array.** This Aim will test whether multifocal imaging generated by a reflective light cavity can be used to capture three-dimensional data with high resolution and will characterize performance of custom image reconstruction algorithms.

1.1 Implement prototype volumetric microscope. A mirror arrangement will be designed to simultaneously focus an array of virtual images onto the camera of a standard epifluorescence microscope.

This new technology has the potential to enable fast, localized, wide volumetric microscopy for advancing neuroscience, and is also widely applicable to any other measurements where high resolution, low complexity multifocal imaging is needed.

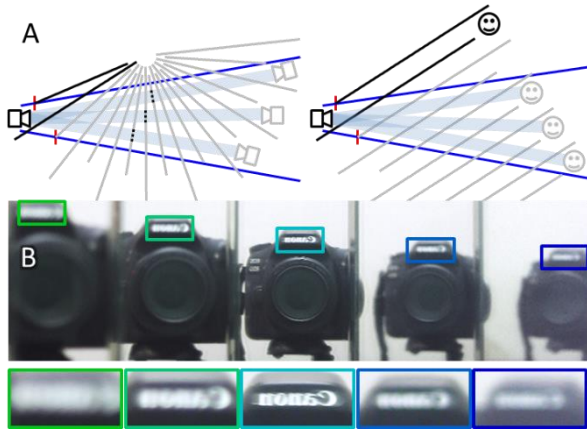
## **D. Approach**

### **D.1. Aim 1. Investigate volumetric image formation using a virtually refocused array.**

This Aim will test whether multifocal imaging based on a reflective light cavity can be used to capture high resolution three-dimensional data at camera-limited framerate and will characterize performance of custom image reconstruction algorithms.

**Aim 1.1. Implement prototype volumetric microscope.** Here we show preliminary data and advances towards successful implementation of a virtual array imaging device. As a first step towards the design of a virtual imaging system, we consider two alternative realizations based on convergent or parallel mirrors. In convergent configuration, the light output path returns through the same space as the input light path, analogous to the case of point source reflections used for kHz-rate laser scanning<sup>20</sup>. Also, a pair of converging mirrors provides a simple macroscopic implementation to demonstrate the virtual array imaging principle, however translation of converging mirrors to an imaging microscope is hindered by the limited space to couple input and output lenses with large optical invariant. Figure 2 illustrates both implementations and demonstrates that a virtual array of images of a single object provides direct multifocal imaging in a single camera image. Preliminary data was obtained using a digital camera (Canon 80D) and two  $80 \times 50 \text{ cm}^2$  mirrors converging at  $\sim 15^\circ$ . Using a lens with 50 mm





**Figure 2.** Principle of virtual array multifocal imaging. A) Diagram of convergent (left) and parallel (right) virtual arrays. Black lines represent physical mirrors. Gray lines and objects represent virtual images of physical mirrors and objects. Blue lines indicate the light acceptance angle of the virtual array. Red marks indicate the focal distance period of the virtual array. Dotted lines indicate perpendicular reflection. B) Experimental demonstration of convergent virtual array. Top: a single photo shows 5 reflections of the camera, at different distances and perspectives. Bottom: colored insets illustrate defocusing as a function of depth.

focal length, the field of view (FOV) of the camera showed 5 reflected images separated in the area of the detector and focused at different distances. The varying focal distance and magnification shown by the virtual images can be attributed to a periodic optical path length offset imposed by the different number of mirror reflections for each virtual image. In a three-dimensional semitransparent sample, this device would enable simultaneous multifocal imaging on a single camera, without the need for separate focusing of each focal depth. In parallel mirror configuration, the imaging path separates the input and output ports of the device, facilitating design of a microscope imaging path. Thus, the proposed microscope will be designed using parallel mirrors.

For a microscope implementation, we follow principles of infinity-corrected systems that simplify the definition of image and pupil planes. In this context, an input image plane is focused at the aperture of the virtual array. Mirror reflections in the cavity fold the expanding beam as it defocuses, creating an array of outputs at the same location but differing in angular content and in path length. The output of the mirror cavity is split into an array of discrete angular ranges, each carrying a complete sample image. A tube lens can then focus the light on a camera, producing an array of separate virtual images focused at a series of depths within the sample. Preliminary optical ray tracing simulations in one dimension show the feasibility of this strategy to form virtual replicate images of the sample. In preliminary work to characterize the proposed parallel mirror geometry, we have also identified a strategy for optically efficient implementation of virtual arrays by applying geometric modeling and invariant-optimized optical design. To design a virtual array device imaging microscope, we first consider experimental needs that define the objective NA, desired imaging FOV, and the depth separation of focal planes in the sample  $u$ , normalized as a fraction of the FOV. Given these values, design parameter choices for a one-dimensional virtual array are the magnification  $M$  at the device input volume, the number of virtual image replicates  $R$ , and the overall length of the virtual array, set by defining the virtual mirror index  $S$  that crosses the virtual optic axis at the output of the system. Using approximations  $1 \ll M^2$  and  $u \ll 1$ , the equation  $\left(\frac{1}{M^2} \frac{NA}{u} + \frac{u}{NA}\right) = \frac{R-1}{S}$  determines the relationship between system design parameters. A choice of integer  $R$  will produce complete sample images that cover the entire virtual array, and a choice of integer  $S$  will result in a centered array of virtual images in the camera. Furthermore, an even  $S$  value will center a virtual image on the camera, while odd  $S$  will place the borders of the FOV centered on the camera.

For example, to design a focal volume microscopy system for fast neuronal activity recording, we select a high space-bandwidth product objective with FOV, resolution, and collection efficiency appropriate for whole-brain zebrafish neuronal recording<sup>5,11</sup> (Olympus XLUMPLFLN-W20). This water immersion objective has a 1.1 mm FOV diameter, NA=1, and magnification  $M=20\times$  when paired with a 180 mm tube lens. Then we select the depth offset of the planes focused in the camera, constrained by a trade-off between in-plane resolution of each replicate focal plane, and number of planes to recover volume data. We select a combination of parameters to maximize collection efficiency and effective NA within a lateral FOV subarea that allows parallel imaging in a camera sensor, while providing multifocal planes that cover a large depth range. In two dimensions, each dimension can be replicated by a virtual array independently with different design parameters, to achieve a regular spacing of 12 focal planes through

the volume. Our chosen combination considers imaging a subset FOV planar area of  $656 \times 492 \mu\text{m}^2$  that will be focused at different depths in a  $3 \times 4$  array in the camera, thus needing a square area of camera detector for the full array of images. We set the magnification at the virtual array input as  $M=10x$ , which can be obtained using a 90 mm lens tube. The chosen plane focal depth separation of  $9 \mu\text{m}$  will allow extending volumetric coverage through a range of  $108 \mu\text{m}$  depth, while attaining at least  $4 \mu\text{m}$  isotropic resolution. These conditions are obtained by setting  $u = 1.8\%$  in the 4-replicate dimension ( $R=4, S=5$ ) and  $u = 5.5\%$  in the 3-replicate dimension ( $R=3, S=8$ ) respectively, relative to the FOV defined for each dimension. Microscopic separations along the optical axis are amplified by a factor  $M^2=100$ , avoiding impractical dimensional adjustments of microscope components. The resulting image array at  $20x$  magnification will need a camera with detector area of  $9.8 \times 9.8 \text{ mm}^2$ .

To implement the virtual array design, we will refine design parameters using wave optics and ray optics modeling and optimization. Preliminary ray tracing simulations (not shown) have supported the feasibility of volumetric virtual array image formation. To test the performance of the custom imaging system and compare with theoretical predictions, we will measure the native focal depth of each virtual image on the camera, the total light throughput obtained at each virtual image, the raw lateral resolution at each focal depth independently, and the raw axial resolution between focal planes. We expect the characterization of this device will be widely interesting to biomedical optics and microscopy communities.

## E. Work plan

Tasks will be organized in a 2-year schedule (4 semesters) as summarized in the following chart.

Specific Aim	Semester	1	2	3	4
<u>1. Investigate volumetric image formation using a virtual array.</u>					
<u>1.1. Implement volumetric microscope.</u>					
1.1.3. Theoretical modeling and parameter design for optical system.		X	X		
1.1.4. Construction of virtual array imaging system.			X	X	
1.1.5. Characterization and testing of optical system.				X	X

## F. References

- Weisenburger, S. & Vaziri, A. *Annu. Rev. Neurosci.* **41**, 431–452 (2018).
- Vanwalleghem, G. *et al. J. Neurosci.* **40**, 4130–4144 (2020).
- Ahrens, M. B., Orger, M. B., Robson, D. N., Li, J. M. & Keller, P. J. *Nat. Methods* **10**, 413–420 (2013).
- Tomer, R. *et al. Cell* **163**, 1796–1806 (2015).
- Kim, D. H. *et al. Nat. Methods* **14**, 1107–1114 (2017).
- Emiliani, V., Cohen, A. E., Deisseroth, K. & Häusser, M. *J. Neurosci.* **35**, 13917–13926 (2015).
- Abrahamsson, S. *et al. Nat. Methods* **10**, 60–63 (2013).
- Voleti, V. *et al. Nat. Methods* **16**, 1054–1062 (2019).
- Wang, D., Zhu, Z., Xu, Z. & Zhang, D. *Eur. Phys. J. Spec. Top.* (2022)
- Prevedel, R. *et al. Nat. Methods* **11**, 727–730 (2014).
- Nöbauer, T. *et al. Nat. Methods* **14**, 811 (2017).
- Adams, J. K. *et al. Sci. Adv.* **3**, e1701548 (2017).
- Broxton, M. *et al. Opt. Express* **21**, 25418–25439 (2013).
- Xue, Y., Davison, I. G., Boas, D. A. & Tian, L. *Sci. Adv.* **6**, eabb7508 (2021).
- Antipa, N. *et al. Optica* **5**, 1 (2018).
- Zhang, Z. *et al. Nat. Biotechnol.* **39**, 74–83 (2021).
- Cong, L. *et al. eLife* **6**, e28158 (2017).
- Pégard, N. C. *et al. Optica* **3**, 517–524 (2016).
- Scarcelli, G. *et al. Nat. Methods* **12**, 1132–1134 (2015).
- Wu, J. *et al. Nat. Methods* **17**, 287–290 (2020).
- Beaulieu, D. R., Davison, I. G., Kılıç, K., Bifano, T. G. & Mertz, J. *Nat. Methods* **17**, 283–286 (2020).
- Ozcan, A., Bilenca, A., Bouma, B. E. & Tearney, G. J. *Appl. Phys. Lett.* **89**, 131124 (2006).

## Executive Summary

### “Retinal Imaging for Retinopathies”

#### New Diagnostics to Explore the Links between Infectious & Non-Communicable Diseases in Low Resource Settings

There is a growing recognition that understanding disease co-morbidities and multi-morbidities is of significance in improving healthcare outcomes, particularly in low-resource settings, where health data is often siloed and held in constrained data bases. For example, there is now a growing recognition that the relationship between communicable and non-communicable diseases (NCDs) in both low- and middle-income countries (LMICs) and high-income countries (HICs) is increasingly important. Evidence shows that endemic infectious diseases (including those caused by parasites such as malaria) interact strongly with non-communicable diseases such as vascular disease and diabetes mellitus. Such multi-morbidities are becoming increasingly important in part due to changes in demographics and lifestyles (including dietary changes).

Despite investments in LMIC healthcare, systems remain vertically integrated by disease group, such that it is challenging for different clinicians, running separate malaria and diabetes clinics in a rural hospital for example, to establish linkages, as records are still primarily held for single disease groups.

My aim is to develop a new tool that will enable scientists to have “a window into the eye” of these two very different and but related diseases – both of which are of increasing in prevalence in LMICs – namely type 2 diabetes and malaria. This will involve creating a low cost instrument that can provide clinically-relevant information in the diagnosis of both diseases using retinal imaging. We propose to interface the instrument with a smart-phone camera and use it to detect the characteristic discoloration, visual features, and oxygenation of the retinal vessels, associated with both diseases. Establishing the linkage between malaria and diabetic retinopathy has the potential to make screening campaigns easier, thus leading to significant increases in early detection, associated with better outcomes. Although there have been research efforts to create easy-to-use instruments, they have suffered from low quality images, making their use challenging, especially with limited training. In order to improve the accessibility and reach of diagnostics, as well as improving performance, we will implement a new three coloured LED illumination, allowing us to obtain high quality images with ultralow cost designs. We will also use a deep-learning tool (running on the phone’s GPU, not requiring wireless access, often unavailable in rural settings) providing diagnostic decision support for healthcare workers. Data will be downloaded later (once networking is available) into digital health records, using privacy-enabled cloud-communication.

We have already developed proof-of-concept instruments and working with clinical partners at the University of Edinburgh, we have started to validate the AI decision support tool using a training database of 300 reference retinal scans, associated with both diabetes and malaria and including controls. In this project, we will complete the technical developments, in close collaboration with our clinical partners in Tanzania and Edinburgh to ensure that the design and implementation are fit-for-deployment. The prototypes will be validated in a field-based study in Tanzania. The project has a number of technical and collaborative risks, that will be mitigated by collaboration with a strong team in Glasgow, with experience of having worked with clinicians at Kilimangaro Christian Medical Centre.

A key goal of this project is to develop a capability in retinal health screening for LMICs that is closer to that provided in high-income countries. We will ensure that our technologies perform across multiple ethnicities, particularly those involving darker skin pigmentations where retinal imaging quality can be different and often with lower signal-to-noise due to the strong absorption of light by melanin. Following this initial study we intend to develop translational pathways through the further engagement of clinicians with the long-term aim of promoting inclusivity in research and technology development for retinal imaging.

## **“Retinal Imaging for Retinopathies”**

New Diagnostics to Explore the Links between  
Infectious & Non-Communicable Diseases in Low Resource Settings

### **Literature Review**

There is a growing recognition that the relationship between communicable and non-communicable diseases (NCDs) in both low- and middle-income countries (LMICs) and high-income countries (HICs) is becoming increasingly important, particularly in low-resource settings, both in terms of the increasing risk of disease and also the wealth disparity in access to screening and management of these conditions (1), (2). Evidence shows that chronic and acute infections (e.g. viral, bacterial and parasitic diseases including tuberculosis, TB, malaria and HIV) interact strongly with non-communicable diseases such as diabetes mellitus, and vascular and chronic lung disease. Such multi-morbidities are emerging as major threats to local health and wellbeing in both HICs and LMICs, with changing demographics and lifestyles.

There is now also compelling evidence that both neonatal NCDs e.g., cardiovascular disease and type II diabetes (3) can be strongly influenced by the infectious disease status of the foetus and/or the mother. Additional factors common in LMICs, such as malnutrition in pregnancy and infancy, coupled with stress arising from chronic inflammation following endemic infections (4) have also been linked both to early-life later-life health outcomes.

Against this evolving backdrop of new understanding, within LMICs, healthcare provision for disease is frequently siloed into “vertical” activities in specialist donor-funded clinics, particularly in semi-urban or rural communities (5), creating a challenge around patient-level “horizontal” data linkages between disease, treatment and outcomes. Despite investments in LMIC healthcare, healthcare systems remain vertically integrated by disease group (5), (6), (7), such that, it is challenging for a clinician running malaria and diabetes clinics in a rural hospital to establish linkages, where records are still primarily held for single disease groups.

Underpinning my vision is the recognition of the tensions between vertical healthcare programmes (with specialist clinics, often donor-funded) and horizontal linkages, focused on the interplay between an individual’s multiple co-morbidities. This paradox is not new (5), (7), although as yet there are no optimised systems implemented that combine a blend of vertical and horizontal activity (a concept that we have termed “diagonal diagnostics”). My aim is to develop new tools that will enable “a window into the eye” of type 2 diabetes and malaria, two very different and related diseases, both increasing in prevalence in LMICs.

The strong interdependency between type 2 diabetes and malaria is already well established, with diabetes greatly increasing the risk of people catching malaria (8). The nature of this interdependence is complex, and is related to an individual’s ability to control parasitaemia being weakened through immune dysfunction (9). The molecular mechanisms linking the diseases are becoming apparent though evidence around dynamics in insulin resistance and inflammation, as well as a link to the reduction in HbA1c (10), (11), where malaria reduces red blood cell integrity with haemolysis, providing an increasing population of young cells which will not have been exposed to glucose. Whether as a consequence of the recent resurgence of malaria, or whether as a result of the proliferation of type 2 diabetes in sub-Saharan Africa, there is now an increasing number of persons at risk for Plasmodium infection and malaria. This is particularly true in pregnant women, where there is a 3–4 times increased risk of miscarriage and a substantially increased risk of stillbirth (12).

### **Problem Statement/Objective**

“Looking into the window of the eye to save lives”.

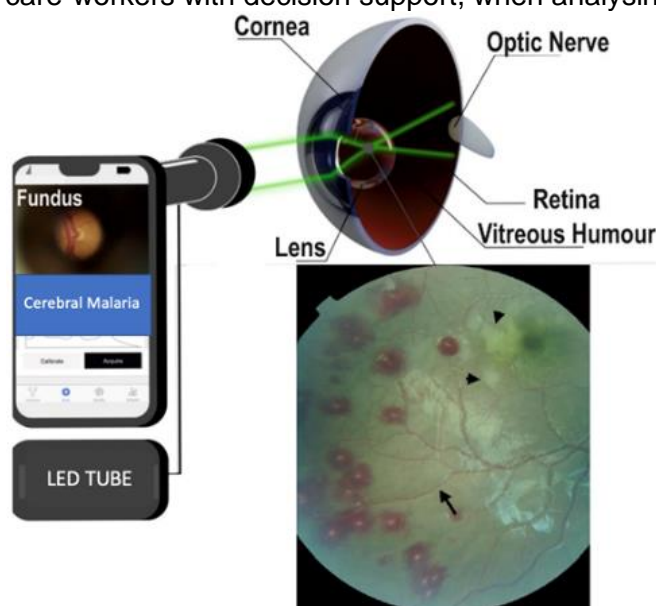
Cerebral malaria is potentially fatal but can be diagnosed to inform treatment towards recovery, whilst diabetes is similarly better treated, the earlier it is detected. Both can be detected and diagnosed using retinal imaging, which is often better accepted than the alternative invasive tests, especially in infants and young children. Our aim is to use a low-cost smart-phone camera to detect the characteristic discoloration, visual features, and

oxygenation of the retinal vessels, associated with both diseases. Being able to detect malaria and diabetic retinopathy at the same time has the potential to make screening campaigns easier, thus leading to early detection, associated with better outcomes.

The device will be combined with a cloud-based deep-learning tool to provide diagnostic decision support for healthcare workers including nurses, caring for adults and children in low-resource rural settings in the Global South, enabling the diagnostic and treatment to be linked with minimal training in image analysis.

Malaria is still considered one of the most common and deadliest diseases. In 2019, malaria led to an estimated 229 million cases and ~409,000 deaths worldwide. In endemic countries, asymptomatic malarial parasitemia is common, and may lead to neurological complications and death, if undiagnosed (13). Children under 5 years are the most vulnerable group affected accounting for 67% (274 000) of all malaria deaths (14). Amongst these individuals, many die from undiagnosed cerebral malaria, resulting from compromised perfusion of the brain due to parasites in the microvasculature (15). An early eye screen can however diagnose cerebral malaria (13), mitigating many of the complications associated with a poor prognosis.

We have previously worked closely with both clinical and industrial experts (including Optos and Nikon) in the field of retinal imaging, examining the retinal vasculature to understand cerebral vascular diseases (16), (17), (18). We now propose that by combining a low cost (fundus) retinal imaging as a new portable optical system, with artificial intelligence/deep learning (19), we will be able to detect the characteristic artefacts associated with the presence of either diabetic or malarial retinopathies in the microvascular network of the retinal tissue. The system will use a privacy enabled cloud communication to provide nurses and care-workers with decision support, when analysing the retinal image.



**Figure 1 - System Concept:** a smart phone camera with a simple interface and positioning system is used to capture pictures of the retina. These are analysed using deep learning methods to identify lesions and features linked to the disease, as well as blood vessels to measure oxygenation.

**The novelty of our approach** that differentiates us from other commercially available mobile phone based systems includes:

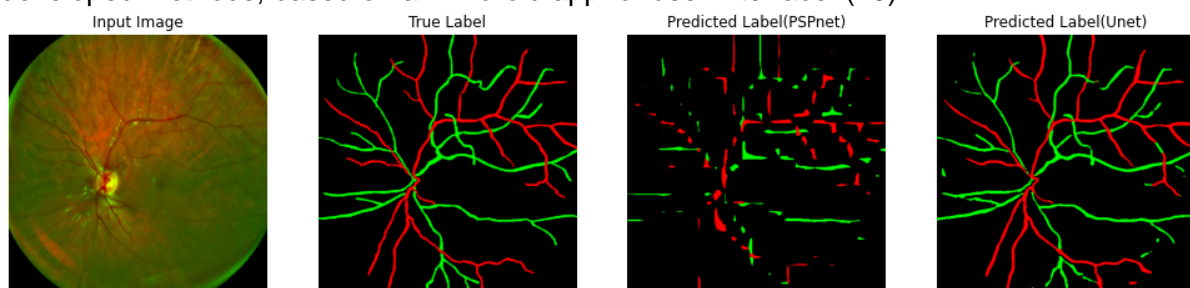
- (i) The use of ultra-low cost optics, based upon three coloured LED illumination, providing high quality images, at a cost of goods affordable in low-resources settings
- (ii) The exploration of new imaging modalities which include the potential for trans-scleral illumination for less-invasive collection of high quality signals
- (iii) The development of a sophisticated image analysis tool, including an AI deep-learning diagnostic decision support, which will be validated in collaboration with clinical ophthalmologists in the UK, prior to being implemented in Tanzania. The tool includes training data collected from appropriate ethnic groupings ensuring (unlike other optical clinical devices, associated with blood oxygenation and temperature measurements) strong diagnostic efficacy across groupings with high skin colouration.

## Outline of tasks/Work Plan

Phase I (month 1 – month 7) – platform development and laboratory validation

**1.1 Hardware:** The design concept will be realised using fundus imaging to collect high resolution retinal scans on a smart phone (see previous image, (17) used for vessel classification, based on wavelength-specific illumination (27)). Measure of success will be around the resolution of the image, and 3-color illumination, sufficient to detect artefacts in the retina (including discolouration) associated with cerebral malaria or diabetes.

**1.2 AI system model prediction:** Using real images from public databases (20), (21), (22), we will train deep-learning tool using a Convolution Neural Network (CNN), enabled on our phone platforms. As a proof-of-concept, we have already shown the development of a blood vessel classification AI supported tool (Figure 2 below), able to assign vascular architecture to retinal images (identifying veins and arteries). We will now adapt this tool for measurement of retinal artefacts and colouration. Measure of success is 99% accuracy on test set. We have access to machine learning development platforms (e.g. TensorFlow) and will use our previously developed methods, based on an Android app for user interface (23)



**Figure 2 – Vessel classification proof-of-concept:** results from our tool, left to right; raw input image, true labelled image and predicted labelled images.

**1.3 Privacy-enabled cloud communication:** We have recently developed a block-chain enabled end-to-end encryption (24), enabling medical images to be uploaded into cloud-based systems, providing entrusted keys to defined users. Images will be uploaded to improve our library/training sets, whilst providing trust and assurance around privacy of medical records.

**1.4 Apply for ethical approval in Tanzania.** We have experience of working in the country and anticipate this process to take 3-6 months.

**Deliverable Phase I (D1 month 7):** a laboratory-validated prototype and analysis pipeline.

Phase II (month 5 – month 15) – field validation and route to deployment

**2.1 Iterated design,** we will iterate on our initial design (deliverable D1) after a first short visit to Tanzania, which will include a co-creation workshop, with 3D-printed prototypes.

**2.2 Using clinical expertise in KCRI, Tanzania,** we will perform a limited field validation study, comparing our proof of concept system against standard of care reference techniques and data. Whilst malaria is endemic in rural communities and many children <5 years in sub-Saharan Africa (>60%) will have the disease during the course of a year, the prevalence of cerebral malaria is much less, ~2.5% in hospitalised children (25). Thus, whilst a statistically powered study falls beyond the scope of the project, we will instead compare retinal images of hospitalised children, diagnosed with cerebral malaria against control children.

**2.3 Route to impact.** Once proof-of-concept is established, we will work with collaborators in Tanzania for wider validation leading to a clinical trial. We will also disseminate the results and the design using the principles of open innovation/open access to enable a more widespread development and adoption of our methods.

**Deliverable Phase II (D2 month 15) –** prototype designs disseminated and data published.



## Gantt Chart

	M1	M2	M3	M4	M5	M6	M7	M8	M9	M10	M11	M12	M13	M14	M15
Phase I - platform development and laboratory validation							D1								
1.1 Hardware															
1.2 AI system model prediction															
1.3 Privacy-enabled cloud communication															
1.4 Apply for ethical approval in Tanzania															
Phase II - field validation and route to deployment															D2
2.1 Iterated design															
2.2 Validation study															
2.4 Route to impact															

**Risk/Project Management.** We will hold monthly meetings on project progress (remotely on Zoom) with all collaborators, in which risk management will form a standing agenda item. We have mitigated most technical risks in our experimental design (above) and initial proof-of-concept experiments, although gaining a useful illumination of the pupil will be important for obtaining high quality images. Should direct illumination reveal challenging to extract features linked with the diseases, we will explore other illumination such as transscleral.

## Team

Victor Ochoa-Gutierrez	University of Glasgow (UoG)	ECR ( <b>Project Lead</b> ) – Retinal Imaging, oximetry, prototype development
Professor Jonathan Cooper	UoG	Research mentor - idea concept and field-based experience on malaria diagnosis
Xin Guo	UoG	AI, Cloud Infrastructure and User Interface.
Dr. Ian MacCormick	University of Edinburgh	Clinical Lecturer – ophthalmology.
Dr. Blandina T. Mmbaga	KCRI Tanzania	Director of Institute (Kilimanjaro Clinical Research Institute), clinical expertise in malaria and diabetes.

## Outcome(s)

- I. The clinical use cases are: i) detection of any retinopathy from screening images (abnormal/normal), and/or ii) detection of diabetic retinopathy severe enough to require referral to ophthalmology according to SIGN guidelines (or other national guidelines such as Tanzania's National Diabetic Retinopathy Management Guidelines, 2018). Both outcomes will also reduce the workload of human graders.
- II. Increased capacity in retinal health screening for LMICs. We will ensure that our technologies perform across multiple ethnicities, particularly those involving darker skin pigmentations where retinal imaging quality can be different and often with lower signal-to-noise due to the strong absorption of light by melanin. Patient selection will follow best practice as per ethics approvals, in particular including a gender-balanced cohort.

## Impact

- Promotion of inclusivity in research and technology development for retinal imaging
- Supporting an informed and collaborative approach to the development, implementation, adoption and exploitation of research outcomes of new medical devices, including technologies, processes, evidence-based policy, community impact or creative outputs
- To provide early-stage investment in a new medical technology with the potential for commercialization, to support the de-risking of these opportunities
- In the longer term, the project will contribute to reduction in patient morbidity (and mortality for malaria), in particular in children under 5, through early diagnosis of retinopathy, leading to sustained, inclusive and sustainable economic growth as well as resilient healthcare infrastructures.

## References

1. Abbafati C et al. Global burden of 369 diseases and injuries in 204 countries and territories, 1990–2019: a systematic analysis for the Global Burden of Disease Study 2019. *The Lancet*.
2. The Malawi NCDI Poverty Commission Report — The NCDI Poverty Network. 2018.
3. Di Bernardo S et al. Assessing the consequences of gestational diabetes mellitus on offspring's cardiovascular health: MySweetHeart Cohort study, *BMJ Open*. 2017.
4. Ogoina D et al.. The role of infections in the emergence of non-communicable diseases (NCDs) *J Infect Public Health* 2009.
5. Marquez PV et al. No more disease silos for sub-Saharan Africa. *BMJ* 2012.
6. Huang F et al. Beyond pilotitis: Taking digital health interventions to the national level in China and Uganda. *Global Health* 2017.
7. Mills A. Mass campaigns versus general health services: What have we learnt in 40 years about vertical versus horizontal approaches? *Bull World Health Organ*. 2005.
8. Danquah I et al. Type 2 diabetes mellitus and increased risk for malaria infection. *Emerging Infectious Diseases*. 2010.
9. Harrington et al. Maternal microchimerism predicts increased infection but decreased disease due to plasmodium falciparum during early childhood. *J. Infect. Dis* 2017.
10. Nakanga WP et al. Personal view: Should haemoglobin A1C be used for diagnosis of diabetes mellitus in Malawi? *Malawi Medical Journal*. 2016.
11. Kalra S et al. Malaria and diabetes. *Journal of the Pakistan Medical Association*. 2017
12. Moore KA et al. Quantification of the association between malaria in pregnancy and stillbirth: a systematic review and meta-analysis. *The Lancet Global Health*. 2017
13. Newton CRJC, et al. Cerebral malaria. *J. Neurol. Neurosurg. Psychiatry* 2000.
14. WHO. Malaria report. 2022.
15. Ogwang R et al. Asymptomatic malaria parasitaemia and seizure control in children with nodding syndrome; A cross-sectional study. *BMJ Open*. 2018.
16. Moss HE. Retinal Vascular Changes are a Marker for Cerebral Vascular Diseases. *Curr Neurol Neurosci Rep*. 2015
17. Carles G et al. Wide-field, illumination-agile, oximetric retinal imaging with a handheld camera. *OSA Imaging and Applied Optics Congress 2021 CTh4E.6*.
18. Ochoa-Gutierrez VJ et al. Multi-spectral vascular oximetry of rat dorsal spinal cord. *Optics and Biophotonics in Low-Resource Settings VI*; 2020
19. Agustin T et al. Optimization Convolutional Neural Network for Classification Diabetic Retinopathy Severity. *ICOIACT 2020*.
20. Drive: Digital Retinal Images for Vessel Extraction - Data Set. 2012.
21. Clinical Data Sets - The Royal College of Ophthalmologists. 2022.
22. Kaggle Repository. 2022.
23. Guo X et al. Smartphone-based DNA diagnostics for malaria detection using deep learning for local decision support and blockchain technology for security. *Nature Electronics*. 2021
24. Singh R et al. Blockchain-enabled End-to-End Encryption for Instant Messaging Applications. In *IEEE 23rd International Symposium on a World of Wireless*; 2022
25. Nkhoma WAC et al. Cerebral malaria in Malawian children hospitalized with Plasmodium falciparum infection. *Annals of Tropical Medicine and Parasitology*. 1999.
26. Carles G et al. Wide-field, illumination-agile, oximetric retinal imaging with a handheld camera. *Conference Papers*; 2021 The Optical Society. CTh4E.6.

## **Electrochemical Zero-mode Waveguides Based Digital Sensing of Biomarkers**

### **Challenge:**

Biomarkers are biological molecules present in bodily fluids and tissues which provide critical knowledge on human health. Detecting and quantifying biomarkers are useful in disease diagnostics, prognosis, evaluating the efficacy of therapy and treatment, and drug discovery and development. Current detection methodologies including enzyme-linked immunosorbent assay (ELISA), polymerase chain reaction, western blotting, and electrochemical sensors lack either a low limit of detection (*i.e.*, quantifying attomolar concentrations) or a low detection time or a combination of both. This limits their use for detecting biomarkers that are found in low concentrations which provides valuable information on human health. Thus, to quantify these biomarkers, it is necessary to develop a new sensing methodology with a low limit of detection and faster sensing time, that is also cost-effective and user-friendly.

### **Proposed project:**

The overarching goal of this project is to develop a digital, ultra-sensitive, cost-effective, and user-friendly sensor system for quantifying biomarkers. We aim to achieve this by employing **an advanced nanophotonic platform called zero-mode waveguides (ZMWs) in combination with optical dark-field microscopy**. In this project, we will develop our sensor targeted to Interleukin-6 (IL-6), one of the common cytokines to understand the condition of several diseases including COVID-19, HIV, and Alzheimer's. ZMWs are cylindrical or conical nanopores in a thin metal film (typically 100 – 200 nm thickness) with a bottom pore diameter smaller than the wavelength of visible light, capable of confining excitation radiation within the nanopore with the intensity decaying exponentially along the axial direction. We will exploit this feature of the ZMW to quantify biomarkers using scattering of plasmonic nanoparticles (NPs) as a readout mechanism. Imaging the ZMW substrate under dark-field mode blocks the trans-illumination but effectively captures the low-angle light scattered by the individual nanopores. The inherent light scattering by the nanopore increases with the insertion of plasmonic NPs such as silver inside the nanopore due to their localized surface plasmon resonance (LSPR). Using this principle, we will quantify the biomarker concentration in two ways: 1) Construct molecular architecture to attract and hold IL-6 in the nanopores and use silver NPs to specifically bind to the nanopores containing IL-6. By monitoring and counting the number of nanopores with the NPs, we can quantify the IL-6 concentration. 2) Immobilize IL-6 on the surface of silver NPs using molecular architecture followed by releasing silver particles and microscopically counting them on the ZMW substrate and relate to IL-6 concentration. Further, we will improve the limit of detection and detection time by increasing the mass transport of silver NPs inside the nanopores using a voltage gate.

### **Outcomes:**

We expect that the proposed nanophotonic-based platform, zero-mode waveguides will quantify IL-6 in the atto molar range ( $\sim 10^{-18}$  M) within 30 minutes including assay formation and readout. Naturally, the platform can be extended to quantify other biomarkers by forming suitable assays. Further, the approach can be transformed into multiplex sensing by co-functionalizing nanopores with multiple recognition elements targeting different analytes and will be sensed by employing different size plasmonic NPs. Lastly, dark-field microscopy can be implemented on a smartphone-based detection setup, making it an easily accessible point-of-care platform. Overall, the proposed sensing platform with an ultra-low limit of detection will push the boundaries of sensing by quantifying new biomarkers and thus improving human health.

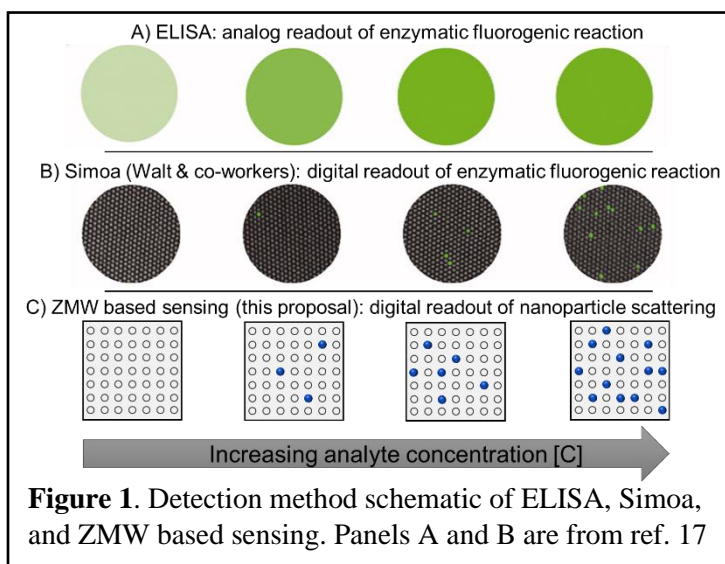
### Electrochemical Zero-mode Waveguides Based Digital Sensing of Biomarkers

**PI:** Vignesh Sundaresan, Assistant Professor of Chemistry and Biochemistry, University of Mississippi

**Current state and problems.** Cytokines are small proteins produced by cells in the immune system that regulate inflammatory responses, making them ideal biomarkers for various pathological states.<sup>1,2</sup> Although cytokines typically guide healthy immune responses, pathogens can trigger excessive immune responses caused by the overproduction of proinflammatory cytokines (‘cytokine storms’), which can rapidly escalate to multi-organ failure and eventually death.<sup>3,4</sup> Treatment requires early detection and intervention. However, there is currently no reliable diagnostic test to detect the onset of cytokine storms. This is a critical issue in the ongoing COVID-19 pandemic as well as a major side-effect of CAR-T cancer therapy, where physicians report the most severe cases, and a large number of deaths (20-30%) correlate with cytokine storms.<sup>5-7</sup> Recent studies suggest elevated levels of interleukin-6 (IL-6), an early-stage proinflammatory cytokine, is a reliable precursor to COVID-19 cytokine storms and adverse patient outcomes.<sup>8,9</sup> IL-6 has also been shown to be an effective marker for a variety of diseases such as HIV, Alzheimer’s, and cytokine release syndrome.<sup>10-14</sup>

Currently, the existing “gold standard” method for quantifying IL-6 in patient samples is enzyme-linked immunosorbent assay (ELISA), where the IL-6 concentration is determined by the intensity of an enzymatic fluorogenic reaction (**Figure 1A**).<sup>15</sup> However, ELISA is not sensitive enough to detect the onset of cytokine storms (limit of detection, LOD - 5.24 fM), and is also time-consuming.<sup>16</sup> Walt and co-workers demonstrated ultra-sensitive detection of IL-6 (0.21 fM) using the single-molecule array (Simoa), where the enzymatic fluorogenic immunoassay is developed within microwells and the analyte concentration is determined by the number of microwells that exhibit fluorescence output (**Figure 1B**).<sup>16,17</sup> Because Simoa is based on single-molecule fluorescence, it requires a large number of microwells (>50000) and utilizes enzymes, lasers, and ultra-sensitive detectors which makes it a costly assay. Moreover, at low analyte concentrations, the fluorescence is shot noise-limited which affects the Simoa sensitivity.

**Research Objectives.** The overarching goal of this proposal is to develop a digital, and ultra-sensitive sensor system for IL-6 that is also cost-effective and user-friendly. We aim to achieve this by employing **an advanced nanophotonic platform called zero-mode waveguides (ZMWs) in combination with optical dark-field microscopy (Figure 1C)**. We envision that this nanophotonic platform will provide diagnostic and prognostic value by quantifying IL-6 digitally and lead to improved health care. The plan to achieve this is divided into three specific aims: 1) detect and determine IL-6 concentration directly by immobilizing nanoparticles (NPs) into ZMWs; 2) quantify IL-6 concentration indirectly by counting the number of captured NPs; 3) achieve rapid and ultra-sensitive detection by electric-field enhanced mass-transport of NPs. Analytical sensitivity, LOD, linear dynamic range, robustness to interferences, and reproducibility will be determined.



**ZMWs and advantages.** ZMWs which, at the most basic level, a cylindrical perforation (diameter < 150 nm) in a thin metal film, capable of trapping optical radiation (**Figure 2A**).<sup>18, 19</sup> The trapped radiation can interact with molecules contained in the zeptoliter-scale ( $1 \text{ zL} = 10^{-21} \text{ L}$ ) volume bounded by the radiation field and enclosed within the nanopore (**Figure 2B**).<sup>20</sup> Although ZMWs have been previously used in single-molecule studies, in this proposal, we will push the boundaries of ZMWs by using them as a digital sensing platform, which can be directly applied in the healthcare setting.

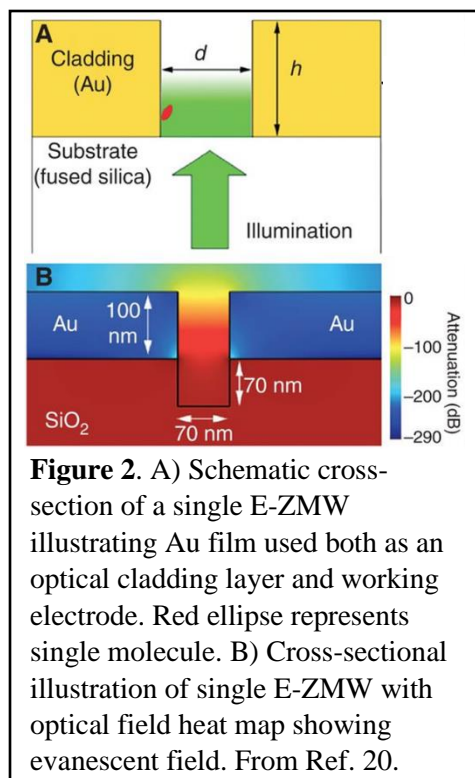
ZMWs based sensing platform offer several advantages:<sup>21</sup> (1) Ultra-low volume. The active volume of individual nanopores is in the order of femto- to attoliters (or  $10^{-18} \text{ m}^3$  to  $10^{-21} \text{ m}^3$ ) which helps to sequester single entities such as molecules or NPs even in relatively high concentrations (i.e., single molecule or NP per pore coverage for 11 aL nanopore can be achieved with  $2 \mu\text{M}$  concentration). Additionally, the nanopore dimension can be easily tuned to accommodate one or a few NPs. (2) Chemical functionalization. The construction of ZMWs with Au cladding layer and a  $\text{SiO}_2$  base can take advantage of the chemical orthogonality of these two materials, so the biorecognition elements can be directed to, and immobilized at either the base of the ZMWs (using organosilane linker chemistry) or the Au layer (using thiol based self-assembly strategies).

(3) Control of local electric field. The gold optical cladding layer in each pore is connected to those in all the other pores which can be used as electrodes. Additionally, another Au layer or electrode can be added on top of the structure, which can be used to change the electric field locally by applying appropriate potentials (*vide infra*, see Aim 3). (4) Massively parallel array and digitization. The capture of NPs can be studied simultaneously over an entire array and can obtain a digitized output using a simple algorithm. (5) Enhanced sensitivity. This sensor platform is based on NPs scattering, which are efficient scatterers, so it is not shot noise limited.

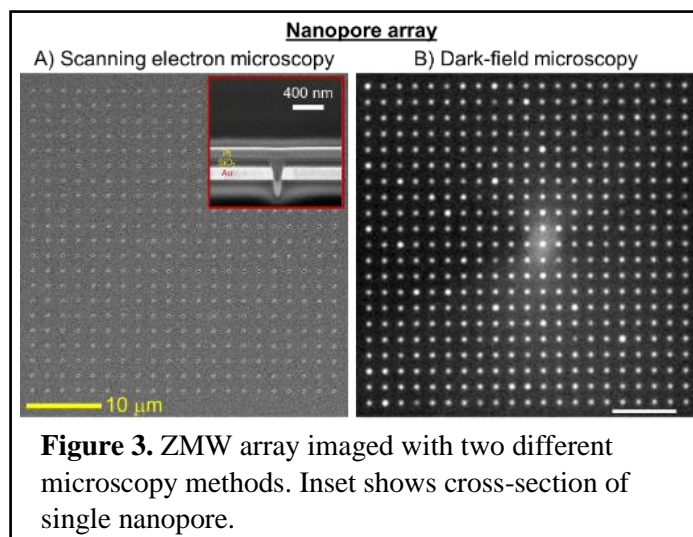
### Research Plan.

**Aim 1: Detect and determine IL-6 concentration directly by immobilizing NPs into ZMWs.** The ZMWs will be fabricated using a combination of deposition and focused ion beam (FIB) techniques.<sup>22, 23</sup> Briefly, a gold layer (200 nm) will be deposited onto a clean glass coverslip using e-beam evaporation followed by the deposition of silicon dioxide (100 nm) using plasma-enhanced chemical vapor deposition (PECVD). Finally FIB will be used to mill an array of conical nanopores on the metal-insulator structure. A representative  $21 \times 21$

nanopore array (pore diameter: top =  $\sim 200 \text{ nm}$  and bottom =  $\sim 100 \text{ nm}$ ) is shown in **Figure 3A**. The optical dark-field image of the nanopore array (**Figure 3B**) shows an array of bright spots in which each bright



**Figure 2.** A) Schematic cross-section of a single E-ZMW illustrating Au film used both as an optical cladding layer and working electrode. Red ellipse represents single molecule. B) Cross-sectional illustration of single E-ZMW with optical field heat map showing evanescent field. From Ref. 20.



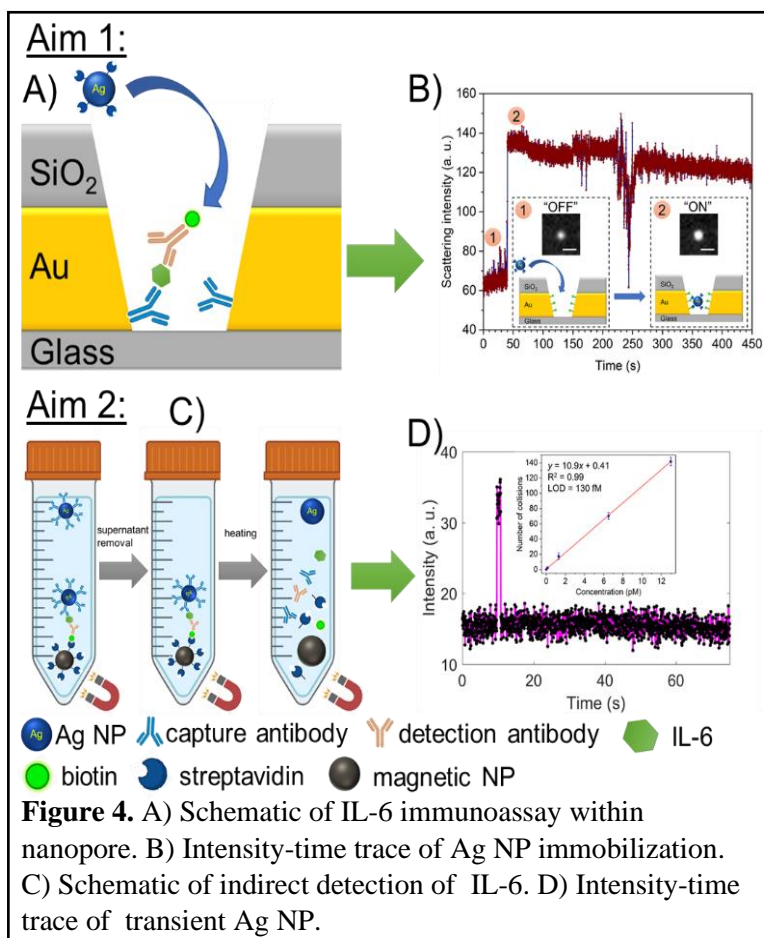
**Figure 3.** ZMW array imaged with two different microscopy methods. Inset shows cross-section of single nanopore.



spot corresponds to the light scattering from individual nanopores. The array size, the interpore distance, and the diameter of the nanopore can easily be optimized by adjusting FIB parameters.

To detect IL-6 directly, we will immobilize a capture antibody in each nanopore (**Figure 4A**). First, the exposed gold surface within the nanopore will be functionalized with thiol/carbodiimide linker chemistry, followed by the immobilization of IL-6 capture antibodies. Ideally, we aim to have a single IL-6 molecule in each nanopore so finite-difference time-domain (FDTD) simulations can be carried out to optimize assay parameters such as incubation time and the number of pores for obtaining single molecule coverage. Then, the nanopore array substrate will be exposed to a standard solution of IL-6 analyte to allow binding to the capture antibody. After the formation of the antibody-antigen complex, a biotinylated secondary antibody will be introduced followed by streptavidin labeled Ag NP (S-Ag NP) and subsequently imaged with dark-field microscopy (**Figure 4A**). If a nanopore contains IL-6 and the recruited biotinylated detection antibody, S-Ag NPs can be captured within the nanopore because of the high-affinity binding of biotin to streptavidin.<sup>24</sup> Because the Ag NPs exhibit enhanced light scattering due to the localized surface plasmon resonance (LSPR), we expect the dark-field scattering intensity of the nanopore to increase due to the insertion of Ag NP. Preliminary results (**Figure 4B**) confirm that the S-Ag NP can be immobilized within the biotin functionalized nanopore as indicated by the step increase in scattering intensity. We will then image the dark-field array, digitize the output, and analyze the results by calculating the ratio of high intensity (with NP) to low intensity (without NP) pores, *i.e.* [ON/OFF]. The limit of detection and dynamic linear range will be obtained by creating a calibration curve relating [ON/OFF] to IL-6 concentration.

**Aim 2: Quantify IL-6 concentration indirectly by counting the number of captured NPs.** This aim focuses on the indirect sensing of IL-6 by quantifying the concentration of Ag NPs. To accomplish this, the IL-6 capture antibodies (described in Aim 1) will be assembled on the surface of Ag NP. After IL-6 recognition, they will be labeled by hybridization to streptavidin-labeled magnetic NPs and separated using a magnetic field (**Figure 4C**).<sup>25</sup> The Ag NPs without IL-6 will not be attracted by the magnetic field; thus, they will be removed with the supernatant. After supernatant removal, the solution will be heated to denature biomolecules that release Ag NPs, whose concentration will be quantified by introducing the solution containing released Ag NPs onto the unlabeled-nanopore array substrate. In these assays, Ag NPs will be allowed to diffuse in and out of the nanopore, and the resulting Ag NPs will be detected by transient





scattering increase, **Figure 4D**. The concentration of Ag NP released during heating is dictated by the IL-6 concentration, so we can calibrate the number of collisions *vs.* the Ag NP/IL-6 concentration. A preliminary experiment performed with citrate-capped Ag NPs on a  $21 \times 21$  nanopore array showed several transient scattering events, proportional to the concentration of free Ag NPs (**Figure 4D, inset**). After creating the calibration curve (# of collisions *vs.* Ag NPs concentration), we determined the LOD as  $130 \times 10^{-15}$  M, and it should be possible to further improve the LOD simply by employing a larger nanopore array.

### Aim 3: Achieve rapid and ultra-sensitive detection by electric-field enhanced mass-transport of NPs.

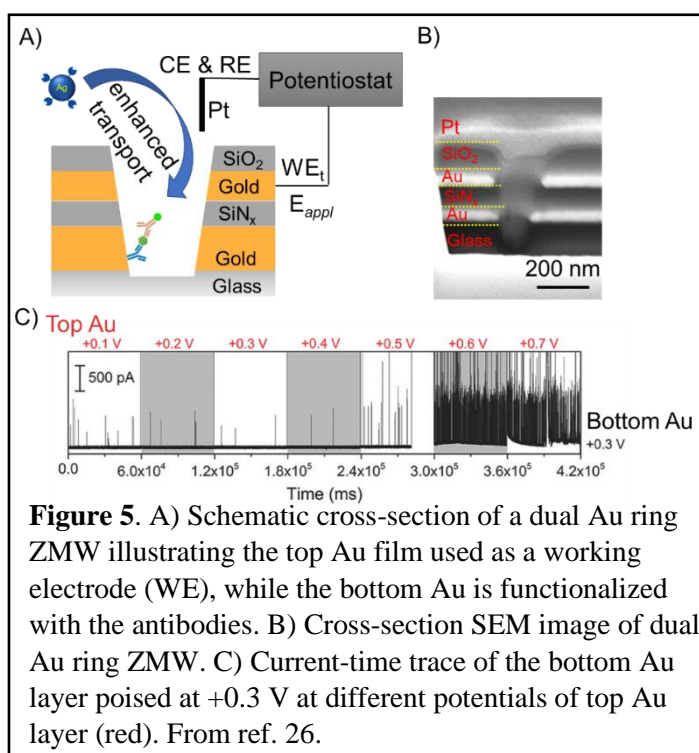
This aim focuses on improving the speed and sensitivity of the nanophotonic sensor platform by introducing another hierarchical gold and silicon dioxide layer such that each pore supports two vertically spaced gold layers as schematically shown in **Figure 5A**.<sup>19</sup> The SEM image of our preliminary fabrication attempt is shown in **Figure 5B**, where the two gold layers (100 nm each) are separated by the silicon nitride insulator layer and the top gold layer is protected by the silicon dioxide layer. As discussed in Aim 1, the bottom gold layer will be used to functionalize biorecognition elements, whereas the top gold layer will be used to apply suitable potentials to control the transport of Ag NPs. For example, applying a small positive potential (+0.3 V) to a solution containing negatively charged citrate-capped Ag NPs enhances the capture of NPs by the nanopore because of the local increase in the electric field within the nanopore. Additionally, the same architecture can be used to improve the detection time for the approach described in Aim 2 without functionalizing the bottom gold layer. Previously, Bohn and co-workers used this architecture to study the oxidation of single Ag NPs electrochemically (Figure 5C).<sup>26</sup> In their experiments, the bottom gold layer was poised to +0.3 V to detect the oxidation of Ag NPs, and the potential of the top gold layer was increased from +0.1 to +0.7 V. The collision frequency of the Ag NPs increased with the potential at the top gold layer. Overall, their approach showed 5×

improvement in NP transport to the nanopore, so it is reasonable to project that by applying an electric field and increasing the nanopore array size, we can achieve LODs in the  $\sim 10^{-18}$  M (aM) range, rendering this an ideal approach for IL-6 and other cytokines that must be measured at  $\sim 10^{-15}$  M concentrations.

### Outcomes and broader impact.

The main expected outcome of this project is an ultra-sensitive, user-friendly digital sensing nanophotonic platform – zero-mode waveguide - for quantifying

biomarkers with LODs in the atto molar ( $\sim 10^{-18}$  M) range. Additionally, the detection or sensing time of



**Figure 5.** A) Schematic cross-section of a dual Au ring ZMW illustrating the top Au film used as a working electrode (WE), while the bottom Au is functionalized with the antibodies. B) Cross-section SEM image of dual Au ring ZMW. C) Current-time trace of the bottom Au layer poised at +0.3 V at different potentials of top Au layer (red). From ref. 26.

Milestones	Time (in months)			
	0 – 6	7 – 12	13 – 18	19 – 24
Aim 1: Detect and determine IL-6 concentration directly by immobilizing NPs into ZMWs				
Aim 2: Quantify IL-6 concentration indirectly by counting the number of captured NPs				
Aim 3: Achieve rapid and ultra-sensitive detection by electric-field enhanced mass-transport of NPs				

the sensor is expected to be faster (<30 minutes) than traditional sensing methodologies enabling its use in point of care (POC) testing. In this proposal we used IL-6 as a model biomarker, naturally one can extend this approach to quantify other biomarkers by utilizing suitable recognition elements such as antibodies and aptamers. Additionally, this platform can be transformed for multiplex sensing by suitably functionalizing ZMWs and employing different size plasmonic NPs (each size targeted for a specific biomarker) to provide a difference in the scattering intensity magnitude (i.e., scattering intensity varies with the NP size).<sup>27</sup> Lastly, the IL-6 -specific assay (and by extension to other specific assays) can be pre-prepared on the nanopore array, and dark-field microscopy can be implemented on a smartphone-based detection setup,<sup>28</sup> making it an easily accessible POC platform.

### References:

1. J.-M. Zhang and J. An, *International Anesthesiology Clinics*, 2007, **45**.
2. G. Arango Duque and A. Descoteaux, *Frontiers in Immunology*, 2014, **5**.
3. N. Mangalmurti and C. A. Hunter, *Immunity*, 2020, **53**, 19-25.
4. D. C. Fajgenbaum and C. H. June, *New England Journal of Medicine*, 2020, **383**, 2255-2273.
5. T. Kishimoto, *International Immunology*, 2021, DOI: 10.1093/intimm/dxab011.
6. T. Giavridis, S. J. C. van der Stegen, J. Eyquem, M. Hamieh, A. Piersigilli and M. Sadelain, *Nature Medicine*, 2018, **24**, 731-738.
7. S. Hojyo, M. Uchida, K. Tanaka, R. Hasebe, Y. Tanaka, M. Murakami and T. Hirano, *Inflammation and Regeneration*, 2020, **40**, 37.
8. C. A. Hunter and S. A. Jones, *Nature Immunology*, 2015, **16**, 448-457.
9. S. A. Jones and C. A. Hunter, *Nature Reviews Immunology*, 2021, **21**, 337-339.
10. J. M. Haissman, L. S. Vestergaard, S. Sembuche, C. Erikstrup, B. Mmbando, S. Mtullu, M. M. Lemnge, J. Gerstoft and H. Ullum, *JAIDS Journal of Acquired Immune Deficiency Syndromes*, 2009, **52**, 493-497.
11. E. Tackey, P. E. Lipsky and G. G. Illei, *Lupus*, 2004, **13**, 339-343.
12. W. Swardfager, K. Lanctôt, L. Rothenburg, A. Wong, J. Cappell and N. Herrmann, *Biological Psychiatry*, 2010, **68**, 930-941.
13. O. P. Kristiansen and T. Mandrup-Poulsen, *The Good, the Bad, or the Indifferent?*, 2005, **54**, S114-S124.
14. H. Murthy, M. Iqbal, J. C. Chavez and M. A. Kharfan-Dabaja, *Immunotargets Ther*, 2019, **8**, 43-52.
15. E. H. Cheteh, V. Sarne, S. Ceder, J. Bianchi, M. Augsten, H. Rundqvist, L. Egevad, A. Östman and K. G. Wiman, *Cell Death Discovery*, 2020, **6**, 42.
16. D. Wu, M. D. Milutinovic and D. R. Walt, *Analyst*, 2015, **140**, 6277-6282.
17. C. Wu, A. M. Maley and D. R. Walt, *Critical Reviews in Clinical Laboratory Sciences*, 2020, **57**, 270-290.
18. L. P. Zaino, D. A. Grismer, D. Han, G. M. Crouch and P. W. Bohn, *Faraday Discussions*, 2015, **184**, 101-115.
19. D. Han, Garrison M. Crouch, K. Fu, L. P. Zaino Iii and P. W. Bohn, *Chemical Science*, 2017, **8**, 5345-5355.
20. K. Fu, W. Xu, J. Hu, A. Lopez and P. W. Bohn, *Cold Spring Harb Perspect Med*, 2019, **9**.
21. K. Fu, S.-R. Kwon, D. Han and P. W. Bohn, *Accounts of Chemical Research*, 2020, **53**, 719-728.
22. V. Sundaresan and P. W. Bohn, *Chemical Science*, 2020, **11**, 10951-10958.
23. S. Baek, D. Han, S.-R. Kwon, V. Sundaresan and P. W. Bohn, *Analytical Chemistry*, 2022, **94**, 3970.
24. K. Aslan, C. C. Luhrs and V. H. Pérez-Luna, *The Journal of Physical Chemistry B*, 2004, **108**, 15631-15639.
25. T. Li, X. Xu, G. Zhang, R. Lin, Y. Chen, C. Li, F. Liu and N. Li, *Analytical Chemistry*, 2016, **88**, 4188.
26. K. Fu, D. Han, G. M. Crouch, S.-R. Kwon and P. W. Bohn, *Small*, 2018, **14**, 1703248.
27. K. A. Willets and R. P. V. Duyne, *Annual Review of Physical Chemistry*, 2007, **58**, 267-297.
28. D. Sun and T. Y. Hu, *Biosensors and Bioelectronics*, 2018, **99**, 513-518.

## **Executive Summary**

### **“An innovative optical fibre device for Micro-pollutants and Greenhouse Gas Monitoring”**

Over the last century, the world's population has increased rapidly leading to an exponentially expansion of industrial manufacturing plants. A by-product of manufacturing is the emission of pollutants into the atmosphere and also river. Fine particles in atmosphere generated from power plants, motor vehicles, and residential wood burning can bypass the nose and throat and penetrate deep into the lungs and some of them can enter to the circulatory system. Studies in the past decade have found that an exposure of fine particle can cause a premature death from heart and lung disease. The report by World Health Organization (WHO) in 2016 showing that the ambient air pollutant due to exposure to fine particulate matter of 2.5 microns are responsible for an estimated 4.2 million premature deaths every year.

Thailand is one of the countries in southeast Asia (ASEAN) that air quality especially in the capital (Bangkok) has been obviously getting worse in the beginning of 2019. The pollution level (PM2.5) and greenhouse gas (CO, CO, NO<sub>2</sub>) remains at hazardous level in many areas of Bangkok and the surrounding provinces. Experts conclude that the combustion from diesel engines, burning of biomass and industrial activities are the main causes of the situations from both inside country and neighbouring countries. According to a report by the Bangkok Metropolitan Administration (BMA) Health Department, it is showing that nearly 40,000 people in the two main districts of Bangkok have gone to hospitals to receive treatment for respiratory diseases since September 2019.

Therefore, the research on the development of air quality monitoring and take mitigating actions to reduce air pollution are of interest. Many air quality sensing methods have been developed over the past decade. While these techniques are widely used for gas sensing applications, monitoring methods based on optics have proven to be an ideal method for remote and real-time particles and gas monitoring. The proposed particles and gas monitoring system in this project include 3 optical systems.

1. Fiberized SPR sensor using the kretschmann configuration for CO<sub>2</sub> and CH<sub>4</sub> detection by depositing a selective material on metal surface of SPR system.
2. Hollow-core polymer optical fiber specific absorption characteristics of CO<sub>2</sub> and CH<sub>4</sub> occurring in the mid-IR region spanning from 2 to 12 microns. The concentration of gas can be deduced from absorption measurements by knowing the absorption strength of ethylene at specific optical frequencies. This approach eliminates functionalization procedure and necessity of regular recalibration. The absolute measurement will be achieved by 1) implementing a reference arm isolated from the environment; 2) using a reference at wavelength far from the peak, or 3) using modulation techniques commonly found in gas sensing.
3. Fiber Bragg grating will be used for fine particles trapped monitoring for PM2.5 detection.

Two simultaneous factors were established within the last decade which enabled this project in this timeline. (a) Advances in the field of photonics and nanotechnology, that enabled the wavelength selectivity proposed in this project. (b) The enormous leap in manufacturing techniques which enabled autonomous technologies and the next generation of compact air-pollutant monitoring. The novel fiber particle and gas sensor proposed in this project offers a step change in both physical size and power consumption compared to existing commercially available gas sensing technology, making it an ideal candidate for low-cost surveying and exploration missions.

**Project title:** An innovative optical fiber device for Micro-pollutants and Greenhouse Gas Monitoring

## 1. Literature Review

Over the last century, the world's population has increased rapidly leading to an exponentially expansion of industrial manufacturing plants. A by-product of manufacturing is the emission of pollutants into the atmosphere and also river. Thus, the development of air quality monitoring and take mitigating actions to reduce air pollution including the particles matter and harmful greenhouse gas become more interesting. Various gas and particle sensing techniques have been developed over the past decade.

The basic concept of optical gas sensing is based on the molecular absorption of light which is call infrared spectroscopy. Infrared (IR) spectroscopy is the interaction of IR light with matter leading to the vibrations on specific bonds for specific wavelength within the molecule. This phenomenon of a molecule causes the decreasing of light energy call absorption.

Among numerous kinds of optical sensing detection technologies such as infrared absorption spectroscopy, photo-acoustic, and spectroscopy, the sensors based on Surface Plasmon Resonance (SPR) sensing technology are favoured by a lot of researchers [1]. Thus, plasmon sensors are gradually becoming one of the highly sensitive and high-precision instruments for sample analysis showed that "Surface Plasmon Resonance (SPR) was used for the real-time detection of small changes in the effective refractive index of metal-dielectric interfaces", which has relatively high sensitivity[2, 3].

Other advance optical techniques that have been develop for particles and gas detection is the optical fiber sensor technology. Hollow-core fiber for gas sensing applications has been developed in years. Mid-infrared gas sensing based on hollow-core MOF has been demonstrated in 2019[4]. The 3.2 m length fiber was used to enhance the time and area of light–gas interaction. In 2020, nitrous oxide detection using the hollow-core MOF was exhibited. In this work, light was propagated inside an air core filled with the analyte gas, in which the microchannel air-core serves as a low-volume and robust absorption cell. Laser-based gas sensors utilize borosilicate fiber because the absorption wavelength of the monitoring nitrous oxide is located at 5.26  $\mu\text{m}$ [5]. Laser-based dual gas sensing of methane and carbon dioxide detection is achieved by using a 1m length of silica hollow-core MOF. The absorption wavelengths of carbon dioxide and methane are 1.574  $\mu\text{m}$  and 3.334  $\mu\text{m}$ , respectively, corresponding to the near- and mid-infrared spectral region. This work showing that, the monitoring crosstalk between methane and carbon dioxides can be well avoided, which paves the way for multi-component gas sensor[6]. In 2019, hollow-core photonic crystal fiber was also developed as the particles trapped for an efficient airborne PM<sub>2.5</sub> monitoring [7]. The micro channel inside the hollow-core MOF is treated as microcells to provide a gas–light interaction platform component gas simultaneous detection due to the broadband guided in the fiber core, nearly covering all molecule absorption lines.

## 2. Problem Statement/Objectives

### Problem Statement

Fine particles in atmosphere can be generated from many sources include power plants, motor vehicles, airplanes, residential wood burning, forest fires, agricultural burning, volcanic eruptions, and dust storms. PM<sub>2.5</sub> is a category of fine particles in atmospheric which brought more concern in the health awareness from people around the world.

PM<sub>2.5</sub> refers to atmospheric particulate matter (PM) that have a diameter of less than 2.5 microns, which is 30 times smaller than the diameter of a human hair. This category of particles

is even smaller than their counterparts PM10, which are particles that are 10 micrometres or less. Therefore, the PM2.5 are called fine particles.

Since the small size and the light weight of fine particles, they tend to stay longer in the air than heavier particles leading to an increasing of the chances of humans and animals inhaling them into the bodies. Due to their diminutive size, PM2.5 can bypass the nose and throat and penetrate deep into the lungs and some of them can enter to the circulatory system.

Studies in the past decade have found that an exposure of fine particle can cause a premature death from heart and lung disease. The medical research published in 2022[4] suggests that long-term exposure to PM2.5 may lead to plaque deposits in arteries, causing vascular inflammation and a hardening of the arteries which can eventually lead to heart attack and worsen chronic disease such as asthma, heart attack, bronchitis, and other respiratory problems. According to the report by World Health Organization (WHO) in 2016 that the ambient air pollutant due to exposure to fine particulate matter of 2.5 microns are responsible for an estimated 4.2 million premature deaths every year.

Apart from the increasing of fine particles in which effect to the global health of humans and animals, greenhouse gas which are the harmful gases can also elevate the premature death of humans from many diseases. Harmful gases found in the air include carbon monoxide (CO), carbon dioxide (CO<sub>2</sub>), methane (CH<sub>4</sub>), and nitrogen dioxide (NO<sub>2</sub>). These poisonous gases are typically created by the same activities to create the PM2.5 such as the burning of wood, oil, coal, charcoal, natural gas, and other fossil fuels are some examples of combustion processes. Exposure to high levels of these gases can cause harmful health conditions, including respiratory infections, heart disease, and lung cancer.

Thailand is one of the countries in southeast Asia (ASEAN) that air quality especially in the capital (Bangkok) has been obviously getting worse in the beginning of 2019. The pollution level (PM2.5) and greenhouse gas (CO<sub>2</sub>, CO, NO<sub>2</sub>) remains at hazardous level in many areas of Bangkok and the surrounding provinces. Experts conclude that the combustion from diesel engines, burning of biomass and industrial activities are the main causes of the situations from both inside country and neighbouring countries. According to a report by the Bangkok Metropolitan Administration (BMA) Health Department, it is showing that nearly 40,000 people in the two main districts of Bangkok have gone to hospitals to receive treatment for respiratory diseases since September 2019. From the study, Bangkok's PM2.5 haze usually occurs in drought season or cold season of Thailand due to the stagnant air movement. The air pollutant crisis also take place in other ASEAN countries such as Myanmar, Laos and Cambodia.

Therefore, the research on the development of air quality monitoring and take mitigating actions to reduce air pollution are of interest. Many air quality sensing methods have been developed over the past decade. Some of the reported techniques include:

- Gas Chromatography (GC) techniques where components of the gas sample are dissolved in a solvent and vaporized to separate the constituents [5].
- Mass Spectrometry technique using the measuring the mass of the compound's molecule to differentiate organic compounds [6].
- Ground Penetrating Radar (GPR) is geophysical technique used for investigations of the earth's subsurface with high resolution, potentially recovering materials that can radiate gases into the environment.

While these techniques are widely used for gas sensing applications, monitoring methods based on optics have proven to be an ideal method for remote and real-time particles and gas monitoring.

The above clearly illustrate the need to develop more reliable in situ measurement to tackle the ever-increasing effects of the PM2.5 and harmful greenhouse gases on the global health awareness. The aim of this research project is to develop and design the optical fiber-based

surface plasmon resonance (SPR), optical fiber grating and hollow-core fiber for the fine particle and gas sensing applications.

**Proposed research programme:** The proposed particles and gas monitoring system will exploit by using 3 main optical systems.

1. Fiberized SPR sensor using the kretschmann configuration for CO<sub>2</sub> and CH<sub>4</sub> detection by depositing a selective material on metal surface of SPR system.
2. Hollow-core polymer optical fiber specific absorption characteristics of CO<sub>2</sub> and CH<sub>4</sub> occurring in the mid-IR region spanning from 2 to 12 microns. The concentration of gas can be deduced from absorption measurements by knowing the absorption strength of ethylene at specific optical frequencies. This approach eliminates functionalization procedure and necessity of regular recalibration. The absolute measurement will be achieved by 1) implementing a reference arm isolated from the environment; 2) using a reference at wavelength far from the peak, or 3) using modulation techniques commonly found in gas sensing.
3. Fiber Bragg grating will be used for fine particles trapped monitoring for PM2.5 detection.

For the hollow-core fiber system, the sensing medium will be based on antiresonant hollow-core optical fibers (ATR), where light is guided by the hollow core which simultaneously acts as a gas chamber. Less than 1 ml of sampled air would be required for absorption measurements allowing to minimize air recycling time decreasing response time of the sensor and helping to maintain compact footprint of the whole system. The sensing part also won't require electrical contacts which can be particularly sensitive in humid environment. The hollow-core geometry of optical fibers relax requirements on the material of the optical fiber as light interaction with the fiber structure is minimal. This is particularly important for the mid-IR region where most materials exhibit strong absorption introducing high losses and screening signal of the target gas. Some materials like chalcogenide glasses are transparent at these wavelengths, but they are expensive, chemically unstable, and frequently involve highly toxic materials.

**Objectives:** A key task of this project is demonstration of three types of particles and gas sensing system based on the optical fiber sensor system.

1. Fiberized-SPR for greenhouse gas detection is the project collaborate with National Oceanography Centre (NOC), Southampton, UK.  
The SPR system with kretschmann configuration will be created by using the small BK7 prism (10x10x10 mm) with specific angle design for the resonance wavelength of 1550nm. Metal layer (Gold, Au) for the generation of SPR effect will be deposit on one of prism surface with the thickness of 40nm. Optical fiber collimators will connect with the prism to launch the light into the prism and also for the collecting the reflected light to the detector. Selective material for specific gas such as PDMS polymer for methane (CH<sub>4</sub>) detection will be deposited on metal surface. Change of the refractive index of material on above metal surface will be used to analyze the concentration of detected gas.
2. Gas sensing using hollow-core fibers. The fibers will be manufactured using an extrusion system based on the fusion deposition modelling 3D printer. The extrusion method for antiresonant fibers was recently demonstrated by our research team. Hollow-core fiber operating in THz spectral region was directly extruded from a micro-structured nozzle. Several types of polymers will be tested for the fiber manufacturing including PET and TOPAS. Subsequent drawing process allows to reduce fiber dimensions to those required for operation in mid-IR. The extrusion system is low-cost and compact.
3. Particle detection using fiber Bragg grating will be fabricated by writing the grating inside the optical fiber core at the fiber tip. The optical fiber tip will be modified to create the thin



membrane which can be vibrate with the flow of particles. Vibration of the membrane can be detected by the close grating resulting in the change in the reflected Bragg wavelength.

### Equipment needed for the project

Activity	Equipment	Availability	
		Yes	Need to order
1. Manufacture of fiber drawing system and fiber fabrication	FDM 3D printer	✓	
	Electronic equipment including a microcontroller, limit switch	✓	
	Mechanical equipment including a stepper motor, linear translation stage	✓	
	Metal 3D printed structure nozzle	✓	
2. Characterization of fabricated hollow-core fiber	Mid-IR light source		✓
	Mid-IR spectrometer		✓
	Optical fiber connector and optical fiber cleaving system		✓
3. Fiberized-SPR	Prism fabrication		✓
	Metal thin film deposition		✓
	Optical fiber collimator		✓
4. Gas sensing system	CO <sub>2</sub> and CH <sub>4</sub> gas source		✓
	Gas controlling and pumping system		✓

### 3. Outline of tasks/Workplan

**Project workflow:** The research group at the Suranaree University of Technology will be working on developing a prototype optical system for particle and gas monitoring. This will include fabrication of the optical fiber, the fabrication of SPR system, integration of light source and detector into a single system.

University of Southampton will be the collaborator to develop the fiber Bragg grating system for particle detection.

Thailand and National Oceanography Centre (NOC) in UK are the stake holder who will test the prototype of the sensing system for both in Thailand and UK.

### 4. Outcomes

At the end of the first year, we expect to achieve the prototype of gas sensing based on SPR system and the optical fiber drawing system to fabricate the hollow-core fiber for gas sensing. The developed fiber drawing system is expected to be able to fabricate the hollow-core fiber with the desired fiber dimension. Moreover, the laboratory-based system of the particle detector based on the fiber Bragg grating should be achieved.

If the project can continue in the second year, the characterization of the optical fiber will be performed in mid-IR region. The guiding performance of the fabricated optical fiber will be analyze. Applications of the fabricated MPOF for ethylene gas sensing will be invented. At least two publications are expected related to the fabrication and experimental validation of mid-IR hollow-core fiber. The second publication will be about the applications in ethylene gas sensing.

### 5. Impact

The novel fiber particle and gas sensor proposed in this project offers a step change in both physical size and power consumption compared to existing commercially available gas sensing technology, making it an ideal candidate for low-cost surveying and exploration missions.

The project will allow to establish academic links between British and Thai scientists working across three different academic institutions. The collaboration will allow to combine expertise in particle and gas sensing to solve a health issue due to the air-pollutant for both in Thailand and UK, optical signal processing and fiber manufacturing to develop gas sensing system. An important part of this project is development various type of sensors including SPR system, fabrication of microstructured polymer fibers for mid-IR spectral region which optically is very challenging. The research programme will not only allow to optimise their design and manufacturing process, but also will investigate effect of the environment on their optical properties, which could be affected by gas absorption and humidity. The proposed fiber manufacturing process will eliminate the need for expensive cleanroom grade equipment traditionally used for optical fiber manufacturing, making them more accessible to interest parties. Although the project aims at developing the system addressing primarily Thailand, it can be also exported to other countries (most of which are on the low- or mid-income countries list) and help them in the improvement of air-quality in their country for better health.

By collaborate this research project with Optoelectronics Research Centre (ORC), University of Southampton will allow the exchange of knowledge and know how through human resources, access to equipment and consumables which will be able to establish and maintain this collaboration.

The Optoelectronics Research Centre (ORC), University of Southampton has a long-established track of record for pioneering work in photonics and is internationally recognised as a world leader in the field of fiber optics and laser devices. It has extensive world class fabrication and experimental facilities and is active across a very broad range of topics and technologies. In 2008 the ORC moved into a new building incorporating a state-of-the-art (>100 million pound) clean room, ensuring that fabrication capabilities remain truly world class. It currently has ~200 research staff and students and over 50 labs focused on optical waveguides and their applications. Within the fields most relevant to this proposal, the ORC has been making fibers and fiber lasers for over 20 years. This expertise has been consistently recognised by EPSRC, most recently when the ORC was selected to host Future Photonics Hub creating a bridge between industry and academia.

## References

1. Torino, S., et al., *PDMS membranes as sensing element in optical sensors for gas detection in water*. Sensing and Bio-Sensing Research, 2017. **16**: p. 74-78.
2. Liu, Z., J. He, and S. He, *Characterization and Sensing of Inert Gases with a High-Resolution SPR Sensor*. Sensors, 2020. **20**(11): p. 3295.
3. Michel, D., et al., *Surface Plasmon Resonance Sensor for In Situ Detection of Xanthan Gum*. IEEE Journal of Selected Topics in Quantum Electronics, 2016. **22**(3): p. 379-382.
4. Pope III, C.A., et al., *Lung Cancer, Cardiopulmonary Mortality, and Long-term Exposure to Fine Particulate Air Pollution*. JAMA, 2002. **287**(9): p. 1132-1141.
5. Loughrin, J.H., S.W. Antle, and J. Polk, *A Gas Chromatographic Method for the Determination of Bicarbonate and Dissolved Gases*. Frontiers in Environmental Science, 2017. **5**.
6. Shimma, S., Toyoda, M. , *Miniaturized Mass Spectrometer in Analysis of Greenhouse Gases: The Performance and Possibilities*. 2012: IntechOpen.

## **Executive Summary for (Health Category)**

### **‘Non-contact cardiac cycle monitoring using microcomb-based dual-frequency terahertz lidar’**

*The challenge.* – Cardiac cycle monitoring, that is the continuous detection of heartbeat rate and its variability, is of critical importance to medical diagnosis and public health observation. To date, the conventional approaches such as electrocardiogram (ECG) device need to maintain contact with human body to work properly, which is not suitable for the increasingly demanding situations where efficiency, comfort, and a high level of hygiene are required. Non-contact techniques have been developed using novel image/video analysis and microwave/radiofrequency radar or laser lidar approaches. However, these new methods suffer from low resolution, high instability or the inconvenience and inefficiency caused by the need to undress, rendering them immature for practical clinical deployment or long-term in-home usage. As such, the development of robust non-contact cardiac cycle monitoring technology that is with a high resolution and a low noise floor and that is also with the capability of penetrating clothes without imposing any health hazard is urgently needed.

*Proposed project.* – Leveraging the cutting-edge microcomb technology and the parallel continuous-wave photomixing multifrequency terahertz (THz) generation method that are at the front line of photonics and THz research, a dual-frequency THz lidar will be developed to perform non-contact cardiac cycle monitoring. Using various microresonator platforms for microcomb generation, low-noise nonlinear optical waves with THz-range oscillation frequencies will be produced with a compact near-infrared laser. A high-speed PIN diode will be adopted to convert the optical waves into two THz signals whose frequency instabilities (or phase noises) are correlated. By applying the frequency-modulated continuous-wave (FMCW) lidar scheme to the pumping laser, the two THz signals would be frequency-swept over multi-gigahertz range with a  $>100$  kHz sweeping rate and an ultrahigh linearity. More importantly, the frequency sweeping directions of the two THz signals are always opposite, which can cancel the microcomb frequency instabilities and the phase noise in the microwave reference during the simultaneous measurement of displacement and velocity. A collimated THz beam containing the two sweeping frequencies will be directed to the target (e.g., the chest wall of a patient) and the reflected THz power will be collected and down-mixed to the radiofrequency (RF) domain. Off-the-shelf RF components including amplifiers, couplers and mixers will be utilized to perform heterodyne operations in real time to derive the accurate distance and velocity from the two RF signals. As a result, the THz lidar can perform highly sensitive ranging and velocimetry without being impacted by the noise contained in the microwave/laser signals, thereby establishing a reliable scheme for non-contact cardiac cycle monitoring. In this project, ranging and velocimetry tests and proof-of-concept heart rate monitoring will be conducted, and the results will be analyzed and compared with ECG measurement to characterize the performance of the developed THz lidar.

*Intended outcomes.* – 1) Because THz waves can penetrate most fabrics without causing potential health hazard, the developed THz lidar can perform convenient and safe non-contact monitoring with a high efficiency and a superior reliability. 2) With the high carrier frequency, the high emission directivity, and the comprehensive sensing capabilities enabled by the FMCW lidar technology, the THz lidar can not only provide clinically practical non-contact heartbeat rate monitoring but also perform high-precision ranging and velocimetry simultaneously in changing situations. 3) Owing to both the unique nonlinear dynamics of microcombs and the multiple-THz-signal generation with parallel photomixing technology, the novel dual-frequency scheme allows the THz lidar to reach a resolution of a few tens of microns in ranging (with the assistance of phase sensitive technique), and a precision of  $100 \mu\text{m/s}$  in velocimetry, showing orders-of-magnitude improvement over prior THz-based measurements. 4) As the THz generation relies on low-cost and compact microcomb technology and the signal processing is executed in the RF domain with off-the-shelf electronics, the developed dual-frequency THz lidar offers remarkable cost-effectiveness and the potential to be widely deployed with low maintenance cost. 5) With several recent breakthroughs in chip-scale microcomb generation and on-chip THz transmitter and receiver integration in the photonic integrated circuit (PIC) industry, the developed dual-frequency THz lidar scheme may be transferred into an all-on-one-chip compact version for mass production. 6) The developed low-noise multifrequency THz waves can be readily used in THz-based environmental monitoring and high-speed wireless communication applications.

## Project Title

Non-contact cardiac cycle monitoring using microcomb-based dual-frequency terahertz lidar

## Literature Review

Coronary artery disease (CAD) is one of the leading causes of death in the world [1], and the direct and indirect costs associated with CAD are major burdens on our already overstretched healthcare systems. Cardiac cycle monitoring (CCM), that is the real-time observation of the heart rate and its variability [2], is regularly utilized to provide early prognosis of CAD, lower the chance of re-hospitalization, and reduce the overall medical cost. Continuous CCM can provide the surveillance for cardiovascular catastrophes and treatment therapies of chronic d

iseases, thus significantly decreasing the morbidity and mortality rates of aged people and patients with a high risk of CAD [1,2]. In addition to its critical importance to the diagnosis and surveillance of CAD, CCM is also a complementary clinical means for examination of COVID-19 symptoms [3], showing the ever-increasing need of the deployment of CCM for mass screening of the population.

To date, low-cost electrical, optical, and mechanical techniques such as electrocardiogram (ECG) [4], photoplethysmography (PPG) [5] and mechanocardiogram (MCG) [6] require the direct or indirect contact to the human body, which not only causes discomfort, inconvenience and hygiene issues but also severely limits the monitoring efficiency. Moreover, these techniques are inappropriate for specific group of patients, such as infants or patients with burns or allergic reactions [7].

To meet the surging need of low-cost and non-contact CCM technologies, new methods based on video analysis [8] and radar/lidar sensing using radiofrequency (RF) and microwaves [9], ultrasound waves [10] and laser light [11] have been developed, showing respective advantages. However, these methods are still far from being reliable or convenient due to the susceptibility to nonideal ambient conditions, the low sensing resolutions and the incapability of penetrating deeply into clothes. Very recently, heart rate detection using terahertz (THz) leaky waves has been demonstrated [12], showing the promise of performing non-contact CCM while eliminating the need for undressing during a health check. Unfortunately, the demonstrated measurement suffers from very low signal-to-noise ratio (SNR  $\sim 2$ ) because of the relatively low sensitivity and the high phase noise level in the THz signal, thus rendering the device impractical for clinical applications.

## Problem Statement/Objective

Terahertz radiation [13,14] represents the electromagnetic waves of frequencies within the range from  $10^{11}$  to  $10^{13}$  Hz. Compared to microwaves and optical waves, terahertz waves are least explored due to the lack of mature methods for generating or detecting signals in this frequency range. Yet, with the non-ionizing nature and the ability to penetrate various non-conducting materials, THz radiation is widely anticipated to play a pivotal role in biological sensing and medical imaging [15].

Adopting the principle of frequency-modulated continuous-wave (FMCW) radar [16], THz leaky waves have been generated to perform heart rate detection [12]. Although the proof-of-concept experiment has been successfully demonstrated, the SNR of the measurement is much lower than that of a conventional ECG. The main reason for the poor performance is that the frequency instabilities and phase noise in the microwave source is translated into the noise in the phase comparison of signals. And the large multiplication factor ( $n > 30$ ) in the microwave-to-THz chain inevitably increases the noise intensity by a factor of  $n^2$ , thus amplifying the noise power by more than three orders of magnitude.

Motivated by the recent achievements of low-noise THz signal generation with microcombs [17] and multifrequency THz wave generation using photomixing of three lasers [18], this proposed project aims at synthesizing multiple ultralow-noise THz waves in a parallel fashion and using novel dual-frequency FMCW THz lidar scheme to perform highly sensitive non-contact CCM in real time.

Figure 1 presents the principle of the dual-frequency THz lidar. A laser is pumping a microresonator resonance of a high quality factor ( $Q$ ), generating nonlinear waves of Turing-roll state [17] that have two intensive optical sidebands with a THz-range frequency difference. In Figure 1 (a), the pumping line is frequency-modulated by an in-phase & quadrature (IQ) modulator (i.e., a single-sideband frequency shifter) and then combined with the sidebands. The multifrequency optical waves are

registered by an optical-to-THz transmitter (Tx), producing two anti-directionally chirped THz frequencies. The frequency difference between the two THz signals is twice of the modulation frequency, which is usually between 5 and 20 GHz. With necessary beam shaping, the dual-frequency THz emission is sent to the sensing target (Figure 1 (b)), and the reflected THz waves are received by a THz receiver (Rx) with the function of downmixing. Using a microwave oscillator with frequency multiplication as the THz local oscillator, the THz frequencies are transferred into two RF frequencies with the same chirping direction. As illustrated in Figure 1 (c), the two RF signals are compared with the linearly chirped modulation frequency with off-the-shelf RF components including bandpass filters, amplifiers, and mixers. Two difference frequencies,  $\Delta f_1$  and  $\Delta f_2$ , can be directly analyzed to derive the information of the displacement and the velocity of the sensing target, as the distance (delay) shifts the two frequencies in an anti-directional fashion, while the velocity (via the Doppler effect) shifts the two frequencies in a co-directional manner. The prominent benefits of the dual-frequency scheme are that *the microcomb oscillation frequency instability is cancelled in the measurement of displacement* and that *the noises contained in the local oscillator for downmixing and the imperfect linearization of frequency modulation are cancelled in the measurement of velocity* because of the mechanism of common noise rejection.

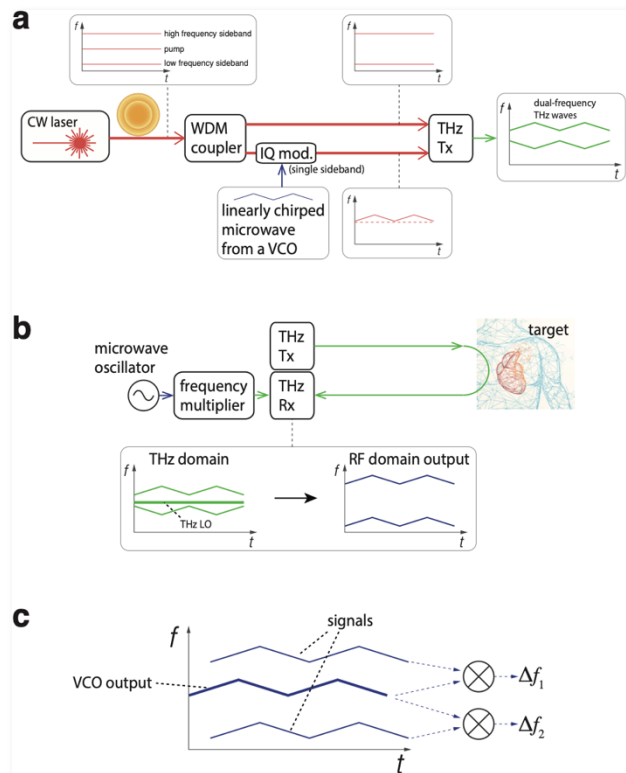


Figure 1. (a) Generation of dual-frequency FMCW THz radiation using a microcomb. (b) Scheme of downmixing the reflected THz signals into the RF domain. (c) Derivation of the measured displacement and velocity using RF signal processing.

Leveraging the unique skillsets of the applicant and his colleagues and the extraordinary infrastructure at the optics and THz laboratories at the University of Adelaide, this project aims to achieve:

- Objective 1: Generate microcombs of THz-range repetition rates with high frequency stabilities and ultralow phase noises.
- Objective 2: Develop a dual-frequency FMCW THz lidar with high ranging resolution and an unprecedented velocimetry precision.
- Objective 3: Demonstrate real-time cardiac cycle monitoring that outperforms the state-of-the-art non-contact technologies.

## Outline of Tasks/Work Plan

Over the 1.5-year (6 quarters) span of the proposed project, three main tasks will be carried out to achieve the aimed objectives. Each main task consists of two to three subtasks. Figure 2 shows the timeline of the course of the project.

Tasks	Subtasks	Q1	Q2	Q3	Q4	Q5	Q6
1. Development of optical microcomb sources	1.1						
	1.2						
	1.3						
2. Dual-frequency FMCW THz generation	2.1						
	2.2						
3. Cardiac cycle monitoring experiment	3.1						
	3.2						

Figure 2. Overview of the work plan.

### Task 1. – Development of optical microcomb sources.

This task lays the foundation of the entire project by developing low-noise optical sources for dual-frequency THz radiation generation with continuous-wave (CW) photomixing technique. Three microresonator platforms will be tested and their performance will be systematically compared.

Subtask 1.1. – Microcomb generation with crystalline whispering gallery mode resonators (Q1).

Multiple crystalline lithium niobate (LN) and magnesium fluoride ( $\text{MgF}_2$ ) microresonators (see Figure 3 (a)) have already been fabricated in Dr Weng's lab, showing  $Q$ s of  $>2 \times 10^8$ . Dispersion measurement will be carried out and a 1550-nm laser will be used to pump mode resonances to generate Kerr comb sidebands. Mode families that can produce microcombs with THz-range repetition rate will be characterized in terms of power threshold, conversion efficiency, and frequency stability.

Subtask 1.2. – Generation of Turing rolls in fiber Bragg grating (FBG) resonators (Q2 – Q3).

To obtain desired resonance numbers and dispersion, grating structures [19] will be designed and fabricated at the Australian National Fabrication Facility (ANFF) Fiber Bragg Grating suite at the University of Sydney (UoSyd) (see Figure 3 (b) for an example). Kerr comb oscillators will be generated in Dr Weng's lab, and the noise performance will be measured using the electrooptic frequency division technique [17]. Active laser locking will be utilized to allow stable long-term operation of the Kerr combs.

Subtask 1.3. – Microcomb generation in on-chip silicon nitride ( $\text{Si}_3\text{N}_4$ ) microresonators (Q3 – Q4).

Integrated  $\text{Si}_3\text{N}_4$  microcombs [20] (see Figure 3 (c)) will be provided by the Integrated Photonics and Applications Center at the Royal Melbourne Institute of Technology (RMIT) led by Prof Arnan Mitchell, who is collaborating with Dr Weng on developing compact frequency comb technology. These chipscale microcombs will be packaged with temperature control and power stabilization. With frequency division, the microcombs will be locked to a microwave reference. Repetition rate phase noise will be measured at both the free-running and the actively locked states. A compact semiconductor amplifying unit will be added on the microcomb packages to ensure that the optical power is above 30 mW to maximize power level of THz radiation from photomixing.

**Task 2. – Dual-frequency FMCW THz generation.**

This task focuses on generating dual-frequency THz signals and applying linear frequency modulation. Receiving and downmixing THz waves will be executed for signal processing in the RF domain.

Subtask 2.1. – Parallel dual-frequency FMCW THz generation in a single PIN diode (Q2 – Q5).

Multiple comb teeth of generated microcombs will be selected by optical filtering and then sent to a PIN-diode-based CW-THz emitter to generate multiple THz frequencies simultaneously [18]. One of the comb teeth will be frequency modulated with an optical IQ modulator. The modulation frequency will be produced by a microwave voltage-controlled oscillator (VCO) that is driven by a high-bandwidth field-programmable gate array (FPGA) unit. The VCO's frequency will be linearly swept by programming the output voltage function of the FPGA unit. The generated THz radiation will be received and mixed down to the microwave domain using a Virginia Diodes Inc. (VDI) Spectrum Analyzer Extension (SAX) module (see Figure 4) at the Terahertz Engineering Lab in the University of Adelaide led by A/Prof Withawat Withayachumnankul, who is currently collaborating with Dr Weng on THz comb generation and spectroscopy. The linearity of the chirping and the phase noise of the down-converted microwave signals will be characterized and optimized.

Subtask 2.2. – THz wave beam forming and characterization (Q4 – Q5).

Using the THz waveguide and beam-forming technique developed at the Terahertz Engineering Lab [21], free space THz waves will be generated. The beam profile will be optimized to maximize the

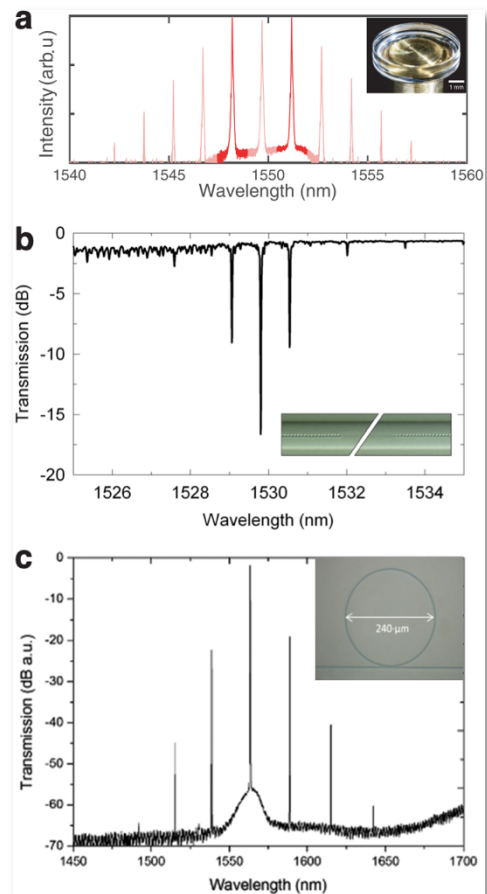


Figure 3. (a) Optical spectrum of the Turing-roll microcomb developed by Dr Weng [17]. (b) The transmission spectrum of a FBG cavity fabricated at UoSyd [19]. (c) Spectrum of a  $\text{Si}_3\text{N}_4$  microcomb developed at RMIT [20]. The insets are the photos of the microresonator samples.



collected power from reflection in sensing applications. The beam quality will be characterized. Diffraction of multifrequency THz waves using the leaky-wave antenna [12] will be explored, and parallel generation of multifrequency THz wave of 4 and 6 frequencies will be attempted.

### **Task 3. – Cardiac cycle monitoring experiment.**

This task is centered on performing the ranging and velocimetry experiments using the developed dual-frequency THz waves. After proper calibration, the THz lidar will be applied in proof-of-concept CCM demonstrations.

#### Subtask 3.1. – Displacement and velocity measurement with dual-frequency THz waves (Q4 – Q5).

The dual-frequency THz beam will be directed to a sensing target such as a rotating metal sphere/disk. With a frequency multiplied low-noise microwave reference as the local oscillator, the SAX module will be used to down-convert the THz frequencies to the microwave domain. The two relevant microwave signals will be amplified and mixed with RF amplifiers and mixers so the two frequencies can be directly compared with the reference signal of the FMCW lidar (i.e., the VCO's sweeping frequency). The distance and the rotating speed of the object will be measured. The results will be used to determine the lidar resolution and precision, and the noise sources will be analyzed and suppressed with setup optimization and post processing.

#### Subtask 3.2. – Human cardiac cycle monitoring using the THz lidar (Q5 – Q6).

The dual-frequency THz lidar will be implemented to demonstrate non-contact CCM. With clothes on, a human's chest wall will be the sensing target. Since both the displacement and the velocity of the chest wall would vary during a cardiac cycle, the data for the ranging and the velocimetry will be analyzed separately and then compared to reveal the best strategy for CCM. Phase comparison between the reflected signal and the reference will be carried out in real time with RF phase comparator, thus dramatically improving the ranging resolution. Long-term continuous measurement under varied physical circumstances will also be conducted to make a comprehensive evaluation of the monitoring performance. A manuscript will be prepared to report the results.

### **Outcomes**

The developed THz lidar is expected to yield ranging and velocimetry performance on a par with or superior to state-of-the-art radar/lidar technologies in terms of measurement resolution and precision. The frequency tuning range of the VCO is around 10 GHz, which corresponds to a resolution of approximately 1.5 cm according to FMCW radar principle. However, the actual frequency tuning range of the microcomb-based lidar can be multiplied using the cascaded four-wave-mixing technique [22] that is fully compatible with the nonlinear photonic platform of the microcomb technology. Assuming a reasonable multiplication factor of 5, the ranging resolution can be improved to  $\sim 3$  mm with the conventional FMCW mechanism. To make further improvement, phase sensitive measurement will be adopted to reach a resolution of  $< 100$   $\mu\text{m}$ .

One of the most remarkable features of the dual-frequency approach is the complete cancellation of the microwave source noise in velocimetry that is usually the dominant noise in FMCW radar/lidar realizations. Owing to this unique feature, the precision of the velocity measurement is ultimately limited by the noise in the optical microcomb oscillation. Based on the recent experimental results showing that the Turing-roll oscillation's phase noise performance is better than that of high-end commercial microwave synthesizers, the velocity measurement precision is expected to reach 100  $\mu\text{m/s}$  using the assumptions that the THz carrier frequency is at  $1 \times 10^{12}$  Hz and that the frequency noise is at 1 Hz/ $\sqrt{\text{Hz}}$  level.

The heart rate monitoring using the developed THz lidar is anticipated to outperform the results in [12] with significantly increased SNR. The parallel measurement of displacement and velocity can potentially deliver more information about the motion of the target, which may assist isolate the cardiac

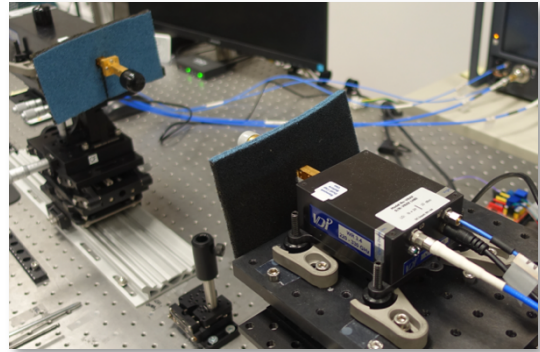


Figure 4. THz receiving and downmixing setup at the Terahertz Engineering Lab.

cycle motion from other physical interferences such as respiration motion artifacts, therefore yielding a more pragmatic and flexible method for long-term CCM with high fidelity. Moreover, as the signal processing after the downmixing of THz waves is exclusively in the RF domain, the sensing results would be directly derived using analog RF and microwave components instead of using digital data acquisition and postprocessing. As a result, the device is cost-effective and robust with a long maintenance-free period, making it not only suitable for fast and efficient clinical implementation but also applicable for all-time in-home health monitoring and physiological surveillance.

In addition to the practical non-contact CCM development, the parallel THz generation with multi-laser CW photomixing will be the first demonstration of THz comb generation using an optical microcomb. The THz comb will be diffracted with the leaky wave antenna to cover a wide angle in space, which could dramatically enhance the acquisition rate and the sensing speed. The low-noise THz comb may even find important applications in high-bandwidth THz near-range wireless communications [23]. This research direction will be immediately explored after the CCM experiment at the Terahertz Engineering Lab with the high-bit-rate THz telecommunication setup established with the strong support from the University of Adelaide and the Australian Research Council.

## Impact

Owing to the versatility of the THz technology and the interdisciplinary nature of the project, the impact is anticipated to be manifold. First, this project will solidify microcomb technology as a competitive and practical solution to cost-effective low-noise THz wave generation. Second, the multifrequency THz generation method will open the road for massively parallel THz radiation generation, potentially leading to the development of metrology-grade THz comb technology. Third, because the entire setup, including microcomb stage, the THz photomixing stage and the microwaved/RF processing stage can be all integrated with existed technologies, the developed device may be further improved to yield a fully integrated version, presenting an all-on-one-chip product. Fourth, the developed CCM technology can be combined with magnetic resonance imaging (MRI), computerized tomography (CT) or X-ray angiography to perform detailed coronary arterial imaging [24,25], thus providing a rich reservoir of physiological information for critical medical applications in an efficient and non-contact manner. Fifth, the developed novel dual-frequency FMCW radar/lidar scheme can be readily applicable in other precision measurements, such as space navigation and advanced manufacturing. Finally, the science and the technological novelties explored in this project is at the convergence of the cutting-edge photonics [26] and terahertz [27] technologies. Besides the direct medical/health usage, they will also find important applications in THz-based environmental monitoring [14] and the next-generation wireless networks [23,28], which shows the overarching significance the proposed project bears in alignment with the purpose of the Optica Foundation 20th Anniversary Challenge.

## Reference

- [1] Austen et al., *Circulation* **51**, 5-40 (1975).
- [2] Kranjec et al., *Biomed. Signal Process. Cont.* **13**, 102-112 (2014).
- [3] Taylor et al, *Sensors* **20**, 5665 (2020).
- [4] Geselowitz, *Proceedings of the IEEE* **77**, 857-876 (1989).
- [5] Allen, *Physiol. Meas.* **28** R1 (2007).
- [6] Iftikhar et al., *Sci. Rep.* **8**, 9344 (2018).
- [7] Galli et al., *Sensors* **22**, 4035 (2022).
- [8] Poh et al., *Opt. Express* **18**, 10762 (2010).
- [9] Lee et al., *Sci. Rep.* **8**, 13053 (2018).
- [10] Kranjec et al., *Sensors* **17**, 2637 (2017).
- [11] Bouazizi et al., *ICC 2022 – IEEE International Conference on Communications*, Seoul, 16-20 May 2022.
- [12] Matsumoto et al., *Nat. Electron.* **3**, 122-129 (2020).
- [13] Siegel, *IEEE Transactions on Microwave Theory and Techniques* **50**, 910-928 (2002).
- [14] Tonouchi, *Nat. Photon.* **1**, 97-105 (2007).
- [15] Siegel, *IEEE Transactions on Microwave Theory and Techniques* **52**, 2438-2447 (2002).
- [16] Stove, *IEE Proceedings F (Radar and Signal Processing)* **139**, 343-350 (1992).
- [17] Weng et al., *Phys. Rev. A* **104**, 023511 (2021).
- [18] Thirunavukkuarasu et al., *Appl. Phys. Lett.* **106**, 031111 (2015).
- [19] Marshall et al., *Opt. Express* **18**, 19844 (2010).
- [20] Frigg et al., *APL Photonics* **5**, 011302 (2020).
- [21] Lees et al., *Opt. Lett.* **46**, 5469-5472 (2021).
- [22] Ishimura et al., *APL Photonics* **7**, 066106 (2022).
- [23] T. Nagatsuma, et al. *Nat. Photon.* **10**, 371–379 (2016).
- [24] Shechter et al., *IEEE Trans. Med. Imag.* **25**, 369-375 (2006).
- [25] Çimen et al., *Medical Image Analysis* **32**, 46-68 (2016).
- [26] Kippenberg et al., *Science* **332**, 555-559 (2011).
- [27] Sengupta et al., *Nat. Electron.* **1**, 622-635 (2018).
- [28] Dang et al., *Nat. Electron.* **3**, 20-29 (2020).

## Executive Summary of “Developing Low-Cost, Portable, Integrated OCT Systems Using Low-Loss Silicon Nitride Platform”

Optical coherence tomography (OCT) is a non-invasive imaging modality that provides depth-resolved, high-resolution images of tissue microstructures. Every year, more than 30 million OCT scans are performed all over the world. It has become the de facto diagnostic and monitoring tool for ophthalmic diseases, and an emerging imaging technology in other areas such as dermatology, gastroenterology and breast cancer imaging. However, the cost of an OCT system is typical from tens of thousands of dollars to easily exceeding \$100,000, the size of an OCT system could be on the order of meter cubic, the parts in the OCT system are separated and need to be actively aligned. The cost, the size and the misalignment of the parts are prohibitive these powerful imaging systems to all but the busiest and most sophisticated practices.

We plan to develop a prototype for a low-cost, portable, integrated OCT system based on silicon photonics, more specifically low loss  $\text{Si}_3\text{N}_4$ . The light source, interferometer and spectrometer of the OCT system will be independently developed and then integrated onto the same carrier to ensure the success of the project. The integration of light source will be developed and achieved through two approaches in parallel: i) The higher risk but higher degree of scalability and integration approach - gain chips and  $\text{Si}_3\text{N}_4$  resonators based frequency combs. ii) The lower risk and more conventional approach - SLD diode and  $\text{Si}_3\text{N}_4$  photonic chip co-package. The integration of the interferometer will be based on the low loss  $\text{Si}_3\text{N}_4$  platform, the reference arm will have a length that is long enough to match the path length of the sample arm. The sample arm will be miniaturized using a co-packaging process with MEMS scanners. The integration of the spectrometers will also be based on  $\text{Si}_3\text{N}_4$  platform and achieved through two approaches in parallel i) The stationary FTS with a  $\text{Si}_3\text{N}_4$  grating. ii)  $\text{Si}_3\text{N}_4$  AWG with lenses integrated on the edge of the chip. All these components will be developed around a central wavelength of 1050 nm, and retinal scans will be taken with our system in collaboration with OCT experts also at Shanghai Jiao Tong University.

The outcome of our proposal is expected to be **a prototype of a low-cost, portable, integrated OCT system**. The device we envision, in final form, will be **two orders of magnitude** reduction in price and **several orders of magnitude** reduction in size and weight. It will have the size and weight less than a typical mobile phone, and will have the capability of providing retinal scans at a resolution of less than 10  $\mu\text{m}$ , comparable to midrange clinical devices currently on the market. The schematic of the OCT system is shown in **Fig. 1**. All three core parts of the OCT system are miniaturized and integrated on the same carrier using components and technologies developed in this project.

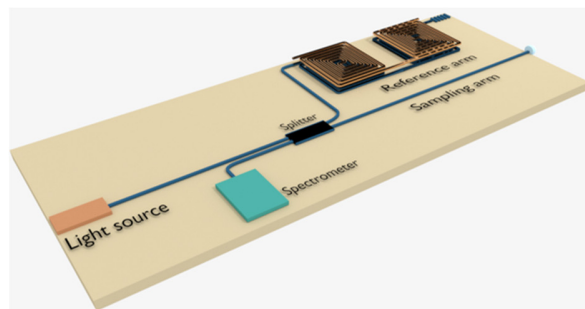


Fig. 1. Schematic of proposed OCT system. All three core parts of the OCT system (light source, interferometer, spectrometer) are miniaturized and integrated on the same carrier.

We expect our systems could be further adapted for imaging and diagnosis of diseases in other specialties using different wavelengths as well, especially in dermatology, dentistry and oncology. Our results will help to reduce costs of the health system while increasing accessibility and compliance for better disease management. We hope that the components and the technologies we developed in this project will help pave the way for low-cost, portable OCT systems and incorporating integrated photonics into optical imaging technologies.

## Developing Low-Cost, Portable, Integrated OCT Systems Using Low-Loss Silicon Nitride Platform

**Literature Review:** Optical coherence tomography (OCT) is a non-invasive imaging modality that provides depth-resolved, high-resolution images of tissue microstructures at high speed. It has become the standard-of-care in medical specialties such as ophthalmology<sup>1-3</sup>, dermatology, and is an emerging imaging technology in other areas such as gastroenterology<sup>4,5</sup> and breast cancer imaging<sup>6,7</sup>. Taking ophthalmology as an example, there are over 30 million OCT scans performed annually around the world<sup>8</sup>. Each generation of OCT machines is more sophisticated and feature-rich than the last, and system prices have continued to rise - today, an OCT machine can easily exceed \$100,000<sup>9</sup>. Given the demand, and high prices, it is no surprise that the market for high end ophthalmic OCT machines is growing at over 8% annually and expected to reach \$1.5 billion by 2023. These powerful imaging systems are cost-prohibitive to all but the busiest and most sophisticated practices. The devices require a dedicated technician to operate them, and quickly become a bottleneck in most offices due to the number of patients that must be scanned on each machine<sup>10</sup>. Additionally, if a machine needs service or becomes misaligned (a common occurrence), office staff must schedule a repair with a biomedical equipment technician (often several days' wait) and reschedule patients whose visits would not be productive without an OCT scan. Therefore, the construction of a portable, handheld, OCT device could increase accessibility, while expanding OCT into settings where use is currently prohibited by its cost and size.

In the past decade, there has been a tremendous growth in the field of integrated photonics. Silicon photonics, in particular, is gaining significant attention. It allows massive fabrication of optical devices at low-cost by utilizing standard fabrication techniques and complementary metal-oxide semiconductor (CMOS) compatible materials. Although the field has its roots in the telecommunications industry, it has expanded to many new applications such as sensing, spectroscopy, nonlinear optics, quantum optics, opto-mechanics, and even neuroscience. Recently, using silicon photonics for miniaturization of different building blocks of OCT systems has been explored by various groups. For example, Yurtsever et al.<sup>11</sup> demonstrated a silicon-based integrated interferometer centered at 1310 nm that had a sensitivity of 62 dB with 115  $\mu$ W power on the sample. Schneider et al.<sup>12</sup> realized an integrated silicon interferometer and an integrated germanium photodiode centered at 1315 nm, which had a sensitivity of 64 dB with 300  $\mu$ W power on the sample, while Eggleston et al.<sup>13</sup> also demonstrated an integrated interferometer with integrated balanced photodiodes and a copackaged MEMS mirror centered at 1310 nm, which had a sensitivity of 90 dB with 550  $\mu$ W power on the sample. Nguyen et al.<sup>14</sup> showed an integrated optics spectrometer centered at 1300 nm that has a sensitivity of 75 dB, and Akca et al.<sup>15</sup> fabricated a miniature spectrometer centered at 1250 nm and a beam splitter system, which had a sensitivity of 74 dB with 500  $\mu$ W power on the sample. We have developed a miniaturized supercontinuum source based on dispersion engineered silicon nitride ( $\text{Si}_3\text{N}_4$ ) centered at 1300 nm, which has a sensitivity of 105 dB with 300  $\mu$ W power on the sample<sup>16</sup>.

However, these works and components are developed for center wavelength around 1300 nm and most platforms are based on silicon which are not suitable for the most widely used ophthalmic systems where the wavelength are commonly around 850 nm or 1050 nm. Very recently, based on  $\text{Si}_3\text{N}_4$  (a promising material to complement silicon at wavelengths below 1.2  $\mu$ m due to its wide optical bandgap and ultra-low loss), Rank et al.<sup>3</sup> demonstrated an arrayed waveguide grating centered around 850 nm, which had a sensitivity of up to 91 dB with 830  $\mu$ W power on the sample. This work shows an increasing interest in the wavelength beyond the telecommunication bands, as well as a step towards realizing integrated OCT system using  $\text{Si}_3\text{N}_4$  platform. However, other key parts of the system, such as the light source, the reference arm, collimating lenses and the CCD, still need to be integrated.

**Objectives:** We plan to develop a prototype for a **low-cost, portable, integrated OCT system** based on silicon photonics, more specifically  $\text{Si}_3\text{N}_4$ , in which the three main



components (light source, interferometer, spectrometer) of the system will be integrated. The center wavelength of the OCT system will first be developed and employed around 1050 nm for diagnosis and management of chronic ophthalmic diseases. Due to the broadband characteristics of  $\text{Si}_3\text{N}_4$  and generalization of the technologies, we expect our systems could be further adapted for imaging and diagnosis of diseases in other specialties using different wavelengths as well, most notably in dermatology, dentistry and oncology. Our objective would be to pave the way toward low-cost, portable OCT and incorporating integrated photonics into optical imaging technologies. Our results will help to reduce costs of the health system while increasing accessibility and compliance for better disease management.

### **Outline of tasks:**

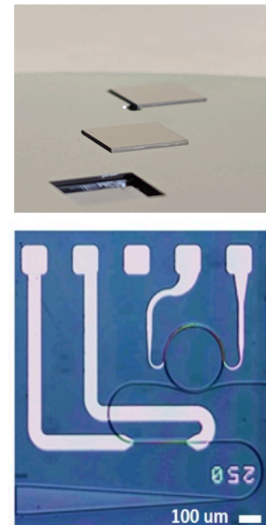
#### **Task 1: Development of $\text{Si}_3\text{N}_4$ platform and the integration of light source chips**

We will utilize the world-leading  $\text{Si}_3\text{N}_4$  fabrication techniques that I developed at the Lipson Group as the base platform for the core of the chip. We propose to use microfabrication techniques such as multipass lithography, chemical mechanical polishing, improved etching and optimized annealing to achieve ultra-low loss in  $\text{Si}_3\text{N}_4$  platform<sup>17</sup>. We will define the passive photonic structures on a silicon wafer, with  $\text{Si}_3\text{N}_4$  grown on  $\text{SiO}_2$  to provide low propagation loss and good coupling to the light source chip. The  $\text{Si}_3\text{N}_4$  chip will be mainly fabricated at the Center for Advanced Electronic Materials and Devices of Shanghai Jiao Tong University. The center is equipped with micro-nano fabrication facilities including e-beam lithography, dual-beam focused ion beam system, double-side alignment UV aligner, spin-coating and developing system, oxidation furnace, nitride low-pressure CVD, rapid thermal processing tool, plasma enhanced CVD, reactive ion etcher, deep-silicon reactive ion etching system, atomic force microscope, etc. These advanced microfabrication equipments can meet the requirements and ensure the successful development of the  $\text{Si}_3\text{N}_4$  platform.

We propose two approaches for the integration of light source chips.

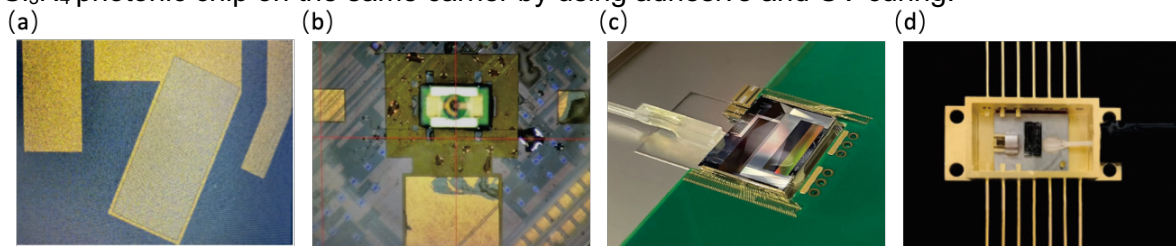
The first approach is to use  $\text{Si}_3\text{N}_4$  resonators to generate frequency combs with and use them as the light source. These resonators are fabricated using the process developed in Task 1. Through self-injection locking and nonlinear processes, it can generate broadband spectrum consisting of discrete lines, and the frequency-spacing is determined by the geometry of the resonator. We have previously shown that that the frequency comb can be generated and used in OCT near 1310 nm by dispersion engineering of  $\text{Si}_3\text{N}_4$  resonator platform. Here, we will use the same technology to generate frequency combs centered around 1050 nm, and further expand the application of OCT with frequency combs.

In order to further reduce the size of the light source, we plan to integrate single-mode gain chips onto the wafer. We plan to pre-etch trenches on the wafer and embed the gain chips in these trenches as shown in Fig. 1 (top). The trenches are defined by lithography, and the silicon substrate is etched by using KOH wet etching. For optical coupling,  $\text{Si}_3\text{N}_4$  waveguides are defined and aligned to the gain chips using pre-defined alignment marks, guaranteeing optimal coupling. The approach ensures, i) good thermal heat dissipation, ii) improved alignment accuracy thus low-loss optical coupling to the photonic structures and iii) ability to use standard silicon processing following the light source chips integration. In addition to integrating single-mode gain chips, we also plan to explore integration of multimode gain chips that are 100  $\mu\text{m}$  wide. We will leverage our recent results on locking longitudinal and spatial multimode gain to low loss  $\text{Si}_3\text{N}_4$  resonators. The large gain waveguide (100  $\mu\text{m}$  x 1 mm long), when butt-coupled to a horn-tapered  $\text{Si}_3\text{N}_4$  waveguide [Fig. 1 (bottom)], ensures high power frequency combs output as well as tolerance of coupling to fabrication variations.



**Fig. 1.** (top) Preliminary demonstration of integration of dies on silicon substrate. (bottom) Ring resonator device with tapered horn coupler for locking multi-mode gain chip.

The second approach is to use conventional superluminescent diode (SLD) as the light source and develop the packaging process with  $\text{Si}_3\text{N}_4$  photonic chips. We plan to utilize the chip packaging and testing platform at Pinghu Institute of Intelligent Optoelectronics of Shanghai Jiao Tong University. This facility is capable of developing widely used chip packaging technologies, such as flip-chip bonding, ultraviolet (UV) curing and butterfly packaging as shown in Fig. 2. For packaging the SLD with  $\text{Si}_3\text{N}_4$  chips, we plan to use the same pre-etch trenches technique described in the previous section to improve the alignment accuracy, and we will design the edge coupler of the  $\text{Si}_3\text{N}_4$  waveguide to match the output mode profile of the SLD, thus increasing the coupling efficiency. Finally, we expect to package SLD diode and  $\text{Si}_3\text{N}_4$  photonic chip on the same carrier by using adhesive and UV curing.

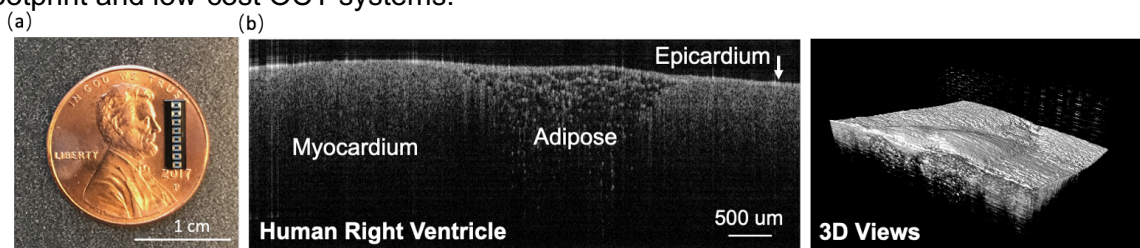


**Fig. 2.** (a) Flip-chip bonding of laser chip. (b) Ultraviolet (UV) curing (c) Packaging of gain chip (RSOA) and silicon chip through edge coupling. (d) Butterfly packaging of laser chip and micro lens.

### **Task 2: Integration of interferometer based on $\text{Si}_3\text{N}_4$ platform**

We propose an interferometer based on  $\text{Si}_3\text{N}_4$  platform. The role of the interferometer in an OCT system, is to generate interference patterns. In today's commercially available OCT systems, for example, Thorlabs Telesto system commonly used in research laboratories and Zeiss Primus OCT system commonly used in clinics, the interferometers consist of free space optics such as beam splitters and mirrors, and normally require hundreds of  $\text{cm}^3$  of volume.

Our proposed interferometer will consist of an input port, an on-chip beam splitter (such as MMI), a long reference arm, a beam output for sampling and an output port to connect to the spectrometer. All these components will be integrated on-chip and can significantly reduce the size of the system down to  $1 \text{ cm}^3$  or even a few  $\text{mm}^3$ . The reference arm will utilize our previous on-chip tunable delay line results<sup>18</sup>. The delay line is composed of a low loss  $\text{Si}_3\text{N}_4$  waveguide up to 0.4 meter long that can be packed into a  $8 \text{ mm}^2$  area as the reference-arm as shown in Fig.3, thus providing great flexibility to match the required path-length for the sample arm. For the low-cost and small-scale of the sample arm, we propose to develop a co-package process for the MEMS scanners. These scans have already been successfully used in other small-footprint and low-cost OCT systems.



**Fig. 3.** (a) Fabricated 0.4 m long  $\text{Si}_3\text{N}_4$  chip in an  $8 \text{ mm}^2$  area. (b) Example of 2D and 3D OCT imaging of a human right ventricle sample from the endocardium side taken with the chip as reference arm<sup>18</sup>.

### **Task 3: Integration of spectrometers**

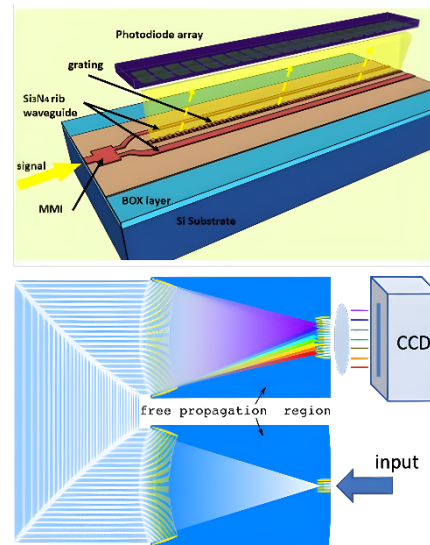
We propose to develop integrated spectrometers and we will try two kinds of independent integrated spectrometer designs.

The first design is using a co-propagative stationary Fourier transform spectrometer (FTS)<sup>19</sup> fabricated with  $\text{Si}_3\text{N}_4$ . The schematic of the FTS is shown in Fig. 4 (top), an optical signal is firstly divided into two parallel  $\text{Si}_3\text{N}_4$  ridge waveguides with different ridge widths. The two waveguides are separated to obtain the required overlap of the evanescent fields of the two excited waveguide modes. Because the excited modes have a slightly different propagation



constant, an interference pattern will be generated between the two waveguides. By placing a grating between the waveguides, the interference pattern can be diffracted upward to a photodiode array. This design provides a solution for broadband operation in combination with high resolution.

The second design is to use an arrayed-waveguide grating (AWG) together with a CCD. AWGs are mainly used for optical communications, but they are also increasingly being used in a range of lab-on-a-chip based photonic sensing systems. AWGs consist of input and output waveguides, input and output star couplers, and an array of waveguides. When broadband light is coupled to the input waveguide, the input star coupler effectively acts as a free propagation region, where the light beam diverges. The divergent beams are coupled to the array of waveguides. The length of the arrayed waveguides increases linearly from one to the next, resulting in different phase delays caused by individual waveguides. At the focal line on the image plane in the output star coupler, only plane waves with the same phase delay interfere constructively. Therefore, each of the output waveguide transmits a single wavelength as shown in Fig.4 (bottom). Several groups have successfully developed AWGs for OCT around 1300 nm and 850 nm. Here, in addition to developing the first AWG centered around 1050 nm for OCT, we will further integrate lenses on the facet of the  $\text{Si}_3\text{N}_4$  chip, and potentially package the line CCD sensor on a PCB.



**Fig. 4.** (top) Schematic of the co-propagative stationary Fourier transform spectrometer (FTS)<sup>19</sup>. (bottom) Schematic of an arrayed-waveguide grating together with a CCD.

**Outcome:** The outcome of our proposal is expected to be a **prototype of a low-cost, portable, integrated OCT system** based on the low loss  $\text{Si}_3\text{N}_4$  platform. The light source, interferometer and spectrometer of the OCT system will be independently developed and then integrated onto the same carrier to ensure the success of the project. The integration of light source will be developed and achieved through two approaches in parallel: i) The higher risk but higher degree of scalability and integration approach - gain chips and  $\text{Si}_3\text{N}_4$  resonators based frequency combs. ii) The lower risk and more conventional approach - SLD diode and  $\text{Si}_3\text{N}_4$  photonic chip co-package. The integration of the interferometer will be based on the low loss  $\text{Si}_3\text{N}_4$  platform, the reference arm will have a length that is long enough to match the path length of the sample arm. The sample arm will be miniaturized using a co-packaging process with MEMS scanners. The integration of the spectrometers will also be based on  $\text{Si}_3\text{N}_4$  platform and achieved through two approaches in parallel i) The stationary FTS with a  $\text{Si}_3\text{N}_4$  grating. ii)  $\text{Si}_3\text{N}_4$  AWG with lenses integrated on the edge of the chip.

All these components will be developed around a central wavelength of 1050 nm, and the integrated OCT system will be employed to take retinal scans in collaboration with OCT experts also at Shanghai Jiao Tong University. We hope that the components and the technologies we developed in this project will help pave the way for low-cost, portable OCTs and incorporating integrated photonics into optical imaging technologies.

**Impact:** The digital and computing revolution of the 20<sup>th</sup> century was driven by the rapid progression from vacuum tubes, to transistors and integrated circuits, and finally to printing computer chips in silicon with millions and now tens of billions of transistors. A quieter, but parallel, revolution has been taking place in optics and photonics that will drive many of the most important innovations of the 21<sup>st</sup> century. One of the main benefits of silicon photonics is that these circuits can be printed alongside, and integrated into, traditional electronic integrated circuits. Therefore, existing foundries, which already operate at scale, can be leveraged to print photonic integrated circuits at high volume and low-cost.

The OCT system that we are proposing to develop in this project is not simply to miniaturize components of existing typical OCT systems, but to reinvent them. The device we envision, in final form, will be **two orders of magnitude** reduction in price and **several orders of magnitude** reduction in size and weight. It will have the size and weight less than a typical mobile phone, and will have the capability of providing retinal scans at a resolution of less than 10  $\mu\text{m}$ , comparable to midrange clinical devices currently on the market. All three core parts of the OCT system will be miniaturized and integrated on the same carrier. Due to the broadband characteristics of  $\text{Si}_3\text{N}_4$  and generalization of the technologies, we expect our systems could be further adapted for imaging and diagnosis of diseases in other specialties using different wavelengths as well, most notably in dermatology, dentistry and oncology. Our results will help to reduce costs of the health system while increasing accessibility and compliance for better disease management.

## **References**

1. Huang, D. *et al.* Optical coherence tomography. *Science* **254**, 1178–1181 (1991).
2. Drexler, W. *et al.* Ultrahigh-resolution ophthalmic optical coherence tomography. *Nat Med* **7**, 502–507 (2001).
3. Rank, E. A. *et al.* Toward optical coherence tomography on a chip: in vivo three-dimensional human retinal imaging using photonic integrated circuit-based arrayed waveguide gratings. *Light: Science & Applications* **10**, 6 (2021).
4. Gora, M. J. *et al.* Tethered capsule endomicroscopy enables less invasive imaging of gastrointestinal tract microstructure. *Nat Med* **19**, 238–240 (2013).
5. Li, K. *et al.* Super-achromatic optical coherence tomography capsule for ultrahigh-resolution imaging of esophagus. *Journal of Biophotonics* **12**, e201800205 (2019).
6. Nguyen, F. T. *et al.* Intraoperative Evaluation of Breast Tumor Margins with Optical Coherence Tomography. *Cancer Res* **69**, 8790–8796 (2009).
7. Kennedy, K. M. *et al.* Diagnostic Accuracy of Quantitative Micro-Elastography for Margin Assessment in Breast-Conserving Surgery. *Cancer Res* **80**, 1773–1783 (2020).
8. Swanson, E. A. & Fujimoto, J. G. The ecosystem that powered the translation of OCT from fundamental research to clinical and commercial impact [Invited]. *Biomed Opt Express* **8**, 1638–1664 (2017).
9. Rosenfeld, P. J., Sadda, S. R. & Waheed, N. K. OCT Angiography: An Economic and Ethical Dilemma for Ophthalmologists in the United States. *Retinal Physician* **15**, 43–44 (2018).
10. Chopra, R., Wagner, S. K. & Keane, P. A. Optical coherence tomography in the 2020s—outside the eye clinic. *Eye* **35**, 236–243 (2021).
11. Yurtsever, G., Weiss, N., Kalkman, J., Leeuwen, T. G. van & Baets, R. Ultra-compact silicon photonic integrated interferometer for swept-source optical coherence tomography. *Opt. Lett.*, **39**, 5228–5231 (2014).
12. Schneider, S. *et al.* Optical coherence tomography system mass-producible on a silicon photonic chip. *Opt. Express*, **24**, 1573–1586 (2016).
13. Eggleston, M. *et al.* 90dB Sensitivity in a Chip-Scale Swept-Source Optical Coherence Tomography System. in *Conference on Lasers and Electro-Optics JTh5C.8* (2018).
14. Nguyen, V. D. *et al.* Spectral domain optical coherence tomography imaging with an integrated optics spectrometer. *Opt. Lett.*, **36**, 1293–1295 (2011).
15. Akca, B. I. *et al.* Miniature spectrometer and beam splitter for an optical coherence tomography on a silicon chip. *Opt. Express*, **21**, 16648–16656 (2013).
16. Ji, X. *et al.* Millimeter-scale chip-based supercontinuum generation for optical coherence tomography. *Science Advances* **7**, eabg8869 (2021).
17. Ji, X. *et al.* Ultra-low-loss on-chip resonators with sub-milliwatt parametric oscillation threshold. *Optica*, **4**, 619–624 (2017).
18. Ji, X. *et al.* On-chip tunable photonic delay line. *APL Photonics* **4**, 090803 (2019).
19. Nie, X., Ryckeboer, E., Roelkens, G. & Baets, R. CMOS-compatible broadband co-propagative stationary Fourier transform spectrometer integrated on a silicon nitride photonics platform. *Opt. Express*, **25**, A409–A418 (2017).

## **Chip-integrated mid-infrared laser and spectroscopy towards scalable environmental monitoring**

Xiyuan Lu, Assistant Research Scientist, University of Maryland Colleague Park | NIST

**The challenge:** In 2022, people around the globe are struggling to deal with heat, tumbling the record stood for over 100 years. Right now, the heat is challenging around the major cities, burdening the electrical grids. Down the line, the extreme weather poses higher risk of other hazards including flooding, superstorms, and diseases. Global warming is one major pressing challenge for our generation.

To solve this environmental challenge, we need to first measure the environmental gases quantitatively, and collect big data with large variety, volume, and velocity. Mid-infrared spectroscopy is the key technology to measure environmental gases, including carbon dioxide and methane, as these gases have absorption signatures at 2-5 micrometers. So far, high-quality mid-infrared spectroscopy, limited by table-top laser and detector setups, can only happen in labs rather than in the field, and is prohibitively expensive to deploy to collect the big data. Satellites can provide an overall analysis of the atmosphere, but lack the local data that is important for regulatory action and enforcement. To collect big data for environmental monitoring from automobiles to drones/air crafts, to farms and factories, we need a scalable spectroscopy technology that is cheap, portable, and manufacturable.

A key challenge for scalable mid-infrared spectroscopy is the laser source, as the mid-infrared gap (2.5-5 micrometers) is not accessible by direct band gap lasers from semiconductors in nature. In recent years, significant efforts have been put in integrating laser sources, with approaches including heterogenous integration and nonlinear photonics. Yet most efforts are focused on visible and near-infrared wavelengths, attracted by commercial interest (virtual/augmented reality, LIDAR for autopiloting etc.) and the thrusts in quantum optics (where quantum systems have emission wavelengths in visible or near-infrared). The mid-infrared spectroscopy, though crucial for environmental monitoring, is comparatively far less explored in the context of integrated photonics. The heterogeneous integration approach, while considered as the favorable path at the visible and near-infrared, does not attract the same level of interest at the mid-infrared, in part because of the lack of direct bandgap materials. Lacking this technical path, nonlinear photonics seems to be the way to go for scalable mid-infrared spectroscopy.

**Proposed project:** I propose to address this challenge using nonlinear optics in the silicon nitride photonics platform, which has been successful in wide-band nonlinear optics, and is supported by wafer-scale foundry fabrication. My proposal contains three parts: developing the photonic chip for efficient generation and vertical emission of the mid-infrared light, and exploring the packaging considerations with laser and detector for spectroscopy.

- The proposed key photonic device ( $< 0.1 \times 0.1$  mm footprint) performs two major functionalities:
  - convert telecom laser light to widely-tunable mid-infrared coherent laser light, through a nonlinear optical process called widely-separated Kerr optical parametric oscillation;
  - emit the generated mid-infrared light vertically out of the chip plane efficiently, through high-quality orbital angular momentum emission.
- Also investigated is the packaging considerations to incorporate the photonic chip with high-power telecom laser diodes by edge coupling, and the infrared detector in flip bonding/expoxy.

**Intended outcomes:** I intend to deliver a functional mid-infrared spectroscopy prototype in 3 steps:

- **0-8 months:** demonstrating telecom-pumped mid-infrared OPO generation on silicon photonics.
- **9-16 months:** demonstrating efficient mid-infrared out-of-plane emission in such OPO devices.
- **17-24 months:** exploring packaging considerations with laser and detector to the photonic chip.

## **Chip-integrated mid-infrared laser and spectroscopy towards scalable environmental monitoring**

Xiyuan Lu, Assistant Research Scientist, University of Maryland College Park | NIST

### **1. Literature Review**

To solve the environmental challenge of global warming, we need to first measure the environmental gases quantitatively, and collect big data with large variety, volume, and velocity. Mid-infrared spectroscopy is the key technology to measure environmental gases. So far, high-quality mid-infrared spectroscopy, limited by table-top laser and detector setups, can only happen in lab rather than in field, and is prohibitively expensive to deploy to collect big data. Satellites can provide an overall analysis of the atmosphere, but lack local data that is important for regulatory action and enforcement. To collect big data for environmental monitoring from automobiles to drones/air crafts, to farms and factories, we need a scalable spectroscopy technology that is cheap, portable, and manufacturable.

A key challenge for scalable mid-infrared spectroscopy is the integrated laser sources, as mid-infrared gap is not assessable by direct band gap lasers from semiconductors, as illustrated in Figure 1(a). The infrared spectrum refers to the electromagnetic spectrum with the wavelength ranging from 0.75  $\mu\text{m}$  to 1 mm, and it is typically divided into near infrared (0.7-1.4  $\mu\text{m}$ ), short-wavelength infrared (1.4-3  $\mu\text{m}$ ), mid-wavelength infrared (3–8  $\mu\text{m}$ ), long-wavelength infrared (8-15  $\mu\text{m}$ ), and far infrared (above 15  $\mu\text{m}$ ). The wavelength range of interest for environmental gas sensing lies across short-wavelength and mid-wavelength infrared, from 2 to 5  $\mu\text{m}$ , as shown by the green box in Figure 1(a), because environmental gases, including carbon dioxide ( $\text{CO}_2$ ) and methane ( $\text{CH}_4$ ), have their distinct absorption features in this wavelength range [1]. Semiconductor lasers have been developed for the range of 2-2.5  $\mu\text{m}$ , with only sparse wavelength coverage because of the limitation of gain material [2]. Beyond 2.5  $\mu\text{m}$ , due to the lack of gain materials, as shown by the gray box in Figure 1(a), direct bandgap lasers are not an option. As a result, we have to resort to either inter-band/quantum cascade lasers [3,4] or nonlinear photonic processes, where the latter approach can naturally provide broad range of wavelength access without the need of epitaxy growth of materials.

In recent years, significant efforts have been put in integrating laser sources, with approaches including heterogenous integration [5] and nonlinear photonics [6]. Yet most efforts are focused on visible and near-infrared wavelengths, attracted by commercial interest (virtual/augmented reality, LIDAR for autopiloting etc.) and the thrusts in quantum optics (where quantum systems have emission wavelengths in visible or near-infrared). The mid-infrared spectroscopy, though crucial for environmental monitoring, is comparatively far less explored in the context of integrated photonics. The heterogeneous integration approach, while considered as the favorable path at the visible and near-infrared, does not attract the same level of interest at the mid-infrared, in part because of the lack of direct bandgap materials. Lacking this technical path, nonlinear photonics seems to be the way to go for scalable mid-infrared spectroscopy.

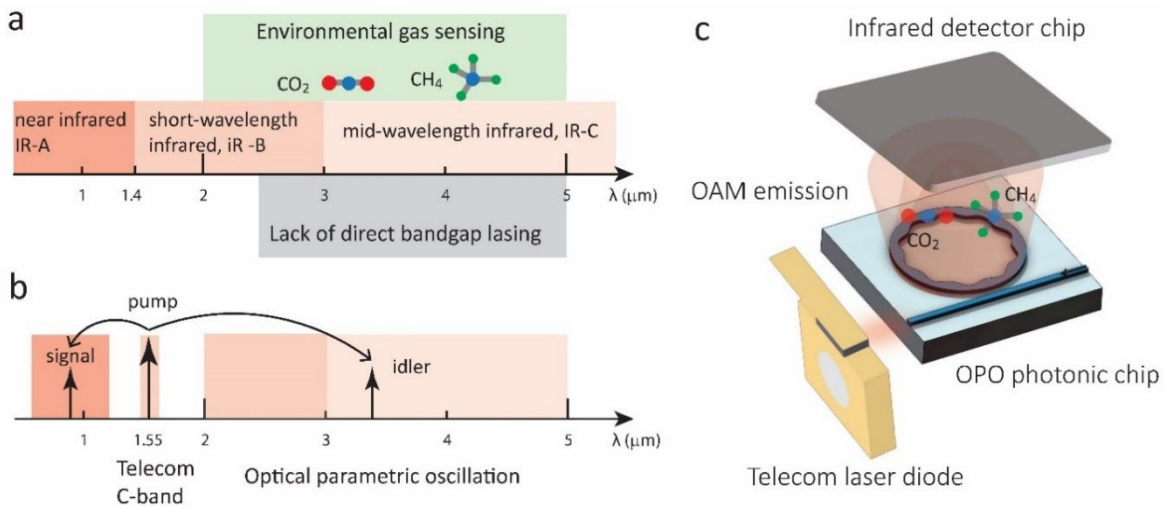
### **2. Problem Statement/Objective**

The objective of this proposal is to solve the scalability problem of the mid-infrared laser and spectroscopy by integrated nonlinear photonics, with proof-of-principle demonstration in two years. The photonics platform used here is high-quality microring resonator in silicon nitride nanophotonics [6], which has been established as a wide-band nonlinear optics platform including frequency combs, optical parametric oscillation (OPO) [7-10], and recently injection locking [11]. Among all the nonlinear

photonic processes, OPO is particularly suitable for generating coherent laser light up to a broad wavelength range by only one single-frequency laser. Significant efforts have been put to generate visible and near-infrared laser lights by integrated OPO, reducing the threshold power at a milliwatts level by a pump laser around 980 nm [7], and generating light from near-infrared to green by a pump laser around 780 nm [8]. Novel engineering approach has been proposed for robust coherent light generation [9].

Beyond visible and near-infrared wavelengths, OPO is also promising in generating short-wavelength infrared light, with a pumped laser and amplifier around 2  $\mu\text{m}$ , and it is possible to extend to mid-wavelength infrared through an advanced dispersion engineering approach [10] using high-quality-factor photonic crystal ring [12]. However, laser and amplifier at 2  $\mu\text{m}$  have large footprint and cannot be integrated so far. Instead, if we pump at telecom band around 1.55  $\mu\text{m}$ , integrated laser technologies are mature and affordable. For example, high-power multi-mode telecom laser diode has been shown to generate up to 150 mW power in single-mode profile using edge coupling and injection locking to a silicon nitride microring [11], in the aforementioned silicon nitride photonics platform. The proposed OPO process is illustrated in Figure 1(b), and access to the full 2-5  $\mu\text{m}$  range is not challenging in dispersion design.

Another challenge for infrared spectroscopy lies at the efficient integration of light emission onto the detector, through the gas in detection. Ejecting the light normal to the chip surface provides easier access to light-gas interaction and also simplify the task for detector integration. Along this line, a packaging scheme is proposed in Figure 1(c) incorporating laser diode, photonic chip, and detector chip. In particular, a high-quality-factor orbital angular momentum (OAM) emission technology [13] is utilized to emit the mid-infrared light generated in the microring vertically, that is, normal to the chip plane. The combination of the OPO and the OAM can be achieved simultaneously in one photonic crystal ring, with similar principles demonstrated previously in [14]. Such packaging scheme may reduce the need of detector chip area and further cut down the cost.



**Figure 1. Challenges of mid-infrared laser and spectroscopy for environmental gas sensing, and the proposed integrate photonics solution.** **a.** Environmental gas sensing occurs at wavelengths from 2 to 5  $\mu\text{m}$ , where direct bandgap lasing materials are lacked. **b.** Optical parametric oscillation (OPO) can provide wavelength access to this broad range by using mature telecom C-band laser technology. **c.** A schematic illustration of the spectroscopy prototype, with telecom laser diodes edge-coupled to the photonic chip, and the mid-infrared light routed vertically by orbital angular momentum (OAM) emission, through the gas species, onto the detector chip.

### 3. Outline of Tasks

The timeline of the tasks is set forth below and is divided into three work packages (WPs), each spanning 8 months. WP1 and WP2 focus on photonic chip technology development and validation, and WP3 focuses on packaging for spectroscopy prototype.

#### **WP 1: Generating mid-infrared laser by telecom pump laser through OPO**

- 1.1 To generate mid-infrared (2-3.5  $\mu\text{m}$ ) by 2  $\mu\text{m}$  pumped laser (*available in lab*). The experimental expectation is to achieve coverage up to 3.5  $\mu\text{m}$ .
- 1.2 To generate mid-infrared (3.5-5  $\mu\text{m}$ ) by 2  $\mu\text{m}$  pumped laser. The experimental expectation is to achieve coverage beyond 3.5  $\mu\text{m}$ , by partial wet-etching of the oxide substrate.
- 1.3 To generate mid-infrared (2-3.5  $\mu\text{m}$ ) by telecom pumped laser (*available in lab*). The experimental expectation is to achieve as broad coverage as possible.
- 1.4 To generate mid-infrared (3.5-5  $\mu\text{m}$ ) by telecom pumped laser. The experimental expectation is to achieve coverage beyond 3.5  $\mu\text{m}$ . If a full coverage proves to be difficult, potential problems and solutions should be analyzed.

#### **WP2. Emitting mid-infrared light vertically in the OPO device**

- 2.1 To calibrate the orbital angular momentum (OAM) grating emission efficiency for the control device geometry without generating OPO.
- 2.2 To design and fabricate the OAM grating with the OPO grating in the same microring.
- 2.3 To demonstrate OAM emission of the mid-infrared light from OPO. The goal is to have an emission efficiency of  $\sim 10\%$  without affecting the threshold power of the OPO within a factor of 3.
- 2.4 To summarize WP1 and WP2, and re-evaluate WP3.

#### **WP3. Exploring the packaging considerations of laser diodes and detectors**

- 3.1 To demonstrate OPO photonic chip with a threshold power below 300 mW.
- 3.2 To couple telecom laser diode to the photonic chip by facet coupling.
- 3.3 To generate mid-infrared light with facet-coupled laser chip.
- 3.4 To explore packaging solutions with the detector chip on top of the photonic chip.

### 4. Work Plan

The table below describes the milestones broken down by work packages, including tentative 6 rounds of fabrication and two manuscripts for peer-reviewed publications. The fabrication rounds can be merged and re-iterated if needed, but should be kept 6 rounds for cost management. The nanofabrication processes of dry etching, oxide lift-off, and postprocessing are merged with other projects to reduce costs. The major remaining costs are for electron beam lithography, which is estimated to be \$2-3k per round.

Ref	Description, fabrication rounds, and deliverables	Target Timeline
WP 1.1	Generate 2-3.5 $\mu\text{m}$ by 2 $\mu\text{m}$ pumped laser. Simulation, <b>1<sup>st</sup> round fabrication</b> , testing, analysis of results.	End of month 2



WP 1.2	Generate 3.5-5 $\mu\text{m}$ by 2 $\mu\text{m}$ pumped laser. Testing, analysis.	End of month 4
WP 1.3	Generate 2-3.5 $\mu\text{m}$ by telecom pumped laser. Simulation, <b>2<sup>rd</sup> round fabrication</b> , testing, analysis of results	End of month 6
WP1.4	Generate 3.5-5 $\mu\text{m}$ by telecom pumped laser. Testing, analysis.	End of month 8
WP 2.1	Calibrate OAM efficiency, set up mid-infrared camera/detector <b>3<sup>rd</sup> round fabrication</b> , testing, analysis.	End of month 10
WP 2.2	Design and get OAM emission working in OPO devices. <b>4<sup>th</sup> round fabrication</b> , testing, analysis.	End of month 12
WP 2.3	Optimize the OAM and OPO for a targeted wavelength. Testing, analysis.	End of month 14
WP 2.4	Summarize WP1 and WP2 in the <b>1<sup>st</sup> manuscript</b> . Re-evaluate WP3 tasks on WP1 and WP2 metrics.	End of month 16
WP 3.1	Improve the power efficiency and output. Testing, analysis.	End of month 18
WP 3.2	Facet couple a laser chip. Simulation, <b>5<sup>th</sup> round fabrication</b> , testing, analysis.	End of month 20
WP 3.3	To couple laser chip and demonstrate OPO. <b>6<sup>th</sup> round fabrication</b> , testing, analysis.	End of month 22
WP 3.4	To explore detector packaging considerations. Report WP3 in the <b>2<sup>nd</sup> manuscript</b> .	End of month 24

## 5. Outcomes

The proposed work has or may have the following outcomes:

- Mid-infrared laser and spectroscopy prototype with technical readiness of 4 is expected, with components and/or breadboard validation in lab or in relevant environment.
- Two manuscripts shall be prepared at the end of each year. The first manuscript summarizes the results of generation and emission of mid-infrared laser light. The second manuscript discusses the packaging considerations for the spectroscopy and future paths.
- Potential intellectual property (IP) might be generated, depending on the level of technical improvement and interest from University of Maryland College Park and NIST.
- Potential collaboration might be attracted to further develop this technology, or to apply the technology in other applications or fields, which will be briefly mentioned in the next section.
- Potential STTR funding might be pursued for product development, depending on the results of this project.

## 6. Impact

The proposed work has broad impacts in many aspects listed in the following:

- The research explores a mid-infrared spectroscopy that fosters the interest of integrated photonics communities to environmental monitoring.
- The research boosts miniaturization of spectroscopy for a broad range of applications, including biology & health, food & agriculture.
- The research examines the path for using integrated nonlinear optics for mid-infrared laser sources, expanding the current focus from visible and near-infrared to mid-infrared wavelengths.
- The research strengthens and helps to improve the fabrication at nanofabrication center at NIST.
- The research sets up an application scenario for wafer-scaled/miniaturized mid-infrared detectors, potentially reducing the surface area needed and therefore further reducing the cost.

## 7. References

- [1] N. Yamazoe and N. Miura, *Environmental gas sensing*, Sens. Actuators B: Chem. 20, 95–102 (1994).
- [2] F. K. Tittel, D. Richter, and A. Fried, *Mid-infrared laser applications in spectroscopy*, in Solid-state mid-infrared laser sources, Springer, 2003.
- [3] R. Q. Yang et al., *Distributed feedback Mid-IR interband cascade lasers at thermoelectric cooler temperatures*, J. Sel. Top. Quantum Electron. 13, 1074–1078 (2007).
- [4] Q. Y. Lu et al., *2.4 W room temperature continuous wave operation of distributed feedback quantum cascade lasers*, Appl. Phys. Lett. 98, 181106 (2011).
- [5] A. Spott et al., *Heterogeneous Integration for mid-infrared silicon photonics*, IEEE J. Sel. Top. Quant. Electron. 23, 1-10 (2017).
- [6] D. J. Moss et al., *New CMOS-compatible platforms based on silicon nitride and Hydex for nonlinear optics*, Nat. Photon. 7, 597-607 (2013).
- [7] X. Lu et al., *Milliwatt-threshold visible-telecom optical parametric oscillation using silicon nanophotonics*, Optica 6, 1535-1541 (2019).
- [8] X. Lu et al., *On-chip optical parametric oscillation into the visible: generating red, orange, yellow, and green from a near-infrared pump*, Optica 7, 1417-1425 (2020).
- [9] F. Zhou et al., *Hybrid-mode-family kerr optical parametric oscillation for robust coherent light generation on chip*, Laser & Photonics Review, 202100582 (2021)
- [10] X. Lu et al., *Infrared Kerr optical parametric oscillation in a photonic crystal microring*, Opt. Lett. 47, 3331-3334 (2022).
- [11] Y. Antman et al., *High power on-chip integrated laser*, arXiv: 2207.06279.
- [12] X. Lu et al., *High-Q slow light and its localization in a photonic crystal microring*, Nat. Photon. 16, 66-71 (2022).
- [13] X. Lu et al., *Highly-twisted states of light from a high quality factor photonic crystal ring*, arXiv: 2208.13075.
- [14] X. Lu et al., *A universal frequency engineering tool for microcavity nonlinear optics: multi-mode selective mode splitting for whispering gallery modes*, Photon. Res. 8, 1676-1686 (2020).

# Mobile Quantum Gravimetry for Near-Surface Geophysics

Xuejian Wu

Department of Physics, Rutgers University, Newark, NJ 07102

Email: [xuejian.wu@rutgers.edu](mailto:xuejian.wu@rutgers.edu)

## Application Information

Application to The Optica Foundation 20th Anniversary Challenge

Category: Environment

Project Duration: 2 years

Budget: \$99,880

## Project Summary

Gravity mapping is important for inertial navigation, resource exploration, refining the geoid, hydrological studies, and hazard monitoring. Gravity cartography, mapping the vertical gravity ( $g_z$ ), gravity gradient ( $\partial g/\partial x$ ), and even its second spatial derivative ( $\partial^2 g/\partial x^2$ ), can access this target directly by sensing minuscule local variations (“anomalies”) in the gravitational field. The strength of these anomalies is typically 0.1-50 E, where 1 E= $10^{-9}/s^2$  (Eötvös unit) is a change in the gravitational acceleration by 1 nm/s<sup>2</sup> over a 1-meter distance.

Exploiting the nature of quantum phenomena, quantum technologies are developing rapidly toward precise sensing. Matter-wave interferometers are robust quantum sensors and are being developed for measuring inertial forces. In contrast to classical sensors, atom interferometers use recoil momentum from photon and matter-wave interactions to coherently split and recombine matter waves. Since laser wavelength defines photon momentum with high precision, atom interferometers are accurate and are thus ideal sensors for precision measurements. Recently, transportable quantum gravimeters have been demonstrated for mobile gravimetry. However, due to complexity and fragility, quantum sensors that are sensitive to the gravity gradient or the second spatial derivative have not yet been tested out of a laboratory.

We propose a scalable quantum gravimeter by dropping multiple cold atomic clouds trapped in diamond-shaped mirrors to simultaneously measure gravity and its high-order derivatives. By combining the beyond state-of-art gravimetry from the recent development of Quantum Information Science and Engineering with application in Near-Surface Geophysics, we aim to demonstrate a shared-use mobile quantum gravimeter that will open new capabilities in geophysical exploration. The quantum gravimeter will allow the application of gravity methods for mineral and water exploration and for the monitoring of subsurface processes that have not previously been available. In Year 1 of this project, we will demonstrate the feasibility of matter-wave interferometry based on diamond-shaped magneto-optical traps and develop an algorithm for modeling gravity distribution for arbitrary underground test objects. In Year 2 of this project, we will demonstrate the prototype of the quantum gravimeter and implement water table leveling measurement in the lab.

Our quantum gravimeter will enable accurate characterization of gravity, the gravity gradient, and the second-order derivative of gravity at the same time. Such measurements will support the discovery and monitoring of previously undetectable structures and processes. The ability to sensitively measure contrasting density in subsurface materials permits the detection and inspection of buried minerals, salt domes, petroleum reservoirs, varying rock types, and bedrock structures. It also permits monitoring of underground fluids, like sequestered CO<sub>2</sub> or the water level in aquifers and other groundwater resources. The low operation cost, high sensitivity, and broad applicability of the instrument will attract usage from a wide range of research fields in academia and industry.

# Mobile Quantum Gravimetry for Near-Surface Geophysics

Xuejian Wu

Department of Physics, Rutgers University, Newark, NJ 07102

Email: xuejian.wu@rutgers.edu

## Background and Motivation (Literature Review)

*Detect underground signal.* As we exhaust resources, it becomes more challenging to discover, characterize, and provide stewardship to underground resources such as ore deposits, aquifers, and sites for carbon sequestration. Traditional methods like borehole analysis and seismic sensing are costly and destructive to the landscape. Nondestructive electromagnetic sensing has made great progress but measures only proxies for the target variable, which is often the mass and size of the formation. Measuring the gravity field can access this target variable directly by sensing minuscule local variations (“anomalies”) in the gravitational field.

*Gravity cartography.* Gravity mapping is important for inertial navigation, resource exploration, refining the geoid, hydrological studies, and hazard monitoring (1). Gravity cartography, mapping the vertical gravity ( $g_z$ ), gravity gradient ( $\partial g/\partial x$ ), and even its second spatial derivative ( $\partial^2 g/\partial x^2$ ), can access this target directly by sensing minuscule local variations (“anomalies”) in the gravitational field (2). The strength of these anomalies is typically 0.1-50 E, where 1 E= $10^{-9}/s^2$  (Eötvös unit) is a change in the gravitational acceleration by 1 nm/ $s^2$  over a 1-meter distance. Spring-based gravimeters and gradiometers have already been used to map geological structures and detect large ore deposits, but their sensitivity is limited (5-50 E/ $\sqrt{Hz}$ ) and they need to be calibrated to compensate for long-term drift (3). To measure the gravity field with

*Quantum sensors.* Exploiting the nature of quantum phenomena, quantum technologies are developing rapidly toward precise sensing. Matter-wave interferometers are robust quantum sensors and are being developed for measuring inertial forces (4, 5). In contrast to classical sensors, atom interferometers use recoil momentum from photon and matter-wave interactions to coherently split and recombine matter waves. Since laser wavelength defines photon momentum with high precision, atom interferometers are accurate and are thus ideal sensors for precision measurements. Recently, transportable quantum gravimeters have been demonstrated for mobile gravimetry (6-9). However, due to complexity and fragility, quantum sensors that are sensitive to the gravity gradient or the second spatial derivative have not yet been tested out of a laboratory.

*Light-pulse atom interferometry.* In a light-pulse atom interferometer, an ensemble of cold atoms (here: rubidium) is prepared in a magneto-optical trap (MOT) and then released into free fall. Each atom’s wave packet is then split coherently by interactions with a light pulse, see Fig. 1. The momentum  $2n\hbar\mathbf{k}$ , where  $n=1,2,3, \dots$  and  $\mathbf{k}$  is the wavenumber, of a photon pair sends the matter wave along two paths. Two more pulses, spaced by intervals  $T$ , redirect the matter waves. Upon interference, the partial waves may add or cancel, depending on the phase difference  $\Delta\varphi$  accumulated along the paths. The probability of detecting the atom at one of the outputs is given by  $\cos^2(\Delta\varphi/2)$ , where  $\Delta\varphi = 2(\mathbf{k}\cdot\mathbf{a}) T^2 + 2(m/\hbar) (\mathbf{A}\cdot\mathbf{\Omega})$ .

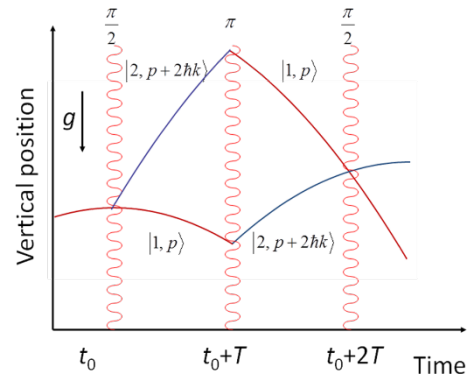


Figure 1. Space-time trajectories of atoms in a light-pulse atom interferometer. The wiggly lines indicate laser pulses, the red and blue lines indicate atoms in two states  $|1\rangle$  and  $|2\rangle$ , respectively (here: the  $F=1$  and  $F=2$  hyperfine sublevels of the rubidium-87 ground state).

Here,  $\mathbf{a}$  denotes linear acceleration,  $\mathbf{A}$  the area enclosed between the interferometer arms, and  $\mathbf{\Omega}$  angular velocity. Detecting the atoms in the outputs A and B thus measure the phase difference.

*Advantages of quantum gravimeters.* Such interferometers have demonstrated state-of-the-art sensitivity for measuring gravity and the gravity gradient. In contrast to instruments based on springs (10), superconducting coils (11), microelectromechanical devices (3), or falling corner cubes (12), they rely on the matter-wave interferometry with a freely falling atomic cloud. Atomic gravimeters are sensitive because of the precise photon momentum defined by the laser wavelength. Besides the large atomic gravimeters in the laboratory, transportable atomic gravimeters are being developed for metrology comparisons (13-16), airborne sensing (17, 18), shipborne surveys (7), and field applications (8, 19). Nowadays, the most sensitive transportable atomic gravimeters can measure gravity in the laboratory with a sensitivity between 10 and 50  $\mu\text{Gal}/\sqrt{\text{Hz}}$  ( $1 \mu\text{Gal}=10 \text{ nm/s}^2$ ) depending on surrounding vibration noise (13, 14). Limited by the environmental vibration noise, the best precision of field-operation atomic gravimeters is still around mGal.

*Challenges of quantum gravimeters.* For geodetic applications, atomic gravimeters must be not only sensitive but also reliable and mobile in field conditions. The high complexity of atom interferometers derives from the fact that they require laser-cooled atoms; in addition to the laser beams required for the interferometer proper, at least six beams at a different frequency, and a repumping frequency are required. This requires a complex system of many lasers, a complex vacuum chamber with many viewports, and an intricate system of laser frequencies stabilized to one another. Mobile atom interferometers have already been built. A compact and simple example is based on a pyramidal magneto-optical trap (MOT). It operates as an accelerometer with a sensitivity of 37 ng at one second of integration time, where  $g$  is the acceleration of free fall (9). Because two gravimeters are required to measure the gravity gradient, the complexity of a quantum gradiometer is double that of a gravimeter. Using two vertically separated MOTs to form to free-fall quantum gravimeters, transportable quantum gradiometers are developed with a resolution of 1-50 E (20-22). However, their mobility and capability of field operation still need to be tested. So far, a compact quantum gravimeter that can measure gravity, the gravity gradient, and the gravity curvature has never been reported.

## Objective

*The goal of this proposal* is to develop the next-generation quantum gravimeter with the capability of simultaneously mapping the vertical gravity, gravity gradient, and its second spatial derivative, and apply the quantum sensor for near-surface geophysics investigations. High-order gravity tensor is more sensitive to density variation, and thus reveals the edge information of the gravity anomaly. We will design and test a diamond-shaped mirror for trapping multiple cold atomic clouds using a single laser beam. This novel mirror geometry will reduce the complexity of multiple atom interferometers. With unprecedented sensitivity as well as miniaturized size, the novel quantum gravimeter will be used for deployable applications, such as detecting tunnels, navigating submarines, sensing underground water storage, and monitoring earthquake or volcano activity.

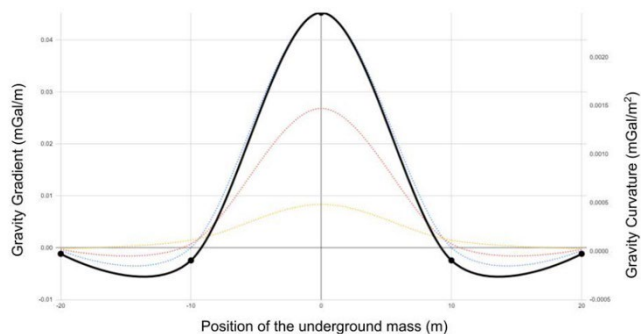


Figure 2. Gravity signal caused by the underground test mass. Yellow: gravity; Red: gravity gradient; Black: gravity curvature.

*Underground tunnel detection.* As an application example, we propose a method of detecting and localizing underground tunnels using the mobile quantum gravimeter. Gauss’s Law shows that the integral of the vertical component of the gravitational acceleration ( $g_z$ ) over the horizontal surface above a confined body is related to the excess mass of the body. This is important in mineral exploration because it allows them to provide a direct estimate of the tonnage of a deposit – a property not derivable from any other exploration technique. In practice, this requires accurate gravity data for the localized deposit from which the anomalies of adjacent bodies or structures have been subtracted. For gradient data, the map of gradient values must be filtered to emphasize the target gradient anomaly and integrated into a map of ( $g_z$ ) before the anomalous mass is calculated. Suppressing near-surface structures by optimum altitude. Near-surface density anomalies have strong effects on ground surveys. They are easily aliased when they are caused by small, high-density formations, polluting the data. In our preliminary simulation (Fig. 2), the gravity gradient has better sensitivity for detecting mass that locates exactly under the sensor and the second-order derivative has better sensitivity for detecting mass that locates around the sensor. By combining these signals, the mobile quantum gravimeter will improve the lateral resolution of the underground object, which may be used for searching for underground tunnels.

### Work Plan

*Diamond-shaped magneto-optical trap (MOT).* To achieve atom interferometry, we first need to cool the atoms to a few  $\mu\text{K}$  to increase the coherence of the matter-wave. Magneto-Optical Trap (MOT) is an efficient method, which can cool millions of rubidium atoms to  $\sim 2 \mu\text{K}$  within a second. However, MOT usually needs six orthogonal laser beams. It is challenging to create three vertically separated MOTs in a compact setup. To do that, we will design and demonstrate diamond-shaped MOTs. A diamond-shaped mirror (Fig. 3) consists of four pieces of gold-coated prisms with an apical angle of  $109.48^\circ$ . A plane laser beam can not only create an overlap trapping volume inside the diamond mirror but also maintain a plane wave while passing the diamond mirror. Using light trace simulation, we found the dimension tolerance is  $\pm 1 \mu\text{m}$  and the angle tolerance is  $\pm 0.025^\circ$ .

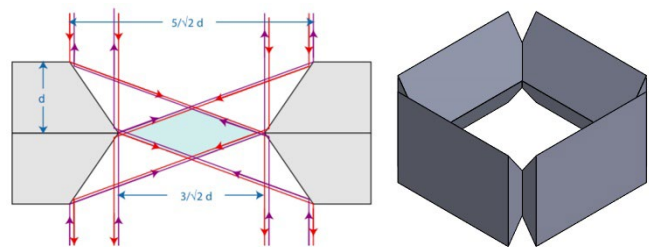


Figure 3. Diamond-shaped mirror. Left: Side view of the mirror illuminating by a plane wave. Right: 3D schematic of the mirror.

To do that, we will design and demonstrate diamond-shaped MOTs. A diamond-shaped mirror (Fig. 3) consists of four pieces of gold-coated prisms with an apical angle of  $109.48^\circ$ . A plane laser beam can not only create an overlap trapping volume inside the diamond mirror but also maintain a plane wave while passing the diamond mirror. Using light trace simulation, we found the dimension tolerance is  $\pm 1 \mu\text{m}$  and the angle tolerance is  $\pm 0.025^\circ$ .

*Three vertically separated atom interferometers.* We will demonstrate three vertically separated atom interferometers illuminated by a single laser beam (Fig. 4 E). Each of the atom interferometers will output a vertical gravity measurement. Using two of the atom interferometers, a vertical gravity gradient can be determined, which can be used to estimate the density of the under-surface rocks. We use ellipse-fitting to read out the difference even if vibrations are so strong that individual gravity measurements are impossible. The output of the three atom interferometers can provide the second derivative of vertical gravity, which can be used to reveal the difference between a basin and an intrusion.



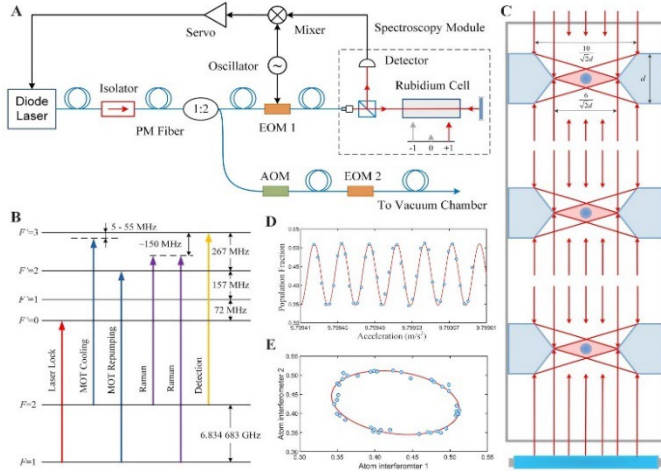


Figure 4. Atomic gravimetry. (A) Fiber-based laser system. (B)  $D_2$  transition of  $^{87}\text{Rb}$ . (C) 2D schematic of atom interferometers with three diamond MOTs. (D) Fringe of one atom interferometer. (E) Ellipse of two atom interferometers.

crystals (AdvR, Inc.) can work with high laser power and generate the repumping frequency and Raman frequency pair, as shown in Fig. 4 (B). Compared with free-space optics, the fiber-based laser system is more reliable and can be packaged in a smaller unit. To obtain Watt-level laser power, existing fiber-based laser systems usually start from telecom wavelength and produce the near-infrared wavelength through frequency doubling. This proposal uses directly a 780-nm wavelength, with a laser beam of  $\sim 40$ -mW power and  $\sim 20$ -mm waist. The available laser power is high enough to drive efficient Raman transitions ( $>60\%$ ) based on a small single photon detuning of  $\sim 150$  MHz to  $F=2 \rightarrow F'=3$  line. Without frequency doubling, the laser system will consume less power and can be powered by batteries.

**Sensor head.** The vacuum system is the sensor head for gravity measurement. The electronic control signals and the laser beam will be delivered to the sensor head remotely. The magneto-optical trap and atom interferometry are inside an ultrahigh vacuum chamber made of aluminum and pumped with an ion pump. As shown in Fig. 5, the length of the vacuum system is about 1 meter. The two quantum gravimeters are evenly separated. The overall weight is less than 20 lb.

**Sensitivity.** Simply releasing the atoms into free fall allows a pulse separation of  $T=0.15$  s. The gradiometer is predicted to achieve a sensitivity of  $1 \text{ E}/\sqrt{\text{Hz}}$  and the gravity curvature is predicted to achieve a sensitivity of  $1 \text{ E}/\text{m}/\sqrt{\text{Hz}}$ , considering a realistic 30% contrast and loss of atoms from state preparation. This figure is based on proven parameters and may be further improved, such as implementing a large photon-atom momentum transfer or launching the atoms upwards with doubling  $T$  and nearly quadrupling the sensitivity.

**Laser system.** Fig. 4 (A) shows the fiber-based laser system, consisting of only one 180-mW distributed Bragg reflector diode laser (Photodigm, Inc.) with a 780-nm wavelength. The +1st order sideband from a fiber-coupled electro-optical phase modulator (EOM1) is frequency-stabilized by frequency modulation spectroscopy in a rubidium vapor cell, nominally to the  $F=1 \rightarrow F'=0$  line. EOM1 can also vary the laser frequency relative to the spectroscopy by  $\pm 200$  MHz to switch between frequencies needed for atom trapping, interferometry, and detection. A fiber-coupled acoustic-optical modulator (AOM) acts as an overall on/off switch for the beam. A fiber-coupled EOM2 based on KTP

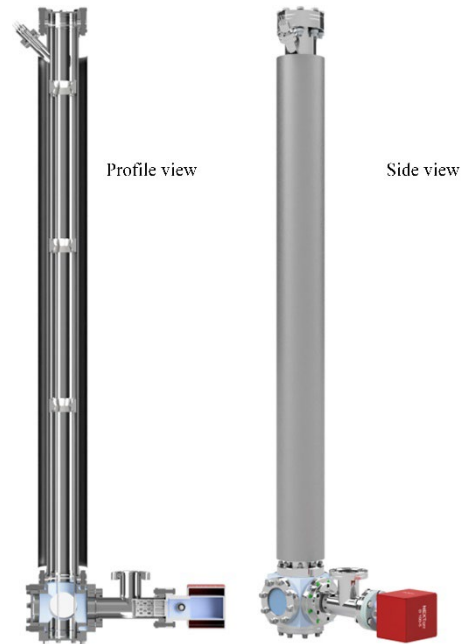


Figure 5. Vacuum chamber 3D model.

## Outcomes

As an interdisciplinary project, it involves atomic physics, quantum information science, engineering, geology, and environmental science. In this 2-year project, the goal is to demonstrate a novel portable quantum gravity sensor, simultaneously measuring vertical gravity and its derivatives. This project will provide strong opportunities for training students for the ongoing second quantum revolution, creating new talent in the emerging field of quantum sensing, computing, communication, and materials. We envision the following specific outcomes:

- Demonstrate a prototype quantum gravimeter, which can measure gravity, gravity gradient, and gravity curvature simultaneously.
- Characterize the sensitivity and resolution of the gravity measurement in the lab.
- Start the collaboration with geophysics groups at Rutgers University and plan field gravity surveys.
- Train one graduate student, one undergraduate student, and two local high school students with cutting-edge quantum physics research
- Publish 2-3 papers in high-impact physics journals, such as *PRL*, *APL*, and *Optica*.
- Apply 1-2 patents.
- Attend 1-2 conferences to report the discovery, such as the 2023 FiO+LS conference.

## Impact

*Impact on research.* We will develop a shared-use mobile gravimeter that will open new capabilities in geophysics exploration. It will allow applying gravity methods for mineral and water exploration and for the monitoring of subsurface processes that have not previously been available. Our quantum gravimeter will enable accurate characterization of gravity, the gravity gradient, and the second-order derivative of gravity at the same time. Such measurements will support the discovery and monitoring of previously undetectable structures and processes. The ability to sensitively measure contrasting density in subsurface materials permits the detection and inspection of buried minerals, salt domes, petroleum reservoirs, varying rock types, and bedrock structures. It also permits the monitoring of underground fluids, like sequestered CO<sub>2</sub> or the water level in aquifers and other groundwater resources. The low operation cost, high sensitivity, and broad applicability of the instrument will attract usage from a wide range of research fields in academia and industry.

*Impact on training students.* Quantum gravimetry has attracted great interest in military navigation, mining, and geosciences in general. Students will be involved in the construction, maintenance, and operation of a new, leading-edge instrument that will serve as a prototype for similar instruments in the industry. This will provide extremely strong opportunities for training the next generation of instrumentalists, creating new talent in emerging fields of nondestructive sensing. The proposed work will provide research experience for undergraduates in leading-edge research. Subprojects will be given to undergraduates, such as developing electro-optical systems and mechanical systems. The PI will work with the Optica Student Chapter at Rutgers University, a student-run suite of support for undergraduates with a focus on women and underrepresented groups, to identify promising undergraduates.

*Outreach.* To enhance diversity in science and engineering, we will continue our successful outreach to local high school students in Newark, New Jersey, one of the nation's most diverse school districts by several quantitative measures. The PI has close collaborations with Dr. Fang, who is a physics teacher at the Union County Magnet High School. In the summer of 2022, the PI mentored three high school students (Juan Chang, Antonio Drakes, and Alek Radak) and demonstrated a Michelson laser interferometer project, among whom one is from an underrepresented group. We will continue to host high school students, particularly students from underrepresented groups in this 2-year project.

## Reference

1. M. Van Camp, et al. Geophysics from terrestrial time-variable gravity measurements. *Rev. Geophys.* 55, 938–992 (2017).
2. D. K. Butler, Microgravimetric and gravity gradient techniques for detection of subsurface cavities. *Geophys.* 49(7), 1084-1096 (1984).
3. R. P. Middlemiss, et al. Measurement of the Earth tides with a MEMS gravimeter. *Nature* 531, 614–617 (2016).
4. A. D. Cronin, et al. Optics and interferometry with atoms and molecules. *Rev. Mod. Phys.* 81, 1051–1129 (2009).
5. K. Bongs, et al. Taking atom interferometric quantum sensors from the laboratory to real-world applications. *Nat. Rev. Phys.* (2019).
6. C. Freier, et al. Mobile quantum gravity sensor with unprecedented stability. *J. Phys. Conf. Ser.* 723, 012050 (2016).
7. Y. Bidel, et al. Absolute marine gravimetry with matter-wave interferometry. *Nat. Commun.* 9, 627 (2018).
8. V. Ménotet, et al. Gravity measurements below  $10^{-9}g$  with a transportable absolute quantum gravimeter. *Sci. Rep.* 8, 12300 (2018).
9. X. Wu, et al. Gravity surveys using a mobile atom interferometer. *Sci. Adv.* 5(9), eaax0800 (2019).
10. M. Lederer, Accuracy of the relative gravity measurement. *Acta Geodyn. Geomater.* 6, 383–390 (2009).
11. J. M. Goodkind, The superconducting gravimeter. *Rev. Sci. Instrum.* 70, 4131-4152 (1999).
12. T. M. Niebauer, et al. A new generation of absolute gravimeters. *Metrologia* 32, 159-180 (1995).
13. C. Freier, et al. Mobile quantum gravity sensor with unprecedented stability. *J. Phys. Conf. Ser.* 723, 012050 (2016).
14. B. Fang, et al. Metrology with atom interferometry: inertial sensors from laboratory to field applications. *J. Phys. Conf. Ser.* 723, 012049 (2016).
15. S.-K. Wang, et al. Shift evaluation of the atomic gravimeter NIM-AGRb-1 and its comparison with FG5X. *Metrologia* 55, 360-365 (2018).
16. Z. Fu, et al. Participation in the absolute gravity comparison with a compact cold atom gravimeter. *Chin. Opt. Lett.* 17, 011204 (2019).
17. R. Geiger, et al. Detecting inertial effects with airborne matter-wave interferometry. *Nat. Commun.* 2, 474 (2011).
18. B. Barrett, et al. Dual-matter-wave inertial sensors in weightlessness. *Nat. Commun.* 7, 13786 (2016).
19. Y. Bidel, et al. Compact cold atom gravimeter for field applications. *Appl. Phys. Lett.* 102, 144107 (2013).
20. W. Lyu, et al. Development of a compact high-resolution absolute gravity gradiometer based on atom interferometers. *arXiv:2202.12021v1* (2022).
21. C. Janvier, et al. Compact differential gravimeter at the quantum projection-noise limit. *Phys. Rev. Lett.* 105, 022801 (2022).
22. B. Stray, et al. Quantum sensing for gravity cartography. *Nature* 602, 590–594 (2022).

## High-power 2- $\mu\text{m}$ frequency combs for rapid greenhouse gas sensing (comb2u)

Carbon dioxide ( $\text{CO}_2$ ), methane ( $\text{CH}_4$ ), and nitrous oxide ( $\text{N}_2\text{O}$ ) compose 98% of global greenhouse gas emissions, and remote, sensitive detection of the concentrations of these gases is critical for understanding and monitoring regional emissions. Dual frequency-comb-based remote sensing has proved to be a unique tool for kilometer open-air path remote monitoring of such gases in the 'eye-safe' wavelength range of 1.6  $\mu\text{m}$ . Despite the remarkable progress in Er-fiber-based laser systems at this wavelength for this application, the 2  $\mu\text{m}$  wavelength region – which is also eye-safe - has many potential advantages since strong absorption lines are present here, as shown in figure 1. For example,  $\text{CO}_2$  shows an almost two times higher absorption coefficient in this wavelength range compared with 1.6  $\mu\text{m}$ , making sensitive tracking of small variations attractive. Although frequency down conversion to this wavelength is possible, Tm, Ho, and Cr-based oscillators directly emitting in this wavelength range are still more attractive due to their simplicity. To cover the minimum broad absorption band of the above gas (about 13 THz from 2000 nm-2200 nm), reducing the repetition rate difference  $\Delta f$ , or increasing the fundamental repetition rate  $f_{\text{rep}}$  can be applied. Later one is more favorable since both measurement speed and bandwidth of dual-comb spectroscopy (DCS) quadratic scales as the fundamental repetition rate. However, state-of-the-art oscillators in the 2-3  $\mu\text{m}$  wavelength range show limited average power within Watt-level, making remote sensing challenging.

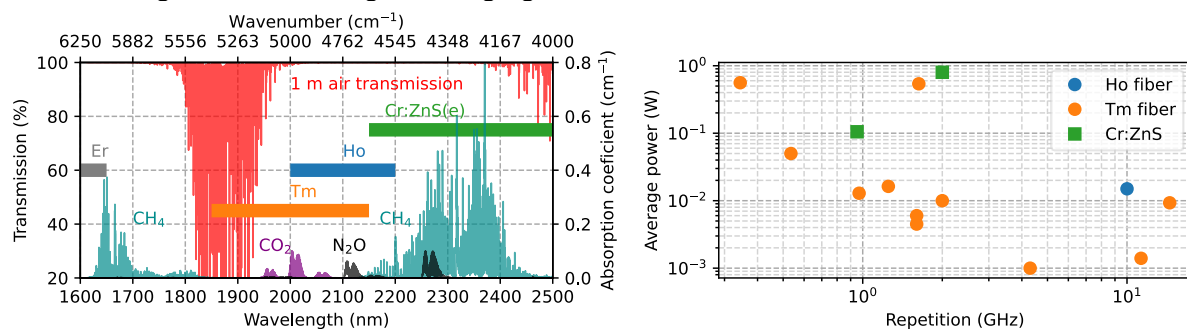


Figure 1. Left, laser emission range illustrated with 1-m air transmission and greenhouse gas absorption coefficient in the 1.6-2.5  $\mu\text{m}$  wavelength range (from HITRAN database). Right, state-of-the-art of high repetition-rate mode-locked oscillators in 2-3  $\mu\text{m}$ .

The current project aims to design and develop industrial-grade, robust, compact, cost-effective, diode-pumped high-power high-repetition-rate mode-locked oscillators around the 2- $\mu\text{m}$  wavelength range based on Tm-doped gain media for rapid greenhouse gas sensing applications. I expect the successful completion of the current project will have the following outcomes and impacts:

- The key specifications I aimed to achieve with the high-power high-repetition-rate 2- $\mu\text{m}$  oscillators are Watt-level average power, repetition rate  $>250$  MHz, and nJ pulse energy. This unique source will further be used to improve greenhouse gas sensing in terms of faster detection speed, high sensitivity, and long-distance detection.
- Within the period of the current project, I expect 1-2 journal publications and  $>2$  submissions for conference proceedings. In addition, one or two master's students will be involved in the current project and get proper training in ultrafast laser development and gas-sensing.
- Establish collaboration with other groups working on the frequency-comb, bridging the laser source development with spectroscopy research.
- Promoting next-generation spectroscopy based on frequency combs at around 2  $\mu\text{m}$  wavelength range. Seeding non-oxide nonlinear crystal based OPO or DFG process further generates MIR radiations. Such MIR comb systems are highly interesting for spectroscopy, environmental monitoring, and medical diagnostics.

## High-power 2- $\mu\text{m}$ frequency combs for rapid greenhouse gas sensing (comb2u)

Applicant: Yicheng Wang

Institution: Ruhr-University-Bochum, Germany

Email: yicheng.wang@ruhr-uni-bochum.de

### Literature Review

**Our motivation: greenhouse gas detection with 2- $\mu\text{m}$  dual-comb** Carbon dioxide ( $\text{CO}_2$ ), methane ( $\text{CH}_4$ ), and nitrous oxide ( $\text{N}_2\text{O}$ ) compose 98% of global greenhouse gas emissions [1], and remote, sensitive detection of the concentrations of these gases is key for understanding and monitoring regional emissions. Dual frequency-comb-based remote sensing has proved to be a unique tool for kilometer open-air path remote monitoring of such gases in the ‘eye-safe’ wavelength range of 1.6  $\mu\text{m}$  [2,3]. Despite the remarkable progress in Er-fiber based laser systems at this wavelength for this application, the 2  $\mu\text{m}$  wavelength region – which is also eye-safe - has many potential advantages, since strong absorption lines are present here, as shown in figure 1. For example,  $\text{CO}_2$  shows an almost two times higher absorption coefficient in this wavelength range compared with 1.6  $\mu\text{m}$ , making sensitive tracking of small variations attractive [4].

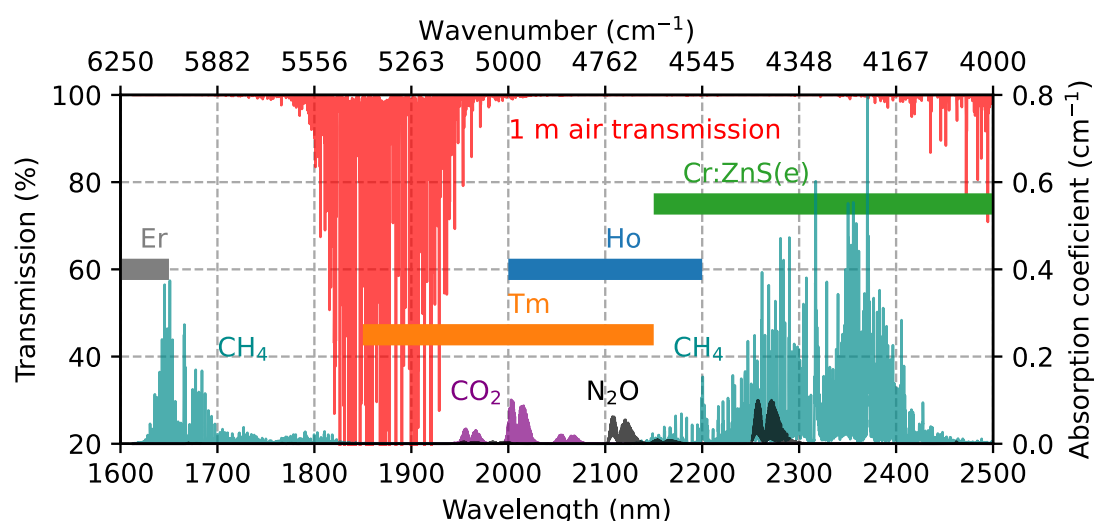


Figure 1. Laser emission range illustrated with 1-m air transmission and greenhouse gas absorption coefficient in the 1.6-2.5  $\mu\text{m}$  wavelength range (from HITRAN database).

As a trade-off, the air absorption coefficient is 1-2 orders of magnitude higher in 2  $\mu\text{m}$  compared with 1.6  $\mu\text{m}$  (HITRAN database). Thus for a km-level 2- $\mu\text{m}$  remote sensing, Watt-scale average power levels are highly desired. In addition, to cover the broad absorption band of the above gases (about 13 THz from 2000 nm-2200 nm), a sufficiently broadband source is desired. These requirements can be achieved in attractive and compact systems using modelocked lasers emitting directly broadband pulses at this wavelength without needing nonlinear conversion stages or amplifiers. In this regard, Tm, Ho, and Cr based lasers have attracted attention recently; and recently, the attractive possibility of a single-laser dual-comb source has confirmed its potential [5]. For such a system highest possible repetition rate is beneficial since both measurement speed and bandwidth of dual-comb spectroscopy (DCS) quadratic scales with the fundamental repetition rate [6]. Furthermore, the power per comb line increases at high repetition rate such that higher detection sensitivity can be reached. However, the average power of high repetition rate oscillators is typically well below Watt-scale, especially in the 2-3  $\mu\text{m}$  region (figure 2), which makes it difficult to apply such systems for remote detection at long distances.

**State-of-the-art 2-3  $\mu\text{m}$  modelocked oscillators** Nowadays, most of the 2-3  $\mu\text{m}$  high repetition-rate oscillators demonstrated are based on Tm or Ho doped fibers. However, due to design constraints, single-mode fibers with a core size of  $\sim 10 \mu\text{m}$  and 10-cm scale length are typically used, which leads to a small overall active media volume. It limits the peak power inside of the cavity for further power scaling. Another reason is such a fiber-based oscillator typically requires a single-mode fiber pump which is power-limited and high-cost. These aspects resulting a typically average power well below Watt-level and pulse energy in pJ-level from such high repetition-rate fiber-oscillators as figure 2 shows. Although harmonic mode-locking techniques or amplifier stages can be applied to bypass these limits, fundamentally mode-locked oscillators are still preferred due to their simplicity, low noise, and robustness. Cr:ZnS(e), known as the MIR-Ti:Sapphire, has shown great potential earlier this year for power-scaling GHz oscillators around 2.4  $\mu\text{m}$  [7]. By applying InGaSb/GaSb SESAM, 0.8 W average power has been recently demonstrated at a repetition rate of 2 GHz representing a promising first realization [7]. However, this laser performance highly depends on the quality of the polycrystalline Cr:ZnS(e) gain medium and the high-performance InGaSb/GaSb SESAM (low saturation fluence and low non-saturable losses), both of which are specialized components that are not widely available. These aspects make commercialization of such a product costly and limit the boost of applications applying such oscillators. Recently, I demonstrated a record-high average power mode-locked laser based on inband-pumped Ho:CALGO, using all commercial components [8]. However, this system is not diode-pumped, significantly increasing complexity and cost. Tm-solid state lasers remain widely unexplored for this application.

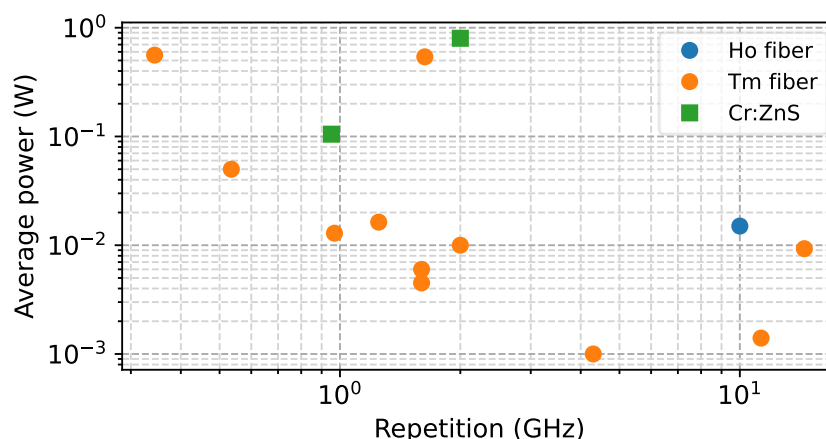


Figure 2. State-of-the-art high-repetition-rate mode-locked oscillators in the 2-3  $\mu\text{m}$  wavelength range.

Here, I aim to design and develop industrial-grade, robust, compact, cost-effective, diode-pumped high-power high-repetition-rate mode-locked oscillators around the 2- $\mu\text{m}$  wavelength range based on diode-pumped Tm-doped gain media for greenhouse gases sensing application. In the following section, I will address some of the challenges and propose solutions and my overall objectives.

### Problem Statement and Objective

#### Problem I: Strong water vapor absorption lines in ambient air preventing broadband mode-locking operation.

The dilemma for mode-locking of so-called 'eye-safe' lasers in bulk geometry around 2  $\mu\text{m}$  is: 'eye-safe' term is mainly due to the strong water-absorption of the lasing wavelength, which results in absorption in cornea reaches minimal depth while the retina is relatively safe. However, these absorption lines in the water vapor in the ambient air will prevent bulk mode-locked oscillators from being stabilized at such wavelength. The following table shows the potential gain media with broadband emission in the 2- $\mu\text{m}$  wavelength range based on Tm. For example, Tm:CaF<sub>2</sub> exhibits an emission bandwidth that exceeds  $>180 \text{ nm}$  [9].



However, the center emission is around 1850 nm, which strongly overlaps with the water vapor absorption lines below 1950 nm.

Table. Properties of broadband Tm-doped media in the 2- $\mu\text{m}$  wavelength range.

Gain material	Emission peak	Emission bandwidth	Nonlinear ref. index
Tm:CALGO	<1950 nm [10]	>254 nm [10]	$8 \times 10^{-20} \text{ m}^2\text{W}^{-1}$ [11]*
Tm:CaF <sub>2</sub>	1850 nm [9]	>180 nm [9]	$1.7 \times 10^{-20} \text{ m}^2\text{W}^{-1}$ [12]
Tm:Lu <sub>2</sub> O <sub>3</sub>	>2070 nm [13]	>200 nm [13]	$3.3 \times 10^{-20} \text{ m}^2\text{W}^{-1}$ [14]

\* value corresponding to  $n_2$  at 1  $\mu\text{m}$

### Possible solutions:

- Introducing wavelength filtering elements such as high-frequency pass filter or Lyot filter. Absorption bands in the ambient air can be avoided by shifting the center emission wavelength. However, this leads to low gain and optical-to-optical efficiency [10,15].
- Sealing the laser. A chamber over the oscillator is required. Vacuum or purging with gas without absorption in the wavelength range would prevent the problem. However, this increases the overall complexity and cost of the laser.
- Introducing low  $n_2$  spacers inside the cavity. One of the project's main ideas originated from a monolithic cavity design [16], where an undoped CaF<sub>2</sub> blank was introduced as spacer for the mode-locked cavity. Although the original idea was for stabilization purposes, the current project could benefit additionally by replacing the air with spacers to avoid water vapor absorption.
- Applying novel sesquioxide ceramics, which emit at the water window and cover the absorption lines of all three greenhouse gases.

### Problem 2: Lack of proper saturable absorbers for 2 $\mu\text{m}$ mode-locking.

GaSb-doped SESAMs with lower bandgap quantum wells have to be applied. Currently, commercialized SESAM with this wavelength range is rare. Parameters of such SESAM also need to be optimized for high-repetition-rate operation in terms of low saturation fluence and low non-saturable losses. Other candidates, such as graphene and SWCNTs, also show relatively unstable quality control, which makes them difficult to use as industrial-grade products.

### Possible solutions:

- The most convenient technique for high repetition rate mode-locking is still based on SESAM techniques. Recently, we were possible to characterize commercial 2- $\mu\text{m}$  SESAM provided by RefleKron, demonstrating excellent properties [8].
- Alternatively, KLM technique can be implemented into the 2- $\mu\text{m}$  oscillators as demonstrated in 1- $\mu\text{m}$  high repetition rate oscillators [17]. Both hard-aperture and soft-aperture techniques can be implemented.

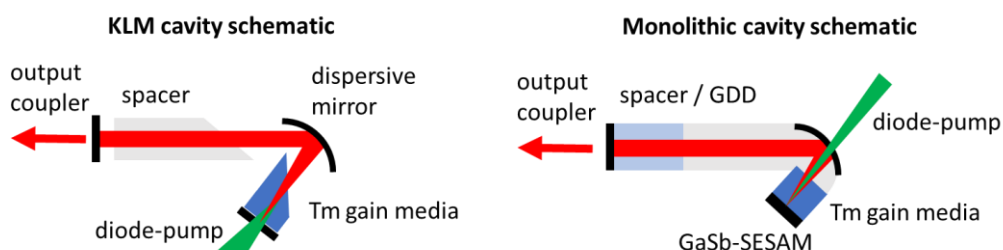


Figure 3. The proposed schematic for free-space soft-aperture KLM cavity and SESAM mode-locked monolithic-cavity which is similar to ref [16].

### Problem 3: Self-focusing and integrated SPM limiting for power scaling.

Self-focusing introduced Q-switching instability is a well-known limit for high-repetition-rate oscillators. This effect will be enhanced if we apply undoped CaF<sub>2</sub> spacers inside the cavity. Additional self-phase modulation might also be enhanced for power scaling.

**Possible solutions:**

- Optimizing cavity design. Specifically, optimizing a larger beam radius inside the spacers and selecting spacer material with a smaller nonlinear refractive index such as CaF<sub>2</sub>.
- Introduce self-defocusing mechanism. As presented in Ref [11], PPLN device can operate as a self-defocusing element with an effective negative  $n_2$ .
- Introduce self-phase modulation cancellation material. As discussed in Ref [18], SHG crystal can be used to cancel out the strong self-phase modulation.

**Objective:**

I aim to develop an industrial-grade, high-repetition-rate, high-power 2- $\mu\text{m}$  dual-combs and demonstrate open-air greenhouse gas sensing based on stabilized frequency combs.

**Outline of tasks and Work Plan**

My main work plan for the current project includes the following two parts:

**Part I: Source development**

- Design and simulation of the cavity. This includes standard ABCD matrix cavity design and simulation against Q-switching instabilities. Spacer materials also need to be calculated appropriately and simulated to determine the combination of nonlinear refractive index and material dispersion inside the cavity.
- Testing the spacer concept with continuous-wave cavity and the birefringent filter. This task is relatively independent of the mode-locked cavity and can be tested in parallel while doing simulations of the final cavity. I expect wavelength tuning curves to show a smoother profile without local absorption valleys below 1950 nm.
- Demonstration of the mode-locked oscillator and further characterization and optimization of the oscillator phase noise and time jitter.
- Stabilization of the frequency combs from the oscillators.

**Part II: Long-distance gas sensing experiment**

- Lab-based demonstration of long-distance gas sensing by applying multi-pass gas cell. The detection can be either done by FTS or DCS.
- Utilizing a detection algorithm with DCS for rapid, sensitive detection.
- Field-based open-air path long-distance gas sensing experiment.

**Outcomes**

- The key specifications I aimed to achieve with the high-power high-repetition-rate 2- $\mu\text{m}$  oscillators are Watt-level average power, repetition rate >250 MHz, and nJ pulse energy.
- Improving greenhouse gas sensing in terms of faster detection speed, high sensitivity, and long-distance detection.
- Within the period of the current project, I expect 1-2 journal publications and >2 submissions for conference proceedings.
- One or two master's students will be involved in the current project and get proper training in ultrafast laser development and gas-sensing.
- Establish collaboration with other groups working on the frequency-comb, bridging the laser source development with spectroscopy research.
- This funding will possibly help prove the laser's prototype and thus support the potential start-up.

## Impact

I expect the successful completion of the current project will not only have a major impact directly on the proposed greenhouse gas sensing applications but also following fields:

- Promoting next-generation spectroscopy based on frequency combs at around 2  $\mu\text{m}$  wavelength range. Seeding non-oxide nonlinear crystal based OPO or DFG process further generates MIR radiations [19]. Such MIR comb systems are highly interesting for spectroscopy, environmental monitoring, and medical diagnostics [20].
- With the growth and development of applications such as lidar sensing, metaverse, and the Internet of Things, more telecom windows are needed before we reach the limited capacity. Therefore, the current project will also promote the exploration of the new 2- $\mu\text{m}$  waveband for fiber communications.

## Reference

1. O. Edenhofer, (Cambridge University Press, 2015), **3**.
2. G. B. Rieker, F. R. Giorgetta, W. C. Swann, J. Kofler, A. M. Zolot, L. C. Sinclair, E. Baumann, C. Cromer, G. Petron, C. Sweeney, P. P. Tans, I. Coddington, and N. R. Newbury, *Optica* **1**, 290 (2014).
3. S. Coburn, C. B. Alden, R. Wright, K. Cossel, E. Baumann, G.-W. Truong, F. Giorgetta, C. Sweeney, N. R. Newbury, K. Prasad, I. Coddington, and G. B. Rieker, *Optica* **5**, 320 (2018).
4. E. Baumann, E. V. Hoenig, E. F. Perez, G. M. Colacion, F. R. Giorgetta, K. C. Cossel, G. Ycas, D. R. Carlson, D. D. Hickstein, K. Srinivasan, S. B. Papp, N. R. Newbury, and I. Coddington, *Opt. Express* **27**, 11869 (2019).
5. R. Liao, H. Tian, W. Liu, R. Li, Y. Song, and M. Hu, *J. Phys. Photonics* **2**, 042006 (2020).
6. I. Coddington, N. Newbury, and W. Swann, *Optica* **3**, 414 (2016).
7. A. Barh, B. Ö. Alaydin, J. Heidrich, M. Gaulke, M. Golling, C. R. Phillips, and U. Keller, *Opt. Express* **30**, 5019 (2022).
8. W. Yao, Y. Wang, S. Tomilov, M. Hoffmann, S. Ahmed, C. Liebald, D. Rytz, M. Peltz, V. Wesemann, and C. J. Saraceno, *Optics Express* accepted (2022).
9. P. Loiko, G. Brasse, L. Basyrova, A. Benayad, J.-L. Doualan, C. Meroni, A. Braud, E. Dunina, A. Kornienko, M. Baranov, G. Daniil, and P. Camy, *Journal of Luminescence* **238**, 118109 (2021).
10. Y. Wang, G. Xie, X. Xu, J. Di, Z. Qin, S. Suomalainen, M. Guina, A. Härkönen, A. Agnesi, U. Griebner, X. Mateos, P. Loiko, and V. Petrov, *Opt. Mater. Express* **6**, 131 (2016).
11. A. S. Mayer, C. R. Phillips, and U. Keller, *Nat Commun* **8**, 1673 (2017).
12. T. R. Ensley and N. K. Bambha, *Opt. Express* **27**, 37940 (2019).
13. C. Krankel, *IEEE J. Select. Topics Quantum Electron.* **21**, 250 (2015).
14. A. A. Lagatsky, O. L. Antipov, and W. Sibbett, *Opt. Express* **20**, 19349 (2012).
15. A. Schmidt, S. Y. Choi, D.-I. Yeom, F. Rotermund, X. Mateos, M. Segura, F. Diaz, V. Petrov, and U. Griebner, *Appl. Phys. Express* **5**, 092704 (2012).
16. T. D. Shoji, W. Xie, K. L. Silverman, A. Feldman, T. Harvey, R. P. Mirin, and T. R. Schibli, *Optica* **3**, 995 (2016).
17. S. Kimura, S. Tani, and Y. Kobayashi, *Optica* **6**, 532 (2019).
18. F. Saltarelli, A. Diebold, I. J. Graumann, C. R. Phillips, and U. Keller, *Optica* **5**, 1603 (2018).
19. S. Vasilyev, V. Smolski, J. Peppers, M. Mirov, I. Moskalev, Y. Barnakov, A. Muraviev, K. Vodopyanov, and S. Mirov, in *Optical Sensors and Sensing Congress 2022 (AIS, LACSEA, Sensors, ES)* (Optica Publishing Group, 2022), p. LM4B.2.
20. A. Schliesser, N. Picqué, and T. W. Hänsch, *Nature Photon* **6**, 440 (2012).

## **In-plane telecom lasers grown on SOI for integrated silicon photonics**

As the crux of next generation communication systems and data interconnects, Si-photonics has been underpinned by the development of some key components such as low-loss Si waveguides and high-speed optical modulators. While Si has been employed to make excellent passive components, efficient light emission still relies on III-V compound semiconductors due to the indirect band structure of Si. Heterogeneous integration approaches such as wafer-bonding and micro-transfer printing have enabled the integration of high-performance III-V lasers on Si-photonics platforms via evanescent coupling strategies. However, the cost and yield of manufacturing is less than optimum compared with monolithic integration, and the large footprint of evanescent coupling limits the scalability of this approach. Monolithic integration of III-V lasers via direct hetero-epitaxy could further benefit Si-photonics in terms of cost, scalability, and integration density. In the past few years, III-V quantum dot lasers with impressive performance have been grown on Si using direct blanket hetero-epitaxy. However, the micrometers thick buffer layers necessary for defect engineering severely impedes the light coupling between the III-V active devices and the passive Si elements underneath. As an alternative, selective hetero-epitaxy of III-V alloys on Si using the aspect ratio trapping (ART) technique enables closer placement and hence more efficient light coupling between the III-V gain material and the Si-waveguides. Limited by required aspect ratio in conventional ART method, the III-V material volume is often at the nanometer scale making the realization of electrically pumped lasers challenging. To solve this dilemma, we have demonstrated an integration scheme named *lateral aspect ratio trapping (LART)* with selectively grown large-area dislocation-free InP membranes on (001) SOI wafers patterned by conventional photolithography. These III-V crystals locate right on top of the buried oxide layer and feature a unique in-plane configuration with the Si device layer, which results in strong light confinement within the epitaxial III-V and allows for compact and efficient butt coupling between III-V and Si in the same plane.

Recently, we have achieved optically pumped lasing of telecom micro-ring lasers and distributed feedback lasers using LART. In this project, we propose to develop electrically pumped telecom lasers on industry-standard SOI wafers through monolithic integration using LART. To achieve practical lasers, we will optimize the parameters to allow lateral growth of defect-free III-V crystals on SOI long enough to support electrically-pumped lasing. Also, to facilitate the lasing unique structure design is necessary for the lateral junction. In this project, we will focus on developing growth techniques and designing laser structures for the integration of practical lasers on SOI using decades of our experience in Metalorganic chemical vapor deposition (MOCVD), device fabrication and characterization. *Putting high-performance lasers exactly where they are needed in the photonic integrated circuit is the most unique and brightest point of this project.*

The proposed in-plane telecom laser on SOI will provide a practical solution for light emitting and efficient coupling with passive components on the Si-photonics platform, the final obstacle between cost-effective integration of electronics and power-efficient photonics. Furthermore, integrating III-V lasers onto SOI substrates will enable the next generation photonic integrated systems to have lower manufacturing cost, as well as be compatible with the well-established Si CMOS electronics.

# **In-plane telecom lasers grown on SOI for integrated silicon photonics**

## **I. Literature Review**

Si-based integrated circuit (IC) is known as the most powerful and mature micro/nano-electronic technology enabling signal processing, memory, and artificial intelligence that are ubiquitous in modern day life. However, Si does not interact efficiently with photons and transports electrons slowly due to the limitations of its inherent crystalline and energy-band structure. In contrast, photonic technologies can be used for data transmission of long reach with large bandwidth and high efficiency. With the continuing exponential growth of internet data traffic, there is a strong motivation to develop technologies for low-cost high-performance photonic integrated circuits which can enable the continued growth of data transmission. Emerging consumer-oriented applications such as automobiles and sensors for robotic platforms are also providing the impetus for the development of energy-efficient, densely integrated and cost-effective photonic integrated circuits (PICs). Silicon photonics (Si-photonics), as the core technology to extend integrated photonics adopting the highly successful Si IC infrastructure for the next-generation of information technology and computing, has been extensively investigated over the years. While Si-photonics has been underpinned by the success of Si-based key components such as low-loss waveguides and high-speed modulators the light emission necessitates the integration of III-V compound semiconductors which have long been employed for lasers in conventional InP-based PICs due to the indirect bandgap nature of silicon [1-3].

To bridge the final gap between the cost-effective electronics and the high-speed photonics, an efficient and scalable on-chip III-V light sources must be integrated on Si which has been the major challenge for Si-photonics. Practical applications in Si-photonics require these light sources to be electrically pumped, efficiently coupled with Si-based passive components, and stably operated at room temperature and elevated temperatures with a long lifetime. Heterogeneous integration approaches such as wafer-bonding and micro-transfer printing have enabled the integration of high-performance III-V lasers on Si-photonics platforms via evanescent coupling strategies [4, 5]. However, the cost and yield of manufacturing is less optimum than monolithic integration, and the large footprint of evanescent coupling limits the scalability of this approach. Monolithic integration of III-V lasers on Si via direct hetero-epitaxy could further enhance Si-photonics in terms of cost, scalability, and integration density. In the past few years, as a result of the low defect sensitivity of quantum dot (QD), we and a few other groups around the world have grown III-V QD lasers on Si using direct blanket hetero-epitaxy with impressive device performance reported [6-8]. Unfortunately, the micrometers thick buffer layers necessary for defect engineering severely impedes the light interfacing between the III-V active devices and the passive Si elements underneath. As an alternative, selective hetero-epitaxy of III-V alloys on Si using the aspect ratio trapping (ART) technique enables closer placement and hence more efficient light coupling between the III-V gain material and the Si-waveguides. The conventional ART method requires a high aspect ratio for the selective growth thereby limiting the epitaxial III-V material volume at nanometer-scale, making the realization of electrically pumped lasers challenging [9-12].

## II. Problem statement/Objective

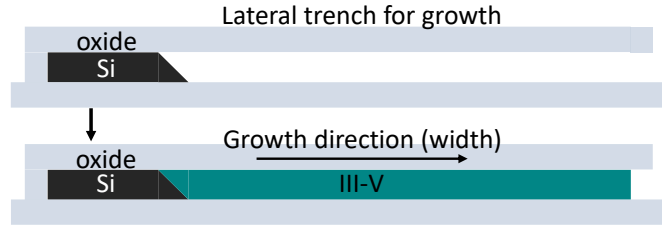


Figure 1. Cross-sectional view schematic illustrating the growth scheme using LART.

To solve this dilemma, we have implemented an integration scheme named lateral aspect ratio trapping (LART) as shown in Figure 1 and demonstrated the selective growth of large-area dislocation-free InP membranes on (001) SOI wafers [13, 14]. These III-V crystals right on top of the buried oxide layer feature an in-plane configuration with the Si device layer, which results in a unique InP-on-insulator architecture and allows for strong light confinement within the epitaxial InP. Moreover, the co-planar configuration between the epitaxial III-V material and the Si device layer leads to compact and efficient butt-coupling schemes. Despite being still in its infancy, the LART approach has been successfully demonstrated by optically pumped InP lasers and Si-waveguides integrated high-performance photodetectors on industry-standard SOI wafers [14-16]. The coupling efficiency between III-V active devices and Si-based passive components was verified to be as high as 70% and can be further improved by optimized fabrication processes enabled by the high-level lithography modules in the foundry [16]. Recently, by incorporating laterally grown multi-quantum wells (QWs) we have achieved telecom band lasing on micro-ring lasers (MRLs) grown on SOI as presented in Figure 2(a) and (b) [17]. Although the III-V material volume for device fabrication has successfully evolved from nano-meter scale to micrometer scale, the device implementation is still limited to nano-lasers and micro-lasers. To further unlock the volume limitation and make a step forward to electrically pumped lasers, we optimized the lateral growth of III-V on SOI and enlarged the volume of the device quality material to around 10  $\mu\text{m}$  wide and 100  $\mu\text{m}$  long. With the enlarged material volume and unique design of lateral gratings for the in-plane lasers, we demonstrated the low threshold distributed feedback (DFB) lasers on SOI using LART as shown in Figure 2(c) and (d) [unpublished]. Extending the epitaxial length requires precise control and tuning of growth conditions and

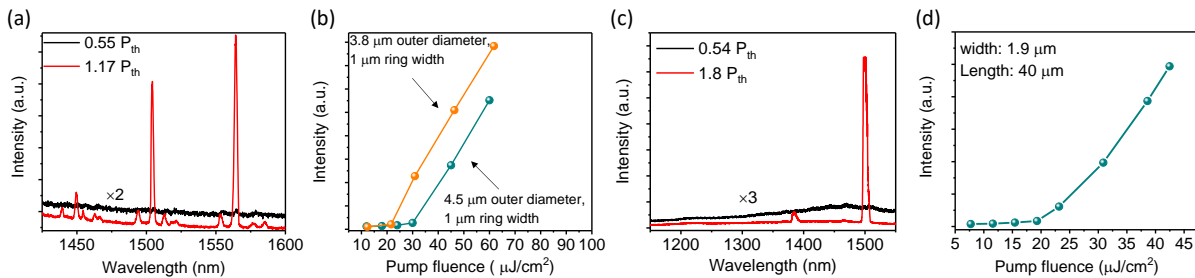


Figure 2. (a) Room temperature spectra of the MRL on SOI with a ring width of 1  $\mu\text{m}$  and an outer diameter of 4.5  $\mu\text{m}$ . (b)  $L-L$  curves of MRLs with the same ring width of 1  $\mu\text{m}$  and various outer diameters of 3.8  $\mu\text{m}$  and 4.5  $\mu\text{m}$ . (c) Room temperature spectra of the DFB laser on SOI. (d)  $L-L$  curves of the DFB laser with a width of 1.9  $\mu\text{m}$  and length of 40  $\mu\text{m}$ . [17]



various defect engineering techniques to achieve device-quality material and morphology. Therefore, sufficiently long III-V material on SOI which are qualified for practical electrically pumped lasers using LART is challenging.

The objective of this program is to investigate and explore the integration of in-plane electrically pumped telecom lasers on SOI using LART. The demonstrated lasers can be coupled with Si-based passive components in a butt-coupling strategy efficiently, thereby serving as the on-chip light sources in Si-photonics.

### III. Outline of tasks/Work plan

Building from our demonstration of optically pumped lasers and telecom photodetectors, we propose to develop electrically pumped telecom lasers on industry-standard SOI wafers through monolithic integration using LART growth, as delineated in Figure 3. Two approaches can be adopted to achieve electrically pumped lasing. The most straightforward method is to pattern the metal contacts on the n-InP and p-InGaAs in the lateral junction (Figure 3(a)). The current-voltage ( $I$ - $V$ ) characteristic of the lateral junctions with shorter lengths has been verified by the demonstration of photodetectors and the resistance for longer junction was calculated to be low enough for lasers. As schematically depicted in Figure 3(b), the laterally grown III-V on SOI can also function as virtual substrates for vertical regrowth. Therefore, another method to realize electrically pumped lasing is to regrow the gain media, upper claddings and p contact layers vertically on the lateral grown InP on SOI. Using this method, both the QWs and QDs can be included as gain media for enhanced device performance. For both methods, we will first optimize the growth parameters to obtain defect-free crystals with sufficiently long wide dimensions. After optimization of the lateral growth, doped cladding and contact layers will be added to the laser structure for the first method. Lateral current injection will be enabled by patterning the p- and n-metal on top of the p-doped InGaAs and n-doped InP, respectively. Shallow etched ridges and SiN gratings can be formed on top of the active region to facilitate lasing. For the latter mentioned method, selective regrowth of QWs, QDs, cladding and contact layers on the laterally grown InP will be developed based on our previous experience of electrically pumped QW and QD lasers on Si using blanket epitaxy [6, 18, 19]. As the laser features a top-down structure, we can leverage on the well-established photonic technology developed for InP based PICs.

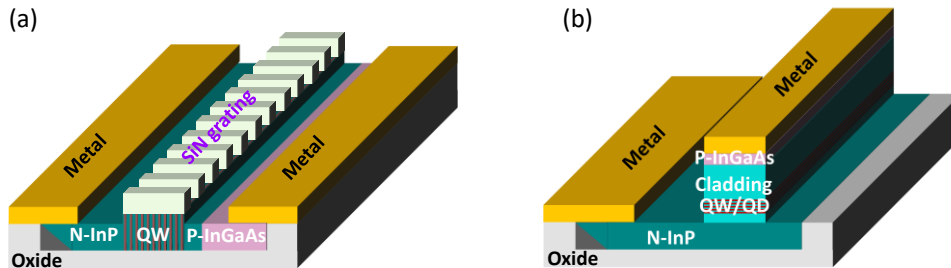


Figure 3. (a) Schematic of electrically pumped DFB laser grown on SOI using LART. (b) Schematic of electrically pumped laser regrown on InP/SOI using LART and selective regrowth.

### IV. Outcome

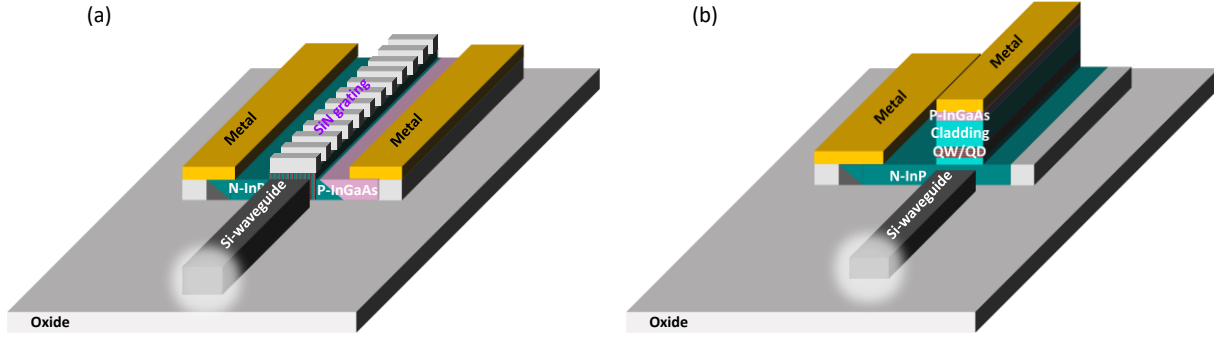


Figure 4. (a) Electrically pumped DFB laser coupled with Si-waveguides using butt-coupling scheme. (b) Light coupling of electrically pumped laser regrown on InP/SOI and Si-waveguides.

The aim of this project is to demonstrate telecom lasers on SOI using the unique selective growth technique of LART. The overarching outcome are to design and experimentally demonstrate (1) growth of InP and other III-V compounds sufficiently long for laser cavity based on our novel and unique LART technique and (2) integrated telecom electrically-pumped lasers on the conventional SOI platform practical for silicon photonics. In this project, we will focus on developing growth techniques and designing laser structures for the integration of practical lasers using decades of our experience in Metalorganic chemical vapor deposition (MOCVD), device fabrication and characterization. This program will allow us to combine the expertise of designing novel MOCVD growth procedures, as well as laser fabrication and characterization technologies. We will address specific issues of integrating high-performance III-V lasers and passive photonic components on SOI which is not available on any demonstrated platform. As schematically illustrated in Figure 4(a), the light from the laser can be butt-coupled to the Si-waveguides in the same plane efficiently for the first method with lateral junction. For the laser structure with regrown gain media, the light can be evanescently coupled to the InP underneath and then butt-coupled to the Si-waveguide, benefitted from the short distance between III-V active region and Si-waveguide (Figure 4(b)). These in-plane lasers can be coupled to our previously demonstrated photodetectors and other components on the SOI.

## V. Impact

The results of this project will facilitate putting high-performance lasers exactly where they are needed in the photonic integrated circuit. This is the most unique and versatile technology to support energy-efficient silicon photonics. Integrating high-performance III-V light sources that can be coupled with Si or SiN passive components and associated integration technologies on the same silicon platform is of paramount importance. First, the proposed in-plane telecom laser on SOI will address the issue of monolithic on-chip laser sources for Si-photonics which is the final gap between the cost-effective electronics and the power-efficient photonics. Furthermore, integrating III-V lasers onto SOI substrates will enable the next generation integrated systems to have lower manufacturing costs, as well as compatible with the well-established Si CMOS electronics. The proposed in-plane telecom lasers integrated on SOI strongly leverage the enormous capabilities and infrastructure of Si CMOS, extending them to photonic and electronic integrated devices/circuits for high speed, wide bandwidth, and energy-efficient applications.

## References:

- [1] M. Near, C. Xiang, Steven M. Bowers, A. Bjorlin, R. Blum, and John E. Bowers, "Perspective on the future of silicon photonics and electronics." *Applied Physics Letters*, 118(22), 220501, (2021).
- [2] D. Thomson, A. Zilkie, John E Bowers, T. Komljenovic, Graham T Reed, L. Vivien, D. Marris-Morini, E. Cassan, L. Viro, Jean-Marc Fédéli, J. Hartmann, Jens H Schmid, D. Xu, F. Boeuf, P. O'Brien, Goran Z Mashanovich and M Nedeljkovic. "Roadmap on silicon photonics." *Journal of Optics*, 18(7), 073003, (2016).
- [3] Y. Han, H. Park, J. Bowers, & K. M. Lau, "Recent advances in light sources on silicon." *Advances in Optics and Photonics*, 14(3), 404-454, (2022).
- [4] Y. Wan, C. Xiang, J. Guo, K. R. oscica, M.J. Kennedy, J. Selvidge, Z. Zhang, L. Chang, W. Xie, D. Huang, and A.C. Gossard, "High Speed Evanescent Quantum-Dot Lasers on Si," *Laser & Photonics Reviews*, 15(8), p.2100057, (2021).
- [5] Y. Hu, D. Liang, K. Mukherjee, Y. Li, C. Zhang, G. Kurczveil, X. Huang, and Raymond G. Beausoleil. "III-V-on-Si MQW lasers by using a novel photonic integration method of regrowth on a bonding template," *Light: Science & Applications* 8(1), 1-9, (2019).
- [6] Y. Xue, W. Luo, S. Zhu, L. Lin, B. Shi, and K. M. Lau, "1.55  $\mu\text{m}$  electrically pumped continuous wave lasing of quantum dash lasers grown on silicon", *Optics Express*, 28(12), pp.18172-18179, (2020).
- [7] C. Shang, E. Hughes, Y. Wan, M. Dumont, R. Koscica, J. Selvidge, R. Herrick, A. C. Gossard, K. Mukherjee, and J. E. Bowers, "High-temperature reliable quantum-dot lasers on Si with misfit and threading dislocation filters," *Optica* 8, 749 (2021).
- [8] S. Chen, W. Li, J. Wu, Q. Jiang, M. Tang, S. Shutts, S. N. Elliot, A. Sobiesierski, A. J. Seeds, I. Ross, P. M. Smowton, and H. Liu, "Electrically pumped continuous-wave III-V quantum dot lasers on silicon," *Nat. Photonics* 10(5), 307-311 (2016).
- [9] Y. Han, Z. Yan, W. K. Ng, Y. Xue, K. S. Wong, and K. M. Lau, "Bufferless 1.5  $\mu\text{m}$  III-V lasers grown on Si-photonics 220 nm silicon-on-insulator platforms," *Optica*, 7(2), 148-153, (2020).
- [10] Y. Shi, Z. Wang, J. Van Campenhout, M. Pantouvaki, W. Guo, B. Kunert, D. Van Thourhout, "Optical pumped InGaAs/GaAs nano-ridge laser epitaxially grown on a standard 300-mm Si wafer," *Optica*, 4(12),1468-73, (2017).
- [11] W. Stephan, Benedikt F. Mayer, H. Schmid, M. Sousa, J. Gooth, H. Riel, and Kirsten E. Moselund. "Room-temperature lasing from monolithically integrated GaAs microdisks on silicon." *ACS nano* 12(3), 2169-2175, (2018).
- [12] S. Mauthe, Y. Baumgartner, M. Sousa, Q. Ding, M.D. Rossell, A. Schenk, L. Czornomaz, K.E. Moselund, "High-speed III-V nanowire photodetector monolithically integrated on Si," *Nature communications*, 11(1), 1-7, (2020).
- [13] Y. Han, Y. Xue, Z. Yan and K. M. Lau, "Selectively grown III-V lasers for integrated Si-photonics," *Journal of Lightwave Technology*, 39(4), pp.940-948, (2021).
- [14] Z. Yan, Y. Han, L. Lin, Y. Xue, C. Ma, W. K. Ng, K. S. Wong, and K. M. Lau, "A monolithic InP/SOI platform for integrated photonics." *Light: Science & Applications* 10(1), 1-10, (2021).
- [15] Y. Xue, Y. Han, Y. Tong, Z.hao Yan, Y. Wang, Z. Zhang, H. K. Tsang, and K. M. Lau, "High-performance III-V photodetectors on a monolithic InP/SOI platform." *Optica* 8(9), 1204-1209, (2021).
- [16] Ying Xue, Yu Han, Yi Wang, Jie Li, Jingyi Wang, Zunyue Zhang, Xinlun Cai, Hon Ki Tsang, and Kei May Lau, "High speed and low dark current Si-waveguide coupled III-V photodetectors selectively grown on SOI", *Optica*, accepted.
- [17] Jie Li, Ying Xue, Liying Lin, Zengshan Xing, Kam Sing Wong and Kei May Lau, "Telecom InGaAs/InP quantum well lasers laterally grown on Silicon-on-Insulator," *Journal of Lightwave Technology*, vol. 40, no. 16, pp. 5631-5635 (2022).
- [18] Si Zhu, Bei Shi, Qiang Li, and Kei May Lau "Room-temperature electrically-pumped 1.5  $\mu\text{m}$  InGaAs/InAlGaAs laser monolithically grown on on-axis (001) Si," *Optics Express*, Vol. 26, No. 11, (2018).
- [19] Y. Xue, Y. Wang, W. Luo, J. Huang, L. Lin, H. K. Tsang, and K. M. Lau, "Telecom InP-based quantum dash photodetectors grown on Si", *Applied Physics Letters*, 118(14), 141101, (2021).

## **Wide-Range Multispectral Imaging for Spatial Ripeness Estimation of Durian Fruits**

The challenge of durian ripeness estimation is the apparent features of durians are not directly relative to their ripeness levels, i.e., color. Moreover, the durian husk is very thick that is difficult to directly investigate the inside qualities, i.e., maturity and ripeness level, without peeling it. The ripeness needs to be estimated before peeling durians for customers. The peeled durians with disappointed ripeness levels will be a waste product in markets. Thus, high accuracy and non-destructive methods are needed for durian's ripeness estimation to satisfy the customers as well as classify the oversupplied fruits for food processing in order to balance demand and supply in the global market

Here, we propose to combine a broad-band multispectral imaging module and machine learning to spatially evaluate the ripeness level of durian fruits. As the machine learning is embedded, the accuracy for ripeness level estimation can also be improved simultaneously through the data collection from our system and retraining of our analytical models. During the change of durian's temperature ( $\Delta T_D$ ) under a surrounding temperature, the images of a durian fruit are obtained by a broad-band multispectral imaging module upon the illumination of ultraviolet light sources (UV-A) and halogen-tungsten light sources, respectively. The captured images consist of a three-dimensional (3D) image and multispectral images covering visible to far-infrared regions that create a data set used for spatial ripeness estimation. The data set is used to train for spatial identifying the ripeness level of the durian into unripe (highlighted as green), ripe (highlighted as yellow), or overripe (highlighted as red) stages by means of a machine learning method. More spectral images can be obtained by placing band-pass filters and/or polarization filters in front of the multispectral imaging module.

The intended outcome of this project is to achieve a field prototype with an accuracy of more than 95% of ripeness estimation for onsite markets to satisfy the demand of customers (waste is expected to be reduced by half or around USD1,500M). The balancing between demand and supply can maintain the economic value (>USD500M) of durian products in the global market. Furthermore, the new platform can be extended to monitor the maturity of durian fruits on trees before harvesting in order to obtain durian fruits with high quality (immature fruits cause the low quality of durian products).

# Wide-Range Multispectral Imaging for Spatial Ripeness Estimation of Durian Fruits

## 1. Literature Review

Durians are edible fruits and commonly grown in Southeast Asia, such as Indonesia, Malaysia, Singapore, Thailand, Cambodia and Vietnam. Thailand is the world's largest durian exporter with over USD500M since 2016. The highest record was in 2020 with over USD2,000M [1]. Usually, customers expect and prefer to buy high-quality durian fruits. The standard parameters used to identify the quality of durian fruits are size, weight, maturity, and ripeness level [2]. Due to the thickness of durian's husk, it is difficult to directly investigate the inside qualities, i.e., maturity and ripeness level, without peeling it.

A widely used method is the analysis of the sound after knocking a stick on the durian fruit. It is typically accomplished by some well-trained or high-experience workers [3] whose results might be different. The ripeness levels can also be measured through the firmness of durian pulp during the ripening stage by using a fruit penetrometer, thus damaging internal pulps [4]. Non-invasive methods with the aid of machine learning have been proposed and demonstrated to accurately identify the ripeness level, including ultrasonics [5] and electronic nose [6]. However, these two techniques have to be performed in a close system in order to prevent the disturbance of the surrounding environment, which is not suitable for practical measurement.

Optical spectroscopy covering visible to near-infrared regions has also been proposed for achieving a rapidly non-invasive measurement of durian fruits [7-10]. Apart from visible to infrared wavelength region, a far infrared (e.g., 8,000-14,000 nm wavelength) spectroscopic imaging module is useful for converting the spectroscopic data into heat for fruit quality control [11]. Especially for thermal imaging, the accuracy of durian ripeness estimation can be up to 97% with the aid of machine learning [12]. Beyond traditional optical spectroscopy, the multispectral imaging technique is cable to simultaneously capture both spectral and spatial information, called a spectral image. But the application of multispectral imaging for spatial ripeness estimation of durian fruits has not been demonstrated yet. Here, we propose to combine a broad-band multispectral imaging module [13] and machine learning to spatially evaluate the ripeness level of durian fruits. As the machine learning is embedded, the accuracy for ripeness level estimation can also be improved simultaneously through the data collection from our system and retraining our analytical models.

## 2. Problem Statement/Objective

Customers favor different ripeness levels due to the different tastes and firmness of durian pulps. However, sellers cannot exactly provide what the customers prefer as the outer features of durians are not directly and completely related to their ripeness levels. The ripeness needs to be estimated before peeling durians for customers. The peeled durians with disappointed ripeness levels will be a waste product in markets. Thus, durian's ripeness is one of the main factors that influence the buying decision of customers in the markets. Therefore, high accuracy and non-destructive methods are needed for durian's ripeness estimation to satisfy the customers as well as to classify the oversupplied fruits for food processing management in order to balance demand and supply in the global market. Here, this project will be focused on a non-destructive method by utilizing multispectral imaging and machine learning to spatially estimate the ripeness level of durian fruits.

### 3. Outline of tasks/Work Plan

#### Proposed concept

The proposed concept is shown in **Figure 1**. During the change of durian's temperature ( $\Delta T_D$ ) under a surrounding temperature, the images of a durian fruit are obtained by a broad-band multispectral imaging module upon the illumination of ultraviolet light sources (UV-A) and halogen-tungsten light sources, respectively. The captured images consist of a three-dimensional (3D) image and multispectral images covering visible to far-infrared regions that create a data set used for spatial ripeness estimation. The data set is used to train for spatial identifying the ripeness level of the durian into unripe (highlighted as green), ripe (highlighted as yellow), or overripe (highlighted as red) stages by means of a machine learning method. More spectral images can be obtained by placing band-pass filters and/or polarization filters in front of the multispectral imaging module.

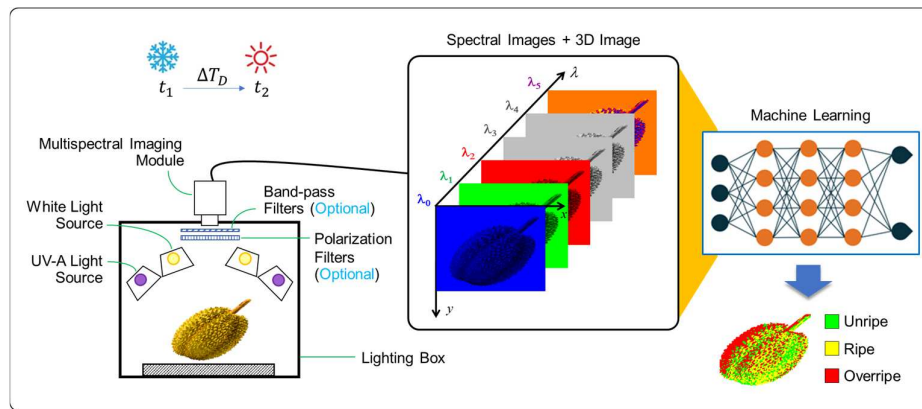


Figure 1 Schematic diagram of broad-band multispectral imaging for spatial ripeness estimation of durian fruits.

#### Broad-band multispectral imaging module

Our broad-band multispectral imaging module consists of an RGB or visible camera (400 – 780 nm), near-infrared (NIR) cameras (800 – 2,500 nm), a far-infrared (FIR) camera (8,000 – 14,000 nm), and a depth sensor. The FIR camera is a thermal imaging sensor having  $160 \times 120$  pixels, thermal sensitivity of  $< 50$  mK, and a frame rate of 9 Hz. For the depth sensor, we exploit a low-cost commercially available imaging optical depth sensor that automatically provides RGB images, IR images and depth information at a fast speed of 60 frames/second (fps) [13]. Our multispectral imaging module can be connected to a typical computer or an electronic controlling unit (e.g., NVIDIA Jetson Nano or a notebook computer) via a universal serial bus (USB).

#### Data acquisition

The data acquisition is divided into two parts as depicted in **Figure 2**. First, durian fruits are suddenly moved from the controlled temperature  $T_{E1}$  to  $T_{E2}$ . Then the acquiring process is performed every 2 mins for 10 mins upon the illumination of UV-A and white light sources, respectively. Band-pass filters are inserted when capturing NIR and FIR spectral images while polarization filters are inserted when an RGB image is obtained under the illumination of the white light sources. Similar to the first method, the second method has the same step for capturing the multispectral images, but the durians are captured every 30 mins in the environmental temperature. By acquiring the data with a cold temperature in the early morning



( $T_{E1}$  at 6 AM) and a warm temperature in the late morning ( $T_{E2}$  at 11 AM), the spectral data with the change of durian's temperature ( $\Delta T_D$ ) can be obtained. 150 "Monthong" durian fruits with different ripeness levels are used for each part. The ripeness will be confirmed by measuring the firmness level with a penetrometer after the durians are peeled. The 3D image will be simultaneously obtained when the white light sources are turned on.

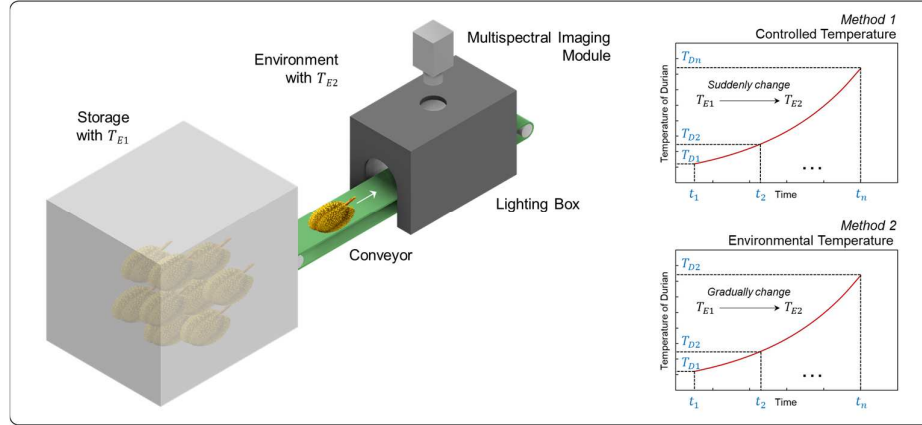


Figure 2 Data acquisition of two different methods.

### Spatial ripeness estimation

The spectral images of durians will be removed background by using thresholding and blob filtering methods to extract an average intensity of whole fruits for each spectral image ( $I_\lambda$ ). After that,  $I_{\lambda_1}$  to  $I_{\lambda_n}$  are used as input data for an artificial neural network to learn the spectral data of all ripeness levels.  $n$  is a number of spectral data. The result of the learning process is applied for spatial ripeness estimation by using each pixel of the durian fruits,  $I_{\lambda(x,y)}$ , as input data. The durian fruit image will be respectively highlighted as green, yellow, and red for unripe, ripe, and overripe stages. At this step,  $t_1$  and  $t_2$  that are significantly relative to  $\Delta T_D$  of durians for each stage, and the principal wavelengths will be determined in order to minimize the number of parameters and optical elements for implementing a field prototype.

### Field operation test

For the field test as illustrated in **Figure 3**, the unwanted optical elements are removed, and a portable version is implemented instead. The multispectral images of durian fruits will be captured in the early morning ( $T_{E1}$ ) and one more time in the late morning ( $T_{E2}$ ). These two sets of spectral images will be used to estimate the ripeness level of durians by sellers before selling to customers.

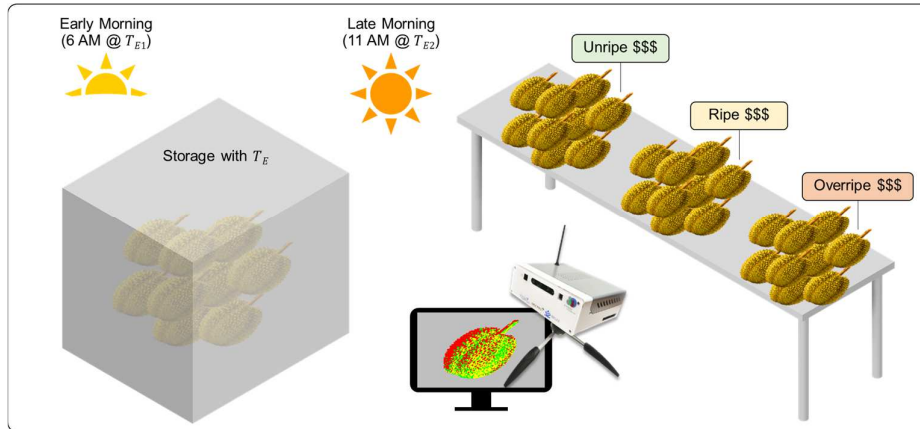


Figure 3 Illustration of a field prototype for durian ripeness estimation.

#### 4. Outcomes

- Achieving a field prototype with an accuracy of more than 95% of ripeness estimation for onsite markets.
- Maintaining the economic value (>USD500M) of durian products in the global market (fresh, frozen, preserved, and dried).
- Arising a new platform of pre- and postharvest technologies for agricultural products.
- Obtaining a 3D model of durian fruits for morphological study.
- Extending this new technology platform for food safety and inspection.
- Extending this platform for monitoring the maturity of durian fruits on trees before harvesting in order to obtain durian fruits with high quality (immature fruits cause the low quality of output products) as illustrated in **Figure 4**.

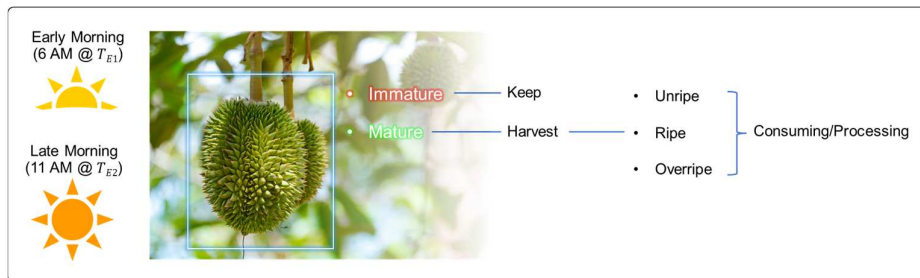


Figure 4 Conceptual diagram of future maturity estimation of durian fruits on trees before harvesting.

#### 5. Impact

From 2022 and beyond, durian production is expected to be more than 1,000,000 metric tons [14] or ~USD3,000M (120 THB/kg or USD3/kg). If the ripeness estimation technology can reduce waste from unwanted durian fruits just by half, the economic value can be saved up to around USD1,500M.

#### References

1. Tridge, "Fresh Durian," [https://www.tridge.com/intelligences/durian/export?utm\\_source=google&utm\\_medium=cpc&utm\\_campaign=fulfillment&utm\\_content=general\\_url\\_mar10&gclid=EAIaIQobChMIsKPU-oqE-QIVIAkrCh1seAX2EAAYASAAEgKYuPD\\_BwE](https://www.tridge.com/intelligences/durian/export?utm_source=google&utm_medium=cpc&utm_campaign=fulfillment&utm_content=general_url_mar10&gclid=EAIaIQobChMIsKPU-oqE-QIVIAkrCh1seAX2EAAYASAAEgKYuPD_BwE).

2. National Bureau of Agricultural Commodity and Food Standards, "Thai Agricultural Standard - TAS 3-2013 - Durian," [https://www.acfs.go.th/files/files/commodity-standard/20190609225641\\_142156.pdf](https://www.acfs.go.th/files/files/commodity-standard/20190609225641_142156.pdf).
3. W. Kharamat, M. Wongsaisuan, and N. Wattanamongkhon, "Durian Ripeness Classification from the Knocking Sounds Using Convolutional Neural Network," in *2020 8th International Electrical Engineering Congress (iEECON)(2020)*, pp. 1-4.
4. C. Bangkok, "Thai Students Invent Tool to Test Durian Ripeness; Claim 100 Percent Accuracy," <https://coconuts.co/bangkok/news/thai-students-invent-tool-test-durian-ripeness-claim-100-percent-accuracy/>.
5. A. Rejo, Suroso, I. W. Budiastara, H. K. Purwadaria, S. Susanto, and Y. Y. Nazaruddin, "Model for Predicting and Classifying Durian Fruit Based on Maturity and Ripeness Using Neural Network," *IFAC Proceedings Volumes* **34**, 321-324 (2001).
6. M. Rivai, F. Budiman, D. Purwanto, M. S. Adil Al Baid, Tukadi, and D. Aulia, "Discrimination of durian ripeness level using gas sensors and neural network," *Procedia Computer Science* **197**, 677-684 (2022).
7. P. Timkhun, and A. Terdwongworakul, "Non-destructive classification of durian maturity of 'Monthong' cultivar by means of visible spectroscopy of the spine," *Journal of Food Engineering* **112**, 263-267 (2012).
8. S. Tangjitwiboonkun, P. Chaiprasart, and R. Rittiron, "Non-destructive measurement of dry matter in mature 'Long-lab-lae' durian fruits using portable NIR spectrometer," in *III Asia Pacific Symposium on Postharvest Research, Education and Extension: APS2014*(International Society for Horticultural Science (ISHS), Leuven, Belgium2018), pp. 517-522.
9. A. M, and P. N. Renjith, "Classification of Durian Fruits based on Ripening with Machine Learning Techniques," in *2020 3rd International Conference on Intelligent Sustainable Systems (ICISS)*(2020), pp. 542-547.
10. P. Onsawai, K. Phetpan, L. Khurnpoon, and P. Sirisomboon, "Evaluation of physiological properties and texture traits of durian pulp using near-infrared spectra of the pulp and intact fruit," *Measurement* **174**, 108684 (2021).
11. S. Sumriddetchkajorn, and Y. Intaravanne, *Two-dimensional fruit ripeness estimation using thermal imaging* (SPIE, 2013).
12. M. Mohd Ali, N. Hashim, and M. I. Shahamshah, "Durian (*Durio zibethinus*) ripeness detection using thermal imaging with multivariate analysis," *Postharvest Biology and Technology* **176**, 111517 (2021).
13. S. Sumriddetchkajorn, S. Rayanasukha, A. Somboonkaew, S. Chanhorm, and U. Wannason, "Low-Cost 3-D Broad-Spectral Imaging Module," in *15th Pacific Rim Conference on Lasers and Electro-Optics*( Hokkaido Japan 2022).
14. Office of Agricultural Economics (Thailand), "Trade Statistics 2022," <https://www.oae.go.th/assets/portals/1/files/journal/2565/trendstat2565-Final-Download.pdf>.

## **Application category: HEALTH**

### **Deep learning-empowered compressive optical coherence tomography for tele-ophthalmology**

#### **What is the challenge?**

The ongoing pandemic of coronavirus disease 2019 (COVID-19) has witnessed an accelerating pivot in the healthcare industry from face-to-face encounters to telehealth: the telehealth's share in US has surged by 2,250% since January 2020. Unfortunately, ophthalmological clinics found themselves in a challenging situation to adapt to this new normal due to the heavy reliance on the diagnostic equipment. In fact, the adoption of telehealth in ophthalmology is among the lagging specialties which is almost tied with physical therapies. Take optical coherence tomography (OCT), the most widely used tools in ophthalmology, as an example, it not only requires on-site operations by trained specialists but also generates immense amount of data, both of which are incompatible with the current telehealth paradigm. Recently, remotely controlled OCT machine that does not require human operation was reported by Izatt Group. However, the second gap remains unfilled: a commercial 200 kHz swept-source OCT (SS-OCT) system could easily produce a raw data bandwidth of ~400 MB/s, which is 20~30-fold larger than the speed of 5G wireless or broadband connection.

#### **How are we going to address it?**

The objective of this project is to develop a compressive SS-OCT system that could support real-time streaming of OCT raw data via current network with satisfactory reconstruction quality. Specifically, we will physically reduce the system's data bandwidth by a factor of 20 (use only 5% of the raw data) and achieve a peak-signal-to-noise ratio (PSNR) of 20 dB during the reconstruction. We plan to achieve this by jointly optimizing the data compression and image reconstruction schemes with the aid of artificial intelligence (AI).

In our proposal, the data bandwidth will be first compressed by reducing the quantization and by performing two-dimensional sub-sampling, and the images will later be recovered by using neural networks. We will use an end-to-end deep learning-based training framework to discover the optimal sub-sampling pattern along with the best performing reconstruction networks. Moreover, the learned sub-sampling pattern will be implemented on an existing retinal SS-OCT system and the trained reconstruction networks will be deployed on a remote host computer. For the system demonstration, human eyes will be imaged and the compressed data will be streamed over the network to a remote host computer. The OCT images will then be reconstructed in real-time to showcase its utility.

#### **What about the outcome and the impact?**

The major outcome of this proposal is a prototype compressive retinal SS-OCT system which would mark the new state-of-the-art performance in terms of using the least data bandwidth to deliver the best reconstruction image quality. This would lead to the real-time streaming of OCT data via common broadband connections for the first time. It should also be noted that the proposed method only requires minimal modifications on the hardware (i.e. re-programming the data acquisition board) and is compatible with most existing SS-OCT systems.

The success of the proposed project would bring us closer towards the realization of the first-generation tele-OCT system: in conjunction with the recently advanced robotic OCT technology, the proposed prototype could be immediately compatible with the current telehealth paradigm. We believe such a progress could be promising remedy to the problems faced by the ophthalmological clinics during this on-going pandemic: millions of patients with eye conditions will no longer need to visit the clinics to receive face-to-face treatments. They can instead visit an unmanned booth with the tele-ophthalmology system installed, while the OCT images of the patient would be streamed real-time on the screens of the tablets or laptops in the ophthalmologists' offices hundreds of miles away.

# Deep learning-empowered compressive optical coherence tomography for tele-ophthalmology

## Problem Statement

The current coronavirus disease 2019 (COVID-19) pandemic witnesses the surge of telehealth thanks to its natural immunity against viral transmission. Based on the US data provided by FAIR Health, the telehealth's share of medical claims once peaked at 13.0% in April 2020 up from merely 0.24% in January 2020, and it currently reads 5.4% in May 2022 despite of the gradual relaxation of social distancing measures [1]. Similar trends are observed in other parts of the globe: reported by Medicare Benefits Schedule (MBS) of Australia, about 27% of MBS services were delivered by telehealth in Q1 2022 [2]. It is evident that telehealth has emerged to become a vital part of the modern healthcare system.

However, ophthalmology is among the lagging specialties during this transformation. According to a recent survey, only 9% of the ophthalmologists has ever tried telemedicine during the pandemic, the total visit decreased by over 50% [3]. These alarming figures remind us of the vulnerability of the patients suffered from various eye conditions such as glaucoma (-52.2% change in total visits, 2.6% telemedicine) and cataracts (-61.2% change in total visits, 1.2% telemedicine) that require regular follow-ups.

One possible reason is that ophthalmology clinics heavily rely on specialized equipment to make diagnostic decisions [4]. Optical coherence tomography (OCT) is among the most widely used tool for diagnosis of retinal diseases. According to the Center's for Medicare & Medicaid Services (CMS), 10.19 million OCT related claims are filed in 2019 compared to a total of 12.54 million comprehensive eye visit claims [5]. In other words, 0.8 OCT procedures are performed per eye visit in average. Unfortunately, the use of OCT not only requires on-site operations by trained specialists but also generates immense amount of data, both of which are hardly compatible with the current telehealth paradigm: (1) the face-to-face imaging procedure would inevitably permit viral transmission and (2) the gigabyte-level data bandwidth could not be supported by current telecommunication infrastructures.

Recently, a series of technological breakthroughs has been made in unmanned operation of OCT. The Izatt Group from Duke University have demonstrated a fully automated OCT system with the aid of robotic arms and computer vision algorithms that could performed unmanned measurement of patients' retina within a minute [6]. However, the real-time (or semi-real-time) streaming of the OCT data (or images) over network remains a challenging task. For example, a commercial SS-OCT system operating at an A-line rate of 200 kHz easily leads to streaming over 400 MB raw data per second. This bandwidth is approximately 23- and 32-fold larger than that of the 5G wireless and broadband connection speed in US, respectively, which greatly hinders the application of OCT for tele-ophthalmology.

The premise of our project is that reducing OCT data bandwidth without compromising image quality is necessary for future tele-ophthalmology applications. We plan to leverage the power of artificial intelligence (AI) technology to jointly optimize the data compression and the image reconstruction schemes via an end-to-end learning approach. Specifically, for the data compression scheme, the analog OCT fringe will be first digitized at a reduced quantization resolution. After that, a small portion of the digitized data will be physically preserved according to a pre-optimized binary 2D mask to compress the bandwidth. High-fidelity images will be later reconstructed from the compressed data via a data-driven approach.

The immediate objective of the project is to demonstrate a prototype retinal OCT system that could support real-time streaming of OCT images with satisfactory quality via current network. In the long term, our vision is to combine the prototype retinal system with the robotic OCT technology developed by Izatt group to enable an unmanned compressive retinal OCT machine that is suitable for the demands of tele-ophthalmology applications.

## Literature Review

The imaging speed of OCT systems is often quantified by the A-line rate, which has been improved dramatically from several hertz to several megahertz in the past decades [7]. While a faster imaging speed has inspired a series of exciting applications such as angiography, elastography, and time-lapse imaging, it also leads to an inflated data bandwidth as computed by the following equation,

$$\text{OCT data bandwidth} = \underbrace{\frac{\text{bit depths}}{\text{sample}}}_{\text{dynamic range}} \times \underbrace{\frac{\text{samples}}{\text{A-line}}}_{\text{spectral sampling}} \times \underbrace{\frac{\text{A-lines}}{\text{second}}}_{\text{A-line rate}} \quad (1)$$

where the bit depths/sample determines the system's quantization resolution and the samples/A-line determines the system's spectral resolution during the fringe digitization.

Numerous efforts have been made to compress the OCT data by (1) decreasing the quantization resolution [8], (2) reducing the spectral resolution or bandwidth [9-13], or (3) sub-sampling the A-lines [14, 15]. Advanced signal processing techniques such as compressed sensing (CS) and deep learning (DL) could be later applied to recover the OCT data from compressed copies. Hao *et al* reported a study to reconstruct the original OCT images from reduce the bit-depth measurements. With the aid of a generative adversarial network (GAN), a peak signal-to-noise ratio (PSNR) of 25.99 dB was obtained at the data compression ratio (DCR, defined as the ratio between uncompressed size and compressed size) of 2 [8]. Liu *et al* proposed a CS-based algorithm to recover the original OCT fringes from its randomly down-sampled measurements by exploiting the sparsity prior [9]. A 9.15 dB improvement in SNR was demonstrated at a DCR of 2.5 on onion samples [10]. Mididoddi *et al* experimentally showcased a compressive time stretched-OCT system by using PRBS to randomly decimate the fringes. A DCR of 1.5 was found to produce a satisfactory reconstruction result. Recently, Zhang *et al* proposed an unsupervised DL-based method to reconstruct the OCT images. A PSNR of 24.66 and 23.40 dB were achieved at a DCR of 2 and 3, respectively [13]. Since conventional OCT relies on raster scanning to acquire images and Lebed *et al* proposed to randomly decimate the A-lines in both fast and slow scanning directions. Subsequently they employed a CS-based algorithm to reconstruct the 3D OCT volumes by promoting the sparsity in the wavelet domain [14]. A DCR of ~1.89 was achieved to render a visually satisfactory reconstruction result.

To summarize, the state-of-the-art (SOTA) compressive OCT system could achieve a PSNR of ~24 dB with a DCR of 2~3. While the image quality of those reconstructed results is mostly satisfactory, the reached DCR is far below the required level for real-time network streaming (DCR~20). In order to further improve the performance, two **innovations** as illustrated in Figure 1 are made in the proposed project.

- (1) **An end-to-end optimization strategy:** Most existing compressive OCT techniques focus on the refinement of the reconstruction algorithm but adopt a non-optimized sub-sampling scheme

(random sub-sampling, regular sub-sampling, or an empirical sub-sampling pattern) during the data compression stage. We propose a deep learning-based end-to-end approach in search of an optimal sub-sampling scheme in conjunction with a high-performance

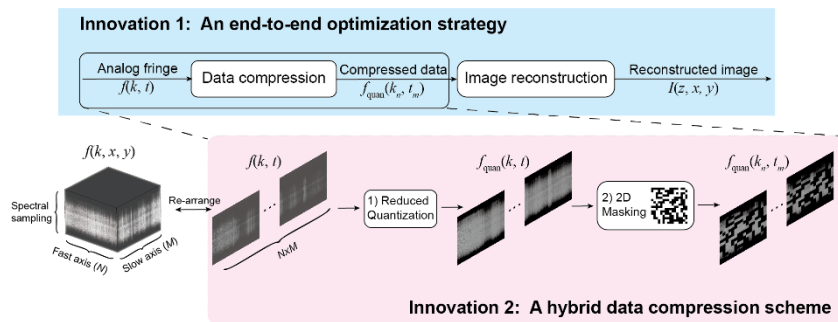


Figure 1. The proposed end-to-end optimization strategy and hybrid data compression scheme

reconstruction algorithm, which could automatically balance the data compression ratio and image reconstruction quality. Here, “end-to-end” means that we combine the data compression and image reconstruction into one optimization problem and use single merit function to regularize it.

- (2) **A hybrid data compression scheme:** Most existing compressive OCT techniques only adopt one compression scheme: compression is performed by either reducing the bit depths, sub-sampling the spectral fringes, or skipping the A-lines. In this project, we suggest that a hybrid scheme which combines multiple compression schemes could offer a better performance.

## Work Plan



**Task 1: Design and validate a jointly optimized compression and reconstruction scheme to recover high-fidelity OCT images from decimated fringe measurements using deep learning**

**Overall strategy:** Conventional approaches to implement compressive OCT are mainly optimized towards image reconstruction but not the data compression. In this study, we plan to jointly optimize the compression scheme and the reconstruction scheme to find the best sub-sampling pattern via an “end-to-end” approach. Specifically, a learnable 2D mask, which could be treated as a shallow layer of a neural network, is incorporated in our signal model to address this issue.

**Data collection and preparation:** We will collect human retinal OCT images via a custom-built swept-source optical coherence tomography system. The system is equipped with 200 kHz Axsun swept source centered at 1060 nm, which possesses an axial resolution of 7.4  $\mu\text{m}$ , lateral resolution of 10  $\mu\text{m}$  and field-of-view of 40°. Twenty volunteers will be recruited and a total of 80 volumes (80,000 B-scans) will be acquired for both eyes as the dataset. During the training, the B-scans will be randomly split into training set, validation set, and testing set in a 6:2:2 manner.

**Preliminary results:** Preliminary results were obtained by using the proposed framework as described in the following method section on a previously obtained human coronary dataset [16]. In our current algorithm development, we have not integrated the quantization reduction yet: only the two-dimensional masking was implemented. The reconstruction results obtained at DCR=2 (50% of the original data), DCR=5 (20% of the original data), and DCR=20 (5% of the original data) are presented in Figure 2. The average PSNR of 86 B-scans in the testing set was 23.87 dB, 22.15 dB, and 19.83 dB, respectively.

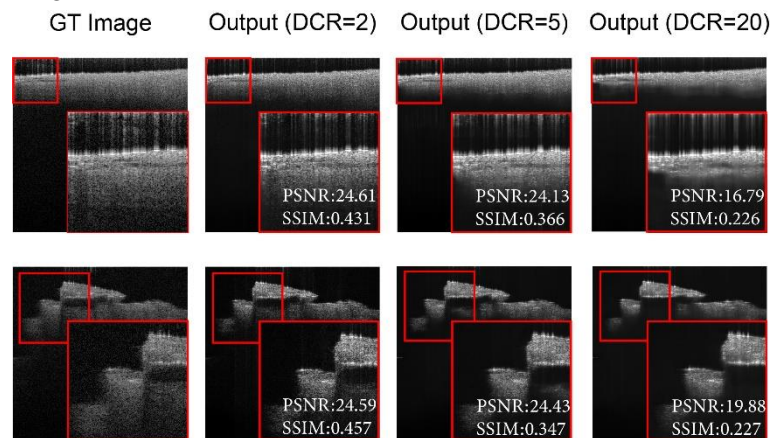


Figure 2. The comparison between the original images and the reconstructed images at different DCRs (DCR=2, 5, and 20).

**Methods and validation:** In order to jointly optimize both data compression and image reconstruction schemes, we use a training framework as illustrated in Figure 3. The framework consists of three trainable blocks: a learnable 2D mask, a fringe inpainting network (Neural network 1, NN1), and an image enhancement network (Neural network 2, NN2). During the network training, we first compress the original fringes by reducing the quantization and 2D sub-sampling the fringes. The compressed data is then inpainted by NN1 to obtain estimated fringes. After that, an IDFT is performed to convert the fringes to image domain and NN2 is used to produce refined images. Three loss functions, including the discrepancy between the original fringes and the estimated fringes ( $\mathcal{L}_{\text{fringe}}$ ), the difference between the refined image and ground truth image ( $\mathcal{L}_{\text{image}}$ ), and the difference between the quantized data and the compressed data ( $\mathcal{L}_{\text{mask}}$ ), are used for training.

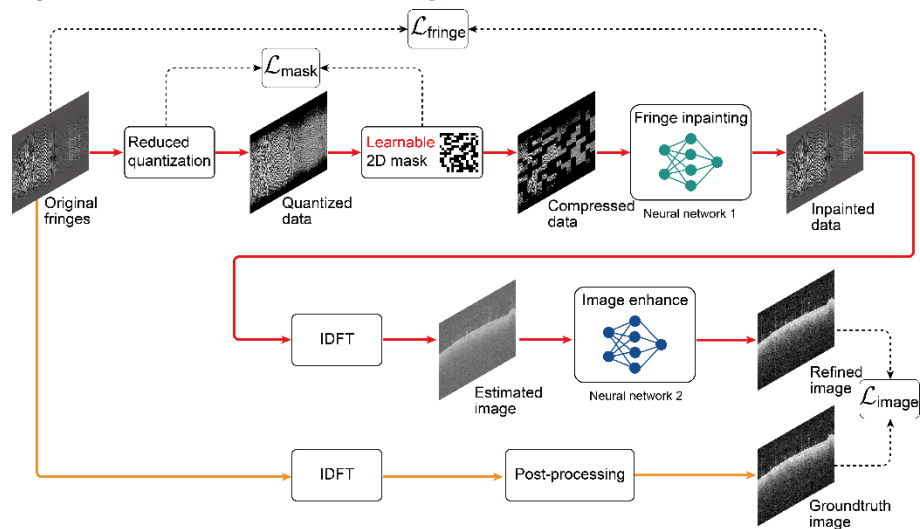


Figure 3. Proposed framework for end-to-end joint optimization of data compression and image reconstruction schemes

fringes. After that, an IDFT is performed to convert the fringes to image domain and NN2 is used to produce refined images. Three loss functions, including the discrepancy between the original fringes and the estimated fringes ( $\mathcal{L}_{\text{fringe}}$ ), the difference between the refined image and ground truth image

( $\mathcal{L}_{\text{image}}$ ), and the data compression ratio ( $\mathcal{L}_{\text{mask}}$ ), are combined to regularize the behavior of the algorithm. By backpropagating the loss functions, we could update both the learnable 2D mask and the neural networks to strike the best balance between the image reconstruction quality and the data compression ratio. In validation, we will use PSNR to evaluate the reconstruction quality and CR to evaluate the data compression performance. A PSNR larger than 20 dB with a DCR of 20 is desired.

## **Task 2: Develop and demonstrate a prototype compressive retinal SS-OCT system for tele-ophthalmology**

**Overall strategy:** We plan to implement the optimized compression scheme in an existing retinal SS-OCT and deploy the trained reconstruction algorithm in a remote host computer as illustrated in Figure 4 : the OCT and the remote computer are connected via network connections. During the operation of the proposed OCT system, the compressed data will be streamed over the network and the OCT images will be reconstructed in the remote host in real-time to showcase its utility in the future tele-ophthalmology applications.

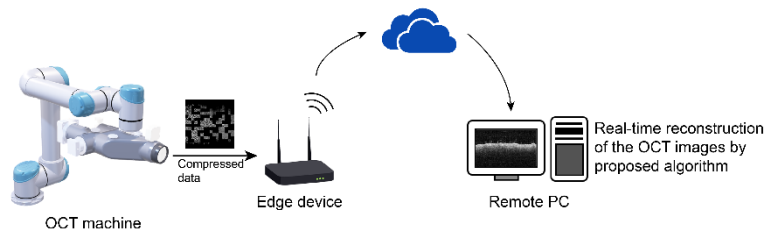


Figure 4. Schematic for the prototype compressive retinal SS-OCT

**Preliminary results:** For the data compression, we have previously demonstrated the capability of performing random skip of the fringe measurement on a commercially available DAQ board (AlazarTech ATS9360) [17]. The schematic diagram and the actually acquired masked fringe (DCR=20) are presented in Figure 5. As to the OCT machine, we will use the same OCT system as previously described in Task 1.

**Methods and validation:** For the compression scheme, we plan to re-program the field programmable gate arrays (FPGA) on a commercially available DAQ board to implement the designed compression scheme: the learned 2D mask from Task 1 will be loaded onto the DAQ board and will be used as a lookup table. The digitized fringe measurements will be either buffered or discarded according to the pattern of the mask to compress the data bandwidth to fit the network connection speed. For the image reconstruction side, we plan to accelerate the network inference speed by network pruning, knowledge distillation and parallel computing to achieve OCT image's real-time reconstruction [18]. Specifically, we will develop a software package that includes the network inference as well as the real-time visualization of the OCT images to provide good user experience. To validate the proposed idea, two DAQ boards will be used simultaneously during the experiment, where one is operated in the compression mode and the other as normal, serving as a reference. We will image both eyes of one volunteer. The discrepancy, which could be quantified by PSNR, between the reconstructed OCT images by using decimated fringe data and full-bandwidth fringe data will be calculated. A PSNR larger than 20 dB will indicate a satisfactory image quality, and the actual bandwidth utilization will be measured to determine the exact compression ratio. On the other hand, the image reconstruction speed as well as the visualization speed could be quantified by the actual frames per second (FPS) that is being displayed; An FPS exceeds 20 via common broadband is desired.

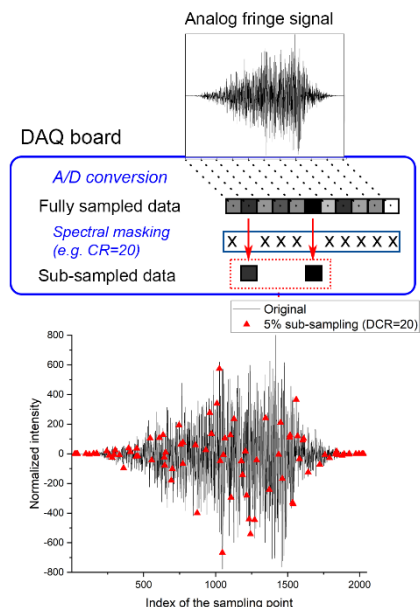


Figure 5. (Top) The implementation of masking on a DAQ board. (Bottom) The acquired sub-sampled fringe.

## **Outcomes**

**The major outcome of the project is a prototype retinal SS-OCT system that is promising for future tele-ophthalmology applications.** With the aid of AI technology, the proposed solution possesses the

potential to significantly reduce the data bandwidth without impairing the image quality, which could then be suitable for transmission over the current network infrastructure. Moreover, the proposed solution could also be optimized for real-time visualization thanks to the fast inference speed of neural networks.

Upon completing this prototype, we will file multiple intellectual properties and translate it into clinical spaces by leveraging existing resources: we have already developed extensive connections with both domestic and international clinical institutions including Shanghai General Hospital and Singapore National Eye Centre via academic collaborations [19, 20].

In addition to the prototype machine, a full package of codes including network training, network inference, and real-time visualization will be delivered. All research progresses will be presented and published in Optica-organized symposiums and Optica open-access journals.

## Impact

***Technological:*** The success of the proposed project would lead to a new state-of-the-art performance of compressive SS-OCT system, which utilizes the lowest data bandwidth with best image quality. In contrast to the prior arts, our solution only involves minimal modifications from hardware's perspective and is compatible with most existing SS-OCT systems. Moreover, the proposed "end-to-end" optimization paradigm could potentially be translated to other medical imaging modality to inspire other format of compressive imaging system. It is also our intent to make the proposed algorithms and software packages as user-friendly as possible to facilitate their dissemination among academic researchers, clinical practitioners and application developers. All the dataset and codes included in this project will be open-sourced pending the permission of Optica Foundation.

***Societal:*** In addition to the quantitative merits, it would also enable the real-time streaming of OCT data via common broadband connections for the first time, which, in combination with the emerging robotic OCT technology, would bring us closer to the realization of the first-generation tele-OCT system. We believe such a progress would also bring a huge societal impact given the ongoing pandemic: millions of patients with eye conditions that requires routine examinations could potentially benefit from this advance.

## Cited References

1. "Monthly Telehealth Regional Tracker," <https://www.fairhealth.org/states-by-the-numbers/telehealth>.
2. C. L. Snoswell, et al., "Telehealth and coronavirus: Medicare Benefits Schedule (MBS) activity in Australia," <https://coh.centre.uq.edu.au/telehealth-and-coronavirus-medicare-benefits-schedule-mbs-activity-australia>.
3. S. Y. Patel, et al., Health Aff. **40**, 349-358 (2021).
4. S. M. Saleem, L. R. Pasquale, P. A. Sidoti, and J. C. Tsai, Am. J. Ophthalmol **216**, 237-242 (2020).
5. CMS, "Part B National Summary Data File," <https://www.cms.gov/Research-Statistics-Data-and-Systems/Downloadable-Public-Use-Files/Part-B-National-Summary-Data-File/Overview>.
6. M. Draelos, et al., Nat. Biomed. Eng **5**, 726-736 (2021).
7. T. Klein, and R. Huber, Biomed. Opt. Express **8**, 828-859 (2017).
8. Q. Hao, et al., J. Biomed. Opt. **25** (2020).
9. X. A. Liu, and J. U. Kang, Opt. Express **18**, 22010-22019 (2010).
10. D. Xu, Y. Huang, and J. U. Kang, Opt. Lett. **39**, 76-79 (2014).
11. C. K. Mididoddi, et al., IEEE Photonics J. **9** (2017).
12. W. Liao, et al., Opt. Lett. **44**, 2955-2958 (2019).
13. Y. Zhang, et al., Light Sci. Appl. **10**, 155 (2021).
14. E. Lebed, S. Lee, M. V. Sarunic, and M. F. Beg, J. Biomed. Opt. **18** (2013).
15. J. Wang, Y. Hu, and J. Wu, Appl. Opt. **57**, 10056-10061 (2018).
16. X. Li, et al., IEEE Trans. Biomed. Eng., 1-1 (2022).
17. Y. Ling, et al., Opt. Express **27**, 855-871 (2019).
18. Q. Zhang, et al., Neurocomputing **323**, 37-51 (2019).
19. J. Li, et al., Biomed. Opt. Express **12**, 2204-2220 (2021).
20. Y. Ling, et al., Opt. Lett. **45**, 6394-6397 (2020).

## Ultra-Compact and Efficient Electro-Optic Modulation Using Nanophotonics (Category: Information)

### Challenge:

Exponential growth of data traffic, information and communication devices, and power-hungry data centers have led to a rapid increase in global electricity consumption. To minimize their energy usage and environmental impact, there is an urgent need to develop miniaturized electro-optic modulators (EOMs) that are more energy-efficient and cost-effective. Over the years, a wide variety of electro-optic materials and photonic designs have been integrated with EOMs on a chip platform to extend the performance boundaries, but their device compactness, modulation efficiency, energy consumption, and optical bandwidth are still limited.

### Proposed Project:

Here we propose to create a hybrid plasmonic-photonic (HPP) EOM incorporating a two-dimensional (2D) polar semiconductor to overcome the limitations. The HPP waveguide structure enables deep-subwavelength transmission with an extreme optical mode confinement down to a nanometer thin dielectric region. A large spatial field overlap with an embedded 2D polar semiconductor is thus possible, and the accompanied plasmonic enhancement will significantly increase the light-matter interaction over a broad range of wavelengths. 2D polar semiconductors have unconventional out-of-plane dipoles that can align with the transverse magnetic (TM) mode of the HPP waveguide, which leads to a gigantic electro-refractive effect. *Our goal is therefore to experimentally realize this new EOM device architecture and demonstrate superior performance in terms of device size, modulation efficiency, energy consumption, and optical bandwidth.* New 2D polar semiconductors with a strong out-of-plane polarization and negligible absorption loss over a broad telecommunication wavelength band will also be identified and tested.

Our research contains two main tasks: (i) *Design of EOMs integrating HPP waveguides and 2D polar semiconductors.* We will explore different HPP waveguide geometries to maximize the mode overlap and model the electrical and optical effects of incorporating 2D out-of-plane dipoles. We will also carry out a system-level design of EOMs and investigate design tradeoffs to optimize the mode overlap, interaction length, modulation efficiency and speed, as well as energy consumption. (ii) *Experimental demonstration of 2D polar semiconductors and high-performance EOMs.* We will exfoliate and transfer 2D polar semiconductors onto substrates to study their crystal structures, surface morphology, and intrinsic optoelectronic properties, besides verifying their out-of-plane dipole characteristics. We will utilize standard cleanroom nanofabrication techniques to realize EOMs and thoroughly characterize their modulator behaviors and performances. These tasks encompass theoretical design and electrical-optical-circuit multiphysics simulations, nanofabrication process development and device integration, as well as rigorous measurement for conceptual validation and performance characterization. The project will have a 1-year duration.

### Research Outcomes and Impacts:

Our research is expected to deliver the following outcomes: (i) Verification of the nanophotonic approach and the demonstration of high-performance EOM devices; (ii) The filing of one patent and the publication of two high-impact journal papers prioritizing Optica open-access journals; (iii) Dissemination of research results in leading conference, invited seminars, and Optica-organized symposiums, Optics & Photonics news magazine, Optica's websites and facebook pages; (iv) Integration of knowledge generated into educational courses and training of students to help their career growth in photonics.

Our nanophotonic approach will overcome EOMs' bottleneck of weak light-matter interaction and enable truly compact EOMs for densely-integrated information processing on chip with superior performance. Ultralow energy consumption can be envisioned, thus reducing the electricity usage in data centers and allowing optical interconnects to compete with electrical interconnect technologies. Low driving voltage and capacitance achievable in our device permits CMOS-compatible operation and higher modulation speed. Wavelength-division multiplexing for high-throughput communication links will be possible owing to our device's broadband operation. Our research will drive the field of energy-saving information processing and accelerate on-chip information networking and computing.

# Ultra-Compact and Efficient Electro-Optic Modulation Using Nanophotonics

## 1. Background and Literature Review

Rapid growth of the world's internet traffic has propelled data centers into the zettabyte era, where annual traffic is projected to exceed 2.2 zettabytes per year<sup>1</sup>. Energy consumption of data centers and information and communication technologies continue to rise at an alarming pace. This calls for an energy-efficient solution to encode data and transmit signals. Central to long-haul optical communication links and short-reach data center interconnects are electro-optic modulators (EOMs), which imprint electrical signals on a light wave to produce an optical encoded data stream. Conventional EOMs rely on nonlinear crystals to modulate light, but they are often too bulky, costly, and inefficient<sup>1,2</sup>. There is thus a growing interest to miniaturize EOMs into waveguides compatible with integrated photonics.

In recent years, a wide variety of electro-optic (EO) materials have been integrated on chip-scale silicon photonic platforms to push for enhanced modulation performances, including silicon, lithium niobate, III-V semiconductors, electro-optic polymers, transparent conducting oxides, phase-change materials, and two-dimensional (2D) materials<sup>1,2</sup>. Different principles had been exploited on these materials to achieve either phase modulation (via Pockels effect or Kerr effect) or absorption modulation (via Franz-Keldysh effect, quantum-confined Stark effect (QCSE), or plasma dispersion effect)<sup>2,3</sup>. Electro-absorption modulators (EAMs) generally have a smaller device footprint and are most energy-efficient due to strong electro-absorption near the band-edge wavelength, as demonstrated in many III-V<sup>4,5</sup> and group-IV<sup>6</sup> waveguide devices. However, to encode information in complex modulation formats for higher bit rates, electro-refractive modulators that rely on *phase modulation* are critically needed<sup>7</sup>.

For phase modulators, a large effective refractive index change  $\Delta n_{eff}$  is sought after, as it governs the amount of phase shift that can be introduced to the light. Its importance is also reflected by the length of the phase shifter  $L$  (or interaction length) and the voltage applied to attain  $\Delta n_{eff}$  sufficient to trigger a  $\pi$  phase shift, denoted as  $V_\pi$ . A key performance metric in modulators is the modulation efficiency  $V_\pi L$ . A small  $V_\pi L$  corresponds to a high modulation efficiency, as it requires less driving voltage and a shorter waveguide length to encode an optical signal. In addition, a broadband low-loss EO material is needed to produce a negligible absorption during the phase modulation. Energy consumption is another important performance indicator, which is manifested by mean energy lost per bit.

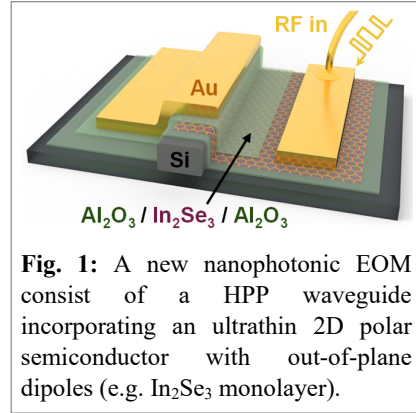
Conventional integrated phase modulators based on silicon, III-V semiconductors, and lithium niobate usually have a large device footprint and a low modulation efficiency<sup>2,8</sup>. This stems from the low  $\Delta n$  achievable in silicon (due to the weak plasma dispersion) and in III-V semiconductors (due to the weak EO coefficient), and the weak optical confinement resulting from the low refractive index contrast in lithium niobate waveguides<sup>1,2,8</sup>. Phase modulators that are more compact and efficient have been realized using transparent conducting oxides (TCOs)<sup>9,10</sup>, electro-optic polymers (EOPs)<sup>11,12</sup>, phase-change materials (PCMs)<sup>13</sup>, and 2D materials<sup>7,14</sup>. However, the performance of state-of-the-art phase modulators still face major limitations: (i) EOP EOMs suffer from a large device footprint (when a silicon slot waveguide is used<sup>12</sup>) or a high propagation loss (when a metal-insulator-metal waveguide is incorporated<sup>11</sup>); (ii) TCO EOMs have a relatively narrow optical bandwidth (*i.e.* spectral response) due to TCO's dispersion and the narrow wavelength range of epsilon-near-zero (ENZ) proximity<sup>9</sup>; (iii) PCM EOMs have a low EO bandwidth due to their intrinsically slow phase transition speed<sup>13</sup>; (iv) EOMs based on graphene<sup>7</sup> and transition metal dichalcogenide (TMDC)<sup>14</sup> suffer from an extremely small mode overlap that leads to a low modulation efficiency and a relatively large interaction length ( $\sim 300 \mu\text{m}$ ). Many high-performance electro-optic phase modulators utilized a microresonator to increase the light-matter interaction to reduce the device length and energy consumption, but this comes at the expense of a narrow optical bandwidth, low thermal stability, and a stringent fabrication tolerance. Therefore, it is essential to address the problems of narrowband operation, large device footprint, and low energy efficiency in existing electro-optic phase modulators.

## 2. Problem Statement, Technical Approach and Research Goal

In light of the above limitations, a pressing **challenge** is identified: *Is it possible to create a new ultra-compact device architecture that maximizes light-matter interaction to attain a small  $V_\pi L$  and reduced energy consumption, without the use of a microresonator?*



Here we propose a new type of non-resonant EOM based on a hybrid plasmonic-photonic (HPP) waveguide with an integrated 2D material (**Fig. 1**). A HPP waveguide makes use of a metal and a high and low refractive index contrast to support a strongly-enhanced optical mode that breaks the diffraction limit<sup>10,15</sup>. Extreme optical mode confinement down to a nanometer is possible, which is two orders of magnitude smaller than the mode size of conventional photonic waveguides. A large spatial field overlap with an embedded 2D monolayer is thus possible, and the accompanied plasmonic enhancement will significantly increase the light-matter interaction over a broad range of wavelengths. In contrast to conventional plasmonic waveguides, a much lower optical loss is expected for HPP waveguides owing to their ability to concentrate electric fields in the dielectric regions away from the metal. HPP waveguides also produce a lower impedance mismatch with standard silicon-on-insulator (SOI) waveguides, thus promises a more efficient coupling and a lower insertion loss. However, HPP modes are transverse magnetic (TM) in nature, meaning the electric field is polarized in the out-of-plane direction, which is orthogonal to in-plane dipoles commonly found in standard 2D materials. We therefore propose the incorporation of a 2D polar semiconductor with out-of-plane dipoles into a HPP waveguide to maximize the field interaction and the electro-refractive effect. We have identified  $\text{In}_2\text{Se}_3$  monolayer as a promising 2D polar crystal candidate with a large intrinsic out-of-plane polarization<sup>16,17</sup>. Additionally,  $\text{In}_2\text{Se}_3$  monolayer has negligible absorption over the entire telecommunication wavelength band. Its integration into HPP waveguides will enable a broadband EO effect that attains a large  $\Delta n_{\text{eff}}$  and a low  $V_{\pi}L$  while retaining a low loss. **Our goal is therefore to experimentally realize this new EOM device architecture and demonstrate superior performance in terms of device size, optical bandwidth, modulation efficiency, and energy consumption.**



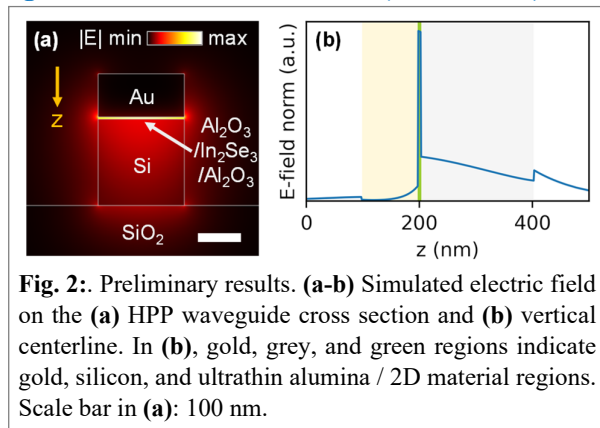
**Fig. 1:** A new nanophotonic EOM consist of a HPP waveguide incorporating an ultrathin 2D polar semiconductor with out-of-plane dipoles (e.g.  $\text{In}_2\text{Se}_3$  monolayer).

### 3. Research Tasks and Work Plan

#### 3.1 Design of EOMs Incorporating HPP Waveguides and Ultrathin 2D Polar Semiconductors

##### 3.1.1 Electromagnetic Simulation and Modeling of 2D Polar Semiconductors (Months: 1-6)

We will engineer the optical mode and propagation properties of the HPP waveguide using electromagnetic simulations based on the finite-element method (FEM) and finite-difference time-domain (FDTD) methods. To highlight the design flow and concept, some preliminary results are shown in **Fig. 2**. The electric field distribution of the HPP waveguide mode is plotted in **Fig. 2a**, wherein the electric field norm within the 2D material region ( $\text{In}_2\text{Se}_3$ ) exhibits a large enhancement compared to the surrounding volume. **Fig. 2b** more quantitatively illustrates this effect by drawing the electric field trace along a vertical line through the waveguide center.



**Fig. 2:** Preliminary results. **(a-b)** Simulated electric field on the **(a)** HPP waveguide cross section and **(b)** vertical centerline. In **(b)**, gold, grey, and green regions indicate gold, silicon, and ultrathin alumina / 2D material regions. Scale bar in **(a)**: 100 nm.

To demonstrate the enhancement offered by the HPP geometry, we also plot the optical field confinement  $\Gamma$  within the  $\text{In}_2\text{Se}_3$  monolayer (modeled to be  $\sim 1$  nm thick) in **Fig. 3**, which shows an accelerating increase in the fraction of optical energy inside the 2D material as the thickness of low index region ( $\text{Al}_2\text{O}_3/\text{In}_2\text{Se}_3/\text{Al}_2\text{O}_3$ ) decreases. At nanoscale gap sizes,  $\Gamma$  reaches 3%, far exceeding the performance of existing 2D materials based modulators that rely on pure silicon waveguides with a small field overlap. For example, *state-of-the-art monolayer  $\text{WS}_2$ -based capacitive modulators only achieved a  $\Gamma$  of 0.016%*<sup>14</sup>, a figure improved by our preliminary waveguide structure by a factor of 187. Furthermore, the light-matter interaction of HPP waveguides is enhanced by a factor of 5 owing to their elevated group index  $n_g=10$  compared to the typical group index of silicon nitride waveguides ( $n_g \sim 2$ ). Building upon this promising result, we will continue optimizing the HPP waveguide geometry to maximize the mode overlap and the strength of light-matter interaction.



Beyond the study of waveguide optics, we will model the effects of incorporating 2D materials with out-of-plane dipoles. Whereas the typical picture of 2D materials' in-plane optical behavior can be modeled using effective sheet conductivities, the optical response of out-of-plane dipoles require a more sophisticated picture to consider the confined electronic wavefunction that exists within the few-angstrom atomic layer. Additionally, the pronounced refractive index change induced through the injection of large amounts of charge carriers may affect the optical energy distribution, which we will also characterize and address computationally.

### 3.1.2 System-level Electro-Optic Modulator Design (Months: 3-9)

We will perform in-depth design of HPP-based EOMs incorporating different 2D polar semiconductors, including the calculation of modulation efficiency, energy consumption, EO bandwidth, and physical footprint. For an  $\text{In}_2\text{Se}_3$  monolayer, since effective mode index shift is determined by the mode confinement  $\Gamma$ , material index change  $\Delta n_{mat}$ , and the waveguide group index, where  $\Delta n_{eff} = \Gamma \times (\Delta n_{mat}/n_{mat}) \times n_g$ , we expect a combined three orders of magnitude ( $187 \times 5$ ) improvement in  $V_\pi L$  over the referenced 2D TMDC-based phase modulator<sup>14</sup>. This reduces  $V_\pi L$  from 8 V mm to below 0.01 V mm, which will mark a record-high modulation efficiency. The strong electro-refractive effect will also reduce the interaction length to  $\sim 4 \mu\text{m}$  while enabling 0.25 V, CMOS-compatible operation. By shrinking the device size, its capacitance, calculated using a parallel plate capacitor model  $C = \epsilon_0 \epsilon_r A/d$ , can be reduced to 7.1 fF. Therefore, the switching energy determined by the capacitive discharge process, where  $U_C = CV^2/2$ , is calculated to be only 2.2 fJ/bit. Given similar 2D material sheet conductivity, gigahertz-scale EO bandwidths similar to existing 2D material modulator performance can be achieved. Beyond calculating the performance metrics, we will leverage both optics and electric current simulations to extract and engineer the contributions of various sources of electrical and optical loss, including optical losses from scattering and plasmonic absorption.

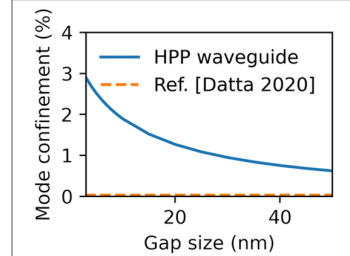
We will identify and address fundamental tradeoffs associated with our proposed modulator design and optimize extrinsic device parameters. To test and characterize the EOM, we will design and optimize the device's supporting electronics and optics. The electrode structure will be designed for good impedance matching to off-chip high-speed driver electronics through microwave engineering. The modulator will also be designed in a Mach-Zehnder interferometer (MZI) configuration to extract  $\Delta n_{eff}$  and  $\Delta k_{eff}$  (effective extinction coefficient). We will split and convert optical signals with multimode interferometers (MMI) and HPP mode converters, respectively, using contemporary FDTD design techniques. Grating couplers will also be designed for low-loss injection and detection of laser light.

## 3.2 Experimental Demonstration of 2D Polar Semiconductors and High-Performance EOMs

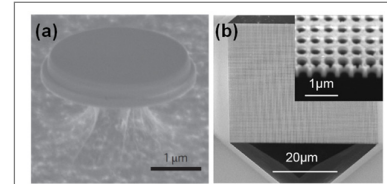
### 3.2.1 Fabrication and Characterization of 2D Polar Semiconductors (Months: 1-9)

Wong will utilize the standard mechanical exfoliation technique to obtain 2D monolayer samples. Bulk crystals will be purchased from a company (e.g. 2D Semiconductors Inc.) and monolayers will be exfoliated onto  $\text{SiO}_2/\text{Si}$  substrates. The presence and position of 2D polar semiconductors will be recorded using Raman spectroscopy and photoluminescence scan. Next, we will transfer the identified  $\text{In}_2\text{Se}_3$  monolayer samples using a capillary-force-assisted clean-stamp method. **Fig. 4** shows our past successful transfer of different 2D monolayers on various micro/nanostructures<sup>18,19</sup>. We will also pattern metal electrodes on the 2D polar semiconductors for electrical characterization.

Wong will characterize the properties of 2D polar semiconductors: (i) Crystal structures, surface morphology, and electrical properties: We will utilize a high-angle annular dark-field scanning transmission electron microscopy (HAADF-STEM) system to visualize the 2D material's crystal structure. Cross-section HAADF-STEM



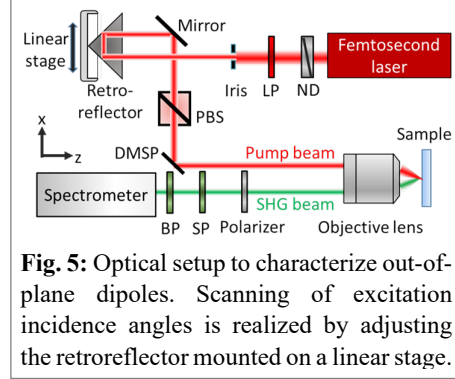
**Fig. 3:** Optical energy confinement within the 2D material for our HPP waveguide far exceeds that of a conventional silicon waveguide published in *Nature Photonics*<sup>14</sup>.



**Fig. 4:** Our previous work integrating (a) a  $\text{WS}_2$  monolayer between  $\text{Si}_3\text{N}_4$  and HSQ to realize a microdisk laser<sup>18</sup>, and (b) a  $\text{WSe}_2$  monolayer on a  $\text{Si}_3\text{N}_4$  photonic crystal slab to demonstrate brightening of dark excitons<sup>19</sup>.

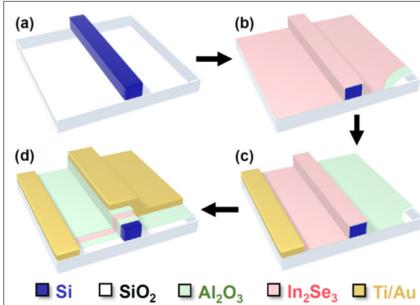
images will reveal the polar structure of the 2D materials. Using a confocal Raman microscopic system, we will analyze Raman characteristic peaks to confirm the quality and phase of 2D polar monolayers. The monolayers' thickness and surface morphology will be examined using an atomic force microscope (AFM). We will utilize a probe station in conjunction with a semiconductor parameter analyzer to measure their electronic properties such as conductivity, carrier density, mobility, and contact resistance.

**(ii) Optical properties and out-of-plane dipoles:** We will perform transmission, absorption, and photoluminescence measurements using a fluorescence microscope to obtain optical response spectrum of the 2D polar monolayers. We will build an angle-resolved polarization-selective second-harmonic generation (SHG) spectroscopy setup to detect the out-of-plane dipoles in the 2D monolayers (**Fig. 5**). The principle lies in the removal of in-plane dipole SHG signals by rotating the monolayer to a certain crystal angle where the specific bond direction becomes perpendicular to both incident and detecting polarization directions. An incoming tilted beam with vertical electric field polarization will excite the out-of-plane dipoles and produce a SHG signal.



**Fig. 5:** Optical setup to characterize out-of-plane dipoles. Scanning of excitation incidence angles is realized by adjusting the retroreflector mounted on a linear stage.

### 3.2.2 Fabrication and Characterization of Electro-Optic Modulators (Months: 3-12)



**Fig. 6:** Fabrication process. (a) EBL and RIE patterning of silicon waveguide. (b) ALD of  $\text{Al}_2\text{O}_3$  and transfer of  $\text{In}_2\text{Se}_3$  monolayer. (c) ALD of  $\text{Al}_2\text{O}_3$ , EBL patterning and liftoff of  $\text{Ti}/\text{Au}$ , and EBL patterning and etching of  $\text{In}_2\text{Se}_3$  monolayer. (d) Masked ALD of  $\text{Al}_2\text{O}_3$ , EBL patterning and liftoff of  $\text{Au}$ .

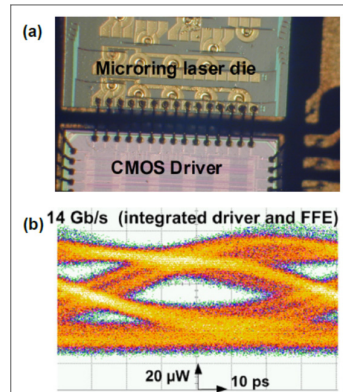
Wong will use a standard silicon-on-insulator (SOI) wafer to fabricate the proposed EOM incorporating a 2D polar semiconductor. **Fig. 6** shows key nanofabrication steps that include electron beam lithography (EBL), reactive ion etching (RIE), atomic layer deposition (ALD), 2D material transfer, electron-beam evaporation, and liftoff. In addition, we will also pattern a Mach-Zehnder interferometer (MZI) embedding the 2D material-integrated HPP waveguide on one arm.

For the characterization of EOM performance, we will couple TM-polarized light from a tunable laser (1500–1620 nm) into and out of the waveguide and MZI via grating couplers. The transmission spectrum for different bias voltages will be recorded to measure the phase shift and absorption change. By measuring the wavelength shift of the MZI transmission spectra and through numerical fitting with simulation results, we can further extract the gating-

induced  $\Delta n_{\text{eff}}$  of our device. We will also utilize the measured extinction ratio of the transmission of the unbalanced MZI to extract the insertion loss of our device. For the measurement of the EOM's dynamic response, electrical signal generated by a network analyzer will be superimposed onto a static drive voltage for small signal measurement. An ultrafast photodiode will be used for the signal detection and a 3 dB electro-optic bandwidth will be measured. **Fig. 7** shows past electro-optic measurement results which confirm our experimental capability to perform high-speed measurement. By measuring the reflection coefficient  $S_{11}$  using the network analyzer, we can further determine the capacitance of our device and understand the origin of the speed limit. Using the measured voltage and capacitance, we will be able to estimate the mean energy loss per bit.

## 4. Research Outcomes

**(i) Idea validation and device demonstration:** The physics and feasibility of our nanophotonic approach will be confirmed via rigorous simulations and experiments. We will demonstrate ultra-compact,



**Fig. 7:** (a) On-chip EO modulation of a multiplexed signal. (b) High-speed optical transmitter eye-diagram.

broadband, and energy-efficient EOMs on an integrated chip platform. New ideas on ways to further improve EOM performances will be developed, which paves the way for subsequent federal funds and academic/industrial collaborations, and hence sustained growth of the technology.

(ii) Patent and publications: We plan to file a patent for our novel HPP EOM integrating 2D materials with out-of-plane dipoles. In addition, we aim to publish two papers in high-impact journals, one on the detailed simulations on our EOM's device architecture and performance tradeoffs, and the other one on the experimental realization. Optica open-access journals will be prioritized in our submissions.

(iii) Conference presentations, invited talks and results dissemination: We will present key research findings in leading photonics conferences such as CLEO and FiO, and deliver invited seminars in universities and industries. We will highlight our work in Optica-organized symposiums, Optics & Photonics news magazine, Optica's websites and facebook pages to promote the photonic solution.

(iv) Education and student training: Knowledge gained in this project will be incorporated into courses taught by the PI, e.g. "*Optoelectronic Materials and Devices*" and "*Metamaterials and Nanophotonics*". Students will be exposed to state-of-the-art nanophotonics and EOM technologies, and will acquire critical skills in simulation, nanofabrication, electrical and optical measurements. This will propel their scientific growth and cultivate their future careers in photonics.

## 5. Research Impact

Our nanophotonic approach explores extreme confinement of light to overcome the weak light-matter interaction bottlenecks in EOMs. This enables truly compact EOMs down to single-digit  $\mu\text{m}$  device length, which allows densely-integrated chip-scale information processing with superior performance at a lower cost. Ultralow energy consumption of 2.2 fJ/bit can be envisioned, which can significantly reduce the electricity usage in power-hungry data centers and minimize the environmental impact. This also addresses the critical demand of <10 fJ/bit required for optical interconnects to compete with future electrical interconnect technologies. Sub-1 Volt modulation and <10 fF capacitance achievable in our device permits CMOS-compatible operation and higher modulation speed. Our non-resonant device architecture further guarantees broadband operation essential for wavelength-division multiplexing (WDM) to deliver high data bandwidths for high-throughput communication links. 2D materials are easy to fabricate on a silicon photonics platform and are conducive for cost-effective and large-scale integration. Our tightly coupled photonic-electronic integration will drive the field of energy-saving information processing and accelerate on-chip information networking and computing. This work will also impact the field of light detection and ranging (LiDAR), display, environmental monitoring, biosensing, and future quantum and neural networks.

## References

1. Rahim, A., et al., **Advanced Photonics**, 2021. 3(2): p. 024003.
2. Sinatkas, G., et al., **Journal of Applied Physics**, 2021. 130(1): p. 010901.
3. Sun, Z., A. Martinez, and F. Wang, **Nature Photonics**, 2016. 10(4): p. 227-238.
4. Nozaki, K., et al., **Nature Photonics**, 2019. 13(7): p. 454-459.
5. Nozaki, K., et al., **APL Photonics**, 2017. 2(5): p. 056105.
6. Timurdogan, E., et al., **Nature communications**, 2014. 5(1): p. 1-11.
7. Sorianello, V., et al., **Nature Photonics**, 2018. 12(1): p. 40-44.
8. Liu, K., et al., **Laser & Photonics Reviews**, 2015. 9(2): p. 172-194.
9. Amin, R., et al., **Optica**, 2020. 7(4): p. 333-335.
10. Sorger, V.J., et al., **Nanophotonics**, 2012. 1(1): p. 17-22.
11. Haffner, C., et al., **Nature**, 2018. 556(7702): p. 483-486.
12. Koeber, S., et al., **Light: Science & Applications**, 2015. 4(2): p. e255-e255.
13. Joushaghani, A., et al., **Optics Express**, 2015. 23(3): p. 3657-3668.
14. Datta, I., et al., **Nature Photonics**, 2020. 14(4): p. 256-262.
15. Oulton, R.F., et al., **Nature Photonics**, 2008. 2(8): p. 496.
16. Xiao, J., et al., **Physical Review Letters**, 2018. 120(22): p. 227601.
17. Ding, W., et al., **Nature Communications**, 2017. 8(1): p. 1-8.
18. Ye, Y., et al., **Nature Photonics**, 2015. 9(11): p. 733-737.
19. Ma, X., et al., **arXiv preprint arXiv:2110.09639**, 2021.